

International Committee for Solvent
Extraction Chemistry and Technology

European Federation of Chemical Engineering



ISEC '86 International Solvent Extraction Conference

Preprints

Volume III

München, Fed. Rep. of Germany
11 — 16 September 1986



Extraction Equipment

Vol. III

Contents

Page

Choice of extraction equipment in chemical processes R. Berger, Ludwigshafen/D	3- 10
Mass transfer characteristics of an agitated column depending on material properties G. Goldmann, E. Blaß, München/D	11- 20
Rapid multistage solvent extraction using the SISAK technique J. Rydberg, G. Skarnemark, Göteborg/S	21- 29
Axial dispersion in pulsed packed columns on both laboratory and industrial scale A.J.F. Simons, R. van Sluys, Geleen; J.C. Göebel, J.M.H. Fortuin, Amsterdam/NL	31- 37
Supercritical fluid extraction in column contactors R.J. Lahiere, J.R. Fair, J.L. Humphrey, Austin, TX/USA	39- 44
Some aspects of high-pressure-extraction process engineering H.J. Gähns, H.J. Beutler, U. Lenhard, F. Lürken, Krefeld/D	51- 53
Hydrodynamics of a section of a large sieve tray extractor R.B. Eldridge, J.L. Humphrey, J.R. Fair, Austin, TX/USA	55- 62
Hydrodynamic behaviour of a rotary agitated column with electrostatic coalescence R.H. Stitt, P.J. Bailes, Bradford/UK	63- 70
The components of the coalescence process in dense dispersions T. Mišek, Praha/CS	71- 79
Measurement of coalescence in agitated dispersions by light transmittance technique V. Hančil, V. Rod, J. Reznicková, Praha/CS	81- 88
An optical fibre probe for the simultaneous measurement of particle size and velocity in two-phase flows J.L. Plawsky, T.A. Hatton, Cambridge, MA/USA	89- 98
Mass transfer effect on hydrodynamics in reciprocating plate extraction column A. Bensalem, L. Steiner, S. Hartland, Zürich/CH	99-106
Influence of dispersed phase on power consumption in vibrating plate columns V. Pavašović, R. Stevanović, Beograd/YU; J. Prochazka, Praha/CS	107-113
Design and application of packed columns for liquid-liquid-extraction R. Billet, A. Grosch, J. Mäckowiak, M. Pajak, Bochum/D	115-121
Gas agitated liquid-liquid extraction in columns filled with regularly arranged Bialecki rings R. Billet, Chr. Braun, Bochum/D	123-128

The effects of dispersed phase mixing on extraction of metals K. Bae, L.L. Tavlarides, Syracuse, NY/USA	129-133
Hydrodynamics in a multistage column extractor; Axial holdup, drop size distribution V. Kirou, J.C. Bonnet, L.L. Tavlarides, Syracuse, NY/USA	135-141
Study on scale up of Kühni column Yu Ming Jiang, Bing Yao Sun, Shanghai/China	143-147
Aspects of pulsed sieve plate column behaviour A. Hussain, N.J. Slater, Bradford/UK; A. Marrocchelli, Rome/I	149-156
Correlation of design parameters for the sieve plate extraction column (SPC) J.O. Oloidi, C.V. Jeffreys, C.J. Mumford, Birmingham/UK	157-165
Scale-up of the Kühni column based on the backflow model K.H. Elsässer, U. Bühlmann, Allschwil/CH	167-174
The effect of column diameter on performance of pulsed plate extractors L.M. Fitzpatrick, H.R.C. Pratt, G.W. Stevens, Melbourne, Vic./AUS	175-181
Power requirement of large pulsed perforated plate column Haijie Chen, Shanghai/China	183-189
Determination of mass transfer rates in an reciprocating-plate extraction column L. Steiner, A.K. Bensalem, S. Hartland, Zürich/CH	191-198
Pilot plant investigation and simulation of a liquid-liquid extraction column I.Colussi, V. Gallo, C. Luciani, U. Preti, Trieste/I	199-206
Experimental design, deconvolution of RTD data and response surface analysis in solvent extraction J.J. Porta, A. Merz, Karlsruhe/D	207-214
Evaluation of mass transfer and axial mixing parameters in pulsed sieve plate extraction columns Xia Lei, Quian Yu, Weiyang Fei, Jiading Wang, Beijing/China	215-222
Separation of unstable emulsions in highly efficient mixer-settler contactor L.I. Sklokin, V.E. Leif, S.M. Masloboeva, Moscow/USSR	223-224
Study on phase separation in settler Yuming Jiang, Bingyao Sun, Qi Zhao, Shanghai/China	225-230
Evaluation of drop size and hold-up in axially agitated plate columns H. Sovová, J. Procházka, Praha/CS	231-237
Thermodynamics modelling of backmixing-effect in an mechanical agitated extraction column R.S. Bes, J. Molinier, Toulouse, J.C. Mora, Odeillo/F	239-246
Axial mixing in pulsed sieve-plate extraction columns E. Auferheide, A. Vogelpohl, Clausthal-Zellerfeld/D	247-254
A new stirred cell M. Waubke, W. Nitsch, Garching/D	255-263

Multicomponent, high flux, interphase mass transfer in liquid-liquid extraction W.J. Korchinsky, C.H. Young, E.D. Negri, Manchester/UK	265-272
Mass transfer on freely suspended single droplets H.-B. Rhein, K. Schügerl, Hannover/D	273-280
Modelling of mass transfer in solvent extraction M. Siebenhofer, R. Marr, Graz/A	281-284
The effect of interfacial turbulence on mass transfer S.H. Zhang, Z.M. Wang, Yuanfu Su, Shanghai/China	285-291
Modelling an apparatus in emulsion liquid membrane operations D. Lorbach, Cambridge, MA/USA; J. Bart, R. Marr, Graz/A	293-300
A comparative performance test for the extraction/re-extraction process and the supported liquid membrane process M. Fröhlich, W. Nitsch, Garching/D	301-308
Simultaneous determination of breakage and coalescence rates in agitated liquid-liquid dispersions M. Laso, L. Steiner, S. Hartland, Zürich/CH	309-316
Drop dispersion in impeller vortex systems M.M. C.G. Warmoeskerken, I. Bouwmans, J.M. Smith, Delft/NL	317-324
The effect of ionic solutions on holdup and flood point for pulsed plate columns L.M. Fitzpatrick, H.R.C. Pratt, G.W. Stevens, Melbourne, Vic./AUS	325-330
Prediction of bulk disengagement rates in continuous solvent extraction settlers P.D. Martin, C.L. Stockwell, Harwell, Oxon/UK	331-338
Hydrodynamics in mixer-settlers with liquid membranes H. Lackner, H.J. Bart, R. Marr, Graz/A	339-344
Behaviour of drops in a centrifugal field D.B. Todd, G.R. Davies, H.A. Lange, Saginaw, MI/USA	345-351
Development of an automatic apparatus for experimental study of drop breakage in a sieve-plate pulsed column K. Eid, C. Gourdon, G. Casamatta, Toulouse; G. Muratet, Paris/F	353-360
Derivation of coalescence model by simulation and experimental study of liquid-liquid fluidized beds C. Gourdon, G. Casamatta, Toulouse; G. Muratet, Paris/F	361-368
Determination of emulsion flooding, local holdup and interfacial area in vertical pulsed solvent extraction columns H.W. Chiang, D. Singh, S. Vijayan, Pinawa, Manitoba/CDN	369-378
Coalescence and motion of drops on inclined plates in liquids W. Meon, E. Blaß, München/D	379-386
A measuring technique for drop diameters in the μm -range in liquid-liquid dispersions F. Rebelein, E. Blaß, München/D	387-396

Studies on phase separation of aqueous-in-organic dispersions in a low-voltage A.C. electric field Li-Min Su, Beijing/China	397-404
Hydraulic studies of a horizontal pulsed solvent-extraction column A.J. Melnyk, S. Vijayan, Pinawa, Manitoba/CDN	405-412
Ob the modelling of the two-phase flow in solvent extraction columns. Radionuclide RTD-analysis as a tool for diagnostics and optimization A. Merz, J.J. Porta, R. Walter, Karlsruhe/D	413-420
Emulsion band thickness in an centrifugal settler M.E. Hodges, Aiken, SC/USA	421-422
Liquid-liquid solid contactors for short and long residential times Jiawen Zhu, Jukang Li, Yuanfu Su, Shanghai/China	423-430
Study of coalescence and settler design in mixer-settler Haihua Shen, Zujun Shen, Shanghai/China	431-436
Breakage ans coalescence of drops in vibrating plate extraction tank Shou-bai Chao, Zheng Fan, Beijing/China	437-444
The residence time distribution of two fluid phases in a centrifugal extractor F. Otillinger, E. Blaß, München/D	445-452
Scale-up of industrial gravity settlers from batch settling data S. A. K. Jeelani, S. Hartland, Zürich/CH	453-460
Electrochemical investigation of axial dispersion in extraction apparatus C. Schaller, G. Kreysa, Frankfurt am Main/D	461-467
Effective interfacial area in the RTL contactor from rates of extraction with chemical reaction E. Alper, Dhahran/Saudi Arabia	469-476

Special Applications: Petrochemicals

Liquid-liquid equilibrium of n-hexane-cyclohexane-methanol mixtures: Influence of water content: P. Alessi, I. Kikic, Trieste/I	479
Extraction of aromatics with different solvents F. Poposka, B. Bliznakovska, V. Mesko, A. Grizo, Skopje/YU	481-489
Butene recovery by extraction G. Emmrich, K. Lackner, Essen/D	491-498
Extraction of Colorado oil share using water as solvent K. Hedden, P. Missal, Karlsruhe/D	499-506
Fundamental investigation of supercritical extraction on coal derived heavy hydrocarbon M. Yanagiuchi, K. Matsubara, T. Ueda, Kawasaki; S. Saito, K. Arai, H. Inomata, Sendai/J	507-514
The effects of the extraction parameters on the chemical composition of extracts obtained from Hungarian brown coals by supercritical extraction G. Deák, Z. Kása, Veszprém/H	515-521

Demetalizing of heavy oil residues with polar solvents J. Höcker, A. Vogelpohl, Clausthal-Zellerfeld/D	523-530
An approach to mathematical description of the permeation of hydrocarbons through liquid membranes P.K. Pluciński, J. Szust, Wrocław/PL	531-537
Influence of emulsion breakage on selectivity in the separation of benzene-heptane mixtures with aqueous surfactant membranes R. Krishna, A.N. Goswami, Dehra Dun/IND	539-548
Hydrodynamics of a non-aqueous liquid extraction system for a packed column R.J. Moore, G.W. Stevens, H.R.C. Pratt, Parkville, Vic./AUS	549-555
Extension of the application of stage additivity method to the calculation of countercurrent extractors with backmixing M. Sovilj, Novi Sad, A. Tolić, Belgrade/YU	557-564

Special Applications: Biotechnology and Natural Products

Application of aqueous two-phase systems for the extraction of biologically active proteins from biomass M.-R. Kula, Düsseldorf/D	567-576
New trends in the extraction of primary and secondary metabolites in biotechnology K. Schügerl, Hannover/D	577-586
Liquid-liquid extraction of proteins using reverse micelles K.E. Goklen, T.A. Matton, Cambridge, MA/USA	587-595
Recovery of microbial proteins by continuous crosscurrent extraction H. Hustedt, K.H. Kroner, N. Papmichael, Braunschweig/D	597-604
Mass transfer of large molecules through phase interfaces M. Seekamp, C. Tiegs, E. Weidner, S. Peter, Erlangen/D	605-611
Solvent extraction of products from the acetone-butanol fermentation S. Dupire, F.C. Thyron, Louvain-la-Neuve/B	613-620
Solvent extraction of metals by oligomeric extraction agents V.I. Bukin, A.M. Reznik, S.A. Semenov, L.D. Yurchenko, Moscow/USSR	621
The principal physio-chemical regularities of extraction in systems with biological fluids G.A. Yagodin, E.V. Yurtov, Moscow/USSR	622
Reactive extraction of d, 1-tryptophane from aqueous solutions by TOMAC/xylene and its back-extraction I. Kirgios, R. Hänsel, H.B. Rhein, K. Schügerl, Hannover/D	623-629
Solvent extraction of succinic acid from aqueous solutions J.A. Tamada, C.J. King, Berkeley, CA/USA; A.S. Kertes, Jerusalem/IL	631-638
Utilisation of green parts of the waste hop plant by solvent extraction V. Grilc, Ljubljana; B. Dobrowsky, Zalec/YU	639-643

Mass transfer problems in high-pressure extraction E. Lack, R. Marr, Graz/A	645-651
Separation of citric acid from aqueous fermentation solutions by extraction-re-extraction processes W. Rückl, M. Siebenhofer, R. Marr, Graz/A	653-658
Ethanol recovery from low-grade fermentates by solvent extraction and extractive distillation: the SEED Process D.W. Tedder, W.Y. Tawfik, S.R. Poehlein, Atlanta, GA/USA	659-666
Extraction of citric acid by N,N-disubstituted alkyl amides Wenqing Wang, Min Yi, Dingfong Chen, Qixiu Pen, Lie Pen, Maoliang Zhang, Xiru Mou, Junbang Chen, Yunxiao Zhong, Beijing/China	667-668
The permeation of phosphonopeptides through liquid membranes P.K. Pluciński, P. Kafarski, B. Lejczak, M. Chichocki, Wrocław/PL	669-676
Liquid membrane extraction of aminoacids G.A. Yagodin, E.V. Yurtov, A.S. Golubkov, Moscow/USSR	677-683
Separation of amino acids from fermentation broth using liquid emulsion membranes M.P. Thien, T.A. Hatton, D.I.C. Wang, Cambridge, MA/USA	685-693
Liquid surfactant membrane emulsions — a new technique for enzyme engineering T. Scheper, K. Makryaleas, Z. Likidis, Ch. Nowotny, E.-R. Meyer, K. Schügerl, Hannover/D	695-702
Separation of aqueous two-phase systems by gravity settling K.H. Kroner, H. Hustedt, Braunschweig/D	703-711

Special applications: Organic Products

Evaluation of the solubility of organic compounds in supercritical fluids P. Alessi, M. Fermiglia, V. Gallo, I. Kikic, Trieste/I	715-722
Liquid-liquid extraction as an alternative to distillation for the recovery of organic material Th. Pilhofer, G. Dichtl, Wiesbaden/D	723-729
Solvent extraction study of tetrahydrofuran from aqueous solutions A.N. Patel, Nsukka, Nigeria	731-738
Purification of glyoxylic acid from glyoxal solutions by tertiary amines extraction D. Pareau, A. Chesné, Paris; A. Schouteeten, Stains/F	739
Isomerism and extractability of organic compounds. Butyl alcohols A.S. Kertes, Jerusalem/IL; D.A. Arenson, C.J. King, Berkeley, CA/USA	741-745
The tricritical point in tetrachloroethylene-ethanediol-nitromethane-n-heptane system V.P. Sazonov, M.F. Chernysheva, Kuibyshev, USSR	747-753
The extraction and separation of phenols by alamine 336 E.N. Basseý, M.A. Hughes, Bradford/UK	755-763

The alcohol/water solubilities A. Szafranski, Z. Lisicki, Warszawa/PL	764
New approach to assessment of molecule aggregation in the organic phase V. Jedinakova, Z. Dvorak, Praha/CS	765-766
Selective oxidation of toluenes to aldehydes by product re-extraction G. Linzbach, G. Kreysa, Frankfurt am Main/D	767-774
The recovery of acetic acid, phenol and ethanol by solvent extraction with a liquid phosphine oxide E.K. Watson, W.A. Rickelton, A.J. Robertson, T.J. Brown, Niagara Falls, ONT/CDN	775-782
Separation of acetic acid and glycerol from aqueous solutions G. Brunner, R. Dohrn, Hamburg/D	783-789
The CO ₂ -trinuclear hydrocarbon solubilities in the supercritical region J. Kwiatkowski, W. Majewski, A. Szafranski, Z. Lisicki, Warszawa/PL	791-797
High pressure extraction of chemically similar substances G. Braun, Frankfurt am Main-Höchst/D	799-805
CPF: Continuous polymer fractionation H. Geerßen, P. Schützeichel, B.A. Wolf, Mainz/D	807-812

Special Applications: Inorganic Products

Solvent extractions of phosphoric acid with long chain tertiary amines S. Stenström, G. Aly, Lund/S, St. Wingefors, Stockholm/S	815-822
On the modelling of multicomponent acid extraction from wet process phosphoric acid with trialkyl amines in kerosene S. Wingefors, Stockholm, S. Stenström, Lund/S	823-830
The extraction characteristics of silicic acid in different systems O.A. Sinegribova, A.Yu. Bobirenko, Moscow/USSR	831-837
The extraction of sulfuric acid and water by primene-JMT dissolved in toluene. Emf and batch studies at 25 °C J.C. Blazquez, J.M. Madariaga, M.C. Sandino, Bilbao/E	839-845
Flow of power-law fluid sheres through newtonian fluids: Hydrodynamics and mass transfer T. Gürkan, Ankara/TR	846
A predictive approach for the determination of composition and temperature dependence of liquid diffusivities T. Gürkan, E. Eroglu, Ankara/TR	847-851
An initio calculation of distribution coefficients of tetraalkylammonium salts St. Jones, S. Khan, B.G. Reuben, London/UK	853-862
Influence of the ionic chloride medium on the transport of HCl through a supported liquid membrane containing tri-n-laurylamine in cumene as carrier M. Valiente, A. Fernandez, M. Munoz, Bellaterra,E	863-871
Facilities transport of acid gases in ion exchange membranes J.D. Way, R.D. Noble, Boulder, CO/USA	873-881

Special Applications: Effluents

- A simple and complete recovery of phenol from waste water by tertiary amines in form of sulfates — a new powerful extractant
G. Braun, W. Grünbein, M. Mayer, B. Wojtech, Frankfurt am Main/D 883-891
- Phenol extraction from cokery waste waters with TAME. Development of the process. Phase equilibrium in the water-TAME-phenols systems
K. Zieborak, T. Porebski, S. Tomzik, Warszawa/PL 893-898
- Acetic acid recovery by liquid-liquid extraction or azeotropic distillation?
Th. Pilhofer, Wiesbaden/D 899
- Process calculation with liquid ion exchangers
H.J. Bart, R. Wachter, R. Marr, Graz/A 901-905
- Recovery of furfural from papermill-effluents by liquid-liquid extraction — economical and technical considerations
G. Bunzenberger, M. Siebenhofer, R. Marr, Graz/A 907-911
- The application of extraction methods in post-distillation residues elimination
M. Zak, Warszawa/PL 913-918
- Liquid-liquid extraction and transport through liquid membranes of metal cyanide complexes ($\text{KAu}(\text{CN})_2$ and $\text{KAg}(\text{CN})_2$) by macrocyclic extractants
M. Tromp, M. Burgard, M.J.F. Leroy, Strasbourg; M. Prevost, Vert-le-Petit/F 919-925
- Behaviour of mass transport by liquid surfactant membrane in a continuous separation column
Jae-Hyung Yoo, Hyun-Soo Park, In-Suk Suh, Chung-Nam/Korea 927-934
- Pertraction of ammonia from waste waters
St. Schlosser, E. Kossaczky, Bratislava/CS 935-942
- Scale-up and performance of 5 Ft.(1.52 m) diameter reciprocating plate extraction column
A.E. Karr, S. Ramanujam Parsippany, NJ/USA 943-949
- Author Index A-1 — A-16

Extraction Equipment

Choice of extraction equipment in chemical processes

R. Berger, BASF AG Ludwigshafen/FRG

Introduction

Liquid/Liquid extraction has some classical fields of application, as for example the nuclear industry, the oil industry and metal extraction. It was these fields, too which stimulated the development of equipment and basic investigations into this separation process. In each of these fields, the problem is a relatively narrowly defined one with certain limiting conditions. The chemical industry was fairly late in making use of this method. In this industry, however, the tasks in question are varied and the physical properties cover a broad range. From this point of view, the question as to which equipment is most suitable for a particular extraction problem takes on a new significance.

Criteria for choosing a suitable extractor

The choice of extractor design is essentially governed by three factors: physical properties, number of theoretical stages and throughput. In addition, some operational aspects are frequently important, for example flexibility with respect to load fluctuations and product quality, sensitivity to solids, suitability for batchwise operation with a number of similar products.

Physical properties which are important with regard to extraction are the difference in the densities of the two phases, the viscosity and the interfacial tension. These three parameters affect the dispersibility on the one hand and the phase separation behavior on the other. Fine dispersion is desirable in order that mass transfer is as complete as possible. On the other hand, complete phase separation is also desirable in order to achieve a satisfactory countercurrent.

A large difference in densities, high viscosity and interfacial tension make it more difficult to carry out dispersing, i.e. they necessitate a higher dissipation of energy than when the reverse is

true. From the point of view of energy dissipation, the various extractors can be classified roughly as follows:

columns without energy input	(packed columns, sieve plate columns ' and columns with corrugated packings)
pulsed columns	(pulsed packed and sieve plate columns and reciprocating plate columns)
rotary columns and centrifuges	
mixer-settlers	

Phase separation is promoted by a large difference in densities and high interfacial tension, whereas high viscosity makes phase separation more difficult. The lower limit for the difference in densities may be given as $\Delta \rho \approx 50 \text{ kg/m}^3$. Mixtures exceeding this value can generally be treated in columns and mixer settlers. If the difference in densities is smaller, a centrifugal extractor has to be used.

A low interfacial tension gives rise to problems in phase separation.

Mixer-settlers are in any case unsuitable for mixtures with a low interfacial tension and owing to the shear field produced, centrifugal extractors too have a dispersing effect which should not be underestimated. In such cases, the energy input should be carefully controlled. Suitable equipments are rotary and pulsed columns in which the energy input can be matched with the physical properties via the rotary speed or the pulsation frequency.

For industrial plants, the lower limit of interfacial tension may be stated as about 1 - 2 mN/m.

The choice of equipment is also influenced by the number of theoretical stages required for a given separation task. Because of their poor separation efficiency, columns without an energy input can only realize a small number of separation stages. Pulsed and rotary columns achieve larger numbers of separation stages. They are limited by the pulsation unit or the length of the through shaft. In the case of the centrifugal extractors, the Robatel design achieves a greater number of separation stages as for example, the Podbielniak extractor. Mixer-settlers are built up according to the modular system. Consequently, there are hardly any limits to the number of separation stages.

The largest diameter built to date can serve indirectly as a preliminary estimate of the maximum possible throughputs in the individual extractor types:

	D_{\max}/m
Reciprocating plate columns	1.0
Pulsed columns	2.7
Kühni extractor	2.5
Asymmetric rotating disc extractor	2.8
Rotating disk contactor	4.0
Mixer-settler column	8.0

Accordingly, the greatest throughputs are clearly to be achieved with the mixer-settler. In the case of the pulsed columns, the pulsation unit imposes a restriction on the diameter. In the rotary columns, the separation efficiency is no longer satisfactory at large diameters. To permit a final statement about the throughput of an equipment, the cross-sectional loadings must be added to the above list. This will be dealt with in a subsequent section when the operating characteristics are discussed.

The importance of standardized test mixtures for comparative investigations of equipments

The literature contains publications which recommend criteria which are necessary for an optimum choice of equipment. However, these recommendations are generally only of qualitative nature and in some cases even contradictory because investigations which allow an objective comparison are not available. The precondition for carrying out investigations into equipments under comparable conditions was first provided by the standardization of test mixtures for extraction, as suggested and worked out in detail by Misek /1/ et al. in connection with the European Federation of Chemical Engineering. The following systems have been recommended:

Toluene/H₂O/acetone
Butyl acetate/H₂O/acetone
n-Butanol/H₂O/succinic acid.

These mixtures not only constitute an objective basis but their presence also acts as a catalyst, stimulating further investigations and encouraging the exchange of scientific information. Consequently, very

successful cooperation took place between university institutes and industry in Austria, Switzerland and the Federal Republic of Germany. As a result of this cooperation, a whole series of investigations into fluid dynamics was carried out, and only a very brief overview of these will be given below.

Operating characteristics of various groups of equipments

Pilhofer /2/ has summarized the most important work carried out with test mixtures over the past eight years in a review, and has made a very clear comparison. This review includes information on the different operating characteristics of the various groups of equipments. Fig. 1 has been taken from this overview and supplemented by a few additional measurements /3/. It shows the separation efficiency, expressed as the number of theoretical stages per meter, as a function of the loading. It contains data for two rotary columns¹⁾, for pulsed sieve plate columns with different fractional free area and for a column with a corrugated packing²⁾ and without energy input. All measurements were carried out using the toluene-system³⁾. It is obvious that the rotary columns achieve the highest separation efficiency but permit only small loadings. The pulsed sieve plate columns permit higher loadings but lower separation efficiency. The fractional free area of the sieve plates, as an additional parameter, extends the range of both characteristics. Finally, the highest loadings are achieved with the columns containing the corrugated packing and without an energy input. However, this advantage is obtained at the expense of a considerable deterioration in the separation efficiency. In general, it may be said that all measures which improve the separation efficiency lead to a reduction in the loading. This discovery is also confirmed by other measurements.

The extent to which the individual groups of equipments are suitable in the event of fluctuations in loading can also be read off from Fig. 1. In the case of the rotary columns, it is true that even a small drop from the optimum design loading leads to a substantial deterioration in the separation efficiency. In contrast, the column containing the corrugated packing covers a very wide loading range, within which the separation efficiency changes only slightly.

1) Kühni, Allschwil, Switzerland and QVF, Wiesbaden/FRG

2) Sulzer, Winterthur, Switzerland

3) in one case, with the butyl acetate-system too /3/

Other parameters of the operating characteristics are the physical properties of the mixture and the geometry of the internals. Using a pulsed sieve plate column as an example, Fig. 2 shows how the fractional free area influences the separation efficiency. The height equivalent of a theoretical stage (HETS) is plotted as a function of the pulsation frequency for two mixtures of high and low interfacial tension. In the toluene system, the plate geometry has a serious effect: the separation efficiency decreases sharply with increasing fractional free area. In contrast, the butanol system, which has a very low interfacial tension, shows no substantial effect. Hence, in the case of systems of low interfacial tension, a plate with a large fractional free area will be chosen in order to take advantage of the higher throughput.

Adapting the column geometry to the separation problem

In the early days of extraction, different types of equipments were associated with very particular geometries, and the various groups therefore differed distinctly from one another. For example, pulsed sieve plate columns had a fractional free area of 15 - 22 %, while reciprocating plate columns had a free cross-section of 50 - 60 %. Recently developed equipments envisage that the geometry will be adapted to the physical properties, in the case of both pulsation columns and rotary columns. This flexibility in designing the internals makes it possible, when studying the fluid dynamics, to combine related equipments into groups, which can be described as a whole. Hence, the separate treatment of a large number of individual equipment in text books is now outmoded.

The extent to which such a method of grouping is viable is illustrated by way of example with pulsed and reciprocating plate columns. Fig. 3 shows the maximum loading as a function of the pulsation for a reciprocating plate column and a pulsed sieve plate column, each of which has a free cross-section of 60 %, and for pulsed packed columns containing 25 mm Pall and Raschig rings. The curves have completely different shapes. Within the frequency range optimum with respect to the design of the equipment, the differences are in no way serious. Fig. 4 compares the equipments in terms of the separation efficiency. Also here the curves for all four types of columns are very close together. In practice, this means that, under otherwise identical conditions, the separation task set can be roughly equally well performed by all of the columns considered here.

This result also shows that optimization of operating conditions and the geometry of the internals are just as important as the choice of a suitable equipment.

The final choice of equipment is often based in practice on limiting conditions which are of a product-specific or operational nature. The following key words may be mentioned in this context: sensitivity to solids, tendency of the product to polymerize, safety aspects. Fluid dynamic investigations over the past decade provide important assistance; nevertheless, the choice of equipment has remained a complex task to be carried out by engineers.

Literatur

- /1/ Misek, T.; Berger, R.; Schröter, J. Standard Test Systems for Liquid Extraction, The Institution of Chemical Engineers 1985
- /2/ Pilhofer, Th.; Schröter J. CIT 56 (1984) 12, 883/890
- /3/ Pommer, St.; Internal Report BASF/ZET 1984, unpublished
- /4/ Berger, R.; Leuckel, W.; Wolf, D. CIT 50 (1978) 544
- /5/ Berger, R. Lecture Jahrestreffen der Verfahrens-Ingenieure, Düsseldorf 1981

Nomenclature

	-	Fractal free area
f	min ⁻¹	Frequency of pulsation
HETS	m	Height equivalent of a theoretical stage
NTS	-	Number of theoretical stages
PM		Pall ring metall
PP		Pulsed packing column
PSP		Pulsed sieve plate column
RK		Raschig ring ceramic
RP		Reciprocating plate column
RZE		Rührzellen-Extraktor Fa. QVF
SMV		Sulzer-Mischerpackung
v _c +v _d	m ³ /m ² h	Column loading

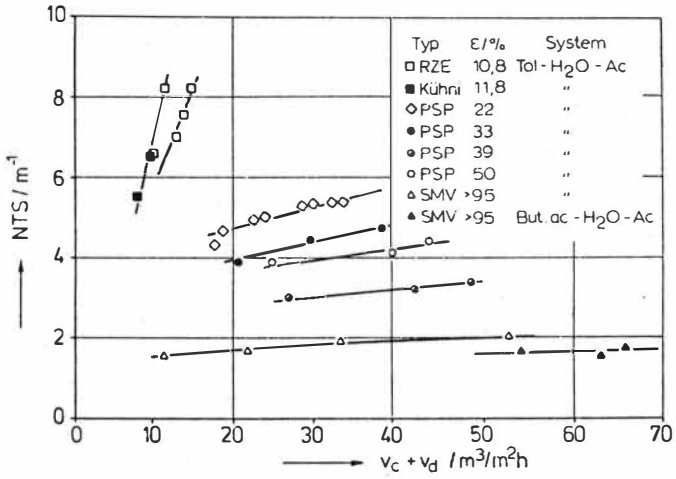


Fig.1: Maximum efficiency as function of loading
Mass transfer cont. → disp. Phase

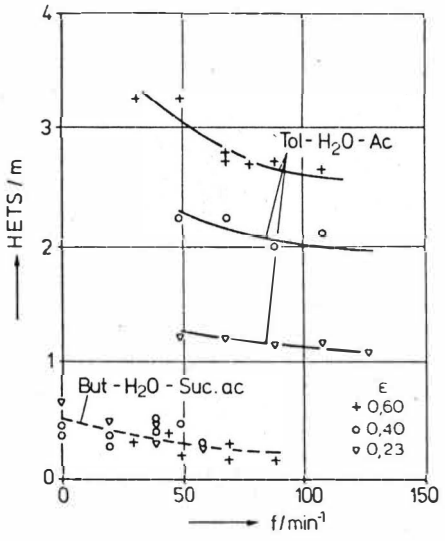


Fig.2: Influence of interfacial tension and fractional free area on separation efficiency
Mass transfer disp. → cont. Phase

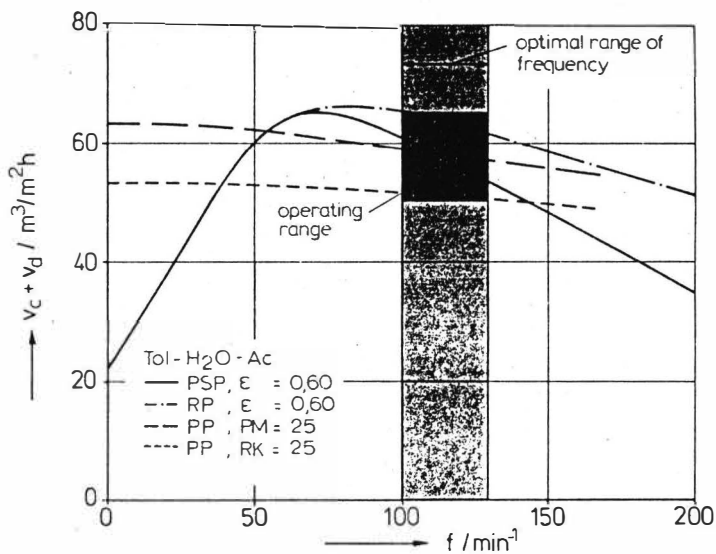


Fig. 3 : Comparison of columns regarding maximum loading
Mass transfer disp. \rightarrow cont. Phase

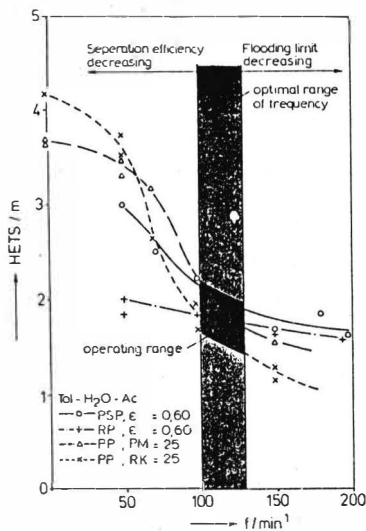


Fig. 4 : Comparison of columns regarding separation efficiency
Mass transfer disp. \rightarrow cont. Phase

Mass Transfer Characteristics of an Agitated Extraction Column Depending on Material Properties

G. Goldmann, E. Blaß
Technische Universität München

1. Problem:

The extraction technique mainly uses relatively simple models for the description of the separation efficiency. Different extractor designs, for example, are often compared with the help of the HETP-Method. Hence the number of theoretical stages for counter-current columns results from the well-known step construction between equilibrium and balance line. In a review of a lot of experiments like these on different pilot columns Pilhofer and Schröter /1/ show, that the respective maximum separation efficiencies rise continuously if the testing system toluene-acetone-water is used and the loading is increased (fig. 1). This insight may lead to the designing norm to run an extractor as close as possible at the flooding point, to strain it to the utmost limit of the capacity. In addition to the mentioned testing system the European Federation of Chemical Engineering recommended butyl-acetate-acetone-water for mean surface tensions. Fig. 2 shows, that the separation efficiency runs through different typical maxima using this material system, if the loading is increased to the flooding rate. Series of exemplary experiments were carried out at a Kühni-column with a diameter of 150 mm, to analyze this influence, which obviously depends on the material system, but not on the apparatus.

2. Balance Model

Balance-models are better than, for example, the simple stage efficiency model, to carry out a scientific engineering analysis of the extractor performance. Balance models like backflow- or dispersion model have proved useful at least for the description of concentration profiles of pilot scaled columns. Equation 1 demon-

strates the differential equation system of the dispersion model, where the mass flow and the mixing values are formulated one-dimensional in axial direction.

$$\begin{aligned}
 -\dot{v}_c \frac{dc_c}{dh} - (1-\epsilon_d) D_{axc} \frac{d^2c_c}{dh^2} &= \beta_{od} \cdot a (c_d^* - c_d) \\
 -\dot{v}_d \frac{dc_d}{dh} + \epsilon_d D_{axd} \frac{d^2c_d}{dh^2} &= \beta_{od} \cdot a (c_d^* - c_d)
 \end{aligned}
 \tag{1}$$

In spite of this restriction concentration profiles in agitated /2,3/ and in pulsed /4/ extractors can be calculated with satisfactory accuracy. The axial dispersion model serves as the main accessory for interpretation in this paper, too.

The equation system (1) shows, that a lot of input values are necessary for the calculation of the concentration profiles of both phases. Besides the axial dispersion coefficients D_{axc} and D_{axd} the holdup ϵ_d and the interfacial area per unit volume a are explicitly needed at fluid dynamic parameters. The equation

$$a = \frac{6 \cdot \epsilon_d}{d_{32}}
 \tag{2}$$

calculates the mean drop diameter according to Sauter. The total mass transfer coefficient, referred to the dispersed phase in our example, multiplied by a represents the volumetric mass transfer coefficient, a coupling element of the differential equation system (1). If the fluid-dynamic parameters can be determined by independent measuring methods, the volumetric mass transfer coefficient is determined by the optimum fitting of the calculated concentration profiles to the measured ones.

If the axial dispersion model can describe the separation problem in question correctly the value $\beta_{od} \cdot a$ can be used as a valuation criterion for the separation efficiency. The subsequent sections report on how it is measured and used for interpreting the separation efficiency profile illustrated in fig. 2.

3. Experiments

The corresponding experiments were carried out with a Kühni-column of the diameter 150 mm (fig. 3). The active column height is 2.52 m, representing 36 mixing cells. The drop size distribution is measured by using the photo-electrical suction method according to Pilhofer /5/. The holdup is determined by the residence time of the dispersed phase. Hence the flow of dispersed phase out of butylacetate is strained with fluorescence colour before it enters the apparatus and the distribution of the tracer concentration is measured with UV light sources and photo multiplier at two downstream spots /6/. However, in addition to the mean residence time the achieved residence time curves include information on the calculation of dispersion coefficients of the dispersed phase. The method of the parameter identification in time domain /7/ offers the Bodenstein-number and the mean residence time as correlation values. NaCl is used as a tracer for the continuous aqueous phase, so that conductivity probes can detect the residence time curves. Along the column height samples are taken at 7 spots per phase, to get the axial concentration profile. Special probes render a proper taking of samples possible, even from the disperse two phase region in the apparatus. The concentration measurement is accomplished by a combination of titration and the density measurement.

All measurement values were recorded at mass transfer conditions (c + d) during one test run, respectively. The parameter field contains a variation of the relative, free stator sectional area of 20 % up to its full aperture and the corresponding loading and speed of rotation settings between 50 % and 90 % of the flooding rate. The ratio of the two phases was set, so that the stripping factor $\lambda = 1$.

4. Results

The correlation of concentration profiles calculated according to eq. (1) to those which were experimentally determined, led to a consistency of satisfactory accuracy in all events. This means that even for the atypical separation behaviour with the material

system butylacetate-acetone-water the axial dispersion model is still valid. Fig. 4 demonstrates the dependence of optimal-fitted volumetric mass transfer coefficients on the loading, at a stator opening of 20 %. Due to fig. 2 the characteristic maximum behaviour of the separation efficiency can also be observed for the model-corrected mass transfer variable $\beta_{od} \cdot a$.

In fig. 5 all the important measured fluid-dynamic and mass transfer properties depending on the loading are plotted for one constant stator geometry $\phi = 40$ %. It lists the number of theoretical stages per meter at a respective optimum speed of rotations, the model-corrected, volumetric mass transfer coefficient, the mixing parameter of both phases and the interfacial area per unit volume. The share of oscillating drops as a qualitative scale for the shifting of the particle spectrum to bigger diameters can be found out by analysis of the drop size distribution according to /12/. The course of $\beta_{od} \cdot a$ is the same as n_{th}/m whereby the maxima of the separation efficiencies hardly differ. The mixing of the continuous phase decreases when the loading is increased, whereas the Bodenstein-numbers of the dispersed phase indicate an increase for the mixing rate of 30 %. A sensitivity analysis for the dispersion model /2/ shows that the mixing influence only affects the column height, i.e. the mass transfer, of pilot plants at 10 %. Hence in the present case the mixing as a main influential parameter for the separation efficiency behaviour is negligible. In any case, this doesn't mean that mixing effects for the column design are generally to be disregarded. They even are of great importance for industrial columns of greater diameters. Hence the further analysis concentrates on the term of mass transfer $\beta_{od} \cdot a$.

The mass transfer coefficient according to eq. 3

$$1/\beta_{od} = 1/\beta_d + m/\beta_c \quad (3)$$

is composed of the partial mass transfer coefficients, if the total residence is mentally shifted to the dispersed phase and resistances in the interface are disregarded. As the transfer component is nearly equally distributed between both phases in the testing system used, the resistances of the inner and outer side

of the drop must be taken into account. For the inner side of the drop /8/ the modified formula according to Handlos/Baron /9/ is recommended:

$$\beta_d = 0,002 \cdot w_{rel} (\eta_c / (\eta_c + \eta_d)) \quad (4)$$

for the outer side of the drop

$$Sh_c = C \cdot Re^{0,5} \cdot Sc^{0,5} \quad (5)$$

when $C = 0.83$ /10/

or $C = 1.21$ /11/, if the potential current round the drop is fully developed.

If the calculation is based on the measured values of the mean drop diameter and the relative velocity, a good accordance to the β_{od} -data is reached, which originate from the fitting of the axial dispersion model to the measured concentration profiles. About 80 % of the calculated values reproduce the 'measured' ones more exact than ± 20 %, 95 % are in the range of ± 40 %. Fig. 5 shows the mass transfer area per unit volume as a fluid-dynamic model property, which runs through a maximum depending on B. As a change of ϵ_d affects the column height at about 60 % /2/, the decline of the separation efficiency next to the flooding point can be quantified approximately.

First the holdup ϵ_d according to eq. 2, which is connected with the relative velocity of both phases, is needed for the calculation of the interfacial area.

$$w_{rel} = \dot{v}_d / \epsilon_d + \dot{v}_c / (1 - \epsilon_d) = f(d_{32}, \epsilon_d) \quad (6)$$

Several authors offer equations for the calculation of the relative velocity, which often include the mean drop diameter and the holdup /10/. Hence the exact knowledge of the drop size is very important, because mistakes propagate from equation (6) and (2).

Basing on many experiments E.A. Fischer /13/ names correlations for the Sauter mean diameter specially fitted to the Kühni column:

$$\frac{d_{32}}{d_R} = C_2 \cdot We^{-0,61} \left(1 + \frac{11}{N_{ST}^{1,22} We^{0,5}} \right) (1+2\epsilon_d) \quad (7a)$$

$$\sigma > 0,012 \text{ N/m}$$

$$\frac{d_{32}}{d_R} = C_3 We^{-0,3} Re^{-0,4} \left(1 + \frac{11}{N_{ST}^{1,22} We^{0,5}} \right) (1+2\epsilon_d) \quad (7b)$$

$$\sigma < 0,012 \text{ N/m}$$

Factor $(1+2\epsilon_d)$ in eq. 7a and 7b respectively considers the increase of the mean drop size for well coalescing material systems.

Eq. 7a reflects about 50 % of the mean drop diameter of our own measurements within ± 10 % and about 70 % within ± 20 %.

Some of the measured mean drop sizes are plotted in fig. 6. They increase at a growing loading. The reason being the substantial extension of that drop class, which is attached to the oscillating region, as found out in an analysis of the drop size distribution (fig.7). This may be caused by the drop-drop-coalescence which is taken into account in the equations 7a and 7b using the holdup term $(1 + 2\epsilon_d)$.

Our own experiments show that the mean drop size is a function of ϵ_d only when the speeds of rotations are low (fig.8). Thus the complex process of drop-drop-coalescence, which is largely unsettled, can't be quantitatively described by the simple empirical formula but this is to be used for qualitative considerations. Hence the subsequent dependences are valid for the determination of the interfacial area:

$$d_{32} = f(\epsilon_d) \quad (8a)$$

$$\epsilon_d = f(d_{32}) \quad (8b)$$

so that errors in the calculation of single terms affect each other. E.g. deviation in the calculation of the drop size of ± 10 % causes a decrease of about 15 % of the holdup according to /12/. If this value is introduced in eq. 2, a changes at -23 %

with an effect of 14.5 % on the column height. Errors of d_{32} in the range of ± 20 %, which are still acceptable, take an aggravating effect on the total height of $+27$ % or -40 % respectively.

Fig. 9 shows, that in spite of the simple formula for the consideration of the coalescence the course of a , depending on the loading, can be calculated qualitatively. Hence from a certain loading onward no more increase of the interfacial area which has any influence on the separation efficiency, is possible in the extractor. The reason being the coalescence effect between the drops.

5. Summary:

As a résumé the essential basis for the calculation of the mass transfer process in an extractor is a deep knowledge of the fluid dynamics in this extractor. The main difficulty is the determination of drop sizes, which mustn't show errors of more than ± 10 % in order to guarantee an accuracy of the calculation of the column height better than 20 %. In addition methods for the calculation of drop size distributions are urgently needed in order to provide a refined model of the fluid dynamics as well as the mass transfer coefficients. Fundamental research shows encouraging results regarding the influence of the coalescence, but we are still far from its quantifying description in turbulent two phase regimes.

Acknowledgement

The authors would like to acknowledge the assistance of the AIF supporting this research program.

Notation

a	interfacial area	m^2/m^3
B	loading	$m^3/(m^2h)$
c	concentration	$kmol/m^3$
C	constant	

d	diameter	m
d_{32}	Sauter mean diameter	m
D_{ax}	ax. dispersion coefficient	m^2/s
D	diffusion coefficient	m^2/s
h	height	m
L	length	m
m	distribution coefficient	
n	rotational speed	1/s
N	number	
\dot{v}	superficial velocity	m/s
w	velocity	m/s
β	mass transfer coefficient	m/s
ϵ_d	holdup	
η	dyn. viscosity	kg/ms
λ	stripping factor	
σ	interfacial tension	N/m

Subscripts

c	continuous
d	dispersed
o	overall
rel	relative
R	impeller
ST	stages

Dimensionless numbers

Bo	= $(w L) / D_{ax}$	Bodenstein number
Re	= $(w d) / \nu$	Reynolds number
Re_R	= $(n d_R) / \nu$	stirrer Reynolds number
Sc	= ν / D	Schmidt-number
Sh	= $(\beta \cdot d) / D$	Sherwood-number
We	= $(w^2 d \rho) / \sigma$	Weber-number

Literature cited:

- /1/ Pilhofer, Th., Schröter, J.: Chem.-Ing.-Tech. 56(1984)12, 883/890
- /2/ Wolschner, B.: Diss., TU Graz 1980
- /3/ Fischer, E.v.: Diss., ETH Zürich 1983
- /4/ Pietzsch, W.: Diss., TU München 1984
- /5/ Pilhofer, Th., Miller, H.D.: Chem.-Ing.-Tech. 44(1972)5, 295/300
- /6/ Niebuhr, D.: Diss., TU Clausthal 1982
- /7/ Bauer, R.: Diss., ETH Zürich 1976
- /8/ Blaß et al.: Chem.-Ing.-Tech. 57(1985)7, 565/581
- /9/ Handlos, A.E., Baron, Th.: AIChE-J. 3(1957), 127/136
- /10/ Boussinesq, J.M.: J. Math. Pure Appl. 6(1905), 285
- /11/ Heertjes, P.M., Holve, W.A., Talsma, H.: Chem. Eng. Sci. 3 (1954), 122
- /12/ Pilhofer, Th.: Habil. TU München 1978
- /13/ Fischer, E.A.: Diss. ETH Zürich 1973

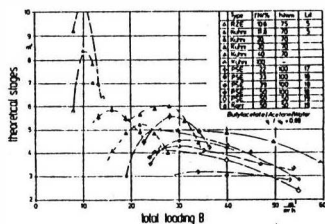
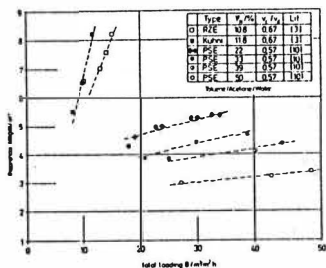


fig.1,2: separation efficiency /1/

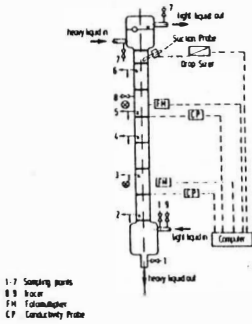


fig.3: Kühni column

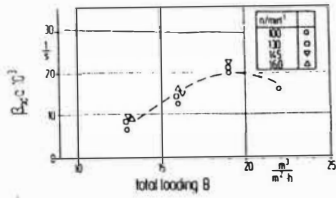


fig.4: mass transfer coefficient

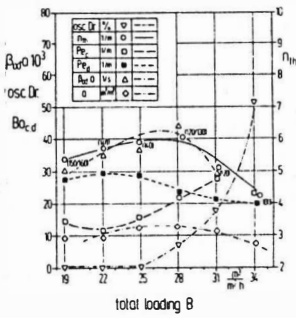


fig.5: parameters studied

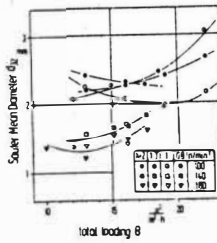


fig.6: drop size distribution

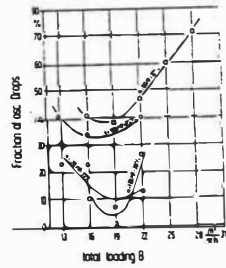


fig.7: drop size distribution

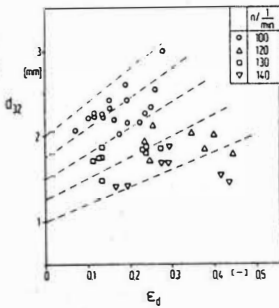


fig.8: drop size

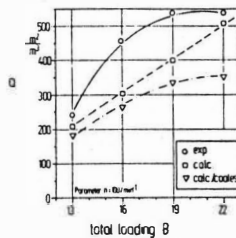


fig.9: interfacial area

J. Rydberg and G. Skarnemark

Department of Nuclear Chemistry, Chalmers University of Technology,
S-412 96 Göteborg, Sweden

1. INTRODUCTION

In the 1960:ies we developed a continuous two-phase liquid flow centrifugal separator, referred to as the H-centrifuge, with some unique properties: >99.9% phase purity of each exit phase with a hold-up time of < 1 s and a hold-up volume of 15-150 ml (1). Its earliest application was in the AKUFVE system (2). This is mainly used for measurement of equilibrium distribution data, either needed for industrial or scientific purposes. It has also been used for studies of chemical kinetics and for following industrial solvent extraction processes (3). In the early 1970:ies the SISAK system was developed (4). It consists of a number of H-centrifuges connected in series to form a multi-stage solvent extraction battery. The SISAK system is used for fast separation and isolation of short-lived chemical species. The H-centrifuge and each of the applications will be described below with emphasis on the SISAK technique.

2. THE H-CENTRIFUGE

2.1 Mechanics

The H-centrifuge has been built in several sizes, of which the H-10 (5) and H-33 (1) versions are commercial; the bowl volumes are 15 and 120 ml, resp. In principle, the design is the same, although the dimensions (both absolutely and relatively) vary. The smaller centrifuge (H-10) operates at higher angular velocity, which results in a considerably shorter holdup time of only 0.3 s, compared with 2 s for the larger one. The flow capacities are 100 and 300 L/h, resp.

Fig. 1 shows the principle of the centrifuge design. The two-phase mixture enters the centrifuge through the central inlet (A); the outlets for the two separated phases from the centrifuge are concentrically located (G and J). The rotating centrifuge bowl consists of (in order of liquid flow): (B) an acceleration chamber; (C-O) a separation chamber where the heavier phase is accumulated at the periphery and the lighter phase centrally; pick-up chambers, (E) one for the heavy phase located below and (H) one for the light located above the separation chamber; and (I and F) stationary turbine-like wheels (scaling disks) that dip down into the rotating liquids in the pick-up chambers. Because of the location of pick-up chambers at each side of the separation chamber, no backmixing can occur. The turbine wheels provide pressure for the outgoing separated phases.

Tests show that absolute phase separation can be achieved by the H-centrifuges for most systems: each phase leaving the centrifuge contains no entrained droplets of the other phase (1). Such absolute phase separation requires optimal adjustment of the liquid flow parameters.

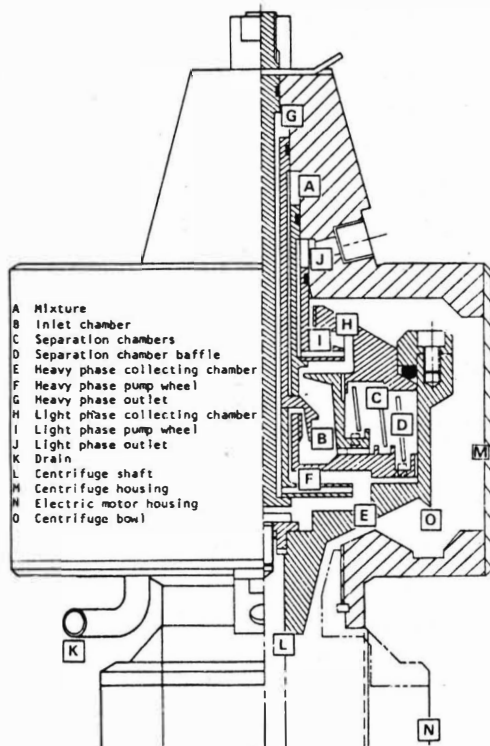


Fig. 1. The H-centrifuge

2.2 Hydrodynamics

By adjustment of the inflow rate, the counterpressure on the outgoing phases and the speed of rotation, the interface between the light and heavy phases in the separation chamber can be forced to move radially. It is necessary to control this interface properly to obtain optimal phase separation. Different solvent extraction systems require different adjustments because of differences in density, surface tension, and viscosity. It may sometimes be necessary to change the dimension of turbine wheels.

Control arrangements are required for the centrifuge: a variable-speed control for the motor, outlet pressure regulating valves and manometers and flow meters.

The H-centrifuge is characterized by a comparatively high speed of rotation (about 25,000 and 10,000 rpm for the H-10 and H-33, resp.), short holdup time (0.3-2 s) and extremely high phase-separation efficiency. A typical result is 0.04% H₂O in benzene and 0.13% benzene in H₂O.

2.3 Materials of construction

The centrifuge has been built in a number of materials. Titanium is chosen as the standard material, because of its resistance to most strong acids at $< 1M$ conc. In some cases it has been desirable to make experiments at higher concentrations on temperatures of these acids, in which case palladium stabilized (1%) titanium is used. It has also been made of PVDF for use in HF media.

Although the centrifuge is free of packings between rotating and stationary parts, some packings are nevertheless needed in other places. For this purpose O-rings of Kel-F have been chosen. After some time these O-rings become deformed and have to be replaced. The O-rings can dissolve extractants like TBP, HDEHP, etc, which then re-dissolve in the organic phase in a later experiment, particularly causing great errors in case of tracer studies. Thus, the O-rings should be changed between different experiments.

The rest of the flow system (valves, heat exchangers, tubes etc) is all made of titanium (or by Pd-Ti). Other materials in contact with the solutions are teflon (parts of the valves) and glass (flow meter, pH-electrode vials). Sampling valves are made of stainless steel and connected to the main flow by small (inner diameter 1 mm) tubings of PVC; these materials do not interfere with the main flow. Construction material, not in contact with the solution, is stainless steel.

The detector cells are described separately below.

3. THE AKUFVE SYSTEM

3.1 Liquid flow system

The AKUFVE system is used for rapid obtaining of distribution and extraction equilibrium curves. It consists of (i) a mixing vessel connected to (ii) the H-centrifuge and (iii) on-line detectors on the exit phases from the centrifuge. The flows are then returned via heat exchangers (for temperature control) to the mixing vessel, so that two closed liquid loops are formed. The liquid flow system also contains valves, flow-meters and thermostats for control. A special vial is used for on-line pH-measurement with dual glass electrodes. Chemical reagents are added to the mixing chamber when desired. The mixing chamber is either of the dynamic stirrer type or is a static Kenics mixer. The latter is used for very short mixing times (< 1 s). Some mixing also occurs at the centrifuge acceleration chamber (B), where high shearing forces occur; this property can only be taken advantage of in very rapid kinetic experiments.

Samplings can be made at the sampling valves, but on-line measurements are preferred.

3.2 On-line detection and data collection

The simplest on-line detection system consists, for each pure phase, of a NaI(Tl) scintillation detector, around which a tubing (usually of teflon) is wound, through which the pure phases from the centrifuge flow. Alternatively, we have used a glass flow-cell inserted in a well-type detector. Both these techniques suffer

from memory effects, i.e. radiotracer sorbed in the flowsystem at the detector produces an undesirable background, which usually increases with pH of the aqueous metal system. This problem cannot be completely eliminated.

Therefore, we have designed 3 new types of detector cells:

(i) The sorption correction cell (6) consists of a bellow system, so that the ratio surface/volume can be changed in a reproducible manner. This allows determination of the surface activity, which then can be deducted from the total activity (surface + volume), so that only volume activity is obtained. In experiments with strongly hydrolyzable metals (U, Am, lanthanides) we have often encountered the situation that all radiotracer is sorbed on the detector and other system walls.

(ii) In the sorption suppression cell (7), a tiny fraction of the pure flow from the centrifuge is withdrawn, rapidly mixed with strong acid (to suppress hydrolysis, and thus sorption, in the cell) and a liquid scintillator, and then pumped to a cell viewed by dual coincidence coupled PMT:s. This technique is advantageous at high pH's (> 7), and also applicable to pure beta and alpha emitters. It is less sensitive for low-energy beta/hard gamma emitting radionuclides.

(iii) The free-flow cell (8) lacks cell walls. The solution to be measured is pumped through a small nozzle in such a way that a geometrically stable stream is obtained. This stream passes in front of a NaI(Tl) crystal without either touching its surface or the walls on the other sides of the free-flowing liquid. This technique has yielded excellent, highly reproducible extraction data. However, it requires large liquid volumes and radioactivities, in addition to an elaborate pumping and flow control system.

The primary purpose of the original AKUFVE system was to obtain accurate distribution data in a minimum of time. Complete mixing equilibrium (but not necessarily chemical equilibrium) is obtained within one minute. In order to measure the concentration of the species of interest in each phase, in addition to pH, temperature, reagents added, and so on, as often as once a minute, a data-logger is required. The data logger can be connected on-line to a computer (9). In elaborate systems, automatic burettes have been connected to the AKUFVE systems.

3.3. Application of the AKUFVE

The AKUFVE system has been described in several publications as well as many of its applications. It has mainly been used to obtain distribution ratios as a function of pH for a large number of metals in the system aqueous nitrate or perchlorate/organic solvent (hexane, chloroform, carbontetrachlorid, benzene, toluene, hexone, etc), in the presence of complex forming ligands (hydrophilic and organophilic amines, adduct formers and chelating agents). From such data stability constants (β_n) and distribution constants (λ_n) have been obtained, as well as the corresponding thermodynamic functions (ΔH and ΔS) (e.g. 10). The AKUFVE has also been used to obtain basic information like McCabe-Thiele diagrams for industrial applications (11).

Though the AKUFVE technique has large potential for kinetic studies in the time range >0.1 s, it has only been rarely used for this purpose (e.g. 12). H-centrifuges have also been connected to industrial mixer-settlers to obtain instant information on the conditions in the mixer (3).

4. THE SISAK SYSTEM

It is obvious that the H-centrifuges also can be used for rapid chemical separations. The main application has been for studies on decay properties of short-lived radioactive nuclides. In this connection the technique is called SISAK (Short-lived Isotopes Studied by the AKUFVE technique). The present SISAK set-up consists of four main parts, namely a target system, a degassing unit, a centrifuge battery for solvent extraction and a detection system.

4.1 Target and degassing

So far we have used three types of targets in combination with the SISAK equipment: a liquid flow cell, the target material sorbed on an ion exchanger and a gas jet target systems. The gas jet target (13) has proven to be the most flexible arrangement, and it is now used in all SISAK experiments.

The nuclear reaction products delivered by the gas jet recoil transportation system are transferred to a liquid phase by intense mixing in a static mixer. The gas/liquid mixture is fed into the degassing unit (5), which consists of a centrifuge specially designed to separate the carrier gas from the liquid phase containing the radionuclides or chemical species of interest. The degassing unit also removes more than 98% of gaseous reaction products like krypton and xenon.

4.2. Centrifuge battery

The solution leaving the degassing unit is pumped to the centrifuge battery (14), which consists of 1 to 4 H-10 centrifuges, depending on the number of steps necessary to obtain a radiochemically pure fraction of the nuclide under investigation. Normally the centrifuges are equipped with static mixers to obtain a proper mixing of the phases, but when investigating very short-lived nuclides (half-life below 3 s) the mixers are removed to decrease the transport time through the equipment. A prerequisite is, however, that the extraction kinetics is fast enough. The phase outlets have throttle valves to maintain a proper pressure balance in the centrifuge, but in contrast to a normal H-centrifuge the pressure meters have been removed to save holdup volume. The solutions are fed into the system via cog-wheel pumps placed in storage vessels. The pumps are constructed to give maximum flow stability. Aqueous phases are usually pumped once-through to avoid contamination problems, while the organic solutions are pumped in closed loops to decrease the amount of organic waste. If necessary, the organic solutions are regenerated in an additional centrifuge or mixer-settler step. It is also possible to heat all solutions before they enter the system. This heating is carried out by using counter-current heat exchangers connected to a 21 kW heating source.

4.3 The detection system

The detection system usually comprises standard equipment for γ -ray spectroscopy, e.g. high purity Ge-detectors and coincidence electronics. All data are stored on magnetic tapes for subsequent computer analysis. The collection source ("detection cell") is either a thin-walled plastic flow cell or a small ion-exchange column on which the nuclide of interest is retained. The ion-exchange column is used for investigating nuclides with half-life >30 s.

5. CHEMICAL SEPARATION SYSTEMS FOR SISAK

One of the most important problems when developing chemical separation systems for SISAK experiments is the need for fast solvent extraction kinetics. If using the static mixers the phase contact time is 0.1 - 0.2 s; if running without mixers it decreases to 40 - 60 ms. The droplet size in the centrifuge acceleration volume becomes very small, < 100 μm ; nevertheless the short hold-up time still allows substantial material transport over the phase boundary. These short times makes it important to choose systems with rapid chemical kinetics (e.g. extraction of species like Br_2 , AsI_3 or PuO_4 into the organic pure solvent) or where the distribution coefficient is high enough to give a sufficient extraction yield, even if the extraction takes place under non-equilibrium conditions. As an example it can be mentioned that the distribution ratios for extraction of UO_2^{2+} from 5 M nitric acid into 0.1 M HDEHP, or 50% TBP, in kerosene are only ~ 2 and ~ 0.1 , respectively, if using one H-centrifuge step without mixer, while the corresponding equilibrium values are several thousand times larger. Although many common reagents and standard extraction procedures cannot be used, slow kinetics have never made the development of any SISAK chemistry impossible. Thus experience shows that chelate extraction usually is too slow for the SISAK technique, while amines and organophosphorous acids in most cases show acceptably fast kinetics.

5.1 Isolation of fission-product zirconium and niobium

The on-line isolation of Zr from a fission product mixture is a typical example of a SISAK separation procedure; see Fig. 2. The fission products carried by the gas jet are dissolved in 1 M H_2SO_4 . The gas/liquid mixture is fed into the degassing unit, in which the carrier gas and the noble gases are removed from the aqueous solution by suction. To enhance the degassing effect the temperature of the solution is kept at 70°C .

In the first extraction step the aqueous phase is contacted with an 0.1 M solution of Alamine-336 in Shellisol-T. The organic phase also contains 5% n-dodecanol to improve the phase separation. Zr and Nb are extracted with high yield into the organic phase, together with a small amount of Tc, I and a few other fission products. In the second extraction stage Zr and Nb are back-extracted almost quantitatively by means of 0.3 M HNO_3 , while Tc and most of the other contaminants remain in the organic phase. A small fraction ($< 1\%$) of the I is, however, back-extracted

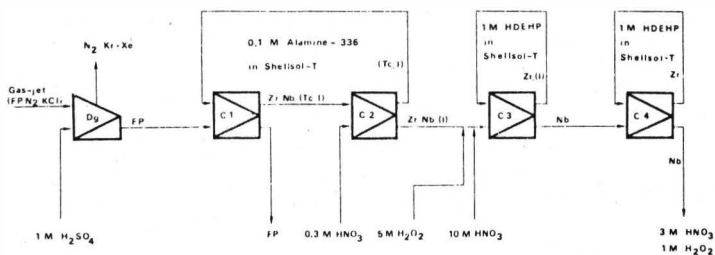


Fig. 2. Chemical separation system for Zr and Nb. Dg = degassing unit, C1 - C4 = mixer-centrifugal separator units, FP = fission products

together with Zr and Nb. After the back-extraction step H_2O_2 is added to the aqueous solution for the complexation of Nb, and 10 M HNO_3 to increase the acidity so that the solution entering the third extraction stage consists of 3 M HNO_3 and 1 M H_2O_2 . In the third stage approximately 95% of the Zr is extracted into 1 M HDEHP in Shellisol-T, whereas Nb as peroxide complex remains in the aqueous phase. In the organic phase only Zr nuclides and their daughter products can be observed, together with a small amount of I. On-line measurements can be carried out on the organic phase (15).

The Zr chemistry can easily be transformed into a Nb chemistry. In this case, the aqueous phase leaving the third stage is contacted once more with 1 M HDEHP in Shellisol-T to remove the last traces of Zr (Zr is not quantitatively extracted in the third step because of kinetic effects). Measurements can then be carried out on the aqueous phase leaving the fourth extraction step (15).

5.2. Isolation of fission-product ruthenium

Another example is the chemical separation system applied to studies of short-lived Ru isotopes; see Fig. 3. In this case the radionuclides transported by the

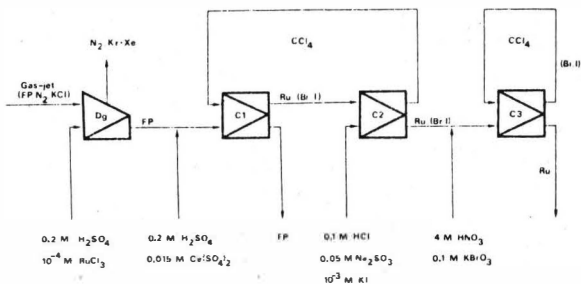


Fig. 3. Chemical separation system for Ru. Dg = degassing unit, C1 - C3 = mixer-centrifugal separator units, FP = fission products

gas jet system are dissolved in 0.2 M H_2SO_4 containing 10^{-3} M $RuCl_3$ carrier. After the degassing step 0.015 M $Ce(SO_4)_2$ is added to oxidize Ru to RuO_4 . In the first extraction step Ru is extracted almost quantitatively into CCl_4 . Ru is then back-extracted into a solution containing 0.05 M Na_2SO_3 and 0.1 M HCl in the second stage. If using a ^{249}Cf target nuclear measurements can be carried out directly on the aqueous phase leaving the second extraction stage; if using ^{235}U or ^{239}Pu as target a decontamination step to remove co-extracted Br has to be installed after the back-extraction stage (the yield of Br is very low in thermal-neutron induced fission of ^{249}Cf). The decontamination is based on an oxidation of Br^- to Br_2 by adding $KBrO_3$ and HNO_3 , followed by extraction into CCl_4 (16).

6. SISAK - PRESENT STATUS AND DEVELOPMENT

The dynamic behavior of the SISAK system has been studied several times by operating the TRIGA reactor in the pulse mode. The results obtained for a set up containing gas jet transport, degassing, extraction and back-extraction show that the first activity reaches the detector site after -2.3 s, while the maximum activity is obtained after -3.8 s.

A central question arising in connection with this fast separation technique is whether it can be improved to give access to even shorter half-lives. One limiting factor is the phase transfer rate in the mixer. This rate depends on several parameters such as chemical kinetics, interfacial tension, the presence of surface active substances, droplet size, temperature, concentration of extractant etc. The smaller the droplets, the shorter can the mixer hold-up time be. In the separation chamber the droplets must spend sufficient time to coalesce. The coalescent time depends on the speed of rotation, the viscosity of the two solvents, the droplet spectrum, and the centrifuge dimensions. The smaller the droplets, the longer time must they spend in the centrifuge. Thus one should avoid mixing the phases too intensely. Under representative conditions it is theoretically possible to separate droplets $>10 \mu m$ in diameter in 0.01 s, while it would take -1 s for $1 \mu m$ droplets. Thus a single mixer-separator stage would require -0.2 s with reasonable material transmission or - for a 3-stage equipment - 0.6 s. This would mean that it should be possible to chemically isolate nuclides with half-lives down to -0.2 s; under favorable circumstances one may reach half-lives down to 0.1 s.

At the present the SISAK technique is applied to investigations of the most neutron-rich Tc, Ru, and Pd isotopes, as well as neutron-rich light actinide isotopes. In the future, we plan to extend these investigations to the heaviest elements, as well as to other nuclides of scientific importance. This work will require a scale-down of the equipment to decrease the consumption of solutions, and development of methods for on-line α -spectroscopy. Such work is in progress.

It should be noticed that studies of short-lived nuclides is not the only application of the SISAK technique. It can be used for studies of other fast phenomena like solvent extraction kinetics and short-lived chemical states. It can also be

applied to the isolation of short-lived radionuclides for medical or industrial purposes, to on-line activation analysis and to industrial solvent extraction processes requiring a short phase contact time, e.g. the reprocessing of highly burnt-out nuclear fuel.

ACKNOWLEDGEMENTS

The work presented has been supported by the Swedish Natural Science Research Council. We also want to thank H. Reinhardt, H. Persson and the members of the SISAK collaboration (J. Alstad, N. Kaffrell, J. Rogowski, M. Skålberg, H. Tetzlaff and N. Trautmann), who all contributed to this work.

REFERENCES

1. H. Reinhardt and J. Rydberg, U.S. Pat. nr 3,442,445, 1969/1971.
2. J. Rydberg, et al. Acta Chem. Scand. 23(1969) 647, 2773, 2781, 2797.
3. H. Reinhardt and J. Rydberg, in Handbook of Solvent Extraction (Eds. T.C. Lo, M.H.I. Baird and C. Hanson), John Wiley & Sons, Inc 1983.
4. P. O. Aronsson, P. E. Johansson, J. Rydberg, G. Skarnemark, J. Alstad, B. Bergersen, E. Kvåle, M. Skarestad. J. Inorg. Nucl. Chem. 36 (1974) 2397.
5. J. Rydberg, H. Persson, P. O. Aronsson, A. Selme and G. Skarnemark, Hydrometallurgy 5 (1980) 273.
6. J. Rydberg, J. O. Liljenzin and Y. Albinsson, Am. Inst. Chem. Eng. Symp. Series 238, Vol. 80 (1984) 47.
7. Y. Albinsson and J. Rydberg, Actinides -85, Aix en Provence, Sept. 1985.
8. H. Ottertun, Int. J. Appl. Rad. Isotopes 23 (1972) 13.
9. S. O. Andersson and D. R. Spinks, Can. Res. and Devel., Nov/Dec (1971)16.
10. B. Allard, S. Johnson, J. Narbutt and R. Lundqvist, In Proc. Int. Solv. Extr. Conf. ISEC 77 (Eds. B. H. Lucas, G. M. Ritcey and H. W. Smith), Canadian Institute of Mining and Metallurgy, Spec. Vol. 21, Toronto 1979.
11. J. O. Liljenzin, In Proc. Int. Solvent Extraction Conf. ISEC 77 (Eds. B. H. Lucas, G. Ritcey and H. W. Smith), Canadian Institute of Mining and Metallurgy, Spec. Vol. 21, Toronto 1979.
12. J. O. Liljenzin, K. Vadasdi and J. Rydberg, in Coord. Chem. in Solution (Ed. E. Högfelt), Swedish Natural Science Research Council, Stockholm 1972. M. Cox and D. S. Flett, in Handbook of solvent extraction (Eds. T. Lo, M. Baird and C. Hanson), J. Wiley 1983.
13. E. Stender, N. Trautmann, G. Herrmann, Radiochem. Radioanal. Lett. 42 (1980)291
14. G Skarnemark, P.O. Aronsson, K. Brodén, J. Rydberg, T. Björnstad, N. Kaffrell, E. Stender, N. Trautmann, Nucl. Instrum. Methods 171 (1980) 323.
15. K. Brodén, G. Skarnemark, T. Björnstad, D. Eriksen, I. Haldorsen, N. Kaffrell, E. Stender, N. Trautmann, J. inorg. nucl. Chem. 43 (1981) 765.
16. G. Skarnemark, K. Brodén, Mao Yun, N. Kaffrell, N. Trautmann, Radiochim. Acta 33 (1983) 97.

by: A.J.F. Simons and R. van Sluys
DSH Research BV; Geleen, The Netherlands

J.C. Göebel and J.M.H. Fortuin
University of Amsterdam; Amsterdam, The Netherlands

1. Introduction

The performance of countercurrent contactors for liquid-liquid extraction is adversely effected by deviation from plug-flow behaviour. Therefore, a good description of the mixing in the phases is required for designing large-scale equipment.

The combined effects that lead to a distribution of residence times of fluid elements of both phases is indicated by the term 'axial dispersion'. Total axial dispersion can be determined with transient methods in which a tracer-concentration pulse or step is introduced near the phase inlet. From the change of the tracer-concentration profile the residence time distribution can be obtained.

In the present paper we shall report about the experimental determination of axial dispersion coefficients of pulsed packed columns ranging in diameter from 0.05 m to 2.4 m, and its dependency on flow rate, pulsation velocity and packing diameter. Further a mathematical model describing the relationship between these physical quantities will be derived.

2. Theory

In the past decades a great number of models for axial dispersion has been published in literature (Wen, 1975).

In these models the axial dispersion has been considered as the result of a number of different phenomena, e.g. molecular diffusion, interaction between distinct ideally mixed regions and the influence of velocity profiles.

Two models often used are:

- the diffusion model, in which a turbulent diffusion of solute is assumed superimposed on plug flow of the phases (Sleicher, 1959; Miyauchi, Vermeulen, 1963)
- the back flow model, in which well-mixed stages are assumed between which backflow occurs (Sleicher, 1960).

2.1. Axial mixing and tracer concentration

In the present paper we shall focus our attention to the axial diffusion model. According to this model axial dispersion in a flow system can be described as a diffusion process, only replacing the molecular diffusion coefficient D_M by the dispersion coefficient E .

The equation governing axial dispersion in phase j then becomes:

$$\frac{\partial c_j}{\partial t} = -v_j \cdot \frac{\partial c_j}{\partial z} + E_j \cdot \frac{\partial^2 c_j}{\partial z^2} \quad (1)$$

As pointed out by Kreft and Zuber (Kreft, 1978), the boundary conditions to this equation are dependent on the physical structure of the column section and its boundaries, as well as on the methods of injection and detection.

In our experimental set-up it was allowed to use open boundary conditions for the calculation of the response to an instantaneous injection. These boundary conditions are:

$$c_j(z, 0) = \frac{n}{A_j} \delta(z) \quad (2a)$$

$$\lim_{z \rightarrow +\infty} c_j(z, t) = 0 \quad (2b)$$

Solving equations (1) and (2) results in:

$$c_j(z, t) = \frac{n}{A_j} \left\{ \frac{1}{4 \pi E_j t} \right\}^{\frac{1}{2}} \cdot \exp \left\{ - \frac{(z - v_j \cdot t)^2}{4 E_j \cdot t} \right\} \quad (3)$$

Eqs. (2) and (3) have often been used to calculate the axial dispersion coefficient E_j , the value of which characterises the axial mixing quantitatively. However, the experimental conditions make it nearly impossible to fulfil condition (2a), owing to the imperfectness of the tracer pulse. In the present case the response of a tracer pulse injected into the feed line to the column at a point P_0 has been measured at different heights P_1 and P_2 in the packed section of the column. The response at point P_2 downstream of P_1 can now be calculated from a response measured at P_1 , applying the equation (Göbel, Fortuin, 1986):

$$c_{j,2}(t) = \int_0^t c_{j,1}(t') \frac{v_j}{(4 \pi E_j (t-t'))^{\frac{1}{2}}} \cdot \exp \left\{ - \frac{(z - v_j (t-t'))^2}{4 E_j (t-t')} \right\} dt' \quad (4)$$

Eq. (4) is a convolution integral. For suitable values of v_j and E_j this equation enables us to relate $c_{j,2}$ and $c_{j,1}$ as function of time for an arbitrary shape of the injected tracer pulse in the feed line to the column. In practice, the integration in Eq. (4) has to be done numerically.

To calculate v_j and E_j from measured values $c_{j,1}(t)$ and $c_{j,2}(t)$, we guess E_j and v_j and calculate $c_{j,2}(t)$ from $c_{j,1}(t)$. We now adjust v_j and E_j in such a way, that the sum of the squared differences between $c_{j,2}(t)$ and $c_{j,2}(t)$ is minimum.

2.2. Axial mixing and local convection

In 1956 Aris (Aris, 1956), extending the work of Taylor (Taylor, 1953), gave a mathematical solution for the case of axial dispersion of a solute in a fluid flowing through a tube, considering the interaction between axial and radial molecular diffusion and the velocity profile.

Göbel and Fortuin (Göbel, Fortuin, 1986) proposed a similar expression for the axial dispersion coefficient E in single-phase flow in pulsed packed columns:

$$\frac{E}{v \cdot d} = \frac{D}{v \cdot d} + \kappa \cdot \frac{v \cdot d}{D} \quad (5)$$

in which D characterises the local radial and axial convection in the liquid flowing through the interstitial space in the packing of the column.

It seems reasonable that D increases with increasing values of both v and s.f. The simplest dependency of D on v and s.f. is of the form:

$$D = A_1 \cdot v + A_2 \cdot s \cdot f \quad (6)$$

in which A_1 and A_2 are empirical parameters. Further D is also dependent on the packing diameter d_p as shown by Spaay et al. (Spaay, 1971):

$$D = C_1 \cdot v \cdot d_p + C_2 \cdot s \cdot f \cdot d_p \quad (7a)$$

C_1 and C_2 being empirical dimensionless parameters. Eq. (7a) can also be represented by the relation:

$$\frac{D}{v \cdot d_p} = C_1 + C_2 \cdot \frac{s \cdot f}{v} \quad (7b)$$

Combination of Eqs. (5) and (7b) gives:

$$\frac{E}{v \cdot d_p} = C_1 + C_2 \frac{s \cdot f}{v} + \frac{\kappa}{C_1 + C_2 \frac{s \cdot f}{v}} \quad (8)$$

From Eqs. (7b) and (8) it can be concluded that for large values of $s \cdot f / v$ the value of E approaches that of D .

An examination of Eq. (8) shows that a minimum value of E is found if E is plotted against $s \cdot f$, keeping v constant. The decrease in E when the pulsation velocity is increased from zero is one of the most striking facts of the axial dispersion coefficients in pulsed packed columns.

The position of this minimum can be obtained from:

$$\left\{ \frac{\partial E}{\partial (s \cdot f)} \right\}_v = 0 \quad (9)$$

From Eqs. (8) and (9) we obtain the pulsation velocity $(s \cdot f)^*$ where E has a minimum value E^* :

$$\frac{(s \cdot f)^*}{v} = \frac{(\kappa^{\frac{1}{2}} - C_1)}{C_2} \quad (10)$$

Substitution of Eq. (10) in Eq. (8) leads to:

$$\frac{E^*}{v \cdot d_p} = 2 \kappa^{\frac{1}{2}} \quad (11)$$

Further, it is important to note that Eq. (8) also agrees with results measured in unpulsed packed columns published in literature (Wen, 1975). In the case of $s \cdot f = 0$, (Eq. 8) reduces to:

$$\frac{E_0}{v \cdot d_p} = C_1 + \frac{\kappa}{C_1} \quad (12)$$

A linear relationship between E and v for large variations in v is a result often reported in literature for systems flowing through unpulsed columns (Wen, 1975) with packing particles of constant size, shape and packing structure.

3. Experimental

Experiments were performed in columns with diameters ranging from 0.05 m and 0.10 m to 2.15 m and 2.40 m and different heights of packed sections (see Table 1).

Both a KCl solution and a solution containing radioactive indium (^{113m}In) have been used as tracer.

The tracers mentioned were soluble in the continuous phase only. In case of the salt solution conductivity cells had been mounted in between packed sections. When using the radioactive tracer, detection of γ radiation took place with intrinsic NaI detectors placed outside the column wall at different heights. At each height two to four detectors were arranged around the column.

The cells and/or the detectors were connected to microcomputer controlled multi-point conductivity and radiation meters respectively, which registered the conductivity or radiation at regular time intervals.

The information was processed on a computer according to the procedure outlined in section 2.

The majority of experiments has been carried out without mass transfer.

4. Results

In Figure 1 an example has been given of experimentally obtained tracer response curves in a 10 cm diameter column, packed with 25 mm stainless steel Raschig rings over a height of 8.4 m, and curves fitted to them following the given procedure. As can be seen from this figure, the agreement between the experimentally determined tracer concentration and the fitted lines is very good.

Axial dispersion coefficient measurements have been performed for different stroke lengths, frequencies and superficial velocities.

In Figure 2 (smoothed) experimental values of the axial dispersion coefficients have been given as plots of $E_c/(v_c d_p)$ versus $s.f/v_c$. For the velocities v_c the best-fit values (nearly always equal to $u_c/(\epsilon(1-\alpha))$) obtained from the calculations on the tracer experiments were taken.

In Figure 3 the points represent experimental values gained in both industrial columns with diameters of 2.15 m and 2.40 m and a 0.10 m diameter laboratory column packed with stainless steel ($\epsilon = 0.92$) Raschig rings.

From the graphs presented the best-fit values of the adjustable parameters C_1 , C_2 and κ have been calculated (see Fig. 3), using a non-linear least-square-fit procedure.

Fig. 2 shows that $E_c/(v_c d_p)$ is dependent on size, type and structure of the packing.

Fig. 3 shows that for a given size, type and structure of the packing $E_c/(v_c d_p)$ is a function of $s.f$ only. Unlike the results of Rosen (Rosen, 1967), whose experiments were carried out at rather small H/D_c values, we found the axial dispersion coefficient being independent of the column diameter.

5. Conclusions

The results presented in this paper show that axial dispersion in a PPC is dependent on the superficial and pulsation velocities of the fluid and size, type and structure of the packing.

Moreover, it has been shown that the axial dispersion coefficient of the continuous phase in pulsed packed columns with diameters ranging from 0.05 m to 2.40 m is independent of the column diameter.

References

1. Aris, R., 1956;
On the dispersion of a solute in a fluid flowing through a tube; Proc. Roy. Soc. London A235, 67-77.
2. Göebel, J.C., Booij, K., Fortuin, J.M.H., 1986;
Axial dispersion in single-phase flow in pulsed packed columns, submitted for publication in Chem. Eng. Sci.
3. Kreft, A., Zuber, A., 1978;
On the physical meaning of the dispersion equation and its solutions for different initial and boundary conditions; Chem. Eng. Sci. 33, 1471-1480.
4. Rosen, A.M., Frylov, V.S., 1967;
The scaling up of mass-transfer equipment and reactors: use of hydraulic model experiments; Chem. Eng. Sci. 22, 407-416.
5. Taylor, G., 1953;
Dispersion of soluble matter in a solvent flowing slowly through a tube; Proc. Roy. Soc. London, A219, 186-203.
6. Wen, C.Y., Fan L.T., 1975;
Models for flow systems and chemical reactors, M. Dekker, New York.

List of symbols

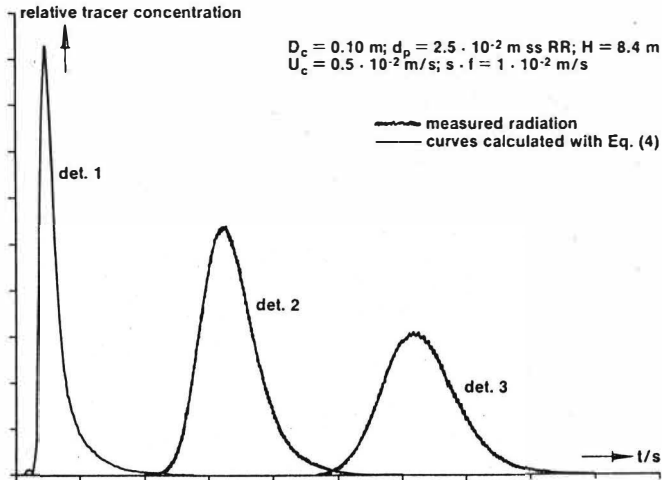
A_j	cross sectional area of the flow of fluid j in the column	m^2
A_1, A_2	parameters in Eq. (6)	m
c_j	tracer concentration in phase j	$mol\ m^{-3}$
$c_{j,1}$	tracer concentration in phase j at reference point P_1	$mol\ m^{-3}$
$c_{j,2}$	tracer concentration in phase j at reference point P_2	$mol\ m^{-3}$
$c_{j,1}^*$	measured value of $c_{j,1}$	$mol\ m^{-3}$
$c_{j,2}^*$	measured value of $c_{j,2}$	$mol\ m^{-3}$
C_1, C_2	parameters in Eq. (7a)	l
D	convection coefficient	$m^2\ s^{-1}$
D_c	diameter of column	m
d_p	diameter of packing particle	m
E	axial dispersion coefficient	$m^2\ s^{-1}$
E_j	axial dispersion coefficient in phase j (see Eq. (1))	$m^2\ s^{-1}$
E^*	minimum value of E	$m^2\ s^{-1}$
E_0	value of E without pulsation	$m^2\ s^{-1}$
f	frequency of pulsation	s^{-1}
H	height of packed section	m
HPO-ipl	Hyam Phosphate Oxime Inorganic process liquor	l
n	amount of tracer injected	mol
s	superficial stroke length of pulsation	m
$(s.f)^*$	pulsation velocity at $E = E^*$	$m\ s^{-1}$
t	time	s
u_c	superficial velocity of continuous phase	$m\ s^{-1}$
v	mean velocity of the fluid flowing through the interstitial space of the packing	$m\ s^{-1}$
v_c	mean velocity of continuous phase in the space occupied by the continuous phase in the packed section ($u_c/\epsilon(1-\alpha)$)	$m\ s^{-1}$
v_j	mean fluid velocity of phase j	$m\ s^{-1}$
w	wall thickness of packing particle	m
z	axial distance	m
α	volume fraction of dispersed phase	l
$\delta(z)$	delta function of space variable	m^{-1}
ϵ	voids in packed section, volume fraction	l
κ	parameter in Eq. (5)	l

Table 1: Dimensions of columns and internals

$\frac{D_c}{m}$	$\frac{h}{m}$	$\frac{d_p}{m}$	$\frac{d_p}{w}$	$\frac{\epsilon}{l}$	tracer	fluid(s)
0.05	1.41	0.005	3.33	0.50	KCl	single
	1.41	0.008	4.00	0.63	KCl	single
	1.41	0.010	5.00	0.65	KCl	single
	1.41	0.010	5.00	0.65	KCl	two
	1.41	0.012	6.00	0.72	KCl	single
0.10	1.32	0.008	4.00	0.61	KCl	single
	1.32	0.012	6.00	0.69	KCl	single
	1.32	0.012	6.00	0.69	KCl	two
	1.32	0.025	8.33	0.74	KCl	single
	1.32	0.025	8.33	0.74	KCl	two
	8.40	0.025	62.50	0.92	In-113m	single
8.40	0.025	62.50	0.92	In-113m	two	
0.23	1.40	0.025	8.33	0.73	KCl	single
	2.35	0.025	8.33	0.73	KCl	single
2.15	9.5	0.025	62.50	0.92	In-113m	two
2.40	12	0.025	62.50	0.92	In-113m	two

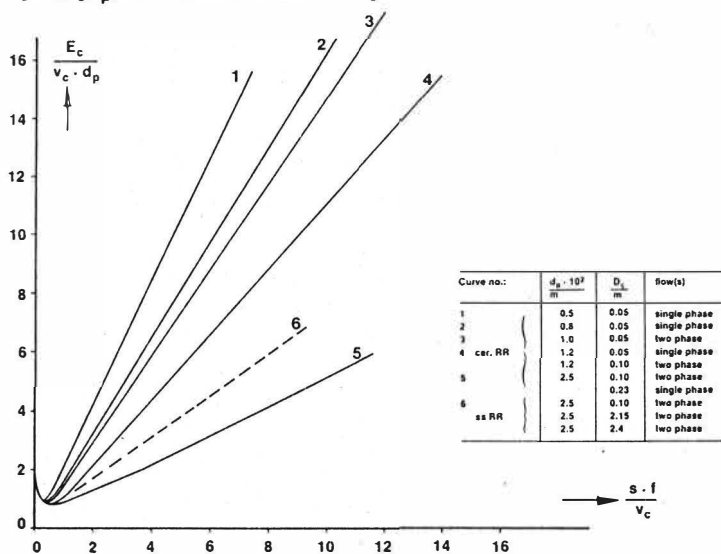
Example of experimentally obtained tracer response curves

fig1



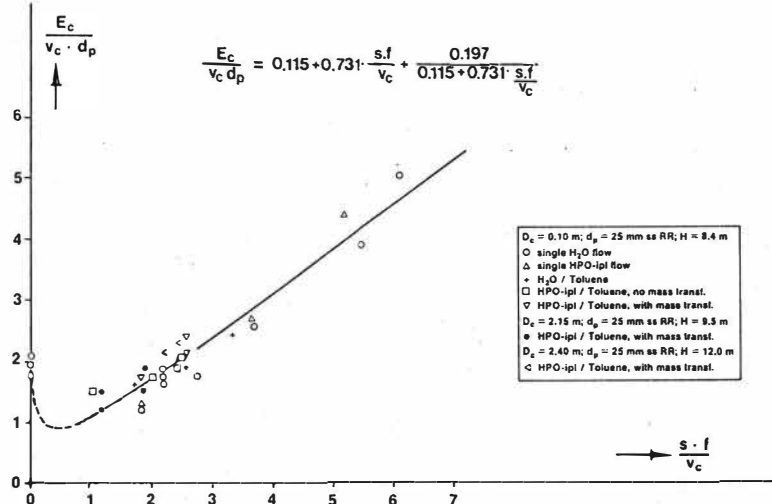
Experimentally determined smoothed values of $E_c / (v_c d_p)$ as a function of $s \cdot f / v_c$

fig2



Experimentally determined values of $E_c / (v_c d_p)$ as a function of $s \cdot f / v_c$

fig3



Supercritical Fluid Extraction in Column Contactors

R.J. Lahiere, J.R. Fair, J.L. Humphrey; The University of Texas; Austin, TX/USA

Once the mechanical design requirements have been addressed the basic design format for extractors used in supercritical fluid extraction (SFE) service is the same as for extractors processing conventional liquids. As in the case of conventional liquid-liquid extraction, there is a need for basic knowledge of phase equilibria, system properties, and the mass transfer and hydraulic performance of extraction devices operating in SFE service.

Whereas some study and investigation have been devoted to the measurement and prediction of both properties and phase equilibria in supercritical fluid systems, relatively little attention has been given to the mass transfer and hydraulic performance of continuous multistage contacting devices that are needed for some commercial applications of SFE.

The purpose of the present study is to address the performance of continuous and countercurrent sieve tray extractors operating in SFE. This will be accomplished through the acquisition of needed experimental data and the subsequent development of models which may be used to predict the performance of industrial scale SFE equipment.

Systems which are being studied are carbon dioxide/ethanol/water and carbon dioxide/isopropanol/water in a 25.4 mm (one inch) and 101.6 mm (four inch) diameter sieve tray columns.

Previous Mass Transfer and Hydraulic Studies

It has been pointed out by others that SFE extractors are expected to give favorable mass transfer rates when compared with conventional liquid-liquid extractors because of higher diffusion coefficients and lower viscosities (1,2).

In one mass transfer study Brunner used supercritical carbon dioxide to separate an aqueous 10 wt.% solution of ethanol in a spray column (3). The effects of pressure, temperature, and solvent/feed ratio on the mass transfer were examined. Mass transfer coefficients almost two orders of magnitude greater than those in conventional liquid extraction were reported.

Experiments to determine separation efficiencies of different packings in a 25.4 mm extraction column were performed by Peter (4). This study showed that a separation of a mixture of glycerides of oleic acids, with carbon dioxide as the supercritical component and acetone as an entrainer, could be made most efficiently with wire

spirals and with a gauze-type (Sulzer) structured packing. At the upper loading limit an efficiency of 3.5 theoretical stages per meter of packing height was achieved.

The same mixture of glycerides was separated in a pilot plant study using compressed propane as the solvent and acetone as an entrainer at 137 bar and 110 C (5). The extraction system consisted of two bubble-cap columns, each with a diameter of 65 mm. The main extraction vessel contained 51 plates and an auxiliary vessel, used for the recovery of solvent, had 34 plates. The authors performed an economic evaluation of the process and concluded that a tall, slim column with low reflux ratios is preferable to a short, large diameter extractor.

A mixture of high-boiling ethyl esters recovered from fish oil was fractionated with supercritical carbon dioxide in spray and packed columns (6). The use of a "hot finger" was employed to optimize the system with respect to temperature and pressure. The best results were obtained at 90 C and 152 bar.

In an investigation by Critical Fluid Systems, Inc., mass transfer efficiency was measured for an alcohol-water separation using near-critical carbon dioxide in a 101.6 mm diameter sieve tray column (7,8). Optimum solvent/feed ratios for the extracted compounds (ethanol, isopropanol, sec-butanol) were determined. However, the main objective of the work was to evaluate the economics of the pilot-plant operation as a whole and not the efficiency of the column, and no mass transfer data per se were reported.

Another pilot scale study at 61 bar and ambient temperature involved use of liquid carbon dioxide as the solvent (9). A 40 mm diameter Scheibel column was used to extract 12 model compounds (such as ethanol, ethyl acetate, 1-hexanol and citronellal) from water. Emphasis was placed on the recovery of each constituent as a function of feed rate, feed composition, and agitator rate.

Flooding in sieve tray extraction devices is due to the entrainment of dispersed phase drops by the continuous phase or by excessive pressure drops which cause the coalesced layer of dispersed phase to back up into the downcomer. Either flooding mechanism will have a detrimental effect on extractor performance. Published flooding studies, even for conventional extraction systems, are few and non-existent for SFE systems. This is an important area of research which deserves attention.

Preliminary Simulation Studies

Presently a model to predict the mass transfer efficiency of a staged supercritical extraction column does not exist. It is logical to assume that the basic principles for models of conventional sieve tray columns could be applied to the supercritical

case. Five previous methods for predicting the efficiency of sieve tray devices operating with conventional extraction systems have been summarized by Fair, et al. (10):

1. Treybal developed an empirical model based on tray spacing, superficial velocities of the phases, and the interfacial tension (11).
2. Skelland and Conger suggested a procedure in which rate equations for mass transfer during drop formation, rise, and coalescence were used to locate a pseudo-equilibrium curve from which the column efficiency could be determined (12).
3. A mechanistic model was proposed by Treybal in which the Murphree stage efficiency was combined with an expression for mass transfer between trays (13).
4. Pilhofer developed a model that predicted column efficiency by applying a calculated point efficiency to one of the two extremes for flow of the continuous phase: completely mixed or plug flow (14, 15).
5. The model proposed by Rocha et al appears to be the most accurate of those published and can predict efficiencies within $\pm 35\%$ (16). In this model the contribution of each step of the total mass transfer is separated and represented by an expression for a mass transfer coefficient. Correction factors for the contribution of drop rise and drop formation were derived from experimental data as functions of the dispersed phase Weber number and the interfacial tension of the system.

The general form of the model proposed by Rocha et al is:

$$E_{md} = \frac{1.1 K_{fd} A_{fd} + K_{rd} A_{rd}}{Q_d \rho_d / M_d + 0.5 K_{rd} A_{rd} + 0.1 K_{fd} A_{fd}} \quad (1)$$

The overall mass transfer coefficients in Equation 1 are determined from individual phase mass transfer coefficients by the two-film model:

$$\frac{1}{K_{id}} = \frac{1}{k_{id}} + \frac{m}{k_{ic}} \quad (2)$$

The approach is modular in that various correlations can be used to predict values of the individual film coefficients. The authors selected a special set of correlations and that set will be used in the analyses given in the present paper. The important property variables are density, viscosity, diffusivity, and interfacial tension.

Predicted values of mass transfer efficiency obtained by use of the model were compared with the data obtained by Critical Fluid Systems on alcohol-water separations using near critical carbon dioxide in a 101.6 mm diameter sieve tray column (7, 8). A comparison between experimental and calculated overall efficiencies for isopropanol and ethanol solutes is presented in Figure 1. When ethanol is the solute, the model

underpredicts efficiency by about 20%; for the isopropanol case it overpredicts by about 40%. Simplifying assumptions in the model and uncertainties in the values of interfacial tensions and diffusion coefficients are contributing causes for these discrepancies.

The model was also used to compare SFE with conventional liquid-liquid extraction. The SFE system was carbon dioxide/ethanol/water at 101 bar and 35 C, and the conventional system was toluene/acetone/water at one atmosphere and 25 C. These two systems have interfacial tensions in the range of 22-25 mN/m and have similar values of aqueous phase diffusion coefficients.

As shown in Figure 2, overall mass transfer efficiencies in the SFE case are almost double those for conventional extraction. The major contributor appears to be the difference in the values for the dispersed phase diffusion coefficients, estimated as $2.1 \times 10^{-8} \text{ m}^2/\text{s}$ for SFE and $2.6 \times 10^{-9} \text{ m}^2/\text{s}$ for the conventional case. Also, the viscosity of the SFE dispersed phase is about one-tenth of that for the conventional system dispersed phase. The transport property advantage of the SFE system appears to be real and bears further discussion.

Phase Equilibrium

The limits for ternary equilibrium studies are provided by the behavior of the corresponding binary systems. Several authors have studied the mutual solubilities of the carbon dioxide system (17, 18). Ternary cases which have been investigated experimentally include: carbon dioxide solvent with water-organics (19, 20, 21), ethane solvent with water-alcohols (22), and ethylene solvent with water-organics (23). Successful attempts to model qualitatively, as well as quantitatively, liquid-fluid systems using the Peng-Robinson (20, 21, 22) and the Redlich-Kwong equations of state (24) have been performed. The interaction constants used in these equations were determined from binary solubility data.

In the present study, the carbon dioxide/ethanol/water and the carbon dioxide/isopropanol/water systems were investigated from a mass transfer concept. Equilibrium data for these systems were obtained from Gilbert (25) and Kander (26), respectively.

Interfacial Tension

The interfacial tension of water-hydrocarbon (including carbon dioxide) systems at high pressures has been measured using the pendant drop method and the capillary rise technique. In the pendant drop method, a pressure cell with glass windows is constructed and photographs are taken of the drops. Interfacial tension is calculated by equating these measurements to the numerical integration of the differential equation for drop shape. Interfacial tension data were obtained for the carbon dioxide water system at temperatures ranging from 24 to 138 C and pressures from 1.03

to 1,030 bar (27, 28).

In the capillary rise technique a single glass capillary is suspended in a thermostated cylindrical brass bomb (29). The height of capillary rise is measured. The capillary rise, the capillary diameter, and the densities of the bulk liquid and gas phases are used to determine the interfacial tension. No measurements of interfacial tensions by this method have been reported for supercritical conditions.

The previous works do not provide a quantitative method for predicting the influence of a third component on the interfacial tension of a high pressure system. In many cases, the addition of the third component will lower the interfacial tension. This would have a very significant impact on the mass transfer efficiency of an extraction device.

In the present study experimental measurements for carbon dioxide/water were used to approximate the value of interfacial tension for the carbon dioxide/alcohol/water ternary. A more accurate estimate of this property is not available when the third component is present.

Diffusion Coefficient

The value of the diffusion coefficient significantly affects the mass transfer efficiency. This is particularly true in the regime of drop formation. Most of the models of this mass transfer mechanism are based on Higbie penetration theory (30). In the present study, the Wilke-Chang equation (31), based on Stokes-Einstein theory, was used to predict binary diffusion coefficients:

$$D_{ab} = 7.4 \times 10^{-8} \frac{(\rho M_b)^{0.5} T}{\mu_B V_A^{0.6}} \quad (3)$$

The results are shown in Table 1. An inspection of the table shows that the Wilke-Chang overpredicts by an average of 26%. At solvent viscosities higher than $0.05 \frac{\text{N}\cdot\text{s}}{\text{m}}$ the performance of the equation improves. The average error in this range of viscosities decreases to 15%.

Table 1
Correlation of Binary Diffusion Coefficients in Supercritical
Carbon Dioxide Solvent With Stokes-Einstein Theory

Solute	°C	D_{WC}/D_{exp} Mean (a)	$D T^{-1}$ Mean (b)	$D T^{-1}$ Maximum % Deviation From Mean	Reference
naphthalene	35-55	1.40	1.91	0.22	36
benzene	35-55	1.18	2.69	0.08	37
n-propyl benzene	35-55	1.09	2.09	0.11	37
tri-methyl benzene	35-55	1.17	1.97	0.11	37
naphthalene	40	1.32	2.00	0.13	38
benzene	40	1.19	2.70	0.17	38
phenol	40	1.44	2.40	0.11	38

(a) Ratio of diffusion coefficients calculated with Wilke-Chang equation to the experimental values.

(b) Units of this term are $((\text{cm}^2/\text{s}) (\text{g}/\text{cm-s}) (\text{°K}^{-1}) \times 10^{-10})$.

The viscosity of the supercritical solvent in the present study was about 0.06 N-s/m within the range of applicability of the Wilke-Chang correlation. A factor of 0.87 (1/1.15) was used to correct for the overprediction of diffusion coefficients with this technique.

A reasonable estimate of the aqueous phase diffusion coefficient was obtained by using the value of this property at atmospheric pressure (32). This phase is not in the supercritical state, and thus should require little if any pressure adjustment. Literature values were corrected for temperature according to Wilke-Chang and assuming 15% overprediction with this equation.

Viscosity

The viscosity of a supercritical solvent is typically one-fourth or less that of a conventional liquid solvent. The less viscous SFE solvent will allow higher throughputs than are possible in liquid extraction.

The viscosity of a supercritical fluid varies directly with pressure. Several attempts to measure the viscosity of carbon dioxide at supercritical conditions have been performed. One of the most accurate studies was by Ulybin and Makarushkin in which this property was measured using a transpiration type capillary viscometer

(33). These authors also evaluated carbon dioxide viscosity data by others.

The viscosity of water at high temperatures and pressures has also been measured extensively. All available data since 1840 were collected and evaluated by Scheffler et al (34). A system of mathematical equations was developed to represent the data in graphical and tabular format.

In the present study viscosities of pure carbon dioxide and water were used to represent the fluid and aqueous phases. This assumption was possible since the solute concentrations in the system were dilute (less than 6 mole %).

Density

Densities of the SFE solvents are in the range of conventional liquid densities though somewhat less. Thus a greater difference in density exists between the extract and raffinate phases in the supercritical case than in a liquid-liquid system. The result is a higher rate of throughput for SFE compared to conventional extraction.

The densities of the most common constituents in SFE, including carbon dioxide, have been tabulated (35). For other components, or for mixtures, estimates may be made using appropriate equations of state and mixing rules. In the dilute system used in this study the density values for the solvent and carrier were substituted for those of the extract and raffinate.

Experimental Equipment

Two 316 ss supercritical extraction test systems have been constructed. The first of these is a simple once-through flow system which incorporates a 25.4 mm (one inch) diameter, 1220 mm (48 inch) high, extractor. The second system is based on a 101.6 mm (four inch) diameter, 2032 mm (80 inch) high, extractor and has more capability than the smaller system (see Figure 3). In addition to being larger it is equipped with a totally automated control system and has total recycle capability.

The extractors in both systems can accommodate either trays or packings. The trays are assembled on threaded rods and are inserted in their correct position. The feed streams are fed to the column by controlled volume liquid pumps. External heat exchangers are used to control the temperature of the feed streams.

At this writing experimental mass transfer and flooding data are being obtained on the carbon dioxide/ethanol/water and carbon dioxide/isopropanol/water systems in the 25.4 mm diameter sieve tray extraction column. Similar data will be taken in the

101.6 mm diameter unit. Mass transfer and hydraulic performance data from the smaller system will be presented at the conference meeting and, to the extent they are available, the larger diameter data will also be presented.

Summary and Conclusions

In order to design an extractor operating in supercritical extraction service one must have accurate information on phase equilibria and system properties as well as knowledge of the mass transfer and hydraulic characteristics of the contactor under consideration.

To date little attention has been given to the mass transfer and hydraulic performance of continuous and multistage contacting devices that are needed for commercial applications of SFE. The purpose of the present and subsequent studies is to add to the knowledge base in these areas. This will be accomplished through the acquisition of experimental data and the subsequent development of mechanistic models useful for predicting the performance of industrial scale equipment.

A review of previous work shows that a few experimental studies on mass transfer have been completed using spray, packed, and tray-type devices with carbon dioxide as the solvent. However for a specific type of device such as the sieve tray, mass transfer and hydraulic studies are either non-existent or not comprehensive enough to allow for the development of generalized models.

It is logical that the basic principles of the models developed for conventional extraction can be extended to SFE. However, the success of simulation will depend in part on the knowledge of accurate phase equilibria and system properties. In the preliminary simulation studies presented earlier the conclusions regarding the accuracy of the model could not be made because of the uncertainty in the values of interfacial tensions and diffusion coefficients. Application of this model did show trends in that one might expect to obtain mass transfer efficiencies in a SFE system significantly higher than in a conventional extraction system.

Results of all experimental and modeling work will be presented at the conference.

Nomenclature

- A_{fd} = Total interfacial area for drop formation, cm^2 .
 A_{rd} = Total interfacial area for drop rise or fall, cm^2 .
 D_{AB} = Mutual diffusion coefficient of solute A at very low concentrations in solvent B, cm^2/s .
 E_{md} = Murphree tray efficiency, fractional.

- Q_c, Q_d = Volumetric flow of continuous and dispersed phases, respectively, cm^3/s .
- K_{fd} = Overall mass transfer coefficient for drop formation based on dispersed phase, $(\text{gm-moles}) / (\text{s-cm}^2)$.
- K_{rd} = Overall mass transfer coefficient for drop rise or fall based on dispersed phase, $(\text{gm-moles}) / (\text{s-cm}^2)$.
- K_{id} = Individual film coefficient for dispersed phase, $(\text{gm-moles}) / (\text{s-cm}^2)$,
 $i = f$ for drop formation, $i = r$ for drop rise or fall.
- K_{ic} = Individual film coefficient for continuous phase, $(\text{gm-moles}) / (\text{s-cm}^2)$,
 $i = f$ for drop formation, $i = r$ for drop rise or fall.
- M_B = Molecular weight of component B, $\text{gm}/(\text{gm-mole})$.
- M_d = Molecular weight of the dispersed phase, $\text{gm}/(\text{gm-mole})$.
- m_{dc} = Slope of the equilibrium curve (mole fraction of solute in dispersed phase) / (mole fraction of solute in continuous phase).
- T = Absolute temperature, degrees Kelvin.
- U_c, U_d = Superficial velocity of continuous and dispersed phases, respectively, cm/s .
- V_A = Molal volume of solute A at its normal boiling temperature, $\text{cm}^3/\text{gm-mole}$.

Greek Letters

- ϕ = Association factor of solvent B, dimensionless.
- η_B = Viscosity of component B, dynes.
- ρ_d = Density of dispersed phase, gm/cm^3 .

Literature Cited

- King, M.B.; Kassim, K.; Bott, T.R.; Fluid Phase Equilibria **10**, 249 (1983).
- Debenedetti, P.G.; Reid, R.C.; paper presented at San Francisco AIChE meeting, November, 1984.
- Brunner, G.; paper presented at San Francisco AIChE meeting, November, 1984.
- Peter, S.; Tiegs, C.; paper presented at International Symposium on High Pressure Chemical Engineering, Erlangen, West Germany, October, 1984.
- Peter, S.; Brunner, G.; Angew. Chem. Int. Ed. Engl. **17**, 746 (1978).
- Eisenbach, G.; Proc., Amer. Chem. Soc., Chicago meeting, **30** (3) 206 (1985).
- Moses, J.M.; Goklen, K.E.; de Felippi, R.P.; paper presented at Los Angeles AIChE meeting, November, 1982.
- Moses, J.M.; de Felippi, R.P.; "Critical-Fluid Extraction of Organics from Water" Contract No. DE-AC01-79CS40258, U.S. Dept. of Commerce (Springfield, VA), June, 1984.
- Schultz, W.G.; Schultz, T.H.; Carleson, R.A.; Hudson, J.S.; Food Technol. **6**, 32 (1974).
- Fair, J.R.; Rocha, J.A.; Humphrey, J.L.; Solv. Extrac. Ion Exchange **2**, No. 7 985 (1984).
- Treybal, R.E.; Liquid Extraction 2nd ed., New York: McGraw-Hill, 1963.
- Skelland, A.H.P.; Conger, W.L.; Ind. Eng. Chem. Process Des. Develop. **12**, 448 (1973).
- Treybal, R.E.; Mass Transfer Operations, 3rd ed., New York: McGraw-Hill, 1980.
- Baker, L.C.W.; Chem. Eng. Commun. **11**, 241 (1981).
- Schultz, L.; Pilhofer, T.; Int. Chem. Eng. **22**, 61 (1982).
- Rocha, J.A.; Humphrey, J.L.; Fair, J.R.; submitted for publication to Ind. Chem. Eng. Process Des. Develop.
- Wiebe, R.; Gaddy, V.L.; J. Amer. Chem. Soc. **63**, 475, (1941).
- Baker, L.C.W.; Anderson, T.F.; J. Amer. Chem. Soc. **79**, 2071 (1957).
- Kuk, M.S.; Montagna, J.C.; in Chemical Engineering at Supercritical Conditions, M.E. Paulaitis, J.M.L. Penninger, R.D. Gray, and P. Davidson (Eds.) 101-112, Ann Arbor, Michigan: Ann Arbor Science, 1983.
- Panagiotopoulos, A.Z.; Reid, R.C.; Proc. Amer. Chem. Soc., Chicago meeting **30**, (3), 46 (1985).
- Paulaitis, M.E.; Kander, R.; J. Phys. Chem. **88**, 869 (1984).

22. McHugh, M.A.; Mallet, M.W.; Kohn, J.P., in Chemical Engineering at Supercritical Conditions, M.E. Paulaitis, J.M.L. Penninger, R.D. Gray, and P. Davidson (Eds.), 113-138, Ann Arbor, Michigan: Ann Arbor Science, 1983.
23. Elgin, J.C.; Winestock, J.J.; J. Chem. Eng. Data **4**, 3 (1959).
24. King, M.B.; Alderson, D.A.; Fallah, F.H.; Kassim, D.M.; Kassim, K; Sheldon, J.J.R.; Mahmud, R.S.; in Chemical Engineering at Supercritical Conditions, M.E. Paulaitis, J.M.L. Penninger, R.D. Gray, and P. Davidson (Eds.), 31-80, Ann Arbor, Michigan: Ann Arbor Science, 1983.
25. Gilbert, M.L.; M.S. Thesis, The University of Delaware, 1985.
26. Kander, R.G.; Ph.D. Dissertation, The University of Delaware, 1986.
27. Hough, E.W.; Heuer, G.J.; Walker, J.W.; Petrol. Trans, AIME **216**, 469 (1959).
28. Heuer, G.J.; Ph.D. Dissertation, The University of Texas (1957).
29. Jho, C.; Nealon, D.; Shogbola, S.; King, A.D.; J. Colloid Interface Sci. **65**, 142 (1978).
30. Higbie, R.; Trans. AIChE **31**, 365 (1935).
31. Wilke, C.R.; Chang, P.; AIChE J. **1**, 264 (1955).
32. Reid, R.C.; Prausnitz, J.M.; Sherwood, T.K.; The Properties of Gases and Liquids, 3rd ed., New York: McGraw-Hill, 1977.
33. Ulybin, S.A.; Makarushkin, W.I.; Proc. Symp. Thermophys. Prop. **7**, 678 (1977).
34. Scheffler, K.; Straub, J.; Grigul, U.; Proc. Symp. Thermophys. Prop. **7**, 684 (1977).
35. International Union of Pure & Applied Chemistry, Int. Thermo. Tables of the Fluid State: Carbon Dioxide, S. Angus, B. Armstrong, and K.M. de Reuck (Eds.), Oxford: Pergamon Press, 1976.
36. Iometev, M.B.; Tsekhanskaya, Y.V.; Russ. J. Phys. Chem. **38**, 485 (1964).
37. Swaid, I.; Schneider, G.M.; Ber. Bunsenges Phys. Chem. **83**, 969 (1979).
38. Feist, R.; Schneider, G.M.; Sep. Sci. Technol. **17**, 261 (1982).

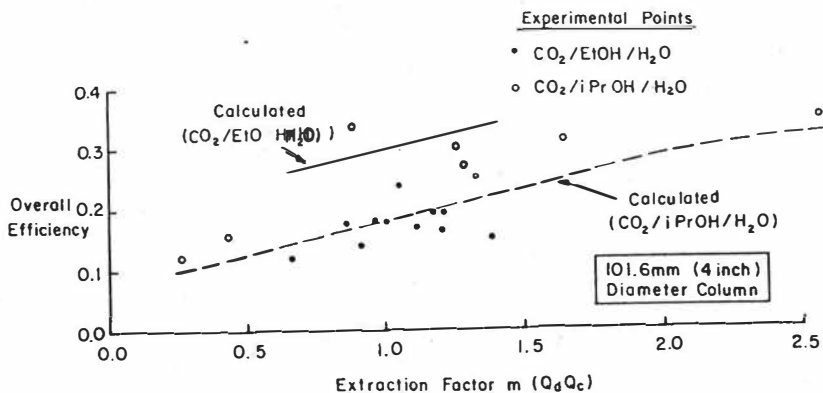


Figure 1. Comparison of Experimental and Calculated Results for the CO₂/EtOH/H₂O and CO₂/iPrOH/H₂O Systems

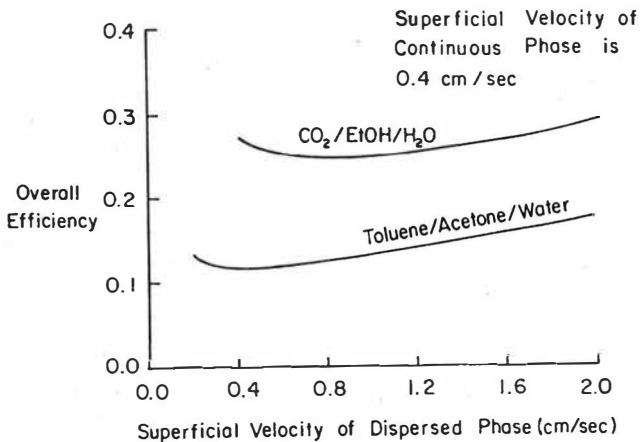


Figure 2. Comparison of Calculated Efficiency for Supercritical and Liquid - Liquid Extraction

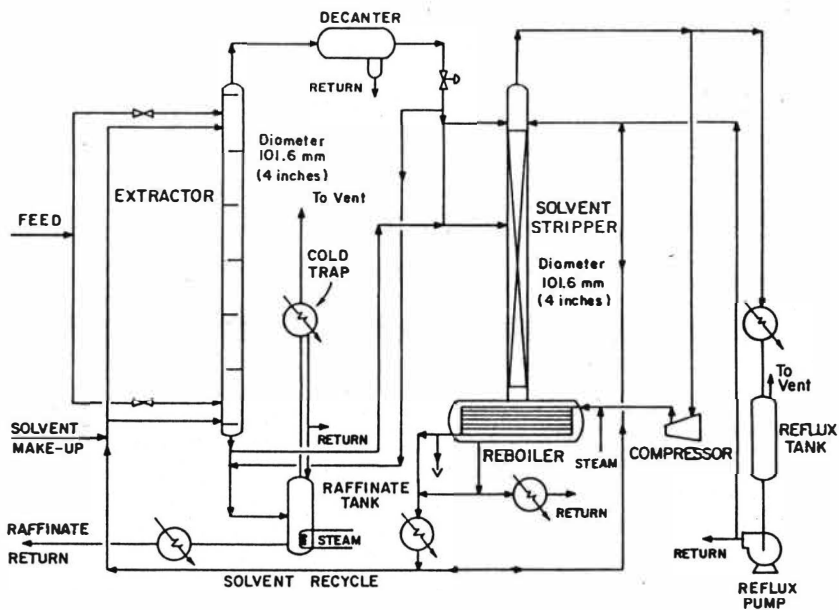


Figure 3. Supercritical Extraction Test System

Gähns, H.J., Beutler, H.J., Lenhard, U. and Lürken, F.
Messer Griesheim GmbH, Krefeld, Germany

1. Introduction

Most of the theoretical work on high-pressure-extraction HPE deals with the solvent power of compressed or supercritical gases, i.e. phase equilibria between single substances and gases of one or more components. Experimental contributions show a broad field of potential application.

This presentation gives results of application-oriented developments focussed on the economy of the HPE-process for a number of different problems. We will concentrate on extractions of natural solid substances because HPE plants in operation today and the near-future applications we see both work with such materials.

2. Solvent power and loading of gases

HPE is based on the solvent power of compressed or supercritical gases, e.g. CO₂. Technically relevant pressures range from 8 to 50 MPa. In this pressure range the solvent power usually increases with increasing density of the gaseous solvent. The solvent power of CO₂ and its dependence on pressure and temperature have been determined for numerous single substances and classes of substances.

Solubility diagrams, however, only give first hints for the choice of HPE-conditions. The loading of the solvent gas (i.e. the concentrations of solute in the supercritical solvent) usually is well below the values of saturation (e.g. 5 to 100 times).

This discrepancy can not be explained by incomplete equilibration but rather by the much more complex situation encountered with natural materials compared with those used to study solubilities. We have to take into account that

- natural materials contain numerous constituents of different solubilities

- the substances to be dissolved are physically or chemically bound to an insoluble solid matrix.
- diffusion as well as adsorption and desorption processes influence the transfer into the solvent phase
- the properties of the solvent are changed by dissolved substances since
- the composition of the solvent changes in the course of extraction because constituents of differing solubility are removed at different rates

These numerous influences result in a manifold of possibilities to optimize the process of extraction some of which are given below. Two cases of typical HPE applications will be considered:

- the production of extracts from natural raw materials
- the refinement of natural products by a selective extraction of unwanted substances.

3. The production of extracts from natural solid materials

The aim of this HPE application is a complete extraction of active principles or valuable constituents from an insoluble solid matrix. For economic reasons it is advantageous to maintain a high loading of the supercritical solvent during the extraction process.

The production of pepper extracts (i.e. oleoresins and piperin) is presented in some detail showing the influences of the pre-treatment (e.g. grinding), of the amount of pepper material (i.e. the height of the autoclave filling), and of the specific CO₂ flow rate on the loading of the gaseous solvent.

In one test a column of previously extracted pepper was put on top of the extractor to investigate the influence of adsorption and desorption on the course and result of an extraction run.

4. Selective Extractions

High selectivity is a basic advantage of HPE. Its achievement, however, may require different solutions in process engineering. Two examples are presented, the decaffeination of tea and the reduction of nicotine in tobacco. Both problems are more difficult to solve than, for instance, the production of caffeine-free coffee because both materials have a full aroma content.

In High Pressure Extraction of caffeine from tea very low loadings of the gas phase were observed under all conditions. Adsorption processes as well as limited diffusion may be the cause. The concentration of caffeine in the solvent gas is only slightly influenced by the contact time between solvent and product, whereas increasing reduction of the aroma content is observed with increasing residence time of the solvent in the extractor. Therefore, the layout of the extractor vessel used for the production of decaffeinated tea had to be modified in a special way to assure short contact time between solvent and product.

An aroma preserving reduction of nicotine from tobacco is based on an extraordinarily high solvent power of mixtures of N_2 and CO_2 with respect to nicotine. Although even small additions of N_2 drastically reduce the solvent power of CO_2 for most substances a maximum solubility of 4 % by weight is found for nicotine even in mixtures of N_2 and CO_2 containing 75 % of Nitrogen. Using such gas mixtures in HPE it is possible to produce tobacco with a reduction of 95 % with respect to nicotine and a loss of aroma components well below 10 %.

5. Outlook

Systematic investigations of process engineering schemes may enhance application of HPE. The multitude of factors that influence the course and result of an extraction require extended trials and scale-up testing. The HPE department at Messer Griesheim Krefeld will install a plant of technical scale at the end of 1986 and thus supplement the smaller test plants already in operation. A close cooperation with manufacturers of HPE equipment is planned to offer the potential user of HPE a complete development of process engineering including basic parameters, layout, and constructional details.

R.B. Eldridge, J.L. Humphrey, J.R. Fair; University of Texas; Austin, TX/USA

Large commercial sieve tray extraction columns do not exhibit the same performance characteristics as their small, pilot-scale counterparts. As might be expected, drop formation and dispersion differ; drop size distributions differ, in part because of changed interfacial characteristics; axial dispersion of the continuous phase is influenced both by longer path length and by forces imparted by the drop field; and the drops may tend to recirculate and thereby depart from the plug flow characteristics observed in small equipment.

It would be expected also that the characteristics of the continuous phase flow in the large extractor would differ from those in the small scale counterpart. As in the case of distillation, a plug flow characteristic might enhance the small column efficiency. Other characteristics, such as retrograde flow and directional velocity gradients would also be expected to influence the effective interphase concentration gradients and thus the observed tray efficiency of the large unit.

The purpose of this work was to examine the axial mixing characteristics of the flow of continuous phase across an active sieve tray. The mixing patterns would be determined as functions of tray geometry, phase flow rates, and fluid physical properties. Once determined quantitatively, the axial dispersion coefficients could then be combined with a point efficiency model, such as that developed by Rocha et al. (1), to enable predictions of large scale extractor tray efficiencies.

Background

The geometry of an extractor sieve tray resembles that of a distillation sieve tray. As indicated in Figure 1, continuous phase enters the tray through a downcomer and passes across the field of moving dispersed phase drops. The mass transfer efficiency of tray n is conveniently expressed as a Murphree efficiency:

$$E_{md} = \frac{Y_n - Y_{n-1}}{Y_n^* - Y_{n-1}} \quad (1)$$

where the Y values refer to solute mole fractions in the dispersed phase and the Y^* term refers to an equilibrium concentration with respect to the continuous phase leaving the tray:

$$Y_n^* = m_{dc} X_n \quad (2)$$

The direct analogy to vapor-liquid equilibrium on distillation trays is apparent.

Depending on phase mixing, the value of E_{md} will be equal to or greater than the local efficiency, which applies to a point on the tray and which can vary with location. For the case of complete continuous phase mixing, $E_{md} = E_{pd}$. For the case of plug flow of continuous phase,

$$E_{md} = \frac{\exp[E_{pd}\lambda] - 1}{\lambda} \quad (3)$$

where E_{pd} = point efficiency, based on dispersed phase concentrations

λ = extraction factor, $m_{dc} F_d / F_c$

F_d / F_c = molar ratio of dispersed to continuous flows

m_{dc} = slope of the equilibrium curve based on molar concentrations, dispersed phase on ordinate scale.

For cases that are intermediate between complete mixing and plug flow, measures of departure from ideal flow are necessary. The pertinent background work leading to such measures has been done largely with homogeneous systems or with gas-liquid systems, and it possible to utilize such work, by direct analogy, for liquid-liquid systems.

A useful method for expressing the degree of tray mixing is the stage model, where the phase in crossflow is presumed to flow through one or more well-mixed stages. This model, originally applied to distillation trays by Gautreaux and O'Connell (2), also relates point and tray efficiencies:

$$E_{md}/E_{pd} = \frac{(1 + \frac{\lambda E_{pd}}{s})^s - 1}{\lambda E_{pd}} \quad (4)$$

where s = number of mixing stages on the tray

When $s = 1$, the continuous phase is completely mixed, and point efficiency equals tray efficiency. For pure plug flow of continuous phase, $s = \infty$. For intermediate cases, a blending of the diffusion and stage models is possible, and

$$s \sim (Pe + 2)/2 \quad (5)$$

The Peclet number, $Pe = \frac{F_c Z}{A_{cm} D_E}$, thus becomes a key dimensionless parameter in assessing the effects of geometry on axial mixing and point efficiency enhancement.

Measurements of Peclet numbers (or eddy diffusion coefficients) for continuous phase flow on sieve trays have not been reported previously. Angelo and Lightfoot (3) considered liquid-liquid system mixing in such a geometry, but limited their work to the completely mixed region. For other extraction devices, however, some

axial mixing studies have been reported, for example the notable work of Myauchi and Vermeulen (4) for packed extractors. It is beyond the scope of the present paper to review mixing studies in the various available extraction devices, since the purpose here is to deal with mixing on crossflow sieve tray devices.

Experimental Equipment

The experimental equipment is shown in Figure 2. The contacting unit was designed to simulate a slice from a larger scale sieve tray extractor and to provide for maximum opportunity for viewing flows of the phases. The design also provides for a broad range of phase flow rates, tray spacings, downcomer dimensions and tray hole patterns. Dimensions of the contacting unit are shown in Figure 3.

Phase interfaces are maintained by adjustment of the height of the atmospheric head tanks. Mesh pads aid in drop coalescence. The injection point for a dye tracer is in the inlet downcomer. A sampling device withdraws fluid from the exit downcomer and feeds the sample to a Beckman spectrophotometer for analysis. For the observation and measurement of mixing effects, a pulse injection technique is used, with the output from the spectrophotometer being recorded on a strip chart. The experimental unit is also equipped for the photographic determination of drop size distribution.

Data Analysis

The unsteady state unidirectional axial dispersion relationship, appropriate for the test method used, is

$$\frac{\partial C}{\partial t} + V_z \frac{\partial C}{\partial Z} = D_E \frac{\partial^2 C}{\partial Z^2} + [\text{source term}] \quad (6)$$

where C = concentration of tracer

t = time

V_z = velocity in the axial direction

D_E = eddy diffusion coefficient

A "source term" is shown in Equation 6 to allow for the injection of tracer in the test section itself. In the present work, an impulse source term was used in the experimentation; this term approximated a perfect delta function.

Equation 7 is the dimensionless solution of Equation 6, subject to plug flow boundary conditions (i.e., no diffusion in the tray inlet or exit downcomer):

$$C_N = (1/t_r)(e^{Pe/2}) \sum_{n=1}^{\infty} \frac{(-1)^{n+1} 8 \alpha_n^2}{4 \alpha_n^2 + 4 Pe + Pe^2} \exp[-A_n(t/t_r)] \quad (7)$$

where C_N = normalized concentration (time)⁻¹

t_r = mean residence time

Pe = Peclet number

$$A_n = \frac{Pe^2 + 4 \alpha_n^2}{4 Pe} \quad (8)$$

$$\tan \alpha_n = \frac{4 Pe \alpha_n}{4 \alpha_n^2 - Pe^2} \quad (9)$$

This solution has been taken from Himmelblau and Bischof (5).

Points were obtained from experimental traces of dye concentration, an example of which is shown in Figure 4. These points were fitted to Equation 7 through a non-linear curve fitting technique. This data regression yielded a Peclet number and a mean residence time which minimized the error between the experimental and calculated concentration profiles; the example shown in Figure 5 is a companion to the raw data of Figure 4. The Peclet number so obtained was combined with the tray length and the continuous phase velocity to yield a value of the eddy diffusion coefficient.

Results

Axial mixing results were obtained for operating sieve trays spaced at 6 and 12 inches, with the geometry shown in Figure 3. Two immiscible systems were used: toluene/water and n-butanol/water, both at room temperature. The interfacial tensions of these systems were 30 mN/m and 1.8 mN/m, respectively. The corresponding Sauter mean drop diameters were 6.3 and 3.2 mm, measured from photographs with a Zidas Digitizer (Karl Zeiss, Inc.).

The experimental data are plotted in Figure 6 as Peclet number versus superficial dispersed phase velocity based on the active (perforated) area of the tray. It is clear that for the lower interfacial tension system (butanol/water) the axial mixing is intense and the tray behaves essentially as a well-mixed stage. Although some plug flow effect might be recognized for large commercial-scale extractors, it appears likely that point efficiencies from small test columns can be scaled up directly.

The butanol/water system has an inherently-high point efficiency because of the small drops and corresponding high interfacial area. One might consider a small tray

spacing in order to promote plug flow, but this in turn would lower the efficiency (shorter drop rise residence time) and thus defeat the attempt to obtain a larger value of Murphree efficiency.

For the higher interfacial tension system (toluene/water), higher Peclet numbers are achieved, as also shown in Figure 6. Downcomer length and hole diameter appear to have a minor influence on axial mixing, but tray spacing has a significant influence. However, the characteristically-low point efficiencies for such systems would show only a small enhancement at the low tray spacings, even with pure plug flow. Again, use of low tray spacings would also impair point efficiency. Thus, also for the high interfacial tension system, scaleup of point efficiency appears to be direct.

Summary and Conclusions

An experimental study has been made of the axial mixing of the continuous phase flowing across a sieve tray that is active with a rising field of light phase drops. Eddy diffusion coefficients as high as $375 \text{ cm}^2/\text{sec}$. were obtained for a tray spacing of 12 inches. This indicates a significant amount of backmixing, even at high flow ratios of continuous to dispersed phase.

One may conclude from this work that for systems with relatively high interfacial tension, which give characteristically low point efficiencies, axial mixing is not an important issue in the design of sieve tray extractors. For systems with relatively low interfacial tension, which give characteristically high point efficiencies, a considerable amount of back-mixing occurs, thus limiting the efficiency enhancement desired for the full crossflow tray. Very low tray spacings can decrease backmixing but in turn limit point efficiency because of lower drop residence time.

Additional work is required to validate completely the effects of all operating and property variables, but the indication is that for most systems, axial mixing plays only a minor role in the optimum design of sieve tray extractors.

Symbols

A	cross sectional area available for continuous phase flow (L)
A_n	variable defined by Equation 8 (dimensionless)
C	concentration of tracer (moles/L ³)
C_n	normalized tracer concentration (1/θ)
D_E	eddy diffusion coefficient (L ² /θ)

E_{md}	Murphree dispersed phase tray efficiency (fractional)
E_{pd}	Point dispersed phase efficiency (fractional)
F_c	continuous phase molar flow rate (moles/ θ)
F_d	dispersed phase molar flow rate (moles/ θ)
m_{dc}	equilibrium distribution coefficient, Y^*/X (dimensionless)
Pe	Peclet number (dimensionless), Equation 5
s	number of mixing stages on tray
t	time (θ)
t_r	mean residence time of tracer on tray (θ)
V_z	velocity of continuous phase in axial direction (L/ θ)
w	dimensionless tray length, dZ/Z
X	mole fraction of solute in continuous phase
X_e^*	mole fraction of solute in continuous phase, in equilibrium with dispersed phase entering the tray
Y	mole fraction of solute in dispersed phase
Y^*	mole fraction of solute in dispersed phase, in equilibrium with continuous phase mole fraction X
Z	distance in direction of continuous phase flow (L)
Z_T	total length of tray flow path (L)

Greek Letters

α_n	variable defined by Equation 9 (dimensionless)
λ	extraction factor, $m_{dc} F_d / F_c$ (dimensionless)
ρ_m	mean molar density of tray mixture (moles/L ³)

Subscripts

n	tray n
$n-1$	tray $n-1$ (below tray n)

Literature Cited

1. Rocha, J.A., Humphrey, J.L., Fair, J.R., "Mass Transfer Efficiency of Sieve Tray Extractors", submitted for publication. Also, J.A.Rocha-Urbe, "Mass Transfer Efficiency of Sieve Tray Extraction Columns", Ph.D. Dissertation, The University of Texas at Austin, USA, December 1984.
2. Gautreaux, M.F., O'Connell, H.E., Chem. Eng. Progr. 51, 232 (1961).
3. Angelo, J.B., Lightfoot, E.N., AIChE J. 14, 531 (1968).
4. Miyauchi, T., Vermeulen, T., Ind. Eng. Chem. Fundam. 2, 113 (1963).
5. Himmelblau, D.H., Bischoff, K.B., Process Analysis and Simulation - Deterministic Systems, Austin, Texas: Sterling Swift, 1968.

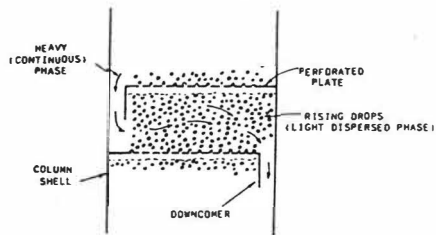


Figure 1. Extraction Sieve Tray

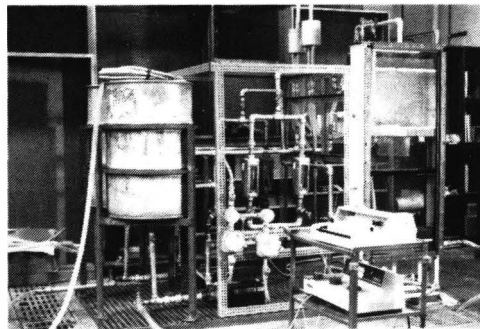


Figure 2. Photograph of equipment

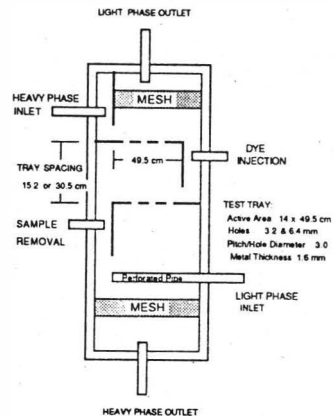


Figure 3. Dimensions of contacting unit

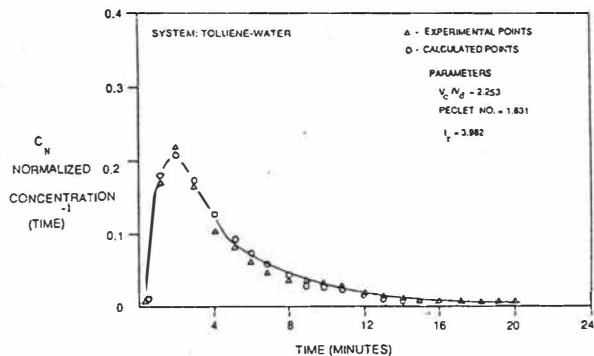


Figure 5. Typical regressed plot of data

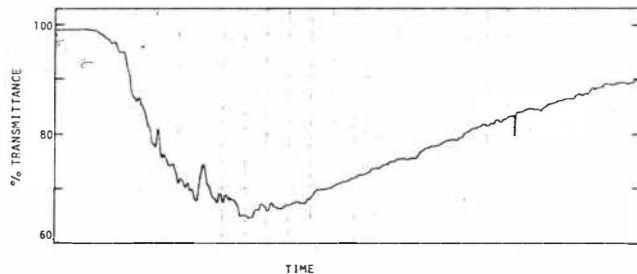


Figure 4. Typical plot of transmittance vs. time

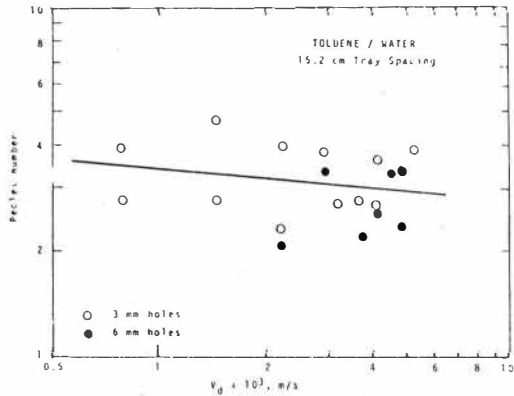


Figure 6A. Pelet numbers for 15.2 cm tray spacing

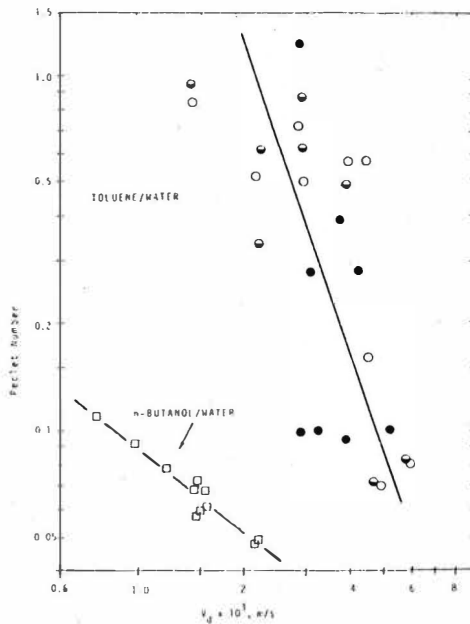


Figure 6B. Pelet numbers for 30.5 cm tray spacing

- toluene/water, 6 mm holes, 7.6 cm downcomer length
- toluene/water, 3 mm holes, 7.6 cm downcomer length
- ◐ toluene/water, 6 mm holes, 15.2 cm downcomer length
- butanol/water, 6 mm holes, 7.6 cm downcomer length

INTRODUCTION

In liquid-liquid extraction the rate of solute transport is determined by the difference in chemical potential in the two phases, the area of interface available and the hydrodynamic conditions at the fluid phase boundary. The resistance to mass transfer provided by the conditions prevailing at the interface comprise, in the absence of chemical reaction, the effects of the two diffusional boundary layers and of the interface itself. For a given system, in order to attain a high rate of solute transfer it is desirable to achieve both large areas of interface and low diffusional resistances by intimately contacting the liquids together. Agitated vessels are useful for this purpose in that the degree of mixing is rarely uniform and therefore, according to the local degree of turbulence, droplet break-up or coalescence may occur. The importance of this process in promoting high rates of mass transfer has long been recognised (1). In cases where droplets undergo rapid successive coalescence and redispersion the observed rates of extraction can be much greater than those which might be predicted from studies of single droplets of the same mean size (2). It has also been observed that the highest rates of mass transfer occur at newly formed interfaces or in cases where the interface can be considered to be undergoing surface renewal (3-6).

From the foregoing it may be deduced that, in order to maximise the rate of solute transfer it is desirable to create, continuously, large areas of new interface between turbulent phases. One means of achieving this is to intensify the coalescence-redispersion cycle by high speed mechanical agitation. This has the additional benefit of increasing the interfacial area. Typically however, small stable droplets give poor mass transfer coefficients because they have stagnant interiors and move slowly. Furthermore, they are so easily entrained by the continuous phase that they severely restrict the allowable throughput of the equipment. The extent to which agitation may be usefully increased is therefore constrained unless droplet coalescence can be independently increased to counteract the production of fine droplets. This requirement can be satisfied for "water in oil" type dispersions by using technology in electrically augmented coalescence recently developed at Bradford (7). Rapid coalescence in such systems can be obtained by the use of pulsed DC fields and insulated electrodes.

A novel rotary agitated differential column has been developed (8,9), the design of which is based upon the concepts discussed above. The objective of the present study is to investigate the effects of enhanced coalescence-redispersion upon column behaviour. The dependence of dispersed phase hold-up upon, firstly the impeller speed and electric field strength and, secondly column loading were studied in the absence of mass transfer. Subsequently, experiments were performed with mass transfer in order to demonstrate the practical value of intensified coalescence-

redispersion with regard to liquid extraction equipment.

EXPERIMENTAL

The extraction column consisted of a 71 mm inside diameter, 0.5 m QVF glass tube with bell ends and mild steel end plates. The column was divided into four mixing compartments and two quiescent end zones by means of five wall mounted stator ring electrodes. The arrangement of the column internals is shown in Figure 1. The active column height was 320 mm.

The ring electrodes were fabricated from PTFE insulated cable. Wire core and insulation diameters were 1.16 mm and 5.10 mm respectively. They were made up to fit closely to the column wall and were each energised by means of a further cable passing through the column wall. The electrode wire core was completely insulated from the process liquids. The nature of the impellers is illustrated in Figure 2. The impeller was located on a rotating shaft, central within the column and surrounded by an immobile slotted cage, or shroud. This design was chosen after initial trials showed that it was not possible to achieve good droplet break-up using conventional column agitators in the presence of an electric field. The slots impart high shear forces on droplets passing through them and also serve to minimise tangential flow. The relative positions of the impeller and shroud were maintained by means of a support collar which was fixed in position by three column length rods. The base of the shroud rested on the support collar and was steadied by "U" shaped locating rods about the column length rods. The flat base of the impeller and the support collar were horizontally aligned. This arrangement ensured that the base of the mixing assembly was effectively sealed and that the mixing induced draught acted only in the region above the collar. The impeller parts were fabricated in mild steel. A supplementary ring electrode was placed in the quiescent zone at the column top in order to enhance "water in oil" de-entrainment.

A liquid test system was selected which would facilitate the laboratory investigation and at the same time demonstrate the applicability of the novel contactor to commercial extractions. In general, the choice of system requires some attention to the physical properties of the liquids, particularly their electrical characteristics since an electrostatic field can only be sustained for a continuous phase which is substantially insulating. The liquid system selected was:

- Continuous, raffinate phase : ISOPAR M[®] (An isoparaffinic hydrocarbon with boiling range 204 to 249°C marketed by Exxon).
- Transferring solute : Cumene (isopropylbenzene supplied by ICI plc).
- Dispersed, solvent phase : an equivolume mixture of N-methyl 2 pyrrolidinone (NMP) and ethylene glycol.

NMP[®] is a cyclic polar solvent marketed by GAF Corp. It is used commercially with a cosolvent, typically ethylene glycol, diethylene glycol or water, for the extraction of aromatics in the Lurgi Arosolvan Process (10). The physical properties of the liquids are given elsewhere (9) but are characterised by an interfacial

tension of 12.8 mN.m^{-1} and a phase density difference of 291 kg.m^{-3} .

The investigation of column hydrodynamics was carried out in the absence of mass transfer using solute free, pre-equilibrated liquids. For the mass transfer experiments fresh liquids were used and the influent continuous phase contained 20% by volume (0.304 mole fraction) cumene. The NMP-ethylene glycol feed was free of solute. Analysis was by G.L.C. and, in the region of interest the equilibrium relationship was shown to be linear and to be described by the equation:

$$y = 0.085x \quad (1)$$

where x and y are the mole fraction of cumene in the raffinate and extract phases respectively (9).

A standard procedure was adopted for the experiments. All work was carried out at ambient temperatures. The column was allowed to operate with a stable interface for a period of three residence times of the minority phase based upon its superficial velocity prior to measurement. For hold-up determination, the feed flows and dispersed phase underflow were shut off simultaneously and the contents of the column were allowed to settle. The column was then drained until the interface was level with the interface marker used for the dynamic situation. The volume drained thus represented the total volume of droplets in the column during operation. Care was taken to recover the dispersed phase prevented from settling by the impeller assemblies. For experiments with mass transfer, samples of the effluent phase flows were taken immediately prior to shut down and hold-up determination. Throughout the mass transfer work a volumetric phase flow ratio, dispersed to continuous, of 4 : 1, was used. This gave an operating line parallel to the equilibrium line.

The electric field for coalescence was obtained by applying a pulsed unidirectional voltage to the electrically insulated electrodes. The impeller assemblies and support rods were electrically grounded. The use of pulsed D.C. fields with coated electrodes for effecting coalescence of "water in oil" type dispersions has previously been reported by Bailes and Larkai (7,11). This study represents the first occasion on which this electrical system has been employed in a non-parallel plate geometry and also for a non-aqueous dispersed phase. The electrical equipment was similar to that used previously (7) and its operational facets are discussed elsewhere (12). Although pulse frequency is known to exert a considerable influence on coalescence performance (13) it was not varied during the present investigation. A pre-determined value of 4 Hz was used throughout the study. This frequency matches the interfacial relaxation time of the column dielectric system (9) and under such circumstances the coalescing effect is likely to be near its maximum.

DISCUSSION OF RESULTS

Figure 3 shows a typical set of results at fixed column loading (1.0 l/min) and phase flow ratio (d/c of 4 : 1) for dispersed phase hold-up as a function of electric field strength and impeller speed. As expected, increasing impeller speed leads to a rise in hold-up and increasing the electrode voltage causes a reduction in the same. It should be noted that only at the lowest flow rates and impeller speeds used could the column be operated in the absence of the electric field.

An alternative means of presenting the data is shown in Figure 4. Here lines of constant hold-up are given as a function of impeller speed and electrode voltage for a different column loading (0.75 l/min). These lines were obtained by interpolation of data similar in form to those shown in Figure 3. This method of data presentation illustrates that the electric field can be effectively used to maintain the droplet coalescence-breakage dynamic equilibrium as impeller speed is increased. Further analysis of all the hold-up results reveals excellent agreement with the empirical relationship:

$$h \propto N^2 V^{-0.5} \quad (2)$$

where h is the dispersed phase fractional hold-up; N is the impeller speed and V is the applied electrode voltage. As an example, the correlation obtained for a column loading of 1.0 l min^{-1} and a phase flow ratio (d/c) of 2 : 1 is given in Figure 5.

The results of experiments carried out at different column loadings are shown in Figure 6. The two impeller speed-electrode voltage combinations used were selected such that, according to Equation (1) they should give similar hold-up values at each given throughput. The data indicate that this is indeed the case over a wide range of operation. The most interesting feature however is that the data exhibit a discontinuity and the line drawn through the experimental points describes an abrupt change of curvature. This finding suggests that the mechanism of droplet break-up and/or coalescence undergoes a change at a certain "critical hold-up" (h_{cr}). Furthermore it is apparent from Figure 7 that this discontinuity corresponds to a maximum in slip velocity (V_{sm}). This fact may be interpreted to mean that droplet size also passes through a maximum at this critical point, if it is assumed that slip velocity is essentially a function of droplet size.

An explanation for this phenomenon has been sought from previous studies of droplet behaviour in agitated systems (14,15). In a stirred tank for example, it appears that droplet size increases with hold-up due to enhanced collision frequencies which, in turn, lead to greater coalescence. This general trend is valid up to the point where the maximum stable droplet size is attained. Droplets of diameter greater than this have a propensity to break-up under the influence of the prevailing shear forces. The maximum stable diameter is, in a given agitated system effectively a function of impeller speed and, for the case of the present study, electric field strength. It is proposed that for hold-up below the critical value (subcritical operation), the fine droplets issuing from the impeller shroud

slots are rapidly coalesced by the electric field and pass subsequently to the next mixing compartment. As throughput, and hence hold-up, is increased, the mean diameter of the droplets, post-coalescence, increases until, at critical behaviour, the maximum stable size is attained. At hold-ups beyond the critical value (supercritical operation), the maximum stable size is surpassed and droplets break-up due to shear forces in the bulk of the column well away from the impeller region. This supplementary break-up occurs in a zone of low electric field intensity and thus re-coalescence is slow resulting in a reducing mean droplet size and slip velocity. Thus two distinct regimes of operation exist.

Results from mass transfer experiments carried out at a constant column loading of 1.0 l/min are presented in Table 1. They indicate that a significant improvement in mass transfer efficiency can be obtained by making concurrent increases in impeller speed and electrode voltage. Hold-up is approximately constant and therefore the balance between coalescence and redispersion is ostensibly invariant. While hold-up may be fairly indicative of the prevailing coalescence-redispersion balance it gives no indication of the frequency with which each occurs. The increasing intensity of the coalescence-redispersion cycle is evident, however, from the marked augmentation in the rate of mass transfer.

In Table 2, data are presented which show that mass transfer efficiency passes through a minimum as column loading is increased. The experiments were carried out using an impeller speed of 1000 rpm and an electrode voltage of 1.5 kV. The hydrodynamic data given were measured with mass transfer occurring. Consideration of these results indicates that the minimum in extraction efficiency is coincident with critical hydrodynamic behaviour. These observations can be explained in terms of the hydrodynamic regimes discussed above. For critical behaviour, droplet size and slip velocity are at a maximum and interfacial area (with respect to dispersed phase volume) and droplet residence times are correspondingly at a minimum. Furthermore, the small droplets created by the impeller are quickly coalesced to produce large droplets which do not redisperse until they pass into the next mixing stage. Overall conditions for mass transfer, in the present context, are poor. In the subcritical regime, the coalescence-redispersion process is the same as for critical operation. Smaller droplet sizes however allow for an increased specific interfacial area (referred to the dispersed phase) and longer residence times which in turn lead to an improved overall mass transfer performance in terms of number of transfer units. In the supercritical regime, not only are the droplets smaller than for critical operation, but also the rate of interface renewal is enhanced. This latter point results from the break-up of unstable droplets in the bulk of the column. Clearly, for optimum column performance, it is desirable to operate in this regime.

CONCLUSIONS

A novel liquid extraction column has been developed which employs high shear mixing in conjunction with electrostatic coalescence. The experimental results obtained show that the electric field can effectively counterbalance the dispersive effects of vigorous agitation. Constant hold-up can be maintained as impeller speed is raised by making suitable increases in the electric field strength. The resulting augmentation of both droplet coalescence and redispersion causes a marked improvement in mass transfer performance. Further hydrodynamic data have shown the existence of two distinct regimes of column behaviour, above and below a critical hold-up. The transition from one regime to the other is characterised by a maximum value of slip velocity and a minimum number of transfer units. The two regimes have been described in terms of their coalescence-redispersion mechanism and the region for optimum operation identified.

REFERENCES

1. Rietema, K., 1958, Chem. Eng. Sci., 8, 103.
2. Thornton, J.D., 1964, Industrial Chemist, January, p. 13.
3. Sherwood, T.K., Evans, J.E. & Longcor, J.V.A., 1939, Trans. A.I.Ch.E., 35, 597.
4. Higbie, R., 1935, Trans. A.I.Ch.E., 31, 365.
5. Dankwerts, P.V., 1951, Ind. Eng. Chem., 43, 1460.
6. Angelo, J.B., Lightfoot, E.N. & Howard, D.W., 1966, A.I.Ch.E.Jl., 12, 751.
7. Bailes, P.J. & Larkai, S.K.L., 1981, Trans. I. Chem. E., 59, (4), 229.
8. Bailes, P.J. & Stitt, E.H., 1985, U.K. Patent Appl., 85 06161.
9. Stitt, E.H., 1985, Ph.D. Thesis, University of Bradford, U.K.
10. Muller, E. & Hoehfeld, G., 1968, Proc. 7th World Pet. Congr. (Mexico, 1967), 4, 13.
11. Bailes, P.J. & Larkai, S.K.L., 1981, Euro. Pat. Appl., 81 305 155.
12. Bailes, P.J. & Dowling, P.D., 1985, Jl. Electrostatics, 17, (3), 321.
13. Bailes, P.J. & Larkai, S.K.L., 1982, Trans. I. Chem. E., 60, (2), 115.
14. Kolmogorov, A.N., 1949, Doklady Akad. Nank, (U.S.S.R.), 60, 825.
15. Vermeulen, T. et al, 1955, Chem. Eng. Prog., 51, 85F.

TABLE 1: Effect of Impeller Speed and Electrode Voltage Upon Column Mass Transfer Performance

Impeller Speed (rpm)	Applied Voltage (kV)	Fractional Dispersed Phase Hold-Up	Number of Transfer Units Per Metre (m^{-1})
1000	1.0	0.143	2.78
1200	1.5	0.151	3.73
1400	2.0	0.149	7.46

FIGURE 1: Drawing of the Experimental Extraction Column

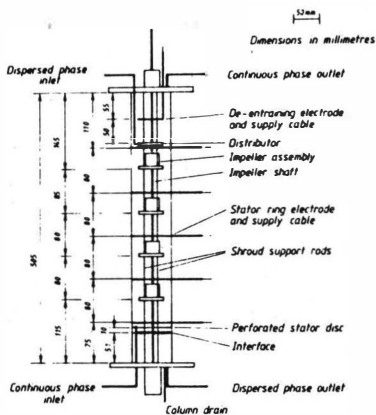


FIGURE 2: Exploded View of an Impeller Assembly

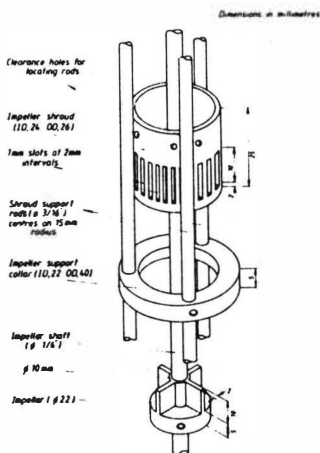


FIGURE 3: Effect of Impeller Speed and Electrode Voltage Upon Hold-Up

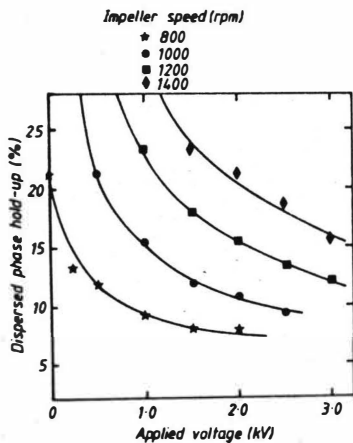


FIGURE 4: Lines of Constant Hold-Up as a Function of Impeller Speed and Electrode Voltage

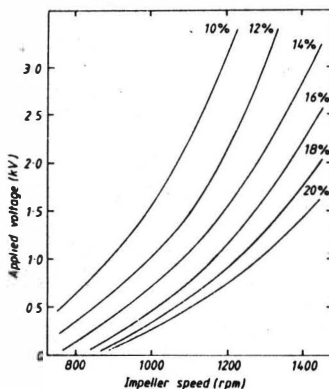


FIGURE 5: Correlation of Hold-Up at Constant Column Loading

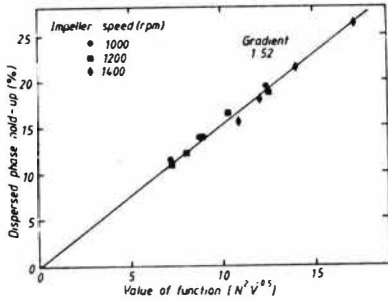


FIGURE 6: Flooding Curve for Experiments at Constant Phase Flow Ratio

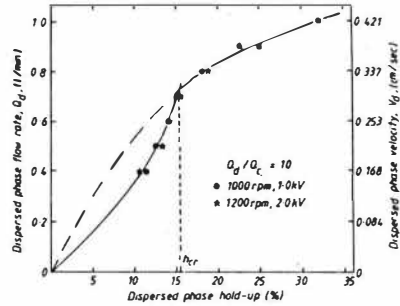


FIGURE 7: Relationship Between Slip Velocity and Hold-Up

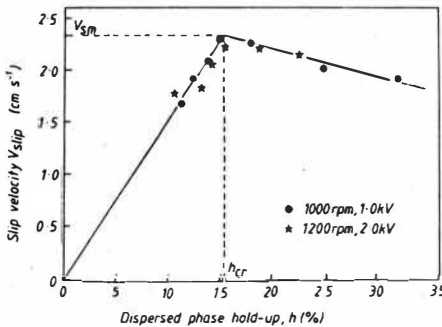


TABLE 2: Effect of Column Loading Upon Mass Transfer Performance

Column Loading		Hold-Up (Fractional)	Slip Velocity (mm.s ⁻¹)	Number of Transfer Units Per Metre (m ⁻¹)
(l.min ⁻¹)	(m ³ .m ⁻² .hr ⁻¹)			
0.5	7.6	0.070	24.5	3.11
0.75	11.4	0.101	25.7	2.44
1.0	15.2	0.135	25.9	2.70
1.25	18.9	0.198	22.6	3.13
1.5	22.7	0.262	21.0	5.13

The Components of the Coalescence Process in Dense Dispersions

T. Míšek, Res.Inst.of Chem.Equipment, Prague, Czechoslovakia

The Liquid Extraction represents a process which takes place in the two-phase liquid mixture. With slight exceptions, there is during the extraction one of both liquids dispersed into the other and must be afterwards coalesced in order it could be removed out of the system. The process of coalescence of liquid dispersion is therefore an inherent part of the extraction process. In comparison with mass transfer, its equilibria and kinetics, and also with studies on drop splitting, the results of coalescence research are very poor, even problematic. This fact refers to both parts of the problem, i.e. drop-to-drop coalescence, as well as drop coalescence at the interface.

This lecture is devoted to coalescence at the interface. The rate of this process is influencing dimensions of the settling parts of column extractors and especially dimensions of settlers in batteries of mixer-settler type. Thus becomes the coalescence, in the majority of cases, a process deciding about the prevailing part of volume, weight, installation area and price of extractors, as well as solvent inventory, and at the same time significantly influencing also their operation cost.

Studies on drop coalescence at the interface have been performed in several stages which are well characterized by the experimental technique used:

- a/ Study of residence time of individual drops at the flat and convex interface /1 - 5/
- b/ A considerable progress has been reached by works of Jeffreys and Davis /6/, who developed the concept of so called coalescence wedge /Fig.2/
- c/ A different procedure used in his pioneer work on dispersion coalescence Ryon /7/. Ryon's approach became, however, a relatively reliable basis for settler modelling, taking in account the drawback that the evaluated layer heights are comparatively small.
- d/ This matter of fact was subject to fundamental comment of Barnea and Mizrahi /8/ who in a comprehensive set of works presented from the engineering point of view the hitherto most significant contribution to theory and practice of industrial settler design.

Short review shows already some of the significant problems and misunderstandings in the coalescence research. I therefore would like to proceed to my own theme, i.e. the individual components of the coalescence process in dense dispersions.

1/ Type of dispersion

Apart from the trivial dispersion characterization by physical properties of phases and by stating which of the phases is continuous and which a dispersed one /sometimes also w/o, o/w/, the dispersions differ according to the hold-up and to the mutual velocity of the dispersed and continuous phases /9/. The relevant characteristics are clearly shown in the graph. Here the hold-up dependence is illustrated, i.e. the volume fraction of the dispersed liquid in the dispersion, on the magnitude, as well as on direction of the vertical drop and continuum flow.

With the increasing velocity of the dispersed phase the hold-up increases until it reaches the value at which all drops start to obstruct each other's motion. Different from the solid particles it does not mean that they really touch each other, but a thin film of the continuous phase remains between them. In that moment character

of the mutual flow of continuum and dispersion changes. The dispersed particles which were till this moment free, and their relative motion was on principle derived from the motion of individual drops in continuum, become at this point on principle immovable and their relative motion against continuum is derived from the pressure drop of the flow of continuum through the interparticle voids. We denominate such a dispersion a dense dispersion. The transition point between both the states /concentrated and dense dispersion/ is a direct analogy of the point of fluidization with solid particles /transition fluid bed - fixed bed/.

The significant difference between solid particles and drops is given by the fact that the hold-up of continuum between solid particles cannot get lower any more, whereas with liquid dense dispersions it is able to further decrease in dependence on dispersion properties almost to zero. If this occurs, then the drops originally of spherical shape gradually deform, flat facets arise on them, receiving finally almost a polyaedric shape. It is suitable to denominate the dense dispersion with drops of spherical shape and the continuum with the shape of inter-spherical channels - the channel dense dispersion. The second limiting case of polyaedric drops and flat layers of continuum between them can be denominated the lamellar dense dispersion. A transition type exists between both cases with both lamellas and channels. Which of the dispersion type will effectively occur, depends on the ratio of pressure P , pressing the drops together and of the internal pressure in the drops

$$P_{in} \sim \sigma_i / d \quad /1/$$

For

$$P \ll P_{in}$$

refers to channel dense dispersion and to drops of spherical shape

and for

$$P \gg P_{in}$$

refers to lamellar dense dispersion and to polyaedric drops

The transition between them is characterized particularly by the ratio P/P_{in} .

2/ Buoyancy pressure in the dispersion

For the buoyancy of the dispersion, the hold-up of which changes with the height of dispersion layer l , the relation

$$\frac{\partial P_b}{\partial l} = \Delta \rho g \chi \quad /2/$$

applies.

For a stagnant dispersion, where both the dispersed and continuous phases do not move, the pressure P would be determined by the buoyancy pressure P_b only. With flowing liquids it is necessary to take also in account the pressure drop, arising by this mutual movement.

3/ Pressure drop in the dispersion

For the pressure P only the vertical components of flow are relevant and the horizontal ones may be neglected. The vertical pressure drop may be estimated using the following reasoning for the lamella type of dense dispersion:

In the theory of laminar flow which takes place in such a dispersion in thin continuum layers, relation between pressure drop / lC / and volume throughput Q is derived

$$Q = - \frac{h^2 z}{12 \mu_c} \cdot \frac{\partial P_f}{\partial l} \quad /3/$$

where h is layer thickness, l its length and z its width. For modelling a flow through lamellar dispersion we assume:

Volume hold-up X is equal to area hold-up, i.e. hold-up in the horizontal cross-section through dense dispersion

$$X = \frac{n \pi d^2 z^2}{4 A} \quad /4/$$

Neglecting the wall effects, the total lamella length corresponding to the width of a lamella is

$$z = \frac{n \pi d z}{2 A} \quad /5/$$

The total area of the lamella is $(1 - X) \cdot A$. The thickness of the layer /area divided by length/ is then

$$h = \frac{1 - X}{X} \cdot \frac{d z}{2} \quad /6/$$

As with the lamellar flow deviations from this model occur, as e.g. local resistances etc., it is necessary to count with a deviated constant of proportionality, into which it is also possible to include the value \mathcal{K} , similarly as with derivation of Kérmán-Kozeny equation. The final relation is then

$$u_R = - \frac{\partial P_f}{\partial l} \cdot \frac{1}{c_f \mu_c} \left(\frac{1 - X}{X} \cdot d \right)^2 \quad /9/$$

4/ Hold-up of the dispersed liquid and its longitudinal profile

As already stated, with the increasing pressure P the shape of drops and the character of flow changes. The change of drop shape, however, brings about in the region of non-spherical drops a further significant change, i.e. change of the hold-up, as shown in Fig.7. The internal pressure is here already related not to the total drop diameter, but to the radius of curvature r of channel walls. A simple geometric consideration /Fig.8/ leads to the opinion that it is possible to correlate the continuous hold-up in dependence of pressure P in the following way:

$$1 - X = \left(c_x \frac{\sigma_i}{d P} \right)^2 \quad /10/$$

for

$$0 < \left(c_x \frac{\sigma_i}{d P} \right)^2 < 0,4 \quad /11/$$

and

$$1 - X = \text{const} = 1 - X_0 \quad /12/$$

for
$$\left(C_x \frac{\delta_i}{dP} \right)^2 > 1 - X_0 \quad /13/$$

This way we arrive at such a course of hold-ups in the layer, as it is depicted in Fig.7.

From the equation /10/ it is possible to obtain by differentiation a relation for increment of pressure with length ℓ

$$\frac{d}{\delta_i} \frac{\partial P}{\partial \ell} = - \frac{1}{2 C_x (1-X)^{1.5}} \cdot \frac{\partial X}{\partial \ell} \quad /14/$$

and by combination with formerly derived relations for buoyancy pressure and friction /2/ /11/ and by rearrangement, separation of variables and by integration we obtain equation

$$d \frac{\int_0^{\ell} X(1-X)^{1.5} \partial \ell}{X_0 - X} = a \frac{U_d}{d} \cdot \frac{\int_0^{\ell} \frac{X}{\sqrt{1-X}} \partial \ell}{X_0 - X} + b \quad /15/$$

which is possible to write as a simple linear relation,

$$y = ax + b$$

where

$$a = \frac{C_f \mu_c}{\Delta \rho g} \quad \text{and} \quad b = \frac{\delta_i}{2 C_x \Delta \rho g} \quad /15 \text{ a, b}/$$

are functions of physical properties of the system and of unknown constants C_f and C_x and

$$y = \frac{d \int_0^{\ell} X(1-X)^{1.5} \partial \ell}{X_0 - X}; \quad x = \frac{U_d \int_0^{\ell} \frac{X}{\sqrt{1-X}} \partial \ell}{d X_0 - X} \quad /15 \text{ c, d}/$$

x and y are functions of variables U_d, d, X and ℓ , which it is possible to find experimentally.

We have carried out measurements with one liquid system in the apparatus according to Fig.8, which with its simplicity is, from the hydrodynamical aspect, unambiguously defined and in the large range of variables we obtained a very good agreement of the experiment with the equation for values of constants

$$C_f = 31,58 \quad , \quad C_x = 0,0071 \quad /16/$$

with a standard deviation less than 20%.

In the monodispersion, where

$$C_x \frac{\sigma_i}{d^p} \gg \sqrt{0,4} \quad /17/$$

the drops are of spherical shape and the hold-up can be considered as constant. The solution is here more simple, the dependence

$$y = ax + b \quad /18/$$

having variables

$$y = d \sqrt{1-x} \cdot X \cdot \ell; \quad x = \frac{U_d}{d} \frac{X}{(1-x)^{1,5}} \ell$$

/18 a, b/

The relations /15/ and /18/ represent a convenient correlation of the hold-up profile in the dense dispersions; their application being complicated by the existence of two regions: of constant hold-up and of hold-up profile and their implicit form in X . However, the calculation of the hold-up profile by numeric integration of the relation

$$\frac{dX}{d\ell} = \frac{1}{b} \left(dX(1-x)^{1,5} - a \frac{U_d}{d} \frac{X}{\sqrt{1-x}} \right) \quad /19/$$

in conveniently chosen boundary conditions is possible.

Discussion on boundary conditions exceed, however, the scope of this lecture.

5/ Model of coalescence at the interface

The equipment according to Fig.7 has been used in several modifications also for the study of drop coalescence intensity at the interface. In accord with the work of Ryon /7/ and Barnea /8/, the layer height was subject to increase with the increased velocity of the dispersed phase U_d and the hold-up profile was subject to change. On the coalescence intensity the following conception has been worked out /11/:

The mean drop residence time at the interface is considered directly proportional to viscosity of continuous liquid and inversely proportional to pressure, acting on drops

$$\bar{t} = C_c \frac{\mu_c}{p} \quad /20/$$

The constant of proportionality C_c is characterizing the intensity of drop coalescence under given physical conditions. The hold-up of the dispersed phase at the interface, with area A , so-called area hold-up, is given by the relation

$$X_L = \frac{n \pi d^2 X^2}{4 A} \quad /21/$$

The flow through the interface of the area A is then

$$U_d = \frac{n \pi d^3}{6 A t} \quad /22/$$

By combining and including α in the constant, we obtain

$$U_d = \frac{d X_i P}{C_c \mu_c} \quad /23/$$

For calculation of P we use the relation /2/ and /9/ derived before

$$P = \int_0^L dP = \Delta \rho g \int_0^L X d\ell - C_f \frac{U_d \mu_c}{d^2} \int_0^L \frac{X}{(1-X)^2} d\ell \quad /24/$$

we define the mean values

$$\int_0^L X d\ell = \bar{X} \ell ; \quad \int_0^L \frac{X}{(1-X)^2} d\ell = \frac{\bar{X} \cdot L}{(1-\bar{X})^2}$$

/24 a,b/

and the whole model can be easily arranged into a simple linear relation between the layer height and the throughput:

$$\frac{U_d}{L} = a (1 - b U_d) \quad /25/$$

in which

$$a = \frac{d X_i \bar{X} \Delta \rho g}{C_c \mu_c} ; \quad b = \frac{C_f \mu_c \left(\frac{\bar{X}}{(1-\bar{X})^2} \right)}{\Delta \rho g d^2 \bar{X}} \quad /25 a,b/$$

Knowing the physical properties and the hold-up, the universal constant C_f and the characteristic coalescence constant C_c can be then calculated.

The Fig.9 shows the agreement of the linear model with the measurements. In all other cases the same good agreement has been achieved.

The coalescence model has been used for the study of quite a number of influences in several experimental series:

- A/ Influence of physical properties /12/ /13/: viscosity /0,9 + 3,9 mPa.s/, interfacial tension /12,7 + 30,3 mN/m/ and density difference /27 + 135 kg/m³/.
 The universal constant C_f has been found in the value of 24,2 ± 5%.
 The coalescence constant C_c in the range of 6930 + 24 94E.

The trends signify the dependence

$$C_c \sim \left(\frac{d^2 \rho_c g}{6_i} \right) \left(\frac{\rho_c}{\Delta \rho} \right)^{4.5}$$

/26/

but the results have high variance and are on a low level of statistical significance.

- B/ Influence of surface active agents /SAA/ in concentrations from C to double of the full surface occupation. The constant C_f found in the value of 33,25. The parameter C_c found at about 12 000, influence of SAA corresponds to the changes of the interfacial tensions according to Eq.26.
- C/ Influence of the mutual contact time of two-phase mixture is small /15/; little significant till about 5 hours, nevertheless during 50 hours the intensity of coalescence decreases by about a half.
- D/ Influence of the temperature exceeds the change which is induced by the change of physical properties. Therefore the temperature itself advances the coalescence.

The experimental research of coalescence, investigation of parameter C_c values etc. is not yet finished. Further measurements are being carried out.

The behaviour of the coalescing layer of polydispersion is further complicated by some further components of the coalescence process. I would like to comment shortly the following:

- 6/ Influence of the polydispersion
- 7/ Drop-to-drop coalescence
- 8/ Entrainment of droplets from the dense dispersion and their generation
- 9/ Mass and heat transfer
- 10/ The coalescence process modelling

The modelling of coalescence process in layers of dense dispersion from model to full scale is at present already very well possible and reliable. The above described models were already with success applied also for batch sedimentation tests from which it is possible to obtain all basic data for design of settlers on industrial scale.

The comments should not give the impression that all coalescence problems are solved. Unfortunately they are not. The own coalescence process is a secret till now, the revealing of which depends first of all on getting more precise and more comprehensive sets of experimental data.

Nomenclature / SI Units/

C_c	coalescence constant	1
C_f	friction constant	1
C_h	hold-up constant	1
d_s	/spherical/ drop diameter	m
g	acceleration due to gravity	m s ⁻²
h	film thickness of continuous liquid	m
z	length coordinate	m
L	height of dense dispersion layer	m
P	pressure acting on drops	Pa
Q	volume throughput	m ³ /s

\bar{t}	mean residence time of drop at the interface	s
u_r	relative velocity	m/s
U	superficial velocity of liquid	m/s
X	hold-up of dispersed liquid	
α	shape factor	l
λ	layer height where the hold-up profile commences	m
μ	viscosity	N.s.m ⁻²
ρ	density	kg/m ³
$\Delta\rho$	density difference	kg/m ³
σ_i	interfacial tension	N/m

I n d e x

c	continuous liquid
d	dispersed liquid
cr	critical value
	mean value
o	initial value / $l = 0$ /
L	finite value / $l = L$ /

L i t e r a t u r e

- 1/ Gillespie T., Fideal E.F., Trans.Farad.Soc. 52, 173 /1956/
- 2/ Cockbain E.G., McRoberts T.C., J.Coll.Sci. 8, 440 /1953/
- 3/ Charles G.F., Mason S.G., J.Coll.Sci., 15, 105, 236 /1960/
- 4/ Mackay G.D.M., Mason S.G., Can.J.Chem.Eng., 41, 203 /1963/
- 5/ Chen J.D., Hahn P.S., Slattery I.C., AIChE J. 30, 622 /1984/
- 6/ Jeffreys G.V., Davis G.A., in Recent Advances in Liquid-liquid Extraction /E.C.Henson/, Pergamon Press, Oxford 1971
- 7/ Ryon A.D., Daley F.L., Lowrie F.S., Chem.Eng.Progr. 55, 70 /1959/
- 8/ Barnea E., Mizrahi J., Trans.Inst.Chem.Engrs., 53, 61, 70, 75, 83 /1975/ and further ones
- 9/ Míšek T., Coll.Czech.Chem.Comm., 28, 1631 /1963/
- 10/ Coulson J.M., Richardson J.F., Chemical Engineering, vol.I., Pergamon Press, Oxford, 1963
- 11/ Rod V., Míšek T., Fes.Inst.Chem.Equipment, report No.536/64, 604/65, Prague 1965
- 12/ Kejř V., Thesis, Prague Inst.of Chemical Technology, 1968
- 13/ Němeček M., Thesis, ditto 1967
- 14/ Heřmanová E., Thesis, ditto 1979
- 15/ Kloud J., Thesis, ditto 1969
- 16/ Hartland S., Jeelani S.A.K., I.Chem.E., Symposium Series No.94, 211
- 17/ Míšek T., Coll.Czech.Chem.Comm., 32, 4018 /1967/

FIG. 6
FLOW IN DENSE
DISPERSION

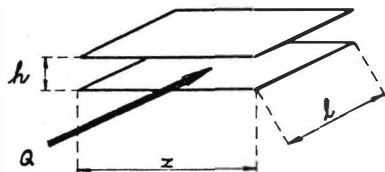


FIG. 8 PRESSURE & HOLD-UP
RELATION IN CHANEL DISPERSION

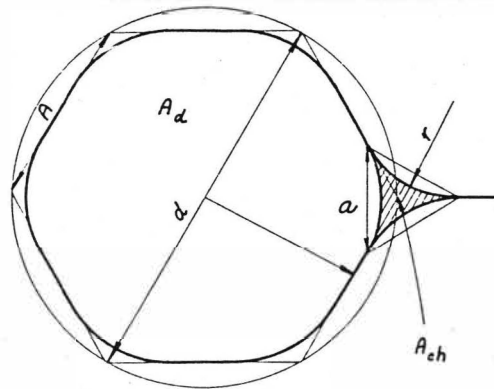


FIG. 7 EXPERIMENTAL APPARATUS - HOLD-UP & PRESSURE
PROFILES IN DENSE DISPERSION

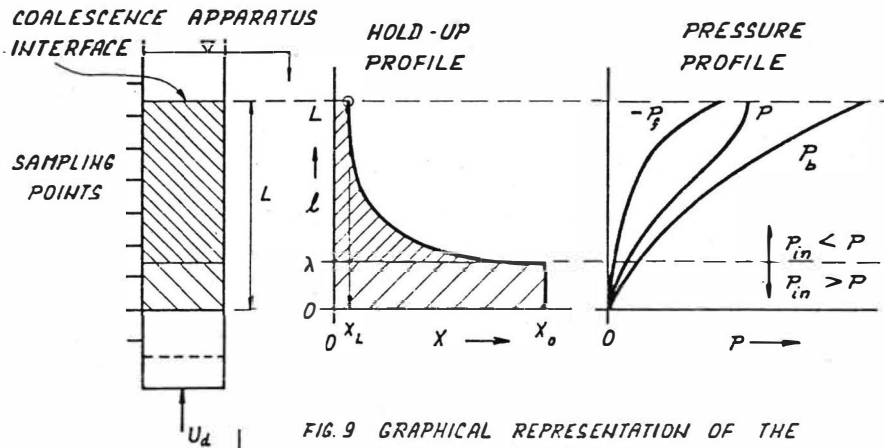
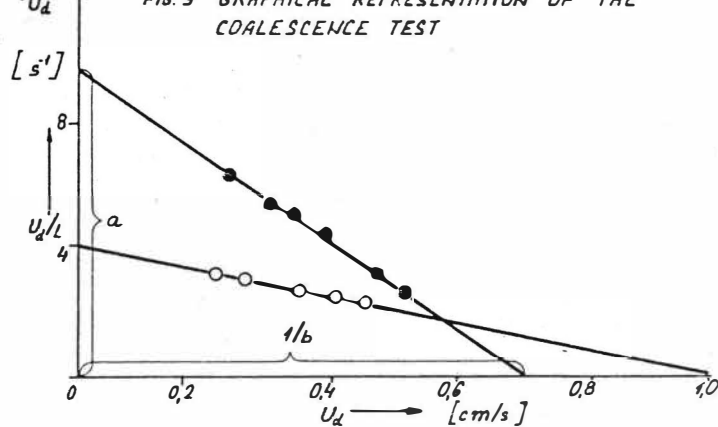


FIG. 9 GRAPHICAL REPRESENTATION OF THE
COALESCENCE TEST



Measurement of Coalescence in Agitated Dispersions by the Light Transmittance Technique

V. Hančil, V. Rod, J. Řezníčková, Institute of Chemical Process Fundamentals, Prague, Czechoslovakia

Knowledge of interparticle mixing in agitated dispersion caused by drop break-up and coalescence could considerably increase the reliability of the chemical engineering calculation of liquid-liquid contactors. Coalescence is globally characterized by the so called volume coalescence frequency, which is defined as the fraction of the volume of the dispersed phase that undergoes coalescence per unit of time. The coalescence frequency depends not only on the hydrodynamic conditions, hold-up and physico-chemical properties of the phases, but also very strongly on the surface properties of the liquid-liquid system. With regard to the complexity of the process and the poor knowledge of the properties of the interface, the coalescence frequency cannot be predicted from basic principles and physico-chemical data.

Several methods have been proposed for measuring the coalescence frequency (1)-(8). The method of direct observation (1), (2), which is experimentally very demanding and yields only isolated data, is not suitable for routine applications. The methods based on tracer technique (3)-(6) yield results affected by the presence of the tracer in the system measured. The approach proposed by Horvarth (7), based on the response of the mean drop size to a change in agitation intensity seems to be the most promising for further development. The aim of this work is to worked out a method based on this principle and develop an experimental technique which would allow to obtain reproducible data for comparative studies of coalescence as well as information on coalescence properties of industrially interesting liquid-liquid systems.

The method is based on the evaluation of the coalescence frequency from the measured rate of the approach of the mean drop diameter to the steady state value in a closed agitated liquid-liquid system. In the system, the change of the drop diameter da/dt depends both on the frequency of coalescence ω_c and on the frequency of break-up ω_b . If the drop break-up prevails ($\omega_b > \omega_c$), the mean drop size decreases ($da/dt < 0$) and vice versa. Since ω_b increases and ω_c decreases with the drop size, the two frequencies finally equalize, $\omega_c = \omega_b = \omega^*$, and the steady state with the equilibrium drop size a^* is reached. Fig. 1 illustrates typical transition curves $a(t)$ in the break-up and the coalescence region. Fig. 2 shows the dependence of the two frequencies on the relative drop size in the region near the steady state. A mathematical model of the dispersion dynamics is needed for the coalescence frequency to be evaluated from the transition curves. Horvarth (7) and Mlynek and Resnick (8) used a highly simplified model of coalescence only, and calculated ω_c from the slope of the transition curve in the coalescence region far from the steady state ($a/a^* \ll 1$) with the assumption of negligible ω_b . This approach permitted them to estimate the coalescence frequency ω_c only in the region far from the steady state and without any check of the adequacy of the assumption. If the more interesting equilibrium value ω^* is to be evaluated, the model must include coalescence as well as break-up and both the coalescence and the break-up transition curves have to be measured. The optical method, introduced by McLaughlin and Rushton (9), proved to be suitable for following the changes of the mean drop size in the dispersion. It is based on the relation between the light absorbance $\ln(I_0/I)$, holdup X , optical path L , and the Sauter mean drop diameter

$$a = 1.5 \times L / \ln(I_0/I) \quad (1)$$

valid if the light is strictly parallel and the diameter of the light beam much greater than a .

The design of the apparatus for coalescence measurement must respect the requirements which follow from the conditions of the derivation of the relation, Eq. (1), and from the sensitivity of coalescence to impurities and temperature fluctuations:

- uniform distribution of the dispersed phase in the volume of the vessel,
- adjustable propeller speed,
- light beam of sufficient cross-section and well defined optical path in the dispersion,
- a direction selective sensor for light intensity measurements,

- e/ construction material preventing any contamination of the system,
- f/ perfect temperature control.

The apparatus is shown in Fig. 3. The measuring cell is a flat all glass vessel (100 mm I.D., 20 mm height), with the bottom and the cover optically polished. The cell is equipped with an inclined blades propeller (35 mm I.D.) which induces strong axial mixing. A glass tube (20 x 3 mm) 25 mm long placed upon the cover over the central opening permits complete filling of the vessel with liquids. Optically polished contact surfaces between the cover and the body of the cell as well as between the cover and the central glass tube provide perfect tightness without any sealing. An inertial wheel, fixed to the propeller and connected with the motor by a flexible shaft, ensures smooth rotational motion of the propeller. A narrow beam of parallel light produced by a He-Ne laser is split into two in a beam divider. After being expanded to 6 mm diameter, the straight beam enters the glass cell as a measuring beam. The intensity of the light that has passed through the cell is measured by a direction selective sensor aligned into the beam axis and provided by a photocell. An optical bench on which all parts of the optical system are mounted facilitates the alignment. Another photocell of the same type, selected so as to have the same characteristics, is used for measuring the light intensity of the reference beam. The signals from the two photocells are introduced into a log-ratio amplifier provided with zero adjustment. The resulting signal from the amplifier, which after the proper adjustment represents the required light absorbance $\ln(I_0/I)$, is filtered by a Butterworth low-pass filter (0.2 Hz) and recorded in the analog as well as in the digital form.

An experimental procedure was developed aimed at obtaining comparable and reproducible data. From the dependence of the mean equilibrium drop size on the propeller speed in the system studied, determined in preliminary experiments, three values n^* , n_b and n_c were selected for the kinetic experiments, corresponding to the equilibrium and the starting values of the drop size diameter a^* , a_b , and a_c resp. on the transition curves, Fig. 1. The cell was completely filled with the known amounts of the presaturated phases and the liquid mixture was agitated for more than two hours. The agitation was then stopped for the phases to separate spontaneously. The light absorbance proved to be negligible under the condition of a clean interface and hence the output signal from the filter was set to zero by the adjustment of the log-ratio amplifier. The mixture was then agitated with propeller speed n_b until the steady state drop size (a_b) was reached. Afterwards the propeller speed was switched down to n^* and the transition of the dispersion to the equilibrium was followed by recording the values of $\ln(I_0/I)$. Then the propeller speed was changed to n_c for the system to reach a new steady state with drop size (a_c) as the initial condition of the other transition to be measured. In a similar way, the rotor speed was switched back to n and the values of $\ln(I_0/I)$ were recorded during the approach of the dispersion to the equilibrium. The procedure was tested on a number of systems. All dynamic experiments were carried out under the following conditions: $X = 0.1$, $a^* \approx 0.5$ mm, $a_b = 3/2 a^*$, $a_c = 2/3 a^*$. The transition curves for three studied systems with greatly different coalescence rates are shown in Fig. 4.

The model describing the dispersion dynamics is based on the population balance, which for binary breakage in a closed system may be written as:

$$\frac{\partial}{\partial t} [N \cdot f_N(v, t)] = B_b(v, t) - D_b(v, t) + B_c(v, t) - D_c(v, t) \quad (2)$$

where

$$B_b(v, t) = 2N(t) \cdot \int_0^{\infty} \beta(v, v') \cdot f_N(v', t) \cdot g(v') \cdot dv' \quad (3)$$

$$D_b(v, t) = N(t) \cdot g(v) \cdot f_N(v, t) \quad (4)$$

$$B_c(v, t) = N^2(t) \int_0^{v/2} h\lambda(v-v', v') \cdot f_N(v-v', t) \cdot f_N(v', t) \cdot dv' \quad (5)$$

$$D_C(v, t) = N^2(t) \cdot f_N(v, t) \int_0^{\infty} h\lambda(v, v') \cdot f_N(v', t) \cdot dv' \quad (6)$$

and

$f_N(v, t)$ is number density of drops.

The functions g , β , $h\lambda$ characterize break-up intensity, daughter drop size distribution and coalescence intensity resp. Integration of Eq. (2) over v yields the overall differential balance of the total number of drops, N . By combining the balance with the relation between the hold-up, total number of drops, and the mean volume of the drop

$$X = N(t) \cdot \bar{v}(t) \quad (7)$$

where

$$\bar{v}(t) = \int_0^{\infty} v \cdot f_N(v, t) dt \quad (8)$$

equation (9) describing the change of the mean drop volume with time is obtained:

$$\frac{d\bar{v}(t)}{dt} = \frac{\bar{v}(t)}{X} \left\{ \frac{1}{2} \int_0^{\infty} D_C(v, t) dv - \int_0^{\infty} D_B(v, t) \cdot dv \right\} \quad (9)$$

It forms the basis for the description of the measured transition curves.

The volume coalescence frequency ω^* , to be evaluated from the transition curves, is defined by the relation:

$$\omega^* = \frac{X}{\bar{v}} \int_0^{\infty} v \cdot f^*(v) \left[\int_0^{\infty} h\lambda(v, v') f_N^*(v') dv' \right] \cdot dv \quad (10)$$

It is evident that the functional forms of g , β and $h\lambda$ must be known for its evaluation. Extensive experiments (10) combined with dynamic simulations (11) enabled us to formulate the functions in the previous study (10)

$$g(v) = \begin{cases} 0 & ; v \leq v_{cr} \\ C_S(v - v_{cr}) & ; v > v_{cr} \end{cases} \quad (11)$$

$$\beta(v, v') = 1/v' ; v < v' \quad (12)$$

$$h\lambda(v, v') = C_C \cdot \left[1 - \exp\left(-\frac{v+v'}{v_{cr}}\right) \right] \quad (13)$$

which together with Eqs (2) to (8) provide plausible description of the transition curves. The above model contains three parameters C_C , C_S , v_{cr} (dependent on the propeller speed), which for a given hold-up X determine also the equilibrium drop size distribution $f^*(v)$. The experiments indicated that the equilibrium distributions corresponding to different propeller speeds are similar in shape, if the hold-up is the same. This is respected by the model if the dimensionless group $C_C/C_S v_{cr}^2$ is independent on the propeller speed.

- There are two possible ways how to estimate ω^* from the measured transition curves:
- 1/ The estimation of the parameters C_C , C_S and v_{cr} by fitting the two transition curves by the model and the subsequent calculation of ω^* from Eq. (10).
 - 2/ The determination of ω^* from a graphical representation of the dependence of ω^* on the selected characteristics of the transition curves constructed on the basis of the numerical solution of the model. The first method, in which correct statistical assumptions can be applied, is computationally extremely demanding. In gene-

ral, it requires multiple solution of the integro-differential equation, Eq. (2), in an iterative optimization cycle. Even if the approximative solution is applied (10) which reduces the problem to the numerical solution of an ordinary differential equation, this approach appears too complicated for routine work. The second method requires standardization of the drop sizes, a_b , a_c at the starts of the transitions. It can be based on the dependence of ω^* either on the slopes of the transition curves at properly defined points a_b , a_c or on the half-times of the transitions. From the analysis of the structure of the mathematical model it follows that, under these conditions, the steady state coalescence frequency ω^* is a unique function of the two slopes (or half times), which can be represented by the relations of the form:

$$\frac{\omega^*}{(da/dt)_{a=a_b}} = F_1 \left(\frac{(da/dt)_{a=a_c}}{(da/dt)_{a=a_b}} \right) \quad (14)$$

or

$$\omega^* \cdot \tau_b = F_2(\tau_b/\tau_c) \quad (15)$$

Curve 1 on Fig. 5 is the graphical representation of Eq. (14) numerically evaluated for $a_b = 3/2 a$, $a_c = 5/4 a$, $a_c' = 4/5 a$, $a_c = 2/3 a$. Curve 2 relates critical diameter a_{CR} to the ratio of the two slopes.

Six aqueous systems differing in interfacial tensions and viscosities were chosen together with one non-aqueous system to show the possibilities of the method presented. A series of experiments with one aqueous system was designed to demonstrate the effect of additives (electrolytes) on coalescence. The physical properties of the systems are summarized in Tab. I. In order to obtain comparable data, the propeller speeds in individual experiments were chosen so that the steady mean drop size a might be approximately the same in all experiments, namely 0.5 mm, which is close to that common in industrial extraction equipment. Generally, the coalescence frequency should be measured at high hold-up to ensure prevailing effect of the coalescence process on the dynamic behaviour of the dispersion. The upper limit is imposed to hold-up by the sensitivity of the light sensors used, as the light intensity decreases exponentially with hold-up X . The value $X = 0.1$ was chosen, which meets these requirements.

The coalescence frequencies were evaluated by the slope method (Figs. 1 and 5). The values of the coalescence frequencies measured under the conditions of constant a are given in Tab. I. The values cover the region of three decimal orders, which is shown in the last column of the table, where frequencies ω^* are related to the frequency of the slowly coalescing system 7, decaline - water. The values ω^* do not show any observable dependence on the physical properties of the phases. It is surprising that the system toluene-ethyleneglycol (system 6) with the highest continuous phase viscosity exhibits the highest coalescence frequency. The presence of electrolytes, even in minute concentrations (systems 7 - 9), significantly increases the coalescence frequency. The dependence of the frequency on the electrolyte concentration exhibits a maximum. Similar dependences were found also for other electrolyte containing systems not shown in Tab. I.

The correct evaluation of ω^* from the transition curves requires an adequate model of the dispersion dynamics. The adequacy of the suggested model is evidenced by the perfect fit of this model to the data $a(t)$ in Fig. 4, which indicates that the error in the evaluation of ω^* due to the inaccuracy of the model is small. The suggested method of the coalescence measurement necessitates perfect wettability of the cell by the continuous phase to prevent any sticking of drops at the surface of the cell. The continuous phase should be transparent to avoid any interference with the optical measurement. The method is comparatively simple. It allows the measurement of coalescence frequency in systems with low as well as with high interfacial tension with very good reproducibility.

Tab. I Volume frequency of coalescence

no.	phase dispersed	phase continuous	ρ_d kg/m ³	ρ_c kg/m ³	μ_d mPa.s	μ_c mPa.s	σ mN/m	n s ⁻¹	a μm	ω^* 10 ⁻⁵ s ⁻¹	ω^*/ω_7
1	benzylalcohol	water	1028	998	5.12	1.20	34.7	3.0	482	150	23
2	cyclohexanol	water	956	998	21.4	1.13	3.1	2.5	527	116	18
3	Me-CO-(n-Bu)	water	815	997	0.65	0.96	9.2	3.2	494	22	3
4	nitrobenzene	water	1194	998	1.89	0.92	24.3	5.5	495	213	32
5	toluene	water	862	997	0.56	0.94	24.8	7.7	468	116	18
6	toluene	ethylene-glycol	852	1096	0.62	16.9	9.1	7.7	503	7808	1200
7	decaline	water	883	998	2.43	0.92	25.8	8.5	423	6	1
8	decaline	0.001 M NaCl	883	1003	2.43	0.92	28.7	8.5	488	31	5
9	decaline	0.005 M NaCl	883	1009	2.43	0.92	29.9	8.5	469	48	7
10	decaline	0.01 M NaCl	883	1009	2.43	0.93	31.0	8.5	492	82	12
11	decaline	0.05 M NaCl	883	1010	2.43	0.96	30.5	8.5	505	168	26
12	decaline	0.01 M NaCl	883	1010	2.43	1.00	29.1	8.5	547	155	24
13	decaline	0.05 M NaCl	883	1011	2.43	1.01	30.7	8.5	498	54	8
14	decaline	1.00 M NaCl	883	1013	2.43	1.02	31.5	8.5	552	51	8
15	decaline	0.005 M KNO ₃	883	999	2.43	0.93	26.4	8.5	597	628	95

In all experiments L = 20 mm, X = 0.1, 20°C

Symbols

- a Sauter mean diameter of drops, m
 a' Sauter mean diameter at which the slopes of $a(t)$ is evaluated, m
 a_{cr} critical diameter of drops $a_{cr} = (6v_{cr}/\pi)^{1/3}$, m
 B_{cr} birth function, m³.s⁻¹
 C_b coefficient of break-up, m⁻³.s⁻¹
 C_c coefficient of coalescence, m³.s⁻¹
 D_c death function, m⁻⁶.s⁻¹
 I light intensity, W.m⁻²
 L optical path, m
 n propeller speed, s⁻¹
 n* propeller speed corresponding to the steady a*, s⁻¹
 N number of drops in unit volume, m⁻³
 t time, s
 v, v' volume of a drop, m³
 v_{cr} critical volume of drops $v_{cr} = \pi a_{cr}^3/6$, drops with a smaller volume than this one do not break under given propeller speed, m³
 X hold-up
 μ_c, μ_d viscosity of continuous and dispersed phase, resp., Pa.s
 ρ_c, ρ_d density of continuous and dispersed phase, resp., kg m⁻³
 σ interfacial tension, N.m⁻¹
 τ half-time, s
 ω coalescence frequency, s⁻¹

Subscripts

- o reference value
 b refers to break-up

c refers to coalescence

Superscripts

- * steady state, hydrodynamic equilibrium
- mean value

References

- 1 Park J.Y., Blair L.M., Chem. Eng. Sci., 30, 1057 (1975).
- 2 Kuboi R., Komasaawa I., Otake T., J. Chem. Eng. Japan 5, 423 (1972).
- 3 Madden A.J., Danerell G.L., AICHE J. 8, 233 (1962).
- 4 van Heuven J.W., Moevenaer J.C., Proceedings Fourth European Symposium on Chemical Reactor Engineering pp. 217, Pergamon Press, N.Y. 1971.
- 5 Komasaawa I., Morioka S., Kuboi R., Otake T., J. Chem. Eng. Japan 4, 319 (1971).
- 6 Miller R.S., Ralph J.L., Curl R.L., Towel O.D., AICHE J. 9, 196 (1963).
- 7 Horwarth W.J., AICHE J. 13, 1007 (1967).
- 8 Mlynek Y., Resnick R., AICHE J. 18, 122 (1972).
- 9 Mc Laughlin C.M., Rushton J.H., AICHE J. 19, 817 (1973).
- 10 Rod V., Hančič V., prepared for publication.
- 11 Rod V., Mišek T., Trans. Inst. Chem. Eng. 60, 49 (1982).

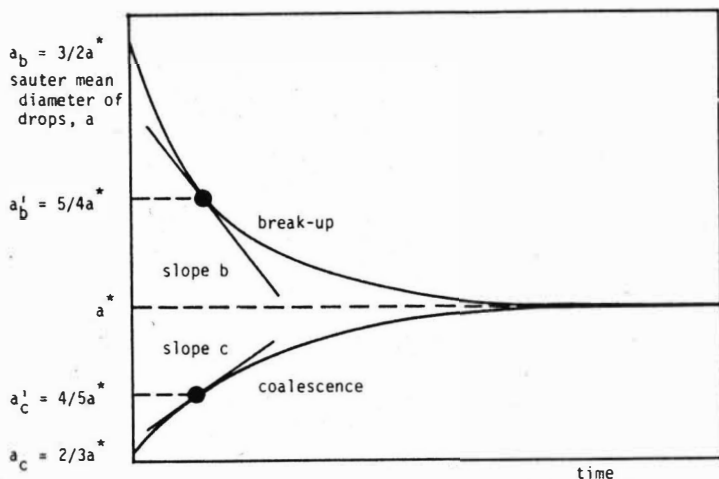


Fig. 1 Transition curves $a(t)$ calculated from light transmittance measurement

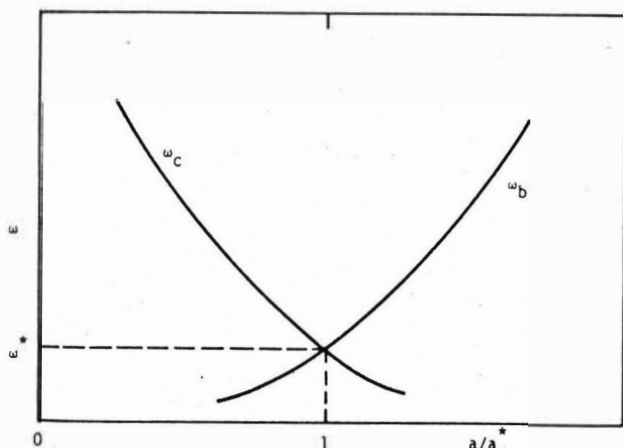


Fig. 2 Schematic dependence of coalescence and break-up frequencies on relative diameter of mean drop

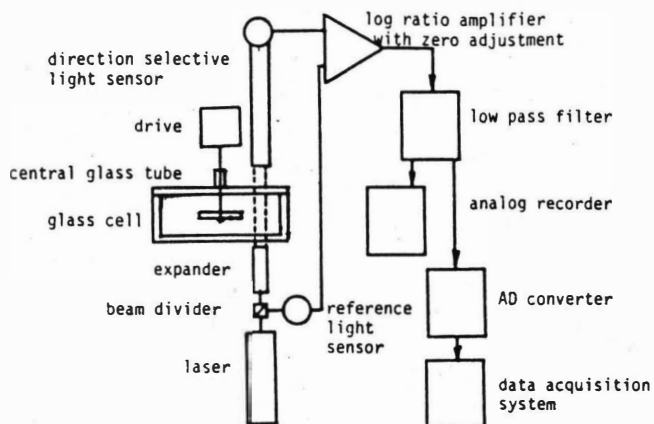


Fig. 3 Apparatus for measurement of transition curves $a(t)$

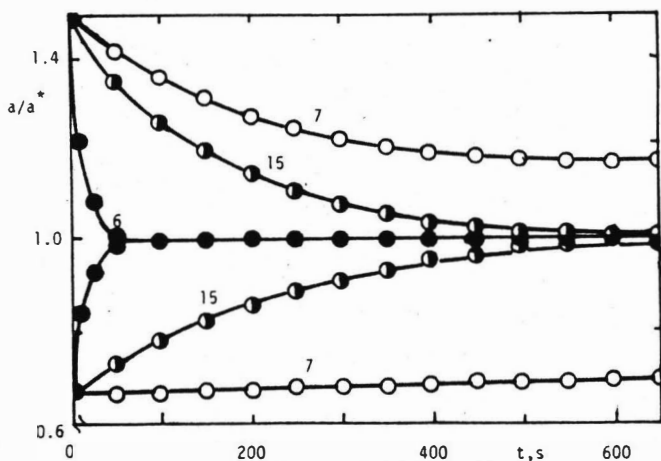


Fig. 4 Dynamic behaviour of dispersions; points are experimental, curves are fitted by the model number denotes systems in Tab. I

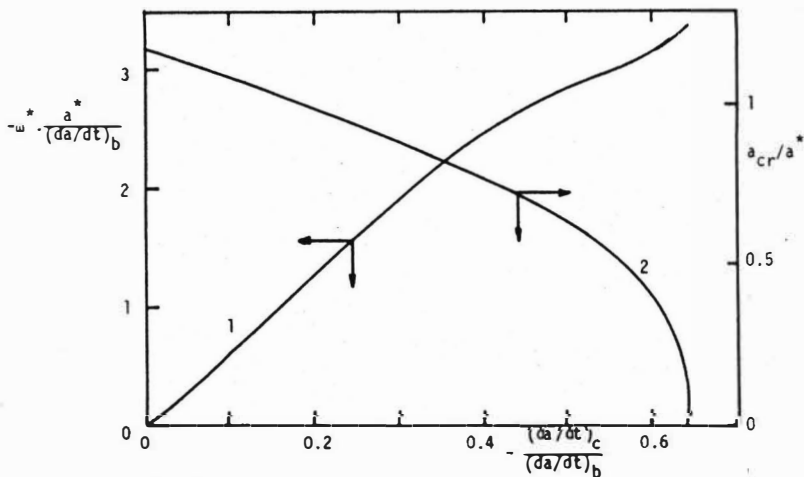


Fig. 5 Determination of coalescence frequency and critical drop size; $a_b = 3/2 a^*$, $a_c = 2/3 a^*$, $(da/dt)_b = (da/dt)_a = 5/4 a^*$, $(da/dt)_c = (da/dt)_a = 4/5 a^*$

An Optical Fiber Probe for the Simultaneous Measurement of Particle Size and Velocity in Two-Phase Flows

J.L. Plawsky T.A. Hatton Massachusetts Institute of Technology, Cambridge, MA, USA

INTRODUCTION

The importance of liquid extraction as a separations operation is reflected in the increasing number of applications to be found in the petrochemical, hydrometallurgical, food and pharmaceutical industries. The intimate contact required between two liquid streams to ensure adequate rates of interphase mass transfer is usually promoted by dispersing one phase as drops in a second, continuous phase. Numerous contacting devices have been developed expressly for this purpose. Some of the more common contactor configurations are mechanically agitated columns of the rotating disk, Kuhnle, Oldshue-Rushton and York-Scheibel types. These extraction columns represent a major capital investment, and their operating costs are not inconsequential. It is therefore desirable to optimize their performance and to develop reliable and accurate design procedures for the sizing of such contactors.

The key to designing extraction columns is a knowledge of the behavior of the dispersed phase, particularly the drop size and velocity distributions which exist in these contactors. These distributions govern the efficiency and success of the mass transfer operation. Most of the recent efforts aimed at measuring these distributions are based on Laser Doppler Velocimetry (LDV) techniques, which use the frequency information contained in light scattered by particles passing through an interference pattern to determine the velocities of the particles and of the continuous fluid. The intensity of the scattered light is related to the particle size, and this effect has been exploited to measure the size and velocity of particles simultaneously.

Most of the early sizing techniques were designed to measure aerosol particles in a size range between 10 and 100 μ m diameter. More recent work has focused on measuring the size of larger particles, especially transparent ones, on the order of a millimeter or more in diameter. These latter techniques are of interest to the Chemical engineer dealing with agitated contacting equipment where particles in this size range predominate. The techniques can be conveniently divided into four classes:

1. Correlation of the drop size with the signal visibility or fringe contrast [1,2,3].
2. Correlation of the drop size with the time difference between signals received from two or more spatially separated detectors [4,5,6].
3. Correlation of the drop size with the overall signal intensity [3,7].
4. Correlation of the drop size using a time of flight approach [8,9,10].

All these techniques suffer from some drawbacks when one attempts to apply them to the measurement of size/velocity distributions in contacting equipment. The most severe restriction is that the contactor must be made from glass or at least have sizable glass portions so that the light can be transmitted and received. In addition, most of these methods are restricted to operation using very low holdups. At higher holdups, the presence of many droplets interferes with the transmission of the light into the contactor and makes measurement extremely difficult. Therefore it is difficult if not impossible to obtain size and velocity measurements at points located far from the contactor wall. To eliminate most of these restrictions, we have developed an optical fiber probe which can be inserted into a column. The probe integrates the necessary transmitting and receiving optics into one package so that measurements can be made without having to realign the system. It is small enough to cause minimal flow disturbance, and can be located far from the laboratory where the data acquisition and the optical equipment would be.

The next few sections will describe the probe and the overall experimental apparatus in detail, and present some data attesting to the accuracy and versatility of the probe system.

APPARATUS DESCRIPTION

Optical Fiber Probe

The probe is an optical fiber device designed to apply LDV techniques for the simultaneous measurement of particle size and velocity. LDV systems were originally designed to measure the velocity of turbulent fluid by measuring the velocity of small seed particles mixed into the fluid. The most widely used systems generate an interference fringe pattern at a point in the fluid by crossing two frequency shifted laser beams at that point. A particle passing through the beam crossing point will scatter light from the two beams. A portion of this light can be collected and the frequency of the recovered signal analyzed to determine the particle and hence the local fluid velocity. The optical fiber probe described here uses a single beam technique developed by Ballik and Chan [11] and Semiat and Dukler [10] to generate a fringe spacing. Large variations in fringe spacing can be obtained quite easily in this system and unlike conventional LDV systems, the fringe spacing can be changed without changing the size of the measurement volume. For large particle sizing applications this system is more versatile and convenient than conventional LDV systems.

The present probe prototype is shown in diagram form in Fig. 1. A detailed schematic of the head assembly of the probe is given in Fig. 2. The probe assembly can be divided into three subunits: the flexible imagescope, the coupling optics, and the head assembly where the signals are generated and detected. The imagescope is a flexible, coherent array of optical fibers having the property that any image incident on one face of the imagescope, is carried along the fibers and appears at the

opposite face undistorted. In the probe system, an image of the grating is projected onto one face of the imagescope and then transferred into the fluid. The primary functions of the imagescope are to carry the image through space unperturbed by atmospheric effects and to isolate the fringe generation equipment from the probe itself. The probe may undergo jarring and vibrations as a result of its attachment to a column.

The imagescope transfers the grating image to the probe body. Here, a relay lens transfers the image onto the face of an image conduit, which is a rigid analog of the imagescope and serves to carry the grating image past the walls of the column and into the fluid. A small gradient index lens is used to project the image from the face of the image conduit into the fluid.

The head assembly of the probe is composed of three components shown in Fig. 2. The first is the lens-image conduit section for image projection. Directly opposite this transmitting section is the first optical fiber detector. This assembly consists of a linear array of optical fibers similar to the system used by Semiat and Dukler [10]. It is used to obtain a transit time signal of a particle passing through the measurement volume. At an angle of 135 degrees with respect to the transmitting section is the second detector, used to obtain a velocity signal from a particle. It is constructed similarly to the image conduit; however, the fibers are arranged to collect light only. They cannot nor do they need to carry an image. The velocity detector uses a bundle of optical fibers coupled to another gradient index lens. Directly behind the lens, and in front of the fiber bundle is a pinhole aperture. The projection of this aperture onto the measurement volume effectively defines the extent of the measurement volume.

Detailed dimensions of the probe system are found in Fig. 2. The probe was designed to be as small as possible to afford minimal flow disturbance. The components are sheathed in rigid stainless steel tubes to withstand harsh environments.

The overall experimental system is shown in Fig. 3. A laser is used to illuminate a Ronchi grating providing a fringe system. The laser provides an extremely intense beam of monochromatic radiation which allows measurements to be taken in room light. An image of the Ronchi grating is projected onto the surface of the imagescope using a distortionless lens system. The transit time and velocity signals are transported via optical fibers to two photodetectors. The resulting electronic signals are captured using a digital waveform recorder. These recorded waveforms can then be sent to a computer and stored for later analysis. The important feature of the apparatus is portability and flexibility of the probe. It can be located many meters from the actual fringe generation and data acquisition equipment and can be manipulated like any other transducer.

DATA ANALYSIS

The probe system can obtain particle size and velocity information using either the transit time technique or the visibility technique. This section will discuss how size and velocity information is extracted using either of the above techniques from signals received from the probe.

Visibility Technique

The visibility technique extracts drop size and velocity from an analysis of the signal from the probe's velocity detector. An actual velocity signal is shown in Fig. 4. This signal is recovered and stored in digitized form. The analysis begins by performing a discrete Fourier transform of the signal, from which the fundamental Doppler frequency of the signal can be recovered and related to the particle velocity as follows:

$$V = F/\sigma \quad (\text{Eqn. 1})$$

Here, F is the fundamental frequency, V is the particle velocity, and σ is the fringe spacing encountered by the particle.

The Doppler or velocity signal consists of two superimposed components: a high frequency or AC component which rides on top of a low frequency or pedestal component. Digital filtering of the FFT waveform and subsequent reinversion enables separation of the two components. The visibility or fringe contrast can then be defined by the following equation:

$$V = \frac{\int AC(t)dt}{\int \text{Pedestal}(t)dt} \quad (\text{Eqn. 2})$$

The visibility is directly related to the size of the particle and so a correlation can be developed to obtain the drop size independently of the drop velocity.

Transit Time Technique

The transit time technique uses both the fundamental Doppler frequency and the time of flight of a particle to obtain size and velocity information. In the probe system, the time of flight is measured by recording the particle's passage past the size detector. The size of the particle can be related to this passage time as follows:

$$R = \frac{V\tau - s}{2} \quad (\text{Eqn. 3})$$

Here, V is the velocity, τ is the time of flight, and s is the height of the linear array of optical fibers making up the size detector.

An actual signal from the size detector is shown in Fig. 5. The passage time is defined as the time between the two circled points, which represent 90% of the base-

line value. The central maximum arises as a result of the particle focusing the light passing through it onto the size detector. It is a phenomenon related to the size of the particle and the refractive index difference between the particle and the surrounding fluid.

In the probe system, a lens is used to project the grating image into the fluid. Therefore, the fringe spacing is not constant along the optic axis, but varies linearly along it, obeying the following equation:

$$\sigma = \frac{B \sigma_0}{B - R \cos \theta} \quad (\text{Eqn. 4})$$

Here, B represents the distance from the center of the measurement volume to the lens surface, σ_0 is the fringe spacing in the center of the measurement volume, R is the particle radius, and θ is the angle the velocity detector makes with respect to the optic axis. Since the fringe spacing varies, the drop size and velocity are interdependent. One must have frequency, and transit time or visibility information to obtain the drop velocity. In the visibility technique, size measurement is independent of velocity so that the velocity can be determined easily once size and visibility have been correlated. In the transit time technique, neither size nor velocity are independent measurements. As long as one has frequency and transit time data, one can calculate velocity and size from the following equations:

$$V = \frac{F(B + s \frac{\cos \theta}{2})}{B \sigma_0 + F \tau \frac{\cos \theta}{2}} \quad (\text{Eqn. 5a})$$

$$R = \frac{B(F \tau - s \sigma_0)}{2(B \sigma_0 - F \tau \frac{\cos \theta}{2})} \quad (\text{Eqn. 5b})$$

These equations were used to calculate all the size and velocity results presented in the next section.

RESULTS

The results presented in this section were derived from a series of demonstration experiments designed to determine the feasibility of the probe system as well as its accuracy. In the first set of experiments, glass beads of known size and velocity were passed through the measurement volume of the probe. At first the bead was passed through the center of the measurement volume and then through various points away from the center, yet still within the field of view of the velocity detector.

Tables 1 and 2 show results of passing the glass beads through the center of the measurement volume. The "actual" quantities are the known values of particle size and velocity, whereas the "measured" quantities are the size and velocity values calculated from probe data. These results are averages of not more than five repeated passages of each bead. The agreement between actual and measured quan-

tities is very good and shows the probe to be an accurate device for measuring particle size and velocity. Moreover, the limited number of bead passages used to form the averages shows the probe to be an accurate measurement tool for single events.

Tables 3 and 4 show the results of passing a bead through the measurement volume at points away from the center, about the optic axis and about the axis perpendicular to the optic axis, respectively. The errors are small, even for beads passing through at points relatively far from the center of the measurement volume. These errors will be reduced further by optimization of the probe's optical system. Errors in the transit time measurements for points corresponding to the results of Tables 3 and 4 were much less than the errors presented in those tables. Optimization of the optical system should also reduce these errors.

Fig. 6 shows the beginning of a correlation relating the signal visibility to the particle size for the glass beads used in Table 1. It is clear that over this size range, the visibility is a single valued function of particle size, and that the probe can be used to obtain particle sizes in the visibility mode. This correlation will be extended in the future once a higher power laser is obtained.

Figs. 7 through 9 show results of an experiment where the probe system was used to measure the size and velocity of air bubbles rising through water. The air bubbles were generated using a glass frit of porosity between 70 and 100 μm . Approximately 150 bubbles were analyzed to generate the following curves. Figure 7 shows a velocity histogram for this experiment. Figure 8 shows the corresponding size histogram. The results look quite reasonable and the average velocity and size values should be accurate even though more measurements are needed to generate a truly statistically significant sample. Figure 9 shows a plot of the velocity-size correlation for this experiment. The general trend of increasing velocity with increasing size is evident. The scatter is a result of the limited number of bubbles analyzed and also an indication that the bubbles had not reached their terminal velocity before being measured. This result was expected due to the proximity of the measurement volume to the frit and jetting of the bubbles from the frit.

CONCLUSIONS AND FUTURE WORK

The results show that the probe is an accurate device for measuring particle size and velocity, and offers a means for measuring these quantities in process equipment far removed from the data acquisition equipment. Since the transmitting and receiving optics are integrated into a single, small package, size and velocity distributions can be obtained at various points in process equipment merely by changing the probe position. No optical realignment is necessary.

Future work on the probe system will involve optimization of the optical system to reduce measurement errors and to extend the range of applicability of the probe. A probe is now being developed to measure particle size using the phase lag approach,

which promises to be more accurate than the transit time or visibility technique and which should greatly extend the size range limits for the probe. Experiments are now underway to determine the holdup limits under which the probe can operate successfully. The system should extend the holdup range over that obtainable with conventional LDV techniques and will definitely be able to reach points in process equipment heretofore inaccessible using conventional LDV equipment regardless of the holdup used.

REFERENCES

- [1] Bachalo, W.D., C.F. Hess. and C.A. Hartwell. 1980. Trans. ASME 102:798.
- [2] Gouesbet, G. and M. Ledoux. 1984. Optical Engineering 23:631.
- [3] Yeoman, M.L., B.J. Azzopardi, H.J. White, C.J. Bates and P.J. Roberts. 1982. AERE Report #10468.
- [4] Durst, F. and M. Zare. 1975. Proc. LDA Symp. (Copenhagen) p.403.
- [5] Bachalo, W.D. and M.J. Houser. 1984. Optical Engineering 23:583.
- [6] Bachalo, W.D. and M.J. Houser. 1985. Reprint ICLASS '85.
- [7] Durst, F. and H. Umhauer. 1975. Proc. LDA Symp. (Copenhagen) p.430.
- [8] Wigley, G. 1977. U.K. AEA Report: AERE-R-8771.
- [9] Lee, S.L. and J. Srinivasan. 1982. Int. J. Mult. Flow 8:47.
- [10] Semiat, R. and A.E. Dukler. 1981. AIChE J. 27:148.
- [11] Ballik, E.A. and J.H.C. Chan. 1973. Applied Optics 12:2607.

Table 1
BEAD VELOCITY CHECK

MEASURED VELOCITY (mm/sec)	ACTUAL VELOCITY (mm/sec)	PERCENT ERROR (%)
254.90	253.71	0.5
272.0	263.31	3.3
257.1	255.88	0.47

Table 2
BEAD SIZE CHECK

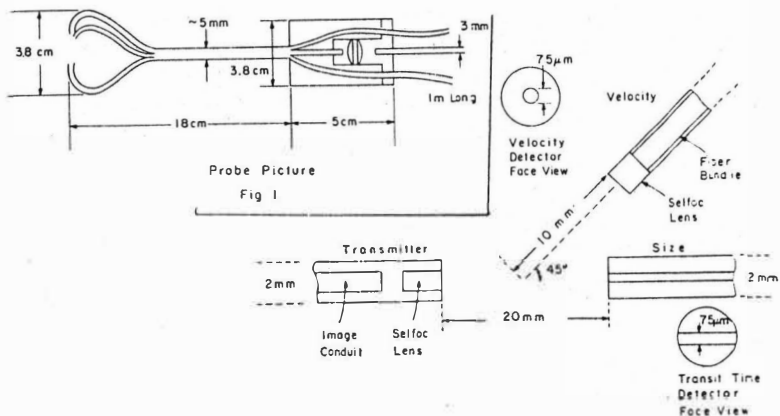
MEASURED SIZE (mm)	ACTUAL SIZE (mm)	PERCENT ERROR (%)
2.954	3.023	2.2
4.419	4.267	3.5
5.06	5.118	1.15

Table 3
OFF-CENTER VELOCITY ERROR - OPTIC AXIS

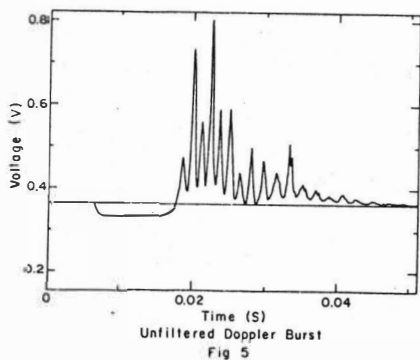
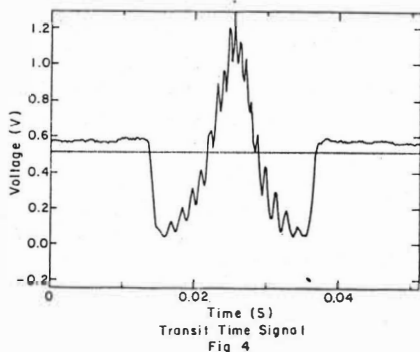
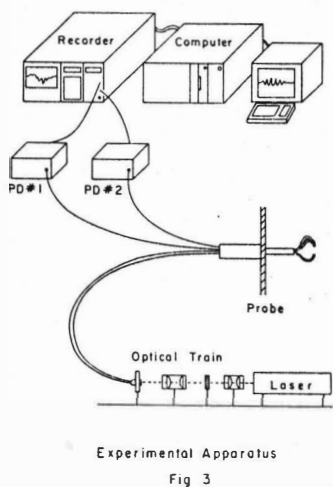
DISTANCE FROM CENTER (mm)	VELOCITY ERROR %
0	0.0
0.10	0.41
0.50	3.07
1.00	7.31

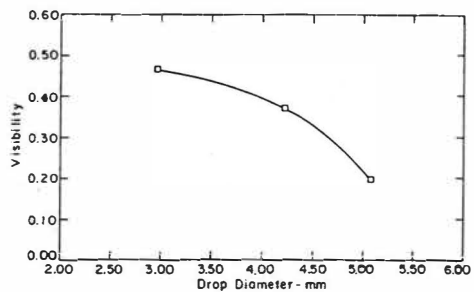
Table 4
OFF-CENTER VELOCITY ERROR - PERPENDICULAR AXIS

DISTANCE FROM CENTER (mm)	VELOCITY ERROR %
0	0.0
0.10	0.90
0.50	3.51

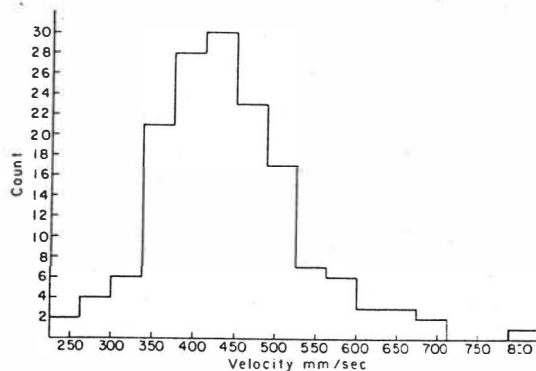


Details of Head Assembly
Fig 2



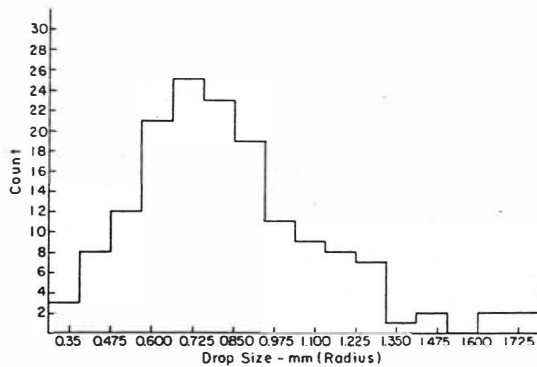


Visibility Correlation
Fig 6



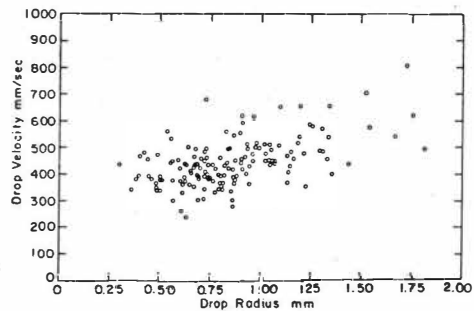
Velocity Histogram

Fig 7



Size Histogram

Fig 8



Velocity - Size Correlation

Fig 9

Mass Transfer Effect On Hydrodynamics In A Reciprocating Plate
Extraction Column

Bensalem, A., Steiner L. and Hartland S.
Dept. of Industrial and Engineering Chemistry
Swiss Federal Institute of Technology
ETH-Zurich, CH-8092 Zurich, Switzerland
ISEC'86, Sept. 1986, Munich, Germany

I. INTRODUCTION

This work considers the hydrodynamic characteristics of a 76.0 mm diameter reciprocating plate extraction column (RPEC) of the type introduced by Van Dijck (1935) and modified by Karr (1955).

Dispersed phase hold-up, flooding, drop size and drop size distribution, and axial dispersion in both phases have been determined, with and without mass transfer, using the liquid system toluene-acetone-water. Comparison of the present results to previous works is given when possible.

There are no published studies concerning the hydrodynamic (flooding, hold-up, axial dispersion in both phases) and mass transfer (including longitudinal concentration profiles) characteristics peculiar to this column (Lo et al., 1983). However, several authors have studied flooding characteristics, dispersed phase hold-up, drop size and axial mixing (only for the continuous phase) in Karr-columns, but only in the absence of mass transfer (Lo et al., 1983; Baird et al., 1971; Baird and Lane, 1973; Kim and Baird, 1976a, 1976b; Hafez et al., 1979).

The present work is part of a comprehensive study on hydrodynamics (with and without mass transfer), and mass transfer (including concentration profiles) in a pilot-plant Karr-column (Bensalem et al., 1982; 1983; 1985; 1986; Bensalem, 1985).

II. EXPERIMENTAL

2.1 Apparatus

The RPEC was constructed from two flanged glass sections with an internal diameter of 76 mm, an overall height of 2650 mm and a reciprocating plate stack of 1900 mm. The dimensions of the column are given in Table I. Further details on this column are presented in some previous publications (Bensalem et al., 1985; Bensalem, 1985).

TABLE I Column Dimensions

Column:	
Diameter (inside)	7.6 cm
Height	200.0 cm
Reciprocating Plate Stack:	
Height	190.0 cm
No. of perforated plates	54
No. of spider plates	2
No. of stainless steel baffle plates	4
No. of Teflon baffle plates	2
Spacing between perforated plates	2.54 cm
Volume fraction occupied by internals	11 %
Hole diameter	1.6 cm

2.2 Operating Procedure

In this study we used one of the test systems suggested by the European Federation of Chemical Engineering, namely, toluene-acetone-water (Misek, 1978). The deionized water phase was discarded after each run and the organic phase distilled after about every five runs. Crud which had formed at the interface during mass transfer experiments was subsequently removed. The outlet concentration of the aqueous phase was monitored with the aid of a density meter. It was found that the steady state was only reached after the contents of the column had been replaced at least five times (not three times as reported by Karr (1959).

III. RESULTS AND DISCUSSIONS

3.1 Hold-up

The disperse phase hold-up is defined as the fraction of the total column volume occupied by the disperse phase. In this work, two different measuring methods were applied: the hydrostatic and the direct sampling method.

The present results show that both measuring techniques give hold-up values, with and without mass transfer, which agree within $\pm 20\%$, with most of the data points agreeing within $\pm 15\%$. However, it is highly recommended that the disperse phase hold-up measurements be carried out with one and the same technique (Bensalem, 1985; Bensalem et al., 1985).

Figure 1 shows the effect of agitation and mass transfer on hold-up. Hold-up values are higher when the direction of mass transfer is from the continuous (water) phase to the disperse (toluene) phase than those measured when acetone transfers from disperse (toluene) to continuous (water) phase. This is due to the change in interfacial tension with the direction of solute transfer (Marangoni effect). When the mass transfer direction is from continuous to disperse, smaller droplets and hence higher hold-ups result. In general the hold-up was found to be higher when the direction of mass transfer is from the continuous to the disperse phase, leading to higher efficiencies but earlier flooding points (Bensalem, 1985).

The correlation of Baird and Lane (1973) does not represent well (average deviation error is more than 40%) the present data. It appears that this model tends to underestimate the power dissipation at high frequencies of reciprocation (data points measured at high agitation gave the largest errors). Other published correlations, among them that of Ramarao et al. (1983), and Kumar and Hartland (1983) did not correlate well the present data (with average deviation errors higher than 70%).

3.2 Flooding

The flooding model of Baird et al. (1971) correlates well (with an average error of 16.4%) the present flooding data, in the absence of mass transfer. However, this model failed to correlate the flooding values measured during mass transfer from disperse to the continuous phase, this being due to enhanced coalescence. Hafez et al. (1979) correlation failed to correlate the present data, even that measured in the absence of mass transfer, giving an average deviation error of more than 78%.

3.3 Drop Size and Drop Size Distributions

Data on mean drop size and hold-up are necessary for the estimation of the interfacial area which is then essential for the efficient operation, design and scale-up of liquid-liquid extraction columns.

In this work the Sauter mean drop diameter (d_{32}) was measured photographically.

Drop Size Distribution

The measured drop size distributions have been plotted as curves of percentage (%) against drop size (d). Figure 2 shows the influence of mass transfer direction on the drop size distribution curves and consequently on d_{32} . The three curves effectively represent data for three different liquid systems because the presence of the solute and direction of mass transfer change the system properties, such as the interfacial tension and density. It is clearly shown that when acetone transfers from disperse (toluene) to continuous (water) phase, the liquid system behaves like a high coalescence system; but for the opposite mass transfer direction, the system behaves like a retarded-coalescing system. The dispersed drops are clearly smaller when the mass transfer direction is from the continuous to disperse phase.

Since there is no published data on drop size distribution in Karr-columns, with or without mass transfer, no comparison with other work is possible.

Mean Drop Size (d_{32})

The present results show that most of the break-up of the dispersed drops is accomplished by the first few plates (Bensalem, 1985; Baird et al., 1971).

Figure 3 shows the strong influence of agitation (AF) on d_{32} , both during and in the absence of mass transfer. When acetone transfers from the continuous (water) to disperse (toluene) phase the interfacial tension is lower and coalescence retarded, thus leading to smaller droplets than for the opposite mass transfer direction. In the absence of mass transfer intermediate coalescence occurs, leading to medium-sized droplets. The results of Chartres and Korchinsky (1978) obtained in a rotating disc column (RDC) agree with the present data.

3.4 Axial Dispersion in Both Phases

In a previous study (Bensalem et al., 1982) we found that the dispersion flow model successfully described and correlated axial mixing in the continuous phase, and fairly well in the disperse phase. And the least-squares method in the frequency (and time) domain is employed for reducing the response curves for both phases, rather than the easier but inaccurate method of moments or the method of the maxima which have been discussed elsewhere (Bensalem, 1985; Clements, 1969 and 1972).

There are no published studies on axial dispersion data in both phases, with and without mass transfer. And as far as the limited published work on axial mixing, measured in the continuous phase, is concerned, there is a significant disagreement in the published data, as shown in Figure 4 (Kim and Baird, 1976 a and b; Nemecek and Prochazka, 1974; Hafez et al., 1979; Ramaro et al., 1983). This is due to the weakness of the published correlations on axial dispersion which are often based on limited data, and do not take into consideration all the operating variables of the column, such agitation (AF), the phase throughputs (Uc and Ud) and the hold-up (or drop size) (Marr and Babb, 1959; Bensalem, 1985).

In general, the axial dispersion coefficients depend on agitation, the phase throughputs, hold-up, the column and plate geometries, and the physical properties of the system (Bensalem, 1985; Bensalem et al., 1983).

IV. CONCLUSIONS

4.1 Hold-up and Flooding

In general, hold-up data obtained, with and without mass transfer, by the hydrostatic and the direct sampling methods give identical values. However, sometimes there were large deviations so that the hold-up should be measured by the same technique. The local hold-up was found to vary with column height due to the variation in drop size distribution along the column. The overall hold-up was found to depend on the agitation speed, phase throughputs and system properties. During mass transfer, hold-up depends on the mass transfer direction (Bensalem, 1985).

The present flooding data, in the absence of mass transfer, was well correlated by the hydrodynamic model of Baird et al. (1971). However, this model failed to correlate the present flooding data measured during mass transfer.

4.2 Drop Size and Drop Size Distribution

Most of the drop break-up occurred in the first few plates, as observed by previous workers (Baird et al., 1971). The agitation rate (and weakly the continuous phase throughput) was found to be the predominant factor in determining the break-up rate and hence the magnitude of the measured d_{32} .

During mass transfer, both the drop size and the drop size distribution curves were found to depend on the mass transfer direction. The mean drop diameter (d_{32}) was smaller when mass transfer occurred from the continuous to the dispersed phase.

4.3 Axial dispersion in Both Phases

The least-squares method in the frequency (or time) domain was found to be more appropriate than both the moments method and the method of maxima (Vergnes, 1976), for estimating the axial dispersion parameters from experimental residence time distribution curves.

Axial dispersion coefficients in both phases, with and without mass transfer, were found to depend on the agitation rate, phase throughputs, hold-up and direction of mass transfer. The authors are unaware of any published studies on axial dispersion in both phases, with and without mass transfer, in RPEC.

Finally, the optimized axial dispersion coefficients in both phases estimated from the experimental concentration profiles were found to compare well ($\pm 20\%$ for the continuous phase; and $\pm 40\%$ for the disperse phase) to those measured by the transient technique (Bensalem, 1985).

Mass transfer has a significant effect on drop size, hold-up, flooding and axial dispersion. Hydrodynamic parameters determined in the absence of mass transfer can lead to appreciable errors in the operation and design of RPEC.

REFERENCES

- Bensalem, A., "The use of the Calco-Oil blue dye and its effect on the hydrodynamics and performance of the RPEC", Internal report, TCL, ETH Zurich, May, (1983).
- Ibid, "Practical axial dispersion measurement techniques in both phases in L/L extractors", Internal report, TCL, ETH-Zurich, Jan., (1984).
- Ibid, "Hydrodynamics and mass transfer in a RPEC", Ph.D. Thesis no.:7721 ETH-Zurich, (1985).
- Bensalem, A., Steiner, L and Hartland, S., "Evaluation et comparaison des parametres de la dispersion axiale dans les deux phases d'une colonne d'extraction a plateaux alternatifs", Can.J.Chem.Eng., 60, 603(1982).
- Ibid, "Axial dispersion, with and without mass transfer, in both phases of a RPEC", proc. of ISEC'83, Denver, AIChE, 130(1983).
- Ibid, "Effect of mass transfer on flooding and holdup in a Karr column", Solvent Extraction and Ion Exchange, New York, 3(5), 697(1985).
- Ibid, "Effect of mass transfer on drop size in a Karr column", Chem.Eng. and Processing, Lausanne,(1986), IN PRESS.

Note: The other cited references cannot be listed here, but they are all listed in the work of Bensalem (1985).

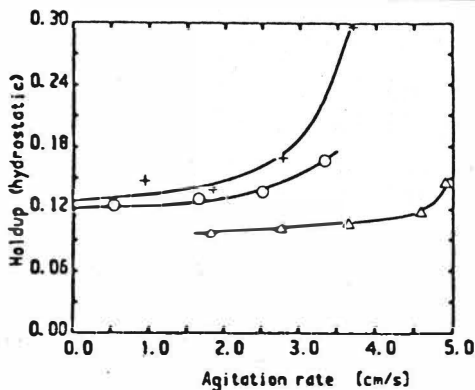


Fig. 1. Influence of mass transfer direction on holdup.
 $U_c = U_d = 0.687$ cm/s, $A = 1.1$ cm. (o) No mass transfer, (Δ) Mass transfer from toluene (d) to water (c), (+) Mass transfer from water (c) to toluene (d).

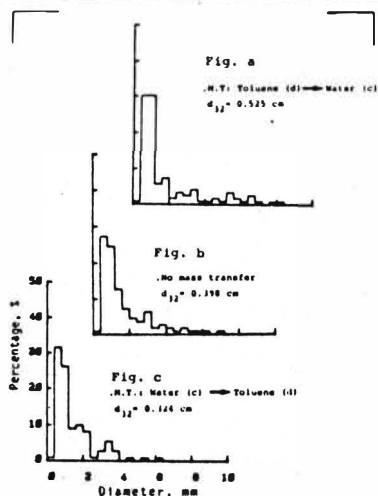


Fig. 2. Effect of mass transfer on the drop size distribution at plate 36 (at 130 cm from the bottom plate).
 $A = 1.10$ cm, $F = 1.67$ s $^{-1}$,
 $U_c = U_d = 0.678$ cm/s.

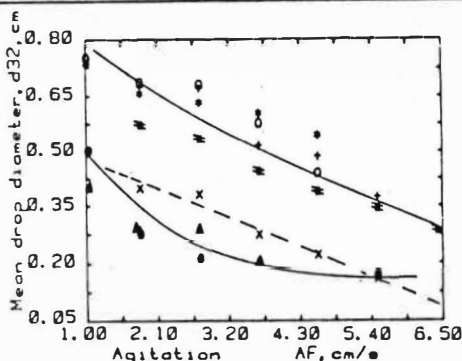


Fig. 3.

Effect of agitation on d_{32} , with and without mass transfer. $H = 130$ cm.

x : no mass transfer

0, +, *, † : MTD Tol. (d) → Water (c)

●, ▲ : m.t.d. Water (c) → Tol. (d)

	0	+	*	†	x	▲	●
U_c , cm/s	0.330	0.532	0.859	0.687	0.687	0.344	0.687
U_d , cm/s	0.550	0.893	1.443	0.687	0.687	0.550	0.687

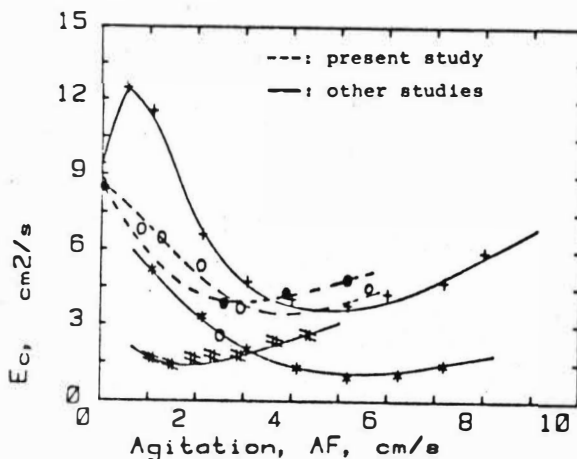


Fig. 4.

Effect of agitation on axial dispersion coefficients measured by various workers.

Reference	symbol	U_c	U_d	d_h	ϕ	h_p (cgs units)
Present study	0 & ●	0.687	0.172	1.6	0.58	2.54 ●: $A = 1.55$ 0: $A = 0.50$
Hafez et al (79)	+	0.50	0.22	1.47	0.58	5.2
Nemecek et al (74)	*	0.31	0.25	0.25	0.19	7.5
Ramarao et al (83)	†	0.24	0.11	0.50	0.19	5.0

Influence of Dispersed Phase on Power Consumption in Vibrating Plate Columns

V. Pavasović, R. Stevanović
Boris Kidrič Institute, Beograd, Yugoslavia

J. Prochazka
Czechoslovak Academy of Science, Institute of Chemical Process
Fundamentals, Prague, Czechoslovakia

Introduction

During the development of a method for continuous determination of the dispersed phase hold-up in a Kaar vibrating plate extractor by a pressure drop, it was observed that the errors were large and systematic (1, 2) at low frequencies of vibration. The hold-up determinations were based on the measurements of pressure changes at the bottom of the extractor, which occurred when the dispersed phase was introduced in the single phase flow. Jiričny and Prochazka (3) also used the pressure drop method for measuring the hold-up profiles in a vibrating plate column. However, they did not notice the difference between the measured and the actual values because the conditions for an application of this method, which they stated in the article, were fulfilled. However, it should be necessary to perform a more detailed analysis of the conditions for application of the method.

In the present work, the macroscopic momentum balance developed for a single phase flow (4, 5, 6) is extended to a two phase flow and the influence of dispersed phase on the power consumption is studied.

Theoretical

The macroscopic momentum balance is applied to a control volume - a segment of the vibrating plate extraction column through which two immiscible and incompressible liquid phases are flowing. All forces acting at the surfaces of the control volume and at a vibrating plate are presented in Fig. 1a and b. The details on the model development are given elsewhere (8). Assuming that all the vectors corresponding to forces, velocities and accelerations are parallel to the control volume axis leads to the following scalar equations:

$$m_s \cdot \frac{dw_s}{dt} + m_c \frac{dw_c}{dt} + m_d \frac{dw_d}{dt} = (p_1 - p_2)A + F_R + (m_s + m_c + m_d)g \quad (1)$$

$$m_p \frac{dw_p}{dt} = F_R - F_p + m_p g - F_B \quad (2)$$

Combining Eqs.(1) and (2) for the particular case of the steady-state

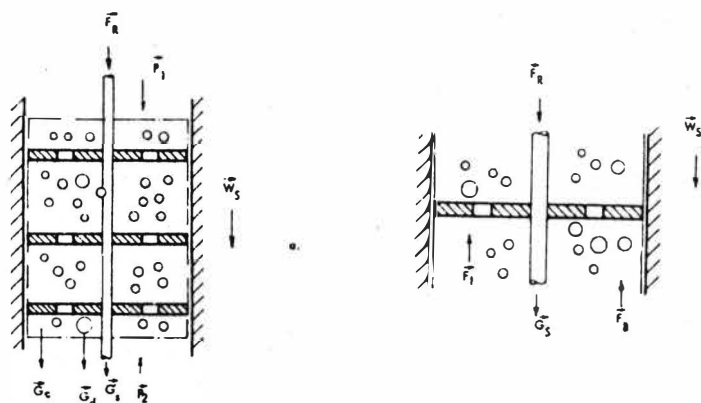


Fig. 1. Forces acting at:
 (a) surfaces of control volume
 (b) vibrating plate.

flow, the following final equation for the force exerted by the liquid-liquid system on the plates is obtained:

$$F_{pv} = \Delta P \cdot A + AH\chi(\rho_c - \rho_d)g \quad (3)$$

where the pressure term ΔP is:

$$\Delta P = (p_2 - p_1) - \rho_c gH \quad (4)$$

The equation for the single phase flow ($x = 0$), equivalent to the equation (3) (5, 6) is:

$$F_{pvo} = \Delta P_o \cdot A \quad (5)$$

The instantaneous power input supplied to the liquid system by motion of the plates is a product of the instantaneous relative velocity between the plates and the liquid, $(w_p - w_c)$, and the force F_{vp} :

$$N_v = w_r \cdot F_{p.v} = (w_p - w_c) \cdot A |\Delta P + \Delta \rho gH| \quad (6)$$

and for the single phase flow ($x = 0$):

$$N_{vo} = (w_p - w_c)A \cdot \Delta P_o \quad (6a)$$

The corresponding average values of the power input can be obtained by integrating equations (6) and (6a) over a period of oscillation T .

The static pressure method of measuring the dispersed phase hold-up is

based on the measurements of pressure drop changes over one period of oscillation in a segment of the column, which occurs when the dispersed phase is introduced in a single phase flow through the column, under the same conditions of vibrating motion of the set of perforated plates, i.e.:

$$\Delta P_o - \Delta P = (F_{pvo} - F_{pv})/A + (\rho_c - \rho_d) \times H \quad (7)$$

The static pressure method can be applied, throughout the whole cycle of reciprocating motion of plates, if:

$$(F_{pvo} - F_{pv})/A = 0 \quad (8)$$

Usually, however, integration over one or more cycles is performed and mean value of Eq.7 is taken. It should be noticed, that the mean values of this equation should be much less influenced and thus the static method based on these mean values may be applied to broader range of conditions.

Experimental

The measurements were performed on a Karr vibrating plate column. The column was of 2.54 cm I.D. and its total height was 2.71 cm. The perforated plates were mounted on a common rod and spaced at equal distances of 2.54 cm. The free area of plates was 51%.

Two binary liquid-liquid systems recommended by the European Federation of Chemical Engineering as official test systems for extraction investigation were used: water-toluene (as a system with high interfacial tension forming large drops) and water-n-butanol alcohol (as a system with low interfacial tension forming small drops) (7). In all experimental runs the aqueous phase was continuous and the organic one was dispersed. Experiments were performed at constant temperature of $20 \pm 0.5^\circ\text{C}$. The physical properties of used systems at 20°C is given in (7).

For the measurements of the instantaneous pressure on the bottom of the extraction column as well as for the continuous determinations of the dispersed phase hold-up, inductive pressure transducers were used (Types S.E.180 and S.E.1150, S.E. Laboratories, Feltham, England). Processing of the signals from the inductive transducers was performed by use of an electronic equipment, the block diagram of which is shown in Fig. 2. By use of a 256 Channel Analyser (Radiation Counter Laboratories, INC., Nucleonic Park, Skokie, U.S.A.), an electrical signal obtained from the pressure transducers, which corresponds to a single vibrating cycle, was digitalised and presented as one hundred

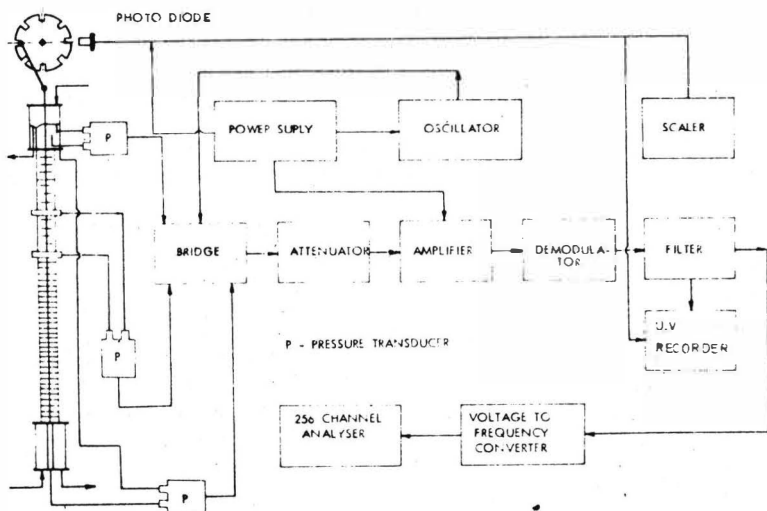


Fig. 2. Schematic of the vibrating column and electronic equipment.

numerical values uniformly spaced in time. For a quantitative evaluation, several hundreds of consecutive electrical signals were used.

Results and discussion

Typical pressure drop signals at lower oscillation frequency for water-toluene system ($f = 0.5$ Hz) are presented in Fig. 3a. Full lines correspond to the pressure variations in single phase flows and the dashed lines present the pressure variations in two phase flows (a term corresponding to the hold-up value is added to the pressure drop of two phase flow according to Eq.3). It is evident from the diagram that there are large differences between the pressure drops in single and two phase flows. These differences are very small when the plates are moving upwards and the largest when the plates are moving downwards with the maximum velocity. It was observed and photographed by a moving camera, that at lower frequencies of vibration the drops were not homogeneously distributed. At these frequencies the vibrating extractor worked in the mixer-settler regime of operation. At the maximum downward plate velocity a large portion of drops was supported by the plates blocking the plate holes.

The increase in friction force over one cycle of oscillation will not be the same for homogeneously and nonhomogeneously distributed dispersions due to a nonlinear (square) relation between the friction force

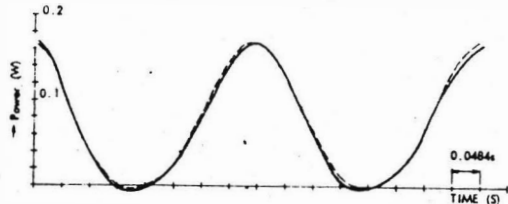
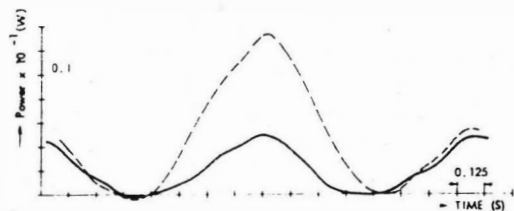
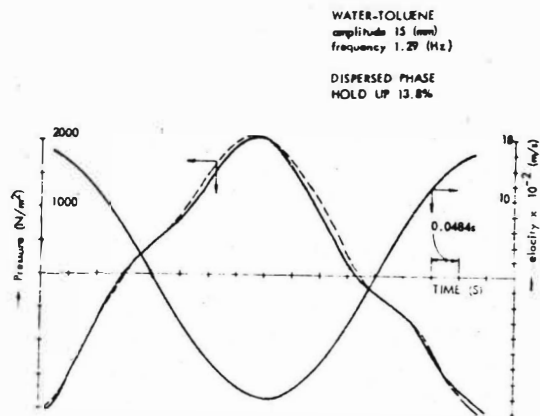
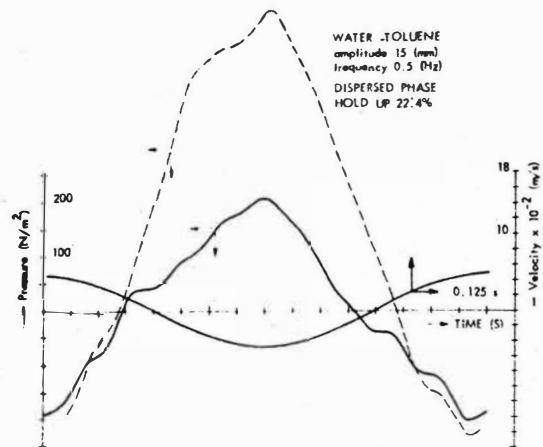


Fig. 3. Typical pressure drop signals for water-toluene system: (a) at lower vibration frequency, (b) at higher vibration frequency.

and the velocity. The friction force between freely moving drops and continuous phase is equal to the buoyancy force acting on drops. This friction force is detected by the pressure drop which is proportional to the dispersed phase hold-up. The decrease in velocities of drops due to their collision with plates and support by the plates will result in lower hold-up detection. Collision and support of drops by the plates are higher for nonhomogeneously distributed dispersion than for the homogeneously distributed one. All of these have as a result a hold-up measurement error. The instantaneous power consumption is also higher for the two phase flow than for the single phase flow, approximately the same when the plates are moving upwards and much higher when the plates are moving downwards.

Typical pressure drop signals at higher vibration frequencies for water-toluene system ($f = 1.29$ Hz) are illustrated in Fig. 3b. At higher oscillation frequencies, the extractor works in the emulsion regime of operation. There are no differences between the single and the two phase pressure drops (if they are presented in this way) as well as in power consumptions.

Typical pressure drop signals at low vibration frequencies for water-n-butanol ($f = 0.5$ Hz) are given in Fig. 4. As can be seen from the diagram, the differences are rather small, practically negligible. The interfacial tension and therefore the drops are small for this system. The drops are homogeneously distributed even at low vibration frequencies and the plate holes at maximum downward plate velocity are not completely blocked. At higher vibration frequencies for this system there also also no differences in pressure drops as well as in power consumption for single and two phase flows.

List of symbols

- A - area of column cross section, m^2
- F - force, N
- g - acceleration gravity constant, ms^{-2}
- H - height of the column, m
- m - mass, kg
- N - instantaneous power input, w
- p - pressure, Nm^{-2}
- t - time, s
- T - period of oscillation, s
- x - dispersed phase hold-up
- w - instantaneous velocity, ms^{-1}
- ρ - density, kgm^{-3}

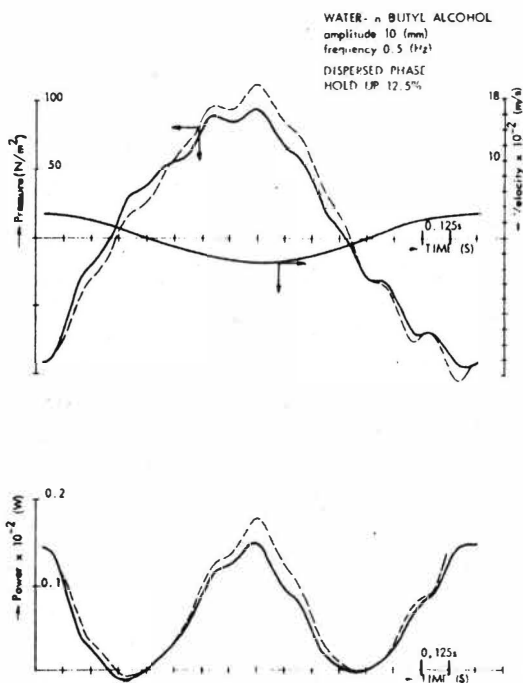


Fig. 4. Typical pressure drop signals for water-n-butanol system.

Subscripts

B - bouyancy	R - rod
c - continuous liquid phase	s - solid
d - dispersed liquid phase	t - two phase flow
o - single phase flow	v - vibrating plate
p - plate	

References

1. Pavasović, V., Ph.D.Thesis, University of Beograd, 1975.
2. Pavasović, V., 5th Int.CHISA Congress, Prague, 1975.
3. Jiričny, V. and Prochazka, J., Chem.Eng.Sci. 35, 2237 (1980).
4. Prochazka, J. and Hafez, M.M., Collection of Czechoslovak Chem. Commun., 138, 505 (1973).
5. Hafez M.M. and Prochazka, J., Chem.Eng.Sci., 29, 1745 (1974).
6. Hafez M.M. and Prochazka J., Chem.Eng.Sci. 29, 1977 (1974).
7. Mišek T., Recommended Systems for Liquid Extraction Studies, The Institution of Chemical Engineers, Rugby 1978.
8. Pavasović, V., Stevanović, R., Prochazka, J., to be published.

R. Billet, A. Gosch, J. Maćkowiak, M. Pająk

1. Introduction

Apart from distillation and absorption, liquid-liquid extraction belongs to the classical process of application for packed columns. Over recent years, the increasing amount of information becoming available on the relations between the hydrodynamics of two-phase flow systems and the mass transfer in such apparatus has led to new calculations facilitating the selection of operating conditions as well as rough calculations on the construction and fitting out (1-4) of packed columns. High loading capacities of packings allow the systems to be operated under extreme phase ratios.

Expensive solvents, which have to be highly enriched with the extracted substance, are often used in extraction processes. In such cases, pilot trials often have to be carried out, whereby their outlay and expense must be kept as low as possible. Therefore, in the light of such considerations, not every installation whose results can be used on an enlarged scale is obviously suitable. The column fitted out with with regularly arranged Bialecki rings is, however, particularly suitable for such tasks (1-3).

Extraction carried out at even low concentrations of transferred components is, in addition, heavily dependent on interfacial factors, the called Marangonie effects, which often make a theoretical prediction of the hydraulic behaviour and the efficiency of the apparatus impossible.

Based on the specific volume of the column, a preselection of the packing material can be undertaken according to constructional or cost-related aspects.

2. Design of packed columns for liquid-liquid extraction

As regards the preparatory calculations for an extraction system, a knowledge of the maximum phase load as well as the efficiency of the fittings within the column is required. A survey of these relationships can be seen for both mass transfer directions C→D and D→C in Table 1, whereas the model constants for their calculation can be found in Table 2.

In deriving the relation for the flood load $u_{C,F1}$ of the continuous phase, Eqn. (1), the two-layer model (4) was taken as a basis in addition to the fact that the characteristic drop velocity is directly proportional to the individual drop velocity (1), (2), (3).

The relations for determining the height HTU_{OC} and HTU_{OD} of a transfer unit in the continuous or disperse phases, Eqn. (6) and (7), were derived under assumption of the validity of the theory of instationary diffusion for short contact times (1-3).

3. The influence of concentration on hydrodynamics and mass transfer

Using a sheet-metal packing of the Montz B1-300 construction type with an element height $h = 0.135$ m, the influence of the acetone concentration on the disperse phase hold-up, the maximum loadability and the mass transfer $D \rightarrow C$ and $C \rightarrow D$ in a toluene (D)-acetone-water system were examined. The results are shown in Figures 1-3. Fig. 1 thus shows the disperse phase hold-up x as a function of the specific throughput u_D of the dispersed phase at different acetone concentrations in toluene. According to this, as the acetone concentration rises, the disperse phase hold-up x increases for the mass transfer direction $C \rightarrow D$ due to changing physical properties of the system. By applying Eqn. (8), we are now in a position to assess these changes of the hold-up quantitatively with the concentration. A sinking of the disperse phase hold-up as the acetone concentration increases has been established for the mass transfer direction $D \rightarrow C$, as shown in the Fig. 1. The loadability of the column also increases when mass transfer of the drops into the continuous phase, $D \rightarrow C$, takes place, see Fig. 1. This behaviour can be attributed to the Marangonie effects, which encourage the formation of bulky dispersed phase flow or flow through created channels.

Evaluation of mass transfer area for $D \rightarrow C$ direction is very difficult because real drops do not exist and thus application of Eqn. (7) for calculation HTU_{OD} can give only approximate results. On the basis of many experiments which have been carried out the following empirical procedure can give more realistic values; to put into Eqn. (7) the greater possible value for interfacial tension σ , i.e. as with pure materials, to increase calculated value HTU_{OD} by the factor 1.15.

Eqn. (6) takes the influence of the physical properties which change with concentration of the mass transfer $C \rightarrow D$ into account. This is illustrated by the numerical example on the end. The relative error in determining the height HTU_{OC} is $\delta(HTU_{OC}) < \pm 15\%$ (1), (2).

This procedure of calculation just described not only applies in the case of the sheet-metal filling (as manufactured by Montz, Type B1-300/ $h = 0.135$ m); it can be applied just as well and to the same extent to both metallic and ceramic packing materials of any desired shape and size.

4. Selection of mass transfer direction and phase throughput ratio

It is advantageous to operate the extraction process with phase ratios of $\lambda = \frac{v_D}{v_C} > 0.5$ when using the mass transfer direction $C \rightarrow D$, as the separating effect of a packed column is always greater, under the operating conditions, than in the opposite direction, i.e. $D \rightarrow C$, see Eqns. (6) and (7). Consequently, those mate-

rials are selected for filling the columns which facilitate dispersion of the excess phase. The general rule applies that an organic phase can be dispersed with practically all technical materials; contrary to this, aqueous phase can not be dispersed when ceramic filling materials are used.

For phase throughput ratios in the range of $\lambda = 0.1 - 0.5$, the mass transfer direction $D \rightarrow C$ can be of advantage, as the statement $HTU_{OD} \neq f(\lambda)$ applies under these operating conditions. However, as regards the exchange direction $C \rightarrow D$, extremely high HTU_{OC} values are reached due to the dependency in $HTU_{OC} = f(\frac{1}{\lambda})$.

Furthermore, when selecting the operating conditions, care should be taken that the specific minimum throughput u_D is greater than $0.1 \cdot u_{D,F1}$. If specific throughputs such as $u_D < 0.1 \cdot u_{D,F1}$ are used, a pronounced reduction in the separating effect due to increased drop size must be reckoned with.

5. Selection of packing

For the given extraction process it is necessary to select such packing which gives the maximum throughput as well as efficiency. Selection of the proper type of packing can be done on the base of the parameter v_0 , Eqn. (10). This parameter was developed using Eqns. (1) and (6) and also the definition Eqn. (9) for the specific column volume v_A , Table 1.

These parameters v_0 have been listed in Table 2 for a number of packing materials; according to this, there are thus considerable differences in v_0 values in the case of the filling materials here considered.

The product of v_0 and the related costs K_0 per m^3 structural volume provided by the manufacturer of the packing material, is a measure for the specific column costs and thus forms the basis for a cost comparison of different packing types.

6. Example

To overall height of a mass transfer unit HTU_{OC} and the hold-up x for the extraction of acetone from water with toluene in a Montz metal sheet packing with an element height of $h = 0.135$ m, operated in the range $u_C < 0.065 \cdot u_{C,F1}$, is to be calculated. Following data are given:

$$D_D = 25.9 \cdot 10^{-10} \text{ m}^2/\text{s}, D_C = 9.8 \cdot 10^{-10} \text{ m}^2/\text{s}, m_{CC} = 0.79 \text{ (kmol/m}^3\text{)/(kmol/m}^3\text{)}$$

$$\rho_C = 988.9 \text{ kg/m}^3, \rho_D = 863 \text{ kg/m}^3, \sigma = 0.020 \text{ N/m and } 0.026 \text{ N/m } \lambda = u_D/u_C = 1.1,$$

$$g = 9.81 \text{ m/s}^2, C_0 = 0.475 \text{ and } \epsilon = 0.93.$$

Solution

For mass transfer direction C → D it is obtained according to Eqn. 6

$$\text{HTU}_{\text{OC}} = \frac{4.45 \cdot 10^{-2}}{1.1} \cdot \frac{0.02^{5/8} \cdot 10^5}{((988.9 - 863) \cdot 9.81)^{3/8} \cdot 988.9^{1/4}} \cdot \left[\frac{1}{9.81^{1/2}} + \frac{1}{0.79 \cdot 25.9^{1/2}} \right] = 1.66 \text{ m}$$

$\text{HTU}_{\text{OC,exp}} = 1.7 \text{ m}$; s. Fig. 3 for $\sigma = 0.020 \text{ N/m}$

Respectively it is received for

$\text{HTU}_{\text{OC}} = 1.96 \text{ m}$, $\text{HTU}_{\text{OC,exp}} = 1.90 \text{ m}$, s. Fig. 3 for $\sigma = 0.026 \text{ N/m}$

On the basis of Eqn. (4) and Eqn. (8) it is calculated the constant

$$C_1 = \frac{988.9^{1/2}}{0.475 \cdot 0.93 \cdot (4.981 \cdot (988.9 - 863) \cdot 0.020)^{1/4}} = 22.7 \text{ s/m}$$

If $u_D = 5.21 \cdot 10^{-3} \text{ m/s}$ it is obtained from Eqn. (8) the disperse phase hold-up

$$x = C_1 \cdot u_D = 22.7 \cdot 0.00521 = 0.118 \text{ m}^3/\text{m}^3$$

$$x_{\text{exp}} = 0.108 \text{ m}^3/\text{m}^3 \quad \delta(x) = +9.5 \%, \text{ s. Fig. 1.}$$

7. Symbols used

c	Constants
$C_{F1, C}$	Constants
C_1, C_3	Parameter, s/m resp. $\text{m}^{+1/2}$
D	Diffusion coefficient of dissolved components, m^2/s
d	Packing diameter, m
d_S	Column diameter, m, for tube column $d_S = d$
g	Acceleration due to gravity, m/s^2
h	Height of packing element, m
H	Column height, m
HTU_0	Overall height of transfer unit, valid for plug flow, m
K_o	Related costs per m^3 structural volume
m_{CC}	Slope of equilibrium line, $(\text{kmol}/\text{m}^3)/(\text{kmol}/\text{m}^3)$
u	Velocity of single drop, m/s
u_C, u_D	Superficial velocity, $\text{m}^3/(\text{m}^2 \cdot \text{s})$
u_K	Characteristic droplet velocity, m/s
v_A	Specific volume of column, $\text{m}^3/(\text{m}^3/\text{s})$
v_0	Parameter
x	Dynamic hold-up of dispersed phase, m^3/m^3

x_{Fj}	Dynamic hold-up of dispersed phase at flooding, m^3/m^3
$\delta(j)$	Relative error for parameter j , % ($j = x, HTU_0$)
ϵ	Void fraction, m^3/m^3
η	Dynamic viscosity, $kg/(m \cdot s)$
ρ	Density, kg/m^3
$\Delta\rho$	Density difference, kg/m^3
σ	Interfacial tension, N/m

Subscription

C	Continuous phase
D	Dispersed phase
F1	Flooding

8. Literature

- (1) Billet, R., Mačkowiak, J., Chem. Ing. Tech. 57 (1985) No. 1, pp. 56/57
- (2) Mačkowiak, J., Billet, R., Germ. Chem. Eng. (1986) No. 1, pp. 48-64
- (3) Billet, R., Mačkowiak, J., Pająk, M.: Chem. Eng. Processing 19 (1985) No. 1, pp. 39/47
- (4) Gayler, R., Roberts, N.W.: Pratt, HRC.: Trans. Inst. Chem. Eng. 31 (1953), pp. 57/68
- (5) Thornton, J.D.: Eng. Sci. 5 (1956), pp. 201/208
- (6) Levich, V.G.: Physicochemical Hydrodynamics, Prentice Hall, New York, 1962

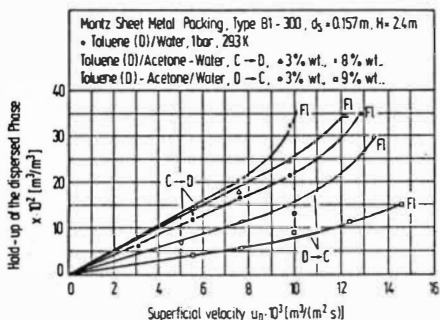


Fig. 2:

Influence of acetone concentration on mass transfer direction D \rightarrow C, valid for sheet metal packing, Montz - Type B1-300, $h = 0.135 \text{ m}$, $\lambda = 1.1$, System: toluene (D)-acetone/water

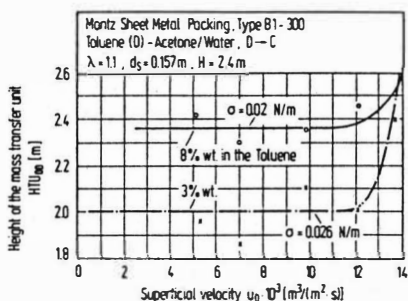
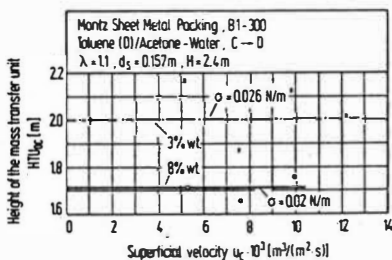


Fig. 3:

Influence of concentration on mass transfer direction C \rightarrow D, valid for sheet metal packing, Montz-Type B1-300, $h = 0.135 \text{ m}$, $\lambda = 1.1$, $\lambda = u_D/u_C$, System: toluene (D)/acetone-water



View of sheet metal packing,
 Montz-Type B1-300

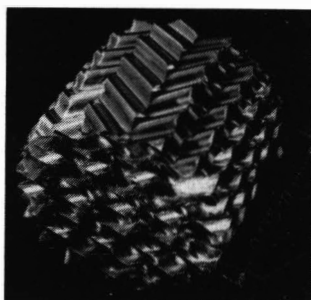


Table 1: Equations for design of packed columns for liquid/liquid extraction processes

Eq	Parameter	Equation	Column type	Lit	Operating range
(1)	$u_{c,fl}$	$\frac{m^2}{m^2 s} u_{c,fl} = C_{fl} u \varepsilon \cdot (1-x_{fl})^2 (1-2x_{fl})$	dumped packing, sheet metal packing	[1,2]	$D \rightarrow C$ $C \rightarrow D$ $u_c = u_{c,fl}$ $u_c = 0.65 u_{c,fl}$
(2)	$u_{c,fl}$	$\frac{m^3}{m^2 s} u_{c,fl} = C u \exp(-b x_{fl}) \varepsilon \cdot (1-x_{fl})^2 (1-b x_{fl})$	tube column with stacked 25 and 50mm Bialeckirings	[3]	$C = 0.586$, $b = 1.17$ for 50mm tube column, $C = 0.488$, $b = 1.31$ for 25mm tube column
(3)	u	$m/s \quad u = (4 g \cdot (\rho_L - \rho_V) \cdot \sigma / \rho_C^2)^{1/4}$	-	[6]	$Re_V = \frac{u \cdot d_{VS} \cdot 1000}{\nu_C}$
(4)	x_{fl}	for Eq.(2) $x_{fl} = \frac{(\lambda^2 - 8 \lambda)^{1/2} - 3 \lambda}{4(1-\lambda)}$	-	[5]	for flooding conditions
(5)		$\lambda = \frac{x_{fl}^2}{(1-x_{fl})^2} \cdot \frac{1-b(1-x_{fl})}{1-b x_{fl}} \cdot \frac{u_D}{u_c}$	evaluated by trial and error method	[3]	
(6)	HU_{DC}	$m \quad HU_{DC} = C_{\lambda 0} \cdot \frac{\sigma^{5/8}}{\lambda (\Delta \rho g)^{3/8} \rho_C^{1/4}} \cdot \left[\frac{1}{D_c \cdot v_2} + \frac{1}{m_{DC} \cdot D_c^{1/2}} \right]$	dumped packing, sheet metal packing	[1,2]	$u_c = 0.65 u_{c,fl}$ $\lambda = 0.4 - 4$
(7)	HU_{DD}	$m \quad HU_{DD} = C_{\lambda 0} \cdot \frac{\sigma^{5/8}}{(\Delta \rho g)^{3/8} \rho_C^{1/4}} \cdot \left[\frac{1}{D_c \cdot v_2} + \frac{m_{DC}}{D_c^{1/2}} \right]$	dumped packing, sheet metal packing	[1,2]	$u_c = u_{c,fl}$
(8)	x	$m^3/m^2 \quad x = \frac{u_D}{C_0 \cdot \varepsilon \cdot u} = C_1 u_D$	dumped and stacked packings	[1,2]	not valid $u_c = 0.65 u_{c,fl}$
(9)	v_A	$\frac{m^3}{m^3 s} \quad a) v_A = \frac{HU_{DC}}{u_D \cdot u_c} \quad b) v_A = \frac{HU_{DD}}{u_D \cdot u_c}$	all types of packings	[7]	
(10)	v_0	$m^{-1/2} \quad \text{acc. to Eq.(1)(6) for } \lambda = \text{const. and } u_c/u_{c,fl} = 1 = \text{const.}$ $v_0 = \frac{C_3}{C_{fl} \cdot \varepsilon}$ whereby $v_A = v_0$			

Table 2: Technical data of the investigated packings and model parameter for evaluation of hold-up, flooding conditions, efficiency of packings and factor v_0

Packing	Material	$d \cdot 10^3$ m	ε m^3/m^3	C_0 Eq.(8)	C_{fl}	$C_3 \cdot 10^2$ $v_0 \cdot 10^2$	
						$\frac{D \rightarrow C}{C \rightarrow D}$	$\frac{D \rightarrow C}{C \rightarrow D}$
Intalox - Saddle	ceramic	25	0.77	0.325	0.40	$\frac{4}{2.7}$	$\frac{13}{8.8}$
Bialeckiring	metal	25	0.94	0.284	0.45	$\frac{3.66}{2.3}$	$\frac{8.2}{5.5}$
Paltring	metal	25	0.94	0.334	0.45	$\frac{3.66}{2.3}$	$\frac{8.2}{5.5}$
Stacked Bialeckiring	metal	25	0.928	0.465	0.67	$\frac{2.67}{1.6}$	$\frac{4.3}{2.9}$
Montz - type sheet metal packing B1-300, h = 0.135m	metal	-	0.93	0.475	0.783	$\frac{4.65}{3.0}$	$\frac{6.1}{4.1}$

Gas Agitated Liquid-Liquid Extraction in Columns Filled with Regularly Arranged Bialecki Rings

R. Billet, Chr. Braun, Ruhr-Universität Bochum, West Germany

Introduction

Steps taken to increase the separation efficiency of liquid-liquid extractors in general refer to devices, which ensure a high dispersion of the droplets of the disperse phase in order to create a sufficiently high mass transfer area. In industry, extractors with mechanically agitated internals such as rotating disk columns (RDC) and pulsating sieve plate extractors (PSE) are preferably used for this purpose. In columns of larger dimension the usage of moving parts requires a relatively large number of industrial instrumentation involving corresponding investment and maintenance costs.

For some time now researches have been carried out into apparatus alternatives, which exclude the disadvantages of moving parts and have comparable separation efficiency. For instance, it could be demonstrated (1) that statical columns with packings suitable for extraction purpose may by all means be able to compete. In addition the efficiency of statical extractors can be considerably increased by introducing an inert gas into the base of the column. This way of energy introduction increase the turbulence within this three-phase liquid-liquid-gas system, which causes an improved dispersion of droplets and consequently a higher hold-up and therefore a greater mass transfer area. These positive effects of gas agitation have been known for many years and observed in various types of extractors. While examining the literature for their treatise, Ziebland and Hackl (2) discovered that a gas agitated extractor was mentioned for the first time as far back as 1937 (3). Publications after 1978 (2), (4), (5), (6), (7), refer time and again to the improved efficiency of gas agitated columns, but only Ziebland and Hackl (3) made first attempts to describe the phenomena in mathematical and physical terms.

The complexity of the three-phase liquid-liquid-gas system therefore requires at first a systematical investigation of the hydraulics, all the more - as the authors' own experiments have shown, the gas influences the physical properties as density and interfacial tension of the solvent and the extract phase.

On the basis of mass transfer experiments in a packed column in order to show the effect of gas agitation on the HTU-values the influence of gas agitation on the hydraulic parameters such as liquid hold-up and droplet size is shown in the following.

System investigated

In order to quantify the influence of gas agitation on the rates of mass transfer, experiments considering both directions of mass transfer were carried out with the system toluene (D)-N₂-acetone-water. For the hydraulic investigations the system

toluene (D)-N₂-water was used.

In the experiments without mass transfer, water from the ion exchanger and toluene were recirculated. Due to the solubility of gas in the liquids the initial interfacial tension between technical pure toluene and water is reduced from 33,3 mN/m during the experiments without gas to a value of approximately 27,5 mN/m. At higher gas flow-rates the intensive mixing and contacting inside the column caused a supersaturation of the liquid phases with nitrogen. The interfacial tension decreased even more and did change with time, for example just after sampling the measured value was less than 23.0 mN/m and after eight minutes the initial value of 27.5 mN/m did return.

Experimental equipment and measuring methods

Because of the good results obtained in columns packed with stacked metallic Bialecki rings (1) the experiments were carried out in such extractors of 100 mm and 154 mm in diameter with a height of packings of 2.62 m and 2.5 m. The total height of liquid above the bottom distributor up to the overflow of the dispersed toluene phase was 3.04 m for the 100 mm and 2.745 m for the 154 mm column.

The specially constructed gas-liquid distributor as well as the distributor for the continuous phase allow a homogeneous distribution of the phase over the whole cross section of the column. The gas and the solvent are fed into the column through common nozzles, while the mixing of these phases already takes place in the distributor itself.

In both columns there is a gauge at a height of approximately 1.6 m for photoelectric droplet size measurements.

In order to determine the gas hold-up x_G the differential pressure between the operating gas agitated column and the static column filled with liquid up to the overflow of the toluene phase is measured. After the estimation of the liquid disperse phase hold-up x_D , the gas hold-up x_G , which is referred to the total volume of the column, can be calculated.

Mass transfer

The results of mass transfer investigations in Fig. 1 show that by feeding inert gas into the column the height of a transfer unit HTU_{OC} can be reduced up to 50 %. This already occurs at relatively small phase ratios $\beta = u_G/u_D$. For the mass transfer direction D \rightarrow C the minimum of the HTU_{OC} values is approximately $\beta = 1.2$, for the direction C \rightarrow D it is 1.5.

As Fig. 2 b shows, the Sauter mean diameter d_{VS} of droplets reaches the minimum value

in this range. For phase ratios greater than $\beta = 1.5$ the energy input by the gas phase doesn't lead to smaller droplet size. The hold-up still increases, but because of the starting circulation of droplets the HTU_{OG} -values increase by longitudinal dispersion, too.

Hydraulic investigations

To determine the hydraulic parameters the hold-up of the dispersed phase x_D , the Sauter mean diameter d_{VS} , Fig. 2 a and 2 b, as well as the gas hold-up x_G , Fig. 3, were measured and plotted against the phase ratio β between the flow rates of the gas phase and the liquid disperse phase.

The investigations were carried out for 4 phase ratios of the liquid phases $\lambda = u_D/u_C$ with 3 or 2 different flow rates of the solvent u_D . The upper 4 curves in Fig. 2 a show results obtained by feeding gas into the column while flooding conditions for the pure toluene (D)-water system were reached. Even few quickly rising gas bubbles immediately prevent banking up of droplets so that the operation limits of the gas agitated column increase. The operation limit with gas was reached, when phase inversion somewhere inside the column or normal flooding occurred.

During the gas agitation, two-phase droplets are formed at the distributor nozzles or created inside the column when a gas bubble attaches to a solvent droplet. The higher density difference between the two-phase droplets and the surroundings continuous phase increases the rising velocity of the droplets. At low gas throughputs this causes an initial sinking of the hold-up as shown in Fig. 2 b. In this range the energy input by the gas phase is not yet so substantial that an increase of the turbulence and thus of the droplets dispersion takes place, Fig. 2 b.

The gas hold-up x_G in Fig. 3 seems to be related to the liquid dispersed phase hold-up in Fig. 2 a. In both Figs. the inclination of the hold-up curves decreases with smaller flow-rates of the solvent-phase u_D . The gas hold-up itself never exceeded a value higher than 12 % of the total column volume, which is probably dependent on the system investigated and on the type of packing. Investigating the system kerosene (D)-air-water in a packed column of 52 mm in diameter filled with 1/4" Raschig rings Diaz, Aguayo and Alvarez (7) found out, that the gas hold-up was always less than 7 %.

Conclusions

The separation efficiency and the capacity of packed columns can be considerably increased by feeding an inert gas into the column. Relatively small gas flow rates give the highest efficiency of the column. The description of the hydraulic and the mass transfer rates in mathematical terms must be the subject of further studies.

Notation:

d_s	Column diameter, m
d_{VS}	Sauter mean diameter of droplets, m
H	Height of the packing, m
HTU_{OC}	Overall height of transfer unit in the continuous phase, m
u_C, u_D	Flow rates of continuous and dispersed phase per unit area of column cross-section, $m^3/(m^2 \cdot s)$
u_G	Flow rates of gas phase per unit of column cross-section, $Nm^3/(m^2 \cdot s)$
β	Phase velocity ratio, $\beta = u_G/u_D, ((Nm^3/(m^2 \cdot s)) / (m^3/(m^2 \cdot s)))$
ϵ	Void volume fraction, m^3/m^3
λ	Phase velocity ratio, $\lambda = u_D/u_C$

References

- (1) Billet, R., Mačkowiak, J., vt "Verfahrenstechnik" 15 (1981) 12, p. 898
- (2) Ziebland, G., Hackl, A., Chem. Ing. Techn. MS586/78
- (3) Tijmstra, S., U.S.-Pat. 2.083.497
- (4) Priestley, R., Ellis, S.R.M., Chem. and Ind. (1978) 19, p. 757
- (5) Milyakh, S.V., Ivanova, V.D., Int. Chem. Eng. 18 (1978) 1, p 112
- (6) Priestley, R., Suppiah, S., Proc. Int. Solvent Extraction Conf., Denver, CO, 1983, p. 139
- (7) Diaz, M., Aguayo, A.T., Alvarez, R., Chem. Ing. Techn. MS 1439/86

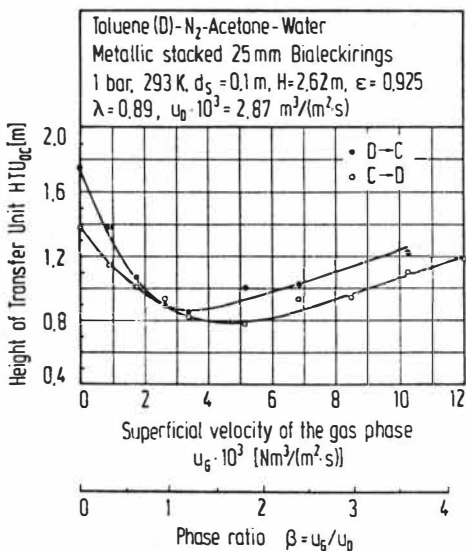
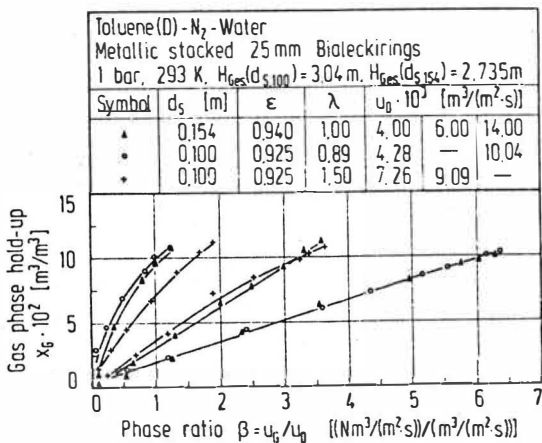


Fig. 1:

Height of a transfer unit
 HTU_{OG} as a function of the
superficial velocity of the
gas phase and of phase ratio
 $\beta = u_g/u_0$

Fig. 3:

Gas phase hold-up x_G
as a function of the
phase ratio $\beta = u_g/u_0$



Toluene(D)-N ₂ -Water						
Metallic stacked 25 mm Bialeckirings						
1 bar, 293 K, H(d _{S,100}) = 2,62 m, H(d _{S,154}) = 2,495 m						
Symbol	d _S [m]	ε	λ	u _D · 10 ² [(m ³)/(m ² ·s)]		
▲	0,154	0,940	1,00	4,00	6,00	14,00
•	0,100	0,925	0,89	4,28	—	10,04
•	0,100	0,925	1,50	7,26	9,09	12,50
•	0,100	0,925	5,00	7,20	11,50	15,50

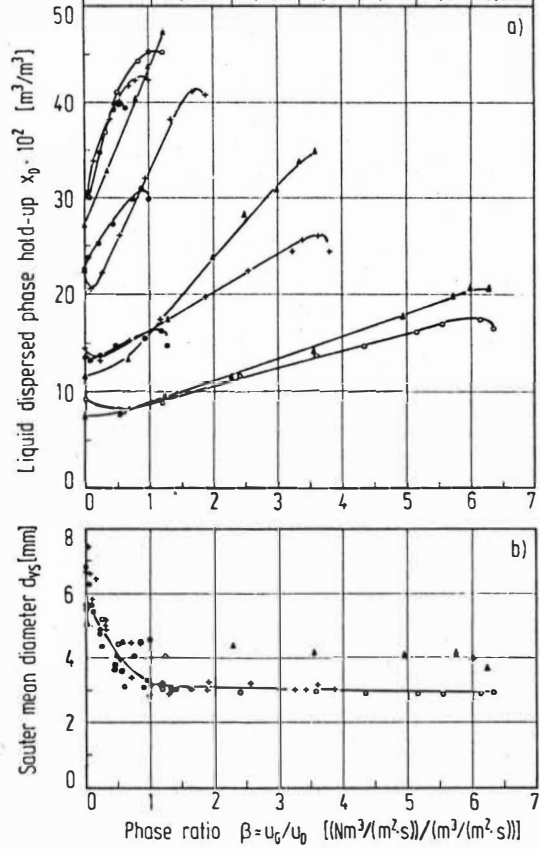


Fig. 2: a) Liquid dispersed phase hold-up x_D
 b) Sauter mean diameter of droplets
 as a function of the phase ratio
 $\beta = u_G/u_D$

J.H. Bae, L.L. Tavlarides, Syracuse, NY/USA

A method for the determination of the bivariate distributions of drop volume and drop metal concentration in a continuous flow agitated dispersion is described to afford a greater comprehension of drop mixing and its effect on the extractor performance. The system considered is cobalt nitrate-acetate buffer/di-(2-ethylhexyl)phosphoric acid-toluene. The chemical equilibria and kinetic models have been determined by Lee and Tavlarides (1,2). A Monte Carlo Simulation procedure, previously developed by Hsia and Tavlarides (3,4), Bapat and Tavlarides (5), and Smith and Tavlarides (6) is employed with the above equilibrium and kinetic models to predict the effect of drop mixing on extraction efficiency for various process variables (1).

In order to obtain bivariate (concentration and size) distribution data experimentally, a special sampling technique is employed. Verhoff et al. (7,8) designed a special sampling probe which was used to withdraw a sample of dispersion from the mixing vessel, protect the sample with a surfactant, and to force the dispersion sample through a photometer assembly which measures both size distributions and dye concentrations of drops. They dissolved a nontransferring dye in the dispersed phase to measure drop mixing frequencies. Janjua (9) developed a laser-capillary probe to measure only drop size for the heptane-water system. Light transmission differences due to different refractive indices of the aqueous and dispersed phases in the capillary were measured. He also compared these drop size distributions with the data obtained from a photographic method. Measurements were made at different locations for three sizes of batch reactors. Weiland et al. (10) developed a photoelectric capillary probe device for the measurement of bubble size distribution using a technique similar to that reported by Pilhofer et al. (11). However, their signal condition was designed to respond to the level of light absorption, rather than the intensity of light transmission. The work discussed here extends these previous studies using the capillary measurement technique to obtain bivariate distribution data (concentration and size) for liquid-liquid extraction systems.

Capillary Measurement Technique

This method involves the use of a fine bore capillary of the order of the smaller droplet sizes in the liquid-liquid dispersions present in solvent extraction processes of interest. A sample stream of the dispersion is drawn from the mixing vessel, and the drops are converted to cylindrical slugs of equivalent volume as they pass through the capillary. Figure 1 shows a light ray diagram for a section through the capillary. An appropriate light source is used to distinguish between the slugs of dispersed and continuous phase as the sample passes

by two detection points. A He-Ne laser of 632.8 nm wavelength is selected as a light source, since cobalt complex in toluene has a molar extinction coefficient of 250 l/mol.cm at 630 nm (12). The laser beam is carefully directed by a system of lenses and slits in such a way that it is focused exactly in the center of the capillary. It is essential that the beam be precisely focused to penetrate the capillary without refraction. The output light beam from the capillary is focused on a photosensitive detector on the other side of the capillary. Since light absorption by the cobalt complex in the dispersed phase is stronger than the absorption by cobalt solution in the continuous phase, a lower light signal is achieved at a photodiode detector if drops cross the light sensor. The output of the photodiode circuit, which consists of amplifiers and comparators, is a voltage signal in a series of random rectangular pulses. The height of each pulse is proportional to the cobalt complex concentration, and the width of each pulse to the drop volume. The dispersed slug volume and equivalent spherical drop diameter are calculated using the known capillary bore diameter (76, 100 or 200 μm) and the drop velocity (1,9,10,11,13). The concentration of the drop is calculated through calibration of the pulse height for a known reference concentration of cobalt complex in toluene.

Capillary Technique Apparatus

Figure 2 shows a flow diagram for the capillary sampling technique. The capillary tube, which has a funnel-shaped entrance with a cone angle of approximately 60° , is immersed at the sampling point in the agitated vessel. The capillary is supported by a capillary adaptor, which is made of viton rubber. A continuous sample of dispersion is withdrawn through the capillary by the vacuum pump. The vacuum jar pressure is controlled by a pressure controller or air bleed valve. An IBM PC with a MetraByte DASH-16 A/D Converter and 2 MegaByte RAM board employing the extended memory specification is used to sample and process the output signals from the photodiode circuit. These signals are also traced on an oscilloscope screen.

For comparisons with the bivariate data obtained above, a photomicrographic system for drop size measurement and two phase separation assemblies for average cobalt concentration measurements in the continuous and dispersed phase are installed in the stirred cell (14,15). The cell is also equipped to measure dispersed phase hold-up with our ultrasonic technique developed by Bonnet and Tavlarides (16).

Future Work and Conclusions

Experiments will be conducted at various operating parameters of residence time, phase fraction and impeller rotational speeds to obtain extraction efficiencies for the cobalt ion in the system mentioned above. The effect of drop mixing frequencies on extraction efficiencies will be measured by the above techniques. These results will be compared with calculated results employing the

kinetic model for the reaction systems (1,2) and the Monte Carlo Simulation methods developed previously (1).

It is expected that these experimental techniques coupled with the computational model for reactive liquid dispersions will permit a detailed analysis of mixing effects on extraction efficiencies and selectivity for liquid-liquid extraction systems.

Acknowledgment

The financial support provided by the Department of Energy, Office of Basic Sciences, Chemical Science Division through the contract DE-AC02-82 ER13002 and Exxon Educational Foundation are gratefully acknowledged.

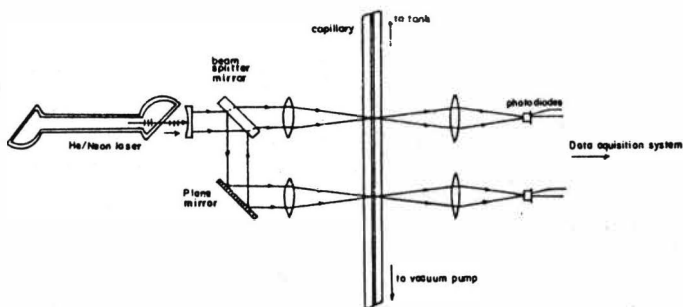


Figure 1 Key Diagram for Capillary Spectroscopy

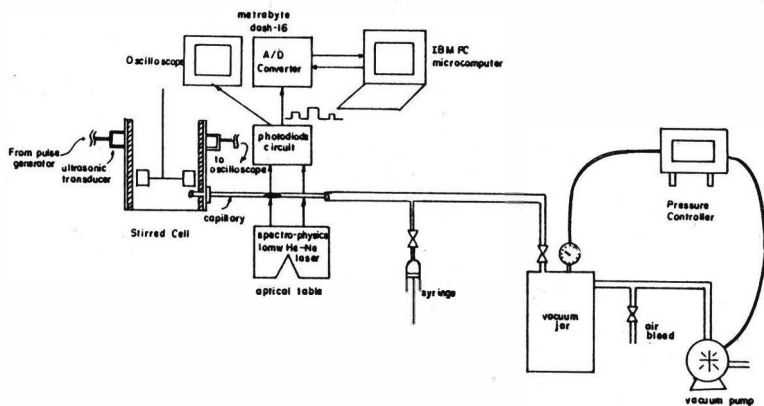


Figure 2 Capillary Spectroscopy Set-up

References

- (1) L.L. Tavlarides, C.K. Lee, S. Mukkavilli, J. Bae, and I. Hahn, paper presented 4th Symposium on Separation Science and Technology for Energy Applications, October 20-24, 1985, Knoxville, Tennessee, To be published in Separation Science and Technology.
- (2) C.K. Lee, Ph.D. Thesis, Syracuse University, Syracuse, NY (1986).
- (3) A. Hsia and L.L. Tavlarides, Chem. Eng. J., 25, 225 (1980).
- (4) A. Hsia and L.L. Tavlarides, Chem. Eng. J., 26, 189 (1983).
- (5) P.M. Bapat and L.L. Tavlarides, Chem. Eng. Sci., 38, 2003 (1983).
- (6) G.W. Smith, L.L. Tavlarides, and J. Placek, paper presented at the Annual AIChE Meeting, Chicago, IL (1985).
- (7) F.H. Verhoff, Ph.D. Thesis, Department of Chemical Engineering, Ann Arbor, Michigan (1969).
- (8) F.H. Verhoff, S.L. Ross, and R.L. Carl, Ind. Eng. Chem., Fundam., 16, 3, 371 (1977).

- (9) K.M. Janjua, Ph.D. Thesis, Imperial College of Science and Technology, London (1982).
- (10) P. Weiland, L. Brentrup and V. Onken, Ger. Chem. Eng. 3, 296 (1980).
- (11) T. Pilhofer and H.P. Miller, Chem.-Ing.-Tech. 44, 295 (1972).
- (12) J.H. Bae, Lab. Notebook, Syracuse University, Syracuse, N.Y. (1985).
- (13) G. Goldman and E. Blass, CHISA '84, V 1.14 (1984).
- (14) P.M. Bapat, Ph.D. Thesis, Illinois Institute of Technology, Chicago, Illinois (1982).
- (15) C.A. Savastano, M.S. Thesis, Syracuse University, Syracuse, N.Y. (1984).
- (16) J.C. Bonnet and L.L. Tavlarides, Ind. Eng. Chem., Fundam., Submitted.

V. Kirou, J.C. Bonnet and L.L. Tavlarides

Department of Chemical Engineering and Materials Science
Syracuse University, Syracuse, NY 13244

Hydrodynamics in a Multistage Column Extractor:
Axial Holdup and Drop Size Distribution

Conventional design of process equipment used in solvent extraction technology involves expensive, time-consuming scale-up techniques. Little consideration is given to recent advances, such as droplet rate processes and hydrodynamic behavior of liquid-liquid systems. A rational design of a liquid-liquid contactor should be based on a fundamental modelling approach. Elimination of the inefficient empiricism can be realized only through implementation of knowledge presently available. In this research program, the interval of quiescence simulation model [1,2] is to be used to account for the effects of drop size distribution, dispersed phase holdup and interdroplet mixing on column performance.

To verify and improve the model during various stages of development, and obtain model parameters, a fully instrumented seven stage counter current extractor has been commissioned. The column features include: glass pipe construction of 12.5 cm diameter and 110 cm in length, seven 12.5 cm height mixing compartments, six-bladed turbine impellers located centrally in each compartment, 316 stainless steel construction of wetted metal parts, five sampling ports for photomicrographic drop size measurements, seven pairs of continuous and dispersed phase sampling heads for concentration measurement, six stations for ultrasonic measurements of dispersed phase holdup, instrumentation for flow measurement and auxiliary equipment. The column station along with the feed storage station is shown in Figure 1.

Drop Size Distribution Measurements

The drop size distribution is being determined by an in situ photomicrographic technique. The probe, a miniaturized adaptation of a previous technique [3], is capable of measuring drop diameters between 50-4000 microns. The photomicrographic probe is shown in Figure 2. A Zeiss MOP-30 particle size analyzer interfaced with an IBM personal computer is being used for data processing.

Ultrasonic Technique for Dispersed Phase Holdup Measurements

An ultrasonic technique developed in our laboratories [4,5] is being used to determine the dispersed phase holdup by measuring the velocity of ultrasound in the dispersion. Two piezoelectric transducers, a pulse generator, an amplifier and an oscilloscope are the basic elements of this technique. Holdup can be estimated simply by measuring the transmission time of the sound pulses. Important features are that the transducers are located on the outside of the column wall and the technique is independent of the shaft position in the acoustical path.

Solute Concentration Measurements

For solute concentration measurements the phases are separated by a modified filtration-coalescence technique developed earlier [6,7]. The sampling probes are shown in Figure 3 and can separate the phases for dispersed phase holdup 4 to 20% and drop diameters between 200-1000 microns.

Preliminary Results

The above described apparatus will permit determination of axial holdup distribution, drop size distribution and concentration distribution (for mass transfer experiments) as a function of operating parameters. Figure 4 shows the axial variation of holdup fraction versus cell position at various rotational speeds, for the toluene/water system (phases mutually saturated). The mode of operation is counter current with the dispersed phase fed at the bottom of the column. In all cases a maximum can be observed in holdup. This maximum shifts to the inlet stage, with increasing impeller speed.

Also, the technique permits the transient evolution of the axial dispersed phase holdup variation to be followed. For future experiments, axial drop size distribution measurements will also be obtained concurrently with backmixing parameters for each phase.

It is expected that the Monte-Carlo simulation technique developed in our laboratories can be extended and expanded upon to model this countercurrent extractor. Such potential capabilities will permit delineation of the effect of operating parameters on column characteristics such as flooding point and maximum throughput. Extension of the above model to extractive/reactive systems is obvious.

Acknowledgement

The financial support provided by the National Science Foundation, Grant No. CPE 8310 223 and partial support by Exxon Educational Foundation are gratefully acknowledged.

References

- (1) Bapat, P.M., L.L. Tavlarides, and G.W. Smith, "Monte Carlo Simulation of Mass Transfer in Liquid-Liquid Dispersions," Chem. Eng. Sci., 38, 2003 (1983).
- (2) Bapat, P.M., and L.L. Tavlarides, "Mass Transfer in a Liquid-Liquid CFSTR," AIChE J., 31, 659 (1985).
- (3) Coualoglou, C.A., and L.L. Tavlarides, "Description of Interaction Processes in Agitated Liquid-Liquid Dispersions," Chem. Eng. Sci., 32, 1289 (1977).(4)
- (4) Bonnet, J. and L.L. Tavlarides, "Determination of Dispersed Phase Holdup in Agitated Extraction Units by an Ultrasonic Technique," 35th Canadian Chemical Engineering Conference, Calgary, Alberta, Canada, Oct. 6-9, 1985, presentation and preprint.
- (5) Bonnet, J., and L.L. Tavlarides, "An Ultrasonic Technique for Dispersed Phase Holdup Measurements," I.E.C. Fundls, submitted for publication.
- (6) Bapat, P.M., and L.L. Tavlarides, "Phase Separation Technique for Liquid Dispersions," I.E.C. Fundls, 23, 120 (1984).
- (7) Bonnet, J., and E.V. Jeffreys, "Hydrodynamic and Mass Transfer Characteristics of a Scheibel Extractor. Part II: Backmixing and Stage Efficiency," AIChE J., 31, 755 (1985).

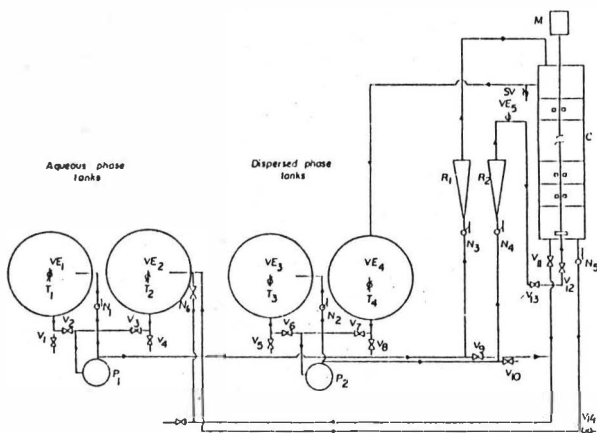


Figure 1:

Liquid-liquid extraction pilot plant

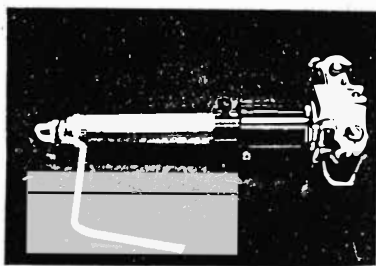
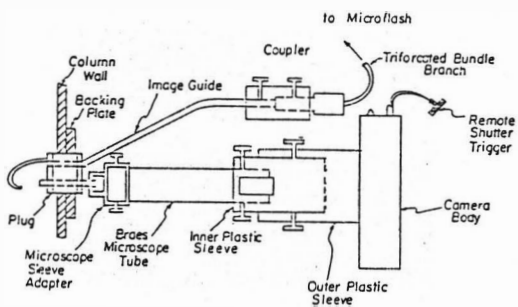


Figure 2:
Photomicrographic Probe

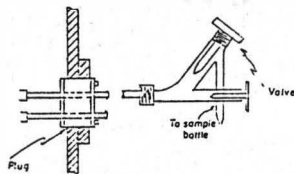
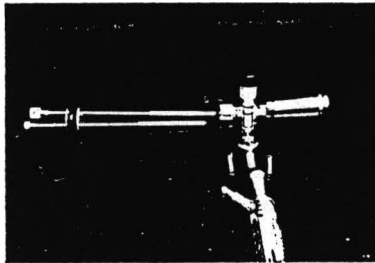


Figure 3:
Concentration Sampling Probe

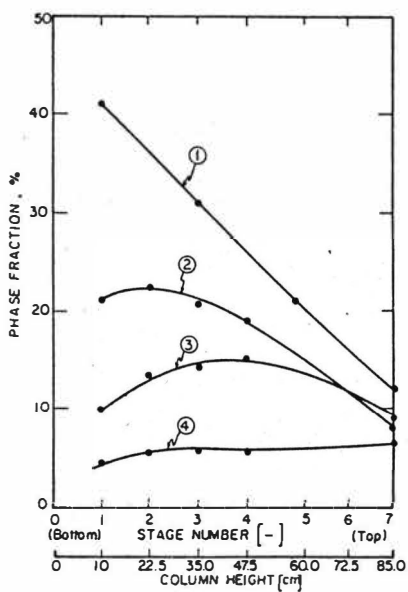


Figure 4

Axial distribution of dispersed phase fraction versus column height at various r.p.m. for counter current operation for mutually saturated water-toluene system: $V_d = .027$ cm/s, $V_c = .163$ cm/s, 1: 250 rpm, 2: 200 rpm, 3: 180 rpm, 4: 160 rpm

Study on Scale Up of Kühni Column

Jiang Yu Ming and Sun Bing Yao

East China Institute of Chemical Technology, Shanghai, China

Introduction

The Kühni column with agitated turbine and multicompartement is an advanced liquid-liquid contactor. The column can be designed to obtain minimal axial mixing, constant hold up of dispersed phase, and maximum capacity for each column section (1). This design capability thus provides a large degree of flexibility and an overall high efficiency for several applications.

Now Kühni column has been extensively applied in many industrial fields, such as petrochemical industry, phosphoric acid and citric acid purification, extraction of vitamins and waste water treatment.

Effectively the largest pilot column ever built has 90 stages (2), the tallest industrial size column has 50 stages, and the diameter has over 2 meters.

Recently many scientists (3,4) have studied hydrodynamics and axial backmixing of Kühni column, but few reports have published on conditions of practical mass transfer. According to the report of the literature (5), the authors have designed two Kühni columns and applied in extraction and stripping separately. Under different operation conditions holdup, dropsize distribution, power consumption and extraction efficiency have been observed so as to find a real procedure of scale up.

Experiment

1, The structure of Kühni column

Two same Kühni columns of 200 mm diameter and 7200 mm total height have been designed and erected for extraction and stripping respectively. Kühni column comprised 40 compartments, and each compartment of 90 mm height has been combined by a six-bladed turbine and a stator plates. The outer and inner diameter are 85 mm and 45 mm.

In order to obtain minimal axial mixing and maximum capacity for each column section, three kinds of stator plates containing the different available free areas of 16%, 34% and 40% have been designed (the experimental data below are by using the stator plate of 16%).

The driver of column is electric motor and shaft speed can be changed by a controller.

2, Flow sheet

A schematic diagram of apparatus is shown in Fig. 1.

The experimental procedure can be divided three stages, the first stage is dynamics test, the water-kerosene system is carried in a single column. Water and kerosene are placed in 2 and 1 separately, then countercurrently contacted in column 4, the rotameter 5 is used for controlling the flow rate of two phases. Holdup, drop size distribution and power consumption are measured so as to optimize the operational conditions. The second stage is mass transfer test, the treated liquid contains organic acid and solvent is mixed by a neutral phosphate compound and diluent. The loaded solvent is stripped by pure water, the extraction and stripping are carried out in column 4 and 6 separately. The third stage is pilot plant test, the loaded solvent from column 4 is directly pumped into column 6 to be stripped by pure water, then the refresh solvent is recycled into column 4 to extract organic acid from material liquor. The purpose of pilot test is to examine the operational stability of two columns.

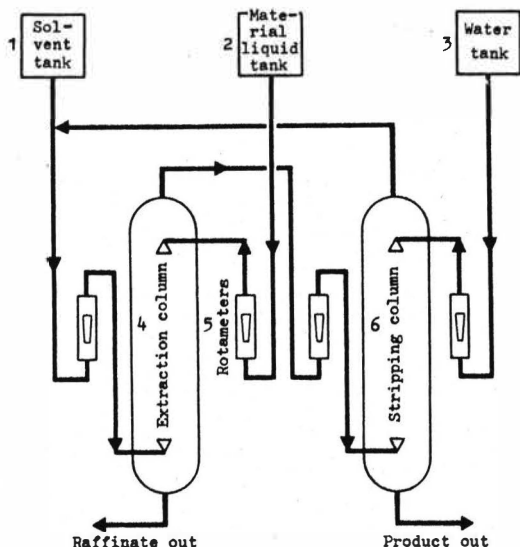


FIG. 1 FLOW SHEET

Experimental results

1, Hold up

The system used for the experimental work were water/kerosene, experiment were carried out at 20°C and the flow rate of water and kerosene were 0.002 and 0.005 m³/min the hold up measured are given in Table 1.

Table 1 Hold-up measurement

N, r.p.m.	V ₀ , liter	x, %
80	5.54	4.20
120	6.50	4.91
155	12.5	9.50
180	18.5	14.0
200	32.8	24.8
260	65.3	49.5

By the eye it is found that when the speed is lower than 155 r.p.m. the drop is larger and clear, increasing the speed will result in decreasing drop size, when the speed is 260 r.p.m., phase inversion will happen.

Hold up was determined by Thornton, J. D. (6) as follows:

$$X_f = \frac{(L^2 + 8L)^{0.5} - 3L}{4 - 4L}$$

here $L = U_d/U_c$.

The hold up at the flooding point was correlated by Thornton's equation, $X_f=0.396$,

it is a reasonable explanation why phase inversion happened at the speed of 260 r.p.m. and the speed between 100 and 200 r.p.m. is suitable for Kuhn column under these operational conditions.

2, Power consumption

Up to now, no literature published refers to the power consumption of Kuhn column, but the empirical equation of Scheible, E. G. (7) is effective for calculation of power consumption of turbine.

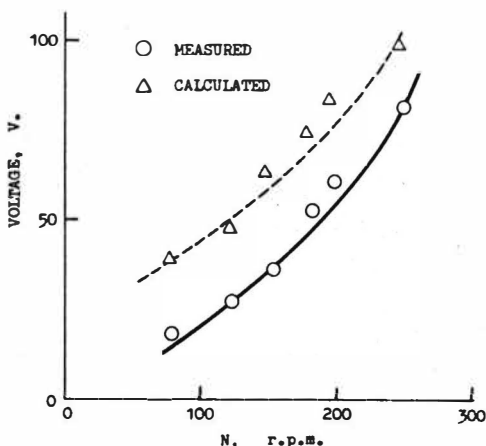


FIG. 2 THE RELATIONSHIP BETWEEN V AND N

$$P = 1.85 \frac{d_1^5 \rho N^3}{g_c} \quad \text{for each turbine.}$$

The data calculated from above equation and measured were plotted in Fig. 2, the slopes of every point are very similar and the difference between two curves can be explained as the friction loss of power.

3, Drop size distribution

Fischer A. (8) measured drop size for a broad range of operational conditions and a wide variety of liquid-liquid systems. A photographic method has been chosen for the determination of drop size, it is found that the drop size distribution in Kuhn column is best approximated by a Mugele-Evens relationship.

The photographic method was also adopted by the author's, the data measured are plotted in Fig. 3 with comparison of Fisher's data under same systems, it is found that the both data are in very close agreement.

4, Extraction

The operational conditions are as follows:

T = 15°C solvent : kerosene + TRPO
 Material liquor containing organic acid 110 g/l.
 Flow rate: org. 0.005 M³/min. aqu. 0.002 M³/min.

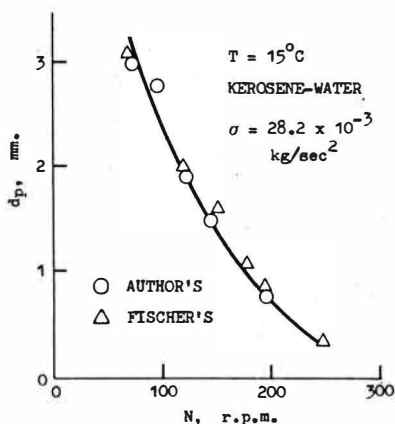


FIG. 3 DROP SIZE DISTRIBUTION

Table 2 Data of extraction

N, r.p.m.	Raffinate, g/l	Solvent loaded, g/l	η , %
85	42.7	8.0	92.7
110	48.3	7.1	93.6
115	53.0	7.1	93.6

It is found from Table 2 that the hold up measured of $X_d=6.85\%$ under these conditions is far away from the flooding point and the design of column could be recognized to meet expectation.

5, Stripping

$T = 90^{\circ}\text{C}$ The loaded solvent containing organic acid 44.2 g/l.

Flow rate: Org. $0.005 \text{ M}^3/\text{min}$.

Aqu. $0.002 \text{ M}^3/\text{min}$.

By using pure water, the aqueous phase from stripping column will be pure organic acid solution.

Table 3 Data of stripping

N, r.p.m.	Org. acid, g/l	Loaded solvent, g/l	η , %
170	97.2	5.3	88.0
170	101	5.0	88.7
170	99.0	5.0	88.7

It is also found from Table 3 that the stripping column would meet the demands of design.

6, Pilot test

The loaded solvent from extraction column was transported into stripping column to be stripped by pure water, then the refresh solvent was recycled into extraction column to extract organic acid from material liquor. So the two Kühni column were linked, the practical data of pilot test were shown as follows:

Extraction: $T = 7^{\circ}\text{C}$ $N = 120$ r.p.m.
Material liquor containing organic acid 99.0 g/l.
Loaded solvent containing organic acid 42.0 g/l.
 $\eta = 97.0\%$

Stripping: $T = 90^{\circ}\text{C}$ $N = 175$ r.p.m.
Pure solution containing organic acid 79.8 g/l.
Solvent from stripping containing organic acid 7.0 g/l.
 $\eta = 82.1\%$

It is shown that Kühni column can provide a large degree of flexibility and an overall high efficiency.

Conclusion

- 1, Kühni column can be designed to obtain lower power consumption, constant hold up of dispersed phase and high mass transfer efficiency, and Kühni column can be also applied in multi-stage (more than 10 stages) liquid-liquid extraction process.
- 2, Dynamics test shows that the calculation of hold up implies Thornton's equation.
- 3, Scheible's equation can be applied for calculation of power consumption of the turbine of Kühni column.

Notation

d_i turbine mixer diameter, m.
 g_c gravity acceleration, m/sec^2 .
 L ratio of phases
 N turbine speed, r.p.m.
 P power consumption, kw
 U_d flow rate of dispersed phase, M^3/min .
 U_c flow rate of continuous phase, M^3/min .
 V_o dispersion volume, M^3
 X hold up efficiency, %
 X_f hold up efficiency at flooding point, %
 ρ density, kg/M^3

References

- (1) Teh. C. Lo, Baird M. H. I., Hanson H. "Handbook of Solvent Extraction", John Wiley & Sons, New York 1983.
- (2) Ingham J., ISEC'74 Proceedings, 1974.
- (3) Vatai G., ISEC'83 Proceedings, 1983.
- (4) Vankatarama J., Can. J. Chem. Eng., 58, 206, 1980.
- (5) The Specification for Kühni Column from Kühni Ltd., 1983.
- (6) Thornton, J. D., Chem. Eng. Sci., 2 (5), 1956.
- (7) Scheible E. G., US Patent 2,856,362, 1958.
- (8) Fisher A., Chemische Rundschau 26, 1, 1973.

Aspects Of Pulsed Sieve Plate Column Behaviour

A. Hussain and M.J. Slater, Schools of Chemical Engineering, University of Bradford, Bradford, U.K.

and

A. Marrocchelli, ENEA, Rome, Italy.

Introduction

Pulsed sieve plate columns have found use in industry, yet there are many aspects of behaviour which are not well understood and design from first principles is not feasible with reasonable certainty of performance⁽¹⁾. We have conducted experiments under well-regulated conditions to establish a better basis for interpretation of hydrodynamic and mass transfer performance. In particular we have studied the motion of single drops through a stack of plates of various geometries, the overall dispersed phase mass transfer coefficient for single drops, and continuous phase axial mixing due to pulsing alone (in the absence of flows).

The glass column used for studying drop behaviour was 76 mm diameter and contained a plate stack of about 1 m high with plates of the following geometries (Figure 1):

Table 1

Free Area, e	0.09	0.22	0.40	0.40	0.40
Hole Size, d_o , mm	3.18	3.18	3.18	4.0	6.5

and plate spacings of 50, 100, 150, 250 mm and no plates. The stainless steel plates were 1.5 mm thick and holes were straight sided. Three steel rods of 6 mm diameter held the plate stack together. The free area values are nominal for the plate since the plate/wall gap has been neglected.

Drop Rise Velocities

Hydrodynamic behaviour of counter-flow columns can be described using a slip velocity correlated with a function of dispersed phase hold-up such that at very low hold-up the slip velocity equals a characteristic velocity.

In this work the characteristic velocity of single, widely-spaced solvent drops of known diameter in water was measured as a function of drop size, plate hole size, plate free area, plate spacing, pulse frequency and amplitude, all under conditions of no mass transfer. Drops were formed at the tip of a horizontal hypodermic needle within the pulsed liquid. The average time of passage of each of 50 drops over 1 m was used to calculate the velocity. Drop sizes were always smaller than plate hole diameter. All the materials used were stainless steel, glass or Teflon. The solvents were hexane, MIBK, n-butanol and toluene; the phases were mutually saturated.

Results have been correlated empirically by separating the influences of pulsation and geometry and in particular using results for no plates with and without pulsing and results for motion of drops through plates without pulsing. The characteristic velocity is compared to measured terminal velocity (no plates, no pulsing). The equations given by Grace⁽²⁾ for mobile drops agree with the terminal velocities measured (using measured physical properties).

An empirical equation which can be used to correlate all results is:

$$V_K/V_T = 1 - [d/(1 + \beta H_c)d_0] - [fA_p/(1 + 0.7\beta H_c) - (fA_p)^2/(1 + 2.6H_c)] \quad (1)$$

$$\beta = 0.275 + 0.365e \quad (\text{cm}^{-1})$$

$d < d_0$, $f \text{ s}^{-1}$, $A_p \text{ cm}$, $H_c \text{ cm}$, $d_0 \text{ cm}$, $d \text{ cm}$. 470 data points are correlated within $\pm 15\%$.

In order to obtain a better understanding of drop behaviour further examination of drop motion has been made using video film. It appears that drop velocity between plates is nearly the same as that achieved in the absence of plates and the time delay suffered at each plate depends on whether the pulse is upwards or downwards when the drop reaches the plate (Figure 2). The time delays vary from plate to plate and there may be a dependence on drop size relative to hole size, and on free area. An empirical correlation of the time delay is still required at present.

The characteristic velocity measured and correlated this way is probably more reliably estimated than with dimensionless group correlations presently available⁽³⁾. However, for practical use the drop size distribution expected needs to be known. The equations proposed by Misk⁽⁴⁾ and Boyadzhiev⁽⁵⁾ might be used to estimate a Sauter mean diameter and the work of Slater⁽⁶⁾ to obtain the consequent parameters of a Mugele-Evans distribution of sizes.

Mass Transfer Coefficients

Drops of cumene were passed through an aqueous solution of 35-40 kg/m³ isobutyric acid. The properties of this system are known⁽⁷⁾. Drops were collected in the neck of an inverted glass funnel at the top of the plate stack. A small diameter stainless steel tube could be moved up and down with the tip in the neck region. The tube was connected to a small sample bottle via p.t.f.e. tubing and then to a rubber bulb for creating vacuum or pressure. The glass tubing leading to the funnel was sealed around the steel tube (using p.t.f.e. tape) so that pulsation from the column liquid was not transmitted to the water/solvent interface in the funnel: disturbance of the interface might enhance mass transfer to an unacceptable degree. Plates of 3.18 mm hole diameter and 22% free area only were used.

An experiment was started by achieving a steady flow of drops: the time to form 50 drops was noted - single drop formation time was less than 1 s. Knowing the solvent flow rate a drop size could be calculated; these were in the range 2.2 to 3.0 mm with most being 2.7 to 2.8 mm. The

interface region in the funnel neck was cleared of solvent then a sample of solvent (2 ml) was collected and analysed for isobutyric acid. The time to form 50 drops was again noted and the rise time of each of 50 drops was measured.

A time-averaged overall mass transfer coefficient K_{od} was calculated from the equation:

$$(y_{out} - y_{in}) / (y^* - y_{in}) = 1 - \exp(-6 K_{od} t/d) \quad (2)$$

The equilibrium value y^* was obtained from the equilibrium curves:

$$y^* = 4.325 - 1.487x + 0.504x^{1.586} \quad (\text{kg/m}^3) \quad (3)$$

putting x equal to the aqueous phase concentration, and y_{in} was zero. The time was taken as rise time plus formation time, the rise time being of the order of ten times larger than formation time.

The data illustrate several interesting features (Figure 3). The value of K_{od} (at constant drop size) varies little with agitation and is not affected by the various combinations of frequency and amplitude used, up to the point at which drops break. The influence of the number of plates in the stack is not marked and experiments in the absence of plates but with pulsation show that the influence of the plates is not great. In the absence of plates and pulsation the value of K_{od} agrees with earlier work done on the system and is only slightly lower than K_{od} values obtained with plates and pulsing. Other workers^(8,9) have noted that agitation influences drop size and hence interfacial area but not the mass transfer coefficient to a marked extent.

Previous work suggests that the mass transfer rate is controlled mainly by the extent of internal motion in the drop and in the present case K_{od} values are intermediate between values appropriate to rigid drop and well-mixed drop conditions. It would appear that substantial increases in K_{od} might be achieved by allowing drops to coalesce and redisperse rather than by agitating more vigorously. In some systems the resistance to mass transfer may be mainly in the continuous phase, a case which remains to be examined for single drops.

Continuous Stationary Phase Axial Mixing

Correlations in the literature for continuous phase axial mixing coefficients for flowing single phase conflict to a large extent and agreement on the influence of hole size, free area, spacing, flow rate and dependence on frequency and amplitude is poor⁽¹⁰⁻¹⁶⁾. In this work we have conducted experiments with no flow to assess the effect of pulsation only.

The column was filled with distilled water. In the base of the column between the bottom plate and the pulse leg was placed the dense liquid trichloro-ethane to prevent acid tracer leaving the section containing plates. A tracer of 10 ml of 1 M hydrochloric acid was injected using a hypodermic needle below the bottom stage and the conductivity change was noted just above

the top stage. For such a closed end system the response according to the dispersion model of axial mixing is^(17,18):

$$\phi = (C - C_i)/(C_f - C_i) = 1 + 2 \sum_{n=1}^{\infty} \exp(-n^2 \pi^2 \alpha) \cos(n\pi) \quad (4)$$

where $\alpha = E_o t/L^2$. When $\phi = 0.506$, $\alpha = 0.14$ and $t = t_{0.506}$, hence $E_o = 0.14L^2/t_{0.506}$.

Experiments have been conducted with columns of three diameters (25, 76, 152 mm) containing plates with holes of three sizes and three free areas, spaced at different intervals.

Equal weighting of data with respect to all the variables was not attempted so computer aided fitting of equations has to be treated with caution. However to ascertain the relative importance of parameters the data were initially fitted by the equation:

$$E_o = 2.360 \times 10^{-3} f^{0.78} A_p^{1.22} e^{-1.19} H_c^{0.57} d_o^{-0.30} D_c^{-0.08} \pm 38 \times 10^{-6} \text{ m}^2/\text{s} \quad (5)$$

The frequency range is 0.5 to 1.78 s⁻¹ and the amplitude range 5.5 to 47.8 mm. It is clear that the axial dispersion coefficient is not a simple function of the product $f A_p$ or of $f A_p^2$ which has dimensions of E_o . The small influence of column diameter and hole size is notable. Reported variations of the axial mixing coefficient with column diameter are therefore probably associated with flow effects rather than geometrical effects alone⁽¹⁹⁾.

Further correlation of the data is based on power consumption calculated from the relationship:

$$P_m = (f^3 A_p^3)(1 - e^2)/2 C_o^2 H_c e^2 \text{ W/kg (or m}^2/\text{s}^3) \quad (6)$$

and dimensional analysis for eddy diffusion⁽²⁰⁾ which gives:

$$E_o \propto P_m^{0.33} l^{1.33} \text{ m}^2/\text{s} \quad (7)$$

where l is an appropriate length parameter. An acceptable equation found to represent the variation of E_o with all the variables in a reasonable manner is (Figure 4):

$$E_o = 2.34 \times 10^{-3} P_m^{0.33} A_p^{0.35} H_c^{0.98} e^{-0.60} \text{ m}^2/\text{s} \quad (8)$$

with a standard deviation of $44 \times 10^{-6} \text{ m}^2/\text{s}$. The numerical coefficient is dimensionless. The range of P_m is 0.3 to 1027 W/kg. Other equations presented in the literature modified by putting continuous phase velocity to zero give inferior results. Data for H_c other than 50 mm are not well-fitted by equation (8).

It must be noted that in calculating P_m the value of the discharge coefficient C_o is taken as 0.6. In the Reynolds number range of interest ($\rho_c d_o f A_p / \mu_c < 400$) C_o is a function of Reynolds number⁽²¹⁾ and further refinement of the correlation is possible using measured values of C_o . However, the improvement is slight.

Once values of E_o are known the further effects of continuous phase flow rate can be assessed. Our own work shows that the continuous phase axial mixing coefficient obtained when the phase is flowing can be adequately correlated in the manner:

$$E = E_o (1 + V_c / 2 f A_p) \quad (9)$$

for column diameters up to 152 mm. However, at larger diameters this equation may not be valid if velocity profiles develop⁽¹⁹⁾.

Conclusions

The simple techniques discussed yield data which are helpful for preliminary design work and for improving understanding of liquid-liquid extraction column performance. The cost of equipment involved is small and much less than a pilot plant, construction of which at present is an expensive proposition in many cases. Use of the techniques discussed in this note could at least reduce the amount of pilot work to be carried out.

Nomenclature

A_p	pulse amplitude (maximum travel)
C	tracer concentration
C_f	final tracer concentration
C_i	initial tracer concentration
C_o	discharge coefficient
d	drop diameter
d_o	plate hole diameter
D_c	column diameter
e	plate free area
E	axial mixing coefficient for flow conditions
E_o	axial mixing coefficient for non-flow conditions
f	frequency
H_c	plate spacing
K_{od}	overall dispersed phase mass transfer coefficient
l	length parameter
L	column length
P_m	power per unit mass
t	time
V_c	superficial continuous phase velocity

V_K	characteristic drop velocity
V_T	terminal velocity
x	aqueous phase concentration
y	solvent phase concentration

References

1. Logsdail, D.H., Slater, M.J., Chapter 11.2 in "Handbook of Solvent Extraction", edit. Lo, T.C., Baird, M.H.I., Hanson, C., pub. Wiley 1983.
2. Grace, J.R., Wairegi, T. and Nguyen, T.H., Trans. I. Chem. E., 167, 54, 1976.
3. Logsdail, D.H., Thornton, J.D., Trans. Inst. Chem. Eng., 331, 35, 1957.
4. Misek, T., Coll. Czech. Chem. Commun., 570, 28, 1963 and 1955, 29, 1964.
5. Boyadzhiiev, L., Spassov, M., Chem. Eng. Sci., 337, 37, 1982.
6. Fei, W-Y., Slater, M.J., J. Sep. Proc. Technol., 5, 1985.
7. Bailes, P.J., Godfrey, J.C., Slater, M.J., Chem. Eng. Res. and Des., 321, 61, 1983.
8. Feick, G., Anderson, H.M., Ind. Eng. Chem., 404, 44, 1952.
9. Coggan, G., Inst. Chem. Eng. Symp. Ser., 138, (26), 1967.
10. Miyauchi, T., Oya, H., Am. Inst. Ch. Eng. J., 395, 11, 1965.
11. Kagan, S.Z., Veisbein, B.A., Trukhanov, V.G., Muzychenko, L.A., Int. Chem. Eng., 217, (2), 13, 1973, (Khim. Prom., 294, 4, 1972).
12. Rozen, A.M., Rubeshnyi, Y.G., Martynov, B.V., Khim. Prom., 132, (1), 46, 1970.
13. Vermeulen, T., Moon, J.S., Hennico, A., Miyauchi, T., Chem. Eng. Prog., 95, (9), 62, 1966.
14. Ryan, L., USAEC Rept. HW36085, 1975.
15. Garg, M.O., Pratt, H.R.C., Ind. Eng. Chem. Proc. Des. Dev., 492, 20, 1981.
16. Niebuhr, D., Vogelpohl, A., Ger. Chem. Eng., 3, 264, 1980.
17. May, W.G., Chem. Eng. Prog., 49, Dec., 55, 1959.
18. Misek, T., Coll. Czech. Chem. Commun., 1686, 40, 1975.
19. Rouyer, H., Lebouhellec, J., Henry, E., Michel, P., Proc. ISEC 1974, Lyon, page 2339, publ. Soc. Chem. Ind., London, 1974.
20. Baird, M.H.I., Rice, R.G., The Chem. Eng. J., 171, 2, 1975.
21. Smith, P.L., van Winkle, M., A. I. Chem. Eng. J., 266, (3), 4, 1958.

Acknowledgements

UKAERE Harwell financed the purchase of equipment.

Dr. Marrocchelli acknowledges the support of ENEA which allowed him to work in Bradford.

S. Marley assisted in measuring axial mixing coefficients.

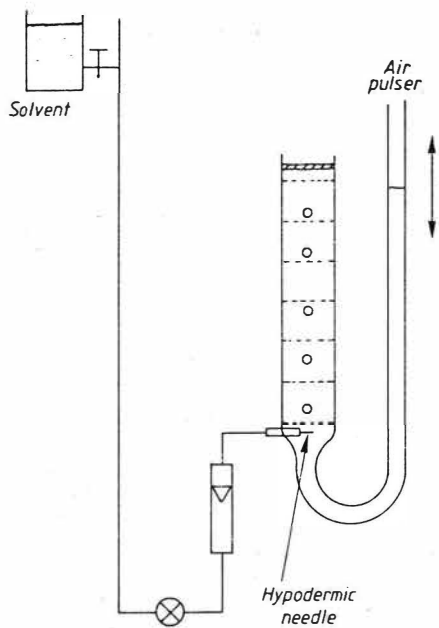


FIGURE 1: Drop formation in the pulsed column

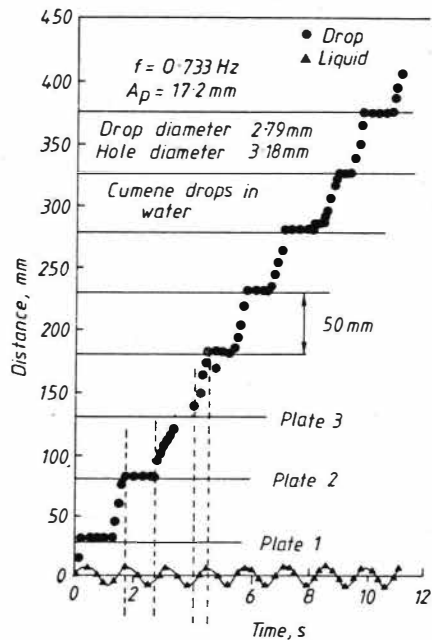


FIGURE 2: Drop motion characteristics

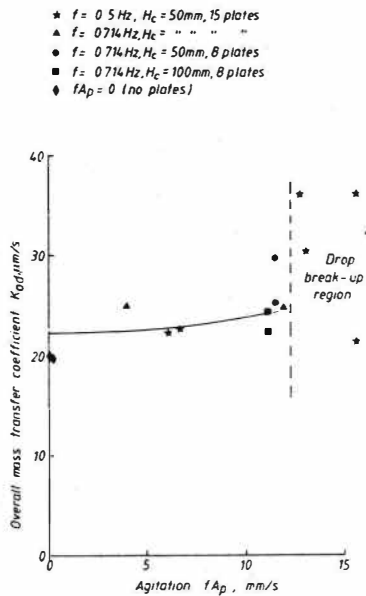


FIGURE 3: Mass transfer coefficients

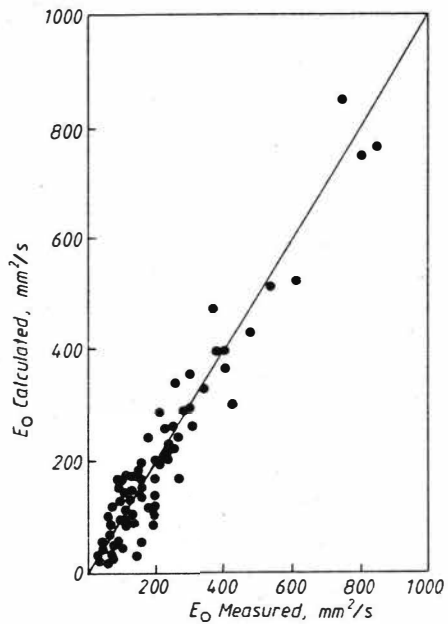


FIGURE 4: Correlation of axial mixing coefficient

 E_o

CORRELATION OF DESIGN PARAMETERS FOR THE SIEVE PLATE EXTRACTION COLUMN (SPC)

JO Oloidi, GV Jeffreys and CJ Mumford. Department of Chemical Engineering, Aston University, Aston Triangle, Birmingham B4 7ET, UK.

The influence of plate spacing and plate hole size upon drop formation mechanisms, drop size distribution, dispersed phase hold-up and flooding phenomena have been investigated in a 0.45 m diameter, 2.3 m high industrial glass Sieve Plate Column (SPC). Correlations are presented for dispersed phase hold-up, coalescence height and drop size (jetting regime). Together with other recommendations, these provide a sound basis for the design of industrial columns.

INTRODUCTION

The sieve plate extraction column (SPC) is widely used in industry, especially in petroleum refining and petrochemical plants (1). Whilst it can be operated with a reasonable efficiency and high throughputs (1-4), there have been some reports of low efficiencies (5) due either to poor design or to operation outside the proper flow regimes. Some hydrodynamic characteristics of the SPC have been reported earlier (6,7). The latter, subsequent work, and literature data (11, 17-19) have been drawn together as a basis for design.

DESIGN PARAMETERS

The important design requirements include:

- (i) Provision for reasonably homogeneous distribution of each phase across any cross section;
- (ii) Generation of a large interfacial area per unit volume of the column;
- (iii) The maximum height of the coalesced layer beneath any plate must be less than the downcomer length;
- (iv) Operation above a certain minimum flow of the dispersed phase, to ensure a minimum head of coalesced layer under any plate and functioning of the majority of the plate holes.

The operation of the SPC is hence strongly influenced by the following design parameters:

Plate and Downcomer Geometry: Dispersion is achieved from each sieve plate provided with a downcomer; holes are omitted from the plate area beneath the downcomer from above. The plate should be constructed such that the surfaces are hydrophobic when water is dispersed and hydrophilic when organic liquid is dispersed (23). Hole diameters are generally in the range 1.5 to 8 mm, located on a square, triangular or circular pitch (8, 9, 14), depending mainly upon the system interfacial tension. Smaller holes are preferred for systems with interfacial tensions > 20 mN/m (dyne/cm) [8].

The pitch size should be approximately 3 times the hole size [9, 10] to avoid coalescence of the drops on the plate at low flowrates, or mutual interference between adjacent jets at high flowrates. A free area of 55% to 60% is therefore desirable, [11, 12], but too large a free area obviously results in a reduced volumetric capacity. The fractional free area of the holes determines the minimum throughput of the dispersed phase to achieve operation of all holes. The plate thickness should not normally be < 1.5 mm,

to ensure rigidity and hence uniform drop coalescence and reformation.

To avoid entrainment, the cross-sectional area of the downcomer is selected to ensure that the average velocity of the continuous phase within it is less than the free rise (terminal/characteristic) velocity of the smallest drops. The minimum downcomer length should be $>h_t$ discussed below.

Plate Spacing: The plate spacing must be sufficient to allow the continuous phase to flow beneath the dispersed phase layer under the plates without causing entrainment. A spacing equal to $2 h_t$ is recommended for small columns or 10 to $12 h_t$ for industrial columns [8]. Plate spacings in industrial columns are between 15 and 60 cm [12]. The plate spacing should also be large enough for uninterrupted jet break up to occur and for subsequent drop rise to be through a sufficient height that the requisite interfacial area is provided for mass transfer.

Flooding: The flooding rate is governed by the system physical properties and column internal design. In addition to the normal factors limiting flow capacity in a gravity-operated extraction column, dispersed phase pressure drop through the holes is also a limiting parameter. Some unfavourable flow characteristics likely to be associated with high volumetric throughputs include excessive entrainment of droplets, overloading of the downcomers, and restriction of flow through the plate holes.

Coalescence Height: The coalescence height, h_t (static hold-up) is the thickness of the dispersed phase layer beneath each plate during steady-state operation and is independent of the plate spacing. It is a measure of flow capacity of the column, ie the greater the thickness, the closer the column is to flooding. The coalescence height should be sufficient to provide the driving force required for the flow of the dispersed phase. The plates should be levelled to ensure uniform coalesced layers beneath them, and hence similar operation of all plate holes across the column cross section. The coalescence height is determined by the drop formation and coalescence characteristics of the dispersed phase, the friction in the orifices for the dispersed phase, and the resistance offered to the continuous phase flow from plate to plate. h_t represents the minimum theoretical height of the downcomer necessary to avoid by-passing of the dispersed phase.

Hold-up and Dropsize: The interfacial area is a function of both the hold-up x and the dropsize distribution generated in each stage, which also determines the mode of mass transfer [13]. The hold-up comprises the static hold-up (coalescence height) and operating hold-up, ie, the total volume of the drops travelling through the continuous phase, expressed as a fraction of column volume.

The interfacial area of contact is given by

$$a = \frac{6x}{d_{32}} \quad \dots (1)$$

$$d_{32} = \frac{\sum nd^3}{\sum nd^2}, \text{ where } n = \text{number of drops} \quad \dots (2)$$

Correlations are therefore required for x and d_{32} , to enable the calculation of the interfacial area, a . Typical drop size distributions and a correlation for the characteristic velocity, U_o , have been reported earlier (6). The characteristic velocity increased with increase in plate hole size or with decrease in plate spacing [6].

Drop Formation and Jetting: Drop formation by jetting is the preferred mode of operation [2, 12]. At reasonably high flowrates depending on system physical properties and plate hole size, ie 0.43 cm/s for Clairsol '350' (d) - water (c) and 23.8 cm/s for CCl_4 (c) - water (d), a jet of the dispersed phase emerges from each hole and subsequently breaks into a series of drops. Operation at jetting velocities near the maximum length has been stated to be two or three times more efficient than when drops are formed directly from sieve plates [15].

Drops formed from any hole may be affected by drops from adjacent holes. Interdrop coalescence may occur on the plate at low flow rates, or interference between jets and their disruption may occur at high flowrates. Only a proportion of holes function at low flowrates and correlations derived for single nozzles do not therefore predict the drop diameters correctly, especially when large diameter holes are used.

EXPERIMENTAL [6, 7]

The SPC comprised a 0.45 m diameter, 2.3 m high industrial glass column with 6 sample points at 0.3 m intervals as shown in Figure 1. The different plate layouts are summarised in Table 1 and satisfied the majority of the above plate design recommendations. The plate spacing was varied between 38 and 20 cm with a downcomer length of between 24 and 6 cm, so that there was always a gap of 14 cm between the end of the downcomer and the plate beneath, ie, the same vertical flow area for the continuous phase above the plate.

The test system was Clairsol '350', a paraffinic hydrocarbon (dispersed) - acetone (solute) - de-ionised water (continuous), which has desirable features as a test system [16]. The de-ionised water had a density of 998.2 kg/m^3 and a viscosity of 0.0011 kg/ms ; Clairsol '350' had a density of 783 kg/m^3 and a viscosity of 0.0018 kg/ms . The system interfacial tension was 35.5 mN/m (dyne/cm).

Prior to each experiment, the column and accessories were thoroughly cleaned and the phases were prepurified and mutually-saturated. All experiments were carried out at $20 \pm 5^\circ\text{C}$. Only work with a mutually-saturated system (ie in the absence of mass transfer) is reported here, but reference is made to later mass transfer experiments.

Drop sizes and jetting phenomena were recorded photographically [6]. A Carl-Zeiss Particle Size Analyser was used to measure drop sizes from two or three replicate photographs. At jetting flowrates 80% to 90% of the holes functioned correctly and allowance was made for the non-jetting holes by introducing an empirical correction factor to obtain the actual jetting velocity.

The coalescence heights beneath each plate were measured during operation and the results averaged. The operating hold-up was measured by the rapid shut-off method [6]. A reduction of plate spacing from 38 to 26 cm was found to significantly reduce the recirculation of drop swarms between adjacent plates.

To determine the flood point the flowrate of one phase was increased incrementally whilst the other was held constant and vice-versa. A period of about 6 mins was allowed after each adjustment to allow steady-state to be re-attained. Flooding was characterised by a rapid increase in the flocculation zone heights beneath the plates, commencing at the top of the column, indicative of unsteady state operation. The flooding data are shown in Figure 2 to indicate the normal operating range but further data are required with different systems.

CORRELATION OF RESULTS

Equal credence was given to data from small diameter columns although, because of wall effects and different inter-plate flow patterns [5-7], the experimental data from the 0.45 m column are more reliable. The experimental data and those in the literature were correlated by multiple regression analysis. All the data were in the absence of mass transfer, since any specific solute affects the system physical properties.

Hold-up, x: The data of this study and of Prabhu *et al* [11] from a 5 cm diameter column with 42, 0.16 hole size plates using the systems water (c) - kerosene (d), water (c) - toluene (d) and water (c) - isoamyl alcohol (d) were correlated to give

$$x = 4.8 \times 10^{-2} \left[\frac{\Delta\rho}{\rho_c} \right]^{-0.01} \left[\frac{U_d}{U_c} \right]^{-0.05} \left[\frac{U_n^2 \rho_c d_n}{\sigma} \right]^{0.73} \left[\frac{U_n^2}{d_n g} \right]^{-0.24} \dots (3)$$

This correlated the results with an average deviation of $\pm 7\%$.

Coalescence height, h_1 : The data of the present study, of Prabhu *et al* [11] and of Fujita *et al* [18] from a 5.6 cm diameter column with 36, 0.20 cm hole size plates using an oil (d) of viscosity 0.00037 kg/ms, density 890 kg/m³ and interfacial tension 25.3 mN/m and water (c), were correlated to give

$$\frac{h_t}{d_n} = 4.49 \times 10^{-4} \left[\frac{U_n^2 \rho_c d_n}{\sigma} \right]^{0.28} \left[\frac{U_c^2 \rho_c d_n}{\sigma} \right]^{0.15} \left[\frac{g \rho_c d_n^2}{\sigma} \right]^{-0.45} \left[\frac{\Delta \rho}{\rho_c} \right]^{0.24} \left[\frac{\mu_c^2}{\rho_c d_n \sigma} \right]^{0.85} \left[\frac{\mu d^2}{\rho_c d_n \sigma} \right]^{-0.37} \dots (4)$$

This correlated the results with an average deviation of $\pm 5\%$.

Drop Size: Droplet size distribution was represented by the functions of Gal-or and Mugele - Evans [6, 13]. Only drop sizes in the jetting regime and with countercurrent continuous phase flow were correlated since cross-flow of continuous phase over the plate has been shown to affect drop size [20].

The data of Vedaiyan *et al* [19] with the system: benzene (d) - water (c), MIBK (d) - water (c) and water (d) - CCl_4 (c), plate hole sizes between 0.20 to 0.37 cm and between 12 to 20 holes per plate and of Garwin and Smith [17] with the system benzene (d) - water (c) with 20, 0.4763 cm plate hole size were combined with those from the present study. Data for the jetting regime were selected from the results of Vedaiyan *et al* [19] by estimating the minimum jetting velocity, U_j , by the equation of Ruff *et al* [21]

$$U_j = \sqrt{\frac{2\sigma}{\rho d_n}} \dots (5)$$

although this predicts a somewhat higher velocity than the minimum observed in the present study. Correlation of the data gave:

$$\frac{d_{32}}{d_n} = 2.81 \left[\frac{\Delta \rho d_n U_n^2}{\sigma} \right]^{0.2} \left[\frac{\Delta \rho d_n^2 g}{\sigma} \right]^{-0.33} \left[\frac{U_n}{U_c} \right]^{-0.19} \dots (6)$$

This proved an unusually accurate correlation with an average deviation of only $\pm 1.6\%$.

The data were also correlated in the form proposed by Kumar and Hartland [22] to give,

$$\frac{d_{32}}{d_n} = 1.45 \left[\frac{\Delta \rho d_n U_n^2}{\sigma} \right]^{0.12} \left[\frac{\Delta \rho d_n^2 g}{\sigma} \right]^{-0.31} \dots (7)$$

The results showed an average deviation of $\pm 2.5\%$ from this correlation. A typical drop size distribution in this jetting regime is shown in Figure 3. In a previous study [6], with the system used here the optimum hole size was 3.175 mm.

CONCLUSIONS

It was concluded that, Equations 3, 4 and 6 or 7 for hold-up, coalescence height and drop size in the

jetting regimes should provide a sound basis for the design of the SPC. However, more data are required with different systems in columns of > 0.2 m diameter.

REFERENCES

- 1 Baird MHI, Lo TC & Hanson C, Handbook of Solvent Extraction, John-Wiley & sons (1983).
- 2 Mayfield FD & Church WL, Ind Eng Chem, 44, 2253 (1952).
- 3 Ponikarov II, Nikolaev AM & Zhavronkov NM, Int Chem Eng, 4(2), 546 (1962).
- 4 Bushnell JD & Fiocco RJ, Hydrocarbon processing 1980, 5, 119 .
- 5 Dawodu FA, PhD Thesis, Aston University, 1983.
- 6 Oloidi JO & Mumford CJ, Paper presented at Research Meeting, Society of Chemical Industry; Solvent Extraction & Ion Exchange Group, University of Aston, 8 May (1985).
- 7 Dawodu FA, Mumford CJ & Jeffreys GV, IChemE Symp 88, 153 (1984).
- 8 Laddha GS & Degallesan TE, Transport Phenomena in Liquid Extraction Tata McGraw-Hull, India (1976).
- 9 Treybal RE, Liquid Extraction, McGraw Hill, 2nd Ed (1963).
- 10 Freshwater DC, in Chemical Engineering Practice Vol 5, Ed. Cremer HW and Davis T, Butterworths, London (1958).
- 11 Prabhu N, Agarwal AK, Degaleesan TE & Laddha GS, Indian JL Tech, 14(2), 55 (1976).
- 12 Jordan DG, Chemical Process Development Interscience Publisher (1968).
- 13 Jeffreys GV, Al-Aswad KKM & Mumford CJ, Sep Sci and Tech, 16(9), 1217 (1981).
- 14 Skelland, AHP, Diffusional Mass Transfer, John Wiley & Sons, (1974).
- 15 Bright A, Chem Eng Res & Dev, 63(1), 59(1985).
- 16 Bailes PJ, Godfrey JC & Slater MJ, Chem Eng Res Des, 61, 321 (1983).
- 17 Garwin L & Smith BD, Chem Eng Prog, 49, 591 (1953).
- 18 Fujita S, Tamixawa E & Chung-gyn Kang, Chem Eng Japan 17 (3), 111 (1953).
- 19 Vedaiyan S, Degallesan TE d& Laddha GS, Indian JL Tech, 12, 135 (1974).
- 20 Kawase YA & Ulbrech JJ, Ind Eng Chem Proc Des & Dev, 20, 636 (1981).
- 21 Ruff K, Pilhofer T & Mersmann A, Chem-Ing-Tech, 48, 759 (1976).
- 22 Kumar A & Hartland S, Trans IChemE, 60, 35 (1982).
- 23 Garner FH, Ellis SRM & Hill JW, AIChEJ, 1(2), 185, (1955).

NOMENCLATURE

- a Surface area per unit volume, m^2/m^3
- d drop diameter, m
- d_{32} Volume-surface, or Sauter, mean drop diameter, m
- d_n Plate hole diameter, m
- g Acceleration due to gravity, m/s^2
- Hc Compartment height or plate spacing, m

- h_t Coalescence height, m
 U Superficial velocity, m/s
 U_n Velocity of dispersed phase at plate hole based on corrected plate hole area, m/s
 x Dispersed phase hold-up

GREEK SYMBOLS

- μ Viscosity, kg/ms
 ρ Density, kg/m³
 $\Delta\rho$ Density difference between phases, kg/m³
 σ Interfacial tension mN/m (dyne/cm)

SUBSCRIPTS

- c Continuous phase
 d Dispersed phase

TABLE 1 PLATE LAYOUT DETAILS

Hole Type	Plate Thickness (mm)	Hole Size (mm)	Number of Holes Per Plate
Drilled	3.175	1.587	1517
Drilled	3.175	3.175	985
Drilled then punched	1.587	4.763	550
Drilled then punched	1.587	6.350	380

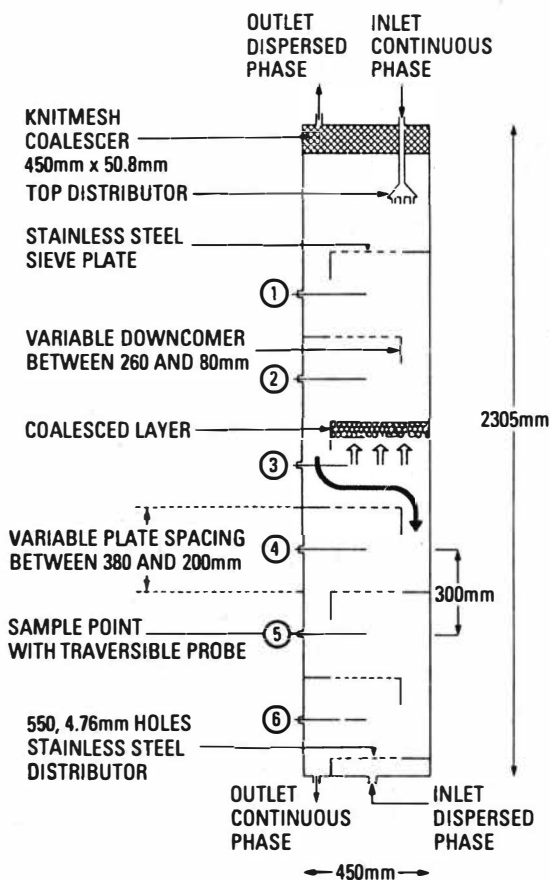
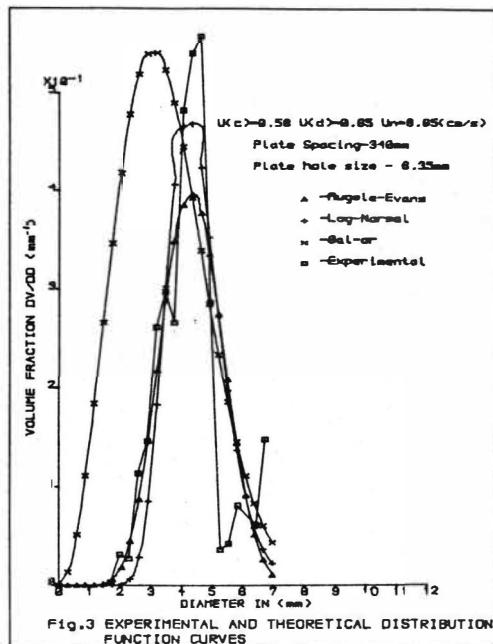
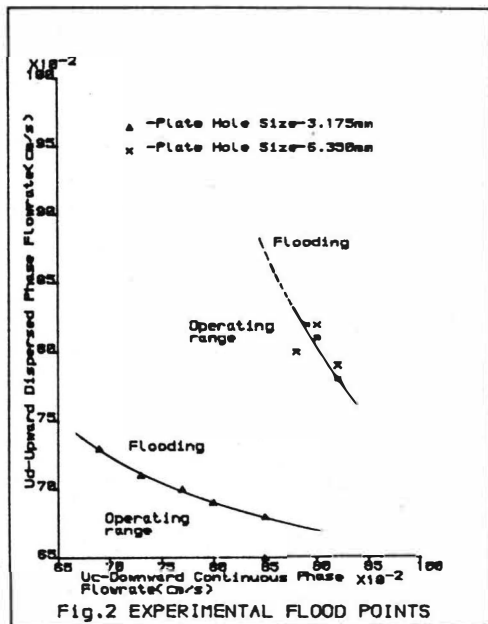


FIGURE 1
GENERAL ARRANGEMENT OF THE
SIEVE-PLATE
EXTRACTION COLUMN (SPC)



Scale-up of the Kühni Column based on the Backflow Model

K.H. Elsässer, U. Bühlmann, Kühni AG, Allschwil/Switzerland

Knowledge of the hydrodynamic behaviour of liquid-liquid extraction columns is important for analysing their actual performance. In particular the effects of axial mixing have to be considered when designing and scaling-up column contactors due to the influence of column scale on this phenomena. The most widely used models to describe axial mixing effects are the backflow and the dispersion model. Several numerical and analytical methods have been published to solve these models.

The Kühni column

The Kühni extraction column belongs to the group of rotary agitated columns and is widely used throughout all industries. Its main characteristics are the Kühni mixing turbine used for agitation and the stator plates bounding each compartment. As shown in figure 1 a characteristic flow pattern is established in each compartment which is maintained independent of column scale. The ability to vary the compartment height, the size of the mixing turbines as well as the free area of flow through the stator plates leads to a high design flexibility as is required to cope with changing physical properties and operational parameters.

The model used

For the present investigations the backflow model was used as described by different authors (1-3). The choice was mainly governed by the fact that the backflow model can be easily adapted to different process conditions. Figure 2 explains the basic set-up of the model. The total column length is divided into N perfectly mixed hypothetical stages each with volume V , axial mixing being allowed for by the backflow coefficients f and e for the continuous and dispersed phases.

To simulate the concentration discontinuities at the end sections no mass transfer was assumed for the two stages $n = 1$ and $n = N$ (4). A system of N nonlinear equations results for each phase. These were solved with a modified Newton iteration (5).

Scaling up

Scaling up column diameter and determining the equivalent rotational speed for industrial scale columns does not raise particular problems. For column diameter normally constant specific throughput is used as the scale-up criterion whereas for rotational speed several approaches are possible e.g. constant tip speed or constant volumetric energy input.

Determination of column height is much more difficult since axial mixing effects have to be considered. A possible route to solve this problem is to maintain the hydrodynamic conditions in the pilot and industrial scale column in such a way that the k.a-values will remain constant. A set of scale-up rules for the Kühni column satisfying this assumption has been published previously (6). The backflow model can now be solved for the unknown column height based on pilot scale data when in addition axial mixing effects are known as a function of scale. The behaviour of the Kühni column has been studied to a great extent in this field, including large scale columns, and is therefore well understood (7).

The principal aim of the present investigation was to evaluate the described procedure and its assumptions by a direct comparison of the performance of a pilot and industrial scale column.

In order to perform scale-up several relations or equations have to be known. The most important ones are listed and commented on below.

. Pe-Number per actual stage, continuous phase (6):

$$\frac{1}{Pe_c} = c_1 + c_2 \left(\frac{H_R}{D_R}\right)^{c_3} \left(\frac{D_k}{H_S}\right)^{c_4} \frac{D_R^2 n_R}{D_k v_c} \phi^{c_5} (1-\epsilon_d) \quad [1]$$

. Pe-Number per actual stage, dispersed phase:

$$Pe_d = Pe_c \frac{v_d}{v_c} \frac{\epsilon_c}{\epsilon_d} \quad [2]$$

This relation is based on the assumption, that the dispersion coefficients of the continuous and dispersed phase can be equated. This was experimentally verified by Kumar (8) for conditions of complete mixing within each compartment corresponding to practical operating conditions.

. equilibrium:

$$Y = mX + c_0 \quad [3]$$

The system used shows a linear dependence in the concentration range investigated. For other applications, especially concentrated solutions, the equilibrium can be approximated by expressing the slope m as a polynomial function of Y or X (8).

transformation of Pe-numbers into backflow coefficients.

$$\frac{Pe_c H_k}{H_s} = \frac{1}{N} (f + \frac{1}{2}), \quad \frac{Pe_d H_k}{H_s} = \frac{1}{N} (e + \frac{1}{2}) \quad [4]$$

for $N \gg 1$

incorporation of column height into model equations

$$\dot{N} = kaV (Y-X), \quad V = \frac{D_k^2 H_k \pi}{4N} \quad [5], [6]$$

Experimental

A Kühni pilot column with diameter 150 mm was operated in parallel on a side stream with an industrial column having a diameter of 800 mm. The column length for the pilot column was chosen independently in order to permit evaluation of the proposed scale-up procedure to be as general as possible. DMF was extracted from an aqueous effluent with Methylene Chloride as solvent.

In a first step the dispersion coefficients, i.e. Pe-numbers, were determined for the industrial column in order to verify the correlation given above for the continuous phase. Steady state and pulse tracer injection technique were used for this purpose. This part of the experimental investigations was done during the start-up period of the overall plant.

When the column was on stream, i.e. during real mass transfer operation, concentration profiles were measured in the continuous and dispersed phases along both columns. Special probes were used to collect the liquid samples as described several times in the literature (8). Parameters investigated were throughput and stirring speed. The samples were analysed using HPLC technology.

Results

Figure 3 shows measured and calculated Pe numbers for the continuous phase. The agreement is good, the maximum deviation reaches only 10 percent. To assess the assumptions made for the dispersed phase, dispersion coefficients were estimated from the concentration profiles using non-linear regression. As expected, deviations are much larger going up to 20 percent. However this is still considered to be a reasonable basis for the model calculations.

For evaluation of the measured concentration profiles, ka -values were determined from the pilot scale data. The profile for the industrial column was then predicted

keeping the k_a -value constant, but taking the changing conditions of axial mixing into account. A typical result is shown in figure 4, where the predicted concentration profile of the industrial column is compared to the measured values. As for other runs the agreement is good and within the required accuracy needed for industrial design purposes. This detailed analysis, which of course could only be done on one extraction system, proves the validity of the described scale-up procedure. This is supported by the successful scale-up of a large number of industrial columns. However it has to be pointed out that each scale-up requires a large amount of information and above all it requires accurate equilibrium data and carefully performed pilot tests.

Summary

A scale-up procedure for the Kühni extraction column is outlined based on the backflow model. For experimental verification a pilot column was operated on a side stream of an industrial scale column. Evaluation of the measured concentration profiles confirmed a scale-up procedure, that has been successfully applied in industrial practise.

Notations

a	interfacial area [m^2/m^3]	N	number of hypothetical stages [-]
c_i	constants	\dot{N}	mass transfer rate [$kg s^{-1}$]
D	diameter [m]	n	rotational speed [s^{-1}]
e	backflow coefficient disp. phase [-]	Pe	Peclet-number [-]
f	backflow coefficient cont. phase [-]	V	volume of hypothetical stage [m^3]
H	height [m]	v	superficial velocity [ms^{-1}]
\dot{H}	mass flow rate dispersed phase [$kg s^{-1}$]	x	mass fraction of dispersed phase [-]
k	mass transfer coefficient [$kg m^{-2} s^{-1}$]	y	mass fraction of continuous phase [-]
\dot{L}	mass flow rate continuous phase [$kg s^{-1}$]	ϵ	hold up of dispersed phase [-]
m	distribution coefficient [-]	ϕ	fractional free area of stator plates [-]

Subscripts

c	continuous phase
d	dispersed phase
k	column
n	stage number
R	impeller
s	stage

Literature

- (1) Miyauchi, T., Vermeulen: *Ind. Eng. Chem., Fund.* 2, 113, 304 (1963)
- (2) Sleicher, C.A.Jr.: *AIChE J* 6 529 (1960)
- (3) Hartland, S., Mecklenburgh: *Chem. Eng. Sci.*, 21, 1209 (1966)
- (4) Ingham, J.: *Advanced solvent extraction technology*, Education course given at University of Bradford, Mai 1985
- (5) Kuester, J.L., Mize, J.H.: *Optimization techniques with fortran*, Mc Graw Hill, New York (1973)
- (6) Bühlmann, U., Mögli, A.: "The Kühni Extraction Column", in *Handbook of Solvent Extraction*, Wiley-Interscience, New York (1983)
- (7) Breyse, J., Bühlmann, U., Godfrey, J.C.: *AIChE Symp. Series*, 238 Vol. 80, 94 (1984)
- (8) Kumar, A.: *Dissertation ETH Zurich, Diss. ETH No. 7806, Zurich (1985)*

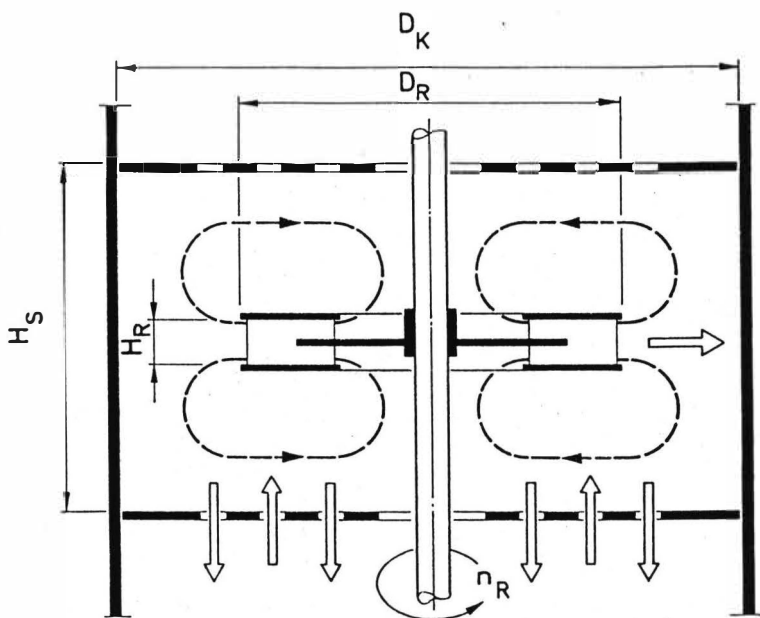


Fig. 1 Characteristic flow pattern and geometry of the Kühni contactor

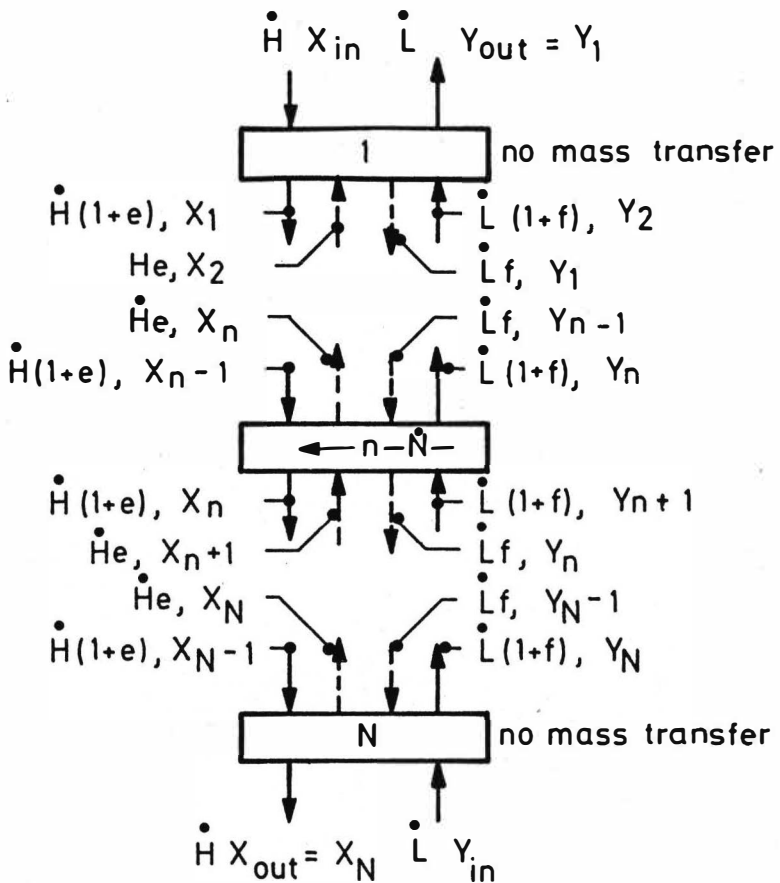


Fig. 2 Backflow model: Material balance over N stages with axial backflow parameters f and e

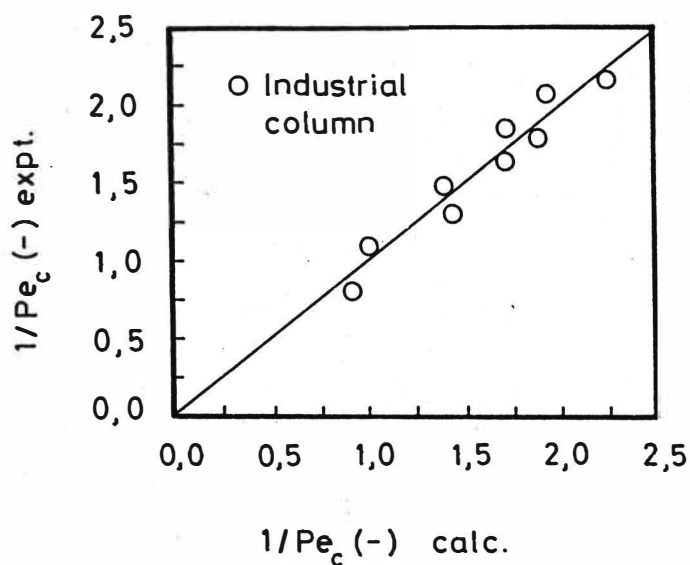
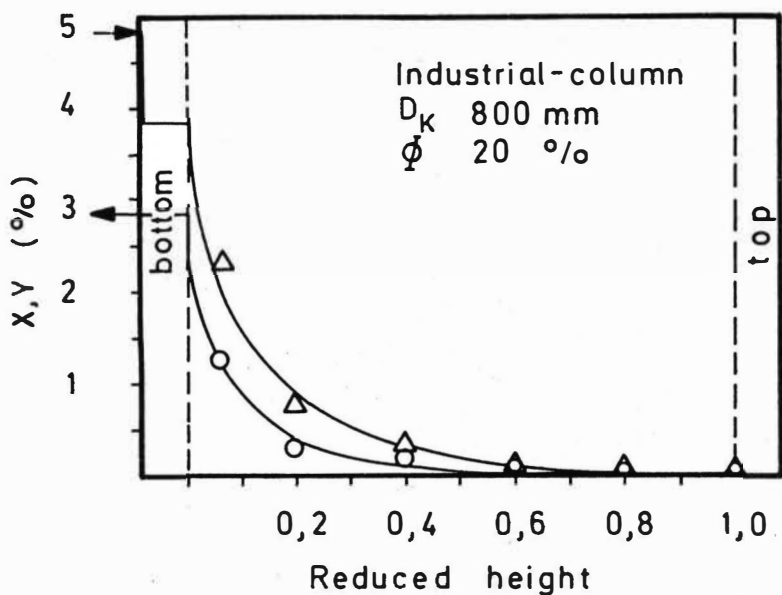


Fig. 3 Reciprocal values of Pe -
number for the continuous phase
 $\phi = 20\%$



Δ -Y, \circ -X experimental
 — predicted

$$1/Pe_c = .41 \quad K_x \cdot a = 15.3 \text{ kg/m}^2 \text{ s}$$

Fig. 4 Predicted conc. profiles for solute transfer from continuous to dispersed phase

The Effect of Column Diameter on Performance of
Pulsed Plate Extractors

Leanne M. Fitzpatrick, H.R. Clive Pratt and Geoffrey W. Stevens
University of Melbourne, Victoria, Australia

ABSTRACT

Continuous phase backmixing coefficients obtained by the steady state tracer injection method are reported for glass pulsed plate columns of 72, 151 and 300 mm diameter using the kerosene-water system. The data indicate that the backmixing coefficients increase with column diameter for single phase operation, but are unaffected when both phases are present. Serious maldistribution and wall streaming occurred with the largest column. The latter was eliminated by sealing the plates, but the former, although considerably reduced, was still present and may be responsible for the reduction in mass transfer rate known to occur on scaling-up the diameter.

INTRODUCTION

The mass transfer performance of pulsed and reciprocating plate columns is known to decrease with increase in column diameter. Sege and Woodfield (1,2) reported a fourfold increase in HTU for a 610 mm diameter pulsed column, as compared with a 76 mm diameter column for the system 3N nitric acid - tributyl phosphate (TBP)/kerosene-uranyl nitrate. The use of louvre-plate redistributors at intervals along the column reduced the difference in HTU to about 10% at the expense of a somewhat reduced throughput (2).

Thornton and Logsdail (3,4) studied mass transfer in four pulsed plate columns of 76 to 305 mm diameter, using the system toluene-water-acetone, and found that the HTU increased as $\exp(d_c)$; it was also found that the interfacial area was unaffected by diameter and it was therefore concluded that the decreased performance arose principally from maldistribution effects.

Rouyer et al (5) studied pulsed columns of various diameters using the system nitric acid - 30% TBP/dodecane - acetic acid. Values of the HTU were found to be identical for 50, 100 and 150 mm diameter columns under the same operating conditions. Continuous phase axial dispersion coefficients, measured by the pulse injection technique, in 45 and 600 mm diameter columns indicated no increase with increasing column diameter.

More recently, Garg and Pratt (6) suggested that the adverse effect of column diameter results from increased continuous phase backmixing. They reinterpreted Thornton and Logsdall's mass transfer data (3,4) in terms of the backflow model (7,8) to determine the effect of column diameter on backmixing. The result was presented as follows

$$a_c = d_c^{0.80} (rA)^{0.10} (0.1703 + 0.3017V_c/V_d) \quad (1)$$

In the present work, continuous phase backmixing coefficients were determined for three columns of different diameter by the steady state tracer injection method using the kerosene-water system.

EXPERIMENTAL

Equipment

Three glass columns with internal diameters of 72, 151 and 300 mm were used. A flat bladed mixing impeller was provided in the tracer injection compartments. Hypodermic SS tubes of 1.6 and 3.2 mm i.d., located 4 to 7 mm below the plates, were used to siphon samples from the column during operation. A schematic diagram of the equipment is shown in Fig. 1, and essential details are given in Table 1.

Materials Used

The system used consisted of water as continuous phase and BP K24 solvent kerosene as dispersed phase; these were mutually saturated prior to use.

Three tracer solutions were used, viz (i), 5.5 wt% NaCl solution, (ii) 3 wt% $K_2Cr_2O_7$ solution and (iii), a 0.5 wt% solution of tartrazine dye (Acid Yellow 22). Methylene blue was also tried, but found to stain the plates and alter the wetting characteristics. All three tracers gave the same backmixing coefficients when used under identical conditions.

Method

The steady state tracer injection technique (8) was used for the measurements. The flowrates for both phases were set and the tracer solution was continuously injected, at a flowrate of 5 to 10% of the continuous phase, into the stirred compartment. After four effective volume changes of the continuous phase the column was assumed to have reached steady state operation. Two or three 80 ml samples were then withdrawn successively from each sample point over a period of 20 or 30 minutes and analysed for the tracer.

Interpretation of Results

A steady state mass balance on tracer around stage n gives (7,8)

$$(1 + \alpha_c)C_{n-1} - (1 + 2\alpha_c)C_n + \alpha_c C_{n+1} = 0 \quad (2)$$

with boundary conditions $n = 0$, $C_n = C_0$ and $n = \infty$, $C_n = 0$. The solution is

$$(C_n/C_0) = [\alpha_c/(1 + \alpha_c)]^n \quad (3)$$

Plots were made of $\ln(C_n/C_0)$ vs n , giving lines of slope $\alpha_c/(1 + \alpha_c)$ from which α_c was obtained.

RESULTS

Measurement Technique

The data obtained in the 72 and 151 mm diameter columns were well represented by Eq. (3). With the 300 mm diameter column, however, initial measurements gave irregular plots which could not be represented by straight lines. Visual observations indicated a variation in the colour of the tracer within each stage. Considerable local streaming of the continuous phase past the plates, due to irregularities in the wall of the glass column, were also noted. This effect was studied further by the addition of six sample tubes to the 4th compartment above the injection stage. An 11-fold variation in tracer concentration was observed for both single and two phase operation.

To eliminate the channelling of continuous phase along the walls, the plates were sealed with 12.7 mm wide rings of 3.2 mm thick nitrile rubber. These completely stopped the wall streaming; however, an 8-10 fold variation for single phase operation, and a 2-3 fold variation for two phase operation in the tracer concentration still occurred. These variations gave uncertainties of $\pm 15\%$ in the resulting backmixing coefficients. This error was reduced to $\pm 10\%$, the same degree of accuracy obtained in the smaller columns, by locating the sample points as closely as possible above each other. The resulting data were then well represented by Eq. (3).

Single Phase Operation

The backmixing ratios obtained for single phase operation in the 72 and 151 mm diameter columns show an increase with increasing column diameter. A similar increase was observed when scaling up from the 151 to the 300 mm diameter column, indicating that the method of measurement in the larger column was appropriate. Some typical results are presented in Fig. 2.

Two Phase Operation

The two-phase backmixing coefficients obtained for the 72 and 151 mm diameter columns, were observed to be similar in all regimes of operation. The 300 mm diameter column data, obtained in the manner previously described, also agreed with these results, as shown in Figs. 3 and 4.

DISCUSSION

The two-phase results indicate that continuous phase backmixing coefficients are unaffected by column diameter over the range studied. The variation of the single phase results is therefore surprising, but it appears probable that this is reduced by the presence of the dispersed phase droplets. Despite this, there was evidence of maldistribution occurring around the plates with the 300 mm diameter column.

The need to mix the tracer in well with the main flow became apparent during this work. Visual observation of the 300 mm column in operation suggested that the variation found in tracer concentration around the plates may have been partly due to incomplete mixing in the injection compartment. It may well be, therefore, that much of the previously reported data for various extractor types, obtained by both the present method and the unsteady state tracer technique, were in error due to failure to mix in the tracer adequately.

The apparent lack of effect of column diameter on the backmixing coefficient is of particular importance in regard to scale-up. Thus, if the deterioration in mass transfer rate is not due to an increase in backmixing with diameter, then the most likely explanation is that it results from increasing maldistribution. This would occur if the same net pressure loss for continuous phase flow could result from a low velocity of the latter coupled with a high dispersed phase holdup in one part of the column cross-section, and vice versa in the other part. Some evidence of this was obtained for the largest column, and if confirmed, steps will need to be taken in the future to minimize this and allow for it during scale-up.

NOMENCLATURE

- A = amplitude, i.e., total excursion of pulse, cm.
 C_n = tracer concentration, $g\ l^{-1}$.
 d_c = column diameter, cm.
 f = pulse frequency, s^{-1} .
 R = phase ratio, V_c/V_d
 n = stage number, counting up from feed compartment.

V_c, V_d = superficial velocity of continuous and dispersed phase respectively, cm s^{-1} .

α_c = continuous phase backmixing coefficient.

REFERENCES

1. Sege, G. and F.W. Woodfield, Chem. Eng. Prog. Symp. Series No. 13, 179 (1954).
2. Woodfield, F.W. and G. Sege, Chem. Eng. Prog. Symp. Series No. 13, 14 (1954).
3. Thornton, J.D., Trans. Inst. Chem. Eng. 35, 317, (1957).
4. Logsdail, D.J. and J.D. Thornton, Trans. Ind. Chem. Eng. 35 331 (1957).
5. Rouyer, H., J. Lebouhelloc, E. Henry and P. Michel, Proc. ISEC '74, 3, 2339 (1974).
6. Garg, M.O. and H.R.C. Pratt, I.E.C. Proc. Des. Develop. 20, 492 (1981).
7. Sleicher, C.A., A.I.Ch.E. Jnl. 6, 529 (1960).
8. Pratt, H.R.C. and M.H.I. Baird, "Handbook of Liquid Extraction" (eds. T.C. Lo, M.H.I. Baird and C. Hanson), Chapter 6, Wiley (1983).

TABLE 1. DETAILS OF COLUMNS

	<u>Column 1</u>	<u>Column 2</u>	<u>Column 3</u>
Column Diameter (mm)	72.45	151.2	299.6(av)
Height of main column section (mm)	1000.	2000.	2000.
Plate Material	SS	SS	SS
Plate Spacing (mm)	50	50	50
Plate Thickness (mm)	1.575	3.2	2.6
Hole Diameter (mm)	3.2	3.2	3.2
Hole Pitch (mm)	6.0	6.0	6.1
(triangular)			
Fractional Free Area	0.213	0.227	0.24(av)
Number of Plates	16	27	26
Plates above tracer inlet	5	13	11
Number of sample points	5	6	6
Method of hole formation	drilled	drilled	punched

- 1 Pulsed Column
- 2 Piston
- 3 Variable Speed Unit
- 4 Variable Eccentric Drive Unit
- 5 Flameproof Electric Motor
- 6 Kerosene Storage Tank
- 7 Water Storage Tank
- 8 Tracer Storage Tank
- 9 Tracer Injection Point
- 10 Sample Points
- 11 Stirrer (operated by air motor)
- 12 Needle or Control Valve

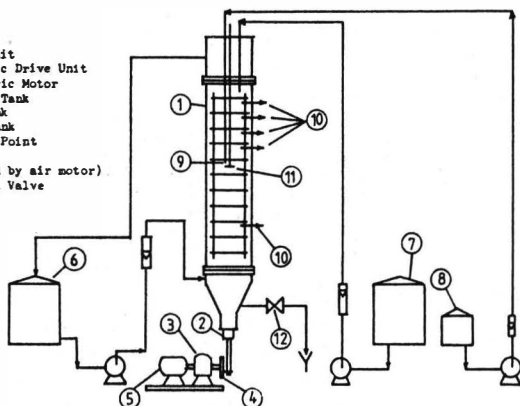


Figure 1: Flowsheet and Equipment

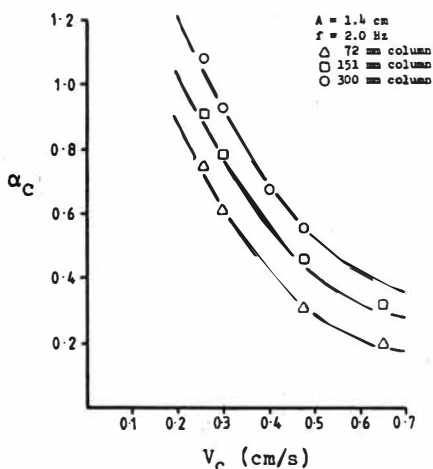


Figure 2: Single Phase Operation Results

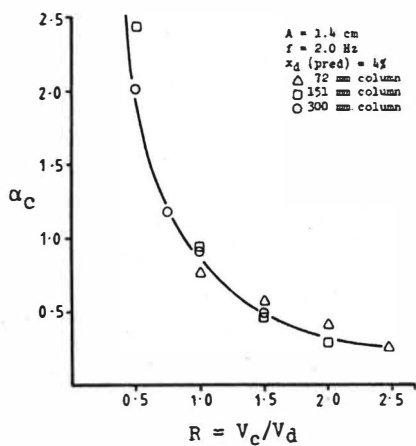


Figure 3: Two Phase Operation Results

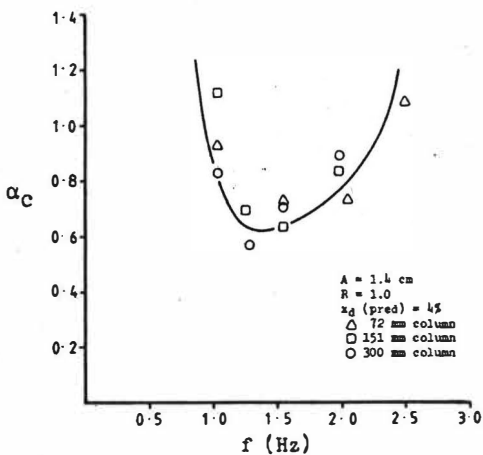


Figure 4: Two Phase Operation Results

POWER REQUIREMENT OF LARGE PULSED PERFORATED PLATE COLUMN

CHEN, Hai-Jie
Shanghai Soap Works, Shanghai (China)

INTRODUCTION

The pulsed perforated plate column is used for a diverse range of extraction processes. Its best known application has probably been in the nuclear fuel industry. However, this type of column has ever been applied to treat liquid-liquid systems of widely varying physical and chemical properties. In China commercial pulsed perforated plate columns were designed to extract uranium and thorium nitrates as well as to separate these two salts in the early nineteen sixties. The plant, in which the mineral monazite has been processed, was put on stream in 1964. It has also been successful for carrying out chemical reaction in the organic field, such as oil splitting under pressure and saponification of fats at a temperature near the boiling point of water. On the other side, it is also effective in pure physical operations such as simple wash of soap stock to recover glycerine. In the latter cases, the amounts of material treated are large and cost of products is relatively cheap. Therefore, the estimation of power consumption is particularly important both in design and in operation.

The present report will concentrate on the power requirement of pulse generator for commercial columns.

COMMERCIAL PULSED PERFORATED PLATE COLUMN (PPPC) SET

The column sets are illustrated by one example in Fig. 1. It consists of the column proper, a U-tube filled with the heavy liquid phase to transmit the pulsation, a pulse generator and an electric motor with all necessary reducing devices.

The dimensions of PPPCs are as follows:

Diameter of column, D	0.6-1.4m
Diameter of holes, d	$3-6 \times 10^{-3}m$
Compartment height	0.047-0.077m
Effective column height	up to 11m
Number of perforations	up to $> 10^4$
Ratio of free area of perforations to cross-sectional area of column	17-30%

Operation conditions:

Frequency	60-200 cycle/min.
Amplitude	$7-30 \times 10^{-3}m$
Apparent speed of heavy phase	$6.4-8.5 \times 10^{-4} m/s$
Apparent speed of light phase	$1.12 \times 10^{-3} m/s$
Temperature	90 °C

POWER MEASUREMENT

The power of electric motor was measured by a voltmeter and an ammeter. To obtain the effective power, a meter for power factor $\cos\phi$ was used. Therefore, the effective power N_j' can be calculated as follows:

$$N_j' = \sqrt{3} V I \cos\phi \quad (1)$$

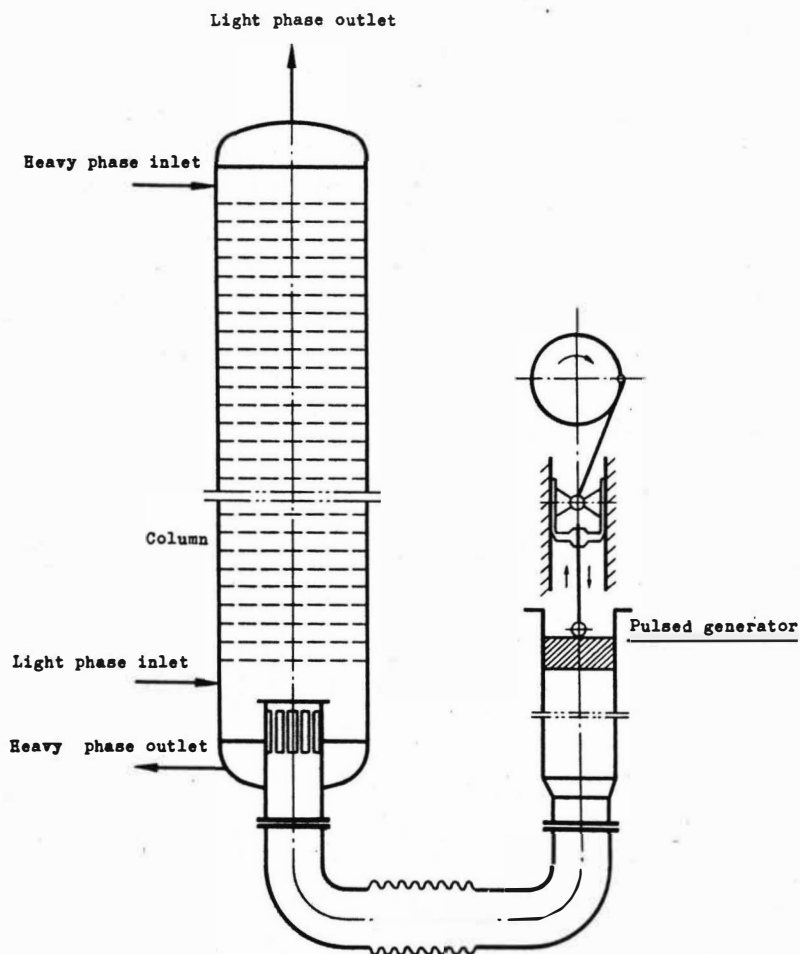


Fig. 1 One of pulsed perforated plate columns

where V is the voltage and I the current in ampere.

All the power losses due to mechanical transmission were included in a factor η . And in the present study $\eta = 0.90$, so the power to drive the fluid in the column can be written as follows:

$$N_j = 0.90 N_j' \quad (2)$$

SYSTEM USED

The brine containing 7-8% NaCl and 1-2% NaOH, which is the washing agent, is used as the continuous phase. Its density is 1100 kg/m^3 and viscosity about 1 c.p. The dispersed phase is the soap stock which contains 7-8% glycerine. Its density is about 900 kg/m^3 and viscosity as high as 1.9×10^4 c.p. These two fluids flow countercurrently in the column.

PREVIOUS WORK FOR THE CALCULATION OF POWER REQUIREMENT

1. Jealous and Johnson Equation⁽¹⁾

Jealous and Johnson (1955) first studied the problem of power requirement of PFFC. They pointed out that the power requirement in PFFC consisted of the following four items, i.e.

- (1) the power to overcome static head of fluid,
- (2) the inertia item,
- (3) the friction loss in the main column, and
- (4) local resistances due to contraction and expansion at the connection between the pulse line and column.

Considering all the above items, Jealous and Johnson proposed the following equation to calculate the power requirement:

$$N_j = S_1 \left\{ (\rho_1 L_1 - \rho_2 L_2) g / g_c + (\rho_1 L_1 + \rho_2 L_2) (d^2 y / dt^2) / g_c + [n(1-\epsilon^2) \rho_1 / (C_0^2 \epsilon^2) + ((S_1/S_2) - 1)^2 \rho_2] (dy/dt)^2 / 2g_c \right\} (dy/dt) \quad (3)$$

where $y = (A/2) \sin 2\pi ft$, the liquid displacement due to pulsation,
 $dy/dt = (A/2) 2\pi f \cdot \cos 2\pi ft$, the velocity of the liquid,
 $d^2y/dt^2 = -(A/2)(2\pi f)^2 \sin 2\pi ft$, the acceleration,
 C_0 = the orifice coefficient.

How to determine the value of C_0 is important to calculate the correct N_j . Jealous and Johnson suggested that the C_0 would be a constant and equal to 0.6.

2. Thornton's Simplified Equation⁽²⁾

In 1957, J.D. Thornton proposed a simplified equation by dropping less important items. It was expressed as follows:

$$\psi_{\max} = \pi^2 n (1-\epsilon^2) (fA)^3 / (2g_c C_0^2 \epsilon^2 L) \quad (4)$$

where the value C_0 is also considered constant and equal to 0.6.

COMPARISON OF CALCULATED VALUES WITH EXPERIMENTAL DATA

The power requirement of the PFC mentioned above was calculated by Eq. (3) and Eq. (4) ($C_0 = 0.6$ as suggested by both authors⁽¹⁾⁽²⁾). The comparison of these values with experimental data was shown in Table 1.

TABLE 1 Comparison of Calculated N_j with Experimental Data

Column diameter m	Frequency s^{-1}	amplitude $10^{-3}m$	Calculated value N_j , kw		Measured value kw
			by Eq.(3)	by Eq.(4)	
1.0	2	7	2.8		11.9
1.0	1.17	25	6.2		19.6
1.0	1.33	25	7.4		23.8
1.0	1.5	25	8.6		24.2
1.0	1.58	25	9.3		19.0
0.7	2.5	30	16.8	7.8	13.3
0.7	3	30	26.7	13.3	17.1

It is apparent from Table 1 that in most cases either Eq.(3) or Eq.(4) do not give accurate values of N_j for industrial PFCs. In consequence, the four items of Eq.(3) were calculated separately and listed in Table 2 in order to see the relative importance of individual ones.

TABLE 2 Four Items of the Power Requirement Calculated by Eq. (3)

Column diameter, m	1.0	1.0	1.0	1.0	1.0	0.7	0.7
Frequency, cycle/s	2	1.17	1.33	1.5	1.58	2.5	3
Amplitude, $10^{-3}m$	7	25	25	25	25	30	30
Power, kw							
(1) static head	2.61	5.44	6.22	6.99	7.38	4.36	5.23
(2) inertia	0.18	0.46	0.69	0.98	1.15	2.03	3.51
(3) friction loss	0.035	0.30	0.45	0.64	0.75	10.42	18.0
(4) local resistance	**	**	**	**	**	**	**
Total	2.8	6.2	7.4	8.6	9.3	16.8	26.7
Measured		11.9	19.6	23.8	24.2	13.3	17.1

** the value is too small to be included

Table 2 shows that the calculated value is deviated much from actual measured power. It seems apparent that most of the deviation is introduced from item (3), i.e. the friction loss. Especially for the column of one metre diameter which had a relative large ϵ ($\epsilon = 0.3$) and low dy/dt , the Reynolds number $Re_0 = d(dy/dt) \cdot \rho / \mu$ is low. Therefore, the value of C_0 should be lower than 0.6 as suggested in references (1) and (2). This may be the cause that the calculated item (3) is much lower than measured data.

THE SIMPLIFIED FORM THE JEALOUS AND JOHNSON EQUATION PROPOSED BY THE PRESENT AUTHOR

Items (2) and (4) are usually small in comparison with total power requirement of industrial PFCs and may be neglected. Most of the power expended are consumed to overcome the static head of liquids and the friction loss for liquids passing through perforations, especially the latter one. Therefore, the following equation using variable C_0 value is recommended:

$$N_j = C_1 \left\{ (\rho_1 L_1 - \rho_2 L_2) g + n(1 - \epsilon^2) \rho_1 (dy/dt)^2 / 2C_0^2 \epsilon^2 \right\} (dy/dt) \quad (5)$$

Since flow rate $Q = \beta_1(dy/dt)$ and

$$(\rho_1 L_1 - \rho_2 L_2)g = H\rho g \quad (6)$$

Eq. (5) can be rewritten as

$$N_j = 2H\rho_1 g / K\eta + n(1-\varepsilon^2)\rho_1 \beta_1 (dy/dt)^3 / (2C_0^2 g^2) \quad (7)$$

The most important thing is to choose a correct C_0 and then Eq. (7) can be used to estimate the power requirement of large PFC.

ORIFICE COEFFICIENT C_0

In large PFC, the Reynolds number $Re_0 = dU\rho/\mu$ in general is not high, and the orifice coefficient should not be taken as a constant, but a function of Re_0 and other parameters. Since the perforated plates of industrial columns consist of more than thousands of orifices and as the fluids eject upwards and downwards through these orifices, the situation becomes very complicated and is almost impossible to be analyzed theoretically. Here the author attempt to make a shortcut by plotting C_0 vs. πAf as shown in Fig. 2. It seems that a linear relation could be obtained.

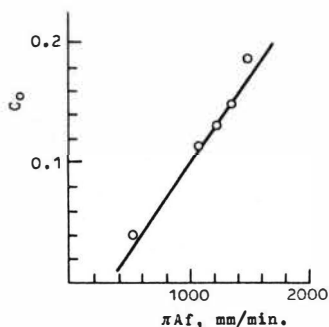


Fig.2 C_0 vs. πAf

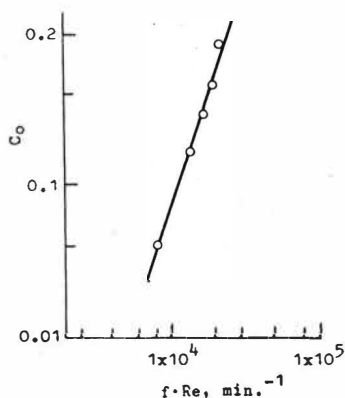


Fig.3 C_0 vs. $f \cdot Re$

Due to that πAf is direct proportional to the fluid velocity U and it has been found by experiments that C_0 increases with increasing f , if Af is fixed (where f varies from 1 to 3.33 s^{-1}), an empirical equation for C_0 is suggested as follows:

$$C_0 = B(f \cdot Re)^m \quad (8)$$

where B and m are two parameters depending on the system treated.

In the system mentioned above,

$$B = 1.7 \times 10^{-5}, \quad m = 1.6$$

The result can be seen in Fig. 3. It shows that the data estimated by Eq.(8) are much close to the measured data. The maximum deviation is less than 6%.

The calculated results of Eq. (7) with varying C_0 values together with the measured data are shown in Fig. 4.

Experiments in other systems made by present author also prove that Eq. (8) is applicable provided the parameters B and m are different.

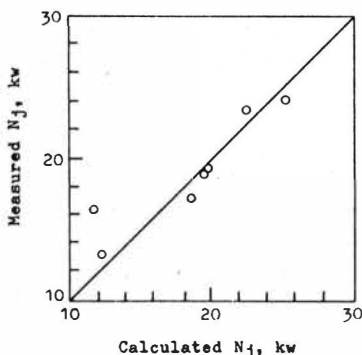


Fig. 4

CONCLUSIONS

1. The simplified Eq. (7)

$$N_j = QH\rho_1g/K\eta + n(1-\epsilon^2)\rho_1S(dy/dt)^3/(2C_0^2\epsilon^2)$$

is applicable for estimating the power requirement of industrial PFCs.

2. Orifice coefficient C_0 is a function of Re and f .
3. C_0 can be calculated by Eq. (8). Parameters B and m depend on the properties of system.

ACKNOWLEDGEMENT

The author gratefully acknowledges the encouragement given by Prof. Y.F. Su, and is willing to thank Mr. J.M. Zhu and Mr. L.K. Li for their kindly help.

NOTATIONS

- A - amplitude of pulsation in the column, m
 C_0 - orifice coefficient
 f - frequency of pulsation, s^{-1}
 g - acceleration due to gravity, m/s^2
 g_c - conversion factor
 H - effective height of the column, m
 K - constant depending upon the units used

L_1 - liquid height in the column, m
 L_2 - length pulse line, m
 n - number of perforated plates in the column
 S_1 - cross-sectional area of the column, m^2
 S_2 - cross-sectional area of the pulse line, m^2
 t - time, s
 y - linear displacement of pulse rod or fluid in column, m

Greek letters

ϵ - free area of perforations to column cross-sectional area.
 η - overall mechanical efficiency
 ρ_1 - density of fluid in column, kg/m^3
 ρ_2 - density of fluid in pulse line, kg/m^3
 μ - viscosity of the continuous phase.

REFERENCES

- (1) Jealous, A.C. and Johnson, H.F., I.E.C., 1159 (1955)
- (2) Thornton, J.D., Trans. Inst. Chem. Eng., 35, 316 (1957)

Determination of Mass Transfer Rates
in a Reciprocating-Plate Extraction Column.

L. Steiner, A.-K. Bensalem and S. Hartland

Swiss Federal Institute of Technology, Zurich, Switzerland.

Introduction: The subject of this study is the reciprocating-plate extraction column as described by Karr (1). It is characterised by large diameter of the plate perforations (typically over 15 mm) and correspondingly large plate free area (over 50 %). The construction is suitable for large phase throughputs and the separation ability is comparable to other intensively agitated extraction columns, though no objective measurements of actual mass transfer performance have been published. To fill this gap, a column in pilot-plant size was constructed and operated with the test-system of toluene, acetone and water. From the measured values of the relevant hydrodynamic parameters and concentration profiles along the column axis the transfer rates were evaluated by a curve fitting technique, generating the concentration profiles on a computer using a suitable model and varying the transfer rate till the best possible agreement between the measured and simulated profiles was achieved. For this purpose models of different sophistication are available, most of them being based either on the principles of back- or forward-mixing.

The backmixing models consider both phases inside a column as continuous fluids and describe their flow patterns by analogy with the theory of molecular diffusion. Additional streams proportional to negative concentration gradients are introduced, the molecular diffusivity being replaced by a dispersion coefficient (which may be some five orders of magnitude greater). To make the model applicable for more complex processes with height-dependent parameters, the differential model may be discretised and converted into stagewise form.

In the forward-mixing models the diffusional concept is used only for the continuous phase. The drops are assumed to keep their identity for longer time intervals, to flow through the column with velocities dependent on their dimensions and exchanging solute with the continuous phase at different rates. These types of model explain the influence of polydispersivity of the drop swarms on the column performance better than the backmixing models. However, they may only

be applied when the individual drop velocities, coalescence frequencies and transfer rates are known. Applying relations valid for single drops to polydisperse swarms is dangerous and can lead to large errors.

Experiment: A typical Karr column of 76 mm diameter with a 2 m active length was used. A stack of 54 plates 70 mm in diameter, with 58 % free area and a hole diameter of 16 mm was reciprocated with variable amplitude (0 to 25 mm) and frequency (0 to 7 Hz). The column was equipped with expanded calming sections (220 mm in diameter) at both ends and connected to a circulation system comprising tanks, pumps, thermostats and flow control. The liquids only came in contact with glass, stainless steel and Teflon. Deionised water was discharged after each use, toluene being distilled after every five runs (2).

The average hold-up of the dispersed phase was measured hydrostatically, local hold-ups were measured by rapidly withdrawing 100 ml of the column contents into a calibrated glass cylinder.

The drop size and its distribution were determined by evaluation of photographs taken through planar windows placed along the column height. The negatives were projected on a screen, the digitalised result being stored on a magnetic tape and transferred to a small computer which evaluated the size distribution and mean Sauter diameter.

Backmixing coefficients in both phases were measured by impulse injection methods, monitoring the response curves in two positions downstream from the injection point. Conductometry was used for the water phase and colorimetry in specially developed on-line cells for the dispersed phase. The response curves were digitalised and the coefficients evaluated on a computer by a curve-fitting technique.

Sampling devices for withdrawal of both phases in pure form were placed at five positions along the active column height. The samples were collected over long time intervals of the order of minutes and analysed for acetone on a gas chromatograph or using a precise density meter.

Evaluation of mass transfer rates: The original intent was to investigate the applicability of both the backmixing- and the forward-mixing models. However, it was found in preliminary evaluations that in many cases the over-all transfer rate increased with distance from the entry-point of the dispersed phase in the column due to changes in the interfacial area. This is difficult to handle using the forward mixing model.

Average mass transfer coefficients based on the backmixing model were therefore evaluated. The procedure previously described (3) was first applied. The active column height was divided into 27 hypothetical stages (i.e. taking two real stages bounded by adjacent stack plates as one hypothetical stage), and the set of balance equations solved by the method of consecutive approximation till the predetermined accuracy was reached. An iterative solution was necessary to allow for the curvature of the equilibrium line. Using measured values for all parameters except the mass transfer coefficient, the curve fitting was performed by single-parameter minimisation of the sum of the deviations between the measured and simulated concentration profiles at all points where experimental measurements were available. Compared to other types of extraction columns investigated earlier, the agreement of the optimised profiles with experimental data was not very good. This was explained by the fact that the drops are not introduced into the column at their final size but produced by breakage from the original large globules in the lower part of the column. Up to half of the column height is required before the stable drop size distribution is reached. To improve the agreement and obtain coefficients related to the actual hydrodynamic regime inside the column, the evaluation procedure was applied for the height between the first and the last intermediate sampling points, rather than for full column height (0.5 to 1.75 m above the lower edge of

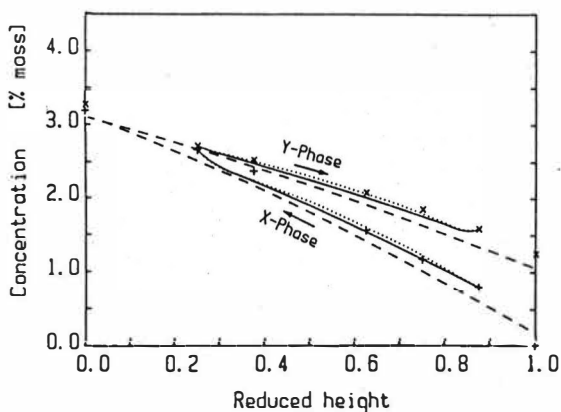


Figure 1: Example of measured and simulated concentration profiles.

Broken lines: Optimised curves for full column length, $K_x = 0.0602$, Mean deviation $s = 1.46(10^{-3})$ (in concentration units). Full lines: One-parameter optimisation for an open system, $K_x = .00566$, $s = 5.91(10^{-4})$. Dotted lines: Three parameter optimisation in an open system. $K_{xB} = 0.0561$, $K_{xM} = 0.0486$, $K_{xT} = 0.0646$, $s = 4.43(10^{-4})$.

the active section). This required a change in the boundary conditions from a closed to an open system. The concentrations measured in the first and the last intermediate sampling points were taken as inlet values and the curves with minimum deviation between the measured and calculated concentrations in the remaining three sampling points (in both phases) were determined. In this way the standard deviations of the simulated profiles were considerably reduced.

To see if the assumption of a constant mass transfer coefficient in the section of interest was justified, a further evaluation was performed splitting the height into three subsections and evaluating the transfer coefficients for each simultaneously by a three-parameter minimisation. Though the statistical confidence is reduced, the results are sufficiently accurate to indicate trends and to check whether the transfer coefficient is constant.

Results: A randomly selected example of measured and optimised concentration profiles is shown in Fig.1, including the values of the optimised coefficients and the mean standard deviations. The optimisation over the full active column height (broken lines) indicates a poor fit and the coefficient is larger than the one determined for the shorter section. The optimisation over a shorter column section (full lines) delivers a better fitting profile with a lower mass transfer coefficient. With a three-parameter optimisation the mean coefficient remained the same as in the previous case, the profile being still closer to the experimental points (dotted lines), but the procedure mainly compensated for the random errors in the experimental measurements. The assumption of a constant mass transfer coefficient was therefore justified in this case.

Fig. 2 compares the coefficients obtained by the two methods against each other, i.e. those calculated for the full length and for the shorter section. The average standard deviations for these two evaluations were $1.77(10^{-3})$ and $9.52(10^{-4})$ respectively. Due to this improvement and elimination of the uncertainties connected with modelling of the end parts of the column, the coefficients evaluated by the second method (open system) are assumed to better represent the over-all hydrodynamic conditions inside the column. They were therefore used in all correlation attempts described here. In three-parameter optimisations the mean standard deviation sank further to $6.03(10^{-4})$ and in 40 % of all measurements (mostly with higher phase throughputs and pulsation intensity), a regular increase of the transfer rate with column height was observed. However, the improved

fit of the profiles was mostly due to better representation of the random scatter of the experimental data. This proves that the assumption of constancy of the transfer rate in the middle part of the column is compatible with the level of experimental accuracy.

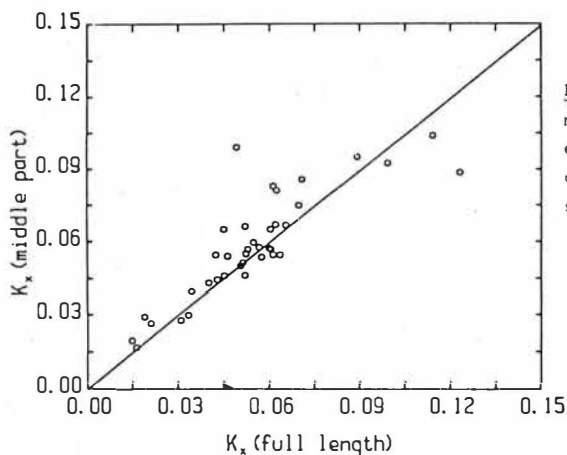


Figure 2: Comparison of mass transfer coefficients evaluated for full column length and over shorter section.

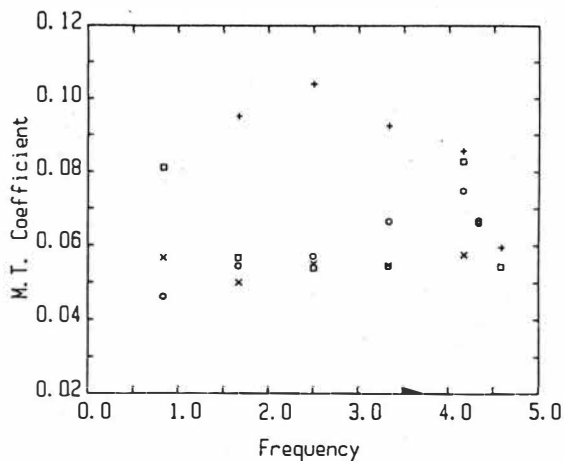


Figure 3: Dependence of mass transfer coefficient on specific throughputs and pulsation frequency. Mass transfer from dispersed toluene (T) to continuous water (W), phase ratio (W/T) is 0.69, specific throughput of both phases in $\text{m}^3/\text{m}^2\text{h}$:

(+) 28.2 (□) 45.7
(x) 63.2 (o) 73.8

As a rule, mass transfer coefficients evaluated from concentration profiles for all types of extraction columns are broadly scattered and cannot be correlated easily. This was observed also in the recent case, some results being shown in Fig. 3 and 4. In the former the variation of the optimised mass transfer coefficient with pulsation frequency is plotted for four experimental series with different specific throughputs (marked by different symbols). Though it is clear that both phase throughputs and pulsation intensity affect the transfer rate, no simple correlation is apparent. The influence of mass transfer direction is demonstrated in Fig. 4 where two series measured with identical phase throughputs are shown. This influence is so significant that only data measured in the same mass transfer direction should be correlated together.

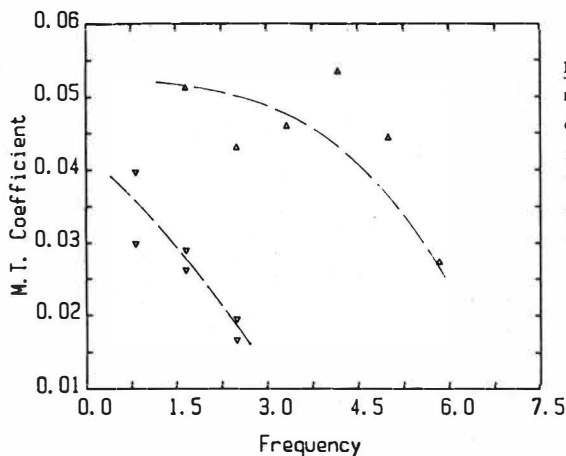


Figure 4: Influence of mass transfer direction on mass transfer coefficient. Phase ratio 1.15, specific throughput $44.1 \text{ m}^3/\text{m}^2\text{h}$, transfer direction: (Δ) T→W, (∇) W→T.

A correlation was first attempted in the common way of plotting the dimensionless mass transfer coefficient (Sherwood number) against the Reynolds number written with mean Sauter drop diameter and the relative drop velocity. Fig. 5 indicates that the Sherwood number varies with the Reynolds number raised to the power 0.8. Drop diameter therefore appears on both axes of the diagram and the correlation is thus meaningless. Fig. 6 shows the same variation when the mass transfer coefficient is used directly on the vertical axis.

A more serious attempt to correlate the parameters influencing the mass transfer rate gave:

$$K_x = 0.46 d_{32}^{0.98} (1-e)^{-2.0} u_c^{-0.68} u_d^{0.39} f^{0.40}$$

This equation is valid for mass transfer from dispersed toluene to a continuous water phase. The agreement with experimental data is shown in Fig. 7.

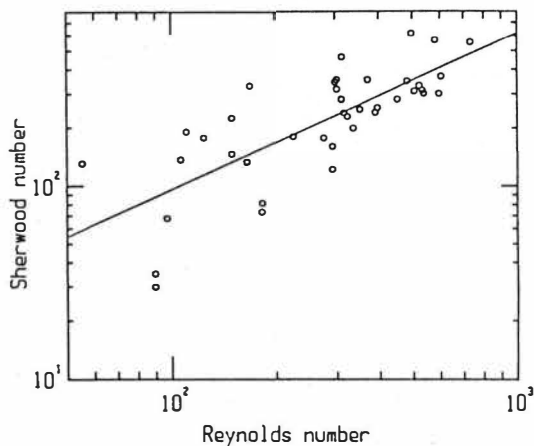


Figure 5: Variation of Sherwood number with Reynolds number (all available data).

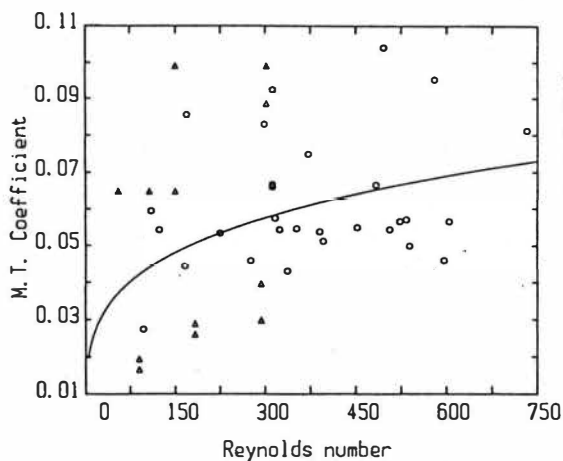


Figure 6: Variation of mass transfer coefficient with Reynolds number (same data as in Fig. 5).

Discussion: The results indicate that the transfer rate depends on mass transfer direction, mean drop diameter, hold-up, continuous and dispersed-phase velocities and frequency of agitation (which influences the transfer rate directly, not only through the drop diameter and the holdup). The strong dependence on continuous-phase holdup

raised to a negative power is rather surprising and may be due to parameter interactions. Unfortunately, all attempts to correlate against the primary parameters only (frequency and phase throughputs) give much worse results.

The magnitude of the measured transfer coefficients is comparable to those determined in stirred columns with intensive agitation. The results indicate that the relative velocity ($u_c + u_d$) is not a suitable correlating parameter and that the energy input directly influences the transfer process. This was also confirmed in a recent study on stirred columns (4) where individual transfer rates several times higher than those observed in undisturbed drop swarms were observed. Therefore, the transfer rates in columns with energy input should not be simulated using relations valid for single drops.

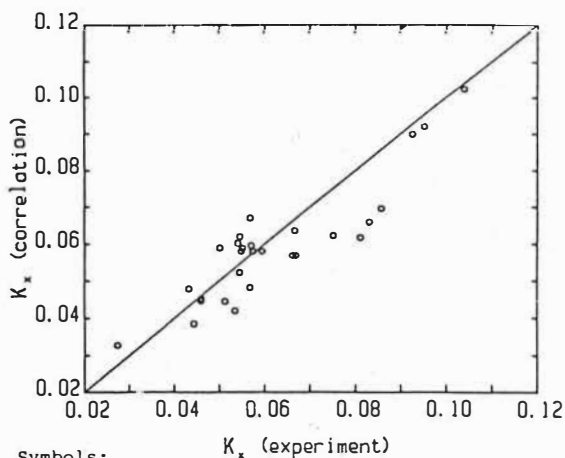


Figure 7: Agreement of proposed correlation with experimental data. Transfer direction T+W, Stand. deviation 10.7%.

Symbols:

- d_{32} - Mean Sauter drop diameter (m)
 - e - Holdup of dispersed phase
 - f - Pulsation frequency (Hz)
 - K_x - Over-all mass transfer coefficient ($\text{kg}/\text{m}^2\text{s}$)
 - u - Actual phase velocity inside column (m/s)
- indices: c - continuous, d - disperse, B - bottom, M - middle,
T - top, x - based on x-phase.

Literature:

1. Karr A.E., A.I.Ch.E. Journal 1959,5,446.
2. Bensalem A.-K., Diss. ETH No.7721, Zurich 1985.
3. Steiner L., Hartland S., Chem.Ing.Tech. 1980,52,MS-819.
4. Steiner L., Kumar A., Hartland S., 4th W.C.of Ch.Eng. Tokyo 1986 (accepted).

I. Colussi, V. Gallo, C. Luciani, U. Preti

Istituto di Chimica Applicata e Industriale - Università di Trieste

Via A. Valerio 2 - 34127 TRIESTE (Italy)

Introduction

The increase in energy costs has renewed interest in liquid-liquid extraction processes for industrial uses. This fact has concerned much research and development work in recent years in order to set up methods and equipments for the extraction of different chemical species from various solutions.

The objective of the present work was the determination of a model suitable for an accurate prediction of the performance of an extraction column, carrying out the experimental tests in a pilot plant composed of two packed columns as extraction and solvent regeneration units.

It is well known that packed liquid-liquid extraction columns suffer from the disadvantage of a difficult dispersion of the two phases. In addition, the performance of most types of liquid-liquid extraction columns is adversely affected by axial dispersion of one or both phases.

Dispersion or backmixing models used for the description of the axial dispersion and of the mass transfer processes in extraction columns have not given satisfactory results. Several authors have demonstrated the strong influence of the droplet size distribution, and theoretical models have been developed in order to predict the effects of size distribution on column performance.

In the present work, these concepts have been applied to the simulation of the extraction pilot plant. In particular, solvent extraction of Fe(III) from hydrochloric acid aqueous solutions was investigated; tributylphosphate (TBP) diluted with Solvesso 100 was used as extractant (1).

The chemical system examined is rather complex, because not only Fe(III) is extracted by TBP according to the following equation (2):



but also HCl is coextracted as (HCl·TBP) complex (3)(4)(5).

Pilot Plant Description

The pilot plant consisted of two glassy packed bed columns: the extraction column, and the washing column in which the organic extractant was regenerated before recycling.

The plant was equipped with a series of tanks for aqueous and organic solutions and with volumetric membrane pumps for the circulation of liquids.

The columns had the following characteristics: external diameter = 90 mm; internal diameter = 80 mm; total height = 2000 mm; distance between light phase and heavy phase distributors = 1560 mm.

The packing consisted of Raschig rings 10 mm diameter. Columns were equipped with lateral taps in order to allow sample withdrawals.

A scheme of the plant is illustrated in Fig. 1.

Plant Simulation

The metal amount transferred per unit time and per unit area of interface from the aqueous phase to the organic phase can be expressed by the following equation:

$$J = K_A \cdot (C_A - C_A^*) \quad (2)$$

The mass transfer model used took into account the variations of the interface area between the fluxes along the column, considering a plug flow condition for both phases.

The use of the model required the knowledge of:

- 1) an analytical expression of the interfacial area as a function of the distance from the inlet and of the flowrates of both phases;
- 2) the volumetric flowrate as a function of the concentration of solute;
- 3) a chemical equilibrium model for iron concentration between aqueous and organic phases;
- 4) an expression of mass transfer coefficient.

For this reason, experimental tests have been planned in order to obtain the following quantities:

- a) interface area values as a function of flowrate at different column heights;

- b) composition of the incoming and outgoing flows during column operation under steady state conditions;
- c) equilibrium data under different conditions.

Interfacial Area per Unit Volume of Dispersion

The interfacial area per unit volume of a dispersion of spherical droplets can be expressed by the following equation (t):

$$a = 6 h / d \quad (3)$$

- in which a = interfacial area/unit volume
 h = dispersed phase hold-up
 d = average drop size (Sauter mean)

As the average diameter of the droplets is relatively large in a packed extraction column, the photographic method was followed, making suitable corrections in order to take into account deformations of the image of the drops due to the vessel wall.

Different pictures were taken in various conditions of continuous and dispersed phase flowrates, varying the height of the packing into the column. Distribution of drop size was then measured by counting and sizing the population of drops. The data obtained were fitted by the following equation:

$$a = \frac{A}{(z+Z_0)^2} + \frac{B}{z+Z_0} + C \quad (4)$$

in which z is the distance from the lower distributor; parameters A, B, Z_0, C depend from the organic phase flowrate Q_0 only, according to the following equations:

$$A = A_1 + A_2 / Q_0 \quad (5)$$

$$B = B_1 + B_2 / Q_0 \quad (6)$$

$$Z_0 = Z_{01} + \exp(Z_{02} * Q_0) \quad (7)$$

$$C = C_1 * Q_0 + C_2 * Q_0 + C_3 * Q_0 \quad (8)$$

The fitting of the experimental data resulted very good; Fig. 2 represents the plot of a vs. z for a particular test.

The evaluation of the hold-up of the dispersed phase was carried out according to the following considerations: when the quantity of continuous phase is constant and the size of the column is known, the dispersed phase volume can be calculated under steady state conditions by measuring the variation of the height of the interface. This value must be referred to the zone of the column in which droplets of the dispersed phase are effectively present, that is the zone between the distributor and the interface during the running of the plant.

Mass Transfer Coefficient Analytical Expression

Eq. (2) can be expressed in the following form:

$$J = K_A^0 \cdot (C_A - C_A^*) \quad (9)$$

in which:

$$\frac{1}{K_A^0} = \frac{1}{K_A} + \frac{1}{k \cdot K_0} + \frac{1}{k \cdot V_i \cdot C_{TBP}^2} \quad (10)$$

This equation can be obtained under the hypothesis of steady state conditions, by combining equilibrium and kinetic expressions for the indicated reaction. The development of the calculations is reported in (7).

Chemical Equilibrium

The correlation of equilibrium data obtained at 298K by the separatory funnel technique is presented in Table 1.

Theoretical considerations which have been made in order to obtain the fitting expression reported in Tab. 1 are discussed in (7).

Experimental

The chemical system considered was composed by hydrochloric acid solution 4.3 M in which iron was dissolved. The organic phase was composed by TBP 20% vol. as extractant, diluted with Solvesso 100 80% vol.

The data obtained from the experiments carried out on the pilot plant are illustrated in Table 2. For each run, material balance calculations have been made; Fig. 3 is an example of such calculations.

The extraction of iron resulted very good; the same, for the organic phase regene-

ration. Fig. 2 illustrates, as an example, the values of: interfacial area per unit height of column, driving force, iron concentration in aqueous phase as a function of the distance from the organic phase distributor, obtained in the experimental tests.

In conclusion, the extraction of iron is complete and good results have been obtained for the simulation of the pilot plant, in particular for the analytical representation of the specific interfacial area and the chemical equilibrium.

Acknowledgement

This work was carried out with the support of "Progetto Finalizzato Metallurgia C.N.R." (Rome).

EQUILIBRIUM DATA

FITTING EXPRESSION

$$C_A^c = K \cdot (C_{TBP} - 2 \cdot C_o)^2$$

CALCULATED K PARAMETER = 9.027

UNCERTAINTY = 0.0086

TEST N.	$C_A^s \cdot 10^3$	$C_A^c \cdot 10^3$	$C_o \cdot 10^3$	C_{TBP}
1	87.6	94.6	121.6	0.60
2	30.3	50.6	88.5	0.60
3	140.5	136.7	134.8	0.60
4	189.2	154.6	139.8	0.60
5	112.6	123.8	129.7	0.60
6	201.3	173.5	146.8	0.60
7	18.0	33.3	70.4	0.60
8	81.1	87.0	119.8	0.60
9	769.4	836.6	228.1	0.63
10	951.3	879.4	229.9	0.63
11	567.7	454.4	203.6	0.63
12	443.2	430.8	201.3	0.63
13	598.4	697.3	221.3	0.63
14	265.9	253.3	176.2	0.63
15	10.1	30.1	67.0	0.63
16	34.4	69.4	110.3	0.63
17	0.81	2.16	9.73	0.63
18	1.37	3.96	15.53	0.63
19	2.34	6.84	30.09	0.63
20	0.13	0.23	1.26	0.63

C_A^c = calculated aqueous phase iron concentration (Kmol/m³)
 C_A^s = experimental aqueous phase iron concentration (Kmol/m³)
 C_o = experimental organic phase iron concentration (Kmol/m³)
 C_{TBP} = experimental organic phase TBP concentration (Kmol/m³)

TABLE 1

PLANT TESTS - EXTRACTION COLUMN

TEST CONDITIONS

packing height = 1.35 m interface height = 1.38 m

inlet organic phase iron concentration = 0.0 Kmol/m³

N.	Q _A	Q _O	C _A ⁱ	C _A ^o	C _O ^o	K
FIRST SERIES			T = 298 K	TBP = .60	Kmol/m ³	
1	6.70	5.56	210.8	88.5	147.5	60.0
2	5.67	4.33	227.0	110.6	152.2	60.4
3	3.28	4.17	230.6	48.3	143.4	58.3
SECOND SERIES			T = 283 K	TBP = .63	Kmol/m ³	
4	6.75	5.56	86.8	6.0	83.1	118.5
5	4.61	4.33	86.8	8.1	86.5	129.8
6	2.18	2.22	86.8	6.0	79.2	126.6

Q_A = aqueous phase flow rate (m³/s*10⁶)

Q_O = organic phase flow rate (m³/s*10⁶)

C_Aⁱ = inlet aqueous phase iron concentration (Kmol/m³*10³)

C_A^o = outlet aqueous phase iron concentration (Kmol/m³*10³)

C_O^o = outlet organic phase iron concentration (Kmol/m³*10³)

K = mass transfer coefficient (m/s*10⁶)

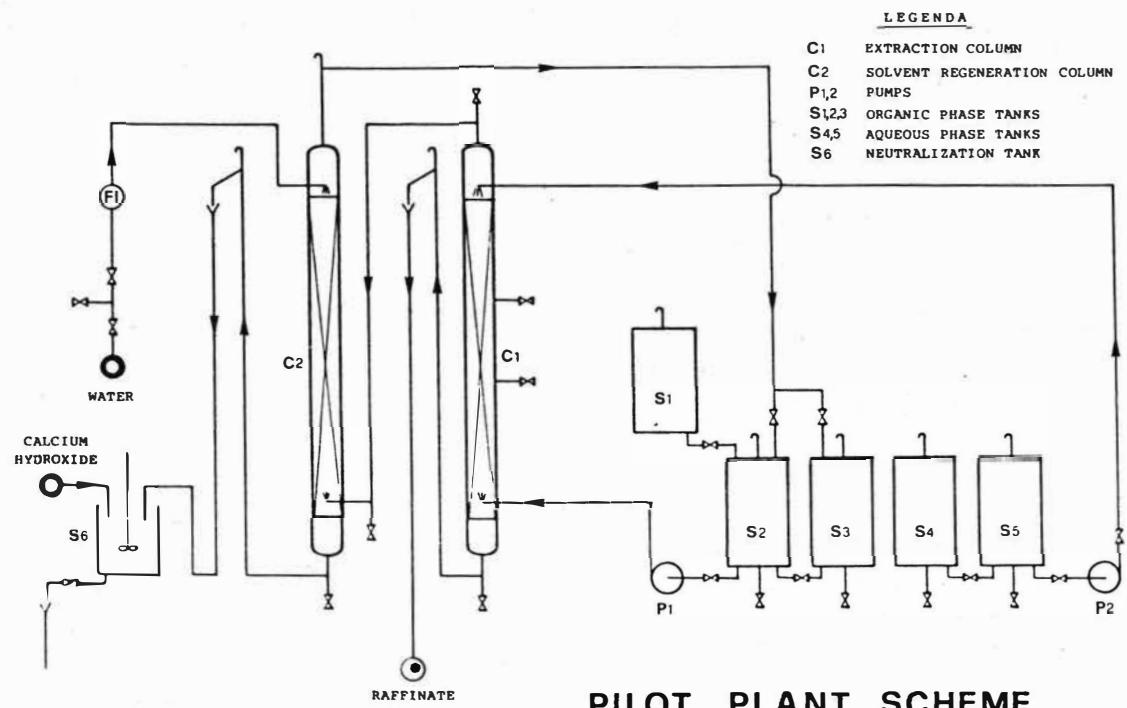
TABLE 2

Nomenclature

C _A	iron concentration in aqueous phase
C _A [*]	equilibrium iron concentration in aqueous phase
C _O	iron concentration in organic phase
J	mass transfer rate
k	equilibrium constant
K _A	aqueous phase mass transfer coefficient
K _A ^o	overall mass transfer coefficient referred to aqueous phase
K _O	organic phase mass transfer coefficient
V	kinetic coefficient
z	distance from organic phase distributor

References

- 1) Colussi, I., Kikic, I., Preti, U., Cocco, A., ISEC 83, 248 (1983).
- 2) Levin, V. I., Meshcherova, I. V., Samrov, U. K., Radiochimia, 3, 417 (1961).
- 3) Hesford, E., McKay, H. A. C., J. Inorg. Nucl. Chem., 13, 156 (1960).
- 4) Baldwin, W. H., Higgins, C. E., Soldano, B. A., J. Phys. Chem., 63, 113 and 118 (1959).
- 5) Nishimura, S., Tokura, I., and Kondo, Y., Mem. Fac. Eng. Kyoto Univ., 27(2), 202 (1965).
- 6) de Carvalho, J. M. R., and Slater, M. J., Chempor '81, 1.170 (1981).
- 7) Luciani, C., Thesis, University of Trieste (Italy) (1986).



LEGENDA

- C1 EXTRACTION COLUMN
- C2 SOLVENT REGENERATION COLUMN
- P1,2 PUMPS
- S1,2,3 ORGANIC PHASE TANKS
- S4,5 AQUEOUS PHASE TANKS
- S6 NEUTRALIZATION TANK

FIG. 1

PILOT PLANT SCHEME

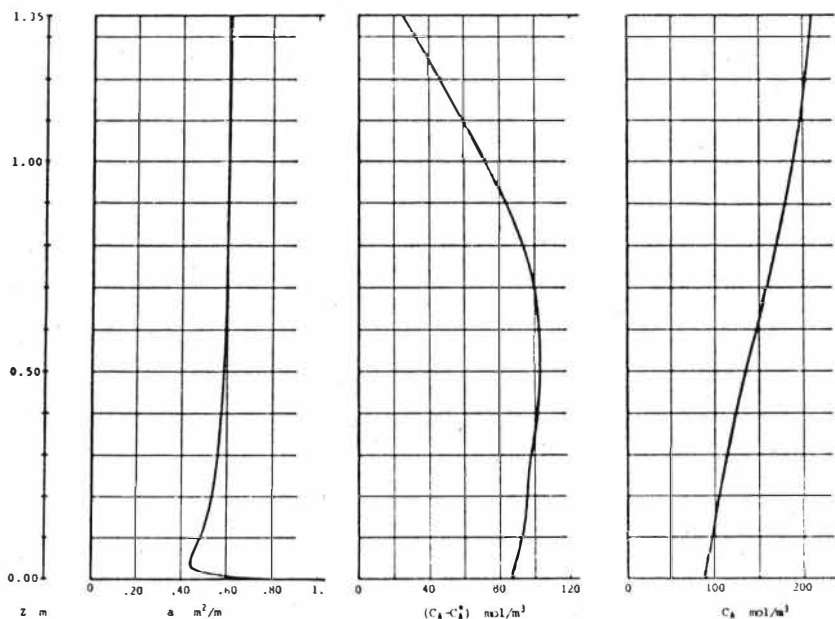


FIG. 2

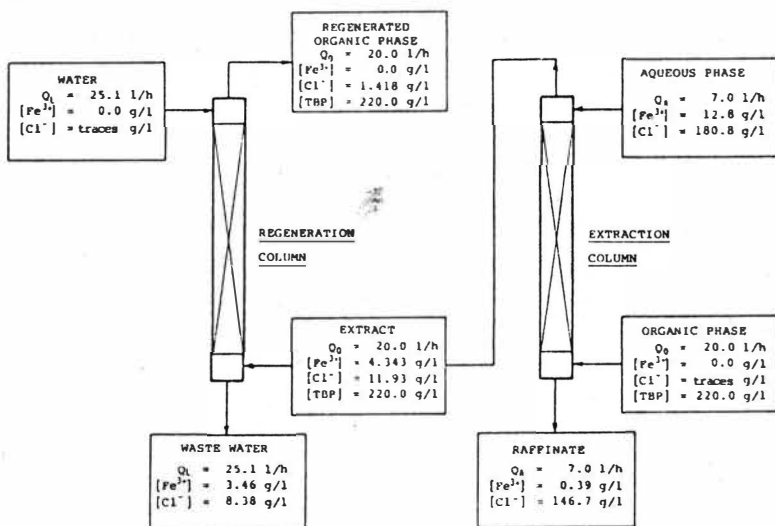


FIG. 3

EXPERIMENTAL DESIGN, DECONVOLUTION OF RTD DATA AND RESPONSE SURFACE ANALYSIS IN SOLVENT EXTRACTION

J.J.Porta and A.Merz
Kernforschungszentrum Karlsruhe GmbH / F.R.G.

SYSTEM IDENTIFICATION

The basic problem in model building is to deduce a structure or a set of equations for a physical system on the basis of experimental observations of the real world. This can be only done by means of a rigorous and systematic mathematical procedure. The model which results is then a quantitative summary of these observations, which, in some sense, can then be used to replace the system itself.

The development of a model can proceed along different routes, depending on the amount of a priori information we have on the functional form of the model. The usual approach in solvent extraction has been to assume a certain model on the base of conservation equations and transport phenomena principles. Here we have to do with a *parameter estimation problem*, where the model output has to match the observed experimental data as closely as possible.

In the unit operation of liquid-liquid extraction, the system and apparatus are so complicated that we are forced to view them as a gray box. We don't have enough a priori information on the form of the model or any parameters that might be important.

The problem of constructing a model purely from input/output data is called the *identification problem* [1]. The common objective of identification and parameter estimation are system diagnosis and control.

Engineering problems can be broadly classified as *direct* or *inverse* problems. To clarify this distinction consider the system illustrated in Figure 1



Figure 1. Systems approach to process identification

If the equations describing the solvent extraction system are known, the direct problem consists of finding the response to a specific input or excitation.

For example, with a given set of equations describing the extraction dynamics of a mixer-settler battery, it may be desired to find the apparatus response to a given feed disturbance. This is a common problem of engineering analysis.

In the much more difficult inverse problem, the response to a particular input or inputs are known, but the equations describing the process are unknown. We have to find a system description which fits such a physically realizable situation as closely as possible. This is a *design problem*, which usually has additional constraints placed upon it, such as time, size, cost, etc. Clearly, there is no unique solution to the design problem, since an infinitely large number of possible processes may show the same input-output behaviour.

Our problem, which may be one of the most difficult inverse problems, is the *modelling or identification problem*: given a set of inputs and corresponding outputs from a system, we want to find a mathematical description (model) for it. For example, concentration, drop-size, hold-up profiles and residence time distributions under several experimental conditions may be given, and it may be desired to find the set of equations which describe the dynamic extraction behaviour of a pulse column.

DECONVOLUTION PROBLEM

The relationship between integral (or energy) methods, differential (or momentum) methods, and linear algebra arises naturally in the field of inverse theory. Like most experiments in applied science we have only *indirect measurements*. That is, the observed data are linear integral (or matrix) transforms of the quantities to be estimated. In RTD process analysis these operators may be approximated by Fredholm integral equations of the first kind of the convolution type.

The inversion of these integral equations is an *ill-posed problem* in the sense of Hadamard /2/. This means that, even for arbitrarily small (but nonzero) noise levels in the data, there still exists a large (typically infinite) set of solutions that all fit the data to within the experimental error. Even worse, solutions in this set can differ from each other by arbitrarily large amounts; i.e., the errors in the solutions are unbounded. Therefore straightforward inversion procedures or iterative algorithms converging to them cannot be directly applied to experimental data and statistical *regularization* techniques are necessary.

The numerical solution of the convolution integral is an extremely difficult problem. The main difficulty is that the solution (system weighting function) does not depend continuously on the data. Therefore, we could have two impulse responses which are radically different and yet produce the same output when convolved with the experimental input signal. It is important to point out that the problem is neither in the digital representation of the signals, nor in the numerical technique used to obtain the solution. The real problem is that *the convolution operator does not have an inverse*, because zero is the accumulating point of its smallest eigenvalues /3/.

A wide distributed method for stabilizing the ill-posedness of convolution integrals consists in reducing the number of degrees of freedom by fitting a parametrized model to the data or to use a coarse grid to represent the solution. Here there is the dilemma that serious errors can result if the number of degrees of freedom is too small (because of an inadequate model) or too large (because of instability of the solution to noise).

A much better alternative imposes *prior knowledge* of the statistical properties of the solution and the *principle of parsimony* to impose constraints in the inversion of the Fredholm integral equation by means of a suitable regularizer /4/. By these means a great increase in accuracy and resolution of the solution can be achieved. This method is very elegant but involves cumbersome computer calculations that have to be tackled with mainframe computers /5/.

Our approach makes use of the convolution theorem that allows numerical discrete Fourier extrapolation techniques with analytic continuation in the frequency space and low-pass filtering of the solution /6,7/. The algorithm was implemented on a PDP-11/60 minicomputer and vectorized for parallel array processing /8/, so that the calculation time for a deconvolution is of the order of 1 s. Figure 2 illustrates the results of a 16K FFT deconvolution for the continuous phase of a 100 mm i.d. pulse column with nozzle plates.

If the entire spectrum after complex division in the Fourier domain is transformed back to the time domain, the result, apparent from Figure 2 is nonsense. One notes by examining the transforms for the input and output signals, that a small residual noise (due to machine roundoff in the computer, noise and error in the original data) extends the whole length of the spectrum. Division in the high frequency region, due to the random nature of the noise, can give rise to enormous numbers. Thus one is forced to bandlimit the DFT data by means of suitable spectral windows /9/, taking the principal solution /10/ as being the correct one.

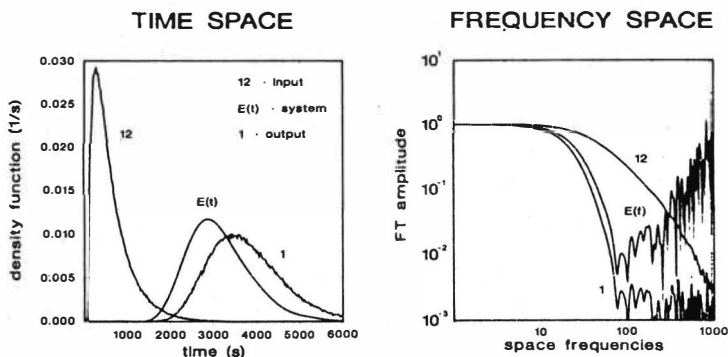


Figure 2. FFT deconvolution in the frequency and time domains

EXPERIMENTAL DESIGN

The experimental program was defined as the study of important parameters of practical significance for the operation of pulsed extraction columns in the reprocessing of nuclear fuel by the PUREX process.

The experimental variables studied were:

- Total flow rate through the pulse columns
- Flow ratio of disperse/continuous phase
- Pulse frequency
- Pulse amplitude
- Axial column position
- Plate geometry (sieve and nozzle plates)

with following response functions:

- Drop size distribution parameters
- Hold-up of the disperse phase
- Axial mixing
- Extraction efficiency for uranium

It should be realized that in the absence of adequate prior work, the choice of the appropriate experimental variables played here a very important role. For instance, many authors /11/ report that the product of puls frequency (f) and amplitude (A), or the quotient of disperse phase velocity to $A.f$ as a dimensionless group are pertinent variables in itself. There is also the

problem regarding the effects of any simultaneous mass transfer action on the fluid-dynamical behaviour.

The statistical design specified the number of runs to be made and the experimental conditions for each one. In order to be able to estimate the coefficients of a second order hypersurface model with 5 independent variables, and to avoid the full 3^5 factorial (81 experiments for every detector), a rotatable central composite design (CCD) /12/ was selected. Figure 3 shows schematically the CCD for 3 independent variables. Now the statistical design was a most important matter, for it served to generate the information desired with a great economy of time and effort.

Central Composite Design

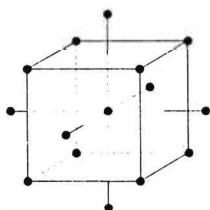


Figure 3. Rotatable design for 3 independent variables

The design employed comprises a delicate balance of properties. It possesses a certain symmetry which facilitates the analysis of variance (ANOVA) and acts to minimize the errors in specifying the constants delineating the responses /13/. The experimentes were so planned as to probe rather evenly the entire field of operations, avoiding both a grouping of runs in a restricted region and a failure to explore the outer reaches.

STATISTICAL ANALYSIS

The statistical analysis required that a selection be made of the functional forms in which the chosen variables were to be expressed. At stake is the ability of an assumed quadratic Taylor's series expansion of the unknown response function to adequately fit the data. The basis for choice of the functional forms of the variables can also be interpreted as the desire for a certain simplicity in the shape of a space model representing the chosen response function. In general the requirements could be best met if the vari-

ables were expressed in those functional forms which have a solid theoretical background. Unfortunately, such a background does not exist for this problem.

Within the range of the experiments, the best relationships fitting the data for second order linear models were determined. In order to visualize the information content of these equations, they can be transformed to their canonical form and presented as response surfaces (see Figure 4) or contour plots. The latter translate the model equations into maps of the response values over two-dimensional slices of the factor space.

SIEVE PLATES

NOZZLE PLATES

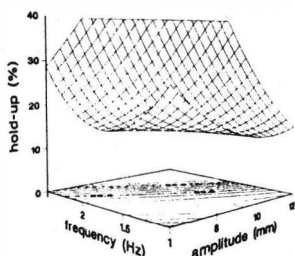
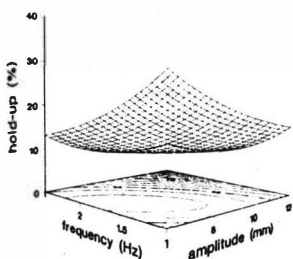


Figure 4. Hold-up response surface analysis for sieve and nozzle plates

SIEVE PLATES

NOZZLE PLATES

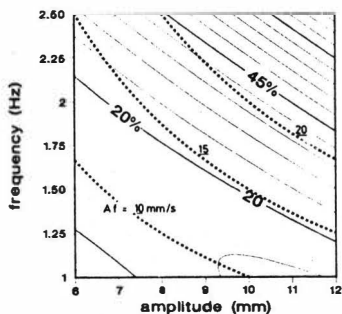
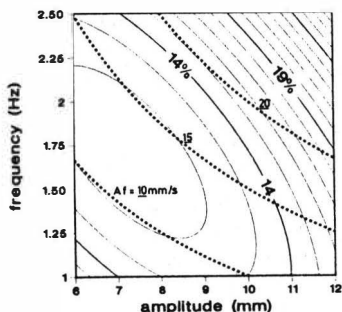


Figure 5. Hold-up contours for sieve and nozzle plates showing constant A.f lines

Figure 5 shows the results for the hold-up as a function of pulse amplitude and frequency. The dashed lines represent the often cited constant A.f hyperbolas.

It can be easily observed that the plate geometry plays a very important role on the hold-up behaviour of a pulse column. A strong interaction between pulse amplitude and frequency is present in both cases. This fact may well be a plausible explanation for the wide variation of experimental results reported in the literature, where the factor treatments are not orthogonal and interactions were not considered. Similar functional dependences on the experimental variables were also observed for the sizes of the droplet phase as response function. Detailed results for the main effects and interactions of all the experimental factors are to be reported later on /14/.

SUMMARY

This paper has attempted to clarify some experimental and computational problems and procedures of process identification relevant in solvent extraction operations.

A method has been presented for inverting the convolution equation arising in the experimental determination of RTD data for extraction systems. The problems of instability and nonuniqueness were minimized by constraining the distribution to be the smoothest nonnegative one that is consistent with the data (parsimony).

The benefits of the experimental and analytical approach can be summarized as:

- the organized approach toward the collection and analysis of data gives maximum information per experimental run
- assesment of information reliability in the light of experimental and analytical variation
- capability to see interactions among experimental variables, leading to more reliable predictions of the response data in areas not directly covered by experimentation

It should be mentioned that a great deal of experimental and theoretical work is currently in progress in this area and by no means can be concluded that the problems have been fully clarified and mathematically solved.

BIBLIOGRAPHICAL REFERENCES

- /1/ Zadeh, L. : I.R.E. Trans. Circuit Theory 3 (1956) 277
- /2/ Courant, R. and Hilbert, D.: "Methods of mathematical physics". Vol. 2, Interscience, New York (1962)
- /3/ Stakgold, I.: "Green's functions and boundary value problems". John Wiley & Sons, New York (1979)
- /4/ Tichonow, A.W. and Arsenin, V.Y.: "Solution of ill-posed problems". John Wiley & Sons, London (1977)
- /5/ Provencher, S.W.: CONTIN Users Manual, EMBL Technical Report DA05, European Molecular Biology Laboratory (1982)
- /6/ Al-Faour, O.M.: Ph.D. Thesis, Univ. College of Wales (1981)
- /7/ Redshaw, T.C.: Ph.D. Thesis, Univ. College of Wales (1982)
- /8/ Merz, A., Porta, J.J. and Walter, R.: ISEC '86 Proceedings
- /9/ Papoulis, A.: "Signal analysis". McGraw-Hill, New York (1984)
- /10/ Bracewell, R.: "The Fourier transform and its applications". McGraw-Hill, New York (1978)
- /11/ Lo, T.C., Baird, M.H.I. and Hanson, C.: "Handbook of solvent extraction". John Wiley & Sons, New York (1983)
- /12/ Box, G.E.P.: Biometrics 10 (1954) 16
- /13/ Box, G.E.P., Hunter, W.G. and Hunter, J.S.: "Statistics for Experimenters". John Wiley & Sons, New York (1978)
- /14/ Porta, J.J. : publication in preparation

Evaluation of Mass Transfer and Axial Mixing Parameters in Pulsed Sieve Plate Extraction Columns

Xia Lei, Yu Qian, Wei-Yang Fei and Jia-Ding Wang
 Chemical Engineering Department
 Tsinghua University, Beijing/China

The "true" height of transfer unit ($HTU_{OX} = V_x/K_{OX}a$) and axial mixing coefficients are considered to be the key parameters in study on mass transfer characteristics and in scale up of differential type contactors. Evaluation of these parameters from measured concentration profiles have been done by many authors (1-7). Measurement of concentration profiles of both phases in a column under steady state is rather time consuming and large quantity of both solution and solvent must be handled during operation and solvent recovery. Besides, it is tedious to acquire pure samples of each phase along a column, especially in experimental columns of rather large diameters. In order to reduce these difficulties in experimental works necessary for development of scale-up procedures for extraction columns, the present work is to examine the possibility of applying a dynamic stimulus-response method for evaluation of the "true" HTU and axial mixing coefficients simultaneously.

Procedure and Modelling: With the same idea as evaluation of axial mixing coefficient of continuous phase in absence of mass transfer by stimulus-response method, solute to be extracted was introduced (as tracer) into the feed stream (solute free or very dilute in solution) while the extraction flow system has attained steady state. Then, the transient solute concentrations in the raffinate were measured and the required parameters evaluated by an algorithm fitting the transient concentration curve. The diffusion model has been used to evaluate mass transfer and axial mixing parameters in a previous work (6,7) by measurement of concentration profiles under steady state. While under unsteady state, intergral equations could be written across a differential section of dimensionless height of Z^1-Z^2 at time interval $t'-t$ according to law of conservation of mass:

$$\int_{Z^1}^{Z^2} \bar{c}_x(x_i - x_i^*) dZ + \int_{t'}^{t''} \left[\left(x - \frac{1}{Pe_x} \frac{\partial x}{\partial Z} \right)_{Z^2} - \left(x - \frac{1}{Pe_x} \frac{\partial x}{\partial Z} \right)_{Z^1} \right] dt + \int_{t'}^{t''} \int_{Z^1}^{Z^2} N_{Ox} (x - x^*) dZ = 0 \quad (1)$$

$$\int_{Z^1}^{Z^2} \bar{c}_y(y_i - y_i^*) dZ - \int_{t'}^{t''} \left[\left(y + \frac{1}{Pe_y} \frac{\partial y}{\partial Z} \right)_{Z^2} - \left(y + \frac{1}{Pe_y} \frac{\partial y}{\partial Z} \right)_{Z^1} \right] dt - \int_{t'}^{t''} \int_{Z^1}^{Z^2} N_{Ox} \frac{V_x}{V_y} (x - x^*) dZ = 0 \quad (2)$$

where

$$\begin{aligned} Z &= l/L, & \tau_x &= L(1-\psi)/V_x, & \tau_y &= L\psi/V_y \\ N_{ox} &= LK_{ox}\alpha/V_x, & Pe_x &= L V_x/E_x, & Pe_y &= L V_y/E_y \end{aligned}$$

For solution of these equations a difference scheme could be derived in the mean implicit form as:

$$\begin{aligned} \tau_x^n (x_j^{n+1} - x_j^n) h &= \frac{\tau}{2} \left[\left(x_{j-1/2}^{n+1} \frac{x_j^n - x_{j-1}^{n+1}}{Pe_{xj-1/2} h} \right) + \left(x_{j-1/2}^n \frac{x_j^n - x_{j-1}^n}{Pe_{xj-1/2} h} \right) \right] - \frac{\tau}{2} \left[\left(x_{j+1/2}^{n+1} \frac{x_{j+1}^{n+1} - x_j^n}{Pe_{xj+1/2} h} \right) + \left(x_{j+1/2}^n \frac{x_{j+1}^n - x_j^n}{Pe_{xj+1/2} h} \right) \right] \\ &\quad - \frac{\tau h}{2} \left[N_{ox,j}^{n+1} (x_j^{n+1} - x_j^n) + N_{ox,j}^n (x_j^n - x_j^{n-1}) \right] \end{aligned} \quad (3)$$

$$\begin{aligned} \tau_y^n (y_j^{n+1} - y_j^n) h &= \frac{\tau}{2} \left[\left(y_{j+1/2}^{n+1} \frac{y_{j+1}^{n+1} - y_j^n}{Pe_{yj+1/2} h} \right) + \left(y_{j+1/2}^n \frac{y_{j+1}^n - y_j^n}{Pe_{yj+1/2} h} \right) \right] - \frac{\tau}{2} \left[\left(y_{j-1/2}^{n+1} \frac{y_j^n - y_{j-1}^{n+1}}{Pe_{yj-1/2} h} \right) + \left(y_{j-1/2}^n \frac{y_j^n - y_{j-1}^n}{Pe_{yj-1/2} h} \right) \right] \\ &\quad + \frac{\tau h}{2} \left[\left(\frac{V_x}{V_y} \right)_j N_{ox,j}^{n+1} (x_j^{n+1} - x_j^n) + \left(\frac{V_x}{V_y} \right)_j N_{ox,j}^n (x_j^n - x_j^{n-1}) \right] \end{aligned} \quad (4)$$

(j = 1, 2, ..., J; n = 1, 2, ...)

This scheme has a stability independent of the value of any parameter and/or step size, and it has a second order precision either to the distance step or to the time step. This scheme is suitable for the condition that the parameters NTU_{ox} (N_{ox} in equation), Pe_x , Pe_y , τ_x , τ_y , V_x and V_y vary with position and time. Simplified assumptions are made that the parameters NTU_{ox} , Pe_x , Pe_y and ψ are constant throughout the extraction section and mass transfer outside the section can be neglected. As the column is to be operated with aqueous (heavy) stream as continuous phase, interphase will be positioned in the upper enlarged decanter, then the upper boundary can be regarded as closed. But, the lower boundary has to be regarded as open, because back mixing in the lower enlarged section would effect the raffinate concentration at the sampling port just below the bottom plate. In this case, approximately perfect mixing is assumed in the lower enlarged section and the lower boundary becomes internal boundary following the same scheme. Based on these simplified assumption, the whole set of difference equations can be written by dividing the sieve plate section and lower decanter into given number of segments respectively. While the inlet concentration of the two phase, x_f and y_s , and an initial profile are given, the transient concentration profiles along the column can be simulated by solving the difference equations step by step in a given time step size, τ . Thus, the parameters NTU_{ox} , Pe_x and Pe_y are evaluated by fitting the measured raffinate concentration with Marquadt's optimisation procedure. Then the HTU_{ox} and HTU_{oxd} are calculated: $HTU_{ox} = L/NTU_{ox}$, and HTU_{oxd} by the approximate method proposed by Miyauchi and

Vermulen (8).

Experimental: Experimental runs were carried out in a glass column of 0.04 m (4 cm) in inside diameter equipped with a "dispersion-coalescence" type cartridge which consisting of one louver plate (organic wettable) situated in between every three "standard" sieve plates made of stainless steel with spacing between plates of 0.025 m (2.5cm). Detail of the cartridge and arrangement of the equipment are given by Lei, et al. (7). HNO_3 was transferred from aqueous (continuous) phase into dispersed 30% TBP (kerosene). In each run, the pre-equilibrated phases with about 0.4N HNO_3 in the aqueous feed stream were brought into steady operation in the column. Then, through a switch valve, situated at the inlet of the feed line, the feed was switched to the "tracer" solution of 2N HNO_3 . The "tracer" feed continued for 5 minutes before the original feed was switched back. This resembled a rectangular stimulus signal to the system. The first raffinate sample was taken from 15 sec. before the "tracer" stream switched on to 15 sec. after it, and marked as sample of zero time. Successive samples were taken in every 30 sec. The error allowed for sample analysis was set to less than 0.01N HNO_3 as required by the simulation algorithm. Runs in the column of 0.04 m in diameter were carried out under pulse amplitude, $A = 0.01$ m (1 cm) and frequency, $f = 2 \text{ sec}^{-1}$ while flow ratio $V_y/V_x = 1; 2; 3$ with the superficial velocity of the aqueous phase, V_x , varies from 1.36×10^{-3} to 4.07×10^{-3} m/sec. Fewer data were taken at $A = 0.005$ m (0.5 cm) and $A = 0.015$ m (1.5 cm). A few runs were carried out in a column of 0.1 m in diameter equipped with the same type of "dispersion-coalescence" cartridge.

Results and Discussion: Fig.1 shows a set of experimental response curves of the raffinate under different total flow rate while other operation conditions are fixed. It is obvious that experimental points on left of the peak point of each curve (i.e. on the rising portion of the curve) carry the most significant and accurate information of mass transfer in the column while points on the falling part of the curve may contain the information of stripping as the original feed of low acid concentration has been switched back after the "tracer" stimulus. In order to minimize any error caused by this local stripping effect, only the rising portion of the curves are fitted by Marquadt's method in the present algorithm. Parameters evaluated by this method are "true" NTU_{OX} (N_{OX}), Peclet number of continuous phase (Pe_x) and Peclet number of dispersed phase (Pe_y). Fig.2 shows the comparison of the "start up" transient curve simulated by use of the parameters

evaluated by this method and the experimental data collected in a testing run using step-input signal (2N HNO₃). Fig.3 shows the comparison of the simulated steady state concentration profiles and the measured data. It can be seen the simulated curves fit the experimental results, and the method of using 5 minutes rectangular signal is justified.

The effect of measurement error of the solute concentration on evaluated results has been examined by Monte-Carlo simulation technique and statistical inference method:

Standard deviation of
measured concentration

0.01 x_r

Parameters	NTU _{OX}	Pe _x	Pe _y
True value	5.00	8.00	8.00
Mean estimated value	5.08	7.95	7.78
Standard deviation	0.23	0.17	0.26
Half of confidence interval (degree of confidence:99%)	0.08	0.06	0.10

The HTU_{OX} and HTU_{OXd} (height of dispersion unit) are calculated from the evaluated NTU_{OX}, Pe_x and Pe_y for each experimental run and the results are plotted as shown in Fig.4 and Fig.5. One set of results obtained by steady state concentration profiles (7) is also shown for comparison.

Results obtained in this work and those obtained in a previous work of Lei, et al. (7) by steady state concentration profiles method are correlated by regression of 60 sets of data into empirical equations:

$$H_{\bullet x} = 5.55 \times 10^{-2} (af^3/v_T)^{-0.66} (v_y/v_x)^{-0.86} \quad (5)$$

Equ.(5) bears the form given by Ziolkowski in 1974 (2).

$$H_{\text{Oxd}} = 0.29 (af/v_T)^{0.60} (v_y/v_x)^{-0.77} \quad (6)$$

Fig.6 shows that 90% of the experimental points fall in the zone of ±20% deviation, and Fig.7 shows that 81% of the experimental points fall in the zone of ±20% deviation.

Conclusion: The dynamic stimulus-response method of applying a rectangular signal to the feed stream is feasible for evaluation of

mass transfer and axial mixing parameters in a pulsed sieve plate column. Experimental technique and the corresponding algorithm suggested have been examined by a single solute extraction system of $\text{HNO}_3(\text{aq.}) - 30\% \text{ TBP (in kerosene)}$. In comparison to the results obtained from steady state concentration profiles, reasonable consistency has been acquired. Extending it's application to multicomponent extraction system would benefit research works for scale up procedure.

Notation:

- A - Pulse amplitude, m
- a - Half of pulse amplitude, $=A/2$, m
- Specific interfacial area, m^2/m^3
- E - Axial dispersion coefficient, m^2/sec
- f - Frequency of pulsation, sec^{-1}
- HTU_{ox} - "True" overall height of transfer unit based on continuous phase, m
- HTU_{oxd} - Height of overall dispersion unit based on continuous phase, m
- h - Distance step size in difference equations, dimensionless
- K_{ox} - overall mass transfer coefficient based on continuous phase, m/sec
- L - Effective extraction height in column, m
- l - Height along the column, m
- NTU_{ox} - "True" overall number of transfer unit
- Pe_{ox} - Peclet number, $= Vl/E$, dimensionless
- t - time, sec
- V - Superficial flow velocity, m/sec
- V_T - Total velocity of two phases, $= V_x + V_y$, m/sec
- x - Solute concentration in continuous phase, N
- y - Solute concentration in dispersed phase, N
- Z - Dimensionless length, $= l/L$
- ψ - Fraction of hold up
- τ - Time step size in difference equations, sec
- τ_x, τ_y - Parameters in equations (1), (2), (3), (4)
- x_0 - initial concentration of aqueous solution, N
- x_f - Concentration of "tracer" feed solution, N
- x_r - Measured concentration of raffinate, N

Superscripts

- * - Equilibrium

Literature Cited:

- (1) Rod, V., British Chem. Engr., 1964, 9(5), 300
- (2) Ziolkowski, Z., Inz. Chem. (Poland), 1974, 4(1), 163
- (3) Sleiner, L., Hartland, S., I&EC, Process Design & Dev., 1978, 17(2), 175
- (4) Rod, V., Fei, W. Y., Hanson, C., Chem. Eng. Res. Des., 1983, 61(9), 290
- (5) Ricker, N. L., King, C. J., et al, AIChE J., 1981, 27(2), 277
- (6) Lei, X., Fei, W. Y., Shen, Z. Y., Wang, J. D., Jour. of CIESC (in Chinese) 1982, 4, 368
- (7) Lei, X., Dai, Y. Y., Shen, Z. Y., Wang, J. D., Proc. CIESC/AIChE Joint Meeting of Chem. Eng., Vol. II, 538, 1982
- (8) Miyauchi, T., Vermeulen, T., I&EC, Fundam., 1963, 2(2), 113

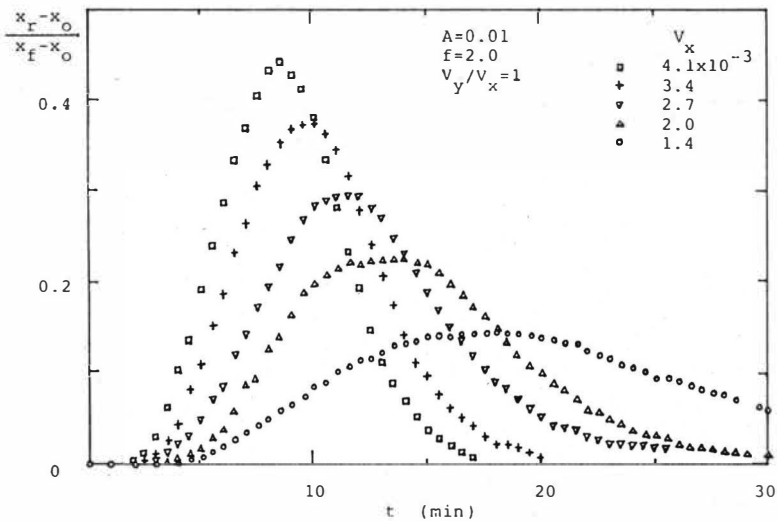


Fig 1. Response Curve of Raffinate
(5 minutes' rectangular signal)

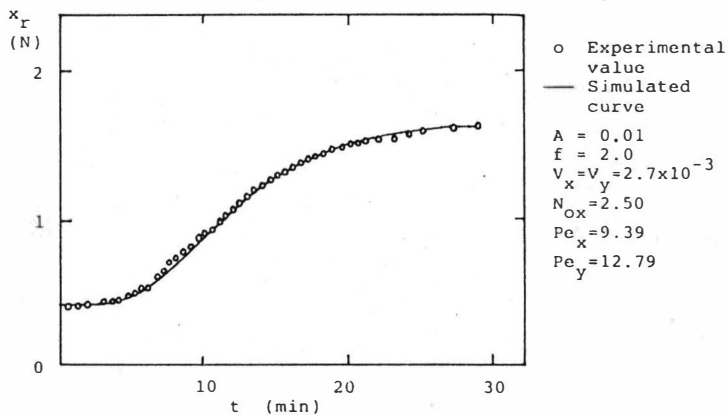


Fig 2. Comparison of Transient Curve Simulated from Evaluated Parameters with Measured Values

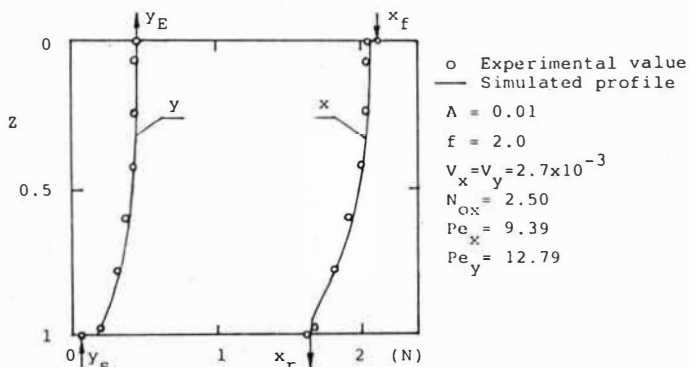


Fig 3. Comparison of the simulated and measured concentration profiles under steady state

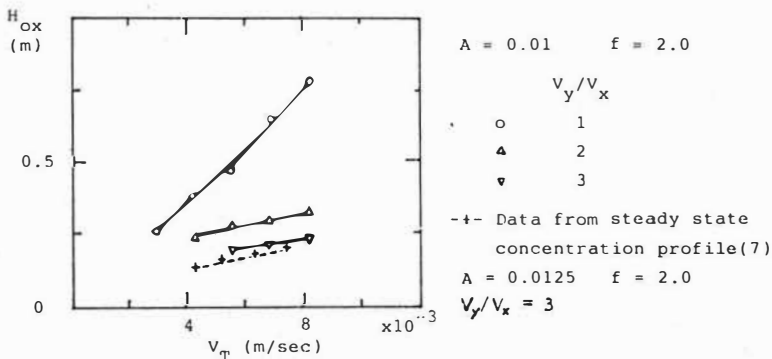


Fig 4. H_{ox} vs. V_T

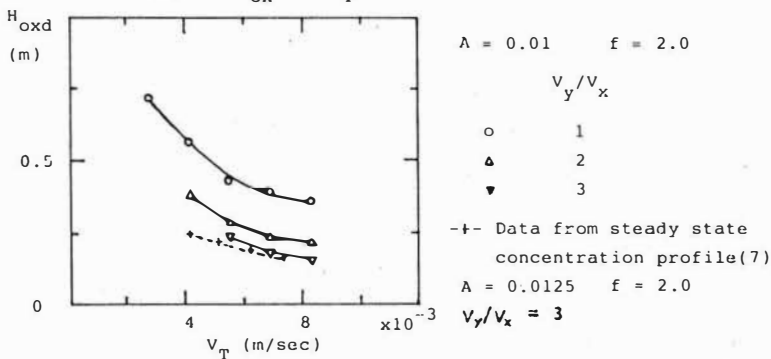


Fig 5. H_{oxd} vs. V_T

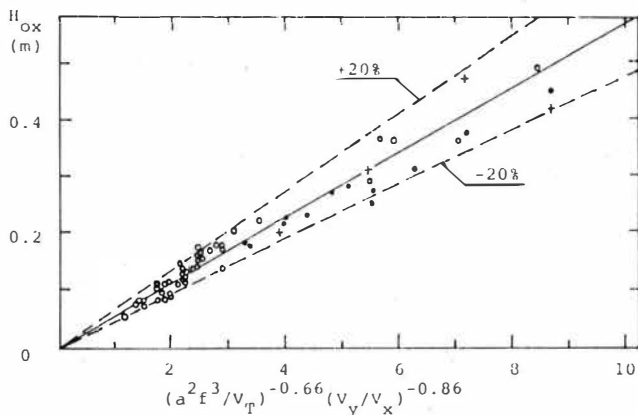


Fig 6. "True" height of transfer unit

- Equ. (5)
 - Exp. value — steady state (7)
 - Exp. value — present work
 - + Exp. value — present work
- (column dia. of 0.1 m)

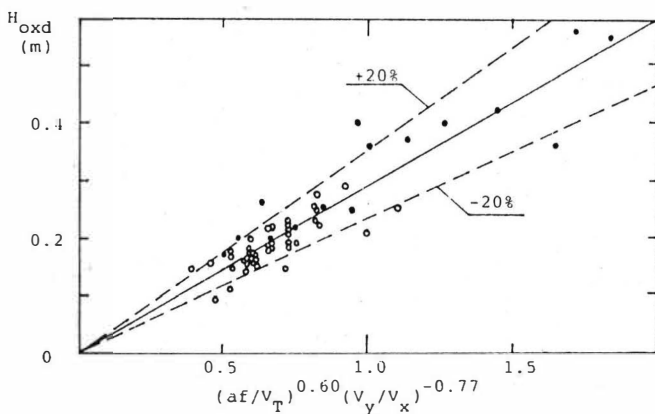


Fig 7. Height of "dispersion" unit

- Equ. (6)
- Exp. value — steady state (7)
- Exp. value — present work

SEPARATION OF UNSTABLE EMULSIONS IN HIGHLY
EFFICIENT MIXER-SETTLER CONTACTOR

L.I.SKLOKIN, V.E.Leif, S.M.Masloboeva

Institute of Chemistry and Technology of Rare
Elements and Mineral Raw Material of the Kola
Branch of the USSR Academy of Sciences

Contactors of the mixer-settler type are still in use as the main equipment for extractive separation of some elements though the column extractive apparatus have greatly developed over two recent decades. Application of such contactors remains stable for both multistage small-tonnage processes (for example, separation of rare earth elements) and large-tonnage processes of few stages (copper extraction).

Economical operation strongly depends on the size reduction of the settling chambers. This problem can be solved in two ways, namely, it is necessary either to alter the properties of the dispersion system or to use special devices in the settling chambers to increase the rate of emulsion separation. The most effective is the combination of both ways.

This paper presents the results of investigation of gravitational separation of emulsions in usual and efficient settlers. Tributylphosphate, petroleum sulfoxides, trialkylamines, cyclohexanol and other dissolvents have been used in the working systems. The hold up of the dispersion phase varied from 0.25 to 0.60. The experiments have been carried out in the settlers with the total loading of 0.01-10 m³/h.

The investigations resulted in defining a two parametric relationship between the specific loading of the settler and the height of the emulsion layer. The techniques of determination of the specific loading and the characteristic height has been worked out. Estimation of the settler's loading per height unit of the emulsion layer has been done.

The effect of different factors on the values of the limit specific loading of the settler has been experimentally studied by the dispersion phase and the characteristic height.

The found relationships have provided description of the working conditions of the sectionalized settling chambers in optimum regimes. Experimental testing of emulsion separation in both laboratory and industrial sectionalized settlers has been carried out. The method of estimation of the sectionalized settlers has been described on the basis of their limit specific loading.

As the manuscript was not available at the 28th May 1986, the deadline for printing this book, we only print the short abstract of the paper.

Study on Phase Separation in Settler

Jiang Yu Ming, Sun Bing Yao and Zhao Qi
East China Institute of Chemical Technology, Shanghai, China

Introduction

One of the most popular equipments for both contacting immiscible liquids on extraction, reaction, mixing and heat transfer is the mixer settler. Now mixer settler has developed a capacity of thousands of gallons in metallurgical and petroleum refineries, and cascades of mixer-settlers with a total of over 100 stages have operated satisfactorily over long periods in nuclear industry (1). In the view of theoretical analysis, the mixer settler may be considered in extraction to be analogous to the bubble cap column in distillation, however, the performance of bubble cap column can be predicted accurately, techniques for the design or analysis of mixer settler are nonexistent.

A mixer settler unit consists essentially of a mixer and a settler, the study on mixing chamber has been well developed, a series of type of impellers, such as turbine type (2), large-delta type (3) etc, has been applied in many systems. In recent years considerable attention has been given to settler design, but the performance characteristics are not easily simulated on a small scale, the large number of variables affecting performance renders the scale up difficult, now the traditional design methods of settler are based on empirical data or enlarging the volume of settler so as to increase residue time, but phase separation in settler is concerned with settling horizontal area, not with the depth of settler, so only the volume enlargement can't attain ideal effect.

Bailes, P. J. (4) has studied the phase separation under electric fields and measured the settling wedge in organic phase. Jeffreys G. V. (5) developed a mathematical model to calculate the volume flow rate of settler, but many constants of the equation proposed by Jeffreys must be obtained by a large number of experiment and even if two settlers have the same volume, the different depth and length will result in distinct settling effect.

In this paper a mathematical model for calculation of settling time has been established by analysis of velocity distribution and assuming that gravity is the main driven force of phase separation. If the thickness of emulsion wedge becomes nought and the settler time from mathematical model is more than the coalescence time of droplets described by Smith and Davies, the design of settlers would be considered suitable.

A new settler type with a horizontal area of tap shape and shallow depth based on the mathematical model has been designed and applied in factories.

Model

A. Analysis of dynamics in settler

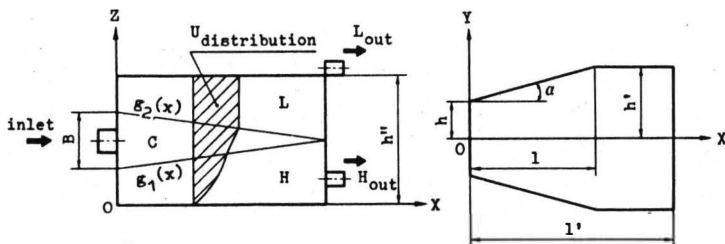


FIG. 1 THE CROSS-SECTION OF SETTLER

A cross-section of settler with a horizontal area of tap shape and shallow depth is shown in Fig. 1, the coalescence layer C is in the middle of L and H phase. Assuming the upper shape $g_1(x)$ and lower shape $g_2(x)$ of C layer as a linear function, according to Jeffrey's arrogation, if heavy phase is dispersion $g_2(x)$ will be a constant, otherwise $g_1(x)$ will be a constant.

Consider the velocity U in Y direction at every cross section of X axis is uniform, the component of velocity in Z direction gives ;

$$(1) \quad U_L = f_1(x)$$

$$(2) \quad U_C = (mz + n) f_2(x)$$

$$(3) \quad U_H = z^2 f_3(x)$$

By the means of continuity law in X direction,

$$(4) \quad Q_L(x) + Q_C(x) + Q_H(x) = Q_T$$

Because no relative slip exists between the layers, the boundary conditions are:

$$(5) \quad U_L|_{z=g_2(x)} = U_C|_{z=g_2(x)}$$

$$(6) \quad U_C|_{z=g_1(x)} = U_H|_{z=g_1(x)}$$

and

$$(7) \quad U_H|_{z=0} = 0$$

$$(8) \quad U_L|_{x=0} = F(U_t), \text{ namely } f_1(x)|_{x=0} = U_t$$

$$(9) \quad U_C|_{x=1} = 0, \text{ namely } f_2(x)|_{x=1} = 0$$

The equation (9) is assumed by the authors, that is to say, the length of settler is just put in the position of the end of coalescence.

Substituting Eqs. (1), (2), (3) into Eqs. (5), (6) and (4).

$$(10) \quad 0 \leq x < 1 \quad g_1^2(x) \cdot f_3(x) = [mg_1(x) + n] f_2(x)$$

$$(11) \quad [mg_2(x) + n] \cdot f_2(x) = f_1(x)$$

$$(12) \quad (tga \cdot x + n) \cdot [2(1 + n)f_1(x) \cdot (h'' - g_2(x)) + mf_2(x) \cdot (g_2^2(x) - g_1^2(x)) + f_3(x) \cdot \frac{2}{3} g_1^3(x)] = Q_T$$

$$(10') \quad 1 \leq x \leq 1' \quad g_1^2(x) \cdot f_3(x) = [mg_1(x) + n] \cdot f_2(x)$$

$$(11') \quad [mg_2(x) + n] \cdot f_2(x) = f_1(x)$$

$$(13) \quad h' [2(1 + n)f_1(x) \cdot (h'' - g_2(x)) + mf_2(x) \cdot (g_2^2(x) - g_1^2(x)) + f_3(x) \cdot \frac{2}{3} g_1^3(x)] = Q_T$$

Simplify Eqs. (10) and (11)

$$(14) \quad f_2(x) = \frac{f_1(x)}{mg_2(x) + n}$$

$$(15) \quad f_3(x) = \frac{f_2(x)[mg_1(x) + n]}{g_1^2(x)} = \frac{f_1(x)[mg_1(x) + n]}{g_1^2(x)[mg_2(x) + n]}$$

Substituting Eqs. (14) and (15) into Eqs. (12) and (13),

$$0 \leq x \leq 1$$

$$(16) \quad [xtga + h] \left[2(1+n)f_1(x)(h''-g_2(x)) + \frac{mf_1(x)}{mg_2(x)+n} (g_2^2(x)-g_1^2(x)) + \frac{2}{3}f_1(x) \cdot g_1(x) \frac{mg_1(x)+n}{mg_2(x)+n} \right] = Q_T$$

$$1 < x \leq 1'$$

$$(17) \quad h' \left[2(1+n)f_1(x)(h''-g_2(x)) + \frac{mf_1(x)}{mg_2(x)+n} (g_2^2(x)-g_1^2(x)) + \frac{2}{3}f_1(x) \frac{g_1(x)(mg_1(x)+n)}{mg_2(x)+n} \right] = Q_T$$

namely,

$$0 \leq x \leq 1$$

$$(18) \quad f_1(x) = \frac{Q_T}{[xtga + h] \left[2(1+n)(h''-g_2(x)) + \frac{m}{mg_2(x)+n} (g_2^2(x)-g_1^2(x)) + \frac{2g_1(x)(mg_1(x)+n)}{3(mg_2(x)+n)} \right]}$$

$$1 < x \leq 1'$$

$$(19) \quad f_1(x) = \frac{Q_T}{h' \left[2(1+n)(h''-g_2(x)) + \frac{m}{mg_2(x)+n} (g_2^2(x)-g_1^2(x)) + \frac{2g_1(x)(mg_1(x)+n)}{3(mg_2(x)+n)} \right]}$$

Hence phase separating time τ_2 in settler is given by:

$$(20) \quad \tau_2 = \int \frac{d(x)}{U(x)} = \int_0^1 \frac{dx}{f_1(x)} = \int_0^1 [xtga + h] \left[2(1+n)(h''-g_2(x)) + \frac{m}{mg_2(x)+n} (g_2^2(x)-g_1^2(x)) \right. \\ \left. + \frac{2g_1(x)(mg_1(x)+n)}{3(mg_2(x)+n)} \right] \frac{dx}{Q_T} + \int_1^1 h' \left[2(1+n)(h''-g_2(x)) + \frac{m}{mg_2(x)+n} (g_2^2(x)-g_1^2(x)) \right. \\ \left. + \frac{2g_1(x)(mg_1(x)+n)}{3(mg_2(x)+n)} \right] \frac{dx}{Q_T}$$

If τ_2 is more than drop coalescence time τ_1 , the design of settler is considered satisfactory, some data of Equ. (2) are known from the geometry of settler, the discussion of τ_1 , $g_1(x)$, $g_2(x)$ and constant m , n is as follows,

B. Drop coalescence time τ_1

The study on a plant or deformable liquid-liquid interface has been the subject of many investigations, Jeffreys and Davies (6) (1971) proposed the coalescence process of fine consecutive stages. The completion time for the five steps is called the coalescence time, but many workers (7,8) have found that the coalescence time in a given liquid-liquid system are not constant, but a distribution curve, and the factors affecting coalescence time include drop size, external forces, density difference, curvature of the interface, interfacial tension, presence of third phase, mutual

solubility, vibration etc. The author's study on coalescence time will be published in another paper.

Davies et al (9) gave a further correlation as:

$$(21) \quad \frac{\tau \sigma}{\mu_c \phi} = 31 \times 10^{-3} \left(\frac{\Delta \rho g \phi^2}{\sigma} \right)^{-1.24} \left(\frac{\mu_d}{\mu_c} \right)$$

The opposite directional effects of various quantities in Equ. (21) are noteworthy.

Here ϕ means drop equivalent sphere diameter and can be calculated by equations of Kumar A (10) which is especially suitable for the drops from mixing chamber.

C. Geometrical shape of coalescence layer

It is found in Fig. 1 that the cross-section of coalescence layer is a triangle whose point is in $x=1'$, when which phase is dispersion is known, the triangle becomes a rectangular triangle. If the height of B can be calculated, $g_1(x)$ and $g_2(x)$ will be obtained.

Barnea and Mizrahi (11) presented a semi-theoretical expression for gravity settlers to estimate the value of B.

$$(22) \quad B = J \left(\frac{Q}{R} \right)^k$$

In the creeping flow, $k=2.5$, the constant J is a function of phase ratio.

D. Primary phase separating velocity U_t

Constant m and n must be solved from the relationship of velocity distribution and boundary conditions $f_1(x)|_{x=0} = U_t$, $f_2(x)|_{x=1} = 0$. The authors considered that gravity is the main driven force of phase separation, so U_t can be obtained from the equation of gravity settling in literature (12).

In sum, the calculation procedure is as follows, firstly coalescence time τ_1 , then $g_1(x)$ and $g_2(x)$ can be obtained from U_t and B, therefore all geometrical shape may be solved step by step through the relationship of $\tau_2 \geq \tau_1$.

Experiment

A. Apparatus and systems

The design sizes of settler shown as Fig. 1 are as follows:

$$\begin{aligned} h &= 135 \text{ mm}, & h'' &= 300 \text{ mm}, \\ l &= 280 \text{ mm}, & l' &= 610 \text{ mm}, & a &= 13^\circ \end{aligned}$$

The experiments of liquid-liquid contacting process are extraction and stripping, the physical properties of both systems are shown in Table 1 and Table 2.

Table 1 Physical properties of extraction

Item	Composition	Density g/cm ³	Viscosity kg-sec/m ²	Interfacial tension kg/m
Aqueous phase	Citric Acid, 10%	1.04	1.52×10^{-4}	9.26×10^{-4}
Organic phase	Kerosene + TBP	0.75	3.46×10^{-4}	

Table 2 Physical properties of stripping system

Item	Composition	Density g/cm ³	Viscosity kg-sec/m ²	Interfacial tension kg/m
Aqueous phase	Pure water	0.971	3.62×10^{-5}	14.51×10^{-4}
Organic phase	Loaded org.	0.683	1.04×10^{-4}	

The total flow rates of extraction and stripping are $0.004\text{m}^3/\text{min}$. the phase ratio Q/A is 2.5.

B. Observation method

By using a float having an adequate density as an indicate, the separating time in settler can be observed, the change of coalescence layer in X-Z cross section can be measured by a glass tube, the entrainment is evaluated by an entrainment apparatus and it is found that if the entrainment is lower than 100 ppm, the separation of phases will be considered satisfactory.

C. Measured data

The drop size ϕ can be calculated from the data of Coulaloglou and Tavlarides (13) in the mixer size of 270 x 270 x 370 mm and at the stirring speed of 250 r.p.m.

Table 3 Comparison of predicted data and measured data

Item	ϕ , cm	B, cm	τ_1 , sec	τ_2 , sec	
Predicted	extraction	0.236	11.6	83	129
	stripping	1.06	11.6	56	102
Measured	extraction	0.30	14.2	—	138
	stripping	0.91	13.1	—	95

It is proven by Table 3 that the predicted and measured data are in very closely agreement, if the above-mentioned procedure is transferred into a computer, the sizes of settler under different operational conditions may be rapidly calculated.

Conclusion

A mathematical model for calculation of settling time has been established by analysis of velocity distribution and assuming that gravity is the main driven force of phase separation. If the thickness of coalescence layer becomes nought and the settler time from mathematical model is more than the coalescence time of droplets described by Smith and Davies, the design of settlers would be considered suitable it is proven that the calculation procedure predicted by the model can be used successful to design a settler with good accuracy.

Notation

- B The thickness of primary coalescence layer, cm.
 C Coalescence layer
 a, b, m, n, J, k Constant
 h, h', h'', l, l' Geometrical size of settler, cm.
 $g_1(x)$, $g_2(x)$ The distribution functions of coalescence layer
 H Heavy phase
 L Light phase

Q	Flow rate, M ³ /min.
Q _T	The overall flow rate, M ³ /min.
U	Phase separation velocity, M/sec.
U _t	Primary phase separation velocity in Z direction, m/sec.
τ ₁	The coalescence time of droplets, sec.
τ ₂	Phase separation time in settler, sec.
σ	Interfacial tension, kg/m.
μ _d , μ _c	The viscosity of dispersion and continuous phase, kg·sec/m ² .
φ	Equivalent drop size, cm.
ρ	Density, g/cm ³ .
R	Section area of settler, m ² .

References

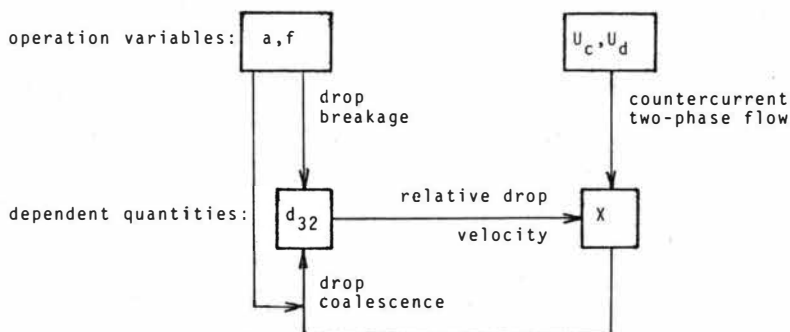
- (1) Lo Teh C., Baird M. M. I., Hanson C., "Handbook of solvent extraction". John Wiley & Sons. New York p.279, 1983.
- (2) McDonald A. R. E., J. South Afr. Inst. Min. Met. 193 (1971).
- (3) Shen Z. J. et al. ISEC'83 proceeding. Denver, USA p.24-5, (1983).
- (4) Bailes, P. J. and Larkai, S. K. L., Trans. I. Chem. E. 59, (4), 229, (1981).
- (5) Jeffreys G. V., Davies G. A. and Pitt K., AIChE Journal Vol. 16, No. 5, pp.823-7, (1970).
- (6) Jeffreys G. V., Davies G. A. "Recent Advances in Liquid-Liquid Extraction", Hanson. C. ed. Pergormen ed. Oxford. (1971).
- (7) Hartland S., Robinson, J. D., Chem. Eng. Sci. 25, 277 (1970).
- (8) Leng S. B., Wilke, C. R., Ind. Eng. Chem. Fundan, 10, 341 (1971).
- (9) Davies G. A., Jeffreys, G. V. and Smith, D. V. Proc. Int. Sol. Extr. Conf., (1971), Society of Chemical Industry, Condon, Vol. 1, 185 (1971).
- (10) Kumar, A., Doctor thesis, Swiss Federal Institute of Technology Zurich. pp.26-8 (1983).
- (11) Barbeem E., Mizrahi, J., Trans. Inst. Chem. Engrs., 53, 70 (1975).
- (12) "Chemical Engineering", East China Inst. of Chem. Tech., China (1983).
- (13) Culaoglon, C. A., Tavlarides, L. L., AIChE J. 22, 289 (1976).

Evaluation of Drop Size and Hold-up in Axially Agitated Plate Columns

H. Sovová, J. Procházka, Institute of Chemical Process Fundamentals, Czechoslovak Academy of Sciences, Prague, ČSSR

Reciprocating plate columns and pulsed sieve-plate columns are studied by a comparison of experimental data with mathematical models. Two types of models are used: detailed polydisperse models, describing different behaviour of individual drop size fractions, and simpler monodisperse models, more appropriate for quick preliminary calculations. Information obtained by one type of model can be transferred easily to another type because both types of models have common parameters.

Monodisperse model equations for calculation of the Sauter mean diameter d_{32} and the volumetric hold-up of the dispersed phase X are given in this text. They apply both to the reciprocating plate columns and to the pulsed sieve-plate columns, the effect of agitation being expressed by the plate reciprocation or liquid pulsation (PR/LP) intensity. The relation between d_{32} and X is as follows.



First, the drop size d_{32} is calculated as a result of drop breakage at a zero coalescence rate. This size can be compared with the drop size evaluated of experiments performed in a dilute dispersion, where the probability of a collision of two drops and their coalescence is low. Drop size and flow rates are input data in evaluation of the hold-up which affects the coalescence rate and the Sauter mean diameter, too. This feedback loop is included in the hold-up equation in a way similar to that used by Mířek¹.

Drop size as a result of drop breakage depends on the relative velocity of drops and plates. At a low PR/LP intensity the relative velocity is determined above all by the slip velocity of drops. With an increasing intensity of agitation the breakage by turbulent eddies starts to prevail. First the eddies are limited to the vicinity of the plate and gradually they spread over the whole stage. The regions of drop breakage are given by the schema:

PR/LP intensity	controlling factor	region of breakage	equation
$0 \leq I \leq I_1$	drop flow through the column	at the plate	(1),(2)
$I > I_1$ and $I < I_2$	periodic motion of the plate/liquid	gradually extends round the plate	(3)
$I > I_1$ and $I \leq I_2$	periodic motion of the plate/liquid	whole stage	(4)

The equations for d_{32} calculation contain empiric constants adjusted to the published experimental data (8 data sources, 189 data points). For d_{32} calculation at low PR/LP intensities the algorithm of Pietzsch and Pilhofer² with two modifications is used. The formula of the drop relative velocity to the plate is changed as marked by the arrow

$$u_t + 4af/\epsilon_p^{0.6} \longrightarrow u_t + pI, \quad p = \begin{cases} 22 & \text{for } \epsilon_p < 0.1, \\ 2.2/\epsilon_p & \text{for } \epsilon_p \geq 0.1 \end{cases} \quad (1)$$

and the result of calculation, maximum drop diameter d_m , is transferred to the Sauter mean diameter according to the relation

$$d_{32} = 0.6 d_m \quad (2)$$

Drop size at a medium intensity of agitation is given by

$$d_{32} = 0.058 \left[\frac{\epsilon_p^2}{(1 - \epsilon_p^2)} \right]^{0.4} (\sigma/\rho_c)^{0.6} I^{-1} \quad (3)$$

At a high intensity of agitation a formula developed by Baird and Lane³ with a modified proportionality constant is used,

$$d_{32} = 0.092 \left[\frac{h\epsilon_p^2}{(1 - \epsilon_p^2)} \right]^{0.4} (\sigma/\rho_c)^{0.6} I^{-1.2} \quad (4)$$

The criterions to separate the three regions are

$$I_1 = \begin{cases} 0.0084 & \text{for } \epsilon_p \leq 0.1 \\ 0.047 \epsilon_p^{0.75} & \text{for } \epsilon_p > 0.1 \end{cases} \quad (5)$$

$$I_2 = 6 h^2 \quad (6)$$

The PR/LP intensity is usually expressed as a product $2af$. An extended definition is used here,

$$I = k_1 a^{k_2} f^{k_3}, \quad k_1 = 1, \quad k_2 = 0.9, \quad k_3 = 1.1 \text{ for a harmonic motion, } (7)$$

which better corresponds to the fact that the effect of agitation on the drop breakage depends not only on the frequency and amplitude, but also on the shape of the periodic motion. The reciprocating plates driven by a motor with a yoke perform a harmonic motion where the effect of frequency on the drop size is stronger than the effect of amplitude. The values of k_1, k_2, k_3 for the pulsed columns cannot be given in general, because they depend on the pulsator characteristics.

If the breakage is limited to the plate vicinity, it's overall rate is low and the drop size decreases along the column. An empiric formula corrects d_{32} calculated according to eq. (2), (3) to the number of the stage N ,

$$d_{32}(N) = d_{32} [1 + 0.7 \exp(-0.1N)] \quad (8)$$

As an example of d_{32} calculation, Sauter mean diameters evaluated for the experimental conditions³ are drawn in Fig.1.

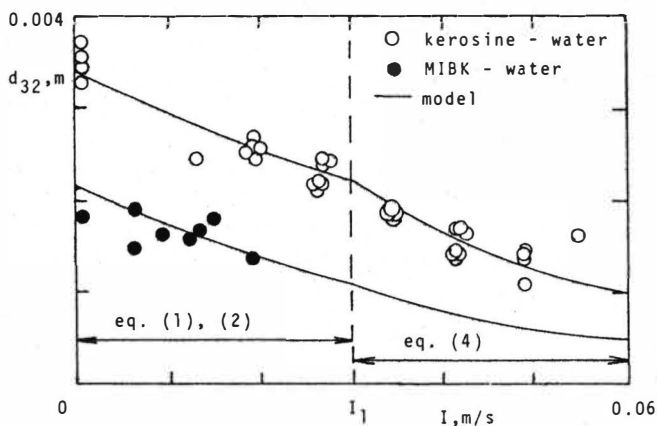


Fig.1. Sauter mean diameter in the Karr column

Volumetric hold-up of the dispersed phase is calculated by the equation of countercurrent two-phase flow in a column with plates

$$u_t(1 - X)^\alpha = U_d/X + k_u U_c/(1 - X) \quad (9)$$

with parameters α , k_u adjusted to the published results of hold-up measurements (13 data sources, 867 data points).

Drop terminal velocity is determined of d_{32} by the formula⁴

$$u_t = 0.249 [(g\Delta\rho)^2/\rho_c u_c]^{1/3} d_{32} \quad (10)$$

with a restriction effective for large oscillating drops⁵

$$u_t \leq u_m = (2/\rho_c)^{0.5} (g\Delta\rho\sigma)^{0.25} \quad (11)$$

Drop size is calculated by eq. (3), (4) even if the condition $I < I_1$ is fulfilled. This simplification speeds up the calculation without introducing any significant error.

The exponent α is connected with the drop coalescence. Let us assume that the left hand side of eq. (9) is $u_t(1-X)^{\alpha_1}$ in a system without coalescence and that the drop diameter enlarges by coalescence to $d_{32}/(1-X)^{\alpha_2}$, where α_2 is a measure of the drop coalescence ability. The drop terminal velocity also increases by this factor and the left hand side of eq. (9) becomes

$$u_t(1 - X)^{\alpha_1 - \alpha_2} = u_t(1 - X)^\alpha, \quad \alpha_1 > 0, \quad \alpha_2 \geq 0 \quad (12)$$

For the experiments simulated the value of α ranges from -1 to 3. Therefore it can be estimated $\alpha_1 = 3$, $0 \leq \alpha_2 \leq 4$. The exponent depends on the interfacial tension and on the purity of liquids. It falls down after a purification of the recycled liquids and then rises slowly, as new impurities accumulate in the system. We have not observed any changes of α with the PR/LP intensity, in contrast to Fei and Slater⁶, who evaluated a strong dependence of α on the intensity of agitation in RDC extractors.

Parameter $k_u \geq 1$ is a measure of the liquid flow retardation by the plates. It is correlated with the specific free area of the plate ϵ_p and with the stage height h ,

$$k_u = 1 + 0.352(1 - \epsilon_p)^{5.15}/h \quad (13)$$

Drops larger than the diameter of plate perforation d_h cannot pass freely and accumulate in front of the plate in a dense-packed layer, which is pumped across the plate by a rate proportional to the PR/LP intensity. The hold-up of the dispersed phase in the layer X_v contributes to the total hold-up in the stage X_t ,

$$X_t = X_v + X(1 - X_v) , \quad (14)$$

$$X_v = (k_v/h) [U_d/(2af-U_c/2)]^{1.5} . \quad (15)$$

As the hold-up X_v diminishes with the growing PR/LP intensity and the hold-up X increases simultaneously, the total hold-up passes through a minimum, as is shown in Fig.2.

A necessary condition for the dense-packed layer formation is $d_{32}/d_h > 0.5$. The coefficient of the layer was evaluated in a range of 0.001 - 0.055 m. It is correlated with parameter α for the most part of experiments,

$$k_v = 0.0023 \exp(0.8\alpha) . \quad (16)$$

However, at higher values of α it diverted several times in both directions. A possible explanation is that α depends above all on the coalescence ability, but the height of the layer is dependent in addition on the plate wettability.

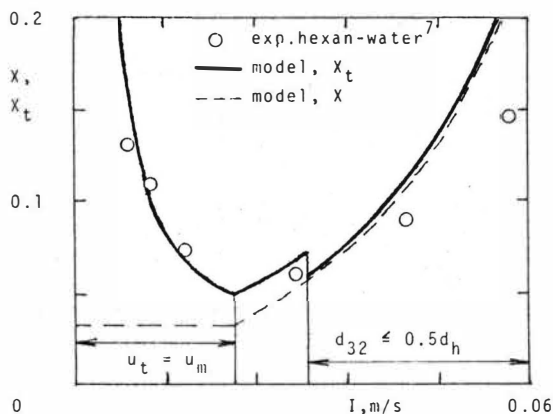


Fig.2. Simulation of hold-up in a pulsed sieve-plate column⁷

A knowledge of the hold-up transient behaviour is important in a hold-up control design. The response of the local hold-up inside the stage to the changes of the vibration intensity and of the phase velocities was measured and evaluated⁸. Similarly to the total hold-up in the column⁹, the dynamics of the local hold-up is approximated by a first order transfer function with time lag

$$F_z(s) = X(s)/z(s) = G_z \exp(-s\tau_z)/(sT_z+1) \quad \text{for } z = I, U_c, U_d, \quad (17)$$

where the values of gain G_z , time lag τ_z and time constant T_z depend on the operation variables I, U_c, U_d .

The hold-up response starts at the end of the column at the drop inlet and spreads through the column with the dispersed phase. Both time constant and time lag correlate with the mean residence time of drops in the section between this end of the column and the locus of hold-up measurement. If the length of this section is L , the mean residence time is

$$\theta = LX_t/U_d \quad (18)$$

and the corresponding correlations based on the measurement⁸ are

$$T_z = 0.6\theta, \quad \tau_z = 0.6\theta \quad \text{for } z = U_c, z = U_d, \quad (19)$$

$$T_z = 0.9\theta, \quad \tau_z = 0.5\theta \quad \text{for } z = I. \quad (20)$$

Gain is calculated of the steady-state hold-up equation (9).

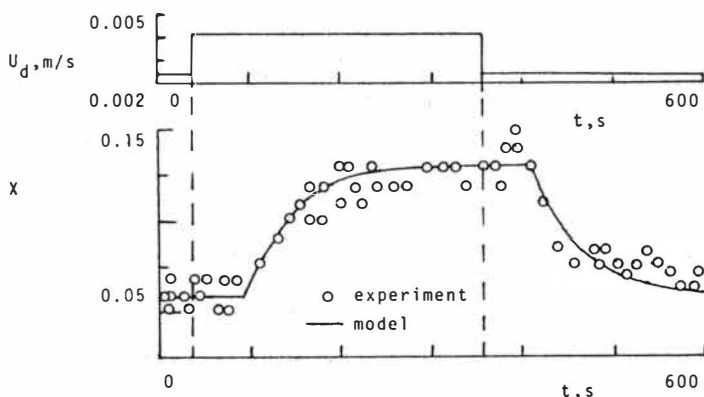


Fig.3. Hold-up response to the dispersed phase flow rate⁸

A good agreement of the calculated and measured response is apparent in Fig.3 with transfer function parameters $G = 39.7$ m/s, $T = \tau = 56$ s. These values were calculated of eq. (9), (18), (19) with parameters $\alpha = 2.2$, $k_v = 0.018$ m evaluated of the steady-state measurements.

A more complex local hold-up response occurs in the mixer-settler regime with a high ratio X_v/X if the intensity of agitation is changed. The height of the layer accommodates immediately to the new level of agitation and the local hold-up inside the stage changes simultaneously in the opposite direction, the total hold-up being kept constant. By a superposition of this response to that described previously a response of zero lag and of the original gain given by eq. (9) arises.

The values of the coefficients in eq. (19), (20) are probably not universal. A further measurement in a broad range of conditions is desirable.

The drop size and hold-up evaluation requires a knowledge of the operation variables a , f , U_c , U_d , of the physical properties of liquids ρ_c , ρ_d , ν_c , σ and of the column geometry ϵ_p , h , d_h . Besides, the effective intensity of the plate reciprocation or of the liquid pulsation should be calculated with respect to the shape of the periodic motion. Finally, the properties of the liquid-liquid and liquid-solid (plate) interface are an important factor affecting the rate of drop coalescence. They are expressed by adjustable parameters α and k_v .

References

1. Míšek T., Collection Czech.Chem.Comm. 28, 1631 (1963).
2. Pietzsch W. and Pilhofer Th., Chem.Eng.Sci. 39, 961 (1984).
3. Baird M.H.I. and Lane S.J., Chem.Eng.Sci. 28, 947 (1973).
4. Míšek T. and Marek J., Brit.Chem.Eng. 15, 202 (1970).
5. Ishii M. and Zuber N., AIChE J. 25, 843 (1979).
6. Fei W.-Y. and Slater M.J., ISEC'83, Denver 1983.
7. Sehmel G.A. and Babb A.L., Ind.Eng.Chem.Proc.Des.Dev. 2, 38 (1963).
8. Sovová H. and Havlíček A., Chem.Eng.Sci. - in print.
9. Taylor P.A., Baird M.H.I. and Kusuma I., Can.J.Chem.Eng. 60, 556 (1982).

Thermodynamics Modelling of Backmixing-Effect in a Mechanical Agitated Extraction Column

Bes R.S., Molinier J., Mora J.C., UA CNRS 192, ENSCT, CNRS Odello
address: ENSIGC-inpt, F 31 078 Toulouse Cedex

1. SUMMARY

A thermodynamics analysis of the irreversible processes in an extraction column is done in order to obtain a synthetic view of the modelling of backmixing effect. This analysis gives a convenient comparison of the various models. It leads to a pragmatic chaotic model which is able to give a reconstitution of the turbulent behaviour of the column.

2. INTRODUCTION

Efficiency of an extraction column is entirely a consequence of energy supplied to the apparatus. This energy permits an increase of the mass transfer coefficient but a backmixing effect gives a limitation of this one. This limitation is a direct consequence of energy dissipation in the column.

The first model proposed for backmixing was based on a second order differential equations /1/. By analogy with a distillation plate /2/ a succession of well mixed reactors with or without recycling between them can be used for the modelisation. More complex models were proposed to take into account a more realistic mechanism: breaking and coalescence of bubbles /3/ or distinction between two types of cells : mixing cells and transfer cells /4/. It is now well known that an overall dispersion coefficient is only a convenient mean for a mathematical representation of backmixing but scaling up is difficult /5,6/. Recently the source of entropy has been introduced in the modelling of the continuous stirred tank reactor /7/, the methodology can be used for extraction. From this short analysis it appears that two ways may be now, used for the modelisation of an extraction column: a mechanistic one and a phenomenological one. The both are complementary. The aim of the latter is to obtain a convenient methodology to choose a model for fitting and using experimental results in order to obtain a convenient tool for chemical engineering.

In this paper a synthetic presentation is done about extraction using a thermodynamic analysis.

3. OVERALL THERMODYNAMIC MODELLING

The overall entropic balance on the apparatus is of the following type: /8/

$$(1) - d L_s - d L'_s + S^* = 0$$

This relation is the result of two equations one for the heavy phase, one for the light one:

$$(2) - d L_s / dz + S = 0 \quad - d L'_s / dz + S' = 0$$

Each one can be obtained as the consequence of a contribution from each components transferred from one phase to the other:

$$(3) - d (L_j s_j) / dz + S_j = 0$$

The source of entropy is the consequence of the simultaneous transfers: mass, momentum, eventually, heat. Each of these transfers have an influence on the others, so a linear decomposition (by analogy with the linear thermodynamics of the irreversible processes) must take into account the coupling and the interactions particularly:

- 1) influence of the others components on the component j, S_{ji}
- 2) hydrodynamics on the component j, S_j^h
- 3) the interaction between the two phases, S_j^i .

so S_j can be as followed:

$$(4) S_j = S_j^* + S_j^h + S_j^i + S_{ji}$$

classically interactions 1 and 3 are not explicitly introduced in the modelisation. The interaction 2 is implicitly introduced by the

concept of "backmixing" through a dispersion coefficient so the piston diffusion model written as a thermodynamic equation may be:

$$(5) - dLj_{sj}/dz + S_j' + S_j'' = 0$$

where S_j' is resulting from mass transfer as: $K(x - X)$ and S_j'' from backmixing $D d^2x/dz^2$.

The ideal flow (plug flow) can be so proposed as the less irreversible model: $S_j'' = 0$ /9/.

From these remarks it has been suggested that a more complete model is obtained from a complete equation which is:

$$(6) - dLj_{sj}/dz + S_j' + S_j'' + S_j''' = 0$$

including an explicit coupling or interaction between the two phases.

In fact the linear decomposition is only a simple convenient mean for the presentation of the thermodynamic decomposition. The following remarks may be done:

- a) if the viscous dissipation is zero there is no extraction even if there is a mass transfer driving force,

- b) if the viscous dissipation is different from zero the mass transfer do not exists necessary; the mass transfer driving force may be zero.

So a non linear equation is necessary, this one may be as follows:

$$(7) - dLj_{sj}/dz + f(S'') S_j' = 0$$

which permits to verify the two above conditions.

4. MECHANISTIC MODEL

For a pulsed sieve trays column:

- when bubbles flow through the tray, the mass transfer area is renewed and the bubbles are divided. The mass transfer is high and the mixing is low,

- on the contrary between plates the phenomena is rather a mixing one. So a cells model can be proposed, a succession of mixing cells and transfer cells alternated /9/ (figure 1). From an experimental point of view it is impossible to have good concentration measurements during the mass transfer. The experimental values are for the mixing cells, it is so necessary to obtain an equation without the concentration in the transfer cells, the corresponding differential equation is

for the dispersed phase:

$$(8) - dx/dz + K(x - X) - k dx/dz = 0$$

for the continuous one:

$$(9) - dy/dz + D' d^2y/dz^2 + K'(y - Y) + k' d^2Y/dz^2 + k'' dy/dz = 0$$

the assumption of the similarity of the two profiles, x and y gives:

$$(10) -(1 + b)dx/dz + K(X - x) = 0$$

$$(11) - (1 + b') dy/dz + (D' + c') d^2y/dz^2 + K'(y - Y) = 0$$

The classical piston diffusion model would be:

$$(12) - dx/dz + D d^2x/dz^2 + K(x - X) = 0$$

$$(13) - dy/dz + D' d^2y/dz^2 + K'(y - Y) = 0$$

The coefficients b , b' and c' are corresponding to the backmixing effect.

So it appears clearly an interaction between the two phases in concordance with the prediction of the overall thermodynamic model. The backmixing effect through a diffusion coefficient is only a convenient mean for fitting experimental results. In spite of backmixing a like piston model is able, in some cases, to fit from a realistic mechanism, experimental results.

5. MECHANICAL ENERGY DISSIPATION

The behaviour of the column is dependant from the mechanical energy, this one is dissipated by the mean of the viscous stress. In the simple case of a pulsed column in laminar flow, a first approximation is that the velocity of fluid has a only axial component. The energy induces a radial velocity gradient (equation 14 table 1').

The energy lost by irreversibility is (great radius) given by the equation 15. For a non steady state the momentum balance is equation 16. According to energy this one is equation 17 or by a derivation versus the coordinate z, equation 18. For a turbulent flow, according to the Prandtl-Taylor turbulent viscosity or for a non newtonian fluid of Ostwald-De Waele type, the above relation 18 is a non linear one: equation 19. With the conditions 20 for the mean dissipation of energy.

The equation 19 is able to have a chaotic behaviour and so it permits the simulation of the transition between laminar and turbulent behaviour/10/.

The energy is a function of time, but the mean value versus time and space is the mean value which can be deduced from the energy consumption of the electric motor a example (equation 20) .

(14)	$Z = \mu \, dv/dr$	(15)	$e = Z \, dv/dr = \mu (dv/dr)^2 = 1/\mu \, \tau^2$
(16)	$\partial \tau / \partial r = -\rho \, \partial v / \partial t$	(17)	$1/\mu \, \partial a / \partial r = \rho \, \partial v / \partial t \quad a = e^{0.5}$
(18)	$(1/(2 \mu \, a)) \, \partial^2 a / \partial r^2 = \rho (\partial v / \partial r) / \partial t = (\rho / \mu) \, \partial a / \partial t$		
(19)	$k \, a^p \, \partial^2 a / \partial r^2 = \partial a / \partial t \quad a = e^m$		
(20)	$\int_{\Delta t} \frac{e}{V} \, dt \, dV = \bar{e} \, V \, \Delta t$		

Table 1 : dissipative modelling, equations

6. DYNAMIC MODELLISATION

The fluctuant behaviour has for consequence the fluctuation of velocity, concentration along the time, but their values are staying in a finite volume of the phase space: (v,x,y).

The dynamic modelisation used from non linear dynamical systems: mechanical or biological can be so adapted in particular the possibility of a direct modelisation by the mean of finite differences equations instead of differential equations or discretized differential one.

The simplest model can the following:

- the column is seen as a single CSTR,
- it is supplied in energy by the mean an agitator,
- the energy supplied to the column from the pulsor is given

by a driving force including dissipation and energy supplied to the motor:

$$(20) \quad E(\bar{e} - e)$$

- according to the analogy with Prandtl Taylor turbulent viscosity the coefficient for the energy dissipation is a function of this energy: a

$$(21) \quad E = E^* e (\bar{e} - e)$$

A part of this energy may be stored, as eddies for example. but the mean values gives a zero time average mean storage. The equation of the model is:

$$(23) \quad E^* e (\bar{e} - e) = e + \Delta e / \Delta t$$

which is of the general kind:

energy transferred = storage + dissipation

e is supposed to be a constant and e a function of the time.

This final equation is a simple particular case for the discretisation of the above differential equation 20. So it is possible to introduce the more general mathematical methodology used for the simulation of the chaotic behaviour through a Feigenbaum's process /11/. The discrete form of the above function is a more general case of the quadratic function used for the illustration of the mathematical turbulence.

7. QUANTUM MODELISATION

The chaotic behaviour has for consequence the impossibility to follow at each time the complete state of the column. Discrete measurements must be done. It is also very difficult to obtain a composition very close to a plate. Measurements show a discontinuity at the inlet of the apparatus. This discontinuity can be seen as an indication of the turbulent state. For a very high mixing state (high energy supplied) the behaviour is like a CSTR. It is not possible to have a distinction between inlet and outlet compositions. From this remark a quantum modelisation has been proposed^{12/}. This may be shown from a piston diffusion model type, with a low value for γ (for simplification):

$$(23) \quad -L \frac{dx}{dz} + D^* \frac{d^2x}{dz^2} + K^*x = 0$$

In fact experiments do not give the value of dx/dz and only difference between the composition at the z position and the inlet composition is obtained. If the composition at the inlet is zero, for simplification:

$$(24) \quad D^* \frac{dx}{dz} + \int_0^z K^*x \, dz = Lx$$

This equation can be written as an operator composed with two mathematical operators acting on x :

$$(26) \quad \hat{P}(x) = \hat{D}(x) + \hat{T}(x) = Lx$$

The physical state of the system is so defined by an eigen value (L) of the overall operator and the composition profile is an eigen function: $x(z)$. This may be compared to the Schrödinger's equation and one consequence is that some postulates from the quantum mechanics are adaptable to some unit operations in chemical engineering. In particular it can be shown that:

$$(26) \quad \hat{D}(\hat{T}(x)) \neq \hat{T}(\hat{D}(x))$$

because of the backmixing effect giving a discontinuity at the inlet. So mass transfer and backmixing gives non compatible parameters which may explain the difficulties for the simultaneous measurements of the two corresponding coefficients.

8. PRAGMATIC MODELISATION

From the above presentation it is necessary to propose a convenient way for using the various type of modelisation. The model must be adapted to the aim: engineering use, design use or knowledge. The use is presented from the simplest one to the more complex one.

The mean calculated position value, at the position z , is deduced from a serie of CSTR without recycling, the number of cells is the representation of the backmixing state. The length of the CSTR can be the length which gives the discontinuity at the inlet (it is a simple proposition, others may be done). The true experimental value of the composition (which is not the mean deduced above from the model) is defined by a statistical process. For time t and the cell number n , there is a probability to obtain the composition from the model at the cell $n-1$ or $n+1$. The maximum of probability is for the mean value of the cell if the measurement is done at the position of the center of the cell.

If it is wanted the fluctuations may be simulated from the above chaotic model (the quadratic function for the simplest case), the maximum dispersion values from experiments in turbulent regime are used for identification of the maximum dispersion of the model.

If the flow in the column is a laminar one, the discontinuity is zero and so the length of each cell are also zero: we have the plug flow model. If the flow is highly turbulent discontinuity is great and only a cell it is the CSTR model (figure 3).

9. CONCLUSION

The modelisation of a mechanical agitated extraction column can be seen from different points of view. The analysis of the equations in connection with the phenomena permits to define various type of models. Each can be compared to the others. For this thermodynamics appears as an useful tool. This gives a general frame, by the mean of some postulates, to place this modelisation in a more complete theoretical surrounding using general physical or thermodynamic laws.

10. NOTATIONS

a dissipative energy indicator, dim defined in the text.
b, b' coefficient, adim
c' coefficient, m
D* backmixing coefficient, mole m / s
D, D' backmixing coefficients, m
D operator
e, e energy, J/s m³
E, E* energy transfer coefficient,
f function
k, k" phenomenological coefficient, m
k' coefficient, adim
K* mass transfer coefficient, mole/m s
K, K' mass transfer coefficient, 1/ m
L, L' liquid flow rate, mole/s
s specific entropy, J/mole K
s phase L, s' phase L', s_j component j
S entropy source, J/s
S* overall, S phase L, S' phase L', S_j due to j, S_j* only mass transfer of j, S_j' influence of hydrodynamic on j, S_j" influence of the other phase on j, S_j" due to hydrodynamic
t time, s
T operator
V volume, m³
x, y, X, Y compositions molar proportions, adim
z coordinate, m
ρ density, kg/m³
μ viscosity, kg/ms
τ momentum density flux, kg/m² s²

11. LITERATURE CITED

1. Miyauchi T., Vermeulen T., Ind. Engng. Chem. Fund. 1963.2.304
2. Gautreaux M.F., O'Connell H.E., Chem. Eng. Prog., 1955.51.232
3. Casamatta G., Doctorat thesis, INPToulouse, sept.1981
4. Djelveh G., Molinier J., Mora J.C., Chisa 81, Praha sept.1981, paper F4.7
5. Hatton T.A., Lightfoot E.N., Chem. Eng. Science, 1982.37.9, 1269-1307
6. Levenspiel O., Fitzgerald T.J., Chem. Eng. Science, 1983, 36, 3, 489-491
7. Kalitzin G.St., Wiss. Z. Techn. Magdebourg, 28, 1984, 114-116
8. Djelveh G., Molinier J., Mora J.C.; 2nd World Cong. Chem. Eng.. Montreal, 9.19.6, oct. 1981
9. Fosy M.; Prevost M.; Mora J.C., Conf. Computers Developp. in Chem. Eng. Ind. Chem., Paris, march 1978
10. Bes R.S., Gabsi S., Molinier J., Mora J.C., Coll. Extraction, échanges d'ions, ENSIGC, Toulouse, paper 11.B1-10, June 1985
11. Bergé P., Pomeau Y., Vidal Ch, L'ordre dans le chaos, Hermann, Paris, 1984
12. Mora J.C.; Chisa 78, Praha, Aug. 1978
13. Bes R.S., Mora J.C., Proc. AMSE Modelling and Simulation, Paris 1982, vol S1, 216-220, Mesnard ed., Paris

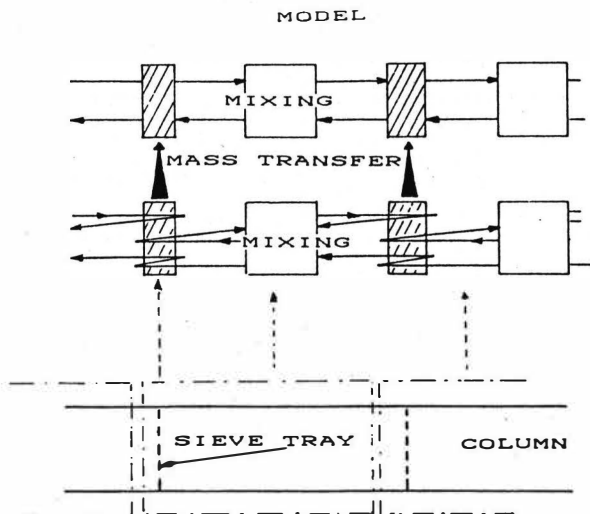


Figure 1: Mechanistic modelisation. Mass transfer occurs when drops are passing through the sieve tray. They are broken and the mass transfer surface is renewed. Between the trays the phenomena are rather mixing type.

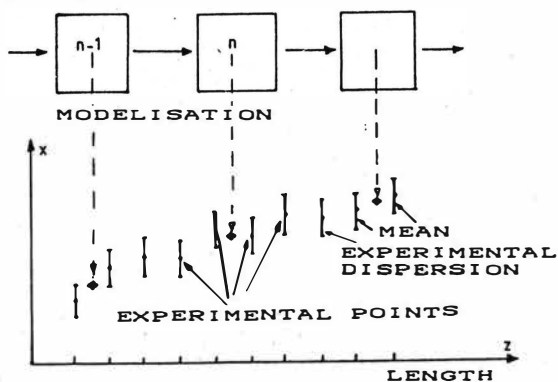


Figure 2: General principle of the quantum type modelisation. The experimental dispersion does not allow to distinguish two successive experimental points.

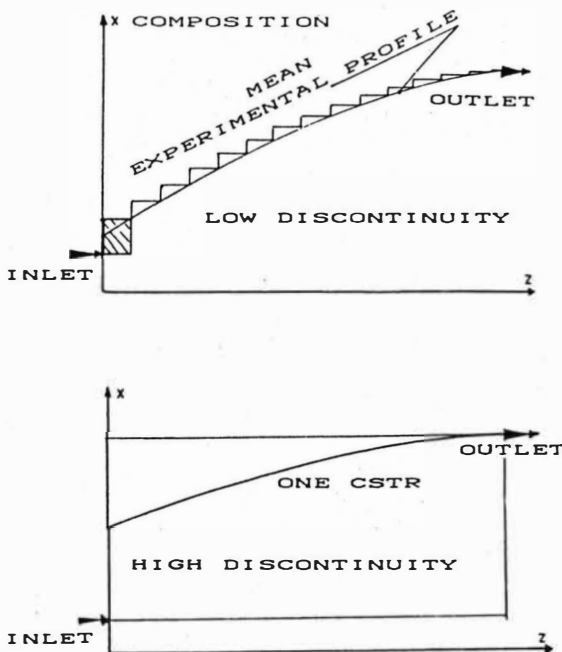


Figure 3: One of the methods to choose the number of CSTR for the quantum modelisation.

12. ANNEX

The quadratic model for one CSTR is the equation 23. This one gives the value of e at time $(t+1)$ from the value of e at time t . It can be written:

$$(27) E^* e (\bar{e} - e) = e + (e(t+1) - e)/t^*$$

t^* is the time step. This equation is also:

$$(28) e \left(E^* \bar{e} - 1 + 1/t^* E^* e \right) t^* = e(t+1)$$

by noting:

$$(29) w = e E^* / (E^* \bar{e} - 1 + 1/t^*) \text{ and}$$

$$(30) u = (E^* \bar{e} - 1 + 1/t^*) t^* / 4$$

The equation (28) is:

$$(31) w(t+1) = 4u w (1 - w)$$

which is the quadratic function used for the simulation of the transition to the chaotic /11/.

From the assumption that the x fluctuations are topologically equivalent to the w fluctuations which are between 0 and 1, it is possible to write the composition, $x'(t)$, as follows:

$$(32) \quad \dot{x} = x + x'(t)$$

The mean value \bar{x} , is given by the CSTR model and the chaotic behaviour of x' may be simulated by the mean of the following equation:

$$(33) \quad x'(t) = \bar{x} w(t) / \bar{w}$$

The figure 4 gives an example for $w(t)$. It must be said that the time step is difficult to identify from experiments. In fact this one is the consequence of an interaction of the column and the measurement apparatus.

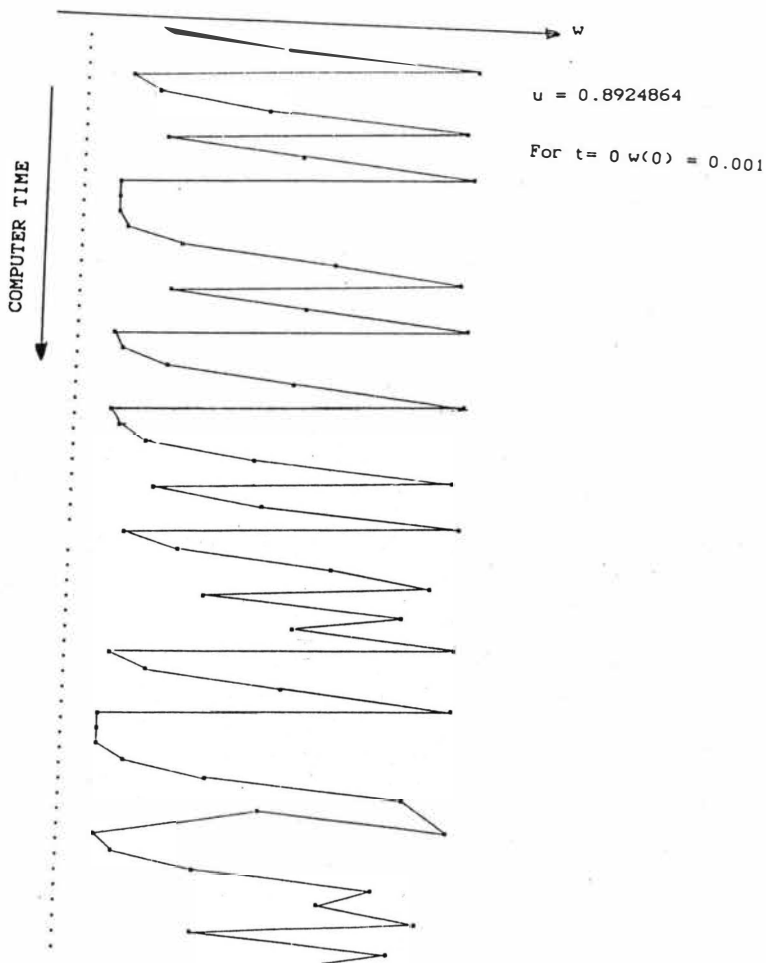


Figure 4: Example of the chaotic behaviour of the only one CSTR energy dissipation quadratic type model

Axial Mixing in Pulsed Sieve-Plate Extraction Columns

Dr.-Ing. E. Aufderheide and Prof. Dr.-Ing. A. Vogelpohl
Institut für Thermische Verfahrenstechnik der TU Clausthal
Leibnizstr. 15, D-3392 Clausthal-Zellerfeld

Introduction

During the last years, extensive research has been done on the hydrodynamic behavior of pulsed sieve-plate extraction columns at our institute. A large amount of data was collected on flooding, dispersed phase holdup, drop size distribution and axial mixing in both phases. The main purpose of our work was to investigate the scale-up of this type of extraction column.

Experimental equipment and measuring techniques

The experiments were performed on two pulsed sieve-plate extraction columns with a nominal diameter of 80 mm and 225 mm (Fig. 1). Water was used as continuous and toluene or butyl-acetate as dispersed phase. The columns were equipped with 43 sieve plates with a plate distance of 100 mm. The sieve plate hole diameter was 2 mm, and the free area was 22 %.

The drop size distribution was measured with a photoelectric suction probe (/1/, /2/). With this method, about 1000 drops can be measured within about 5 minutes. The reliability of the results was checked using the photographic method.

For the residence time measurements a pulse injection method was applied. For the dispersed phase, a luminescent tracer was used (see Fig. 1). With this method, the tracer concentration can be measured through the wall of the glass column without disturbance of the flow. For the continuous phase, a salt tracer was used which allows measuring the concentration with conductivity probes.

Residence time measurements - continuous phase

The decrease of column performance with increasing column diameter has often been attributed to the existence of non-ideal flow pat-

terns. Therefore, much effort has been spent to measure dispersion coefficients in the continuous phase. Most of the results, however, were obtained on small columns and with limited variation of parameters. Often the resulting correlations are contradictory.

Careful analysis of our tracer signals proved that the dispersion model is applicable for the continuous phase. Therefore, the dispersion model is used in this study to evaluate the mixing experiments.

For the smaller column, the dispersion coefficient of the continuous phase proved to be almost independent of throughput, amplitude and pulsing intensity. For the toluene/water-system, however, a large influence of the column diameter was found (Fig. 2). For the larger column, dispersion coefficients increased almost by a factor of two. The same values were found for a lower flow rate, too.

Although the averaged data points for the larger column follow a rather smooth line, the single measurements scatter much more compared to the small column. This indicates that the flow in the large column is somewhat unstable. Visual observation confirms the existence of large eddies and radial velocity differences. A comparison with results obtained in a previous study proved that the formation of eddies is influenced by inadequate sealing between the plates and the column wall.

Some additional runs were carried out using butyl-acetate instead of toluene as the dispersed phase (Fig. 3). In this case, only a slight increase of the dispersion coefficient is found when the larger column is used. At the lower volumetric flow rate, however, a few data points exhibit the same increase of mixing intensity as in the toluene studies.

Residence time measurements - dispersed phase

Dispersed phase axial mixing is often analyzed by the dispersion model, too. In the dispersed phase, however, deviations from plug flow are mainly caused by the existence of drop size distributions resulting in a spread of drop velocities. Therefore, residence time distributions of the dispersed phase should rather be interpreted as a convective process (Levenspiel & Fitzgerald /3/). This was done, for example, by the forward mixing model as given by Misesk and

Rod /4/. Still, Steiner & Hartland /5/ recommend using the dispersion model for both phases to reduce calculation time. They state that for practical design purposes sufficiently accurate results may also be obtained with the dispersion model.

Although careful analysis of the tracer signals showed that indeed the dispersion model does not describe the dispersed phase behavior adequately, this model was at first used for data evaluation. Compared with the continuous phase, the scatter of the data is much more pronounced.

In accordance with the results of the continuous phase, the dispersed phase dispersion coefficients are found to increase in the larger column, particularly at low pulsing intensities (Fig. 4). At the lower flow rate extremely high dispersion coefficients are obtained in the larger column at low pulsing intensities. Obviously, at these operating conditions the two-phase flow is somewhat unstable.

If butyl-acetate is used instead of toluene, an increase of the dispersion coefficient of the dispersed phase with growing column diameter is found only at high pulsing intensities.

Convective modelling of dispersed phase behavior

In the next step, the dispersed phase tracer signals were analyzed by a convective model. This model which was presented in detail elsewhere /6/ follows the forward mixing concept. Based on several assumptions each class of drop sizes can be attributed to a certain section of the inlet tracer concentration curve. Therefore we know at which time drops of a certain size pass the entrance of the test section. From this information we can calculate the concentration signal at the outlet, too, if the velocity of the drops is known.

If the pulsing intensity is high, the velocity of the drops can be calculated as for spray columns; else, the influence of the plates must be considered. In our model, this was achieved by subdividing the distance between two neighboring plates into three stages with different dispersed phase holdups. For each of these zones the height and the holdup can be calculated with the aid of some simplifying assumptions.

Figure 5 gives an example for the convective modeling of tracer curves obtained in the smaller column. The calculated response curve exhibits an almost perfect fit to the experimental curve. Very good agreement was found for lower pulsing intensities, too. The results justify the simplifications which had to be made to describe the movement of the drops.

For the larger column and lower pulsing intensities, the experimental curve turned out to be considerably smoother than the theoretical one. In accordance with the results obtained with the dispersion model, this can be attributed to the existence of large eddies.

The convective model just presented is based on several assumptions some of which are rather stringent. If these assumptions are valid, no adjustable parameter is needed such as the dispersion coefficient which has to be fitted to the experimental data. If one of these assumptions must be relaxed, however, model parameters have to be introduced. For instance, channeling can be included following the ideas of Jiricny, Kratky & Prochazka /7/. Several calculation methods based on a convective description of the dispersed phase behavior have been given by Steiner & Hartland /5/.

The point should be stressed that in the great majority of applications the dispersion model will be sufficiently accurate. From a scientific standpoint, however, it is incorrect to measure dispersed phase dispersion coefficients by fitting tracer signals to the dispersion model. Instead, an effective dispersion coefficient should be used for column design which causes the same reduction of column performance as the forward mixing effect. A simplified approach was developed to estimate the order of magnitude of such an effective dispersion coefficient by combining equations by Rod /8/ and by Stemerding and Zuiderweg /9/. Although the underlying simplifications do not allow a generalization of the results, it can be demonstrated that reasonable results can be obtained by calculating an effective dispersion coefficient from drop size data.

Notation

a	pulse amplitude (stroke)
c	normalized tracer concentration
D	axial dispersion coefficient
f	pulse frequency
t	time
v	superficial velocity

Subscripts

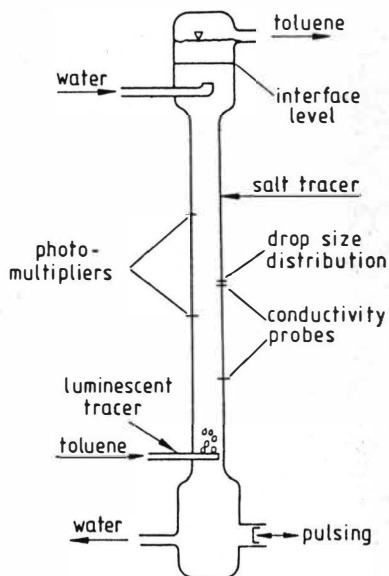
c	continuous phase
d	dispersed phase

References

- /1/ Pilhofer, T., H. Jekat, H.-D. Miller, J.H. Müller: Messung der Größenverteilung fluider Partikel in Blasensäulen und Sprühkolonnen. Chem.-Ing.-Tech. 46 (1974) MS 149/74
- /2/ Rauen, D., E. Aufderheide, A. Vogelpohl: Automatischer Abgleich der Absaugsonde zur Tropfengrößenmessung. Technisches Messen 51 (1984) 408/412
- /3/ Levenspiel, O., T.J. Fitzgerald: A warning on the misuse of the dispersion model. Chem.Eng.Sci. 38 (1983) 489/491
- /4/ Misek, T., Rod, V.: Calculation of contactors with longitudinal mixing. in Hanson, C. (Hrsg.): Recent advances in liquid-liquid extraction. Pergamon Press, Oxford 1971, 197/237
- /5/ Steiner, L., S. Hartland: Neues zur mathematischen Modellierung von Flüssig/Flüssig-Extraktionskolonnen. Chem.-Ing.-Tech. 55 (1983) 194/201
- /6/ Aufderheide, E., A. Vogelpohl: A convective model to interpret dispersed phase residence time measurements in pulsed liquid/liquid extractors. Chem.Eng.Sci., in press

- /7/ Jiricny, V., M. Kratky, J. Prochazka: Counter-current flow of dispersed and continuous phase. Chem.Eng.Sci. 34 (1979) 1141/1149, 1151/1158
- /8/ Rod, V.: Calculating mass transfer with longitudinal mixing. Brit.Chem.Eng. 11 (1966) 483/487
- /9/ Stemerding, S., F.J. Zuiderweg: Axial mixing and its influence on extraction efficiency: A simplified approximation method for design calculations. The Chem.Eng. (1963) 156/160

Figures



column diameter : 72mm, 212mm

active height : 4.4m

plate distance : 100mm

hole diameter : 2mm

free area : 22%

liquid systems :

toluene / water

butylacetate / water

Figure 1: Experimental setup and measuring techniques

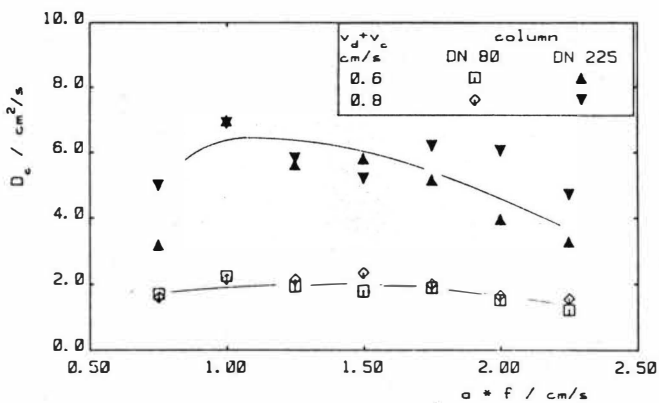


Figure 2: Continuous phase dispersion coefficients vs. pulsing intensity (toluene/water, $a = 8$ mm)

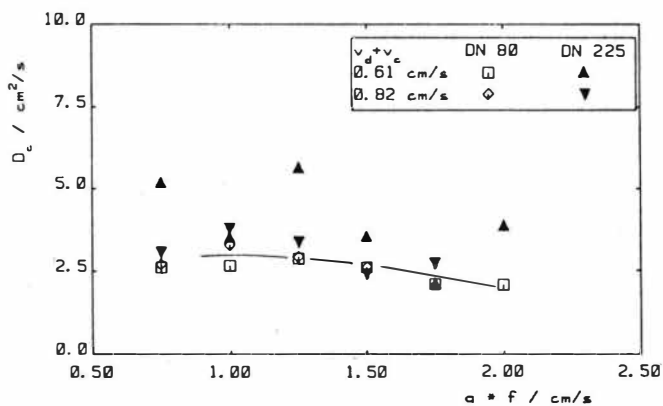


Figure 3: Continuous phase dispersion coefficients vs. pulsing intensity ($a = 8$ mm, butyl-acetate/water)

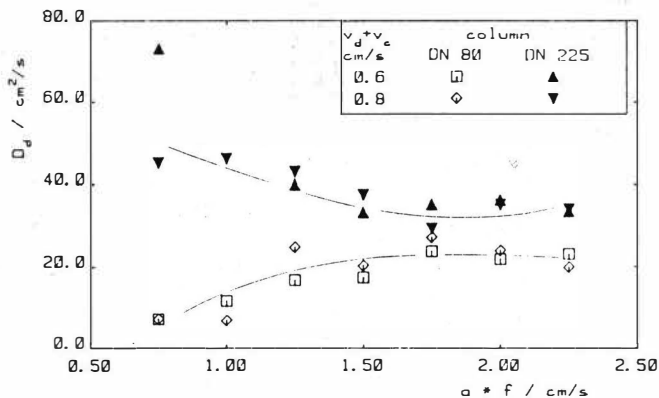


Figure 4: Dispersed phase dispersion coefficients vs. pulsing intensity (toluene/water, $a = 8 \text{ mm}$)

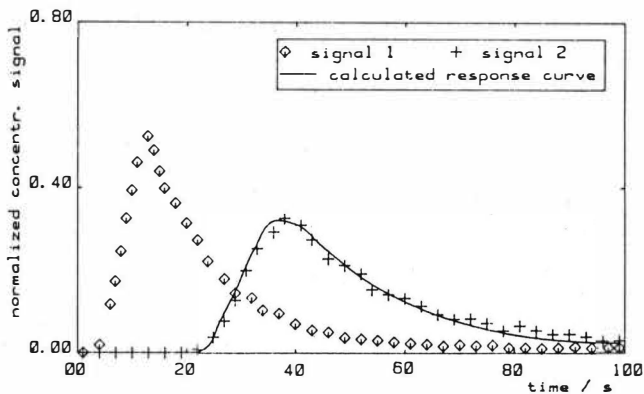


Figure 5: Tracer signals and response curve calculated by the convective model ($v_d + v_c = 0.81 \text{ cm/s}$, $a = 8 \text{ mm}$, $f = 2.5 \text{ s}^{-1}$, column DN 80, toluene/water)

A new stirred cell

M. Waubke, W. Nitsch, Technical University of Munich, Garching/D

1. Introduction

In the main stirred cells are being used today in order to solve problems arising from kinetics. Working on kinetics of mass transfer with chemical reaction in liquid-liquid-systems, one distinguishes processes controlled by reaction and processes limited by transport by observing the influence of forced convection on mass transfer. Being able to adjust convection in both phases separately, stirred cells are the most appropriate devices to identify the rate controlling step.

2. Conception

The main intention was, to design a new type of stirred cell with a great efficiency. Improving by try and error we developed a suitable form, which makes sure when considering processes controlled by chemical reaction independence of mass transfer on forced convection is not caused by the special geometry of the stirred cell.

Deciding on the efficiency was made by measuring mass transfer.

Processes controlled by chemical reactions have fluxes which are independent of forced convection and therefore an optimum stirred cell must be judged by the extent of dependence upon convection of processes governed by transport : These transport coefficients should have a maximum dependence on forced convection.

The above mentioned improving by try and error was performed using a binary system (Toluene-water), which for sure is controlled by transport.

Fig.1 shows a stirred cell, which is known in principle (1), which however has been changed in details to make possible an easy and precise copy, but above all has been modified to make it most efficient.

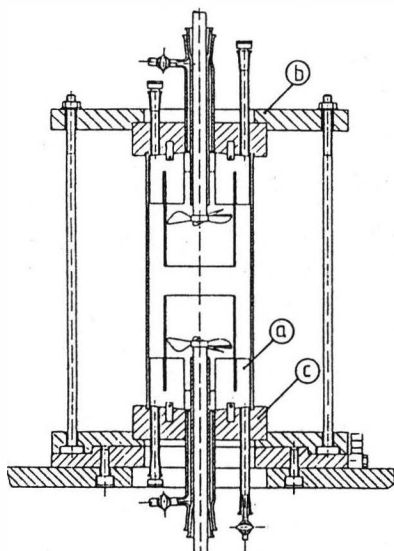


Fig. 1 The proposal of a new stirred cell as a standard apparatus.

There are straight, not treated glasses being used. The stirrers produced by simple processes are positioned in the midst of the inner glass tube having defined distance to the wall.

Tangential components of the velocity will be compensated by metal plates (a). In order to tighten the outer glass there are two metal disks (b) screwed together and holding two teflon disks (c). These teflon parts fix the metal plates (a) and the bearings of the stirrer shafts. In order to be sure, that no material will pollute the cell, as well as to be able to use strong detergents, we use exclusively glass, teflon and stainless steel (1.4301).

3. The convection inside the stirred cell

This stirred cell has been designed to make possible an intense mass-transfer by a small residence time of fluid elements at the interface. Therefore there are no devices inside the interface in contrast to Lewis (2). By changing the direction of the tangential velocity-component into the vertical and by using an inner glass tube the stream in this cell consists in the main of axial velocity-components. It is of interest for this flow to know the distribution of velocity in the annular clearance, which allows to calculate the rate of flow per time. Another important feature is the flow in vicinity of the interface so as to understand mass-transfer and its affection by the forced convection as well as the affection of the forced convection by mass-transfer.

Velocities have been measured using Laser-Doppler-Velocimetry (LDV). Additionally we used a light scattering device, which gives a global overview thus supporting LDV.

3.1. The convection in the annular clearance

In the annular clearance there is a lightly displaced, parabolic distribution of the axial component of velocity, which is known in hydrodynamics for laminar flow in annular clearances. By calculating the integral of the axial velocity over radius and angle we gain the volumetric rate of flow per time. This means another as yet not available characteristic of the flow inside the stirred cell, which up to now could only be described by the rotation speed of the stirrer. By systematic variation the volumetric flow could be found to be dependent on the rotation speed (n^1) and on specific gravity ($\rho^{0.05}$). Furtheron we found, that viscosity does not influence by a large degree. Knowing the volumetric throughput per time modelling of mass-transfer can be approached.

3.2. The convection near the interface

Besides the special geometry of the stirred cell, which is important for distinguishing processes limited by transport and those limited by chemical reaction, adsorbates in the interface influence mass transfer heavily. Since stirred cells have long-lived interfaces, this apparatus is most sensitive concerning adsorbates, which can be induced by impurities. By adding deliberately tensides the states of maximum and minimum influence of the forced convection near the interface by adsorbates can be reached.

3.2.1 Maximum influence by the monolayer in the interface ($c < cmc$)

In the region between the interface and that end of the inner glass tube, which is directed towards the interface, in the main radial components of velocity can be observed. Applying concentration of tensides below the critical micellation concentration (cmc) results in radial velocity-profiles, as for example is shown in Fig.2 .

Starting with zero in the interface the radial velocity increases with growing distance from the interface with a linear gradient, which changes into a parabolic profile in a distance, that is dependent on viscosity.

As Fig.2 also shows, over the whole interface there are strongly differing gradients of the radial velocity near the interface.

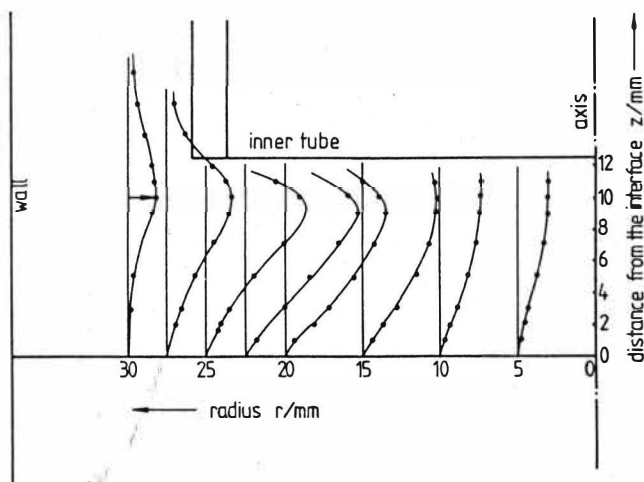


Fig. 2 Typical radial development of radial velocity-components in the stirred cell along the interface (reading example: $r = 30\text{mm}$, $z = 10\text{mm}$: $v_r(z = 10\text{mm}) = 0,85 \text{ cm/s}$)

The above shown hydrodynamic slow-down in the interface can be compared with the flow along a plate and thus explains the retardation of mass transfer at tenside concentrations below the critical micellation concentration.

3.2.2 Minimum influence by the monolayer in the interface ($c > c_{mc}$)

When increasing the addition of tensides above the c_{mc} the fluxes of mass transfer in systems that are limited by transport reach again the level of fluids with no adsorbates inside the interface (4,5). This so-called c_{mc} -effect, that has been reported several times by us (4,6) has also macroscopic effects on the profiles of the radial velocity near the interface. Above the c_{mc} there are radial velocities different from zero in the interface and smaller gradients of the radial

velocity. Measuring these profiles aims to find that ratio of rotational speed of stirrers, which enables us to get the same radial velocity and an even distribution on both sides of the interface. We think that this state of flow, called plug-flow is an essential requirement for a correlation of mass transfer fluxes in systems controlled by transport. First results lead to the assumption, that this state can be reached by adjusting the rotational speed of the stirrer in such a way resulting in equal rates of flow in the organic and the water-phase.

3.2.3 Regions of flow near the interface

Considering flow near the interface in absence and presence of monolayer, immense differences of the mean radial velocity along the radius can be observed (averaged at a radius between interface and the end of the inner glass tube). This finding can be explained using photographs from an axial sectional view, made with help of a light-scattering technique applying different systems and rotational speeds. These photographs show, that there are three different regions of flow in the interface, as Fig.3 demonstrates in principle :

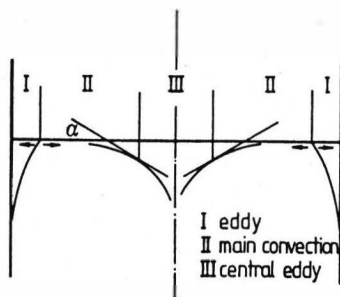


Fig. 3 The areas of flow near the interface

This means, that the surface along which mass transfer is occurring, is not homogeneous concerning hydrodynamics.

Analysing the above mentioned photographs revealed, that the region contacted by the main current occupies independent of rotational speeds 60% of the whole interface. This result was acquired using a construction of tangents and defining a limit angle of $\pi/6$ for measuring the central eddy.

It should be pointed out, that the difference of radii, which delimit this area is equal twice the space of the annular clearance.

4. Film pressure

In order to characterize monolayers of adsorbates, as well as to illuminate questions of stability and permeability of monolayers it is important to know the magnitude of shear stress caused by forced convection at a certain rotation speed.

Knowing which local states of compression occur and knowing the π/A -isotherm it is possible to decide whether a monolayer will collapse or not. Interpretation of measurements of permeation makes it essential to have knowledge of the behaviour of monolayers in the field of forced convection.

4.1. The radial dependence of the film pressure

In contrast to former methods Laser-Doppler-Velocimetry makes possible measurements of punctual, local velocities and thus enables it to evaluate the compression of the monolayer of adsorbates induced by the flow: By measuring profiles of the radial velocity-component in both phases local shear stresses in the interface can be calculated. This enables us to determinate the gradient of interfacial tension along the interface, based on an equation for the motion of newtonian surfaces as delivered by Scriven (7).

Integration of the shear stress over the radius results in the film pressure, which is shown in its typical form in Fig.4.

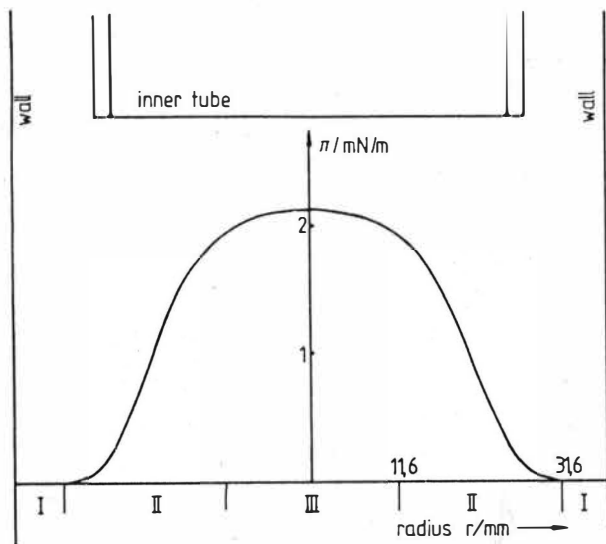


Fig. 4 Typical radial development of the film pressure

The magnitude of film pressure, determined in the above mentioned procedure is the same as that resulting from other methods (8,9). Remembering of the regions of flow near the interface (Fig.3) the radial development of the film pressure in Fig.4 becomes clear. In the regions of the eddies near the wall, as well as in the region of the central eddy there are only small contributions to the total film pressure, since in these areas exists just small gradients of the radial velocity. The main contribution arises from that region, which is denoted III in Fig.3 and which represents the main flow.

Literature

- (1) Nitsch, W.; Kähni, J.G.: Chem.-Ing.-Techn. 15(1979)S.890/1 MS729/79
- (2) Lewis, J.B.: Chem. Eng. Sci. 3(1954)S.248/59
- (3) Brauer, H.: Grundl. der Ein- und Mehrphasenströmung, Sauerländer 1971
- (4) Hoffmann, A.: Diploma Thesis TU München, 1980
- (5) Weber, G.: Doctoral Thesis TU München, 1976
- (6) Nitsch, W.; Heck, K.D.: Wärme- und Stoffübertragung 9(1976)S.53/4
- (7) Scriven, L.E.: Chem. Eng. Sci. 12(1960)S.98/108
- (8) Navazio, L.: Doctoral Thesis TU München, 1979
- (9) Kremnitz, W.: Doctoral Thesis TU München, 1981

Multicomponent, High Flux, Interphase Mass Transfer in Liquid-Liquid Extraction

W.J. Korchinsky, C.H. Young, E.D. Negri

Department of Chemical Engineering, UMIST, P.O.Box 88, Manchester M60 1QD, England.

INTRODUCTION

Mass transfer inside liquid droplets has been studied extensively. Several models for the mechanism have been proposed and the resulting model equations have been solved, with varying degrees of accuracy depending on boundary conditions assumed, to predict mass transfer rates to/from drops. These studies have assumed, without exception, single solute transfer at low concentrations.

Mass transfer of single solutes at high concentrations, involving convective flux contributions to the total solute flux between phases, has been studied in a variety of physical situations but not inside a drop. Multicomponent transfer studies too have been extensively reported, but not applied specifically to transfer with drops.

Presented here are the modifications to the theories required to extend their application to high flux of a single component in rigid¹ and turbulent circulating² (Handlos-Baron³) drops and to multicomponent mass transfer in rigid drops⁴.

Experimental results for single solute transfer at high flux are compared with the predictions of the Handlos-Baron (high flux) model.

THEORY

Rigid Drop - Single Solute

Assuming spherical symmetry, solute and total mass balances around a differential spherical shell inside a drop give,

$$\text{for the solute} \quad \frac{\partial(\rho y)}{\partial t} + \frac{1}{r^2} \frac{\partial(r^2 N)}{\partial r} = 0 \quad (1)$$

$$\text{and for the mixture} \quad \frac{\partial \rho}{\partial t} + \frac{1}{r^2} \frac{\partial(r^2 N_T)}{\partial r} = 0 \quad (2)$$

where the solute flux in the radial direction is given by the sum of convective and diffusive fluxes,

$$\begin{aligned} N &= N_T y + J \\ &= N_T y - \rho D \frac{\partial y}{\partial r} \end{aligned} \quad (3)$$

With the assumptions of constant mixture density and of non-transferring solvents at the interface Equation (2) gives $r^2 N_T = 0$. But as there is no source or sink in the centre of the drop, the radial total flux, N_T , within the drop must be zero, and therefore there are only equal and opposite diffusive fluxes of solute and solvent to consider, as in the low flux case! The solute mass balance therefore gives, simply, the following (if constant D is also assumed),

$$\frac{\partial y}{\partial r} = D \frac{\partial^2 y}{\partial r^2} + \frac{2}{r} \frac{\partial y}{\partial r} \quad (4)$$

If constant drop radius is assumed the analytical solution of Newman⁵ may be applied, for the case of constant drop surface composition, to obtain drop solute concentration variation with radial position and time.

For the case of finite resistance in the continuous phase, the film theory is applied. At the interface the equality of mass fluxes on either side is assumed. The existence of high fluxes implies that a correction for them using the film theory must be made. An expression similar to that predicted by the film model for steady state is proposed. Assuming a linear equilibrium relationship, the boundary condition at the interface is:

$$\left. \frac{\partial y}{\partial r} \right|_I = \frac{\rho_c k_c}{\rho_D D} (1 - y_I) \ln \frac{1 - x_b}{1 - y_I/m} \quad (5)$$

where k_c is the "low flux" continuous phase mass transfer coefficient. Now it is not possible to obtain an analytical solution to Eq. 4 and a numerical solution is required.

So, though the mass transfer mechanism within the drop remains the same, what is different for the high flux case is that the significant convective flux through the drop surface must be added to the diffusive flux; the resulting total flux out of (or into) the drop causes the drop boundary to contract (or expand). A mass balance at the boundary gives:

$$N_{TI} \cdot 4 R^2 = - \frac{4}{3} \rho_D \pi \frac{d(R^3)}{dt} \quad \text{or} \quad \frac{dR}{dt} = - \frac{N_{TI}}{\rho_D} = - \frac{J_I}{\rho_D (1 - y_I)} \quad (6)$$

The changing drop radius can therefore be computed simultaneously with the drop concentration profile.

Rigid Drop - Multicomponent Transfer

With spherical symmetry the multicomponent balances equivalent to Eqs.(1) and (2) may be written in matrix form as

$$\frac{\partial}{\partial t} [\rho y] + \frac{1}{r^2} \frac{\partial}{\partial r} [r^2 (N)] = (0) \quad (1M)$$

$$\frac{\partial \rho}{\partial t} + \frac{1}{r} \frac{\partial}{\partial r} (r^2 N_T) = 0 \quad (2M)$$

The solute fluxes, (N), are obtained as the sum of convective and diffusive fluxes as follows

$$(N) = N_T(y) + (J) = N_T(y) - r [D] \frac{\partial(\hat{y})}{\partial r} \quad (3M)$$

Here the Linearised Theory of Toor⁶ or Stewart and Procter⁷ is applied to write the generalized Fick equation for (J) in matrix form, hence to obtain Eq.(3M).

As in the binary case, for constant density the total radial flux, N_T , within the drop must be zero. For constant [D] the matrix equivalent of Eq.(1) is obtained. The resulting system of partial differential equations is coupled through [D], but may be de-coupled if [D] is constant and non-singular to obtain.

$$\frac{\partial(\hat{y})}{\partial t} = r \lambda_J \left(\frac{\partial^2(\hat{y})}{\partial r^2} + \frac{2}{r} \frac{\partial(\hat{y})}{\partial r} \right) \quad (4M)$$

where $(\hat{y}) = [P]^{-1}(y)$ and $r \lambda_J = [P]^{-1}[D][P]$.

This system of partial differential equations may be solved for the 'pseudo-compositions', \hat{y}_i , and then these can be converted back to y_i . In fact, for constant drop surface composition (y_I), the Newman solution applies - with \hat{y}_i and λ_i replacing y_i and D respectively.

At the drop surface, the convective flux must be considered so the total flux is given by

$$(N)_I = -\rho_D [\beta_y]_I [D] \frac{\partial(\hat{y})}{\partial r} \Big|_{r=R} \quad (5M)$$

For variable surface composition, these fluxes must be equated to those through the continuous phase 'film', i.e.

$$(N)_I = \rho_c [\beta_x] [k_c] (x_I - x_b) \quad (6M)$$

To obtain the high flux $[k_c]$, the low flux $[k_c]$ matrix must be corrected, i.e. using the film theory. The changing radius may be calculated as before, using Eq.(6).

Handlos-Baron Drop - Single Solute

The continuity equation for one dimensional mass transfer that is to be solved in this case is³,

$$\frac{\partial y}{\partial t} = \frac{1}{\rho_D} \frac{4}{d} \frac{1}{\xi} \frac{\partial}{\partial \xi} (N\xi) \quad (7)$$

As in the rigid drop case, regardless of concentration level, we may substitute the (eddy) diffusive flux for the total flux, in the model given by,

$$J = N = -D_e^* \rho_D \frac{\partial y}{\partial \xi} + \frac{4}{d} \quad (8)$$

$$\text{where } D_e^* = \frac{d v_s}{2048} \left(\frac{6\xi^2}{1} - \frac{8\xi}{\mu_D/\mu_C} + 3 \right) \quad (9)$$

At the drop surface ($\xi = 1$) combining Eqs.(8) and (9) gives the diffusive flux as

$$J_I = \frac{v_s D}{512 (1 + \mu_D/\mu_C)} \frac{\partial y}{\partial \xi} \Big|_R \quad (10)$$

and the total flux as

$$N_I = J_I / (1 - y_I) \\ = \frac{v_s D}{512 (1 + \mu_D/\mu_C) (1 - y_I)} \frac{\partial y}{\partial \xi} \Big|_R = k_c \rho_c \ln \frac{(1 - x_b)}{(1 - x_I)} \quad (11)$$

The changing drop radius may be obtained through Eq.(6).

Column Model

Assuming the usual axial dispersion model for the continuous phase, and the 'forward mixing' model for the dispersed phase, a differential solute mass balance based on the continuous phase gives the following⁸,

$$\frac{d(Wx)}{dz} + SE_c \rho_c \frac{d^2 x}{dz^2} = \sum_{i=1}^{IN} (N_{AI,i} a_i) S \quad (12)$$

where the interphase fluxes, $N_{AI,i}$, must be determined by the simultaneous solution of the above and the appropriate drop model equations. The Handlos-Baron model has consistently proved most appropriate in previous studies⁹⁻¹¹.

RESULTS

RIGID DROPS

The effects on predicted rigid drop extraction efficiencies of increasing solute concentration level and driving force are illustrated for a binary system in Fig.1 and for a ternary system in Fig.2. In both, constant diffusion coefficients are assumed, with the matrix of coefficients in the latter case containing a significant negative off-diagonal (D_{12}) value, so that component 1 diffusion rates are significantly reduced by component 2 concentration gradients (see later). These results are for constant surface composition.

The results in Figs.1 and 2 are typical in demonstrating a slight decrease in extraction efficiencies with increasing solute content. The increasing convecting flux simply increases (or decreases) the drop size and the diffusion flux-dependent

internal solute concentrations are little affected by solute levels. In fact analytical solutions which are for low solute concentrations may be used with accuracy at much higher concentrations.

The influence of solute concentration level independent of initial driving force and (at low, 0.01 driving force) independent of drop size effects is illustrated for rigid drops in Figs.3 and 4 (binary and ternary system respectively). Now extraction efficiencies increase with solute levels as expected. The possible influence of molecular interaction is illustrated in Fig.4 where efficiencies (for $y_{11} = 0.02$) are also plotted for a lower value of the off-diagonal diffusion coefficient, D_{12} .

Any variation in molecular diffusivities with solute concentration levels will modify these results and should be taken into consideration when known.

HANDLOS-BARON DROPS

The predictions of this model at a constant low, initial overall driving force ($m_{x_b} - y_o = 0.01$) are shown in Fig.5. In this case the properties of the toluene-acetone-water system are used in the model solution, with variation with concentration taken into account. The increase in total flux has not resulted in increases in extraction efficiency with solute levels in this case because of the variation with concentration of the distribution coefficient. A significant increase (~40%) in the distribution coefficient has virtually eliminated the influence of the increasing total flux, so that the extraction efficiencies vary little with solute levels.

Drop mass transfer predictions were combined with the column model equations to predict the performance of a 21.9 cm diameter Rotating Disc Contactor, details of which may be found elsewhere². These results were compared with experimental results obtained over a range of acetone concentrations in a continuous aqueous feed. Acetone concentrations in the dispersed toluene phase were increased simultaneously to maintain relatively low (0.04) driving forces and limit the influence of drop size change due to changing solute content. An extraction factor of about one was maintained.

Nine runs with acetone content in the aqueous phase feed varying from 6 to 28 wt% were carried out. Experimental extraction efficiencies and theoretical predictions agreed very closely, as shown below.

RUN		1	2	3	4	5	6	7	8	9
E_{oc}	Exp.	.580	.647	.737	.850	.912	.820	.866	.934	.934
	Theor.	.583	.617	.692	.812	.916	.755	.831	.915	.928

Experimental concentration profiles did not compare well with theoretically predicted ones at higher solute concentrations. Very low interfacial tensions and small drops at these solute levels apparently resulted in a greater influence of axial mixing than predicted from the low flux run E_c values, as illustrated in Fig. 6. Higher mass transfer rates, than predicted from low flux run results, must also be present to account for the accuracy in prediction of the efficiencies. The reason for this is under investigation.

SUMMARY

Rigid drop mass transfer may now be made for high solute concentrations and for multiple solute transfer.

Column mass transfer rates are best predicted by the application of the Handlos-Baron model, whose predictions are now extended to higher solute concentrations. Because the mechanism is one of turbulence inside the drops, an influence of interaction in multicomponent systems is unlikely so that the theory should be applicable to individual components in a multicomponent system.

NOTATION

a	interfacial area
D	molecular diffusion coefficient
$[D]$	$(n-1) \times (n-1)$ matrix of generalized Fickian diffusivities
D	Handlos-Baron eddy diffusivity
E_c^c	axial dispersion coefficient, continuous phase
E_i^c	solute i -based efficiency
E_i^{oc}	extraction efficiency, continuous phase basis
J^{oc}	solute diffusion flux
(J)	vector of solute diffusive fluxes ($\text{kg}/\text{m}^2/\text{s}$)
k	mass transfer coefficient, continuous phase
$[k_c], [k_c]$	$(n-1) \times (n-1)$ matrices of mass transfer coefficients, low flux and high flux
m	solute distribution coefficient
(N)	vector of total solute mass fluxes ($\text{kg}/\text{m}^2/\text{s}$)
N, N_T	total mass flux of solute, all components
n	number of components
$[P], [P]^{-1}$	$(n-1) \times (n-1)$ modal matrix of matrix $[D]$, and the inverse
r	drop radial coordinate
R	drop radius
S	column cross-sectional area
t	time
V	slip velocity
$x_{i,y}$	weight fraction solute, continuous, dispersed phases
(y)	vector of dispersed composition
(\bar{y})	vector of dispersed phase pseudo-composition
z	column vertical position

GREEK SYMBOLS

$[\beta]$	$(n-1) \times (n-1)$ matrix of elements, $\beta_{ij} = \delta_{ij} + y_i/y_n$
δ_{ik}	Kronecker delta
ρ_{ik}	density
ν_C, ν_D	viscosities, continuous and dispersed phases
	dimensionless time, Dt/R^2

SUBSCRIPTS

l	component l in ternary system
A	solute
b	bulk
C	continuous phase
D	dispersed phase
i	pertaining to drops of diameter, d_i
I	interface
o	initial value
R	evaluated at drop surface
s	slip

REFERENCES

1. Korchinsky, W.J., Negri, E.D. and Young, C.H., Chem. Eng. Sci., 1986.
2. Korchinsky, W.J. and Young, C.H., Chem. Eng. Sci., 1986.
3. Handlos, A.E. and Baron, T., A.I.Ch.E.J., 1957, 3, 127.
4. Korchinsky, W.J. and Negri, E.D., Chem. Eng. Sci., 1986.
5. Newman, A.B., Trans. A.I.Ch.E., 1931, 27, 310.
6. Toor, H.L., A.I.Ch.E.J., 1964, 10, 448.
7. Stewart, N.E. and Prober, R., Ind. Eng. Chem. Fund., 1964, 3, 224.
8. Young, C.H., Ph.D. Thesis, Victoria University of Manchester, 1985.
9. Korchinsky, W.J., Loke, C.T. and Cruz-Pinto, J.J.C., Chem. Eng. Sci., 1982, 37, 781
10. Cruz-Pinto, J.J.C. and Korchinsky, W.J., Comp. Chem. Eng., 1983, 7, 19-25.
11. Korchinsky, W.J. and Young, C.H., J. Chem. Tech. Biotech., 1985, 35A, 347.

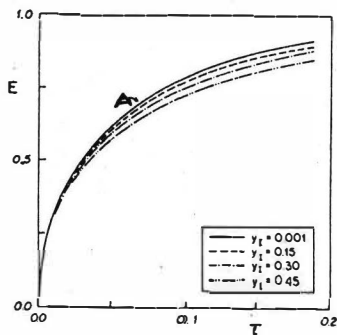


FIGURE 1: Rigid drop extraction efficiencies ($y_{oi} = 0.0$, $D = 2.972 (10^{-9}) \text{ m}^2/\text{s}$, $R = 0.001 \text{ m}$), including analytical solution (A).

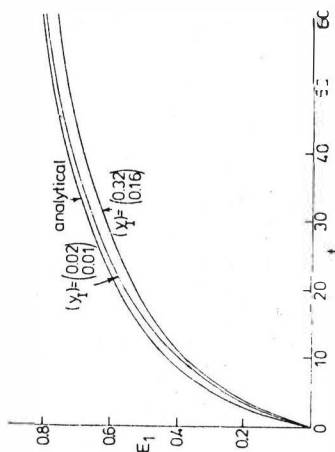


FIGURE 2: Comp. 1 (of ternary) extraction efficiencies at constant (y_I), $y_{oi} = 0.001$.

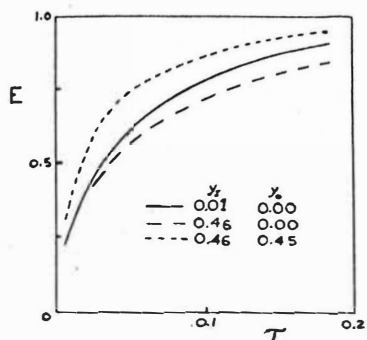


FIGURE 3: Rigid drop extraction efficiencies at constant initial driving force ($y_1 - y_0 = 0.01$).

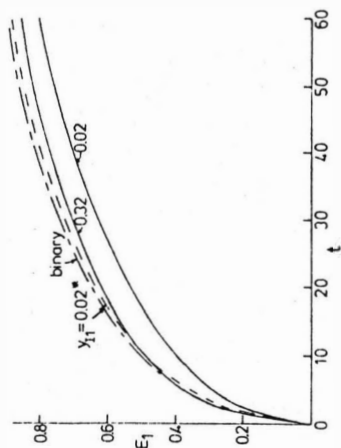


FIGURE 4: Component 1 (of ternary) extraction efficiencies at constant (y_1) and constant initial driving force - *reduced D_{12} value.

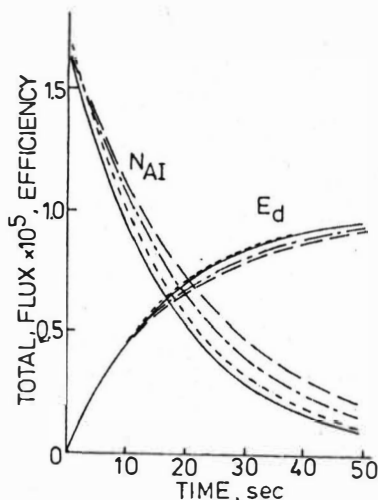


FIGURE 5: High flux Mandlos-Baron drop total interfacial solute fluxes & efficiencies: $y_0 = 0.0$ (—), 0.1 (---), 0.2 (— · —), 0.3 (— · — · —); $k_c = 0.00$ cm/s; $d = 0.2$ cm.

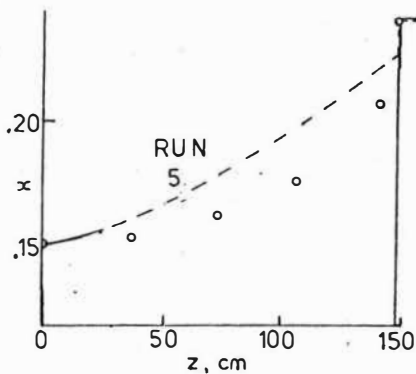


FIGURE 6: Experimental (o) and theoretically predicted (---) continuous phase concentration profiles.

H.-B. Rhein, K. Schügerl*

Introduction

Investigations in mass-transfer of liquid-liquid extraction on freely suspended single droplets present unexpected results about the influence of special fluid dynamics and interface stability on the kinetics of mass transfer.

The phenomena of mass transfer on single droplets characterized by comparison with the results of experiments in a semi-continuous two-phase stirring cell.

Short review

Twenty years ago Mensing and Schügerl performed their basic work in mass transfer on freely suspended single droplets /1,2/. Later, a modified scintillation-counting method was developed by Halwachs /3/. This method allowed the contactless determination of the concentration in freely suspended single droplets by use of low energetic Am-241- γ -rays as an external source by means of high resolution in regard to the time aspect /3,4/. The two-phase system xylene/water is well applicable for the investigations of many transferred compounds by liquid-liquid extraction.

However, modelling of non-stationary mass transfer requires the possibility of differentiating single parameters of a given system in regard to their influence on mass-transfer. In this way, Hänsel /5,6,7/ showed that the interface-relating mass transfer coefficients in amino-acid extraction are higher in larger than in smaller droplets and, therefore, contrary to the expected tendency. Such effects are caused by the special fluid dynamics and are not predictable by two-phase STR experiments.

Dipl.-Chem. Hans-Bernhard Rhein, Prof. Dr. Karl Schügerl,
Institut für Technische Chemie, Universität Hannover,
Callinstr. 3, D-3000 Hannover

For the systematic characterisation of droplet phenomena and on account of their relevance to column scale-up, two isomer chlorobenzoicacids were investigated, which are different according to their degree of solvation.

Mass transfer and association effects /8,9/

Based on the pK_a -values of 2-chloro-benzoic-acid and 3-chloro-benzoic-acid (2.94 and 3.83), the extraction in the system xylene/water is greatly dependent on the pH. Extraction reaches from the sole physical distribution of non-dissociated acid HB between the phases at pH 1 to conditions of reactive coupling at pH 12. Under such conditions - at pH 12 - the mass transfer resistance in the aqueous phase is totally eliminated. On the other hand, polar organic carbonic-acids are dissolved in apolar solvents such as xylene by dimerisation. The equilibrium between monomer and dimer is dependent on the total acid concentration and estimable by IR-spectroscopy or by the extraction distribution coefficient. A new variable, which is defined by equation (1) using the distribution coefficient

$$H = \frac{C_{org,tot}}{C_{aq,tot}}$$

is only dependent on the non-dissociated acid HB in the aqueous phase (eq. 2):

$$Q := H (1 + 10^{pH-pK_a}) \quad (1)$$

$$Q = K_E + 2 K_D K_E^2 [HB]_{aq} \quad (2)$$

where K_E and K_D are the thermodynamic equilibrium constants of physical extraction and dimerisation reaction.

Kinetics of mass transfer

Even though the non-steady state of mass-transfer - caused by the fluid dynamics of the droplet, i. e. circulations and oscillations - forbids a stationary kinetic evaluation, we can discuss the divergence of steady state by definition of momentary quasi-steady state by definition of momentary quasi-steady state mass transfer coefficients k_t /3,8/.

Caused by the phase ratio $V_{org}/V_{aq} \approx 10^{-6}$ in the case of a single droplet, evaluation becomes easier. Based on Lewis' two-film-theory, the overall-coefficient k_t is computable from continuously measured concentrations of chloro-benzoic acid in the droplet during the extraction process:

from xylene to water (extraction to quasi-continuum)

$$k_t = - \frac{dc_{org}}{dt} \cdot \frac{V_{dr}}{A} \cdot \frac{1}{c_{org}(t)} \quad (3)$$

from water to xylene (extraction from quasi-continuum)

$$k_t = \frac{dc_{org}}{dt} \cdot \frac{V_{dr}}{A} \cdot \frac{1}{\frac{K_E \cdot c_{w,0}}{1+10^{pH-pK_s}} \left(0,5 + 2K_D \sqrt{\frac{1}{16K_D} + \frac{c_{org}(t)}}{2K_D}} \right)} - c_{org}(t)} \quad (4)$$

Fig. 1 shows k_t of 2-chloro-benzoic acid as a function of equilibrium conversion in dependence on pH for xylene-to-water extraction ($K_D = 255$ l/mol).

Fig. 2 shows the corresponding curve for 3-chloro-benzoic acid ($K_D = 543$ l/mol).

The distinct non-stationary state of stronger dimerizing 3-CBA, namely under pH-12-conditions, at first let us consider the mass-transfer-resistance on the side of the dimerisation reaction. The acceptance is underlined by water-to-xylene extraction into the droplet, where monomer/dimer-ratio modification induces remarkable changes of k_t , when dimerisation is decreasing /8/. k_t -value is influenced by the dimerisation equilibrium as well by the sole reaction and by fluid dynamic properties. Differentiation of these effects is not possible, if only k_t is known.

Semi-continuous two-phase stirred cell

For the determination of extraction kinetics normally two-phase stirred cells are suitable. Their construction are oriented according to the one developed by Lewis. The disadvantage of such vessels with $V_{aq} \approx V_{org}$ is that the results are not necessarily transferable to droplet-phase ratio, i. e. principally not, if coupled reactions (dimerisation, dissociation) are possibly involved in fluid dynamic or interface stability.

Therefore, a new kind of two-phase stirred cell was constructed, in which the water phase is a continuum ($V_{org}/V_{aq} \approx 10^{-3}$). The water phase is lead as continuous through flow, via stirred cell input/output, connected to tank reservoir. The degree of mixing was characterized by residence time distribution. Corresponding to the droplet, the concentration of chloro-benzoic acid was continuously determined in the xylene-phase by UV-spectroscopy as $C_{org,tot}$.

Residence time distributions show that in the used vessel the average residence time of the continuous water phase for flow rates $V_{aq}^* = 4.8$ to 9.0 l/h is independent on stirrer frequency $n = 0-500$ rpm.

The deviation of average residence time or of variance of residence time distribution becomes only significant when flow rates are below 2.4 l/h and at the same time, stirrer frequencies must be lower than 70 rpm. In all other cases, the degree of mixing of the water phase in the cell is independent on stirrer frequency. This fact is not necessarily transferable to the organic phase.

According to these hydrodynamic effects, the mass transfer - represented by k_t using eq. (3) - of 3-chloro-benzoic acid at pH-12 was investigated with the flow rate and stirrer frequency as parameters.

The following results were obtained:

1. The steady state condition can be maintained as long as the total concentration C_{org} is high enough, so that $dx_{monomer}/dc_{org}$ is constant and there is no increase of monomer concentration produced by dissociation of dimer ($x_{monomer}$ - molfraction monomer corresponding to dimerisation equilibrium). The steady state condition is nearly undisturbed by n and V_{aq}^* , if $n > 70$ rpm and $V_{aq}^* > 3.6$ l/h.
2. If monomer/dimer ratio increases, k_t also increases slowly to a maximum point. After this point, it is observed that the value of k_t falls down to a minimum. Soon afterward the mass transfer coefficient suddenly increases to a value greater than the maximum point before. The minimum is lower than k_t at the steady state condition. This characteristic maximum/minimum course of k_t is dependent on n as well as dependent on V_{aq}^* . Experimental data with V_{aq}^* as a parameter and $n = \text{const.} = 250$ rpm are shown in fig. 3 (k_t vs monomer acid conversion).

Conclusions

In the reactive extraction the mass transfer of 3-chloro-benzoic-acid into the aqueous phase at high total concentration is controlled by the solvation equilibrium in xylene, which is related to the lower tendency of dimer to transfer to the interface because of its "apolar" nature.

Since the monomer/dimer ratio increases during extraction, mass transfer becomes faster. However, it is limited because of loading effects at the interface, produced by polarity/tensid character of the monomer.

It seems that the loaded interface can renew itself by opening the monomer-layer there. Then mass transfer begins to rise again. The opening process is dependent on hydrodynamics in the organic phase (influenced by n) as well as in the aqueous phase (influenced by V_{aq}^*).

Both the experiments in single droplet system or in stirred cell show that mass transfer of chloro-benzoic acid - as a representative of carbonic acids - is limited by the interactions at the interface produced by the acid solvation. Proposals for modelling will be given.

References

- /1/ Mensing, W.
Dissertation, University of Hanover, 1968
- /2/ Mensing, W., Schügerl, K.
Chem. Ing. Tech., 42 (1970), 837
- /3/ Halwachs, W.
Habilitationsschrift, University of Hanover, 1981
- /4/ Halwachs, W., Schügerl, K.
Chem. Eng. Sci., 38 (1982), 1073
- /5/ Hänsel, R.
Dissertation, University of Hanover, 1984
- /6/ Hänsel, R., Halwachs, W., Schügerl, K.
Chem. Eng. Sci., 41 (1986), 555
- /7/ Hänsel, R., Halwachs, W., Schügerl, K.
Chem. Eng. Sci., 41 (1986), 135
- /8/ Rhein, H.-B.
Diploma thesis, University of Hanover, 1984
- /9/ Rhein, H.-B., Hänsel, R., Schügerl, K.
Chem. Ing. Tech., 57 (1985), 798

Fig. 1 Freely suspended single droplet:
 coefficient k_e as a function of equilibrium
 conversion of the extraction of 2-chloro-
 benzoic acid from xylene to water
 parameter: pH of aq. phase
 droplet volume 55 μ l, $c_{org,0} = 30$ mM/l

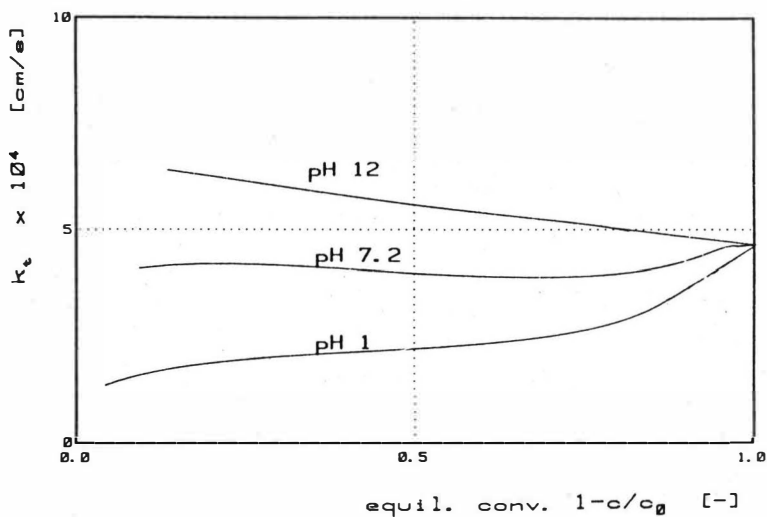


Fig. 2 Freely suspended single droplet:
 coefficient k_e as a function of equilibrium
 conversion of the extraction of 3-chloro-
 benzoic acid from xylene to water
 parameter: pH of aq. phase
 droplet volume 55 μ l, $c_{org,0} = 40$ mM/l

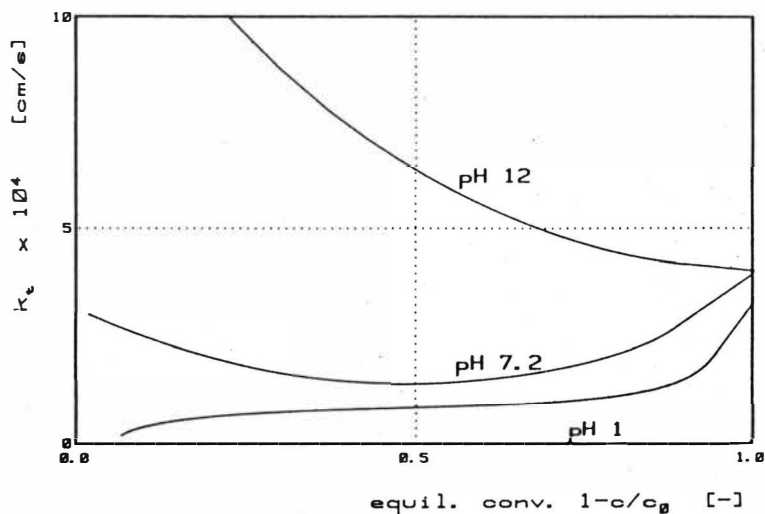
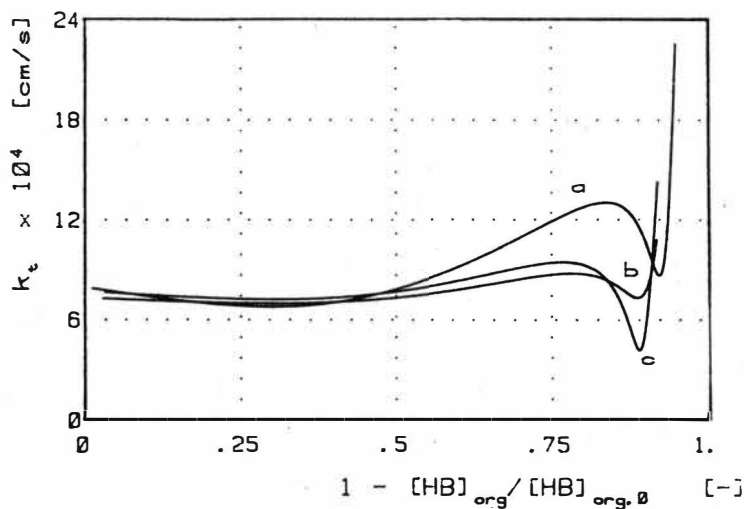


Fig. 3 Semi-continuous stirred cell:
 coefficient k_t as a function of monomer
 equilibrium conversion.
 3-chloro-benzoic acid extracted from xylene
 to water at pH 12
 stirrer frequency 250 rpm, $c_{org,0} = 30$ mM/l
 parameter: flow rate aq. phase
 $a = 40$, $b = 60$, $c = 80$ [ml/min]



Modelling of mass transfer in solvent extraction

M. Siebenhofer, R. Marr, Technische Universität Graz,
Graz/Austria

When doing a literature screen in solvent extraction at the present state one has to accept that the centre of interest is located in the development of solvents and solvent mixtures with optimum distribution properties. Sure this field of investigation has to be considered increasingly as the futural level of technology will be very connected with the recovery and separation of various substances from raw materials with low concentration.

Besides the influence of the solvent composition and the mechanism of separation on apparatus design and apparatus selection have to be considered as well as these properties directly fix constructive boundaries.

Evaluation of an extraction process ordinary starts with the description of the problem. Then solvent selection and mechanism studies occur. At this state the optimum separation properties of the selected solvent mixtures are tested to find out the solvent with the best loading capacity under consideration of modifier and diluent effects on the separation behaviour. Further the complete process, starting with the extraction step and ending with the solvent regeneration step must be tested for to guarantee the practicability of the process. All these steps can be tested in laboratory scale size. During this period of investigation only poor information on apparatus design is evaluated. But serious information about data needed for a succesful apparatus design are at least as necessary as principle information about the practicability of the complete process. Although the apparatus qualities of most of the industrially used extraction apparatus are tested and compared by so called test systems these informations don't offer much help for the apparatus design for systems that don't show very similiar properties compared with these test systems. Therefore fundamental investigation in this field is sure necessary for the evaluation of general information on the parameters that have to be considered when constructing an extraction apparatus.

The main parameter that influences the apparatus height is the mass transfer determining step of the separation process. Under consideration of this a research program on the investigation of the mass determining step in solvent extraction has been started with the objective to work out representantive transfer models based on the mechanism of

separation. Beside the possibility of rate determination by diffusion in both phase layers rate determination by the transfer in the boundary layer shows different properties mainly based on the separation mechanism itself. These phenomena influence the apparatus design and -selection and they can cause bad experiences if not considered or neglected. On principle these phenomena determine what apparatus type has to be used with regard to the manner of phase contact. Therefore the class of continuously working extraction apparatus has to be subdivided into the group of apparatus with continuous phase contact corresponding to the spray column type and into the group of apparatus with discontinuous phase contact corresponding to the mixer settler type.

In case of mass transfer control by diffusion apparatus efficiency is mainly affected by the energy input. Therefore the optimum design is very connected with the knowledge on hydrodynamic properties. Except the consideration of minimum drop size fraction apparatus selection is not limited by further significant parameters. If phase transfer is controlled by chemical reaction rate determination may be located at both sides of the phase boundary layer. The manner of phase contact then depends on the type of barrier that limits the mass transfer. Independent of the species to be separated the majority of reaction controlled transfer processes may be described by equation 1.

$$A_I \approx A_i \approx A_{II} \quad (1)$$

Application of this equation is connected with the assumption that the transfer of the reactive substance of the solvent to the interface does not affect mass transfer. This ordinary happens as reactive substances used in solvent extraction preferably set up at the interface caused by their polar nature. Then rate determination is either caused by the rate ratio of solute-solvent complex formation or by the separation of the formed complex from the interface. If the complex formation is rate determining, the separation problem can be treated similar to diffusion controlled processes.

When separation of the loaded reactive substance of the solvent from the interface into the bulk of the solvent is blocked, the solvent will be loaded up to the interface equilibrium concentration which is less than the corresponding total solvent equilibrium concentration. For a complete loading of the solvent the interface has to be disturbed or destroyed to enable the interface saturation with non reacted active substance of the solvent /1/. Therefore the solvent either has to be used as the continuous phase in the apparatus, which is hardly to be

realized in most cases when extraction columns are used, or the dispersed solvent drops have to be coalesced and redispersed again after a determined mass transfer duration for the single droplet. For the second way apparatus of the mixer settler type are needed.

Shift of mass transfer order /2/

With increasing loading of the solvent a shift of the order of reaction is possible. Again this mass transfer type should preferably be treated in mixer settler apparatus types. Ordinary hydrodynamic effects do not influence the mass transfer behaviour of the above mentioned mass transfer types. This is in agreement with the fact that most of the experiments in this field have been worked out with conventional solvent systems with molecular interaction of less power than hydrogen bondings. Therefore practical treatment of processes corresponding to the above mentioned deviations from diffusion controlled mass transfer processes is better done in mixer settler type apparatus.

Quantitative investigation

The major problem at the present state is how to assign the various types of reaction in solvent extraction to one of these process types based on the stoichiometric mass transfer equation. On principle the experimental set up for quantitative information about mass transfer can either be a pilot plant experiment which causes the highest demand for the needed information or experiments can be worked out in a single droplet column or in a small volume batch vessel /3/. The latter methods guarantee satisfactory results for the investigation of the mass transfer type of an investigated system while the information from experiments of the first possibility only leads to mean mass transfer coefficients. As observed from single droplet experiments a mean upper residence time of about 30 seconds is advantageous for serious information as data estimation for a mechanism to be tested becomes easier. Based on equation 1 following rate equations have already shown to be representative:

$$-dc_A/dt = k_1 \cdot c_A / (1 + k_2 \cdot c_A) \quad (2)$$

Mass transfer processes according to this type of reaction consider both the rate of the complex formation and the separation of the solvent-solute product from the interface /4/. The general rate form to equation 2 is given in equation 3.

$$-dc_A/dt = k_1 \cdot c_A^m / (1 + c_A^n) \quad (m > n) \quad (3)$$

Both mechanism presume the formation of an active group of solute at the interface in the first step and any further interaction with the solvent in the following steps.

Although these rate equations don't necessarily surround the whole variety of possible mechanism they may describe several processes better than the common mass transfer equation. To test what mechanism better fits an experimentally found data set, the integral rate coefficient evaluation shows good properties.

Nomenclature

A	solute - any substance
c	concentration (mol/l)
k	rate coefficient
m,n	reaction order
t	time

Indices

I,II	phase I or II
i	interface

Literature cited

- /1/ Yagodin, G.A., Tarasov, V.V., Formin, A.V., Ivakhov, S.: CIM Special, Vol 21, ISEC 77, p 260 - 265
- /2/ Levenspiel O.: Chemical Reaction Engineering, John Wiley & Sons, Inc., New York, 2nd edition, p 64 ff
- /3/ Aprahamian, E., Freiser, H.: Role of Interfacial Areas in Vigorously Stirred Solvent Extraction Systems; Fourth Symp. on Separ. Science and Techn., Oct 20 - 24, 1985, Knoxville (Tenn)
- /4/ Siebenhofer, M., Marr, R.: Auswirkungen der Extraktionsmittelzusammensetzung auf den Stoffaustausch und die Apparateauswahl; GVC- Jahrestreffen der Verfahrens-Ingenieure, Sept 19 - 24, 1984, Munich

THE EFFECT OF INTERFACIAL TURBULENCE ON MASS TRANSFER

Study of Transfer of Two Solutes Separately and Simultaneously Through Liquid-Liquid Interface

S.H. Zhang, Z.M. Wang and Y.F. Su

East China Institute of Chemical Technology, Shanghai, China

Introduction

In the process of liquid-liquid or gas-liquid mass transfer, it is oftentime observed that there are spontaneous interfacial convection, eruption and emulsification which promote the mass transfer rate substantially. The interfacial convection resulting from local changes in interfacial tension may manifest in a variety of ways. Rippling of the interface, localized eruptions and cellular convection are the terms most frequently mentioned.

Most experiments have been carried out either in the quiescent condition or in the flow condition. Each term associated with others relates to a particular hydrodynamic state of the bulk liquid. It could not be made a clearcut, because they affect each other and make the interfacial phenomena very complicated.

Glender and Reddy (1964) measured that the enhancement factors of the mass transfer coefficient were 1.5 to 4 in a stirred cell. Bakker (1966) obtained the factors of 2-3 in a parallel flow condition. Berg and Morig (1969) point out that if there is a stable density gradient when solute transfers through the interface, the interfacial turbulence induced by Marangoni effect will be confined in the area close to the interface. On the contrary, if there exists an instable density gradient, the interfacial turbulence will penetrate into the bulk phase as a manner of turbulent eddies. Besides, some experiments were done by Sawistowski (1963) and Ostrovskii (1974). As yet it still has not been clear that what kind of effects will happen when there is specific bulk flow as well as interfacial turbulence. Since some extractors relate to the film flow pattern, a specific cell has been built for the investigation.

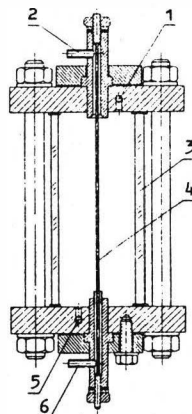


Fig. 1 Transfer cell

1-water inlet 2-solvent outlet
3-quartz cell 4-solvent film
5-water outlet 6-solvent inlet

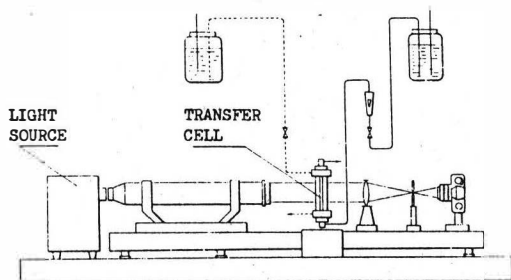


Fig. 2 Schlieren system

Experimental

A. Equipment

A transfer cell is shown in Fig. 1. The outside dimensions of the cell are $2.4 \times 6 \times 10, 10^{-2}$ m. At the center of the cell, there is a stainless steel wire sleeved with a Teflon tube of 0.23 cm in diameter. As the organic phase likely wets the surface of the Teflon, a quite uniform film of the organic phase has been obtained. The cell was made of quartz and had a very good optical characteristic. It was placed in the optical path of a Schlieren apparatus so that the interfacial phenomena can be observed visually and recorded photographically. The Schlieren system is shown in Fig. 2.

The experimental systems are shown in Table 1. In addition the system carbon tetrachloride-acetic acid and iodine-water was used in simultaneous counter transfer process. Distilled water and analytical reagents were used in these experiments. The equilibria are shown in Figs. 3 and 4. In the latter the presence of I_2 has no influence on the distribution of HAC. The physical properties of the solvents and interfacial tension are related to the concentrations of the solute in both phases. Therefore, those data have to be measured experimentally. The interfacial tension data were measured with the drop weight method and the viscosity data were determined by the Ostwald viscometer. The physical properties are listed in Table 1 and the plots of interfacial tension versus the concentration of the solute are shown in Fig. 5. The concentrations of the solute were measured either by titration or spectrophotometry.

Table 1 Physical properties of the phases (293°K)

Systems	Properties						
	m $C_0 \cdot C_w$	D_o $10^{-9} \text{ m}^2/\text{s}$	D_w $10^{-9} \text{ m}^2/\text{s}$	ρ_o kg/m^3	ρ_w kg/m^3	μ_o $10^{-3} \text{ kg/m}\cdot\text{s}$	μ_w $10^{-3} \text{ kg/m}\cdot\text{s}$
$C_6H_5CH_3$ -HAc- H_2O	FIG. 3	2.10	1.08	888	998	0.582	1.043
$C_6H_5CH_3$ -HAc-20% glyc.	FIG. 3	1.97	0.531	892	1.085	0.621	2.120
$C_6H_5CH_3$ -HAc-40% glyc.	FIG. 3	1.87	0.272	917	1.145	0.652	4.137
CCl_4 -HAc- H_2O	Fig. 4	1.37	1.08	1.595	998	0.969	1.005
CCl_4 - I_2 - H_2O	89.9	1.36	1.09	1.595	998	0.964	1.005

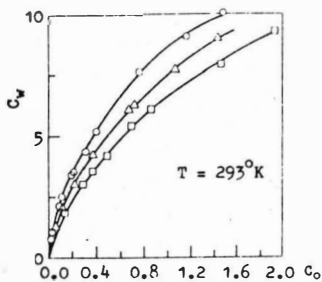


FIG. 3 DISTRIBUTION OF HAC BETWEEN Aq. AND ORG. PHASES

- $C_6H_5CH_3$ -HAc- H_2O
- △ $C_6H_5CH_3$ -HAc-80% H_2O -20%GLYCEROL
- $C_6H_5CH_3$ -HAc-60% H_2O -40%GLYCEROL

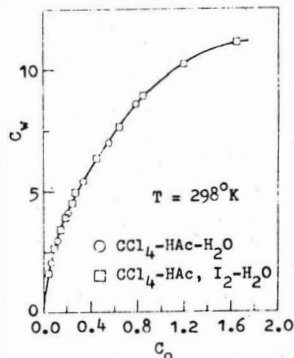


Fig. 4 Distribution of HAC between Aq. and Org. phases

B. Procedure

Two solvents were mutual saturated before starting experiments in order to ensure that only the solute was transferring during the experiments. There were two kinds of procedures. The first one was semi-batch style i.e., the organic phase flowed as a film through the cell and then was collected in a flask. After a period of time, the flow was switched off. The average concentration of both phases were analysed. The second one was continuous operation i.e., both phases passed through the cell continuously. After the process had reached stable condition, the samples were taken and analysed. The thickness of the film was measured by a microscope.

Results

A. Hydrodynamics of the film flow

In a liquid-liquid system, when one of the liquid moves vertically as a film passing through another liquid, it is subject not only to the gravitational force but also to the buoyant force. If the viscosity of the surrounding liquid is very low, the thickness of the film can be calculated by Eq. (1).

$$b = (3 \mu_o q_o / \Delta \rho g)^{1/3} \quad (1)$$

where q_o is the periphery flow rate of the organic phase, and $q_o = V_o / \pi d$; $\Delta \rho = \rho_w - \rho_o$ and the average velocity of the liquid film is

$$U_o = V_o / \pi b(d + b) \quad (2)$$

The Reynolds number of the liquid film is

$$Re = 4 U_o b \rho_o / \mu_o \quad (3)$$

A good agreement of the experimental data of film thickness with the calculated ones by using Eq. (1) is shown in Fig. 6. According to the observation of authors, only when $Re > 150$, the ripple of the liquid film will occur.

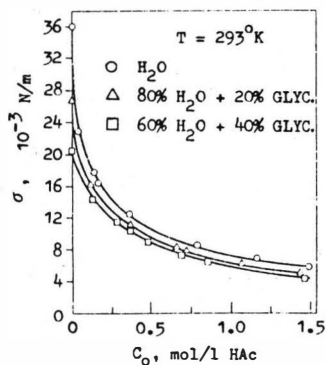


Fig. 5 b vs. C_o

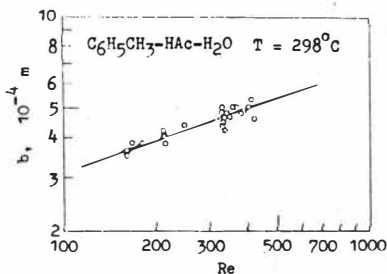


Fig. 6 b vs. Re

— Calculated from Eq. 1
 O Experimental

B. Mass transfer

The overall mass transfer coefficient based on organic phase K_o can be calculated by Eq. (4) in semi-batch operation, or Eq. (5) in the continuous operation.

$$K_o = \frac{V_o}{S} \ln \left(\frac{C_{o1} - m \bar{C}_w}{C_{o2} - m \bar{C}_w} \right) \quad (4)$$

$$K_o = \frac{V_o}{S} \frac{(C_{o1} - C_{o2})}{(C_o - C_o^*)_{1m}} \quad (5)$$

Where $(C_o - C_o^*)_{1m}$ is the logarithmic mean driving force of the concentrations between inlet and outlet.

If there is no interfacial turbulence, it is assumed that there is no radial velocity gradient, the contact time is very short and the penetrate depth of the molecular diffusion is small. Thus the convective mass transfer equation reduces to Eq. (6).

$$U_o \frac{\partial C_o}{\partial X} = D_o \frac{\partial^2 C_o}{\partial y^2}$$

$$U_o \frac{\partial C_w}{\partial X} = D_w \frac{\partial^2 C_w}{\partial y^2} \quad (6)$$

Solving Eq. (6) by combining the boundary condition, the solution similar to the penetration theory was obtained.

$$k_o = \sqrt{\frac{D_o U_o}{\pi X}} \quad (7)$$

The average mass transfer coefficient is

$$k_o = 2 \sqrt{\frac{D_o U_o}{\pi L}} = 2 \sqrt{\frac{D_o}{\pi \tau}} \quad (8)$$

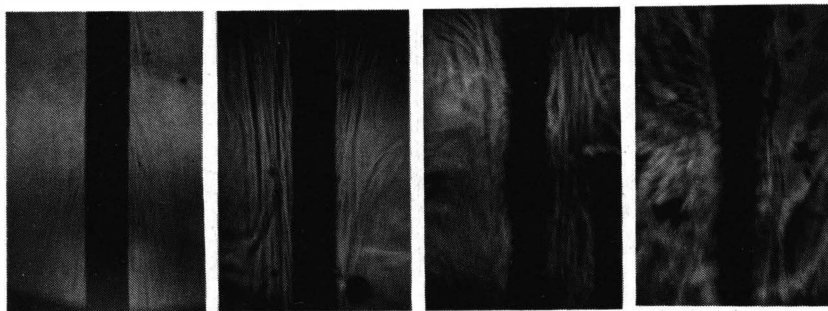
The concentration of the solute at interface is

$$C_{oi} = \frac{\bar{C}_w}{\frac{1}{m} + \sqrt{\left(\frac{D_o}{D_w}\right)}} \quad (9)$$

and $C_{oi} = m C_{wi}$

There are four Schlieren photos shown on Fig. 7. If the initial concentration of acetic acid in toluene is low (Fig. 7a) e.g., 0.0431 k mol/m³, the interface looks calm. As the concentration of acetic acid increases beyond a certain value, "critical", the eruption and spontaneous convection will occur (Fig. 7b). Further increasing the concentration of acetic acid, the interfacial motion will develop to strong turbulence which will increase the mass transfer rate substantially (Figs. 7c,d).

The experimental data of mass transfer coefficient at low solute concentration and without interfacial turbulence are agree well with Eq. (8), which shows that the mass transfer coefficient k_o is inversely proportional to $\tau^{1/2}$. Figs. 8 and 9 also show that the mass transfer coefficient increases substantially as the concentration of acetic acid increases. It is also shown, in Fig. 10, that the enhancement factor F increases with the increase of the value of Reynolds number. The fact that the experiments, in which acetic acid transfers from CCl₄ to water and from toluene to water, have interfacial turbulence is in contradiction with the Sternling and Scriven (1959) criterion. It seems that such kind interfacial turbulence is a disorder one.



$C_{0,1} = 0.203$

$C_{0,1} = 0.423$

$C_{0,1} = 0.978$

$C_{0,1} = 1.57$

Fig. 7 Schlieren photographs show that the intensity of interfacial turbulence depends upon the initial acetic acid concentration in the toluene phase $C_{0,1}$ (in $\text{kg}\cdot\text{mol}/\text{m}^3$) for the system $\text{C}_6\text{H}_5\text{CH}_3\text{-HAC-H}_2\text{O}$. $C_{A,1} = 0$, $C_{A,b} \approx 0$

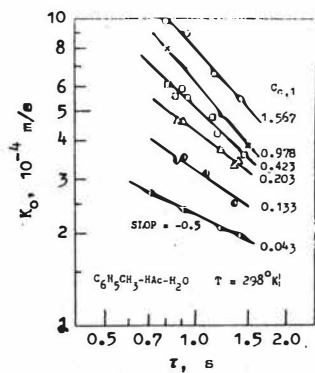


Fig. 8 K_0 vs. τ

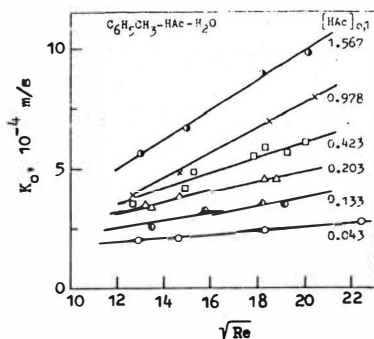


Fig. 9 $K_0(\text{HAC})$ vs. $\sqrt{\text{Re}}$

C. Interfacial pressure and Marangoni number

It is considered that the difference of the interfacial pressure, $\Delta\pi = \pi^* - \pi = \sigma(C_{0,1}) - \sigma(C_{0,b})$, is the driving force of the interfacial turbulence and the viscosities of the liquids are the resistant force. The mass transfer data can be correlated with the Marangoni number. Based on the organic phase, the Marangoni number is

$$\text{Ma} = (\sigma_{01} - \sigma_{0b}) / \mu_0 K_{0R} \quad (10)$$

Where K_{0R} is the mass transfer coefficient without interfacial turbulence as a reference. The data are shown in Fig. 10. For the systems of toluene-acetic acid-water and toluene-acetic acid-40% glycerine, the correlation is as follows

$$F = (\text{Ma}/\text{Ma}_c)^n \quad (11)$$

Where $\text{Ma}_c = 0.912 \times 10^5$; $n = 1.2 \pm 0.3$

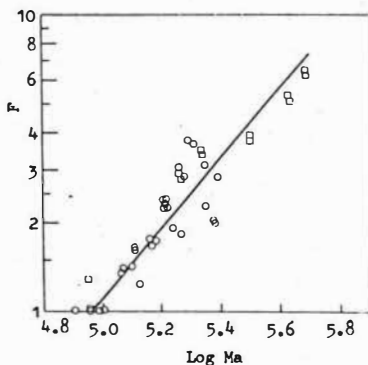


Fig. 10 Enhancement factor F vs. $\text{Log } Ma$

- $C_6H_5CH_3-HAc-H_2O$
- $C_6H_5CH_3-HAc-40\% \text{ GLYCEROL}$

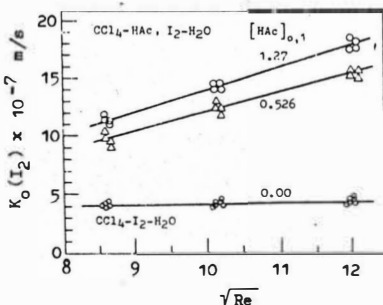


Fig. 11 $K_o(I_2) \times 10^{-7}$ vs. \sqrt{Re}
Initial Aq. Conc.

$$[I_2]_A = 7.98 \times 10^{-4} \text{ kmol/m}^3$$

D. Simultaneous counter transfer processes

No interfacial turbulence has been observed at any concentration of iodine which transfers from aqueous to CCl_4 phase alone. It seems interesting to know what will happen to the transfer of iodine if HAC is transferring at the same time in the opposite direction.

From Fig. 11 the lowest line indicates that the transfer of iodine is "normal". But in the presence of simultaneous transfer of HAC from CCl_4 to aqueous phase the mass transfer coefficients of iodine are enhanced almost to the same extent, i.e. $F=2.2-4.7$, as those of HAC, despite the main resistance resides either in the water phase in the first case or in the organic phase in the second case.

A conclusion may be drawn that interfacial turbulence induced by transfer of one solute will also promote that of the other irrespective of the direction of transfer. It becomes also evident that the influence due to Marangoni effect on both sides of the interface is of the same order of magnitude, either on hydrodynamics or on mass transfer.

Notation

- | | | | |
|-------|---|-------|--|
| b | average thickness of the film, m. | m | distribution coefficient, (C_o^*/C_w) . |
| C | solute concentration, kmol/m^3 . | q_o | periphery flow rate of organic phase, $\text{m}^3/\text{m}\cdot\text{s}$. |
| D | diffusivity coefficient, m^2/s . | Re | Reynolds number of the film, dimensionless. |
| d | diameter of the Teflon column, m. | S | interfacial area of the film, m^2 . |
| F | enhancement factor of mass transfer coefficient. | U_o | average velocity of the film, m/s . |
| K_o | over-all mass transfer coefficient based on organic phase, m/s . | V | volumetric flow rate, m^3/s . |
| k | individual mass transfer coefficient, m/s . | X | distance from the inlet of the film, m. |
| L | total height of the column, m. | y | radial coordinate of the film, m. |
| Ma | Marangoni number, dimensionless. | | |

Greek letters

- μ viscosity, $\text{kg/m}\cdot\text{s}$.
- π interfacial pressure, N/m .
- ρ density, kg/m^3 .
- σ interfacial tension, N/m .
- τ contact time, s.

Subscripts

- 1 inlet.
- 2 outlet.
- b bulk flow.
- c critical state.
- i at interface.
- o organic phase.
- r reference state.
- w aqueous phase.
- lm logarithmic mean.

References

- Bakker, C.A.P., Van Buytenen, P.M. and Beek, W.J., Chem. Eng. Sci., 21, 1039 (1966).
- Berg, J.C. and Morig, C.R., Chem. Eng. Sci., 24, 937 (1969).
- Imaishi, N. and Fujinawa, K., Inter. Chem. Eng., 20, 226 (1980).
- Imaishi, N., Suzuki, Y., Hozawa, M. and Fujinawa, K., Inter. Chem. Eng., 22, 659 (1982).
- Olander, D.R. and Reddy, L.E., Chem. Eng. Sci., 19, 67 (1964).
- Ostrovski, M.V., Inter. Chem. Eng., 14, 431 (1974).
- Sawistowski, H., Trans. Instn. Chem. Engrs., 41, 174 (1963).
- Sternling, C.V. and Scriven, L.E., AIChE J., 5, 514 (1959).

Modelling An Apparatus In Emulsion Liquid Membrane Operations

D.Lorbach, H.J.Bart, R.Marr, Graz, Austria

The present work is an investigation of mass transfer in an emulsion liquid membrane process for the extraction of Zn^{++} from aqueous solutions with a liquid ion exchanger. A diffusion and reaction controlled mass transfer model is developed and experimentally tested in a single drop apparatus. This mass transfer model is extended to continuous emulsion liquid membrane (ELM) operations in a mixer settler device (CSTR). Calculated solutions are presented in a performance diagram.

ELM technology is relatively new, but growing demand in high performance separation techniques helps to increase potential industrial applications e.g. in the recovery of heavy metals [1,2], amines [3], and in the field of biochemical engineering [4].

The general principles of an ELM - process are as follows: The solute present in the continuous phase is extracted by an emulsion which is dispersed in an agitated feed solution. An emulsion globule consists of an oil phase in which the aqueous droplets of the stripping solution are embedded. The oil phase acts as the membrane. It is composed of an oil solvent, a stabilizing surface active agent, and a reactive carrier, if the solute itself is insoluble in the membrane. The internal droplets vary in size between 0.5 - 8.0 μm . It has been suggested by earlier experimental evidence [5] that most of the tenside is bound at the internal droplet interface. Any circulation in an emulsion globule is therefore suppressed because of the steric resistance of the lipophilic chains of the tenside molecules inside the emulsion globule. The globules generally are sized between 0.2 and 1.2 mm.

The two most important types of mass transport are simple diffusion type transport of the solute and carrier facilitated transport. Facilitated transport, the subject matter of this work, involves a chemical reagent in the membrane phase. This reagent reacts with the solute at the external globule interface and transports the solute to the internal stripping phase, where the reverse reaction occurs. Numerous mass transfer models have been proposed for the simple diffusion case. It has been shown that the most successful explanation of the experimental results was attained by taking into account the transient nature of the diffusional transport of the solute inside the emulsion globule [3].

Despite the great potential for commercial application of carrier facilitated transport little has been undertaken to develop reliable mass transfer models for this case. The only exception to this lack in developed theory is for the extraction of Cu^{++} with chelating reagents, a system for which transient diffusion models have been recently proposed [5,6]. It was therefore desirable to investigate the validity of a diffusion and reaction controlled mass transfer model for carrier facilitated

systems with different types of carriers. Carriers such as liquid ion exchangers have much faster kinetics than chelating reagents. For the present study the extraction of Zn^{++} by a cation exchanger was chosen because of its importance as the first large scale ELM process [7].

Experimental Set Up and Reactants

Experiments were performed in a single drop apparatus similar to that for previous studies of Cu^{++} extraction and a detailed description may be found elsewhere [5]. This device was expected to give the most reliable data for actual mass transfer because there is no interference of polydispersity effects. After contact with the $ZnSO_4$ containing continuous phase the emulsion phase was split by means of an electric coalescer. The internal stripping phase was then analyzed in an atomic absorption spectrophotometer. Chemicals used were p.a. grade except for the membrane phase which consisted largely of kerosine like solvent Shell-Sol T. The surfactant used was commercial grade polyamine ECA-4360 from Exxon. The carrier reagent was the ester bis-2-ethyl-hexyl-dithiophosphoric acid as supplied by HOECHST Ag. The pH of the continuous phase was controlled with sulfuric acid. 50 g/l $NaSO_4$ was added to the continuous phase to maintain a relatively constant ionic strength throughout the experiments and to guarantee negligible osmotic swelling. The internal phase was 2.5 M sulfuric acid.

The Diffusion And Reaction Controlled Mass Transfer Model

As pointed out above, a reliable model should take the transient nature of the diffusion process into account. Furthermore, the resistance of the chemical reaction of the carrier and the mass transport resistance at the outer interface have to be included. The model which is presented here tries to take these effects into account. The simplifying assumptions are as follows: The first and probably most restrictive one is the assumption of ideal solutions, so that concentrations instead of activities can be used. The extraction reaction and stripping reaction are located exactly at the outer and internal interfaces. It is assumed that a Sauter mean diameter could be used to describe the internal droplet size distribution and the Diffusion inside an emulsion globule is described with an effective diffusivity.

The stoichiometry of the reaction is:



The equations governing mass transfer are:

- continuous phase:

$$\dot{n} = k_A (C_{A3} - C_{A3}^*) \quad (2)$$

- extraction reaction:

$$\dot{n} = k_f \left\{ \frac{C_{A3}^* C_B^*}{C_{H3}^*} - \frac{1}{K_{ex}} \cdot \frac{C_C^* C_{H3}^*}{C_B^*} \right\} \quad (3)$$

- globules:

$$\frac{v_2}{v_1 + v_2} \frac{\partial C}{\partial t} = D_{\text{eff}} \frac{1}{r^2} \cdot \frac{\partial}{\partial r} r^2 \frac{\partial C}{\partial r} - \frac{3 v_1 k_r}{R_1 (v_1 + v_2)} \cdot \left(C_C C_{H1} - K_{\text{ex}} \frac{C_{A1} C_B^2}{C_{H1}} \right) \quad (4)$$

$$\frac{\partial C_{A1}}{\partial t} = \frac{3k_r}{R_1} \cdot \left(C_C C_{H1} - K_{\text{ex}} \frac{C_{A1} C_B^2}{C_{H1}} \right) \quad (5)$$

$$C_B = C_B^0 - 2C_C \quad (6)$$

$$C_{H1} = C_{H1}^0 - 2(C_{A1} - C_{A1}^0) \quad (7)$$

- boundary conditions:

$$r = 0 : \quad \frac{\partial C}{\partial r} = 0. \quad (8)$$

$$r = R : \quad \dot{n} = D_{\text{eff}} \frac{\partial C}{\partial r} \Big|_{r=R} \quad (9)$$

In equation (6) the inherent assumption is that the carrier and the carriercomplex have equal diffusivities. In terms of dimensionless variables the equations scale as:

$$\dot{v} = (y_1 - y_5) \quad (10)$$

$$\dot{v} = Da \left\{ \frac{y_5 y_2^{R_{BH}}}{y_6} - \frac{R_{BA}}{K_{\text{ex}} R_{BH}} \frac{y_3 y_6}{y_2} \right\} \quad (11)$$

-globules:

$$\frac{\partial y_3}{\partial \tau} = \frac{1}{(1-\phi')} \frac{1}{\eta^2} \frac{\partial}{\partial \eta} \eta^2 \frac{\partial y_3}{\partial \eta} - \frac{3}{\rho} \frac{\phi'}{(1-\phi')} \theta_R^2 \cdot \left(R_{HB} y_3 y_7 - \frac{K_{\text{ex}}}{R_{HB}} \frac{y_4 y_2^2}{y_7} \right) \quad (12)$$

$$\frac{\partial y_4}{\partial \tau} = \frac{3}{\rho} \theta_R^2 \left(R_{HB} y_3 y_7 - \frac{K_{\text{ex}}}{R_{HB}} \frac{y_4 y_2^2}{y_7} \right) \quad (13)$$

$$y_2 = 1 - 2y_3 \quad (14)$$

$$y_7 = 1 - \frac{2}{R_{HB}} (y_4 - y_4^0) \quad (15)$$

- boundary conditions:

$$\eta = 0 : \quad \frac{\partial y_3}{\partial \eta} = 0. \quad (16)$$

$$\eta = 1 : \quad \dot{v} = \frac{R_{BA}}{Bi} \frac{\partial y_3}{\partial \eta} \Big|_{\eta=1} \quad (17)$$

The above equations were solved numerically, since there is no known analytical solution. The solution was obtained in a straightforward fashion by the method of lines [8] in combination with an ODE-solving routine. In the case of the single drop experiments the concentrations C_{H_3} and C_{A_3} are held constant due to the fact that the phase ratio of continuous phase to the emulsion phase is very large.

Parameters Of The Model

All model parameters have a physical meaning and thus can be derived from first principles. The kinetic parameters of the stripping reaction were measured in a constant interface cell and the experimental procedure and the evaluation of the parameters were similar to those previously reported for the extraction of Cu^{++} [5]. The external mass transfer coefficient, the reaction rate constant of the extraction reaction and the effective diffusivity, however were measured in the single drop apparatus. There are transport- and reaction-controlled regimes in the range of high pH and low Zn^{++} concentrations which allow the independent determination of k_A and k_f in a procedure similar to that previously reported [5]. All parameters determined for the extraction of Zn^{++} with the chemical system under consideration are presented in Table 1.

Experimental Results In The Single Drop Apparatus

Experimental results are shown in Figures 1 and 2, where the influence of the continuous phase pH and Zn^{++} concentration are shown, respectively. The experiments depicted in Figure 1 were carried out in the kinetic regime and the influence of different pH values as reflected in the extraction reaction kinetics can clearly be recognized. Figure 2 reveals that a transport regime of the carrier complex is reached if the Zn^{++} concentration in the continuous phase becomes higher than 0.0153 mol/l. This regime determines the extraction rate. In the case of 0.0765 mol/l Zn^{++} mass transfer soon becomes slower than in the case of 0.0153 mol/l Zn^{++} . This is in sharp contrast to the kinetics, but becomes clear if the nature of the diffusional transport is taken into account. In the case of higher Zn^{++} concentration, the outer layers of an emulsion globule are saturated faster and the diffusional resistance becomes larger.

Extrapolation Of The Experimental Results To A CSTR

The good description of experimental results in the single drop apparatus encouraged us to extrapolate our calculations to continuous stirred tank reactors, reactors which represent the mixer settler type apparatus widely used in liquid-liquid

extraction. The only equation which has to be changed in order to describe the permeation process is eq.(2). The equation for the continuous phase now reads

$$v_w (C_{Ai} - C_{Ae}) = \frac{N}{T} 4\pi \int_0^{\infty} R^2 k_A (C_{Ae} - C_A^*) e^{-t/T} dt \quad (18)$$

with:

$$\dot{n} = k_A \cdot (C_{Ae} - C_A^*) \quad (19)$$

In dimensionless parameters these equations can be rewritten:

$$f_1 = \frac{v}{v_e} \left(\frac{C_{Ai} - C_{Ae}}{C_{Ai}} \right) = 3Bi \int_0^{\infty} (y_e - y_B) e^{-\theta\tau} d\tau \quad (20)$$

$$\dot{v} = (y_e - y_B) \quad (21)$$

Equations (20) and (21) express the functional dependence of the utilization factor f_1 which is not only a function of the Bi number and θ , but also of y_e and y_B . Assuming that all chemical and physical parameters of the model remain constant, the general functional relationship for the utilization factor can be written as

$$f_1 = f(\theta, Bi, R_{BH}, R_{BA}, \frac{A_{3e}}{A_{3i}}) \quad (22)$$

where R_{BA} now is C_B^0/C_{Ai} and R_{BH} is C_B^0/C_{He} .

This function is shown in Figure 3 with R_{BA} and R_{BH} held constant. Figure 3 is actually a diagram which gives a first estimate of mixer settler performance using emulsion liquid membranes. The most important fact revealed by this diagram is that equilibrium considerations are negligible in comparison to the transient nature of ELM processes.

Conclusion

The applicability of the diffusion and reaction model was shown for an ELM process recovering Zn^{++} from aqueous solutions. The model very well describes the reaction with a liquid ion exchanging reagent and the diffusional transport inside the globule. The transient nature of the diffusional transport inside the globule could be experimentally verified by the characteristic mass transport rates for various Zn^{++} concentrations in the continuous phase. A calculated diagram was presented to extrapolate the experimental results to a continuous process (CSTR) which showed that ELM-apparatus performance is determined by the residence time of the emulsion and not by equilibrium considerations.

Literature cited:

- (1) Fyles, T. M.; J. Membr. Sci., 24 (1985), 229.
- (2) Izatt, R.M.; McBride, D.W.; Christensen, J.J.; Bradshaw, J.S.; Clark, K.A.; J. Membr. Sci.; 22 (1985), 31.

- (3) Baird, R.S.; Bunge, A.L.; J. Membr. Sci., in press (1986).
 (4) Thien, M.P.; Hatton, A.T.; Wang, I.C.; Proceedings of the ACS Symposium, Chicago, IL, 1985.
 (5) Lorbach, D.M.; Bart, H.J.; Marr, R.; Ger. Chem. Eng., in press (1986).
 (6) Teramoto, M.; Sakai, T.; Yanagawa, K.; Ohsuga, M.; Miyake, Y.; Sep.Sci. Technol., 18 (1983), 735.
 (7) Draxler, J.; Marr, R.; Bouvier, A.; Kriechbaumer, A.; Proetsch, M.; ISEC, Denver, CO, 1983.
 (8) Madsen, N.K.; Sincovec, R.F.; Computational Methods in Nonlinear Mechanics; J.T. Oden et al., Eds., Texas Inst. for Computational Mechanics, Austin, TX, 1974.

List of Symbols:

- Bi Biot number = Rk_A/D_{eff}
 C_{A1} Zn^{++} concentration, dispersed phase [mol/l]
 C_{A3} Zn^{++} concentration, continuous phase [mol/l]
 C_{Ae} Zn^{++} effluent concentration, CSTR [mol/l]
 C_{A1} Zn^{++} inlet concentration, CSTR [mol/l]
 C_B Carrier concentration, membrane phase [mol/l]
 C_C Carrier-complex concentration, membrane phase [mol/l]
 C_{H1} H^+ concentration, internal phase [mol/l]
 C_{H3} H^+ concentration, continuous phase [mol/l]
 C_{He} H^+ effluent concentration, CSTR [mol/l]
 Da Damkohler number = k_f/k_A
 D_{eff} effective diffusivity [m^2/s]
 f_1 performance factor, defined by eq. (19)
 k_A mass transfer coefficient, continuous phase [m/s]
 K_{ex} equilibrium constant = $C_C C_H^2 / C_A C_B^2$
 k_f extraction reaction rate coefficient [m/s]
 \dot{n} specific molar flux [$mol/m^2/s$]
 N total number of droplets, CSTR
 r radial coordinate in a globule [m]
 R emulsion globule radius [m]
 R_1 internal droplet sauter mean radius [m]
 R_{BA} = C_B^0 / C_{A3}^0
 R_{BH} = C_B^0 / C_{H3}^0
 R_{HB} = C_{H1}^0 / C_B^0

 t time [s]
 T mean residence time of emulsion globules, CSTR [s]
 V_1 internal phase volume [m^3]
 V_2 membrane phase volume [m^3]
 V_E emulsion hold up, CSTR [m^3]
 v_e emulsion flowrate, CSTR [m^3]
 v_w continuous phase flowrate, CSTR [m^3]
 y_1 = C_{A3}^0 / C_{A3}^0
 y_2 = C_B^0 / C_B^0
 y_3 = C_C^0 / C_B^0
 y_4 = C_{A1}^0 / C_B^0
 y_5 = C_A^* / C_{A3}^0
 y_6 = C_{H3}^0 / C_{H3}^0
 y_7 = C_{H1}^0 / C_{H1}^0

$$y_B \dots = C_A^* / C_{Ai}$$

$$y_e \dots = C_{Ae} / C_{Ai}$$

Greek symbols:

$$\eta \dots \text{dimensionless radial coordinate in the globule} = r/R$$

$$\theta \dots = R^2 / D_{eff} \cdot v_e / V_E$$

$$\theta_R^2 \dots \text{Thiele modulus} = k_R R C_B^0 / D_{eff}$$

$$\dot{v} \dots \text{dimensionless specific molar flux} = A / C_{A3}^0 / k_A$$

$$\rho \dots = R_1 / R$$

$$\tau \dots = D_{eff} t / R^2$$

$$\phi' \dots = V_1 / (V_1 + V_2)$$

Indices:

0 at time 0.
 * at the interface

Table 1: Parameters for the extraction of Zn^{++} .

$D_{eff} = 1.9 \cdot 10^{-10}$ [m ² /s]	$k_A = 3.0 \cdot 10^{-7}$ [m ² /s]
$C_B^0 = 0.055$ [mol/l]	$k_f = 2.5 \cdot 10^{-7}$ [m ² /s]
$C_{H1}^0 = 2.5$ [mol/l]	$k_r = 1.1 \cdot 10^{-9}$ [m ⁴ /mol/s]
$C_{A1}^0 = 0.0$ [mol/l]	$K_{ex} = 106$
$R = 1.3 \cdot 10^{-3}$ [m]	$R_1 = 3.0 \cdot 10^{-6}$ [m]
$\phi' = 0.33$	

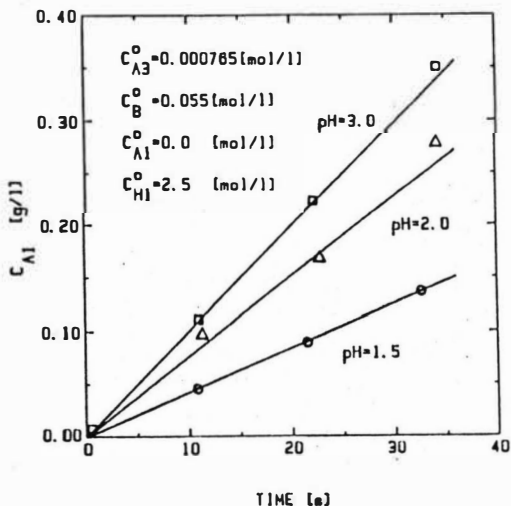


FIGURE 1 : Influence of the continuous phase pH in the reaction regime; Experiments in the Single Drop Apparatus.

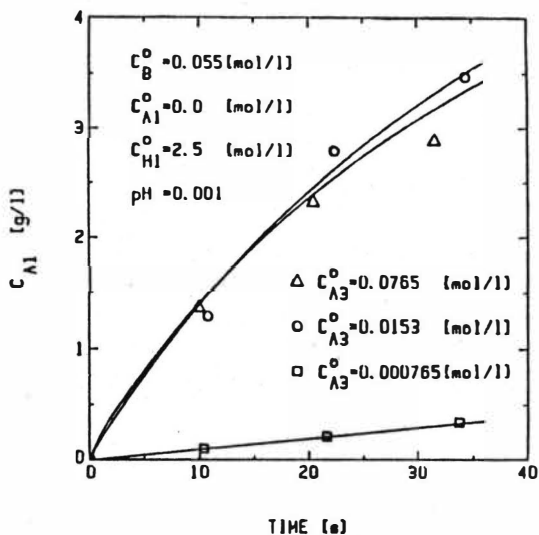


FIGURE 2 : Influence of the continuous phase Zn^{++} concentration; Experiments in the Single Drop Apparatus.

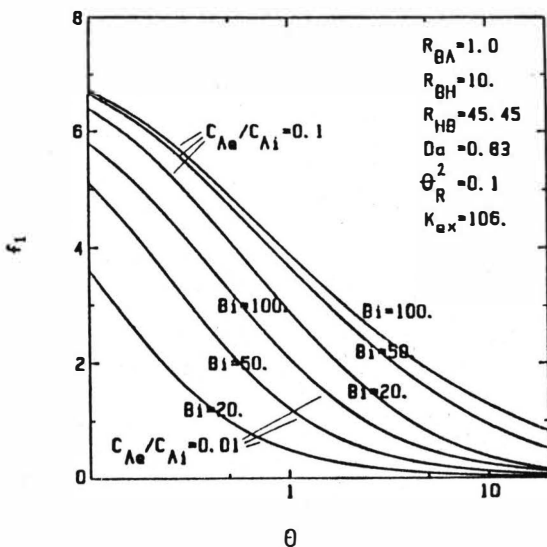


FIGURE 3 : Performance curves of ELM operation in a continuous stirred tank reactor (CSTR).

A comparative performance test for the extraction/re-extraction process and the supported liquid membrane process.

M. Fröhlich, W. Nitsch, TUM D 8046 Garching, Lichtenbergstr 4

During the last twenty years there have been some new extraction processes proposed. The common principle of these new processes lies in a close linkage of an extraction step with a re-extraction step. Some frequently mentioned examples are the "liquid surfactant membrane" (LSM) process, the "supported liquid membrane" (SLM) process and less frequently, the creeping film (CF) process. These membrane processes, however still compete with the conventional "extraction/re-extraction" (ExRe) process. The aim of this project is a quantitative comparison between the ExRe- and the SLM-process. The SLM process has been chosen, because this process seems to be well calculable.

1. Mathematical treatment of the ExRe process.

For a ternary system with equilibrium at the interface and concentration independent partition coefficients the individual approach can be reduced to a global approach, which leads to the known equations :

$$\dot{n} = \beta_{\text{tot}}^e (c_w^e - c_o^e / K^e) \quad (1)$$

$$1/\beta_{\text{tot}}^e = 1/\beta_w + 1/(\beta_o * K^e) \quad (2)$$

for the extraction process and:

$$\dot{n} = \beta_{\text{tot}}^r (c_o^r - c_w^r / K^r) \quad (3)$$

$$1/\beta_{\text{tot}}^r = 1/\beta_o + 1/(\beta_w * K^r) \quad (4)$$

for the re-extraction process. The first order differential equations (1 and 3) have an analytic solution. The integral of the drops' mean lifetime t^E resp. t^R leads to equation 5 and 6:

$$c_o^e(t^e) = c_o^r(t^r) + E^e (c_w^e K^e - c_o^r(t^r)) \quad (5)$$

$$c_o^r(t^r) = c_o^e(t^e) + E^r (c_o^r(t^r) - c_w^r/K^r) \quad (6)$$

$$\text{with: } E^e = 1 - \exp(-t^e * 6 * \beta_{\text{tot}}^e / K^e / d^e) \quad (7)$$

$$E^r = 1 - \exp(-t^r * 6 * \beta_{\text{tot}}^r / d^r) \quad (8)$$

The mass balances of the ExRe-device are described by equations 9, 10 and 11:

$$\dot{N} = V_O (c_O^e(t^e) - c_O^r(t^r)) \quad (9)$$

$$\dot{N} = V_w^e (c_w^{e,f} - c_w^e) \quad (10)$$

$$\dot{N} = V_w^r (c_w^r - c_w^{r,f}) \quad (11)$$

Usually the system parameters and the operating parameters $\dot{V}_w^e, \dot{V}_w^r, \dot{V}_O, c_w^{e,f}$ and $c_w^{r,f}$ are known quantities. For such a set of parameters equations 5,6,9,10,11 can be solved with respect of the five unknown variables $c_w^e = c_w^{e,l}, c_w^r = c_w^{r,l}, c_O^e(t^e), c_O^r(t^r)$ and \dot{N} .

As the equations are linear in respect of this set of unknown variables, the solution has been obtained by applying the gaussian elimination method.

This model has been also investigated by own experiments. These experiments were done by extraction of phenol in the system water/dibutyl ether/0.1 n NaOH. Experiments with 15 different operating conditions could be described by the transport coefficients:

$$\beta_w = (20 \pm 5) \cdot 10^{-3} \text{ cm/s} \quad (12)$$

$$\beta_O = (19 \pm 4) \cdot 10^{-3} \text{ cm/s} \quad (13)$$

These values tend about those, which are familiar for circulating drops.

Mathematical treatment of the SLM process

For the SLM process a model has been assumed with three individual transport coefficients. Two outside coefficients describe the mass transport through the boundary layers on both sides of the membrane. These coefficients depend on the linear flow velocity. The third transport coefficient describes the membrane transport. The magnitude of the membrane transport coefficient has been estimated using the diffusion approach. According to the commercial flat sheet membrane cellgard 2500 a thickness of $\delta = 25 \mu$ and a membrane porosity of $\epsilon = 0,45$ has been assumed:

$$\beta_M = D / \delta = 10^{-5} \text{ cm}^2 \text{ s}^{-1} / 2.5 \cdot 10^{-3} \text{ cm} = 4 \cdot 10^{-3} \text{ cm s}^{-1} \quad (14)$$

The outside coefficients have been tentatively estimated using results of liquid-liquid stirred cell measurements:

$$\beta_B^e = \beta_B^r = 0.3 \cdot 7 \cdot 10^{-3} \cdot v \quad (15)$$

The linear flow velocity v depends not only on the flowrates \dot{V}_w^e and \dot{V}_w^r but also on the "slimness" S of the device:

$$S = Q/L = v * (v/\dot{V})^2 \quad (16)$$

The table below shows the effect of the slimness on the linear flow velocity, the outside membrane coefficients and the global coefficient β_{glb} defined in equation 23:

L (m)	\dot{V}_w^e (m ³ /h)	v^e (cm/s)	Re ^e	$\beta_B^e * 10^{-3}$ (cm/s)	v^r (cm/s)	Re ^r	$\beta_B^r * 10^{-3}$ (cm/s)	$\beta_{glb} * 10^{-3}$ (cm/s)
2	2	0.222	8.8	0.46	0.0222	0.88	0.046	0.457
2	16	1.777	71.1	3.73	0.1777	7.11	0.373	3.394
10	2	1.111	44.4	2.33	0.1111	4.44	0.233	2.187
10	16	8.888	355.5	18.66	0.8888	35.55	1.866	12.824

This example has been calculated for an apparatus with an total volume of 1 m³, a membrane area of 500 m² and a flow ratio of 10:1. The effect of the slimness and the linear flow velocity on the transport coefficients is quite obvious. The reynold numbers indicate, that it is very difficult to achieve turbulent flow in a flat sheet device. As the calculations imply a turbulent flow they have to be considered as best case calculations for the flat sheet membranes. This restriction does not hold for hollow-fibers as it is possible to achieve high values for the slimness inside the hollow-fiber.

First of all the individual approach has been reduced to a global approach. This is possible without restrictions for a problem with one transfer component, with equilibrium at the interface and with partition coefficients K^e and K^r independent of the concentrations. The starting equations are:

$$\dot{n} = \beta_B^e (c_w^e - c_w^{e*}) \quad (17)$$

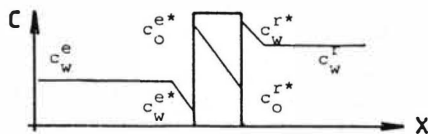
$$\dot{n} = \beta_M (c_o^{e*} - c_o^{r*}) \quad (18)$$

$$\dot{n} = \beta_B^r (c_w^{r*} - c_w^r) \quad (19)$$

$$K^e = c_o^{e*} / c_w^{e*} \quad (20)$$

$$K^r = c_w^{r*} / c_o^{r*} \quad (21)$$

The concentration gradients are illustrated in the following figure:



The global transport equation has been derived using only algebraic laws:

$$\dot{N} = \frac{d c_w^e}{d t} \frac{V}{F \varepsilon} = \beta_{glb} (c_w^e - c_w^r / (K^e K^r)) \quad (22)$$

$$1/\beta_{glb} = 1/\beta_B^e + 1/(\beta_B K^e) + 1/(\beta_B K^e K^r) \quad (23)$$

As the analytic integration will be performed over the apparatus length, equation 22 has been transformed from time to local coordinates:

$$\frac{d c_w^e}{d x} = \beta_{glb} \frac{B \varepsilon}{\dot{V}_w^e} (c_w^e(x) - c_w^r(x) / (K^e K^r)) \quad (24)$$

Equation 24 has been integrated by analytic and numeric methods for all five basic flow variants. The decisive assumption is that the transport coefficients are independent of the location inside the device. For reasons of limited space, only the final solutions are cited below.

1) Plugflow in the extraction- and the re-extraction phase, counter flow : e. g. flat sheet unit:

$$c_w^{e,l} = \frac{c_w^{e,f} \exp(-a*L) + c_w^{r,f} k / (a * K^e * K^r) * (1 - \exp(-a*L))}{1 + k / (a * K^e * K^r) * (\dot{V}_w^e / \dot{V}_w^r) * (1 - \exp(-a*L))} \quad (25)$$

$$c_w^{r,l} = c_w^{r,f} + (c_w^{e,f} - c_w^{e,l}) * (\dot{V}_w^e / \dot{V}_w^r) \quad (26)$$

$$k = \beta_{glb} * (B * n * \varepsilon) / \dot{V}_w^e \quad (27)$$

$$a = k * (1 - 1 / (K^e K^r)) * (\dot{V}_w^e / \dot{V}_w^r) \quad (28)$$

2) Plugflow in the extraction- phase and the re-extraction phase, parallel flow : e. g. flat sheet unit:

$$c_w^{e,l} = c_w^{e,f} \exp(-a*L) + (c_w^{e,f} (\dot{V}_w^e / \dot{V}_w^r) + c_w^{r,f}) * k / (a * K^e K^r) * (1 - \exp(-a*L)) \quad (29)$$

$$c_w^{r,l} = c_w^{r,f} + (c_w^{e,f} - c_w^{e,l}) * (\dot{V}_w^e / \dot{V}_w^r) \quad (30)$$

$$k = \beta_{glb} * (B * n * \varepsilon) / \dot{V}_w^e \quad (31)$$

$$a = k * (1 + 1 / (K^e K^r)) * (\dot{V}_w^e / \dot{V}_w^r) \quad (32)$$

3) Plugflow in the re-extraction phase, backmixing in the extraction phase : e. g. hollow fiber unit:

$$c_w^{r,1} = \frac{(c_w^{e,f} + c_w^{r,f} * (\dot{V}_w^r / \dot{V}_w^e)) * (k/a) * (1 - \exp(-a * L)) + c_w^{r,f} * \exp(-a * L)}{1 + (k/a) * (\dot{V}_w^r / \dot{V}_w^e) * (1 - \exp(-a * L))} \quad (33)$$

$$c_w^{e,1} = c_w^{e,f} - (c_w^{r,1} - c_w^{r,f}) * (\dot{V}_w^r / \dot{V}_w^e) \quad (34)$$

$$k = \beta_{glb} * (\pi * d_m * n * \epsilon) / \dot{V}_w^r \quad (35)$$

$$a = k / (K^e * K^r) \quad (36)$$

4) Plugflow in the extraction phase, backmixing in the re-extraction phase : e. g. hollow fiber unit :

$$c_w^{e,1} = \frac{c_w^{e,f} * \exp(-a * L) + (c_w^{e,f} * (\dot{V}_w^e / \dot{V}_w^r) + c_w^{r,f}) * k / (a * K^e * K^r) * (1 - \exp(-a * L))}{1 + k / (a * K^e * K^r) * (\dot{V}_w^e / \dot{V}_w^r) * (1 - \exp(-a * L))} \quad (37)$$

$$c_w^{r,1} = c_w^{r,f} + (c_w^{e,1} - c_w^{e,f}) * (\dot{V}_w^e / \dot{V}_w^r) \quad (38)$$

$$k = a = \beta_{glb} * (\pi * d_m * n * \epsilon) / \dot{V}_w^e \quad (39)$$

5) Backmixing in the extraction and in the re-extraction phase : e. g. stirred membrane cell:

$$c_w^{e,1} = c_w^{e,f} - [k * L * (c_w^{e,f} - c_w^{r,f} / (K^e * K^r))] / [1 + k * L * (1 + 1 / (K^e * K^r)) * (\dot{V}_w^e / \dot{V}_w^r)] \quad (40)$$

$$c_w^{r,1} = c_w^{r,f} + (c_w^{e,1} - c_w^{e,f}) * (\dot{V}_w^e / \dot{V}_w^r) \quad (41)$$

$$k = \beta_{glb} * (B * n * \epsilon) / \dot{V}_w^e \quad (42)$$

Discussion and first results

In order to get a survey of the separation performance the relevant parameters have been varied in a wide range:

\dot{V}_w^e	:	1 m ³ /h	32 m ³ /h
F	:	125 m ²	2000 m ²
β_B^e	:	0.05 * 10 ⁻³ cm/s	9.0 * 10 ⁻³ cm/s

The calculations showed, that both the ExRe-process and the LSM process have a chance. The most important barrier for a clear delimitation lies in the poorly estimated outside coefficients β_B^e and β_B^r . Therefore own experiments are being prepared, which clarify the influence of the flow conditions on outside coefficients.

Nevertheless a first result of the calculations may be told now. The strong point of the SLM process seem to lie in it's little

backmixing. This specific advantage can be used best, if an almost complete separation is necessary or if a bad extracting agent is involved. Both points are known from other separation processes and are confirmed by the calculations. In diagram I and II the phenol concentrations leaving the different devices with the extraction phase are plotted as a function of β_B^e . This has been done for the five LSM process variants and for the ExRe process. The ExRe process has been calculated with three different disperse phase flow rates. Diagram I has been calculated with the true value of $K^e (=10.5)$ and $K^r (=86.0)$. In order to simulate a bad extracting agent, diagram II has been calculated with $K^e=1.05$. Both diagrams show the effect the backmixing clearly. The separation performance of the SLM process is for $\beta_B^e > 0.001$ cm/s equal or better than the performance of the ExRe process. A comparison between the different SLM variants shows, that the influence of backmixing is important. Only the SLM variants, which do not allow backmixing in the extraction phase, are superior to the ExRe process. The variants, which allow backmixing in the extraction phase are inferior or at best equal. The limited influence of backmixing in the re-extraction phase can be explained by equation 24. As c_w^r is divided by $K^e \cdot K^r$ this concentration is not of great importance. Thus the influence of backmixing is limited too. The comparatively better performance of the SLM process with bad extracting agents shall be demonstrated by comparing diagram I and II. The following considerations below $\beta_B^e = 0.001$ cm/s. For $K^e = 10.5$ the ExRe process can compete with the SLM process if a disperse phase flow $\dot{V}_O = 40$ m³/h is applied. For $K^e = 1.05$ a disperse phase flow of $\dot{V}_O = 80$ m³/h is necessary for a separation performance equal to that of the membrane process.

List of symbols :

- B (cm) width of membrane
- c_B^e (g/cm³) conc. of phenol in dibutyl ether, extraction column
- $c_B^{e,0}$ (g/cm³) conc. of phenol in dibutyl ether, re-extraction col.
- c_W^e (g/cm³) conc. in water phase, extraction
- $c_W^{e,r}$ (g/cm³) conc. in water phase, re-extraction
- $c_{W,f}^e$ (g/cm³) conc. in feed of extraction phase
- $c_{W,f}^r$ (g/cm³) conc. in feed of reextraction phase
- $c_w^{e,l}$ (g/cm³) efflux cocentration in the extraction phase

$c_{w}^{r,1}$	(g/cm ³)	efflux concentration in the re-extraction phase
d_{d}^e	(cm)	diameter of drops in extraction column
d^r	(cm)	diameter of drops in re-extraction column
d_m	(cm)	diameter of hollow fibers
F	(cm ²)	membrane area
K^e	(-)	partition coefficient of extr. step
K^r	(-)	partition coefficient of the reextr. step
L	(cm)	length of membrane
n	(-)	number of fibers or sheets in a membrane unit
\dot{n}	(g/cm ² ,s)	specific mass flux
\dot{N}	(g/s)	mass flux
Q	(cm ²)	cross sectional area of membrane units
v	(cm/s)	linear flow velocity
V	(cm ³)	volume of an device
\dot{V}_w^e	(cm ³ /s)	feed stream of the extraction phase
\dot{V}_w^r	(cm ³ /s)	feed stream of the re-extraction phase
\dot{V}_o	(cm ³ /s)	disperse phase flow of the ExRe device
β_w	(cm/s)	indiv. coeff. in water phase
β_o	(cm/s)	indiv. coeff. in organic phase
β_o^{tot}	(cm/s)	total coeff. of extraction of ExRe device
β_r^{tot}	(cm/s)	total coeff. of re-extraction of ExRe device
β_e^e	(cm/s)	individual coeff. of extraction phase (SLM)
β_B^r	(cm/s)	individual coeff. of re-extraction phase (SLM)
β_M	(cm/s)	individual coeff. of membrane phase
β_{glb}	(cm/s)	global transp. coeff. of membrane process
ϵ	(-)	porosity of membranes

Diagram I : Efflux concentration for different devices and for variable individual transport coefficients:

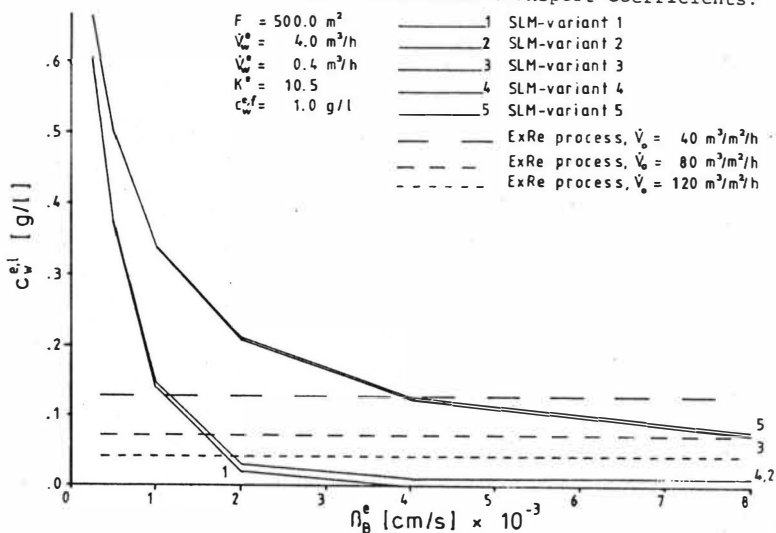
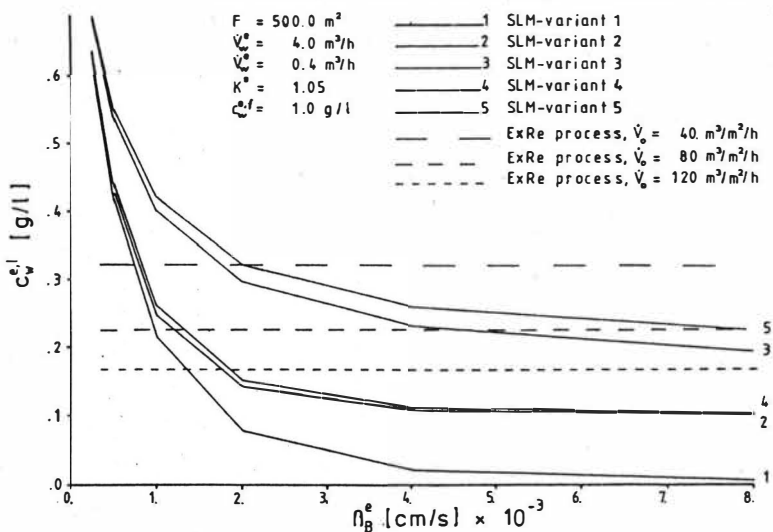


Diagram II: Efflux concentration for different devices and for variable individual transport coefficients:



Simultaneous Determination of Breakage and Coalescence
Rates in Agitated Liquid-liquid Dispersions.

M. Laso, L. Steiner, S. Hartland

Swiss Federal Institute of Technology, Zurich, Switzerland

In the last two decades, several attempts to predict the behaviour of dispersed phase agitated systems have been made, usually involving the population balance equation. This was first explicitly formulated by Curl 1963, Valentas and Amundson 1966, 1968, and Valentas et al. 1966. Being an integro-differential equation for which no analytical solution has been found, complicated numerical procedures must be used which limit its applicability. Interesting alternative approaches have been proposed: Narsimhan et al. 1980 used an alternative formulation of the population balance equation based on a 'similarity' hypothesis which seemed to be validated by experimental evidence. Other authors (Spielman and Levenspiel 1965, Zeitlin and Tavlarides 1972, Bapat et al. 1983) used Monte Carlo digital simulation techniques in an attempt to bypass the difficulties of the general population balance. These methods have been shown to be very flexible and free of numerical instability but are very time consuming.

Theoretical

The numerical solution procedures are time consuming because the drop size range is discretised using a mesh with regular spacing and because drop interactions (breakage and coalescence) have to be taken into account for all possible size combinations. This leads to a very fast growth in problem size as the number of mesh points is increased. Since the breakage and coalescence functions appearing in the drop population equation fall rapidly to zero for drop interactions off the $v=v'/2$ and $v=v'$ diagonals respectively, significant time savings can be gained by considering only high probability events. This is achieved by using a geometrical mesh in which the volume of drops in a given class is twice the volume of drops in the previous class. Coalescence is assumed to occur only between two equally sized drops and a given drop to break up into two daughter droplets of equal size. Breakage and coalescence are represented by rate

constants, K^d and K^c respectively. With these assumptions, the following number balance equations for each drop class can be written

$$\begin{aligned}
 v_T \frac{dn_1}{dt} &= I_1(t) - O_1(t, n_1, \dots, n_M) + v_T [2K_2^d n_2 - 2K_1^c n_1^2] \\
 v_T \frac{dn_2}{dt} &= I_2(t) - O_2(t, n_1, \dots, n_M) + v_T [2K_3^d n_3 - 2K_2^c n_2^2 + \\
 &\quad + K_1^c n_1^2 - K_2^d n_2] \\
 \vdots & \\
 \vdots & \\
 \vdots &
 \end{aligned}
 \tag{1}$$

$$\begin{aligned}
 v_T \frac{dn_i}{dt} &= I_i(t) - O_i(t, n_1, \dots, n_M) + v_T [2K_{i+1}^d n_{i+1} - \\
 &\quad - 2K_i^c n_i^2 + K_{i-1}^c n_{i-1}^2 - K_i^d n_i] \\
 \vdots & \\
 \vdots & \\
 \vdots & \\
 v_T \frac{dn_M}{dt} &= I_M(t) - O_M(t, n_1, \dots, n_M) + v_T [K_{M-1}^c n_{M-1}^2 - K_M^d n_M]
 \end{aligned}$$

The I_i and O_i terms correspond to source and sink terms which may appear in the general case. System (1) does not have a general analytical solution and has to be numerically integrated, which can be done in a few seconds with any standard computer subroutine for solution of ordinary differential equations. (1) has the advantage that it gives the dynamic behaviour of the dispersion as well as the steady state (asymptotic) solution. It has been shown (Laso 1986) that the solution of (1) is close to that of the full population balance equation and is obtained with a small fraction of the computational effort.

Apart from offering the possibility of simulating the dynamic behaviour of the dispersion, the present model makes it possible to determine breakage and coalescence rates from the transient behaviour of the drop size distribution. The basis of the method

has been explained by Ramkrishna 1981 and relies on the determination of the drop size distribution at several instants during the transient that follows a step change in agitation speed. Narsimhan et al. 1984 were able to determine breakage rates in this way for very lean dispersions (in which coalescence was negligible). Considering the K^C and K^D constants as unknown parameters in (1), it is possible to estimate simultaneously their values by regression. The individual breakage and coalescence rate constants can then be correlated with physical properties and operating conditions in order to obtain generalized correlations. These correlations are directly comparable with phenomenological drop interaction functions proposed by other authors (Coulaloglou and Tavlarides 1976).

Average volumetric breakage w_v^b and coalescence w_v^c frequencies are defined as:

$$w_v^b = \frac{\sum_{i=2}^M K_i^d n_i v_i}{\sum_{i=1}^M n_i v_i} \qquad w_v^c = \frac{\sum_{i=1}^{M-1} 2K_i^c n_i^2 v_i}{\sum_{i=1}^M n_i v_i}$$

It can be shown that at the steady state both are equal to the equilibrium volumetric interaction frequency which is characteristic for each system and operating conditions.

If the experimental drop size distribution during the transient is plotted as a function of time, a three dimensional surface Ω is obtained. The solution of (1), that is, the evolution of the drop concentration for each class as a function of time defines a surface Ω_F , in a way loosely related to the classical method of lines for the solution of partial differential equations (fig. 1). K^C and K^D parameters producing the optimum fit between both surfaces are taken as coalescence and breakage rate constants respectively.

Experimental

A total of 50 transient behaviour experiments were performed in a 1.1 lt standard stirred tank with a six flat-blade impeller in the hold-up range 0.01 to 0.42 and for three organic dispersed phases. Drop size was photographically determined by means of the

capillary suction method. Dispersion samples were immediately returned to the vessel after having been photographed in order to avoid altering the contents of the vessel.

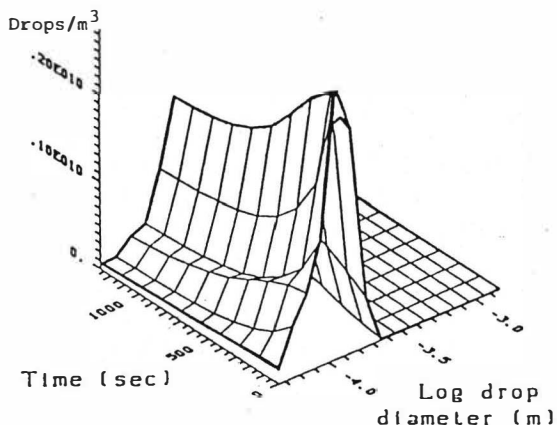


Fig. 1

Ω_F -surface (optimum fit) in the t-v-n space

The dispersion was sampled 10 times during the transient and the corresponding drop size distribution determined by manually digitising an enlarged projection of the negative. Interfacial area of the dispersion was continuously monitored by a scattered light probe consisting of a halogen light source and a photodiode immersed in the dispersion. Detailed information on the experimental procedure as well as the complete data set can be found elsewhere (Laso 1986).

The capillary suction technique was found to deliver accurate results if a minimum of 300 drops was counted for each photograph. However, two factors were encountered which were responsible for bad reproducibility of measurements of the drop size distribution. The first has been described by Verhoff et al. 1977 and is caused by the periodic formation and detachment of dispersed phase aggregates in relatively calm zones of the vessel (behind the baffles, for example). Such aggregates significantly modify the local drop size distribution and hinder an accurate determination of drop size distribution. In order to detect such periodic fluctuations in the drop size distribution,

a special technique was developed. It is based on the analysis of the output signal of a scattered light detector. Any periodic modification of the drop size distribution would affect in a periodic way the amount of light scattered by the dispersion, and this variation can be extracted from the background noise by Fourier (spectral) analysis. In fig. 2 the spectrum of the detector signal during dispersed phase aggregate formation is shown.

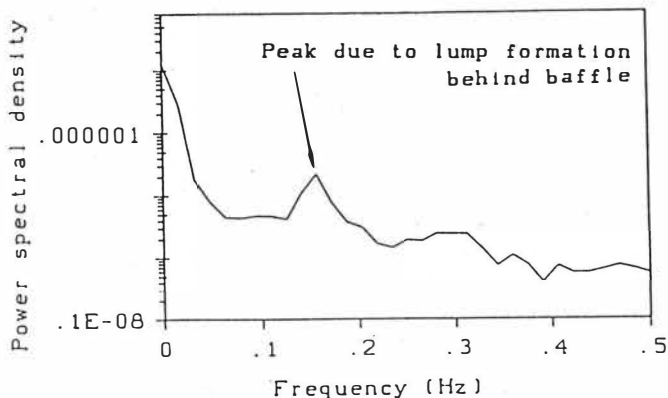


Fig. 2

Power spectrum of photodiode output signal.

Peak at 0.15 Hz corresponds to a periodic fluctuation in the drop size distribution.

The second factor is the presence of electrolytes in the aqueous phase, which render the dispersion more tractable but reduce coalescence to an unknown extent. Furthermore, the presence of even very low amounts of ionic compounds (which are often added to improve reproducibility) cause hysteresis of the drop size distribution with respect to changes in agitation speed. That is, the drop size distribution is not uniquely related to operating conditions (in particular to agitation speed). Hysteresis could be prevented by careful cleaning of the vessel and its internal parts. Experiments performed under very clean conditions and in the absence of lump detachment phenomena were found to be very reproducible. In all experimental runs checks were made for the absence of hysteresis and aggregate formation phenomena.

Breakage and coalescence functions

From the 48 experimental runs, 96 values for the average volume-surface diameter d_{32} , 48 values for the average volumetric interaction frequency and 416 values for each K^C and K^d were obtained. From these experimental data, the following correlations were derived:

Sauter diameter d_{32} :

$$\frac{d_{32}}{D} = 0.118 w_e^{-0.40} X^{0.27} \left(\frac{u_d}{u_c} \right)^{-0.056} \quad (2)$$

Average volumetric interaction frequency:

$$w_v^* = 1.0085 \cdot 10^{-4} w_e^{1.38} X^{0.63} \quad (3)$$

Breakage rate constant:

$$\frac{K^d}{N} = 4.04 \cdot 10^{-6} \left(\frac{v}{D^3} \right)^{0.91} w_e^{3.67} (1+X)^{-1.94} z^{-0.19} \quad (4)$$

Coalescence rate constant:

$$\frac{K^C}{ND^3} = 2.18 \cdot 10^{-10} \left(\frac{v}{D^3} \right)^{-0.49} w_e^{-0.51} X^{0.90} z^{-0.05} \quad (5)$$

The last two are compared with the experimental values of Narsimhan et al. 1980 for breakage, with Coualaloglou's 1976 and with Sovova's 1983 phenomenological models for breakage and coalescence in figs. 3a and 3b. The dependence of K^d on drop volume is in good agreement with Narsimhan's 1980 correlation, whereas both phenomenological models for breakage and coalescence predict a dependence on drop volume which seems to contradict experimental evidence. In particular, drop breakage was experimentally found to be strongly dependent on agitation speed.

Equations (4) and (5) were also applied in the 288-300 K temperature range and for a 5.8 lt flow vessel for which residence times varied between 15 and 23 minutes. This strongly validates the generality of (4) and (5). These correlations can be used to predict breakage and coalescence rates for droplets in agitated liquid-liquid extraction columns.

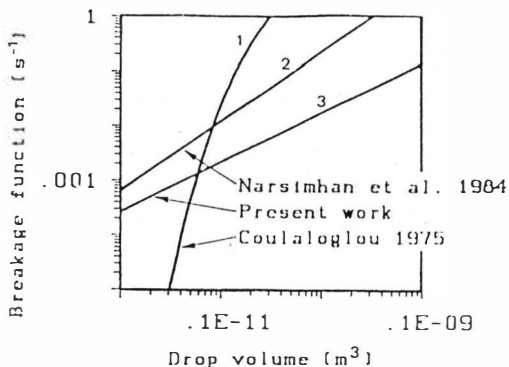


Fig. 3a

Breakage rate as a function of drop volume v .
 Comparison between two experimental correlations and
 a phenomenological model (Coulaloglou 1975).

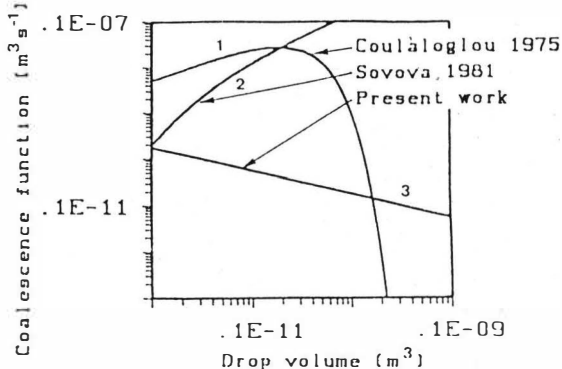


Fig. 3b

Coalescence rate as a function of drop volume.
 Comparison between present work and two phenomenological models.

Literature cited

Bapat et al.

Chem. Eng. Sci. 38, 2003 (1983)

Coulaloglou, C.A.

PhD Thesis, Illinois Institute of Technology (1975)

Coulaloglou, C.A., Tavlarides, L.

Chem. Eng. Sci. 32, 1289 (1976)

Curl,R.L.

AICHEJ 9, 175 (1963)

Laso,M.

PhD Thesis, Swiss Federal Institute of Technology,
Zurich (1986)

Narsimhan,G. Nejfelt,G., Ramkrishna,D.

AICHEJ 30, 457 (1984)

Spielman,L.A., Levenspiel,O.

Chem.Eng.Sci. 20, 247 (1965)

Valentas,K.J., Amundson,N.R.

Ind.Eng.Chem.Fund. 5, 533 (1966)

Valentas,K.J., Amundson,N.R.

ibid. 7, 66 (1968)

Valentas,K.J., Bilous,O., Amundson,N.R.

ibid. 5, 271 (1966)

Verhoff,F.H., Ross,S.L., Curl,R.L.

ibid. 16, 371 (1977)

Zeitlin,M.A., Tavlarides,L.L.

Can.J.Chem.Eng. 50, 207 (1972)

Symbols used

d_{32}	Sauter mean diameter	L
D	Impeller diameter	L
K^C	Coalescence rate constant	$L^3 T^{-1}$
K^D	Breakage rate constant	T^{-1}
I_i	Dispersed phase source intensity	T^{-1}
n	Number concentration of drops	L^{-3}
N	Agitation speed	T^{-1}
O_i	Dispersed phase sink intensity	T^{-1}
t	Time	T
v	Drop volume	L^3
V_T	Tank volume	L^3
X	Dispersed phase hold-up	
w_V	Volumetric average interaction frequency	T^{-1}
σ	Interfacial tension	MT^{-2}
μ	Viscosity	$ML^{-1}T^{-1}$
We	Weber number	$W_e = \frac{\rho N^2 D^3}{\sigma}$
Z	Ohnesorge number	$Z = \frac{u_{d1}}{\sqrt{\rho D \sigma}}$

DROP DISPERSION IN IMPELLER VORTEX SYSTEMS

M.M.C.G. Warmoeskerken, I, Bouwmans and J.M. Smith

Laboratory for Physical Technology

Delft University of Technology

Prins Bernhardlaan 6

2628 BW Delft, The Netherlands

SUMMARY

The flow field generated near flat or pitched blade impellers is dominated by trailing vortices. These are responsible for most of the drop breakup when the lighter phase of a liquid-liquid system is dispersed. In view of the large centrifugal and elongational forces associated with these vortices, the dispersion process is greatly affected by the density difference between the two liquid phases, though the importance of this effect has not generally been recognised.

When the heavier phase is dispersed, the rotation in the trailing vortices tends to remove the drops from the regions of greatest stress. Different breakup mechanisms are then relevant and the resulting drop size distribution will no longer be described by the more usually accepted correlations.

INTRODUCTION

A turbine stirred tank is frequently used for batchwise producing a liquid-liquid dispersion. In the literature many relations can be found which predict the drop size in such systems. In a review Mersmann & Grossman, (1), present 18 relations for the Sauter mean diameter, d_{32} . All these relations could be summarized by

$$d_{32} = C We^{-0.6} \quad (1)$$

in which C is a factor which depends on the system involved. Assuming isotropic turbulence in the stirred tank and a homogeneous energy dissipation, equation (1) can also be derived following the theory of Kolmogoroff, (2) and Hinze, (3).

Since the work of Van 't Riet, (4) and Biesecker, (5), it is known that the flow pattern in a stirred tank is complex. In particular the flow around the impeller is complicated by the presence of roll vortices behind the impeller blades. It is fully accepted that these vortices play a dominant role in the dispersion mechanism of gases in liquids by mechanical agitators. As a result of the density difference between gas and liquid the gas is drawn into the low pressure region within the vortices. On this basis it is surprising that the only density involved in Eq. (1) for predicting the drop size in stirred liquid-liquid dispersions is that of the continuous phase. It is to be expected that if the density difference between continuous and dispersed phases is positive the drops will be drawn into the vortex and when this difference is negative the drops will be flung out of the impeller region.

This supposition leads to the conclusion that the dispersion of lighter liquid drops will take place in the impeller region while denser drops will be broken up elsewhere. This should lead to a difference in drop size distribution not only because the energy dissipation in the impeller region is greater than in the rest of the tank but also as a result of less isotropic turbulence structure near the impeller.

THE IMPELLER FLOW FIELD

The flow pattern behind the blades of a Rushton turbine is characterised by pairs of roll vortices, described by Van 't Riet (4), Figure 1. Each blade produces two roll-vortices, one at the upper and one at the lower side. Tattersson et al. (6) found that pitched blade turbines produce a similar vortex system, though in that case there is only a single tip vortex from each blade, as shown in figure 2. In both geometries the rotation of the fluid within the vortices generates a pressure gradient and

results in a centripetal force away from the axis of the vortex. Stephenson, (7), was the first to relate the dispersion mechanism of droplets to the vortex system behind the impeller blades. Using high speed cine film he showed that the vortex is the cause of droplet break up for dispersed fluid that is swept into this zone. Konno et al., (8), also observed different break up mechanisms in a stirred tank: near the impeller and in the bulk fluid. They explained their observations in terms of non-isotropic turbulence in the impeller zone and isotropic turbulence in the rest of the tank. Chang et al. (9) also observed two different dispersion mechanisms which they called ligament stretching and turbulent fragmentation. However data relating the influence of the density differences to the vortex system are not available. Recently Eckert et al., (10), have reported some effect of ρ_d and ρ_c on the interfacial area. However they only performed measurements with $\rho_d < \rho_c$. From their data it can be concluded that the interfacial area increases with increasing values of $(\rho_c - \rho_d)$ for constant ρ_c . The authors ascribed this effect to an increase of the kinematic viscosity of the dispersed phase. Increasing values of $(\rho_c - \rho_d)$ for constant ρ_d resulted, contrary to our expectations, in a decreasing interfacial area, e.g. larger drops. Because the authors do not give experimental details as impeller speed, Reynolds Number and power input, care is needed in the interpretation of these data.

THEORY

The rotation of the fluid within the vortex is maintained by a pressure gradient which can be expressed as

$$\frac{dP}{dr} = \rho_c \frac{v_0^2}{r} \quad (2)$$

in which r represents the radius of the vortex and v_0 the tangential velocity of the fluid, fig.3.

As a result of this pressure gradient a fluid element with the dimensions dr , $r d\theta$ and dz , fig.4, within the vortex experiences a force

$$F_D = -\rho_c \frac{v_0^2}{r} V \quad (3)$$

in which V is the volume of the fluid element.

Due to the rotation of the vortex, a fluid element also experiences a centripetal force:

$$F_p = \rho_d V \frac{v_\theta^2}{r} \quad (4)$$

in which ρ_d is the density of the fluid element, or the dispersed phase. The total force acting in the r direction on the fluid element follows from Eq.(3) and Eq.(4):

$$F_{\text{tot}} = \rho_d V \frac{v_\theta^2}{r} - \rho_c V \frac{v_\theta^2}{r} \quad (5)$$

or

$$F_{\text{tot}} = \frac{v_\theta^2}{r} V (\rho_d - \rho_c) \quad (6)$$

When $\rho_d < \rho_c$ the resulting force will move the fluid element to the core of the vortex while when $\rho_d > \rho_c$ this force will move the fluid element out of the vortex. Lighter drops are therefore subjected to the large centripetal and elongational forces associated with the roll vortices and may break up as a result. On the other hand, when the dispersed phase is heavier than the continuous phase the rotation in the trailing vortices tends to remove the drops from this region of greatest stress.

NUMERICAL SIMULATION

A numerical simulation gives some insight into the behaviour of a droplet in the impeller region. In the first instance a two dimensional model in a plane perpendicular to the vortex axis has been applied. The calculations are based on a six blade Rushton turbine with a diameter of 10 cm. For calculating the velocities of the vortex the model proposed by Van 't Riet (4) has been used.

Besides the pressure and centrifugal forces given by Eq.(3) and Eq.(4), there is also a friction term which acts on the droplet in a direction opposite to the direction of the velocity difference of the continuous fluid and the droplet:

$$F_f = \frac{1}{2} \rho_c (\Delta v)^2 C_d \frac{\pi}{4} d^2 \quad (7)$$

in which Δv is the velocity difference between the fluid and the droplet.

C_d is the drag coefficient, which depends on the geometry of the droplet and the Reynolds Number. For our present purpose the droplet is assumed to behave as a rigid sphere for which C_d has been approximated by

$$C_d = 0.43 + \frac{24 \eta_c}{\rho_c \Delta v d} \quad (8)$$

With these three forces and the vortex velocity model of Van 't Riet the movement of a drop released near the vortex could be calculated. The numerical procedure of Heun has been applied here.

Figures 5 and 6 show some preliminary results of the calculations for water as the continuous phase, $\rho_c = 1000 \text{ kg/m}^3$, and an impeller rotational speed of 1 s^{-1} . Fig.5 shows the path followed by a drop of nonane, $d = 5.5 \text{ mm}$, $\rho_d = 720 \text{ kg/m}^3$, which is released near the vortex. From this figure it is clear that the drop follows the rotation of the vortex and moves towards the centre of the vortex. The total duration of the movement drawn is about 0.2 second. Figure 6 shows the movement path that would be followed by a drop of carbontetrachloride, $d = 5 \text{ mm}$, $\rho_d = 1400 \text{ kg/m}^3$, released near the vortex. In this case the duration of the movement drawn is about 0.05 second. From this figure it is clear that in this case the drop is immediately flung out of the vortex region.

Though the model used is still incomplete, these results confirm our opinion that the density difference between the continuous and the dispersed phases must play an important role in the dispersion mechanism, especially in determining the region where drops are most likely to be broken up.

We hope to show quantitatively the importance of the density difference on the characteristics of stirred liquid-liquid dispersion, including the minimal impeller speed for dispersion, phase inversion and drop diameter in our future experimental programme together with a more sophisticated three dimensional numerical model.

SYMBOLS USED

C	constant defined in Eq.(1)	(m)
C_d	drag coefficient	(-)
d	drop diameter	(m)
d_{32}	sauter mean diameter	(m)
F_c	centripetal force	(N)
F_f	force due to friction	(N)
F_p	force due to pressure	(N)
F_{tot}	total force	(N)
P	pressure	(Pa)
r	radius of the vortex	(m)
V	volume of a fluid element	(m ³)
v_{θ}	tangential velocity	(m/s)
Δv	velocity difference between the phases	(m/s)
We	Weber Number	(-)
η_c	continuous phase viscosity	(Pa s)
ρ_c	continuous phase density	(kg/m ³)
ρ_d	dispersed phase density	(kg/m ³)

LITERATURE CITED

1. Mersmann, A. and H. Grossman, *Int. Chem. Eng.*, 22, (1982), 581-590
2. Kolmogoroff, A.N., *Dok. Acad. Sci. URSS*, 30, (1941), 301
3. Hinze, J.O., *AIChE Journal*, 1, (1955), 289-295
4. Riet, K. van 't, PhD-thesis, Delft University of Technology, The Netherlands, (1985)
5. Biesecker, B.O., *VDI-Forschungsheft*, 554, (1972)
6. Tatterson, G.B., H.H.S. Yuan and R.S. Brodkey, *Chem Eng. Sci.*, 35, (1980), 1369
7. Stephenson, R., *Inst. Chem. E. Symp. Series*, 38, (1974), paper C4
8. Konno, M., M. Aiko and S. Saito, *J. Chem. Eng. Japan*, 16, (1983), 312-319
9. Chang, T.P.K., Y.H.E. Sheu, G.B. Tatterson and D.S. Dickey, *Chem. Eng. Comm.*, 10, (1981), 215-222
10. Eckert, R.E., C.M. McLaughlin and J.H. Rushton, *AIChE Journal*, (1985), 31, 1811-1821

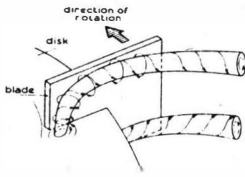


Fig.1 The roll vortices behind a blade of the Rushton turbine. After van 't Riet, (4)

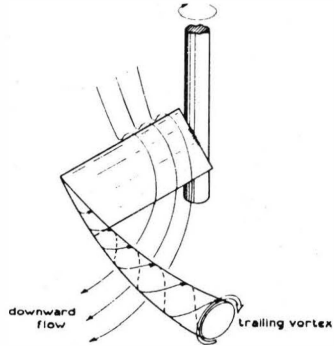


Fig.2 The roll vortex produced by a pitched blade turbine. After Tatterson et al., (6)

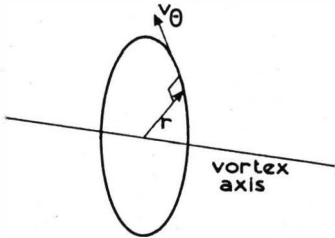


Fig.3 The coordinate system used to describe the movement of the vortex.

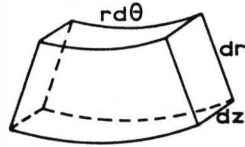


Fig.4 The fluid element within the vortex

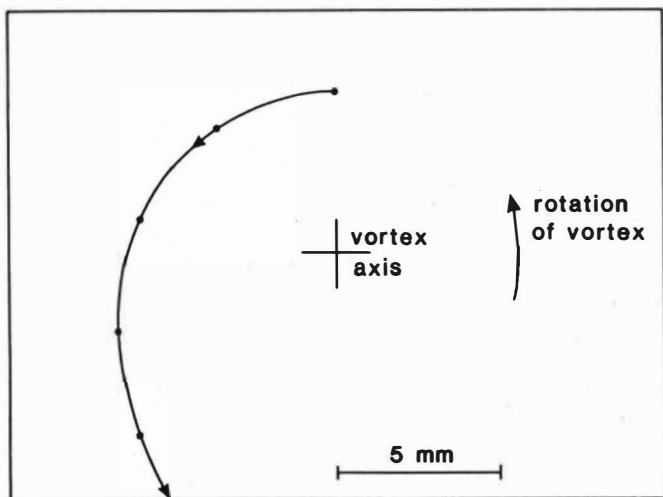


Fig.5 The calculated path followed by a drop of nonane.

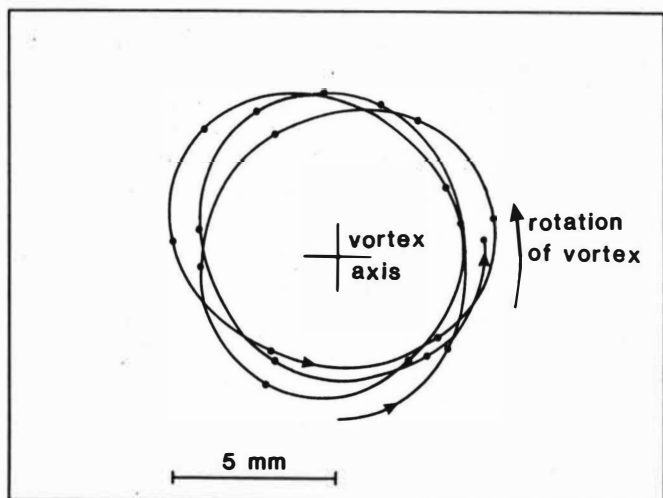


Fig.6 The calculated path followed by a drop of carbontetrachloride.

The Effect of Ionic Solutions on Holdup and Flood Point
for Pulsed Plate Columns

Leanne M. Fitzpatrick, H.R. Clive Pratt and Geoffrey W. Stevens,
University of Melbourne, Victoria, Australia.

ABSTRACT

An unexpected "salt effect" has been observed for the butyl acetate-water system in a pulsed perforated plate column. This takes the form of an increased holdup and a reduction in flood point when ionizing salts are present in low concentration, as compared with those for salt-free water. This effect is particularly marked in the transition and emulsion regions of operation, and has been observed with other polar, but not non-polar, solvents. Discrepancies in the available correlations for holdup are also noted.

INTRODUCTION

The holdup of dispersed phase and the flood point are important hydrodynamic parameters in the interpretation of the performance of liquid extraction columns, and reliable methods for their prediction are essential in design. For many contactor types the "slip velocity" equation, or simple modifications of it, has proved invaluable. In its original form this is as follows (1):

$$\frac{V_d}{\epsilon\phi} + \frac{V_c}{\epsilon(1-\phi)} = v_s = \bar{v}_0(1-\phi) \quad (1)$$

where \bar{v}_0 the "characteristic velocity", is defined as the mean velocity of the dispersed phase droplets when $V_c = 0$ and $V_d \rightarrow 0$. Differentiation of this expression, and setting $dV_c/d\phi = dV_d/d\phi = 0$ determines the flood point, so that both this and the holdup can be predicted if a reliable method of correlation of \bar{v}_0 is available.

Thornton and Logsdail (2,3) obtained flood point together with some holdup data for pulsed plate columns of 76 to 305 mm diameter and derived a correlation of \bar{v}_0 in terms of physical properties, pulsation characteristics and column geometry which appeared to fit the data well for the emulsion regime. Other workers have proposed correlations of a more empirical nature which cover in addition the mixer-settler and transition ("dispersion") regimes (4-6). However, as will be shown later, agreement between the various correlations is not always good.

In the course of work on the measurement of continuous phase backmixing for a pulsed column using the steady state tracer injection technique, premature flooding was observed with the butyl acetate-water system when an ionic tracer was added. The column was first operated with no tracer present at fairly high holdup (ca 8-18%)

and upon addition of the tracer solution at a rate of about 10% of the continuous phase flow rate, the column flooded immediately. Both a 3 wt. % potassium dichromate and a 5.5 wt. % sodium chloride tracer gave this effect. A 0.5 wt. % solution of tartrazine dye was observed not to alter the holdup significantly or to cause flooding, and was therefore used in further work on backmixing with this system.

Some further work has been done with the butyl acetate system to determine the extent of this effect, and is described below. The same effect was observed when sodium chloride tracer was used with the methyl isobutyl ketone-water system; however, it was not observed with the non-polar solvents n-heptane, kerosene and toluene.

EXPERIMENTAL

Equipment

The column comprised a 1.0 m length of 72.5 mm internal diameter precision bore glass tube together with an upper interface section and a lower section expanded to 100 mm diam., containing the solvent distributor. This was fitted with a stack of 16 x 1.575 mm thick S.S. plates drilled with 3.2 mm holes on a 6.0 mm triangular pitch, giving a free area of 23%. Pulsing was provided by a variable stroke valveless pump driven through a variable speed gearbox, mounted vertically directly below the column.

Materials

The aqueous phase consisted of deionized water, to which was added NaCl as required. Commercial grades of solvents were used, and the phases were circulated repeatedly around the column before use to ensure mutual saturation.

Procedure

Holdup was determined by the standard drainage method (7). The column was operated continuously and after five effective volume changes of the continuous phase steady state operation was assumed to have been achieved. The aqueous and solvent inlet flows and the aqueous outlet flow were then shut off simultaneously. When drainage of dispersed phase droplets was complete, the solvent layer was displaced into a measuring cylinder until the interface returned to its original position. A correction was applied for the solvent content of the interface emulsion prior to drainage. The precision of the measurements was rather low at about $\pm 10\%$; this was due to the relatively short column used.

The flood points were obtained by setting one of the flows, generally the continuous phase, and increasing the flow of the other in steps until a second interface formed and remained stationary just below the bottom plate. The precision of the measurements was about $\pm 5\%$.

Results

The holdup data for butyl acetate are summarized in Table 1. These show a marked increase in holdup and a reduction in flood point, especially in the emulsion and transition regions, with even small NaCl concentrations present. In some runs, after steady state operation had been achieved at fairly high holdup with deionized aqueous phase, change-over to a dilute NaCl solution resulted in immediate flooding, as indicated in the Table 1.

The flood point measurements are compared in Fig. 1 with the correlations of Thornton (2) and Smoot et al (8) for the emulsion regime together with the relationship $V_d + V_c = 2fA$ for the mixer settler regime. These show clearly the reduction in throughput resulting from the presence of NaCl.

DISCUSSION

The fact that the "salt effect" apparently occurs only with polar solvents suggests that it must have an electrostatic origin. Both the increased holdup and reduced flood point indicate that the droplet velocity is reduced; this could occur either by repulsion of the droplet by the plates as they pass through the holes, or by reduced coalescence (and possibly also increased breakage) of the droplets, thus reducing their size and hence their terminal velocities. The first possibility could result from repulsion of the charged polar droplets due to the zeta potential resulting from adsorption of ions by the oxide layer around the interior surface of the holes. This is probably unlikely, however, as the zeta potential is greatest for very small ionic concentrations, of the order of 10^{-3} M, and diminishes at higher concentrations.

The alternative possibility would result if ions were adsorbed around the droplet surface by the charges on the polar groups in the solvent molecules. These could result in mutual repulsion of the droplets and reduced coalescence; however, breakage of droplets on passage through the holes in the plates would still occur, so that the mean droplet size would be reduced. If this explanation were correct, a reduction in interfacial tension would be expected due to the adsorption. However, measurements of interfacial tension by the drop weight method gave no indication of this; thus, the measured values were found to be 14.4 dynes/cm for deionized water and 14.7 ± 0.4 dynes/cm for NaCl concentrations of 10^{-9} to 10^{-1} M. Some photographic evidence was obtained of a substantial reduction in Sauter mean diameter of the

droplets, but this requires further study.

In Table 2, a comparison is given of the holdup predicted by the various available correlations, together with the measured values for salt-free conditions, and with salt present; the calculated values indicate a negligible effect of salt due to changes in physical properties. These indicate substantial discrepancies for all the correlations, and it is clear that further work is required to resolve the problems for this important type of extractor.

NOMENCLATURE

- A = pulse amplitude (total excursion in the column), cm
f = pulse frequency, s^{-1}
R = phase flow ratio, (V_c/V_d)
 V_c = continuous phase velocity, $cm\ s^{-1}$
 V_d = dispersed phase velocity, $cm\ s^{-1}$
 v_s = slip velocity, $cm\ s^{-1}$
 \bar{V}_O = "characteristic velocity" of droplets, $cm\ s^{-1}$
 ϕ = fractional volumetric dispersed phase holdup
e = fractional voidage of packing.

REFERENCES

1. Gayler, R., N.W. Roberts and H.R.C. Pratt, Trans. Inst. Chem. Eng. 31, 57 (1953).
2. Thornton, J.D., Trans. Inst. Chem. Eng. 35, 316 (1957).
3. Logsdail, D.H. and J.D. Thornton, Trans. Inst. Chem. Eng. 35, 331 (1957).
4. Miyauchi, T. and H. Oya, A.I.Ch.E. Jnl. 11, 395 (1965).
5. Kumar, A. and S. Hartland, Chem. Eng. R. and D. (Trans. Inst. Chem. Eng.) 61, 248 (1983).
6. Garg, M.O. and H.R.C. Pratt, A.I.Ch.E. Jnl. 30, 432 (1984).
7. Gayler, R. and H.R.C. Pratt, Trans. Inst. Chem. Eng. 29, 110 (1951).
8. Smoot, L.D., B.W. Mar and A.L. Babb, I.E.C. 51, 1005 (1959).

Table 1: Butyl acetate and Water Dispersed Phase Holdup as a Function of Phase Flowrates and Pulsation Frequency ($A = 1.4 \text{ cm}$)

V_c cm s^{-1}	V_d cm s^{-1}	fA cm s^{-1}	% Holdup, $100 \phi^{\#}$			
			No	0.48%	0.24%	0.13%
			NaCl	NaCl	NaCl	NaCl
0.40	0.40	1.4 ^a	13.2	17.9	11.9	15.8
0.40	0.20	1.4	5.2	6.4	-	-
0.20	0.20	1.4	6.33	-	-	7.1
0.16	0.16	2.1 ^b	5.6	8.3	8.3	8.8
0.32	0.16	2.1	5.9	8.9	-	-
0.16	0.32	2.1	13.3	F	-	-
0.32	0.32	2.1	12.1	F	17.3	F
0.31	0.31	2.8 ^c	17.7	F	-	F
0.26	0.26	2.8	14.2	F	F	F
0.26	0.13	2.8	8.6	F	-	-
0.13	0.26	2.8	13.5	F	-	-
0.13	0.13	2.8	8.0	13.7	13.5	12.3

*F = flooded

a = Mixer settler Region

b = Transition (Dispersion) Region

c = Emulsion Region

Table 2: Predicted Holdup With and Without Salt Added. ($A = 1.4 \text{ cm}$)

V_c cm s^{-1}	V_d cm s^{-1}	fA	NaCl pre- sent	% Holdup, $100 \phi^{\#}$				
				Measured	Thornton ^{2,3}	M & O ⁴	K & H ⁵	Garg ⁶
				0.40	0.40	1.4	No	13.2
"	"	"	Yes	15.2	N/A	4.2	11.0	8.0
0.40	0.20	1.4	No	5.2	N/A	2.7	5.1	4.0
"	"	"	Yes	6.4	N/A	2.7	5.1	4.0
0.16	0.16	2.1	No	5.6	4.1	3.2	5.4	N/A
"	"	"	Yes	8.3	4.1	3.2	5.3	N/A
0.32	0.16	2.1	No	5.9	4.3	3.2	5.7	N/A
"	"	"	Yes	8.9	4.3	3.2	5.7	N/A
0.13	0.13	2.8	No	8.0	4.1	3.6	5.5	N/A
"	"	"	Yes	13.2	4.2	3.6	5.5	N/A

*N/A = Not Applicable

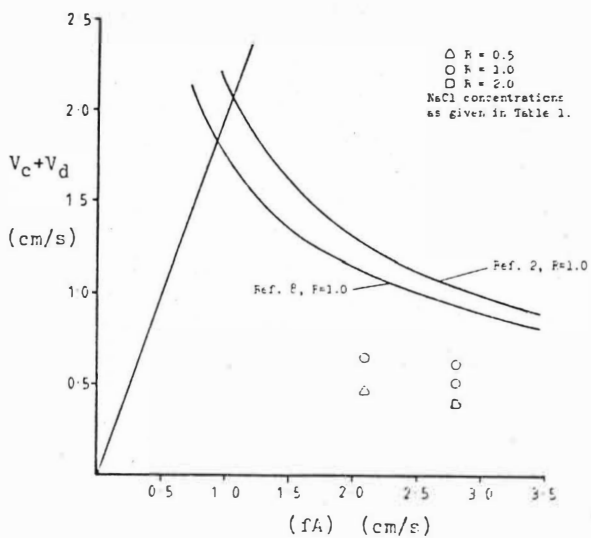


Figure 1: Comparison of floodpoint data with various correlations.

P.D. Martin and C.L. Stockwell, Harwell Laboratory, Oxon, UK

1. Introduction

A knowledge of the rate of disengagement of liquid-liquid dispersions is crucial to the efficient design of solvent extraction equipment, such as mixer-settlers or the disengaging zones of column contactors; failure properly to account for finite disengagement time can result in flooding and contamination of outlet streams. Disengagement rates of bulk dispersions have proved impossible to predict from physical property and drop size data alone, largely because the rate of drop-drop coalescence, which plays a key rôle in disengagement, is profoundly influenced by small quantities of surface-active material. The subtle effects of such adventitious minor components on interfacial viscosity and elasticity is very difficult to characterise, and when extended to large random assemblages of drops make prediction from fundamental data impossible.

An alternative approach adopted by a number of authors with varying success has been to attempt to predict the performance of an industrial continuous settler from a transient ('batch') coalescence test performed in the laboratory on a sample of the identical dispersion. The coalescence time or rate of coalescence is then used to derive parameters from which the performance of a continuous settler, expressed as the depth of dispersion as a function of the superficial coalescence velocity of the dispersed phase, can be predicted. The form of this dependence is such that an asymptote, i.e. infinite dispersion depth, is reached at a flooding point, though at lower throughputs a power-law approximation can be used; i.e. $H \propto (Q_d/A)^Y$. In predicting this dependence the theory must take account of the three separate zones of coalescence shown in Figure 1a).

The most comprehensive and systematic approach to this design problem has been given by Jeelani and Hartland⁽¹⁾. Drawing on both previous and original work, they show how the observed bulk behaviour can be derived from a fundamental consideration of interdrop and drop/interface coalescence defined by the minimum number of parameters. Jeelani and Hartland's work (and that of most previous workers, except Barnea and Mizrahi⁽²⁾) has largely concentrated on dispersions in which the constituent drops are relatively closely spaced; drops progress from a feed point to the final horizontal coalescing interface in an orderly fashion, undergoing interdrop coalescence in the process. However, as settler depth becomes greater it is the sedimenting zone which grows the more rapidly with increased throughput and which is responsible for flooding (Figure 1b)) there is therefore a need to concentrate more attention than hitherto on this zone.

For the Separation Processes Service at Harwell Laboratory, theoretical models have been derived to describe the sedimentation/coalescence zone. The parameters used to quantify the rate of coalescence are the same as those used by Hartland, but settling of growing drops under the full range of sedimenting regimes is taken into account.

2. Sedimentation with Interdrop Coalescence

In the most elementary case that could be considered, drops do not coalesce at all whilst sedimenting, but coalesce immediately with the homophase on reaching the interface. In this trivial case clearly there is no distinguishable dispersion band until the 'hindered' settling velocity of the drops is exceeded, when dilution of the incoming dispersion and rapid flooding result. However, in practice there is coalescence between the sedimenting drops whose growing size counteracts the effect of hydrodynamic drag and gives the observed smooth increase in dispersion depth with throughput. Any model which aims to predict this dependence must therefore use the well-established correlations for sedimentation as a basis from which to determine from a batch test the parameters of coalescence. The situation is complicated by the fact that as drop size increases there are changes both in the sedimentation regime (i.e. Stokes' Law \rightarrow transitional \rightarrow turbulent) and in the time taken for individual interdrop coalescence events.

3. Outline of the Method of Prediction

The procedure is as follows (Figure 2). A tall vessel is filled with a dispersion of the two liquids to be studied, and the position of the upper and lower dispersion band interfaces measured and plotted as a function of time as the dispersion collapses to give two clear phases. The movement of the sedimenting interface is of particular interest; its gradient is measured at a number of points, and from the rate of change of gradient is deduced the rate of growth of drops by coalescence. If ϕ is the drop diameter and V is the slip velocity:

$$\phi = K_2 V^2 + (K_2 V^2 + K_1 V)^{1/2}$$

where K_1 , K_2 are constants defined by Stokes' Law, and turbulent (i.e. constant friction factor), settling respectively, corrected for the 'crowding' or interference of one drop with another. From a log-log plot of diameter ϕ versus t are derived two coalescence parameters Φ and s . Φ defines the rate of growth of a drop of a specific size, while s quantifies the way in which increasing drop size increases the time taken for coalescence, viz:

$$\tau = \tau_0 \left(\frac{\phi}{\phi_0} \right)^s$$

The parameter s has been found to take values of up to $3^{(3)}$.

In order to proceed to calculate the continuous flow data it is necessary to have an appropriate model for the bed of liquid particles which make up the sedimenting zone of the dispersion. This can be thought of as a fluidised bed in which the velocity of the continuous phase is large enough to maintain a suspension of the largest drops at the observed dispersed phase hold-up (typically 0.3 to 0.5) but is smaller than the terminal velocity of the smallest drops. It is possible then to calculate the time taken for a drop to grow until it cannot be hydrodynamically supported, and to equate this to its residence time in the sedimenting zone of the dispersion band, the volume of which at the throughput in question is thereby defined. The relationship between the sedimenting zone thickness H and throughput so obtained is:

$$H = \left(\frac{Q_d}{A}\right) \frac{1}{\epsilon \Phi} \left[\frac{K_2(Q_d/A)^2}{R^2(1-\epsilon)^2} + \left(\frac{K_2^2(Q_d/A)^4}{R^4(1-\epsilon)^4} + \frac{K_1(Q_d/A)^2}{R(1-\epsilon)}\right)^{1/2} \right]^s$$

The relative magnitudes of K_1 , K_2 , Q_d/A and Φ determine the settling regime; if a variable i were defined, such that $V \propto \phi^i$ where $i = \frac{1}{2}$ (turbulent) to $i = 2$ (Stokes' Law) then apparently:

$$H = \left(\frac{Q_d}{A}\right)^{\left(\frac{s}{i} + 1\right)}$$

where the index $(s/i + 1)$ can then take the wide range of values shown in the table and covering most of the correlations observed industrially.

Table Typical Values of the Index Y

$$H \propto (Q_d/A)^Y, \quad Y = (s/i + 1)$$

$s =$	1.0	1.5	2.0	3.0	
$i = 0.5$	3	4	5	7	Turbulent
1.0	2	2.5	3	4	Transitional
2.0	1.5	1.75	2	2.5	Stokes' Law

This approach to the modelling of deep dispersion bands in settlers and columns has been shown to apply to industrial systems in which dispersion feeds the

sedimenting front and drop movement is unidirectional⁽⁴⁾. However in practice even among 'vertical' settlers (as opposed to those in which a horizontal progression is dominant) a variety of flow patterns can be found (Figure 3). A common flow regime is that shown in Figure 3c) in which the dispersion feed is made near the base of the sedimenting zone, a regime often favoured as providing the opportunity for very small haze droplets to be collected. For this situation the model described above needs refinement to allow for encounters between non-equisized drops, and work to this end is in progress.

4. Conclusion

By using sound theoretically-based models which draw carefully chosen empirical constants from batch experiments, it is now possible to predict the behaviour of deep band settlers, at least in certain limited geometries; further work will extend this. At the same time it is becoming clear that the correct selection of appropriate forms of batch disengagement test will become an increasingly important part of this research if the method is to become attractive to industrial users.

References

- 1) Jeelani, S.A.K. and Hartland, S. *AIChEJ* 31 (1985) 711.
- 2) Barnea, E. and Mizrahi, J. *Trans. I. Chem. E.* 53 (1977) 61, 70, 75, 83.
- 3) Charles, G.E. and Mason, S.G. *J. Colloid Sci.* 15 (1960) 236.
- 4) Pring, S. Industrial Experience Report, University of Bradford (1984).

Notation

A	Settler horizontal area
H	Thickness of dispersion band; approximate thickness of sedimenting zone of deep dispersion
i	Sedimentation index
K_1, K_2	Constants
Q_c	Throughput of continuous phase
Q_d	Throughput of dispersed phase
R	Phase flow ratio = Q_d/Q_c
s	Coalescence index
V	Drop-continuous phase slip velocity
Y	Dispersion thickness index

ϵ Dispersed phase hold-up
 Φ Coalescence parameter
 ϕ, ϕ_0 Drop diameter, reference
 τ, τ_0 Interdrop coalescence time, standard.

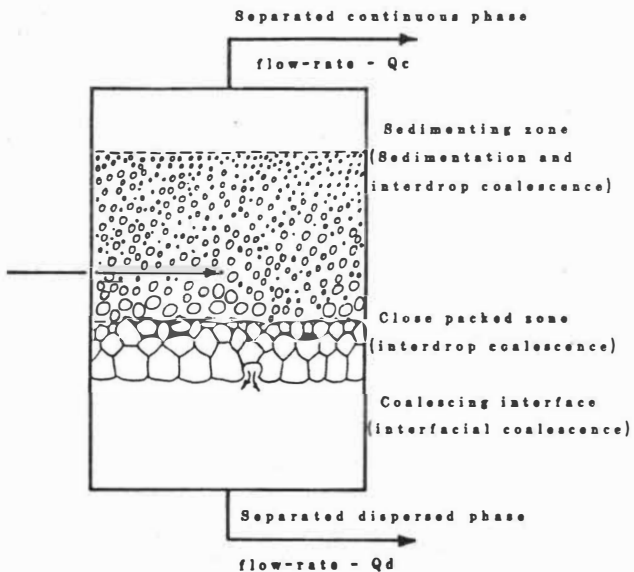


FIGURE 1a) COALESCENCE ZONES IN A DEEP BAND GRAVITY SETTLER (HEAVY PHASE DISPERSED)

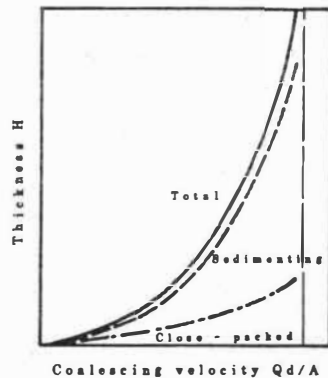
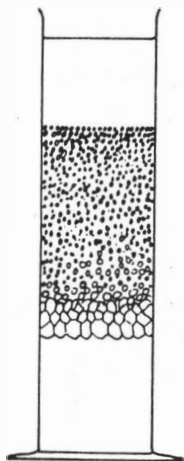
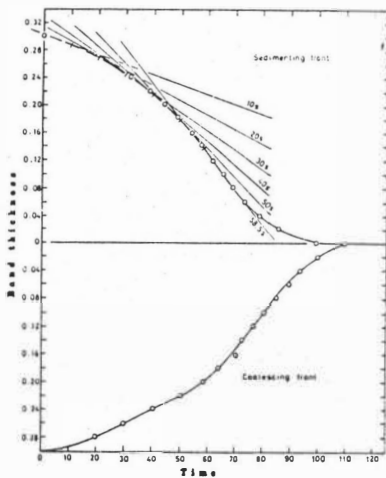


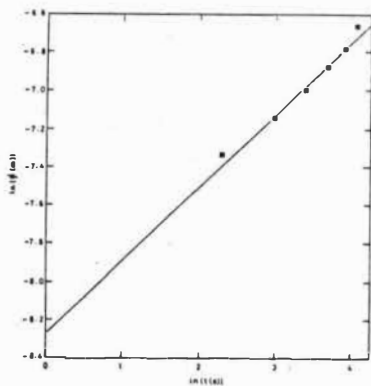
FIGURE 1 b) COMPARATIVE GROWTH OF ZONES WITH THROUGHPUT



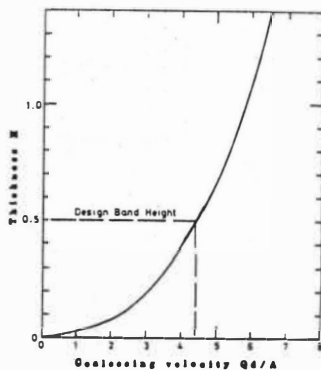
a) Batch test



b) Sedimentation Velocities



c) Derivation of coalescence parameters



d) Predicted settler performance

FIGURE 2. OUTLINE OF PREDICTIVE METHOD.

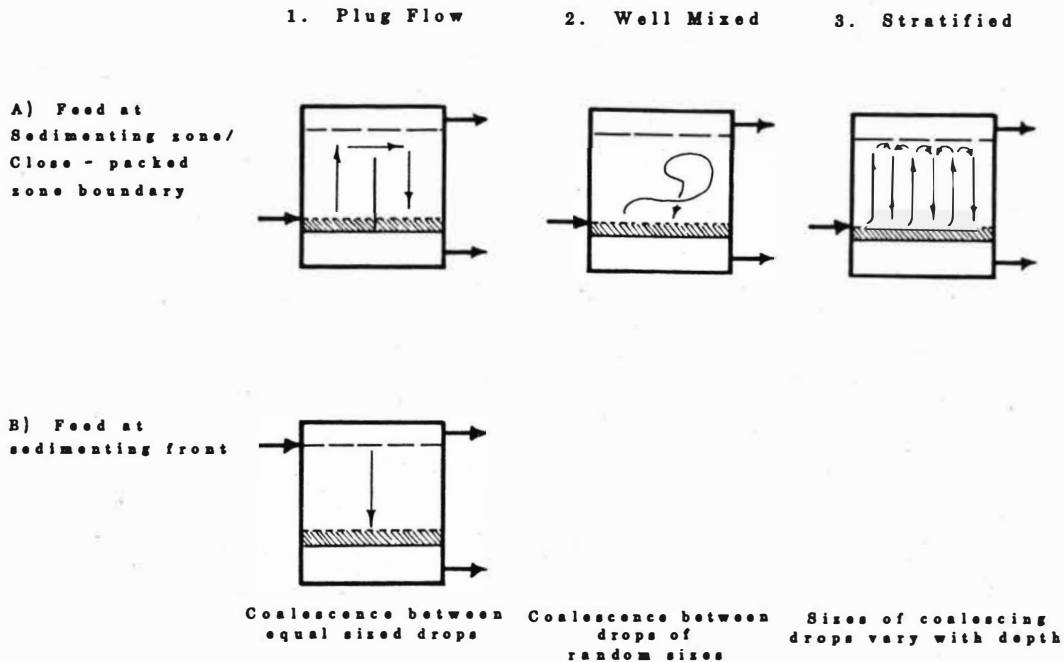


FIGURE 3. FLOW PATTERNS IN CONTINUOUS SETTLERS - NATURE OF
DROP-DROP INTERACTIONS

Hydrodynamics in Mixer-Settlers with Liquid Membranes

H.Lackner, H.-J.Bart, R.Marr, Technische Universität Graz, Austria

Liquid Membrane Permeation (LMP) has been noted as a new technique for metals recovery (1). Up to now a number of metals have been tested. Industrial implementation is in the case of zinc recovery from spinning baths (2).

A product plant is under construction now. The LMP realizes a combined extraction and stripping process. Both steps occur simultaneously. Preparation of an emulsion for LMP is done as follows. An aqueous Phase I (receiving phase) is emulsified by high speed agitation in an organic Phase II which consists of a diluent, an extractant and a surfactant to stabilize the emulsion.

Subsequent to this the emulsion is dispersed by slow stirring in an aqueous Phase III (feed phase), which contains the metal ions to be separated.

As soon as the agitation is stopped the emulsion coalesces, Phase III and emulsion separate. After that the emulsion (Phase II and I) is broken by a splitter. The organic membrane phase can be used for preparation of emulsion phase again.

During phase separation a sedimentation process in the emulsion can be observed. This is due the differences in density of Phase II and Phase I, respectively.

These phenomena occur the more the longer

- the coalescence time of the concerned phases
- the contacting time of the phases
- the residence time of the non broken emulsion in the settler is.

This adversely affect converts a homogeneous emulsion phase into a pure organic Phase II, emulsion and "heavy organic phase".

The heavy organic phase consists of compact Phase I droplets surrounded by organic phase. It's density is higher than the density of Phase III, it is not splittable and cannot be used again.

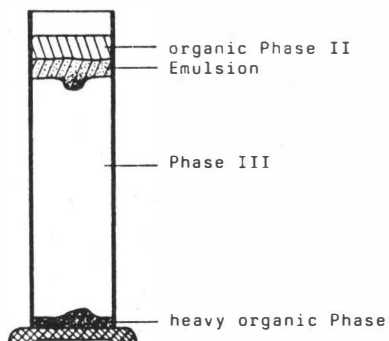


Fig. 1: Sedimentation process after coalescence

This phenomenon occurs different in different apparatus and should be exemplified in case of a column and a mixer-settler.

Column: Sedimentation processes are negligible. The coalescence of emulsion droplets moves continuously the interface between emulsion and Phase III.

Mixer-Settler: Higher residence time of the emulsion in the settler.
 No movement of the interface between emulsion and Phase III.
 Growth of a "heavy organic phase" due to sedimentation.

Because of the growth of a heavy organic phase in a conventional horizontal mixer-settler a new settler must be designed to stop these sedimentation processes.

A new design of mixer-settler

Instead of a horizontal settler, which normally is used in liquid-liquid extraction a vertical standing settler, similar to CMS was designed.

The advantages of this settler for LMP are

- short residence time of the emulsion in the settler
- continuously moved interface between the emulsion and Phase III
- hydrodynamic advantage for mass transfer
- smaller size of the plant
- the coalescence of the dispersed phase already starts in the coupling between mixer and settler

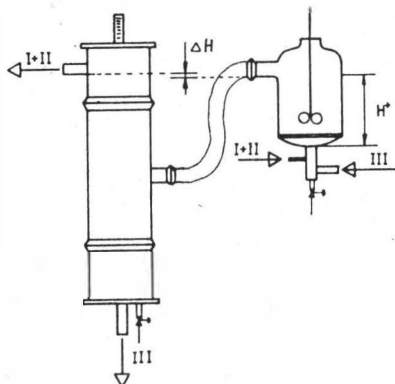


Fig. 2: Mixer-settler with horizontal standing settler

Experiments

The emulsion and the feed phase were contacted continuously into the mixer. The volume of the mixer was 1,6 (l).

The hydrodynamic and the mass transfer dependent variables (e.g. hold up) were varied by

- varying agitator speed
- varying ΔH (see fig. 2)

(this variation is done easily, because the mixer is assembled on riffle bars and all pipes are made of flexible tubes).

The height of the impeller above the bottom of the mixer was kept constant at $H'/3$.

Results

Variation of ΔH

The speed of agitation was constant at 350 rpm. By varying the height of ΔH between mixer and settler the hold up change was studied in dependence of phase ratio in the emulsion.

It can be shown, that the phase ratio has a significant effect on hydrodynamics and mass transfer because of physical parameters of the emulsion.

The viscosity of the emulsion increases with the decrease of the phase ratio Phase I: Phase II.

These differences in emulsion viscosity effect a wide change in hold-up (4 % to 22 %).

Measurements were done under steady state conditions after three hours continuously running.

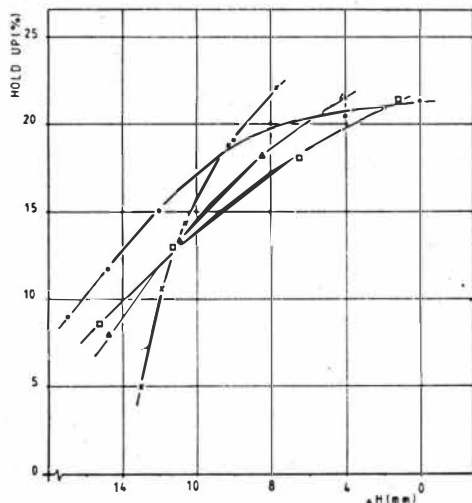


Fig. 3: Hold-up as a function of ΔH and phase ratio I:II

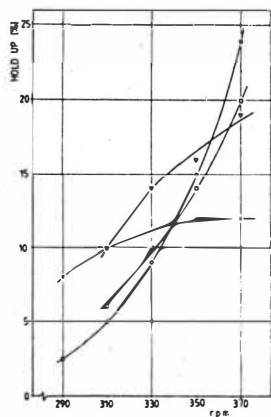
Variation of agitator speed

Studies were carried out within an impeller speed range of 290 to 370 rpm. ΔH was kept constant.

Influences of phase ratio I:II are shown in fig. 4.

Hold up increase becomes inadequate at phase ratio I:II higher than 1:5.

At this high phase ratio an emulsion layer was formed at the top of the mixer. Higher impeller speed could not disperse this emulsion layer again.



o phase ratio I:II = 1:3
 □ phase ratio I:II = 1:4
 ▽ phase ratio I:II = 1:5
 × phase ratio I:II = 1:6

Fig. 4: Hold-up as a function of agitator speed and phase ratio I:II

Operation behaviour of mixer-settlers

The steady state conditions for a continuously working two stage counter current mixer settler pilot plant for LMP were investigated. Fig. 5 shows obviously that those conditions were obtained after a periode of 9 hours.

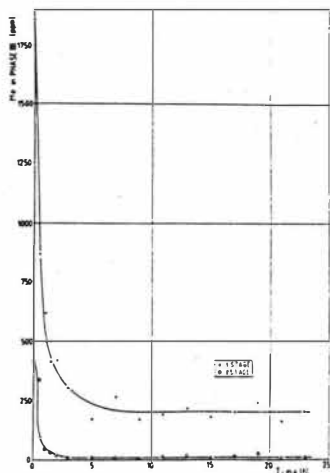


Fig. 5: Concentration in phase III vs. time

Conclusion

Mixer-settlers used for Liquid Membrane Permeation demand a new design. Because of sedimentation processes based on the differences in density between Phase I and Phase II conventional horizontal settler are not suitable and show poor efficiency. This is why a vertical standing settler was designed and constructed.

Studies were carried out for hydrodynamics in mixer. Settler characteristics will be investigated in the future.

References

- /1/ N.N.Li, US Patent 3779907
- /2/ J.Draxler, R.Marr, Chem.Eng. and Proc., in press

Behavior of Drops in a Centrifugal Field

D. B. Todd, G. R. Davies, H. A. Lange, Baker Perkins Inc., Saginaw, MI, U.S.A.

Centrifugal extractors have been employed for liquid-liquid extraction processes over the last forty years. The most common centrifugal extractor consists of a series of perforated plates housed in a rotating assembly, as shown in Figure 1. When initially introduced, the commercial extractors had limited capacity, and pilot testing could be done on the full scale model. As the size and capacity of the commercial equipment was increased, the manufacturers developed empirical scale-up rules for both capacity and efficiency. Today, pilot size centrifugal extractors (1), 180 mm internal diameter by 25₃ mm internal width, rotating at up to 10,000 rev/min, with a capacity of 0.1 m³/h, are used to define the requirements for commercial size extractors with capacities of 100 m³/h.

There has been little effort to relate scale-up criteria to fundamental principles of drop size and behavior of two liquids in countercurrent flow under centrifugal force through perforated plates. Such fluid dynamic behavior has been studied by Blass and coworkers (2,3) utilizing a similar sized extractor equipped with a transparent side. Stölting and Blass (2) studied the formation of drops at a nozzle and the trajectory of these drops through a non-flowing lighter phase. Schilp and Blass (3) studied higher centrifugal forces (to 500 G's) in a rotor without internals except for one tray with either one orifice or 10% perforation. The Sauter mean drop diameters were determined to vary with centrifugal field intensity ($R \omega^2$) as follows:

$$d_{32} = K(R \omega^2)^{-0.48} V_d^a$$

For a single hole, the dependence of the dispersed phase superficial velocity (V_d) was almost non-existent ($a = 0.03$). With the 10% perforated plate, the dependence on V_d was stronger ($a = 0.15$), possibly reflecting more interdrop coalescence.

Our studies have been done with a 400 mm I.D. rotor, 13 mm wide, with eighteen 40 mm D windows on both sides (Figure 2). We find that at higher V_d from a single orifice, a jet instability exists, as shown in Figure 3, and that the drops were smaller than we could measure. We also find that under countercurrent flow, there is evidence of vortices within the continuous phase that can be strong enough to reverse the expected spiralling inward flow of the dispersed lighter phase. This is shown in Figures 4 and 5. Maximum drop size in these figures is less than 1 mm diameter. It had been noted earlier (4,5) that liquids passing through a centrifugal extractor experience additional pressure drop in proportion to both flow rate and rotor speed. It is this turbulent energy dissipation, above and beyond that attributed to the drop across the orifices, that contributes to the further reduction in droplet size.

With perforated cylindrical trays in place, the dispersed phase jet stream from one tray may impinge against the next tray, frequently leading simultaneously to more dispersion by impact as well as to coalescence before that phase flows to the next orifice(s) for redispersion. Typical radial spacings of the cylindrical trays are only 4 to 12 mm apart, and the degree of perforation is usually less than 5%. Thus, the contribution of impingement to drop size may be a significant factor. After many years of operation, slightly differently colored polished areas have been observed on the cylindrical trays corresponding to the perforation pattern of the next outboard tray for high flow rates of dispersed light phase.

A somewhat similar phenomena occurs when the principal interface is located close to the issuing jet. This is illustrated in Figure 6, wherein the dispersed phase creates a mini-emulsion at the interface by impingement and bounce back.

We conclude that fundamental studies of the fluid dynamics of counterflowing liquids in centrifugal extractors are very beneficial towards understanding the phenomena involved. However, the as-yet intractable effects of vortex flow and impingement preclude a complete mathematical modeling of drop formation and flow. Thus, prediction of commercial performance must continue to rely on actual pilot performance as interpreted on the basis of the accumulated experience of the equipment suppliers. Nevertheless, we expect to continue our efforts to reduce the art to science.

References

- (1) Todd, D.B., GVC/AlChE Joint Meeting Preprints D4-4, Munchem, Sept. 17-20, (1974)
- (2) Stölting, M., Blass, E., Ger. Chem. Engr. 2 (1979) 14-17.
- (3) Schilp, R., Blass, E., Ger. Chem. Engr. 5 (1982) 364-368.
- (4) Todd, D.B., Chem. Engr. Prog. 42 No. 9, 119-124 (1966).
- (5) Todd, D.B., Davies, G.R., Proc. ISEC (1974) Lyon 3 2379-2398.

Nomenclature

- a - exponent of dependence of drop diameter on flow rate.
- d_{32} - Sauter mean drop diameter.
- K - constant in reference (2).
- R - Radius within centrifugal rotor.
- V_d - Superficial velocity of dispersed phase through orifice(s).
- ω - radial velocity.

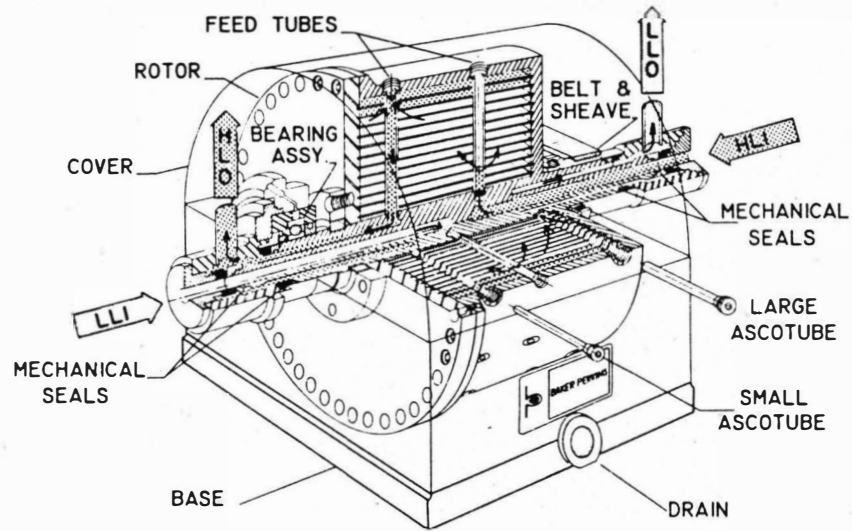


FIGURE 1: CUTAWAY OF CENTRIFUGAL EXTRACTOR

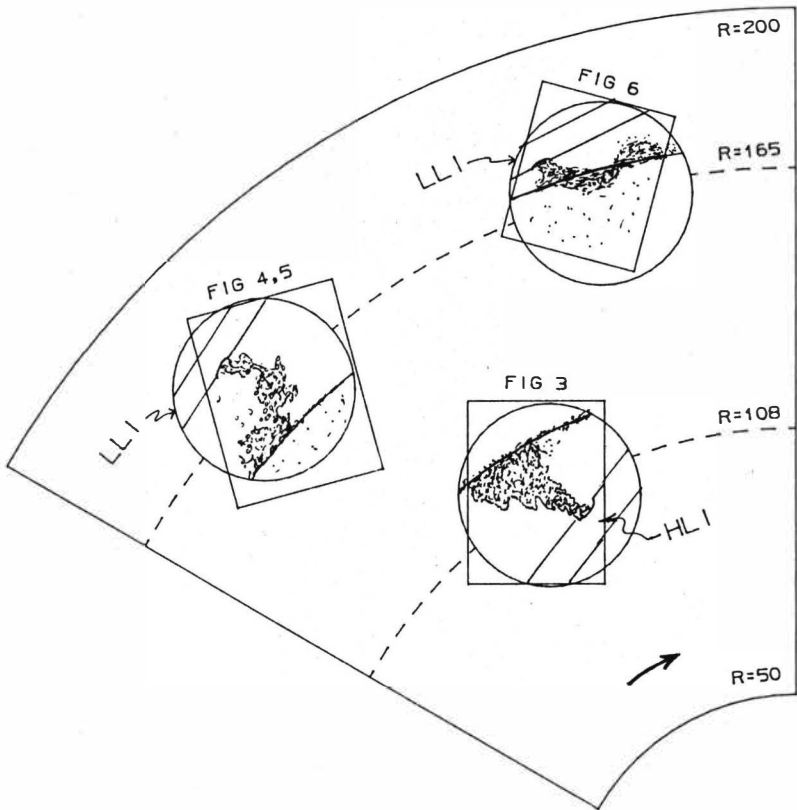


FIGURE 2: SECTION OF EXPERIMENTAL EXTRACTOR SHOWING WINDOWS AND LOCATION OF FIGURES 3-6



FIGURE 3: JET BREAKUP OF
WATER INTO KEROSENE, 1730 RPM

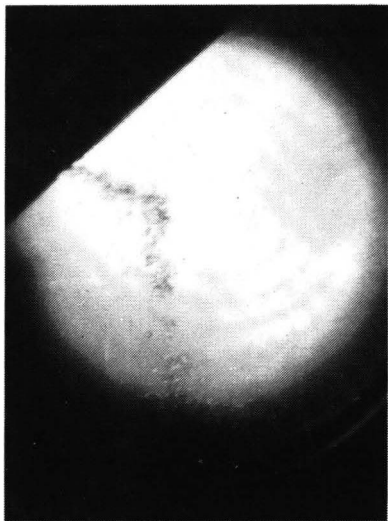


FIGURE 4: FLOW PATH REVERSAL
OF KEROSENE DISPERSED IN WATER
AT LOW KEROSENE RATE

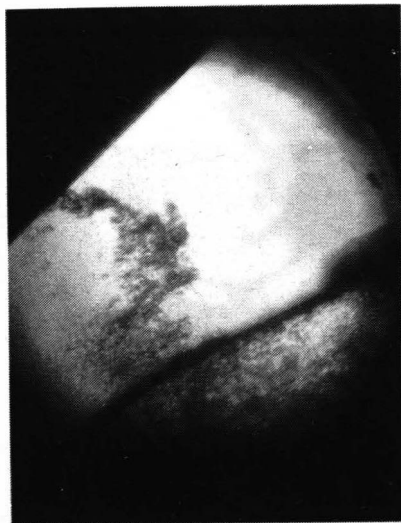


FIGURE 5: FLOW PATH REVERSAL
OF KEROSENE DISPERSED IN WATER
AT HIGHER KEROSENE RATE

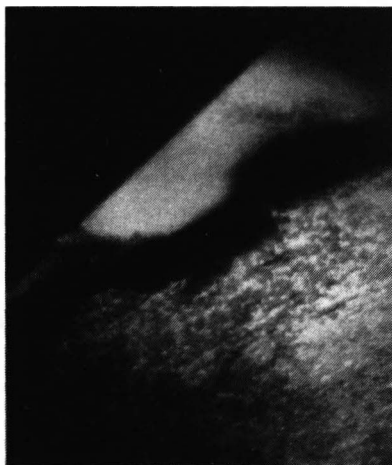


FIGURE 6: KEROSENE IMPINGEMENT
INTO PRINCIPLE INTERFACE WITH
WATER, 1640 RPM

K.EID, C. GOURDON, G. CASAMATTA, G. MURATET
Institut du Génie Chimique, U.A. 192 C.N.R.S., Chemin de la Loge
31078 TOULOUSE CEDEX/France

1. INTRODUCTION

In order to design liquid-liquid extraction columns, it is required to predict hydrodynamics of the counter-current flow, as far as it determines interfacial area, drop residence time, therefore transfer between both phases in contact. Three mechanisms are involved in the description of the behaviour of dispersed phase: transport, breakage and coalescence of drops (1). As these mechanisms depend strongly on the two-phase system and on the type of the contactor, it seems to be difficult and inappropriate to establish general laws that could pretend to being suitable for the whole systems that are under consideration in solvent extraction. It is yet well received that drop breakage and coalescence are particularly very sensitive to hydrodynamics, nature of materials, interfacial properties, mass transfer, presence of surfactants or impurities (2,3,4) ...

Therefore, it is likely more convenient to restrict pilot tests to simple experiments that will allow to study separately, as far as it is possible, the trend of a liquid-liquid system to break or coalesce under specified conditions of counter-current flow. The present paper contributes in suggesting a methodology for achieving the study of drop breakage in a pulsed sieve-plate column.

2. EXPERIMENTAL DEVICE

Our objective is to predict breakage ability of any liquid-liquid system in a pulsed column. Experiments have to be simple, repetitive, automatic, and have to consume a little of products in such a way as to reduce costs in comparison with pilot tests.

In the present study, we are interested in determining breakage of drops through a sieve-plate. The experimental device consists of (Fig. 1):

- a part of a column with a sieve-plate and the pulsator:
 - it corresponds to an actual stage of a pulsed sieve-plate pilot column;
- an injection system of calibrated drops;
- a control unit for specifying drop injection times according to the pulsation period;
- a measuring system of daughter drop sizes;
- a micro-computer APPLE II for real time data acquisition and data processing.

2.1 Description of the column stage

The column stage is out of glass, 200 mm high, and its diameter D is 50 mm. As in the present study only liquid-liquid systems, for which the continuous phase is the heavy one and the dispersed one is light, are concerned, the column is placed like it appears in Fig. 1. At the top of column are located two funnels for drop collection. At the bottom, a guide tube leads the drop up to sieve-plate compartment, that consists of two stainless steel sieve-plates free area of which is about 23% and hole diameter is 2 mm. The distance between the plates can be easily modified.

Agitation is achieved with a lateral pulsator, made out of P.T.F.E. The pulsator is driven by a motor, rotation speed of which can vary so that pulsation frequency can easily be modified. Pulsation amplitude is also variable. Hydrodynamical pressures are counter-balanced from the one and the other side of the pulsator.

Except for the permanent pulsating movement of the continuous phase inside the column, there are no inlet and outlet flowrates.

2.2 Drop calibration and injection system

The principle of drop calibration unit consists in pushing as accurately as possible the axis of a micro-syringe containing the light phase that will form a drop at the tip of a nozzle.

After the drop has been formed at the nozzle, it will be broken away by means of a little hammer that will hit the nozzle at a precise time controlled by the same unit. It is possible to synchronize with high accuracy this time with any given instant during pulsation period.

2.3 Description of the measurement system

It is required to collect drops at the top of the device and to measure the sizes, whatever happens to the calibrated mother drop, that is traveling inside the compartment.

The principle of the measuring system (Fig.2) consists of a capillary tube of 0.2 mm diameter, in which the collected drops are stretched, and of a photoelectric cell, that detects passage of drops into the capillary tube by means of a differential measurement of refractive index. This system is convenient for a large range of liquid-liquid systems that present a relative slight difference of refractive index and was often employed in past works (5,6). It is easy to select a suction flowrate into the capillary tube by means of a micro-pump, so that drop velocity is accurately determined. Therefore, the measurement of passage times in front of the photoelectric cell is a direct measurement of drop sizes. It is also possible to determine simultaneously whether the mother drop has broken or not.

2.4 Data acquisition and processing

Data acquisition and processing are achieved by means of a micro-computer APPLE II. Acquisition frequency is 4 kHz. Data are converted with an analog/digital converter into 12 bits words. Two input channels of the converter are selected :

- the first one is intended to get the signal delivered by the step-by-step motor during a mother drop formation ; this information is needed for differentiating two successive experiments ;
- the second one is intended to detect for every mother drop the number of signal peaks (that is daughter drop number) and the duration of each one (that is daughter drop size).

Data processing results in the determination of the following statistical quantities :

- breakage probability ;
- daughter drop size distribution.

During every experience, a balance test is achieved for determining whether or not the collected volume is equal (with an accuracy of 10 %) to the injected mother drop volume. Only 10 % of our experiments were rejected because this test was not guaranteed.

3. EXPERIMENTS PROCEDURES

Experiments presented in this paper are concerned with the following liquid-liquid system : Water-Decane. Physical properties are collected in the Table 1. There is no mass transfer. Operating conditions are :

- mother drop diameter d_{md}
- pulsation intensity, characterized by the product amplitude-frequency : $A.f$
- drop injection time as regards to pulsation period T
- distance between both plates : compartment height H .

Mother drop diameters range from 1.0 mm up to 2.5 mm. Pulsation intensity covers a range from 19 mm.s⁻¹ up to 48 mm.s⁻¹ that corresponds to industrial operating conditions. In most of experiments, distance between both plates is constant and equal to 50 mm, that is precisely the one of an actual stage in one of our laboratory pilot column.

During our experiments two particular breakage mechanisms are exhibited :

- drop is breaking after one or more crossings through the sieve-plate ;
- drop is breaking without crossing through the sieve-plate ; this one is observed as the drop is located under the plate at the precise time when the pulsated flow is starting to go in the opposite direction ; at this time, shear stresses are rather so strong that drop is stretched until it breaks.

4. BREAKAGE PROBABILITY

4.1 Breakage probability according to agitation intensity

Breakage probability is defined as the ratio of the number of drops that are breaking over the total number of mother drops, that are injected. Agitation intensity is characterised by the product amplitude-frequency of pulsation. Results are presented in the Fig.3, where breakage probability Pr is plotted versus A.f. For three mother drop sizes (1.0 mm; 1.5 mm; 2.0 mm) breakage probability is increased with A.f. The larger drop size (2.5 mm) leads to breakage probability that is nearly constant and very high (83 % around) in the A.f range from 25 up to 40 mm.s⁻¹. As A.f reaches 45 mm.s⁻¹, breakage probability tends to unity for the whole drops.

In conclusion :

- as concerns drops larger than plate hole diameter, breakage probability is ever high even in the case of low A.f ; the evolution is not very sensitive to pulsation intensity ;
- as concerns drops smaller than plate hole diameter, breakage probability is highly sensitive to pulsation conditions and our results are compatible with the notion of maximum stable drop diameter (7,8,9), below which breakage probability is near zero ;
- under high agitation conditions, breakage probability tends to unity for the whole investigated drop sizes.

4.2 Breakage probability according to cross velocity

From experiments, we have noticed that breakage probability did not only depend on the pulsation intensity, but also on the distance X between the nozzle and the perforated plate. This result has put into evidence that breakage had to be expressed in terms of cross velocity, i.e. the velocity of the drop as it is crossing the plate Vd, or in a slightly different manner the continuous phase pulsated velocity Vc.

In order to estimate cross velocity, we have derived a simple kinematic relationship giving the instantaneous drop velocity Vd inside the compartment :

$$V_d = V_c + V_r \quad (1)$$

Vr is the relative velocity of a single drop in stagnant fluid. Vr was measured for different drop diameters and we have checked that Vignes' law used to fit our data with good agreement :

$$V_r = 1/4.2 (g \cdot \Delta e / e_c)^{2/3} \cdot (e_c / \mu_c)^{1/3} \cdot (1 - E_0/6) \cdot d \quad (2)$$

Eo means Eötvös number and is : $g \Delta e d^2 / \sigma$

Vc is the instantaneous pulsated flow velocity, expressed by :

$$V_c = \pi A f \cos (2 \pi f t - \pi/2) \quad (3)$$

It is then assumed that a drop is subject to a rectilinear oscillating movement where instantaneous displacement x(t) is expressed by :

$$x(t) = V_r t + A/2 \sin(2 \pi f t - \pi/2) + \Lambda/2 \quad (4)$$

Time t at which drop is crossing the plate is deduced from relationship (4) where x is the equal to the distance X between inlet guide tube level and sieve-plate level. Therefore, as V_r and X are fixed, it is possible to estimate easily V_c from equations (3) and (4). On Fig. 4, we have plotted the experimental breakage probability versus V_c . Difference of behaviour among the drops, diameter of which is larger than a plate hole (2.0 mm) and the ones smaller than 2.0 mm, is clearly exhibited on Fig. 5. Drops of 2.0 mm diameter include likely an intermediate behaviour.

5. DAUGHTER DROP DISTRIBUTION

On Fig. 5, we have plotted number probability P_n versus normalized diameter d/d_{md} .

Let us simply notice that, as pulsation intensity is increased, distributions are shifted from a left (negative) asymmetry to a right one (positive), for breakage provides more and more smaller drops at increasing cross velocity. The evolution according to intensity pulsation is related to the change of daughter drops number N_{dd} . The larger the mother drops are, the greater the number of daughter drops is. For instance, 1.5 mm mother drop breakage provides between 2 and 3 drops; for the other mother drops, daughter drops number is increasing rapidly up to 6 and more.

After investigating the first distribution moments, it is demonstrated that:

- at lower cross velocities, there is a little of daughter drops and mean diameter is near the one of mother drop: for instance, $d_{10} = 0.6$ up to $0.8 d_{md}$;
- at intermediate cross velocities, daughter drops number is increased, mean diameter is decreased and population is rather uniformly polydispersed;
- at higher cross velocities, daughter drops number is strongly increasing, but population is less polydispersed as far as population mean diameter is strongly decreasing: for instance, $d_{10} = 0.4 d_{md}$.

Whatever the mother drop size may be, population tends to the same mean diameter as cross velocity is increasing. This is emulsion regime of liquid-liquid extraction columns at high pulsation intensity for which dispersed phase can be characterized by a stable diameter.

NOTATION

A	pulsation amplitude, m
d	drop diameter, m
D	column diameter, m
d_{10}	mean diameter, m
f	pulsation frequency, s ⁻¹
g	gravitational acceleration, m.s ⁻²
H	stage height, m
N	number
Pr	breakage probability
$P(X_i)$	probability function of variable X_i
t	time, s
T	pulsation period, s
Vd	instantaneous drop velocity, m.s ⁻¹
Vc	instantaneous pulsation velocity, m.s ⁻¹
Vr	single drop relative velocity, m.s ⁻¹
x	drop axial position, m
X	distance between nozzle and sieved plate

Greek symbols

ρ	liquid density, Kg.m ⁻³
$\Delta\rho$	liquid-liquid density difference, Kg.m ⁻³
ν	kinematic viscosity, m ² .s ⁻¹
σ	interfacial tension, Nm ⁻¹

Subscripts

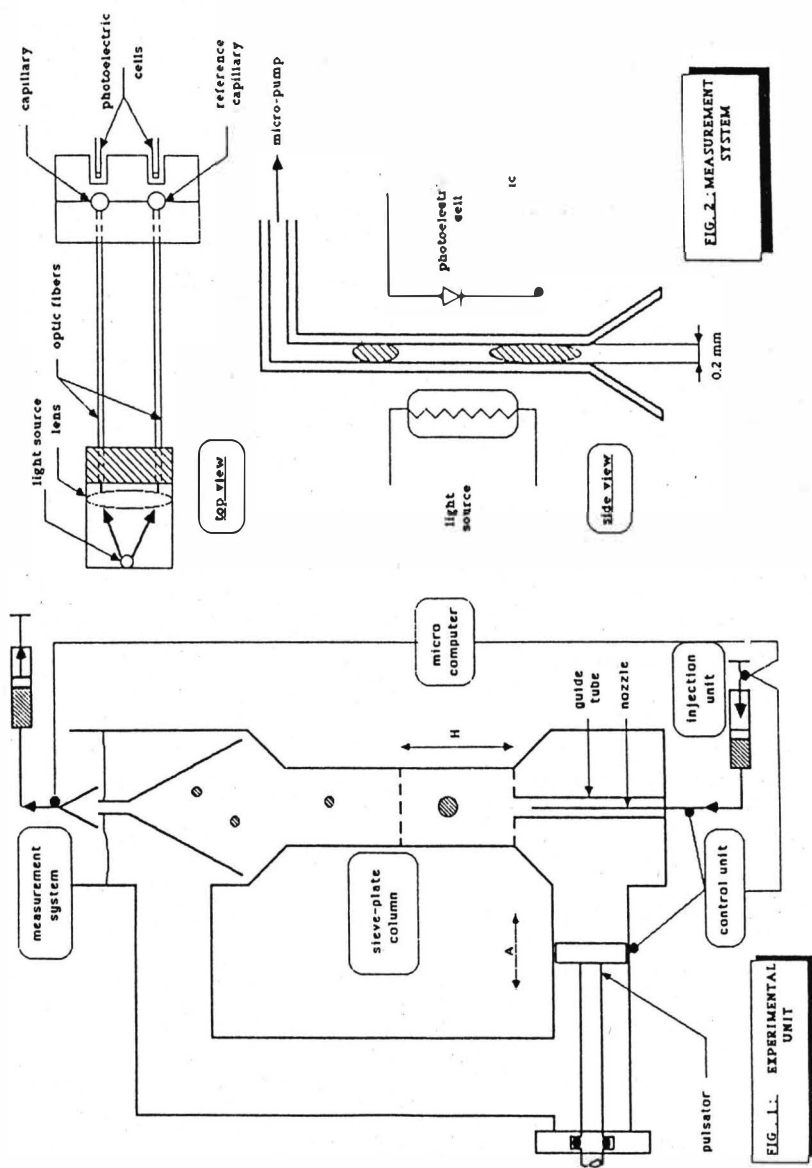
- c continuous phase
- d dispersed phase
- dd daughter drop
- md mother drop
- n relative to a number property

REFERENCES

- (1) CASAMATTA G., VOGELPOHL A., Ger.Chem.Eng.,8(2),96, 1985
- (2) ZUIDERWEG F.J., GROOTHUIS H., Chem.Eng.Sci.,12,288, 1960
- (3) JEFFREYS G.V., DAVIES G.A., "Recent Advances in Liquid-Liquid Extraction", (HANSON ed.), 1971
- (4) TAVLARIDES L.L., COULALOGLOU C.A., ZEITLIN M.A., KLINZING G.E., GAL-OR B., Ind.Eng.Chem.,62,6, 1970
- (5) WIJFFELS J.B., RIETEMA K., Proc. ISEC,1, 1971
- (6) ROSS S.L., VERHOFF F.H., CURL R.L., Ind.Eng.Chem.Fund., 16,771, 1977
- (7) HINZE J.O., AICHE J., 1(3), 289, 1955
- (8) SHINNAR R., CHURCH J.M., Ind.Eng.Chem.Fund., 52,253, 1960
- (9) MOLAG M., JOOSTEN G.E.M., DRINKENBURG A.A.H., Ind.Eng.Chem.Fund.,19,275, 1980.

	WATER	DECANE
Volumic weight kg m^{-3}	1000	730
Interfacial tension 10^{-3} N m^{-1}	49	
Solubility (H₂O)	-	0
Refractive index	1.3325	1.4130

TABLE 1 Chemical and physical properties of
Water-Decane system (at T= 18° C)



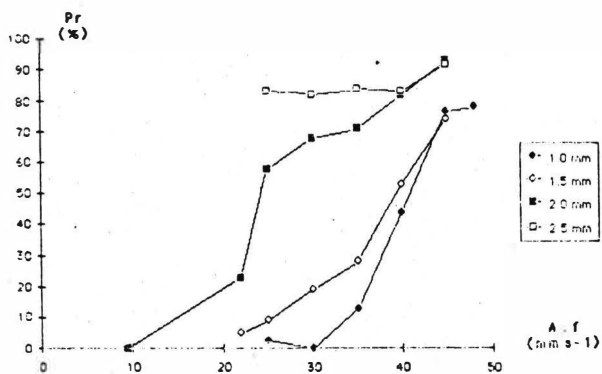


FIG 3 BREAKAGE PROBABILITY VERSUS PULSATION INTENSITY

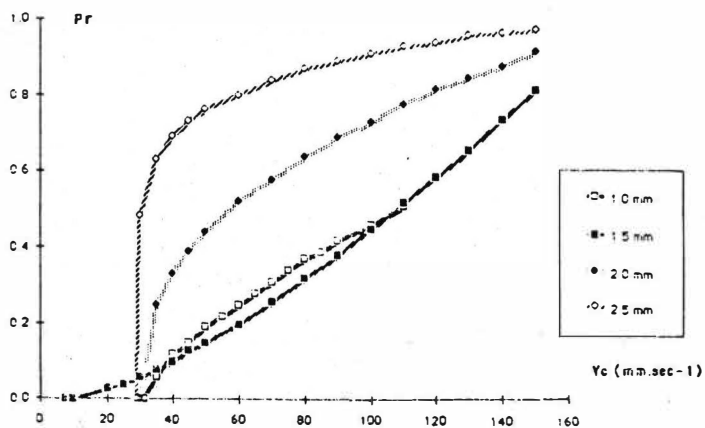
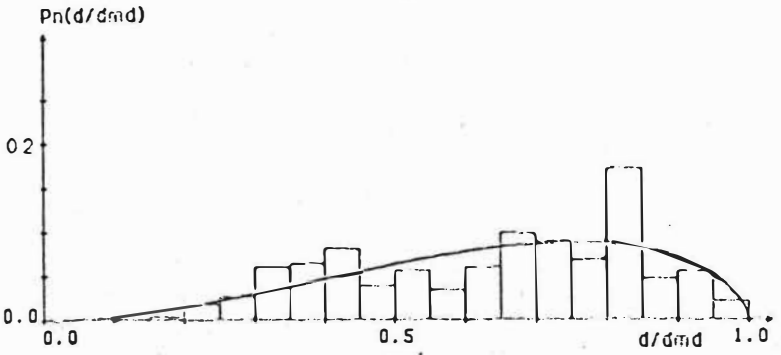


FIG 4 BREAKAGE PROBABILITY VERSUS PULSATION VELOCITY

A.f = 25 mm.s⁻¹ Pr = 0.584
 $\bar{d}_{md} = 1.990$ mm



A.f = 45 mm.s⁻¹ Pr = 0.936
 $\bar{d}_{md} = 1.945$ mm

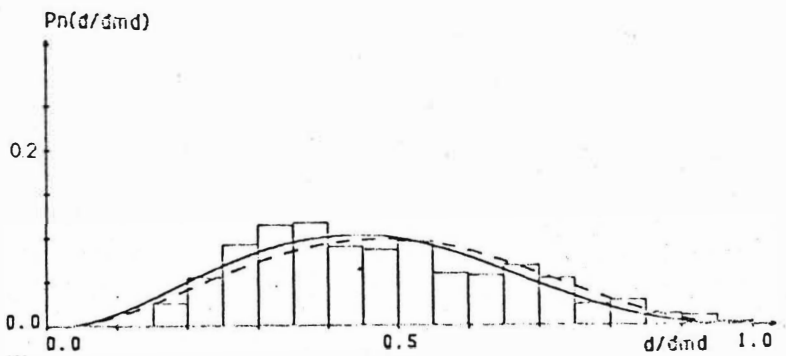


FIG. 5 : DAUGHTER DROP NUMBER DISTRIBUTIONS FROM 2.0 mm MOTHER DROP BREAKAGE

Derivation of coalescence model by simulation and experimental study of liquid-liquid fluidized beds

C. GOURDON, G. MURATET*, G. CASAMATTA
ENSIGC, U.A. 192 CNRS., Chemin de la Loge
31078 TOULOUSE CEDEX/France
* Univ. PARIS VI, Paris/France

1. INTRODUCTION :

Design and working of industrial liquid-liquid extraction columns are linked to the behaviour of dispersed phase, for it determines interfacial area, therefore efficiency in terms of total throughput and mass transfer. In the last years, many results were consistent with the fact according as it is important to take into account hold-up gradients and drop size distributions all along a column ; much work has been yet devoted to the description of drop population characteristics.

Casamatta (1) has recently proposed a drop population balance model in which the three basic mechanisms affecting dispersed phase are described : transport, breakage, coalescence. In order to predict industrial working conditions, it is required to define laws that are representative of the former mechanisms for any kind of liquid-liquid system under any kind of agitation type. Even though it is possible to study separately breakage of a single drop (2), it seems difficult to follow the same approach for the study about drop coalescence, because both mechanisms are ever coupled in a column.

In this paper, we present an experimental way to determine the ability to coalesce of a given system under specified hydrodynamical conditions. The principle consists in the formation of a liquid-liquid fluidized bed. Besides such a study may be applied to the description of flooding conditions for which a dense swarm appears between drop distributor and continuous phase outlet.

2. EXPERIMENTAL DEVICE (Fig.1) :

The liquid-liquid fluidized bed is maintained inside a part of 50 mm diameter column, downstream a perforated plate. This one is out of stainless steel with 23% free area and 2 mm hole diameter. The column is 340 mm high (height quoted later H_0). Aqueous phase inlet is at the top, organic dispersed phase inlet is located at the bottom. Droplet slip velocity is counterbalanced by the continuous flow rate. Because of rather high aqueous flowrates and because of lack of mechanical agitation, drops can not pass through the perforated plate. As drop velocity is obviously related to drop size, larger drops tend to raise and stay at the top of the bed up to reach the sieve-plate, while the smaller ones are located at the bottom.

By means of a drop injection system, that was developed in earlier work (2), it is possible to calibrate very accurately drops that are coloured and used as tracers inside the droplet bed.

In the present work, the liquid-liquid system is the following one : water-hexane. By adding up glycerol into water (27% in volume around) and by influence of temperature it is easy to match refractive index of both phases ; by this way, it is possible to make the bed completely transparent and therefore to follow by means of video technique the events to which the coloured drop is subject : coalescence, trajectory fluctuations, eventually breakage just below the sieve-plate where shear stresses are rather strong. Physical properties of the involved system are collected in the Table 1.

3. EXPERIMENTAL PROCEDURE :

Operating conditions are the following ones :

- continuous flowrates in the range of 200 l/h (10.2 l/h.cm²) up to 400 l/h (20.4 l/h.cm²),
- dispersed phase volume injected, comprised between 50 cm³ and 200 cm³ (corresponding to total hold-ups included between 10% and 40%)
- calibrated coloured drop diameters from 2 up to 3.5 mm.

A change in aqueous flowrate acts directly on droplet bed expansion and on local hold-ups, therefore on drop size and turbulence intensity.

A change in dispersed phase volume acts on total hold-up and obviously on drop size and turbulent flow.

For steady-state hydrodynamics and dispersed phase volume conditions the more probable levels of a given coloured drop are detected into the droplet bed. By this way from axial positions of drops of different diameters, it is possible to deduce drop size segregation all along the column. The total height of droplet bed is also measured.

Besides, it is possible simultaneously to record whether coalescence has occurred or not because it brings about a change in initial coloured drop size, therefore in former drop stabilization level. We define the coalescence time as being the time that a drop spends into the bed until it is coalescing. We have determined mean coalescence times for varying conditions.

4. EXPERIMENTAL RESULT :

4.1 Drop size segregation

On Fig.2, we have plotted the extreme values of residence levels covered by drops of different diameters. These levels are relative to column height and are comprised between the sieve-plate (level 0) and the injection level (at a distance of 260 mm from the sieve-plate).

At a lower continuous flowrate (10.2 l/h.cm^2), droplet bed is relatively dense, concentrated just under the sieve-plate (Fig.2A). For more important total hold-ups, droplet bed height is increased and drop size segregation is well emphasized, smaller drops being strictly located at the bottom. At a higher continuous flowrate (15.3 l/h.cm^2), droplet bed expansion is more pronounced along the column and drop size distributions are clearly exhibited as total hold-up reaches 30% (Fig.2B). Obviously, there is an upper limit above which the whole dispersed phase may be swept along by the continuous phase.

4.2 Drop bed height

For varied values of operating parameters, we have measured droplet bed heights H , that are presented in the Fig.3. For a fixed dispersed phase volume, this height depends strongly on continuous flowrate and on breakage and coalescence rates. Let us simply notice that if flowrate is increased (10.2 l/h.cm^2), bed increase is nonlinear according to dispersed phase volumes. Breakage influence being assumed constant in this case, this observation means that coalescence effects are implied.

4.3 Mean coalescence times

We have measured the mean coalescence times T for varied drop sizes, dispersed phase volumes and continuous flowrates. The results are collected in the Table 2. For the whole sizes that are under investigation, coalescence times decrease either with higher total hold-up or with higher flowrate, i.e. at higher turbulent intensity. Coalescence is naturally enhanced because in both cases drop collision probability is increased.

During the whole experiments, coalescence events have been mostly observed when drops were stabilized at levels relative to its proper sizes. Mean values of these coalescence levels corresponding to each case are also mentioned in Table 2. These values are needed for interpreting results according to turbulent intensity gradients along the column.

4.4 Hydrodynamics

It seems convenient to investigate the previous results in terms of hydrodynamical conditions, particularly turbulent intensity. A first step of this study consists in measuring at different levels of the column mean and turbulent flow velocities by means of Laser Doppler Anemometry.

We have noticed that downstream a perforated plate, turbulent regime is rather homogeneous and isotropic, nearly similar to grid turbulence conditions. On Fig.4, axial turbulent intensity is plotted versus distance to the sieve-plate for different flowrates in the range of fluidized bed conditions.

Beyond a turbulent production region below the plate, turbulent intensity decreases rapidly and its order of magnitude is about 10% in the lower region of the column.

The larger the drops are, the higher they go up and the more turbulent motions they are submitted to. As regards coalescence times that decrease with drop size, it is suggested that coalescence frequency is enhanced by turbulence as much as vortices are large enough relative to drops for being able to carry on the drops. On the other hand, at the top below the plate, drops are expected to break, for turbulent vortices are small in comparison with drop sizes (around equal to hole diameter) and contain relative high associated energy.

5. FLUIDIZED BED SIMULATION :

We have adapted the drop population model that was earlier developed in our laboratory (1) for simulating the fluidized bed under the varied previous conditions.

5.1 Model description

The column is considered as a series of N stages. In accordance with our experiments, breakage is assumed to be only active just below the plate ; coalescence is brought into effect everywhere else.

The model is relying on a population balance : drop classes are defined according to drop sizes and at each stage, inputs and outputs into and out of a given drop class are investigated, either due to drop transport up from the lower stage or back from the upper one, or due to loss or formation by breakage and coalescence. For transport terms, the dispersion-plug flow is applied to the continuous phase flow. Drop motion is traduced by a slip velocity that was subject to many earlier works (3), (4), (5).

For breakage law, we have referred to earlier works about drop breakage in pulsed sieve-plate columns (2), (3). Two parameters are determined :

- breakage rate
- daughter drop size distribution

For coalescence mechanism, we have noticed that coalescence into the fluidized bed is due to random collisions according to flow conditions.

5.2 Coalescence law

The former consideration advised us to propose a simple relationship between coalescence frequency of a given drop and hydrodynamics characterized by turbulent intensity.

Let ω be the coalescence frequency of one drop diameter d with any drop diameter d' ; in an elementary stage volume V_0 , ω can be expressed by :

$$\omega = \lambda \pi (d+d')^2 u' N(d') / V_0 \quad (1)$$

$N(d')$ is the number of drops diameter d' present in the volume V_0 , deduced simply from the mean hold-up H by :

$$N(d') = V_0 H / V(d') \quad (2)$$

μ' indicates the relative drop collision velocity and is assumed to be equal to mean turbulent velocity (R.M.S. value) at the respective drop residence level. At this one, it is assumed that the drop diameter d may only collide with drops of same size. Under these assumptions, (1) can be simplified and the comparison of $1/\omega$ with coalescence time T (Table 2) allows to adjust the coefficient λ that is similar to a collision efficiency factor in equ. (1)

As example, a simulation result is demonstrated in Fig.5. Hold-ups and drop population mean diameters are plotted versus distance from the sieve-plate.

NOTATION

d, d'	drop diameter, m
d_{32}	Sauter mean diameter, m
H	Column level (distance to the sieve-plate), m
H_0	Column height, m
I_t	axial turbulent intensity
$N(d)$	number of drops diameter d
Q	continuous phase flowrate, ($l/h.cm^2$)
T	coalescence time, s

u' turbulent velocity, $m.s^{-1}$
 V_0 stage volume, m^3
 $V(d)$ drop volume, m^3

Greek symbols

ϕ dispersed phase hold-up
 λ coalescence efficiency coefficient (Eq. (1))
 ω coalescence frequency, s^{-1} (Eq. (1))

REFERENCES

- (1) CASAMATTA G., VOGELPOHL A., Ger. Chem.Eng., 8(2), 96, 1985
- (2) EID K., GOURDON C., CASAMATTA G., MURATET G., ISEC'86, MÜNCHEN
- (3) VIGNES A., Gen.Chim., 93(5), 1969
- (4) PAKDEE - PATRAKORN S., Doc.Eng.Thesis, TOULOUSE, 1980
- (5) PERRUT M., Doctor of Sciences Thesis NANCY, 1972

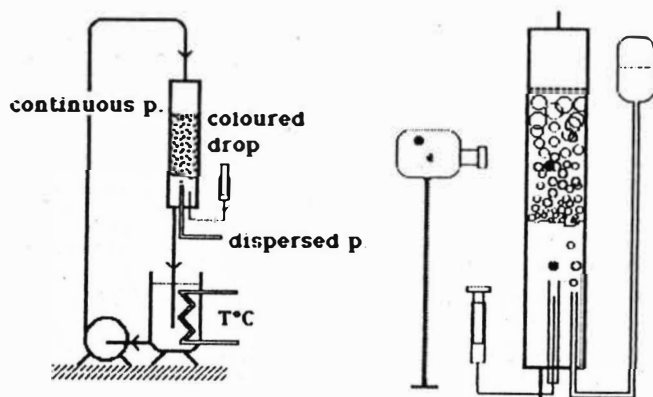


Fig. 1 : DESCRIPTION OF INSTALLATION

TOP (SIEVE-PLATE)

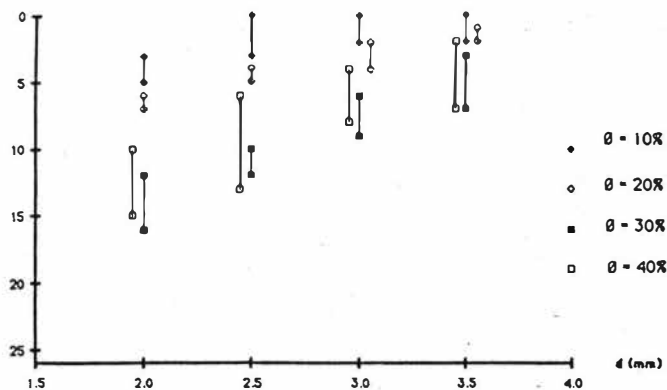


FIG. 2A : DROP SIZE SEGREGATION ($Q = 10.2 \text{ l/h.cm}^2$)

TOP (SIEVE-PLATE)

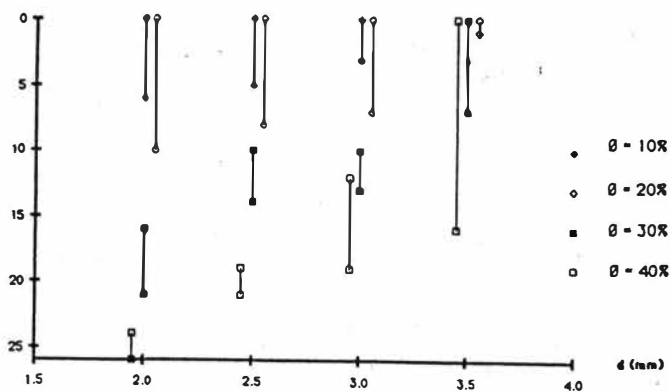


FIG. 2B : DROP SIZE SEGREGATION ($Q = 15.3 \text{ l/h.cm}^2$)

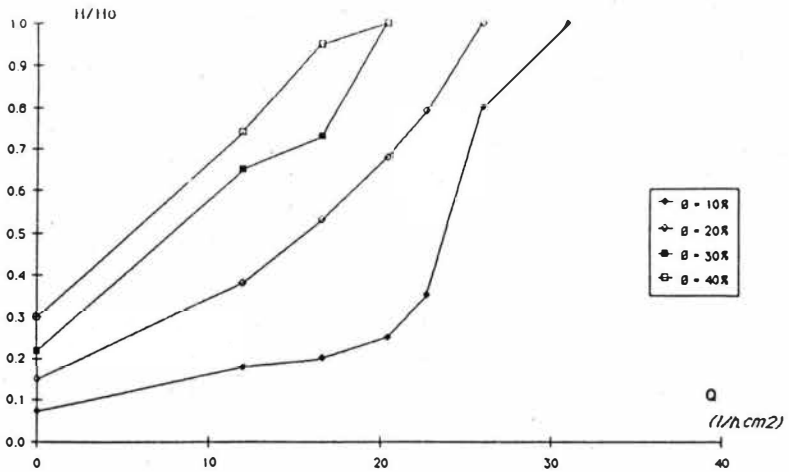


FIG. 3 : STEADY-STATE DROPLET BED HEIGHT

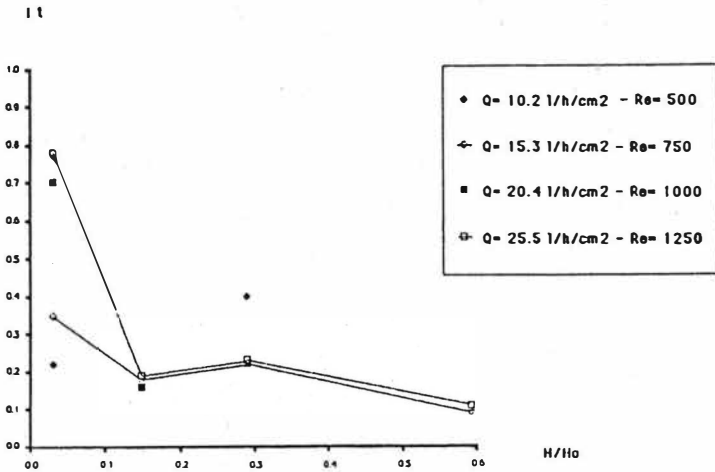


FIG. 4 : AXIAL TURBULENT INTENSITY VERSUS DISTANCE TO THE SIEVE-PLATE

	WATER	HEXANE	WATER + GLYCEROL
Volumic weight kg m^{-3}	1000	659	1082
Interfacial tension 10^{-3} N m^{-1}	43		37
Refractive index	1.3325	1.3745	1.3745

TABLE 1 Physical properties of
Water-Hexane system (at $T = 20^\circ \text{ C}$)

EXPER. CONDITIONS	DROP SIZE (mm)			
	2	2.5	3	3.5
$Q = 12 \text{ l/h} \cdot \text{cm}^2$ $\theta = 30\%$	104	35	22	-
	5.5	4.5	3.5	
$Q = 12 \text{ l/h} \cdot \text{cm}^2$ $\theta = 40\%$	4.7	5.3	2.7	3.2
	21	19	17	14
$Q = 16.6 \text{ l/h} \cdot \text{cm}^2$ $\theta = 30\%$	43	19	5.9	-
	8	6	2	

T
H

T (s) : coalescence time

H (cm) : coalescence level downstream
the sieve-plate

TABLE 2 : Coalescence times for different drop
sizes and operating conditions

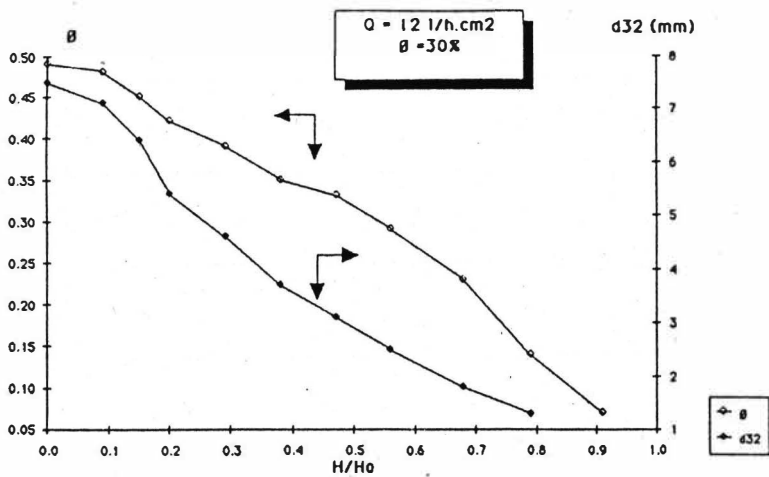


FIG. 5 : SIMULATION of FLUIDIZED BED

Determination of Emulsion Flooding, Local Holdup and Interfacial Area in Vertical Pulsed Solvent Extraction Columns

H.W. Chiang, D. Singh, S. Vijayan, Atomic Energy of Canada Limited, Pinawa, Manitoba, Canada

Abstract

Emulsion flooding studies were carried out by measuring local pressure drop, holdup and entrainment parameters using a 0.1-m diameter by 1-m-high perforated-plate column. For a solvent-dispersed case, it was found that the holdup and pressure-drop at the bottom plate section showed S-shaped variations with throughput velocity. Within this curve, the region of stable operation was bounded by the 'loading point' and the 'total flooding point'. To establish the practical limit for the operation of the column, and to define control strategies, it was shown that the column must be operated at a set of conditions within this region. The additional constraint was dictated by the magnitude of the 'allowable' entrainment loss. The loss of solvent due to entrainment was found to be influenced by the geometry of the bottom settling chamber, in addition to liquid properties.

Local dispersed-phase holdup and interfacial area were also investigated by differential-pressure and light-transmittance methods, respectively, using a 0.05-m diameter by 1.5-m-high perforated-plate pulsed column.

Measurements of the total and dynamic differential pressure gave the static pressure-drop component, from which the dispersed-phase holdup was calculated. This method was verified with a 'drainage' method. The agreement between the two methods was good (within ± 7.0 percent), confirming the viability of the pressure-drop method for on-line measurements of local holdup.

The light-transmittance measurements along the column were transformed into a semi-empirical relationship for interfacial area using a modified form of Beer's law. The interfacial area values required to obtain the constants in the empirical relation were obtained independently by holdup measurements and by droplet-size studies by still photography. The empirical relationship was found to be valid for holdup values up to 27.0 percent and interfacial areas in the range $300\text{--}2700 \text{ m}^2/\text{m}^3$.

1. Introduction

The occurrence of total throughput capacity limit or flooding in extraction columns has received little systematic experimental investigation. Blanding and Elgin (1) reported flooding limits for packed and spray extraction columns, and suggested the importance of the 'end-section' design of the column in the determination of flooding. Recently, Berger and Walter (2) addressed flooding measurements by a differential-pressure method using a pulsed perforated-plate column. Several flooding correlations have appeared in the literature (3) on pulsed perforated-plate columns during 1950-1980. In general, the lack of precise measurements together with the methodology employed by the majority of workers make such data

questionable. In addition, the detection methods used for flooding determinations have been qualitative and speculative.

Several on-line methods for measuring holdup in column contactors have appeared in recent literature. Ultrasonic techniques have been tested (4,5) on small-scale equipment with some success. Cermak (6) presented an empirical correlation for determining holdup from column dimensions and liquid density as measured by a weight recorder. Jiricny and Prochazka (7) estimated holdup from differential-pressure measurements on a Karr contactor. Jenkins and Myers (8) calculated holdup from differential-pressure measurements and compared the results with those obtained by a volume-displacement method. The agreement between these two methods has been within $\pm 22\%$.

Techniques for estimating interfacial area in liquid-liquid systems have been investigated (see review by Vassallo (3)). These methods fall into two major categories (a) indirect (e.g., light transmittance and chemical) methods, and (b) direct (e.g., photographic measurements of droplet-size) methods. The majority of the studies on the light-transmittance method has been investigated using agitated vessels (9). Inherent in these studies are several assumptions and limitations which make them unsuitable for direct application to pilot-scale extraction equipment.

In this paper, we summarize results on the determinations of flooding, and local holdup and interfacial area in vertical pulsed perforated-plate columns, using bulk-sampling, differential-pressure, light-transmittance, still-photography and liquid-drainage methods.

2. Experimental Apparatus and Materials

The liquid-liquid system employed in this investigation consisted of 30 vol% tributylphosphate + 70% Isopar M - 2.0 mol/L nitric acid. The solvent was kept as dispersed phase in all measurements. The mutually saturated liquid phases had a density difference of 223.3 kg/m^3 and interfacial tension of 10.8 mN/m at 25°C .

A schematic diagram of the test equipment is shown in Figure 1. Flooding studies were carried out using a 0.1-m diameter by 1-m-high (plate section) column. A 0.05-m diameter by 1.5-m-high column was used for holdup and interfacial area measurements. An assembly of perforated stainless steel plates, each 1.5 mm thick, was supported in the column on a central stringer rod, and separated by stainless steel tube spacers having an outer diameter of 1.2 cm. The plate perforations were 3.175-mm holes arranged on a triangular pitch to give a 23.0 percent free area. The plates were spaced at 0.05-m intervals. The ends of the main plate section were connected by means of stainless steel collars to phase disengagement vessels. These collars were drilled radially to provide four openings for housing sample ports, differential-pressure transducers, and photodiodes-collimated light source assemblies.

flooding point ($\phi_B = \phi_{SP} = \phi_{FP}$), for high frequency and low flow-ratio operation suggest reduced probability of droplet coalescence and hence a lower degree of dispersed phase buildup in the bottom section of the column. The high probability of droplet coalescence at high flow-ratio and low-frequency operation, and also at all flow ratios at low frequency, leads to a large buildup of the dispersed phase in the bottom plate section.

For a given phase flow ratio and pulse velocity, the solvent entrainment (defined as the volume fraction of the solvent phase in the aqueous effluent) was found to increase gradually beyond the loading point as the total throughput was increased. At high frequencies (> 1 Hz) as the flooding point was approached, this entrainment increased abruptly from 0.005 to 0.4. The magnitude of the entrainment was dictated by the flow ratio of phases. For low-frequency operations, entrainment increased monotonically from 0.005 up to about 0.02 independent of flow ratio. This suggests that the production of small droplets at high frequency and the carry-over of the droplets by the aqueous phase appears to be the dominant mechanism for the observed increase in the entrainment. It appears that the size of the bottom settling-vessel (0.22-m diameter by 0.5-m high) is reasonably adequate to settle out small droplets produced at low frequency operations.

The local pressure-drop behaviour with U_T was found to be similar to that of the bottom holdup.

The S-shaped pattern of bottom holdup (similarly the local pressure drop) with total throughput as characterized by the loading and flooding points (Figure 3) essentially determines the region of stable operation. However, the scale of this region in terms of the total throughput velocity is about 0.1 cm/s or, in terms of pulse frequency, about 0.15-0.3 Hz. Despite the large changes in the ϕ_B values between the loading and flooding points, the relatively very small change in the throughput velocity or pulse frequency suggests that the precision and control of operating variables are critical in determining reproducible flooding point data in column studies. In reality, the total throughput capacity limit will be determined by the allowable entrainment loss between the loading and flooding points.

To illustrate this flooding methodology, a comparison of the flooding curves predicted by five different correlations is shown in Figure 4. The lower curve represents throughput values at 'loading point' while the upper experimental curve shows data at the 'flooding point'. If the constraint of allowable entrainment loss is imposed, then the actual capacity limit for stable operation will be in between the two experimental curves. Among the empirical correlations for emulsion flooding (10-13), correlations by Smoot et al. (12), and modified Thornton and Smoot equations by Groenier et al. (13), best predict the current flooding data at low and intermediate frequencies (0.7-1.2 Hz). All published correlations overpredict flooding data at higher frequencies.

3. Flooding

3.1 Method of Measurement

Measurements of maximum throughput (flooding) capacity of the column were made indirectly by measuring holdup at three positions along the column via two-phase sampling and the differential-pressure methods. (Details of holdup determination by the differential-pressure method are described in Section 4.2). In addition, effluent streams were sampled and analyzed for phase-entrainment.

During a typical experimental run, holdup and entrainment values were recorded about one hour after reaching steady state. The hydraulic steady state was ascertained by the steady differential-pressure reading. The operating conditions were restricted to dispersion and emulsion regions: pulse frequency = 0.5-1.7 Hz; amplitude = 0.032 m; total superficial velocity = 0.001-0.014 m/s; and dispersed to continuous phase flow and ratio = 0.25-5.

3.2 Flooding Results and Discussion

Over 100 experiments were carried out to determine the effect of operating variables on local holdup at three points along the column and solvent entrainment in the aqueous effluent stream. The general trends observed in the holdup behaviour are common to all experiments. As the total throughput velocity, U_T , was increased, the bottom holdup, $\hat{\theta}_B$ (just below the first plate near the solvent inlet), increased gradually at low values of throughput, increased abruptly at intermediate values and then levelled off at higher throughput values. Holdup in the middle plate section of the column showed a similar but less pronounced trend. At the top plate section (near the aqueous inlet), the holdup did not show any such variations with throughput velocity.

Figure 2 shows typical results of $\hat{\theta}_B$ variations with total throughput. Most experiments were carried out by gradually increasing the total throughput until the bottom holdup value reached a maximum, designated by the saturation holdup point, $\hat{\theta}_{SP}$, or holdup at flooding, $\hat{\theta}_{FP}$ (see Figure 3). This value is essentially a constant and lies in the range 0.8-0.9. The experiment at 0.5 Hz was terminated before $\hat{\theta}_B$ could reach the maximum value because of limited feed-pump capacity. The appearance of a second liquid/liquid interface below the bottom plate section of the column is indicated in Figure 2 by a pair of arrows for each frequency condition. The right arrow of the pair shows the first appearance of the second interface while the left arrow reveals the maximum value of total throughput at which the second interface is not observed. The throughput scale between these two points is primarily dictated by the smallest increment of the U_T value (0.05 cm/s) employed in the experiments.

For low flow ratios (0.25-1) and high frequency operation (> 1 Hz), the maximum $\hat{\theta}_B$ values were in the range 0.4-0.6. However, for pulse frequencies less than 1 Hz, the maximum holdup attainable was in the range 0.8-0.9. The low values of $\hat{\theta}_B$ at

4. Dispersed Phase Holdup and Interfacial Area

4.1 Methods of Measurement

A schematic of the pulsed column with differential-pressure cells and butterfly valves for measuring holdup is shown in Figure 5. All other ancillary equipment are the same as shown in Figure 1.

Differential-pressure measurements over the plate section of the column were obtained from differential pressure (DP) transducers connected across three sections of the column, as shown in Figure 5. The transducer across the top section (DPC 1) was a Rosemount cell, while the other two cells (DPC 2 and 3) were Foxboro units. Output voltage signals from the transducers were stored on an Apple microprocessor.

Experiments were performed by recording the differential-pressure signals of each transducer at hydraulic steady state for no pulsing, pulsing only, pulsing with single continuous-phase flow and pulsing with two-phase flow, for each of the operating conditions studied.

Holdup measurements were also performed by two other methods. One method, generally referred to as the drainage method, involved the instantaneous isolation of the column contents by closing two butterfly valves (Figure 5) followed by draining of the column contents and measuring the volumes of the two phases. The second method involves withdrawal of two-phase samples (approximately 100 mL/sample) at four positions along the column and calculation of the holdup.

Interfacial area experiments by the light-transmittance method were also carried out using the light-source detector system (Figure 5). The light source consisted of a 21 V/45 W halogen lamp mounted in a black cylindrical casing to which a lens collimator tube was attached. This arrangement provided a parallel beam of light. The detector used was a cadmium sulphide photoconductive cell. The above arrangement was installed across the diameter of the column at two locations along the column.

Light-transmittance measurements were made by recording the incident light intensity, I_0 , as measured by the photodiode for pure aqueous phase and transmitted light intensity, I , in the presence of two-phase dispersion at the two locations. In addition, local dispersed-phase holdup measurement by the sample withdrawal method, and mean droplet size by still photography were performed at each location.

4.2 Results and Discussion

Analysis of Differential-Pressure Data for Holdup Determination

The total pressure drop (ΔP_T) measured in a pulsed extraction under conditions of two-phase flow and pulsing can be resolved into three major components (14) as follows:

$$\Delta P_T = \Delta P_{\text{static}} + \Delta P_{\text{inertia}} + \Delta P_{\text{friction}} \quad (1)$$

For the current work, the following simplifying assumptions have been made: (a) the inertial and friction terms in equation (1) are lumped together as the dynamic pressure-drop term, ΔP_{dyn} , (b) ΔP_{dyn} for the two-phase flow with pulsing can be estimated for a given operating condition by measuring ΔP_{dyn} for single continuous-phase flow with pulsing, and (c) the dispersed phase holdup ϕ_d is calculated from ΔP_{static} by a simple hydrostatic balance as follows:

$$\phi = (\Delta P_{static} \cdot \rho_c \cdot g) / g \cdot h (\rho_c - \rho_d) \quad (2)$$

where

$$\Delta P_{static} = \Delta P_T - \Delta P_{dyn} \quad (3)$$

and

ρ_c and ρ_d = density of continuous and dispersed phases, respectively; g = acceleration due to gravity; and h = distance over which ΔP cells are mounted. ΔP_T and ΔP_{dyn} are determined experimentally, as described above.

A total of 20 experiments were performed. Values of holdup for each of the three sections and the entire plate section were calculated from pressure-drop measurements using equations (2) and (3).

Holdup

The drainage method was used as a standard for assessing holdup by the differential-pressure method. Figure 6 shows a comparison of holdup data by the differential-pressure and drainage methods, and the agreement between the two sets of data is good. However, the consistent bias shown by the differential-pressure technique in underpredicting holdup cannot be readily accounted for and may be due to microdynamic processes that have been assumed to be negligible in the analysis methodology. The percentage deviation between the two sets of holdup is of the order of 7%, and is well within the range of experimental error. In a recent study, Jenkins and Myers (8) estimated holdup in a pulsed column using differential-pressure and interface-displacement methods. The agreement between the data by the two methods was reported to be within $\pm 22\%$. Local dispersed-phase holdup values by the pressure-drop method obtained for each of the three plate sections are shown in Figure 7. The holdup profiles shown are consistent with the published literature as reviewed in reference 15.

Interfacial Area

For the current work, a total of 20 experiments were carried out to obtain data for the fraction of light transmitted, I/I_0 , local dispersed phase holdup and mean droplet size. The latter two measurements were performed at the same location where the light-transmittance measurements were made.

The interfacial area, a_i , for each experimental condition was calculated using the relationship:

$$a_i = 6\phi_d/d_{32} \quad (4)$$

where ϕ_d (holdup) and d_{32} (sauter mean droplet diameter) were determined experimentally.

The Beer's law (9) for light transmittance in a polydisperse media relates the fraction of light transmitted to interfacial area:

$$\ln(I/I_0) = -k a_i l \quad (5)$$

Thus, a plot of $\ln(I/I_0)$ versus a_i yields a straight line with an intercept of 1. This relationship, however, is only valid for dilute dispersions and situations where forward scattering of light reaching the photodetector is absent.

Figure 8 shows the presence of two distinct regions, each represented by a straight line. The first region represents interfacial area values up to $1200 \text{ m}^2/\text{m}^3$ with an intercept of 1, while the second region represents interfacial area greater than $1200 \text{ m}^2/\text{m}^3$. The first region is evidently consistent with the light transmittance theory for low interfacial areas. The second region, however, is inconsistent with the theory. This is expected, as the density of the dispersion in this region falls outside the dilute dispersion assumption.

The experimental data were correlated by a modified form of equation (5) that includes a weighting term to account for the effects due to concentrated dispersions. The correlation used to fit the data takes the form:

$$\frac{I}{I_0} = (1 + K_1 a_i^{K_2} l) \exp(-K_3 a_i l) \quad (6)$$

where l is the internal diameter of the column ($=5.0 \text{ cm}$) and the parameters K_1 , K_2 and K_3 were determined by a nonlinear least-square regression analysis, giving the following parameter estimates at the 95% confidence limit:

$$\begin{aligned} K_1 &= 8.6487 \times 10^{-11} (\pm 4.1795 \times 10^{-11}); & K_2 &= 4.1550 (\pm 0.3465); \\ K_3 &= 0.0102 (\pm 2.892 \times 10^{-4}) \end{aligned}$$

For low interfacial area values (or dilute dispersions) the first term in equation (6) approaches unity, thus reducing the relationship to a form that is consistent with the Beer's law (eqn. 5).

5. Conclusions

- The local holdup in the bottom plate section of the column (closer to the solvent inlet) with throughput velocity exhibits an S-shaped pattern. This pattern is less pronounced when overall holdup of the column is used.
- The local and overall pressure-drop values across the bottom section of the column exhibit trends similar to those of holdup.
- The S-shaped holdup curve contains two characteristic boundaries represented by 'loading' and 'flooding' points. Stable operation of the column is achieved at any point within the region bounded by the loading and flooding points. The exact location of the operation is dictated by the allowable loss of solvent as entrainment in the aqueous phase.

- The abrupt increase in dispersed-phase holdup between the loading and flooding points occurs in a narrow region. In terms of pulse frequency and throughput velocity, the scale of this region is typically 0.15-0.3 Hz and 0.001 m/s, respectively. This illustrates the importance of the precision and control of operating variables in flooding determinations.
- To report throughput capacity limits, it is essential to specify both loading and flooding points, and the entrainment loss. In addition, equipment specifications must also include the geometry of all components in the column, as they influence the entrainment levels.
- Differential-pressure measurements using single- and two-phase flows can be resolved by simple analysis to provide local and overall dispersed-phase holdup in vertical pulsed columns.
- Holdup values determined by the differential-pressure method agree within 2-7 percent of those obtained by the volume-displacement method.
- The light-transmittance method for interfacial area determination is extended up to a holdup of 0.27. A correlation relating the fraction of transmitted light to interfacial area adequately describes the experimental data.
- For holdup values less than 0.124 and interfacial area up to $1200 \text{ m}^2/\text{m}^3$, the light-transmittance change with interfacial area is consistent with Beer's law for polydisperse media.

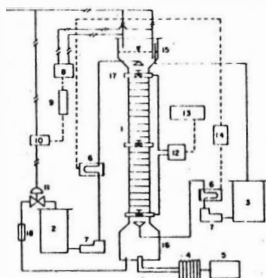
Acknowledgement

The authors gratefully acknowledge Messrs. R.J. Lucas and A.S. Palson for their assistance with the experiments.

References

1. Blanding, P.H. and J.C. Elgin, *Trans. A.I.Ch.E.*, **38**, 305 (1942).
2. Berger, R. and K. Walter, *Chem. Eng. Sci.*, **40**(12), 2175 (1985).
3. Vassallo, G., *The Hydrodynamic Behaviour of a Pulsed Column*, Commission of the European Communities, Report No. EUR-8597, Luxembourg (1983).
4. Bonnet, J.C. and L.L. Tavlarides, *Determination of Dispersed Phase Holdup in Agitated Extraction Units by an Ultrasonic Technique*, Proc. 35th Canadian Chem. Eng. Conf., Calgary, Canada, Oct. 6-9, 1985, vol. 2, p. 58.
5. Havlicek, A. and H. Sovov'a, *Coll. Szeck. Chem. Com.*, **49**, 378 (1984).
6. Cermak, A.P., *Techniques for Determination of the Dispersed Phase Holdup in Pulsed Columns Used in a Nuclear Fuel Reprocessing Plant*, International Solvent Extraction Conference, Liege, Belgium, Sept. 6-12, 1980.
7. Jiricny, V. and J. Prochazka, *Chem. Eng. Sci.*, **35**, 2237 (1980).
8. Jenkins, J.A. and P.E. Myers, *Estimation of the Dispersed Phase Holdup in a Pulsed Perforated-Plate Column from Pressure Drop Measurements*, I.Ch.E. Symposium Series, No. 88, Dounreay, U.K., Nov. 27-29, 1984.
9. McLaughlin, G.M. and J.H. Rushton, *A.I. Ch. E. J.*, **19**(4), 817 (1973).

10. Thornton, J.D., *Trans. Inst. Chem. Engrs.*, **35**, 316 (1957).
11. Pratt, H.R.C., *Ind. Chem.*, **31**, 552 (1955).
12. Smoot, L.D., B.W. Mar and A.L. Babb, *Ind. Eng. Chem.*, **51**, 1005 (1959).
13. Groenier, W.S., R.A. McAllister and A.D. Ryon, *Flooding in Perforated-Plate Pulsed Extraction Columns*, U.S. AEC, Oak Ridge National Laboratory Report, ORNL-3890 (1966).
14. Jealous, A.C. and H.F. Johnson, *Ind. and Eng. Chem.*, **47**(6), 1159 (1955).
15. Shin, Y.J., H.W. Chiang and S. Vijayan, *Dispersed Phase Droplet-Size Distribution and Holdup in a Pulsed Perforated-Plate Extraction Column*, Proc. 35th Canadian Chem. Eng. Conf., Calgary, Canada, Oct. 6-9, 1985, vol. 2, p. 83.



1. 10-cm perforated plate column
2. Organic storage tank
3. Gear box and motor drive
4. Constant volume feed pump
5. Proportional integral controller
6. Pneumatic control valve
7. Recorder
8. Upper disengagement section
9. Stainless-steel collar
10. Aqueous storage tank
11. Teflon bellows system for pulsing
12. Remote mass flow meter
13. Pneumatic transmitter
14. Pneumatic transducer
15. Pressure transducer
16. Digital indicator for mass flow
17. Lower disengagement section
18. Electric conductivity probe

Figure 1: A Schematic Diagram of the Pulsed Column and Accessories

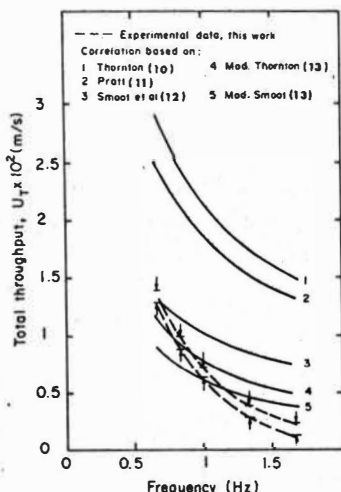


Figure 4: Comparison of Experimental Flooding Data with Published Empirical Correlations

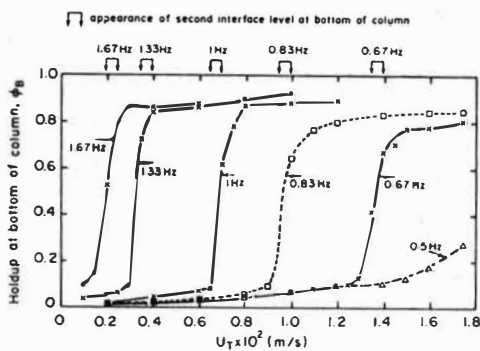


Figure 2: Bottom Holdup Variations with Total Throughput Velocity

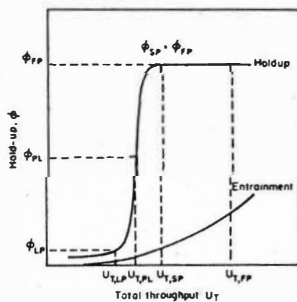


Figure 3: A Schematic Diagram of Holdup and Entrainment Variations with Throughput Velocity

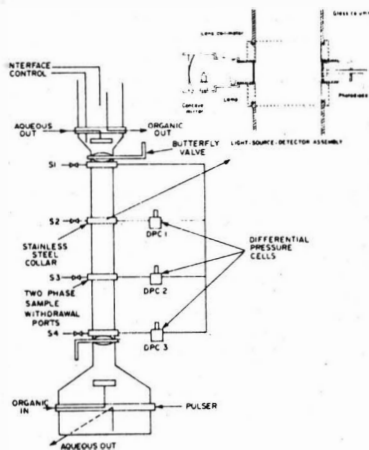


Figure 5: A Schematic Diagram of the Pulsed Column Showing Locations of Instruments for Local Holdup and Interfacial Area Measurements

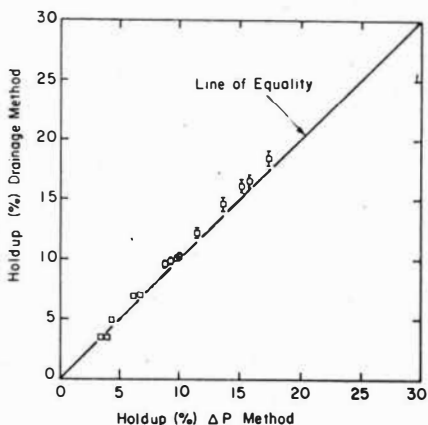


Figure 6: Comparison of Holdup Data by Differential Pressure and Drainage Methods

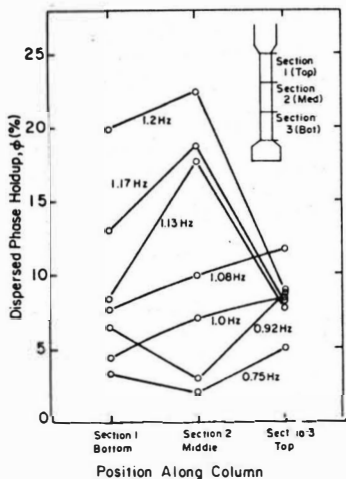


Figure 7: Effect of Pulse Frequency on Holdup Profile by Differential Pressure Method

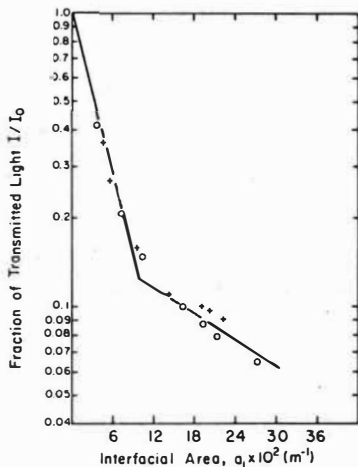


Figure 8: Effect of Interfacial Area on Fraction of Transmitted Light

Coalescence and Motion of Drops on Inclined Plates in Liquids

Dipl.-Ing. W. Meon, Prof. Dr.-Ing. E. Blaß,

Lehrstuhl A für Verfahrenstechnik, Technische Universität München

1. Introduction:

The coalescence of drops on even interfaces in liquid-liquid systems is determined by a multitude of factors, whose complex interactions have not yet been sufficiently clarified to allow a reliable predetermination. If for the present the drop diameter is restricted to the range of millimeters, proximity forces on the function of determining factors are almost eliminated. If in addition an enrichment of tensides and therefore interfacial energy effects at the point of coalescence are excluded, the problem of coalescence is reduced to the hydrodynamic problem at the draining of a thin layer consisting of continuous phase between the drop and its originating phase. The use of inclined plates as coalescers in a settler wetted well by the drop fluid, is a simple technical realization of this ideas (figure 1). Resulting from the drop coalescence a thin liquid film (trickling film) is formed on the plate, which constantly flows off the plate to the surface of the continuous phase forced by the buoyant lift. Thus no tensids can concentrate at the surface of the trickling film (points of coalescence), because the tensid molecules are constantly transported at the principle phase boundary. But even from the hydrodynamic point of view plate packages, which are used successfully in gravity settlers to separate solid-liquid and liquid-liquid systems for a long time, favor the coalescence. In this case the drop motion with respect to the static inclined plate is an important reason for the rapid coalescence on the plate. In order to get a basis for the dimensioning of settlers with plate packages, the coalescence of single drops and chains of drops on inclined plates are studied.

The present fundamental experimental and theoretical results point out the fact that it is possible to describe the principle of the coalescence on plate packages by the means of scientific engineering.

2. Experiments on the drop coalescence on inclined plates

It is necessary for the dimensioning of a settler to know about the separation time of the dispersion in its clear phases. It consists of the approaching time of the drop to the inclined plate and the residence time on the trickling film until complete or partial coalescence has

occured. The following considerations are restricted to the residence time of the drops on the inclined trickling film, which is called the time of coalescence. Once the time of coalescence has been worked out, the dimensioning of the settler is possible, if the behavior of drops in a swarm is known. Therefore the emphasis of the fundamental experiments on coalescence is put on the experimental and theoretical determination of the time of the coalescence of single drops and chains of drops on an inclined plate.

3. Mathematical model for the determination of the coalescence time

In the introduction the coalescence was described as the process of the draining of the thin layer of continuous phase, which is either enclosed by two drops or one drop and the horizontal interface (see figure 2):

figure 2: Process of coalescence

If the thin layer manages to undergo a critical thickness δ_{crit} during its draining out, it tears up and the drop can coalesce. This draining process is to be modelled physically. The important physical factors for the development of the model are plotted in figure 3. A trickling film, resulting from coalesced drops, flows up an inclined plate. A drop, which rose from the dispersion to the plate, has reached the trickling film, deforms its surface and moves with its velocity v_p towards the flow of the trickling film. Thus the enclosed thin layer drains between the drop and the trickling film over the line contact ($2 \cdot r_f \cdot \Pi$), showing a special flow-profile, while the drop approaches with the velocity $d\delta/dt$ to the surface of the trickling film.

figure 3: Process of coalescence on an inclined plate (the thin layer $\delta(t)$ is plotted much enlarged)

For the model derivation an initial value of 10^{-4} m for the layer draining is defined. This presumption hardly reflects on the result of the time of coalescence, as the critical thickness of the thin film is the order of 10^{-7} m (Vrij and Overbeck /4/). If the inertia force is neglected, an equilibrium of forces can be set up for a fluid element during a stationary flow-process in the draining layer and the following equation can be derivated:

$$\frac{dp}{dr} + \frac{dr}{dz} = 0 \quad (1)$$

If the Newton formula for shearing stress is valid, the term $d\tau/dz$ can be replaced by $-\eta_c \cdot d^2u/dz^2$. If the thin layer drains symmetrically and ring-shaped the overpressure p in the middle of the spherically shaped thin layer under the drop ($r=0$) is $2 \cdot \sigma/R$, whereas R corresponds to the radius of curvature (Princen /5/). This overpressure is meant to sink to $p=0$ at $r=r_f$ because of the loss of flow-pressure /3/. These assumptions allow the integration of the pressure p versus the radius r during the solving of the differential equation (1).

The velocity profile $u(z)$ of the draining thin layer can be worked out by integrating the equation (1) two times versus dz :

$$u = \frac{1}{2\eta_c} \cdot \frac{dp}{dr} \cdot (z^2 - z \cdot \delta) + v_r \cdot \frac{z}{\delta} \quad (2)$$

The relative velocity for the determination of the profile of velocity $u(z)$ were deduced from the observation of the drop movement. If the Newton formula for shearing stress is used for the liquid layer and the trickling film between drop and plate (figure 3) the relative velocity v_r between the two boundary faces of the thin layer is:

$$v_r = v_p \left(1 - \frac{1}{\frac{\eta_d}{\eta_c} \cdot \frac{\delta}{(\delta_R - L_E)} + 1} \right) \quad (3)$$

The difference between the thickness of the trickling film and the depth of immersion L_E of the drop in an interface can be calculated with Rautenberg's /3/ and Princen's /5/ mathematical models. The velocity of drops v_p is figured out by a physical model which we developed ourselves and which will shortly be described in the following. The flow profile $u(z)$, calculated from equations 2 and 3, can be introduced in the continuity equations (eq. 4a,b) for ringshaped symmetrical draining:

$$\dot{V}_{aus} = 2 \pi \cdot r_f \cdot \int_0^{\delta} u(z) \cdot dz \quad (4a)$$

$$\dot{V}_{aus} = - \pi \cdot r_f^2 \cdot \frac{d\delta}{dt} \quad (4b)$$

Out of this we obtain the differential equation for the approaching velocity between a drop and the surface of a trickling film, which can be interpreted using the factors of influence shown in eq. 5.

$$\frac{d\delta}{dt} = - \underbrace{\frac{2\sigma \cdot \delta^3}{3R \cdot \eta_c \cdot r_f^2}}_{\text{capillarity pressure}} - \underbrace{\frac{2 \cdot \delta \cdot v_p}{r_f}}_{\text{drop movement}} \left(1 - \underbrace{\frac{1}{\frac{\eta_d}{\eta_c} \cdot \frac{\delta}{(\delta_R - L_E)} + 1}}_{\text{plate influence}} \right) \quad (5)$$

An integration*) of the term within the limits of $\delta = 0,1 \text{ mm}$ ($t=0$) to $\delta = \delta_{\text{crit.}}$ leads to the desired time of coalescence t_k of a drop with a trickling film on an inclined plate. The integrated form of this equation is extensive and hard to follow up. Each of the physical influential factors is one by one discussed by using the equation of the velocity of the approach of the drop (eq. 5).

4. Discussion and interpretation of the theoretical and experimental results

In eq. 4 the 1st term ($2\sigma \cdot \delta^3 / 3R \cdot \eta_c \cdot r_f^2$) indicates the contact pressure of the drop on the surface of the trickling film. This term gains greater influence mainly with small drops, which is clearly to be seen, as in this case the contact surface r_f^2 of the drop and the interface, as well as the radius of curvature R^{**}) adopts very small value. In this case the 1st term and thus the velocity of approach is great. Therefore, for small drops this results in a short time of coalescence (with reference to a hydrodynamic point of view). This was wholly confirmed by the experimental investigations with small single drops conducted for this reason.

The second term ($2v_p \cdot \delta / r_f$) considers the influence of the absolute velocity between the drops and the static plate. A high velocity of drops causes a faster approach of the drops to the surface of the trickling film, and thus a shorter time of coalescence. The velocity of the drops is calculated for the stationary drop movement on a trickling film. Figure 4 marks the forces acting on the drop.

figure 4: Acting forces on a single drop in the trickling film flow

The equation of motion can be figured out by producing the equilibrium of forces out of the dead weight $F_g(x)$, the buoyant forces $F_A(x)$, the

*) Bronstein-Semendjajew, Taschenbuch der Mathematik, Zürich and Frankfurt/M. 1975, 15. Auflage, S. 300 Nr. 52 and 54, S. 299 Nr. 40

***) Pressure of curvature: $2\sigma/R$

hydrodynamic resistance $F_{\zeta}(x)$ and the shearing force $F_{\tau}(x)$, which describes the induction of the drop and the plate:

$$v_{pr} = -4 \cdot C \cdot (-) \left(16C^2 - (8 \cdot \bar{v}_c \cdot C - \frac{4 \cdot g \cdot d_p \cdot (\rho_c - \rho_d) \cdot \sin \alpha}{3 \cdot \zeta \cdot \rho_c}) \right)^{1/2} \quad (6)$$

with

$$C = \frac{r_f^2 \cdot \eta_d}{\zeta \cdot \rho_c \cdot d_p^2 (\delta_R - L_E)} \quad (7)$$

The absolute velocity of drops can then be figured out of a superposition of the mean ambient velocity \bar{v}_c of the drop (calculated according to Rautenberg /3/) and the velocity v_{pr} , which is the relative velocity between the drop and its environment.

$$v_p = v_{pr} + \bar{v}_c \quad (8)$$

A detailed derivation of this model of motion is shown in /6/.

The third term describes the influence of the plate on the process of coalescence. This term evaluates the influence of the drop movement using the shear stress which is removed between the moving drop and the stationary plate throughout the trickling film and the draining layer. The term tends to zero when the distance between the drop and the plate is small ($\delta_{R-L_E} \rightarrow 0$) and the viscosity of the continuous phase is low. This causes the maximal velocity of approach and thus a fast coalescence. This, among other factors, has been experimentally investigated in details and could be verified with the help of a lot of datas. One factor, which has thus been found out, offers a quantitative delimitation for favorable conditions for the coalescence on a plate. Figure 5 shows a typical diagram of the results of the investigations on the influence at the plate. Single drops coalesce with a trickling film from drop phase on an inclined plate within a specific range of volumetric flow rate.

figure 5: Influence of the plate on the coalescence

Within this range of volumetric flow rate a constant time of coalescence is given for a constant drop diameter. The exceeding of a certain volumetric flow rate results in the sudden rise of the time of coalescence. There is hardly any zone of transition between the short and the

long time of coalescence. Figure 5 points out the physical background of this behavior of coalescence. The thickness of the trickling film δ_R grows according to the increasing volumetric flow rate \dot{V}_R . If the thickness of the trickling film δ_R corresponds to the depth of immersion of the drop ($\delta_R = L_E$), the drop is lifted from the plate. In the range of $\delta_R = L_E$ a strong shear stress favors the process of coalescence because of a high relative velocity between the drop and the plate. If the drop removes from the plate ($\delta_R > L_E$) the shear stress is strongly reduced because of the increasing distance to the plate. The small relative velocity of the interface v_r , thus figured out, becomes low, while the process of draining becomes much slower. Thus the time of coalescence quickly increases. The model calculation in figure 5 clearly shows that the model of coalescence is able to predict correctly the strong hydrodynamic influence on the process of coalescence. One important result of this investigation can be drawn up by a simple criterion, which gives the boundaries of the operation conditions for a plate as coalescer with a short obtainable time of coalescence.

Criterion on the fast coalescence on a plate:

$$\delta_R / L_E \leq 1$$

δ_R calculated according to Rautenberg /3/
 L_E calculated according to Princen /5/

Thus a calculation of the time of coalescence for single drops on an inclined plate can be interpreted with reference to hydrodynamics according to the figure following.

figure 6: Calculated time of coalescence depending on the drop diameter

In the range of small drops the time of coalescence highly increases according to growing drop diameters, because the contact pressure of the drop on the thin layer decreases with an increasing drop diameter. If the size of the drop grows even more, the decreasing contact pressure is compensated by the rising velocity of the drops. (eq. 5, IInd term) The result is a characteristic maximum for the time of coalescence. Big drops more and more press through the trickling film and start an interaction with the plate in case of $L_E = \delta_R$. In this case the drop movement causes a very strong shear stress field in the thin layer and favors a fast draining. The time of coalescence falls all of a sudden and sets to a constant level.

5. Summary and outlook:

Our research method for coalescence phenomena, the drop coalescence on inclined plates, allows a reflection the coalescence process from the hydrodynamical point of view. That is why a mathematical model could be introduced, which calculates the coalescence process of single drops on a trickling film as the draining of a thin layer of continuous phase under a drop, based on fluidmechanical principles. This model enables to interpret hydrodynamically the behavior of the single drop coalescence of various drop diameters at different volumetric flow rates of the trickling film and angles of inclination of the plate. Thus the short time of coalescence of small single drops ($Bo < 0.116$) can be attributed to the high contact or capillarity pressure. Contrary to this, strong shear stress between drop and plate causes a short time of coalescence for big single drops. This high plate influence only occurs when the drops are able to press almost through the trickling film to the plate ($L_E = \delta_R$). A simple criterion, which gives the boundaries of short times of coalescence, is obtainable from these results. In this field the theoretical results correspond very well to the experimental data. Further research on the drop swarm coalescence on inclined plates shall create a basis for the dimensioning of plate separators for liquid-liquid systems in addition to the results of the single drop coalescence.

Literature:

- /1/ T.D. Hodgson, D.R. Woods: J. of Coll. and Int. Sci. 30 (1969) 429-446
- /2/ J. Stauff: Kolloidchemie, Springer Verlag 1960
- /3/ D. Rautenberg: Dissertation, TU München 1983
- /4/ A. Vrij, J. Th. G. Overbeck: J. of the American Chem. Soc. 90 (1968) 3074-3078
- /5/ H. M. Princen: Surface and Colloid Science, Vol. 2, 1-84, Wiley 1969
- /6/ W. Meon: Diplomarbeit, TU-München 1983, Lehrstuhl A für Verfahrenstechnik

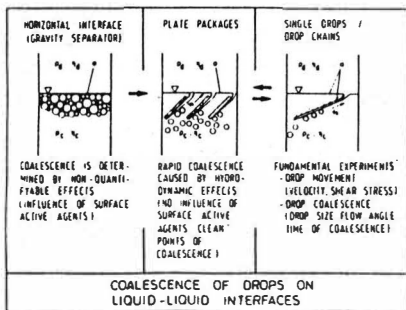


figure 1:

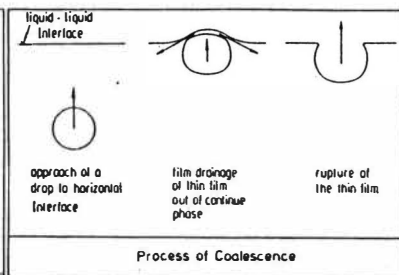


figure 2:

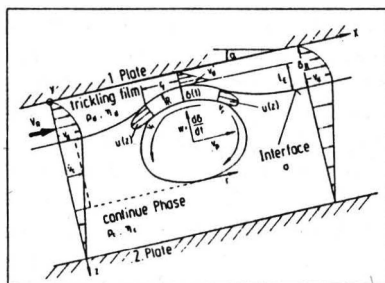


figure 3:

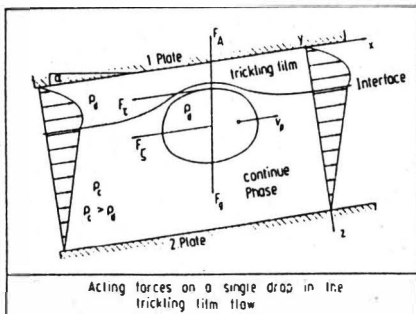


figure 4:

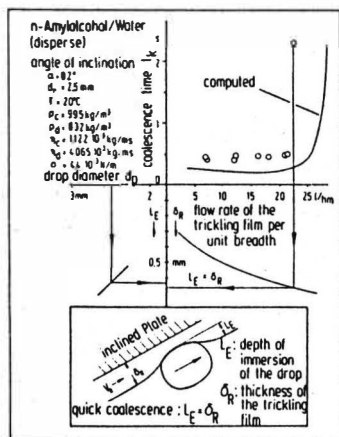


figure 5:

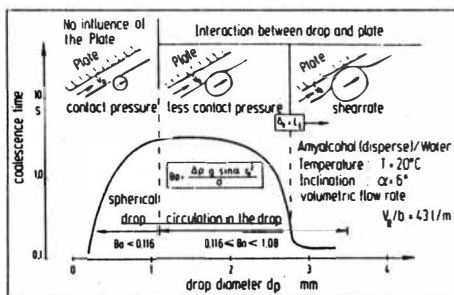


figure 6:

A Measuring Technique for Drop Diameters in the μm -range in
Liquid-Liquid Dispersions

Dipl.Ing. Fritz Rebelein, Prof. Dr.-Ing. E. Blaß,
Lehrstuhl A für Verfahrenstechnik, Technische Universität München

Introduction:

Liquid-liquid dispersions occur in many fluid-dynamic processes, wanted or unwanted, like in the liquid-liquid extraction, at the condensation of heteroazeotropics, at the solubility reduction caused by changes of temperature and so on. The separation of the dispersions causes a lot of technical problems and isn't still predeterminable up to now. The scientific engineering treatment of the separation of liquid-liquid dispersions by drop coalescence must be based on the single drop diameter and on the drop size distribution of the droplet swarm respectively. Especially for micro-dispersions of drop sizes below $100 \mu\text{m}$ the experimental determination of drop diameters turns out to be difficult.

The only methods of measurement which are more or less suitable are based on sedimentation processes and light diffraction at the particle surface. E.g. the Laser-Doppler Methods, the detection of light diffraction at the single particle and the analysis of Fraunhofer's diffraction patterns belong to the latter group. Each of these methods has its optimum actional range and only few of them are really suitable for the usage in liquid-liquid systems.

This paper introduces a measuring method which is based on the analysis of Fraunhofer's diffraction patterns. This method was chosen because it allows drop size measurements from drop sizes of about $2 \mu\text{m}$ up to $800 \mu\text{m}$ which can be done in a fast and easy to handle way and in addition is good value.

The measuring technique:

The measuring method is based on the interpretation of Fraunhofer's diffraction patterns, which is where the name diffraction spectrometry comes from. As early as 1817 J. Fraunhofer described the optical installation to produce diffraction patterns /1/. Fig. 1.1. shows the installation used today to produce these diffraction patterns by drops in liquids.

If ball-shaped drops of equivalent size which are dispersed in a liquid, are moved across the defocussed laser beam on their way through the cuvette of the optical installation illustrated in fig. 1.1, the result being a radial-symmetric Fraunhofer's diffraction pattern in the focal plane of the lense, which is arranged at the outlet side (fig. 1.2.). Fraunhofer's diffraction patterns for drops of equivalent size consists of a very light central circle which is surrounded by concentric light and dark rings. The light-intensity distribution of the diffraction patterns on the radius depends on the drop diameter. If the drops in the light beam are not monodisperse, but a drop size distribution is existent, the diffraction patterns of the respective diameters superpose and result in a radial-symmetric diffused diffraction pattern with an intensity distribution dependend on the radius. Basing on the measured intensity distribution the drop size distribution is figured out by a large-scale numeric calculation method /2/.

In order to measure the drop size a liquid-liquid dispersion is continually removed of the stirred tank by suction through a short pipe, like for example is illustrated in fig. 1.1. After that the dispersion flows through the space between the two cuvette windows in the form of a layer of a width of 2 mm and a depth of 30 mm (the radius of these windows being about 15 mm). The laser beam penetrates the cuvette in vertical direction to the dispersion layer and in doing so is partly diffracted.

The rate of the diffracted light increases according to the number of the drops and, after a certain concentration is reached, it causes the "blinding" of the detector. To avoid this a drop

concentration of 1 to 5% of volumetric concentration mustn't be transgressed at a thickness of the dispersion layer of 2 mm and drop diameters of about 50 to 100 μm . If the probe, which has to be analyzed, shows a considerable higher volumetric concentration, i.e. up to several percent, it must be diluted to a suitable concentration by adding continuous phase on its way to the measuring cuvette. The pipe length is not critical for drop coalescence, as long as the drop concentration lies within the mentioned range of a few parts promille. Experiments testing several meters of pipe length between the sampling point and the measuring point in the diffraction spectrometer didn't show any changes on the drop spectrum. The pipe material didn't effect the results, as the usages of pipes which were well-wetted and unwetted by the drop phase didn't show any difference. Nevertheless an influence of the pipe material can't be excluded in the case of higher concentrations of the dispersed phase. Even during the analysis the samples should be transported continuously as static probes tend to separate and therefore the drops size distribution changes within seconds. The drop velocity at the measuring point doesn't affect the testing result. Using the described method one complete measuring cycle lasts about 10 to 15 minutes preparations and report printing included.

Comparison of the results of diffraction spectrometry and photography

As there was no experience available for drop size measurement using the measuring technique described, its fitness has to be proved. On this purpose identic dispersions were analyzed by photography and diffraction spectrometry almost at the same time and the results compared afterwards.

The testing materials used were Tributylphosphat/n-Alkan (refractive index 1.4183), Shellsol T (refractive index 1.421) and Benzene (refractive index 1.5014) as dispers phases and distilled water (refractive index 1.3321) as continuous phase. The drop diameters varied in a range below 500 μm .

The photographs were taken by a 35 mm single lens reflex camera supplied with a balwo and a macro lens. The films used were "Ilford HP4/HP5" and "Kodak Technical Pan". A magnification factor of about 5 was obtained between the real drop size and its image on the film. In addition the photographed drops were magnified by projection, so that a total magnification factor of now about 200 was reached and the drop size could be measured by metering. The drop size distribution was determined from a magnitude of such single drop measurements. The photographs of the dispersion samples were taken through the windows of the same measuring cuvette which was used for the diffraction spectrometry. This guaranteed identic boundary conditions for the two measuring methods.

The results of this comparison

The measurements showed the result that the obtained drop size distributions corresponds very well to the well-known RRS-distribution. Therefore, the measured values were plotted in corresponding RRS-graph-papers and then compared. This comparison yields a typical difference of the distributions obtained from the two methods. Fig. 2 shows one typical result graphically. As can be seen, the diffraction spectrometry (curve 1) shows a very high rate of smallest drops, which doesn't exist in the photographs, as can be proved; this is the range on the left side of the plotted inflection point in fig. 2 and therefore smaller than $10 \mu\text{m}$ (this effect can also be seen at smaller and bigger drop diameters). An optical anomaly of the diffraction behaviour in the inside of the drops proved to be the reason for this aberration of the diffraction spectrometry. Some explanations are necessary to understand this anomaly: The measuring method described in this context is well-suitable in the region of the geometrical optic; that means that the particles to be measured must be bigger than $2 \mu\text{m}$ if light in the luminous spectrum is used. Then the diffraction behaviour can be described by means of geometrical optics. In this range it is quite normal, that parallelly incident light leaves the drop strongly divergent. This diffraction is so strong, that almost no light from the inside of the drop can reach the detector of the measuring system. Only the

light diffracted at the surface joins the detector and is analyzed. A limiting area of geometrical optics is approached the more the drops and their surrounding phase are fluids of similar refractive indices. The 'normal' refraction behaviour previously described changes and becomes more and more anomalous: The focussed light beam is hardly affected any more; it leaves the drop with a minimum divergency and a highly increased intensity. This light from the inside of the drop superposes the diffracted light from the drop surface and also incidences the detector of the measuring instrument. The measuring system isn't able to discriminate the origin of the incoming light and therefore all the light which reaches the detector is analyzed as diffractive light of drops. As a consequence the light coming from the inside of the drops is reproduced as a fraction of smallest drops, which isn't really existent. Therefore, the non-existent fraction of smallest drops shown in fig. 2 is caused by the great similarity of the refractive indices of the fluids used. As a rule these refractive indices are predetermined by the fluid samples to be analyzed and cannot be controlled. Therefore, we looked for a way to correct the distribution which was measured by the diffraction spectrometer, so that it conforms with reality, which, for example, is reflected in photography. Out of different alternatives the following proved to be the best one: The inflection point in the course of the volume cumulative distribution curve (curve 1) measured by the diffraction spectrometry has to be found out and then the simulated fraction of smaller drop diameters is cut off the distribution in question starting from the inflection point of the curve. The rest of the distribution of the higher drop diameters is normalized once again, so that the volume cumulative distribution once more reaches 100 %. The new distribution (curve 2) plotted in the RRS-graph paper shows a definite RRS-distribution and thus corresponds to the real distribution type (curve 4). The distributions corrected this way on an average showed for all experiments smaller particle diameters of about 10-12 % compared to the photographed distributions. This deviation can be neutralized by simple replacing the corrected distribution by a distribution of a particle diameter which is 10-12 % bigger (curve 3). (This is illustrated by a translatory shift in the RRS-graph paper.)

The suitability of this empirical correction method must be verified for the usage of the diffraction spectrometry in case of other refractive indices than the investigated ones. We expect the quality of the testing results to increase with a greater difference of the refractive indices between drop phase and surrounding phase; unfortunately, however, it is impossible to state to what degree the quality of the testing results will improve. For doing this a calibration with drops must be done, as has been described.

Summary

The usage of diffraction spectrometry was tested for liquid-liquid dispersions. It proved suitable but nevertheless a systematic deviation of the measuring results compared to those taken from photographs is obvious. Because of the very similar refractive indices a rate of micro drops is feigned. We developed an empirical method according to which the results of the diffraction spectrometry must be corrected, so that they reflect the distributions in question offering a similar quality than photographs.

References

- /1/ Fraunhofer, I.: Bestimmung des Brechungs- und Farbzerstreuungsvermögens verschiedener Glasarten. Gilbert Annalen der Physik 56 (1817) S. 193 ff.
- /2/ M. Heuer, K. Leschonski: Erfahrungen mit einem neuen Gerät zur Messung von Partikelgrößenverteilungen aus Beugungsspektren. Preprints, 3. Europäisches Symposium Partikelmeßtechnik, Nürnberger Messe und Ausstellungsgesellschaft mbH, S. 515 ff.
- /3/ H.C. van de Hulst: Light scattering by small Particles, John Wiley, New York, S. 131 ff.

figure 1.1

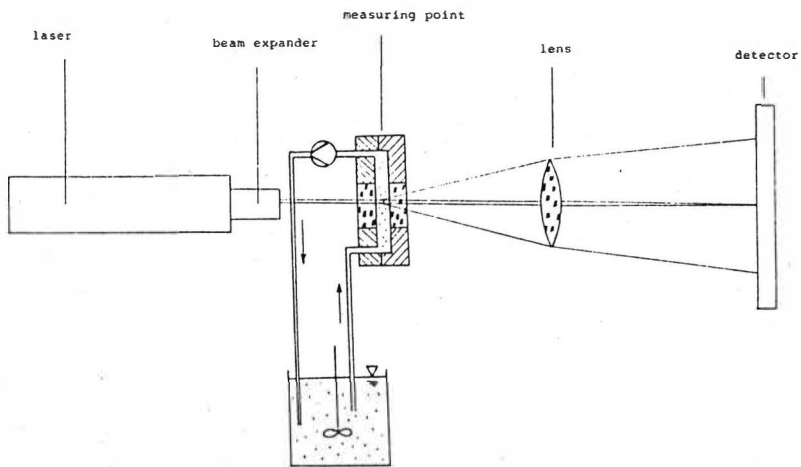
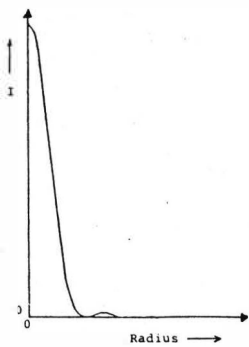
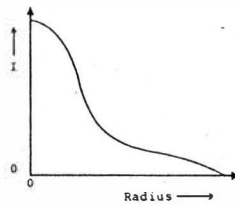


figure 1.2



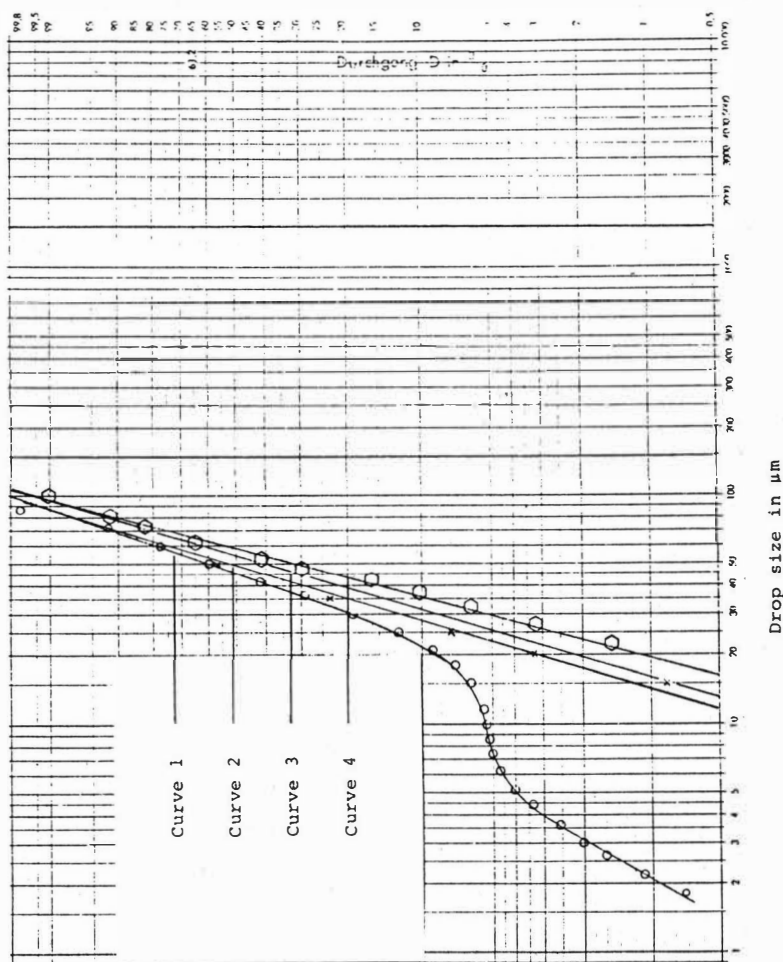
Intensity distribution
of mono-dispersed particles
over the radius



Intensity distribution
of poly-dispersed particles
over the radius

figure 2.

CUMULATIVE VOLUME



Studies on Phase Separation of Aqueous-in-Organic Dispersion in a Low-Voltage A.C. Electric Field

L.M. Su, Institute of Chemical Metallurgy, Academia Sinica,
Beijing, China

Investigations on the improvement of phase separation of aqueous-in-organic dispersion have been made using a low-voltage A.C. electric field generated by a pair or two pairs of electrodes placed in the settler of mixer-settlers of two different scales on three extraction systems.

1. Introduction

The phase separation of aqueous-in-organic dispersion i.e. organic continuous dispersion (OCD) of liquid-liquid extraction is generally more difficult than that of aqueous continuous dispersion (ACD). The dispersion separation can be improved by adding some special baffle sets into the settler, but the effects for OCD are usually not so good as those for ACD. So people tried to use some more powerful techniques in the settler to promote the phase separation of OCD.

The application of electric field has very good effects on the improvement of phase separation of OCD, but up to now, most of the electric field applied commercially or experimentally are all of high static D.C. or high-voltage A.C. (1-9). Besides, the electrostatic field is provided by an electric coalescer located between the mixer and the settler and the two poles consist of a high voltage electrode closed to the top cover of the coalescer and a metal plate settled into the aqueous phase (3-4).

In the present work, a low-voltage electric field was applied in the settler of a mixer-settler (MS) or a mixer-settler with double mixers in each stage (DMMS) to promote the phase separation of OCD for the purpose of enhancing the coalescence of conductive aqueous droplets, simplifying the construction of the unit, saving total costs and achieving much more operation safety. Some significant parameters that have not been reported in literatures, for instance, the position of electrodes in settler, distance between the two poles, combinations of multi-electrodes and the direction of electric field relative to fluid flow, etc, have also been investigated.

2. Analysis of phase separation process under the action of electric field

Similar to the phase separation process in the gravitative settler, the phase separation process under the action of electric field may still include the coalescences between droplets of the dispersed phase, agglomerations between the droplets and interface between the dispersed bulk phase and dispersion band. In addition to those mentioned above, the two coalescence processes both contain several steps, and under the rule of electric field the velocities of charged droplets moving forward to the centre of the electric field may be largely accelerated, the membrane of the organic continuous phase may be dragged and split-
ted intensely. So the frequencies of colliding and coalescing between the aqueous conductive droplets which were surrounded by two electric layers may be increased largely, even the coalescing steps may also be reduced and the whole phase separation process may be completed in a moment. If the electrodes were not coated with an insulating layer or if the intensity of the electric field was so strong that the aqueous droplets were made dispersed again rather than coalesced or the charged aqueous droplets formed into a string and arranged in a straight line, short circuit of electric field would occur and result in failure of the improving of the phase separation of OCD.

Experimental systems and their physical properties Table 1

Organic phase (% v)	aqueous phase (kg/m ³)	ρ_a (kg/m ³)	ρ_o	μ_a (kg/m·s)	μ_o	γ (kg/s ²)	λ_a (1/·m)	λ_o
D ₂ EHPA 29.2	CuSO ₄ Soln.	1012	856	0.106	0.376	3.8×10^{-3}	8.5×10^{-5}	1.1×10^{-9}
Kerosene 70.8	Cu 8							
D ₂ EHPA 29.2	NiSO ₄ Soln.	1156	828	0.176	0.272	1.9×10^{-3}	2×10^{-4}	1.1×10^{-9}
Kerosene 70.8	Ni 60.4							
P507 50	RECl ₃ Soln.	1046	887	0.136	1.356	14.9×10^{-3}	4.8×10^{-4}	1×10^{-9}
Kerosene 50	RE 25.8							

P507=2-ethylhexyl-phosphoric acid mono-2-ethylhexyl ester

RE=rare earths

D₂EHPA=P204

3. Systems, equipments and experimental methods

The systems tested and their physical properties are listed in Table 1. The experiments were carried out in the settler of a 0.001 m³ MS or a 0.01 m³ DMMS and the electrodes were made of nickel sheet coated with a perspex insulating layer. The experimental parameters such as properties of electric power, values of electric voltage, distance between the two poles, thickness of dielectric layer for the electrodes, position of electrodes placed in the settler, combinations of multi-elec-

trodes, directions of electric field relative to the fluid flow and extraction systems, etc. were varied in the experiment respectively. OCD was formed at the beginning of the test and then the aqueous dispersed phase was pumped into the mixer. The volumes of dispersion band or emulsion band (v) and the entrainments of aqueous in organic (z) were measured.

Effects of properties of electric field

Table 2.

electric field tested	P204/CuSO ₄ *		P204/NiSO ₄ *		P507/RECl ₃ **	
	v (ml)	z (ppm)	v (ml)	z (ppm)	v (ml)	z (ppm)
empty	160	294	181	264	> 6540	flooding
A.C. 40v	73	948	91		598	1679
D.C. 40v	6	1023	10	93	586	1037
A.C. 10v					515	2323
D.C. 10v					658	1525

* Small poles l/L 0 d/W 0.8 on 0.001m³ MS

** Mid poles " 0.6 " 0.3 on 0.01 m³ DMMS

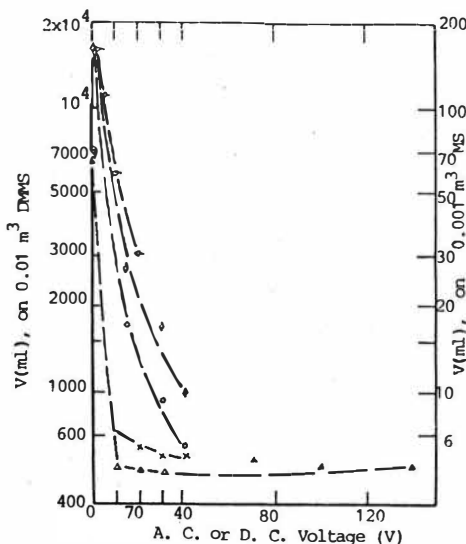


Figure 1 Effect of voltage values and properties of electric field on dispersion bands

- P204/NiSO₄ Open poles A.C.)*
 - ◇ P204/NiSO₄ enclosed poles D.C.}
 - P204/CuSO₄ enclosed poles D.C.}
 - × P507/RECl₃ enclosed poles D.C.)*
 - △ P507/RECl₃ enclosed poles A.C.}
- * on 0.001 m³ MS
** on 0.01 DMMS

4. Experimental results

4.1 The effects of properties and voltage values of electric field on phase separation of OCD

Experimental results shown in Table 2 and Figs. 1-3 illustrate:

(1) For the three extraction systems tested, a low-voltage electric field with a voltage below A.C. 220 V or D.C. 40 V may improve the

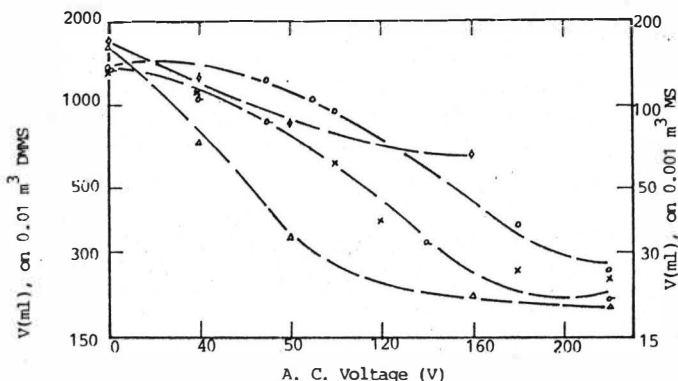


Figure 2 Effect of voltage values and properties of electric field on dispersion bands

▲ P204/CuSO₄ small poles } * ○ P204/NiSO₄ mid poles } **
 ◇ P204/NiSO₄ small poles } x P204/NiSO₄ mid poles }
 * on 0.001 m³ MS, ** on 0.01 m³ DMMS

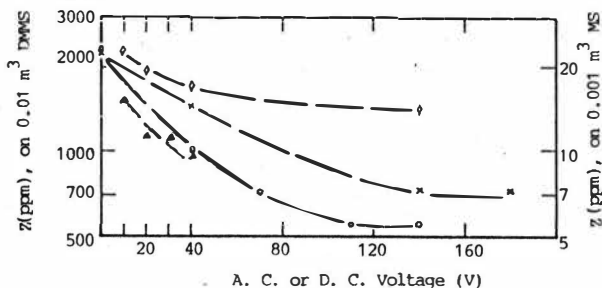


Figure 3 Effect of voltage values and properties of electric field on entrainments of aqueous in organic

○ P204/NiSO₄ A.C. ◇ P507/RECl₃ A.C.
 x P204/NiSO₄ A.C. △ P507/RECl₃ D.C.

* on 0.01 m³ DMMS, mid and enclosed poles

phase separation of OCD largely, and for P507/RECl₃ system the dispersion band (v) was reduced to less than one tenth, even though the voltage was lowered to A.C. 10 V or D.C. 10 V.

(2) Provided there were no variations in other parameters, the effects of D.C. field applied for decreasing the entrainments of aqueous in organic (z) were better than with A.C. field. But for the reduction of v , the effects of the application of D.C. field was similar to those with A.C. field for P507/RECl₃ system.

(3) Generally speaking, the v and z decrease with the increase of the

voltage, because an increase in voltage may cause intensification of electric field, thus enhancing the phase separation of OCD.

(4) The comparison of experimental results for P507/RECl₃ with those for P204/NiSO₄ or P204/CuSO₄ system indicated that the use of a low-voltage electric field for promoting the phase separation of OCD for P507/RECl₃ had much better effects than for P204/NiSO₄ or P204/CuSO₄ system, which may be explained by the following facts: Since the Pka of P507 (Pka=4.10), is higher than that of P204 (Pka=3.32) and the conductivity of RECl₃ solution is higher than that of CuSO₄ or NiSO₄ solution, leakage and short circuit of electric current in P507 are less than in P204 and moving velocities of aqueous droplets and colliding velocities between aqueous droplets in P507/RECl₃ are larger than in P204/CuSO₄ or P204/NiSO₄ system.

4.2 The effects of electrode sizes, insulating layer thickness of electrode and distance between the two poles tested on phase separation of OCD

The experimental results shown in Tables 3 and 4 and Figs. 4 and 5 indicate:

Effects of insulating layer thickness of electrodes Table 3

δ/δ_0	P204/NiSO ₄			P507/RECl ₃		
	Conditions tested	V (ml)	Z (ppm)	Conditions tested	V (ml)	Z (ppm)
1	mid poles	204	681	mid poles	485	1679
2	A.C. 220V 1/L	224	1080	A.C. 220V 1/L	526	1440
4	0.06 d/W	0.2	318	0.06 d/W	0.3	656

δ/δ_0 = relative thickness of insulating layer on 0.01 m³ DMMS

Effects of sizes of electrode 0.01 m³ DMMS 1/L 0.06 d/W 0.3 Table 4

Sizes of electrode tested	P204/NiSO ₄ A.C. 220 V		P507/RECl ₃ A.C. 220 V		D.C. 40 V	
	V (ml)	Z (ppm)	V (ml)	Z (ppm)	V (ml)	Z (ppm)
empty	1290	2375	> 6540	flooding	> 6540	flooding
small	298	905	609	1031	765	
mid	244	875	526	1440	586	1679
large	209	665	490	1939	526	2578

(1) V decreases with the decrease of insulating layer thickness (δ) of electrode, but z varies with δ , depending on the system tested (see Table 3). When $\delta=0$, i.e. open electrode used, v may be reduced to the minimum (refer to Figs. 1 and 2). It is, however, not practical for

the industrial production.

(2) V decreases with the increase of electrode dimension, but z varies with the systems and conditions tested (see Table 4). During the coalescence of droplets they generate many small droplets or hazes and are very difficult to coalesce again. So, if the intensity of the electric field is too strong, z may increase. When the intensity of the electric field is over certain limit, the chief rule of electric field is to disperse droplets rather than promoting coalescence. These viewpoints may well explain the results of z for P507/RECl₃ system tested.

(3) V decreases with the decrease of distance (d) between the two poles, but z increases with the decrease of d (see Figs. 4 and 5). The smaller the d is, the stronger the intensity of electric field will be. Therefore, too small d is not suitable for a lower z .

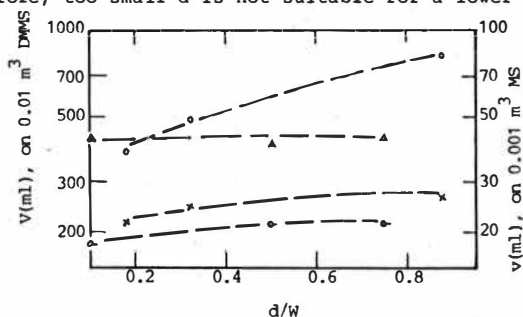


Figure 4 Effect of distance between two poles on dispersion bands

○	P204/CuSO ₄	A.C. 160 V	open poles	}	*
△	P204/NiSO ₄	D.C. 15 V	enclosed poles		
×	P204/NiSO ₄	A.C. 220 V	enclosed poles	}	**
○	P507/RECl ₃	A.C. 220 V	enclosed poles		

* on 0.001 m³ MS ** on 0.01 m³ DMMS

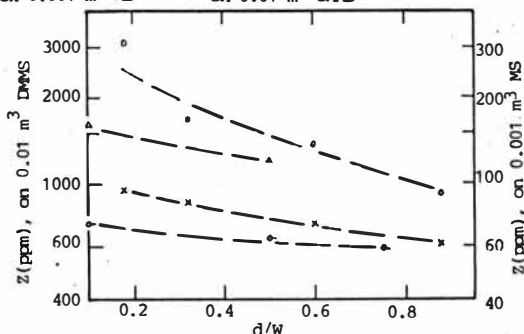


Figure 5 Effect of distance between two poles on entrainmentments of aqueous in organic

○	P204/CuSO ₄	A.C. 160 V	open poles	}	on 0.001 m ³ MS
△	P204/NiSO ₄	D.C. 15 V	enclosed poles		
×	P204/NiSO ₄	A.C. 220 V	enclosed poles	}	on 0.01 m ³ DMMS
○	P507/RECl ₃	A.C. 220 V	enclosed poles		

4.3 The effects of location of electrode and direction of electric field in the settler on phase separation of OCD

Experimental results illustrated in Tables 5 and 6 indicate:

- (1) It is not desirable to place the electrodes at the inlet for both v and z are large (see Table 5). At the inlet the action of electric field is interfered by the disturbance of flow, so the electrodes should better be placed near the inlet, instead of at the inlet.
- (2) When the location of electrode (1) is far from the inlet, v would become large and the larger the l is, the higher the v would be. It is well known that when the electric field is as close to the inlet as possible, its rule acts as early as possible that its effects to improve phase separation of OCD will be much better.
- (3) Comparison of the experimental results of two directions of electric field shows that as the electric field is vertical to fluid flow, v is smaller, but z is larger (see Table 6).

Effects of relative locations of electrode

Table 5

l/L	P204/CuSO ₄ * A.C. 160 V		P204/NiSO ₄ ** A.C. 220 V		P507/RBCl ₃ ** A.C. 220 V		A.C. 10 V	
	V (ml)	Z (ppm)	V (ml)	Z (ppm)	V (ml)	Z (ppm)	V (ml)	V (ml)
empty	160	294	1290	2375			76540	
0 (inlet)			595	830			1814	
0.06	21	1194	298	905	260	609	515	485
0.08					343	212		580
0.25					512	161		925
0.50	40	1251						
1.0	55	8508	note: d/w 0.3		d/w 0.9		d/w 0.3	

* A.C. 160 V 0.001 m³ MS ** A.C. 220 V 0.01 m³ DMS

Effects of directions of electric field relative to fluid flow

Table 6

electric field relative to fluid flow	P204/NiSO ₄ * Conditions tested			P507/RBCl ₃ ** Conditions tested		
	V (ml)	Z (ppm)	Z (ppm)	V (ml)	Z (ppm)	Z (ppm)
Parallel	A.C. 220 V 1/L 0.06 d/w 0.2	218	1040	two pair poles 1/L 0.06 d/w 0.3	562	1031
Vertical		170	1040		478	1939
Parallel	A.C. 220 V 1/L 0.06 d/w 0.3	742	1280	single pair poles 1/L 0.06 d/w 0.3	526	1525
Vertical		415	1930		485	1679

0.01 m³ DMS

* two pair poles

** A. C. 220 V

4.4 Comparison on the performance of the single and two-pair electrodes tested

The results are listed in Table 7 and show:

- (1) The two-pair electrodes can decrease v slightly and increase z obviously, but the case for P507/ RECl_3 system and D.C. field was right converse.
- (2) Considering the increasing extent for z and the decreasing extent for v and the intensity of electric field, an over-strong field is not suitable for phase separation. So the selection of compound electrodes must be very careful.

Comparison on the performances of the single- and two-pair poles Table 7

electrodes tested	P204/ NiSO_4 *				P507/ RECl_3 **		
	conditions tested	v (ml)	z (ppm)		conditions tested	v (ml)	z (ppm)
mid	{ 1/L d/W	0.06	244	1078	A.C. 220V	{ 526 478	1440 1939
mid + small		0.3	235	1330			
mid	{ 1/L d/W	0.06	204	681	D.C. 40 V	{ 586 725	1679 1207
mid + small		0.2	170	1040			
0.01 m ³ DMMS		* A.C. 220V	** 1/L 0.06	d/w 0.3			

5. Conclusions

- (1) A low-voltage D.C. field or A.C. field may largely improve phase separation of aqueous-in-organic dispersion, even though the voltage applied is as low as 10 V for certain systems, particularly the dispersion band may be reduced to less than one tenth.
- (2) In addition to the above, it has been found that there should be a proper location of a single-pair electrodes, a suitable distance between the electrodes, a desirable thickness of insulating layer for electrodes and a right direction of electric field.
- (3) An over-strong intensity of electric field is not suitable for phase separation of an organic continuous dispersion, so the selection of electrode dimension and number should be very careful.
- (4) For certain system, when constant voltage is applied, the D.C. field is more effective in decreasing the entrainments of aqueous in organic, but its effects are the same or less in reducing the dispersion band compared with A.C. field.

Nomenclature

- d distance between a pair of poles (m)
- l location of poles far from the inlet of settler (m)
- L length of settler (m)
- v volume of dispersion band or emulsion band (ml)
- w width of settler (m)
- z entrainment of aqueous phase in organic phase (ppm)

References

- (1) Bailes P.J. et al.; Chem. Eng. Res. Des. Vol.2,1, 33, (1984)
- (2) Martin L. et al.; Separation Science and Technology, 18 (14&15) 1455, (1983)
- (3) Bailes P.J. et al.; Trans. Inst. Chem. Eng. Vol.60, 2, 115, (1982)
- (4) Bailes P.J. et al.; Trans. Inst. Chem. Eng. Vol.59, 4, 229, (1981)
- (5) Bailes P.J. et al.; ISEC'74, Vol.2, 1011 (1974)
- (6) Shafik E.S. et al.; IEC Fundam. Vol.13, 2, 139 (1974)
- (7) Hanson C.; "Recent advance in liquid-liquid Extn." pergamon press, oxford, 505-510 (1971)
- (8) Brown A.H. et al.; Chem. Eng. Sci. Vol.23, 841 (1968)
- (9) Allan R.S. et al.; Trans. Farady Soc. Vol.57, 2027 (1961)

A.J. Melnyk and S. Vijayan, Atomic Energy of Canada Limited,
Whiteshell Nuclear Research Establishment, Pinawa, Manitoba, Canada ROE 1LO

Abstract

A horizontal configuration for a pulsed extraction column has been recognized as having a great potential in replacing vertical pulsed columns (VPC) in the separation of heavy elements in the nuclear industry. Published work examining the performance of the horizontal pulsed column (HPC) has been sparse to date, thus preventing the design of large-scale units. A research program was started in 1982 at the Whiteshell Nuclear Research Establishment to study the importance of hydraulic factors in the performance of the HPC.

The hydraulic experiments were carried out in a 0.075-m diameter by 1-m long column with a 'standard' perforated-plate cartridge using a 30% tributylphosphate + 70% Isopar M - 2 mol/L nitric acid system. The flooding experiments showed that the flooding capacity limitations can be represented in terms of a Sege-Woodfield type flooding diagram. The nature of this flooding diagram was found to be strongly dependent on both pulse amplitude and frequency independently, as well as on the coupled pulse effect represented by the pulse velocity. The phase flow ratio was found to have only a minor effect on the maximum total throughput. The influence of the physical properties of the systems on flooding capacity is also reported.

The effects of individual phase flow rates, and pulse amplitude and frequency on the dispersed-phase holdup and axial mixing, in both the organic and aqueous phases were examined. The aqueous phase was the dispersed phase in the majority of experiments. The holdup behaviour for different operating conditions exhibited trends similar to those observed for the VPC. Axial mixing in the aqueous phase, determined by a discrete-stage model, was negligible over the range of operating conditions studied. However, axial mixing in the organic phase was found to be significant, and the influence of operating variables is described. Measurements of the single-phase power dissipation were found to be adequately correlated by a quasi-steady-state power equation commonly used for the VPC.

Introduction

The horizontal pulsed column (HPC) has been identified as a possible alternative to the vertical pulsed column (VPC) in the reprocessing of nuclear fuels. The HPC appears to retain all the major advantages of the VPC, while offering the additional major advantage of substantially reduced shielding and associated building costs. The potential merits of the HPC were first realized in the early 1950s (1). The

original design of the HPC was flawed, however, due to the interdependence of individual extraction cells. This interdependence of cells caused the propagation of local disturbances throughout the column, which had the effect of severely reducing mass transfer efficiency (2). To overcome this problem, Thornton (3) developed a new plate configuration that allowed adjacent extraction cells to be hydrodynamically independent. This plate configuration design has been adopted as the standard by several investigators over the last three decades (4-7). Most of the published work to date has been in the form of preliminary investigations into the behaviour of the HPC. These results suggest that the column displays throughput capacity limitations similar to the VPC and has a higher mass transfer efficiency (7). However, there is insufficient published data regarding the operation of the HPC to allow proper scale-up of the column to industrial-scale units.

Experimental

A modified version of Thornton's design (3) was used in this study (see Figure 1). The column was 0.075 m in diameter by 1 m long and was divided into fourteen 0.05-m long extraction cells. Plate perforations were 3.2 mm in diameter, located only over half the plate, resulting in a net free area of 11.7% per plate. The systems studied and their physical properties are summarized in Table 1.

Throughput capacity measurements were made by determining the pulse frequency at which the column was observed to flood for a fixed total superficial velocity, phase flow ratio and pulse amplitude. Local holdup measurements were made by measuring the volume fraction occupied by each phase in every cell when all flows and pulsing action were terminated. Axial mixing was examined using two colourimeter probes to measure the transient response of a tracer injected into one of the phases. Power dissipation in the HPC was measured using the standard force-displacement hysteresis method (8).

Results and Discussion

Throughput Capacity

The throughput capacity limitations of the HPC were found to be well represented by a Sege-Woodfield flooding diagram as shown in Figure 2. The HPC behaved hydraulically as a mixer-settler under all stable operating conditions. However, the flooding curve could be divided into three distinct operating regions.

At low pulse velocities ($af < 0.006$ m/s), a 'Fully Separated Flow' (FSF) region was observed where both phases were completely stratified with no significant dispersion of either phase present. Flooding in this region appears to be due to

inadequate pulsation and is described by

$$U_A + U_0 = af \quad (1)$$

At mid-pulse velocities ($0.006 \text{ m/s} < af < 0.01 \text{ m/s}$), a small, but stable, dispersion band formed in the centre of the column. In this region, referred to as the 'Dispersion Transition' (DT) region, the throughput capacity reached a maximum. This maximum throughput (U_T^*) is dependent on the pulse amplitude, phase flow ratio, and physical properties of the system studied.

At high pulse velocities ($af > 0.01 \text{ m/s}$), a large stable dispersion band was observed, which occupied up to 70% of the total cell volume. In this region, referred to as the 'Pseudo-Dispersion' (PD) region, the total throughput decreased with pulse velocity. The flooding curve in this region is adequately correlated by

$$U_T = C_1(1 - \exp[(a - 0.0064)/C_2]) \cdot (af)^{C_3} \quad (2)$$

where $C_1 = 3.753 \times 10^{-7}$, $C_2 = -0.0077$ and $C_3 = -3.09$ for system 1. The exponent on the pulse velocity term, C_3 , was found to be independent of the system studied, whereas the other coefficients, C_1 and C_2 , were dependent on the physical properties of the system studied. Flooding in this region appears to be caused by the lack of stratification of the two phases, resulting in a large degree of internal recycling.

For low pulse amplitudes ($a < 0.02 \text{ m}$), the column flooded at high pulse frequencies ($f > 0.5 \text{ Hz}$) and, as a consequence, the period of one pulse cycle was small ($\tau < 2 \text{ s}$). Calculations based on the terminal velocity of droplets produced at these conditions indicate that there is insufficient time available for the droplets to settle to the two-phase interface in one pulse cycle. Consequently, these droplets are readily entrained in the reverse flow action, reducing the net throughput. At higher pulse amplitudes ($a > 0.02 \text{ m}$), the resulting lower pulse frequencies ($f < 0.5 \text{ Hz}$) provide a sufficient period of pulsation for the droplets to settle. At these pulse velocities, however, the droplets do not readily coalesce. This leads to a buildup of the dispersion band. It has been found that the pulse velocity at which the total throughput begins to decrease can be reasonably estimated by equating the residence time based on pulse velocity to the coalescence time obtained from correlations (9) for all systems studied. This mechanism explains the exclusive dependence of the flooding curve on pulse velocity at high pulse amplitudes. Anomalous regions in the flooding curve (range of pulse velocities for which throughput is constant) were also observed (see Figure 2). The location of these regions is correlated by

$$f = 0.184 (a)^{-0.43} \cdot (\Delta\rho/\rho_A)^{1/2} \quad (3)$$

Flooding curves were determined for a range of phase flow ratios from $U_A/U_0 = 7/1$ to $1/7$. The phase flow ratio was found to have no influence on the flooding curves in the FSF and PD regions. The phase flow ratio was found to influence the maximum throughput, U_T^* , with a minimum value for U_T^* observed at a $1/1$ phase flow ratio.

The effects of physical properties of the system were also studied. Generally, the throughput limitations of the column improved with increasing density difference and interfacial tension, as shown in Figure 3.

Dispersed Phase Holdup

The aqueous phase dispersed under all stable operating conditions. In this study, the total aqueous holdup was measured although the aqueous phase was present in three different states. One state consisted of a bulk aqueous layer located at the bottom of each cell. This aqueous layer was present for all stable operating regions and was the only state observed in the FSF region. In the DT and PD regions, the aqueous phase was also present as randomly dispersed droplets in the organic phase. A third state was found in the DT and PD regions, where aqueous droplets were present in a tightly packed dispersion band located between the aqueous- and organic-continuous regions. At high pulse velocities approaching flooding, this state appears to be the dominant contributor to the total holdup.

The total aqueous holdup was constant throughout the pulse cycle although the contributions from the above described states varied. The local cell holdup did not vary significantly throughout the column from cell to cell. Consequently, an overall average total holdup, $\bar{\theta}_T$, was used to correlate the effects of the operating variables on holdup. The resulting correlation for system 2 is

$$\bar{\theta}_T = 0.698 \alpha^{-0.534} \cdot f^{-0.3717} \cdot U_A^{0.576} \cdot (1 + U_0/U_A)^{0.3098} \quad (4)$$

The average holdup varied from 0.16 to 0.50 over the range of operating conditions studied. Although not reflected in equation (4), a slight increase in holdup was observed at high pulse velocities prior to flooding. The form of equation (4) is similar to that used by Kumar and Hartland (10) to correlate the dispersed phase holdup in the mixer-settler region of operation for the VPC.

Axial Mixing

Axial mixing results obtained from transient tracer response curves were analyzed by a discrete-stage backflow model (11). A backflow coefficient (α) was determined by performing a non-linear least-squares regression analysis to determine the best statistical parameter estimate. An approximate relation between the backflow and dispersion coefficients can be shown to be (11)

$$E_1 = U_1 \alpha_1 S_p \quad (5)$$

Experimental results indicate that axial mixing is not an important factor in the aqueous phase (dispersed phase). Statistically significant backflow coefficients, were only found at low aqueous flowrates ($U_A < 0.00125$ m/s) and low pulse velocities ($af < 0.004$ m/s). The largest aqueous backflow coefficient measured was 0.695. This corresponds to a dispersion coefficient (E_A) of about 3.9×10^{-5} m²/s. As opposed to the dispersed phase, axial mixing in the continuous phase (organic phase) was found to be significant. Backflow coefficients as large as 25.4 (or $E_O = 1.8 \times 10^{-3}$ m²/s) were obtained. The organic-phase backflow coefficient was a strong function of pulse amplitude, frequency, and the organic flowrate, but independent of aqueous flowrate. The relative dependency of these terms is demonstrated in the following correlation:

$$\alpha_O = 0.426 \cdot a^{2.74} \cdot f^{1.04} \cdot U_O^{-2.03} \quad (6)$$

Power Dissipation

Power dissipation due to pulsation in the HPC was studied for three different single phases (water, dodecane and 30% TBP + 70% isopar M), with and without external flows. It was found that the average power dissipation ($\bar{\psi}$) was insensitive to single-phase flow and, thus, adequately described in terms of the pulse amplitude and frequency.

The average power dissipation in pulsed and reciprocating plate columns is usually estimated from a quasi-steady-state model for frictional losses (12) by the following expression:

$$\bar{\psi} = \frac{2\pi}{3} \rho n A_C \frac{1-\epsilon}{C_0 \epsilon} (af)^3 \quad (7)$$

Using an orifice coefficient (C_0) determined from steady-state pressure-drop experiments, it was found that the predicted power dissipation from equation (7) was consistently greater by 5 to 20% than the experimentally measured power dissipation (see Figure 4). However, the general trend describing the influence of pulse velocity given in equation (7) was in good agreement with experimental data over the range of stable operating conditions as dictated by the flooding curves. At high pulse frequencies, a sudden drop in the measured power dissipation was observed (Figure 4). The frequency (f_c) corresponding to this drop in power dissipation was dependent on the pulse amplitude:

$$f_c = 0.184 a^{-0.43} \quad (8)$$

This minimum power dissipation appears to be due to the formation of turbulent eddies that may absorb and release the energy imparted on the fluid by the pulser. It is interesting to note that the characteristic frequency (equation (8)) appears to be related to flooding anomalies by a $(\Delta\rho/\rho_A)^{1/2}$ ratio (equation (3)). This ratio is common to hydraulic models for horizontal two-phase flow systems (13). The cause for the observed flooding curve anomalies is not presently understood, although it is speculated that these anomalies might be attributed to a Kelvin-Helmholtz type instability phenomenon (13).

Conclusions

- (1) The throughput capacity limitations of the HPC can be represented by a Segewoodfield type flooding curve similar to that used for the VPC. The flooding curve can be divided into three regions: a Fully Separated Flow region at low pulse velocities, a Dispersion Transition region at mid-pulse velocities, and a Pseudo-Dispersion region at high pulse velocities.
- (2) Flooding at low pulse velocities is due to inadequate pulsation. Flooding at high pulse velocities is due to lack of stratification of the two phases caused by either (a) insufficient time for droplets to settle to the interface at high pulse frequencies ($f > 0.5$ Hz) or (b) insufficient time for droplets to coalesce at low pulse frequencies ($f < 0.5$ Hz).
- (3) The flooding curve is strongly influenced by the physical properties of the system in the mid- to high-pulse velocity regions.
- (4) The total aqueous holdup is constant throughout the column and consists of three components: (a) a bulk, aqueous, continuous layer, (b) randomly dispersed, aqueous droplets in the organic continuous region, and (c) a tightly packed, dispersion band.
- (5) Axial mixing in the dispersed phase (aqueous phase) is negligible, while axial mixing in the continuous phase (organic phase) is significant and is adequately correlated.
- (6) Experimentally determined, time-averaged power dissipation is 5 to 20% lower than the value predicted from a quasi-steady-state model.
- (7) An anomaly in the form of a minimum power dissipation occurs at a characteristic frequency, which is a function of pulse amplitude. This anomalous behaviour appears to be related to the flooding curve anomaly.

Acknowledgement

The authors gratefully acknowledge Mr. M.D. Pellow for his assistance with the experiments. Results presented in this paper are part of a doctoral thesis being submitted by A.J. Melnyk to McMaster University, Hamilton, Canada.

Nomenclature

A_C	- cross sectional area (m)	$\bar{\psi}$	- power dissipation (W)
a	- pulse amplitude - full stroke (m)	S_p	- plate spacing (m)
af	- pulse velocity (amplitude-frequency products, m/s)	U^p	- superficial velocity (m/s)
C_0	- orifice coefficient	α	- backflow coefficient
E	- dispersion coefficient (m/s)	γ	- interfacial tension (mN/m)
f	- pulse frequency (Hz)	ϵ	- plate-free area
n	- number of plates	\emptyset	- aqueous phase holdup
		ρ	- density (kg/m)

Superscripts

$\bar{\quad}$	- average value
*	- maximum value

Subscripts

A	- aqueous phase
O	- organic phase
T	- total

References

- (1) Olney, R.B., Methods and Apparatus for Contacting Fluids, U.S. Patent No. 2,629,654 (1953).
- (2) Schneider, H., Proposed New Design for a Liquid-Liquid Contactor, California Research and Development Co., Livermore, U.S.A., Report No. LWS-2460 (1952).
- (3) Thornton, J.D., Improvements in or Relating to Methods and Apparatus for Contacting Liquids, British Patent No. 39899/57 (1957).
- (4) Logsdail, D.H. and J.D. Thornton, J. Nucl. Energy, Part B, Reactor Technology, 1, 15 (1957).
- (5) Meznik, F. and V. Sraier, Ceskoslav. Akad. Ved., Rez/Prague, Czech. UJV-1919 (1967).
- (6) Vdovenko, V.M. and S.M. Kulikov, Radiokhimiya, 8, 525 (1966).
- (7) Cermak, A.F., Contactors for a Nuclear Fuel Reprocessing Plant, Development of the Horizontal Pulsed Column, Paper presented at the 2nd World Conference of Chemical Engineering, Montreal, Canada, October 1981.
- (8) Hafez, M.M. and M.H.I. Baird, Trans. I. Chem. Eng., 56, 229 (1978).
- (9) Smith, D.V. and G.A. Davies, A.I.Ch.E. Symp. Ser., 68, 124 (1972).
- (10) Kumar, A. and S. Hartland, Chem. Eng. Res. Des., 61, 285 (1983).
- (11) Wen, C.Y. and L.T. Fan, Models for Flow Systems and Chemical Reactors, Marcel Dekker, New York, 1975.
- (12) Jealous, A.C. and R.F. Johnson, Ind. Eng. Chem., 47, 1159 (1955).
- (13) Taitel, Y. and A.E. Dukler, A.I.Ch.E. J., 22, 47 (1976).

Table 1. Summary of Physical Properties

System No.	Description	ρ_0 (kg/m ³)	ρ_A (kg/m ³)	$\Delta\rho$ (kg/m ³)	γ (mN/m)	μ_A (mPa·s)	H_0 (mPa·s)
1	30% TBP + 70% Isopar M -Distilled Water	833.6	997.0	163.4	10.8	0.89	2.69
2	30% TBP + 70% Isopar M -2.0 mol/L HNO ₃	849.1	1055.3	206.2	11.5	0.92	2.59
3	Dodecane -Distilled Water	746.1	997.4	251.3	52.4	0.89	1.35

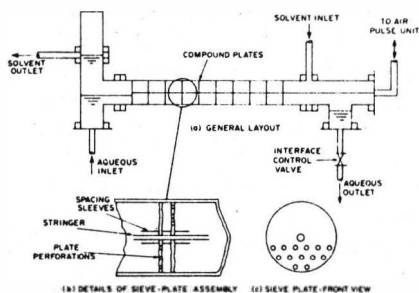


FIGURE 1: A Schematic of the Horizontal Pulsed Column

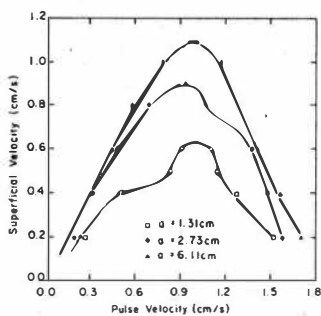


FIGURE 2: Effect of Pulse Amplitude on Throughput Capacity

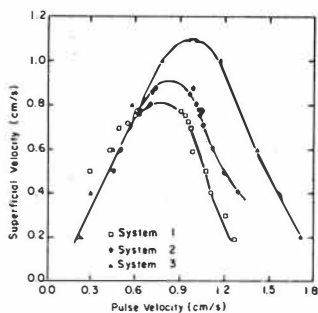


FIGURE 3: Effect of Physical Properties on Throughput Capacity

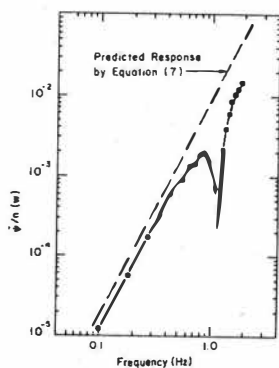


FIGURE 4: Effect of Frequency on Power Dissipation

ON THE MODELLING OF THE TWO-PHASE FLOW IN SOLVENT EXTRACTION COLUMNS

Radionuclide RTD-Analysis as a tool for diagnostics and optimization

A. Merz, J.J. Porta and R. Walter

Kernforschungszentrum Karlsruhe GmbH / F.R.G.

INTRODUCTION

This report is concerned with the dual problem of generating and analyzing data in experimental investigations in the quest for a suitable mechanistic model for the fluid dynamics of two-phase flow in pulsed extraction columns. The one-dimensional axial dispersion model is still often used for the description of the two-phase fluid dynamics in solvent extraction apparatus, although physical considerations cast considerable doubt on this approach /1-4/.

In the dispersed phase of a solvent extraction column we have a population of coalescing, partial coalescing and non-coalescing droplets moving counter-current to the continuous phase. Different-sized droplets will move with different velocities through the active column length and will have different residence probabilities in contradiction with the most basic assumption of the dispersion model.

One essential hurdle for an improvement in the understanding of local fluid-dynamical phenomena is frequently the lack of adequate diagnostic measurement methods. This is specially important for the identification of the dispersed phase.

The experimental findings reported in this paper result from RTD-experiments using radiotracers. For this purpose the radiotracing techniques were adapted to the specific requirements of the PUREX system (TBP-kerosene/nitric acid). This system is of capital importance for the reprocessing of nuclear fuel.

RADIONUCLIDE DIAGNOSTICS

A radionuclide diagnostic method was developed and applied in conjunction with a computer-controlled multi-detector measuring system. By these means, the flow patterns and the axial phase distribution can be followed on-line without disturbing the process.

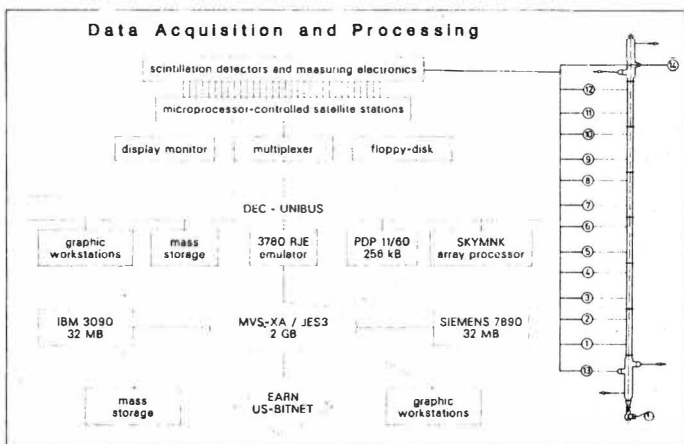


Figure 1. Data acquisition system for radiotracer experiments in solvent extraction columns

The upper half of Figure 1 shows schematically the digital data acquisition system. The system was designed for a maximum of 32 scintillation detectors. The experimental data can be stored in real time on floppy-disk or mass-storage devices of a PDP-11/60 process computer. This machine can also be used for the first data processing steps. For this objective special array processing hardware is used in parallel. The PDP machine is connected as RJE-station to the mainframe computers of the Karlsruhe Nuclear Research Center. Time and memory consuming extensive mathematical computations (model parameter estimation, deconvolution operations, statistical analysis) /5/ can by means of this LAN concept be distributed to different processors, thus enabling a rapid solution of the problem.

Radiotracer compounds and special irradiation techniques were developed for the specific labeling of the organic phase (TBP-kerosene). F-18 perfluor-

carbon compounds (perfluorbenzene and perfluorkerosene), as well as radioiodine-labeled dodecane /6/, were found to be suitable tracers for the organic phase. For the radiotracing of the aqueous phase (nitric acid) generator-produced radioisotopes were used ($^{87}\text{-Y}/^{87\text{m}}\text{-Sr}$, $^{113}\text{-Sn}/^{113\text{m}}\text{-In}$).

The radiotracers were injected into the feed stream for the corresponding phase. Injection points along the active column were available for special investigations of radial mixing effects.

Basic two-phase flow phenomena and specific problems of plate geometry were investigated on a test facility (pulsed plate column: 100 mm i.d., 6 m active length) with equilibrated phases to assure the absence of mass-transfer effects. Corresponding measurements under mass-transfer conditions on industrial columns are reported in /7/.

RTD-ANALYSIS

Model comparison

Considering the extraction column, as a first approximation, as a linear time-invariant ergodic system, the weighting function $E(t)$ describes its fluid-dynamical behaviour. Unexpected effects, not covered in the model (i.e. entrainment, tailing, etc) may be thus identified. The system weighting function can be evaluated by means of DFT deconvolution techniques.

Most authors try to stabilize the ill-posed deconvolution problem by fitting a parametrized model to the data and optimizing these parameters (i.e. Bodenstein number or dispersion coefficients) over iterative convolution. Here there is the dilemma that serious errors can result if the number of degrees of freedom is too small (because of an inadequate model) or too large (because of instability of the solution to noise /5/.

Figure 2 shows the system weighting functions $E(t)$ evaluated from radionuclide RTD experiments for the organic dispersed and aqueous continuous phase respectively.

The input-output signals correspond with the detectors represented on Figure 1. The experimental conditions (total flow rate $\dot{V}_o + \dot{V}_a = 200$ l/h, phase flow ratio $\dot{V}_o/\dot{V}_a = 5.5$, amplitude $A = 8.4$ mm, puls frequency $f = 1.75$ Hz, 25°C) correspond to the central point of the experimental design /5/. Figure 3 shows a comparison of the system weighting functions $E(t)$ with the probability distribution function of the 2-parameter axial dispersion model

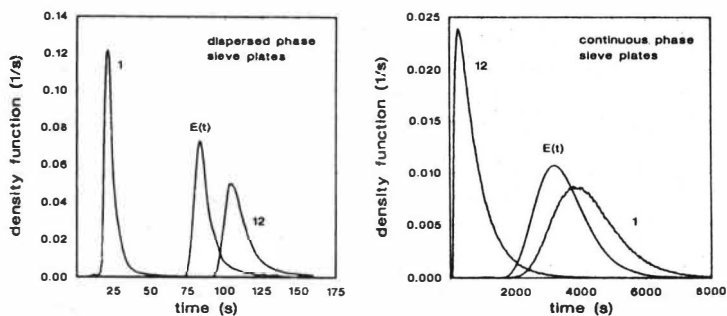


Figure 2. Deconvolution of radiotracer signals

(DM) and the log-normal distribution model (LN). The latter is reported to be able to describe pulsating blood flow /8/ as well as rising bubbles in gas-liquid columns /4/. As seen from Figure 3 the fluid dynamics of the dispersed phase can also be well approximated by this stochastic model. The weakness of the constant-coefficients axial dispersion model become thus evident: A better fit of the model parameters to the weighting function is not possible. On the other side (see Figure 5) both models can well describe the phenomena in the continuous phase. In this case convective transport effects dominate in relation to the much smaller dispersion effects. This good description for the continuous phase should although not be taken as a validation of the axial dispersion model for the description of two-phase fluid dynamics in pulsed columns.

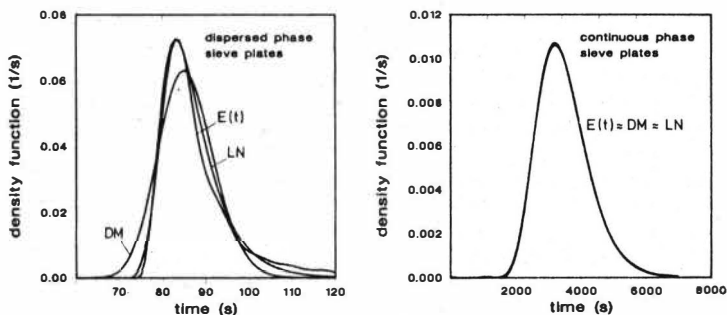


Figure 3. Model comparison

Special problems of axial and radial mixing

The lack of knowledge on the radial mixing and the effects of backmixing of the continuous phase at the fluid interphase in the settler chamber are fundamental causes for the uncertainty in the scale-up of extraction columns. These aspects have been neglected in the fluid dynamic modelling of columns because of the considerable higher sophistication of the mathematical methods involved therein.

These questions were investigated on a pulsed column with nozzle and sieve plates respectively (see Figure 5).

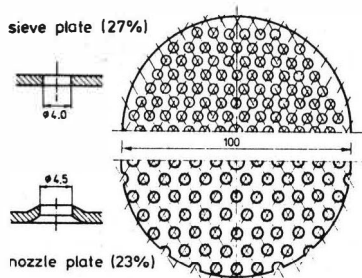


Figure 4. Plate geometry

The column was equipped with 60 nozzle and 61 sieve plates with a constant spacing of 50 mm.

The results obtained from two radiotracer experiments (dispersed phase σ_d , continuous phase σ_c) are presented by the mean values $\bar{\nu}$ of the measured RTD. The influence of the plate geometry on the behaviour of the dispersed phase is evident. The drop size distribution with nozzle plates is finer as the one with sieve plates. Because of this fact the mean droplet rise velocity $\bar{\nu}_0$ is smaller, the hold-up larger and the axial mixing more intensive. The statistical parameters were determined by means of the system weighting function between detector positions 1 and 6, and 7 and 12 respectively. The plate geometry shows almost no effect on the fluid dynamics of the continuous phase. The latter will be although intensively backmixed by the rising bubbles of the dispersed phase. The RTD of the continuous phase in the liquid settler interphase (detector 14) can thus be well described by an ideal mixed vessel /9/. This fact can be of crucial importance for the

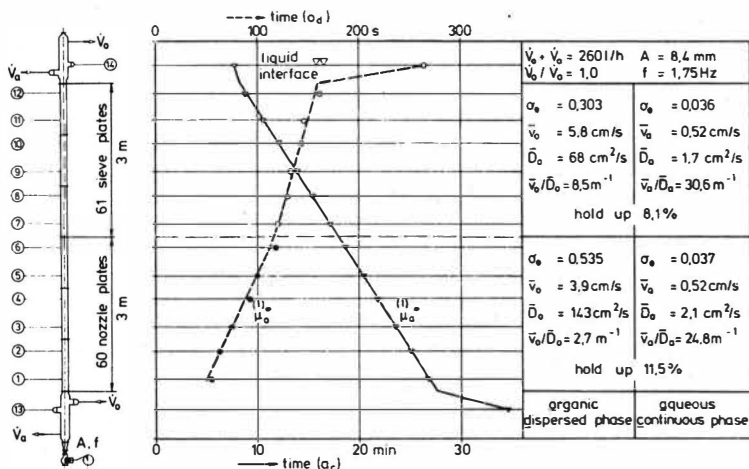


Figure 5. Effect of the plate geometry on the fluid dynamics

extraction of uranium from the continuous into the dispersed phase (i.e. /7/). Two clearly different fluid-dynamical regions must be considered here: the active column and the region up to the liquid interphase.

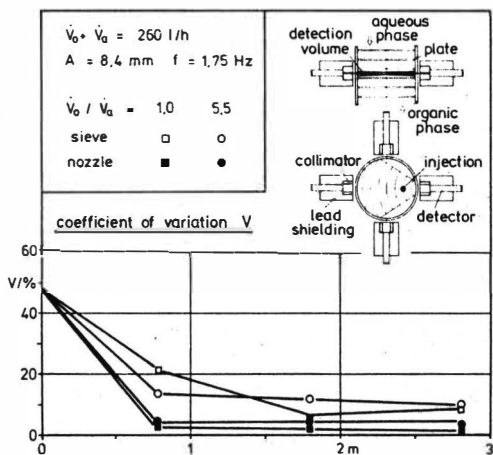


Figure 6. Radial mixing effects

The quality of radial mixing was further investigated. Up to now this problem has only been taken into consideration for the design of large industrial columns /7,10/. The influence of plate geometry had not been up to now evaluated. This problem was investigated in this experimental program too. With the experimental arrangement shown in Figure 6 detectors were installed at the measuring levels 2,4,6 and 8,10,12 respectively (see Figure 5).

Channeling effects were simulated by means of excentric tracer injections. Radial mixing effects of the plate geometry could thus be studied.

The variation coefficient along the flow path can be considered as a characteristic measure of plate homogenization effects /9/. Starting with a calculated asymmetry of 48% (see Figure 6), nozzle plates show a better radial mixing effect than sieve plates. The reason for this behaviour can be seen on a finer distribution of the droplet phase and a larger residence time between two adjacent plates. The lack of radial mixing is also, according to this result, a plate-specific problem. This may also have in slim columns an increase of the necessary extraction length as a consequence.

BIBLIOGRAPHICAL REFERENCES

- /1/ Levenspiel, O. and Fitzgerald, T.J.: Chem.Eng.Sci.38 (1983)489
- /2/ Hatton, T.A. and Lightfoot, E.N.: Chem.Eng.Sci. 37 (1982) 1289
- /3/ Schuegerl, K.: Fortschr.-Ber. VDI-Z., Reihe 7, Nr.8 (1968)
- /4/ Kurtin, M. and Molerus, O.: Chem.-Ing.-Tech. 58 (1986) 252
- /5/ Porta, J.J. and Merz, A.: ISEC '86 Proceedings
- /6/ Porta, J.J. et al.: Ger. Pat. DE 3346723 A1
- /7/ Eiben, K. et al.: ISEC '86 Proceedings
- /8/ Wise, M.E.: Acta Phys. Pharm. Neerlandica 14 (1966) 175
- /9/ Merz, A.: KfK-Nachr. 18 (1986) 2
- /10/ Zimmermann, H. et al.: Chem.-Ing.-Tech. 75 (1985) 540
- /11/ Merz, A. and Zimmermann, H.: ANS Fuel Reprocessing and Waste Management, Proceedings (1984) ISBN 0-89 448-118-5

EMULSION BAND THICKNESS IN A CENTRIFUGAL SETTLER

by

M. E. Hodges

E. I. du Pont de Nemours and Company
Savannah River Laboratory
Aiken, SC 29808

To properly design centrifugal settlers, an estimate of the emulsion band thickness is required. Emulsion band thickness can be easily estimated at the maximum throughput for a centrifugal settler since at those conditions the emulsion band completely covers the area between the heavy and light liquid exit weirs.

The emulsion band thickness is a function of liquid densities, interfacial tension, rotor speed, and rotor dimensions. For emulsion band thickness to be characterized in terms of these variables, it must be estimated at conditions other than at the maximum throughput.

Centrifugal settlers of the type used at the Savannah River Plant use air pressure in a chamber containing a series of weirs to control placement of the interface within the settler. Determination of the air pressures at which aqueous material just starts to flow over the organic weir and at which organic material just starts to flow over the aqueous weir provides a means of estimating band thickness over a wide range of operating conditions. This paper presents a correlation of calculated emulsion band thicknesses with operating variables.

This work was done under Contract No. DE-AC09-76SR00001 with the U.S. Department of Energy.

An abstract of a paper proposed for presentation at the
ISEC '86 International Solvent Extraction Conference
Munich, FRG
September 11-16, 1986

and for publication in the proceedings

This paper was prepared in connection with work done under Contract No. DE-AC09-76SR00001 with the U.S. Department of Energy. By acceptance of this paper, the publisher and/or recipient acknowledges the U.S. Government's right to retain a nonexclusive, royalty-free license in and to any copyright covering this paper, along with the right to reproduce and to authorize others to reproduce all or part of the copyrighted paper.

LIQUID-LIQUID-SOLID CONTACTORS FOR SHORT AND LONG RESIDENTIAL TIMES

ZHU Jia-Wen, LI Jo-Kang and SU Yuan-Fu (Y.F. SU)

East China Institute of Chemical Technology, Shanghai, China

Some of liquid-liquid contactors can be applied to the system containing solids. Therefore, possibilities exist also for their uses in leaching, slurry extraction and LEACHEX (leaching and extraction being carried out simultaneously)⁽¹⁾ which has been demonstrated feasible and efficient in certain systems. Because there exists relative large amount of solid particles besides the organic and aqueous phases, the conventional designs of the extraction equipment have to be modified to meet the operation requirement. The present authors used the design of RDC for short residential time and the RTL contactor for long residential time of liquid-liquid-solid contacting. The results of hydrodynamic studies are reported as follows.

A. THE RDC FOR SHORT RESIDENTIAL TIME

The RDCs are in use world wide and have been investigated by a large number of researchers. It is said that the RDC can be applied for systems with one solid phase and one or two liquid phases. This type of equipment was chosen to treat systems containing an organic phase and an aqueous phase which carries a relatively high content of solids. Preliminary test indicated that when solid particles had an average diameter $1.3 \times 10^{-4} \text{m}$ and a density 2640kg/m^3 , the particles could not pass the column freely but deposited on the stator rings. Therefore, the rotors were modified by welding three narrow strips to each of the lower surfaces of rotating discs so that the stirring intensity might be enhanced and all the solid particles could pass through the column together with the continuous heavy phase in tortuous path quite freely provided that the rotor speed exceeds 5s^{-1} . As the rotors so modified behave more or less like open turbine impellers, the column is named "Open Turbine Rotating Disc Contactor" or OTRDC.

The OTRDC Column

A typical compartment of OTRDC is shown in Fig. 1. Its structural dimensions is given as follows:

Column diameter D	0.050m
Compartment height H _p	0.025m
Diameter of disc D _R	0.028m
Width of paddle	0.002m
Number of paddles	3
Stator ring opening D _g	0.030m
Total height of column	1.025m
Number of compartments	41

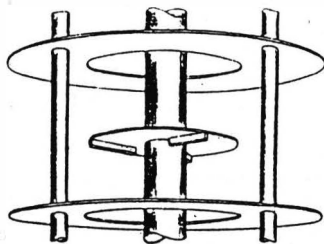


FIG. 1 A Typical Compartment of OTRDC

Systems Used

1. Liquid-liquid system:

Phase	Material	Velocity U, m/s	Rotor Speed, s ⁻¹
Continuous (c)	Deionized water	0.914 - 2.875×10^{-3}	4.17 - 9.83
Dispersed (d)	Kerosene	0.799 - 2.920×10^{-3}	
Solute	Butyric Acid		

2. Liquid-liquid-solid System

Sand was used in liquid-liquid-solid experiments. Its av. diameter is $1.3 \times 10^{-4} \text{ m}$ and density is 2640 kg/m^3 . The ratio of solid to continuous phase varied from 0.151 to 0.348 (by weight). Other parameters are shown as follows.

Phase	Material	Velocity U, m/s	Rotor Speed ω^{-1}
Continuous (c)	Deionized Water	$1.372 - 2.780 \times 10^{-3}$	5-8
Dispersed (d)	Kerosene	1.262×10^{-3}	
Solid (s)	Sand		

Result and Discussion

1. Liquid-liquid System

Characteristic Velocity U_0 and Dispersed Phase Hold-up h

Characteristic velocity U_0 was first correlated with Froude number $Fr = D_R^2 \omega^2 / g$, physical properties and the column geometry by Logsdail, Thornton and Fratt⁽²⁾. Then Kung and Beckmann⁽³⁾, Laddha et al.⁽⁴⁾ and Zhang, Ni and Su⁽⁵⁾ studied the same problem and observed there exist different hydrodynamic regions demarcated by critical rotor speeds (or critical Fr).

From experimental data on OTRDC a plot of $U_d + U_{ch}/(1-h)$ vs. $h/(1-h)$ for different rotor speeds all gives straight lines passing through the origin. And the characteristic velocities thus obtained have been correlated as follows:

$$U_0 / (\sigma \Delta \rho / \rho_c^2)^{0.25} = a (Fr^{-1} \psi^b)^p \quad (1)$$

where σ is interfacial tension, $\Delta \rho$ is density difference, ρ_c is density of continuous phase, $\psi = (\sigma^3 \rho_c / \mu_c^4 g)^{0.25} (\Delta \rho / \rho_c)^{0.6}$ and μ_c is viscosity of the continuous phase.

For the cases of no mass transfer:

Region I, $a = 0.374$, $p = 0$, when $Fr^{-1} \psi > 717$;
 Region II, $a = 4.12 \times 10^{-4}$, $b = 1$, $p = 1.04$ when $Fr^{-1} \psi < 717$.

For the cases with mass transfer:

Region I, both c \rightarrow d and d \rightarrow c directions of transfer,
 $a = 0.402$, $p = 0$, when $Fr^{-1} \psi^{1/2} > 85$;
 Region II,
 c \rightarrow d direction, $a = 6.82 \times 10^{-3}$, $b = 1/2$, $p = 0.915$, when $Fr^{-1} \psi^{1/2} < 85$;
 d \rightarrow c direction, $a = 14.4 \times 10^{-3}$, $b = 1/2$, $p = 0.742$, when $Fr^{-1} \psi^{1/2} < 85$.

These results are shown in Fig. 2 and Fig. 3. From these figures it has been observed that the existence of two regions divided by "critical" point is apparent. And due to the Marangoni effect, the exponent p for direction d \rightarrow c is lower than direction c \rightarrow d in region II.

Axial Mixing

The pulse-inject and response method was used to determine the axial mixing in OTRDC. The results were correlated by using optimum method.

Continuous phase axial mixing,

$$E_c(1-h)/H_T U_c = 0.5 + 0.0235 [D_R N(1-h)/U_c]^{0.928} [(U_d + U_c)/U_c]^{0.563} \quad (2)$$

As it is in RDC⁽⁵⁾, the influence of apparent velocity of dispersed phase U_d on the continuous phase axial mixing could not be neglected.

The comparison of the continuous phase axial mixing in OTRDC with that in RDC is shown in Fig. 4. With increasing rotor speed, the eddy diffusion

coefficient E_c in OTRDC will increase more rapidly than that in RDC. But within the lower rotor speed region for ordinary operating conditions of OTRDC, the difference of E_c between OTRDC and RDC is not significant.

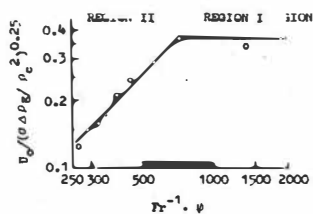


FIG. 2 Correlation of U_0 - no Mass Transfer

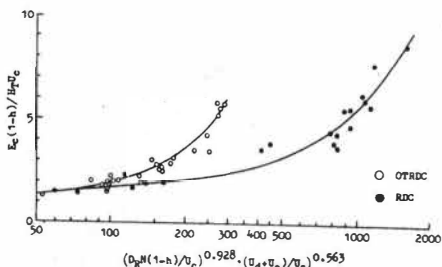


FIG. 4 Continuous Phase Axial Mixing

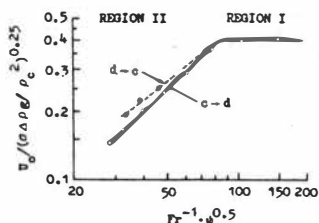


FIG. 3 Correlation of U_0 - with Mass Transfer

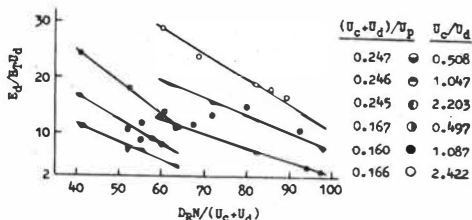


FIG. 5 Dispersed Phase Axial Mixing

Dispersed phase axial mixing,

$$E_d/HU_d = 20.3 [(U_c + U_d)/U_p]^{-0.355} (U_c/U_d)^{0.440} - [(U_c + U_d)/U_p]^{0.610} (U_c/U_d)^{0.364} D_p H / (U_c + U_d) \quad (3)$$

where $U_p = 1.55 \times 10^{-2}$ m/s is a parameter corresponding to the throughput and the physical properties of materials.

It is interesting that the eddy diffusion coefficient E_d decreases with increasing rotor speed, see Fig. 5. Because this phase is dispersed in the continuous phase as droplets, the use of diffusion model is considered appropriate. The axial mixing seems to be determined by drop size distribution. With increasing rotor speed the drop size of the dispersed phase becomes uniform and drop velocity profile flattens, so the apparent E_d decreases.

2. Liquid-liquid-solid System

As stated before, when the rotor speed is higher than 5 s^{-1} , the solid particles can pass through the column freely. At high rotor speed the flow pattern of solid particles becomes turbulent, which can be visible to the naked eyes.

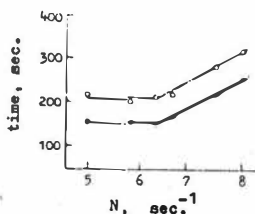
Solid phase Residential Time and Axial Mixing

It has been observed that the relationship between residential time of solid

in column and the rotor speed is separated into two regions:

- Region 1 (low speed) in this region the residential time is independent of the rotor speed (or Fr).
- Region 2 (high speed) the residential time increases with increasing rotor speed (Fig. 6).

By tracer method it was observed that the moving rate of solid U_s relative to the heavy continuous phase $[U_s - U_c / (1-h)]$ will not change if the rotor speed is fixed. The correlation of these two regions are gives as follows (see Fig.7):



flow rate		
$L(m^3/s)$	$V(m^3/s)$	$S(kg/s)$
○ 2.54×10^{-6}	2.34×10^{-6}	8.83×10^{-4}
● 5.14×10^{-6}	2.34×10^{-6}	8.83×10^{-4}

FIG. 6 Residential Time of Solid Phase in Column

- Region 1, $[U_s - U_c / (1-h)] / U_t = 0.265(S / \rho_s L) - 0.23$, when $8.7 < Fr^{-1} < 14$;
- Region 2, $[U_s - U_c / (1-h)] / U_t = 0.00632 Fr^{-2} - 0.03$, when $Fr^{-1} < 7.9$ (4)

where U_t is the mean settling velocity of solid particle (m/s); S the flow rate of solid phase (kg/s); L the heavy phase flow rate (m^3/s) and ρ_s the density of solid (kg/m^3).

The axial mixing of solid phase approaches constant when the rotating speed of disc is high. It seems that it is determined mainly by the particle size distribution.

Influence of Solid on Liquid Phase Behaviors

It has been found that the influence of the presence of solid phase on liquid phase behaviors can not be neglected.

Due to the stirring action of solid particles, the dispersed phase hold-up is higher than the simple liquid-liquid system even when the rotor speed is low. And the characteristic velocity U_0 is lowered by the presence of solid. These results are shown in Fig. 8.

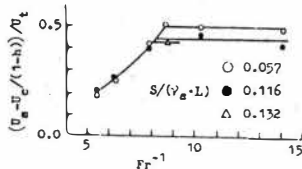


FIG. 7 Correlation of Solid Phase Residential Time

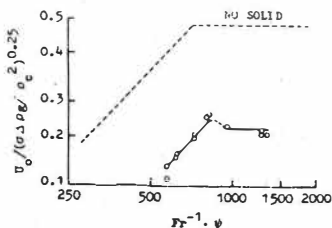


FIG. 8 Influence of the Solid Phase on U_0

The existence of solid particles restrains the liquid phase axial mixing, both continuous and dispersed phases. Comparison of experimental data of these two cases (with and without solid particles), the following relation is obtained:

$$E' = (0.1 \sim 0.45)E$$

(5)

where E' and E are the diffusion coefficients in the presence and absence of solid respectively.

However, the interface between two liquid phases might be contaminated with fine solid particles. Therefore, it is important to select proper systems to achieve successful operation.

B. THE RTL CONTACTOR FOR LONG AVERAGE RESIDENTIAL TIME

The RTL contactor has been known to apply to extraction system with low density difference, low interfacial tension and prone to emulsification. In addition, possibilities exist also for its application to systems containing solid particles. Despite its successful use over the past 20 years, the fundamentals of the operation of the RTL contactor have not been studied as extensively as have those of the other industrial contactors, and only some preliminary studies have been made on axial mixing and mass transfer in a pilot-scale unit^(6,7).

The authors have inclined to use the RTL contactor to handle systems consisting of an organic solvent and an aqueous phase which contains relatively high content of solid particles, so that leaching of the solid and extraction of the soluble valuables are expected to proceed almost simultaneously. In this contactor the residential time for various phases will be significantly longer than the previous type of vertical column. Here a preliminary study of hydrodynamic behaviors of organic and aqueous phases flowing counter-currently and of aqueous and solid phases flowing co-currently in the contactor under different conditions will be reported.

The RTL Contactor

The shell of the contactor was 0.1m in diameter and total length of 0.86m. The rotor consisted of 24 discs. Six buckets were mounted on each of all discs and the distance between adjacent discs was 0.03m. The aqueous phase, which might carry solid particles, flowed countercurrently against the organic phase. The interface between two liquid phases was controlled by a solenoid valve. In order to assist the movement of solid particles through and out of the contactor, the major modifications were made as follows⁽⁸⁾.

1. On each compartmental disc there were three passages for solid particles between two buckets (Fig. 9). The passages between the adjacent discs were staggered so that the solid residential time might be increased.
2. To reduce the stagnant region at the bottom and assist the movement of all solids, on the edges of every other buckets were mounted pieces of baffle, as also shown in Fig. 9.
3. The common axis of the shell and the rotor might be incline to horizontal, and the angle of inclination β could be adjusted.

Mathematical Model

Due to the inclination of the contactor and the pressure drop from one end of the contactor to the other, the interface between two liquid phases may not coincide with the axis. Therefore, the flow cross-sectional area of each liquid phase varies continuously and the superficial flow rate changes accordingly. It does not meet the assumption of the diffusion model, so a modified model has been used.

1. Relationship Between Cross-sectional Area and Axial Dimension

If the angle α , which is formed by the axis of the contactor with the interface between two liquid phases, is small, the cross section area A for the flow of either liquid phase is approximately linear with axial dimension l , i.e.

$$A/A_0 = (1-0.0041 \alpha L/2) + 0.0041 \alpha l \quad (6)$$

where A_0 is datum cross-sectional area and L total length of the contactor.

2. Equation for Unsteady Injection to Determine Axial Mixing

If the fluid velocity is U , the flow per unit cross-sectional area entering a section l with a component of concentration c may be defined as

$$UX = Uc - E \cdot dc/dl \quad (7)$$

where E is the axial diffusion coefficient.

Applying this concept to any process in which the component accumulates at rate r per unit volume, a material balance over an element dl as shown in Fig. 10 gives

$$UX \cdot A = [UX + d(UX)] (A + dA) + r \cdot A \cdot dl \quad (8)$$

With the unsteady injection method to determine E , r is the tracer accumulation rate $\partial c/\partial t$. Combining Eqs. (6), (7) and (8), it follows

$$\frac{1}{Pe} \frac{\partial^2 c}{\partial Z^2} - \frac{1-0.0041 \alpha L/2e}{(1-0.0041 \alpha L/2) + 0.0041 \alpha LZ} \frac{\partial c}{\partial Z} = r \frac{\partial c}{\partial t} \quad (9)$$

where $Pe = U_0 L/E$, Z is dimensionless length, τ residential time and t time. Pe and α are two parameters of the model. The coefficient of the term $\partial c/\partial Z$ represents the effect of changing cross-sectional area and, therefore, the changing superficial flow rate on the concentration gradient in the contactor.

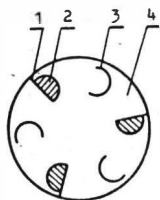


FIG. 9 Sectional View Showing Structure of the Rotor

1. baffle
2. opening
3. bucket
4. disc

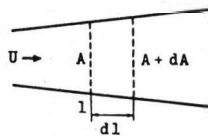


FIG. 10 Flow in Changing Cross-Sectional Area with Axial Dispersion

3. Equations for Countercurrent Extraction with Axial Mixing

Using the same method, the following equations can be obtained

$$\frac{d^2 x}{dz^2} - \frac{Pe_x - 0.0041 \alpha L}{(1-0.0041 \alpha L/2) + 0.0041 \alpha LZ} \frac{dx}{dz} - l' e_x N_{Ox} (x-x^*) = 0 \quad (10)$$

$$\frac{d^2 y}{dz^2} + \frac{Pe_y - 0.0041 \alpha L}{(1+0.0041 \alpha L/2) - 0.0041 \alpha LZ} \frac{dy}{dz} + Pe_y N_{Ox} \frac{F_x}{F_y} (x-x^*) = 0 \quad (11)$$

where x and y are solute concentrations in organic and aqueous phases respectively, N_{Ox} overall number of transfer units based on organic phase, F_x and F_y are volumetric flow rates of organic and aqueous phases, and x' is concentration in equilibrium with y . The coefficients of the first order differential term also represent the effect of the changing flow rate on the concentration gradient. If the cross-sectional area does not change, the Eqs. (9), (10) and (11) are reduced to the normal form of the diffusion model.

In the present case the phase equilibrium is not linear, and a numerical method, similar to that proposed by Ricker (9) using back-flow model, is used and demonstrated to be stable and efficient.

Results and Discussion

1. Test of the Proposed Model

Using two RTD curves obtained under the same conditions except for different inclinations, it is obvious that there are some differences between two diffusion coefficients calculated by normal diffusion model, which may be due to that the normal model does not adapt to the changing superficial flow rate. But, if the modified diffusion model is used, the differences are insignificant.

By comparison of the calculated concentration profile along the contactor with measured volumes (see Fig. 11), one can see that the modified model ($a=2$) fits better than the normal model ($a=0$).

2. Axial Diffusion

In the present work, tap water and kerosene were used as the aqueous and organic phases respectively.

As the agitation intensity in the contactor is usually low and the flow is obstructed by the rotating discs, the entrainment of dispersed phase by continuous phase is small. And as the moving direction of droplets of dispersed phase is perpendicular to the flow direction of the bulk of continuous phase, the eddies attached to the wakes of the dispersed phase droplets are not liable to cause the continuous phase to flow in an adverse direction. For these reasons, a change of the flow rate of one phase does not affect the axial mixing of the other.

The differences of wetting characteristics and other physical properties of water and kerosene may induce the droplets of the two to move in different ways, which in turn may be the cause of the phenomena that the axial diffusion coefficient of the aqueous phase is basically independent of its own flow rate while that of the organic phase increases with increasing its own flow rate.

The experiments also indicate that the diffusion coefficients of both phases increase linearly with the rotating speed n . The following correlations were obtained:

$$E_y/(U_{Oy}H) = 0.1369 + 0.1093 R \cdot n/U_{Oy} \quad (12)$$

$$E_x/(U_{Ox}H) = 0.3456 + 0.05189 R \cdot n/U_{Ox} \quad (13)$$

where U_0 is datum flow rate, H distance between two adjacent discs and R inside diameter of the contactor.

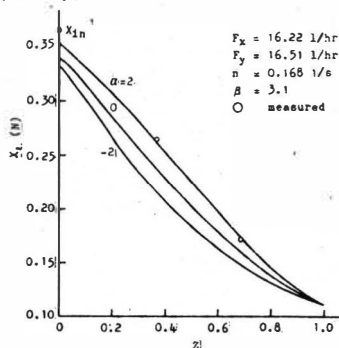


FIG. 11 Comparison of Concentration Profile

3. Behavior of Solid Particles

Sand of $2.8-4.5 \times 10^{-4} \text{m}$ and tap water flowed co-currently in the contactor, and marble particles were used as the tracer. The average residential time (ART) of sand in the contactor varies from 10 to 20 minutes. As either the speed of the rotor or the angle of inclination β of the contactor increases, ART decreases (Fig. 12). The flow rate of sand and consequently, the hold-up of sand in the contactor do not significantly affect the value of ART. High hold-up of sand and high rotor speed will enhance the intensity of the solid mixing (Fig. 13). The variance σ^2 of the RTD curves is about 0.03 to 0.05. A variance analysis of the results of perpendicularity tests reveals that the flow rate of aqueous phase has no marked influence on either the ART or the intensity of solid mixing. This fact may be due to the low flow rate of aqueous phase and the high density of sand.

Application

As a bench-scale test, the RTL contactor was successfully used for the recovery of metal value from spent vanadium catalyst by LEACHEX process⁽¹⁰⁾. The experiments revealed that the overall efficiency of leaching and extraction was high and that the operation was stable and organic solvent was seldom entrained by solid particles and aqueous phase or vice versa.

REFERENCES

- (1) Tang, S.Z., Zhao, C. and Su, Y.F., Chemical World, 26, 263 (1985) (in Chinese).
- (2) Logsdail, D.H., Thornton, J.D. and Pratt, H.R.C., Trans. Inst. Chem. Engrs., 36, 301 (1957).
- (3) Kung, E.Y. and Beckmann, R.B., AIChE J., 7, 319 (1961).
- (4) Laddha, G.S., Degaleesan, E.E. and Kannappan, P., Can. J. Chem. Eng., 56, 137 (1978).
- (5) Zhang, S.H., X.D. Ni and Y.F. Su, Can. J. Chem. Eng., 59, 573 (1981).
- (6) Sheikn, A.R., Ingham, J. and Hanson, C., Trans. Inst. Chem. Engrs., 50 (3), 199 (1972).
- (7) Wang, P.S.M., Ingham, J. and Hanson, C., ibid, 55 (3), 196 (1977).
- (8) Robinson, L.F., Brit. Pat. 2033244 (1980).
- (9) Ricker, N.L., Fumiyuki Nakashio and King, C.J., AIChE J., 27 (2), 277 (1981).
- (10) Cai, S.H., "Recovery of Vanadium from Spent Catalyst LEACHEX Process", M.S. Thesis, East China Inst. of Chem. Tech., Shanghai, China (1985).

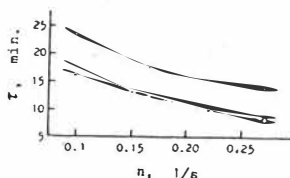


FIG. 12 Average Residential Time of Solids vs. Rotor Speed

- △ $F_S = 2.77 \text{ kg/hr}$ $\beta = 3.9$
- $F_B = 1.96 \text{ kg/hr}$ $\beta = 3.9$
- $F_B = 1.96 \text{ kg/hr}$ $\beta = 1.04$
- $F_y = 21.9 \text{ l/hr}$

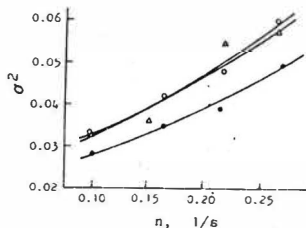


FIG. 13 Variance of RTD curves for Solids vs. Rotor Speed

- $F_S = 2.77 \text{ kg/hr}$ $\beta = 3.9$
- $F_B = 1.96 \text{ kg/hr}$ $A = 3.9$
- △ $F_B = 1.96 \text{ kg/hr}$ $\beta = 1.04$
- $F_y = 21.9 \text{ l/hr}$

STUDY OF COALESCENCE AND SETTLER DESIGN IN MIXER-SETTLER

H. H. Shen* and Z. J. Shen
Chemical Engineering Research Centre,
East China Institute of Chemical Technology

SCOPE

Mixer-settler is widely used in solvent extraction process due to its higher stage efficiency, broad operating flexibility and simple construction. However, the most drawback of the mixer-settler is its large area occupation and thus large solvent inventory particularly in gravity settler. This is probably due to the presence of indeterminate amounts of surface-active agents, the behavior of drops coalescence is only qualitatively understood, thus making the reproducible data very difficult to obtain. Subsequently, a conservative settler designation was an inevitable trend in general.

In this study, a correlation of the height of dispersion band with other operating conditions has been proposed based on the Hartland's model (1978). Since it is not necessary to achieve complete separation of the phases with a dispersion band that diminishes in height to zero at the settler's offtake, hence, a reasonable stable height of dispersion band is desired. In present investigation, it can be calculated based on an analytical mathematical model for optimum volumetric flow-rate of dispersed phase containing the meaning of minimum operating cost per unit volumetric capacity incorporated with the solvent inventory and settling area requirement.

INTRODUCTION

Recent decades, along with the better understanding of the separation mechanism of liquid-liquid dispersion, the relationship between the behaviour of dispersion band in settler and the ability of phase separation and the inter-drops effect has been considered. Jeffreys et al. (1971) proposed a detail coalescence procedure of a single drop to interface and raised a separation model about a thin wedge dispersion band related with the settling area. Couglou (1976) proposed a similar coalescence procedure between drops. The effects of height of dispersion band have been studied. Warner (1965), Barnes & Mizrahi (1975) and Su Li-Ming (1984) pointed out that settling also related with the volume of dispersion band. Some models were suggested to describe the behaviour of thick dispersion band. Not as same as wedge dispersion band, the thick band is rectangle in shape. Barnes & Mizrahi (1975) measured the holdup distribution and divided the thick dispersion band into several sub-layers. Allak & Jeffreys (1974) described the construction of the thick band and noticed that in the sub-layer near the coalescence front, the drops are dodecahedra in shape. They all raised that the effect between drops influences the ability of settling of unit area and reduces the coalescence time. This might be the reason why the thick dispersion band is in researchers' good graces. Hartland et al. (1978) proposed a model more accurately to describe the relationship of the height of dispersion band to the factors of dispersion throughput, drop size, coalescence time and holdup of dispersion. The main aim of present paper is to develop a more practicable model based on Hartland's model for the purpose of settler's design.

EXPERIMENTAL

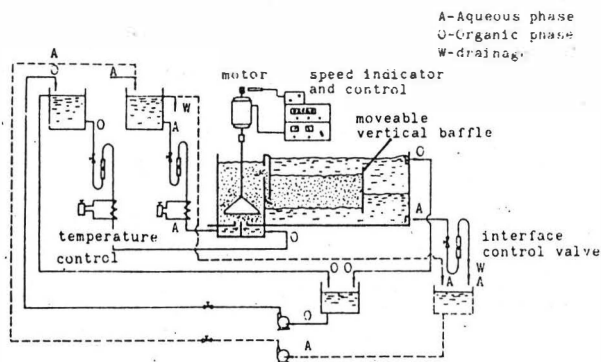


Fig. 1 The schematic diagram of experimental apparatus

* Present address: Nanjing Institute of Chemical Technology

The experiment was carried out by measuring the height of dispersion band in steady state under different operating conditions in a single stage plexiglass mixer-settler. Fig. 1 shows the schematic diagram of experimental apparatus. The effective volume of mixer was 5.6 liters, while the settling area could be varied from 0.0306 m² to 0.144 m² by moving the vertical baffle in the settler. The flow rate of aqueous outlet was controlled by the valve to maintain the interface level in stable. Two types of agitator were used i.e. large delta impeller developed by Shen et al. (1980, 1983) and Rushton 6-blade open type turbine. Two systems: kerosene/water and butanol/water, were employed in this work without mass transfer in different temperature, 150°C and 250°C and different rotating speed in the range of 250 to 350 rpm and 150 to 250 rpm respectively. Table 1 lists the properties of systems used. The phase ratio O/A varied from 2 to 0.5. The organic phase was dispersed in all cases. The entrainment of organic phase was measured by glass capillary tube.

Table 1 Properties of systems

System	Kerosene	Water	Butanol*	Water**
ρ (kg m ⁻³)	800	1000	840	990
μ (mpa s)	1.64	1.13	2.9	1.14
r (mN m ⁻¹)	28.2(150°C)		2.8(250°C)	

* be saturated by water

** be saturated by butanol

THEORY AND MODEL

In a gravity continuous settler, the coalescence process of the dispersion band is very complicated. It chiefly consists a procedure of drops sedimentation in companied with a drainage of the continuous phase film between drops. As long as the drops packed closer and dense and the film turns into a critical thickness, along with the film breaking, the drops coalesce to the mother phase or other drops. Obviously, many factors might effect this coalescence process, such as: the drop size thus the agitating strength, physical properties of the system, phase ratio, disturbance of the dispersion movement and the height of the dispersion band etc. The effect of temperature can be considered in physical properties. Based on the coalescence mechanism, Hartland and Vohra (1978) derived a model as follows:

$$(1) \quad H = \frac{6 V_d \tau_b}{\bar{\tau}} \ln \left(\frac{3 V_d \tau_1}{2 \epsilon_1 d_0} \right)$$

Where H is the height of dispersion band, V_d is the volumetric flow rate of dispersion phase Q_d per unit area A, d_0 is drop diameter, τ_b and τ_1 are coalescence time between drops and between drop and mother phase respectively, $\bar{\tau}$ is average dispersed holdup, ϵ_1 is holdup at coalescence front. $\epsilon_1 \geq 1$. Comparing with the dimensional analysis method;

$$H \propto (Q_d/A)^m$$

Eq. (1) describes the relationship of H and V_d more accurately.

Owing to:

$$(2) \quad d_0 \propto (We)^{-0.6} \quad \text{or}$$

$$(3) \quad d_0 \propto N^{-1.2}$$

We is Weber's number and N is agitator's rotating speed, and because τ_b and τ_1 are the functions of d_0 , assuming:

$$(4) \quad \tau_1 \propto d_0^{-m} \quad \text{and}$$

$$(5) \quad \tau_b \propto d_0^{-m}$$

Substituting (2) (3) (4) and (5) into Eq. (1) and rearrangement, it gives:

$$(6) \quad H = B_1 V_d N^{1.2m} (\ln V_d + 1.2(1+m) \ln B_2)$$

Where B_1 and B_2 are constants relating to system properties and phase ratio. Here τ_b can be effected by the disturbance of the dispersion movement, so, τ_b is also related to V_d , Hartland (1978) treated this relationship by introducing a correction factor V_d^p , assuming:

$$\tau_b \propto V_d^p$$

Thus, Eq. (6) can be rewritten as:

$$(7) \quad H = C_1 V_d^{p+1} N^{1.2m} \ln(C_2 V_d N^{1.2(1+m)})$$

Where C_1 and C_2 are constants only relating to system properties and phase ratio, m and p are all constants.

The present Eq. (7) describes the relationship not only between the height of dispersion band and the dispersion throughput but agitating speed also. Moreover, it can be avoidable to calculate the items of coalescence time τ_b and τ_1 .

If all variables except V_d are known, Eq. (7) can be simplified as:

$$(8) \quad H = A V_d^{p+1} (\ln V_d + B)$$

when $\ln V_d < -(B+1)/(p+1)$
then,

$$\frac{\partial H}{\partial V_d} < 0$$

However, $\partial H/\partial V_d$ is great than 0 in fact (Jeffreys, ISEC'74). So, it is clear that Eq. (7) can't be used in the case of lower flow rate, because in such case, the dispersion band is wedge in shape and doesn't flow only in parallel direction.

RESULTS AND DISCUSSIONS

The height of dispersion band was measured under given operating conditions (N , V_d , O/A) and systems. Then the constants C_1 , C_2 , p and m in Eq. (7) could be computerized from the experimental data. Table 2 shows the results of present work with butanol/water and kerosene/water systems. The deviation of this model lists on the item D_v in Table 2.

Table 2

Equation	$H = C_1 V_d^{p+1} N^{1.2m} \ln(C_2 V_d N^{1.2(1+m)})$						
System	O/A	T(°C)	C_1	C_2	p	m	D_v
Butanol/H ₂ O	2/1	25	0.03	-3.9	2	0	5.8%
Butanol/H ₂ O	3/2	25	0.054	-3.8	2	0	5.0%
Butanol/H ₂ O	1/1	25	0.135	-5.1	2	0	3.5%
Kerosene/H ₂ O	2/1	15	9.9×10^{-7}	1.5	1	1.5	11.4%
Kerosene/H ₂ O	3/2	15	7.2×10^{-7}	1.8	1	1.5	13.5%
Kerosene/H ₂ O	1/1	15	1.2×10^{-6}	1.8	1	1.5	13.5%

The effect of dispersed phase throughput per unit settling area V_d and agitating speed N against the height of dispersion band H at different phase ratio with large delta impeller are shown in Figs. 2, 3 and 4. It can be seen that H increases with the increasing of V_d and N in all cases. However, the curves become steeper at the higher agitating speed or lower phase ratio in most cases.

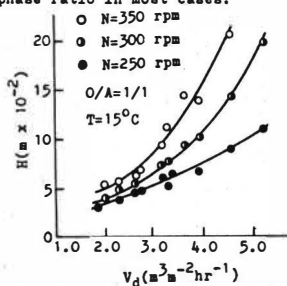


Fig. 2 The effect of V_d on H in different N , kerosene/water system, kerosene dispersed with large delta impeller

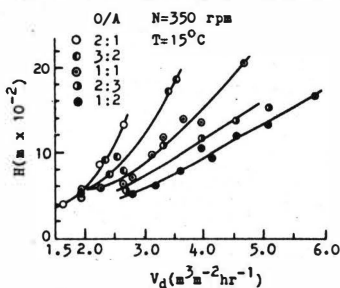


Fig. 3 The effect of V_d on H in different phase ratio, kerosene/water system, kerosene dispersed with large delta impeller

Different systems reveal different performance shown in Figs. 2 and 4. Much higher H can be seen for butanol/water system than that of kerosene/water system at same N and phase ratio due to its much lower interfacial tension. Consequently, the values of the constant of Eq. (7) reveal big difference at different systems particularly C_1 . But, the effect of N on H for butanol/water system is not so sensitive as for kerosene/water system shown in

Fig. 4, where the sets of curves are closer each other in different N and reflecting on the value of constant m is zero for item N at Eq. (?). In experiment, it was observed that for butanol/water system, the drop size was more uniform and the height of dispersion band was more stable with less wave motions.

It seems quite different effect of phase ratio on H for two systems studied. For butanol/water system, phase ratio shows having a simple effect. According to the mixing theory, the dispersed drop size increases with the increasing of the dispersed phase holdup at higher phase ratio ($d_0 \propto (1+B)^3$, here B is a constant). Consequently, the thickness of the continuous phase film between drops might be thinner in thicker dispersion band and easier to be broken. Therefore, the coalescence process is improved and the H decreases with increasing of phase ratio. The butanol/water system is a typical system which shows this phenomenon clearly in Fig. 4. But the effect of phase ratio on kerosene/water system shows more complicate and interesting. The curves of H versus O/A have an inflection points and fall in a valley around $O/A=2/3$ as seen in Fig. 5. Reference to Hartland's work, the coalescence time of drops is proportional to the volume force of the below drop (or upper drop, depend on which phase is dispersed) exerted on the upper (below) drop. The volume force of the dispersion band exerted on the drops near the coalescence front makes the shape of the drops change into dodecahedra, consequently, the process of coalescence is improved. When the phase ratio increased, the drop size and the speed of phase separation are all increased, so the dispersion band become thinner. However, at the same time, the volume force of the thinner dispersion band exerted on the coalescence front is decreased. So that, a tendency of increasing the height of dispersion band is existed. As the phase ratio further increasing, the height of dispersion band increased again. This is the explanation for the appearance of the valley on the curve of H versus O/A in kerosene/water system.

It was also found experimentally that the height of dispersion band was effected remarkably by the center position of the dispersion band (h_1) related to the position of the dispersion inlet passageway (h_f) (Figs. 6 and 7). When h_1 higher than h_f , the entering dispersion fluid might flow upwards and disturb the dispersion band, thus increase its height in the settler. When h_1 much lower than h_f , because the holdup difference, the relative gravity of the entering dispersion might be higher than that of the dense packed layer of the dispersion band in the settler, so, a part of dense packed dispersion phase will flow back into the inlet passageway and cause an uncontrolled recycle and than increase the settling load. It can be seen in Fig. 7, where the H - h_1 curve goes upwards again as the h_1 is less than 8 cm. Of cause, this phenomenon was only seen in the case of light phase dispersed and the position of the dispersion inlet passageway h_f was 12 cm. in present work.

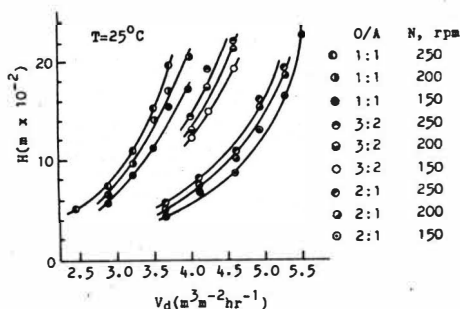


Fig. 4 The effect of V_d on H in different N and O/A , butanol/water system, butanol dispersed with large delta impeller

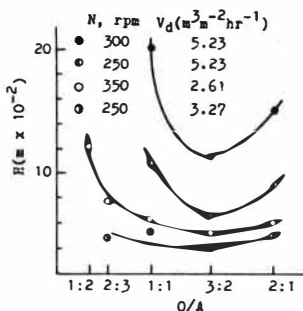


Fig. 5 The effect of phase ratio on H for kerosene/water system

The comparison of two types of agitator is shown in Fig. 8 ($H - V_d$) and Fig. 9 ($\bar{v} - V_d$). The experiment was carried out at different rotating speed according the different characters of the agitators. The large delta impeller is a big area type agitator, it can be seen to be more efficient in transporting larger scale turbulence to a main flow stream and thus in creating more local turbulence intensity and circulation throughout the mixer. Compare with the smaller area multi-bladed type Rushton turbine, for doing same job, uniform distribution of the drop size can be obtained in a much lower rotating speed by large delta impeller. For example, the experiment had been done for kerosene/water system ($O/A=1$) in previous study (1952), the optimum rotating speed was 204 rpm for large delta impeller and 545 rpm for Rushton turbine respectively. Thus in the view point of settling referring to Figs. 8 and 9, the large delta impeller creating lower dispersion height and particularly much lower entrainment (w) might be the considerable result.

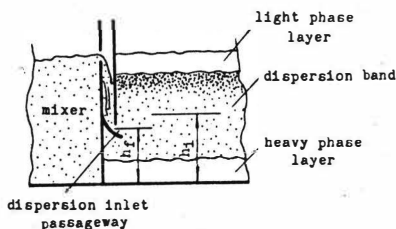


Fig. 6 The position of dispersion inlet passageway in settler

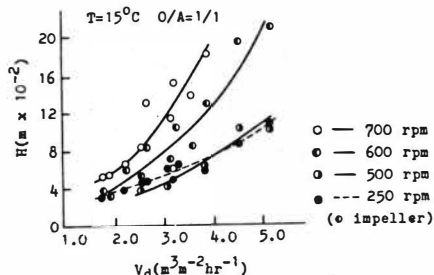


Fig. 8 The effect of V_d on H in different type of agitator. System: kerosene/water

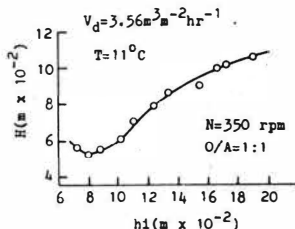


Fig. 7 The effect of the position of dispersion inlet on H . System: kerosene/water
 ● delta impeller $N=250$ rpm
 ○ Rushton turbine $N=500$ rpm
 $T=15^\circ\text{C}$ $O/A=1:1$

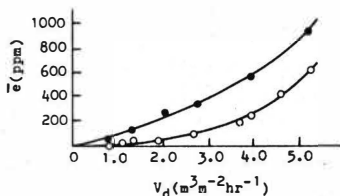


Fig. 9 The effect of V_d on entrainment in different type of agitator. System: kerosene/water

SETTLER DESIGN

In present investigation, the design of a settler is only limited within the principle of the behavior of dispersion coalescence itself without any coalescence aid. However, it aims to offer the basis for further reduce the settler's area and solvent inventory by means of different kind of coalescence aid in settler design.

Since the height of dispersion band is proportional to the increasing of dispersion throughput. In other work, to improve the settling throughput by adopting a desire dispersion height in the settler is one of the way to overcome the mixer-settler's drawback on large area occupation and large solvent inventory.

Assuming the cost of solvent per m^3 is C_0 and the cost of settler's construction per m^2 is C_s , then gives the total cost C_a as:

$$(9) \quad C_a = Q_d(C_0R + C_sS + C_p)$$

Where R is solvent inventory per m^3 of dispersion throughput per hr, S is settling area requirement per m^3 of dispersion throughput per hr, C_p is constant of the other costs. Assuming:

$$(10) \quad R = (H\bar{\phi}_d + h_d)/V_d$$

$$(11) \quad S = 1/V_d$$

$\bar{\phi}_d$ is average holdup of dispersion band, h_d is height of a light phase layer above the dispersion band for safety purpose. Substituting (10), (11) into Eq. (9), then the minimum cost requirement can be estimated, when:

$$(12) \quad \frac{\partial C_a}{\partial V_d} = \frac{Q_d}{V_d^2} (C_0(\bar{\phi}_d V_d H - H\bar{\phi}_d - h_d) - C_s) = 0$$

Simplifying Eq. (12) as:

$$(13) \quad C_s/C_0 = \bar{\phi}_d V_d H - H\bar{\phi}_d - h_d$$

Substituting Eq. (7) into Eq. (13) and rearrangement as:

$$(14) \quad C_1 \bar{V}_d V_d^2 + P N^{1.2m} (p(\ln V_d + 1.2(1+m)\ln N + C_2) + 1) = C_B/C_0 + h_d$$

To sum up, a design procedure of a settler containing the meaning of minimum operating cost per unit volumetric capacity incorporated with the solvent inventory and settling area requirement is suggested as follows:

1, From Eq. (7), compute the constants C_1 , C_2 , p and m from small scale experiment for a given system.

2, Specify C_B , C_0 , h_d and N (from mixing operation).

3, Calculate V_d from Eq. (14).

4, Calculate the desired H from Eq. (7). The total height of the settler H_B is as follows:

$$(15) \quad H_B = H + h_d + h_c$$

Where h_c is height of a heavy phase layer under the dispersion band for safety purpose.

5, For given Q_d , calculate settling area:

$$(16) \quad A = Q_d/V_d$$

CONCLUSIONS

1, In present work, a more practicable model, Eq. (7), based on Hartland's model is proposed containing the important parameter N for the purpose of settler's design.

2, A procedure for settler design is suggested for the optimum dispersed phase flow rate per unit settling area and the minimum solvent inventory on the basis of adopting a reasonable stable thick dispersion band.

3, It is further confirmed that large delta impeller shows its good characters also in settling process due to its lower power consumption requirement and thus lower dispersion height and less entrainment for accomplishing a same job.

ACKNOWLEDGEMENT

The authors express thanks to Dr. Tah C. Lo for many helpful discussions to Professor Dr. S. Hartland for supply of reference and Professor Y. F. Su for continuous encouragement.

REFERENCES

- 1, Hartland, S. & D.K. Vohra, Chem-Eng-Tech, 50(19), 673 (1978).
- 2, Jeffreys, G.V. & G.A. Davies in C. Hanson ed. Recent Advances in Liquid-Liquid Extraction, Pergamon Press, Oxford (1971).
- 3, Coulaglou, G.A. et al. AIChE J, 22, 289 (1976).
- 4, Warner, B.F. et al. Proc. 3rd Inter. Conf. Peaceful Uses of Atomic Energy, 10, 224, Geneva (1964), U.N. New York (1965).
- 5, Barner E. & J. Mizrahi, Trans. IChemE., 53, 61-83 (1975).
- 6, Su Li-ming et al. Inter-change material (in Chinese) (1984).
- 7, Allak, A.M.A. & G.V. Jeffreys, AIChE J., 20, 564 (1974).
- 8, Shen, Z.J., B.Y. Sun, J. Li & J. Bachelart, J. ECICT, 1, 47-61 (1982).
- 9, Shèn, Z.J. et al., ISEC'83, 24-5, Denver (1983).
- 10, Calderbank, P.H., in V.W. Uhl and J.B. Gray ed. Mixing-Theory and Practice, V2, Chap. 6, Academic Press, New York, (1967).

Breakage and Coalescence of Drops in Vibrating Plate Extraction Tank

Chao Shou-bai & Fan Zheng

Institute of Chemical Metallurgy, Academia, Sinica Beijing, China

1. INTRODUCTION

Apart from distillation, liquid-liquid extraction is the most important separation process in chemical engineering. However, in contrast to distillation, the knowledge regarding the design and performance of extraction columns is still far from satisfactory. The cause lies mainly in the complex behaviour of polydispersion resulted from the drop size distribution, breakup and coalescence process of drops as well as the influence of these parameters on axial mixing and mass transfer. Up to now, the results of extraction research show that a safe design of extraction columns based on fundamentals is impossible unless these factors have been taken into account.

The mutual relation among drop breakage, coalescence and the drop size distribution can be represented by a population balance equation[1]. Some works[2,3] have been done on the theoretical modelling of droplet breakage and coalescence rate in dispersed systems in terms of continuous population balance. Experimental data on drop breakage and coalescence rate are sparse and have been confined mostly to agitated vessels at low holdup of dispersed phase. It has been assumed that the drop breakage is resulted from the turbulent pressure[4]. In vibrating plate extraction columns, the effect of turbulent shear force near the hole edge in the plate is very obvious on drop breakup. It is different from that in the agitated vessels.

The scope of this work is to formulate the drop breakup and coalescence rate in vibrating plate extraction tank, using Monte-Carlo simulation method for estimation of kinetic parameters in population balance equation. For reasons of simplicity, we restrict ourselves to a batch system. This does by no means limit the method to be applied to modelling of more complicated flow system.

2. EXPERIMENTAL

EQUIPMENT AND MATERIALS

The experiments were performed in a vibrating plate tank with three sieve plates. The glass tank is 100 mm in diameter and 110 mm in height.

With three different free areas and hole diameter of plates, the experiments were designed for investigating of the effects of the structure of sieve plates. Table 1 gives features of the plates:

Table 1

free area	58%	45%	32%
hole diameter	8,10,12	10	10

The drop size measurement system consisted of a camera, an electronic flash unit, and a light probe. The light transmittance method was employed to measure the Sauter diameter of drops, consisted of a light source and receiver. The range of operating conditions studied were: vibrating frequency 136r.p.m. <math><f<586\text{r.p.m.}</math>, amplitude

Two systems, toluene(81.6% in volume)+carbon tetrachloride (18.4% in volume, dispersed)-.001 M Na_3PO_4 aqueous (continuous) and xylene(82.6% in volume)+carbon tetrachloride(17.4% in volume, dispersed)-.002 M Na_3PO_4 aqueous(continuous) were selected, the chemicals used being analysis grade. Measurements of interfacial tension between phases using the drop weight method gave values to 38 dyne/cm for the first system, and 34.4 dyne/cm for the second system.

METHOD

The parallel light transmittance method proposed by McLaughlin [5], was used to measure the mean drop size (d_{32}). The relation between d_{32} and fraction of light transmittance was:

$$\ln(I_0/I) = 1.5 \cdot l_x \cdot X / d_{32} \quad (1)$$

From measurement of I_0/I , d_{32} could be calculated.

The step change in mixing intensity was used to trace drop breakage and coalescence processes[6]. Through measuring of d_{32} in these transitional processes, The drop breakage and coalescence rate could be estimated by comparing the simulation results with experimental data.

PROCEDURE

After stabilising conditions in the tank, four or five photographs were taken using a camera with F2.5 lens and 1/1000 s exposure. Illumination was provided by means of 1000 W photoflood light. Then step changing in the vibrating frequency, samples were taken from light receiver by a microcomputer. When another steady condition was established, the sampling was stopped and the data needed stored.

3. THEORY

DROP POPULATION BALANCE

Let us consider a closed two-phase system with dispersed phase holdup

X. The population balance expressing the change in concentration of drops of diameter d with time can be written in the form

$$\begin{aligned} \frac{\partial [N(t)f_n(d,t)]}{\partial t} = & 2N(t) \int_0^\infty \beta(d,d')g(d')f_n(d',t)d(d') - N(t)g(d)f_n(d,t) \\ & + \frac{[N(t)]^2}{2} \int_0^d w[(d^3-d'^3)^{1/3}, d'] \times \frac{d^2 f_n[(d^3-d'^3)^{1/3}, t] f_n(d',t)}{(d^3 - d'^3)^{2/3}} d(d') \\ & - [N(t)]^2 f_n(d,t) \int_0^\infty w(d,d') f_n(d',t) d(d') \end{aligned}$$

(2)

In relation (2), the function $g(d)$ denotes breakage intensity of drops of diameter d , $\beta(d,d')$ conditional probability density of the formation of a daughter drop d by break-up of a drop of diameter d' and $w(d,d')$ coalescence intensity of drops of diameter d and d' , given by the product of the relative collision frequency and the coalescence efficiency.

If the functions g, β, w and the initial distribution $f_n(d,0)$ are known, the evolution of the drop size distribution, the instantaneous breakage and coalescence frequencies, as well as steady-state values of these variables, can be estimated.

BREAKAGE RATE

The breakage of a drop in vibrating plate tank depends on the relative velocity of the drop to the sieve plate. Most investigation focused on prediction of droplet deformation in isotropic turbulent flow[7] or in simple shear field[8]. These investigation give an insight into the breakage process. It appears that the drop breakup in turbulent fields occurs by three possible mechanisms: laminar shear, turbulent pressure fracturation, and turbulent shear.

Through experimental observation, it could be seen that drop breakup occurred mainly in the field near the holes in the plates. It could be assumed that turbulent shear forces near the holes in the plate control the breakage processes.

The space of a stage can be divided into two zones: the breakage zone (between $\pm A$ of equilibrium position of the plate), and the coalescence zone (beyond $\pm A$ of equilibrium position of the plate in a stage) The fraction of breakage zone is

$$B_f = 3A/2H \quad (3)$$

The number of drops of diameter d in breakage zone is

$$3A/2H*n(d) \quad (4)$$

The breakage rate is assumed to be equal to multiplication of collision rate $r(d)$ between drops in the breakage zone and sieve plate by breakage efficiency $r(d)$.

$$G(d) = g(d) * n(d) = r_c(d) * r(d) \quad (5)$$

Through analysis of droplet movement in the tank, $r_c(d)$ can be written as

$$r_c(d) = C_I \frac{2Af}{H} (1-\phi)^2 \phi (d/d_h)^3 (d_h/H)^{\frac{1}{2}} (1+X)^{-2} n(d) \quad (6)$$

Breakage efficiency is assumed proportional to the fraction of colliding which has kinetic energy greater than the droplet surface energy. The fraction of these "energetic collisions" can be derived by considering the relative velocity between drops and sieve plates, and position in the tank.

Let $u_{pd}^2(d)$ represent mean square of relative velocity between drop (size d) and sieve plate, consisting of two parts, the sieve plate velocity and the drop velocity passing through the hole in the plate.

$$u_{pd}^2(d) = u_p^2 + u_f^2 \quad (7)$$

It could be represented by the following empirical equation

$$u_{pd}^2(d) = K_1 u_p^2 (d/d_h)^{n_1} (d_h/H)^{n_3} (1+n_2X) \quad (8)$$

The mean square of relative velocity between two points separated by distance d in the turbulent flow, given by [9]

$$u_d^2(d) = K_2 d^{2/3} \epsilon^{2/3} \quad (9)$$

If

$$u_{pd}^2 > U \quad (10)$$

satisfied, breakage will take place. (U is critical breaking velocity)

$$U = (Nwe, cr \sigma / \rho_d d) \quad (11)$$

In terms of statistical analysis of droplet and assumption stated above, $r(d)$ can be expressed as

$$r(d) = [1 - (d_{cr}/d)^{2n_1+1}]^{\frac{1}{2}} \quad d > d_{cr} \quad (12)$$

substitution of Eqs. (6) and (12) into Eq. (5), the breakage rate becomes

$$G(d) = C_I (2Af/H) (1-\phi)^2 \phi (d/d_h)^3 (d_h/H)^{\frac{1}{2}} (1+X)^{-2} [1 - (d_{cr}/d)^{2n_1+1}]^{\frac{1}{2}} n(d) \quad d > d_{cr} \quad (13)$$

DAUGHTER DROP SIZE DISTRIBUTION

A little information is available to permit definition of the functional form of the daughter drop size distribution (d, d') and the number of droplet formed per breakage (d') in a vibrating plate tank. Rod and Hancil [10] observed drop breakup in an agitated vessel and found that daughter drop size distribution could be characterized by distribution function

$$\beta(d^3, d'^3) = (\gamma - 1) (1 - (d/d')^3)^{\gamma - 2} \quad (14)$$

They have also obtained the number of daughter droplets formed per breakage

$$\gamma(d') = 2 + .41[(d'/d_{cr})^3 - 1] \quad (15)$$

L. Fan[11] has reported the results regarding the daughter droplet number in the agitated vessel with high speed cinephotography. He found that two unequal droplets were formed in the cause of a mother drop breakage. In this work, β distribution function was used as the daughter drop size distribution

$$\beta(d^3, d'^3) = 30(d/d')^6 [1 - (d/d')^3]^2 \quad (16)$$

COALESCENCE RATE

Fundamental investigation on drop coalescence mainly focused on droplet coalescing at flat interface. For coalescence of droplets to occur in a turbulent flow field the droplets must collide and have sufficient collision energy so that the processes of film drainage, film rupture and coalescence may occur. The binary coalescence rate between drops of size d and d'

$$\omega(d, d') = \lambda(d, d') h(d, d') n(d) n(d') \quad (17)$$

an expression for the collision rate of drops $h(d, d')n(d)n(d')$ could be derived by assuming that the mechanism of collision in a locally isotropic turbulent flow field is analogous to the collision between gas molecules. The collision rate is

$$h(d, d')n(d)n(d') = 3.14/4 K_3^2 (d+d')^{7/3} \Sigma^{1/3} \quad (18)$$

where K is the constant in following eqn.

$$u = K_3 \Sigma^{2/3} (d+d')^{2/3} \quad (19)$$

The expression for coalescence efficiency $\lambda(d, d')$ of binary collision in dispersion can be related to the ratio of collision energy and interfacial energy. The following empirical equation was used to describe the coalescence efficiency

$$\lambda(d, d') = [K_4 \rho_d \Sigma^{2/3} d d' / K_5 \sigma (d+d')]^{1/3}]^{1/2} \quad (20)$$

where Σ is energy dissipation in vibrating plate extraction column.

T.C. Lo[12] suggested the following relation

$$\Sigma = 2\pi/3 [(1-\phi^2)/C_0^2 \phi^2] (Af/H)^3 \quad (21)$$

substitution of Eqs. (18), (20), and (21) into Eq. (17), the coalescence rate can be written in terms of droplet diameters

$$\omega(d, d') = c_{II} (d+d')^{7/3} \Sigma^{1/3} [\rho_d \Sigma^{2/3} d d' / \sigma (d+d')]^{1/3, 1/2} n(d) n(d') \quad (22)$$

DROP SIZE

In the system of dispersion, there seems to exist a maximum drop size d above which breakage is assured and a minimum drop size d below which no breakage occurs. The maximum drop size is determined by the correlation

$$\rho_d u_{pd}^2 d_{max} / = Nwe, cr \quad (23)$$

substitution of eqn.(8) into eqn.(23), one can obtain

$$d_{\max}^{2n_1+1} = K_6 (2Af)^{-2} d^{2n_1} (H/d_h)^{2n_3} (1+n_2x)^2 \phi^{-2} (\sigma/\rho_d) \quad (24)$$

However, no such information exists for d_{cr} . An equation of the form

$$d_{\max} = K_7 d_{32} \quad (25)$$

was assumed, where K_7 estimated to be equal to 1.52 from the experimental data.

PARAMETER ESTIMATION VIA COMPARISON WITH DATA

Experimental drop size distribution data for vibrating plate tank were compared with three distribution models. It was found that volume-log-Normal distribution could fit the experimental data fairly well

$$f_v(d) = 1 / (.231 \sqrt{2\pi} d) \exp[-(\ln d - \ln 1.107 d_{32})^2 / 2 * .231^2] \quad (26)$$

Experimental Sauter diameter of drops been fitted by Eq.(24), and gave $n_1=.167$, $n_2=1.140$, $n_3=-.187$, $K_6=1.224$. Figures (1) and (2) show drop size distribution and Sauter diameter of drops.

From Eq. (2), it can be seen that population balance equation balance equation is very complicated. Statistical Monte-Carlo techniques have been developed in attempts to bypass the difficulties of using integrodifferential equations in the description of dispersed phase system. Spielman and Levenspiel [13] used pure Monte-Carlo digital simulation technique which removed the limitation of studying simple reaction kinetics and could be applied to unsteady state analysis. Recently, Rod[14] extended the work to simulate drop breakage and coalescence in a dispersion system. In this work, the combination of the basic fundamental concept of drop breakage and coalescence in dispersion system with a stochastic Monte-Carlo simulation method permits us to evaluate the parameters in breakage and coalescence frequency function, by fitting the experimental Sauter diameter of drops in the transitional processes over the entire range of the operating condition. It gave values to 66.0 of C_1 and $5.27 * 10^{-4} \text{ cm}^{-3}$ of C_2 with variation of 20.0% and 25.2% respectively. The final form of breakage and coalescence rate could be written as

$$G(d) = 66.0 (1-\phi)^2 \phi (d_h/H)^{1/2} (1-x)^{-2} (2Af/H) (d/d_h)^3 [1 - (d_{cr}/d)^{4/3}]^{1/2} n(d) \quad d > d_{cr}$$

$$\omega(d, d') = 5.27 \times 10^{-4} (d+d')^{13/6} (d d')^{1/2} (2Af)^2 / H^{2/3} (\rho_d/\sigma)^{1/2} (1-\phi^2) / \phi^{4/3} \frac{n(d) n(d')}{n(d) n(d')} \quad (28)$$

A comparison of the experimental data and calculated mean drop size, and drop size distribution in transitional processes are shown in Figs. (3) and (4). Considering the assumption made for deriving the breakage and coalescence rate, the experimental data are correlated satisfactorily.

In Fig. (5), the experimental Sauter diameters of drops in steady state are correlated to the vibrating intensity ($2Af$). It can be seen that d_{32} is proportional to the 1.5 power of $2Af$.

NOTATION

A	vibrating amplitude of the plate, cm	$\overline{u_p^2}$	mean square velocity of plate, cm^2/s^2
B_f	fraction of breakage zone	$\overline{u_{pd}^2}$	mean square of relative velocity between drop of size d and plate, cm^2/s^2
C_D	drag coefficient	X	holdup of dispersed phase
CI	breakage constant		
CI	coalescence constant, cm^{-3}		
d	drop diameter, cm		
d_{32}	Sauter mean diameter, cm		
dh	diameter of the hole in plate, cm		
d_{max}	maximum steady drop diameter, cm		
f	vibrating frequency, 1/s		
G(d)	breakage rate, 1/s		
g(d)	breakage frequency, 1/s		
H	plate spacing height, cm		
$h(d, d')$	collision frequency of drops, 1/s		
I, I_0	light intensity		
K_i	constant		
l_x	light path length, cm		
N_{We}	Weber number = $\rho u^2 d / \sigma$		
n(d)	number of drops of size d		
r(d)	breakup probability		
$r_c(d)$	collision frequency of drop with plate, 1/s		
t	time, s		
$\overline{u_c}$	critical breakage velocity cm/s		
$\overline{u_d^2}(d)$	mean square of relative velocity between two points separated by a distance d, cm^2/s^2		
$\overline{u_f^2}$	mean square velocity of drops through the hole in plate cm^2/s^2		
			Greek symbol
		$\beta(d, d')$	daughter drop size distribution
		$\gamma(d')$	daughter droplet number
		Σ	energy dissipation per unit mass, $\text{erg}/\text{g}/\text{s}$
		$\lambda(d, d')$	coalescence efficiency
		ρ	density g/cm^3
		σ	interfacial tension, dyne/cm
		ϕ	free area of plate
		$\omega(d, d')$	coalescence rate, 1/s
			Subscripts
		cr	critical value
		c	continuous phase
		d	dispersed phase
		n	number

REFERENCE

- Valentes, K.J. et al, Ind. Eng. Chem. Fundl., 5, 271 (1966)
- Valentes, K.J. et al, Ind. Eng. Chem. Fundl., 5, 533 (1966)
- Coulaloglou, C.A. et al, Chem. Eng. Sci., 32, 1289 (1977)
- Shinnar, R.J., Fluid Mech., 10, 259 (1961)
- McLaughlin, C.M. et al, A.I. Ch. E.J., 19, 417 (1973)
- Howarth, W.J., A.I. Ch.E.J., 13, 1007 (1967)
- Jares, J. et al, Paper Presented at the 8th Int. CHISA congress, Prague, 1984.
- Karm, H.J. et al Ind. Eng. Chem. Fundl., 7, 576 (1968)
- Hinze, J.O., A.I.Ch.E.J., 1, 289 (1955)
- Rod, V. et al, Paper Presented at 7th Int. CHISA Congress, Prague, 1981
- Fan, L., Private Communication, 1985
- Lo, T.C. et al, "Handbook of Solvent Extraction.", Wiley, New York, 1983
- Spielman, L.A. et al, Chem. Eng. Sci., 20, 247 (1965)
- Rod, V. et al, Trans. Ind. Chem. Enger., 60, 48 (1981)

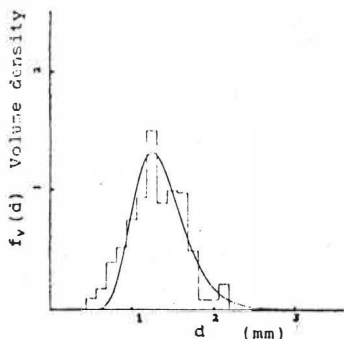


Fig. 1 Theoretical and experimental size distribution.
 $A=3.5$; $f_1=305\text{rpm}$; $f_2=420\text{rpm}$;
 $X=.17$; $H=2.5$; $d_h=1.2$; $\varphi=.56$
 $d_m=1.2$ (exper.) vs 1.18 (calc.)

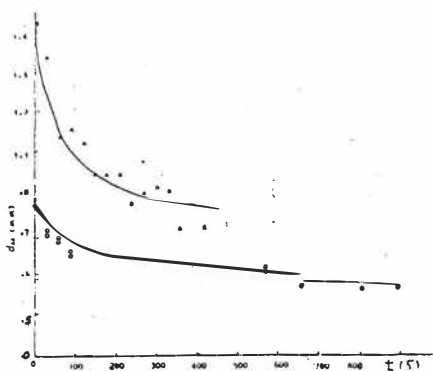
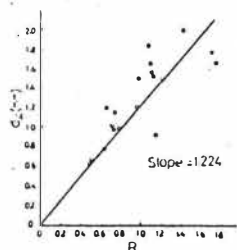


Fig. 3 Simulation and experimental mean diameter (response to a change of mixing intensity). Solid line are calculated. Symbols are experimental data for which \star $f_1=185\text{rpm}$; $A=3.5$; $f_2=320\text{rpm}$; $X=.057$; $H=2.5$; $d_h=1.2$; $\varphi=.56$, \circ $f_1=325\text{rpm}$; $f_2=445\text{rpm}$; $A=3.5$; $H=2.5$; $d_h=1.2$; $\varphi=.56$;



$$R = \left(\frac{d_{32}}{1.1} \right)^3 (2A)^{1.5} \varphi^{.5} d_h^{1.5} (1.14A)^{1.5} \left(\frac{f_2}{f_1} \right)^{.5}$$

Fig. 2 Correlation of Sauter diameter

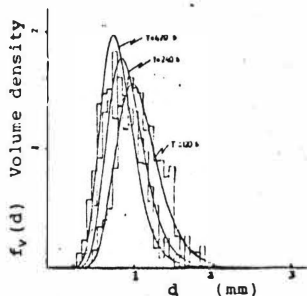


Fig. 4 Response of drop size distribution to a change of mixing intensity. $f_1=185\text{rpm}$; $f_2=320\text{rpm}$; $X=.057$; $H=2.5$; $d_h=1.2$; $\varphi=.56$; $A=3.5$.

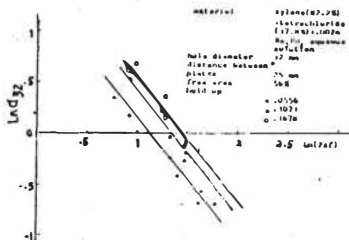


Fig. 5 Experimental Sauter diameters vs mixing intensity.

The Residence Time Distribution of Two Fluid Phases in a
Centrifugal Extractor

Dipl.-Ing. F. Otillinger, Prof. Dr.-Ing. E. Blaß,
Lehrstuhl A für Verfahrenstechnik, Technische Universität München

INTRODUCTION

High intensity of centrifugal field is extremely useful for accelerating the mixing and separating process during an extraction. This is of particular interest when one is dealing with liquid systems of very small differences in density, or when short contact time is necessary. Hydrodynamics and mass transfer of the dispersed fluid-fluid systems in centrifugal extractors cannot yet be fully calculated.

For the last few years Schilp and Blass /1/ have clarified the flow through perforated sheets, drop sizes and the radial settling motion. The experimental and theoretical research is now concentrating on the residence time distribution of the two fluid phases.

The following presents methods of how to measure the Residence Time Distribution (RTD) and how to evaluate these measurements. Two different mixing models - the well-known Dispersion Model and a combined model - are used to interpret the hydrodynamic behavior of the fluid phases. Both models are critically valued with respect to their suitability for scaling up different types of centrifugal extractors.

METHODS OF RESEARCH

The experimental research was conducted with a model centrifuge with a thick glass disc front (figure 1). Perforated sheets with different hole diameters and hole pitches can be inserted into the centrifuge. There are various radii possible. The centrifuge is surrounded by the required measuring and supply equipment. The flow process is recorded and measured by a high speed camera as well as a stroboscopic camera. In order to determinate the RTD it was necessary to trace the heavy liquid (water) at the input with KCl, the light liquid with a red organic dye. With the help of a conductivity probe (heavy liquid) and a spectral photometer (light liquid) the answer to the tracer impulse was continuously measured at the outlet. Two different methods were used to evaluate the tracer curves: Firstly the mean and variance (\bar{t} , σ^2) of the pulse response curve were determined and related to the Dispersion Model; secondly the Dispersion Model was fitted to the experimental data in time domain. In addition to the Dispersion Model we derived a combined model for a centrifugal extractor and compared the resulting system transfer function of the combined model with the standardized experimental pulse response data.

RESULTS

1. EVALUATION BY USING THE DISPERSION MODEL

1.1 Fitting in the Time Domain

The system transfer function in the time domain was used for fitting the Dispersion Model to the experimental data /2/. The boundary conditions were those of a closed-closed system. The model was fitted by varying both the Peclet number and the mean residence time.

The function for fitting is:

$$\phi = \sum_{t=0}^{t=t_n} (C(t)_{\text{exp}} - C(t)_{\text{mod}})^2 \stackrel{!}{=} \text{Min}$$

The quality of the fitting is determined by the Relative Standard Deviation (RSD)

$$\text{RSD} = \frac{\sqrt{\phi_{\text{opt}} / (N-2)}}{C(t)_{\text{exp,max}}} \cdot 100 \%$$

so that N marks the number of measuring points.

1.2 Motion of a fluid element (dispersed phase) as a function of time
The first living phase of a fluid element is to be part of a primary drop formed directly at the perforated cylindrical sheet. Increasing the field intensity causes the primary drop to disintegrate into secondary drops. Once these drops have reached the stationary layer of the dispersed phase, the regarded fluid element is part of the coalescing drops. These coalescing drops flow into the stationary layer of the dispersed phase. Hence the last living phase of the fluid element in one stage is to be a part of the stationary layer (figure 2). While drop formation and settling motion only take a few milliseconds, coalescing and staying in the stationary layer takes about 1-3 seconds. Therefore the dominating living phases are coalescence and the being part of the stationary layer, whereas settling paths of different length don't have any noticeable influence on the RTD data.

1.3 The Peclet number of the dispersed and continuous phase

The heavy as well as the light fluid can be dispersed or continuous. With the help of the pressure difference at the outlet of the heavy and the light fluid ($p_{1,\omega} - p_{h,\omega}$) the centrifugal extractor can be filled with the heavy fluid ($p_{1,\omega} - p_{h,\omega} \approx 0$; light fluid dispersed), or the light fluid ($p_{1,\omega} - p_{h,\omega} = \text{max}$; heavy fluid dispersed). In case of dual-flow sheets the stationary layers of the dispersed fluid are usually very small, whereas the stationary layers of the continuous phase fill up the whole space between the stationary layer of the dispersed phase and the next perforated sheet.

The evaluation of the experimental data shows, that in case of normally values of working parameters as field intensity and through-put the stationary layers of both the dispersed and the continuous phase are well mixed ($Pe \approx 0$) and the very fast settling motion of the dispersed phase is similar to plug flow.

The Peclet number of the continuous phase:

$$Pe_c = \frac{\bar{v}_c \cdot R}{(1-\epsilon_d)} \cdot D_{ax,c}$$

Figure 3 shows the Peclet number of the continuous phase versus the number of stages in a centrifugal extractor. There is a significant increase of the Peclet number resulting from an increased number of well mixed stationary layers. In case of well mixed layers of nearly the same size the Tanks in Series Model conforms well with the experimental data.

The Peclet number of the dispersed phase:

Though the motion of drop swarms in centrifugal fields is similar to plug flow and the number of stages is increasing, the Peclet number of the dispersed phase is remarkably low, corresponding to great backmixing (figure 3). What is the reason for low Peclet numbers in case of dispersed phase? Experimental investigations of a single stationary layer showed, that the low Peclet number is the result of the dominating mixing effect of the great clarification zone in relation to the mixing effects of the small stationary layers. The plug-flow-like motion of the drop swarm shows no remarkable influence on the RTD-data.

2. COMBINED MODEL FOR A CENTRIFUGAL EXTRACTOR

2.1 The structure of the Combined Model

It was necessary to develop a better mixing model, because the Dispersion Model only gives one integral Peclet Number over the whole apparatus and no information about one single stage in the extractor. Based on the Tank in Series Model a Combined Model with different sized compartments was developed. The elements of this model are completely stirred tanks (CSTR) of different sizes and a plug-flow element as shown in fig. 4. The CSTRs are similar to the different sized stationary layers of the regarded liquid and the ring seals of the inlet and outlet of the extractor. The plug-flow element, which is composed of several different sized single plug-flow elements, is similar to the inlet and outlet borings, while the settling motion (plug-flow) is neglected. Figure 4 shows the Combined Model for a different number of stages. $F(0)$ is the system transfer function in the time domain. The

main advantage of this model is its modular structure. Single elements can be taken away or fitted in, depending on the structure of the apparatus. This means that the combined model only needs geometric information like the number of perforated sheets and the volume of the layers and the clearing zone. In the Combined Model are no fitting parameters like the Peclet number or the Mean Residence Time \bar{t} . The volume of the layers can be calculated by using working parameters and liquid data.

2.2 Height of the stationary layers of the dispersed phase

The calculation of the volume of the liquid layers is based on the height h of these layers, which is /3/

$$h = \left(\frac{w_N}{\mu}\right)^2 \frac{1}{r_N \omega^2} \frac{\rho_d}{\Delta \rho}$$

$$\mu = 0,63$$

in which $r_N \cdot \omega^2$ is the intensity of the centrifugal field, w_N the velocity of the dispersed jet and $\Delta \rho$ the difference of densities ($\rho_d - \rho_c$). Substituting the velocity of the dispersed phase w_N by the maximum velocity at the 3rd flooding point in case of dual-flow borings one can calculate the maximum height of the stationary layers h_{\max} of the dispersed phase:

$$h_{\max} = \left[\frac{K \cdot (Bo'')^{0.13}}{\mu \cdot \left(1 + \frac{\dot{v}_c}{\dot{v}_d}\right)} \right]^2 \frac{\rho_d}{2\Delta \rho} \quad K = 6.07 \cdot 10^{-3} \sqrt{m}$$

$\frac{\dot{v}_c}{\dot{v}_d}$ = throughput ratio

Bo'' is the modified Bond-Number in the centrifugal field:

$$Bo'' = d_N^2 \cdot \frac{\Delta \rho \cdot r_N \omega^2}{\sigma} \quad \sigma = \text{interfacial tension}$$

d_N = nozzle diameter

2.3 Comparison of the Combined Model and own experimental data basing on Peclet numbers

Figure 5 shows the Peclet number of the heavy liquid versus the dimensionless height of the principal interphase h_j/H . The minimum height $h_{j\min}$ is the height of the clarification zone added to the height of the very small layers of heavy liquid. In this case ($p_{1,\omega} - p_{h,\omega} = \max$) the heavy liquid is dispersed, whereas the light liquid is the continuous phase. If the pressure difference between the heavy and the light liquid decreases at the outlet, the height of the principal interphase h_j increases. In this case the heavy liquid in the inner stages is dispersed and the light liquid is continuous, whereas in the outer stages the heavy liquid is continuous and the light liquid dispersed. If the pressure difference ($p_{1,\omega} - p_{h,\omega} = 0$) is zero, the heavy liquid becomes the continuous phase in the whole extractor and the height of the principal

interphase is at its maximum (h_{Jmax}). In case of a continuous heavy phase the Peclet number has got its maximum value. Figure 5 shows the good consistency of computed values of the Combined Model with experimental data even in all intermediate stages. An examination of the light phase provides the same well-fitting results of the Combined Model.

2.4 Comparison of the Combined Model and literature data

The RTD-data of two different pilot centrifuges (Pod A-1, Pod B-10) /4,5/ could be simulated with the presented Combined Model (table 1). The fitting of the model in the varied parameter field was better than RSD < 7.5 %.

SUMMARY

Valuation of the different methods of evaluation respectively mixing models and their importance for the practice:

Using the mean \bar{t} and variance σ^2 of the pulse response curve is insufficient for RTD curves with long tailings ($Pe < 5$). But the mean and variance are useful as starting values for parameter fitting of the Dispersion Model in the time domain and for the elimination of the mixing effects of inlet and outlet facilities. Though the Dispersion Model could be fitted very well (RSD < 3%), it can hardly be used for scaling up, and thus it is of no importance for industrial practice.

The advantage of the Combined Model is its modular structure. Thus it is possible to develop a mixing model of satisfactory fitting (RSD < 10%) for all kinds of centrifugal extractors with radial phase flow, based on geometrical data and working parameters. The Combined Model seems to be suitable for scaling up different types of centrifugal extractors with radial phase flow.

Literature:

- /1/ Schilp, R.; Blaß, E.: Drop Formation at Rotating Orifices in a Centrifugal Field; Fluid Mechanics, Phase Separation and Interfacial Phenomena, ISEC '83, Denver
- /2/ Wen, C.Y.; Fan, C.T.: Models for Flow Systems and Chemical Reactors, Marcel Dekker, Inc., New York 10016, 1975
- /3/ Schilp, R.; Blaß, E.: The Flooding Capacity of Perforated Plates in Rotating Liquid-Liquid-Systems; Chem. Eng. Commun., Vol. 28 (1984) p. 85 ff.
- /4/ Todd, D.B.: Multiple Functions in a Centrifugal Extractor, Chem. Engn. Prog., Vol. 62 (1966) No. 8, p. 119 ff
- /5/ Todd, D.B.: Predicting Performance of Centrifugal Liquid Liquid Extractions; Baker Perkins Inc., Saginaw, Michigan, USA 48601

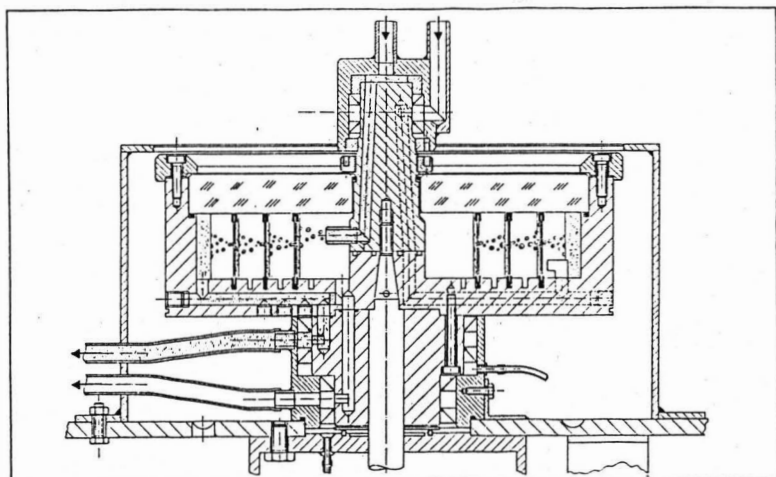


fig. 1 : Cross Section through the Model Extractor

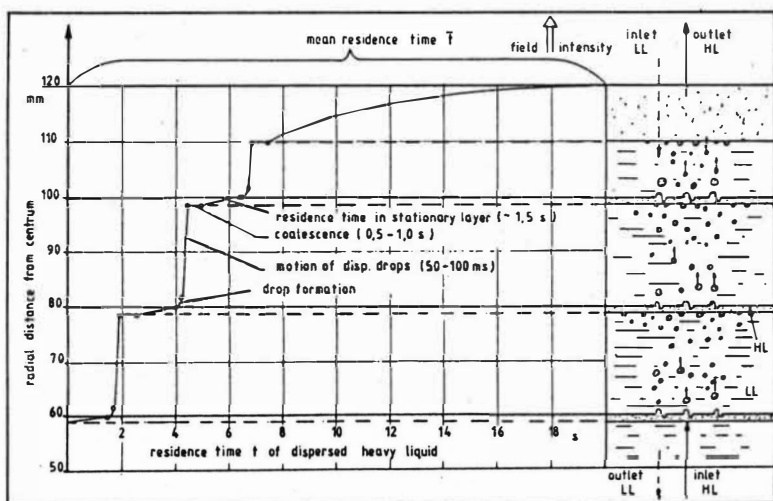


fig. 2 : Motion of a Fluid Particle as a Function of Time

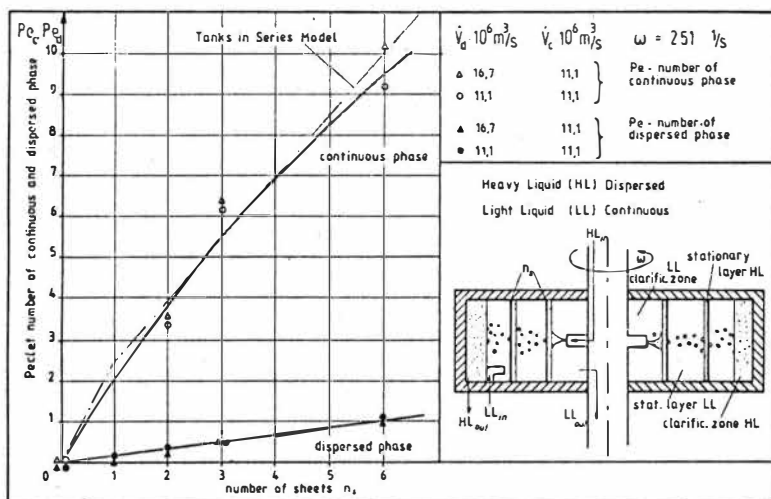


fig. 3 : Pelet Number of the Continuous and Dispersed Phase (HL dispersed)

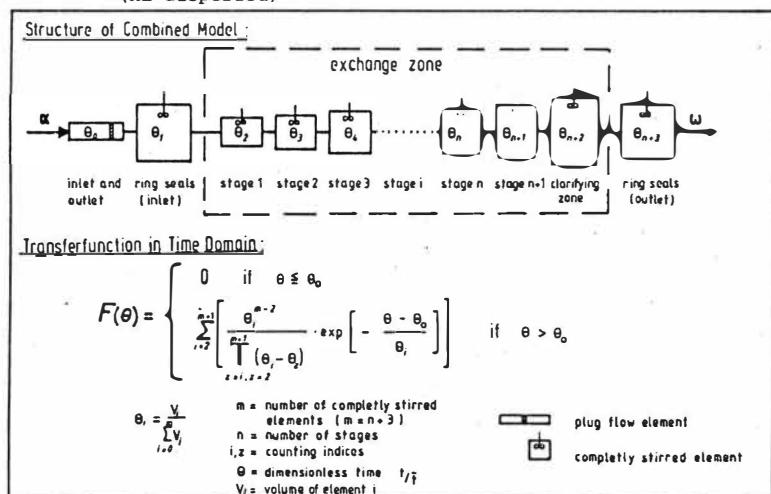


fig. 4 : Combined Model for a Centrifugal Extractor

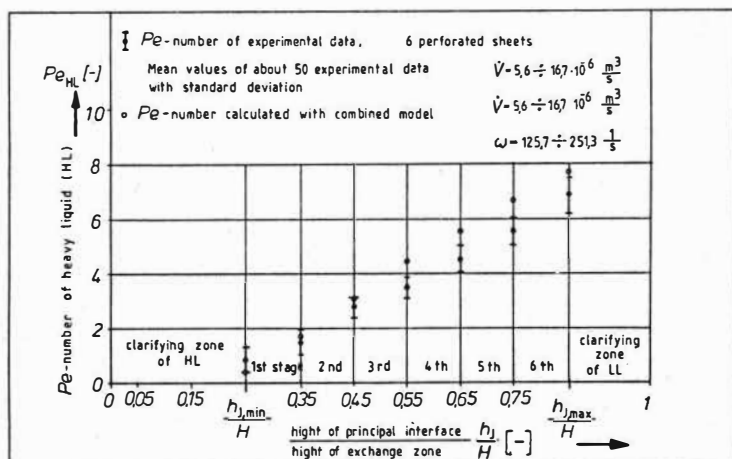


fig. 5 : Combined Model Compared to Experimental Data

Pod A-1, 7 perforated sheets, 2 sheets clarifying zone

\dot{V}_{HL} (water) m^3/s	\dot{V}_{LL} (kerosene) m^3/s	w $1/s$	$\frac{w^2}{\rho w}$ m/s^2	quality of fitting RSD %
$4.2 \cdot 10^{-6}$	$(0.5 \dot{V}_{LL} = 8.3 \cdot 10^{-6})$	1046	54775	1.6
$16.7 \cdot 10^{-6}$	*	1046	54775	4.0
$33.3 \cdot 10^{-6}$	*	1046	54775	4.81

Pod B-10, 28 perforated sheets, 2 sheets clarifying zone

\dot{V}_{HL} (water) m^3/s	\dot{V}_{LL} (kerosene) m^3/s	w $1/s$	$\frac{w^2}{\rho w}$ m/s^2	quality of fitting RSD %
$315 \cdot 10^{-6}$	$315 \cdot 10^{-6}$	209,3	6552	3.5
630	630	209,3	*	7.1
315	315	261,7	10270	6.3
1262	315	261,7	*	4.7
1073	1073	261,7	*	6.1
315	315	314,0	14789	7.5
1262	315	314,0	*	5.1
1262	1262	314,0	*	5.1

Table 1: Comparison between experimental RTD-data by Todd /4.5/ and the RTD-data computed with help of the Combined Model.

Scale-up of Industrial Gravity Settlers from Batch Settling Data

S.A.K. Jeelani, S. Hartland, TCL, ETH, Zürich, Switzerland.

The design of large scale liquid/liquid continuous gravity settlers from small scale batch settling tests is discussed. Batch experimental data for two liquid/liquid systems are used to predict the variation in the steady-state dispersion height with the volume rate of flow and the results obtained compared with experimental data on a continuous settler. The models employed are also successfully applied to published data on the kerosene/water system for a 122 cm diameter continuous settler and a 30.5 cm diameter batch settler.

Introduction

Liquid/liquid continuous vertical gravity settlers can be designed from batch settling tests (1,2), thereby eliminating the need for expensive pilot plant work. Generalized models applicable to both batch and continuous settlers are proposed (3,4), depending on whether the interfacial coalescence rate is controlled by the drop size, the height of the dense-packed zone or the total dispersion height. The aim of this paper is to demonstrate that even large gravity settlers can be designed from relatively small scale batch settling tests. Published experimental data on large settlers, together with our own data obtained using two different liquid/liquid systems, are utilized to verify the models employed.

Modelling

The theoretical models predicting the steady-state dispersion heights of the sedimentation and dense-packed zones from batch sedimentation and coalescence fronts are discussed in detail elsewhere (1-4) but are summarized here before applying them to the experimental data.

Height of Sedimentation Zone:

The sedimentation velocity of drops relative to the continuous phase, u_{sB} in an unsteady - state batch settler is :

$$u_{sB} = (-dx/dt)/(1-\bar{\epsilon}_s) = k_s t^{1/s}/(1-\bar{\epsilon}_s) \quad (1)$$

where $\bar{\epsilon}_s$ is the average dispersed phase hold-up fraction in the sedimentation zone, t the elapsed time and x the position of the sedimenting interface with respect to the final undisturbed interface. The exponent $1/s$ and constant k_s depend on the extent of binary coalescence and the physical properties of the liquid/liquid system. Integrating with $x = x_0$ when $t = 0$ and expressing in logarithmic form yields a straight line of slope $(1 + 1/s)$ and intercept $\ln(k_s/(1+1/s))$.

In a steady-state dispersion of cross-sectional area A the relative sedimentation velocity of drops u_{sC} is :

$$u_{sC} = (Q_d \beta / A \bar{\epsilon}_s) \{1 + \bar{\epsilon}_s (R-1)\} / (1 - \bar{\epsilon}_s) \quad (2)$$

where R is the ratio of volume flow rate of continuous phase Q_c to that of the dispersed phase Q_d and the drop residence time $t = \bar{\epsilon}_s H_s A / Q_d$, so that the equivalent of equation (1) in terms of the steady-state height of the sedimentation zone H_s is :

$$H_s = K_s (Q_d / A \bar{\epsilon}_s K_s)^{1/\beta} \quad (3)$$

where $K_s = k_s / \{1 + \bar{\epsilon}_s (R-1)\} \beta$. The value of β depends on the circulation and settler geometry, being unity when there is no circulation (which is generally true for a continuous settler with baffles at the dispersion feed inlet). In an unbaffled settler with circulation, $\beta = 1/(1 - \bar{\epsilon}_s)$. The value of $\bar{\epsilon}_s$ is usually greater than the hold-up fraction in the dispersion feed ϵ_f . Inspection of the above equation shows that H_s increases as $\bar{\epsilon}_s$ decreases, so inserting the feed hold-up ϵ_f leads to conservative values of H_s . Thus values of $1/s$ and k_s found from the experimental batch sedimentation profile up to the inflection point can be used in equation (3) to predict the variation in height of the sedimentation zone H_s with the volume rate of flow of the dispersed phase per unit area Q_d/A in the steady-state continuous settler.

Height of Dense-Packed Zone:

Interfacial coalescence rate; Dense-packed height controlled; Power function of dense-packed height.

When the volume rate of interfacial coalescence per unit area ψ_i is independent of the drop size and depends only on the dense-packed height (3)

$$\psi_i = -dy/dt = k_p h_p^p \quad (4a)$$

for a batch settler in which $h_p = (y - \bar{\epsilon}_s h) / (\bar{\epsilon}_p - \bar{\epsilon}_s)$ is the height of the dense-packed zone, with hold-up $\bar{\epsilon}_p$, h the total dispersion height and y the position of the coalescing interface with respect to the final undisturbed interface, and

$$\psi_i = Q_d/A = k_p H_p^p \quad (5a)$$

for a continuous settler in which the steady-state value of the dense-packed height is H_p . The experimental variation in $-dy/dt$ with h_p up to the inflection point t_{c*} of the batch coalescence profile gives k_p and p , which can be used to predict the variation in dense-packed height H_p with Q_d/A in a continuous settler.

Linear Function of Dense-Packed Height :

When the volume rate of interfacial coalescence ψ_i is a linear function of the dense-packed height so that $p = 1$, equations (4a) and (5a) reduce to :

$$\psi_i = -dy/dt = k_p h_p \quad (4b)$$

for a batch settler (2), and

$$\psi_i = Q_d/A = k_p H_p \quad (5b)$$

for a continuous settler. Furthermore, in a batch decaying dispersion, if the sedimentation is almost complete before interfacial coalescence commences (2), or if sedimentation is almost complete after the inflection point t_{c^*} , then for $t > t_{c^*}$ $x \approx 0$ and $h_p = y$, so that

$$-dy/dt = c_2 y \quad (6a)$$

$$\text{or } y = c_1 e^{-c_2 t} \quad \text{for } t > t_{c^*} \quad (6b)$$

$$\text{and } k_p = c_2 (\bar{\epsilon}_p - \bar{\epsilon}_s) / (1 - \bar{\epsilon}_s) \quad (6c)$$

Thus k_p determined from the experimental batch coalescence profile after t_{c^*} can be utilized in equation (5b) to predict the variation in the dense-packed height H_p with Q_d/A in a steady-state continuous settler. The total dispersion height H is then $H_s + H_p$.

Experimental:

A single-stage mechanically agitated mixer-settler unit with the following dimensions was used to investigate the settling characteristics of dispersions :

Perspex mixer	:	22 x 22 x 39 cm
Height to overflow	:	21.5 cm
Glass steady-state settler	:	20 cm diameter x 50 cm
Height to feed inlet	:	24 cm
Dispersion inlet feed diameter:	:	2.5 cm
Stainless steel impeller	:	6 straight flat-bladed turbine, 10 cm in diameter.

The closed loop arrangement and the experimental procedure have been discussed in detail elsewhere (2). The measurements investigated the effects of impeller speed and phase flow ratio on the variation in steady-state height with specific volume flow rate of dispersed phase Q_d/A using two liquid/liquid systems. Unsteady-state batch sedimentation and coalescence tests were also performed in the mixing tank of the mixer-settler unit.

Application to Experimental Data - Data of Ryon et al. (5)

The shapes of the experimental sedimentation and coalescence profiles (batch mixer decay) obtained by these authors using a 304.8 mm diameter unsteady-state batch settler with 0.1 M di(2-ethylhexyl) phosphoric acid in kerosene containing 30 g of tributyl phosphate per liter dispersed in aqueous 1 M sodium carbonate and 0.5 M sulphuric acid solution at 25°C with initial hold-up $\bar{\epsilon}_0 = 0.5$ can be seen from

Figure 1a to be sigmoidal in both x and y , inferring that the interfacial coalescence rate is a power function of the dense-packed height (1,3,4). Assuming $\bar{\epsilon}_s = \bar{\epsilon}_{s0} = \bar{\epsilon}_0 = 0.5$ ($\bar{\epsilon}_{s0}$ being the initial hold-up in the sedimentation zone) and $\bar{\epsilon}_p = 1.0$, the values of the parameters determined by least squares fits from sedimentation (equation (1)) and coalescence (equation (4a)) fronts up to the respective inflection points for the data of Ryon et al. (5) as shown in Figure 1a, are

$$k_s = 0.0449 \text{ cm/s}^{1+1/s} ; \quad 1/s = 0.4$$

$$k_p = 0.0071 \text{ s}^{-1} ; \quad 1/p = 0.47$$

The variation in the steady-state dispersion height H with the specific volume flow rate of dispersed phase Q_d/A obtained experimentally by these authors, using a 1220 mm diameter continuous settler with the above mentioned liquid/liquid system at 25°C ($0/W, \epsilon_f = 0.5$) is shown in Figure 1b (solid circles). The variations in the steady-state heights of the sedimentation and dense-packed zones H_s and H_p with Q_d/A are predicted by using equations (3) and (5a), with $\beta = 1$ and the values of the parameters given above. The predicted variation in steady-state dispersion height H with Q_d/A (full line), which is the sum of the predicted variations in H_s and H_p with Q_d/A , is shown in Figure 1b (also shown is the variation in H_p with Q_d/A). The agreement between the experimental and predicted variations in H with Q_d/A can be seen to be very good, despite the fact that the steady-state settler is 16 times larger in area than the unsteady-state batch settler.

Present Data :

Figures 2a and 3a show the variations in the positions x and y of the sedimenting and coalescing interfaces relative to the final undisturbed interface obtained from flow (FMD) and batch (BMD) mixer decay unsteady-state batch settling experiments ($\bar{\epsilon}_0 = 0.5$) corresponding to steady-state runs SR 105 and SR 202 for the systems 50% n-heptane in paraffin oil dispersed in water (System A) and 40% toluene in paraffin oil dispersed in water (System B) at 20°C. As can be seen, the sedimenting front in each of the Figures has an inflection point, so equation (2) is used to compute the values of k_s and $1/s$, listed in Table 1.

Table 1

System :	A		B	
$k_s, \text{cm/s}^{1+1/s}$	FMD	BMD	FMD	BMD
	0.0131	0.0079	0.0066	0.0046
$1/s$	0.6242	0.7443	0.6030	0.6390
k_p, s^{-1}	0.0149	0.0100	0.0071	0.0073

These values of $1/s$ and k_s are utilized in equation (3) to predict the variation in height of the sedimentation zone H_s with specific flow rate of dispersed phase Q_d/A in a steady-state settler, using $\bar{\epsilon}_s = \bar{\epsilon}_{s0} = \bar{\epsilon}_0 = 0.5$ and with $\beta = 1/(1-\bar{\epsilon}_s)$, since

no baffles are used.

It can also be seen from Figures 2a and 3a that although the value of y varies with time, the value of $-dy/dt$, up to the inflection point t_{c*} is less than Q_d/A in the corresponding steady-state experiments, but that after the inflection point the variation in y with t is exponential, during which sedimentation is almost complete. This is confirmed by the low average deviations between the measured values of y and those predicted by equation (6b) for $t > t_{c*}$ for both flow and batch mixer decay (8.8% and 9.8%; 4.3% and 2.6%). This means that the interfacial coalescence is a linear function of the dense-packed height. So the values of k_p computed from equation (6c) are listed in Table 1 and utilized in equation (5b), using $\bar{\epsilon}_s = \bar{\epsilon}_{s0} = 0.5$, and with values of $\bar{\epsilon}_p = 0.75$ and 0.875 for phase systems A and B respectively to predict the variation in steady-state dense-packed height H_p with Q_d/A .

Figures 2b and 3b show comparisons between the variation in steady-state height H ($=H_s + H_p$) with the specific volume flow rate of dispersed phase Q_d/A , predicted from typical unsteady-state batch settling experiments (both flow and batch mixer decay in Figures 2a and 3a), corresponding to steady-state runs SR 105 and SR 202, and that determined experimentally (full lines represent the curves generated by the power law $H = K(Q_d/A)^W$, with the constants obtained by least squares fits of the experimental steady-state runs: 6 for phase system A and 4 for phase system B). The open and solid circles refer to the predicted variation in H with Q_d/A from FMD and BMD experiments respectively. The predicted variation in H_p is also shown. Agreement between the predicted and experimental variations in H with Q_d/A is once again very good.

References

1. S.A.K. Jeelani and S. Hartland, *AIChE J.* **31**, 711-720 (1985)
2. S.A.K. Jeelani and S. Hartland, *Chem.Eng.Res.Des.*, in Press (1986)
3. S. Hartland and S.A.K. Jeelani, *I.Ch.E.Symp.Series No. 94*, Vol.II, 211-223 (1985)
4. S.A.K. Jeelani, *Ph.D.Thesis*, ETH Zürich (1985)
5. A.D.Ryon, F.L. Daley and R.S.Lowrie, Report No.ORNL-2951, Oak Ridge National Laboratory, Tennessee, 1960.

Acknowledgement

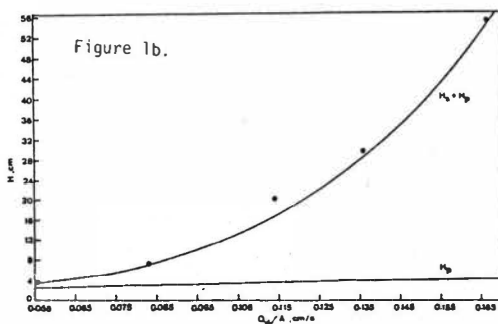
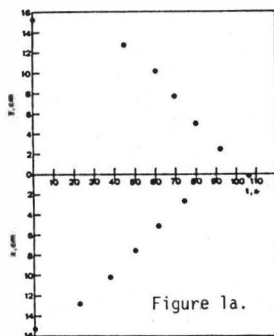
The experiments for phase system B were performed by Pius Abgottspon.

Nomenclature

A	cross-sectional area of settler
c_1, c_2	constants in exponential decay of the batch coalescence front
h_s, h_p	heights of sedimentation and dense-packed zones in a batch dispersion
H_s, H_p	heights of sedimentation and dense-packed zones in a continuous dispersion
H	sum of heights of sedimentation and dense-packed zones in a continuous dispersion
k_s, K_s, k_p	constants in sedimentation and coalescence equations
p	exponent in equations for interfacial coalescence rate
Q_c, Q_d	volume rates of flow of continuous and dispersed phases in a continuous settler
R	ratio of volume rate of flow of continuous phase to that of dispersed phase
s	exponent in sedimentation equations
t	elapsed or residence time
u_{sB}, u_{sC}	relative velocities of drops in batch and continuous settlers
x, y	positions of sedimenting and coalescing interfaces relative to the final undisturbed interface in a batch dispersion

Greek Symbols

β	parameter accounting for the degree of circulation in a continuous settler
$\bar{\epsilon}_s, \bar{\epsilon}_p$	average hold-up fraction of dispersed phase in sedimentation and dense-packed zones
$\bar{\epsilon}_0$	initial hold-up in a batch dispersion
$\bar{\epsilon}_{s0}$	initial hold-up in sedimentation zone in a batch dispersion
ϵ_F	hold-up in feed to a continuous settler
ψ_i	volume rate of interfacial coalescence per unit area



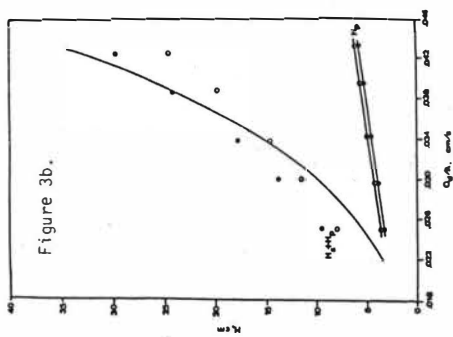
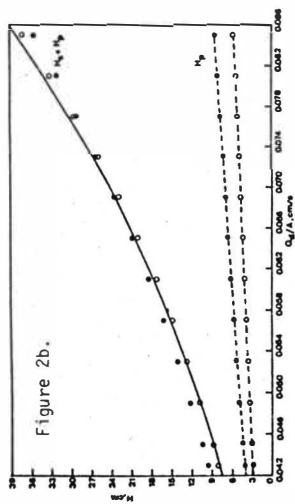
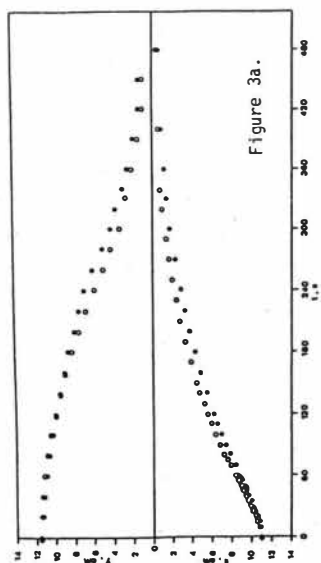
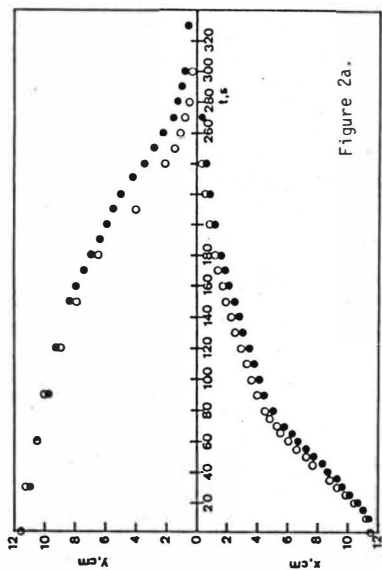


Figure Captions:

Figure 1a : Variation in the positions of sedimenting and coalescing interfaces, x and y with time, t (solid circles) obtained in a 30.5cm diameter batch settler. Data of Ryon et al.(5).

Figure 1b : Variation in H with Q_d/A obtained experimentally (solid circles) from a 122cm diameter steady-state settler by Ryon et al.(5) compared with that predicted from the batch settling data shown in Figure 1a (full line). The predicted variation in H_p is also shown.

Figure 2a : Variation in the positions of sedimenting and coalescing interfaces, x and y with time, t for phase system A. Open and solid circles represent Flow and Batch Mixer unsteady-state decay data corresponding to the steady-state run SR 105.

Figure 2b : Comparison between predicted and experimental variation in H with Q_d/A . Full line is the power law curve for the experimental steady-state runs SR 101 to SR 106. Open and solid circles represent the predicted variations in H and H_p (joined by the straight lines) with Q_d/A from the Flow and Batch Mixer decay experiments shown in Figure 2a.

Figure 3a : Variation in the positions of sedimenting and coalescing interfaces, x and y with time, t for phase system B. Open and solid circles represent Flow and Batch Mixer unsteady-state decay data corresponding to the steady-state run SR 202.

Figure 3b : Comparison between predicted and experimental variation in H with Q_d/A . Full line is the power law curve for the experimental steady-state runs SR 202 to SR 205. Open and solid circles represent the predicted variations in H and H_p (joined by the straight lines) with Q_d/A from the Flow and Batch Mixer decay experiments shown in Figure 3a.

C. Schaller and G. Kreysa

Dechema-Institut, Frankfurt/Main

Axial dispersion describes the deviation of the real reactor behaviour from that of the ideal plug flow reactor, i.e. the degree of axial mixing within the reactor. It is the crucial factor which determines product yield and selectivity of the reactor. Particularly scale-up problems are strongly related to the influence of axial dispersion. Traditionally axial dispersion is investigated by tracer methods. A clearly defined tracer signal (eg. a pulse) is modulated at the reactor inlet. The response of the reactor to this signal detected at the outlet is a direct measure of the axial dispersion.

Obviously there are two extreme cases: the ideal mixer and the plug flow reactor. The response of the ideal mixer to a pulse inlet signal is an exponentially decreasing transient without time delay. The plug flow reactor response on the other hand is the unchanged inlet signal delayed by the reactor residence time. The response of a real reactor shows a time-delayed and modulated signal. However, the interpretation of the outlet response can be difficult as a result of a non-ideal input signal. Furthermore the tracer method is not suitable for measurements of the dispersed phase of a two phase reactor.

This paper describes a new method to measure the axial dispersion of a reactor. The experimental set up is a loop consisting of the reactor and an electrochemical stirred cell (see Figure 1).

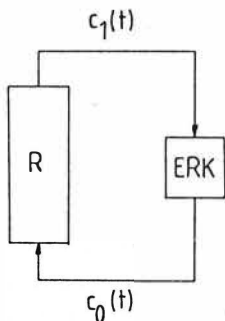


Fig. 1: Non-steady state reactor loop for the investigation of the axial dispersion of reactor R

The active species of the electrolyte is converted in the stirred cell only while there is no conversion within the reactor. Hence, the reactor only imprints its hydrodynamic behaviour on the concentration transient which can be measured without time delay via the current of the cell if it is operated within the diffusion controlled range.

In order to be able to interpret the experimental transient the mathematic modelling of the loop is essential. The modelling of a steady state recycle reactor does not cause any problems /1/. However, study of the transient behaviour of reactor circuits is still under development /2/ and the present loop (see Figure 1) requires the consideration of its transient behaviour.

The following dynamic modelling of the loop regards the reactor as a cascade of N ideal mixers. The solution is then capable to calculate the concentration transient of the stirred cell as a function of the number of ideal mixers forming the reactor. Fitting the theoretical to the experimental concentration transient yields the number of ideal mixers of the cascade which describes the investigated reactor best. The well-known relation

$$B_0 = \frac{\sqrt{4(N-1)^2 - 1}}{D_{ax}} = \frac{u}{D_{ax}} \quad (1)$$

allows the calculation of the axial dispersion.

Dynamic modelling

The modelling of the loop bases on the material balances of the individual ideal mixers of the cascade and of the stirred cell.

The Laplace-transformation appears most suitable for finding the solution of this system of differential equations /3/.

The material balance for the active species in the stirred cell yields:

$$V_B \frac{dc_0}{dt} = Q(c_1 - c_0) - A_e k_e c_0 \quad (2)$$

Eq. (2) can be transformed into the Laplace region /3/ describing the relationship between inlet and outlet concentration of the stirred cell:

$$\bar{c}_1 = \tau_B \left(s + \frac{1}{\tau_B} + \frac{A_e k_e}{V_B} \right) \bar{c}_0 - \tau_B c^* \quad (3)$$

The material balance for the i^{th} mixer of the cascade (no conversion) is:

$$\frac{V_R}{N} \frac{dc_i}{dt} = Q(c_{i-1} - c_i) \quad (4)$$

The Laplace-transformation yields the successive relationship between the transformed concentrations of adjacent mixers:

$$\bar{c}_i = \frac{c^\circ}{s + \frac{N}{\tau_R}} + \frac{\frac{N}{\tau_R}}{s + \frac{N}{\tau_R}} \bar{c}_{i-1} \quad (5)$$

Eliminating all concentrations of the internal mixers of the cascade forms the transformed balance of the cascade:

$$\bar{c}_1 = \frac{c^\circ}{s + \frac{N}{\tau_R}} \sum_{i=0}^{N-1} \left(\frac{\frac{N}{\tau_R}}{s + \frac{N}{\tau_R}} \right)^i + \left(\frac{\frac{N}{\tau_R}}{s + \frac{N}{\tau_R}} \right)^N \bar{c}_0 \quad (6)$$

According to dynamic systems analysis /4/ the recycle of the reactor outlet via the stirred cell imprints a particular perturbation function on the reactor inlet. Mathematically this means to find the solution of the differential equation describing the cascade taking into account the boundary value conditions for inlet and outlet caused by the recycle through the stirred cell. This complex procedure can be handled in the Laplace region fairly comfortably.

Eq. (3) in eq. (6) eliminates \bar{c}_1 finally yielding an equation for \bar{c}_0 representing the transformation of the concentration in the stirred cell:

$$\bar{c}_0 = c^\circ \left[\frac{1}{s} - \frac{A_e k_e}{v_B} \left\{ \frac{1}{s} \frac{1}{s+a} + \sum_{i=1}^{\infty} \frac{1}{\tau_B^i} \left(\frac{N}{\tau_R} \right)^{iN} \frac{1}{s} \frac{1}{(s+a)^{i+1}} \frac{1}{(s+b)^{iN}} \right\} \right] \quad (7)$$

$$a = \frac{1}{\tau_B} + \frac{A_e k_e}{v_B}, \quad b = \frac{N}{\tau_R}$$

A rather complex retransformation allows the calculation of the concentration of the stirred cell at any time and for any number of mixers forming the reactor cascade:

$$\frac{c_o(t)}{c^o} = 1 - \frac{A_e k_e}{V_B} \frac{1}{a} \left[1 - \exp(-at) \right]$$

$$- \frac{A_e k_e}{V_B} \sum_{i=1}^{\infty} \left\{ \frac{1}{\tau_B^i} \left(\frac{N}{\tau_R} \right)^{iN} \times \int_0^t \left[\int_0^u \frac{p^i \exp(-ap)}{i!} dp \frac{u^{iN-1} \exp(-bu)}{(iN-1)!} \right] du \right\}$$

$$a = \frac{1}{\tau_B} + \frac{A_e k_e}{V_B} \quad b = \frac{N}{\tau_R} \quad (8)$$

Under the given experimental conditions this concentration transient is directly accessible via the current of the stirred cell.

Assuming that the reactor is an ideal plug flow reactor without conversion (i.e. no axial dispersion) the material balance for the active species is:

$$\frac{\partial c(t,x)}{\partial t} + u \frac{\partial c(t,x)}{\partial x} = 0 \quad (9)$$

Transforming the t variable and solving the resulting differential equation in x yields the equation for the transformed outlet concentration of the plug flow reactor:

$$\bar{c}(s,L) = c^o \frac{1 - \exp(-\tau_R s)}{s} + \bar{c}(s,0) \exp(-\tau_R s) \quad (10)$$

where $\bar{c}(s,L) = \bar{c}_1$
 $\bar{c}(s,0) = \bar{c}_0$

The combination of eq. (3) and eq. (10) eliminates \bar{c}_1 yielding the transformed stirred cell concentration for the loop:

$$\bar{c}_0 = c^o \frac{\tau_B s + 1 - \exp(-\tau_R s)}{s \left[\tau_B s + 1 + a_e k_e \tau_B \exp(-\tau_R s) \right]} \quad (11)$$

The retransformation of eq. (11) allows the calculation of the stirred cell concentration at any time for the loop with ideal plug flow reactor:

$$\frac{c_0(t)}{c^*} = 1 - a_e k_e \tau_B \sum_{i=0}^{\infty} \left(\frac{1}{\tau_B}\right)^{i+1} \frac{1}{i!} \int_0^t \langle t - i\tau_R \rangle^i \exp\left[-\frac{a}{\tau_B} \langle t - i\tau_R \rangle\right] dt \quad (12)$$

$$a = 1 + a_e k_e \tau_B$$

Figure 2 illustrates the performance of eq. (8) and (12) for a loop of a large reactor and a relatively small electrochemical stirred cell. The influence of axial mixing within the reactor is clearly visible.

The steep decline of the concentration at the beginning is a result of the rapid disappearance of the active species in the stirred cell. For the case of the ideally mixed reactor the concentration transient changes into a smooth decline for any time after the residence time of the stirred cell. This is because changes at the inlet of the ideally mixed reactor cause immediate changes at the outlet (see Figure 1).

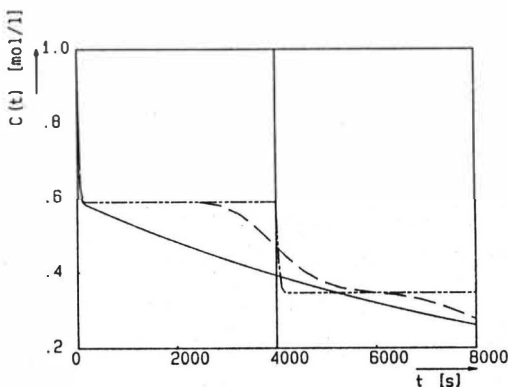


Fig. 2: Influence of axial dispersion on the concentration transient of the electrochemical stirred cell

- $D \rightarrow \infty$, equivalent number of mixers $N = 1$
- - - - - $0 < D < \infty$, equivalent number of mixers $N = 30$
- · - · - $D = 0$, equivalent number of mixers $N = \infty$

parameters: $a_e = 5 \text{ cm}^{-1}$; $k_e = 3.5 \cdot 10^{-3} \text{ cm s}^{-1}$;

$$V_B = 200 \text{ cm}^3 ; V_R = 20,000 \text{ cm}^3 ; Q = 5 \text{ cm}^3 \text{ s}^{-1}$$

The other extreme, the ideal plug flow reactor, shows a stepwise decline of the concentration in the stirred cell (see Figure 2). Until the reactor residence time of 4,000 s the feed of the stirred cell is the unchanged initial concentration c^* of the loop, hence, the horizontal course of the cell concentration until 4,000 s.

As expected the transient for the loop with a real reactor lies between both extremes.

Figure 2 proves that it should be possible to fit a theoretical transient to the experimental transient by varying the number of equivalent mixers forming the reactor as a direct measure of the axial dispersion of the investigated reactor (eq. (1)). Furthermore this new method is not restricted to a single phase reactor but it allows the quantitative measurement of the axial dispersion of both phases of an extractor assuming that both phases are conductive. Experiments to analyse the performance of this method are in progress.

The authors acknowledge Deutsche Forschungsgemeinschaft (DFG) for the financial support of this work.

Symbols

a_e	cm^{-1}	specific electrode surface
A_e	cm^2	electrode surface
Bo	-	Bo-number
c	mol cm^{-3}	concentration
D_{ax}	$\text{cm}^2 \text{s}^{-1}$	axial dispersion coefficient
k_e	cm s^{-1}	electrochemical mass transfer coefficient
L	cm	reactor length
N	-	number of mixers of the cascade
Q	$\text{cm}^3 \text{s}^{-1}$	flow rate
s	s^{-1}	Laplace transformed time
t	s	time
u	cm s^{-1}	supervicial velocity
V	cm^3	volume
x	cm	locus
τ	s	residence time

Indices

B	stirred cell
R	reactor
*	initial
-	Laplace transformed form
o	inlet
l	outlet

Step function

$$f(x) \begin{cases} = f(x) & \text{for } x \geq 0 \\ = 0 & \text{for } x < 0 \end{cases}$$

Literature

- /1/ Levenspiel, O.: Chemical Reaction Engineering, John Wiley & Sons, New York 1972
- /2/ Fahidy, T.Z.: Principles of Electrochemical Reactor Analysis, Chapter 10, Elsevier, Amsterdam 1985
- /3/ Holbrook, J.G.: Laplace-Transformation, Friedr. Vieweg + Sohn, Braunschweig, 1973
- /4/ Stephanopoulos, G.: Chemical Process Control, Part III, Prentice-Hall, Englewood, Cliffs/New Jersey 1984

Effective Interfacial Area In the RTL Contactor From Rates of Extraction With Chemical Reaction

E. Alper

Chemical Engineering Department, University of Petroleum
and Minerals, Dhahran 31261, Saudi Arabia

Summary

The values of aqueous phase physical transfer coefficient and effective interfacial area of RTL (formerly Graesser) extractor were obtained at different rotor speeds. For the latter, the methodology of liquid extraction accompanied by fast pseudo - first order reaction was used. It was confirmed that the alkaline hydrolysis of n-butyl formate could be conveniently employed for this purpose.

Values of the aqueous phase mass transfer coefficient varied between 2.5×10^{-5} m/s and was highest at rotor speeds of about 0.2 rev/s. The effective interfacial area varied between 90-140 m^2/m^3 for rotor speeds of 0.06 - 0.25 rev/s.

Introduction

The RTL (formerly Graesser raining-bucket) extractor consists of a single rotor operating on a substantially horizontal axis in a cylindrical stator (see Figure 1). The rotor comprises a series of circular baffles, between which are mounted a number of cylindrical buckets, partly open in the direction of rotation. The extractor is filled with two liquid phases and the interface level is controlled at the equatorial position. Thus the slow motion of the rotor causes each phase to cascade through the other to provide the contacting (1).

The fundamentals of the operation of the RTL contactor have not been studied as extensively as have those of other commercial contactors, but some preliminary studies have been made on axial mixing and overall mass transfer rate in a glass pilot-scale unit (0.15m diameter and 0.76 m long) by Sheikh et. al. (2) and Wang et. al (3). However no information is available about the individual mass transfer coefficients and the effective interfacial area. The latter has been often obtained by physical methods, such as light transmission, photography and the concept local isotropy for liquid-liquid systems (4). On the other hand, for gas-liquid systems it is common and indeed convenient to use chemical methods for measuring interfacial area (5, 6). Extraction with reaction was first used by Nanda and Sharma (7) for measuring effective interfacial area in liquid-liquid extractors. A convenient system for such studies is the alkaline hydrolysis of n-butyl formate. In this investigation, individual volumetric mass transfer coefficient and the effective interfacial area of a pilot-plant scale Graesser extractor have been obtained from the measured extraction rates of pure n-butyl formate into either water or sodium hydroxide solutions respectively.

Equipment

Graesser Extractor: The basic construction of the experimental contactor is as illustrated in Figure 1. It was based on a 0.15m (6 inch) diameter by 1 meter long QVF precision bore glass pipe section with buttress ends to which stainless steel end plates were fixed using QVF cast iron backing rings. The stainless steel rotor assembly consisted of 36 compartments, each one 0.025m (one inch) long and containing eight buckets. The annular gap between the rotor and shell was 2.36×10^{-3} m (3/32 inch). The rotor assembly was driven by a constant speed motor and using a gear-box the speed could be varied between 4-20 rev/min accurately. The pilot plant facilities contained also two overhead tanks which allowed normally flowrates of each phase between $3-15 \times 10^{-6}$ m³/s. The temperatures of both phases at both ends were also measured by using thermocouples.

Stirred Cell: The kinetics of the alkaline hydrolysis of n-butyl formate was investigated in a 0.075m inside diameter stirred cell where the organic phase and the aqueous phase were stirred independently. The stirrers were mounted on concentric shafts which were driven by separate variable speed motors. They were turbine type on a 0.03m diameter disk and had 6 paddles of 0.01m x 0.01m each. The cell contained also four rectangular baffles and at the stirring speeds employed (60-90 rev/min), the interface remained plane so that the interfacial area could be taken as the cross sectional area of the cell minus that of the shaft. The stirred cell contained a jacket through which constant temperature water was circulated which gave a temperature control of $\pm 0.5^\circ\text{C}$.

Aqueous Phase Mass Transfer Coefficient

Aqueous phase mass transfer coefficient ($k_L A$) of the Graesser extractor was measured by extracting pure n-butyl formate into water at different rotor speeds. Experimental difficulties and economical considerations necessiated a procedure where only water flowed, however the level was kept near equatorial position by the addition of pure n-butyl formate intermittently. Samples were taken from the outlet water phase and analysed for n-butyl formate content by the saponification method which was found to be satisfactory. The present equipment (which is currently being modified) does not allow sampling anywhere except at the outlet. This necessiated employment of a liquid flowrate (31.55×10^{-6} m³/s) which was considerably higher than the normally recommended flowrate range, but of course, prevented the saturation of the leaving water.

Because of the highly complex and ill-defined nature of the existing two-phase flow in the contactor, it seems reasonable to propose a simplified model. Thus we may assume that the complete mixing takes place at the annular gap between compartments and the bulk concentration of the dissolved n-butyl formate in any compartment could be taken as the average concentration of liquid entering to this compartment.

This leads to the following difference equation for the nth compartment:

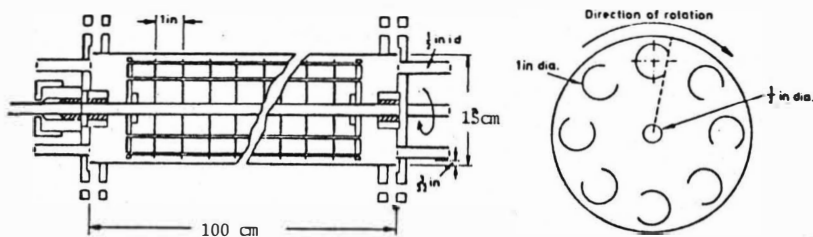


Figure 1. Constructional details of raining-bucket extractor.

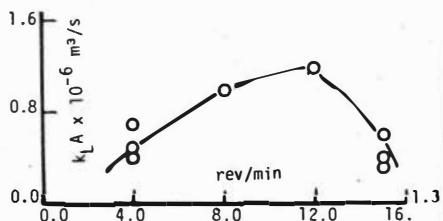


Figure 2. Aqueous phase physical mass transfer coefficient as function of rotor speed.

Figure 3. Typical results of hydrolysis of n-butyl formate in the stirred cell.

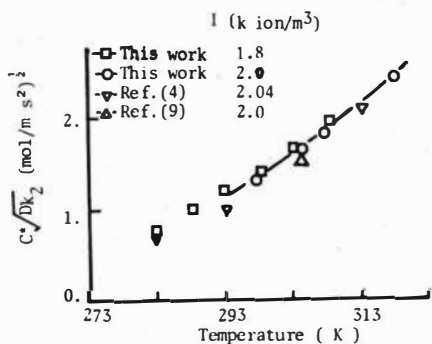
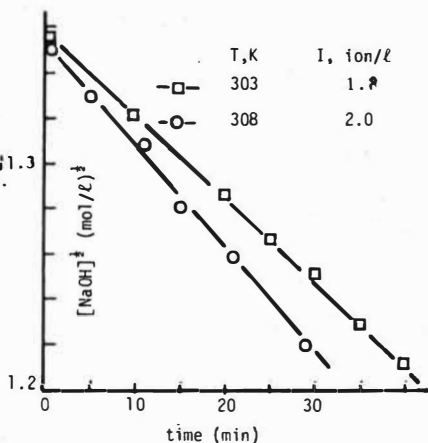


Figure 4. $C^* \sqrt{Dk_2}$ against temp.

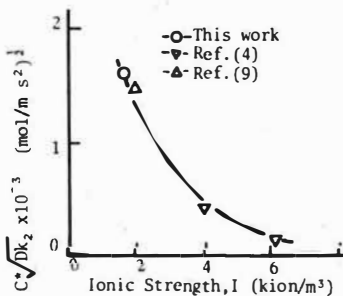


Figure 5. $C^* \sqrt{Dk_2}$ at different concentrations of NaOH as function of I.

$$k_{Ln} A_n (C^* - C_{n-1}) = L(C_n - C_{n-1}) \quad (1)$$

where L is the volumetric flowrate of water, k_{Ln} is the aqueous phase mass transfer coefficient, A_n is the effective interfacial per compartment, C^* is the solubility of *n*-butyl formate in water and C_n is the concentration of *n*-butyl formate in the water stream which is leaving the *n*th compartment. Since k_L and A are likely to be independent of n , we may take $k_{Ln} A_n$ as constant throughout the extractor. Then Eqn. (3) becomes linear and can be solved to give (Alper (8)):

$$\ln \frac{C^* - C_0}{C^* - C_N} = -N \ln \left(1 - \frac{k_L A}{L} \right) \quad (2)$$

where C_0 and C_N are concentrations of *n*-butyl formate in the aqueous phase at the inlet and outlet of the extractor. It can easily be shown that Eqn. (2) becomes identical with that obtained from the plug flow model only if $(k_L A/L) \ll 1$. In order to calculate $k_L A$ from the measured inlet and outlet concentrations of C_0 and C_N , the solubility C^* is also required. However, such solubility data for esters are not only scarce but also erroneous since *n*-butyl formate hydrolyses slowly in water. The value of C^* was obtained experimentally taking care to avoid hydrolysis of *n*-butyl formate, that is by not allowing the pH to drop below 4. Table 1 shows the results which compare well with that of Nanda and Sharma (4).

Figure 2 shows the experimental results at one flowrate for different stirring speeds which were calculated using Eqn. (2). These results represent the most unexpected behaviour which is quite contrary to that found in other form of mechanically agitated extractor. These results are to some extent difficult to reproduce and the exact reason for the above mentioned behaviour is not clear. However this may be due to change in the droplet mass transfer regime as suggested by Wang et. al. (3) to explain their results of similar behaviour. The range of k_L values (which was estimated using the measured interfacial area per compartment, A) lies in the order of around $2 - 5 \times 10^{-5}$ m/s which correspond, for instance, to those obtained in spray columns for the same chemical system (4, 9).

Effective Interfacial Area from Chemical Methods

Reaction Kinetics of Alkaline Hydrolysis of *n*-Butyl Formate: The chemical reaction follows:



and it is known to be first order with respect to both ester and the OH^- ions (4, 10, 11). The kinetic data and the second order rate constant k_2 are available both at infinite dilution (12) and also for concentrated solutions (4, 9-11). However for the analysis of extraction with reaction experiments in the Graesser extractor it is necessary to know the value of $C^* \sqrt{Dk_2}$. The solubility (C^*) and the diffusivity (D) of the dissolved component cannot of course, be measured directly in reactive solutions. On the other hand $C^* \sqrt{Dk_2}$ can conveniently be measured in a contactor

with a known interfacial area (13). Therefore for the purpose of both checking the kinetics and obtaining $C^* \sqrt{D k_2}$ data for the relevant solution, certain number of experiments were carried in the stirred cell.

In the experiments, pure n-butyl formate and approximately 2N NaOH were contacted in the cell and 3 ml aqueous phase samples were withdrawn at intervals of 5 - 15 minutes. Since the liquid extraction is accompanied by fast pseudo first order reaction, the extraction rate per unit interfacial area is given by (13):

$$R = C^* \sqrt{D k_2} B^0 \quad (2)$$

where B^0 is the bulk concentration of OH ions. Thus, the integration of a mass balance equation gives:

$$\sqrt{B^0} = \sqrt{B_1^0} - \left(\frac{S}{2V} C^* \sqrt{D k_2} \right) t \quad (4)$$

where S is the interfacial area (which is taken as the cross-sectional area minus that of the shaft) and V is the aqueous phase volume (which was always $2 \times 10^{-4} \text{ m}^3$). Figure 3 shows two typical results at two different temperatures as $\sqrt{B^0}$ against time plots. Similar results have been obtained at different temperatures and from the slopes of these straight lines $C^* \sqrt{D k_2}$ was calculated according to Eqn. (4). Figure 4 shows $C^* \sqrt{D k_2}$ as function of temperature. The same figure shows also the results of other workers. Our results compare well with those of the others, however they are consistently higher. The value of $C^* \sqrt{D k_2}$ is strongly influenced by the concentration of the solution since C^* , D and k_2 are all decreased in concentrated solutions. Figure 5 shows the effect of ionic strength.

Measurement of the Effective Interfacial Area from the Rates of Extraction with Reaction

For this purpose, initially a solution of approximately 2N NaOH and pure n-butyl formate were flowed counter-currently for the flow ranges of the pilot-plant as supplied by the manufacturer, that is between $5-10 \times 10^{-6} \text{ m}^3/\text{s}$. However due to highly exothermic reaction, the temperature of leaving liquid raised to about 318 to 323 K from about 295 K. Later, the extractor operation was modified so that the organic phase was always batchwise and 0.6 m^3 of aqueous solution was recirculated at the flowrate of $3.15 \times 10^{-5} \text{ m}^3/\text{s}$. However, this high flowrate allowed an operation only at low stirring speeds; otherwise the organic phase was entrapped in the leaving liquid.

Making a mass balance around the n -th compartment by assuming complete mixing at the annular gap and by taking the bulk concentration as that of entering from the previous one gives:

$$-L(B_n^0 - B_{n-1}^0) = A_n C^* \sqrt{D k_2} B_{n-1}^0 \quad (5)$$

Eqn. (5) assumes fast pseudo first order reaction regime which is justified since the necessary condition is satisfied everywhere (13):

$$(B^0/C^*) \gg \sqrt{DK_2} B^0/k_L > 5 \quad (6)$$

Taking A_n as constant and noting that $C^*\sqrt{DK_2}$ increases along the contactor due to the temperature rise Eqn. (5) can be rewritten as:

$$B_{n+1}^0 = B_n^0 - (Ak_n/L)(B_n^0)^{\frac{1}{2}} \quad (7)$$

where

$$K_n = (C^*\sqrt{DK_2})_n \quad (8)$$

Eqn. (7) is already nonlinear even for isothermal condition; in addition, because of the temperature increase the value of $C^*\sqrt{DK_2}$ varies significantly. The value of A was obtained from the measured concentrations (B_0 and B_{36}^0) and temperatures at the inlet and outlet respectively and using Eqn. (7). In the calculations the value of K was evaluated from Figure 4 either at the arithmetic mean temperature or from an assumption that the temperature rise is linear. Both procedures are, of course, justified at high flowrates (or for low temperature increases) and the latter should yield more accurate results when the temperature rise is significant. In this case, Eqn. (7) was solved numerically assuming a value for A and optimising it so that the calculated B_{36}^0 was within 1% of the measured one.

Table 2 shows the results of experiments and the calculated values of effective interfacial area per compartment (A) at different rotor speeds. These data are, of course, very limited, however it covers the range which is of practical interest for Graesser extractor. It shows also that the variation with rotor speed is not substantial. It was not possible to compare these results with any other data since no published information could be found in the literature. However, the work in our laboratory is in progress and will involve both the hydrolysis of another ester (n-propyl chloroacetate) and a physical method, i.e. photography.

Conclusions

This work confirmed that the extraction of pure n-butyl formate into water or alkaline solutions is a very convenient system for determining aqueous phase mass transfer coefficient $k_L a$ and also effective interfacial area a in pilot-scale extractors. Both the parameter $C^*\sqrt{D}$ and the second order reaction rate constant k_2 are strongly affected by the ionic strength. It is therefore recommended that rather than estimating these values, the parameter $A^*\sqrt{D_A k_2}$ may best be measured in a model extractor with a rigorously defined liquid-liquid contact area, such as a stirred cell with plane interface. k_L values lie in the range of 2.5×10^{-5} m/s which compare favourably with those of other extractors. It has been found that the maximum value of k_L corresponds to a rotor speed of approximately 0.2 rev/s. This finding

Table 1. Solubility of n-butyl formate in water at different temperatures

Temperature (K)	299.5	303.0	303.5	313.0	314.0
Solubility $\times 10^2$ (k mol/m ³)	7.2	7.8	7.5*	8.1*	8.6

*From Ref. (4)

Table 2. Effective Interfacial area per compartment in the raining - bucket extractor, A

Run	B**(kmol/m ³)		Flowrates $\times 10^6$ (m ³ /s)		Rotor Speed rev/s	Temp(K)		A $\times 10^2$, m ²	
	In	Out	Aqueous	Organic		Inlet	Outlet		
1	1.94	0.16	6.25	6.25	0.25	297	319	5.18*	5.53+
2	1.94	0.60	10.0	10.0	0.25	296	323	4.92*	5.31+
3	1.05	0.03	9.0	9.0	0.19	296	324	6.10*	6.81+
4	1.61	1.26	31.5	-	0.067	302	305	4.78*	4.93+
5	1.47	1.10	31.5	-	0.067	303	307	5.04*	5.23+
6	1.35	1.02	31.5	-	0.067	303.5	307	4.63*	4.83+
7	1.13	0.83	31.5	-	0.10	305	307.5	4.63*	4.45+

*K was estimated at the arithmetic mean temperature

+K_n was estimated assuming a linear temperature increase

**Initial NaOH concentration was always 2.0 kmol/m³.

Runs (4-7): Organic phase was batchwise.

supports the results of Wang et. al. and confirms the most unusual dependency on the stirring rate (3).

The effective interfacial area per compartment was between 0.044 - 0.068 m² for rotor speeds of 0.06 - 0.25 rev/s. The corresponding interfacial area per unit volume of extractor lies in the range of 90 - 140 m²/m³ and these values correspond to those obtained in spray columns and packed columns (1/2" Raschig rings) when the dispersed aqueous phase hold-up is approximately in the range of 0.05 - 0.1 (4, 9). However these values are conservative since the interfacial temperature rise will be considerably higher than the bulk temperature rise necessitating higher values of K_n than those used in Eqn. (7).

Finally, the effect of flowrates were not specifically investigated, but the experimental results indicate that its effect may not be critical of critical importance.

Acknowledgement

This work was carried out at the Chemical Engineering Department of University of Petroleum & Minerals, Dhahran, Saudi Arabia. The research facilities and the support are gratefully acknowledged.

Notation

- a Interfacial area per unit volume of extractor, m^2/m^3
A Interfacial area per compartment in the Graesser extractor, m^2
 B^0 Bulk concentration of sodium hydroxide, mol/m^3
 C^* Solubility of ester in aqueous phase, mol/m^3
D Diffusion coefficient of dissolved ester, m^2/s
 k_2 Second order rate constant, $m^3/mol\ s$
 k_L Aqueous phase physical mass transfer coefficient, m/s
K Parameter defined by Eqn. (8), $(mol/ms^2)^{1/2}$
L Aqueous phase flowrate, m^3/s
N Number of compartments in the Graesser extractor
S Contact area in the stirred cell, m^2
V Aqueous phase volume in the stirred cell, m^3
t time, s

References

1. Coleby, J. "The RTL (formerly Graesser Raining-Bucket) Contactor", in "Handbook of Solvent Extraction" (Ed. Lo, T.C., M.H.I. Baird and C. Hanson), Wiley (1983) pp. 449-452.
2. Sheikh, A.R., J. Ingham and C. Hanson, Trans. Instn. Chem. Eng. 50, 199 (1972).
3. Wang, P.S.M., J. Ingham and C. Hanson, Trans. Instn. Chem. Eng. 55, 196 (1977).
4. Nanda, A.K. and M.M. Sharma, Chem. Eng. Sci. 21, 707 (1966).
5. Alper, E. Trans. Instn. Chem. Engr. 64 (1979).
6. Alper, E. (Ed.) "Mass Transfer with Chemical Reaction in Multiphase Systems", Martinus-Nijhoff (1983).
7. Fernames, J.B. and M.M. Sharma, Chem. Eng. Sci. 22, 1267 (1967).
8. Alper, E. AIChE 25, 545 (1979).
9. Laddha, G.S. and T.E. Degaleesan, "Transport Phenomena in Liquid Extraction", Tata McGraw-Hill (1976).
10. Nanda, A.K. and M.M. Sharma, Chem. Eng. Sci. 22, 769 (1967).
11. Bidner, M.S and de Santiago, M., Chem. Eng. Sci. 26, 1484 (1971).
12. Leimu, R., R. Korte, E. Laaksoren and U. Lehnuskoi, Acta Chem. Fenn. 1913, 93 (1964).
13. Sharma, M.M. "Extraction With Reaction", in "Handbook of Solvent Extraction" (Ed. Lo, T.C., M.I.H. Baird and C. Hanson), Wiley (1983) pp. 37-52.

Special Applications: Petrochemicals

LIQUID-LIQUID EQUILIBRIUM OF N. HEXANE-CYCLOHEXANE-METHANOL MIXTURES:
INFLUENCE OF WATER CONTENT.

Alessi P., Kikic I.

Istituto di Chimica Applicata e Industriale, Università di Trieste, Trieste - Italy.

ABSTRACT

In the literature we cannot find liquid-liquid equilibrium data for the ternary system n-hexane-cyclohexane-methanol; otherwise many different set of data for the binaries n-hexane-methanol and cyclohexane-methanol are reported.

These data are scattered, especially those relative to the binary methanol-n-hexane. In this case it seems that the data are lying on two solubility curves with different values of the mutual solubilities and different values of the upper critical miscibility temperature: the difference between the two critical temperatures is about 10 C (between 35 and 45 C).

The possible explanation for these scattering is the presence of water in the methanol. For this reason we are carrying out experimental work with the aim of investigating the influence of small quantities of water on the binary and ternary liquid-liquid equilibrium.

Since it is very difficult to maintain during the runs methanol anhydrous, the data relative to the system with zero water content are obtained by extrapolating the experimental data obtained with different and known amount of water. The range of water content investigated is 0.5 - 4.5 wt.% at temperatures ranging between 15 and 35 C.

In this manner the effect of water on the critical upper temperature of the binaries is explained and an empirical relationship between these two quantities is presented.

INTRODUCTION

Although many solvents are known for recovery of aromatics from reformed naphthas, the need of completing the equilibrium data of such systems still exists. Data concerning the influence of the paraffin on the binodal curves, selectivity and distribution curves are still investigated (1,2,3,4,5,6,7,8). One of the aim of this investigation is the better understanding of this influence.

In order to complete the equilibrium data two empirical correlations of Hand and Othmer-Tobias were used (9,10).

RESULTS AND DISCUSSION

Experiments were carried out in mixers provided with mixing device of 1000 rpm which allowed equilibrium to be attained in 10 min. The hydrocarbon feed mixture was varied from 0-100 Vol%, with phase ratio 1:1 (aromatic+paraffin versus solvent) in all the investigated cases. The investigated temperature range was $20-60^{\circ}\text{C} \pm 0,5^{\circ}\text{C}$. After attainment of equilibrium the phases were allowed sufficient time for separation.

Using as paraffins: n-heptane (n-H), iso-octane (IO) and methylcyclohexane (MCH), the following groups of systems were investigated:

- I. furfural-benzene/toluene-MCH/IO;
- II. n-methylpyrrolidone (NMP)-benzene/toluene-IO/n-H;
- III. sulfolane-benzene/toluene-MCH/IO/n-H;
- IV. dimethylsulfoxide (DMSO)-benzene/toluene-IO/n-H;
- V. diethyleneglycole (DEG) -benzene/toluene-IO/n-H;

The composition of the extract and raffinate phase were determined using Gas-Chromatograph.

The efficiency and selectivity of the solvent in the presence of different paraffins were determined according to the equilibrium data, distribution curves and selectivity curves.

The influence of the present paraffin on the equilibrium state was investigated with the three first groups of systems and the results obtained at 40°C are compared.

Figure 1 shows the distribution curves for the systems furfural-MCH/IO-benzene. The temperature effect on the equilibrium over the investigated range was negligible. Therefore the experimental points are avoided, but the curve corresponds to the whole investigated temperature region.

It is evident that the distribution curve related to the system with MCH as a paraffin lies nearer to $K_D=1$, which leads to conclusion that the solubility of the paraffin in the solvent i.e. the extractability of the solvent for the solute increases. This can be in connection with the molecular structure of the paraffin and with its molecular mass. The ternary diagram for these systems shows a larger heterogeneous region in the case of iso-octane. Nevertheless in both cases (iso-octane or MCH) this region is very narrow. Such results lead to the conclusion of an increase of the solvent selectivity with the increase of the number of C-atoms in the molecule of the paraffin i.e. with the increase of his molecular mass. At the same time the region of the concentration of benzene in the starting mixture is narrow (Table 1). The results obtained with the systems furfural-iso-octane/MCH-toluene are analogous. The distribution curve for the system furfural-iso-octane-toluene points to higher K_D -values compared with those for the system furfural-MCH-toluene and produces a binodal curve with larger heterogeneous region.

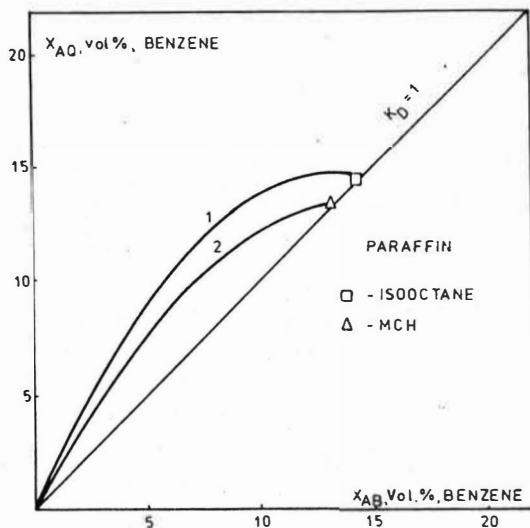


Figure 1, Distribution curves for the systems: 1-furfural-benzene-IO; 2-furfural-benzene-MCH

The influence of the aromatics and paraffins in the equilibrium state are shown in Figure 2. An enlargement of the heterogeneous region with the increase of the molecular mass of the paraffin, as well as the molecular mass of the aromatic is noticeable. The possible aromatic con-

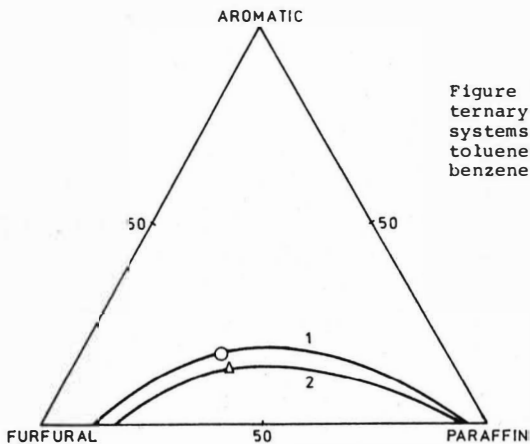


Figure 2. Phase equilibrium ternary diagrams for the systems: 1-furfural-IO-toluene; 2-furfural-MCH-benzene.

centration in the starting mixture is wider in the case of toluene compared with that of benzene. The selectivity of furfural towards toluene relative to that of benzene, in the presence of the same paraffin is higher although the extractability of the solvent is higher for the lighter aromatic-benzene-which means also higher K_D -values (Tab.1.)

For all these systems is characteristic the narrow heterogenous region. This limits the application of furfural as a solvent only to starting mixtures with low aromatic concentration, which is in connection with the high mutual solubility of furfural in the investigated paraffins.

The results of equilibrium obtained with the systems belonging to the second group are analogous to those of the first group i.e:

- a) for the same aromatic the K_D -values as well as the heterogenous regions are higher and larger in the presence of paraffins containing larger number of C-atoms in the molecule,
- b) in the case of the same paraffin the K_D -values are higher in the presence of a lighter aromatic, and
- c) in the case of the presence of the same paraffin, the heterogenous region is larger in the presence of toluene as aromatic.

Figure 3 represents an illustration on the influence of the present paraffin in the systems: NMP-iso-octane/n-heptane-toluene.

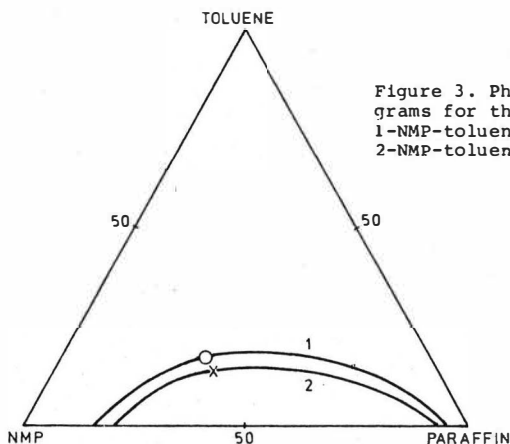


Figure 3. Phase ternary diagrams for the systems:
1-NMP-toluene-iso-octane,
2-NMP-toluene-n-heptane

The limited applicability of this solvent at lower aromatic concentration in the starting mixture is also a characteristic resulting from its high solubility in n-heptane and iso-octane (Table 1).

On the other hand sulfolane can be used for extraction of aromatics from mixtures containing very high aromatics concentration in the starting mixtures, as can be seen from Figure 4, which represents a plot of the concentration of toluene in the extract phase versus the initial concentration. The curve "C" which serves for comparison corresponds to 100% extraction. Accordingly the highest extent of extraction was attained with the systems containing higher molecular mass i.e iso-octane.

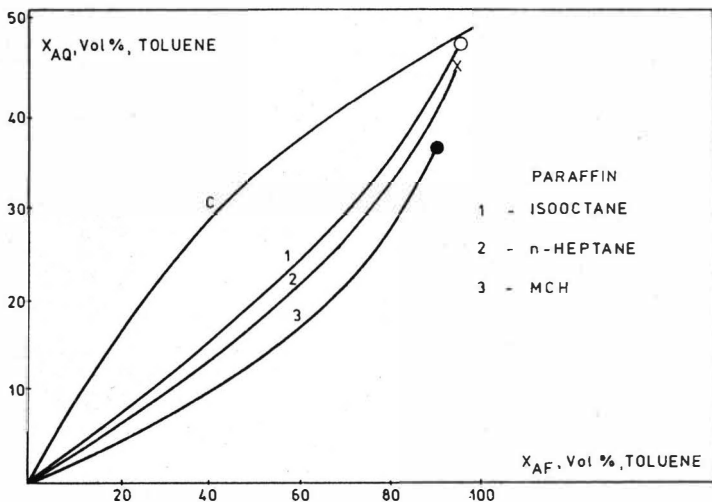


Figure 4. Dependence of aromatic equilibrium concentration ⁴ in the extract phase on the initial concentration for the systems of the group III.

The same dependence for benzene is analogous with the difference that the analogical curves 1, 2 and 3 are disposed nearer to the curve "C", which confirms the assumption of the higher ability of the solvent to extract lighter aromatics. The distribution curves for the system sulfolane-iso-octane/n-heptane/MCH-toluene are presented in Figure 5.

Compared with the same dependence for the systems of the first two groups, the distribution curves are situated below $K_D=1$. From the position of the curves 1, 2 and 3 it can be seen that the extractability of sulfolane increases with the increase of the number of C-atoms, as well as the molecular mass of the paraffin used, as a result of a decrease of the mutual solubility of sulfolane with the investigated paraffin. The disposition of the distribution curves is analogous with that of toluene, but lies nearer to $K_D=1$.

Figure 6 represents the ternary equilibrium diagram for the systems sulfolane-iso-octane/n-heptane/MCH-toluene.

As a general conclusion for this system is the large heterogenous region for all the three paraffins, the largest one being obtained with iso-octane. A large heterogenous region of the systems containing benzene is characteristic as well. A bigger difference in the wide of the heterogenous region, in respect to the same paraffin, is evident in the case of systems with higher aromatic concentration i.e. benzene.

According to the distribution curves, as well as to the ternary diagrams of the systems of the third group it arises a higher extractability of sulfolane towards lighter aromatics, but a higher selectivity towards heavier aromatic in the mixture with paraffin with the highest number of C-atoms in the molecule.

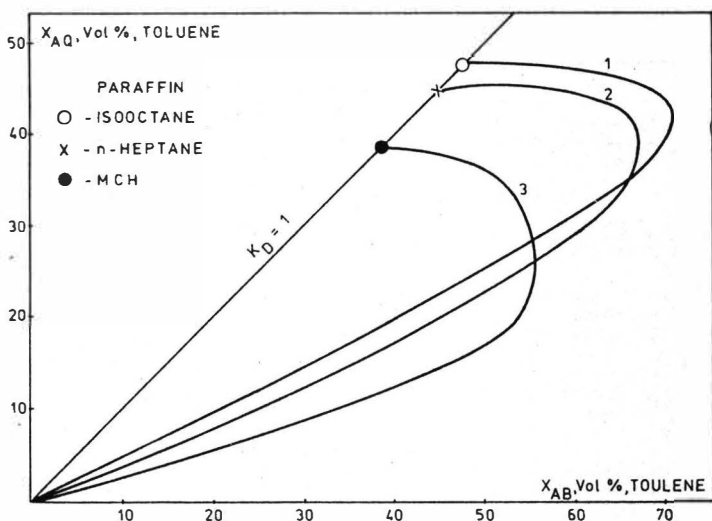


Figure 5. Distribution curves for the systems of the group III

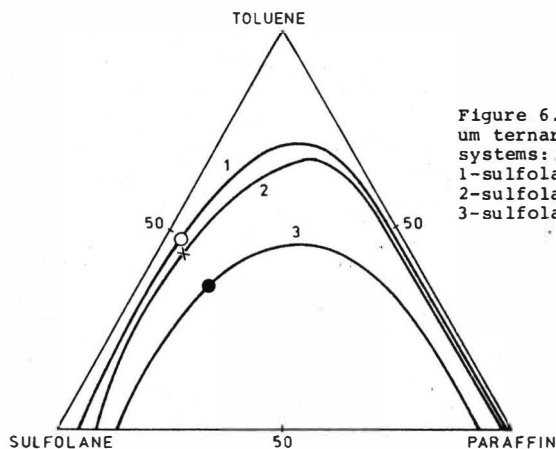


Figure 6. Phase equilibrium ternary diagrams for the systems:

- 1-sulfolane-toluene-IO
- 2-sulfolane-toluene-n-H
- 3-sulfolane-toluene-MCH

In order to make a definitive conclusion concerning the influence of the paraffin, as a criteria the K_D -values as well as the plait points were chosen. These are presented in Table 1. According to the obtained results the following increasing order of the favourable paraffin could be established:

MCH, n-heptane, iso-octane

Table 1. Calculated K_D values ($X_{AF} 20 \text{ Vol}\%$), Plat point data and max. initial aromatic concentration

No	S y s t e m	K_D	PPVol%	X_{AF} Vol %
1	benzene-MCH-furfural	-	13,2	18,2
2	tolene-MCH-furfural	1,05	16,1	23,7
3	benzene-IO-furfural	1,71	14,4	31,3
4	toluene-IO-furfural	1,17	17,0	34,0
5	benzene-MCH-sulfolane	0,42	33,8	72,0
6	toluene-MCH-sulfolane	0,36	36,0	78,0
7	benzene-IO-sulfolane	0,95	45,6	87,0
8	toluene-IO-sulfolane	0,64	48,0	90,2
9	benzene-MCH-DMSO	0,90	40,6	85,0
10	toluene-MCH-DMSO	0,53	45,2	88,0
11	benzene-IO-NMP	2,29	13,6	25,5
12	toluene-IO-NMP	1,25	14,9	28,0
13	benzene-MCH-NMP	-	13,0	18,0
14	toluene-MCH-NMP	-	13,4	20,0
15	benzene-IO-DEG	0,38	-	-
16	toluene-IO-DEG	0,28	-	-
17	benzene-IO-DMSO	0,84	31,2	74,4
18	toluene-IO-DMSO	0,78	34,4	78,0
19	benzene-MCH-DMSO	0,76	29,7	71,3
20	toluene-MCH-DMSO	0,52	33,0	75,6

On the basis of the results obtained for all the five groups of systems, the selection of the most convenient solvent was made with respect to iso-octane, as the most convenient paraffin. The dependences concerning toluene are chosen for illustration (Figures 7,8,9).

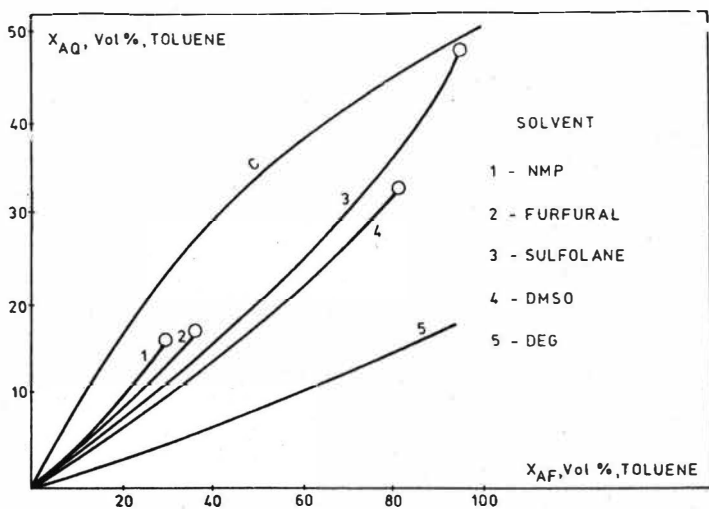


Figure 7. Dependence of toluene equilibrium concentration in extract phase on the initial concentration for the systems with iso-octane as a paraffin.

The dependence of the equilibrium concentration of toluene in the extract phase on his initial concentration, for all the investigated solvents is shown in Figure 7. The curves related to NMP and furfural lies nearest to the curve "C", while the curve referred to DEG is the lowest one, which points to the small extractability of this solvent for aromatics. On the other side such statement is based on the existence of a region of low initial aromatic concentrations as with NMP and furfural it was impossible the extraction of the aromatics from mixtures with higher aromatics content.

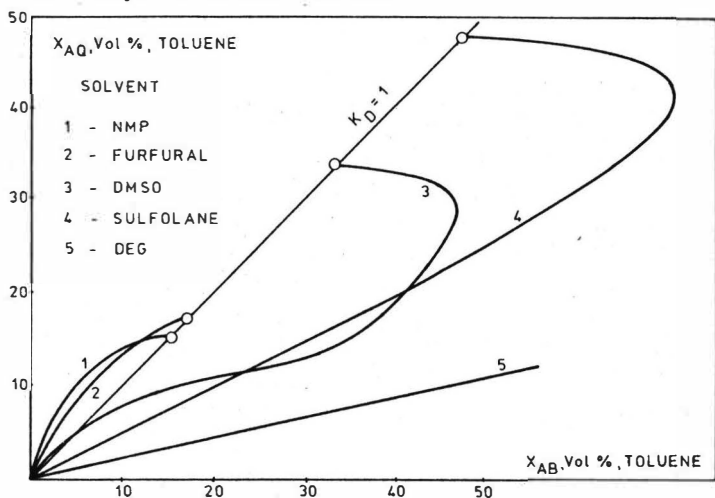


Figure 8. Distribution curves for the systems with iso-octane as a paraffin.

From the position of the distribution curves with reference to $K_D=1$, (Figure 8) the most favourable aromatic distribution arises in the case of NMP as a result of a good mutual solubility of NMP and aromatic in all the ratios. The order of the curves was analogous also in the case of benzene as aromatic. Accordingly the following decreasing order of extractability, related to both of the paraffins arises:

NMP, furfural, DMSO, sulfolane, DEG

In Figure 9 are presented the phase-equilibrium curves for systems containing toluene as an aromatic. As it can be seen the phase-equilibrium curve related to the system containing DEG is open due to its limited solubility with the aromatics, as well as the low solubility with the paraffins.

The systems with DMSO and sulfolane are characterized with a large heterogeneous region. The systems with furfural and NMP give very narrow heterogeneous region in the ternary diagram. An analogous dependence was obtained using benzene as an aromatic. Accordingly the increasing order of selectivity of the solvents arises as follows:

NMP, furfural, DMSO, sulfolane, DEG

Because of the completely opposite orders regarding to the extractability and selectivity, the selection of the solvent should be made according to the particularities of the starting mixture.

DEG as sole solvent can not be recommended regardless to the type of the aromatic and its initial concentration in the starting mixture, besides his high selectivity and ability to form the largest heterogeneous region, because of its limited mutual solubility with the aromatics. As a

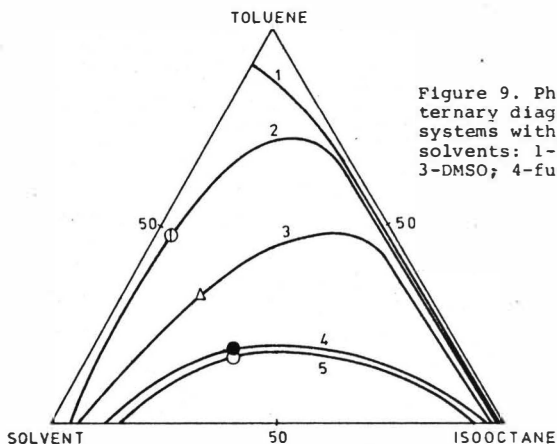


Figure 9. Phase equilibrium ternary diagrams for the systems with different solvents: 1-DEG; 2-sulfolane; 3-DMSO; 4-furfural; 5-NMP.

suitable solvents, for systems with low initial aromatic concentration arise furfural and NMP because of their high K_D -values regardless to the narrow heterogeneous regions they produce.

For the extraction of aromatics from systems with high initial aromatic concentration, sulfolane or DMSO can be considered as the most convenient solvents because of their ability to recover aromatics from such mixtures.

The experimental equilibrium data were correlated using the empirical correlations of Hand and Othmer-Tobias. The calculated values of the coefficients and exponents were used to correlate the experimental equilibrium data (9,10).

The values of the root mean square deviation (σ) are determined and presented in Table 2.

Table 2 Root mean square deviation at 30°C

No	System	σ	
		Hand	Othmer-Tobias
1	benzene-MCH-furfural	0,0278	0,0202
2	benzene-IO-sulfolane	0,0219	0,0270
3	toluene-IO-sulfolane	0,0476	0,0847
4	benzene-MCH-sulfolane	0,0768	0,0690
5	toluene-MCH-sulfolane	0,1563	0,0582
6	benzene-IO-NMP	0,0330	0,0496
7	toluene-IO-NMP	0,0053	0,0453
8	benzene-MCH-NMP	0,0136	0,0341
9	toluene-MCH-NMP	0,0027	0,1004
10	toluene-IO-DMSO	0,0082	0,0342
11	toluene-IO-furfural	0,0048	0,0393

The obtained results lead to consideration that for more of the investigated systems the correlation of Hand shows better agreement between the experimental and calculated data.

REFERENCES

1. R.P.Tripathi, A.Raja Ram and P.B.Rao, J.Chem.Eng.Data 1975,20(3),261
2. P.Gurtner, J.Fuhrmann und W.Spielmann, Chem.Techn.,31, Jg.,Heft 5, Mai 1979
3. Zavidov V.I., Shapchenko,N.I., Dal,V.I., Khim.Tekhnol,Topl. Masel., 11 (1) 29 (1966)
4. Renon,H., Raimbault,C., Jeanjean,P., Paper presented at the Eight World. Pet. Congr., Moscow, 4 (1971), 197
5. A.Z.Bikkulov,R.K.Khazipov, Khim.Techol.Topl .Masel. 16)10),15(1971)
6. Z.Maksimović,A.Tolić,and M.Sovilj, Bull.Soc.Chemique,Beograd,46(11) 663-670 (1981)
7. Von S.Van Pham, I.Priboth, R.Hennig und K.Quitzcsh, Z.phys.Chemie, Leipzig 264 (1983), 2 S. 305-317.
8. F.Poposka, B.Bliznakovska and A.Grizo, Paper presented at the Yug. Simp. Chem.Biochem.Eng., 14-15 Feb., 1985, Zagreb, S-B/4,18
9. Othmer,D.F., Tobias, P.E., Ind.Eng.Chem, 34,690 (1942)
10. Hand,D.B., J.Phys.Chem., 34, 1961 (1930)

Butene Recovery by Extraction

Gerd Emmrich, Klaus Lackner, Krupp Koppers, Essen, FR Germany

1. INTRODUCTION

Large streams of C_4 hydrocarbons are yielded from naphtha-based steamcrackers and catalytic crackers, among others. Such streams have established low-commercial values in recent years, compared to other olefin streams, and may be even used as fuel. They contain, apart from highly unsaturated C_4 hydrocarbons, particularly C_4 paraffins and C_4 mono olefins. Because of their high reactivity, the C_4 mono olefins are increasingly being used as feedstock for further reactions. This fact was an incentive for Krupp Koppers to look for a simple and economical process for separation of C_4 mono olefins from C_4 hydrocarbon mixtures. The result is a new process developed to separate butenes from a butene/ butane mixture, based on Krupp Koppers' proven Morphylane extractive distillation technology. The new process is called BUTENEX.

The BUTENEX process is highly flexible with regard to feedstock composition, product purities and yields. The following two cases have been selected to demonstrate the capabilities of the process:

Case 1 Separation of butene-2 from an n-butane/butene-2 mixture, as obtained from an oligomerization unit or from a butene-1 separation unit. Butene-2 is to be concentrated to 80 % for recycling to the oligomerisation unit.

Case 2 Separation of butene-2 from an n-butane/butene-2 mixture, as obtained from an oligomerization unit or from a butene-1 separation unit. Butene-2 and n-butane are to be recovered as pure products.

The data contained in this paper have been prepared in order to give an initial impression of the economy of the process. They apply to a unit designed for a feedstock capacity of 5.0 t/h n-butane/butene-2 mixture (44,000 tpy for 8,760 hours operation per year) with a butene-2 content of 41 wt.%.

2. PROCESS DESCRIPTION

(see attached flow-sheet)

The feedstock is charged into the extractive distillation (ED) column C-101, which is fitted with valve trays. The solvent, entering at the top section of the column, causes extensive separation of n-butane and butene-2. The n-butane vapours leaving the top of the ED column are sent to the small butane column C-103 for solvent recovery.

The bottom product of the ED column, consisting of solvent and butene concentrate, is pumped to the butene column C-102 by the bottom pump P-101.

The heat requirement of the ED column C-101 is supplied by heat exchange with hot solvent in the reboilers E-102 and E-103 and by steam in the reboiler E-101.

The solvent, remaining in the ED column overhead vapour, is separated from the n-butane in the packed butane column C-103. The solvent, withdrawn at the bottom, is recycled to the feedstock of the ED column by bottom pump P-104.

The top vapour (n-butane) is condensed in the air cooler E-108 and collected in the reflux drum D-102. Pump P-105 returns a part of the n-butane condensate to the column C-103 as reflux, the remainder is sent to battery limits.

The heat requirement of the butane column C-103 is supplied by heat exchange with hot solvent in the reboiler E-107.

In the butene column C-102 the butene-2 concentrate is separated from the solvent by distillation. Like the butane column, the butene column is also packed.

The butene-2 vapour leaving the top of the column C-102 is condensed in the water cooler E-106 and collected in the reflux drum D-101. Pump P-103 returns a part of the condensate back to the column as reflux, while the rest (butene-2 concentrate) is sent to battery limits as product.

Hot solvent is the bottom product of the butene column. Used as a heating medium it is pumped to the reboilers E-102, E-103, E-107 and E-105 by the butene column bottom pump P-102. The solvent is then cooled down to the required temperature in the air cooler E-109 before it again enters the top of the extractive distillation column.

A part of the heat requirement of the butene column C-102 is supplied by heat exchange with hot solvent in the reboiler E-105. The remainder is supplied by steam in the reboiler E-104.

3. THE SOLVENT

The efficiency of a modern extraction process depends on the physical properties of the solvent applied. The BUTENEX process uses a solvent which is widely used in the chemical industries. It offers a combination of high selectivity for olefins with sufficient solvent efficiency for non-olefins, which is nearly optimal for use in an extractive distillation plant.

The solvent has a high degree of permanent thermal stability and also good chemical stability. Solvent consumption and expenditure for regeneration of the solvent are low. The solvent is inexpensive and manufactured on a large scale.

The solvent is slightly basic and is widely used as an inhibitor to prevent corrosion. No corrosion occurs in the equipment of a BUTENEX plant.

4. FEEDSTOCK COMPOSITION

The process data are based on the following feedstock composition (Case 1 and 2):

Components

n-Butane	wt. %	58
Butene-1	"	1
trans Butene-2	"	24
cis Butene-2	"	17

5. PRODUCT SPECIFICATION

5.1 Case 1

5.1.1 Butene-2 Concentrate Composition:

n-Butane	wt. %	20.0
Butene-1	"	1.3
trans Butene-2	"	46.0
cis Butene-2	"	32.7
Solvent	ppm	< 1

5.1.2 n-Butane Composition

n-Butane	wt. %	98.3
Butene-1	"	0.7
trans Butene-2	"	0.8
cis Butene-2	"	0.2
Solvent	ppm	< 1

5.1.3 Yields

Based on the feedstock composition shown in Section 4, the expected yields are as follows:

n-Butane	82.0 wt. %
Butene-2	99.0 wt. %

5.2 Case 2

5.2.1 Butene-2 Composition:

n-Butane	wt. %	1.0
trans Butene-2	"	57.9
cis Butene-2	"	41.1
Solvent	ppm	< 1

5.2.2 n-Butane composition:

n-Butane	wt. %	99.0
Butene-1	"	1.0
Solvent	ppm	< 1

5.2.3 Yields

Based on the feedstock composition shown in Section 4, the expected yields are as follows:

n-Butane	98.95 wt. %
Butene-2	99.0 wt. %

5.3 Utilities Specification

It is assumed that the following utilities are available at battery limits:

	Pressure (bar abs.)	Temp. (°C)
Cooling water	3.5	26
Steam	20	212

6. CONSUMPTION FIGURES

(Expected figures per metric ton of feedstock)

6.1 Case 1

Electric power	kWh	22
Cooling water ($t = 8^{\circ}\text{C}$)	m^3	15
Steam, 20 bar	kg	840
Solvent	g	< 50 (resp. DM 0.25)

6.2 Case 2

Electric power	kWh	22
Cooling water (t = 8°C)	m ³	17
Steam, 20 bar	kg	945
Solvent	g	< 50 (resp. DM 0.25)

7. INVESTMENT COST ESTIMATE

The cost estimated for the BUTENEX plant including all equipment, construction, erection and basic and detailed engineering, amounts to approx. DM 9.500.000,-- for Case 1 and for Case 2.

The cost is a preliminary budgetary estimate based on cost factors valid in the Federal Republic of Germany in December 1985.

The investment cost does not include spare parts and the licence fee.

8. PERSONNEL REQUIREMENTS

For continuous plant operation the personnel requirement amounts to 2 operators per shift.

9. EXPERIENCE

The BUTENEX process is based on Krupp Koppers' proprietary extractive distillation technology, the MORPHYLANE process for the recovery of BTX aromatics. This process has been applied in ten commercial plants with a total capacity of more than 1.6 million tons pure aromatics per year. For more than 10 years, all new clients employing aromatics extraction in West Germany have decided in favour of the Krupp Koppers Morphylane technology.

Extraction of Colorado Oil Shale Using Water as Solvent

K. Hedden, P. Missal, Engler-Bunte Institute, Division of Gas, Oil, and Coal, University of Karlsruhe, F.R.G.

INTRODUCTION

Besides fossil fuels like coal, oil, or natural gas oil shale represents a considerable energy potential (1). This potential can be used in the future when the reserves of oil and natural gas become more and more difficult to exploit.

Up to now all technical processes being developed for the upgrading of oil shale are retorting processes. The extraction of oil shale could be an attractive alternative. Earlier investigations have shown that high conversion degrees are obtainable for sub- and supercritical extraction of coal and oil shales with various organic solvents (2,3).

This report describes a new investigation on the extraction of Colorado oil shale using water as solvent. The aim of the investigation is to get design parameters for the development of an extraction process. Conversion of oil shale, yields of extract and gas as well as compositions of extract and of formed gas are measured in dependence of extraction temperature, duration of extraction, particle size of the oil shale, and amount of solvent.

EXPERIMENTAL

Material

The oil shale used for the extraction with water originates from the Piceance Creek Basin, Rio Blanco County, Colorado. Elementary analysis has shown that the kerogen content of the oil shale amounts to about 17.5 wt. % (m.f.). By Fischer assay analysis oil shale conversions of about 13 wt. % (m.f.) and extract yields of 9 wt. % (m.f.) were obtained. The formed gases, 3 wt. % (m.f.), consisted of H_2 (34.5 vol. %), CO_2 (24.1 vol. %), CH_4 (18.7 vol. %), C_2-C_4 (18.1 vol. %), and CO (4.1 vol. %). Only 0.5 vol. % H_2S were found.

Apparatus and procedure

The experiments were carried out in an autoclave constructed of stainless steel, designed for pressures up to 330 bar and temperatures up to 500 °C, and with a volume of 69 ml.

Before the experiment was started oil shale and water were filled into the autoclave and the system was flushed with nitrogen to remove the remaining air. Then the autoclave was heated up in a short time to the chosen extraction temperature.

At the end of the experiment the reactor was expanded to atmospheric pressure. The formed extract and the water were collected in an ice-bath cooled extract separator and the gas was collected in a burette. The residue remained in the autoclave until the reactor was cooled down to room temperature.

For all experiments the amount of formed extract was small in comparison to the used water. Therefore, a quantitative separation of the extract from water was only possible with the help of a solvent consisted of tetrahydrofuran (thf) and toluene. The solvent was then removed from the extract in a rotation evaporator. Subsequently the weighed extract was further separated into n-pentane soluble oils, into asphaltenes (toluene soluble), and into preasphaltenes (thf soluble). Again the solvents were removed from the fractions in a rotation evaporator. The gas was analysed in a Janak/Orsat gas chromatograph. The residue was extracted with thf in a Soxhlet apparatus and after removal of thf this extract was further separated into oil, asphaltenes, and preasphaltenes.

RESULTS AND DISCUSSION

Effect of temperature

In a series of experiments batches of 16 g oil shale each (0.5 wt.% moisture) were extracted with 8.5 ml water at temperatures between 300 °C and 450 °C. The time of extraction was 60 min. The pressure varied in dependence of the extraction temperature from 88 bar (300 °C) up to 313 bar (450 °C). The conditions and results are shown in Fig. 1.

The experiments show that the extraction temperature and pressure have a great influence on oil shale conversion, extract yield, extract composition, and gas yield. Whereas the degree of oil shale conversion is small at low extraction temperatures, it increases up to 17.5 wt.% (m.f.) at extraction temperatures above 400 °C. At temperatures above 450 °C some coke was formed so that less liquid products were collected. These results are not shown in Fig. 1. The extract yield passes through a maximum of 12 wt.% (m.f.) at 390 °C and decreases with further temperature increase. The reason is that at high temperatures the long-chain hydrocarbons are cracked to lighter products which partly disappear with the mixture of thf/toluene in the rotation evaporator. At low extraction temperatures the content of n-pentane soluble oils in the extract is high. With increasing temperature more asphaltenes are formed from kerogen and the content of oil decreases. At high temperatures the cracking of asphaltenes is dominant, lighter products are formed, and the content of oil increases again. Compared to this fact the content of preasphaltenes in the extract remains constant throughout the measured temperature region. A steady increase in the gas yield with increasing extraction temperature up to 5.4 wt.% (m.f.) can be observed. The main component of the gas is CO₂ (70 vol.%). Other components

are H_2 , CH_4 , and a small amount of CO . At high temperatures cracking of the extract influences the composition and the amount of gas.

Effect of time of experiment

Fig. 2 shows the influence of time of experiment on oil shale extraction. It can be seen that an extraction time of 30 min is sufficient to get high conversion of oil shale (17.5 wt. % (m.f.)). The extract yield decreases from 12 wt. % (m.f.) to 9 wt. % (m.f.) with increasing time of experiment because lighter products are formed by cracking of the extract and these are lost in the rotation evaporator. The oil content in the extract and the amount of formed gases increase with duration of extraction.

Effect of particle size

Increase in particle size up to 5 mm shows no influence on oil shale conversion (Fig. 3). The degree of conversion is about 17 wt. % (m.f.). Only for particles larger than 5 mm the conversion of oil shale decreases. It can also be seen that small particles (<0.2 mm) give a large amount of short-chain hydrocarbons. These are removed with the organic solvents in the rotation evaporator. Therefore, the extract yield is only 6 wt. % (m.f.). Larger particles give extract yields of 11 wt. % (m.f.). In the experiments with larger particles the extract contains nearly 50 wt. % asphaltenes. The reason for this is the short time of experiment which is not sufficient to crack the asphaltenes to lighter products.

Effect of amount of solvent

The effect of the amount of solvent on extraction was investigated in a further series of experiments (Fig. 4). It can be seen that the amount of solvent has an influence on the oil shale conversion. Whereas the degree of conversion is 15 wt. % (m.f.) for 1.5 ml water, it increases up to 17.5 wt. % (m.f.) for 8.5 ml water and than remains constant by further increase of the amount of water. With increasing amount of water the extract yield changes from 7 wt. % (m.f.) to 11 wt. % (m.f.) and higher yields of asphaltenes are obtained. The amount of formed gas is nearly constant (5 wt. % (m.f.)). The experiments showed that reaction takes place between CO and H_2O . The content of CO in the gas decreases from 3 vol. % to 0.6 vol. % with increasing amount of water in the reactor.

CONCLUSIONS

From the experimental results described above it can be concluded that the following extraction conditions give high degrees of conversion of oil shale and high extract yields:

The extraction temperature should be above 400 °C but not higher than 450 °C. The time of extraction has to be at least 30 min to get a high content of oil in

the extract. The particle size should not exceed 5 mm. Normally, high density of the solvent is advantageous for extraction. In autoclave experiments increasing amount of solvent always leads to an correspondingly increasing pressure and thereby the density. With water as solvent the minimum ratio of water to oil shale by weight should be about 0.5. Under these conditions the kerogen can be completely extracted with water as solvent.

REFERENCES

1. R. Rammler et al.: Chemie-Ingenieur-Technik 53, 96-104 (1981).
2. A. Wilhelm, K. Hedden: "Extraktion von Kohle und Lösungsmitteln in unterkritischer und überkritischer Phase unter hydrierenden und nichthydrierenden Bedingungen", Forschungsbericht FB-T-82-177, Bundesministerium für Forschung und Technologie, 1982.
3. S.C. Guo et al.: Erdöl und Kohle - Erdgas - Petrochemie, 39 (1986), submitted for publication.

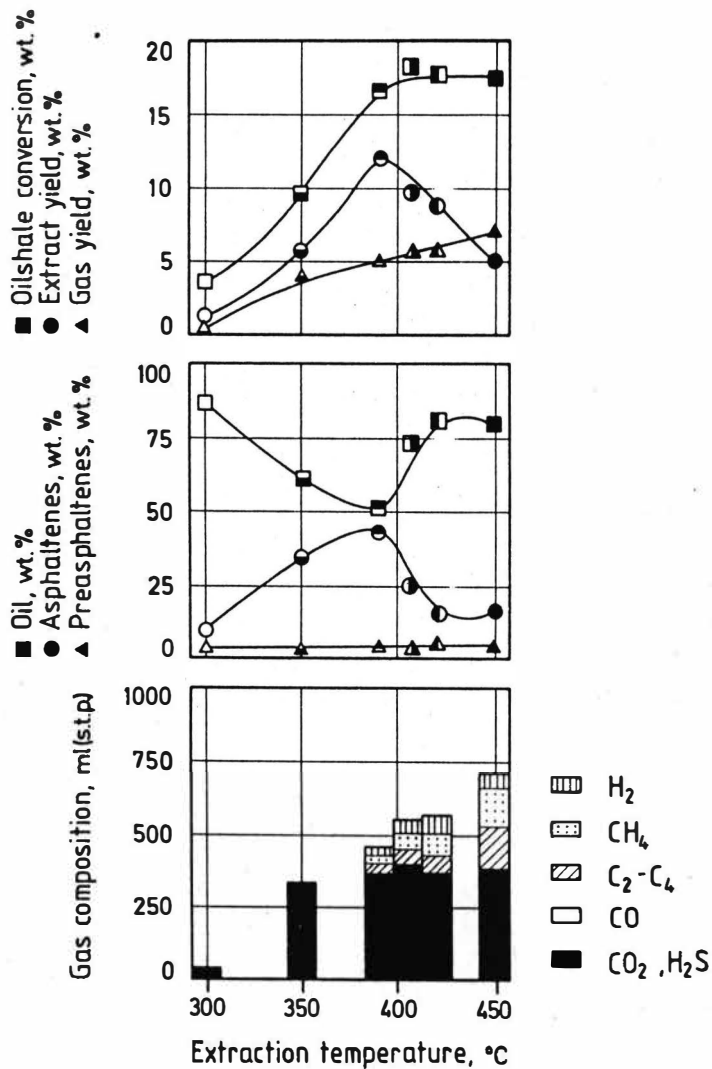


Figure 1 Influence of extraction temperature on oil shale conversion, extract yield, gas yield, extract composition and gas composition: 16 g oil shale (2-2.5 mm); 8.5 ml water; 60 min. (□ 300 °C, 88 bar; ◻ 350 °C, 181 bar; ◻ 390 °C, 228 bar; ◻ 410 °C, 260 bar; ◻ 420 °C, 278 bar; ◻ 450 °C, 313 bar).

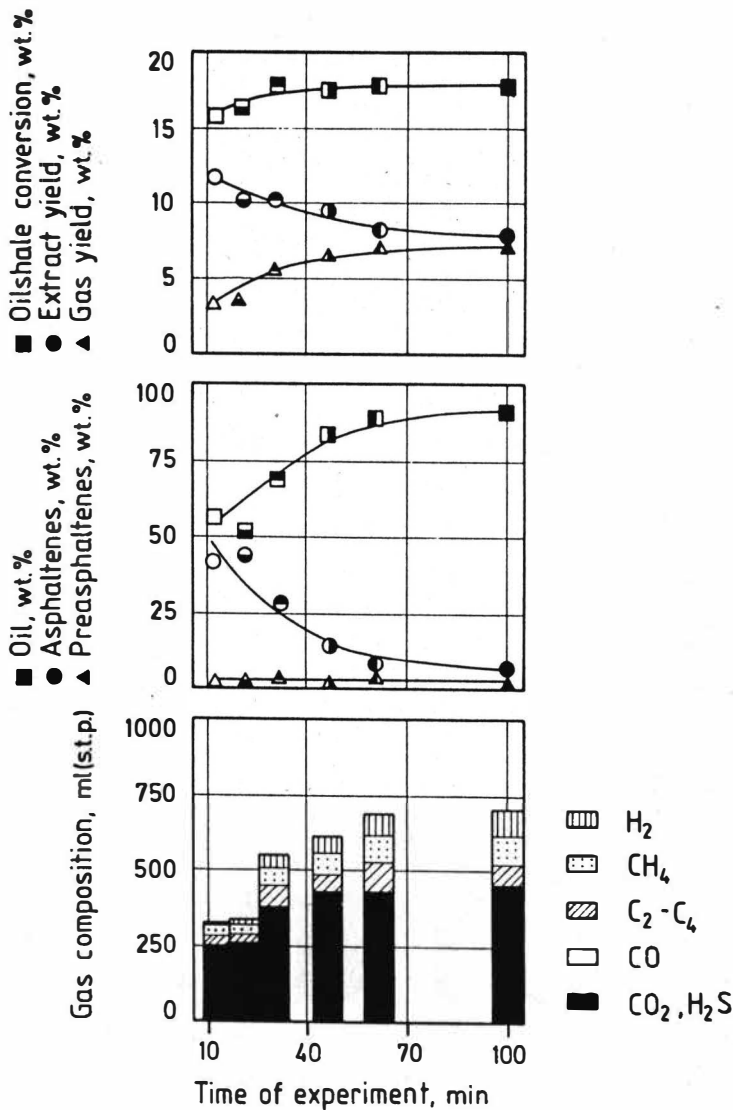


Figure 2 Influence of time of experiment on oil shale conversion, extract yield, gas yield, extract composition and gas composition: 16 g oil shale (2-2.5 mm); 8.5 ml water; 425 °C. (□ 13 min, 285 bar; ◻ 20 min, 284 bar; ◼ 30 min, 291 bar; ◽ 45 min, 293 bar; ◾ 60 min, 296 bar; ◿ 100 min, 296 bar).

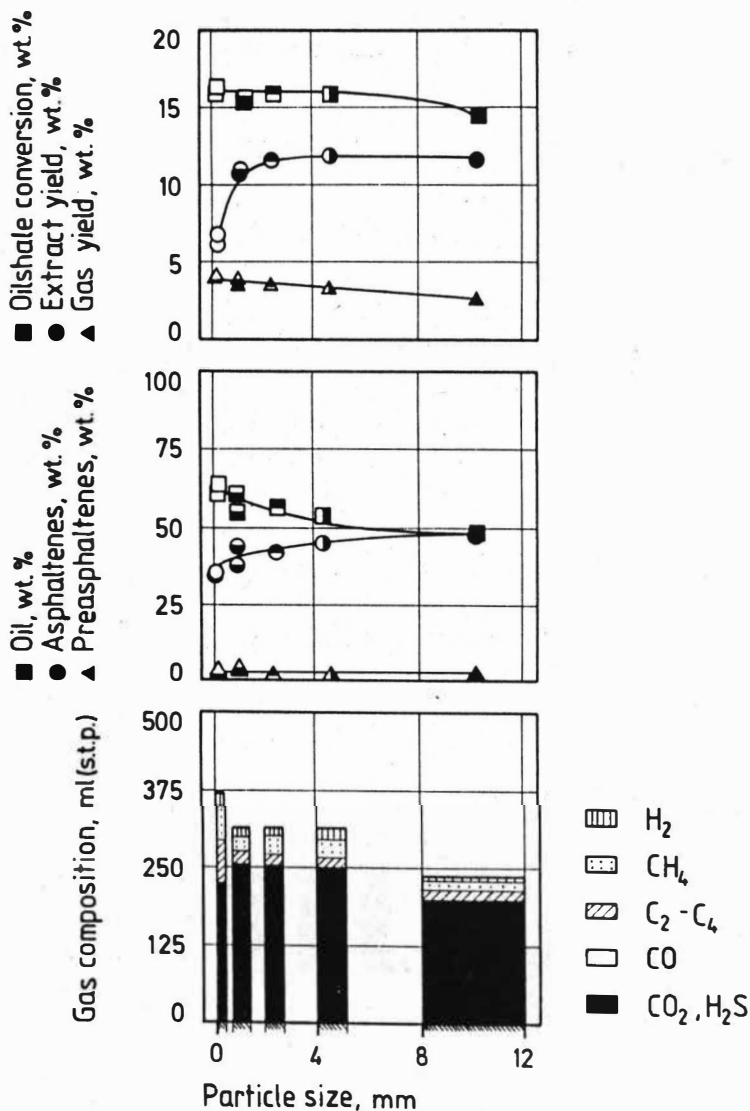


Figure 3 Influence of particle size on oil shale conversion, extract yield, gas yield, extract composition and gas composition: 16 g oil shale; 8.5 ml water; 425 °C; 15 min.

(□ <0.2 mm, 290 bar; ▣ 0.6-1.2 mm, 285 bar; ▤ 2-2.5 mm, 285 bar; ▥ 4-5 mm, 284 bar; ▦ 8-12 mm, 281 bar).

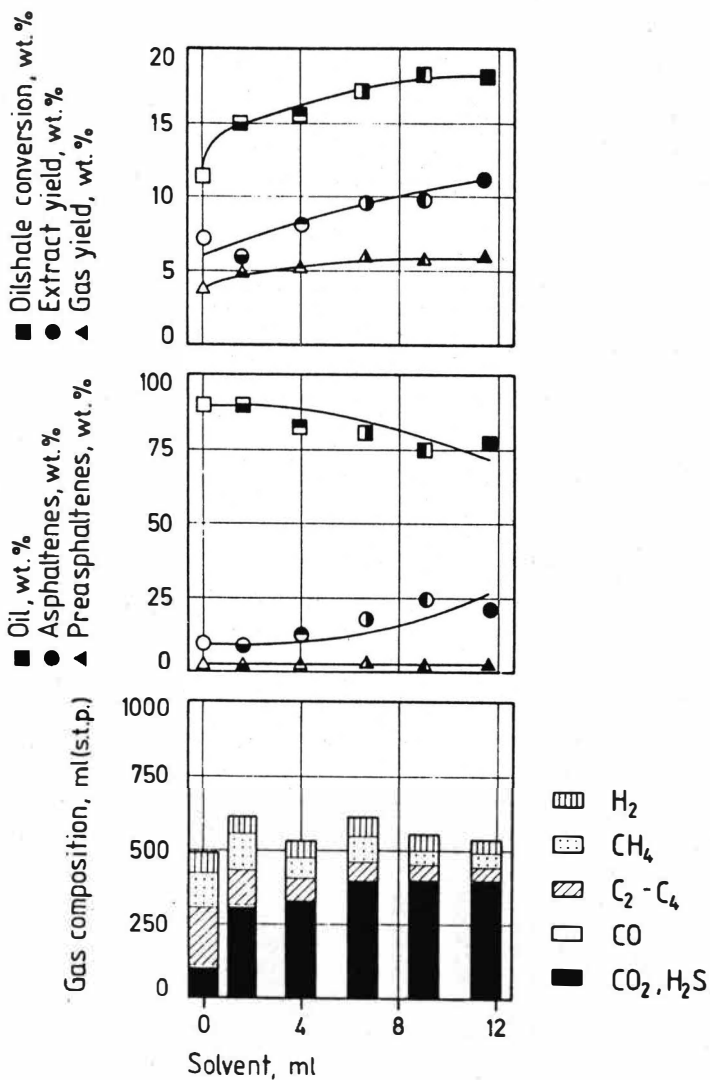


Figure 4 Influence of amount of solvent on oil conversion, extract yield, gas yield, extract composition and gas composition: 16 g oil shale (2-2.5 mm); 410 °C; 60 min. (□ 0 ml, 25 bar; ◐ 1.5 ml, 115 bar; ◑ 4 ml, 170 bar; ◒ 6.5 ml, 246 bar; ◓ 8.5 ml, 260 bar; ◔ 11.5 ml, 271 bar).

Fundamental Investigation of Supercritical Extraction on Coal Derived
Heavy Hydrocarbon

M. Yanagiuchi^{*}, K. Matsubara^{*}, T. Ueda^{*}
S. Saito^{**}, K. Arai^{**}, H. Inomata^{**}

* Technical Research Center, Nippon Kokan K.K.
Kawasaki, 210, JAPAN

** Department of Chemical Engineering
Tohoku University, Sendai, 980, JAPAN

INTRODUCTION

In the Japanese iron and steel industry and chemical industry, the effective utilization of by-products coal tar and pitch has been enthusiastically sought. The effective separation of the useful component of coal tar is the very important topic from the standpoint of high value by-products.

Supercritical extraction technology is an attractive method as the separation technology has many operational and economic advantages in comparison with conventional distillation and liquid-liquid extraction as follows :

- (1) The solubility can be controlled by solvent and extraction conditions.
- (2) Solvent recovery can be done with ease with low energy consumption.

Therefore, research on supercritical extraction with engineering application has been sought. Supercritical extraction technology is applied to the separation of the valuable components of coal tar.

At the first stage, the selection of the optimum solvent was done by the measurement of vapor-liquid phase equilibrium on CO₂-tar derived components system using CO₂ as the supercritical gas (1,2,3). The correlation between calculated and observed data has been carried out by the conventional equations of state.

EXPERIMENTAL

Table 1 shows the main components of coal tar. In the extraction of the valuable components from coal tar, the target components are as follows :

- (1) The compounds in large quantity and having some value (e.g. naphthalene, methylnaphthalene, anthracene, etc).

- (2) The compounds in small quantity and having high value (e.g. indole, quinoline, etc)

Naphthalene, methylnaphthalene and quinoline mixtures were selected as test system. The measurement of binary and ternary systems including CO₂-naphthalene, metylnaphthalene,quinoline was conducted.

The experiment was carried out in the static apparatus shown in Figure 1 (4,5,6). The apparatus is a combination of static and recycle methods and is composed of an equilibrium cell with observation window, a sampling section, a sampling injection section and an analysis section. The equilibrium cell has two observation windows made of borosilicate glass and is constructed of SUS 316 steel. The inner volume is about one liter. The maximum temperature and pressure for the cell is 500 K and 20 MPa. A helical ribbon impeller is used to promote vapor-liquid contact. High temperature packing material is used. The line between two constant temperature ovens is heated up to prevent condensation of the high boiling compounds during the measurement.

After the equilibrium cell is completely evacuated and cleaned, the sample is supplied and equilibrium is promoted through stirring. Then, the sampling from both vapor and liquid phases is taken.

Gas chromatography is used for the composition analysis.

RESULTS AND DISCUSSION

The result of phase equilibrium data of the CO₂-naphthalene system is shown in Figure 2. Data up to 16 MPa were obtained. Vapor phase is shown by the magnified figure. The solubility of naphthalene in vapor phase is about 1 mol % or 4 wt %. Experimental results for CO₂-quinoline and CO₂-Metylnaphthalene systems are indicated in Figures 3 and 4. The solubility of quinoline in the vapor phase is the same as that of naphthalene. The solubility of 2-Metylnaphthalene in the vapor phase is around 2 mol % or 10 wt % at about 15 MPa.

The general idea of extraction of solute 1 from the mixture of solute 1 and 2 using solvent is shown in Figure 5. The tie-line is indicated by solid line. The apex (solvent) and both ends of tie-line are connected. The points of intersection indicates the extract and raffinate composition. The steeper the slope of the tie-line, the higher the separation efficiency or selectivity becomes. For example, the results of the CO₂-naphthalene-quinoline ternary system is shown in Figure 6. Naphthalene is condensed into the gas phase. The same result is also obtained in case of other pressure conditions.

The experimental data were correlated with the calculated results.

In our calculations, the Peng-Robinson (PR) and Soave-Redlich-Kwong (SRK) equations shown in Table 2 were used.

The following conventional mixing rules were used. (7)

$$a_m = \sum_i \sum_j X_i X_j a_{ij} \quad b_m = \sum_i X_i b_i \quad a_{ij} = (1 - K_{ij}) (a_i a_j)^{0.5}$$

where K_{ij} is a binary interaction parameter and is determined in order to minimize the calculation error. Figures 2,3 and 4 show the result of binary systems. The solid line indicates the predicted value. The experimental data are well correlated with the calculations by the introduction of binary interaction parameters K_{ij} in the mixing rules. Then vapor and liquid equilibrium calculation for CO_2 -naphthalene-quinoline ternary system is done using K_{ij} parameters determined from the binary systems (Figure 6). The K_{ij} parameter of the naphthalene-quinoline binary system was determined by the fitting of data of the ternary system.

The correlation error of the solubility in gas phase was not small, but the slope of tie-line is correlated well. Therefore, it should be noted that the selectivity qualitatively may be predicted with PR equation for supercritical extraction processes. The calculation for the various solvents (gases) is carried out assuming the extraction of naphthalene from the mixture of naphthalene and quinoline. The selection of optimum solvent was tried. The calculation was conducted near the critical pressure varying temperature. Each binary interaction parameter K_{ij} was assumed to be zero.

The following two criteria were considered to select optimum solvent.

(1) The solubility of naphthalene in gas phase Y (naphthalene) [mol %]

$$(2) \text{ Selectivity } \beta = \frac{Y(\text{naphthalene}) / Y(\text{quinoline})}{X(\text{naphthalene}) / X(\text{quinoline})}$$

X: Liquid phase Y: Vapor phase

A solvent with high solubility and selectivity is best. Figure 7 shows the result of our calculations. Selectivity is plotted against solubility Y (naphthalene). Practically, selectivity decreases with the increase of solubility. This is a general trend in case of the extraction of mixtures of similar compounds in terms of molecular structure. Among the solvents or gases considered in our calculations, ethylene, ethane and carbon dioxide have a higher selectivity in comparison with other solvents (gases).

In the case of supercritical extraction in coal conversion processes, the following two cases are assumed.

- (1) The deashing of coal
- (2) The selective extraction of the valuable compounds from coal liquids

In case (1) aromatic solvents such as benzene or toluene with high solvating power may be effective.

In case (2) the solvent or gas such as CO_2 , C_2H_4 with low solvating power and high selectivity may be optimum. The phase equilibrium data obtained in this paper is fundamental data of case (1) and (2).

CONCLUSIONS

The fundamental investigation on the supercritical extraction of coal tar or pitch was conducted. The prediction of vapor-liquid equilibrium of binary or ternary systems including polyaromatic compounds can be accomplished with conventional equations of state (e.g. PR equation, SRK equation). At the present, the fractionation of the mixture of polyaromatic compounds has not been accomplished and the resolution of this problem will be future research. Therefore, the acquisition of vapor-liquid equilibrium data on various supercritical gas and heavy hydrocarbon is important. The acquisition of these data cost vast amount of time and work, so the development of the equations of state applicable to the mixture of multicomponents is also required.

REFERENCES

1. C.P. Chai and M.E. Paulaitis, J. Chem. Data, 26, 277 (1981)
2. H.M. Sebastian, H.M. Lin and K.C. Chao, J. Chem. Eng. Data, 25, 381(1980)
3. M. McHugh and M. E. Paulaitis, J. Chem. Eng. Data, 25, 329, (1980)
4. H. Inomata, Y. Takeuchi, C. Yokoyama, K. Arai and S. Saito,
The 48 th Annual Conference of the Society of Chemical Engineers, Japan
5. H. Inomata, K. Arai and S. Saito, J. Chem. Eng. of Japan, 11, 722 (1983)
6. H. Inomata, K. Arai, S. Saito, T. Ueda and M. Yanagiuchi,
The 50 th Annual Conference of the Society of Chemical Engineers, Japan
7. G. Soave, Chem. Eng. Soci., 27, 1197 (1972)

TABLE 1. THE COMPONENTS OF COAL TAR

Name	Boiling Point Range (°C)	Percentage (wt %)	Main Components	Use
Light Oil	~170	1	Benzene Toluene Xylene Pyridine	Miscellaneous
Carbolic Oil	170 ~ 200	3	Phenol Cresol	Medicine Plastics
Naphthalene Oil	200 ~ 230	12	Naphthalene	Pesticide Dyestuff
Creosote Oil	230 ~ 280	6	Metylnaphthalene Naphthalene Quinoline Indole	Dyestuff Medicine Medicine
Anthracene Oil	280 ~ 350	18	Anthracene Carbazole Phenanthlene	Dyestuff Plastics
Pitch	350 ~	55	-	
Total (5 % Moisture) excluded		95		

TABLE 2. A GENERAL FORMULA OF EQUATIONS OF STATE

SRK EQUATION	PR EQUATION
$P = \frac{RT}{v-b} - \frac{a}{v(v+b)}$ <p>where</p> $a = a_c \cdot \alpha, \quad a_c = \frac{0.42747 R^2 T_c^2}{P_c}$ $\alpha^{0.5} = 1 + m (1 - \sqrt{T_r})$ $b = \frac{0.08664 R T_c}{P_c}$ $m = 0.480 + 1.574 \omega - 0.176 \omega^2$	$P = \frac{RT}{(v-b)} - \frac{a}{v(v+b) + b(v-b)}$ $a = a_c \cdot \alpha, \quad a_c = \frac{0.45724 R^2 T_c^2}{P_c}$ $\alpha^{0.5} = 1 + m (1 - \sqrt{T_r})$ $b = \frac{0.07780 R T_c}{P_c}$ $m = 0.37464 + 1.54226 \omega - 0.26992 \omega^2$

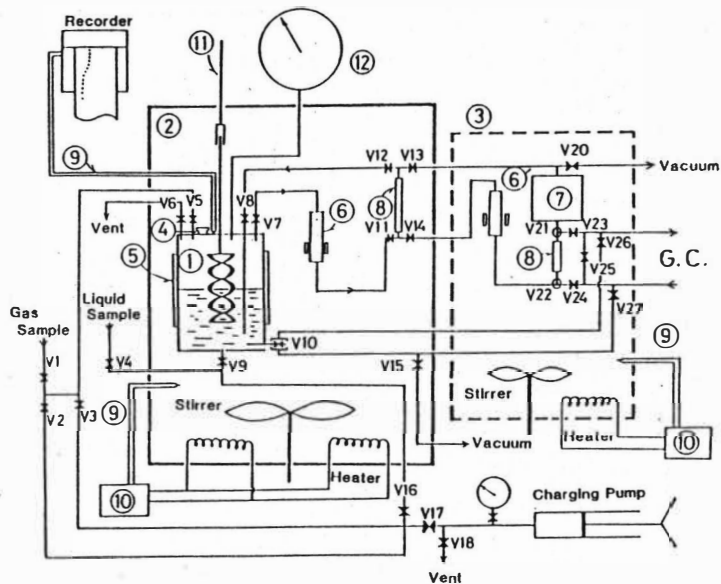


FIGURE 1. Schematic diagram of experimental apparatus

- | | | | |
|------------------------------|-----------------------|-------------------|--------------------------|
| ① Equilibrium Cell | ④ Solid Charging Port | ⑦ Expansion Tank | ⑩ Temperature Controller |
| ② Air Bath | ⑤ Window | ⑧ Sampler | ⑪ Magnetic Stirrer |
| ③ Air Bath (Sampling System) | ⑥ Magnetic Pump | ⑨ CA Thermocouple | ⑫ Pressure Gauge |

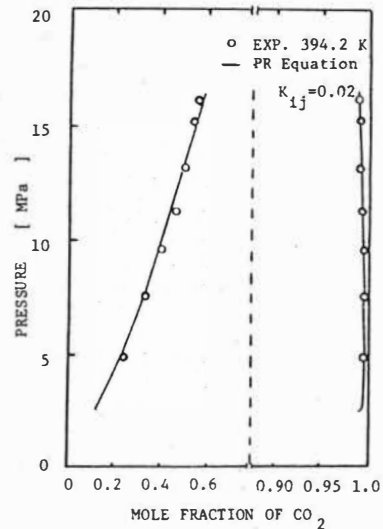


FIGURE 2. VAPOR-LIQUID EQUILIBRIA FOR CO₂-NAPHTHALENE SYSTEM

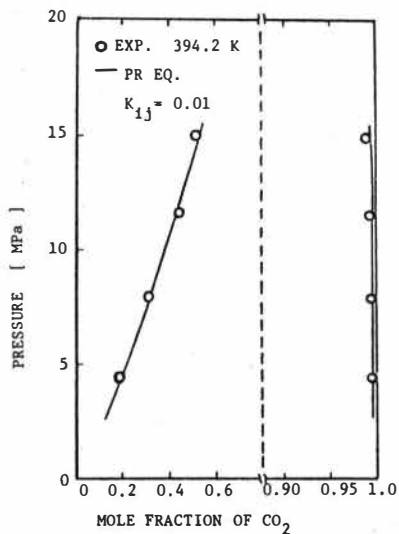


FIGURE 3. VAPOR-LIQUID EQUILIBRIA FOR CO₂-QUINOLINE SYSTEM

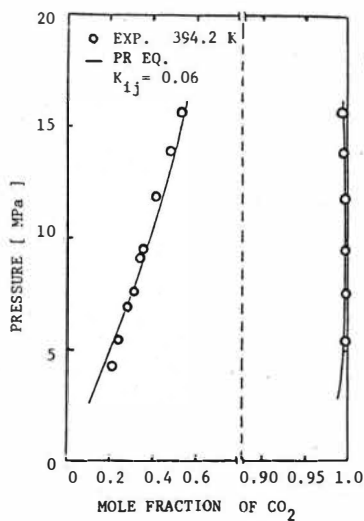


FIGURE 4. VAPOR-LIQUID EQUILIBRIA FOR CO₂-2-METHYLNAPHTHALENE SYSTEM

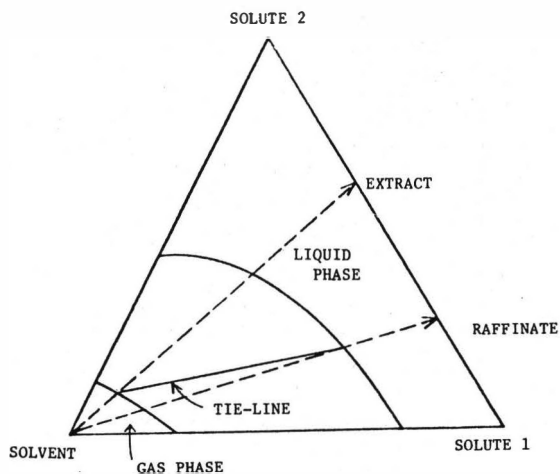


FIGURE 5. A GENERAL IDEA OF GAS EXTRACTION

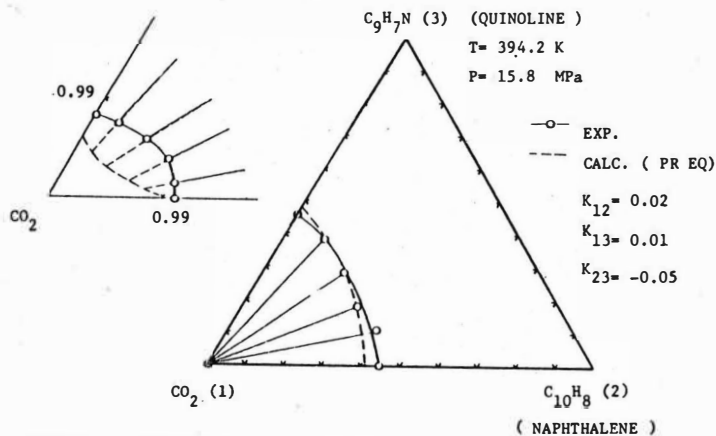


FIGURE 6. TERNARY PHASE DIAGRAM FOR $CO_2(1)-C_{10}H_8(2)-C_9H_7N(3)$ SYSTEM

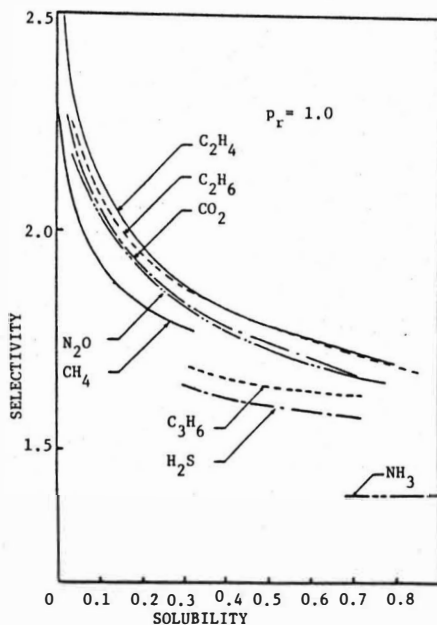


FIGURE 7. RELATIONSHIP BETWEEN SOLUBILITY AND SELECTIVITY

The effects of the extraction parameters on the chemical composition of extracts obtained from Hungarian brown coals by supercritical extraction

Gy. Deák, Z. Kása, Veszprém University, Veszprém, Hungary

One possibility for the liquefaction of coal is its extraction with supercritical gas followed by hydrocracking of the extract. This process was developed by the British National Coal Board and its main advantages are as follows: the capacity and selectivity of the solvent can be varied not only by the temperature but by the pressure as well; the separation of the solvent is simple; coal particle size is of lesser importance (1).

The composition of the extracts obtained by this process had been investigated by several authors (1-3). Most of the data are on coals but some Turkish and Chinese lignites were also studied. The results show that below 400 °C very little degradation is taking place during extraction and at such temperatures the supercritical solvent is extracting molecules held in the coal pores, in agreement with Vahrman's molecular sieve theory of coal. At higher temperatures, however, the supercritical solvent is extracting the product formed on pyrolysis of coal.

Extracts are generally separated according to a scheme of Bartle into pentane-soluble (PS), pentane-insoluble but benzene-soluble (BS) and pentane and benzene insoluble (BI) fractions and these fractions are further separated by adsorption chromatography (4).

In the Coal Research Establishment, Stoke Orchard, England it was found with bituminous coals that the increase of the extraction time and temperature increased the amount of both the PS and BS fractions, while the effect of the pressure was rather insignificant. The amount of the benzene-insoluble fraction, on the other hand increased with an increase in each of the variables (1).

In the present paper we summarize the results of our investigations on the effects of the extraction parameters on the composition of extracts obtained from Dudar lignite, Hungary. It was extracted in a semicontinuous extractor with toluene in the pressure range of 2.5-16.0 MPa, temperature range of 280-420 °C.

Experimental

The proximate and ultimate analyses of Dudar coal are given in Table 1.

Table 1
Analysis of Dudar lignite, Hungary

Air-dried basis %		Dry, ash-free basis %				
Moisture	Ash	Volatiles	C	H	N	S
8.3	15.6	51.5	70.1	5.3	0.7	5.9

Toluene was obtained from the Danube Refinery, Százhalombatta, Hungary, and used without further purification.

Supercritical gas extraction

The supercritical gas extraction was carried out in a 1 dm³ semi-continuous extractor with toluene as solvent. The extractor was charged with coal (700 g), flushed with nitrogen and heated. When the temperature reached 300 °C, toluene was pumped via a preheater into the bottom of the extractor and through the coal bed. The pressure was maintained at the required value by adjusting the amount of the withdrawn products. The gaseous phase was condensed by a water cooled condenser and the solvent and extract collected. On reaching the final temperature the extraction was continued until the given solvent/coal ratio was reached.

Fractionation of the extracts

The gas extracts were liquid extracted with pentane and the insoluble material was further extracted with benzene to yield an asphaltene fraction. The pentane soluble were separated by adsorption chromatography on silica gel. Fractions were eluted successively with n-pentane, benzene and methanol giving fractions PSPE, PSBE, PSME resp. A similar method was adopted to separate the asphaltenes into benzene and methanol eluates, BSBE, BSME resp.

Analyses

Ultimate analyses were made for C,H. Molecular weights were determined by osmometry. ¹H-nuclear magnetic resonance spectra of the fractions were recorded in CDCl₃ in the case of PSPE, PSBE, PSME and pyridine-d₅ in the case of BSBE, BSME and BI fractions.

Results and discussion

Extractions were carried out in the pressure range of 2.5-16 MPa, temperature range of 280-420 °C and toluene/coal mass ratio of 8.6. At 360 °C and 10 MPa five extract fractions were collected separately that contained identical amount of toluene, to study the effect of the time on the yield and composition of the extract.

Yields of the extract fractions are given in Tables 2-4.

Table 2.

Extract yields in function of pressure at 360 °C

P, MPa	Extract yield %, daf	PS ^x	PS [§]			BS ^x	BS ^{xx}		BI ^x
			PE	BE	ME		BE	ME	
2.5	13	94	62	23	12	2	1	97	1
10	18	77	36	40	21	17	12	85	3
16	27	74	34	36	26	20	17	80	4

Basis: x extract; § PS; xx BS;

Table 3.

Extract yields in function of temperature at 10 MPa

T, °C	Extract yield %, daf	PS ^x	PS [§]			BS ^x	BS ^{xx}		BI ^{x'}
			PE	BE	ME		BE	ME	
280	6	64	12	33	53	30	4	91	4
360	18	77	36	40	21	17	12	85	3
420	18	84	57	31	11	11	35	66	2

Basis: x extract; § PS; xx BS;

Table 4.

Extract yields in function of time 360 °C, 10 MPa

Time	Extract yield %, daf	PS ^x	PS [§]			BS ^x	BS ^{xx}		BI ^x
			PE	BE	ME		BE	ME	
1. hour	7	83	40	34	24	12	13	85	2
2. hour	6	79	32	37	27	16	11	84	3
3. hour	3	75	32	37	28	20	11	87	4
4. hour	1	62	29	42	28	28	22	77	8
5. hour	1	58	32	41	26	30	22	77	9

Basis: x extract; § PS; xx BS

The pressure has a significant effect on the supercritical extraction. An increase of the pressure increases the extract yield while the relative amount of the PS fraction of the extract decreases and that of the benzene soluble fraction increases. A marked change can be seen in the composition of the PS and BS fractions as well. At 2.5 MPa there are more PSPE and BSME than under supercritical conditions.

In the case of the temperature a significant change was found at the critical point of the toluene. At 280 °C the extract yield is small, and its BS content is relatively high. At 420 °C both the extract yield and the composition of the extract prove the cracking of coal.

The data in Table 4 show that most of the extraction takes place in the first two hours of the process and while the PS content of the extract decreases with time and its BS and BI content increases, the compositions of the PS and BS fractions do not change significantly. The properties of the extracts and their fractions are given in Tables 5-7.

At 360 °C the atomic C/H ratios and the molecular weights are rather similar under supercritical pressures, while at 2.5 MPa they are significantly smaller. The distribution of the protons is independent of the pressure (Table 5.).

Table 5.

The properties of extract in function of pressure at 360 °C

P, MPa	Sample	Types of protons						Atomic C/H ratio	Molecular weight
		H _{ar}	H _{OH}	H _F	H _α	H _β	H _γ		
2,5	Extract	-	-	-	-	-	-	0,633	377
	PS	-	-	-	-	-	-	0,631	374
	PE	8	0	0	19	54	19	0,589	382
	BE	11	1	2	27	43	16	0,735	378
	ME	8	0	6	29	43	14	0,719	329
	BS	-	-	-	-	-	-	0,881	469
	BE	7	0	1	16	54	22	0,630	361
	ME	21	0	16	27	24	12	0,888	471
	BI	17	0	0	16	64	3	0,652	720
10	Extract	-	-	-	-	-	-	0,732	551
	PS	-	-	-	-	-	-	0,691	465
	PE	6	0	0	16	59	19	0,604	391
	BE	8	0	2	26	49	15	0,789	529
	ME	10	0	12	23	40	15	0,716	472
	BS	-	-	-	-	-	-	0,966	847
	BE	16	12	7	19	31	15	0,952	809
	ME	21	0	9	28	31	11	0,969	854
	BI	12	31	2	16	27	12	0,926	1029
16	Extract	-	-	-	-	-	-	0,759	543
	PS	-	-	-	-	-	-	0,702	329
	PE	6	0	0	16	58	20	0,625	314
	BE	12	0	1	23	47	17	0,787	345
	ME	9	3	1	23	50	14	0,728	327
	BS	-	-	-	-	-	-	1,007	979
	BE	18	10	3	26	31	12	1,064	975
	ME	22	12	5	23	27	11	0,991	981
	BI	17	25	1	19	28	10	0,978	1921

Table 6.

The properties of extracts in function of temperature at 10 MPa

Temp. °C	Sample	Types of protons						Atomic C/H ratio	Molecular weight
		H _{ar}	H _{OH}	H _F	H _α	H _β	H _γ		
280	Extract	-	-	-	-	-	-	0,678	873
	PS	-	-	-	-	-	-	0,650	512
	PE	3	0	0	12	57	28	0,591	285
	BE	4	0	0	13	58	25	0,662	488
	ME	4	0	4	18	54	20	0,659	591
	BS	-	-	-	-	-	-	0,740	1405
	BE	11	7	0	15	47	20	0,689	870
	ME	9	9	4	20	43	15	0,741	1421
	BI	15	16	4	15	33	17	0,771	2540
360	Extract	-	-	-	-	-	-	0,732	551
	PS	-	-	-	-	-	-	0,691	465
	PE	6	0	0	16	59	19	0,604	391
	BE	8	0	2	26	49	15	0,789	529
	ME	10	0	12	23	40	15	0,716	472
	BS	-	-	-	-	-	-	0,966	847
	BE	16	12	7	19	31	15	0,952	809
	ME	21	0	9	28	31	11	0,969	854
	BI	12	31	2	16	27	12	0,926	1029
420	Extract	-	-	-	-	-	-	0,745	417
	PS	-	-	-	-	-	-	0,714	372
	PE	11	0	0	17	56	16	0,629	329
	BE	28	0	0	30	32	10	0,926	442
	ME	17	0	10	28	34	11	0,77	401
	BS	-	-	-	-	-	-	1,080	678
	BE	33	0	1	32	26	8	1,107	520
	ME	27	0	10	28	21	14	1,061	781
	BI	15	30	5	11	31	8	0,913	862

Table 7.
The properties of extracts in function of time at 360 °C and 10 MPa

Time	Sample	Types of protons						Atomic C/H ratio	Molecular weight,
		H _{ar}	H _{OH}	H _F	H _α	H _β	H _γ		
1. hour	Extract	-	-	-	-	-	-	0,702	492
	PS	-	-	-	-	-	-	0,680	409
	PE	6	0	0	20	55	19	0,631	387
	BE	12	0	5	21	46	16	0,721	394
	ME	12	2	9	22	41	14	0,693	485
	BS	-	-	-	-	-	-	0,890	983
	BE	16	13	7	18	33	13	0,810	707
	ME	18	7	5	23	35	12	0,906	1030
	BI	22	8	4	21	39	6	0,906	1072
2. hour	Extract	-	-	-	-	-	-	0,736	489
	PS	-	-	-	-	-	-	0,696	417
	PE	6	0	0	17	57	20	0,636	285
	BE	14	0	2	25	45	14	0,753	559
	ME	6	0	3	21	54	16	0,703	368
	BS	-	-	-	-	-	-	0,989	785
	BE	21	21	3	21	23	11	1,013	741
	ME	13	34	5	17	22	9	0,984	794
	BI	26	0	4	23	37	10	1,003	868
3. hour	Extract	-	-	-	-	-	-	0,778	467
	PS	-	-	-	-	-	-	0,723	349
	PE	11	0	1	20	52	16	0,658	270
	BE	11	0	0	26	49	14	0,790	327
	ME	14	4	0	25	44	13	0,726	534
	BS	-	-	-	-	-	-	1,041	748
	BE	24	23	5	21	21	6	1,090	533
	ME	20	27	0	24	24	5	1,030	795
	BI	23	11	2	23	37	4	1,038	1272
4. hour	Extract	-	-	-	-	-	-	0,848	538
	PS	-	-	-	-	-	-	0,761	395
	PE	9	0	0	15	57	19	0,660	369
	BE	20	0	3	30	35	12	0,897	351
	ME	6	0	6	26	48	14	0,715	490
	BS	-	-	-	-	-	-	1,071	706
	BE	26	5	5	27	29	8	1,079	771
	ME	32	6	8	27	22	5	1,068	686
	BI	31	0	5	23	33	8	1,045	1046
5. hour	Extract	-	-	-	-	-	-	0,831	494
	PS	-	-	-	-	-	-	0,739	356
	PE	11	0	0	13	56	20	0,644	272
	BE	24	0	3	30	33	10	0,857	342
	ME	10	3	3	23	47	14	0,705	481
	BS	-	-	-	-	-	-	1,041	592
	BE	27	2	4	27	31	9	1,018	527
	ME	32	0	5	28	27	8	1,049	613
	BI	32	24	0	12	28	3	1,020	1073

The dependence of the extract composition on the temperature is rather complicated. There are greater differences in the distributions of the proton types, in the C/H atomic ratios and in the molecular weights in function of the temperature. Molecular weights decrease with temperature at 420 °C it is a clear sign of cracking, while the proton distribution and C/H ratio are more similar in the supercritical temperature range and differ to that at 280 °C.

Data in Table 7 prove that the composition of the extract does not change significantly during the course of the extraction.

References

- 1 National Coal Board: Conversion of coal to liquid products using supercritical extraction. Final report to the European Coal and Steel Community Contract No. 6220-EC/8/805 1978.
- 2 T. Tugrul and A. Olcay: Supercritical-gas extraction of two lignites. *Fuel*, 57 (1978) 415-420.
- 3 H. Yang, K. Xiong, W. Xue and Y. Zhu: Investigation on supercritical-gas extraction of Chinese brown coals, in Proc. - Jt. Meet. Chem. Ind. Eng. Soc. China Am. Inst. Chem. Eng., Chem. Ind. Press, Beijing 1982, 2, pp. 583-595.
- 4 K.D. Bartle: The chemical nature of supercritical-gas extracts of coal and lignite. *Compend.- Dtsch. Ges. Mineraloelwiss. Kohlechem.* 77-78 (1977) 252-267.

Demetalizing of Heavy Oil Residues with Polar Solvents

Dipl.-Ing. J. Höcker (speaker), Prof. Dr.-Ing. A. Vogelpohl
Institut für Thermische Verfahrenstechnik, TU Clausthal
Leibnizstraße 15
D-3392 Clausthal-Zellerfeld

1. Introduction

The amount of residue left after vacuum distillation is about 30% of the crude oil feed. Its portion will increase, as the supply of light crude oil will decrease within the next decades. On the other hand the demand of light hydrocarbons will increase while the sale of heavy fuel oil dropped from 1973 to 1983 by 70 %.

Thus, there is a strong demand for economical conversion processes which upgrade heavy hydrocarbons into more valuable light hydrocarbons. Hydrocracking processes are widely used for this purpose. But the high content of heteroatoms in the residue prevents an economical application of processes where catalysts are involved. Heavy residues contain up to 2000 ppm of vanadium and 200 ppm of nickel. The metals are associated mainly with the asphaltenes. The IP 143 procedure defines asphaltenes as the oil compounds that are insoluble in n-heptane. They are understood as colloidal micelles which are solvated in the surrounding oil. Their precipitation can be achieved by disturbing the solvation with the result of flocculation and settling of the asphaltenes.

Industrial processes use light n-paraffines such as propane or butane for deasphalting. But all processes using light hydrocarbons have the disadvantage of poor selectivity with respect to metal content.

Searching for better precipitants, researchers at the German "Institut für Erdölforschung" discovered polar solvents lead to a better demetalization, especially liquid CO₂ and ethyl acetate as shown in Fig. 1.

The major goal of our work presented here is to develop continuously operating deasphalting processes employing CO₂ or ethyl acetate based

on the experience from batchwise experiments at the "Instiut für Erdölforschung". Such process involve the unit operations as shown in Fig. 2.

Both routes have their specific difficulties. First we will discuss some problems that occurred while putting a CO_2 -deasphalting process into operation. Second, a process will be introduced capable of demetalizing heavy vacuum residues using ethyl acetate.

2. Deasphalting with CO_2

The encounter of asphaltenes during enhanced oil recovery with CO_2 led to the idea of using CO_2 for precipitating asphaltenes and thereby demetalizing heavy residues. The optimum conditions for demetalizing were explored to be 55 bar and 29 °C at a residence time of 2 h.

CO_2 is hardly miscible with a vacuum residue due to the high viscosity of about 100 mPas at room temperature. Thus, the residue has to be diluted. We used kerosene as an appropriate diluent. It lowers the viscosity to 5 mPas, hardly affects the colloidal structure and is easily available. In an industrial deasphalting process one would use directly the liquid stream from the stripping section of the atmospheric tower with the appropriate viscosity.

Up to now there are relatively few experimental data available on the demetalizing effect of CO_2 and none that deal with chemical engineering aspects. Thus, in a first step batch measurements were carried out in the autoclave on the far left of Fig. 3 to obtain data essential for designing a continuous process such as phase equilibria and the effect of residence time and CO_2 /oil ratio. The other two autoclaves can be combined with the first one to a mixer-settler. The volumes of the autoclaves are 1, 2 and 4 l, respectively. Another arrangement of the autoclaves permits to run them as a rotating disc contactor, a column type frequently used in industrial deasphalting operations.

In the experiments three phases exist in the autoclave: a CO_2 rich phase with little kerosene, an oil phase with dissolved CO_2 and finally the asphaltenes. The upper phase could be analyzed very accurately.

At 55 bar and 28 °C it contains 98 % CO₂. The rest are the lighter components of the kerosene.

The analysis of the lower phase is much more difficult. Two samples are taken, one to measure the amount of CO₂ dissolved in the oil and a second to filtrate the asphaltenes from the oil. The filtercake is washed with n-heptane to distinguish IP 143 asphaltenes from other precipitated hydrocarbons.

The experimental work done so far pinpoints the separation of the precipitated asphaltenes from the oil as the major problem. They are very sticky and difficult to release from the autoclave.

As phase equilibria measurements by sampling are very time consuming, a system is under development to detect flocculated asphaltenes by absorption of infrared light. This procedure will enable us to quickly determine the ranges of pressure, temperature and composition in which asphaltenes precipitate.

3. Demetalizing with ethyl acetate

3.1 Experimental work

As pointed out before, the main problem is the high viscosity of the vacuum residues. In addition, the solubility of oil in ethyl acetate is very poor, so that an efficient mixing of the residue and the solvent is the key to a continuous process.

For these reasons, a twin-screw extruder was chosen as a promising mixing device. Since both screws have the same direction of rotation, selfcleaning is a very important feature of this type of extruder. The type of extruder and the operating conditions were chosen in close cooperation with its manufacturer Werner & Pfleiderer in Stuttgart which has earned a worldwide reputation for its extruder technology. The typical throughput was 5 kg/h of heavy residue, mainly "Orinoco" and "Boscan" (Tab. 1). The main variables were the number of revolutions, the type of solvent (ethyl acetate, pentane, heptane and mixtures thereof), the ratio of solvent to residue and the temperature.

The observed properties where the amount of insolubles, the efficiency of precipitation (i.e. the filtercake from the samples was washed for two hours with the solvent in a Soxhlet extractor and the mass of the washed over the unwashed cake is taken as an indication of the efficiency of the precipitation in the extruder), the degree of demetalization and the behaviour of the insolubles during filtration. This last observation gives at least some hints whether the following operation, i.e. the solid-liquid separation can be achieved easily.

3.2 Results

The influence of the number of revolutions is relatively small, but the higher the speed, the better is the filtration and the structure of the filtercake. This is due to the increased mass transfer and the higher shear-rates. The solvent more readily separates the insolubles from the oil at higher speeds ($n=400$ l/min). As to be expected, the amount precipitated by ethyl acetate is slightly higher but the demetalization is better (Tab. 2). Mixtures can improve the yield or the degree of demetalization, but the separation can no longer be achieved by simple filtration as the filtercake becomes very sticky and the solvent/oil ratio has to be increased (12/1 instead of 10/1). As shown in Fig. 4, rising the temperature from 20°C to 40°C does not effect yield or demetalization very much, but the filtration is easier at 40°C . This also follows from the precipitation efficiency. The closer it is to unity, the better is the performance of the extruder and the easier is the filtration.

The remaining metal content was generally higher for nickel than for vanadium. Typical results were 40-45% for nickel and 35-40% for vanadium. The yield of demetalized oil was about 75% in most cases.

4. Summary

Many efforts are made to be prepared for the foreseeable shortage of light hydrocarbon crudes. One possibility of stretching the existing resources is deasphalting and thereby demetalizing vacuum residues in order to get a suitable hydrocracking feedstock. CO_2 and ethyl acetate are promising precipitants for aphaltenes because of their strong de-

metalization effect. But many practical problems arise due to the uncommon physical behaviour of heavy oils, above all its high viscosity. A high pressure apparatus was built in order to study different types of continuous processes for demetalizing with CO₂. The deasphalting of heavy residues with ethyl acetate can be achieved using an extruder to overcome the problem of mixing the poorly soluble acetate into the highly viscous residues. Operating conditions were established for easy separation of the asphaltenes by filtration.

This work was made possible by the "Sonderforschungsbereich 134: Erdöltechnik-Erdölchemie", a special research program on the technology and chemistry of petroleum at the TU Clausthal.

		VR Orinoco	VR Boscan
C	/wt.-%	84.0	82.2
H	/wt.-%	10.0	10.1
S	/wt.-%	4.5	5.8
N	/wt.-%	0.8	0.85
O	/wt.-%	0.7	0.5
Nickel	/ppm	140	144
Vanadium	/ppm	650	1485
Asphaltenes (C ₇ -insol.)	/wt.-%	13.0	15.5
Conradson Coke	/wt.-%	20.0	18.4

Tab. 1 Composition of the Vacuum Residues (VR)

		n-Heptane	Ethyl Acetate
Insolubles	/wt.-%	13,5	23,8
Efficiency of precipitation		0,77	0,88
residual metal content	V / % Ni	43,0 53,8	36,9 43,0

Tab. 2 Comparison of Demetalization with n-Heptane and Ethyl Acetate

ORINOCO Vacuum Residue	
Rotation Velocity	400 rpm
Temperature Solvent	20°C
Solvent/Residue Ratio	10/1 by volume
Overall Throughput	50 kg/h

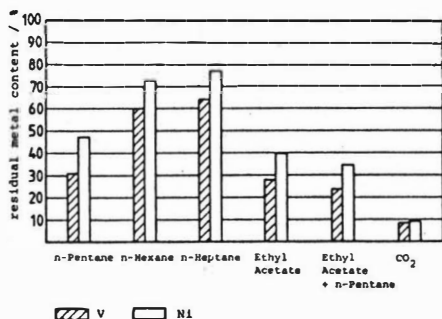


Fig. 1 Demetalization Effect of different Solvents and Kuwait Vacuum Residue

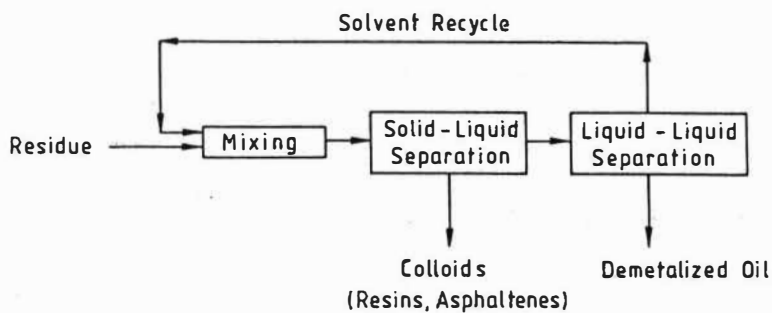


Fig. 2 Unit Operations of a Continuous Deasphalting Process

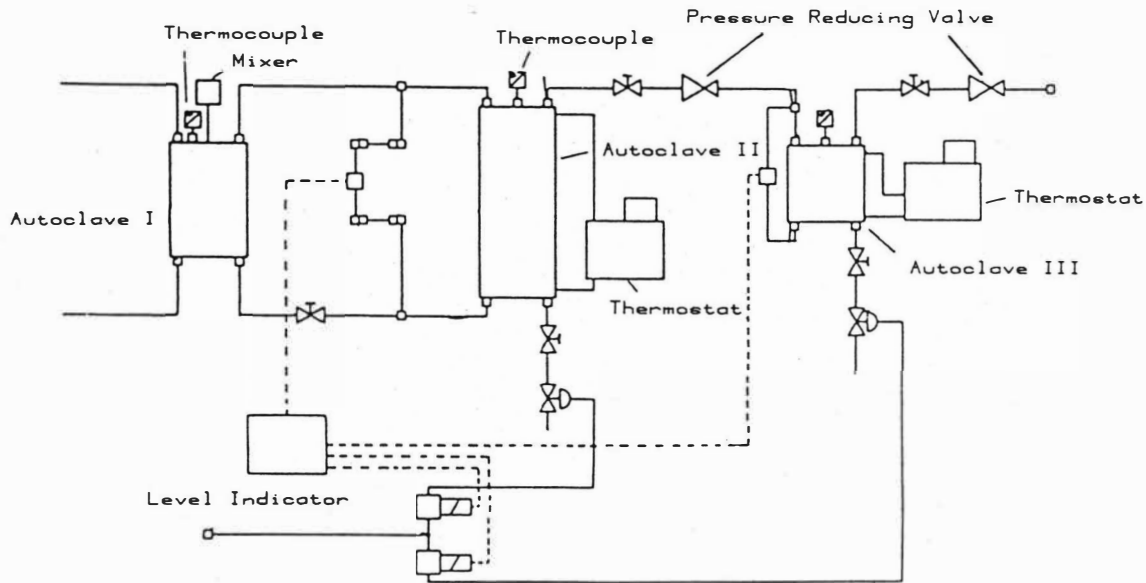


Fig. 3 Experimental Arrangement for Deasphalting with CO₂

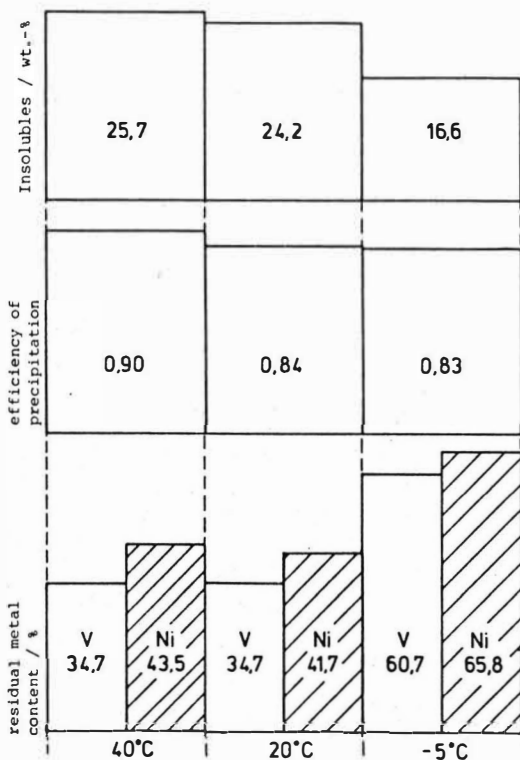


Fig. 4 Influence of Temperature on Demetalization with Ethyl Acetate

BOSCAN Vacuum Residue

Rotation velocity 400 rpm

Solvent/Residue Ratio 10/1 by volume

Overall Throughput 50 kg/h

An Approach to the Mathematical Description of the Permeation of Hydrocarbons through Liquid Membranes.

P. Pluciński*, J. Szust

Institute of Chemical Engineering and Heating Equipment,
Technical University, Wrocław, Poland.

*) present address: Technische Universität München,
Institut für Technische Chemie,
Lehrstuhl I, F.R.G.

The mathematical model of permeations of hydrocarbons through liquid surfactant membranes is proposed. This model describes the influence of the surfactant and feed kind and its concentrations on the transport through the interfacial surfactant barrier availing itself on Eyring theory of processes rate, on the equilibria (based on Scatchard and Hildebrand's theory of solubility) and on the mass transfer inside the membrane. In the last case the Cussler's model of solubilization kinetics is used. It also gives an explanation to the experimental results found in the literature.

The literature data on the permeation of hydrocarbons through liquid membranes (1-4) indicate, that this process depends on the diffusion and solubility of hydrocarbons both in aqueous phase of membrane, as well as in surface layers of surfactants molecules adsorbed onto the oil-water interface. So far, the transport of hydrocarbons through liquid membranes has been considered as a "simple diffusion", in which the surfactant used stabilized only the liquid membrane. In the previous papers (5,6) author showed the possibility of the solubilization of diffusing hydrocarbons inside the membrane. In this case the micelles act as typical carrier.

General thermodynamical considerations:

1) Diffusion of hydrocarbons through palisade layers of surfactants adsorbed on oil-water interface.

The transition of hydrocarbon molecules through the surface layer of surfactant according to Eyring theory (7) can be described as follows:

$$j_A = \lambda \cdot k_{OA} \cdot x_{Ai} \cdot c_O \quad ; \quad k_{OA} = \frac{k \cdot T}{h} \cdot \exp\left(\frac{-\Delta G_A^*}{R \cdot T}\right) \quad (1)$$

By defining the selectivity coefficient of the separation of two components (A and B) mixture as a ratio of mass transfer fluxes we set:

$$\alpha_{A/B} = \exp\left(\frac{-\Delta G_A^* - (-\Delta G_B^*)}{R \cdot T}\right) \quad (2)$$

Having in mind that the selectivity coefficient depends on cohesion energies in the investigated system (8) and that "regular solutions" theory can be used for the description of extraction processes (9,10) we obtain:

$$-\Delta G_A = RT \cdot \ln x_A + v_A \sum_{i=1}^m \sum_{j=1}^m \Phi_i \cdot \Phi_j (D_{iA} - 0,5 D_{ij}) \quad (3)$$

Relations 2 and 3 enable us to estimate the influence of both: feed composition (kind of hydrocarbons) and kind of surfactant used on the selectivity of separation due solely of the transport through the layer of adsorbed surfactant.

2) Equilibria in the core of membrane.

Equilibrium at the feed-membrane (p.t = const) can be described by the commonly used equation:

$$dG = \sum_{i=1}^{\alpha} \sum_{j=1}^{\beta} \mu_i^j dm_i = 0 \quad (4)$$

According to the Hill's thermodynamics of microsystems, which was applied to the micellar systems by Hall and Pethica (11), the standard chemical potential of the substance solubilized by micelles depends not only on pressure and temperature, but also on the number of micelles. Assuming that the selectivity coefficient is proportional to the ration of partition coefficients K , equations 3,4 enable us to predict the influence of the kind and concentration of feed components as well as the kind of surfactant used on the separation effects.

3) Diffusion of micelles in the aqueous layer of the membrane.

According to Cussler's and co. (2) model of solubilization, the permeation mechanism consists of the following steps:

- diffusion of micelles to the feed-membrane interface
- adsorption of micelles onto the interface
- reaction of the solubilization i.e. absorption of the solubilize inside the micelles
- desorption and further diffusion of complexes: micelle-solubilize through the membrane
- adsorption of complexes onto the membrane-permeate interface
- release the solubilized molecules form the micelles
- desorption of empty micelles from the interface

Additionally we must assume that the total number of available sides for adsorption is constant for both interfaces and the total concentration of micelles in membrane is also constant.

Discussion:

1) Diffusion through surfactant layers.

Equations 2 and 3 show that the selectivity coefficient for the two-component mixture of aromatic (A) and aliphatic (B) hydrocarbons is less than 1 ($v_A < v_B$, $\beta_A > \beta_B$ for $\phi_A^O = \phi_B^O = 0,5$ (13)). Thus, the aliphatic hydrocarbons diffuse through surfactant membrane faster then the aromatic ones. The

equivalent (i.e. dependent on model parameters only) selectivity coefficient $\alpha_{A/B}$ versus the kind of surfactants used is presented in Table 1. Since a stable liquid membrane consisting of only two molecular layers of adsorbed surfactant can not be formed, the verification of the model made difficult. Therefore, the presented verification is indirect and based on the fact that selectivity coefficient decreases with the decreasing of membrane thickness i.e. increasing the role of surfactant layers in overall permeation process.

Table 1

The influence of surfactant kind on the transport of toluene and heptane through surfactant liquid membranes (8,14)

Surfactant	interfacial layer			bulk of membrane	
	δ_s $4,89 \cdot 10^{-4}$ $\sqrt{J/m^3}$	α_{PL}	$\frac{\Delta \alpha}{\alpha_{max}}$	K'	α_{max}
Sodium dodecylsulfate	14,10	0,041	43,0	26,24	11,00
Sodium dodecylbenzenesulfonate	13,00	0,084	39,8	12,80	4,60
Potassium palmitate	9,60	0,528	34,3	2,03	4,55
Sodium laureate	9,60	0,528	35,3	2,03	4,12
Sodium oleate	9,30	0,604	29,7	1,78	3,65
Rokwinol 60 (Tween 60)	9,05	0,674	18,1	1,59	2,42
Rokanol K 20*	9,00	0,688	15,4	1,56	2,95
Rokafenol N10**	8,91	0,715	13,1	1,50	3,06
Rokafenol N8**	8,86	0,730	6,6	1,47	3,23

*) polyoxyethylene (20) alcohols obtained from coconut oil

**) Rokafenol - polyoxyethylene nonylphenol

PL - palisade layer, max - for thick membrane

$\Delta \alpha = \alpha_{1/20} - \alpha_{max}$ / δ - solubility parameter

The values of relative decrease of the selectivity coefficient for equimolar mixture of toluene-heptane taken from (8) are also presented in Table 1. The values of selectivity coefficient found for the 1:20 membrane to oil volume ratio (i.e. for most thin membranes so far obtained) reflects most strongly the influence of diffusion through surfactant layers. The difference between the values of selectivity coefficients, for the process governed by the diffusion through aqueous phase, and that for which the contribution of both aqueous and surfactant layers are nearly the same, can be treated as a direct measure of the influence of surfactant palisade layers on the permeation process.

2) Equilibria in the core in membrane:

Equations 3,4 allow us to estimate the influence of kinds of surfactant as well as feed on the value of micellar supplementary equilibrium coefficient. The relation between experimental and supplementary coefficients is presented in Table 1. A simple relation, confirming presented model, between these coefficients and solubility parameter of surfactants is found. While calculating the values of supplementary equilibrium the values of volume fractions of toluene and heptane in micelles were assumed arbitrarily (equal to 1,2) by analogy of those found for the mixture of benzene and hexane (13). Presented model (eqs. 3,4) allows us also to estimate the role of feed composition (volume ration β^0) on the selectivity of separation. Calculated values of K decrease with increasing of the amount of benzene in the feed, and the character of this dependency changes when the concentration of toluene reaches 0,4 kmol/kmol (i.e. for $\beta_A = 0,5$). The calculated pattern of this relation is very close to that obtained experimentally by Shah and Owens (2).

3) Diffusion of micelles in aqueous layer of the membrane.

From the proposed in this work model of the diffusion it is evident, that only two steps: reactions onto the interfaces, can change the selectivity of the separations. Therefore, it was assumed that these two steps govern the process. If we assumed equilibria in the rest steps, and we include the flux of free hydrocarbon molecules dissolved in water, according to (13) we obtain:

$$j_A = \frac{c_T [S_0] k_2^A K_1 ([A]_1^A - [A]_2^A)}{K_1 K_2 (K_3 + c_T) ([A]_1^A + [A]_2^A) + 2(1 + c_T K_1)} + \frac{D_A}{s} ([A]_1 - [A]_2) \quad (5)$$

where:

$K_i = k_i/k_{-i}$; $[S_0]$ - number of sites onto interface

The dependence of mass transfer flux on micelles concentration (c_T) = resulting from eq 5 is with a good qualitative agreement with experiments (14). Analysing the influence of surfactant concentration on the selectivity coefficient ($\alpha_{A/B} = j_A/j_B$) we can easily find the dependence:

$$\alpha_{A/B} = \frac{X_1 c_T^2 + X_2 c_T + X_3}{Y_1 c_T^2 + Y_2 c_T + Y_3} \quad (6)$$

This dependence does not preclude the existence of maximum which was experimentally observed (2). From eq.5 we can also find the dependence of $\alpha_{A/B}$ versus feed composition (for $[A]_2 = [B]_2 = 0$)

$$\alpha_{A/B} = \frac{X_1' ([A]_1/[B]_1)^2 + X_2' ([A]_1/[B]_1)}{Y_1' ([A]_1/[B]_1) + Y_2'} \quad (7)$$

Decreasing concentration of A (benzene) in a feed mixture with B (hexane) we decrease the ration $[A]_1/[B]_1$ (equilibria eq. 3 and 4) and decrease the selectivity of separation. This facts was also experimentally observed (2).

Literature

1. N.N.Li, *Ind.Eng.Chem., Process Des.Dev.*, 10(1971)215.
2. N.D.Shah, T.C.Owens, *Ind.Eng.Chem., Prod.Res.Dev.*, 11(1972)58.
3. G.Casamatta, L.Boyadzhiev, H.Angelino, *Chem.Eng.Sci.* 29(1974) 2005.
4. P.Alessi, I.Kikic, M.Orlandini, *Chem.Eng.J.* 19(1980)221.
5. P.Plucinski, *Tenside Detergents*, 22(1985)18.
6. P.Plucinski, *J.Membrane Sci.*, 23(1985)105.
7. A.A.Frost, R.G.Pearson, *Kinetics and Mechanism*, J.Willey, New York, 1961.
8. P.Plucinski, *Europe-Japan Congress on Membranes and Membrane Technology*, Stresa, Italy, 18-22 June, 1984.
9. S.Siekierski, R.Olszer, J.Inorg.Nuclear Chem., 25(1963)1351.
10. T.Wakayashi, S.Oki, T.Omori, N.Suzuki, *ibid.*, 26(1962)2255, 2265.
11. D.G.Hall, S.A.Pethica, in *Nonionic Surfactants* (edited by M.J.Schick), pp.516-557, M.Dekker, New York, 1967.
12. J.A.Shaeiwitz, A.F-C.Chan, E.L.Cussler, D.F.Evans, *J.Colloid Interface Sci.*, 84(1981)47.
13. M.A.Chaiko, R.Nagarajan, E.Ruckenstein, *ibid.*, 99(1984)168.
14. Z.Fądział, M.Sc.thesis, T.U.Wrocław, Poland, 1983.

Influence of Emulsion Breakage on Selectivity in the Separation of Benzene-Heptane Mixtures with Aqueous Surfactant Membranes

R. Krishna and A.N. Goswami, Indian Institute of Petroleum, Dehra Dun 248005, India

Introduction

Liquid Membranes provide a powerful, energy efficient, tool for effecting separations in diverse areas such as waste water treatment⁽¹⁾, hydrocarbon separations^(2,3) and hydrometallurgy⁽⁴⁾. The focus in this paper is on separation of hydrocarbon mixtures, specifically the selective removal of aromatics from a mixture containing aromatics and paraffins. A liquid membrane hydrocarbon separation process uses thin aqueous films stabilized by emulsification; this membrane permits a selective passage of the aromatics from the feed phase into the receiving, or solvent, phase. The selectivity in transport of aromatics is primarily due to the much higher solubility in the aqueous, intervening, phase^(2,5,6). Ideally speaking, the membrane phase should be stable and prevent the feed hydrocarbon mixture from physically mixing with the solvent phase because such mixing would entail loss of selectivity. Under conditions in which there is no such physical mixing due to breakage of the emulsion, the selectivity is governed solely by the relative rates of transfer of the compound types across the aqueous membrane; these relative rates are determined by the ratio of the product of solubility and molecular diffusivity of the transferring species in the aqueous phase. But such ideal conditions do not always prevail and what happens in practice is that due to emulsion instability, the membrane can rupture so that there is non-selective transport, of a portion of the feed hydrocarbon mixture, into the solvent, resulting in a loss of selectivity⁽⁷⁾. The "overall" mass transfer coefficient obtained in the permeation process reflects not only selective, diffusive, transport across the membrane but also the non-selective physical mixing of feed with solvent. Mass transfer coefficients should therefore be corrected for the emulsion breakage phenomena in order to draw meaningful conclusions; this has been insufficiently recognised in the literature^(8,9,10).

In this paper we will develop a model for the liquid membrane separation process taking proper account of emulsion breakage. Using this theoretical model we have interpreted mass transfer measurements for the separation of mixtures of benzene - n-heptane to give an estimate of the extent of non-selective transport due to emulsion breakage. This estimated breakage is further verified by independent measurements using water-insoluble dye "tracers". The study reported here should provide a more rational approach to the interpretation of liquid membrane separation data and also provide a more soundly based scale-up methodology.

Development of Model

The liquid membrane permeation process is modelled as a parallel-step process:

1. selective diffusional transmembrane transport

2. non-selective transport due to emulsion breakage.

A schematic diagram of the model is given in Figure 1 where we consider the feed mixture to be made up of two compound types: aromatics(A) and non-aromatics(NA). The fraction of the feed mixture which gets transferred to the solvent phase due to emulsion breakage is denoted by ϵ_b .

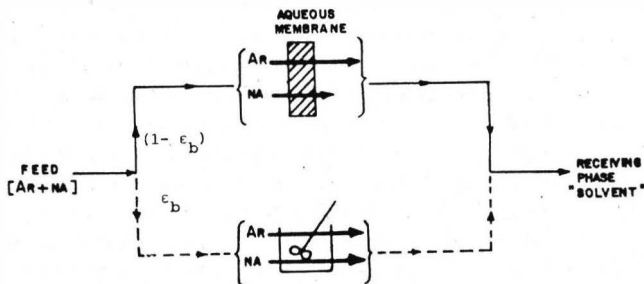


Figure 1. Model of Transfer Process across Liquid Membrane.

Let us first consider the diffusive transmembrane mass transfer process. At time t the concentration profile of the transferring aromatic species A is shown pictorially in Figure 2.

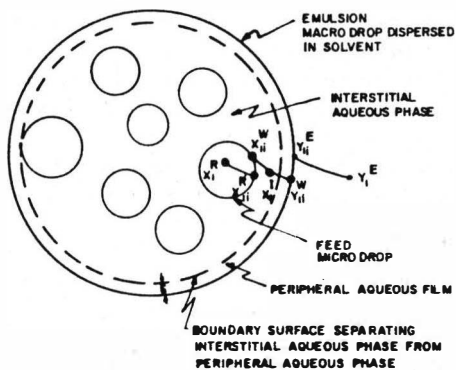


Figure 2. Concentration Profiles at Time t for Transmembrane Transport

We can distinguish four sequential steps in the mass transfer process:

- (i) transfer within the microdrop of the emulsion; mass transfer coefficient denoted by k_1^R (superscript R referring to feed or raffinate phase)
- (ii) transfer from the surface of the microdrop to the bulk aqueous surfactant

(interstitial) phase; transfer coefficient $k_1^{W(1)}$

(iii) transfer from the bulk interstitial aqueous phase to the surface of the macrodroplet; transfer coefficient $k_1^{W(2)}$. This transfer process is presumed to be governed by molecular diffusion across a peripheral film as depicted in Figure 2.

(iv) transfer from the surface of the macrodroplet to the bulk solvent phase; transfer coefficient k_1^E .

There are two interfacial areas (reckoned per unit volume of extract phase): $a^{(1)}$ referring to that between the feed microdrop - water interface and $a^{(2)}$ at the emulsion - solvent interface. If we define an overall mass transfer coefficient K_1^E for the feed - solvent mass transfer process by

$$N^{(1)} a^{(1)} = N^{(2)} a^{(2)} = K_1^E a^{(2)} \rho^E (x_1 - x_1) \quad (1)$$

where x_1^R and x_1^E refer to the mass fractions of A (aromatics) in raffinate and extract phases respectively. We can derive the following expression for the overall coefficient K_1^E

$$\frac{1}{K_1^E a^{(2)} \rho^E} = \frac{1}{k_1^R a^{(1)} \rho^R} + \frac{1}{M_1 k_1^{W(1)} a^{(1)} \rho^W} + \frac{1}{M_1 k_1^{W(2)} a^{(2)} \rho^W} + \frac{1}{k_1^E a^{(2)} \rho^E} \quad (2)$$

The small sizes of the microdrops (usually in the range 1 - 10 μm) and the macrodrops (of diameters of about 1-3 mm), coupled with the fact that surfactants are present would suggest that rigid drop (both micro- and macro-) may be assumed. For transfer within and outside rigid spheres, the Newman model gives, for sufficiently high Fourier numbers, the Sherwood numbers to be respectively 6.58 and 2 respectively. This, along with diffusivity data, allows estimation of the coefficients k_1^R , $k_1^{W(1)}$ and k_1^E . For estimating $k_1^{W(2)}$, an estimate is required of the effective thickness of the peripheral film across the mass transfer can be expected to be controlled. This film thickness can be taken to be of the same order of magnitude as the intermicrodrop distance. From a knowledge of the microdrop diameter and microdrop holdup, this effective film thickness can be estimated and so the coefficient $k^{W(2)}$ is

$$k^{W(2)} = D_1^W / \delta \quad (3)$$

The differential material balance for component 1 (aromatic A) in the extract phase is

$$\frac{dE_1}{d\xi} = \frac{d(Ey_1)}{d\xi} = N_1^{(2)} a^{(2)} V E_\tau = \rho^E K_1^E (x_1 - y_1) a^{(2)} V E_\tau + y_1 (N_1^{(2)} + N_2^{(2)}) a^{(2)} V E_\tau \quad (4)$$

An overall balance gives

$$\frac{dE}{d\xi} = (N_1^{(2)} + N_1^{(2)}) a^{(2)} V E_\tau \quad (5)$$

Combination of Equations (4) and (5) yields

$$\frac{dy_1}{d\xi} = \frac{\rho E K_1^E a^{(2)} V^E \tau}{E} (x_1 - y_1) \quad (6)$$

Next, consider the non-selective transfer due to emulsion breakage. We have the following relation at any instant

$$\frac{dE}{d\xi} = -\frac{dR}{d\xi}; \quad \frac{d(Ey_1)}{d\xi} = -\frac{d(Rx_1)}{d\xi} \quad (7)$$

There is no change in the raffinate phase composition due to the non-selective transfer process and so $dx_1/d\xi = 0$. Thus from Equation (7) we get the change in the extract phase composition due to emulsion breakage as

$$E \frac{dy_1}{d\xi} = -(x_1 - y_1) \frac{dR}{d\xi} \quad (8)$$

Using the model depicted in Figure 1, we may write the composition change of the extract phase due to both diffusive and mixing transfer processes as

$$\frac{dy_1}{d\xi} = -\epsilon_b \frac{(x_1 - y_1)}{E} \frac{dR}{d\xi} + \frac{(1 - \epsilon_b) \rho E K_1^E a^{(2)} V^E \tau}{E} (x_1 - y_1) \quad (9)$$

Both the raffinate and extract phase amounts, R and E respectively, vary with time. Let R_0 and E_0 represent the initial amounts. Also define the number of overall mass transfer units NTU_1 as

$$NTU_1 = \frac{\rho E K_1^E a^{(2)} V^E \tau}{E_0} \quad (10)$$

The variation of R with time can be expressed empirically as

$$R = R_0 f(\xi) \quad (11)$$

where $f(\xi)$ is a function which can be determined from the experimental data.

Equation (13) can be integrated from $\xi = 0$ to $\xi = 1$ to give

$$NTU_1 = \frac{\frac{1}{1+m} \ln \left(\frac{mx_{10}}{mx_{10} - y_1(1+m)} \right) + \epsilon_b \int_0^1 \frac{f'(\xi) d\xi}{f(\xi)(1+m - mf(\xi))}}{\frac{(1 - \epsilon_b)}{m} \int_0^1 \frac{d\xi}{f(\xi)(1+m - mf(\xi))}} \quad (12)$$

where $m = E_0/R_0$ is the initial solvent/feed ratio. If we denote β as the selectivity defined as $\beta = NTU_1/NTU_2$, then the fractional breakage can be calculated from

$$\epsilon_b = \frac{\frac{\beta}{1+m} \ln \left(\frac{mx_{20}}{mx_{20} - y_2(1+m)} \right) - \frac{1}{1+m} \ln \left(\frac{mx_{10}}{mx_{10} - y_1(1+m)} \right)}{(1 - \beta) \int_0^1 \frac{f'(\xi) d\xi}{f(\xi)(1+m - mf(\xi))}} \quad (13)$$

Equation (13) was used to estimate the fractional breakage from the mass transfer permeation data and assuming that the selectivity β is equal to the ratio of the products of the solubilities and diffusivities of species 1 (aromatics) and 2 (non-aromatics) in water, i.e. $\beta = M_1 D_1 / M_2 D_2$. This simplification follows from the fact that the mass transfer process is controlled by the third term on the right hand side of Equation (2). This can be checked by substituting the values for the various parameters as listed in Table 1.

Experimental

The mass transfer measurements were made at 30°C in a thermostatted glass mixer-settler unit of 300 ml capacity as shown in Figure 3 below.

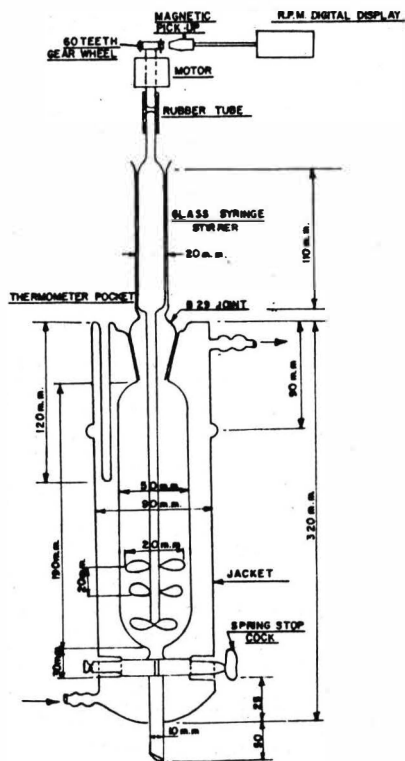


Figure 3. Mixer-Settler Unit in Liquid Membrane Permeation Experiments

Model mixtures of benzene - n-heptane (50:50) were used as feed and an alkyl phenol polyoxyethylene compound HYOXYD X200 as surfactant. The oil-in-water emulsions were formed by vigorous agitation of the feed with surfactant solution at 4000 rpm for 15 minutes and then mixed with "solvent" - kerosine - at 650 rpm in the same unit. The phases were then settled and analysed by an azeotropic distillation procedure standardized and reported earlier⁽¹⁴⁾. Four parameters: surfactant concentration, permeation time, feed/water ratio in emulsion and emulsion to kerosine ratio were studied. In addition to these mass transfer measurements, the fractional breakage ϵ_b was measured independently using a water insoluble dye tracer technique following Li (2)

Results and Discussions

Table 2 gives the set of experimentally measured compositions of benzene (1) and n-heptane (2) in the extract phase under a varying set of conditions. Using the diffusivity and solubility data of benzene and n-heptane in water as given in Table 1 the theoretical selectivity β was calculated to be 878. The form of the function $f(\xi)$ was evaluated from a curve fit of the actual measured data and taken to be of the form

$$f(\xi) = \frac{7.37}{R_0} + 1 \quad (14)$$

$$1 + 6.29 \xi$$

Using the above functional relationship the fractional breakage ϵ_b was calculated from the measured data and the values are reported in Table 2, along with the the experimental overall mass transfer coefficients $K_1^E a^{(2)}$ calculated using Equation (10) and (12). The values of the fractional breakage ϵ_b calculated above are compared with direct measurement of this parameter using dye tracer technique in Figure 4.

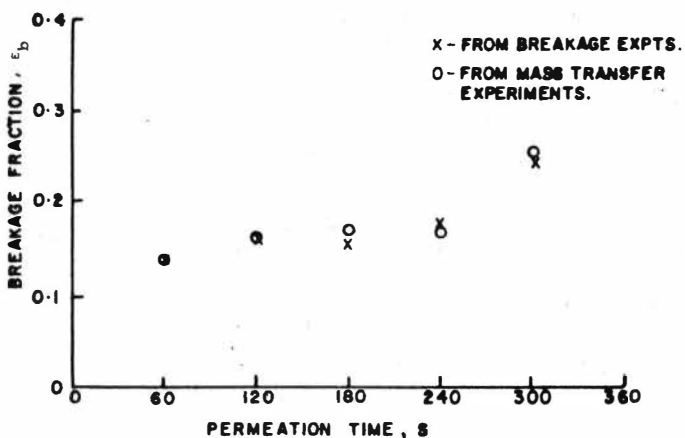


Figure 4. Fractional Breakage from Direct Measurements and from Calculations.

The excellent agreement between the directly measured fractional breakage and that estimated from mass transfer data provides a strong proof of the validity of the model set forth in this paper. Also, using the values of the various parameters as listed in Table 1, the overall volumetric mass transfer coefficient $K_1^E a^{(2)}$ is calculated to be 0.002 s^{-1} , of the same order as observed in the experiments. This provides further proof of the assumptions made in the estimates of the drops sizes.

From Table 2 it can be seen that the fractional breakage is fairly insensitive to changing surfactant concentration, which would suggest that this parameter, over the range studied, does not have an effect on the system mass transfer behaviour.

ϵ_b is seen to increase with permeation time suggesting that emulsion stability decreases with contact time. With increasing hydrocarbon/water ratio in the emulsion it should be expected that the membrane thickness would decrease. Therefore $K_1^E a^{(2)}$ should increase as is observed to be the case, in Table 2. With decreasing emulsion/solvent ratio the same mixing energy is used to disperse emulsion in an increasingly large volume of solvent. Hence with decreasing ratio, the interfacial area $a^{(2)}$ (and hence also $K_1^E a^{(2)}$) will decrease; this is borne out in the results of Table 2.

Concluding Remarks

A parallel two-step model consisting of diffusive and non-selective mixing transport has been developed to describe the mass transfer process during membrane permeation. The model has been verified by comparing the fractional breakage predicted from mass transfer measurements with direct measurements of this parameter. It can be expected that this better insight into the mechanism of interphase mass transfer will aid the scale-up of liquid membrane separation processes.

References

- (1) R.P. Cahn and N.Li, Separation Science, **9**, 505 (1974)
- (2) N. Li, A.I.Ch.E.J., **17**, 459 (1971)
- (3) N. Li, Ind.Eng.Chem.Proc Des and Dev., **10**, 215 (1971)
- (4) K. Kondo, K. Kita, I. Koida, J. Irie and F. Nakashio, J.Chem.Eng(Japan), **12**, 203 (1979)
- (5) J. Stelmazek, J.Membrane Science, **2**, 197 (1977)
- (6) G. Casamatta, C. Chavarie and H. Angelino, A.I.Ch.E.J., **24**, 945 (1978)
- (7) L. Boyadzhiev, T. Sapundzhiev and K. Bezenshek, Separation Science, **12**, 541 (1978)
- (8) N. Shah and T. Owens, Ind.Eng.Chem.Prod.Res.Dev., **11**, 58 (1972)
- (9) P. Alessi, B. Canepa and I. Kikic, Canad.J.Chem.Engng, **57**, 54 (1979)
- (10) J. Stelmazek and B. Borkowska, Inz.Chem., **5**, 869 (1975)
- (11) A. Newman, Trans.Am.Inst.Chem.Engrs, **27**, 203 (1931)
- (12) C. McAuliffe, J.Phys.Chem., **70**, 1267 (1966)
- (13) C.R. Wilke and P. Chang, A.I.Ch.E.J., **1**, 264 (1955)
- (14) A.N. Goswami and B.S. Rawat, J.Chem.Tech.Biotechnol., **34A**, 174 (1984)

Nomenclature

a	interfacial area per unit volume of extract phase, m^{-1}
D	molecular diffusivity, $m^2 s^{-1}$
d	diameter, m
E	mass of extract phase, kg
K	overall mass transfer coefficient, $m s^{-1}$
M	partition coefficient between aqueous and organic phases, -
m	initial solvent/feed ratio
N	flux of component across interface, $kg m^{-2} s^{-1}$
R	mass of raffinate phase, kg
Sh	Sherwood number, -
t	time, s
V	volume, m^3
x	mass fraction of component in raffinate phase
y	mass fraction of component in extract phase

Greek symbols

β	selectivity; $\beta = NTU_1/NTU_2$, -
δ	effective film thickness, m
ρ	mass density, $kg m^{-3}$
ϵ_b	fractional breakage, -
ξ	dimensionless time, $\xi = t/\tau$
τ	permeation time, s

Subscripts

1,2	aromatic and non-aromatic compound respectively
i	interfacial value
I	denotes boundary surface separating interstitial aqueous phase from peripheral film (see Figure 2).

Superscripts

E	extract phase
R	raffinate phase
W	aqueous phase
(1),(2)	denotes interfaces at feed microdrop - water and emulsion macrodrop - solvent respectively

Acknowledgement

The authors are extremely grateful to Miss Anshu Sharma who provided assistance in carrying out the experiments. Discussions with Dr B.S. Rawat were fruitful.

Table 1. Hydrodynamic, Thermodynamic and Physical Property Values Used in the Calculations Quoted in the Text

Property	Value Used	Data Source
Dispersed phase microdrop diameter	8 μm	Own measurements
Emulsion macrodrop diameter	2 mm	Own measurements
Volume fraction dispersed phase in emulsion	0.5	Own data
Volume fraction emulsion in solvent	0.5	Own data
Density of extract phase	820 kg m^{-3}	Own measurements
Density of raffinate phase	790 kg m^{-3}	Own measurements
Partition coefficient of Benzene in water at 30 $^{\circ}\text{C}$	1.78×10^{-3}	Reference 12
Partition coefficient of heptane in water at 30 $^{\circ}\text{C}$	2.94×10^{-6}	Reference 12
Diffusivity of Benzene in hydrocarbon phase	$3.42 \times 10^{-9} \text{ m}^2 \text{ s}^{-1}$	Reference 13
Diffusivity of benzene in water	$1.32 \times 10^{-9} \text{ m}^2 \text{ s}^{-1}$	Reference 13
Diffusivity of heptane in water	$0.91 \times 10^{-9} \text{ m}^2 \text{ s}^{-1}$	Reference 13
Volume of extract phase	$6.25 \times 10^{-5} \text{ m}^3$	Experimental value
Thickness of peripheral aqueous film,	1 μm	Estimated

Table 2. Experimental data on separation obtained in batch mixer-settler unit for the system: benzene - n-heptane. The fractional breakage ϵ_b , calculated from the theoretical model using $\beta = 878$ are also given in the Table along with the breakage corrected volumetric overall mass transfer coefficient $K_{1a}^{E(2)}$.

Parameter Varied in Expt †	m	R_0	y_1	y_2	ϵ_b	$K_{1a}^{E(2)}$
Surfactant Conc. (wt%)	$g\ g^{-1}$	g	-	-	-	s^{-1}
0.1	0.493	24.66	0.1346	0.0226	0.18	0.00277
0.2	0.480	24.00	0.1345	0.0253	0.21	0.00299
0.3	0.510	25.29	0.1377	0.0226	0.17	0.00277
0.4	0.500	25.06	0.1388	0.0224	0.17	0.00291
0.5	0.497	24.88	0.1377	0.0208	0.16	0.00284
Permeation time (s)						
60	0.484	24.19	0.1072	0.0170	0.14	0.00493
120	0.495	24.72	0.1345	0.0200	0.16	0.00403
180	0.516	25.84	0.1421	0.0245	0.18	0.00299
240	0.520	26.02	0.1472	0.0229	0.16	0.00242
300	0.500	25.04	0.1423	0.0312	0.25	0.00206
Hydrocarbon Feed						
Water						
1.0	0.510	25.24	0.1377	0.0226	0.17	0.00277
1.25	0.550	27.41	0.1499	0.0227	0.15	0.00309
1.50	0.612	30.62	0.1571	0.0295	0.16	0.00310
Emulsion Solvent						
0.50	0.256	25.67	0.0897	0.0157	0.22	0.00205
0.75	0.361	23.81	0.1077	0.0198	0.22	0.00224
1.00	0.510	25.29	0.1377	0.0226	0.17	0.00278
1.50	0.78	25.63	0.1805	0.0258	0.13	0.00367

NOTE: In all the above experiments the following parameters were kept constant:

- benzene mass fraction in feed = 0.5
- RPM during emulsification step = 4000
- RPM during permeation step = 650

Hydrodynamics of a Non-Aqueous Liquid Extraction System for a Packed Column

R.J. Moore, G.W. Stevens and H.R.C. Pratt,
University of Melbourne, Victoria, Australia.

ABSTRACT

Holdup and flood-point data are reported for the non-aqueous system Sulfolane-heptane. A plot of the holdup data in the form used to obtain the characteristic velocity was concave upwards, indicating an increase in droplet velocity and a lower rate of increase of holdup with increasing throughput, as compared with aqueous systems. The flood points were also appreciably higher than the values predicted using a correlation which allows for the effect of continuous phase viscosity. Possible reasons for these discrepancies are proposed.

INTRODUCTION

Industrial liquid extraction operations sometimes involve the use of non-aqueous systems, the most common examples being aromatics separation and lubricating oil extraction as practised in petroleum refineries. Very little information is available in the literature about such systems, apart from equilibrium data, and the design of plants has necessarily been effected by empirical scale-up from pilot plant data.

The present work has been directed towards remedying this deficiency. This paper presents hydrodynamic data involving dispersed phase holdup and flood point for the system Sulfolane-heptane in a packed column; this system was selected as an idealized form of the Shell "Sulfolane" process which is used extensively for aromatics (BTX) separation from petroleum reformatate.

EXPERIMENTAL

Equipment

The column was constructed from two 75 mm diameter QVF glass sections together with solvent inlet and interface sections, the former expanded to 100 mm diameter; it was packed to a height of 1.7 m with 12.6 mm ceramic or 15.0 mm glass Raschig rings. The light phase (heptane) distributor consisted of 8×4 mm i.d. SS tubes which passed through the packing support plate directly into the packing. The arrangement of the remainder of the equipment is shown in Fig. 1.

Materials Used

The Sulfolane (tetrahydrothiophene 1,1 dioxide) was supplied by Shell Chemicals Ltd. and was the industrial grade, containing 3% water to improve its selectivity. It was yellow-brown in colour due to the presence of decomposition products. Initial runs with the Sulfolane as supplied showed that an emulsion developed at the interface and increased in volume progressively. Tests in separating funnels indicated that the tendency to emulsify was reduced greatly by treatment with activated carbon, leaving the Sulfolane almost colourless. Before further use, therefore, it was passed 20 times through two 1.0 m x 0.10 m i.d. columns in series containing activated carbon.

The heptane was an industrial grade, with 95% by weight distilling between 95°C and 100°C. The properties of the solvents are summarized in Table 1, and those of the packings in Table 2.

TABLE 1: PROPERTIES OF SYSTEM

Phase	B. Pt. °C	Density kg m ⁻³	Viscosity kg m ⁻¹ s ⁻¹	Interfacial tension [*] , kg s ⁻²
Sulfolane	287	1,258	8.35 x 10 ⁻³	12.7 x 10 ⁻³
n-heptane	95-100	682	0.407 x 10 ⁻³	

* Between mutually saturated Sulfolane and heptane

TABLE 2: PROPERTIES OF PACKINGS

Type	Size [*] mm	No./m ³ †	Voidage ε	a m ² m ⁻³	a/ε ³ m ⁻¹
12.5mm ceramic	12.6x12.6x2.3	298,000	0.717	285	773
15.0mm glass	15.0x14.7x1.2	207,000	0.842	284	476

* Length x height x thickness

† As packed

Procedure

Dispersed phase holdup was determined by the normal drainage method (1). Thus, the phases were circulated until the column contents had been changed at least 3 to 4 times, when the flows were shut off simultaneously and the droplets allowed to settle. The dispersed phase was then run off through valve H into a measuring cylinder, and the volume determined. Corrections were applied for the presence of dispersed phase in the emulsion region at the interface, and for the "spray" section between the top of the packing and the interface. A total of 44 runs was carried out with the ceramic packing, covering a range of superficial flow rates of each phase up to 0.011 m s^{-1} .

The most satisfactory method for the determination of the flood-point was found to be to set the heptane flow, and to increase the Sulfolane flow until flooding occurred. This was always preceded by phase reversal in the middle of the column, which extended downwards as the flow was increased. The flood-point was taken as that for which a second interface formed below the packing and remained steady.

RESULTS

Holdup

The holdup data are shown in Fig. 2, plotted in the form suggested by the well-known slip velocity equation (2), viz

$$V_d + V_c \frac{\phi}{1 - \phi} = \epsilon \bar{v}_0 \phi(1 - \phi) \quad (1)$$

in which \bar{v}_0 , the "characteristic velocity", is defined as the mean droplet velocity when $V_c = 0$ and $V_d \rightarrow 0$.

Eq. (1) was originally applied to aqueous systems (2), for which a plot of the data in the form of the left hand side against $\phi(1 - \phi)$ gave a straight line of slope $\epsilon \bar{v}_0$ through the origin. However the present data did not follow this behaviour, but gave a line of gradually increasing slope at values of $\phi(1 - \phi)$ above about 0.1, as shown in Fig. 2.

The overall accuracy of the data varied from about $\pm 6\%$ to $\pm 10\%$, the major uncertainty being the measurement of the Sulfolane content of the emulsion at the interface. The height of this emulsion varied over a period of several weeks, due to a build-up of impurities on the packing. These were removed at intervals through valve H.

Flood Point

The flooding data are plotted in Fig. 3 in the form $V_{cf}^{1/2}$ vs $V_{df}^{1/2}$. These had an accuracy varying between ± 2 and $\pm 8\%$, depending upon the flow rate. Also shown in Fig. 3 are the lines representing values predicted by the correlation recommended by Houlihan and Landau (3), viz

$$1 + 0.835 \left(\frac{\rho_d}{\rho_c}\right)^{0.25} \left(\frac{V_d}{V_c}\right)^{0.50} = 0.92 \frac{\epsilon}{a 0.043} \left[\left(\frac{V_{cf} a}{g \epsilon^3}\right) \left(\frac{\rho_c}{\Delta \rho}\right)^{0.25} (\mu_c \gamma)^{0.25} \right]^{-0.25} \quad (2)$$

DISCUSSION

Fig. 2 also shows the line predicted from holdup data for aqueous systems by the "collision theory" of Gayler et al (2). The slope of this line, corresponding to $\epsilon \bar{v}_0$, is about 11% above that of the line representing the measured holdup values up to about 0.14 (i.e., for $\phi(1-\phi) \leq 0.12$) and is close to the upper error limit found for the aqueous data. However, at higher holdup values the line deviates upwards at an increasingly rapid rate, corresponding to an increasing value of the effective characteristic velocity as given by the slope of the line joining any point on the curve with the origin. This in turn leads to a decreasing rate of increase of the holdup.

There has been speculation in the literature that the exponent of the $(1-\phi)$ term on the right of Eq. (1) might differ from unity. This was therefore examined for the data presented in Fig. 2 by plotting $V_d/\phi + V_c/(1-\phi)$ vs. $(1-\phi)$ on logarithmic coordinates. Although there was considerable scatter of the points, it was concluded that the data were best represented by an exponent of unity.

Consideration was given to the possibility that these effects resulted from an increase in droplet diameter, and hence of velocity, due to coalescence. However, photographic measurements showed that this was not the case, and in fact the measured d_{32} values were in reasonable agreement with those predicted by the correlation in ref. 4. for aqueous systems. It was observed in operation at the higher holdup values, however, that the droplets followed exactly in one another's wakes, forming "chains" which passed through preferential tortuous channels in the packing. These would sometimes appear to coalesce to form a complete stream flow which would break up later into droplets higher up the column. It is apparent that the resistance to flow would be reduced in this mode, thus accounting for the increasing velocity and reducing holdup, analogous to that described by Arrowsmith and Foster (5) for multi-droplet flow.

The reason for the dominance of such a flow mechanism with the Sulfolane-heptane system may be related to the combination in this system of a high continuous phase viscosity with a moderately low interfacial tension. The effect of such forces has been represented by a dimensionless "M" group defined as (6),

$$M = g\mu_c^4 \Delta\rho / \gamma^3 \rho_c^2$$

The value of this group for Sulfolane-heptane is 8.5×10^{-6} , that is, two or more orders of magnitude greater than for aqueous systems, which range from 8.3×10^{-8} to 3.0×10^{-11} .

It might be expected that the increasing droplet velocity and consequent reducing holdup would lead to an increase in flood-point, as compared with aqueous systems. This is borne out by Fig. 3, which shows an appreciable increase in the measured values of the flood-point as compared with those predicted by Eq. (2), in which allowance is made for the effect of continuous phase viscosity.

NOTATION

- a = superficial area of packing, m^{-1}
 d_{32} = Sauter mean diameter of droplets, m^{-1}
 V_c, V_d = superficial velocity of phase, $m s^{-1}$
 \bar{v}_o = characteristic velocity of droplets in packing, $m s^{-1}$
 ϵ = fractional voidage of packing
 ϕ = fractional holdup of dispersed phase in packing voids
 ρ_c, ρ_d = density of phase, $kg m^{-3}$.

Subscripts

- c = continuous phase
d = dispersed phase
f = flood-point value

REFERENCES

- (1) Gayler, R. and H.R.C. Pratt, Trans. Inst. Chem. Eng. 29, 110 (1951).
- (2) Gayler, R., N.W. Roberts and H.R.C. Pratt, Trans. Inst. Chem. Eng. 31, 57 (1953).

- (3) Houlihan, R. and J. Landau, *Can. J. Chem. Eng.* 52, 758 (1974).
- (4) Gayler, R. and H.R.C. Pratt, *Trans. Inst. Chem. Eng.* 31, 69 (1953).
- (5) Arrowsmith, A. and P.J. Foster, *Trans. Inst. Chem. Eng.* 52, 211 (1974).
- (6) Clift, R., J.R. Grace and M.E. Weber, "Bubbles, Drops and Particles", Academic Press (1978).

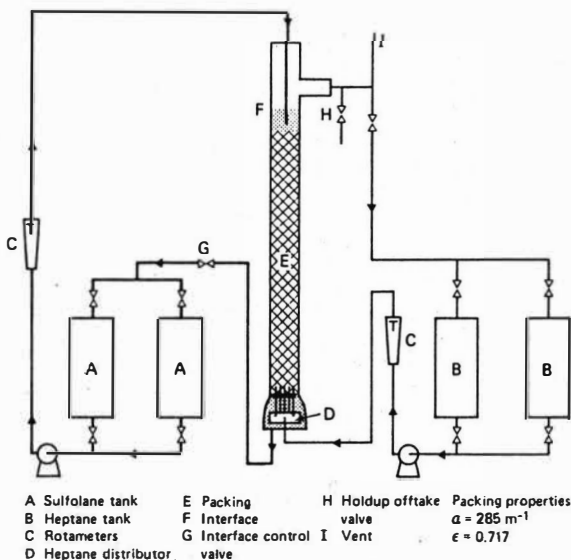


Figure 1 Arrangement of equipment

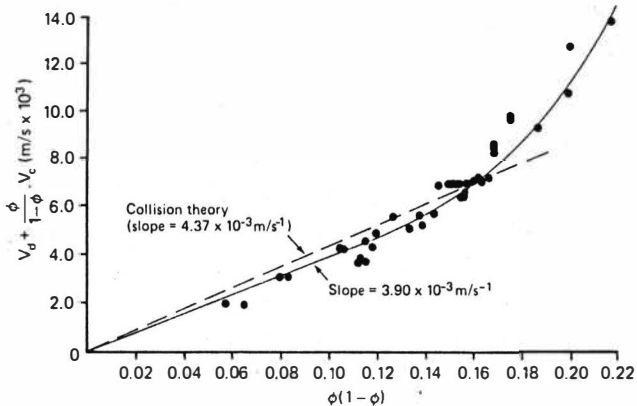


Figure 2 Plot of holdup data

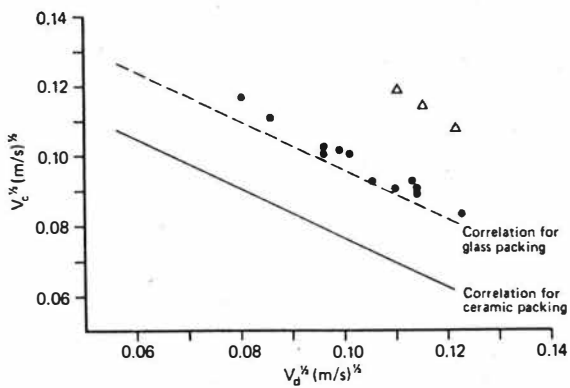


Figure 3 Comparison of flood-point data with Eq. 2:

- ceramic rings
- △ glass rings

Extension of the Application of Stage Additivity Method to the Calculation of Countercurrent Extractors with Backmixing

M. Sovilj, Institute of Petrochemistry, Gas, Oil and Chemical Engineering, Novi Sad, Yugoslavia

A. Tolić, Institute for Technology of Nuclear and Other Raw Materials, Belgrade, Yugoslavia

The basic methods published for the design of countercurrent extractors with backmixing are based on two models, the so-called differential backmixing model (1,2) and stagewise backmixing model (3,4). However, the analytical solutions for both models are restricted only to the linear case of solute distribution (5,6). The solution of the general case with non-linear equilibrium distribution requires a numerical procedure applying either boundary iteration (7,8) or a method of simultaneous solution of the set of non-linear equations (9). For the solution of the set of equations for differential backmixing model the numerically-graphical procedure has been developed (10) but the application of this procedure is restricted to the case with extremely great backmixing in one phase. However, for the calculation of equilibrium stages for countercurrent extractors with backmixing two graphical methods have been developed (11). One method is used for the calculation of equilibrium stages for one-solute distribution and the other is used for two dependent solutes distribution.

Since the solutions of exact methods of differential and stagewise backmixing model are very complex, the approximate methods for the calculation of countercurrent extractors with backmixing were proposed (6). The solutions of these methods are quite simple but the application of the majority of the methods is restricted primarily to the linear case of equilibrium distribution, or to the scale of backmixing in both phases (6).

One of the recent approximate methods for the calculation of countercurrent extractors with backmixing, the so-called stage additivity method, is developed on the basis of stagewise backmixing model (12-14). The application of this method to the calculation of countercurrent extractors with backmixing for the general case of equilibrium distribution (15) and to the calculation in the compound countercurrent extractors (16) have given satisfactory results.

In this paper extension of the application of stage additivity method to the calculation of countercurrent extractors with backmixing for the general case of multicomponent extraction will be discussed.

Stage Additivity Method

The stage additivity method (12-14) can be used for the calculation of the total number of stages in countercurrent extractors with backmixing. The stage additivity method is quantitatively described by the following equation:

$$(1) \quad N = N_M + (N_D - N_T) + \Delta N$$

The correction number of stages was obtained by equation:

$$(2) \quad \Delta N = \frac{[1 - (0.79 + 0.14 F)(N_T - 1) \ln F] f}{1 + t(1 + F f)} + \frac{[1 + (0.79 + 0.14/F)(N_T - 1) \ln F] s}{1 + t(s + F)}$$

Extraction factor was derived in the implicit form:

$$(3) \quad \ln F = \frac{N_M}{N_T} \ln \frac{1 + F t}{1 + t}$$

Numerical Procedure for a General Case of Equilibrium Distribution

The proposed numerical procedure for the calculation of total number of stages by Eq. (1), for a given value of: $f, s, t, Q, x_{in}, y_{in}, x_{out}, y_{out}$ and for a general case of equilibrium distribution: $x_n^* = x_n (y_n)$, was simply obtained by applying the derived numerical procedures for the calculation of fictive number of stages (N_M, N_D, N_T) and the correction number of stages (ΔN).

The procedure for calculation of the fictive number of stages is of general validity and is based on successive solutions of the system of material balance equation for steady state for phase (x) around n-th stage - Eq. (4) and for for both phases for the first n-stages - Eq. (5) and equilibrium equation - Eq. (6), introducing the corresponding conditions for the definition of N_M, N_D and N_T . The procedure for calculation of correction number of stages (ΔN) is based on - Eq. (2), using - Eq. (3) for the calculation of extraction factor (12-14).

$$(4) \quad (1 + f) x_{n-1} - (1 + 2f) x_n + f x_{n+1} - t (x_n - x_n^*) = 0$$

$$(5) \quad x_0 + f x_{n+1} - (1 + f) x_n - (1/Q) y_1 - (s/Q) y_n + \\ + (1/Q)(1 + s) y_{n+1} = 0$$

$$(6) \quad x_n^* = x_n (y_n)$$

Extension of the Application of Stage Additivity Method

Since the stage additivity method was developed only for the calculation for the case of one-solute distribution or for two dependent solutes distribution, it was necessary to extend the application of stage additivity method to the calculation for the case of multicomponent equilibrium distribution.

In this paper the extension of stage additivity method is proposed and for a description of the equilibria in multicomponent liquid - liquid system the following type of function is used (17):

$$(7) \quad \ln w_i = \sum_{j=1}^3 b_{ij} (x_j - p)^j, \quad i = 1, 2, 3$$

The numerical procedure for the calculation of the total number of stages, i. e. stage additivity method including - Eq. (7) for equilibrium distribution, was tested for the calculation in the case of multicomponent liquid - liquid system of the following type : aromatics - paraffins - sulfolane at 100°C. The multicomponent liquid - liquid system was treated as pseudoternary one. In this paper all the components were classified, according to their chemical similarities, as aromatics (the first), paraffins (the second) and sulfolane (the third component).

The constants in - Eq. (7) were obtained on the basis of experimental data for equilibrium distribution of the pseudoternary system : aromatics - paraffins - sulfolane at 100°C (18) by Marquardt's optimization procedure (19) and given in Table 1.

Table 1. The value of constants in Eq. (7) for the pseudoternary system of the type : aromatics (1) - paraffins (2) - sulfolane (3) at 100°C

Component, i :	b_{i1}	b_{i2}	b_{i3}
1	-0.2248	13.9210	28.7202
2	15.0800	42.4591	69.2015
3	-21.9090	-43.2901	-39.5194

The initial data for the numerical procedure of total number of stages were obtained by method of calculation of multicomponent liquid - liquid extraction (20). In all investigated cases the feed flowrate of raffinate before its entry to countercurrent extractor (the first stage) was prepared from 0.011 kg/s aromatics and 0.017 kg/s paraffins. At the same time the feed flowrate of extract at the other side of column was 0.028 kg/s of sulfolane.

The partial mass transfer coefficients related to raffinate (k_{xi}) and to extract (k_{yi}) are assumed constant throughout the column for component i , Table 2. The numerical value of partial mass transfer coefficient for all pseudocomponents were selected so that they were the same as those for single characteristic component (20).

Table 2. The value of partial mass transfer coefficient for pseudocomponents of the system : aromatics (1) - paraffins (2) - sulfolane (3)

Component, i	Partial mass transfer coefficient, $\text{kg m}^{-2} \text{s}^{-1}$	
	Raffinate, $k_{xi} \cdot 10^3$	Extract, $k_{yi} \cdot 10^3$
1	2.780	1.390
2	4.170	2.085
3	4.170	2.085

In order to test the proposed numerical procedure, included the data of concentration profile for multicomponent liquid - liquid system : aromatics - paraffins - sulfolane, the total number of stages in 80 runs were calculated.

In all investigated cases the parameters were varied in the following regions :

exact number of stages	3 - 10
backmixing coefficient in phase (x)	0 - 10
backmixing coefficient in phase (y)	0 - 10

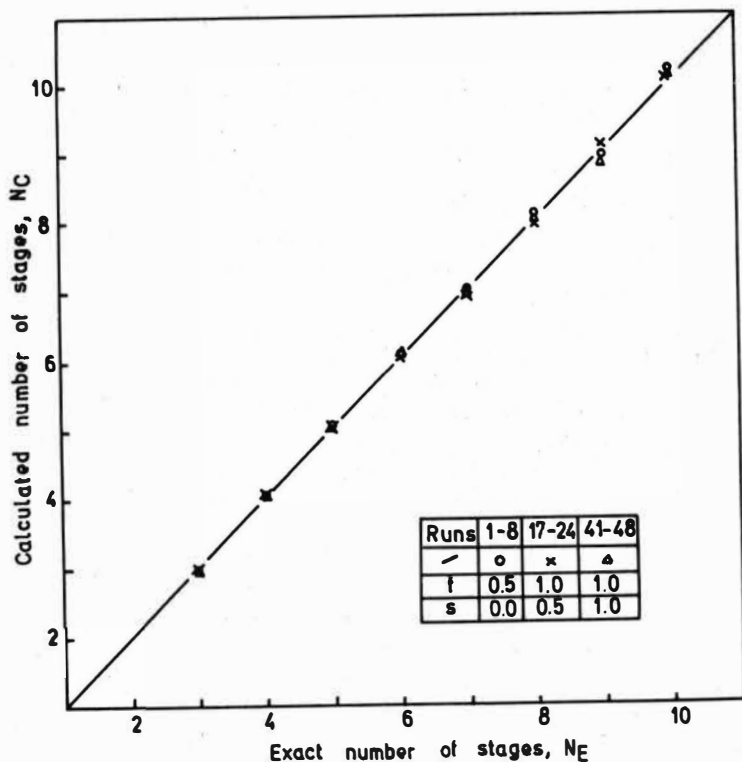


Figure 1. Comparison of calculated (N_C) with exact number of stages (N_E) for the selected runs

The calculated number of stages for selected runs are compared graphically with exact number of stages in Figure 1. As it is obvious from the given results, the agreement is very good for all selected cases. The relative deviations between calculated and exact values of the number of stages for all investigated cases (δ) was from - 1.85 to + 11.84 %. The sum of square deviations between calculated and exact values of the number of stages (δ^2) was 0.54.

Nomenclature

- b_{ij} - constants in Eq. (7),
- f - backmixing coefficient in phase (x),
- F - extraction factor,
- i - pseudocomponent (1-aromatics; 2-paraffins; 3-sulfolane),
- k_x - partial coefficient in phase (x), $\text{kg m}^{-2} \text{s}^{-1}$,
- k_y - partial coefficient in phase (y), $\text{kg m}^{-2} \text{s}^{-1}$,
- m - distribution coefficient,
- N - total number of stages,
- N_C - calculated number of stages,
- N_D - number of equilibrium stages,
- N_E - exact number of stages,
- N_H - number of stages when backmixing is absent in both phases,
- N_T - number of theoretical stages,
- ΔN - correction number of stages,
- p - concentration of component (1) in plait-point, kg kg^{-1} ,
- Q - flow rate of phase (x) and phase (y),
- s - backmixing coefficient in phase (y),
- t - true number of transfer unit in a stage,
- x - concentration of solute in phase (x), kg kg^{-1} ,
- x_1 - concentration of component (1) in phase (x), kg kg^{-1} ,
- x^* - concentration of solute in phase (x) for equilibrium, kg kg^{-1} ,
- y - concentration of solute in phase (y), kg kg^{-1} ,
- δ^2 - sum of the square deviations,
- δ - relative deviations.

Subscripts

- i - number of components,
- in - before entry to extractor,
- j - degree of function in Eq. (7),
- n - typical stage of extractor,
- out - at exit from extractor.

References

1. Miyauchi, T., Vermeulen, T., *Ind. Eng. Chem., Fundamentals*, 2, 113 (1963)
2. Sleicher, C.A., *AIChE J.*, 5, 145 (1959)
3. Miyauchi, T., Vermeulen, T., *Ind. Eng. Chem., Fundamentals*, 2, 304 (1963)
4. Sleicher, C.A., *AIChE J.*, 6, 529 (1960)
5. Hartland, S., Mecklenburgh, J.C., *Chem. Eng. Sci.*, 21, 1209 (1966)
6. Mišek, T., Rod, V., in Hanson, C., (Ed.), *Recent Advances in Liquid-Liquid Extraction*, Chap. 7., Pergamon Press, London, 1971
7. Mecklenburgh, J.C., Hartland, S., *Inst. Chem. Engrs., Symp. Ser.*, No. 26, 115 (1967)
8. Mecklenburgh, J.C., Hartland, S., *Can. J. Chem. Eng.*, 47, 453 (1969)
9. McSwain, C.V., Durbin, L.D., *Separation Science*, 1, 677 (1966)
10. Rod, V., *Brit. Chem. Eng.*, 9, 300 (1964)
11. Tolić, A., Miyauchi, T., *J. Chem. Eng. Japan*, 6, 241 (1973)
12. Tolić, A., Rod, V., Jevtović, V., *Bull. Soc. Chim. Beograd*, 38, 571 (1973)
13. *Ibid.*, *Idem.*, 38, 581 (1973)
14. Tolić, A., Rod, V., Konšar-Djurđević, S., Petković, D., *Bull. Soc. Chim. Beograd*, 38, 591 (1973)
15. Tolić, A., ISEC'83, Denver, U.S.A., p. 117
16. Tolić, A., Kocić, S., CHISA'78, Prague, Czechoslovakia, p. H 3.2.
17. Rod, V., *The Chem. Eng. J.*, 11, 105 (1976)
18. Sovilj, M., *PhD Diss., Univ., Novi Sad, Novi Sad*, 1984
19. Marquardt, D.W., *J. Soc. Indust. Appl. Math.*, 11, 431 (1963)
20. Vrba, J., *Coll. Czech. Chem. Commun.*, 42, 1786 (1977)

Special Applications: Biotechnology and Natural Products

Application of aqueous two-phase systems for the extraction of biologically active proteins from biomass

Maria-Regina Kula

Institut für Enzymtechnologie der Universität Düsseldorf
5170 Jülich

Introduction:

The most valuable biotechnological products today are biologically active proteins, which as a rule are insoluble in common organic solvents. Proteins are linear polymers of 20 different aminoacids, which are tightly folded in a specific way shielding the majority of hydrophobic sidechains in the interior of the macromolecular structure and exposing charged groups on the outside towards the natural solvent water. At the same time very specific surface structures are formed, vital for the catalytic or biological activity of the single protein and allowing precise recognition of corresponding structures in molecular dimensions. To maintain the integrity of the complex structure is therefore of utmost importance in any recovery process of enzymes, proteohormones, immunomodulators, antibodies etc.

By their very nature proteins are not suitable for the conventional solvent extraction systems. However they can be handled very well in aqueous two-phase systems, making use of the incompatibility of hydrophilic polymers such as polyethylen glycol (PEG) and dextran in water or by salting out PEG with alkali phosphates or sulphates, respectively (1-5). The phases formed are distinguished by their high water content and very low interfacial tension. Both properties contribute to the observed stability of biologically active proteins and cells in aqueous two-phase systems and the high activity yield obtained in extraction. Application of the special solvent systems allows one to exploit liquid-liquid extraction technology for the isolation, concentration and partial purification of proteins.

The phase diagram of a frequently employed system, PEG 1540 and potassium phosphate is presented in fig. 1. The following discussion will concentrate on the recovery of proteins which has reached an advanced state during the last decade. A detailed discussion of basic and applied aspects of aqueous two-phase systems can be found in recent monographs and reviews (1-5).

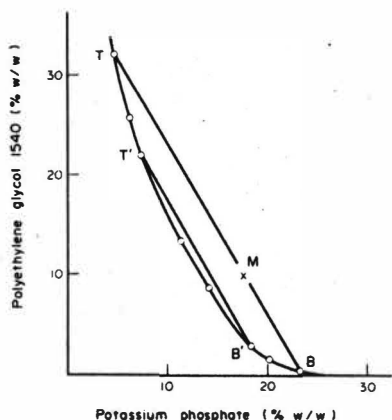


Fig. 1: Phase diagram of a PEG 1540 - potassium phosphate system at 20° C (data taken from Albertsson, ref. 1)

Partition of proteins:

Partition of macromolecules in aqueous phase systems can be described by a partition coefficient K which is defined by the ratio of the concentration of the compound of interest in top and bottom phase. The experimentally observed value of K will depend on surface properties such as surface free energy and surface charge and is an integral over all possible interactions taking place between the compound of interest and the different phases. It can be visualized as a sum of increments (6):

$$\log K = \log K_{\text{charge}} + \log K_{\text{hydrophob}} + \log K_{\text{hydrophil}} + \log K_{\text{ligand}} \dots 1$$

Equation 1 provides a framework to predict changes in K in a qualitative way by alteration of the environmental parameters, eg the pH-value, salt addition, choice of phase forming polymers and their molecular weight. Since these parameters are not independent of each other a quantitative description of partition based on molecular properties of the compound of interest is not possible at present. Changes in pH for example will not only influence the surface charge of the protein of interest, the surface free energy may be altered and also the phase potential at the same time.

The choice of the polymers and in addition their average molecular weight and the molecular weight distribution offer possibilities to set experimentally very subtle changes in the relative hydrophobicity of the phases thereby influencing the surface free energy. The difference between the phases may be very small, but will become apparent for particles and macromolecules since it is multiplied with a large surface area. Another way to affect the relative difference between the phases is given by selecting the length of the tie line for the desired separation. At the plait point - where the length of the tie line approaches zero - the phase compositions should be identical and the partition coefficients converge to 1. Away from the plait point K values deviate from 1.

Partition of cell homogenates:

For particles such as cells, subcellular organelles and insoluble cell wall fragments found in a cell homogenate a one-sided partition is expected because of the exponential relation between the partition coefficient and the surface area or molecular weight, respectively. This property allows one to substitute a very difficult mechanical separation step encountered in the isolation of any intracellular protein by a thermodynamically controlled partition step.

The difficulty in the mechanical separation step arises from the small size and rather wide size distribution of particles present in the homogenate after disintegration of microorganisms and extending from about 5×10^{-6} m to well below $0,3 \times 10^{-6}$ m into the colloidal range. For a successful extraction process conditions have to be found whereby the insoluble material and the desired protein partition into opposite phases. Cell fragments and unbroken cells should preferentially be collected in the lower phase to facilitate phase separation later on. For reasons discussed above an experimental approach is needed to devise a suitable extraction. Examples are summarized in table 1. It should be noted, that the method of cell disintegration does not influence the partition and the separation of enzymes from cell debris. Results from small scale experiments can be used to design a process and predict large scale performance. This is demonstrated in table 2. The results document that equilibrium has been achieved in large volumes and the phase separation was adequate. For economic reasons the amount of cell homogenate extracted in an aqueous two-phase system should be as high as possible (7). This leads rapidly to a situation where the concentration of polymers introduced into the

Table 1: Summarized data for the extractive separation of enzymes from disrupted cells.

Enzyme	Organism	Kind of phase system	Cell concentration (%)	Yield (%)	Purification factor
α -glucosidase	Saccharomyces cerevisiae	PEG/salt	30	95	3.2
Glucose-6-phosphate dehydrogenase	"	PEG/salt	30	91	1.8
Alcohol dehydrogenase	"	PEG/salt	30	96	2.5
Hexokinase	"	PEG/salt	30	92	1.6
Fumarase	"	PEG/salt	25	83	4.6
Formaldehyde dehydrogenase	Candida boidinii	PEG/crude dextran	20	94	n.d.
Formate dehydrogenase	"	PEG/crude dextran	20	91	n.d.
Formate dehydrogenase	"	PEG/salt	33	90	2.0
Isopropanol dehydrogenase	"	PEG/salt	20	98	2.6
Glucose isomerase	Streptomyces species	PEG/salt	20	86	2.5
Pullulanase	Klebsiella pneumoniae	PEG/dextran	25	91	2
Phosphorylase	"	PEG/dextran	16	85	1
Fumarase	Escherichia coli	PEG/salt	25	93	3.4
Aspartase	"	PEG/salt	25	96	6.6
Penicillin acylase	"	PEG/salt	20	90	8.2
Leucine dehydrogenase	Bacillus sphaericus	PEG/crude dextran	20	98	2.4
Leucine dehydrogenase	Bacillus cereus	PEG/salt	20	98	1.3
Glucose-6-phosphate dehydrogenase	Leuconostoc species	PEG/salt	35	94	1.3
D-Lactate dehydrogenase	Lactobacillus confusus	PEG/salt	20	95	1.5
L-2-hydroxy isocaproate dehydrogenase	"	PEG/salt	20	93	17.0
D-2-hydroxy isocaproate dehydrogenase	Lactobacillus casei	PEG/salt	20	95	4.9
NAD-Kinase	Lactobacillus cellobiosus	PEG/salt	20	100	3.0
Fumarase	Brevibacterium ammoniagenes	PEG/salt	20	83	7.5

Table 2: Large scale performance of enzyme extractions from cell homogenates

Enzyme	Phase system	Yield 10 ml scale	Yield in process scale	volume
Formate dehydrogenase	PEG/salt	95%	94%	250 l
Leucine dehydrogenase	PEG/salt	99%	98%	127 l
Leucine dehydrogenase	PEG/crude dextran	99%	97%	160 l

carrier aqueous two-phase system is no longer neglectable but in the same order of magnitude. Starting concentrations of 200-400 gr. wet cells per kg final phase systems are manageable (table 1), which corresponds to 5-10% dry matter added to the carrier system. This will perturb the aqueous phase system, but the basic features of partition and liquid-liquid separation are maintained. The resulting extraction system certainly does not behave anymore in an ideal way but the partition coefficients and performance are very reproducible even in such complex systems. The polymers introduced with the cell homogenate will shift the binodal of the carrier system to the left and contribute to the phase separation. A system composed of 20% broken cells, 18% PEG 1550/7% potassium phosphate—clearly below the binodal of the carrier system (see fig. 1) - has been used very successfully to partition cell debris to the bottom phase (4). The addition of large amounts of cell homogenate will alter the volume ratio of the phase system which in turn will influence the yield, depending on the partition coefficient as well as the volume ratio as shown by equation 2:

$$y_T = \frac{100}{1 + (V_B/V_T)(1/K)} \quad 2$$

The accumulation of solids in the bottom phase will lead to a considerable increase in the viscosity (4). This is also a consequence using crude dextran as a phase forming polymer. As long as $V_T > V_B$ the lower phase will be dispersed in the much less viscous top phase and the viscosity of the dispersion will be low. During separation eg in a centrifugal separator the dispersion will be broken and two phases exhibiting very diverse rheological properties may result. For such systems a nozzle separator may be used with advantage for the liquid-liquid separation as shown in fig. 2. Otherwise conventional separators can be employed to achieve the necessary phase separation (4).

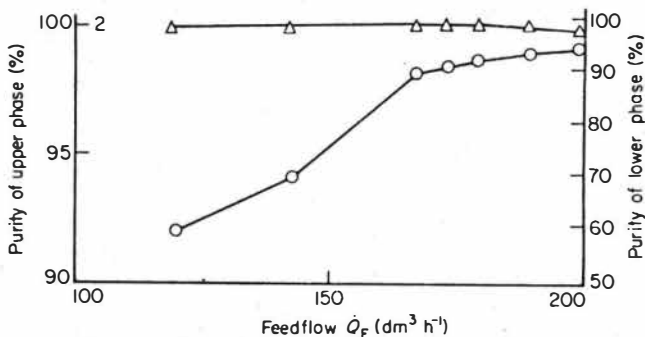


Fig. 2: Extraction of formate dehydrogenase from *Candida boidinii*, separation of the phase system (18% PEG 400, 7% PEG 1550, 8% potassium phosphate, pH 7,8, 20% broken cells) in a nozzle separator (YEB 1334 from α -Laval, 3 nozzles \varnothing 0,5 mm, $\eta_B = 1400$ mPasec) Δ top phase, \circ bottom phase. Fig. taken from ref. 9.

Under turbulent mixing equilibrium is established surprisingly fast, considering that macromolecules are involved and rather viscous bottom phases. First measuring points after less than 1 minute fail to detect deviation from the equilibrium value. The mass transport is facilitated by the low interfacial tension and the fast coalescence and redispersion of the phase system (8). Large volumes can be easily and rapidly processed with a minimal expenditure of energy. Extracting enzymes from biomass up to 25 fold purification has been achieved besides the initial objective, to clarify the crude extract and remove all solid matter. This will improve any subsequent chromatographic separation which will not be burdened with an excess of foreign protein (10). Besides undesired proteins also nucleic acids can be easily removed by partition. The product is usually partitioned in the PEG rich top phase, which may be applied directly onto reverse phase columns, hydrophobic matrices, or ion exchange resins, to recover the product and separate the neutral hydrophilic polymer. This may be the preferred course if a homogeneous, highly purified protein is the ultimate goal (10). For the isolation of a technical catalyst it is preferable to repartition the desired enzyme into the salt rich bottom

phase of a second aqueous two-phase system recovering the majority of the polymer introduced in the top phase. The product may be concentrated and desalted in an ultrafiltration plant. Economic analyses of processes indicates that the extractive recovery of biologically active proteins from cell homogenates is superior to mechanical separation steps (7, 4). For very large processes the high consumable costs for the chemicals introduced have to be considered. The major portion of PEG and also part of the salt can be recovered by the process described above. The further development of efficient recycle system for the phase forming components will make extraction for proteins a very attractive technology. In contrast to most other methods employed in protein recovery extraction can be performed in continuous mode. Development and performance of such processes is described by Hustedt et al elsewhere in this volume.

Reactive extraction:

Inspection of equation 1 indicates several possibilities to dominate the partition coefficient of a desired protein by a strong interaction with a ligand confined to one of the phases by covalent linkage to a phase forming polymer. This ligand may be an liquid ionexchanger such as DEAE Dextran, a hydrophobic ester eg PEG-palmitate or a biospecific ligand. The alteration of K with increasing DEAE Dextran concentrations in a PEG/dextran system is shown in fig. 3 taking partition of pullulanase as an example. In the absence of the ionexchanger the enzyme prefers the top phase, but it will be shifted to the bottom phase at rather low DEAE-dextran concentrations, K becomes < 1 around 0,04% DEAE-dextran. Ionexchange relies on a general property, the difference in charged groups in proteins and has only limited resolving power. However proteins will form very specific complexes with substrates, products, inhibitors, antibodies or receptors. These interactions are called bioaffinity and can form the basis of very selective purification schemes such as affinity chromatography. The principle can be exploited also with partition confining the ligand preferentially to the PEG rich top phase of a PEG/dextran system (11, 12).

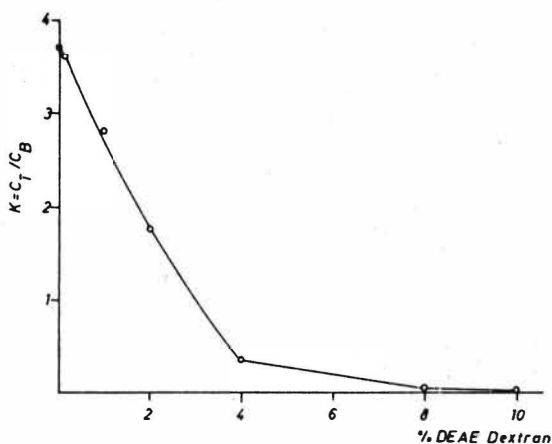


Fig. 3: Partition coefficient of pullulanase as a function of DEAE-dextran concentration. Phase system: 9% PEG 4000, 1,25% total dextran T 500 concentration, 100 mM sodium phosphate, pH 7,8. The relative amount of DEAE dextran is plotted as abscissa.

For economic reasons the specific interactions of traizine dyes with proteins have recently received much attention. PEG-derivatives are easily prepared. From a large number of readily available reactive dyes the best affinity agent can be selected measuring the dissociation constant of the protein-dye complex, which will determine the selectivity of the extraction (13). The yield of a single partition will be strongly influenced by the number of binding sites of the protein. Since enzymes frequently exhibit several binding sites affinity extraction should be an efficient separation technique. Extraction of formate dehydrogenase from *Candida boidinii* cells has been investigated in detail (12). Some results are summarized in table 3 to demonstrate that good yields can be realized with improved selectivity compared to conventional extraction (specific activity only =2U/mg). Recycling of the ligand is also possible, which is vital for the economy of such a process. It can be expected that affinity extraction will find increased application since equilibrium is established fast and there is no mass transfer resistance as in chromatographic separations. Therefore it should be especially suited for large scale processes.

Table 3: Affinity extraction of formate dehydrogenase from the cell homogenate of *Candida boidinii* (data from reference 12)

Scale of phase system ^a	Yield %	specific activity (U/mg)	Number of experiments	recycling of ligand
0.005	72±3	5.9±0.06	5	4
5.0	78±2	5.0±0.05	5	4
50.0	65	3.7 ^b	1	-
220.0	74	3.5 ^b	1	-

a) composition: 9% PEG 10.000, 1% crude dextran, 20% cells, 1 mMol/l ligand in top phase, 5% ammonium formate, 25 mM potassium phosphate, pH 8

b) batches of *Candida boidinii* differing in the starting activity were used in the large scale experiments.

Conclusions:

Aqueous two-phase systems can be employed with advantage for the extraction of biologically active proteins from biomass. This way chemical engineering knowledge and concepts from solvent extraction can be applied to products otherwise not amenable to the technique. Biological activity of proteins and cells is well preserved in such systems. Experiments with up to 1000 kg phase system have not revealed technical problems in equilibration and separation with scale up. A few processes are already established in industry.

Acknowledgements:

The work described has been performed at the Gesellschaft für Biotechnologische Forschung mbH, Braunschweig. The contributions from my collaborators A. Cordes, P.F. Fauquex, H. Hustedt, K.H. Kroner, U. Menge and H. Schütte are gratefully acknowledged.

References:

- 1) P.A. Albertsson, Partition of cell particles and macromolecules, 2nd edition 1971, 3rd edition 1986 Wiley (Interscience), New York.
- 2) M.-R. Kula, Liquid-liquid extraction of Biopolymers, in: Comprehensive Biotechnology, Vol. 2 (eds. C.L. Cooney and A.E. Humphrey) p 451-471, Pergamon Press New York, 1985
- 3) H. Walter, D.E. Brooks and D. Fisher (eds.), Partitioning in aqueous two-phase systems, Theory, methods, uses and application to Biotechnology, Academic Press, New York, 1985
- 4) H. Hustedt, K.H. Kroner and M.-R. Kula, Application of Phase Partitioning in Biotechnology, in reference 4, p 529-587
- 5) M.-R. Kula, K.H. Kroner and H. Hustedt (1982), Purification of enzymes by liquid-liquid extraction, Adv. Biochem. Eng. Vol. 24, p 73-118
- 6) P.A. Albertsson (1977), Separation of particles and macromolecules by phase partition, Endeavour 1, 69-74
- 7) K.H. Kroner, H. Hustedt and M.-R. Kula (1984), Extractive enzyme recovery - economic considerations, Process Biochem. 19, 170-179
- 8) P.F. Fauquex, H. Hustedt and M.-R. Kula (1985), Phase equilibration in agitated vessels during extraction enzyme recovery J.Chem. Tech.Biotechnol. 35 B, 51-59
- 9) K.H. Kroner, H. Schütte, W. Stach and M.-R. Kula (1982), Scale up of formate dehydrogenase isolation by partition, J.Chem.Tech.Biotechnol. 32, 130-137
- 10) U. Menge, E. Fraune, J. Lehmann and M.-R. Kula, Purification of proteins from cell culture supernatants, Proceedings of the ESACT Meeting, Baden bei Wien, 1985, in press
- 11) G. Johansson, Hydrophobic and affinity partitioning, in reference 4, p 187-196
- 12) A. Cordes and M.-R. Kula, Process design for large-scale purification of formate dehydrogenase from *Candida boidinii* by affinity partition, J. Chromatography in press
- 13) A. Cordes, J. Flossdorf and M.-R. Kula, Affinity partitioning - development of a mathematical model describing the behaviour of biomolecules in aqueous two-phase systems. Submitted Biotechnol. Bioeng.

New trends in the extraction of primary and secondary metabolites in biotechnology

K. Schügerl, Hannover, FRG

Introduction

Most metabolites with low molecular weight are excreted by the microorganisms into the fermentation broth. The downstream processing usually begins with their enrichment and isolation. After this first recovery step, the raw product is usually purified in many stages. The extraction can be one of these recovery or purification processes.

Physical extraction of metabolites

Physical extraction of metabolites is fairly popular in biotechnology. However, its application is restricted to solutes with a high partition coefficient between organic and aqueous phases /1-19/. In the case of acids or bases, their salts are not soluble in the organic solvent. Therefore, the pH of their aqueous solution has to be adjusted to values below pK_a (for acid) or above pK_b (for bases), since only the free acids or bases can be extracted with organic solvents. The physical extraction has several drawbacks. Some shall be illustrated here in the light of three different examples:

The solvent extraction of acetic acid from dilute aqueous solutions is combined with azeotropic distillation. Above 30-40 % acid concentration, the azeotropic distillation alone is more economical than the combined process. The extraction alone is not economical because of the low equilibrium distribution coefficient K_D (weight fraction of the solute in the aqueous phase).

With the increasing chain length of the organic solvents, their loss, due to their decreasing solubility in water, is reduced, however, the K_D of acetic acid and several other solutes diminishes as well. The extraction is not practicable.

Penicillin G is the raw material of semisynthetic penicillins. Its recovery from the fermentation broth is performed according to a nearly 40-year-old process. For the extraction of Penicillin G, a weak acid with $pK_a = 2.75$, the pH of mycel-free broth is set at 2.0 - 2.5 to bring the acid anion into an undissociated free state. Before the acidification, the cell-free medium is cooled to 0 - 3 °C to reduce

the decomposition rate of Penicillin G. The free acid is extracted by n-butylacetate in centrifugal extractors (e.g. Podbelniak, Luwesta, Alfa-Laval). At these low temperatures and short contact times, the losses of Penicillin G - due to decomposition - are reduced, but still amount to 15 - 20 % /21/.

Several amino acids are practically insoluble in apolar organic solvents. Therefore, their extraction from the aqueous solution by organic solvents - sparingly soluble in water - is not possible /22/.

Supercritical extraction becomes increasingly popular in the food industry. However, it is only suitable to extract lipophilic organic components, like esters and ether lactones. Solutes with strong polar functional groups, like OH and COOH makes the extraction difficult. Strong polar solutes, like sugar and amino acids cannot be extracted below 500 bar. Therefore, the drawbacks of physical extraction cannot be avoided by the use of liquified gases as solvents. Unlike supercritical extraction, these drawbacks can be avoided by using carriers in the organic solvent, which form a complex or act as ion exchangers.

In the following, three examples for the use of carriers are considered:

- acetic and citric acids
- Penicillin G and
- amino acids

Acetic and citric acids

Carrier extraction of acetic and citric acids were investigated by several research groups. Different carriers were used with appropriate organic diluents /20,23-29/. The diluent serves to provide suitable physical properties (viscosity, density, etc.) for the extraction process. The formation of the third phase can be avoided by a so-called "modifier". The extraction mechanism is an acid-base neutralization. Acid in the aqueous phase transfers to the solvent phase, where it forms a complex with the base (amine). If the base is sufficiently insoluble, the reaction complex stays almost entirely in the solvent phase. The complex is usually termed a salt or ion pair. Phosphoryl compounds and amines are popular complexing extractants for acetic acid. From the phosphoryl compounds, trioctyl phosphine oxide (TOPO) in a hydrocarbon diluent seems to be the most suitable reactive extractant. At low aqueous acid concentration, the K_D value is high (3.12 at 0.189 wt%), but it diminishes with increasing acid concentra-

tion (to 0.45 at 7.45 wt%) /23/. Amines are stronger extractants for acetic acid than phosphine oxides. However, primary amines are too soluble in water. Secondary amines with long hydrocarbon chains are excellent extractants, but they are able to react with acetic acid during regeneration of the complexing agent. The water solubility and reactivity of tertiary amines with acetic acid are low enough, and they are very good complexing agents. Unfortunately, the published investigations only evaluated K_D values, but did not consider the kinetics of the extraction.

Similar investigations were carried out with citric acid /27-29/.

Tertiary amines are the preferred complexing agents with different diluents. There is a strong effect of the diluent type on the K_D values, especially in the low acid concentration range, where the complex-diluent interaction appears to have a dominant effect. The K_D value is a function of the polarity of the diluent. At higher acid concentrations, however, the diluent effect is slight /27/. With increasing temperature, the K_D values are reduced, e.g. in Alamine 336 + Isopar H (1:1 v/v)-water system from $K_D = 7.97$ at 25 °C to 1.86 at 60 °C /27/.

Penicillin G

The main problem of the physical extraction of Penicillin G is its instability at pH 2.0-2.5. By the application of complexing agents, the reactive extraction can be performed in the pH range 5 to 7, in which Penicillin G is stable. In Fig. 1, the degree of extraction is plotted as a function of the pH value for physical extraction with n-butylacetate and with LA-2 (N-lauryl-N-trialkyl-methyl-amine) as a complexing agent in n-butylacetate at different LA-2 concentrations. Reactive extraction can be performed in the pH range 5 to 6 with the same degree of extraction which can be attained by physical extraction only at pH 3 to 4.

In Fig. 2, the scheme of physical and reactive extraction of Penicillin G with aliphatic amines is shown. The partition of the free acid at $\text{pH} < \text{pK}_a$ is given by the partition coefficient

$$C = C_{\text{HP}_0} / C_{\text{HP}_a} \quad (1),$$

where HP_0 and HP_a are the free acids in the organic and aqueous phases. At higher pH values ($\text{pH} > \text{pK}_a$), a fraction of the acid is dissociated into acid anion P_a^- and proton H_a^+ . For the concentration of free acid, eq(2) is valid:

$$C_{\text{P}_a^-} = C_{\text{HP}_a} \cdot 10^{(\text{pH} - \text{pK}_s)} \quad (2)$$

The distribution coefficient of the partly dissociate acid is given by eq(3):

$$K_{Phy} = \frac{C_{HP_O}}{C_{HP_a} + C_{P_a^-}} \quad (3)$$

Eq(4) shows the relationship between the partition coefficient of nondissociated acid C and the distribution coefficient of the partly dissociated acid K_{Phy} :

$$K_{Phy} = C \frac{1}{1 + 10^{(pH-pK_s)}} \quad (4)$$

In the presence of amine A in the organic phase, the anion P_a^- and the proton H_a^+ in the aqueous phase react at the interface with A_O and form the complex AHP_O , which is only soluble in the organic phase:



The equilibrium constant is given by eq(6):

$$K_G = \frac{C_{AHP}}{C_A \cdot C_P \cdot C_H} \quad (6)$$

For the concentration of penicillin anion $C_{P_a^-}$ in the aqueous phase, eq(7) holds true:

$$c_p = -0,5 \cdot \left(\frac{C_{A,G} - C_{P,G}}{2} + \frac{1}{K_G \cdot C_H} \right) + \sqrt{0,25 \cdot \left(\frac{C_{A,G} - C_{P,G}}{2} + \frac{1}{K_G \cdot C_H} \right)^2 + \frac{C_{P,G}}{K_G \cdot C_H} \cdot Z} \quad (7)$$

$$\text{with} \quad Z = 1 + 10^{(pK_s - pH)} + C \cdot 10^{(pK_s - pH)} \quad (8)$$

(Here $C_{P_a^-}$ was replaced by C_P for the sake of simplicity.) The degree of extraction E is given by eq(9):

$$E = \frac{C_{HP_O}}{C_{P_G}} 100 = \frac{100}{1 + \frac{1 + 10^{(pH-pK_a)}}{C}} \quad (9)$$

where C_{P_G} is the sum of the penicillin concentrations

$$C_{P_G} = C_P + C_{HP_a} + C_{HP_O} + C_{AHP_O}$$

The degree of extraction E can be calculated as a function of the pH value with this relationship (curves in Fig. 1).

Since the chemical reaction at the interface is an instantaneous one, the extraction rate depends only on the mass transfer of anion and amine to the interface. For the extraction rate, the following rela-

tionship was evaluated /21/:

$$-dc_p/dt = k_p \cdot a_p [c_p + 0,5 \cdot \left(\frac{k_A}{k_{AHP} \cdot K_G \cdot C_H} + \frac{k_A \cdot C_A}{k_p} - c_p \right) - \sqrt{0,25 \cdot \left(\frac{k_A}{k_{AHP} \cdot K_G \cdot C_H} + \frac{k_A \cdot C_A}{k_p} - c_p \right)^2 + \left(\frac{k_A \cdot c_p}{k_{AHP} \cdot K_G \cdot C_H} + \frac{k_A \cdot C_{AHP}}{k_p \cdot K_G \cdot C_H} \right)}] \quad (10)$$

In Fig. 3, the dimensionless penicillin concentration with regard to its initial concentration is plotted as a function of time for different amine concentrations in a stirred cell. (At pH 6, the concentration of the free acid can be neglected). The good agreement between measured (symbols) and calculated (curves) data is obvious. By means of Fig. 3, the mass transfer coefficients were identified as $K_p = 4.5 \cdot 10^{-4}$ cm/s (penicillin), $K_A = 1.0 \cdot 10^{-4}$ cm/s (amine) and $K_{AHP} = 6.5 \cdot 10^{-4}$ cm/s (complex).

The reactive extractions of Penicillin G were carried out in different extraction columns /21,30,31/.

In Fig. 4, longitudinal concentration profiles of Penicillin G in the aqueous phase of the laboratory Karr-column at different stroke frequencies are plotted. The combination of the kinetic model (eq 10) with a cascade model yields eq(11):

$$c_{p,0} - c_p = \tau \cdot k_p \cdot a_p \left[c_p + 0,5 \cdot \left(\frac{k_A}{k_{AHP} \cdot K_G \cdot C_H} + \frac{k_A \cdot C_A}{k_p} - c_p \right) - \sqrt{0,25 \cdot \left(\frac{k_A}{k_{AHP} \cdot K_G \cdot C_H} + \frac{k_A \cdot C_A}{k_p} - c_p \right)^2 + \left(\frac{k_A \cdot c_p}{k_{AHP} \cdot K_G \cdot C_H} + \frac{k_A \cdot C_{AHP}}{k_p \cdot K_G \cdot C_H} \right)} \right] \quad (11)$$

where τ is the mean residence time and n the number of stages which were evaluated from the measured residence time distribution (RTD) of the aqueous phase, and a_p is the specific interfacial area which was evaluated according to eq(12) from the measured holdup ϵ_0 and Sauter diameter d_{23} of the droplets of the organic phase

$$a_p = \frac{6\epsilon_0}{d_{23}(1-\epsilon_0)} \quad (12)$$

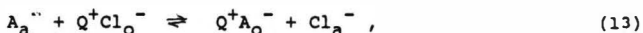
The agreement between the measured (symbols) and by means of eq(11) calculated (curves) longitudinal concentration profiles is satisfactory (Fig. 4). The investigations on the 7.6 m high pilot plant column confirmed the results evaluated on the laboratory column. In all investigated columns, high degrees of extraction were attained. The Kühni-column exhibited the highest performance, probably due to the highest specific power input applied in that column.

Countercurrent extraction and reextraction were also performed in a three-stage centrifugal extractor (Type TA-7-01-506 of Westfalia) at 8000 rpm. Mycel-free, citrate-buffered broth (500 l/h) was contacted with the solvent phase (250 l/h LA-2 in n-butylacetate) at an initial pH of 5.0. At an enrichment degree of two, a 98.2 % degree of extraction was attained. In all these investigations, satisfactory degrees of extraction were achieved and the loss of Penicillin G was reduced from 15 - 20 % (for physical extraction) to less than 1 %.

Amino acids

Amino acids have at least two pK values: pK₁ (COOH) and pK₂ (NH₃⁺). Because of the relatively high pK₂ (9 to 10), a large excess of buffer- or OH⁻-anions is necessary to maintain a sufficient amount of amino acid anions in the aqueous phase, which is necessary for their reactive extraction. The coextraction of these anions considerably influences the amino acid extraction.

When a liquid ion exchanger, e.g. quaternary ammonium chloride, is used as a carrier, chloride ions become free during the complex formation, and the extraction of amino acid and buffer anions into the organic phase is accompanied by the countertransport of the chloride anion into the aqueous phase. (The difference between the moles of transferred chloride- and amino acid-anions yields the coextracted moles of buffer anions.) Let us consider the extraction of d,l-phenylalanine by Adogen 464 (trioctyl, methyl-ammonium chloride, TOMAC) in xylene as an example:



where A_a^- is the amino acid anion in the aqueous phase
 $Q^+Cl_o^-$ quaternary ammonium salt in the organic phase
 $Q^+A_o^-$ complex in the organic phase
 Cl_a^- chloride ion in the aqueous phase

The flux of the amino acid anion is a function of the mass transfer coefficients k of the above components and the equilibrium constant $K_A^* = C_{QAoi}^2 / C_{QCl oi} C_{Aai} / 32$, neglecting the effects of coextraction:

$$-J_{A_a} = -\frac{dC_{A_a}}{dt} \cdot \frac{1}{a_s} = k_{A_a} (C_{A_a} + 0.5 B - \sqrt{0.25 B^2 - R}), \quad (14)$$

where

$$B = \frac{k_{QC1} k_{QA}^2 k_A^* C_{QC1} + 2k_{Aa}^2 k_{QC1} \cdot C_{Aa}}{k_{Aa} k_{QA}^2 k_A^* - k_{Aa}^2 k_{QC1}} + \frac{2k_{Aa} k_{QC1} k_{QA} C_{QA} - k_{Aa} k_{QA}^2 k_A^* C_{Aa}}{k_{Aa} k_{QA}^2 k_A^* - k_{Aa}^2 k_{QC1}}$$

$$R = \frac{-k_{QC1} (k_{QA} C_{QA} + k_{Aa} C_{Aa})^2}{k_{Aa} k_{QA}^2 k_A^* - k_{Aa}^2 k_{QC1}}$$

The agreement between measured and by eq(14) calculated concentration time functions is satisfactory.

However, the reactive extraction of amino acids by quaternary ammonium salts as carriers in extraction columns is not always unproblematic. Since the metallic parts of the column are wetted by the carrier solution, the latter was used as continuous phase. Furthermore, because of the high interfacial activity of the quaternary ammonium salts, the reactive extraction of d,l-phenylalanine in a pulsed sieve plate extraction column is restricted to low throughputs of the phases and to low stroke amplitudes and frequencies. Therefore, the performance of this column for this extraction is lower than that of the Penicillin G extraction.

Conclusions

By means of reactive extraction, several drawbacks in the physical extraction can be avoided. Reactive extraction in biotechnology has a bright future, because

- the capacity of the solvent phase can be considerably increased by the consecutive reaction
- the extraction rate can be increased by instantaneous reaction
- the selectivity of extraction can be increased by chemical reaction
- separation progresses are possible, which were not amenable up to now because of the insolubility of the solute in the common organic solvents.

At present, suitable carriers are still not available. Most commercial carriers were developed for chemical analytics and hydrometallurgical processes or for the reprocessing of nuclear fuels. Systematic investigations are necessary to develop highly specific carriers for the enantioselective separation of biotechnological products.

Literature

- (1) G. Machell, *Ind. Chemist* **35** (1959) 412
- (2) R.E. Treybal, *Liquid Extraction*, Section 15 in R.H. Perry and C.H. Chilton, Eds., *Chemical Engineers' Handbook*, 5th ed., Mc Graw-Hill, New York 1973, p. 15-8
- (3) M. Souders, G.J. Pierotti, C.L. Dunn, *The Recovery of Penicillin by Extraction with a pH gradient*; in: *The History of Penicillin Production*, Chem. Eng. Progress Symp. Series, Vol 66, No 100, 1970, Chapter V
- (4) *Biotechnology of Industrial Antibiotics*. Ed. E.J. Vandamme, Marcel Dekker, Inc., New York, 1984
- (4a) G. Herschbach, C.P. van der Beck, P.W.M. van Dijk, *The Penicillin*; in: 4, p. 45
- (5) M.G. Kostareva, N.P. Bednyagina, G.A. Bitynskaya, *Khim. Zh.* **8** (8) 44 (1974)
- (6) M.G. Kostareva, N.I. Vyatkina, *USSR Patent* 306 669 (Oct. 25, 1977)
- (7) B.A. Sobin, A.C. Finlay, J.H. Kane, *US Patent* 2 516 080 (July 18, 1950) Charles Pitzer Co, Inc.
- (8) G.M. Mischer, *US Patent* 3 795 663 (March 5, 1974)
- (9) C. Vezina, S.N. Sehgal, *Antimycin A*; in: 4, p.629
- (10) D. Butterworth, *Clavulonic acid*; in: 4, p. 225
- (11) M. Podojil, M. Blumanerova, Z. Vanek, K. Kulik, *The Tetracyclines*; in: 4, p. 259
- (12) L.C. Vining, D.W.S. Westlake, *Chloramphenicol*; in: 4, p. 386
- (13) W. von Daehne, S. Jahnsen, I. Kirk, R. Larsen, H. Lörck, *Fusidic acid*; in: 4, p. 427
- (14) E. Higashide, *The Macrolides: Properties, Biosynthesis and Fermentation*, in: 4, p. 451
- (15) J.L. Jost, L.A. Kominek, G.S. Hyatt, H.Y. Wang, *Cycloheximide: Properties, Biosynthesis and Fermentation*, in: 4, p. 531
- (16) F.M. Huber, A.J. Tietz, *Griseofulvin: Properties, Biosynthesis and Fermentation*, in: 4, p. 551
- (17) R.J. White, R.M. Stroshane, *Daunoribicin and Adriamycin: Properties, Biosynthesis and Fermentation*, in: 4, p. 569
- (18) P.P. Gray, S. Bhuwathanapun, *Tylosin: Properties, Biosynthesis and Fermentation* in: 4, p. 743
- (19) A.M. Biot, *Virginiamycin: Properties, Biosynthesis and Fermentation*, in: 4, p. 695
- (20) C.J. King, *Acetic Acid Extraction*, in "Handbook of Solvent Extraction", Ed. T.C. Lo, M.H.I. Baird, C. Hanson, John Wiley & Sons, New York, 1983, p. 567

- (21) M. Reschke, K. Schügerl, Chem. Eng. J. 28 (1984) B1-B9, B11-B20, 29 (1985) B25-B29, 31 (1985) B19-B26
- (22) I. Kirgios, Master Thesis, 1985, University of Hanover
- (23) N.L. Ricker, J.N. Michaels, C.J. King, J. Separ. Proc. Technol. 1 (1) (1979) 36-41
- (24) M. Siebenhofer, R. Marr, Acid extraction by amines, ISEC '83
- (25) M. Siebenhofer, R. Marr, Chem. Ing. Tech. 57 (1985) 558-559
- (26) B. Wojtech, M. Mayer, Chem. Ing. Tech. 57 (1985) 134-136
- (27) R. Wennersten, J. Chem. Technol. Biotechnol. 33B (1983) 85-94
- (28) R. Wennersten, ISEC '80, Vol 2 (1980) 80-63, 1-7
- (29) Jian Yu-Ming, Li Dao-Chen, Su Yuan-Fu, ISEC '83, 517-518
- (30) B. Müller, Dissertation, 1985, University of Hanover
- (31) Z. Likidis, Ongoing Dissertation, University of Hanover
- (32) R. Haensel, W. Halwachs, K. Schügerl, Reactive extraction of d,l-phenylalanine with TOMAC as carrier. Equilibrium and mass transfer investigations. Chem. Eng. Sci. (in press)

Figures

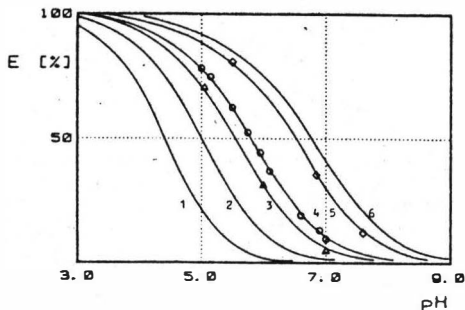


Fig. 1 Extraction of Penicillin G with Amberlite LA-2-n-butylacetate. Degree of extraction as a function of the pH for stoichiometric concentrations of Penicillin G and carrier /21/

1 $c_P = 10 \text{ mmol/l}, c_A = 0$	4 $\circ c_P = c_A = 10 \text{ mmol/l}$
2 $c_P = c_A = 1 \text{ mmol/l}$	5 $\diamond c_P = c_A = 50 \text{ mmol/l}$
3 $\triangle c_P = c_A = 5 \text{ mmol/l}$	6 $c_P = c_A = 100 \text{ mmol/l}$

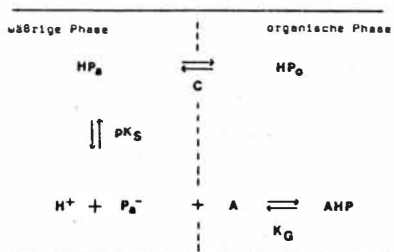


Fig. 2 Scheme of extraction of Penicillin G with aliphatic amines /21/

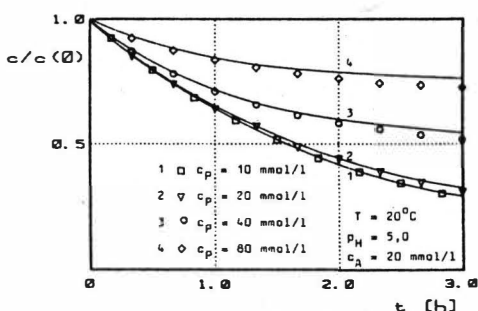


Fig. 3 Kinetics of extraction of Penicillin G with Amberlite LA-2-n-butylacetate. Dimensionless penicillin concentration with regard to its initial concentration c/c_0 as function of the extraction time /21/ - calculated, measured $\circ \nabla \square$

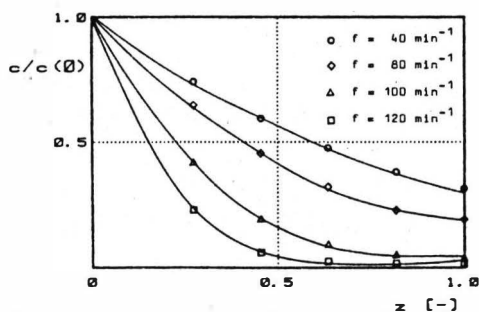


Fig. 4 Longitudinal concentration profiles of penicillin in the laboratory Karr-column. Dimensionless concentration with regard to the feed concentration as a function of the dimensionless length with regard to the active length of the column at different stroke frequencies /21/

INTRODUCTION

Liquid extraction has been employed in many different sectors of the chemical process industries, and would seem to be a strong candidate to meet the burgeoning recovery and separation demands made by the new biotechnology industries. The lack of a suitable solvent system capable of exhibiting the required selectivity for one molecular species over another, and which is not harmful to labile solutes, has limited the implementation of extraction techniques in protein recovery operations, however. Substantial progress has been made in the use of two-phase aqueous polymer systems, introduced by Albertsson and co-workers [1], and studied on a larger scale by the group of Kula [2].

An alternative to the two-phase polymer systems is the use of organic solvents, which have been employed successfully in the recovery of organic acids, but which have not been considered for proteins because of their general propensity to be either insoluble in such solvents, or to denature when brought into contact with them. These problems can be overcome by shielding the proteins within the polar cores of surfactant aggregates, or "reversed micelles," in apolar solvents such as isooctane.

We summarize here some of our recent findings on the use of reversed micelle solutions for the solubilization and selective recovery of proteins from aqueous solutions. The results will be published in a more comprehensive compilation [3].

PROTEIN SOLUBILIZATION

Surfactants which exhibit high solubility in organic solvents often form reversed micelles, aggregates in which the surfactant head groups form a polar core, and the hydrocarbon tails orient themselves outwards. These aggregates are capable of solubilizing substantial quantities of aqueous solution in their polar cores, forming an aqueous pool which is shielded from the hostile organic environment by the surfactant shell. In addition to water, other polar solutes can also be solubilized, including proteins, as depicted schematically in Figure 1.

Early experiments with cytochrome-c showed a strong dependence of the extent of protein solubilization on the ionic strength of the system [4,5]. Other workers had observed a dependence of the solubilization of α -amylase on system pH [6]. These results suggest that an electrostatic interaction between the protein surface charge and the micelle inner double layer dominates the protein solubilization behavior. As such, the effect of pH is to vary the ionization state of amino acid side chains on the protein surface, changing the net charge on a protein. Varying the ionic strength of a solution modifies its ability to screen electrostatic

interactions between surfaces of charge, and thus modifies the strength of the interaction between the protein and the micelle inner double layer.

We have probed the validity of these concepts by investigating the solubilization response of several proteins of widely varying structural characteristics to changes in system pH and ionic strength.

EXPERIMENTAL PROCEDURE

Materials and methods used in this work have been described in detail in previous papers [4,5]. A general outline of the procedure is given here.

Solubilization experiments were performed by contacting 5 ml of a 1 mg/ml protein solution of the desired pH and ionic strength with an equal volume of 50 mM AOT in isooctane solution, in a 30 ml agitated beaker for 5 minutes. (Aerosol OT, or AOT, is an anionic surfactant commonly used in protein solubilization studies.) The dispersion was centrifuged at 2000 rpm for 15 minutes to obtain a distinct phase boundary. The separated phases were assayed for protein content using absorption at 280 nm. In some cases, protein content was also determined by the Lowry assay. The pH of the aqueous phase was measured before and after contacting with the micellar phase, and the final, "equilibrium," pH is used in reporting solubilization results. Water content of the organic phase was determined by Karl-Fischer titration.

Stripping experiments were conducted by contacting the protein-loaded organic phase with an equal volume of aqueous solution having the desired ionic strength and pH, for 15 minutes.

Several experiments were conducted in which the aqueous feed solution contained a mixture of proteins, and a separation of the proteins was attempted. The techniques for these experiments were identical to those for single protein experiments, except that the aqueous phases were also analyzed by HPLC, with UV detection.

RESULTS AND DISCUSSION

Effect of pH:

The solubilization of several proteins at low ionic strength with varying pH has been studied. Data for three representative proteins are shown in Figure 2. Their molecular weights and pI 's are given in Table 1. When $pH > pI$, such that the proteins have a net negative charge, the electrostatic interaction between the protein and the negatively charged micelle inner double layer (AOT is an anionic surfactant) is repulsive and solubilization is disfavored. As the system pH is lowered below 10.6, a rapid change in the solubilization behavior of cytochrome is observed, with complete solubilization occurring for $6 < pH < 10$. Below the lower bound, the cytochrome solubilization is diminished, possibly due to a denaturation of the protein at low pH and in the presence of surfactant. This conclusion is supported

by the presence of a solid precipitate at the interface at lower pH values.

The larger α -chymotrypsin begins to solubilize only at pH-values significantly lower than the pI of the protein, and the range over which solubilization is essentially complete is reduced substantially relative to that for cytochrome-c. At low pH values, the apparent denaturation of the protein observed with cytochrome-c is also observed with α -chymotrypsin. It is plausible that the solubilization of the larger chymotrypsin molecule requires a more significant electrostatic interaction, and this is obtained at pH's lower than the pI, at which a greater protein surface charge density is present.

The very large bovine serum albumin (BSA) does not solubilize in 50 mM AOT for any pH value tested. It appears that the electrostatic interaction cannot be made sufficiently large by lowering the pH to counteract the apparently unfavorable interactions which disfavor solubilization.

In summary, it appears that pH values lower than the pI of a given protein are required to effect its solubilization in a micellar solution of anionic surfactant. Significantly lower pH values must be employed for larger proteins, most probably to overcome a size exclusion effect by enhancing the favorable electrostatic interaction. Very large proteins cannot be solubilized in 50 mM AOT solutions at any pH, as the size exclusion effect completely dominates over the electrostatic interaction.

Effect of Ionic Strength:

The major effect of variations in the ionic strength of the aqueous solution is expected to be the electrostatic screening of interactions between the charged groups on the protein surface and the surfactant head groups. These are reduced as the ionic strength is increased. It is also possible that such variations can affect protein solubilization through the protein hydrophobic energy, and by shifting ionization equilibria.

The ability of ionic solutions to modify the repulsive electrostatic interactions felt by neighboring surfactant molecules in a reversed micelle is reflected in the data presented in Figure 3, showing the water content of the micellar solution, expressed as the molar ratio of water to surfactant, w_0 , as a function of potassium chloride concentration of the aqueous phase. The ratio w_0 is, to a first approximation, proportional to the size of the reversed micelle, so these data indicate that increasing the ionic strength of the solubilized aqueous solution results in a decrease in the equilibrium micelle size. An explanation of this behavior is that at the higher ionic strengths, the repulsive electrostatic interactions between adjacent surfactant polar heads are screened (reduced), and thus a smaller micelle results.

The effect of ionic strength on the solubilization of cytochrome-c and α -chymotrypsin is shown in Figure 4. The pH of each system was such that at low ionic strength, 0.1 M KCl, total solubilization of each protein was observed. For cytochrome-c the solubilization diminished as KCl concentration was increased above 0.1 M, with solubilization completely suppressed for $[KCl] > 0.5$ M. It is of interest to note that this transition occurred at values of $[KCl]$ for which w_0 is relatively constant, the major change in micelle size having occurred over the range $0.1 < [KCl] < 0.2$ M.

The solubilization of the larger α -chymotrypsin is reduced when $[KCl] > 0.1$ M, with transfer of the protein being almost completely suppressed for $[KCl] > 0.3$ M. As this transition occurs over the same range of KCl concentration for which the empty micelles are observed to decrease in size, this suggests that the increase in ionic strength reduces the attractive electrostatic interaction between protein and micelle, as well as inducing a size exclusion of the protein from the micelle.

Thus, increased ionic strength appears to reduce the favorable electrostatic interaction between protein and micelle for all sizes of protein, and to aggravate any size exclusion effect experienced by larger proteins. Data obtained with several other proteins support these conclusions, but also lead one to suspect that ionic strength has other effects, in addition to those mentioned here.

Effect of Surfactant Concentration:

It is expected that over a range of surfactant concentration, starting at low concentrations, the surfactant is present as reversed micelles, and the addition of surfactant results in an increase in the number of micelles, rather than any substantial change in micelle size. As the surfactant concentration is increased to higher values, it is expected that equilibration with an aqueous phase will result in the formation of other, more complex aggregate structures [7,8]. These structures are ill-defined for AOT-isooctane-water systems, especially those containing salts and proteins.

It seems quite likely that changes in aggregate structure will lead to a change in a solubilization behavior of a given protein. We report here preliminary data for the proteins cytochrome-c and BSA.

Cytochrome-c, at a concentration of 1 mg/ml in 0.1 M KCl, was contacted with isooctane containing varying AOT concentrations. The resulting micellar phase was then contacted with 1.0 M KCl to recover the protein in an aqueous phase. Solubilization of the protein was complete for $[AOT] = 0.025, 0.050, 0.075, 0.100,$ and 0.200 M. For 0.500 M AOT, most of the protein was obtained in the micellar phase but the overall concentration of protein in organic was lower, ~ 0.80 mg/ml, because of the substantial quantity of water solubilized with the protein. The aqueous phase was an emulsion

which could not be analyzed for protein content. Almost complete recovery of cytochrome was obtained by contacting the protein-loaded AOT solutions with 1.0 M KCl, except for the case of 0.50 M AOT. In that case, a substantial quantity of protein, approximately 50%, remained trapped in the organic phase. Further understanding of these effects will require a more complete knowledge of the surfactant aggregation behavior at these higher concentrations.

The solubilization of BSA in 0.20 and 0.50 M AOT in isooctane solutions was also investigated. The system pH was controlled in the range 3.5 to 5.3 using a citrate/phosphate buffer of 0.01 M total molarity in 0.1 M KCl. It was observed that approximately 10% of the protein was transferred to the organic phase using 0.2 M AOT, with no clear functionality on pH. At 0.50 M AOT, almost all the protein could be solubilized at a pH of 4.75, slightly below the protein's pI of 4.9. Solubilization quickly drops off as the pH is varied about this point, as seen in Figure 5. Considering the complete lack of solubilization in 0.05 M AOT (see Figure 2), and the above cytochrome data using 0.50 M AOT, these results are difficult to explain. While the pH functionality is similar to that of other proteins, it is unclear why such a high AOT concentration is required. Furthermore, it is known that citrate can complex with protein, making it possible that the observed behavior is that of a BSA-citrate complex.

In general, it appears that varying the concentration of AOT between 0.025 and 0.20 M does not affect the solubilization of proteins, the primary effect being to increase the number density of micelles present in the organic phase. At AOT concentrations of 0.50 M (~30 wt %), substantial perturbations in solubilization behavior are observed, which may be due to changes in the aggregation behavior of AOT at these higher concentrations, with the possible formation of rod-like micelles or liquid, crystalline structures. Information on aggregate structure under the conditions of interest has yet to be determined.

Protein Separations:

It is possible to exploit these solubilization phenomena in the separation of mixtures of proteins. In general, two factors may be employed -- the differences in the charge-pH functionalities of different proteins, and differences in size. An example separation is shown in Figure 6, which illustrates the separation of cytochrome-c from BSA. In this case, the size exclusion effect which prevents the solubilization of BSA in 0.05 M AOT solution is responsible for its retention in the raffinate, with the cytochrome-c being first solubilized in the organic phase and then recovered in a second aqueous phase of higher ionic strength.

A more difficult separation is between the ternary mixture of cytochrome-c, lysozyme and ribonuclease-a. In this case, differences in the electrostatic interactions of the protein with the micelle, as controlled by pH and ionic strength, were exploited

to separate this mixture of equally-sized proteins. Details of the response of each protein to changes in system pH and [KCl] have been described previously [5]. The scheme used to take advantage of these differences is shown in Figure 7, with the compositions of the resulting aqueous phases, as analyzed by reversed phase C 18 HPLC, shown in Figure 8. Excellent separation and recovery were achieved, but it should be noted that the differences in response to changes in ionic strength which exist between lysozyme and cytochrome-c cannot be explained by our simple electrostatic interaction model. Clearly other interactions are affecting the solubilization behavior of proteins.

In summary, it appears that differences in protein size and charge can be employed to attain selective solubilization, and thus separation of proteins. Other less well understood interactions can also can play a role in obtaining separation.

CONCLUSIONS

The selective partitioning of proteins between an aqueous solution and an organic phase containing reversed micelle surfactant aggregates has been studied as a potential extraction process for protein recovery and separation. It is apparent that the electrostatic interaction model can explain many of the trends observed with changing pH and ionic strength. It is also clear that a size exclusion effect is important for higher molecular weight proteins, which must be interpreted in terms of possible limitations on the stability of the larger micelles which would be required to solubilize large proteins. These limitations may arise from structural aspects of the surfactant, entropic considerations, and other interactions as yet not considered.

High surfactant concentrations yield solubilization behavior of a substantially different nature than obtained at relatively dilute concentrations which may possibly be attributed to changes in the surfactant aggregate structure at higher concentration.

Finally, it appears that protein separations can be effected by this technique and the possibility for its application appears very broad.

ACKNOWLEDGEMENT

This work was supported by grants from the W.R. Grace Co., the National Science Foundation, and Alfa-Laval, Inc. We thank Juan Alvarez, Mark MacNicholas, Anne Dillon and Dr. Heinz Bader for their technical assistance in this work.

REFERENCES

- [1] Albertsson, P.-A., Partition of Cell Particles and Macromolecules, 3rd Edn., John Wiley Sons, NY, 1986.
- [2] Kula, M.-R., K.H. Kroner and H. Husted, Advances in Biochemical Engineering, v. 24, Reaction Engineering, A. Fiechter, ed., Springer-Verlag, NY, 1982,

p. 73-118.

- [3] Goklen, K.E. and T.A. Hatton, Biotech. and Bioeng., (in preparation).
- [4] Goklen, K.E. and T.A. Hatton, Biotech. Prog., 1, 69-74 (1985).
- [5] Goklen, K.E. and T.A. Hatton, Sep. Sci. Tech., in press (1986).
- [6] van't Riet, K. and M. Dekker, Proc. 3rd Europ. Congr. on Biotech., Munich, 10-14 September 1984.
- [7] Tamamushi, B. and N. Watanabe, Colloid and Polymer Science, 258, 174-178 (1980).
- [8] Ekwall, P., L. Mandel and K. Fontell, J. Colloid and Polymer Sci., 33, 215-235 (1970).

Table 1
Protein Properties

Protein	Molecular Weight	pI
Cytochrome-c	12,384	10.6
α -Chymotrypsin	25,000	9.7
Bovine Serum Albumin (BSA)	65,000	4.9
Ribonuclease-a	13,683	7.8
Lysozyme	14,300	11.1

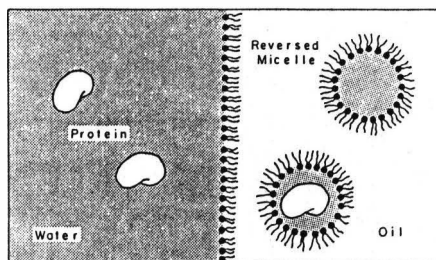


Figure 1. Schematic Diagram of Protein Solubilization in Reversed Micelles.

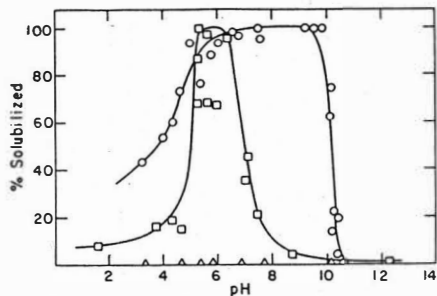


Figure 2. Protein Solubilization as a Function of pH (o) = Cytochrome-c; (□) = α -Chymotrypsin; (Δ) = Bovine Serum Albumin (BSA)

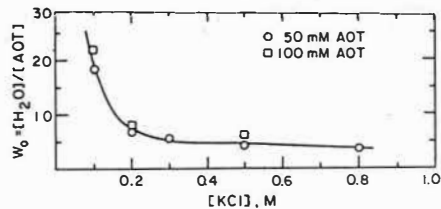


Figure 3. Effect of Salt Concentration on Water Solubilization by Reversed Micelles.

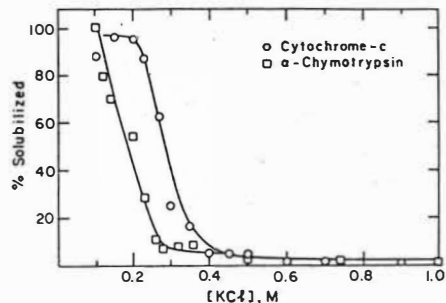


Figure 4. Protein Solubilization as a Function of Salt Concentration.

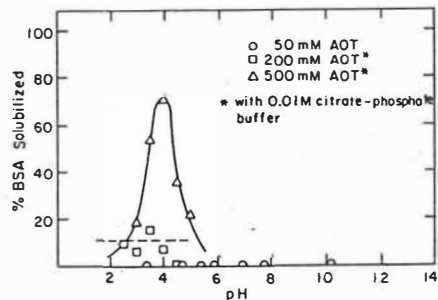


Figure 5. Solubilization of BSA as a Function of pH and AOT-Concentration.

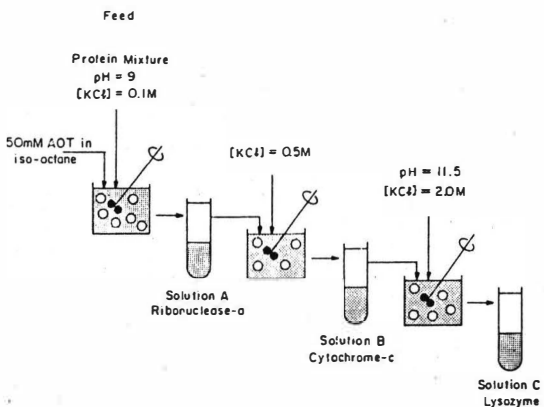


Figure 7. Experimental Procedure for the Separation of a Ternary Protein Mixture.

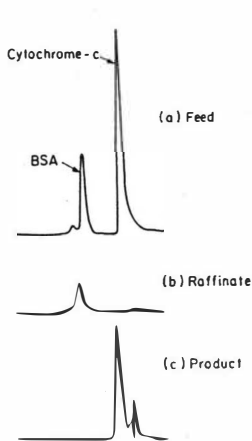


Figure 6. GPC Chromatograms of Aqueous Solutions Demonstrating the Separation of BSA and Cytochrome-c.

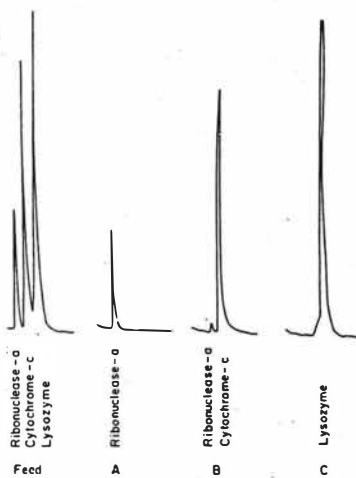


Figure 8. HPLC Chromatograms Demonstrating Resolution of a Ternary Protein Mixture Using Conditions of Fig. 7.

RECOVERY OF MICROBIAL PROTEINS BY CONTINUOUS CROSSCURRENT EXTRACTION

H. Hustedt, K.H. Kroner, N. Papamichael, GBF, Gesellschaft für Biotechnologische Forschung mbH., D-3300 Braunschweig, FRG.

Introduction

During past years extraction in aqueous phase systems has been developed to a versatile technology for the large-scale recovery of microbial enzymes and other biologically active proteins. Actual reviews are given in ref. 1 and 2. A recent development is continuous processing according to the principle of crosscurrent extraction with the principal advantages of

- enhanced space time yield
- fully automated operation
- increased number of extraction parameters
- more homogeneous product
- increased yields for labile products.

First process developments have been carried out on the enzyme fumarase from *Brevibacterium ammoniagenes*, a 2-stage process, and aspartase from *E.coli*, which is a 3-stage procedure (3-5). The results obtained have led to the development of a compact two-stage extraction plant (dimensions $l \times w \times h \sim 2 \times 1 \times 2$ m) built by Westfalia Separator AG. (Oelde, F.R.G.). In this paper the principles of continuous crosscurrent extraction in aqueous phase systems and first experiences made with this plant are described. Further recycling of the phase chemicals in a simple mode is discussed briefly.

Principle of continuous crosscurrent extraction in aqueous phase systems.

The transformation of batchwise aqueous phase extraction into continuous operation is relatively easy, because - as generally in extraction - only mixing, phase dispersion and phase separation are required as unit operations. The general scheme is shown in fig. 1 for a two-stage process, which is the usual mode of operation; in the scheme cell disruption by wet milling is included.

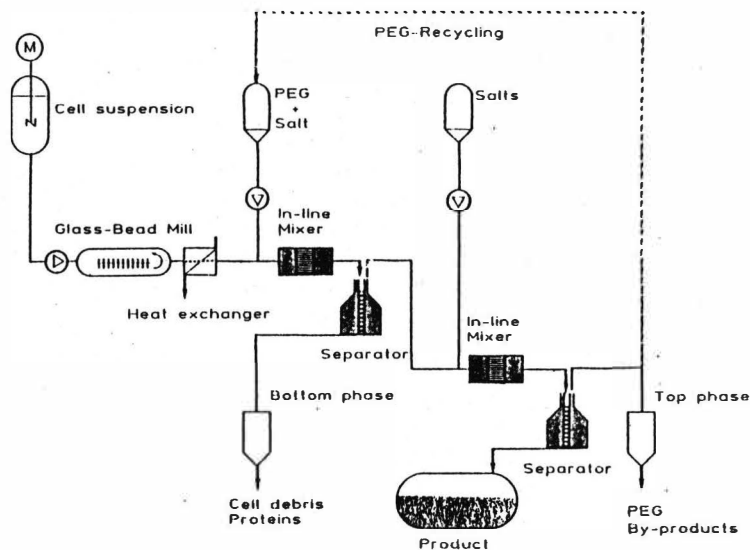


Fig. 1: Flow scheme of continuous crosscurrent extraction with aqueous phase system

Table 1: Examples of two-step extraction processes developed in the GBF

enzyme	organism	enrichment factor	final (%) yield
penicillin acylase	<i>E. coli</i>	10	78
D-2-hydroxy-isocaproate dehydrogenase	<i>Lactobacillus casei</i>	7	85
fumarase	<i>Brevibacterium ammoniagenes</i>	22	75
L-2-hydroxy-isocaproate dehydrogenase	<i>Lactobacillus confusus</i>	21	90
leucine dehydrogenase	<i>Bacillus cereus</i>	6	83
fumarase	baker's yeast	13	76

In the extraction plant mentioned above the principle outlined in fig. 1 is exploited. It contains two pilot-size separators type SA-1 (Westfalia Separator AG) with an equivalent clarifying area of 1460 m². Mixing is performed at the 1st stage in an agitated flow through cell or by a static mixer; the latter is applied generally at the 2nd stage. Besides magnetically inductive flow-meters no special equipment for measuring and control is included in the basic plant.

In tab. 1 a number of two-step enzyme extraction processes are summarized; all of these appear suitable for continuous processing.

Continuous extraction of fumarase

Taking into account the high consumption of biomass (ca. 600 kg per day) during long-term continuous processing an extraction process for the enzyme fumarase from baker's yeast - commercially available in any scale at low cost - has been developed as a model process. Data of the recovery process are included in tab.1.

The main physico-chemical data of the process liquids are collected in tab. 2. The viscosities of the process streams are moderate facilitating mixing and equilibration in a matter of seconds. To this contributes mainly the low interfacial tension of these systems, for which about 0.5 mN/m can be assumed from measurements of comparable processes (6). The very fast equilibration of the phases is reflected by the data in tab. 3 for the first extraction step, using a static mixer for mixing and phase dispersion. In this connection it should be noted that during the mixing process at first the phase system has to be established - cf. extraction in water/organic systems - before equilibrium of partition can be obtained.

Besides attainment of equilibrium of partition, phase separation with high and constant purity is necessary to establish a reliable continuous process. This is generally possible by the use of common disk stack separators operated either in a liquid-liquid mode or, at high bottom phase viscosities ($\eta > 500$ mPa's), as solid-liquid (nozzle) separator (2).

Tab. 2: Physico-chemical data of the process liquids //
fumarase from baker's yeast extraction process

Liquid	Volume ratio	Density g/cm ³	Viscosity ³⁾ mPa·s	pH
cell homogenate	1.14	1.052	6.5	7.0
PEG/salt mixture		1.202	22	10.7
1. extraction: 1)				
dispersion		1.122	20	
top phase		1.088	4.5	8.6
bottom phase	1.47	1.143	210	
2. extraction: 2)				
top phase I		1.088	4.5	8.6
salt solution	2.52	1.176	~ 1	5.92
dispersion		1.114	6.5	6.84
top phase		1.089	3.3	6.97
bottom phase	2.88	1.177	~ 1.5	6.62

1) conditions:

17 % PEG 1550

8 % K₂HPO₄

25 % biomass (wet weight)

2) conditions:

70 % top I

6.7 % potassium phosphate

pH 5.9

3) relative viscosity at 200 rpm

Much experience has already been accumulated during past years in this field showing that phase separation can be performed with phase purities of 98 to 100 %. This applies also for the separation of solid biomass (1st extraction step) and for this step phase purities close to 100 % can be attained especially for the product containing top phase. Conversely a phase purity of e.g. 97 % for the bottom phase would result in a loss of only 1.5 % of product with this phase at an average volume ratio of 2. An example is shown in fig. 2 for the fumarase / baker's yeast process using a laboratory size separator.

In the two-stage extraction plant first runs of the baker's yeast process have been carried out processing up to 400 kg of broken biomass per run. Further experiments have been carried out extracting fumarase from *Brevibacterium ammoniagenes*. In this case ~150 kg biomass (wet weight) has been processed within 7 h with the same final product yield and purity as in the comparable batch process. The results obtained gave evidence that the plant is functionable in the basic form. However, more sophisticated process control appeared desirable to allow fully automated operation; for this aim a microcomputer with interface hardware has been adapted. Further a common time-based sludge discharge control unit has been installed.

In first experiments the computer has been used for control of the flows and monitoring of the pressure before both mixers, which served as alarm functions. Results of a preliminary fully automated run lasting 7 h are shown in fig. 3; after starting no manual operation was required. The data reflect the stability of the process; further the enzyme concentrations in the product-enriched phases were approximately identical with those obtained in the batch process confirming a stage efficiency of ~100 % for both stages. Cell disruption by wet milling (see fig. 1) was included in the continuous process.

The concept has now to be approved by long-term operation, where recycling of the phase chemicals should be included to reduce the consumption of chemicals (see below).

Table 3 : Phase equilibration by static mixing/dispersing - fumarase / baker's yeast process, 1. extraction step (Kenics mixer. i.d. 4.9 mm, 21 mixing elements)

flow rate (ml/min)	flow rate (cm/sec)	rel. fum.- act. in t.p.* (%)	rel. protein conc. in t.p.* (%)	Δp (bar)	Re
356	31.5	99.0	92.1	~ 0.17	88
724	64.1	97.8	92.7	0.41	179
1086	96.1	96.7	90.1	0.87	268
1447	128	96.8	94.4	1.3	357
1783	158	97.5	94.1	1.8	442

*) in relation to the equilibrium concentration / t.p. = top phase

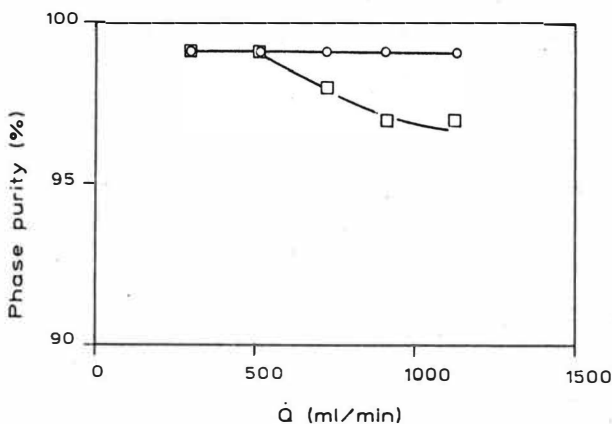


Fig. 2: Separation of fumarase from baker's yeast cells, 1st extraction step - phase purity in dependence on the feedflow \dot{Q}
(Separator: Gyrotester B (Alfa-Laval), Σ -factor 700 m²;
o — o top phase, □ — □ bottom phase

Recycling of phase chemicals

A drawback of the aqueous phase extraction technology appears to be the relatively high consumption of chemicals, which becomes evident when processing in technical scale (7). For the processing of 1 t of baker's yeast extracting fumarase in the mode described, for example, 680 kg PEG 1550 and 533 kg potassium phosphate would be necessary. Therefore recycling of the chemicals appears desirable for operation in such scale. Several ways have been discussed in ref. 2. Here only the most convenient mode is described briefly: At appropriate process development the majority of the PEG can be recycled by direct reuse of the secondary PEG-rich upper phase in the first extraction step as outlined in fig. 1 (dotted line). This way a part of the salt is also recycled. The majority of the salt in the secondary bottom phase could be recycled after concentration of this phase by ultrafiltration and reusing the permeate again in the 2nd extraction. For the fumarase/baker's yeast process this approach has been found feasible at least four times without negative effects on product yield and purity and would reduce the consumption of PEG to a quarter and that of salt to about the half.

The mode of recycling described would be efficient especially for continuous processing; for batchwise operation the benefits would be reduced partly by the requirement of storage of the process liquids. For process control during continuous extraction with automated recycling on-line monitoring of product concentration and quality appears necessary; this could be performed advantageously by coupling an appropriate analytic system to the micro-computer used already for control of the basic process parameters (8).

Final remarks

Fully automated continuous crosscurrent extraction of proteins appears feasible with high efficiency. The technique offers the potential for easy continuous downstream processing of microbial proteins from cell harvesting to purities appropriate for technical biocatalysts. For products requiring high final purity the development of continuously operating high resolution techniques appears desirable to allow fully continuous protein purification.

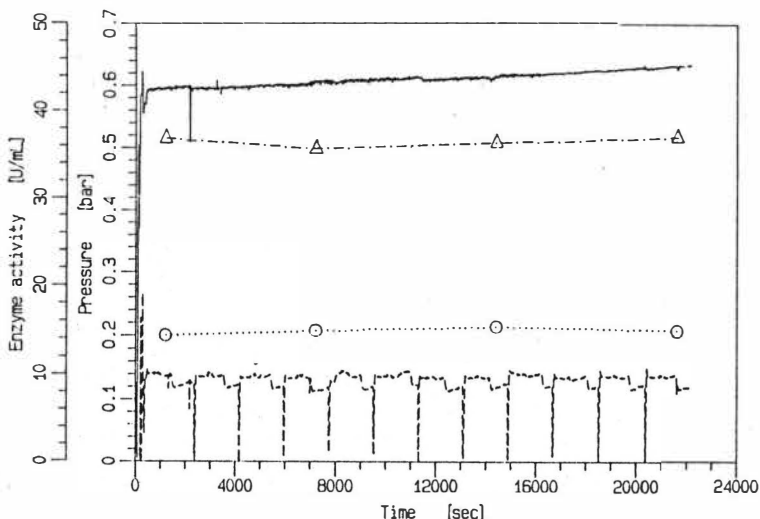


Fig. 3: Computer controlled crosscurrent extraction in the two-stage extraction plant (Westfalia Separator AG)
 - fumarase / baker's yeast process
 (feed to separator 1: 100 l/h; Kenics mixer, i.d. 8.1 mm, 27 mixing elements)
 o.....o fumarase activity in the 1. top phase
 Δ---Δ fumarase activity in the 2. bottom phase
 — pressure before mixer 1, --- pressure before mixer 2

REFERENCES

1. H. Hustedt, K. H. Kroner, U. Menge, M.-R. Kula: Trends in Biotechnol. 3 (1985), 139
2. H. Hustedt, K. H. Kroner, M.-R. Kula: "Application of Phase Partitioning in Biotechnology", in: Phase Partitioning - Theory, Methods, Uses and Applications to Biotechnology (eds. H. Walter, D. Fisher, D. Brooks), Academic Press, New York, 1986
3. H. Hustedt, K. H. Kroner, H. Schütte, M.-R. Kula: "Extractive Purification of Enzymes", in: Enzyme Technology (ed. R. M. Lafferty), p. 135, Springer, Berlin, 1983
4. H. Hustedt, K. H. Kroner, M.-R. Kula: Proc. 3rd Eur. Congr. Biotechnol. Vol. 1, p. 597, Verlag Chemie, Weinheim (1984)
5. H. Hustedt, K. H. Kroner, M.-R. Kula: Chem. Ind. 108 (1985), 527
6. P. F. Fauquex, H. Hustedt, M.-R. Kula: J. Chem. Technol. Biotechnol. 35 B (1985), 51
7. K. H. Kroner, H. Hustedt, M.-R. Kula: Proc. Biochem. 19 (1984), 170-179
8. H. Hustedt, K. H. Kroner, M.-R. Kula: Biotech Forum 2 (1985), 56

Mass transfer of large molecules through phase interfaces

by M. Seekamp, C. Tiegs, E. Weidner and S. Peter, Erlangen, FRG

Introduction

Although in some industrial processes substances of high molecular weight are handled, there is only little known about their transport through the phase interfaces. When a mixture containing 88 wt.-% glyceryloleate and 10 wt.-% acetone is dissolved in carbon dioxide at 135 bar and 70 °C the equilibrium concentration of acetone is obtained within 3 minutes [1]. On the other hand the equilibrium concentration of glyceryloleate is reached after 27 minutes as shown in fig. 1. Before the solving experiment started carbon dioxide had been dissolved in the liquid phase up to saturation. Often the low rate of dissolution of low volatile substances limits the space-time-yield of separation processes like e. g. extraction processes.

The rate of dissolution of glyceryloleate is about eight times lower than the same of acetone. This difference cannot simply be explained by the difference of the diffusion rates, because the phase interface is mostly covered by glyceryloleate molecules due to the high concentration of glyceryloleate. We rather presume that not the transport of the molecules to the boundary layer but the crossing of the phase interface is the limiting partial step.

Therefore it appeared to be of interest to investigate the transport phenomena of large molecules through phase interfaces.

Mass transfer coefficients

The dissolution of oleic and stearic acid in a dense gas was investigated. Mixtures of oleic and stearic acid were saturated with the dense gas at 60 °C. The dense gas flew over a falling film of the latter with constant speed. Hence in the experiments only oleic and stearic acid was transferred from the falling film into the gaseous phase.

The change of the concentration of the fatty acids in the dense gas on passing the falling film was measured. The mass transfer coefficient is calculated by the equation.

$$n_i = (C_{i,e} - C_i)_{lm} \cdot A \cdot B_i$$

with n_i = dissolved amount of mass per unit time

A = contact surface

B = mass transfer coefficient

$(C_{i,e} - C_i)_{lm}$ = logarithmic average value of the driving concentration difference

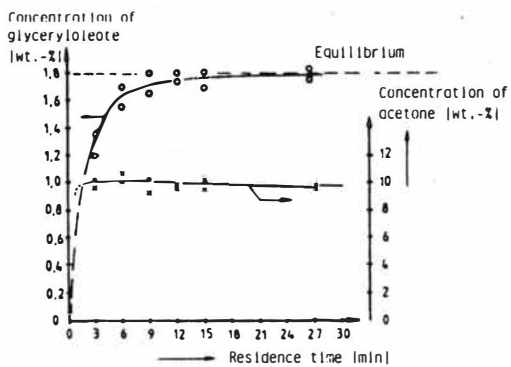


Fig. 1: Dissolution of a glyceryloleate-acetonmixture in CO_2 at 135 bar and 70 °C

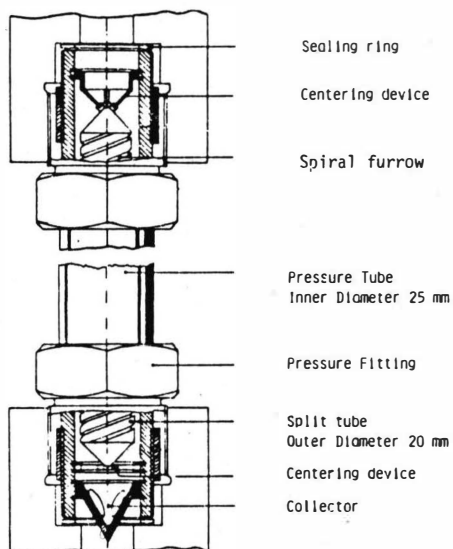


Fig. 2: Split tube column

To accomplish the measurements a split-tube column with a split width of 5 mm was available. The concentric fixed inner tube had two, helical furrows with a square cross section, one fitted into the other (deep = 1 mm, width = 1 mm, inclination = 10 mm per turn). The distance between the two furrows was 5 mm. In this way trickle generation was avoided. In the split tube the contact surface of the liquid phase was determined to be $90 \pm 18 \text{ cm}^2$. The alignment of the split-tube in the column tube was achieved by the devices as shown in fig. 2.

Mixtures containing different amounts of oleic and stearic acid were used as low volatile substances to be dissolved; as supercritical solvents carbon dioxide and ethane were taken. The gas-saturated liquid phase was circulated from the bottom to the top of the split tube column. The supercritical solvent was introduced a short distance above the bottom of the column and made to flow upwards through the column. The liquid fatty acid flowed down in the furrows. The Reynolds-Number of the gas stream was 75. Samples were taken and analysed from the incoming and outgoing solvent stream.

The solvent stream leaving the top of the column was fed into a regeneration column. There the pressure of the dense gas was reduced, whereby the dissolved low volatile components precipitated. The regenerated gas was recompressed and recycled to the split-tube column. The precipitated product was fed to the top of the split-tube column.

Fig. 3 shows the binodal curves of a 50 %-mixture of oleic and stearic acid with carbon dioxide and ethane in a p,x-diagram at 60 °C.

The obtained mass transfer coefficients are presented in table 1.

No.	Gas	Mixture ol./st.	pressure [bar]	Temp. [°C]	$\beta_{\text{oleic acid}}$ [m/h · 10 ⁻³]	$\beta_{\text{stearic acid}}$ [m/h · 10 ⁻³]	$\bar{\beta}$
1	CO ₂	9 : 1	200	60	76 ± 8	62 ± 8	69 ± 8
2	CO ₂	1 : 1	200	60	90 ± 22	62 ± 11	76 ± 16
3	CO ₂	1 : 1	250	60	55 ± 2	33 ± 3	44 ± 3
4	Ethane	1 : 1	120	60	216 ± 30	141 ± 30	178 ± 30
5	CO ₂	9 : 1	200	75	51 ± 3	23 ± 3	48 ± 3
6	CO ₂	1 : 1	200	75	63 ± 4	42 ± 2	52 ± 2
7	CO ₂	1 : 4	200	75	60 ± 4	56 ± 3	57 ± 3

The mass transfer coefficient for oleic acid is higher than the mass transfer coefficient for stearic acid. At 200 bar the mass transfer coefficients at 75 °C are smaller than at 60 °C. The mass transfer coefficients at 60 °C decrease with rising pressure. At 60 °C the mass transfer coefficient using ethane as solvent at 115 bar is 4 times greater than using carbon dioxide as solvent at 250 bar.

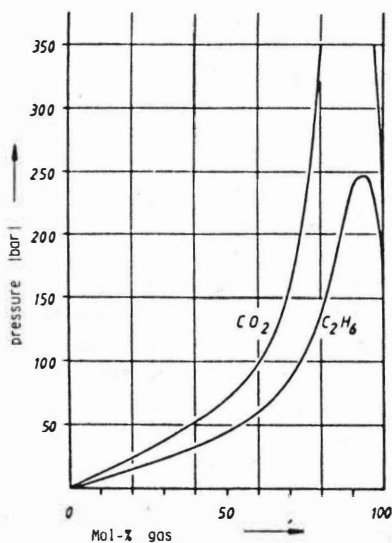


Fig. 3: Phase equilibria of a mixture of oleic-/stearic acid (80 wt.-%/20 wt.-%) with carbon dioxide and ethane at 60 °C

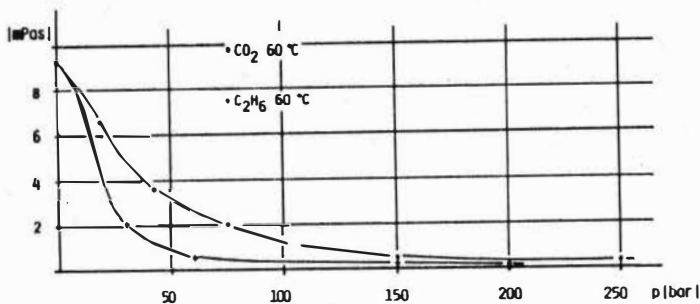


Fig. 4: Dynamic viscosity of a 50 wt.-% mixture of oleic-/stearic acid with carbon dioxide and ethane at 60 °C as a function of pressure

although in both cases the concentration gradients are not very different.

The mass transfer coefficient of oleic acid depends less on the composition of the mixture than the mass transfer coefficient of stearic acid.

Viscosity of the coexisting liquid phases

The viscosity of a 50 %-mixture of oleic and stearic acid was measured at 60 °C as a function of the saturation pressure by means of a capillary viscometer. The liquid to be measured is pumped through the capillary with constant flow rate. The pressure difference between the ends of the capillary is determined. From the rate of flow and the pressure difference caused by it, the viscosity of the liquid sample is determined using the well known Poiseuille equation.

In fig. 4 the measured viscosity of the liquid phase at 60 °C is plotted as a function of the gas pressure, at which the mixture of oleic and stearic acid was saturated with CO₂ or ethane respectively.

At a given pressure the decrease of the viscosity of the oleic and stearic acid mixture is larger for ethane than for carbon dioxide. At 60 °C in equilibrium, the solvent capacity of ethane at 120 bar is nearly the same as for carbon dioxide at 250 bar. Therefore the driving forces for the mass transfer from the liquid into the gas phase are nearly equal. Hence, the viscosities of the liquid oleic and stearic acid mixture in equilibrium with the respective gases under these conditions are of interest. When saturated at 250 bar and 60 °C with carbon dioxide the viscosity of the mixture of the fatty acids was determined to 0.34 mPas. The viscosity of the mixture at 60 °C was found to be 0.33 mPas, when saturated with ethane at 120 bar.

Discussion

For the mass transfer through interfaces it is assumed that the mass transfer resistances are arranged in series. Therefore the largest resistance determines the overall rate of mass transfer. In the gas phase the diffusion rate is higher than in the coexisting liquid phase by one order of magnitude or more. Therefore the diffusion in the liquid phase and the mass transfer through the interface remain the limiting steps. Under the conditions of the mass transfer experiments the liquid phase and the gas phase exhibit laminar flow. Due to this it can be assumed as a first approximation that the mass transfer takes place only in a direction vertical to the flow direction, and similarly to a static system, no convective flow has to be considered. The driving concentration difference is of about the same magnitude for the dissolution of the fatty acids in carbon dioxide at 250 bar and their dissolution in ethane at 120 bar. The logarithmic average value of the concentration difference amounts in the case of carbon dioxide to $0.081 \cdot 10^{-6} \text{ kmol/m}^3$ and in the case of ethane to $0.077 \cdot 10^{-6} \text{ kmol/m}^3$.

The theories of diffusion [2] lead to the result that at a given temperature the product of diffusion coefficient and viscosity should be constant if substance-specific effects are negligible

$$D_{i,j} \cdot \eta_j = \text{const}$$

$D_{i,j}$ = Diffusion coefficient of substance
i in the medium j

η_j = dynamic viscosity of the medium j

According to the two-film theory the mass transfer coefficient β should be directly proportional to the diffusion coefficient [3]. Therefore the equation

$$\beta_i \cdot \eta_j = \text{const}$$

should be satisfied. The surface renewal theories obey to the relation $\beta_j \sim \sqrt{D_{i,j}}$ which leads to the equation

$$\beta_i^2 \cdot \eta = \text{const}$$

In table 2 the mass transfer coefficients of the experiments No. 3 and 4 (table 1) and the viscosities of the corresponding liquid phases at 60 °C are represented.

Table 2

Experiment No.	Solvent	Pressure [bar]	mass transfer coefficient		Viscosity of the liquid phase mPas	$\beta \cdot \eta$	
			oleic acid	stearic acid		oleic acid	stearic acid
3	CO ₂	250	55	33	0.34	18.7	11.2
4	ethane	120	216	141	0.33	71.3	46.5

The product of the mass transfer coefficient of the fatty acids and the viscosity of the liquid phase is by no means constant as one would expect on account of the little differences between the viscosity of the liquid phases and the driving concentration differences.

On the contrary, an increase of the product ($\beta \cdot \eta$) by a factor of about 4 is found, if ethane is used as a solvent instead of carbon dioxide. Referring to the surface-renewal-theories the difference will become even greater. The van der Waals' co-volume of carbon dioxide is $42.67 \cdot 10^{-3} \text{ m}^3/\text{kmol}$ and that of ethane $63.80 \cdot 10^{-3} \text{ m}^3/\text{kmol}$. The large deviation of the product $\beta \cdot \eta$ cannot be explained by the difference of the molecule diameters of the solvents. Hence it seems improbable that the mass transfer by diffusion is the limiting partial step for the mass transfer. Finally there remains the mass transfer through the phase interface itself as the limiting transport resistance.

A molecule crossing the phase boundary is forced to change the composition of its solvating envelope. The bigger a molecule the longer is the time which is needed for this process. Probably the change of the solvating envelope of the large molecule is limiting the rate of crossing the phase boundary as shown schematically in fig. 5.

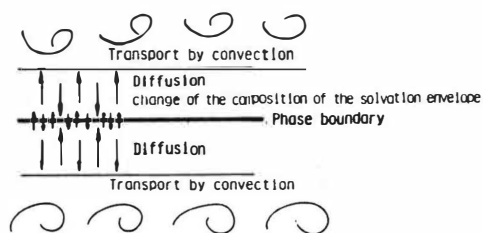


Fig. 5: Schematic graph of the mass transfer through a phase interface

Literature:

- [1] Diss. C. Tiegs, Erlangen 1985
- [2] DECHEMA Seminar of advanced separation technologies, DECHEMA, Frankfurt 1981
- [3] Ullmann's Enzyklopädie der techn. Chemie, Verlag Chemie Weinheim/Burgstr, 4th edition, Volume 1, 1974
- [4] Handbook of Chemistry and Physics 62nd edition, CRC Press 1981/1982

Solvent Extraction of Products from the Acetone-Butanol Fermentation

S. Dupire, F.C. Thyron, Louvain University, Louvain-la-Neuve, BELGIUM

Fermentation processes based on renewable raw materials have the potential for producing important large tonnage organic chemicals. Like ethanol, butanol can be obtained through fermentation of grain, molasses or suitable waste materials that may be a source of sugars.

By-products like acetone, ethanol and acetic/butyric acids are also formed during the fermentation process.

Although economically attractive when based on waste-type materials, the acetone-butanol fermentation has a number of drawbacks which must be addressed before any attempt for commercial production is made.

The major one is the very low levels of butanol that are observed in the final fermented broth. With current technology such levels are only about 1.9 % (w/v).

This results in the need for large size vessels for fermentation and an energy-intensive distillation recovery of the products.

The removal of highly polar organics from dilute aqueous solution is one of the most difficult industrial separations problems. Distillation is frequently used for recovery of polar organics from water; that class of distillations accounts for a substantial portion of the world's energy consumption (1). However distillation processes often encounter low relative volatilities and azeotropes and the cost per unit quantity of solute recovered therefore increases greatly as the solute becomes more dilute in the feed. For such situations there is considerable incentive for a recovery process which removes the solute from the water at lower energy cost. Solvent extraction is such a process.

GENERAL CONSIDERATIONS

The most important factor in generation of a process for extraction of polar organics from a dilute water stream is solvent selection. Since water flows are often large, it is important to choose a solvent which will give a high distribution ratio for the solutes in question; this is needed to keep solvent circulation rates from becoming excessive. An effective solvent for highly polar organics frequently has a substantial solubility in water itself. In such cases, the dissolved solvent must be removed somehow from the raffinate water, and the solvent properties must be well suited to whatever process is used for that purpose.

Methods for removal and recovery of residual dissolved solvent include atmospheric steam stripping, inert-gas stripping, vacuum steam stripping and re-extraction. Alternatively, one can seek a solvent with a combination of low enough solubility, emulsification tendency, and cost so that removal and recovery of solvent from the

raffinate water are not necessary. The solvent must not be toxic or refractory itself. For any but the lowest concentrations of soluble organics in the feed water, it will be necessary to regenerate and reuse the solvent. Regenerability - often by distillation or stripping - and chemical stability of the solvent under regeneration conditions thereby become important attributes so as to keep solvent consumption economically low.

PRODUCTS OF THE ACETONE-BUTANOL FERMENTATION (ABF)

The acetone-butanol fermentation is carried on by bacteria belonging to the genus clostridium. It is known that the final product ratios obtained are a strong function of the clostridium species utilized for the fermentation process (2). As butyric acid accumulates in the medium, the pH of the fermentation will continue to drop to about 4.0 at which time a new enzyme system is activated leading to the formation of acetone and butanol and small amounts of end products - carbon dioxide, acetoin, water, hydrogen, acetic acid and butyric acid in addition to the two main products. A typical ABF yield is (in % w/w glucose): butanol, 23-acetone, 7-acetoin, 2.9 - butyric acid 2 - acetic acid 1.3. - ethanol, 1.2 - hydrogen, 1.5 (3). When the butanol reaches concentration higher than 13 g.L^{-1} , the fermentation process is stopped due to the inhibition on the microorganisms.

DISTRIBUTION AND SEPARATION FACTORS OF BUTANOL AND ACETONE IN SEVERAL SOLVENTS

Extraction studies of butanol and acetone from aqueous solutions were performed by placing equal volume of water phase and solvent in a thermostated cell equipped with a mechanical stirring device. The mixture was shaken for 15 min. After the two layers has separated for 1/2h aliquot of both phases were withdrawn and analyzed on a FID gas chromatograph.

The results are presented in table I. The distribution coefficient K is defined as

$$K_s = \left[\frac{\% \text{ w solute in organic phase}}{\% \text{ w solute in aqueous phase}} \right]_{\text{equil}}$$

and the separation factor α as

$$\alpha = \frac{K_s}{K_{\text{H}_2\text{O}}}$$

They are calculated for solutions containing 0.6 % w/w acetone and 1.2 % w/w butanol in water.

TABLE I. Experimental values of K_s and α for various solvents

Solvents	T(°C)	ACETONE		BUTANOL	
		K_s	α	K_s	α
Ethyl ether	20	0,76	51	5,14	412
n-Hexanol	20	0,67	9	9,47	129
	40	1,19	16	14	191
i-Nonanol	20	0,63	23	7,73	286
	40	0,87	28	8,69	277
i-Decanol	20	0,50	19	6,88	259
	40	0,66	26	7,87	307
n-Decanol	20	0,41	11	5,86	153
Tetradecanol	40	0,61	19	5,22	160
Diisobutylketone	20	0,72	120	2,55	427
Anisole	20	0,85	643	0,99	750
	40	1,04	334	1,77	570
Phenetole	20	0,66	393	0,88	506
Xylene	20	0,49	806	0,53	878
Mesitylene	20	0,38	1900	0,47	2300
Methylbenzoate	20	0,79	96	1,84	222
Dibutylphtalate	20	0,52	88	1,21	207

Several conclusions can be drawn from these results: at first, the distribution coefficients for acetone are always lower than for butanol and in the extreme cases there is an order of magnitude between them. Secondly, alcohols with 6 to 9 carbon atoms are very efficient to extract butanol.

The increase of temperature and the choice of a branched alcohol always favour the extraction. Unfortunately, the distribution coefficient for acetone is too low to allow an economical extraction.

On the other hand, it is well known that ethanol (4,5) and acetic acid (6,7) display distribution coefficients generally lower than unity in conventional solvents. That is the reason why the choice of an extraction solvent shall not be made in function of these two solutes in low concentration in the fermentation broth.

In fact, we found the following correlation between butanol and ethanol distribution coefficient for most solvents:

$$\log K_{\text{BuOH}} = \log K_{\text{EtOH}} + 1,25$$

DISTRIBUTION OF BUTANOL AND ACETONE IN MIXED SOLVENTS

Since the extraction of butanol seems to be realised without difficulty, the main problem remains to improve the acetone extraction. If we discard the symmetric te-

trichloroethane which displays a good distribution ratio (7.31) and a high separation factor (3463) for acetone but is highly toxic, one way to increase the distribution coefficient of acetone could result in mixed solvents. Several solvent mixtures were tested and the most promising one consists of anisole or toluene (cheaper but slightly less efficient) with $C_6 - C_9$ alcohols.

The results obtained with the anisole-alcohols mixtures are plotted in figure 1 and 2. Comparison of these figures shows an exaltation of K_s for acetone while the butanol distribution varies nearly linearly with composition.

Results obtained at 40 °C with isononanol- anisole mixtures are also presented in dotted lines and still show an improvement of the partition.

On the other hand, the values of distribution coefficient of acetic and butyric acids between water and 60 % (by volume) isononanol - 40 % anisole at 20 °C are respectively 0.575 and 17.1 with separation factors of 30 and 893.

Under the same conditions, K_s and α for ethanol have been shown to be 0,375 and 20.3.

When considering isononanol (40 % by volume) - toluene mixture as solvent, K_s and α have been found to be 1.08 and 115 for acetone at 20°C. These values are comparable to those found in isononanol (40 % v) - anisole mixture.

PROCESS DESIGN

Selection of the appropriate solvent or solvent mixture reflects a compromise not only among relative volatility, solubility in water but also among number of theoretical stages and solvent/feed (S/F) ratio. Taking into account all these features, computations have been made in order to determine the values of S/F for various solvents at 40 °C. The number of theoretical stages and the percentage to be extracted were taken to be 9 and 99 %.

The results are presented in table II.

TABLE II. Solvent to feed ratios (S/F) and percentage of solute in extract (% E) (w/w)

T: 40 °C - 9 theoretical stages - $S/F = S/F_{theor.} \times 1,25$

SOLVENTS	SOLUTES					
	K_s	BUTANOL			ACETONE	
		S/F	% E	K_s	S/F	% E
i-nonanol	8,69	0,21	5,6			
i-decanol	7,87	0,23	5,1			
n-hexanol	14	0,13	9,1			
i-nonanol + toluene (40 - 60 % v)				1,28	1,43	0,46
n-hexanol + anisole (40 - 60 % v)				1,73	1,06	0,56

BUTANOL + ACETONE

	K_S	S/F		% E	
		But	Acet	But	Acet
i-nonanol + anisole (40-60)	6.2	1.57	1.17	1.02	0.51
i-decanol + anisole (20-80)	3.4	1.37	1.34	0.9	0.44

Although a mixture of heavy alcohol with anisole could extract simultaneously butanol, acetone and an important part of other solutes with a solvent feed ratio near 1, energetic consumption calculations show that there is no gain in choosing separation by extraction rather than conventional distillation. That is the reason why an other alternative has been considered based on two extraction columns the first one assigned to butanol and the second to acetone separation.

The extraction of butanol with i-nonanol, i-decanol or hexanol and its separation from the solvent will consume five time less energy than its separation from water solutions. Afterwards, the effluent from the first extraction column will undergo a second extraction with hexanol-anisole mixture to remove acetone and ethanol. In order to maintain the loss of solvent under maximum limits it will be necessary to remove these solvents from the effluent by a third column using a solvent such as decanol which is practically insoluble in water (0,003 % W at 20 °C). The flow-sheet of this installation is presented in figure 3.

CONCLUSION

It has been shown that it is advisable to extract solutes from the acetonebutanol fermentation with the help of three extraction columns in order to optimize the recovery of the products and the energetic consumption.

REFERENCES

1. T.W. MIX, J.S. DWECK, M. WEINBERG and R.C. ARMSTRONG, Chem. Eng. Prog. (1978) 74 (4), 49.
2. S.C. BEESCH, Ind. Eng. Chem. (1952) 44 (7), 1677
3. T.G. LENZ and A.R. MOREIRA, Ind. Eng. Chem. Prod. Res. Dev. (1980) 19 (4) 478
4. A. SOUISSI and F.C. THYRION, Prod. 2nd World Congr. Chem. Eng. (1981) 4, 443
5. C.L. MUNSON and C.J. KING, Ind. Eng. Chem. Process Des. Dev. (1984) 23, 109
6. N.L. RICKER, E.F. PITTMAN and C.J. KING, J. Separ. Proc. Technol. (1980, 1 (2) 23
7. D.H. SHAH and K.K. TIWARI, I. Chem. E. Symposium Series Alternatives to distillation (1978) n° 54, 257

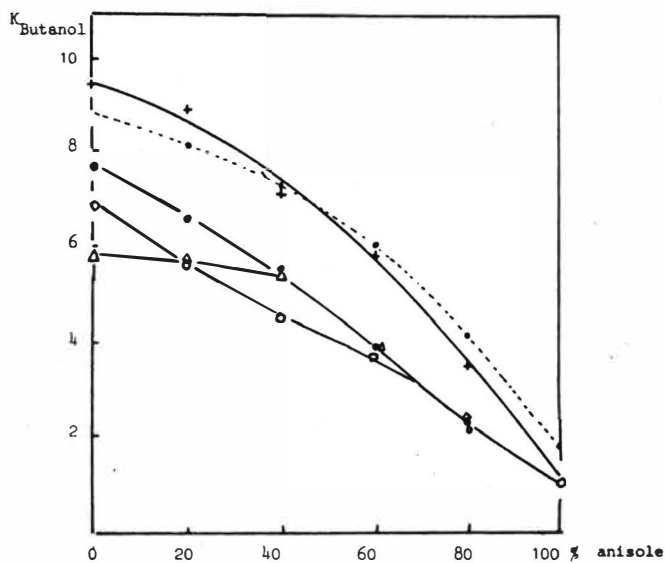


Fig. 2. Distribution coefficients of butanol in various alcohol-anisole mixtures (1.2 % W Butanol in water, 20°C except (...) 40°C).

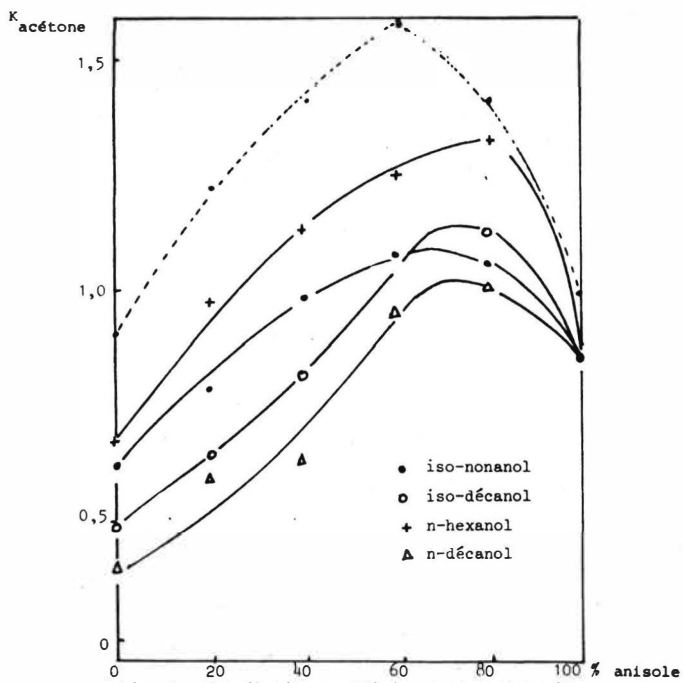


Fig. 1. Distribution coefficients of acetone in various alcohol - anisole mixtures.
 (0.6 % W in water, 20°C except (...) 40°C)

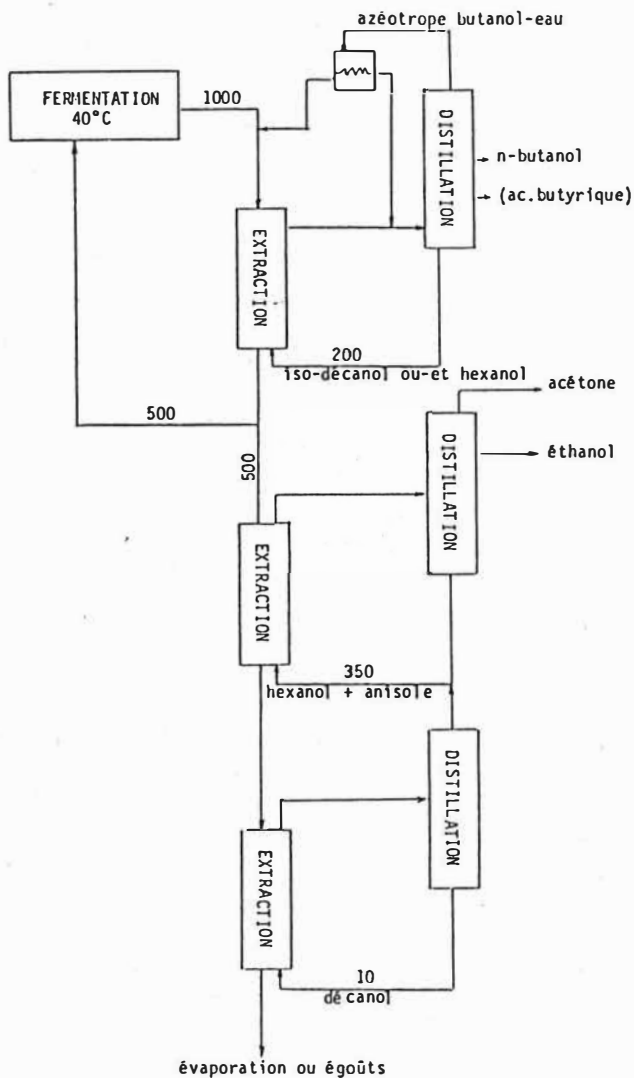


Fig. 3. Flow sheet of the process of extraction of solutes from acetone-butanol fermentation

Solvent extraction of metals by oligomeric extracting agents

V.I. Bukin, A.M. Reznik, S.A. Semenov, L.D. Yurchenko, Moscow
Lamonosov Moscow Institute of Fine Chemical Technology
M. Pirigovskaya I, USSR-435 Moscow

No manuscript available

THE PRINCIPAL PHYSICO-CHEMICAL REGULARITIES OF EXTRACTION
IN SYSTEM WITH BIOLOGICAL FLUIDS.

G.A.Yagodin, S.V.Yurtov.

Mendeleev institute of chemical technology, Moscow, USSR.

The elaboration of medical methods of detoxication and biotechnological methods has awaked interest in the problem of extraction from biological fluids. There are some peculiarities of extraction from biological fluids, which are caused by the presence of biological phase. The biological phase may be blood (plasma, lymph and so on) or culture liquid.

These peculiarities can be come to several points:

Nonequilibrium - The systems with biological fluids are non-equilibrium, but owing to homeostasis connections in the system there is the region where the system parameters are independent of time. This region may be described in terms of quasi-equilibrium.

Multicomponent - The multi-component system not only complicates the study of process, but causes some cooperative phenomena.

Protein - On the one hand the presence of protein in biological fluids is one of the causes of homeostasis, on the other hand protein is a surfactant. And in heterogeneous systems it forms films on the interface. That is why the renewing of surface is necessity in such systems.

Dispersion - The biological fluids are not homogeneous. There are dispersions, in some cases like lyophobic colloid. Sometimes this comes to irreversibility of process. The critical phenomena of dispersed particles often influence on equilibrium and kinetic.

Fontoxicity - Apart from the complication connected with toxicity it must be secured the minimum damages of the biological phase components. It limits the choice of extractants and diluents.

As the manuscript was not available at the 28th May 1986, the deadline for printing this book, we only print the short abstract of the paper.

REACTIVE EXTRACTION OF D,L-TRYPTOPHANE FROM AQUEOUS SOLUTIONS BY TOMAC/XYLENE AND ITS BACK-EXTRACTION

I. Kirgios, R. Hänsel, H.B. Rhein, K. Schügerl
Institut für Technische Chemie, Universität Hannover

Introduction

One of the separation processes which may be used in amino acid production to recover a relatively pure product is the reactive extraction process. In this process, the reactive component is added to the liquid-liquid extraction system, so that under certain conditions only specific amino acids will be extracted. The selection of suitable conditions is important to attain a high selectivity. Therefore, it is necessary to observe the thermodynamic and kinetic behaviour of the reactive extraction process /1,2/.

In this work thermodynamic and kinetic behaviour of the reactive extraction of tryptophane was observed. Xylene and TOMAC (trioctylmethylammoniumchloride) were used as solvent and as carrier respectively. For comparison, the thermodynamic behaviour of the reactive extraction of tyrosine was also examined.

Equilibrium thermodynamic.

Equilibrium constants of the reactive extraction of tryptophane were calculated, based on the reaction equations (1), (2), (3), and (4) in Fig.1. For tyrosine, it is necessary to consider the dianions at pH greater than 12.

According to the reaction equations above, it is clear that the pH values of the aqueous phase decrease as the amino acids and OH-ions are extracted from this phase, however, excessively low pH values cause the undesirable repression of the amino acid protolyse. This problem can be avoided if the buffer capacity is large enough and if the co-extraction of the buffer anions is much lower than the co-extraction of the hydroxyl anions.

The isotherm distributions of d,l-tryptophane and tyrosine are shown in Fig.2 and Fig.3, with carrier concentration as a

parameter. From the figures it can be seen that by increasing the molar ratio between the carrier concentration and the amino acid concentration from 1 to 3, the distribution coefficient of tryptophane was increased by about four times, and tyrosine about twice. It is also shown that at a molar ratio equal to 3, the distribution coefficient of tryptophane was almost ten times larger than of tyrosine. This fact allows the possibility for the separation of both amino acids through the reactive extraction method.

Fig.4 shows the experimentally determined equilibrium constants of tryptophane and tyrosine obtained through the reactive extraction. Fig.4a describes the influence of the chloride concentration to the yield in the back-extraction process.

Extraction kinetics.

The experiment to characterize the kinetic parameters of extraction of amino acid, tryptophane, was conducted in a batch stirred cell, as shown in Fig.5.

The reactive extraction of tryptophane took place when the anions exchanged at the interface. The reaction interface is constant, because the amino acid anions in the extract phase, xylene, are physically insoluble.

Fig.6 shows the relationship between the remaining tryptophane and time with the mixer frequency as parameter.

Fig.7 describes the influence of the carrier concentration to the amount of tryptophane and OH⁻ ions extracted.

Conclusions

From the data obtained one is able to draw the following conclusions:

1. Tryptophane in aqueous phase could only be extracted by reactive extraction method using TOMAC as the carrier.

2. The extraction yield was dependent upon the molar ratio between carrier and amino acid concentration. The maximal yield could be reached after one hour.

3. By raising the carrier concentration to excessive levels, the co-extraction also increases.

References

- /1/ Hänsel, R.
Dissertation, University of Hanover, 1984
- /2/ Kirgios, I.
Diploma thesis, University of Hanover, 1985

Fig. 1: Equilibrium reactions in the system of xylene+TOMAC/NaOH+amino acid

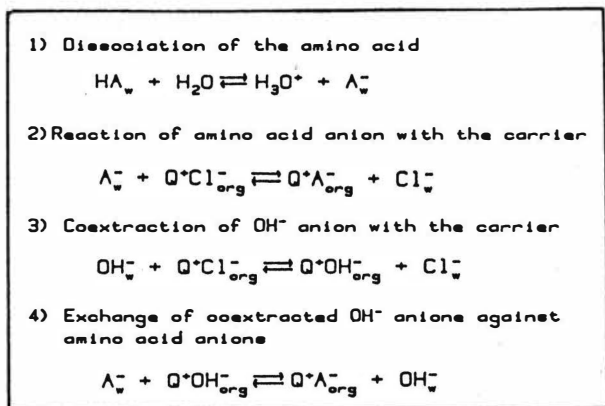


Fig. 2: Isotherm distribution of d.l-tryptophan in buffer/xylol+TOMAC
Parameter: Carrier concentration
Amino acid concentration: 5 mM/l

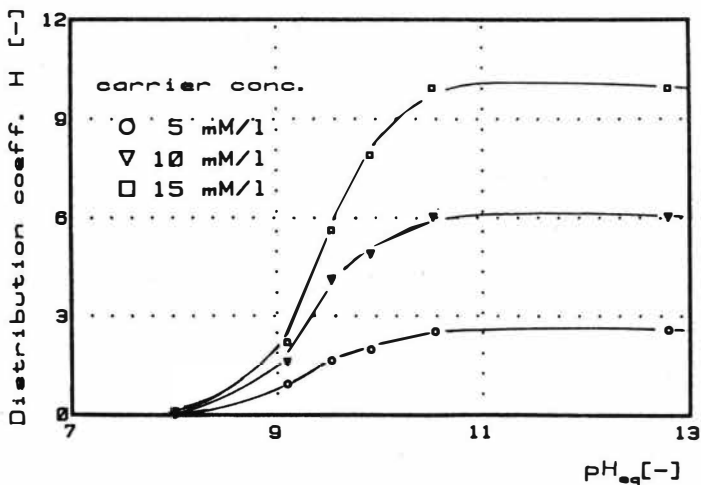


Fig. 3: Isotherm distribution of d.l-tyrosine in buffer/xylol+TOMAC
 Parameter: Carrier concentration
 Amino acid concentration: 5 mM/l

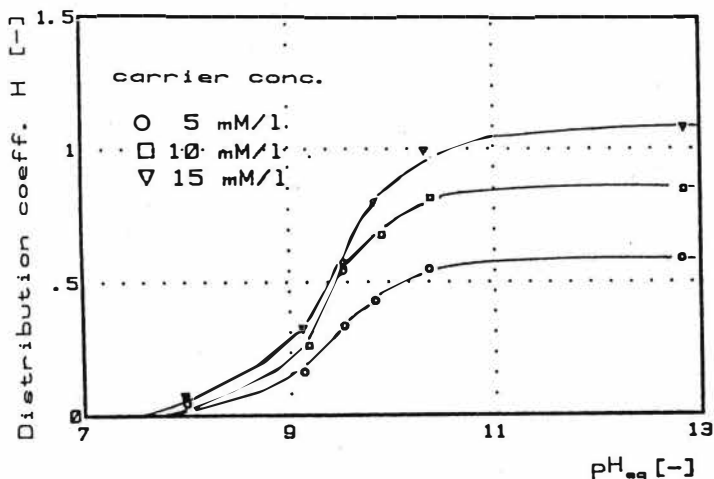


Fig. 4: Experimentally derived equilibrium constants of tryptophane and tyrosine

d.l-tryptophane	d.l-tyrosine
$K_{T_r} = \frac{[O^+A_{tr}^-] [C]_0}{[O^+C]_{tr}^- [A^-]}$	$K_{T_y} = \frac{[O_2^+A_{tr}^{2-}] [C]_0^2}{[A^{2-}] [O^+C]_{tr}^-^2}$
$K_{T_r} = 7.0 [-]$	$K_{T_y} = 0.056 [-]$
$K_{\text{const}} = \frac{[O^+OH_{tr}^-] [C]_0}{[OH^-] [O^+C]_{tr}^-}$	$K_{\text{const}} = \frac{[O^+OH_{tr}^-] [C]_0}{[OH^-] [O^+C]_{tr}^-}$
$K_{\text{const}} = 4.5 [-]$	$K_{\text{const}} = 4.5 [-]$
$K_{\text{const}} = \frac{[O^+A_{tr}^-] [OH^-]}{[A^-] [O^+OH_{tr}^-]}$	$K_{\text{const}} = \frac{[O_2^+A_{tr}^{2-}] [OH^-]^2}{[O^+OH_{tr}^-]^2 [A^{2-}]}$
$K_{\text{const}} = 1.56 [-]$	$K_{\text{const}} = 0.0027 [-]$

Fig. 4a: Back-extraction of tryptophane from xylene. Parameter: variation of the aqueous phase
 O NaCl-solution Δ HCl-solution

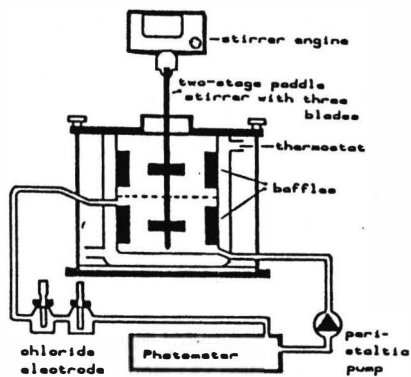
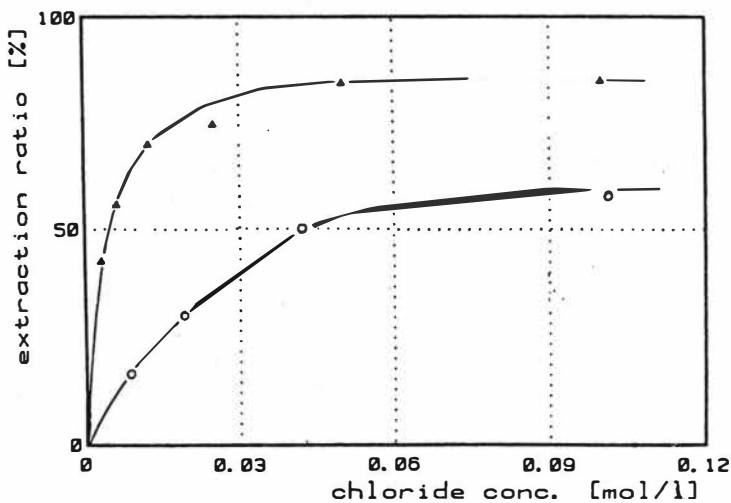


Fig 5 STIRRED CELL

Fig. 6: Remaining amino acids in aqueous raffinate phase as a function of time
 C_0 , TOMAC=6 [mM/l], C_0 , TRY=2 [mM/l]
 parameters: mixing speed

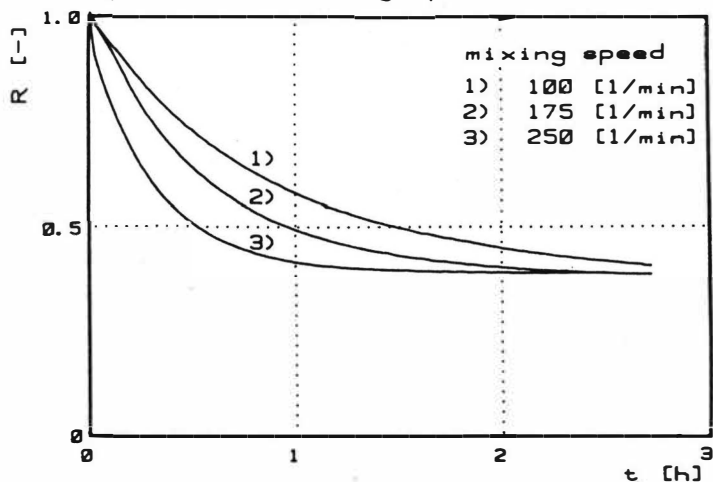
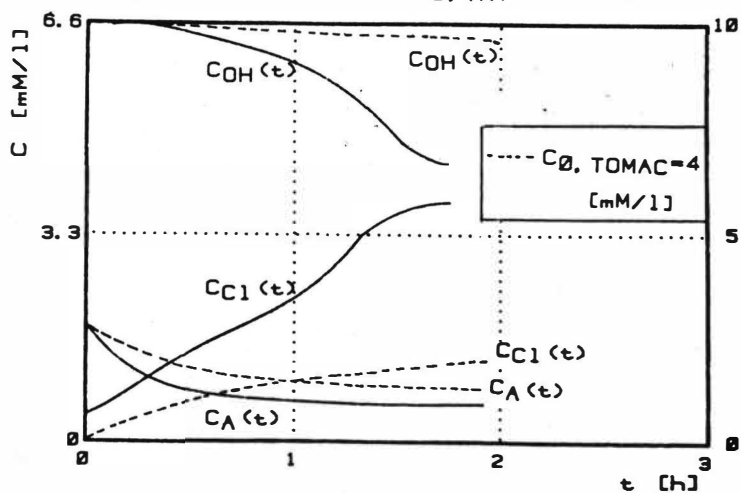


Fig. 7: Concentration-time course diagram for all components in aqueous raffinate phase
 C_0 , TOMAC=8 [mM/l], C_0 , TRY=2 [mM/l]



Solvent Extraction of Succinic Acid from Aqueous Solutions

J.A. Tamada, A.S. Kertes, C.J. King, University of California Berkeley, California, USA 94720.

In the production of carboxylic acids, processes such as fermentation yield low concentrations of carboxylic acids in an aqueous multicomponent solution. The subsequent separation, purification, and concentration of the carboxylic acids is often difficult due to the nature of the solute. Carboxylic acids interact strongly with water, resulting in low solute activity coefficients in aqueous solution. The affinity of the acids for water is often manifested as low volatility of the solute relative to water, which makes conventional distillation difficult. The low aqueous solute activities result in low equilibrium distribution ratios of the acid into most organic solvents, making conventional solvent extraction difficult or impractical.

Solvent extraction with mass separating agents which can reversibly form a chemical complex with the solute is being examined as a means of separating the acids from aqueous solution. A mass-action-law analysis shows that extraction through a complexation reaction has the capability of producing high distribution ratios at low solute concentrations. Reversibility of the weak bond formed in the complex facilitates regeneration of the extractant and recovery of the solute.

Solvent Phase Selection

Long-chain tertiary amines are known to possess many desirable qualities for extraction of carboxylic acids [1]. Studies on extraction of citric [2], acetic [3] and various other carboxylic acids [4] have shown that extraction with tertiary amines results in high distribution ratios for acid extraction. The ability to extract is attributable to the Lewis-base functionality of the amine, which interacts with the carboxylic acid functionality to form an acid-base ion pair. In addition, tertiary amines with sufficiently long hydrocarbon chains are minimally soluble in water, preventing costly losses of the extractant. Tertiary amines have not been found to undergo undesirable side reactions. They appear to be thermally stable, allowing distillation or other high temperature regeneration methods to be implemented.

The extractant is generally mixed with a diluent, an organic solvent which imparts to the organic phase desirable physical qualities which the extractant alone may lack. The diluent may be used to reduce viscosity, regulate density, or dilute the extractant to reduce extractant losses to the aqueous phase. The diluent can play another important and less obvious role in the extraction process, in that it can have a profound effect on the extractive power of the amine [3]. The

extractant itself may be an inhospitable environment for the polar acid-base ion pair. The diluent may possess functional groups which give it the ability to solvate the acid-base ion pair in the organic phase and greatly enhance the extractability of the solute.

Experimental Results

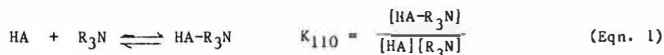
Batch extraction experiments were performed with succinic acid (Mallinckrodt), a dicarboxylic acid ($pK_{a1} = 4.2$, $pK_{a2} = 5.6$) [5] as the solute. The extractant was Alamine 336 (Henkel Corp.), an 8- to 10-carbon chain tertiary amine, with an average molecular weight of 392 gm/mole. Methyl iso-butyl ketone (MIBK) and chloroform (both Mallinckrodt) were the diluents. The chloroform was washed with water before use to remove any ethanol used as a stabilizer. A known concentration of the aqueous acid solution was contacted with known concentrations of the extractant in the diluent in a one-to-one solvent-to-water volumetric phase ratio. Samples were equilibrated in a shaker bath at 25°C. Contact time was for a period of at least 12 hours, which preliminary tests showed to be ample time for equilibration. Results of experiments on the extraction of succinic acid with Alamine 336 in MIBK and chloroform are given in Figures 1a and 1b. The results are given as D , the distribution ratio, which is the molar concentration of solute in the organic phase divided by the molar concentration of solute in the aqueous phase at equilibrium, versus the initial Alamine 336 molarity in the organic phase, at various constant initial aqueous acid concentrations. Initial extractant concentrations ranged from 0.0 M (no amine) to 2.05 M (100% amine).

The results indicate that chloroform used as a diluent gives much higher distribution ratios than MIBK when results are compared at the same initial acid and initial amine concentrations. However, MIBK alone is capable of extracting small amounts of acid, indicated by a non-zero distribution coefficient at zero amine concentration, while chloroform used alone extracts very little acid. Another observation is that a solvent phase with both the diluent and extractant produces larger distribution ratios than either the extractant or diluent alone; i.e., the distribution ratio exhibits a maximum at an intermediate amine concentration. These results strongly suggest some type of diluent-complex interaction.

MIBK is a Lewis base, with electron-donating groups on the carbonyl oxygen. This enables MIBK to extract some acid without the aid of a complexing extractant. Chloroform is a Lewis acid, which may interact with the carboxyl group on the acid-base complex to solvate the complex favorably. Spectroscopic evidence [5] suggests that the acidic chloroform may itself complex with the ion pair. Probably MIBK also has interactions which solvate the complex better than the extractant itself does.

Mechanism

The main mechanism for extraction is generally recognized to be ion pair formation:



where R_3N is the amine, HA is the undissociated aqueous acid, and $\text{HA-R}_3\text{N}$ is the acid-amine ion-pair. An equilibrium constant, K_{110} , where the first subscript denotes the number of acids in the complex, the second subscript denotes the number of base molecules in the complex, and the third number denotes the number of diluent molecules in the complex, can be assigned to this reaction. $[\text{HA}]$ and $[\text{R}_3\text{N}]$ are the equilibrium concentrations of the undissociated aqueous acid and uncomplexed organic amine. It can be seen from Eqn. 1 that when the pH is high, the dissociation of the weak carboxylic acid reduces the undissociated acid concentration and reduces the effective extractive power of the extractant. Even in a medium with no added base, at low solute concentration (<0.02 M), the self-dissociation of the acid is sufficient to reduce the extractability of the solute greatly. Therefore the pH of the final solution is important in the extraction process, especially at low solute concentration. In the chloroform-Alamine 336 system, the high distribution coefficients, and hence low aqueous solute concentrations, make pH a particularly important factor. pH measurements of the equilibrium aqueous phase were taken, and found to deviate on the high side from values predicted using the pK_a values of succinic acid, when amine concentration was relatively high and acid concentration was relatively low. This deviation is attributable to the slight solubility of either a basic organic-phase impurity or the basic amine extractant itself in the aqueous phase at high amine concentration.

Some spectroscopic evidence [7] suggests that additional complexes may be formed, such as two acids complexed to one amine $(\text{HA})_2\text{-R}_3\text{N}$, with an equilibrium constant K_{210} . With a dicarboxylic acid it could also be speculated that two bases can enter the complex for each acid, forming a $(\text{HA})\text{-(R}_3\text{N)}_2$ complex, with an equilibrium constant K_{120} . Extending these concepts, the formation of additional higher complexes could also be speculated. Additionally, the diluent may have sufficiently strong interactions to be considered a component of the complex.

Chemical Modelling

In systems in which "chemical" interactions between the complex components are strong compared to the "physical" interactions between components, a "chemical model" can be developed to fit experimental data. The apparent strength of the acid-amine ion pairing suggests the use of a chemical model may be a good approach

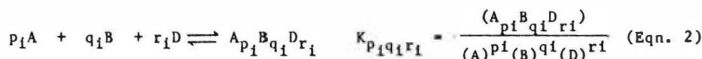
for the systems studied in this paper.

The chemical modelling approach has two major assumptions:

1. Multiple complex formation of acid and amines (and possibly diluent), in which each complex is assigned its own empirically determined equilibrium constant, accounts for all the acid extraction.
2. Activity coefficient ratios of organic-phase species are unity over the concentration range of the extraction.

This modelling approach does have some limitations. In ignoring "physical" interactions between components, the model may be less realistic than models which account for organic phase nonidealities in other ways. Minimizing the error between the extraction data and a hypothesized model may imply that complexes of a specific stoichiometry are formed. Without independent evidence, such as spectroscopic data, the existence of these complexes must be viewed with caution, since they may be artifacts of the nature of the model. Despite these limitations, if complexation interactions are strong, chemical modelling can be a useful tool in fitting data and in deepening understanding of the mechanisms of extraction.

In mathematically developing the chemical model, the formation of i complexes is postulated. These can be represented by i equations of the form:



where p_i , q_i , and r_i are the number of acid, base, and diluent molecules in complex i , $[A]$ is the concentration of undissociated acid at equilibrium in the aqueous phase, $[B]$ is the concentration of uncomplexed, or "free", base in the organic phase, and $[D]$ is the concentration of the uncomplexed diluent in the organic phase.

There are mass balance constraints on the system:

$$[B]_T = [B] + \sum q_i [A_{p_i} B_{q_i} D_{r_i}] \quad (\text{Eqn. 3a})$$

$$[A]_T = [A] + \sum p_i [A_{p_i} B_{q_i} D_{r_i}] + [\text{dissociated A}] \quad (\text{Eqn. 3b})$$

$$[D]_T = [D] + \sum r_i [A_{p_i} B_{q_i} D_{r_i}] \quad (\text{Eqn. 3c})$$

The proposed complexes, the data on pH, total base, total diluent, and equilibrium aqueous acid and organic acid concentrations were put into a computer program. The concentration of undissociated acid was computed from the measured pH, the total aqueous acid concentration, and the pK_a values of the acid. The amount of

acid extracted by MiBK by "physical" extraction was accounted for subtracting the product of the volume percent MiBK by the amount of acid extracted by the MiBK alone at the equilibrium aqueous acid concentration. The least sum of squares error, taken as $\log(D+1)_{\text{expt}} - \log(D+1)_{\text{theory}}$, was minimized.

At low extractant concentrations, the percent change in diluent concentration is small and the diluent effects can be absorbed into the equilibrium constants by making the number of diluent molecules per complex zero. Also, less acid is extracted, reducing the amount of dissociation. A comparison of theoretical predictions and experimental data at low Alamine 336 concentration are given in Figures 2a and 2b. The loading, the molarity of acid in the organic phase divided by the molarity of amine initially, is plotted against the equilibrium aqueous undissociated acid molarity at various constant initial amine concentrations.

Some interesting differences between the two diluents are noticeable. First of all, chloroform shows a much larger K_{110} than MiBK, indicating that chloroform has a greater ability to solvate the complex. Secondly, a 1:1 complex fits the chloroform data quite well, while the MiBK data require a 2:1 as well as a 1:1 complex to fit the data. Another interesting aspect of these curves is the lack of dependence of loading on the initial amine concentration. This implies that any complexes formed have only one amine molecule per complex, as multi-base complexes would have a concentration dependence.

At higher extractant concentrations, diluent concentration effects must be considered. Additionally, the dissociation of acid becomes an important factor. For the chloroform data a modified D , defined as molarity of organic phase divided by the molarity of undissociated aqueous acid, was used in the minimization program, rather than the actual D . A comparison of theoretical and experimental results, plotted as loading versus equilibrium undissociated acid concentration at constant amine concentration, is given in Figure 3. A one complex model with 1:1:2 acid:base:diluent stoichiometry gives reasonably good agreement to the data, and demonstrates that a very simple chemical model is able to represent these experimental results. Addition of more complexes to the model did not appreciably reduce the error, and the use of additional parameters in a model was not reasonably justified.

Conclusions

1. Experiments with the extraction of succinic acid by Alamine 336/MiBK and Alamine 336/chloroform demonstrate that diluent-complex interactions affect the power of the extractant greatly. Chloroform was found to allow much higher distribution ratios than MiBK.

- Simple chemical models involving 1:1 and 2:1 acid-amine ion pairs are capable of modelling extraction data at low amine concentrations.
- At high amine concentrations, diluent effects must be more expressly considered in the model.

Acknowledgments

This work was supported by the Assistant Secretary for Conservation and Renewable Energy, Office of Energy Systems Research, Energy Conservation and Utilization Technologies (ECUT) Division of the U.S. Department of Energy under Contract No. DE-AC03-76SF00098. One of the authors (J.A. Tamada) was the recipient of a fellowship from the National Science Foundation.

References

- A.S. Kertes and C.J. King, *Biotechnol. Bioeng.*, **28**, 269, (1986)
- P. Vanura and L. Kuca, *Coll. Czech. Chem. Comm.*, **41**, 2857, (1976).
- N.L. Ricker, J.N. Michaels, and C.J. King, *J. Separ. Process Technol.*, **1**, (1979).
- A.S. Vieux, N. Rutagengwa, J.B. Rulinda, and A. Balikangeri, *Anal. Chim. Acta*, **68**, 415, (1974).
- J.A. Dean, (ed), *Lange's Handbook of Chemistry*, 13th ed., McGraw Hill, p.5-56, (1985)
- G.M. Barrow and A.E. Yerger, *J. Amer. Chem. Soc.*, **76**, 5211, (1954).
- D.F. Detar and R.W. Novak, *J. Amer. Chem. Soc.*, **92**, 1361, (1970).

Fig. 1a
Extraction of Succinic Acid by
Alamine 336 in MIBK

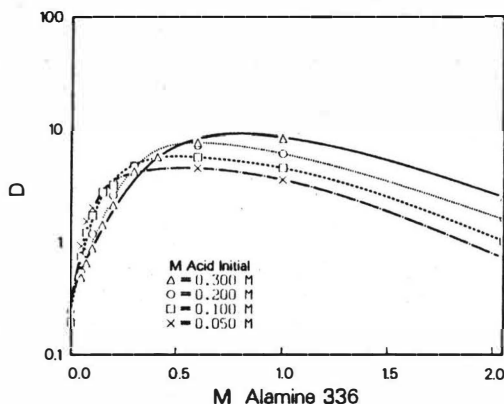


Fig. 1b

Extraction of Succinic Acid by
Alamine 336 in Chloroform

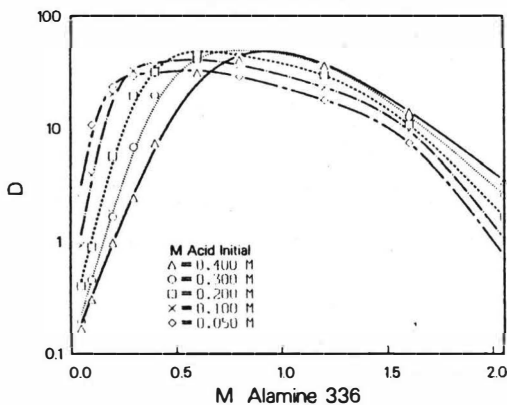


Fig. 2a

Extraction of Succinic Acid by
Dilute Alamine 336 in MiBK
(Solid Line Is Model Prediction)

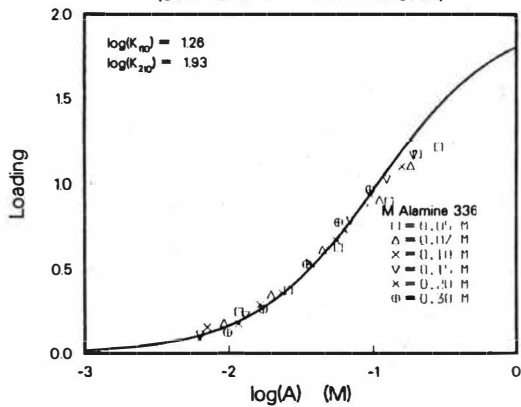


Fig. 2b

Extraction of Succinic Acid by
Dilute Alamine 336 in Chloroform
(Solid Line Is Model Prediction)

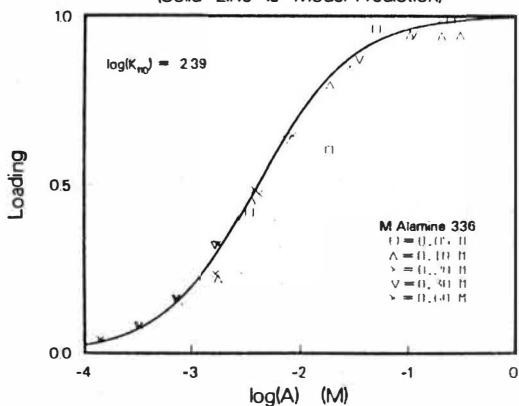
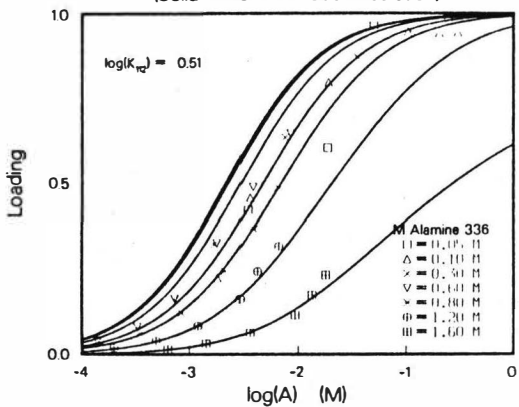


Fig. 3

Extraction of Succinic Acid by
Alamine 336 in Chloroform
(Solid Line Is Model Prediction)



Utilisation of green parts of the waste hop plant by solvent extraction

V. Grilc, "Boris Kidrič" Institute of Chemistry, Ljubljana, Yugoslavia
B. Dobrowsky, Hmezad-Agrina, Zalec, Yugoslavia

Summary

The process for extraction of bitter constituents from dry waste hop plant (after cones had been removed) is presented. It consists of: (a) drying of fresh hop foliage, (b) grinding of dry material, (c) extraction of organic soluble substances (d) stripping of organic solvent from the solid residue and (e) separation of the solvent from the extract by evaporation. Ten different solvents were used. The extraction efficiency is a function of type of extraction process, phase ratio, solid phase humidity etc. The bitterness of the hop green material was completely removed, rendering the material very rich on proteins (about 23 %). The extract contains hop resins, essential oils, waxes and dyes, which can be, after separation, used for various purposes.

1. Introduction

The hop (*Humulus lupulus*) is cultivated to provide raw material for the brewing industry (1). When the cones get ripe, the whole plants are collected and taken from the field.

The cones are mechanically torn down and separated from the leaves. The residual mixture consists of leaves and disintegrated cones (so called "green mass") and represents troublesome agricultural waste. There are records (2-4) about ill side effects on animals, which were fed with the fresh green mass, despite well known valuable composition the hop plant (1-3).

From obvious reasons extensive data exist in literature about the chemical composition of hop cones. Data on the rest part of the hop plant are scarce. Summary of the literature survey is presented in Table 1.

TABLE 1: Summary of the literature data of hop plant composition (1-4)

	Water (%)	Proteins (%)	Fatt (%)	Cellulose (%)	Extractable m. (%)	Ash (%)
Fresh plant	66.0	4.7	1.3	9.2	14.6	4.2
Fresh leaves	68.0	5.1	1.4	6.3	13.7	5.5
Dry plant	10.6	12.5	3.5	24.5	38.1	10.8
Dry leaves	12.0	14.0	4.0	17.4	37.7	14.9

The aim of this study was to evaluate the waste hop mass as a raw material for various useful products. Particular of our concern was the relatively high content of proteins as well as natural pigments in the hop leaves. The hypothesis was to eliminate bitter substances and dyes by means of an organic solvent to isolate the dyes from the extract and finally to prepare the residual hop mass in quality suitable for animal food.

2. Experimental and results

The green mass, obtained from a mechanical picking of the cones was first dried at 60° C with air in a typical three - stage hop drying unit. Careful separation by hand revealed that the material is a mixture of leaves (85 %), stalks (5 %) and about 10 % of disintegrated cones. The drying process is described elsewhere (5). Humidity of the obtained dry material was about 10 wt %. The fragile material was disintegrated in a hammer mill, yielding particles less than 3 mm in size and simultaneously eliminating ferrous (wire) particles by means of a magnet. Analysis of the material, called "the hop meal" is presented in Table 2. The material was overdried, after some days storage the equilibrium content of water was reached, about 10 % per weight, having bulk density of 414 kg/m³.

The extraction experiments were carried out using ten different organic solvents and five mixtures of them. At room temperature the process was effected in a stirred vessel, while at boiling point temperature in the Soxleth apparatus. Separation of solvent from the extract was achieved by means of laboratory rotating evaporator under vacuum. The results of extraction tests are presented in Table 3.

Rather extraordinary high extraction efficiency of methanol at boiling point is the net effect of consecutive washing of the hop meal with 20 - 30 portions of hot, fresh solvent. When the same system is consecutively washed with fresh portions of cold methanol (weight ratio being 1:4,2), the resulting extractivities were: 11.7, 6.0, 4.0, 2.4 and 1.0, respectively. The net extractivity equals 25.1 %, which is practically the same as at boiling point temperature. Since the cross-flow process is not economical in practice, a countercurrent extraction was performed, by means of a series of separation funnels(6), simulating a three stage process. The results are shown in the diagram 1.

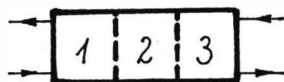
TABLE 2: Percent extracted from dry waste hop material using various solvents

Solvent type	solid:liquid weight ratio ⁺	% extracted at room temp.	% extracted at boiling point temp.	T _B (°C)
n-hexane	-	-	8.1	68.8
petrolether	1:2.5	6.4	13.2	30-50
benzin	-	-	12.9	60-90
dichloromethane	1:5.3	7.9	10.1	39.7
trichloroethylene	1:5.9	7.5	11.0	86.9
methanol, abs.	1:4.8	11.0	25.8	64.7
methanol, 90 wt %	1:4.9	13.1	-	-
ethanol, abs.	-	-	9.7	78.5
ethanol, 95 wt %	1:4.8	4.8	-	-
diethylether	1:2.9	6.8	10.7	34.6
acetone, abs.	1:3.2	9.1	11.7	56.2
acetone, 80 wt %	1:5.0	11.2	-	-
ethylacetate	1:5.4	6.3	10.9	77.2

Diagram 1: Results of the simulation of three stage countercurrent extraction process

37 g of extract/kg of solvent

4.75 kg of fresh solvent/kg of solid phase at the inlet



333 g of extract/1 kg of inert solid

90 g of extract/kg of inert solid

The yield of the three stage extraction battery with respect to the amount of extract is 73 %. Theoretical calculation reveals, that 3.6 ideal stages are required for 90 % efficiency, which means 4 to 5 practical stages are needed.

The extract and the residual solid were analyzed and the composition is presented in Tables 3 and 4. Standard analysis for evaluation of hop extract was used for the extract. The latter was obtained by mixture of methanol and benzene. For comparison, composition of extract from hop cones (the same solvent was used), is also shown.

TABLE 3: Composition of the extract (wt %)

Component	waste hop green mass	hop cones
water	6.6	2.1
chlorophyll	2.1	-
total resins	35.4	81.2
soft resins	29.4	68.2
alpha acids	4.7	33.1
beta fraction	24.7	35.1
hard resins	6.0	13.0
bitterness (Wöllmer)	7.9	37.9

TABLE 4: Composition of the extracted meal

Component	content (wt %)	component	content (%)
water	8.96	Na	0.014
ash	15.64	K	1.0
cellulose	17.2	Ca	4.8
tot. proteins	22.3	Mg	0.9
		Fe	0.03
		Zn	0.007
		Mn	0.008
		Cu	0.095
		P	0.20
		N ₂	3.42

3. Conclusions

The results of this investigation show that extraction of dry waste hop green mass can resolve problems with utilisation of this material. Both products (the extract and the residual meal) consist valuable components and can be used as the basis for various applications in agriculture, food industry and elsewhere. Economics of the

whole process depends particularly on the value of the final products.

Literature

1. Modern Methods of Plant Analysis, Vol. 6, p. 135, Spinger Verlag, 1963
2. A.Stählin; Die Beurteilung der Futtermittel 2. Teil, Neumann Verlag, Radebeul und Berlin, 1957
3. Handbuch der Futtermittel, 1.-3. Teil, Paul Parcy Verlag, Hamburg und Berlin, 1969
4. M.Kirchgessner; Tiernahrung, 6. Aufl., DLG Verlag, Frankfurt 1985
5. V.Grilc, B.Dobrowsky; B. Kidrič Institute of Chemistry, Internal documentation, 1984
6. R. Treybal, Liquid Extraction, 2 Ed., Mc Graw Hill, New York, 1963
7. Brautechnische Analysemetoden, Band I, 212, Mebak, Feising - Weichen Stephan, 1979

Mass Transfer Problems in High-Pressure Extraction

E.Lack, R.Marr, Technische Universität Graz, Graz/Austria

Introduction

The advantage of high-pressure extraction (HPE) to produce extracts without residual solvents leads to an increasing interest for this technology. Since the size of HPE plants has changed from laboratory scale to industrial production, investigation on mass-transfer has become more important. A sufficient knowledge about the mass-transfer of natural substances from solid materials into the solvent is necessary for the design of economical production plants /1/.

Mass Transfer in HPE

The objectives of mass-transfer investigations is to find out an optimum of the specific solvent flow rate of the process. The specific solvent flow rate is defined as mass flow of the solvent per amount and solid feed and extraction time for a desired extraction efficiency. This parameter varies between 5 and 100 kg CO₂/kg feed and extraction time. The energy consumption is linear dependent on the mass flow rate of the solvent for all processes with a complete solvent recirculation and this energy can be calculated with the aid of T,s-diagram /2/.

Compared to the conventional solvent extraction hydrodynamics and diffusion are the main influences on mass transfer.

Diffusion: It should be mentioned that we decide between two different sections in diffusion when extracting plant raw material. At the beginning of the extraction process mass transfer is controlled by leaching of the desired substances from the surface of the raw material. The substances can diffuse into the solvent similar to liquid-liquid extraction. With increasing extraction time mass transfer is controlled by the diffusion of the extractable substances from the center of particle to the surface. Because of this long diffusion path and other properties of the solid raw materials such as adsorption bondings the mass transfer rate is reduced and this is the reason for the long extraction times.

Hydrodynamics: The hydrodynamics influences mainly the geometry of the extractor. It is necessary to reach a homogeneous velocity profile over the whole cross sectional area of the extractor.

An other parameter which has to be optimized is the particle size-distribution. Big particles yield a good flow distribution but

cause a slow diffusion. Two small particles lead to a higher backmixing and to the formation of solvent channels.

Experiments

For studying the mass transfer behaviour a lot of experiments were made to measure the loading of the solvent in dependence on extraction time and height of bed. All experiments were made in our laboratory plant.

The technical data of the plant are:

the volume of the extractor is 10 l

the maximum working pressure is 325 bar

the maximum working temperature is 200° C

the flow rate can be varied between 5 and 60 kg CO₂/h

Flaked seed of rape seed and milled press cake of rape seed were used as feed material. To avoid the influence of different properties preparation of the raw material was done in the same way for all experiments.

The thermodynamic conditions for all extraction runs are:

Extraction pressure 290 bar

Extraction temperature 40° C

Separation pressure 50 bar

Separation temperature 25° C

In the following some results of these measurements are shown.

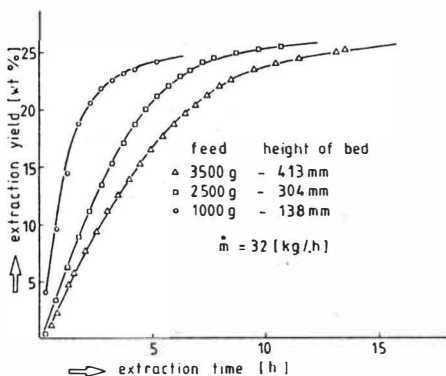


Fig. 1: Extraction yield versus extraction time

Fig. 1 shows the extraction yield curves in dependence of the total solvent throughput. Because of the low solubility of vegetable oil in CO_2 and the low solvent velocities in the extractor the extraction times are rather long.

For each height of bed an own experiment is necessary because it is not possible to take out solid samples of the bed at different heights during the extraction run.

As written before, the extraction experiments should show the loading behaviour and the extraction yield of the solvent at different extraction time and at different levels of the solid bed.

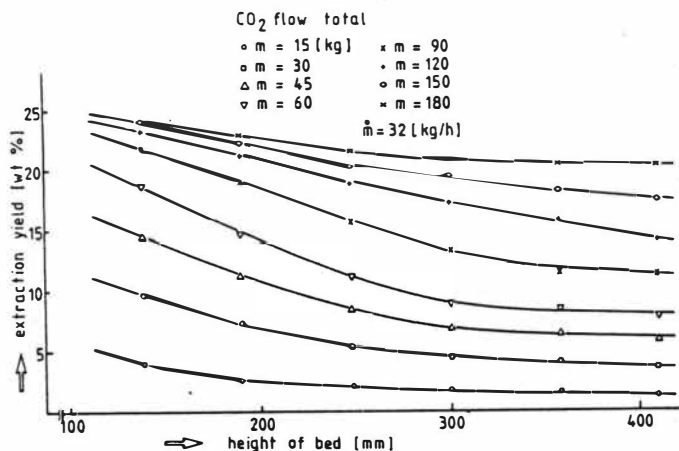


Fig. 2: Extraction yield dependent on height of the solid bed

Figures 2 and 3 show the extraction yield versus height of bed and extraction time. The moving of the mass transfer zone from the bottom to the top of the extractor is clearly shown in figure 3 by the logarithmic plot of the extraction time.

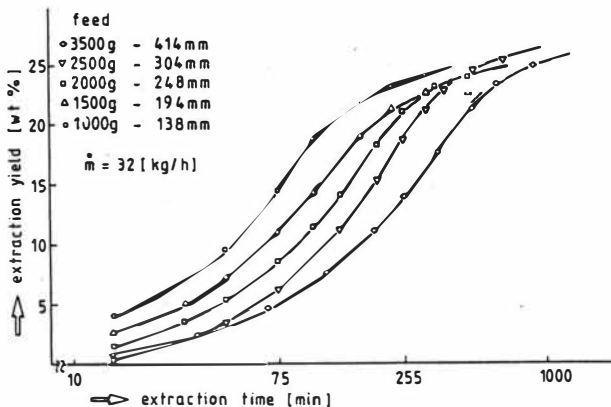


Fig. 3: Extraction yield dependent on extraction time for different height of bed

A three dimensional projection of fig. 3 in fig. 2 shows the three dimensional dependence of the extraction yield on extraction time and height of bed. These relations are important for the evaluation of the optimum mass transfer rate.

Modelling of Mass transfer

One of the objectives of these investigations were to collect a lot of data for the modelling of mass transfer. The models of perkoliation which are used in the extraction of plant materials are not successful in HPE.

A useful model to describe the mass transfer should offer the following possibilities. It should be able to describe the differential mass transfer dependent on time, height of bed, solvent flow rate and concentration gradient with two mass transfer coefficients (one for the first mass transfer section and one for the diffusion section).

There are very few models in literature to describe mass transfer in high pressure extraction. Two well known models are from Brunner and King /3,4/.

Analysis of HPE of rape seed and other natural raw materials show that there is a lot of analogy between the drying processes and HPE. The mass transfer is separated into two sections - one for the direct contact between water and air (constant drying velocity) or extract-able substance and supercritical solvent (constant mass transfer rate) - one for the diffusion of water through the cell membrane or extract through the cell membrane (decreasing mass transfer rate). Another point is that the solubility of water in air or extract in supercritical solvent is dependent on the thermodynamic conditions of the solvent.

The drying model which is described in the book of Otto Krischer "The fundamentals of the drying technique" /5/ was very useful to be applied in a mass transfer model for HPE.

The model starts with the local and chronological distribution of the extract in the solid given by the following differential equation.

$$\frac{\partial^2 r}{\partial \tau \partial z} - \frac{1}{v} \cdot \frac{dv}{dr} \cdot \frac{\partial r}{\partial \tau} \cdot \frac{\partial r}{\partial z} + v \frac{\partial r}{\partial z} = 0$$

This equation can be solved by derivating to τ , the dimensionless time.

$$\frac{1}{v} \cdot \frac{\partial r}{\partial z} + r = r(z, \tau = 0)$$

$r(z, \tau = 0)$ is the extract content at the beginning of the extraction.

v = dimensionless mass transfer rate

r = dimensionless extract content

z = dimensionless position

By separating the variables, the differential equation can be solved by integration and reaches the following form:

$$\int_{r_1}^r \frac{dr}{v(r)(r_0 - r)} = \int_{z_1}^z dz$$

For the first extraction section the distribution of the local and chronological extract content is described as following,

$$r(z, \tau) = r_0 - \tau \cdot e^{-z}$$

In this section the mass transfer rate is constant. The integral can be solved in the diffusion section if the function of $v(r)$ is given by a mathematical equation. The integral must be solved graphically if the function $v(r)$ cannot be described with a mathematical equation. A computer program was made for solving such integrals in a short time.

The assumed boundary conditions between drying processes and HPE are:

- similar geometry of the extraction yield curve and the drying rate curve
- constant breaking point loading for different feed amounts
- plug flow can be assumed for both processes
- constant diameter for the whole height of bed

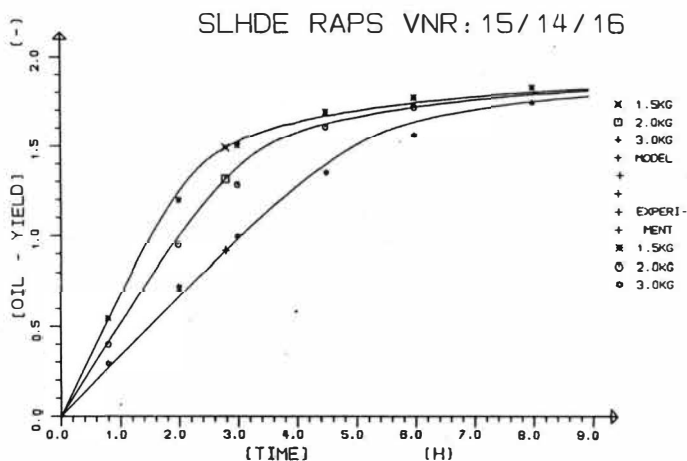


Fig. 4: The calculated and the experimental extraction yield curves dependent on the extraction time for a feed amount of 1,5 kg, 2 kg and 3 kg rape seed

The results show a quite good description of the HPE extraction according to the drying model as shown in fig. 4.

A disadvantage of the model is, that it is very sensitive to back mixing.

Summary

The objective of the modelling of mass transfer is to describe the extraction process in the extractor and to offer the possibility to calculate the mass transfer for industrial extraction processes out of experiments in a pilot plant.

References

- /1/ Brunner, G. and S. Peter, Chem.Ing.Techn.53, 7, 529 (1981)
- /2/ Bunzenberger, G., E.Lack and R.Marr, Ger.Chem.Eng.7, 25 (1984)
- /3/ Brunner, G., Ber.Bunsenges.Phys.Chem.88, 887 (1984)
- /4/ King, M.B., T.R.Bott, K.Kassim and M.Barr, Preprints High Pressure Chemical Engineering, Erlangen, 301 (1984)
- /5/ Krischer, O. and W.Kast, The fundamentals of drying technique, Springer Verlag (1978)

Separation of Citric Acid from Aqueous Fermentation Solutions by Extraction-Reextraction Processes

W.Rückl, M.Siebenhofer, R.Marr, Technische Universität Graz,
Graz/Austria

Introduction

Citric acid is a very important bio-product. It is mainly used in food- and beverage industry but also added to pharmaceutical and chemical products. Today's world production is about 400.000 t/a. The production is commonly done through fermentation of suitable raw materials such as sugar, molasse, cell hydrolysate a.s.o. The fermentation process is performed by "aspergillus niger". Problems and technical advances in this fermentation step should not be part of this paper. The isolation of citric acid from the fermentation broth was investigated and a new technique using liquid liquid extraction and distillation was developed.

Common Process

The commonly used process for the removal of citric acid from the fermentation broth is forming the nearly insoluble calcium citrate by addition of lime water to the broth after separation of the micro-organism. The solubility of the calcium citrate in water is dependent on temperature and pH-value. It is in the range of some g/l. From the calcium salt the citric acid is obtained through a hydroly-sation step using sulfuric acid. The remaining calcium sulfate is an unsaleable waste because of its bad quality. The total amount of waste in this process is about 2,5 tons per ton of citric acid with about 65 % of calcium sulfate /1/.

As these chemicals, lime water and sulfuric acid are main factors in production costs of citric acid, many working groups have tried to find new ways to isolate the citric acid from the fermentation broth /2,3,4/.

Extraction Processes

The extraction processes have become the most important ways of the newer technologies. Many investigators have tried to find solvents which are applicable to those extraction processes. The main demand in this solvent selection process is, besides the well known parameters such as high capacity or high distribution coefficient, selectivity a.s.o., is to find a non toxic substance because of the use in food industry.

Early works brought up n-butanol, ethylacetate, ethylether, MIBK, MEK. All these solvents have very low distribution coefficients (c_{org} / c_{aqu}) as a main disadvantage. They are in ranges between 0,1 and 0,3 /5,6/. Wennersten already reported long chain aliphatic amines and phosphoryl group containing substances suitable for these problems. The distribution coefficients are 10 to 20 times higher. He also reported the possibility of reextraction by temperature change as distribution coefficients decrease with increasing temperature. Wennersten reported reextraction temperatures of 60 to 80° C. He also reported already problems of diluting reactive components in aromatics or in alkanes to reach hydrodynamic parameters which make the solvents usefull in columns or mixer-settlers. The influences of diluent on distribution coefficients are also reported /7,8/.

Experimental Work

In our work, the only use of non toxic substances was the main demand. The optimal mixture of reactive component, diluent and modifier had to be found. The fact made e.g. the use of benzene as diluent absolutely impossible. Solvent developing experiments were performed in separation funnels and agitated vessels. The following substances were used: as the reactive component, a tertiary amine (HOSTAREX A 324), as the modifier Isodecanol, and as the diluent a medium fraction of alkanes (Shellsol I). For composition of these three substances the following aims had to be observed.

Maximum capacity, max. interfacial tension, min. density, min. coalescence time, min. losses (through solubility or distruction) min. costs.

A composition of 30 % amine, 30 % isodecanol and 40 % alkanes was found as an optimum. With this solvent all experiments from equilibrium curve estimation to column experiments containing extraction and reextraction step were done. All steps of the process, extraction from fermentation broth, reextraction with stripping acid and thermal regeneration were performed in technicum scale plants.

Column diameter for liquid-liquid contacting was 20 mm (Karr) and 80 mm (SHE-self stabilizing high performance extractor). Each column had a height of 2 m. For vapour liquid contacting a 50 mm Raschig-ring packed distillation column was used.

Equilibrium data

Fig. 1 shows the equilibrium curve for citric acid between water and the above mentioned solvent. From there it can be seen that the

distribution coefficient is heavily influenced by the aqueous feed concentration. This dependence derives from the type of extraction based on chemical reaction forming the ammonium salt. The maximum loading limited by the stoichiometry can be seen at a organic concentration of about 0,58 mol/l.

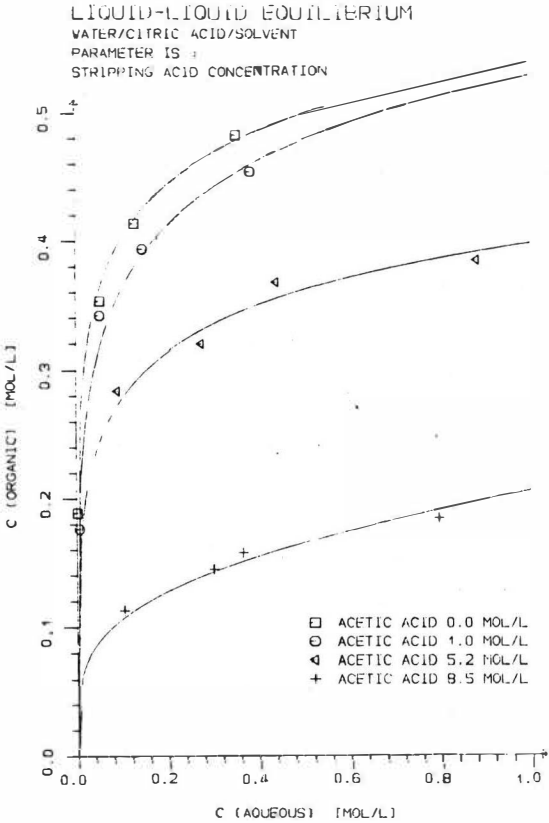


Fig. 1: Liquid-Liquid Equilibrium for citric acid

On the other hand it can be seen, that the concentration of a stripping acid influences the equilibrium distribution so much, that an economical reextraction process can be performed. Acetic acid was used as a representative species because on one hand it shows good reextraction behaviour, on the other hand it is relatively easily handled compared e.g. to formic acid. As stripping reagent an acid must be used which can be removed from the solvent by distillation. Any other acid (e.g. mineral acids) which cannot be removed by thermal regeneration of the solvent would cause a process similar to the conventional technique. That means, that the acid has to be removed from the solvent by forming an insoluble salt. This would cause losses in chemicals and solvent.

The stripping acid should decrease the distribution coefficient to a minimum to reduce the amount of citric acid in circulation and minimize the losses which could occur through thermal destruction in the distillation step. The distillation of acetic acid from this solvent was reported in former works /9/.

Extraction-Reextraction Process

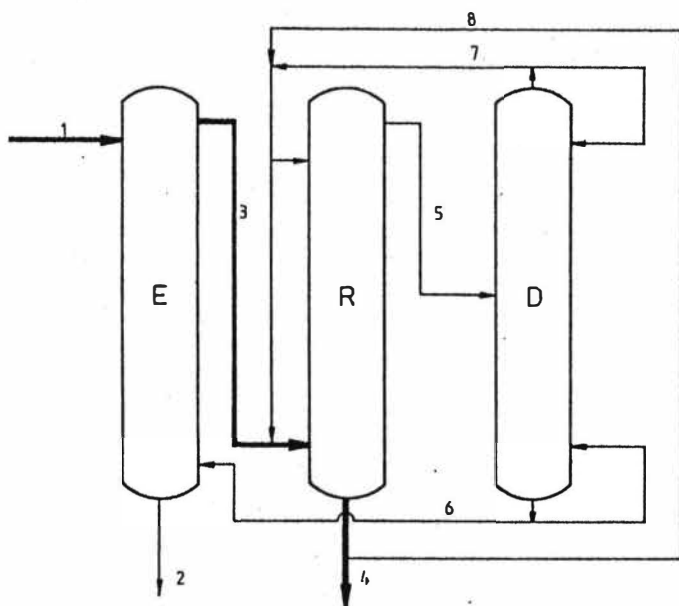


Fig. 2: Extraction-Reextraction-Distillation

Fig. 2 shows the flow sheet of the extraction-reextraction-process. The regeneration of the solvent is done by distillation only. The precleaned fermentation broth (1) is pumped as continuous phase through the extractor from the top to the bottom. The raffinate leaves the apparatus with a minimum rest loading of citric acid according to plant design. The solvent (6) is the dispersed phase and goes from the bottom to the top of the column. The solvent (3) loaded with citric acid leaves the extraction column and enters the reextraction column at the bottom again. The exchange of citric acid and stripping acid occurs. The raffinate (4) is a mixture of citric acid and stripping acid. The solvent which is now loaded with stripping acid (5) goes to the distillation plant. At the top of the column the stripping acid leaves the distillation and goes back to the reextraction column (7), the cleaned solvent (6) is brought back to the extraction column.

For better selectivity it can be useful to reflux the product stream (4) partially into the reextraction column which is indicated by stream 8.

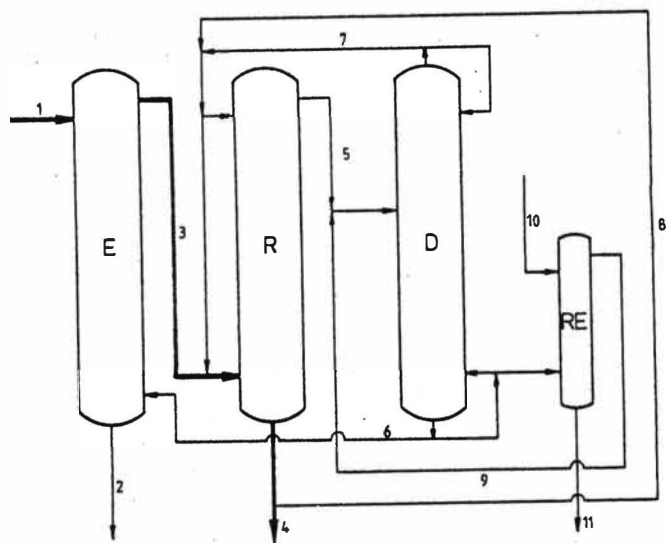


Fig. 3: Extraction-Reextraction-Distillation-Regeneration

Fig. 3 shows the same process as fig. 2, but includes a regeneration step. This step can be necessary if substances (e.g. stronger acids caused by impurities) remain in the solvent and cannot be separated by distillation. The regeneration plant is commonly a liquid-liquid-contactor like an extraction column. The regeneration medium (e.g. a sodium hydroxide solution) (10) is contacted with the bottom product (6) of the distillation. That means the solvent reaches the regeneration step after distillation to minimize the necessary amount of chemicals. The waste stream (11) is the used regeneration medium and can be made up again.

Streams in Fig. 2 and 3

- (1) Fermentation broth
- (2) Raffinate
- (3) Solvent + citric acid
- (4) Citric acid + stripping acid
- (5) Solvent + stripping acid
- (6) Solvent + impurities*
- (7) Stripping acid
- (8) Citric acid + stripping acid
- (9) Solvent
- (10)*Regeneration agent inlet
- (11)*Regeneration agent outlet

* means only in Fig.3.

Literature

- /1/ Ullmann: Enzyklopädie der Technischen Chemie, 4. Auflage, Band 9, S 624, Verlag Chemie
- /2/ FR-Patent 1127820
- /3/ FR-Patent 1211066
- /4/ DT-Patent 1055483
- /5/ Marvel, C.S. and Richards, J.C.: Anal.Chem.21 (1949), p 1480
- /6/ Gordon, F.K.: Ind.Eng.Chem. 45 (1953), page 1813
- /7/ Wennersten, R.: ISEC '80, Liege, Proc.80/63 (1980)
- /8/ Wennersten, R.: J.Chem.Techn.Biotechnol. 338 (1983), p 85
- /9/ Siebenhofer, M. and R.Marr: ISEC '83, Denver, Col., Proc.18e (1983)

**ETHANOL RECOVERY FROM LOW-GRADE FERMENTATES BY SOLVENT
EXTRACTION AND EXTRACTIVE DISTILLATION: THE SEED PROCESS**

D.W. Tedder, W.Y. Tawfik, and S.R. Poehlein
School of Chemical Engineering
Chemical Process Design Institute
Georgia Institute of Technology
Atlanta, GA 30332--0100 U.S.A

ABSTRACT

Solvent extraction may be coupled with extractive distillation to recover ethanol from low-grade fermentates. Water coextracts with ethanol from dilute aqueous mixtures, but the resulting extracts can be dehydrated by extractive distillation. Such dehydrated extracts can then be selectively stripped to produce fuel grade ethanol and regenerated solvent.

INTRODUCTION

Liquid/liquid extraction may be used to separate ethanol from water. Earlier measurements were reported by several investigators (1-8). When the relative effects of various molecular functionalities are considered, water immiscible alcohols exhibit higher distribution coefficients. However, solvents containing phosphate groups, ester, and carbonyl groups are also usable. On the other hand, those solvents with higher distribution coefficients (e.g. 2-ethylhexanol) also exhibit lower selectivities. Moreover, the selectivities of all solvents examined tend to decrease with increasing aqueous ethanol concentrations.

Solvents that are capable of achieving high ethanol recoveries from dilute mixtures, yield selectivities high enough to produce fuel-grade ethanol from dilute aqueous mixtures, and also exhibit adequate solute loadings have not been found. Typically, extracts contain 3 to 5 wt% ethanol and about equal amounts of water. In such cases a single cycle (i.e. solvent extraction followed by regeneration) will not yield a fuel grade product (i.e. 98-99 wt% ethanol).

However, the higher boiling solvents (e.g. tridecyl alcohol) also radically change the ethanol/water relative volatility and can be used in extractive distillation where water is selectively removed from the liquid/liquid extract. In this case, those solvents with higher capacities but lower selectivities can still be used to recover a fuel-grade product.

In the case of the higher boiling solvents, Solvent Extraction and Extractive Distillation (SEED) can be coupled as indicated in Fig. 1 to achieve the desired separation. The resulting process consists of three columns: a liquid/liquid extraction column, an extractive distillation column, and a solvent regeneration column. The last column recovers the desired fuel-grade ethanol product and provides regenerated solvent for the liquid/liquid extraction and the extractive distillation columns as indicated.

THERMODYNAMIC MEASUREMENTS

The equilibrium compositions of vapor and liquid phases were measured using gas chromatography and internal standards. The modifier/diluent ratio for blended solvents was assumed not to change appreciably due to equilibration. For selected solvent blends, the liquid/liquid mutual solubility curve was also tritrated.

Liquid-Liquid Equilibria

Fermentates typically contain small amounts of dissolved salts and species like sugars. Synthetic feeds containing dextrose as a substitute for all nonionic, inextractable dissolved fermentate solids were used to measure liquid/liquid equilibria and to develop the given correlations.

Ethanol and water distribution coefficients in the solvent were measured as a function of ethanol and dextrose weight fractions, the temperature, and the volume fraction of the modifier (either TBP or tridecyl alcohol) initially in the organic diluent (Isopar M). Data analysis then led to the following empirical correlations which are valid over the indicated ranges.

Tridecyl Alcohol/Isopar-M Blends

$$\ln D_e = 7.644 - 3.23 X_e^2 + 1.76 X_e + 0.849 X_D$$

$$\begin{aligned}
 & + 2.89 V_{\text{TDOH}} - 3153.4/T \\
 \ln D_W = & 2.664 - 18.941 X_e^2 + 9.26 X_e + 1.86 X_D \\
 & + 3.73 V_{\text{TDOH}} - 1383.3/T \\
 X_e < & 0.33 & 301 < T < 342 \text{ K} \\
 X_D < & 0.60 & V_{\text{TDOH}} < 1.0
 \end{aligned}$$

These correlations for ethanol and water extraction are based upon 23 equilibrations in which the independent variables were adjusted over the range indicated.

Tri-n-butyl phosphate/Isopar-M Blends

$$\begin{aligned}
 \ln D_e = & 1.6 + 58.5 X_e^2 - 19.3 X_e + 0.985 X_D + 3.78 V_{\text{TBP}} - 1007.5/T \\
 \ln D_W = & -5.31 - 6.96 X_e^2 + 5.36 X_e + 1.18 X_D \\
 & + 4.95 V_{\text{TBP}} - 465.1/T \\
 X_e < & 0.33 & 301 < T < 342 \text{ K} \\
 X_D < & 0.6 & V_{\text{TBP}} < 0.5
 \end{aligned}$$

These correlations are based upon 27 equilibrations.

Vapor Liquid Equilibria

Vapor/liquid equilibria were measured for all binary pairs. Analysis of the data using the Uniquac (9) model led to the parameter estimates that are summarized in Table 1.

$$\text{where } \ln \tau_{ij} = -A_{ij}/RT$$

Table 1. Uniquac binary interaction parameters for the ETOH/H₂O/TDOH/ISOPAR M system estimated from binary VLE data.

i	H2O	ETOH	ISOPAR M	TDOH
H2O	0	329.49	348.66	326.1
ETOH	-29.43	0	-117.10	332.80
ISOPAR M	762.37	1839.5	0	887.14
TDOH	326.10	35.2	-348.89	0

LABORATORY APPARATUS

Laboratory extraction tests were carried out using a 2.54 cm diameter glass reciprocating plate column. This unit included 92 stainless steel reciprocating plates and had an active contact height of 244 cm. It is sold by the Chem Pro Corp., New Jersey, U.S.A. as Model KC 1-8.

Two glass vapor/liquid bubble cap columns were built to test the SEED process. Both columns had 7.6 cm diameters. The extractive distillation column consisted of three bubble cap trays above the feed and three below. The solvent regeneration column included four bubble cap trays below the feed and two above.

RECIPROCATING PLATE COLUMN MODEL

A generalized correlation for the height equivalent to a theoretical stage to diameter ratio (HETS/D) was developed using experimental and literature (10,11) data. This ratio is correlated in terms of several dimensionless groups as indicated below. Additional details about the model are given elsewhere (12).

$$\frac{\text{HETS}}{D} = 1.03 \left(\frac{D \Delta \rho g}{\rho_c U_T^2} \right)^{-0.075} \left(\frac{A F t_m}{H U_T} \right)^{-1.30} \left(\frac{\sigma}{D \rho_c U_T^2} \right)^{0.625} \pm 16.4\%$$

TOXICITY TESTS

Earlier studies (13) on solvent toxicity suggested that solvent species with at least a ten carbon chain exhibit sufficiently low aqueous solubilities that they no longer interfere with the fermentation process. Studies at Georgia Tech confirmed this observation. For example, 2-ethylhexanol strongly suppresses biological activity while species such as decyl and tridecyl alcohols exhibit very little effect.

FERMENTATE EXTRACTION

Actual fermentates were produced using sucrose, media, and brewers' yeast. These fermentates typically contained about 5 wt% ethanol and 10 wt% inextractable solids. Tri-n-butyl phosphate and diluent (Isopar-M) blends were used as the solvent.

In these tests, whole fermentate was pumped into the top of the reciprocating plate column which was operated organic continuous (i.e. with the liquid/liquid interface below the contact zone).

Fermentate droplets containing biomass passed downward through the column and were observed to coalesce at the bottom of the column. Extract was passed through a coalescer, preheater, and into the middle of a bubble cap column containing 6 trays.

Steady state with solvent recycle could be achieved in about 2 hours of continuous operation. Actual ethanol product recovered from the solvent regeneration column averaged to about 45 wt% ethanol and the column performance was comparable to operation with synthetic feed mixtures.

During these tests no significant accumulation of interfacial debris was observed to accumulate. The biomass passed through the column without accumulation.

SOLVENT EXTRACTION/EXTRACTIVE DISTILLATION TESTS

In these cases the reciprocating plate column and two bubble cap VLE columns were used. Several hours of continuous operation with solvent recycle were required to achieve steady state. The aqueous solvent extraction feed contained from 3 to 9 wt% ethanol. Solvents consisted of tridecyl alcohol/Isopar-M mixtures. Product recovered from the top of the extractive distillation column typically contained from 1 to 20 wt% ethanol. Product recovered from the solvent regeneration column ranged from 85 to 98 wt% ethanol.

COMPUTER AND ECONOMIC ASSESSMENT

Computations using both a rating simulator (PROCESS) and a design estimator (RUNOPT) were completed. The rating simulator was developed by Simulation Sciences, In., in Fullerton, CA. The design estimator is available at Georgia Tech on the CYBER.

Generally, the computer models and the actual process runs agree. For example, an analysis of the second test described above indicates that the plates below the feed in the EDC exhibited about 60% overall efficiency. The predicted temperatures and pressures also agreed well with the actual experiment. At specified pressures, the temperatures of EDC and SRC bottoms and distillates were within 5°C of the predicted values.

Cost analysis was completed in which three beers (5.15, 1.9, and 0.57 wt%) were processed using the SEED process. Comparisons

were then made with Berkeley optimized distillation (14) concept using their net energy balances, cooling water, and theoretical tray estimates. Azeotropic distillation costs were modelled using the data provided by Black (15). All cases assumed a 99% ethanol recovery and purity (mole basis).

Computer modelling studies suggest that energy savings are possible compared to conventional distillation. Economic comparisons suggest that the SEED process may save 3 U.S. cents/liter when processing to 10 wt% beer up to 13 U.S. cents/liter for a 3 wt% fermentate feed. Ethanol recovery via this route become more attractive as the mixture quality decreases.

DISCUSSION

The solvent polarity and the ethanol/water loading both affect the water/ethanol relative volatility in the presence of the solvent. In the presence of solvents, the water/ethanol relative volatility ranges from 10 to 30. Pure diluent (Isopar-M) yields the highest water/ethanol relative volatility whereas 2-ethylhexanol yields lower values. Blended mixtures of tridecyl alcohol and Isopar-M exhibit intermediate volatilities, but water is always more volatile than ethanol in the presence of high-boiling solvents.

The cell viability after solvent extraction was not studied in this work. Hence, these tests do not prove that the raffinate could be recycled to the fermenter while still maintaining the culture. However, they do suggest that fermentates can be effectively processed by solvent extraction without adverse effects from biomass accumulation in the column.

Optimization studies in which the solvent blend was treated as a variable led to a solvent consisting of pure tridecyl alcohol. This result suggests that solvent loading is more economically important than selectivity during solvent extraction and relative volatility during extractive distillation. Further solvent improvements may be achieved through the use of high-boiling mixtures that exhibit even higher loadings than pure tridecyl alcohol.

NOMENCLATURE

A	=	Amplitude of reiprocation
A_{ij}	=	Uniquac binary interaction parameter
D	=	column diameter
D_e	=	ethanol distribution coefficient (ratio of weight fractions)
D_W	=	water distribution coefficient (ratio of weight fractions)
F	=	frequency of reciprocation
g	=	gravity constant
H	=	plate spacing
R	=	gas constant
t_m	=	plate thickness
T	=	temperature, K
U_T	=	phase relative velocity
V_{TDOH}	=	volume fraction of tridecyl alcohol in solvent
V_{TBP}	=	volume fraction of TBP in solvent
X_D	=	weight fraction dextrose in equilibrated aqueous phase
X_e	=	weight fraction ethanol in equilibrated aqueous phase.
$\Delta\rho$	=	phase density difference
ρ_C	=	continuous phase density
σ	=	liquid/liquid interfacial tension

REFERENCES

1. D.F. Othermer, R.F. White and E. Trueger, Ind. and Eng. Chem., vol 33, No. 10 (1941) 1240.
2. A.V. Brancker and T.G. Hunter, ibid, vol. 32, No. 1 (1940) 38.
3. I. Bachman, ibid, vol 32, No. 1 (1940) 35.
4. J.L. Schweepe and J.R. Lorach, ibid, vol. 46, No. 11 (1941) 2391.
5. D.F. Othmer and P.E. Tobias, ibid, vol. 34, No. 6 (1942) 696.
6. C.M. Qualline and Van Winkle, ibid, vol. 44 No. 2 (1952) 1668.
7. J.W. Roddy, Ind. Eng. Chem. Proc. Des. Dev., vol. 20 (1981) 104.

Extraction of Citric Acid

by N,N-disubstituted Alkyl Amides

Wang Wenqing , Yi Min , Chen Dingfong , Pen Qixiu ,
Pen Lie , Zhang Maoliang , Mou Xiru , Chen Jinbang

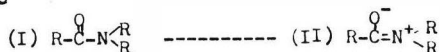
(Department of Technical Physics , Peking University ,
Beijing , China)

ABSTRACT

Citric acid has been produced commercially from fermentation aqueous solution by the procedure of adding lime to form calcium citrate then reacting with sulfuric acid to form citric acid solution and insoluble calcium sulfate. This procedure has the disadvantages of requiring expendable lime and producing the disposal of calcium sulfate. The present paper provides a process for the extraction of citric acid with N,N disubstituted alkyl amides from fermentation broth.

Disubstituted amides is to be expected strong extract

-ants



The contribution of (II) should not only weaken the carbonyl bond but should also increase the availability of the electrons of the oxygen atom for bond formation. A systematic investigation of the use of N,N disubstituted alkylacetamide as an extractant for the extraction of citric acid has been studied.

The citric acid can be conveniently recovered from the amide phase by back-extraction with water. The extraction process is exothermic, so the extraction is favorably carried out at lower temperature (10°C - 20°C) and strippings at higher temperature (60 - 70°C). Provided that a proper value of distribution ratio is adjusted by adding sweet odor diluent. The theoretical stages of counter-current extraction and back extraction required to attain high percentage recovery are kept at reasonable numbers.

As the manuscript was not available at the 28th May 1986, the deadline for printing this book, we only print the short abstract of the paper.

The Permeation of Phosphonodipeptides through Liquid Membranes

P. Pluciński,** P. Kafarski,* B. Lejczak,* M. Cichocki

Institute of Chemical Engineering and Heating Equipment

*) Institute of Organic and Physical Chemistry
Technical University of Wrocław, Poland

***) present address: Technische Universität München
Institut für Technische Chemie
Lehrstuhl I

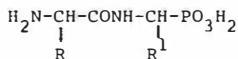
Amino acids, their phosphonic analogues and phosphonodipeptides were found to be easily transported through thin (1-10 μm) organic membranes formed by emulsion treating technique. This transport is stereoselective. Thus, L-L isomer of 1-(N-valylamino)ethanephosphonate is transported faster than L-D isomer.

Carrier-mediated transport of amino acids and their derivatives plays essential role in many biochemical processes (1). Therefore, it is of great importance to construct the model systems of biological transport not only for simulating the biochemical processes, but also for developing new methodologies in separation science.

Such artificial transport of alkali metal, transition metal and ammonium cations has already been realized by the use of many kinds of crown ethers and related molecules (2). Surprisingly only scattered examples of amino acid transport mediated by macrocyclic compounds are given in the literature (3-9). Moreover, the studies were carried out using bulk liquid membranes which are not good mimetics of biological ones.

In this communication we report the preliminary studies on transport of dipeptides and amino acids through thin (1-10 μm) membranes formed by emulsion treating technique (10). These membranes better resemble the biological membranes and offer the potential of moving large amount of these derivatives in a short time from source to the receiving phase.

During several years we have been engaged in the synthesis of phosphonodipeptides 1, a new class of promising antibacterials, and their separation into diastereomers (11-13).



1

Such diastereomeric peptides are indispensable for biological studies. Consequently, we have focused our interest on their transport.

EXPERIMENTAL

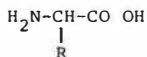
The emulsion system was formulated from the organic membrane phase and the aqueous receiving and source phases. The organic phase consisted of carbon tetrachloride in which carrier (18-crown-6, Kryptofix 5, Kryptofix 22 or Kryptofix 222) was dissolved and of Rokwin 60 (1-8% per weight; Rokwin 60 is the mixture of esters of higher fatty acids and sorbit, produced by NZPO Rokita, Poland), chosen among several nonionic surfactants. The source phase contained peptide or amino acid in water (2.5 mM solution), while water saturated with carbon tetrachloride was the receiving phase.

Emulsion (obtained by stirring $5 \cdot 10^{-5} \text{ m}^3$ (50 ml) of source phase and $2,5 \cdot 10^{-5} \text{ m}^3$ (25 ml) of carbon tetrachloride at 83,3 1/s (5000 rpm) for 180 s and receiving phase $1,5 \cdot 10^{-4} \text{ m}^3$ (150 ml) were stirred continuously at 33,3 1/s (200 rpm). Samples of permeate were collected between 300s (5 min) to $1,26 \cdot 10^4$ s (3.5 h) and were analysed spectrophotometrically monitoring the appearance of peptide bond or carboxylate absorption (between 230 and 275 nm, individually for each compound). The

composition of permeate was also determined by thin layer chromatography using Merck s HP-TLC plates pre-coated with 60 F₂₅₄ silica gel. The chromatograms were developed using n-butanol - acetic acid - water (12:3:5) as the solvent and the spots were visualized with ninhydrin spray reagent.

RESULTS AND DISCUSSION

The studies presented here clearly demonstrate that amino acids, peptides and their phosphonic analogues are easily transported through organic membranes formed by emulsion treating technique. The detailed studies of the transport kinetics, the influence of surfactant (used to stabilize the membrane), as well as the role of carrier were carried out using valine 2a (R = CH(CH₃)₂) and 1-(N-valylamino) ethane-phosphonate 1a (R = CH(CH₃)₂, R¹ = CH₃).



2

Both of them rapidly permeated through membrane during first 10 minutes (Fig. 1 and 2) and then the permeation velocity achieved constant value, thus showing standard rate-time dependence. Quite surprisingly the permeation rates strongly depend on surfactant (Rokwin 60) concentration, while the dependence on the kind of carrier used is less significant (Fig. 3). This is probably due to the existence of combined-type transport: transport mediated by reversed micelles formed in the membrane phase (similarly to the phenomenon described previously (14, 15) and the transport mediated by the presence of macrocyclic carrier. To eliminate the first effect we have used surfactants not forming reversed micelles in organic media (16), i.e. block copolymers of propylene and ethylene oxides (Pluronic 62 and Pluronic 2600/20, produced by Institute of Organic Technology and Polymer Science of the Technical University of Wrocław, Poland). Unfortunately also in this case the peptide 1a was transported through carbon tetrachloride in the absence of carrier. This is originated from the ability of these surfactants to serve as carriers by binding the ammonium

(NH_3^+) group of the peptide via oxygen atoms of copolymer in a manner similar to crown ethers (structural building blocks of copolymers and crown ethers are the same). The influence of the carrier type and concentration on permeation rates of 1a is shown in Table 1. Analogous dependence was observed in the case of valine 2a. The transporting abilities of macrocyclic ligands used are as follow: Kryptofix 5 > Kryptofix 222 > Kryptofix 22 > 18-crown-6, and are with a good agreement with those reported in the literature (2).

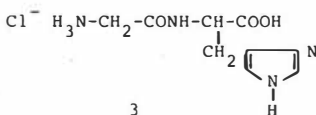
Table 1. The dependence of the permeation rate (mM per 3600s) on the carrier used.

Rokwin 60 concentration	Kryptofix 5		18-crown-6		without carrier
	0,83mM	0,02mM	1,8mM	0,02mM	
4%	0,225	0,192	0,185	0,175	0,182
8%	0,375	0,298	0,225	0,220	0,220

The phosphonopeptides (Table 2) and glycyl-L-histidine hydrochloride 3 were efficiently and nearly to the same degree transported through membrane containing Kryptofix 5. The only exception was (N-L-alanyl-amino)-4-methoxyphenylmethanephosphonic acid 1d.

Table 2. The permeation rates (mM per 3600 s) of dipeptides through carbon tetrachloride membrane stabilized with Rokwin 60 and containing Kryptofix 5 (0,83 mM solution)

Peptide	R	R ¹	Concentration of Rokwin 60			
			with Kryptofix 5		without carrier	
			2%	4%	2%	4%
1a	(CH ₃) ₂ CH	CH ₃	0,625	0,625	0,155	0,225
1b	CH ₃	c-C ₆ H ₁₁	0,495	0,625	0,370	0,505
1c	(CH ₃) ₂ CH ₂ CH	CH ₂ C ₆ H ₅	0,430	0,510	0,155	0,235
1d	CH ₃	p-CH ₃ OC ₆ H ₄	-	0,070	-	0,030
<u>3</u>			0,420	0,430	0,160	0,250



The bigger differences of transport rates appeared when no carrier was present. However, there is no visible structure-transport ability relationship and we are unable to discuss these differences, at this stage of studies. May be the use of the wider variety of peptide structures would help for better understanding of this problem.

The transport stereoselectivity is the vital problem in this study. Thus, we have compared the transport rates of diastereomeric forms of 2a (Table 3). In all cases the L-L(S-R) isomer was transported faster than L-D(S-S)isomer, thus showing the diastereoselectivity of the system studied. In the extreme case this selectivity reached 2,71. This result is quite promising and indicate the possibility of the use of this system for separation of diastereomeric mixtures.

Table 3. Stereoselectivity of 1a transport.

1a isomer	Rokwin 60 concentration					
	with Kryptofix 5				without carrier	
	0,83 mM		0,02 mM			
	2 ‰	4 ‰	2 ‰	4 ‰	2 ‰	4 ‰
a)						
L-L	0,62	0,62	0,25	0,32	0,16	0,38
L-D	0,62	0,60	0,18	0,28	0,08	0,14
b)						
Stereoselectivity	1,00	1,03	1,38	1,14	2,00	2,71

a) rate of permeation in mM per 3600 s.

b) defined as the ratio of L-L and L-D isomers permeation rates.

It is worth nothing, that the addition of carrier to the membrane phase accelerated the transport with simultaneous decrease of its stereoselectivity.

We have also studied the possibility of separation of amino acids from their mixtures with their phosphonic analogues. If the mixtures of valine and peptide 1a, or leucine 2b ($R=CH_2CH(CH_3)_2$) were used the separation was achieved. The tlc studies indicate that amino acids are better transported than their phosphonic counterparts regardless of the presence or absence of carrier.

REFERENCES

1. K.King, *Angew.Chem.*, 82, 343 (1970)
2. E.Weber, *Kontakte (Darmstadt)*, 1, 26 (1984)
3. J.P.Behr, J.M.Lehn, *J.Am.Chem.Soc.*, 95, 6108 (1973)
4. K.Maruyama, H.Tsukabe, *J.Chem.Soc.Chem.Commun.*, 966 (1980)
5. M.Newcomb, J.L.Toner, R.C.Hegelson, D.J.Cram, *J.Am.Chem.Soc.*, 101, 494 (1979)
6. H.Tsukabe, *Tetrahedron Lett.*, 22, 3981 (1981)
7. H.Tsukabe, *Tetrahedron Lett.*, 22, 1519 (1981)
8. K.Maruyama, H.Tsukabe, T.Araki, *J.Am.Chem.Soc.*, 104, 5197 (1982)
9. K.Maruyama, H.Tsukabe, T.Araki, *Tetrahedron Lett.* 22, 2001 (1981)
10. N.N.Li, *Ind.Eng.Chem.Process Des.Dev.*, 10, 215 (1971)
11. P.Kafarski, B.Lejczak, P.Mastalerz, J.Szewczyk, C.Wasielewski, *Can.J.Chem.*, 60, 3081 (1982)
12. B.Lejczak, P.Kafarski, J.Szewczyk, *Synthesis* 412 (1982)
13. B.Lejczak, P.Kafarski, P.Matalerz, *J.Chromatogr.* 324, 455 (1985)
14. P.Pluciński, *Tenside Detergents* 22, 18 (1985)
15. P.Pluciński, *J.Membr.Sci.*, 23, 105 (1985)
16. N.J.Schick, *Nonionic Surfactants*, M.Dekker Inc., New York 1967

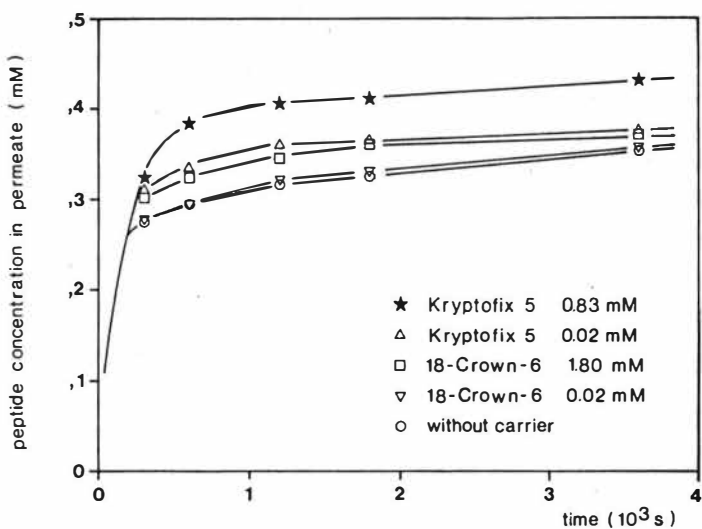


Fig.1 Concentration of valine (2a) in permeate during the process.
Concentration of Rokwin 60 - 4%.

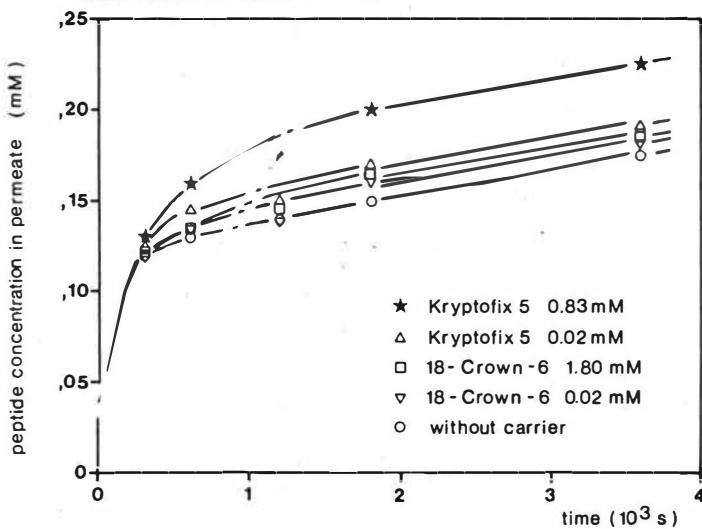


Fig.2 Concentration of 1-(N-L-valylamino)ethanephosphonic acid (1a) in permeate during the process.
Rokwin 60 concentration - 4%.

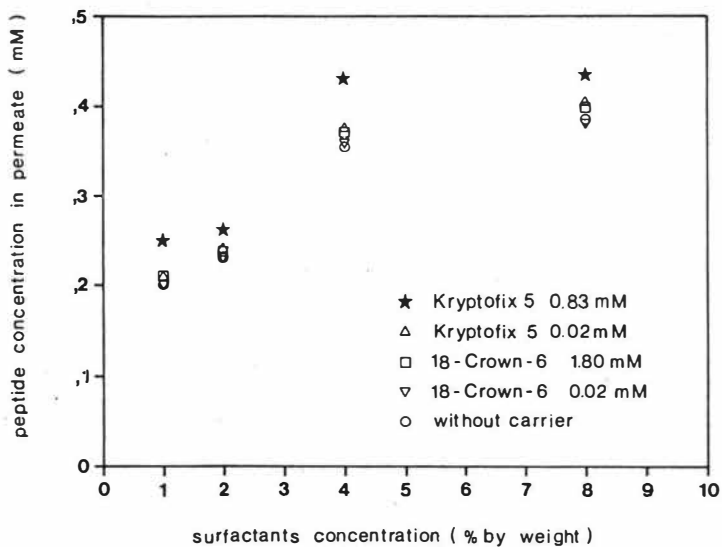


Fig.3 The influence of Rokwin 60 concentration on permeation of valine (2a) after 3600 s of the process.

Liquid Membrane Extraction of Aminoacids

G.A.Yagodin, E.V.Yurtov, A.S.Golubkov, Moscow Mendeleev College of Chemical Engineering, Moscow, USSR

The modern development of biotechnology is closely connected not only with the improvement of microbiological synthesis but also with the creation of new separation methods of microbiological products. One of the characteristic features of the fermentation liquids formed is a relatively low content of the end product. Therefore separation and concentrating operations contribute considerably (over 20 %) to the cost of the final product. In order to improve such operations and to decrease losses with waste water the method of membrane extraction has been suggested, in particular, its multi-emulsion modification. Multi-emulsions for extracting organic substances are extensively studied of late (1,2).

The potentialities of the method for extraction of aminoacids from their aqueous solutions of low concentrations have been studied in the case of one of indispensable aminoacids, viz. lysin (LYS). The liquid membrane for the emulsion preparation consists of vaseline and non-toxic vacuum oils with additions of surfactants, namely sorbitanoleate and some others.

In solution LYS exists as an ion with different net charge depending on the pH of the medium. At 2 + 3 pH (as is the case in those experiments) LYS is a cation. Consequently di (2-ethylhexyl) phosphoric acid (D2EHPA) is used as a carrier in membrane phase which results in the cation mechanism of LYS transport through the membrane. 1 N hydrochloric acid is used as the internal phase of the emulsion since inorganic acids are effective stripping agents for LYS re-extraction from the membrane phase and LYS monochlorhydrate resulting from HCl stripping is a commodity output of microbiological production (Fig. 1).

The percentage of the components was determined on the basis of the appropriate rate of LYS mass transport and the emulsion stability. Thus an increase in D2EHPA concentration in the

membrane and that of HCl in the internal phase results in a decrease of the semi-breakdown time ($\tau_{1/2}$) of the emulsion. The concentration of HCl over the range from 0.5 N to 1 N should be made up for by an increase in the surfactant concentration in the membrane from 4 to 9 volum.% (v.%) respectively. At the surfactant concentration of 7 + 10 v.% sufficient stability is found for emulsions whose D2EHPA concentration in the membrane does not exceed 15 v.%. Emulsions containing 6 + 9 v.% of surfactant and 10 + 15 v.% of D2EHPA in the membrane phase are best suited for LYS extraction.

The stability of liquid membranes is influenced by the phase ratio in emulsion. For the same surfactant concentration in membrane $\tau_{1/2}$ increases with increase of internal phase volume then there is a peak on the plot (76 + 77 v.% of internal phase for 10 v.% of surfactant in membrane) and then it begins to decrease. In the case of breakdown of emulsion with significant HCl volume the "excess" of internal phase (more than 76 + 77 v.%) is quickly separated at first, then the rate of breakdown becomes lower.

The presence of the carrier in the membrane phase practically has no effect on the purity of the LYS obtained. It is the distribution coefficient between the aqueous phase and the membrane and not the solubility of D2EHPA that determine its concentration in the external and internal phases. Thus, during LYS extraction with emulsion containing 10 v.% of D2EHPA the concentration of the latter amounts to 0.01 kg/m^3 , an order of magnitude below its solubility.

LYS extraction from model solutions of low concentrations (about 1 kg/m^3) has been carried out. For performing the emulsion extraction process it is essential that the process of the emulsion semi-breakdown should last much longer than that of extraction. However, the emulsion should be liable to ready breaking after the extraction in order to obtain the internal phase enriched in the end component. The thermal breakdown is a two-stage process: at a temperature as low as 60°C over 95 v.% of the emulsion is broken down in 10 + 15 min.

while at 80 °C it takes 4 + 5 min. The remainder of the emulsion containing 3 + 4 v.% of the internal phase breaks in the course of a few days irrespective of temperature (Fig. 2 - a).

The two stages of the breakdown confirm the presence of a microemulsion in the liquid membrane that may be responsible along with molecular diffusion for LYS transport through liquid membrane.

The breakdown of emulsions at elevated temperatures appears to be caused by two factors. First, as the temperature rises surfactant adsorption on the surface of the internal phase droplets decreases, i.e. desorption from this surface increases. Losing their protective cover the internal phase droplets coalesce. On the other hand, the breakdown of the emulsions is accounted for their thermodynamic instability. A temperature increase results in the relaxation of surface tension at the interface. Coalescence causes reduction in the interfacial area, i.e. in this case the process is spontaneous.

The stabilization of the emulsion is observed in the course of extraction: after the extraction the emulsion proves to be more viscous as compared with the initial one. As the extraction time increases up to a certain limit, the viscosity also increases. One of the factors responsible for the stabilization is the shift of pH values in the internal phase of the emulsion to a neutral range resulting from the swelling phenomenon (water permeation into the internal phase) caused by the osmotic pressure gradient through the membrane. LYS transport through a surfactant-containing membrane was observed in the absence of an extracting carrier, it can be regarded as evidence for the micellar mechanism of water transport through the liquid membrane (3).

The emulsion stabilization enables its residence time in the apparatus to be prolonged on account of an increase of the semi-breakdown period. On the other hand, extreme stabilization adversely affects the ability of the emulsion to break after the extraction (Fig. 2 - b,c,d).

The emulsion swelling (S) was estimated as per cent ratio between the change of the volume of the internal emulsion phase during extraction and its original volume.

The emulsion swelling exerts a considerable influence on the LYS concentration in the course of the extraction. Provided the water transport were completely eliminated, LYS concentration in the internal phase could be several times higher. If 1 N HCl is constantly used as an internal phase swelling is dependent on the surfactant concentration and phase ratio in the emulsion. A 1 % decrease in the surfactant content in the membrane results in a 20 + 30 % reduction in the emulsion swelling.

However emulsions where the surfactant concentration is below 5 + 6 v.% exhibit low stability (their semi-breakdown period is as little as 50 min. and even less). Provided the surfactant concentration is fixed water transport can be regulated by changing the emulsion phase ratio. Thus, the addition of another 5 ml of an acid to an emulsion containing 8 v.% of surfactant during its preparation causes a 35 % increase in its swelling.

For the suggested emulsion compositions where the membrane phase makes up 78 v.% of vacuum oil, D2EHFA makes up 15 v.% and the surfactant - 7 v.% and with 1 N HCl as the internal phase (the ratio between the membrane and internal phases is 1 : 2), swelling constitutes 95 %, the fraction extracted of LYS is 94 %, LYS concentration in the internal phase after extraction is 15 kg/m^3 , and the yield of crystalline LYS monochlorhydrate is 70 %.

Experiments show the extraction to proceed much faster than the emulsion swelling (the correspondind mass transfer coefficients have different orders of magnitude). Therefore, it is necessary to choose the optimum time of the emulsion residence in the extractor, that would ensure the most complete extraction of the end component and prevent further swelling (Fig. 3). For this purpose, we used the Harrington method according to the generalized desirability function. The optimal time of the emulsion residence in the apparatus proved to be much lower than

its semi-breakdown period. Thus, for the "LYS solution - extracting emulsion" phase ratio equal to 1 : 1, the residence time of the emulsion in the extractor is 2.0 ± 0.3 min.

Thus, liquid membrane extraction may be an effective means of extracting aminiocids, LYS in particular. In combination with other separation and purification techniques it may be used as one of the elements of wasteless technological schemes. The combination of extraction and stripping in one stage may replace multi-stage separation processes in microbiological production. The choice of the optimal composition of the membrane and internal emulsion phases may ensure the suitable extraction rate and the process selectivity with the simultaneous of the end product.

REFERENCES

- (1) Halwachs W., Völkel W., Schugerl K., Proceedings ISEC'80, pap. 80 - 88.
- (2) Yagodin G., Lopukhin Y., Yurtov E. et al, Proceedings ISEC'83, pap. 385 - 386.
- (3) Yagodin G., Ivakhno S., Gusev V., et al, "Doklady Akademii Nauk SSSR", USSR, Moscow, vol.226, № 5, p. 1198 -1201 (1982).

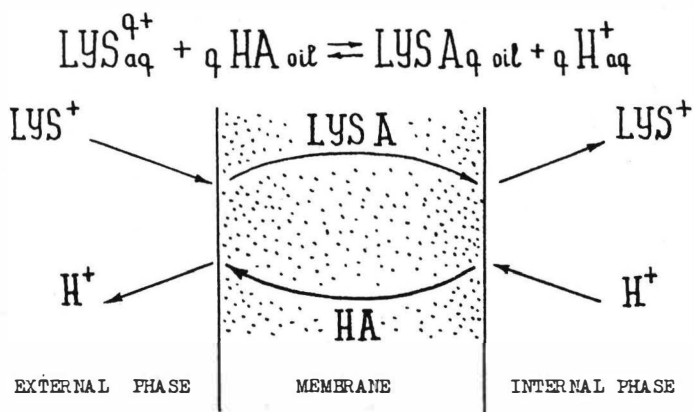


FIG. 1. SCHEMATIC REPRESENTATION OF LYS TRANSFER THROUGH LIQUID MEMBRANE.

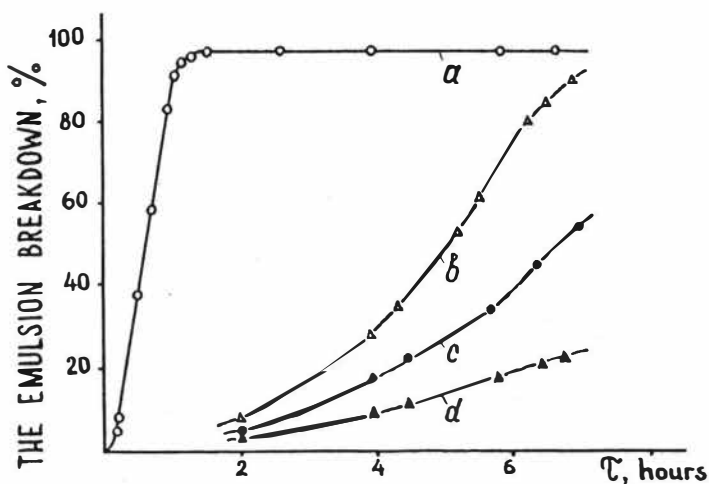


FIG. 2. THE EMULSION BREAKDOWN AT 40 °C.

a - INITIAL EMULSION,
 b, c, d - THE EMULSION AFTER 1, 2, 3-HOUR EXTRACTION,
 RESPECTIVELY.

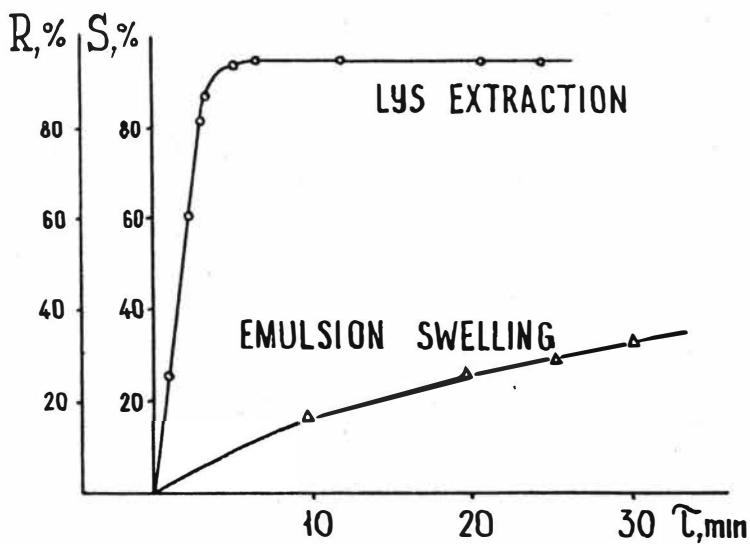


FIG. 3. THE COMPARISON OF THE EXTRACTION AND THE SWELLING RATES.
 (R - RECOVERY FACTOR, S - EMULSION SWELLING).

Separation of Amino Acids from Fermentation Broth Using Liquid Emulsion Membranes

M.P. Thien, T.A. Hatton, D.I.C. Wang, M.I.T., Cambridge, MA, U.S.A.

Traditionally, the "downstream processing" of biochemicals has had the two-fold goals of separation and purification. Liquid emulsion membranes are well-suited for both of these functions. Since their introduction in 1968 (1), liquid emulsion membranes (LEMs) have been considered for the commercial separation of heavy metals (2), the recovery of rare earths and fission products from process streams (3), and the removal of organics from wastewater streams (4). To date, however, biochemical separations using LEMs have been limited to biomedical applications (5,6). The apparent potential for the applications of LEMs in the area of biotechnology has prompted us to examine the LEM-mediated separation of several biochemicals. In this paper we report our progress in applying LEMs to the separation of α -amino acids from fermentation broths. An extended account of our work is to be published elsewhere (7). While exploring this system, we also hope to delineate further the role of various process parameters on LEM-mediated separations as well as establishing the importance of osmotic swelling in LEM separation processes.

FACILITATED TRANSPORT SYSTEMS FOR AMINO ACID SEPARATIONS

Most of the LEM systems studied for metal separations have been of the facilitated transport or "TYPE II" (8) class. These systems typically utilize an oil-soluble carrier in the oil phase and either a high concentration of counter-ion or a solute-specific reagent in the interior phase as driving forces for the separation. Amino acids, due to their zwitterionic nature, are not by themselves appreciably soluble in organic solvents. At high pH, they are predominantly present as anions (as opposed to zwitterions). We have thus considered a simple carrier-mediated chloride counter-transport system which separates the amino acid in its anionic form (see Figure 1). This system uses a chloride gradient across the membrane as the driving force. A non-specific anion complexing agent is used as the carrier and facilitates the separation of the amino acid.

EXPERIMENTAL

All experiments were conducted batch-wise in a two-liter baffled glass vessel at 25°C as reported elsewhere (9). Agitation speed was kept constant at 400 RPM. Membrane phases consisted of a long-chain paraffinic solvent (Solvent 100 Neutral; Exxon USA), decyl alcohol as a co-surfactant (Sigma Chemical, USA), a poly-amine (Paranox 100, Exxon Chemical) or sorbitan mono-oleate (Span 80, Atlas Chemical, USA) as the emulsion-stabilizing surfactant, and tri-capryl ammonium chloride as the carrier (Aliquat 336, Henkel Corporation, USA). Exterior phases typically consisted of L-Phenylalanine (Sigma Chemical, USA) brought to pH 11 with NaOH. All chemicals were used as supplied. Phase compositions for the experiments are given in Table I. All membranes containing 4% v/v Paranox 100 had similar internal droplet size distributions after emulsification.

Exterior phase phenylalanine concentrations were measured using UV spectrophotometry

at a wavelength of 257.7 nm. Interior droplet size distributions were measured by centrifugal analysis using a CAPA-500 particle size analyser (Horiba Corporation, Japan). Osmotic swelling of the emulsion and interior phenylalanine concentration were estimated by mass and material balances. These estimates were corroborated by thermal demulsification of the emulsion and direct measurement of phenylalanine and potassium concentrations. Estimates agreed with direct measurements to within 10%.

RESULTS

The process currently being examined is the separation of amino acids from fermentation broth. These broths typically contain mineral salts required for microbial growth at concentrations ranging from 0.01 to 0.2 M. This being the case, an especially important concern in applying LEMs to biochemical separations is the influence of ions other than those of the desired solute on separation. Previous authors have examined the influence of "competing" solutes in LEM separations both for simple diffusion type membranes (10) and for the separation of one heavy metal from another in facilitated transport LEM separations (11). To date, however, no effort has been made to assess the effect of competitive ions on nonspecific carriers in biochemical LEM processes. In order to assess the effects of "contaminating" ions in the exterior phase on LEM facilitated transport separations, we conducted a series of experiments in which anionic phenylalanine was separated in the presence of various concentrations of sulfate anion, SO_4^{2-} (present as sodium sulfate, Na_2SO_4). The concentration range studied, 0.0 to 0.2 M SO_4^{2-} , was typical of the salt concentration present in fermentation broth. The results of this study are shown in Figures 2 and 3. The percent extraction $[\text{Phe}]^0 - [\text{Phe}]^f / [\text{Phe}]^0$ of phenylalanine from the exterior phase after forty minutes is plotted versus initial exterior phase sulfate concentration in Figure 2. As can be seen from the figure, the final extraction decreases markedly as the sulfate concentration is increased. It appears that at low sulfate concentrations, increases in $[\text{SO}_4^{2-}]$ cause significant decreases in the amount of amino acid extracted. As the concentration of sulfate is increased, the rate of change of amino acid extracted becomes smaller and eventually appears to reach a constant value.

It has been noted (9) that although exterior concentration profiles are useful in determining the extent of extraction from an LEM separation, such profiles contain no information regarding the possibility of changes in the various phase volumes (changes caused by membrane breakage and membrane swelling). In addition, biochemical downstream processing is concerned with the amount of extraction as well as with the concentration of the separated solute. The latter parameter is a quantity that can be drastically affected by changes in interior volume. With this in mind, Figure 3 shows what happens to the interior phase as a function of sulfate concentration. V_{mem} is the percent change in volume of the interior phase based on original interior phase volume. Negative values of V_{mem} correspond to membrane breakage while positive values correspond to membrane swelling. $[\text{Phe}]^{\text{int}}$ is the final interior phenylalanine concentration after 40 minutes contact time. As can be seen, both V_{mem} (always a positive quantity) and the interior phenylalanine concentrations appear to decrease

linearly with increases in initial exterior sulfate.

Another concern of those wishing to apply LEM technology to bioseparations is the maintenance of membrane integrity. Previous workers have noted that membrane stability (12) and, purportedly to a lesser extent, membrane swelling (13,14) are two of the most significant process problems in the application of LEM to commercial scale separations. Both of these potential difficulties can be attributed, in part, to the formulation of the membrane phase (15). This being the case, the next parameter we studied was that of non-ionic surfactant type and concentration. The standard formulation given in Table I for emulsion and exterior phase compositions was used for the surfactant trials and the results are given in Table II. In this table, V_{mem} is as defined previously and $[Phe]^f$ is the concentration of phenylalanine in the exterior phase measured in grams per liter after forty minutes contact time.

Although no quantitative conclusions can be made from Table II, several quantitative observations can be stated. First, from the data using Span 80 in the absence of Paranox 100, the negative values of V_{mem} indicate significant breakage occurs for almost all concentrations of Span 80. This breakage results in essentially no separation (as is reflected by the essentially unchanged $[Phe]^f$). In contrast to the negative values of V_{mem} for Span 80, the positive values of V_{mem} for Paranox 100 indicate that the interior phase has experienced swelling. Previous experiments (9) have indicated that membrane swelling is due to water transported across the membrane by the surfactant and that this swelling increases monotonically as a function of contact time. The data for Paranox 100 readily indicate that the amount of swelling increases (up to a point) with increases in the concentration of surfactant. Finally, the data for mixed surfactants in the membrane phase indicate that, while separation is not drastically affected by the addition of any particular surfactant (as is seen in the insignificant change in $[Phe]^f$ for the surfactant mixtures), the amount of swelling (and presumably the concentration of solute in the interior phase) is affected significantly as indicated by the considerable changes in V_{mem} .

Another parameter of importance is that of the carrier concentration. While other workers have examined the effects of varying carrier concentration on separation (16), none has examined the effect of carrier concentration on interior phase solute concentration. More appropriately stated, no effort to date has been made to examine the effects of carrier concentration on membrane breakage and membrane swell. We conducted experiments in which only the carrier concentration was varied. Figure 4 shows the exterior phase concentration versus time profile for several different concentrations of carriers. Initial solute transfer rates increase as the concentration of carrier is increased. The separation effected for the higher carrier concentrations approaches what appears to be an equilibrium value after a sufficient period of time. As stated previously, however, the exterior concentration versus time profile gives no information as to the possible changes in the volumes of the various phases as a function of time. In Figure 5 is plotted the estimated interior phase

phenylalanine concentration and V_{mem} (percentage based on initial interior phase volume) after 40 minutes contact time for the various concentrations of carrier. The data indicate that the volume of the interior phase increases dramatically as the amount of carrier increases. The non-zero intercept on the V_{mem} versus carrier concentration curve can no doubt be attributed to swelling mediated by the non-ionic surfactant.

Discussion

We believe that the results shown above have several important ramifications on the possible application of LEMs to biochemical separations, and to LEM-mediated separations in general. The effect of competitive ions in the exterior phase represents an interesting combination of opposing effects. Due to the solute non-specific nature of the carrier (17), the chloride gradient, the driving force for the separation of amino acids from the exterior phase, is also used in part to effect transport of the undesired sulfate anion across the membrane. The resulting competition between the amino acid and the sulfate anion reduces both the initial flux of the amino acid and reduces the overall extraction and interior phase concentration of the desired solute. The importance as to the nature of the solute is demonstrated by the fact that although the "contaminating" anion becomes as much as ten times as concentrated as the desired solute, the total extraction of the desired solute is only decreased by about 30%.

Lessening the severity of the decrease in extraction caused by competition is the decrease in swelling which occurs with increases in exterior phase total ion concentration. As the initial amount of sulfate in the exterior phase is increased, the difference in ionic strength across the membrane is decreased. In decreasing the difference in ionic strength and thus decreasing the difference in water activities across the membrane, the driving force for membrane swell is diminished. It is unfortunate that the magnitude of the decrease in swell does not make up for the decrease in the amount of phenylalanine extracted.

The surfactant studies also have significant implications for LEM-mediated separations. The results from the Span 80 experiments show that, at least for the system in question, Span 80 does not properly stabilize the LEM. This is an interesting finding, being that many of the membrane formulations in the LEM literature utilize Span 80 as the sole stabilizing surfactant. With the pervasive use of Span 80 in past LEM experiments, it is not difficult to see why Stroeve and Varanasi were (12) prompted to remark in 1982: "At present, the widespread use of LEM's as a separation system in industrial processes has not been possible due to problems of (membrane) stability." It is obvious from the results of the Paranox 100 formulation experiments above as well as data reported elsewhere (14) that stability is not a problem if the proper surfactant is used. Indeed, from the Paranox 100 results above, it appears that membrane swell is much more of a problem than is membrane breakage.

Several mechanisms for emulsion swell have been proposed in the emulsion and LEM literature (18,19). All of these mechanisms incorporate the assumption that water

transport across the membrane is somehow mediated by the emulsion-stabilizing surfactant and that the driving force for this transport is the difference in water activities across the membrane resulting from the vastly different ionic strengths on either side of the membrane. Thus, the increase in swell with increase in surfactant concentration shown in Table II is not a surprising observation.

Also not surprising are the increases in initial solute transport rates as the concentration of carrier is increased (Figure 3). This result has been shown by previous authors (16). Much more interesting is the change in swell with changes in carrier concentration. The increase in membrane swell with increases in carrier concentration has not, to our knowledge, been reported in the literature. It is our conjecture that carrier-induced swell is caused by the hydration of carrier at the exterior/membrane interface and the subsequent transport of water across the membrane by the carrier/solute/water complex. This scenario is essentially the proposed model for surfactant-induced swelling of Colinart *et al.* (18) with the surfactant being replaced by the carrier/solute complex. The ramifications of this development focus on the formulation of the membrane phase. When finding the "optimum" concentration of carrier in the membrane phase, the adverse effects of increased swelling and the resulting more dilute interior phase solute concentration must be weighed against the increases in initial solute transport rates resulting from increases in carrier concentration.

Conclusions

Liquid emulsion membrane systems can be applied to the separation of biochemicals from fermentation broth. A significant process consideration for such applications is the competitive effect produced by anions other than the desired solute. In addition, both surfactant-mediated and carrier-mediated swelling of the membrane are important to consider.

Acknowledgements

This work was funded in part by a Monsanto Junior Faculty Award to T.A. Hatton. The authors would like to express their appreciation for the laboratory assistance of Linda Marinilli, Todd Renshaw, and Byron Stewart.

Literature

1. N.N. Li; U.S. Patent #3410794 (1968).
2. J. Frankenfeld, R.P. Cahn, and N.N. Li, Sep. Sci. Tech., **16**, p. 385 (1981).
3. H. Hayworth, W.S. Ho, and W.A. Burns, Sep. Sci. Tech., **18**, p. 493 (1983).
4. N.N. Li and A.L. Shrier, Rec. Dev. Sep. Sci., Vol. I, p. 163 (1972).
5. C.W. Chang, C.C. Fuce, J. Frankenfeld, and C.T. Rhodes, J. Pharm. Sci., **67**, p. 63 (1978).
6. T.T. Yang and C.T. Rhodes, J. App. Biochem., **2**, p. 7 (1980).
7. M.P. Thien, T.A. Hatton, and D.I.C. Wang, to be published in Biotech. and Bioeng.
8. E.S. Matulevicius and N.N. Li, Sep. Pur. Meth., **4**, p. 73 (1975).
9. M.P. Thien, T.A. Hatton, and D.I.C. Wang, ACS Symp. Series, in press.
10. R.S. Baird, A.L. Bunge, and R.D. Noble, "Batch Extraction of Amines Using Emulsion Liquid Membranes: Importance of Reaction Reversibility," to be published.

11. E.J. Fuller and N.N. Li, J. Mem. Sci., **19**, p. 155 (1984).
12. P. Stroeve and P. Varanasi, Sep. Pur. Meth., **11**, p. 29 (1982).
13. R.E. Terry, N.N. Li, and W.S. Ho, J. Mem. Sci., **10**, p. 305 (1982).
14. R.P. Cahn, J. Frankenfeld, N.N. Li, D. Naden, and K.N. Subramanian, Rec. Dev. Sep. Sci., Vol. VI, p. 51 (1982).
15. F. Marr and A. Kopp, Int. Chem. Eng., **22**, p. 44 (1982).
16. W. Volkel, W. Halwachs, and K. Schugerl, J. Mem. Sci., **6**, p. 19 (1981).
17. J.M. Lehn and J.P. Behr, J.A.C.S., **95**, p. 6108 (1973).
18. P. Colinart, S. Delepire, G. Trouve, and H. Renon, J. Mem. Sci., **20**, p. 167 (1984).
19. A.T. Florence and D. Whitehill, J. Coll. Int. Sci., **79**, p. 243-256.

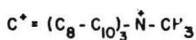
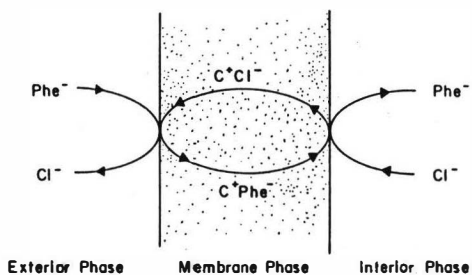


Figure 1. Schematic diagram of a chloride counter-transport LEM process for L-phenylalanine separation.

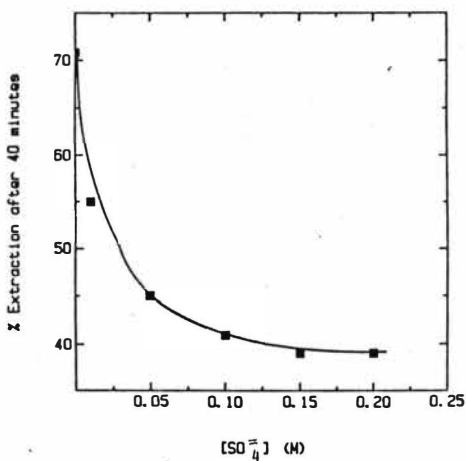


Figure 2. % Extraction of phenylalanine from Exterior phase versus initial exterior phase sulfate concentration.

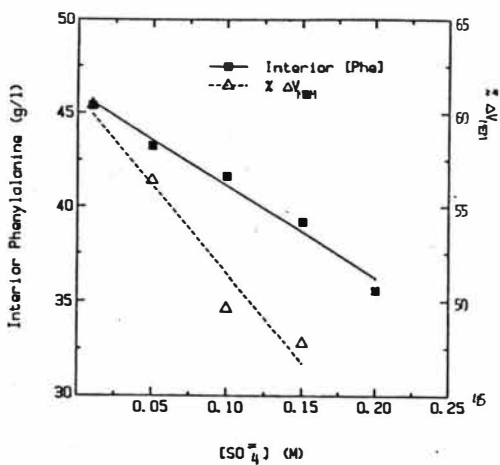


Figure 3. % V_{mem} and interior phase phenylalanine concentration versus initial exterior phase sulfate concentration.

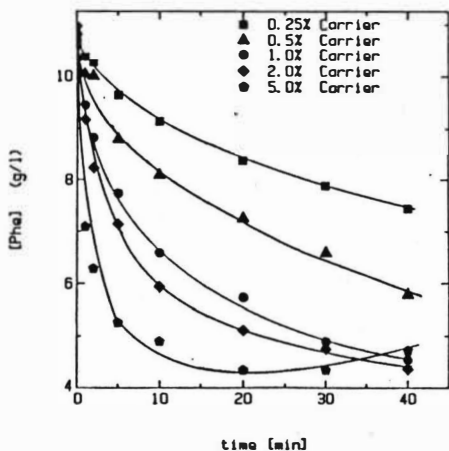


Figure 4. % Extraction of phenylalanine from exterior phase versus carrier concentration (% v/v).

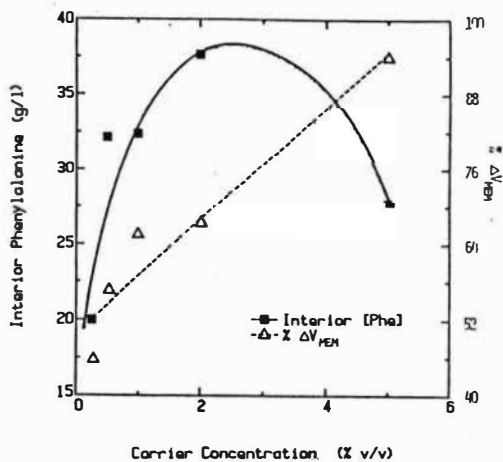


Figure 5. % V_{mem} and interior phenylalanine concentration versus carrier concentration (% v/v).

Table I: Typical Composition of System for LEM Separation of Phenylalanine

Interior Phase (70 milliliters):

2.0 M KCl
pH 11.0 with KOH

Membrane Phase* (100 milliliters):

92 % Solvent 100 Neutral
5 % Decyl Alcohol
4 % Paranox 100
1 % Aliquat 336

* % v/v

Exterior Phase (700 milliliters):

11.5 g/l L-phenylalanine
pH 11.0 with NaOH

Table II: Effect of Surfactant Type and Concentration on LEM Separation of Phenylalanine

<u>% Span 80*</u>	<u>% Paranox 100*</u>	<u>%V_{mem}</u>	<u>[Phe]^{f**}</u>
1.0	0.0	- 82	9.52
2.0	0.0	- 33	10.66
4.0	0.0	- 16	10.51
6.0	0.0	+ 21	10.12
0.0	1.0	+ 19	6.68
0.0	2.0	+ 35	5.74
0.0	4.0	+ 56	5.46
0.0	6.0	+ 58	5.86
1.0	1.0	+ 17	6.65
1.0	2.0	+ 52	5.68
2.0	1.0	+ 55	6.00
2.0	2.0	+ 69	5.73

* % v/v

** Measured in g/l; initial exterior phase [Phe] = 11.5 g/l

Liquid Surfactant Membrane Emulsions - A New Technique for
Enzyme Engineering

T.Scheper, K.Makryaleas, Z.Likidis, Ch.Nowotny, E.-R.Meyer, K. Schügerl

Institut für Technische Chemie, Universität Hannover

Liquid membranes are suitable to encapsulate enzymes. The liquid membrane immobilizes the enzymes, protects them from proteases, keeps them in their native environment and through the use of carriers, preselects the substrates permeating into the enzyme phase. It is also possible to obtain selective enrichment of one of the products of the enzymatic reaction. The use of liquid membrane reactors for enzymatic bioconversions has several advantages in comparison to solid membrane reactors and conventional immobilization techniques; there is no membrane fouling, enzyme emulsions can be used in cell-free fermentation broths, and substances which might decrease the enzyme activity can be excluded. The separation effect is not based on differences in molecular weight but in the chemical behaviour of the substances to be separated. Thus, it is not necessary to use cofactors with increased molecular weight for enzymatic reactions, since the coenzyme cannot permeate the liquid membrane. This cofactor can be regenerated continuously in the enzyme emulsion.

In the early 1970's N.N.Li first reported about the possibility to immobilize enzymes in liquid surfactant membrane emulsions. The results of our research work for different applications of enzyme emulsions are presented in this paper.

One of the most simple systems is the encapsulation of α -chymotrypsin in a kerosene organic phase. This enzyme emulsion hydrolyzes D,L-phenylalanine methyl ester into L-amino acid and D-ester /1/.

The second system is the encapsulation of penicillin-G-acylase. Penicillin permeates through the membrane (this transport is accelerated by the carrier LA-2 a secondary amine) and is hydrolyzed by the enzyme (Fig.1). 6-Amino-penicillanic acid is

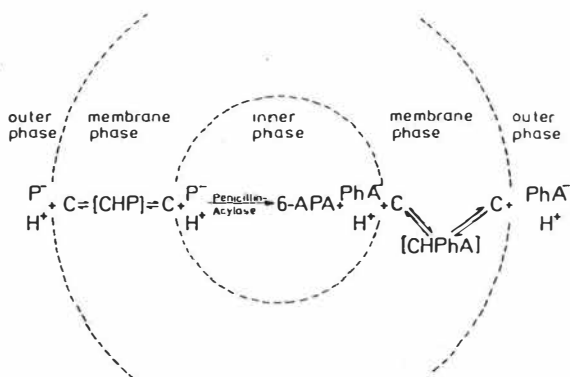


Figure 1 Reaction scheme of Penicillin-G-acylase

produced and enriched in the inner phase. The phenylacetic acid anion is transported to the outer phase by the anion exchanger LA-2. Batch tests for the extraction of Penicillin G from model solutions as well as from cell-free fermentation broths were performed.

The membrane composition is an important parameter for enrichment effectivity, as shown in Fig. 2. The concentration

courses of phenylacetic acid (PhA), 6-APA and Penicillin G (PG) in the outer phase are plotted for different types of membranes. In the upper plot, 7.5% Span 80 and 1.5% LA-2 were dissolved in the organic phase while in the lower plot 5% Span 80 and 1.5% LA-2 were utilized. Penicillin G decrease in the latter case is about 70% in 150 min. and in the former about 55% (however the undesired increase of 6-APA is nearly negligible using 7.5% 80 and 1.5% LA-2).

The variation of the carrier concentration also influences the membrane stability and the enrichment effectivity. A carrier concentration of 1% in the organic membrane phase is very favourable with regard to the high extraction (PG) and enrichment (6-APA) grade. All tests were performed with a membrane type of kerosene, 7.5% Span 80 and 1% LA-2.

It was also possible to work with this type of enzyme emulsion in a Kühni extractor column (10.5-l active volume) for the Penicillin G extraction in larger scale. After the extraction the emulsion was broken down in a continuously working electrocoalescence unit and the enzyme containing inner phase was used for the enzymatic synthesis of ampicillin by adding a precursor (D-phenylglycine methyl ester) and changing the pH-value of the inner phase.

As a more complex enzyme system, L-leucine-dehydrogenase and formatdehydrogenase were encapsulated with the coenzyme NAD^+ (native) in a paraffin emulsion (Fig.3). L-leucine-dehydrogenase catalyses the reductive amination of α -ketoisocaproate into L-leucine. During this reaction, NAD^+ is produced and it becomes reduced continuously by the second enzyme, the formate dehydrogenase. The same system is used by Wandrey and Kula for the L-Leucine production in a solid membrane reactor.

A suitable membrane phase is paraffin with 5% Span 80 (emulsifier) and 1% Adogen 464. Mass transfer limits the overall reaction rate. This is why the permeation coefficients of the

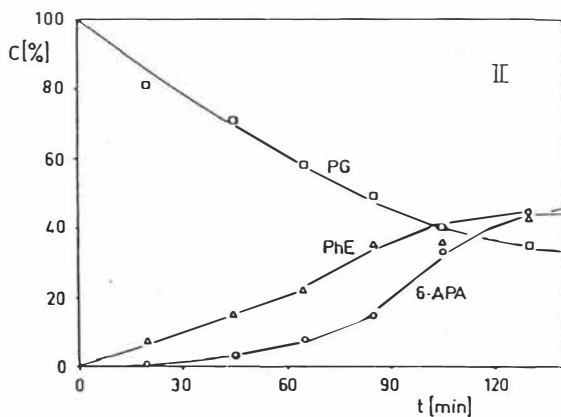
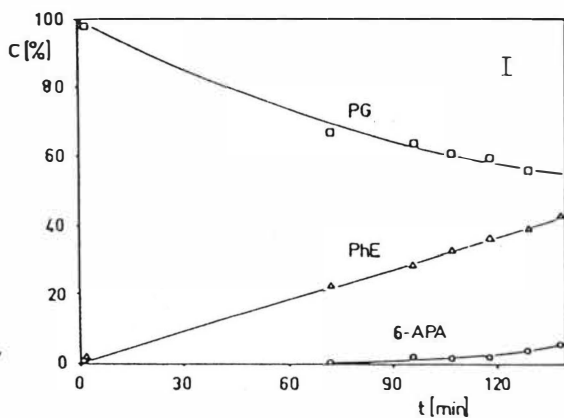


Figure 2 Influence of membrane composition (concentrations of Penicillin (PG), phenylacetic acid (PhE) and 6-Amino-penicillanic acid (6-APA) in the outer phase)

substrates and products were determined by solid-supported liquid membranes. Ammonium and formate have the lowest permeation coefficients and their permeation through the membrane limit the reaction (Fig.4). In continuous tests, the effluent was analyzed by means of a polarimeter (L-Leucine), a UV-photometer (α -ketoisocaproate), and a NH_3 -sensor (ammonium). Samples were analyzed in an amino acid analyzer. In Fig. 5 the results of a continuous test for the L-Leucine production is shown ($\approx 170\text{min}$; $\text{pH}=8.3$; $T=25^\circ\text{C}$; concentration caproate: 40mM/l ; concentration of LEUDH and FDH: 20 U/ml each; concentration NAD^+ : 3mM/l ; concentration ammonium formate: 440mM/l). A steady state is attained after 4 residence times.

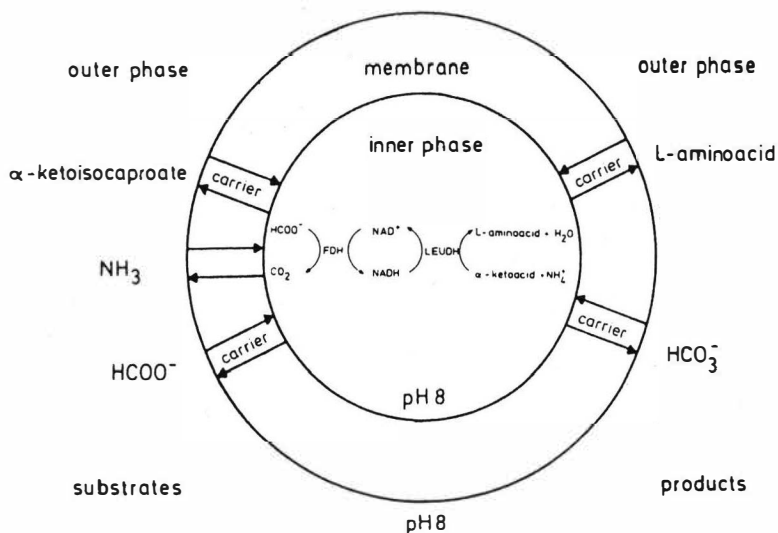


Figure 3 Reaction scheme of LEUDH-emulsion

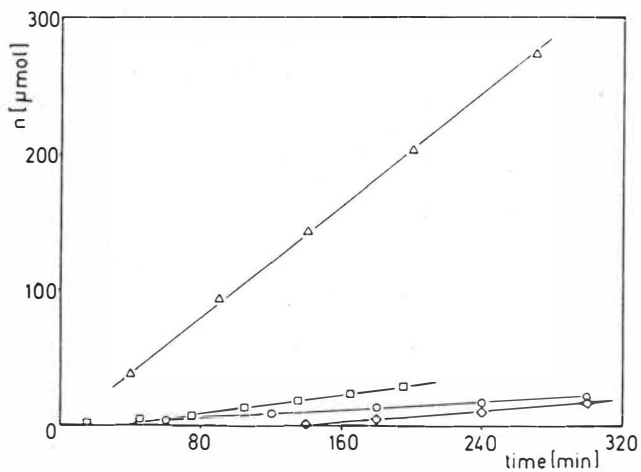


Figure 4 Permeation rates (Δ -L-leucine, \square - α -ketoglutarate, \diamond - ammonium, \circ - formate)

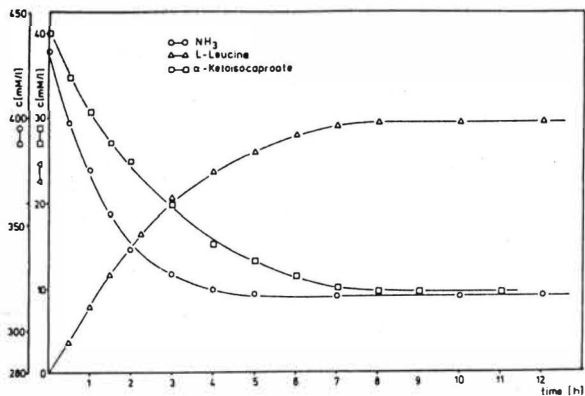


Figure 5 Concentration of substrate and products during a continuous test

Another system was tested for the enantioselective hydrolysis of a racemic mixture of 4-Acetoxycyclopent-2-en-1-ol. For this purpose, pig-liver-esterase was encapsulated. During the reaction the (R)-carbinol and the (S)-ester are formed. Both products are highly interesting for prostaglandin synthesis. The carbinol is produced and enriched in the inner phase of the enzyme emulsion. The reaction scheme is shown in Fig.6 and some of the results are shown in Fig.7 (○ 133 μ l enzyme in the inner paraffin phase, ▼ 200 μ l native enzyme, □ 200 μ l enzyme after contact to organic phase, Δ 100 mg esterase from *Trichoderma reesei*). The conversion rate with the pig-liver-esterase emulsion is lower compared to the native enzyme but the enantiomeric excess is higher (over 50% compared to 30% with native enzyme)

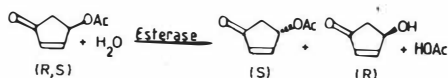


Figure 6 Reaction scheme for enantioselective hydrolysis

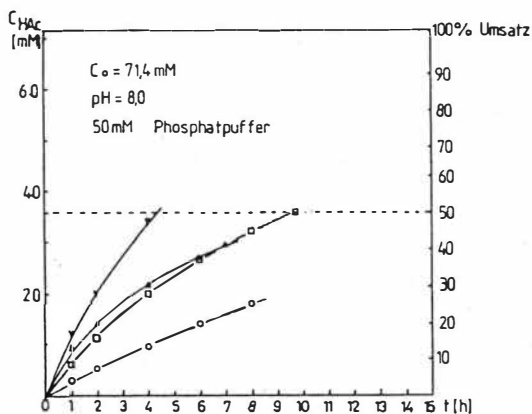


Figure 7 Conversion of substrate under different conditions

References:

/1/ Th. Scheper, W. Halwachs, K. Schügerl, (1983), Preparation of L-amino acids by means of continuous enzyme catalyzed D,L-amino acid ester hydrolysis inside liquid surfactant membranes, ISEC 83, Denver/Colorado

SEPARATION OF AQUEOUS TWO-PHASE SYSTEMS BY GRAVITY SETTLING

K.H. Kroner, H. Hustedt, GBF, Gesellschaft für Biotechnologische Forschung mbH., D-3300 Braunschweig, FRG.

Introduction

Aqueous two-phase systems (APS) have been described as useful for the extractive purification of enzymes in large scale (1) and also applications in bioconversion processes (2). Albertsson (3) has described these systems and their use in biochemical research basically. The speciality of these ternary phase systems is that both phases contain a large amount of water which makes them very suitable for partition of biomolecules. But for technical processing of such systems the differences in the physico-chemical parameters in comparison to other common extraction systems have to be considered; mainly the interfacial tension is low and the viscosity difference between the phases can be large, especially when solid biomass is included. In spite of this APS behave generally as true liquid-liquid dispersions (also when including cell material) and the use of common techniques and equipment from extraction technology can be adapted. Under this view gravity settling may be of interest, because of its simple design and low cost equipment to improve the economy of protein extraction in APS. So far, only few data has been reported with respect to gravity settling and the implications of the physico-chemical parameters of APS. The aim of this work was to carry out some basic studies, determining the influencing parameters and describing the behaviour in batchwise and continuous settling experiments.

Results

1. Physico-chemical parameters

For the basic studies two model systems have been selected, which are representative for the most of the technical used APS

- PEG 1550, potassium phosphate (pH 7.0)
- PEG 4000, Dextran 500.

First a set of systems with different compositions are prepared and analyzed (for details see ref. 3). The interfacial tension was measured with a Spinning drop tensiometer (Krüss, Hamburg, FRG), the densities of the phases were determined with an Oscillodensitometer (Parr, Graz, Austria) and viscosities of the phases were measured with a Cuvette viscosimeter (Contraves, Stuttgart, FRG). Table 1 and 2 show the collected data. All parameters examined changes with increasing tie-line length. In the case of the PEG-Dextran systems the data show quite low interfacial tensions in the range from $3.1 \cdot 10^{-4}$ - $4.1 \cdot 10^{-2}$ mN/m and density differences between the phases of $18-79 \text{ kg/m}^3$. The viscosity of the continuous PEG-rich phase changes only slightly ($\sim 4 \text{ mPa}\cdot\text{s}$).

Table 1: Physico-chemical data of PEG 1550 / potassium phosphate*
two-phase systems

PEG (%)	potassium phosphate (%)	tie-line length (%)	volume ratio (V_t/V_b)	$\Delta\rho$ (kg/m^3)	η_{top} ($\text{mPa}\cdot\text{s}$)	η_{bott} ($\text{mPa}\cdot\text{s}$)	σ (mN/m)
11.0	12.4	5.6	0.9	38	5.7	2.0	$0.1 \cdot 10^{-1}$
14.0	12.0	21.9	1.3	70	7.8	1.9	$1 \cdot 10^{-1}$
16.0	12.0	27.8	1.4	82	9.7	1.9	$2.2 \cdot 10^{-1}$
19.0	12.0	35.7	1.4	108	12.9	2.4	$5.1 \cdot 10^{-1}$

*) pH = 7.0

Table 2: Physico-chemical data of PEG 4000 / Dextran 500* two-phase systems

PEG (%)	dextran (%)	tie-line length (%)	volume ratio (V_t/V_b)	$\Delta\rho$ (kg/m^3)	η_{top} ($\text{mPa}\cdot\text{s}$)	η_{bott} ($\text{mPa}\cdot\text{s}$)	σ (mN/m)
6.0	5.8	6.2	1.5	18	4.1	43	$0.03 \cdot 10^{-2}$
6.5	6.1	10.5	1.4	32	3.6	100	$0.12 \cdot 10^{-2}$
7.0	6.6	14.4	1.5	48	3.7	145	$0.81 \cdot 10^{-2}$
8.0	7.6	19.8	1.7	64	4.3	303	$2.0 \cdot 10^{-2}$
9.0	8.5	24.8	1.9	79	4.4	364	$4.1 \cdot 10^{-2}$

*) systems include 1 mM-potassium phosphate buffer, pH 7.0;

Dextran 500 was purchased from Pfeiffer & Langen, Dormagen, FRG

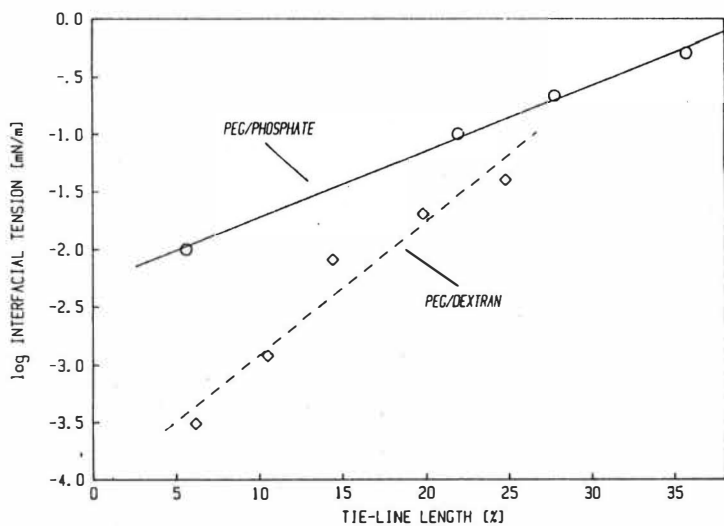


Fig. 1: Interfacial tension of APS in dependence on tie-line length

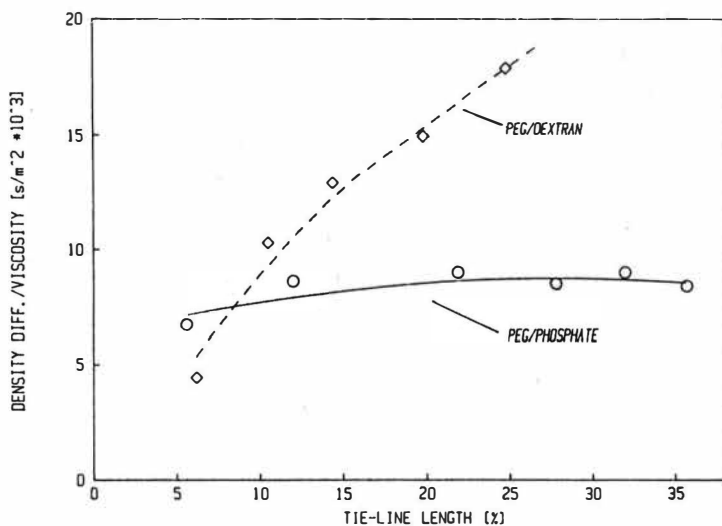


Fig. 2: Change of density difference / viscosity quotient with the tie-line length

In the case of the PEG/salt system the interfacial tension is 1-2 orders of magnitude higher (10^{-2} - $5.1 \cdot 10^{-1}$ mN/m); the density differences and viscosities are slightly higher (38-108 kg/m³, resp. 5.7 - 12.9 mPa·s). Thus, a different settling behaviour for both types of systems can be expected and are generally observed.

Fig. 1 shows a linear relation between the logarithm of the interfacial tension and the length of the tie-line, this agrees well with other data from Albertson (3). Because of the fact, that the density difference of the phases change linearly with increasing tie-line length (see tables) a rough estimation of the interfacial tension can be carried out from a plot of logarithm of the interfacial tension versus the density differences (see tables).

The behaviour of the density difference/viscosity quotient from Stoke's law is different, too, for both systems observed. In the PEG/Dextran systems this quotient increases considerably over the full range, more steeper and to higher values as compared to the PEG/salt system. Here the increase in viscosity of the continuous PEG-rich phase due to higher PEG concentrations counteracts the increase in density differences (see fig. 2). One has to note that for PEG/dextran systems the viscosity of the disperse bottom phase is much higher as that of the continuous phase.

2. Settling behaviour

The basic settling behaviour was studied with the both 'model-systems' described in simple glass cylinders in laboratory scale (0.1 - 1 l), with a height to diameter ratio of around 2-3. The bottom phase was the disperse one in both cases; the volume of settled disperse phase was read over time. Fig. 3 shows the typical settling curves for two systems of the type PEG/salt and PEG/Dextran. Phase separation starts immediately in the PEG/salt system and the amount of settled volume increases nearly linearly. In contrast the PEG/Dextran systems show a large 'lag-time' before separation starts and a more sigmoidal settling curve. This depends mostly on the lower interfacial tension. After mixing very small droplets are obtained ($\leq 10 \mu\text{m}$), which have to be enlarged by coalescence, before settling can occur, and finally the rate of coalescence at the interface line is low, too. Further some hindrances for the separation near the interface line must be considered, due to the high viscosity of the lower dextran-rich phase. Similar behaviour has been observed with PEG/salt systems including large amounts of cell mass in the disperse bottom phase (see under sect. 3 and ref. 4).

Generally the settling behaviour depends on the length of the tie-line of the systems. Settling times are in the range of 5-10 minutes for the PEG/salt system and 15-40 min for PEG/Dextran systems, respectively (for comparison see ref. 3). The change of the settling velocity is nearly linear in the range of 10-30 % for the tie-line length and with similar steepness for both systems. In this range

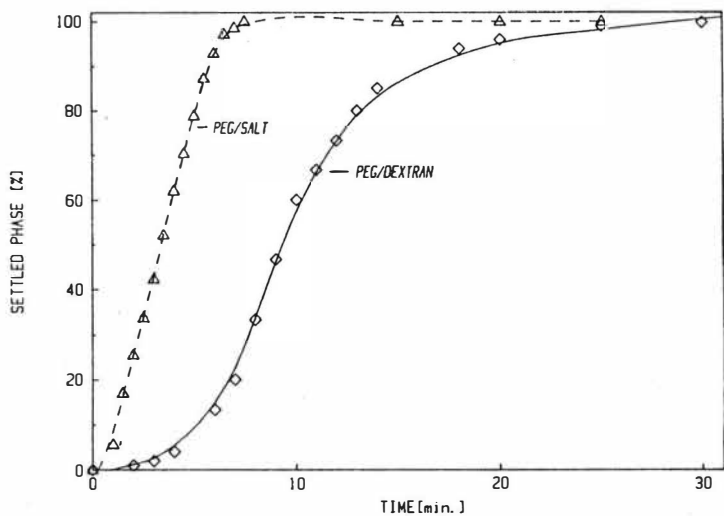


Fig. 3: Comparison of the settling behaviour between a PEG/salt and a PEG/Dextran system.

Volume = 0.8 l, volume ratio top/bott = 1.5, H/D = 2
 systems: No. 2/Table 1 and No. 3/Table 2

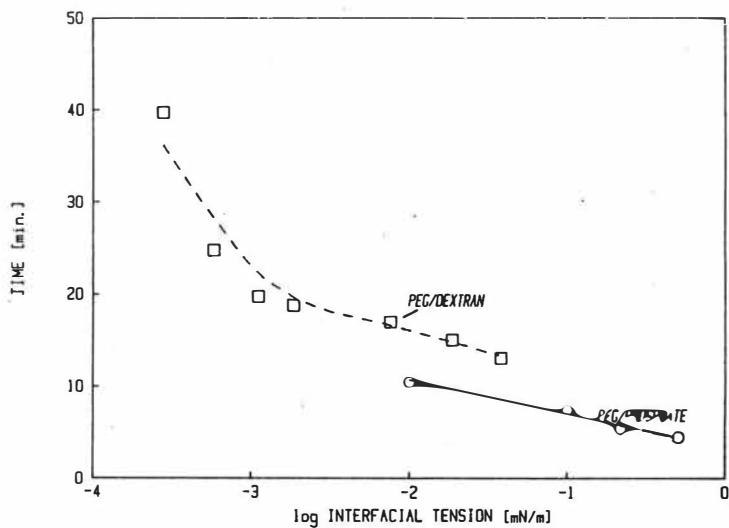


Fig. 4: Settling time in dependence on interfacial tension

the separation velocity of the PEG/dextran system is about a factor of 2-3 lower comparing to the PEG-salt system, although the density difference/viscosity quotient is higher. This reflects the strong influence of the interfacial tension with respect to the above mentioned points of discussion. (Fig. 4 shows for comparison the settling time plotted versus the logarithm of the interfacial tension).

The absolute values for the settling times given here are only for discussion. For calculation of the separation performance and comparison with other data, one has to consider the geometric parameters, for example the height of the liquid column. Further the type of dispersion used has to be considered because settling time depends on whether the lighter phase or the heavier phase is the disperse one, due to the differences in the viscosity of the phases. In the case of the PEG/Dextran system gravity settling is restricted from practical consideration to systems with the lighter phase as the continuous one and is more useful in small scale for laboratory purposes (see for example the counter-current distribution apparatus from Albertsson, ref. 3).

3. Technical use of gravity settling

The use of gravity settling for large-scale preparations has been described already in the literature, mostly in subsequent partition steps without solid cell material present. Few data are published also with phase systems including cell homogenates (collected data see ref. 4). As mentioned above the practical applications are restricted mainly to PEG/salt systems. Commonly simple cylindrical vessels are used in 100 l scale operating in a batchwise mode. With cell containing systems separation values between 85-93 % have been reported with time needed between 10-20 h (4). These times are one order of magnitude higher as with cell free systems (30-90 min) in the same scale. The decrease in separation performance depends on the change of the physico-chemical parameters of the systems, mainly on the strong increase in viscosity of the lower phase (see tab. 3). The settling behaviour of such systems is similar to those with pure PEG/Dextran systems. Fig. 5 shows this feature in a lab-scale experiment, comparing the settling time of a pure PEG/salt system with the same system including 20 % wet cell mass (broken *Candida boidinii* cells). The initial settling velocity is rather high, but the final separation is hindered by the high viscosity of the lower phase. The main geometrical parameter for the settling performance is the height of the liquid column, especially when solid biomass is processed. Some similarities to cell sludge sedimentation exists with regard to hindered settling (4).

The overall volumetric performance in the experiment described here can be calculated roughly to about $80-100 \text{ l/h}\cdot\text{m}^2$. Using a cylinder with 1 m^2 settling area (cross section) these values are comparable to the performance of a disc stack separator with a Σ -value of ~ 1000 (equivalent area). In the case of the pure salt system one can compare the performance ($1000 \text{ l/h}\cdot\text{m}^2$) with a Σ -value of

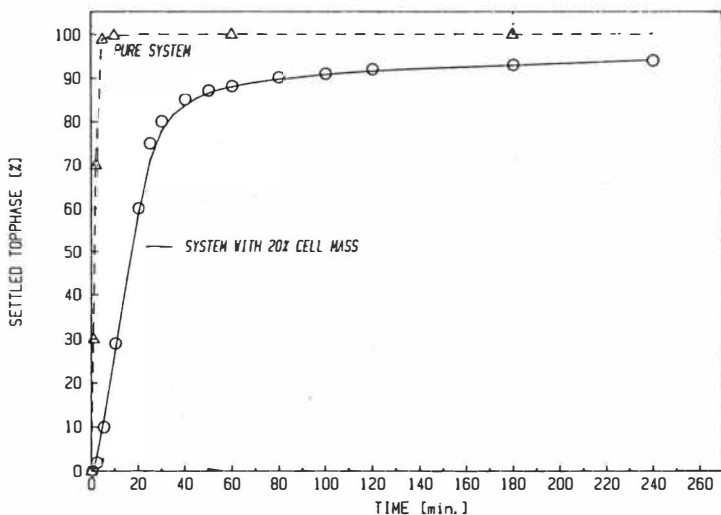


Fig. 5: Comparison of the settling behaviour of a PEG/salt system without and with biomass.
System: Mixed PEG 1550/PEG 400, see Table 3

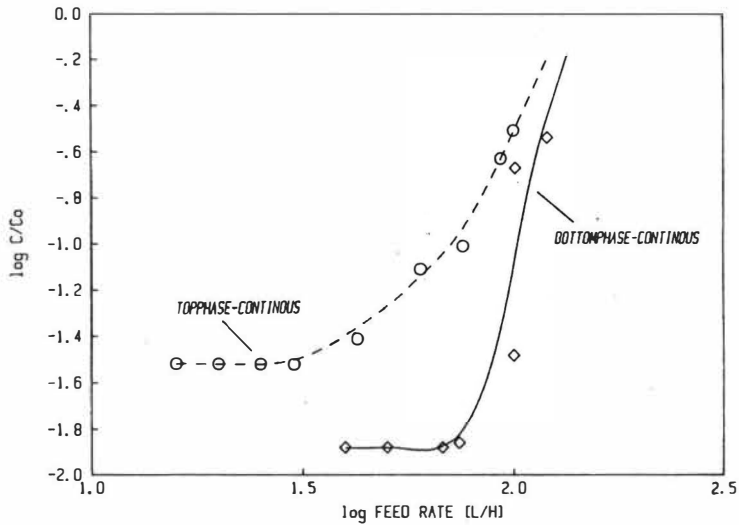


Fig. 6: Continuous settling of a PEG/phosphate system in a horizontal settler (system corresponds to No. 3/ Table 1) (C_0, C = conc. of disperse phase in feed and effluent)

around 7000 (for comparing separator performance see ref. 4). However, in most cases the settling behaviour of phase systems including cell mass do not allow separation under gravity, and product losses and long residence times have to be taken into account. But for separation of solid-free systems gravity settling is an alternative method, especially with regard to the low investment costs.

Continuous operation with gravity settlers is generally possible, too, mainly with the pure systems. Fig. 6 shows as an example the separation performance of a horizontal tube settler (glass-tube settler, Quickfit, Wiesbaden, FRG). This settler has a length of 1 m and a diameter of 10 cm. With the PEG/phosphate system the performance was 40-50 l/h when operating with the top phase as continuous phase and 70-80 l/h respectively, when operated the bottom phase as the continuous phase. The difference in performance is due to the difference of the viscosities of the phases. The area related performance was 400-500 l/h·m² and 700-800 l/h·m², respectively. These values are around a factor of two lower as can be assumed from static settling experiments (2). Some influence of the flow through the apparatus must be considered such as disturbance of the settling field, redispersion due to the low interfacial tension and entrapping of very small droplets of the disperse phase in the more viscous phase. This problems can be reduced by introducing weirs or baffels and some of such improvements are reported (4).

Conclusions

Some basic studies are presented describing the settling behaviour of aqueous two-phase systems with regard to their physico-chemical parameters. The results show that the parameters interfacial tension (which is quite low) and viscosity of the phases (namely the difference in viscosity between the phases) influences strongly the separation behaviour of such systems. The overall performance of settling can be rather high, especially in the case of PEG/salt systems and settling under gravity has to be considered as an alternative method to centrifugation. But this holds mostly for solid free systems.

The different behaviour of aqueous phase systems with respect to their physico-chemical parameters have to be taken into account when using common equipment from extraction technology. In the case of continuous settling some constructional modifications have to be performed to improve the performance.

Table 3: Comparison of physico-chemical parameters of pure aqueous phase systems and corresponding systems including cell mass (see also ref.4)

system composition	volume ratio (-)	$\Delta\rho$ (kg/m ³)	$\eta_{top}^{1)}$ (mPa·s)	$\eta_{bott}^{1)}$ (mPa·s)	σ (mN/m)
PEG 4000 9 % ²⁾ Dextran T-500 2 %	8.8	47	3.0	94	-0.03
system with <i>K. pneumoniae</i> 20 %	2.5	96	10.0	1100	n.d.
PEG 1550 18 % ³⁾ phosphate 11 % ³⁾	3.2	83	9.0	2.0	0.55
system with phosphate 7 % disrupted cells baker's yeast 20 %	3.1	90	10.0	450	n.d.
PEG 400 18 % PEG 1550 7 % ⁴⁾ phosphate 10 % ⁴⁾	3.2	110	7.0	2.5	1.3
system with phosphate 8 % disrupted cells <i>C. boidinii</i> 20 %	3.3	184	12.0	1400	n.d.

1) relative viscosity at 200 rpm

2) systems include 0.3 M potassium phosphate, pH 7.5

3) sodium/potassium phosphate, pH 7.5

4) potassium phosphate, pH 7.8

References

- (1) M.-R. Kula, K.H. Kroner, H. Hustedt, Purification of enzymes by liquid-liquid extraction, in: *Advances in Biochemical Engineering* (ed. A. Fiechter) Vol. 24, 73-118, Springer, Berlin, 1982
- (2) B. Mattiasson, M. Larsson, Bioconversion in aqueous two-phase systems, in: *Third Europ. Congress on Biotechnol.*, Vol. II, 187-193, Verlag Chemie, Weinheim, 1984
- (3) P.A. Albertsson, Partition of cell particles and macromolecules. Wiley Interscience, New York, 1971
- (4) H. Hustedt, K.H. Kroner, M.-R. Kula, Applications of Phase Partitioning in Biotechnology, in: *Partitioning in Aqueous Two-phase Systems - Theory, Methods, Uses and Applications to Biotechnology* (eds. H. Walter, D. E. Brooks, D. Fisher), Academic Press, New York, 1986.

Special Applications: Organic Products

EVALUATION OF THE SOLUBILITY OF ORGANIC COMPOUNDS IN SUPERCRITICAL FLUIDS

P. Alessi, M. Fermeglia, V. Gallo, I. Kikic
Istituto di Chimica Applicata, University of Trieste, ITALY

INTRODUCTION

Supercritical fluid extraction (SFE) is a separation process in which a liquid or solid mixture and an extractive agent are brought in contact at temperature and pressure above the critical point of the extractive agent. A fluid in supercritical condition (SF) has the peculiarity to solubilize different amounts of relative not volatile substances and in this respect it does not differ from a normal 'liquid' solvent. The solubility in the supercritical fluid cannot be evaluated only from pure component properties such as vapour pressure or sublimation pressure.

Temperature, pressure and molecular structure of all the components are equally important in determining the separation of a given mixture by means of SFE. All these variables contribute to determine the value of the density which is of extreme interest because the solubility in SF is very sensitive to its variation.

The operating pressure and temperature ranges for the extraction are mainly influenced by the critical temperature and pressure of the SF. Since very high temperature and pressure are in general to be avoided for economical reasons, special attention is paid to the fluids with the lowest critical temperature and pressure (CO₂ or lower terms of hydrocarbon families). All these fluids are not polar or slightly polar so not polar substances are preferably dissolved. In order to modify this situation one can change the properties of the SF by adding small amounts of polar substances (water for example) (1). Due to the potentiality of this separation process many studies have been published in the last years (2). In view of the peculiar characteristics of carbon dioxide, natural product separations and in general food product treatments are the most common applications of

the SFE (3).

From a theoretical point of view, the knowledge of the equilibrium between two phases is essential in evaluating the feasibility of a separation process. In this respect we are concerned with the evaluation of high pressure equilibrium for binary or ternary mixtures.

Unfortunately literature reports very few data (3) not allowing thus a comprehensive evaluation of the capability of the supercritical fluid extraction processes.

In this work we present an analysis of the experimental methods for the determination of SFE conditions and some suggestions for reducing time consuming experiments by a theoretical treatment of the data.

THEORY

From basic thermodynamics (4) the equilibrium conditions expressed by the isofugacity criterion are:

$$f_i^\alpha = f_i^{\Delta P} \quad (1)$$

for all the components i in the mixture, including the SF. In this equation ΔP indicates the supercritical phase in which the major quantity of supercritical fluid is present and α indicates the phase in which the original mixture to be separated is present. Since the fugacities should be evaluated at high pressure an equation of state (5) approach should be used; it follows:

$$\phi_i^\alpha x_i^\alpha = \phi_i^{\Delta P} x_i^{\Delta P} \quad (2)$$

where ϕ_i are the fugacity coefficients and x_i the compositions in the two phases.

Now we consider a pure component i in equilibrium with the supercritical fluid:

$$\phi_i^\alpha x_{i0}^\alpha = \phi_{i0}^{\Delta P} x_{i0}^{\Delta P} \quad (3)$$

where x_{i0}^{SP} is the mole fraction of component i in the supercritical phase and x_{i0}^m is the mole fraction of component i in the substrate. Since the SF has a negligible solubility in the substrate x_{i0}^α can be reasonably considered equal to 1, so that:

$$x_{i0}^{SP} = \phi_i^{SP} / \phi_i^\alpha \quad (4)$$

ϕ_{i0}^α and ϕ_{i0}^{SP} in equation (3) are function of the temperature, pressure and the interaction between the SF and the component i , while ϕ_i^α and ϕ_i^{SP} in equation (2) are still function of temperature and pressure and of the interactions between the SF and the component i plus the mutual interactions of all the others components in the mixture.

The behaviour of a multicomponent mixture is known, in principle, if all the interactions among the molecules are known, so in first approximation the mixture can be characterized by knowing only the solubilities in the supercritical fluid.

Any other thermodynamic information about the binary mixtures (component i -supercritical fluid) can be used for the identification of the interactions and for the calculation of the fugacity coefficients. At low pressures (below the critical pressure of the SF) and low temperatures (below the critical temperature of the SF) the equilibrium conditions for the binary mixture component i - supercritical fluid (a gas in these conditions) are still represented by an equation similar to equation (3):

$$\phi_{SF}^\alpha x_{SF}^\alpha = \phi_{SF}^G x_{SF}^G \quad (5)$$

where α and G are the phases in equilibrium. In this case:

$$x_{SF}^G \approx 1$$

$$x_{SF}^G = \phi_{SF}^G / \phi_{SF}^\alpha \quad (6)$$

x_{SF}^m represents the solubility (mole fraction) of the SF in the component i .

Also x_{SF}^m is a property of the binary mixture i -SF and it can be used for the evaluation of the fugacity coefficients; ϕ_{SF}^α and ϕ_{SF}^G differ

from the fugacity coefficients contained in equation (4) for the following reasons:

- the properties contained in equations (4) are evaluated at higher pressures;
- the properties contained in equations (4) and (6) are evaluated for the same binary mixture but for the opposite diluted regions (equation (4) for mixtures rich in SF component, equation (6) for mixtures containing mainly component i).

Therefore the use of one kind of information for the evaluation of the other one needs two types of extrapolations: with respect to pressure and to composition and it should be carefully checked.

EXPERIMENTAL METHODS

Solubilty in supercritical fluids

Different apparatus normally used for VLE determinations can be successfully applied for determining solubility in supercritical fluids (i.e. static or circulating apparatus).

Particular attention is devoted to the determination of the solubility of organic compounds in SF. The apparatus used in this investigation is similar to that suggested by Paulaitis (6). A flow technique is used to bring in contact supercritical fluid with the organic substratum packed in the two equilibrium cells; sampling of the saturated fluid phase mixture is accomplished with a switching valve between the second equilibrium cell and the metering valve.

Solubility of gases in liquids or solids

Volumetric and chromatographic methods are the most appealing experimental techniques for the determination of the solubility of gases in liquids or solids because of their rapidity and reliability. Due to the low volatility of the substances involved in SFE, gaschromatographic methods are particularly suitable. The experimental apparatus does not differ from a commercial gas - chromatograph in which the liquids are the stationary phase in the columns and the gases are the solutes injected. An improvement on the classical experimental apparatus can be considered a high pressure gas

- chromatograph. In this case one can obtain experimentally the solubility of gases at different pressures (up to 60 bar) so that the extrapolation needed in order to obtain the solubility (i.e. the solubility of liquid in SF) can be reduced.

Advantages of this technique in comparison with direct determination of the solubility in SF are the rapidity of the experiments and the small amount of organic solvents needed in determining binary information.

RESULTS AND DISCUSSION

Direct determination of the solubility of organics in compressed gases (such as CO₂) is a difficult and time consuming task and, especially in the initial steps of a process development may not be justified. We investigate the possibility of calculating the solubility in compressed gases starting from experimental data determined in different, and more favorable, conditions, namely low pressure Henry's constants of the gases in the liquids. This approach has the advantage of much less time consuming experimental determination, but rises the problem of two extrapolations (with respect to pressure and composition) which have to be done by means of an appropriate model.

Theoretically speaking an equation of state should be used in order to verify the compatibility between different experimental information. The equation of state considered should have the following features:

- to be able to correlate gas - solubility data
- to be suitable for the description of equilibrium properties in supercritical conditions: from previous investigations (7) a repulsive term of Carnahan - Starling type should be preferred.
- group contribution concept should be included in the equation

For these reasons the group contribution equation of state (GCEOS) developed by Skjold - Jorgensen (8) and applied by Brignole et al (9) in supercritical conditions for a particular problem satisfies all the requirements stated above. The details concerning the derivation of the equation and parameter tables are reported in the original paper by the author (8), in this paper we point out that this model contains

parameters, some of them calculable from pure component properties and some other calculable from binary data.

Since the model was developed for predicting gas - solubility data, some group interaction parameters have already been determined allowing us to calculate phase equilibria in conditions in which the supercritical extraction can be applied.

In order to check the approach proposed we have measured the solubility (Henry's constant) of a supercritical fluid such as CO₂ and light paraffines in two different classes, taken as representative of two different behaviour: alcohols and paraffines. These data were determined at atmospheric pressure and at temperature ranging between 50 and 100 degree C, by chromatographic method.

The calculations are performed by using the computer program developed by Skjold - Jorgensen modified for treating high boiling substances: the hard sphere diameter, which originally was calculated to match the normal boiling point of the pure component, is calculated to match a vapour pressure data in the range of temperature considered in this investigation.

This modification is essential when treating high boiling substances because of the extreme difficulty in extrapolating vapour pressure data of these substances up to the normal boiling point. Calculation performed on Henry's constants (Table 1) for high boiling compounds shows a dramatic effect of the hard sphere diameter on the equilibrium properties due to the fact that the repulsive term of the equation of state is function essentially of the hard sphere diameter. Table 2 reports the experimental data of CO₂ in such classes: these data are compared with those calculated by means of the GCEOS with the group interaction parameters published in the original paper. The agreement obtained is good, even if some deviation could be expected due to the long chain molecules of the solvent, as it was pointed out by the author.

The equation, with the same values of the group interaction parameters, is then applied for the prediction of the solubility of organic compounds (alcohols and paraffines) in supercritical fluids.

Table 3 reports the comparison between experimental and predicted data; by remembering the two extrapolations performed in this calculation the agreement found should be considered satisfactory and

the results promising for further application of the method in preliminary investigations on the feasibility of a supercritical fluid extraction process.

Unfortunately the test cannot be carried out on an wider data base because few data are available in the literature for both cases: solubility of CO₂ and solubility of organic compounds. Consequently the number of characterized groups is, at present, rather low and therefore new experimental data should be measured. Different long chain solvent has been used as stationary phases for gas - liquid chromatography in order to extend the parameter table of the GCEOS model and to test the model in the prediction of solubility at supercritical conditions.

ACKNOWLEDGMENT

The authors thanks Steen Skjod Jorgensen for making his computer program available and MPI " Ministero Publica Istruzione" for financial support.

LITERATURE CITED

- (1) Peter S., Ber. Bunsenges. Phis. Chem. 88, 875(1984).
- (2) Bertucco A., Fermeiglia M., Guarise G.B., Kikic I., Ing. Chim. Ital. 21, 45 (1985).
- (3) Paulaitis M.F., Krukonis V.J., Kurnik T.R., Reid R.C., Rev. Chem. Eng. 1, 2 (1983).
- (4) Prausnitz J.M., Lichtentaler R.N., Azevedo E.G., " Molecular Thermodynamic of Fluid Phase Equilibria", Prentice Hall 1986.
- (5) Vidal J., Ber. Bunsenges. Phis. Chem. 88, 784 (1984).
- (6) Paulaitis M.E., McHugh M.A., Chai C.P., in "Chemical Engineering at Supercritical Fluid Conditions", Ann Arbor Science 1983.
- (7) Bertucco A., Fermeiglia M., Kikic I., Chem. Eng. J., 32,21(1986).
- (8) Skjold - Jorgensen S., Fluid Phase Equilibria, 16, 784 (1984).
- (9) Brignole E., Skjold-Jorgensen S., Fredenslund Aa, Ber. Bunsenges. Phis. Chem. 88, 801 (1984).

Table 1: influence of vapour pressure on the Henry's constants;
first row H, second row hard sphere diameter:

Solvent	T (K)	H (atm)		H (atm)	
			T=330	T=400	T=560
C16	333.7	115.5	116.79	93.29	73.47
			6.7934	6.989	7.245
C18	313.4	75.60	79.12	63.44	59.11
			6.941	7.014	7.599

Table 2: Henry's constants of CO2 in organics:

Solvent	T (K)	H exp.	H cal.
hexadecane	304.10	67.40	66.11
	333.70	115.50	116.79
octadecane	309.40	67.40	66.40
	334.50	84.50	87.50
dodecanol	309.40	103.20	101.12
	333.70	136.60	133.25
tetradecanol	320.30	99.70	100.72
	339.60	126.20	122.33

Table 3: solubility of organics (y2) in compressed CO2

Solvent	T (K)	P(atm)	Y2 exp	Y2 cal
ethanol	298.0	20.0	.0048	.0042
		30.0	.0036	.0031
	348.0	30.0	.0321	.0379
butanol	313.0	40.0	.0290	.0311
		28.7	.0030	.0035
	42.7	.0010	.0011	
hexadecane	463.0	19.8	.0047	.0047
		40.7	.0030	.0030

Liquid-liquid extraction as an alternative to distillation for the recovery of organic material

Th. Pilhofer, G. Dichtl

QVF Glastechnik GmbH, 6200 Wiesbaden 13, FRG

In the chemical and pharmaceutical industry a lot of homogeneous liquid mixtures are produced where one component has to be removed. The classical process for that problem is distillation. Today, however, a decision for distillation is not made before the possible use of alternative processes has been checked.

That paper deals with the liquid-liquid extraction as alternative to distillation. Application of liquid-liquid extraction seems to be suitable if distillation can be applied only under difficult conditions or if the operating costs for the separation process are lower than for distillation.

The following problems are representative for the first group of processes:

- a) Separation of high boiling components requires low pressures and thus greater diameter of distillation columns. Example: Purification of high boiling organic acids.
- b) Separation of a homogeneous azeotropic mixture. The azeotrope can be overcome by selection of a suitable solvent. Example: Pyridine/water.
- c) Separation of mixtures with high concentrations of dissolved salts gives incrustation problems on boiler surface of distillation columns. In the course of extraction, the salts remain in the raffinate phase and separation of solvent and solute can be easily achieved. Example: Recovery of acetic acid from mother liquors.

The possibility of reducing the operating costs is given for the following problems:

- a) Systems to be separated have low separating factors in the VL-equilibrium either in a limited concentration range

(example: acetone/water) or in the whole concentration range (example: acetic acid/water). By applying a suitable solvent with a favourable VL-equilibrium with the solute, the operating costs can be reduced drastically.

- b) Removal of a high boiling component preferentially from water. The high evaporation costs of water can be reduced if the solute is extracted in an organic solvent with lower heat of evaporation and more favourable VL-equilibrium. (Example: phenol/water).
- c) If a component like dimethylformamide or dimethylacetamide suffers from hydrolysis in aqueous surroundings, the product loss especially under higher temperature during distillation can be overcome by extracting that component in an organic solvent and subsequently separating solvent and solute in the absence of water.

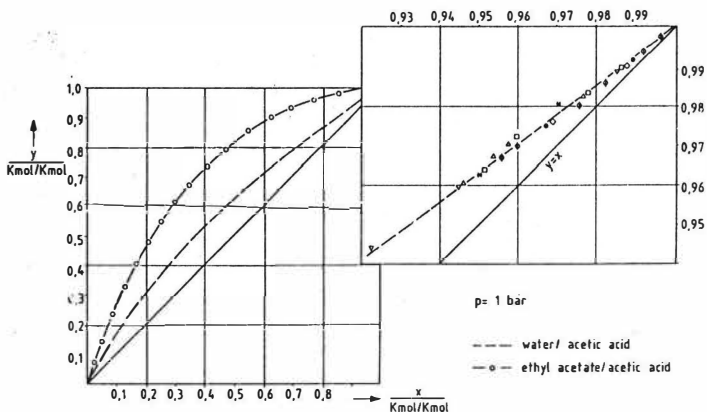


Fig. 1: VL-equilibrium water/acetic acid and ethyl-acetate/acetic acid

For demonstration reasons, in fig. 1 the VL-equilibrium of the system acetic acid/water is represented. It can be seen that in the whole concentration range there are small differences between vapour and liquid phase compositions. Additionally, there are still smaller concentration differences in the water corner which is plotted in an enlarged scale. Opposite to that, the VL-equilibrium between acetic acid and a suitable solvent like ethyl acetate, which is

also represented in fig. 1, shows high separation factors. Consequently, the operating costs can be reduced distinctly by extraction of the acetic acid, e.g. with ethylacetate and subsequent distillation of the acetic acid/ethyl acetate mixture.

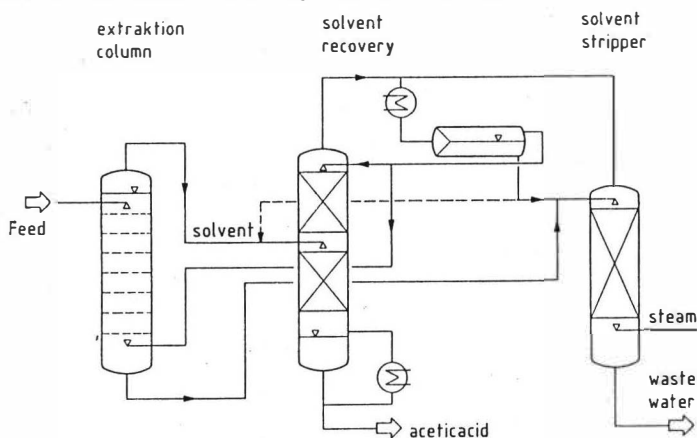


Fig. 2: Flowsheet of an acetic acid extraction plant

In fig. 2 a flowsheet of the acetic acid recovery process via liquid-liquid extraction is represented. The solvent, e.g. ethylacetate, is assumed to have a lower density than the acetic acid/water mixture. It is thus fed at the bottom of the extraction column whereas the aqueous phase enters the column at the top. The solvent extracts the acetic acid in the contact zone of the extraction column and leaves the column at the top. The mixture acetic acid/solvent with a small amount of water enters the solvent recovery column. If, as assumed in fig. 2, the solvent is lower boiling than acetic acid, it appears at the top of the distillation column together with the water. The vapours are condensed. The heterogeneous mixture is separated in a settler. The organic phase will be partly refused to the column or recycled to the extraction. The aqueous layer together with the raffinate of the extraction column is fed to the top of the stripping column where residual solvent is removed usually by live steam. The product acetic acid is removed at the bottom of the distillation column.

The structure of the flowsheet is similar in all other processes as long as the solvent recovery is carried out by distillation. As an

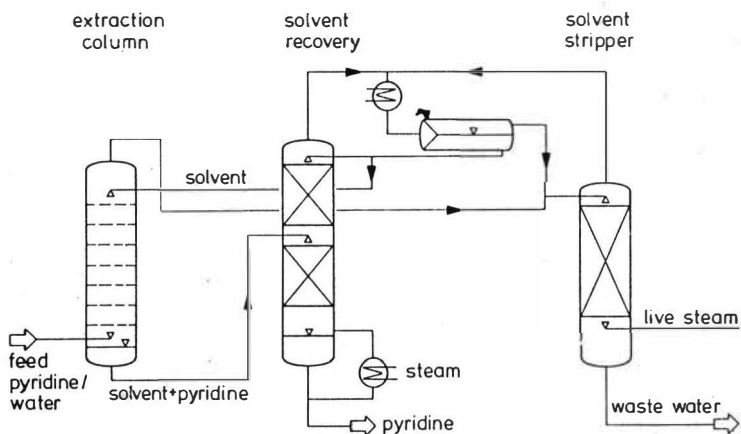


Fig. 3: Flowsheet of a pyridine extraction plant

example, in fig. 3 the flowsheet for the pyridine recovery is demonstrated. The only change is the fact that the solvents for that process usually have a higher density than the aqueous feed. Consequently, the solvent is fed to the top and the aqueous stream is fed to the bottom of the extraction columns. Some other small modifications arise if the solvent is higher boiling than the recovered solute.

The feasibility of an extraction process mainly depends on the availability of a suitable solvent. Suitable means that

- a) the solvent exhibits a high distribution coefficient for the component to be recovered and
- b) the VL-equilibrium of the system solvent/solute is favourable with respect to the operating costs of the solvent recovery.

For liquid-liquid systems, equilibrium curves exhibit three principal shapes. They are represented in fig. 4 with the concentration of the solute in the extracting phase on the y-axis and the concentration of the solute in the feed on the x-axis. The ratio of the two concentrations is usually designated as distribution coefficient. The left hand diagram shows the ideal case of a linear dependency which holds only for dilute solutions. The middle curve is representative e.g. for solutes which form dimers in the organic

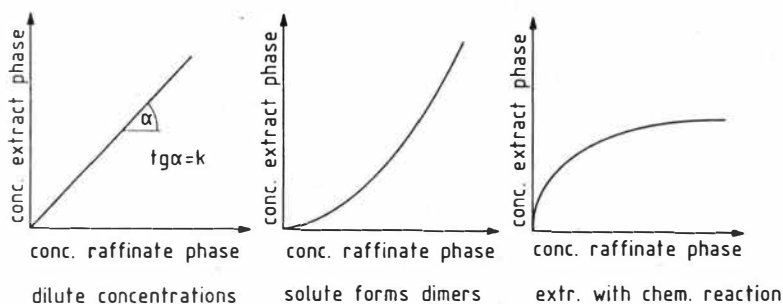


Fig. 4: Types of LL-equilibrium curves

phase like organic acids. The right curve is mainly valid for extraction with chemical reaction. In the asymptotic region stoichiometric conditions exist. According to the McCabe-Thiele construction the flow ratio of solvent phase to feed phase is inverse proportional to the slope of the distribution curve. For non-linear conditions the slope for low concentrations is relevant. Consequently, a high distribution coefficient results in a low solvent to feed ratio and hence in a lower energy input to the solvent recovery column.

The problem of a favourable VL-equilibrium for the system solute/solvent was discussed extensively together with the acetic acid recovery. Here only some special problems in connection with the solvent recovery should be discussed. The first problem deals with the presence of the second solvent - usually water - in the extract phase. Thereof some considerations result for the design of the process.

Fig. 5 shows the ternary liquid-liquid equilibrium diagram for the system solute C - solvent A - water. A feed according to point F should be extracted thus that a final concentration according to point RE results. The point AZ designates the binary azeotrope between water and solvent A. The separation of the extract phase between solvent, solute and water from the point of energy requires an extract phase concentration on the line between pure solute and the point AZ. For equilibrium reasons only the point SA fulfills

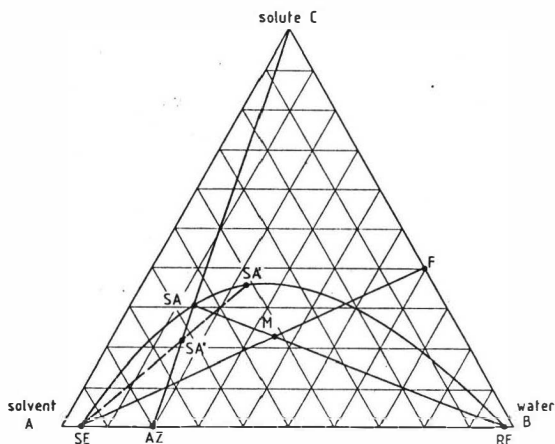


Fig. 5: Representation of the interdependence of the mass balances for extraction and solvent recovery

that condition. For balance reasons that point SA can only be reached if the ratio of solvent to feed corresponds to the length of the lines FM and MSE. From the point of view of the liquid-liquid equilibrium it may be appropriate to choose another solvent to feed ratio. In that case an extract phase concentration left or right of point SA results. Then care has to be taken that the control of the distillation allows to mix the extract phase with either solvent or aqueous phase in order to reach a feed point on the line CAZ. Such a possibility is outlined in the flowsheet of fig. 2.

Another problem arises if a solvent is applied where the solvent recovery cannot be carried out by conventional distillation. The extraction of acetic acid with methylisobutylketon (MIBK) may serve as an example. For several reasons it is useful to use that solvent. The solvent recovery is not possible by conventional distillation because MIBK and acetic acid exhibit nearly the same boiling point.

However, it is possible to use the coextracted water as an entrainer for the removal of the MIBK from water. The process should be described by means of fig. 6. It shows the same diagram like fig. 5. The MIBK azeotrope is denoted by AZ. It contains approximately 25 % water and boils at approximately 87 °C. The theoretical point SA cannot be reached because the liquid-liquid equilibrium requires a higher solvent to feed ratio resulting in a point SA'. Therefore, the separation can only be achieved if the extract phase according

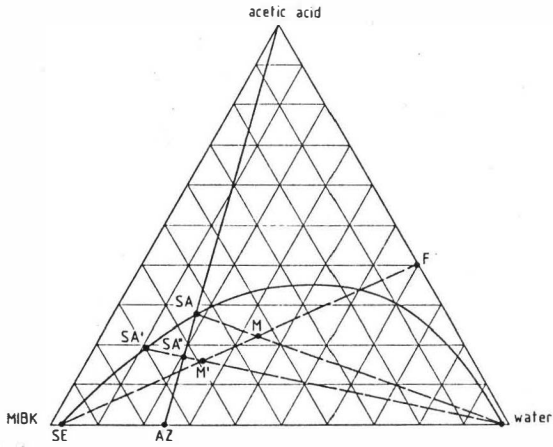


Fig. 6: Mass balances of extraction and solvent recovery for acetic acid extraction with MIBK to point SA' is mixed with water thus that a mixture according to point SA'' results. The control equipment of the distillation column has to be equipped accordingly.

Solvent Extraction Study of Tetrahydrofuran From Aqueous Solutions.

Amrit N. Patel, Department of Pure and Industrial Chemistry, University of Nigeria, Nsukka, Nigeria.

Summary: The data for the study of salt effect on the distribution of tetrahydrofuran (THF) between benzene and water for the seven inorganic salts are reported. The salting out coefficients of the seven salts follow the decreasing order as under:

Magnesium chloride > lithium chloride > sodium chloride >
sodium bromide > sodium iodide > sodium sulphate >
potassium chloride.

The decreasing order of the salting out coefficients is explained in terms of ionic charges and radii which also have significant influence on the enthalpy and entropy of hydrations of these salts. The salting out coefficients follow the similar decreasing trend to that of the enthalpy and entropy of hydrations for these salts as indicated by the table 1.

The cross-current two stage laboratory extraction of THF from this aqueous mixture in a weight ratio of 40 (THF) : 60 (H₂O) carried out with benzene and cyclohexane as extracting solvents achieved 96.0 and 96.5 percent recovery of THF respectively.

Introduction: The separation of THF from its aqueous mixtures is of particular interest due to the significant demand of THF as solvent for polymer and for extraction of alkaloids and physiologically active compounds. Also THF is a reactive intermediate in the synthesis of a number of organic compounds (1,2).

THF forms an azeotrope with water which makes its separation rather difficult by distillation. However as THF and water have different solubilities in organic solvents, the solvent extraction technique which invokes such property can be a suitable industrial method for the recovery of THF from aqueous solutions. Of the number of hydrocarbons studied (3) benzene showed the highest distribution coefficient and selectivity for the THF followed by toluene and cyclohexane. Benzene, therefore was chosen as an extracting solvent to study the salt effect on the distribution coefficient of THF between water and benzene.

The salt effect on the distribution data for a number of tertiary systems namely: ethylacetate - ethyl alcohol - water (4), benzene - carboxylic acids - water (5,6) and organic solvents-acetic acid - water (7) has been extensively reported in literature. However the data concerning the salt effect on the distribution of THF between two immiscible solvents such as benzene and water, a problem of engineering applications has received little attention. The present study therefore deals with the salt effect of magnesium chloride (MgCl₂), lithium chloride (LiCl), sodium chloride (NaCl), sodium bromide (NaBr), sodium iodide (NaI), sodium sulphate (Na₂SO₄) and potassium chloride (KCl) on the distribution coefficients of THF between benzene and water.

The cross-current two stage laboratory separation of THF from its aqueous mixtures with benzene and cyclohexane as extracting solvents is reported in this paper.

Experimental Methods: All materials used in the present study were of laboratory reagent grade. All measurements were carried out at 29-30°C. Of the several methods (8) described in literature for the determination of tertiary phase equilibrium and tie-line data, the most widely employed is probably the synthetic method of Othmer et al (9) which was followed in our earlier work (10,11) was adopted for this study. The tie-line data in the presence of inorganic salts were determined by equilibrating equal volumes of aqueous phase containing THF and inorganic salt added and the benzene phase. The equilibrating of the two phases was followed by separation. The benzene phase was analysed for THF concentration by the refractive index measurements in conjugation with the calibration curve prepared by systems of known compositions on the solubility curves. The THF concentration in the aqueous phase was found by mass balance. The solubilities of the inorganic salts under study were found to be negligible in benzene as compared to salts concentrations in the aqueous phases. The amounts of salts initially added to the aqueous phases were assumed to be present in the aqueous phases only. The seven inorganic salts at 5,10,15 and 20 wt.% concentrations were studied.

The cross-current two stage laboratory scale extraction of THF from its aqueous mixture in a weight ratio of 40 (THF): 60 (H₂O) with benzene and cyclohexane as extracting solvent was carried out by equilibrating the two phases in a separating funnel. The two phases then were separated and analysed for the THF concentrations. 100gms of the aqueous phase when equilibrated with 25.5gms. of benzene gave an extract phase, E₁ and a raffinate phase, R₁. The raffinate phase, R₁ when equilibrated with the same amount of benzene as in the first stage, gave the extract phase E₂ and the raffinate phase, R₂. The extract phases E₁ and E₂ were combined and distilled. 38.4gms. of THF was recovered thereby showing its percentage extraction of 96.00. Cyclohexane when replaced benzene, the extraction of THF was 96.5 percent.

Theory: There is a general agreement on the physical phenomena responsible for the salt effect on the distribution of a non-electrolyte solute between two relatively immiscible solvents such as benzene and water. The addition of a salt to an aqueous solution of a non-electrolyte results in the change of activity coefficient of the non-electrolyte solute. The increase in the activity coefficient is termed as 'salting out' while the decrease in the activity coefficient is termed 'salting in'. These phenomena may be explained on the basis of three main theories namely: the hydration theory (14), the electrostatic theory (15, 16) and the internal pressure concept (17,18).

As to the hydration theory the salting out results owing to the preferential orientation of water molecules around salt ions which in effect remove these molecules from their effective role as solvent for the non-electrolyte. The number of water molecules so influenced by each salt ion is known as the hydration number. The hydration number of an ion is dependent on its ionic charge and radius. The ionic charge when spread over a relatively small area has a high degree of solvation by water molecules due to greater ion-dipole interaction resulting in a higher hydration number which in turn affect the salting out influence of the ion. The hydration theory permits only qualitative estimate of the magnitude of the salt effect but it fails to explain the wide variation in the hydration numbers reported

in literature.

The electrostatic theory, which considers only the action of coulombic forces only and omits other factors, explains the salting out effect on the basis of the alteration in the dielectric constant of the solution. Debye and McAulay (15) and Butler (16) have derived equations for the activity coefficient of non-electrolyte in dilute salt solutions. These equations predict that salting out will occur if the dielectric constant of the non-electrolyte solution is less than that of water and salting in if the reverse is true. The theory also predicts that the logarithm of the activity coefficient of the non-electrolyte is a linear function of the ionic strength.

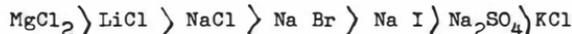
According to the concept of internal pressure, the concentration in total volume upon the addition of salt to water can be thought of as a compression of the solvent which makes it more difficult for the introduction of molecules of a non-electrolyte which results in salting out. An increase in total volume upon the addition of a salt would have the counter effect known as salting in.

Of the many semiquantitative empirical correlations derived on the basis of the above theories to predict the salt effect on the distribution of a solute between two relatively immiscible solvents, the expression proposed by Setschnow (12):

$$\ln \frac{C_T^0}{C_T} = k_S C_{SA} \quad \text{-----} \quad (1)$$

which was reported to be valid up to 3M salt concentration is used for the present study. For a given solvent phase, the solute concentration C_T and C_T^0 are aqueous phase solute concentrations with and without salt present respectively. C_{SA} is salt concentration in the aqueous phase and k_S is the salting out coefficient. This equation was also used by Swebb and Morgan (19) and McAteer (20) to present their data.

Results and Discussion: The experimental data for the distribution of THF between the benzene and the aqueous phases are presented in Figures 1 to 7 for the seven inorganic salts at 0, 5, 10, and 20% by weight salt concentrations in the aqueous phases. The increase in salt concentration in the aqueous phase was observed to enhance the transfer of THF to the benzene phase. The enhancement in the transfer of THF to the benzene phase is due to the salting out effect of the salt ions. The increased salt concentration in the aqueous phase is likely to provide more free ions which in turn remove more number of water molecules from their effective role as solvent. A definite trend in the salting out effect of the seven salts was observed in the Figure 8. The trend follows the following decreasing order for the salting out effect:



The salting out coefficients of the seven salts at 6 wt.% salt concentration in the aqueous phase were determined from the plots of

$$\ln \frac{C_T^0}{C_T} \quad \text{VS} \quad C_{SA} \quad \text{presented in the Figure 8. The}$$

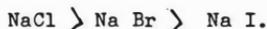
values of the salting out coefficients of the seven salts along with ionic radii and charges of ions, enthalpy and entropy of hydrations of the salts are presented in Table 1.

The observed order of the salting out coefficients of the salts can be explained on the basis of ionic charges and radii which have significant influence on the behaviour of ions in solution.

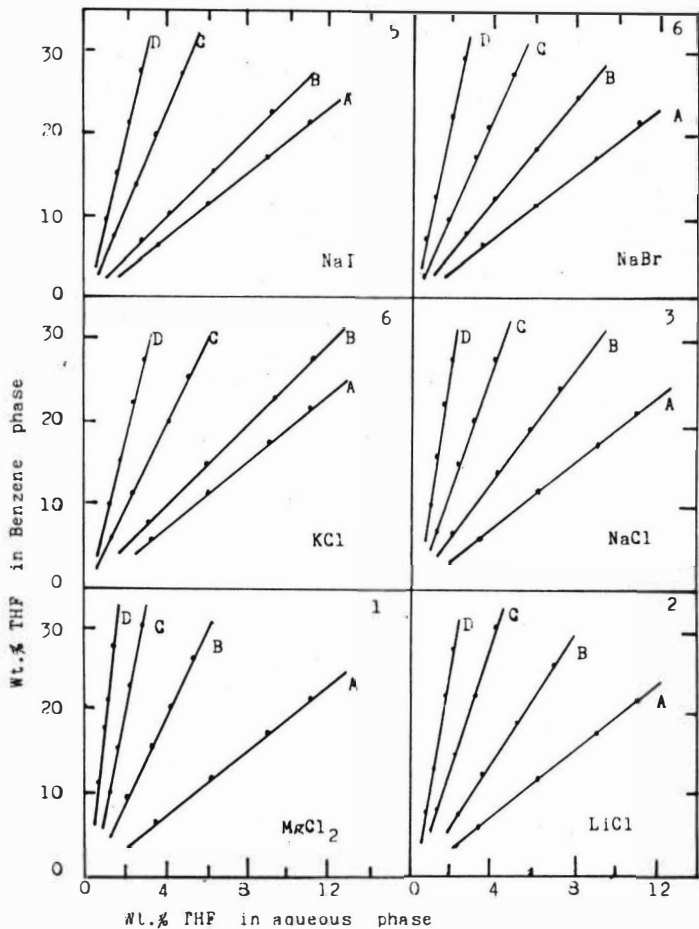
Table 1 : Salting Out Coefficients Enthalpy and Entropy of Hydrations and Ionic Radii(13)

Salt	Salting Out Coefficient k_S	Enthalpy and Entropy of Hydration		Ionic Radius (r) and Charge (z)	
		H K Cal/mole	S Cal/mole/ degree	z	r Å
MgCl ₂	0.105	-635.60	-110.90	Mg ²⁺ 0.65 Cl ⁻ 1.81	0.813
LiCl	0.095	-210.20	- 52.00	Li ⁺ 0.68 Cl ⁻ 1.81	0.402
NaCl	0.085	-181.60	- 44.10	Na ⁺ 0.95 Cl ⁻ 1.81	0.362
NaBr	0.082	-176.80	- 40.10	Na ⁺ 0.95 Br ⁻ 1.96	0.344
Na I	0.080	-166.50	- 35.10	Na ⁺ 0.95 I ⁻ 2.16	0.322
Na ₂ SO ₄	0.076	-	-	-	-
KCl	0.073	-164.90	- 36.0	K ⁺ 1.35 Cl ⁻ 1.81	0.316

In the case of magnesium chloride, bivalent charge on the magnesium ion with small ionic radius is spready over a relatively small area and as such a strong ion-dipole interaction between Mg²⁺ ion and water molecules is expected. The Mg²⁺ ions thus orient preferentially more number of water molecules than monovalent Li⁺, Na⁺, and K⁺ ions with large ionic radius. The monovalent charge on Li⁺, Na⁺ and K⁺ ions is dispersed over a relatively large area and thereby weakening the ion-dipole interaction between the ions and water molecules. The Mg²⁺ ions thus likely to remove more number of water molecules from their role as effective solvent for the solute THF compared to Li⁺, Na⁺ and K⁺ ions. Thus the removal of water molecules from their role as effective solvent for the solute, by the salt ions largely determines the salt effect. The salting out effect of the monovalent anions Cl⁻, Br⁻ and I⁻ can also be explained in the similar order as under:



The salting out coefficients of the salts as shown in table 1



Figures 1 to 7 Distribution of THF plots.

A: Salt free : B: 5 wt.% salt: C: 10 wt.% salt:

D: 20 wt.% salt.

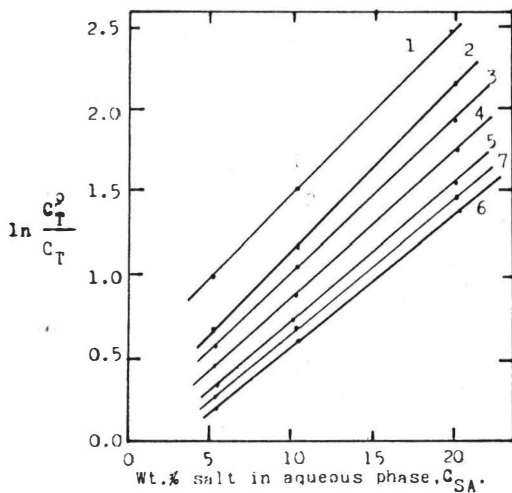
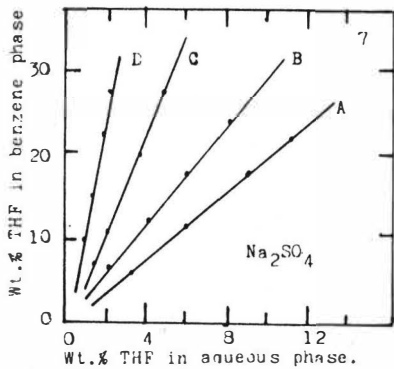


Figure 3.



follow the similar decreasing order for the enthalpy and entropy of hydration of the salts. The entropy of hydration largely results from coulombic interactions between the ions and the solvent molecules and it depends on both charge. The high charge density over a small ionic radius of an ion usually negative entropy of hydration. The orientation of water molecules around ions restricts their motion compared with their freedom in the bulk of the water. It is ordering process around an ion that largely determines the entropy change. The large monovalent anion like I^- have more positive entropy than is expected. From the magnitude of the entropy change it can be deduced that the ions with large ionic radii causes a break down in the structure of liquid water. This effect is probably present with other ions as well but is over shadowed by the strong orientation effect of high charge density and small ion size. Thus it can be concluded that both the salting out coefficient and the entropy of hydration of a salt are dependent on the ionic charges and radii of the salt ions.

The salt effect of di and trivalent salts like calcium chloride, barium chloride, aluminium chloride, chromium chloride and ferric chloride is under study for the THF-benzene-water system.

The experimental results of the extraction of THF with benzene and cyclohexane gave 96.00 and 96.50 percent extraction of THF in correspondence with those results obtained by the graphical construction method for the two stage cross-current extraction process.

References:

1. Kirk, R.E.; Othmer, D.E. Encyclopedia of Chemical Technology, Vol.10 Interscience, New York, 1966, 2nd Edn. p.249.
2. Jose, Coca; Ramona, M. Diaz. J.Chem.Tech.Biotechnol. 1979, 29, 694.
3. Patel, A. N. J.Chem.Tech.Biotechnol. 1983, 33A, 245.
4. Pai, M.V.; Rao, K. Madhusudana. J.Chem.Eng.Data. 1966,II,353.
5. Eisen, E. O.; Joffe, J. J.Chem.Eng.Data. 1966, II, 480.
6. Eisen, E. O.; Desai, M. L. J.Chem.Eng.Data. 1971, 16, 200.
7. Shah, D. J.; Tiwari, K. K. J.Chem.Eng.Data. 1981, 26, 375.
8. Alders, L. In Liquid-Liquid Extraction Chapter II, Elsevier Publishing Company, Amsterdam, 1958, 2nd. Edn. p.35.
9. Othmer, D. F.; White, R.E.; Trueger, E. Ind.Eng.Chem.1941, 35, 1240.
10. Hanson, C.; Patel, A. N. J.Appl.Chem. 1966, 16, 341.
11. Patel, A. N. J.Chem. Tech.Biotechnol. 1979, 29, 51.
12. Setschenow, J.Z. Physik.Chem. 1889, 4, 117.
13. Harvey, K. B.; Porter, C.B. Introduction to Physical Inorganic Chemistry, Chapter 9, p.316, Published by Addison Wesley Publishing Company, London, 1962.

14. Glasstone, S.; Found A. J.Chem.Soc. 1925, 127, 2660.
15. Debye, P.; McAulay, J. Physik Z. 1925, 26, 22.
16. Butler, J.A.V. J.Phy.Chem. 1929, 33, 1015.
17. Tammann, G. Z. Physic.Chem. 1893, 71, 676.
18. McDevitt, W. F.; Long, F. A. J.Amer.Chem.Soc. 1952,24,1773.
19. Swabb, Jr. L.E.; Morgan, E.L. Chem.Eng.Prog.Symp. ser. 1952, 48(3), 40.
20. McAteer, P.J.; Cox, R. W.; Geankoplis, C.J. A.I.Che.E.J. 1961, 2, 456.

Purification of glyoxylic acid from glyoxal solutions by tertiary amines extraction

D. Pareau, A. Chesné (Ecole Centrale de Paris, France)

A. Schoeteeten (Société Française HOECHST, Stains, France)

Manuscript will be available in München

A.S. Kertes,¹ D.R. Arenson,² C.J. King²

1. Institute of Chemistry, The Hebrew University, Jerusalem, Israel
2. Department of Chemical Engineering and Lawrence Berkeley Laboratory, University of California, Berkeley, CA, U.S.A.

Liquid-liquid extraction, in conjunction with extractive distillation or without it, has been a powerful tool in the separation technology of organic chemicals, and many industrial processes are based on the distribution technique. The interest in the process continues, and perhaps even intensifies, as new and sophisticated chemical engineering improvements achieve better and cleaner extractive separation methods, with higher yields and increased purities of the chemicals recovered (1). The program of the last two ISEC meetings, 1983 and 1986, as well as the listings in the Bibliography Section of the trade periodical (2) appearing since 1983, testify to the significantly increased interest in the chemistry of extraction of organic compounds. We have recently reviewed the field of fermentation product carboxylic acids (3) and low-molecular weight alcohols (4). The conclusions reached were clear in emphasizing that if further improvement in the extractive separation technology is to be achieved, the level of knowledge and understanding of the chemistry of extraction of organic compounds has to be brought up to that of inorganic compounds and metal complexes. Motivated accordingly, we have embarked on a multifaceted program which calls for basic chemical and chemical engineering investigations of the extractive separation of organic compounds.

We report here specifically our initial results on the extraction of the four isomers of butyl alcohol, 1-butanol (n - BU), 2-butanol (s - BU), 1-propanol-2-methyl (i - BU), and 2-propanol-2-methyl (t - BU) from their aqueous solutions by m-cresol dissolved in n-octane, at 25°C. The aim is to develop an extractive separation method for the isomers.

Working hypothesis

There is not a great deal of data in the literature on the effect of structural isomers on the partition coefficient, P , or distribution ratios, D , of organic compounds. As a matter of fact, we know of no explicit or systematic study of the effect. Several fragmentary observations are recorded in the compilation of Hansch and Leo (5) which lists $\log P$ data for the four butanols, in addition to the two propanols and three out of eight pentyl alcohols. We summarize the butyl alcohol data in the table. A difference in P values by a factor of three or four is common, though that in benzene of almost an order of magnitude, appears to be exceptional.

Log P of isomeric butyl alcohols between water and organic solvents, 25°C

Solvent/Extractant	n - BU	i - BU	s - BU	t - BU
Carbon tetrachloride (6)	-0.29	-0.32	-0.46	-0.77
Benzene (6)	-0.07	-0.11	-0.24	-0.57
Diethyl ether (7)	0.57	0.53	0.30	-0.08
n-Octanol (8)	0.88	0.65	0.61	0.37
n-Octanol (9)	0.87	0.74	0.65	0.43
Oleyl alcohol (9)	0.50	0.46	0.29	0.06

Numerous correlations between the partition coefficient of organic nonelectrolytes and various chemical, physical and thermodynamic properties of their aqueous solutions such as the partial vapor pressure, enthalpies and entropies of solution, energies of hydration, partial molar volumes, heat capacities, degrees of association, size of the molecule and its surface area, and others were attempted (4,5). Some are more successful than others, but always fail in correlating branched compounds. Even aqueous solubility of the nonelectrolytes, the property most closely related to the partition coefficient through the hydration process, intrinsic hydrophilicity and H-bonding, successfully defies attempts to make P values of isomers predictable (9 - 13). None of the differences in these properties between isomers are dramatic. It is even not sure whether they are statistically significant when correlated to the partition coefficient. The transfer process is obviously much more complex than it is reflected by either the crudity of the formal activity coefficient of the solute or its partition between two phases, or both.

The general failure of the aqueous-phase solution properties to correlate with the partition coefficient of isomeric compounds forces us to look elsewhere for explanation. We will attempt a correlation with organic phase properties of the extraction system. Specifically to the butyl alcohols, there is a wide variety of ways in which they can interact with the extractant and/or diluent and/or water. Some of these interactions are bound to be rather complex, some strong, some weak, and several mutually competing. In order to simplify the system in chemical terms by reducing the number of, or even eliminating, competing interactions, we have chosen to study the extractive behavior of a reactive extractant, m-cresol. There is considerable evidence (4) of relatively strong specific interactions between butyl alcohols and OH-bearing extractants, such as octyl or oleyl alcohols and phenols.

It is our working hypothesis that the interactions between cresol and butyl alcohols are significantly stronger than those between either of the components and water or octane, the diluent employed. For that matter, even stronger than those leading to the formation of self-associates, such as the tetrameric butanol in octane, for

example (4). Differences in the octyl and oleyl alcohol log P values for the isomers shown in the table suggest a considerable effect of the structural and steric characteristics on the proton-donating and proton-accepting ability of the hydroxyl groups (14) in the butyl alcohol isomers. Our present data, shown below, appear to confirm that.

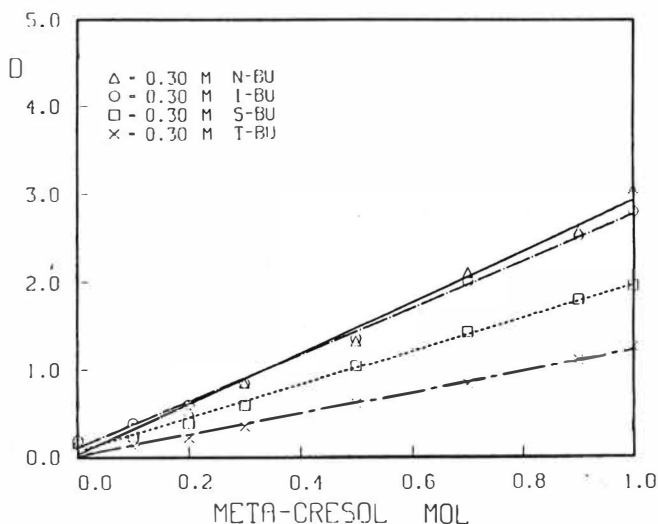


Figure 1. Distribution ratio of butyl alcohols between water and m-cresol solution in n-octane, 25°C.

Results

Two sets of distribution data are the least amount of information required to establish, by way of slope analysis, the stoichiometry of the adduct formed between cresol (CR) and butanol (BU) via the reaction



assumed to represent the transfer process from the aqueous into the organic (barred) phase. One, at constant initial concentration of each of the four alcohols and varying initial concentration of cresol in octane; and, another set, the way around, constant cresol concentration and varying initial aqueous alcohol concentration. A few samples of the results collected so far on the first set are shown in Figures 1 and 2 in the form of the distribution ratio, D, against the mole/L concentration of m-cresol in n-octane at 25°C. The first one shows the D values for the four

isomers at seven cresol concentrations in the 0.1 to 1.0 mole/L range, and Fig. 2 represents the effect of the alcohol concentration, in the case of *t*-BU, in the initial aqueous solution upon the *D* values.

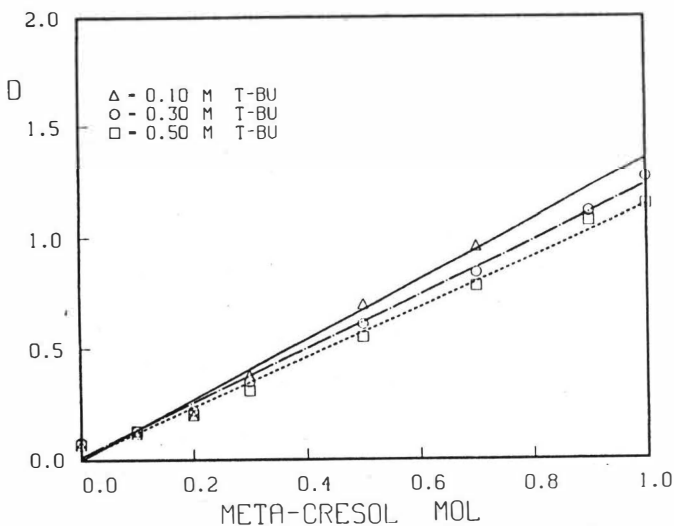


Figure 2. Distribution ratio of tert-butyl alcohol between water and *m*-cresol solution in *n*-octane at three different initial aqueous alcohol concentrations, 25°C.

The data points, admittedly showing considerable scatter, as given in the figures, were not corrected for the solubility/extraction of the isomers by the diluent alone. Additionally, and this is far more important, no corrections were made for the loss of *m*-cresol to the equilibrium aqueous phase. It is known (15) that the partition coefficient at infinite dilution of *m*-cresol between water and *n*-octane is around 1.6 at 25°C. This is a disturbingly low value. It means a considerable transfer, some 40%, of the extractant to the aqueous solution, especially at its higher initial concentration in octane. We have no data yet on that loss, thus no data to apply the corrections needed for a mass-action law interpretation of the extraction equilibrium [1] in the form of the conventional logarithmic plot of *D* versus the mole/L concentration of cresol and butanol in order to obtain the numerical values of *p* and *q*, as well as the formation constant K_{pq} of the cresol-butanol adduct.

More detailed experimental information is expected to be presented at the meeting and published subsequently.

Acknowledgement

This work is supported by the Assistant Secretary for Conservation and Renewable Energy, Office of Energy Systems Research, Energy Conservation and Utilization Technologies (ECUT) Division of the U.S. Department of Energy under Contract No. DE-AC03-76SF00098.

References

- (1) C.J. King, "Separation Processes", Second Edition, McGraw-Hill, New York, 1980.
- (2) E.P. Horwitz and J.D. Navratil, eds., "Solvent Extraction and Ion Exchange", M. Dekker, Publ., New York.
- (3) A.S. Kertes and C.J. King, *Biotech. Bioeng.*, 28, 269 (1986).
- (4) A.S. Kertes and C.J. King, *Angew. Chem. Intern. Ed.*, in press.
- (5) C. Hansch and A. Leo, "Substituent Constants for Correlation Analysis in Chemistry and Biology", Wiley, New York, 1979.
- (6) J. Mullens, I. Hanssens and P. Huyskens, *Bull. Soc. Chim. Belge*, 79, 539 (1971).
- (7) K.B. Sandell, *Naturwissen.*, 51, 336 (1964).
- (8) C. Hansch et al., unpublished data quoted in Ref. (5).
- (9) R. Kühne, K. Bocek, P. Scharfenberg and R. Frank, *Eur. J. Med. Chem.-Chim. Therapeutica*, 16, 7 (1981).
- (10) G.L. Amidon, S.H. Yalkowsky, S.T. Anik and S.C. Valvani, *J. Phys. Chem.*, 79, 2239 (1975).
- (11) S.H. Yalkowsky and S.C. Valvani, *J. Pharm. Sci.*, 69, 912 (1980).
- (12) R.D. Cramer, *J. Amer. Chem. Soc.*, 99, 5408 (1977).
- (13) J. Hine and P.K. Mookerjee, *J. Org. Chem.*, 40, 292 (1975).
- (14) G.L. Amidon, S.H. Yalkowsky and S. Leung, *J. Pharm. Sci.*, 63, 1858 (1974).
- (15) Ya. I. Korenman and V.V. Pereshein, *Zhurn. Prikl. Khim.*, 43, 1410 (1970).

The Tricritical Point in Tetrachloroethylene-Ethenediol-Nitromethane-n-Heptane System

V.P.Sazonov, M.F.Chernysheva, Polytechnical Institute, Kuibyshev/USSR

The equilibrium of three liquid phases in the composition tetrahedron is represented geometrically by some volume. The given volume may be enclosed between the faces of the tetrahedron, Fig. 1 (a), or between the free and the limiting tie-line, Fig. 1 (b), or between the two limiting tie-lines, Fig. 1 (c,d). The limiting tie-line is a tie-line which connects the figuration points of critical and noncritical phases on the composition diagram of the multicomponent system.

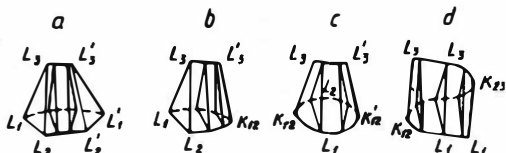


Fig. 1

Different volume shapes of three liquid phase equilibrium of the quaternary system.

For the first time the equilibrium of three liquid phases in quaternary systems was found in the system Ethyl Ether-Water-Potassium Jodide-Mercuric Jodide^[1] and was investigated at a temperature of 293.1 K. The volume shape of the three-phase equilibrium in this system corresponds to the Fig. 1 (d).

With the increase of temperature the compositions of the liquid phases change and it leads to the change of the shape and volume position of the three-phase equilibrium. One of the possible modifications of the three-phase volume, shown on Fig. 1(d), is its contraction to a point. This transformation corresponds to the transition of the three liquid phase equilibrium to the critical one-phase state. Konstamm^[2] was the first to show the principal possibility of simultaneous critical phenomena between three coexistent phases. Later^[3] it was noted in this work that such phenomena may be carried out in the systems with the number of components $n \geq 3$. Tricritical phenomena were found during equilibrium investigation of liquid-liquid-gas in the ternary systems^[4] and of liquid-liquid-liquid in the quaternary water-organic systems^[5]. At present several quaternary systems with tricritical phenomena between the three liquid phases are investi-

gated to a different extent.

It was mentioned in the works^[6,7] that the emergence of the tricritical phenomena in the quaternary systems is possible if the tie-lines of the two boundary ternary systems are located in the space crosswise. Besides^[8], according to the theory of the tricritical phenomena of Griffiths^[8], the figuration point of heterogeneous mixture which corresponds to the tricritical point composition at temperatures somewhat lower than critical is to be situated outside the three-phase equilibrium region.

The cleaning of nitromethane, tetrachloroethylene and ethanediol was carried out in accord with the procedures described earlier^[9]. The purity of obtained agents was considered by the results of chromatographic analysis. n-Heptane of "for chromatography" grade was used without additional cleaning. The temperatures of phase transformations were determined by the polythermal method in the range of 313-360 K. Heterogeneous mixtures with mass of 8g in closed glass ampoules were fixed in pairs in a special holder and were placed into the thermostat for the determination of phase transition temperatures. The temperature was measured by a thermometer graduated in 0.01 and 0.02° divisions.

The quaternary system includes six binary and four ternary boundary systems. Tetrachloroethylene, Ethanediol, Nitromethane and n-Heptane are designated by indexes /T/, /E/, /N/ and /H/ respectively. The system T-H is homogeneous from the six binary boundary systems, the rest are characterized by the limited solubility of the components. In ternary systems T-E-N and E-N-H there exists the equilibrium of the three liquid phases in a certain range of temperatures. Maximum temperatures of the existence of three phase equilibrium in these systems are equal to 329.8 and 315.02 K respectively. When the equilibrium of three liquid phases changes to the two-phase state, nitromethane and tetrachloroethylene phases take part in the critical phenomena in the first system, and ethanediol and nitromethane phases - in the second.

By preliminary experiments the region of the three-phase equilibrium in quaternary systems was determined. For the mixtures in quaternary systems the transition of the equilibrium of three liquid phases to the two-phase state was accomplished at temperatures higher than 329.8 K. Heterogeneous mixtures of a given region contain no more than 2.0 mass % of heptane. In accord with the density of pure components the liquid phases were conventionally named and designated as: the upper - (L₁) - ethanediol, the central - (L₂) - nitromethane, the

lower - (L_3) - tetrachloroethylene phases. When the equilibrium of three liquid phase changed into two-phase state of the quaternary system, critical phenomena took place either between phases L_1 and L_2 or between phases L_2 and L_3 , therefore, the volume shape of three-phase equilibrium in this system corresponds to the Fig. 1 (d).

The literature data^[4,5] point to the fact that a precision determination of the tricritical point coordinates is extremely difficult as in n-component systems ($n \geq 3$) the infinite set of methods concerning the change of the composition of heterogeneous mixtures is possible. This is the reason why it is necessary to work out an optimal procedure of coordinate search of a given critical point. In this case the following properties of this point must be taken into consideration. With any method of the composition change of heterogeneous mixture, tricritical point must correspond to the maximum temperature of the existence of three-phase equilibrium. Besides, this point must correspond to the contact point of dissolution polytherms of the third and second liquid phases, constructed in the coordinates of temperature - mass % component of the quaternary mixture. We applied a method which is conventionally named a method of the local extremums. The main point of the method lies in the search of such heterogeneous mixtures which would have the greatest temperature of the existence of the three-phase equilibrium and the least temperature difference of dissolution the third and the second liquid phases with a certain method of changing the composition of the quaternary mixture. The method of the local extremums was used for the search of the coordinates of the tricritical point in the system tetrachloroethylene-ethanediol-nitromethane-n-heptane.

On the basis of the preliminary experiments the relationship of the temperatures of phase transformations and the content of heptane in quaternary mixtures was determined. The composition of these mixtures changed along several secant lines, Fig. 2. From a given set of experiments the mixture was chosen with the content of 0.5 mass % heptane and a certain relationship of three other components. This mixture has the greatest temperature of the existence of three-phase equilibrium (339.3 K) and the least temperature difference of dissolution of the third and second liquid phases.

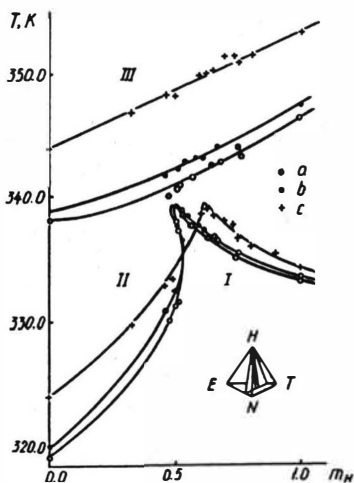


Fig. 2

Effect of heptane on the phase transformation temperatures

of the heterogeneous mixtures: a) $m_E:m_N:m_T = 1.0:2.2:1.8$;

b) $m_E:m_N:m_T = 1.00:2.18:1.82$; c) $m_E:m_N:m_T = 1.0:2.1:1.9$.

Regions: I - three liquid phase equilibrium,

II - two liquid phase equilibrium,

III - one-phase state.

In the next set of heterogeneous mixtures the content of heptane was 0.5 mass %, the relationship of tetrachloroethylene and nitromethane was constant, but the content of ethanediol was variable. The maximum temperatures of the existence of three-phase equilibrium, respectively, 339.6 and 339.8 K have the mixtures with the content of ethanediol 19.6 mass % and the ratio $m_1:m_2=0.82:1.00$ and $0.835:1.000$. The least temperature difference of the dissolution of the third and second liquid phases (0.2) corresponds to the mixture with the ratio $0.82:1.00$.

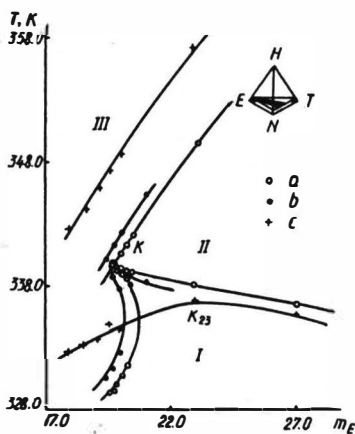


Fig. 3

Solubility isotherms of the quaternary heterogeneous mixtures with the content of heptane 0.5 mass %:

a) $m_H:m_T = 1.00:0.82$; b) $m_H:m_T = 1.000:0.835$; c) $m_H:m_T = 1.000:0.905$.

Regions: I - three liquid phase equilibrium,

II - two liquid phase equilibrium,

III - one-phase state.

In heterogeneous mixtures of the other set of experiments the content of heptane (0.5 mass %) and ethanediol (19.5 mass %) was constant, but the concentration of the rest substances was variable. In this set of experiments the greatest temperature of the existence of three-phase equilibrium (339.8 K) and the least temperature difference of the dissolution of the third and second liquid phases (0.4) has the quaternary mixture with the content of tetrachloroethylene 36.25 mass %.

Fig. 4 shows the polytherms of the solubility of heterogeneous mixtures with constant content of nitromethane and variable content of tetrachloroethylene and ethanediol. The polytherms of the dissolution of the second liquid phase have almost flat maximum, and with the increase of the content of heptane in the sections - the maximums shift to the area of higher temperatures. The quaternary mixture which belongs to the section () of the given set has the highest temperature of the existence of three phase equilibrium (339.8 K) and the least temperature difference of the dissolution of the third and second liquid phases (0.4).

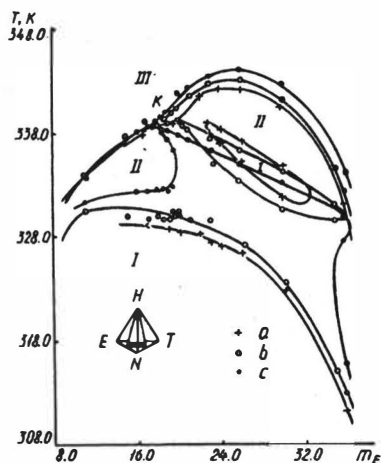


Fig. 4

Solubility isotherms of the quaternary heterogeneous mixtures with constant content of nitromethane and heptane (mass %): a) $m_N = 43.8, m_H = 0.45$; b) $m_N = 43.78, m_H = 0.50$; c) $m_N = 43.75, m_H = 0.56$.

Regions: I - three liquid phase equilibrium,
 II - two liquid phase equilibrium,
 III - one-phase state.

During investigation of some quaternary mixtures the phenomenon was found not noticed earlier in other works. When such mixtures were heated successively we observed the dissolution at first and then again the occurrence of the third liquid phase with its succeeding dissolution by the further increase of temperature. Such sequence of phase transformations points to the fact that the figuration point of the heterogeneous mixture which corresponds to the composition of tricritical point at temperatures somewhat lower than the critical must be located outside the region of three-phase equilibrium. This fact not earlier established under polythermal investigations [5, 6] is in agreement with the prediction of the theory of tricritical phenomena [8] and investigations of similar systems under isothermal conditions [10, 11].

For the determination of approximate parameter values of tricritical point its characteristic properties were used. The starting data for the calculation were the figuration point parameters of the mixtures with maximum dissolution temperatures of the third liquid phase and

the least temperature difference of dissolution of the third and second liquid phases. Tricritical point of the given system has the following parameters: $T = 340.1 \pm 0.3$ K and critical concentrations of tetrachloroethylene, ethanediol, nitromethane and n-heptane respectively 36.3 ± 0.2 , 19.5 ± 0.2 , 43.7 ± 0.1 and 0.5 ± 0.02 mass %.

REFERENCES:

1. Dunningham A.G. - J. Chem. Soc., 1914, vol.105, N 11, p.2623-2639.
2. Konstamm Ph. - Handbuch der Physik, 1926, Bd.10, S.271.
3. Zernike J. - Rec. Trav. Chim., 1949, vol.68, N 6, p.585-594.
4. Crychevsky I.R., Ephremova G.D., Pryanikova R.O., Serebryakova A.V. - J. Phys. Chem., USSR, 1963, vol.37, N 8, p.1924-1925.
5. Radyshevskaya G.S., Nikyrashina N.I., Merzhlin R.V. - J. Gen. Chem. USSR, 1962, vol. 32, N 3, p.673-676.
6. Machanek V.K., Mochalov K.I. - Scientific Notes. Perm's University, 1968, N 178, p.3-9.
7. Sazonov V.P., Gydkyna L.V., Gromakovskaya A.G., Kargova S.A. - J. Phys. Chem. USSR, vol. 50, 1976, N 2, p.560-561.
8. Griffiths R.B. - J. Chem. Phys. 1974, vol.60, N 1, p.195-206.
9. Sazonov V.P., Chernysheva M.F. - J. Gen. Chem. USSR, 1985, vol.55, N 11, p.2440-2446.
10. Lang I.C., Widom B. - Physica, 1975, vol.81A, N 2, p.190-213.
11. Bocko P. - Physica, 1980, vol.103A, N 1-2, p.140-171.

THE EXTRACTION AND SEPARATION OF PHENOLS BY ALAMINE 336

by

E.N. Bassey and M.A. Hughes

University of Bradford
Bradford, BD7 1DP
West Yorkshire
England

There are two main commercial liquid-liquid extraction processes for the recovery of phenols from aqueous waste streams, these are the Phenosolvan and Chem-Pro systems which use di-isopropyl ether and methyl isobutyl ketone respectively. In both processes the phenols are recovered from the organic extract by distillation and provide a single product, e.g. a mixture of monohydric and dihydric phenols. Indeed a variety of solvents are capable of extracting the phenols from aqueous solutions. They have been the subject of many studies and K_d values have been published. In general, the solvents which have the highest polarity and lowest molecular weight extract phenols the best. However, such solvents do suffer from the disadvantage that at too low a molecular weight the losses to aqueous raffinate are prohibitive.

In recent times, workers have shown considerable interest in exploring alternative extractants which have high enough distribution coefficients, low emulsion tendency and more importantly, low solubility in water to make solvent recovery from raffinate unnecessary.

It might be of advantage to find a solvent which could differentiate between the two main phenol groups, e.g. monohydric and dihydric and at the same time have some of the advantages of the simple solvents. It is known that because phenols are weak acids the distribution of phenols between water and a classical solvent is very much pH dependent. Such acid-base behaviour might be further explored if an organic base were incorporated into an inert diluent and used as solvent.

High molecular weight amines have been used before to extract weak acids such as carboxylic acids, chloroacetic acids. Pollio et al¹, Mukherjee et al² and Pittman³ extracted phenols by using primary, secondary and tertiary amines. King⁴ lists the K_d values for various phenols extracted by the tertiary amine Alamine 336. Other Lewis bases such as trioctylphosphine oxide and tributylphosphate have been reported as extractants.

The purpose of the present work was to explore the differing behaviour of the extraction of phenols by Alamine 336. Consequent upon this a new flowsheet was

developed and tested.

EXPERIMENTAL

Chemicals Alamine 336 was obtained from Henkel Inc., U.S.A. and used with either Analar hexane (BDH Ltd., U.K.) or odourless kerosene. The phenols were obtained mostly from BDH Ltd. but standards for chromatography originated from Polyscience Corporation, Netherlands.

Analysis HPLC has been used to quantitatively analyse both organic and aqueous phases for phenol content. A Du Pont Zorbax or Spherisorb ODS column was used with Gilson equipment. The mobile phase was acetonitrile buffered with a 2% v/v acetic acid solution in water. The system employed isocratic elution on a 45% acetonitrile flow.

The Effect Of pH On Extraction By Alamine 336

Phenol and resorcinol were chosen to represent the monohydric and dihydric phenols respectively. Shake out experiments were carried out on a 5 g/l phenol or a 2 g/l resorcinol solution at pH 6-7. The organic phase chosen after several trials was 20% v/v Alamine 336. The extraction at 1:1 phase ratio is shown in Table 1.

TABLE 1 - Properties Of Extractants

Extractant	Solubility in Water (weight %)	K_d (g/l/g/l)	K_d (from literature)
<u>Extraction of phenol</u>			
methyl isobutyl ketone	2 ⁵ , 1.9 ⁶	70	110 ⁶ , 100 ⁷ , 89 ⁸
ethyl acetate	9.7 ⁵	49	36 ⁹ , 24.7 ¹⁰ , 27.5 ¹
tributyl phosphate	0.042 ¹¹	433	> 99 ¹
toluene	0.05 ¹² , 0.06 ⁶	1.77	0.2 ¹² , 1.8 ¹
odourless kerosene		1.22	0.16 ¹³ , 0.2 ¹
n-hexane	0.00095 ¹²	0.08	0.13 ¹³
Alamine 336	< 0.005 ¹⁴		
20 vol % Alamine 336/n-hexane		2.28	
20 vol % Alamine 336/odourless kerosene		2.7	
<u>Extraction of resorcinol</u>			
20 vol % Alamine 336/n-hexane		0.29	

The K_d values may be compared with some selected from the literature for other solvents, and it is shown that the amine does not extract better than polar solvents. However, the K_d values show that phenol could be separated from resorcinol at this pH and they are not sufficiently low to preclude a commercial liquid-liquid extraction process.

Further experiments, where the pH was varied gave the results shown in Figure 1.

The usual shape of the graph for the extraction of phenol by a simple solvent at various pH has been reported on by Greminger et al.⁷ and Korenman¹⁵. We note here that in the case of extraction of phenol by the amine, there is a plateau in the range pH 6-9.

Further inspection of Figure 1 shows that phenol could be separated from resorcinol by a "pH swing" method.

It was confirmed that the phenols were readily stripped from the amine by contacting with approximately 30% v/v or 6-7% v/v ammonia for monohydric and dihydric phenols respectively.

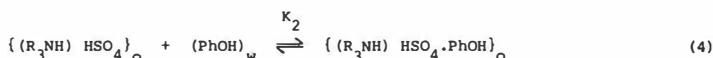
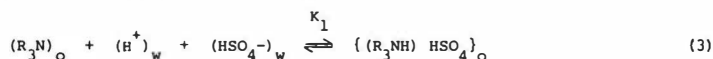
A DISTRIBUTION MODEL FOR PHENOLS EXTRACTION BY ALAMINE 336

(i) Monohydric phenols

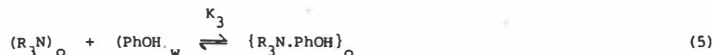
Dissociation occurs according to:



Sulphuric acid complexes the amine according to:



Additionally, phenol associates with the amine:



If $\{(\text{R}_3\text{NH})\text{HSO}_4\cdot\text{PhOH}\}_o = \text{complex 1}$

and $\{\text{R}_3\text{N} : \text{PhOH}\}_o = \text{complex 2}$

then the distribution coefficient for a monohydric phenol $K_{d,m}$ is given by:

$$K_{d,m} = \frac{\{\text{complex 1}\} + \{\text{complex 2}\}}{\{\text{PhOH}\}_w + \{\text{PhO}^-\}_w} \quad (6)$$

It can now be shown by algebra that:

$$K_{d,m} = \frac{K_1 K_2 K_H C_O C_{HW} C_{1W} + K_3 C_O C_{1W}}{C_{1W} + K_{a1} C_{1W} / (H^+)_w} \quad (7)$$

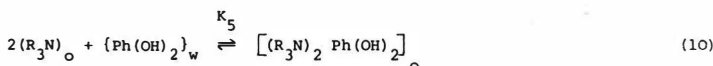
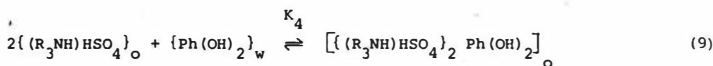
which reduces to:

$$K_{d,m} = C_O [(AC_{HW} + B) / (1 + K_{a1} 10^{pH})] \quad (8)$$

where C_{1W} , C_{HW} , C_O are the analytical concentrations of the aqueous phase phenol, aqueous phase sulphuric acid and organic phase amine respectively; $K_1 K_2 K_H = A$, $K_3 = B$, $(H^+)_w = 10^{-pH}$. The degree of fit of equation (8) to the analytical data is shown in Figure 1.

(ii) Dihydric phenols

Similar reasoning is used for modelling equilibria in the dihydric phenols system; but now:



and by algebra the distribution constant for the dihydric is given by:

$$K_{d,d} = \frac{\{\text{complex 3}\} + \{\text{complex 4}\}}{\{Ph(OH)_2\}_W + \{PhCHO^-\}_W + \{PhO_2^-\}_W} \quad (11)$$

where complex 3 = $[\{(R_3NH)HSO_4\}_2 Ph(OH)_2]_O$

complex 4 = $[(R_3N)_2 Ph(OH)_2]_O$

then:

$$K_{d,d} = \frac{K_1^2 K_H^2 K_4 C_{HW}^2 C_{2W} + K_5 C_O C_{2W}}{C_{2W} + K_{a2} C_{2W} / (H^+)_w + K_{a2} K_{a3} C_{2W} / (H^+)_w^2} \quad (12)$$

reducing to:

$$K_{d,d} = C_O^2 [(\epsilon C_{HW}^2 + \phi) / (1 + K_{a2} 10^{pH} (1 + K_{a3} 10^{pH}))] \quad (13)$$

where $\epsilon = K_1^2 K_H^2 K_4$, $\phi = K_5$

The fit is demonstrated in Figure 1.

A FLOWSHEET TO EXTRACT AND SEPARATE MONOHYDRIC AND DIHYDRIC PHENOLS

We have developed the following flow sheet, Figure 2, which delivers two main products, e.g. monohydric and dihydric phenols as a ammonium phenolate solution. The organic extractant is regenerated by contacts with ammonia. The number of stages required for each duty was calculated using McCabe-Thiele type diagrams.

The circuit has been tested on bench scale mixer settlers both on simulated ammoniacal liquors and on a liquor arising from coke-ovens. Space does not permit here the full analysis of the products but the Tables 2 and 3 show quantitative results from a simulated liquor and the chromatograms in Figure 3 demonstrate how the phenols were separated from a coke-oven liquor as aqueous feed to the equipment.

REFERENCES

1. Pollio, F.X., Kunin, R. and Pruess, A.F., Environmental Science and Technology, 1, (6), 495-498, June 1967.
2. Mukherjee, P.N., Bhattacharya, R.N. and Ray, S.K., Urja, 211-240, April 1982.
3. Pittman, E.F., M.S. Thesis, University of California, Berkeley, U.S.A., 1979.
4. King, C.J., Proc. Intern. Solv. Extr. Conf., Vol. 2, 80-86, Liege-Belgium, 1980.
5. Perry, E.S. and Weissberger, A., Techniques of Chemistry, Vol. XII, 181, John Wiley and Sons, 3rd Ed., 1978.
6. Erhart, J.P., Won, K.W., Wong, H.Y., Prausnitz, J.M. and King, C.J., CEP, 67-73, May 1977.
7. Greminger, D.C., Burns, G.P., Lynn, S., Hanson, D.H. and King, C.J., A.I.Ch.E. Meeting, Philadelphia, June 1980.
8. Won, K.W. and Prausnitz, J.M., J. Chem. Thermodynamics, (7), 661-670, 1975.
9. Shelkov, A.K., Spravochnik Koksokhimika (Coal Chemist Handbook), Vol. III, 167, Metalurgia, Moscow, 1966.
10. Leucke, R.H., Rep. DE81 O28104, Dept. of Chem. Eng., Missouri University, Columbia, U.S.A., 1981.
11. Hala, J. and Tuck, D.G., Proc. Intern. Solv. Extr. Conf., Vol. I, 198, The Hague, 1971.
12. Kiezyk, P.R. and Mackay, D., Canadian J. Chem. Eng., 49, 747-752, 1971.
13. Medir, M. and Mackay, D., Canadian J. Chem. Eng., 53, 274-277, June 1975.
14. Private communication of Dr. M.A. Hughes with General Mills of U.S.A. (now Henkel Inc.), June 1962.
15. Korenman, Ya I., Ekstraksiya Fenolov. (Extraction of Phenols), Gorkii, 1973.

Table 2 Phase composition in monohydric phenol operating circuit

Organic: 20 vol.% Alamine 336 in kerosene
 Strip solution: 4.7 M NH₃ (\cong 30% v/v NH₃)

stage number	Aqueous pH	Phenolic compound	Phase composition, g/l		% Phenol extracted or stripped
			Aqueous	Organic	
<u>Extraction, Aqueous/organic ratio = 1.07</u>					
	Feed	Phenol Resorcinol	5.0 2.0		
1	8.82	Phenol Resorcinol	2.96 2.0	5.03	
2	8.81	Phenol Resorcinol	1.62 1.90	2.85 0.17	
3	8.70	Phenol Resorcinol	0.84 1.90	1.41 0.06	94
4	8.97	Phenol Resorcinol	0.30 1.84	0.58 0.06	
<u>Stripping, strip/org ratio = 1.17</u>					
1	11.70	Phenol Resorcinol	4.2 -	0.54 -	
2	12.20	Phenol Resorcinol	0.36 -	0.12 -	97.6

- not found

Table 3 Phase composition in dihydric operating circuit

Organic: 20 vol.% Alamine 336 in kerosene
 Strip solution: 1M NH₃ (\cong 7% v/v NH₃)

stage number	Aqueous pH	Phenolic compound	Phase composition, g/l		% Phenol extracted or stripped
			Aqueous	Organic	
<u>Extraction, Aqueous/organic ratio = 1.06</u>					
	Feed	Resorcinol Phenol	1.84 0.30		
1	2.88	Resorcinol Phenol	0.03 0.006	1.95 0.36	
2	3.43	Resorcinol Phenol	0.003 0.001	0.032 0.005	99.84
<u>Stripping, strip/organic ratio = 1.06</u>					
1	10.42	Resorcinol Phenol	1.76 0.32	0.31 0.13	
2	10.67	Resorcinol Phenol	0.21 0.1	0.08 0.02	95.9

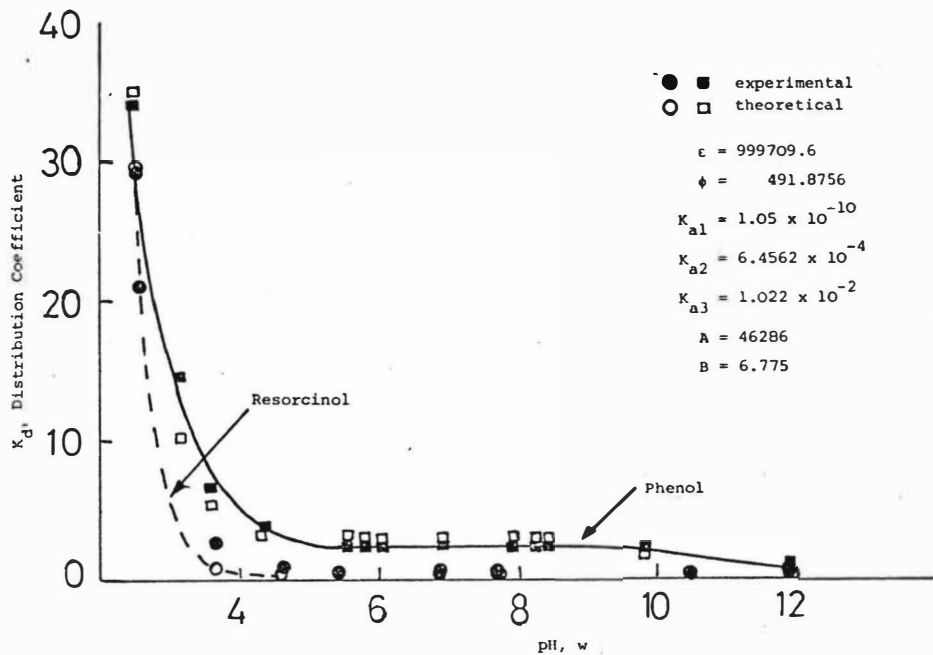
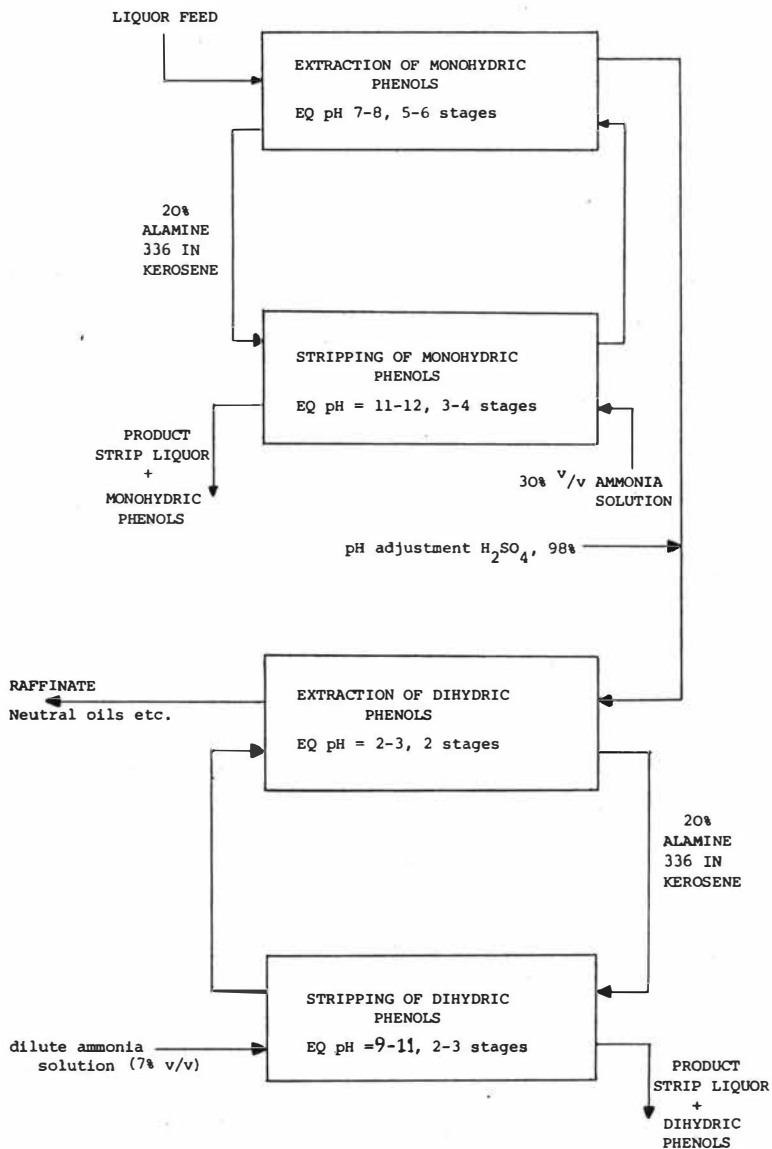


FIGURE 1: Graph showing how extraction of monohydric and dihydric phenols varies with pH. Mathematical models are shown by — for phenol and --- for resorcinol.

FIGURE 2 SCHEME FOR EXTRACTION AND SEPARATION OF PHENOLS FROM CARBONIZATION LIQUORS



R - Resorcinol
 P - Phenol
 a - dihydric zone
 b - monohydric zone

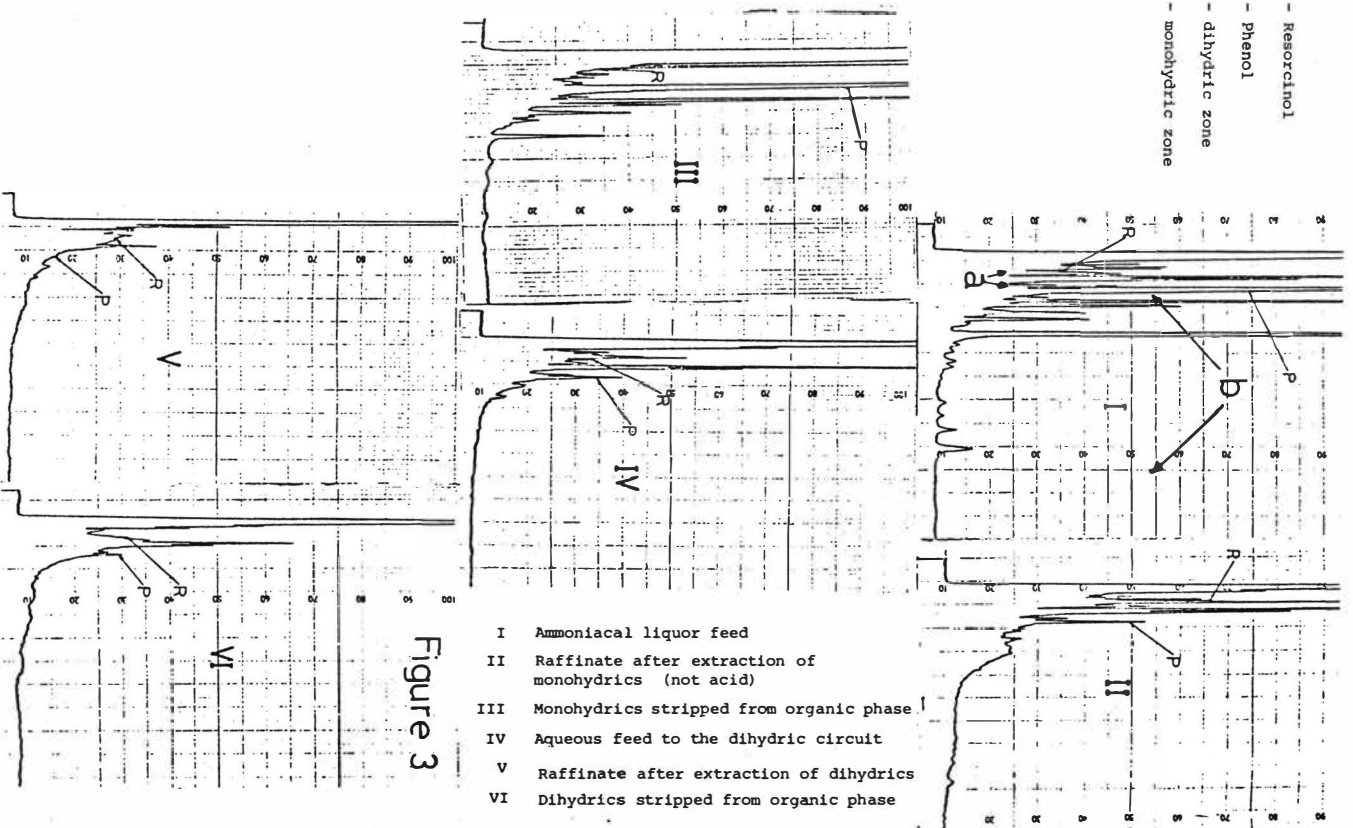


Figure 3

THE ALCOHOL/WATER SOLUBILITIES

Andrzej SZAFRAŃSKI and Zygmunt LISICKI

Industrial Chemistry Research Institute (Instytut Chemii Przemysłowej), Department KB-6, Rydygiera 8, 01-793 Warsaw
POLAND

Abstract:

Solubility data including miscibility gaps in binary alcohol/water systems have been considered for almost 80 monohydroxy alcohols ranging from propanol to octadecanol, based on about 200 literature references.

The alcohol-in-water solubilities range from complete (methanol, ethanol) or very high (for 1-propanol miscibility gap occurs only between -10.5° and -1.7°C) to as low as 10^{-7} mol L^{-1} (e.g. for hexadecanol). As the alcohol chain length is increased in arithmetic progression, the proportion of alcohol in the aqueous phase diminishes in geometric progression, the ratio of water solubility of one homologous member to that of the next being of the order of four. In the alcohol-rich phase the proportion of water remains relatively high, e.g. for 1-dodecanol a water/alcohol ratio as high as 0.3 is observed, compared to 1 for 1-butanol.

For 1-alkanols, empirical relations of the linear or quadratic type, $\log c/\text{mol L}^{-1} = a + bN_{\text{C}}$ or $\log c/\text{mol L}^{-1} = a + bN_{\text{C}} + cN_{\text{C}}^2$, that correlate the solubility in water (c) with the carbon number of the alcohol (N_{C}), a , b and c being regression parameters, yield estimates which in some cases seem to be more reliable than the currently available experimental data. Correlations involving gamma model equations (e.g. HPTL) have also been tested.

For most of the higher and also for some of the lower alcohols data gaps are acute. For most lower alcohols the reported data are often imprecise or conflicting so that accurate reinvestigation is in order.

As the manuscript was not available at the 28th May 1986, the deadline for printing this book, we only print the short abstract of the paper.

New Approach to Assessment of Molecule Aggregation in the Organic Phase

JEDINÁKOVÁ V., DVOŘÁK Z., Institute of Chemical Technology, Dept. Nuclear Fuel Technology and Radiochemistry, Prague

Association constants of tertiary amino nitrates were determined from a colligative properties - cryoscopic and osmometric data. The association degree and association constants of amines, R_3N , or their salts R_3NMX ($X = NO_3^-, ClO_4^-, Cl^-, Br^-$), were calculated by means of the computer program MOP, a modification of the Swedish program LETAGROP SUMPA. The approach is based on the assumption that the ion pair B associate by the following equation



to give the n-mers.

The equilibrium constant is thus

$$\beta_n = \left\{ \gamma_{(B_n)} [B_n] \right\} / \left\{ \gamma_B^n [B]^n \right\},$$

where γ^i are the activity coefficients. The activity coefficient ratios for low concentration of B are generally assumed to be constant.

The analytical concentration of substance B is then

$$c = b + \sum_{(n)} \beta_n b^n$$

whereas the total concentration representing the sum of concentrations of the various associate species is

$$B = b + \sum_{(n)} n \beta_n b^n,$$

where b is the monomer concentration.

An assessment method has been developed for the model of the

solution containing ⁿ complete sequence of associates whose relative representation in the solution drops proportionally. In view of the fact that the model embodies the experimental data with sufficient accuracy, the concept of a solution without dominant structures seems to be in a better agreement with the real state of the solution.

As the manuscript was not available at the 28th May 1986, the deadline for printing this book, we only print the short abstract of the paper.

Selective Oxidation of Toluenes to Aldehydes by Product Reextraction

G. Linzbach, G. Kreysa

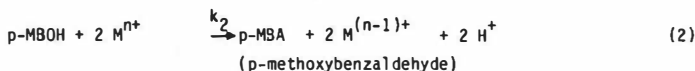
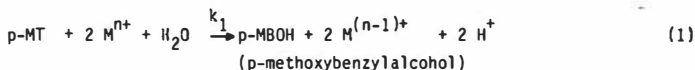
Dechema-Institut, Frankfurt/Main

The mediated oxidation of organic compounds by a redox system which is regenerated electrochemically in a separate reactor has been investigated repeatedly. This method decreases problems like insolubility of the organic substrate in electrolytes or the consumption of costly conducting salts. For the oxidation of aromatic compounds (toluene or substituted toluenes) to aromatic aldehydes some authors found Mn^{3+} and Ce^{4+} to be suitable mediators /1-3/. The main problem for using this reaction as a technical approach for the synthesis of aldehydes is the undesired formation of the corresponding carboxylic acid by further oxidation of the aldehyde. Kinetic studies about the indirect oxidation of p-methoxy-toluene (p-MT) to p-methoxybenzaldehyde (anisaldehyde, p-MBA) have shown, that the chemical reaction takes place in the aqueous phase. Therefore the formed aldehyde may be protected against further oxidation by re-extraction into the organic phase. Methylenechloride has found to be a satisfactory reagent for this purpose /2/. The aim of the present paper is the description of experimental investigations on microkinetics, the mathematical modelling of the reaction system and first calculations with different reactor models.

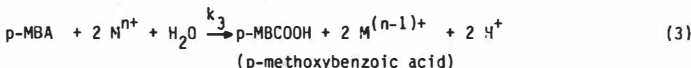
Microkinetic Investigations

The oxidation of p-MT by metal ions like Ce^{4+} or Mn^{3+} proceed in a sequence of consecutive reaction steps:

Aldehyde formation via benzylalcohol



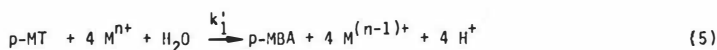
Oxidation to carboxylic acid



Another undesired parallel reaction is the oligomerisation of p-MT via a cation radical mechanism /2,4/:



Due to the fact that reaction (1) is very fast, one can summarize (1) and (2):



All experimental investigations were performed in a stirred vessel. The tested variables have been the concentrations of Ce^{4+} / Ce^{3+} , H_2SO_4 and p-MT (in CH_2Cl_2 or n-hexane), the temperature and the degree of dispersion.

The concentration of p-MT in the aqueous phase has found to be the most important factor for the selectivity of the aldehyde formation. In dependence on the experimental conditions this concentration is determined by mass transfer or reaction rates. Fig. 1 illustrates this by experimental and calculated results for the change of the p-MT and Ce^{4+} concentrations in the aqueous phase with time. In run 1 the reaction rate is partially controlled by the mass transfer until the p-MT concentration reaches its equilibrium value (see Fig. 1b).

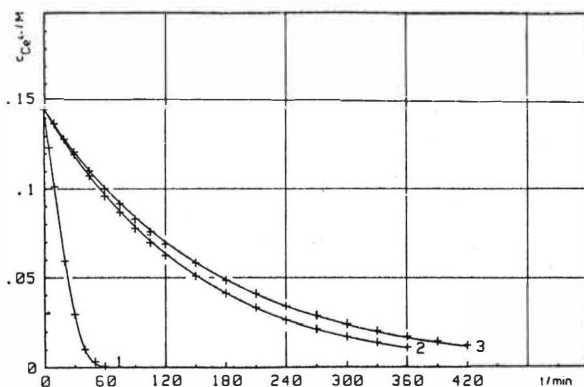


Fig. 1a: Concentration time function of $\text{Ce}^{4+} / 4$
 (+ experimental results, - fitted curves, curve numbers indicate the runs in table 1)

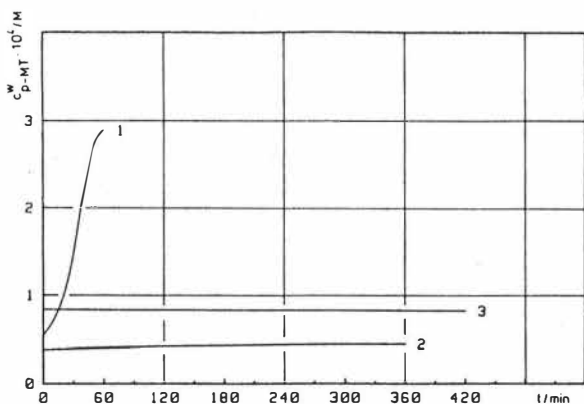


Fig. 1b: Concentration time functions of p-MT in the aqueous phase (curve numbers indicate the runs in table 1)

Table 1: Conditions and results of the kinetic experiments

RUN	$C_{H_2SO_4} / \text{mol l}^{-1}$	$T / ^\circ\text{C}$	$k_p A_p / 10^{-3} / \text{cm}^3 \text{s}^{-1}$	$K_V \cdot 10^{-3} / \text{l}$	$k / \text{l mol}^{-1} \text{s}^{-1}$
1	1.5	35	0.074	4.95	2.468
2	1.5	5	0.348	26.4	0.713
3	0.5	5	0.495	14.5	0.305

$C_{p\text{-MT}}$	= 1.322 mol/l in CH_2Cl_2
V_{org}	= 227.3 ml
C_{Ce}	= 0.15 mol/l $\text{Ce}(\text{SO}_4)_2$ + 0.025 mol/l $\text{Ce}_2(\text{SO}_4)_3$
V_{aqu}	= 900 ml

For modelling the kinetics of the system one has to know the correct values for the rate constants, mass transfer coefficients and equilibrium concentrations of all species.

The time dependance of the concentration as function of experimental conditions is described then by the following system of differential equations:

$$\text{Phase transfer term: } \frac{dc}{dt} = \frac{k_p A_p}{V} \left[\frac{C_{\text{org}}}{K_V} - C_{\text{aqu}} \right] \quad (6)$$

$$\text{Flow term (continuous process): } \frac{dc}{dt} = \frac{q}{V} [C_{\text{inlet}} - C] \quad (7)$$

Both terms have to be calculated for each species which participates in the reaction.

The reaction terms itself depend on the particular reaction equations and the stoichiometric coefficients of the species. For the computation of a reaction system including reaction (3) and (5) the differential equation for the time function of the Ce^{4+} concentration yields for instance:

$$\frac{dCe^{4+}}{dt} = -4 k_1' [Ce^{4+}] [p-MT_{aq}] - 2 k_3 [Ce^{4+}] [p-MBA] \quad (8)$$

Based on these equations some theoretical results for different types of reactors (Stirred Tank Reactor, Continuous Stirred Tank Reactor, Co-current Extraction Column and Counter Current Extraction Column) will give first ideas about an optimal reactor design for the described system. The required kinetic data which are not known from investigations are taken from publications on similar systems /3/. The exact values will be determined in further microkinetic studies.

The considered reactions are the formation of aldehyde (5) and the further oxidation to the p-methoxybenzoic acid (3).

Table 2: Kinetic and experimental data

Temperature /°C	35	Species	$K_V/1$	$k_{p-p}^A/1/s$
Spec. Interfacial area /cm ⁻¹	51	Ce ⁴⁺	-	-
V _{org} /l	0.2273	p-MT	4150	} 0.074
V _{aqu} /l	0.9	p-MBA	415	
[H ₂ SO ₄]/Mol/l	1.5	p-MBCOOH	4.15	
k ₁ ' /l/mol/s	2.46			
k ₃ /l/mol/s	0.0295 /3/			

Stirred Tank Reactor

Fig. 2 shows the calculated concentration variations of Ce⁴⁺, p-MT and the formed aldehyde (aqueous and organic phase) with time. Due to the high reaction rate and the discontinuous operation mode the Ce⁴⁺ concentration decreases rapidly (see Fig. 1). After 45 min. Ce⁴⁺ is completely consumed and the p-MT concentration in the aqueous phase increases to the equilibrium concentration (0.283mmol/l). The concentration of the aldehyde in this phase runs through a light maximum which is caused by the competitive aldehyde formation and consumption by further oxidation. The selectivity for the aldehyde formation amounts 0.967 (with p-methoxybenzoic acid as by-product).

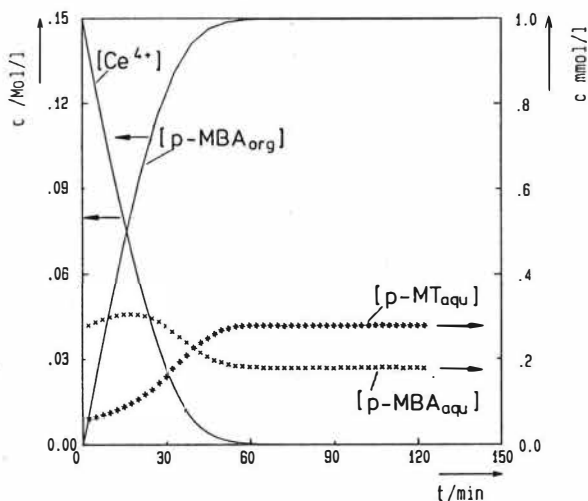


Fig. 2: Concentration time functions of p-MT oxidation by Ce⁴⁺

Continuous Stirred Tank Reactor

The simulation results of a continuous stirred tank reactor, calculated with the same conditions as in the previous described STR and flow rates of 1 l/h for the organic and 4 l/h for the aqueous phase, are illustrated in Fig. 3. Again after 45 min. stationary working conditions are reached with an outlet concentration of 0.06 Mol/l for the aldehyde (organic phase) and 0.089 Mol/l for the Ce⁴⁺ (aqueous phase). In contrast to the discontinuous batch procedure there is no complete conversion of the Ce⁴⁺ and only a few percent of the p-MT become oxidised. Due to the decrease of the reaction rate with lowered Ce⁴⁺ concentration the space-time yield is reduced with increasing fractional conversion.

An efficient and economic separation step for winning the pure product and regenerating the reaction solutions may overcome the problem of low product concentrations but the following comparative calculations for co- and counter current reactive - extraction columns will show another way of efficient process design for the described system.

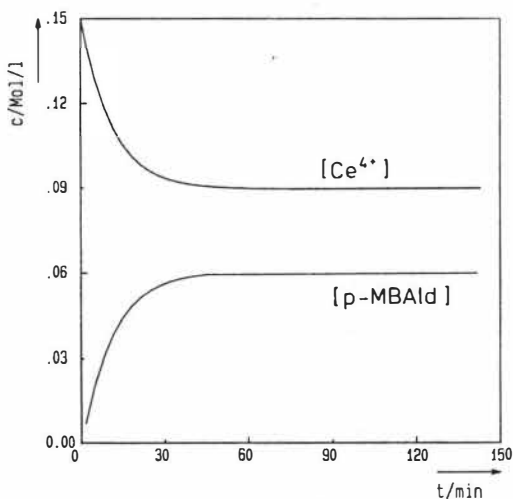


Fig. 3: Concentration time functions of Ce^{4+} and p-MT (same conditions as Fig. 1 and 2)

Co- and Counter Current Columns

Fig. 4 and Fig. 5 illustrate the improvement of the conversion degree by using a column (numerically approximated by 20 vessels) instead of a stirred tank. Of course all conditions (volume, flow rates, kinetic data etc.) are the same as in the previous calculations. The product concentration has been more than doubled and also the selectivity of the aldehyd formation is enhanced obviously (Table 3).

Table 3: Selectivity and fractional conversion for different operation modes

Operation mode	Selectivity p-MBA	Fractional conversion	
		Ce(4+)	p-MT
Discontinuous stirred tank:	0.958	1.000	0.110
Continuous stirred tank :	0.971	0.405	0.045
Co-current column :	0.991	0.870	0.098
Counter current column :	0.998	0.887	0.105

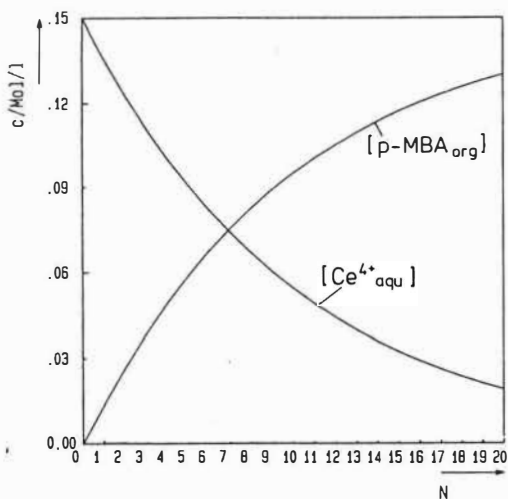


Fig. 4: Concentration time functions of Ce^{4+} and p-MT (Co-current column), same conditions as above

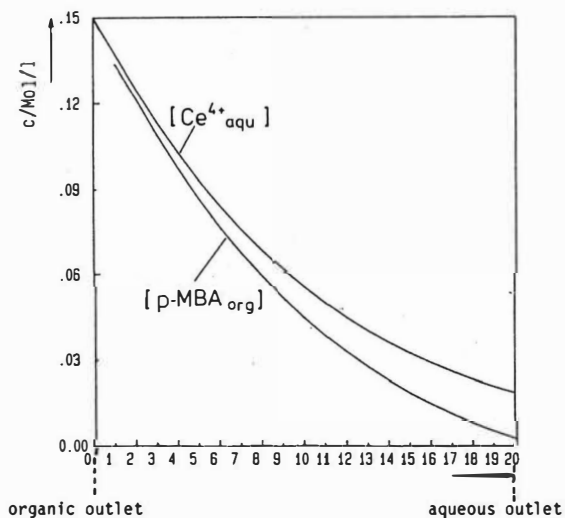


Fig. 5: Concentration time functions of Ce^{4+} and p-MT (Counter current column, same conditions as above)

Each of the calculated selectivities is quite high due to the optimized working conditions, but for systems without an additional extractant like methyl-enechloride and lower temperatures the difference in selectivity between single tanks and cascades may become more than 0.3.

With a complex model based on experimental data and mechanistic assumptions all of these alternative routes can be compared in an efficient and time saving manner.

Furthermore the model enables the calculation of reactor design and optimized working conditions. It will be used not only for stationary but also for dynamic modelling of the system and therefore it will be helpful for controlling the process in instationary states.

Acknowledgement

The authors wish to thank AIF Arbeitsgemeinschaft Industrieller Forschungsvereinigungen for the financial support of this work.

References:

- /1/ K. Kramer; P. Robertson; N. Ibl; J. Appl. Electrochem. 10,29 (1980)
- /2/ G. Kreysa; H. Medin; J. Appl. Electrochem. (in press)
- /3/ H. Wendt; H. Schneider; J. Appl. Electrochem. 16, 134, (1986)
- /4/ H. Medin; Dissertation; TU München 1983

Nomenclature:

A_p	specific interfacial area (cm^{-2})
C	concentration (Mol/l)
k_p	mass transfer coefficient (cm s^{-1})
k	rate constant ($\text{l mol}^{-1} \text{s}^{-1}$)
K_v	distribution coefficient (1)
V	Volume (cm^3)

THE RECOVERY OF ACETIC ACID, PHENOL AND ETHANOL BY SOLVENT EXTRACTION WITH A LIQUID PHOSPHINE OXIDE

E.K. Watson, W.A. Rickelton, A.J. Robertson, T.J. Brown, Cyanamid Canada Inc.,
Niagara Falls, Canada

INTRODUCTION

CYANEX®923 extractant is a liquid mixture of trialkylphosphine oxides containing C6 and C8 alkyl groups (Table 1). It was designed to overcome limitations encountered in the use of trioctylphosphine oxide (TOPO) while developing processes for the recovery of acetic acid, phenol and ethanol from aqueous solutions in this laboratory. TOPO, melting at 47-52°C, must be dissolved in a diluent. High-boiling diluents are used to facilitate solute recovery from the extract by distillation. The solubility of TOPO in such diluents is 150-200 kg/m³ at 25°C and 300-400 kg/m³ at 50°C. Dilution reduces the extraction coefficient (K) and increases the separation factor (α) relative to water. Volume of solvent required increases. Further, heavy compounds as in synthetic fuel plant effluents that were co-extracted with the acetic acid were not removed with the acetic acid from even the highest-boiling TOPO solution by straightforward distillation, requiring extra processing steps to be considered. CYANEX 923 extractant needs no diluent. It is liquid to 2°C. Observed K_D values are 2-5 times greater than those in diluted TOPO. The high boiling point of 310°C at 345 kPa ensures that the heaviest compound encountered to date can be distilled from the extract.

Acetic acid extraction with TOPO has been studied by King (1,2) and patented by Grinstead (3) and Kanzler (4). Development of a process using TOPO was described by Helsel (5). Phenol extraction with TOPO was patented by Savides (6). Ethanol extraction with TOPO was patented by Bright (7). This paper compares the performance of CYANEX 923 extractant with that of diluted TOPO solvents in single-contact extractions of the three solutes from aqueous solutions. Comparison is made with other potential extractants for ethanol.

EXPERIMENTAL

The acetic acid aqueous feed was a real sample of synthetic fuel plant effluent. It contained 6.15 kg/m³ acetic, 1.5 kg/m³ propionic, 0.6 kg/m³ butyric and still smaller concentrations of higher molecular weight acids. The phenol aqueous feed was prepared from laboratory grade chemicals to simulate the effluent from a phenol/bisphenol plant. It contained 10 kg/m³ phenol and 30 kg/m³ Na₂SO₄. Ethanol solutions were made up from denatured alcohol and distilled water. CYANEX 923 extractant was commercial grade, used without dilution.

TOPO was dissolved in alkylated benzene diluents. Equilibrations used a solution of 400 kg/m³ in Conoco*DPA diluent for acetic acid, of 325 kg/m³ in Conoco*500 diluent for phenol, and of 300 kg/m³ in Aromatic**100 diluent for ethanol. These TOPO concentrations were close to saturation in the respective diluent at the experimental temperature. One kinetic run used a TOPO solution of 150 kg/m³ in Conoco DPA.

Equilibrations were conducted in shake flasks immersed in a temperature controlled water bath. Kinetic runs used a stirred water-jacketed beaker. Temperature was 50°C in the acetic acid and phenol experiments, 25°C in the CYANEX 923 extractant/ethanol runs and 30°C in the TOPO/ethanol experiments. Contact time was 15 min. except in the kinetic runs where it was varied. Separated phases were filtered, organic through phase separation paper and aqueous through filter paper, before analysis. Aqueous phases were analyzed for acetic acid by titration, for phenol by UV and for ethanol by GC. Organic phases were analyzed for acetic acid by titration, for phenol by GC and for water by Karl Fischer. Ethanol in the organic phase was determined by three-component material balance.

RESULTS AND DISCUSSION

Extraction isotherms are compared in Figure 1. The better isotherm in each case for CYANEX 923 can be expected to reduce extraction stages and/or solvent circulation rate. For example, extraction of acetic acid from a 5 kg/m³ feed by CYANEX 923 extractant is complete in 3 stages with an O/A of 0.5. Diluted TOPO requires an O/A of 1.0 in 3 stages. With this O/A ratio, the CYANEX 923 needs only 2 stages.

Kinetics of acetic acid extraction are compared in Figure 2. The rate in CYANEX 923 extractant was slightly higher than in the TOPO solutions. Presumably, the added resistance to diffusion presented by the TOPO diluent is responsible. The rate for both solvents is fast enough for mixer-settler or column extractors.

K_D and α values for the extractant/substrate combinations are shown in Table 2. K_D is wt% solute in organic/wt% solute in aqueous; α is K_D for solute/ K_D for water. α for Phenol was not measured. The values tabled were determined by extrapolating experimental results to an aqueous solute concentration of zero for a common comparison basis. CYANEX 923 exhibited consistently higher K_D and lower α than the TOPO solutions, reflecting the trade-off effect discussed by King (8) of dilution with inert solvents.

In the special case of ethanol extraction from fermentation broths, the goal is a 20% solvent-free ethanol concentration in the extract. Higher values make no further reduction in the energy required in the subsequent distillation (Eakin, 9)(Figure 3). This sets a hypothetical minimum for required α corresponding to an infinite extractor, and a maximum useful value beyond which there is no further reduction in extractor volume or energy consumption. Both depend on feed concentration. These limits were computed and are shown in Figure 4 beside the value for CYANEX 923 extractant and ranges of values reported for several classes of potential extractants by Roddy (10) and King (11). In Figure 5 the K for the new extractant is positioned with respect to the range of reported values on a plot showing the effect of K_0 on extractor size. Clearly, CYANEX 923 is a serious candidate for ethanol extraction.

Solubility in water affects solvent losses and/or the need for extra processing steps to recover solvent from raffinate. The new extractant has no advantage over TOPO, and particularly diluted TOPO, in this regard, but it ranks high in the list of potential extractants shown in Table 3. Solubilities in Table 3 not available from the literature were estimated by the UNIFAC method (12).

ACKNOWLEDGEMENTS

The authors would like to express their thanks to American Cyanamid Company, in particular Drs. R.J. Boyle and J.B. Gallivan, for permission to publish this paper.

- * Product of the Continental Oil Co.
- ** Product of Exxon Corporation

REFERENCES

- (1) Wardell, J.M. and King, C.J., *Journal of Chemical and Engineering Data* 23, (2), 144 (1978)
- (2) Ricker, N.M., Michaels, J.N., King, C.J., *J. Separ. Proc. Technol.*, 1(1) 36 (1979)
- (3) Grinstead, R.R., US Patent 3,816,524 (1974)
- (4) Kanzler, W., Austrian Patent 365,080 (1981)
- (5) Helsel, R.W., *Chem. Eng. Prog.* 73 (5), 55 (1977)
- (6) Savides et. al., US Patent 4,420,643 (1983)
- (7) Bright, J.H., US Patent 4,544,779 (1985)
- (8) King, C.J., "Separation Processes", 2nd Ed., McGraw Hill, New York (1980), p. 757-763
- (9) Eakin, D.E. et. al., Preliminary Evaluation of Alternative Ethanol/Water Separation Processes, Battelle, Pacific Northwest Laboratory, Report No. PNL-3823 (1981)
- (10) Roddy, J.W., *Ind. Eng. Chem. Process Des. Dev.* 20, 104 (1981)
- (11) Munson, C.J., King, C.J., *Ind. Eng. Chem. Process Des. Dev.* 23, 109 (1984)
- (12) Magnussen, T. et. al., *Ind. Eng. Chem. Process Des. Dev.* 20, 331 (1981)
- (13) Sorenson, J.M., Arlt, W., "Liquid-Liquid Equilibrium Data Collection", DECHEMA, Vol V, Part 1 (1979)
- (14) Schulz, W.W., Navratil, J.P., "Science and Technology of Tributyl Phosphate", CRC Press (1982)

TABLE 1. PROPERTIES OF CYANEX 923 EXTRACTANT

Average Molecular Weight	= 348
Trialkylphosphine oxides:	93%
Specific Gravity:	0.88 @ 25°C
Freezing Point:	-5 to +2°C
Viscosity:	.04 Pa.s @ 25°C .014 Pa.s @ 50°C
Boiling Point:	310°C @ 345 kPa
Solubility in Water:	10 mg/kg
Solubility of Water in:	8 w/o

TABLE 2. K_D AND α

CYANEX 923 EXTRACTANT	T O P O					
	K_D	α	Diluent	Conc. kg/m ³	K_D	α
Acetic Acid	8.9	46	Conoco DPA	400	4.9	170
Phenol	1200	---	Conoco 500	325	240	---
Ethanol	1.0	15	Aromatic 100	300	0.48	40

TABLE 3. POTENTIAL ETHANOL EXTRACTANTS SOLUBILITY IN WATER, WT%

	<u>Exptl(1)</u>	<u>UNIFAC</u>
CYANEX 923 Extractant	0.001 (2)	
Tri-n-Butyl Phosphate	0.042 (3)	
n-Butyl Acetate	0.64	
i-Butyl Acetate	0.85	
Methyl Isobutyl Ketone	1.9	
Diisobutyl Ketone	0.083	
Isophorone		0.19
3-Phenyl-1-Propanol		0.15
2-Ethyl-1-Butanol		0.88
3-Methyl-3-Pentanol	4.3	
4-Methyl-2-Pentanol	1.6	
3-Ethyl-3-Pentanol	1.7	
2,4-Dimethyl-3-Pentanol	0.7	
2,3,4-Trimethyl-1-Pentanol		0.12
2-Ethyl-1-Hexanol		0.12
3-Methyl Cyclohexanol		0.55
2-Ethyl-1-Heptanol		0.045
3-Ethyl-3-Heptanol		0.048
2,4-Dimethyl-3-Heptanol		0.044
2,6-Dimethyl-4-Heptanol		0.044
1-Octanol	0.051	
2,2-Dimethyl-3-Octanol		0.017
3,7-Dimethyl-3-Octanol		0.017
1-Nonanol	0.013	
1-Decanol	0.0037	
4-Decanol		0.016
1-Dodecanol	0.00023	
1-Tridecanol		0.00072
2-Ethyl-4-Methyl Pentanoic Acid		0.24
n-Hexanoic Acid	1.1	
2-Ethyl Hexanoic Acid		0.24
n-Octanoic Acid		0.24
Neodecanoic Acid		0.032

(1) Sorenson and Arlt (13) except as noted

(2) This work

(3) Schulz and Navratil (14)

Fig.1 EQUILIBRIA

Acetic Acid

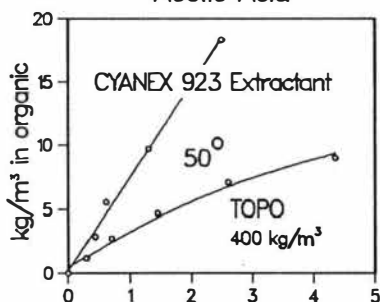
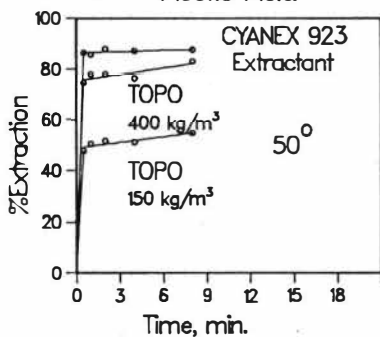


Fig.2 KINETICS

Acetic Acid



Phenol

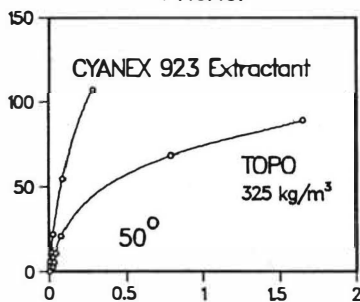


Fig.3 ENERGY

Ethanol

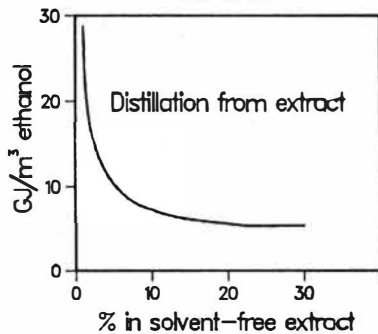
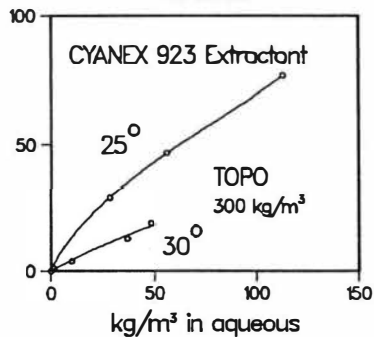


Fig.4 α IN ETHANOL/WATER

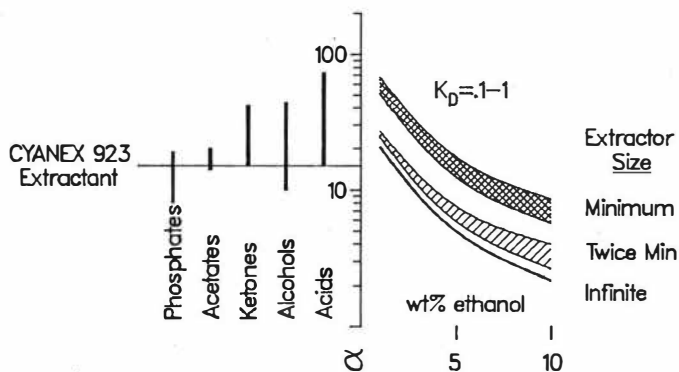
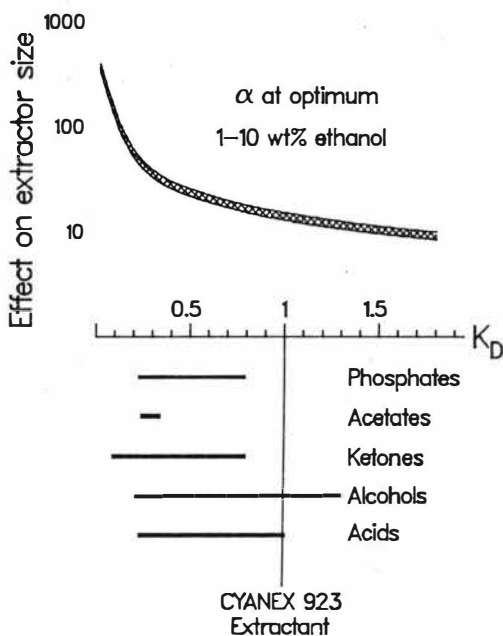


Fig.5 K_D IN ETHANOL/WATER



Separation of Acetic Acid and Glycerol from Aqueous Solutions

Gerd Brunner and Ralf Döhrn **

** Prof. Dr.-Ing. G. Brunner and Dipl.-Ing. R. Döhrn, Arbeitsbereich Verfahrenstechnik II, Technical University of Hamburg-Harburg, Eissendorfer Strasse 38, D-2100 Hamburg 90, Federal Republic of Germany.

The separation process of supercritical gas extraction can be regarded as an extraction process in which the extractant or solvent is a supercritical dense gas. The well-known basic flow diagram of an extraction process can be applied on the extraction with supercritical gases (fig.1).

A mixture of substances A and B, which are to be separated, is introduced into a separating stage. Within this process stage, component A is preferentially taken up by the solvent (supercritical gas). At an adequately selectivity or with a sufficient number of theoretical stages, component A is largely removed by the supercritical solvent and component B essentially remains in the residue (P2 in fig 1.).

The solvent properties of the supercritical solvent can be altered by a temperature or pressure change. By this way component A can be separated from the solvent by precipitation in the second process stage. Subsequently, the regenerated supercritical gas is pressurized, thermostated and pumped again to the separation stage. The

extract P1, which consists mainly of component A is removed from the second and product P2 from the first stage.

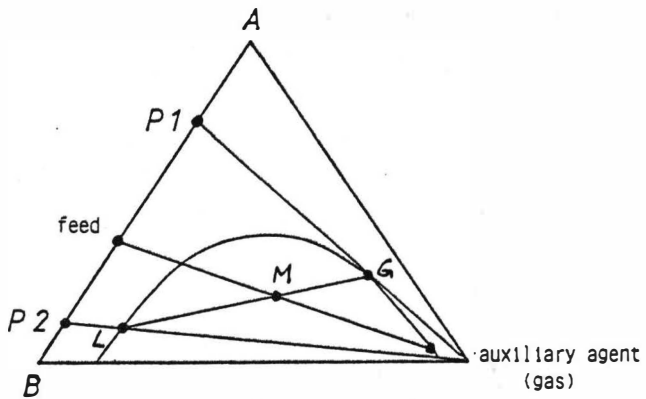
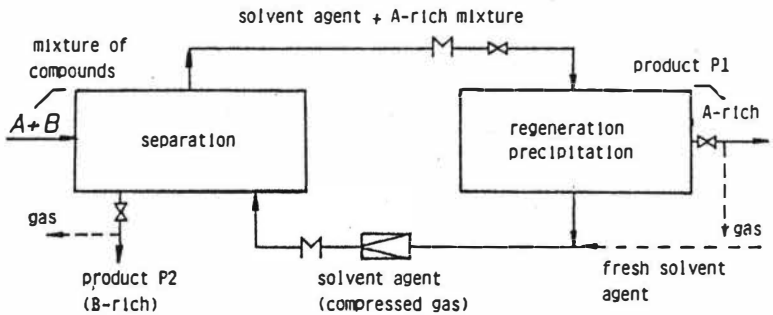


Fig. 1: Flow scheme of a separation process using supercritical solvents

The extraction can be also illustrated in a standard triangular diagram (fig 1). The feed F, consisting of the substances A and B is mixed with the solvent S that the overall composition corresponds to the point M. The mixture separates into a gaseous phase G and a liquid phase L. When the supercritical gas is removed these

equilibrium phases result in the products P1 and P2. So far, extraction processes with either a liquid or a supercritical gaseous solvent hardly differ.

The investigation for separating organic substances and water have been carried out in an apparatus in which the phases can be contacted countercurrently. The set up consists essentially of two columns and the necessary pumps to provide the mass flows.

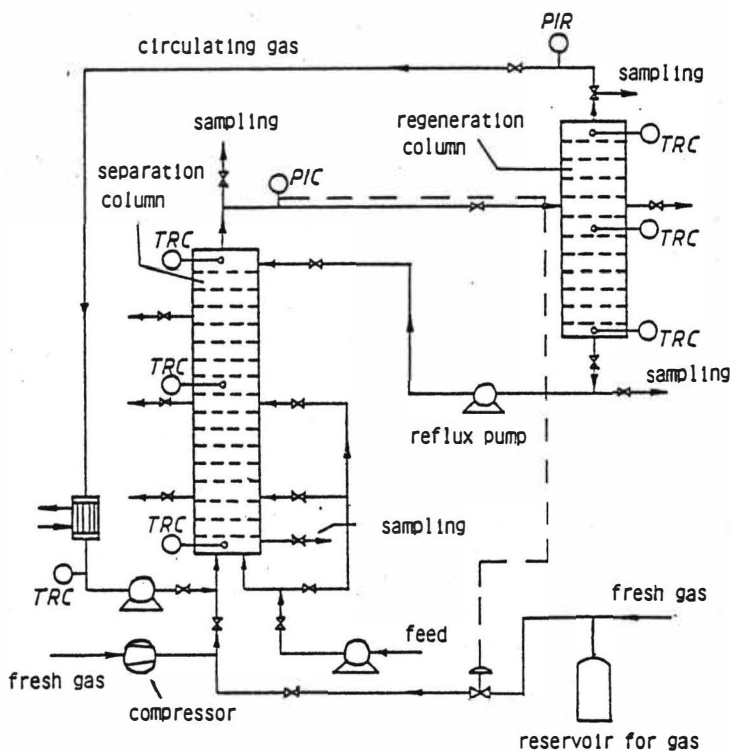


Fig. 2: Flow scheme of the experimental apparatus

For the investigation of the separation of organic substances from aqueous solutions one column was operated as a bubble column. For this purpose the column (height 3.4 m, inner diameter $17 \cdot 10^{-3}$ m) was filled at operating pressure up to one third of its height with the mixture to be separated. Then pure gas was bubbled from the bottom through the column. The gas was removed at the top of the column, depressurized and separated in a liquid and a gaseous part.

Dimensions and column internals are shown in fig 3. The column contains wire networks. A collecting ring is installed after every tenth network.

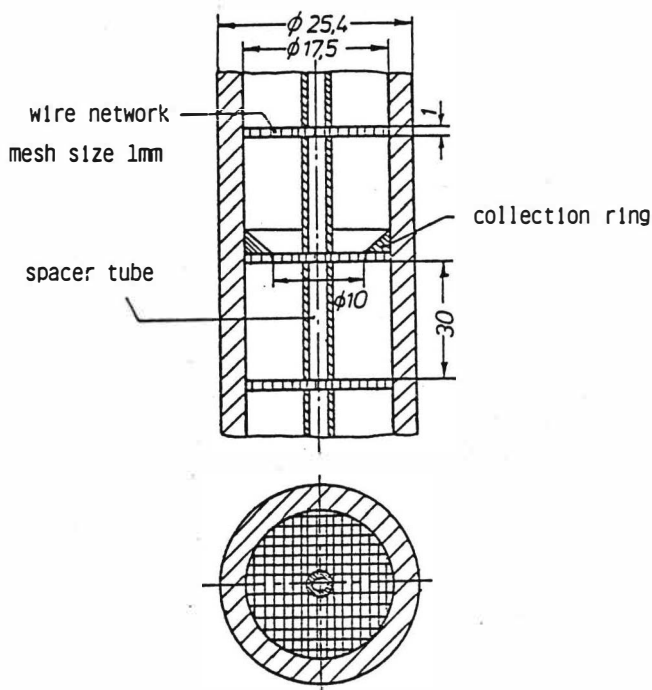


Fig. 3 : Detail of the experimental column

In fig. 4 the depletion in ethanol of the liquid is shown for temperatures between 20°C and 95°C at a pressure of 155 bar. Gas flow was 1000 cm³/h corresponding to a mean linear velocity of the gas, related to the free column area, of 1.2 mm/s. With increasing temperature the extraction accelerates. This is due to the like wise effects of enhanced diffusivity and enhanced solubility of ethanol in carbon dioxide at higher temperatures.

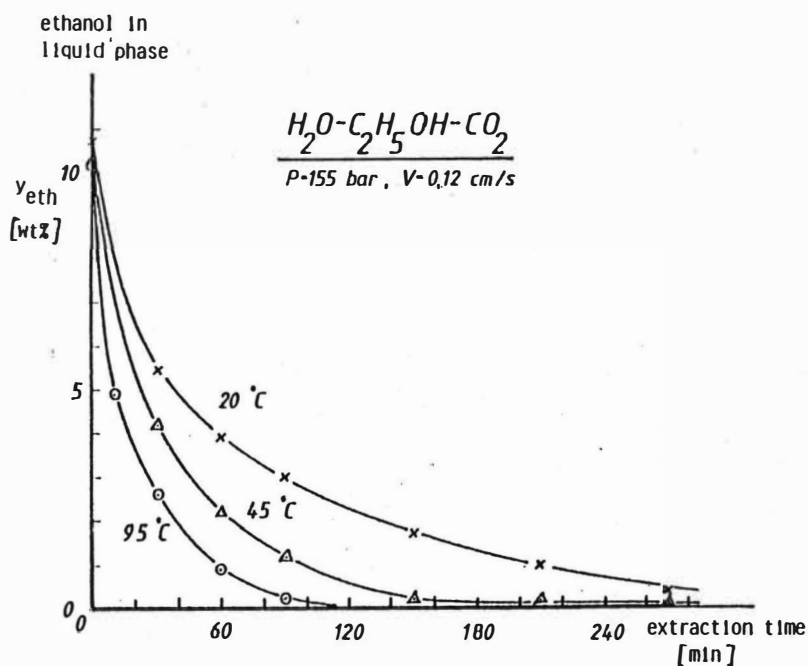


Fig. 4: Content of ethanol in the liquid phase as function of the extraction time

In further experiments the extraction of other organic substances from aqueous solutions has been investigated. Fig.5 shows the depletion in acetic acid and glycerol of the liquid at a temperature of 60°C and a pressure of 150 bar.

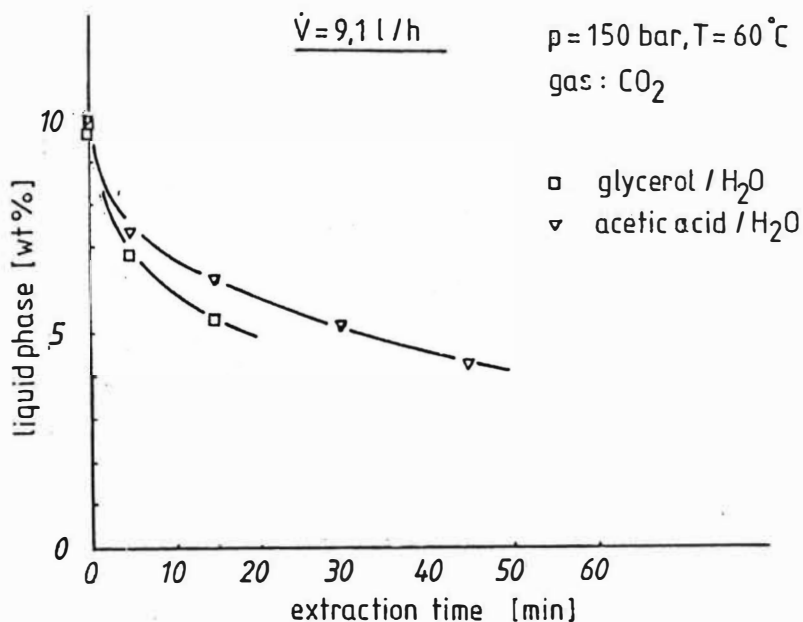


Fig. 5: Separation of organical substances by means of supercritical gas extraction

In table 1 the extraction by means of a supercritical gas mixture of carbon dioxide and propane ($P = 150 \text{ bar}, T = 60^\circ\text{C}$) is compared with a distillation process for the acetic acid - water separation.

In the gas extraction process the acetic acid concentration can be

increased after one theoretical stage from 10 to 60 wt% (distillation: 16.4 wt%) with a separation factor of 13.5 (distillation: 1.77). To increase the concentration from 10 to 67 wt% the gas extraction process needs 1.3 theoretical stages while a distillation process needs 6.

Table 1

Comparison of the supercritical gas extraction (CO₂-propane, 150 bar, 60°C) with a distillation process of a acetic acid - water mixture

	distillation process	gas extraction process
Feed concentration, acetic acid	10 wt%	10 wt%
Concentration after one theoretical stage	16.4 wt%	60 wt%
separation factor	1.77	13.5
number of theoretical stages needed for a concentration increase from 10 to 67 wt%	6	1.3

J. Kwiatkowski, W. Majewski, A.M. Szafranski, Z. Lisicki

Industrial Chemistry Research Institute, Rydygiera 8, 01-793 Warsaw, POLAND

The solvency of a supercritical fluid (SCF) for low-volatile coal-liquids constituents like naphthalene, methyl naphthalenes, anthracene, fluorene and numerous other two- and three-ring compounds, is by a factor of 10⁴ to 10¹⁰ in excess of that of an ideal-gas mixture. This enhancement underlies the SCF extraction process which has recently been gaining more and more in industrial interest.

We have measured the solubilities of naphthalene, anthracene, phenanthrene, fluorene and carbazole and of some binary mixtures thereof, viz., phenanthrene-anthracene, fluorene-anthracene, anthracene-carbazole and phenanthrene-carbazole, in carbon dioxide at pressures of 100-200 bar (100-180 bar for C₁₀H₈) and at a temperature of 313.1 K (308.1 K for C₁₀H₈). The flow technique was used as described at more length elsewhere /2/. The experimental assembly (Fig. 1) comprised a solvent purification and supply system, a pressure and flow control system, expansion valve, cold trap, and a flow rate and volume measuring system. For experimental procedure see ref. /2/.

For simple fluid mixtures considerable progress has been achieved in the EoS-based description of the solubility in SCF solvents /3-5/. For mixtures containing species with large molecular size and shape differences and/or permanent polarity, equations of state (EoS) are still at an early stage of development. At present, a more practical approach is to use mixing rules for developing mixture EoS from pure fluid EoS. The conformal solution theory and the density expansion expression of the radial distribution function of fluids has recently been used to derive a set of mixing rules /6/.

The solubility of a solid 2, y₂, in an SCF solvent is expressed /7/ as

$$y_2 = (p_2^s/p)(\beta_2^s/\beta_2) \exp \int_{p_2^s}^p (v_2^s/RT) dp \quad (1)$$

where β_2^s is the fugacity coefficient of solid 2 at the saturation pressure and β_2 is the vapor phase fugacity coefficient of the solute 2 at pressure p. With the solid volume v_2^s assumed to be independent of pressure and p_2^s very small (β_2^s tending to unity), Eq.(1) becomes

$$y_2 = (p_2^s/p) \beta_2^{-1} \exp(v_2^s(p - p_2^s)/RT) \quad (2)$$

For the calculation of β_2 an EoS must be chosen, the simplest choice being the van der Waals equation,

$$(p + a/v^2)(v - b) = RT \quad (3)$$

Numerous mixing rules have been suggested /9/, among which the following

$$I. \quad a = \sum_i \sum_j x_i x_j a_{ij} \quad (4a)$$

$$b = \sum_i x_i b_i \quad (4b)$$

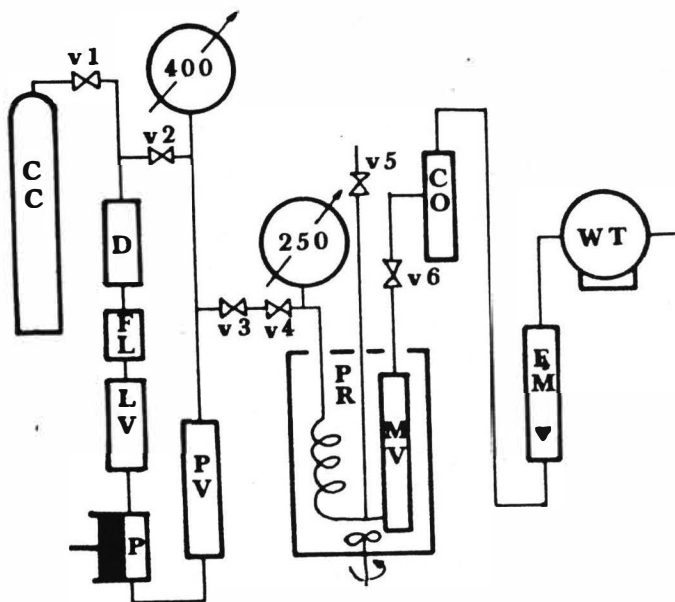


Fig. 1. Line diagram of the flow-method assembly for measuring solubility of organic solids. CC - compressed gas cylinder, D - drier, FL - fine filter, LV - liquefaction vessel, PR - preheater, CO - condenser, MV - measuring vessel including equilibrium cell kept in water bath, FM - flow meter, WT - wet test meter, V1 thru V6 - pressure valves

are the common practice in EoS engineering applications /1, 8/. With the unlike-interaction parameter a_{ij} ($i \neq j$) assumed as

$$a_{ij} = (1 - k_{ij})(a_{ii}a_{jj})^{0.5} \quad (4c)$$

and with Eq.(3) chosen as the EoS, the fugacity coefficient of solute 2 in an SCF solvent is

$$\phi_2 = (RT/(v - b)) P^{-1} \exp(b_2/(v - b) - 2 \sum_j x_j a_{2j}/vRT) \quad (5)$$

$$\text{II. } a = \sum_i \sum_j x_i x_j a_{ij} \quad (6a)$$

$$b = \sum_i \sum_j x_i x_j b_{ij} \quad (6b)$$

The difference between Case I and Case II mixing rules is in the expression for b . The unlike-interaction parameters are expressed as

$$a_{ij} = (1 - k_{ij})(a_{ii}a_{jj})^{0.5} \quad (7a)$$

$$b_{ij} = ((b_{ii}^{1/3} + b_{jj}^{1/3})/2)^3 \quad (7b)$$

The fugacity coefficient then becomes

$$p_2 = (RT/(v - b))P^{-1} \exp((-b + 2 \sum_j x_j b_{2j})/(v - b) - 2 \sum_j x_j a_{2j}/vRT) \quad (8)$$

III. A third set is the set of the DEX mixing rules /6/ which with the van der Waals equation (3) are

$$a = (b/2)((D - vRT)/C + ((D - vRT)^2/C^2 + 4vRT/b)) \quad (9a)$$

$$b = \sum_i \sum_j x_i x_j b_{ij} \quad (9b)$$

$$\text{where } C = \sum_i \sum_j x_i x_j a_{ij} \quad \text{and} \quad D = \sum_i \sum_j x_i x_j a_{ij}^2/b_{ij}$$

The fugacity coefficient is

$$p_2 = (RT/(v - b))P^{-1} \exp(-b + 2 \sum_j x_j b_{2j})/(v - b) - \int_v^\infty (A_2/v^2 RT) dv \quad (10)$$

$$\text{where } A_2 = (1/n)((\partial(n^2 a)/\partial n_2))_{T, v, n}$$

For the unlike-interaction parameters in these mixing rules the same expressions as Eqs.(9a) and (9b) are used.

The sets I and II proved to be inferior to the set III of mixing rules in the prediction of the solubilities of the pure solids studied in this work in much the same way as they were for 2,3- and 2,6-dimethyl-naphthalene in supercritical CO_2 and C_2H_6 /6/. Therefore, set III was adhered to in the present calculations.

With the interaction parameter k_{12} adjusted to one experimental solubility data the predictions obtained are all consistent to within 1-5% with the observed values (Figs. 2-5). With binary solid phases the agreement is less satisfactory.

The solubilities of fluorene, anthracene and phenanthrene in CO_2 rise considerably as the pressure is increased and at 200 bar the values are about twice as high as those at 100 bar. The three compounds exhibit highly diverse saturated vapor pressures and critical evaluation of the available experimental pure-compound property data has disclosed considerable discrepancies /10, 11/. Pure-compound data uncertainties may well have at least partly affected the solubility predictions for the binary solid phases examined.

In the ternary systems studied (two solids + SCF solvent), the effect of pressure on the solubility is quite similar to that observed in the binary systems: the solubility rises as the pressure is increased. It is thus easy to see that the solutes interact with each other to enhance their solubilities in CO_2 . Whether a pure solute or cosolute with anthracene, fluorene is soluble to a similar extent. Anthracene, however, as a cosolute with fluorene is much more soluble than it is in the binary system (Fig. 3). It behaves likewise in the systems

involving phenanthrene (Fig. 4) and carbazole (Fig. 5). The solubilities of phenanthrene in the two ternary systems involving anthracene (Fig. 4) and carbazole (Fig. 5) are lower than the solubility of phenanthrene alone. The solubilities of carbazole in the ternary systems examined are close to the values established for pure carbazole as a solute in CO_2 . The selectivity of supercritical carbon dioxide in the ternary systems investigated increases as the pressure is raised.

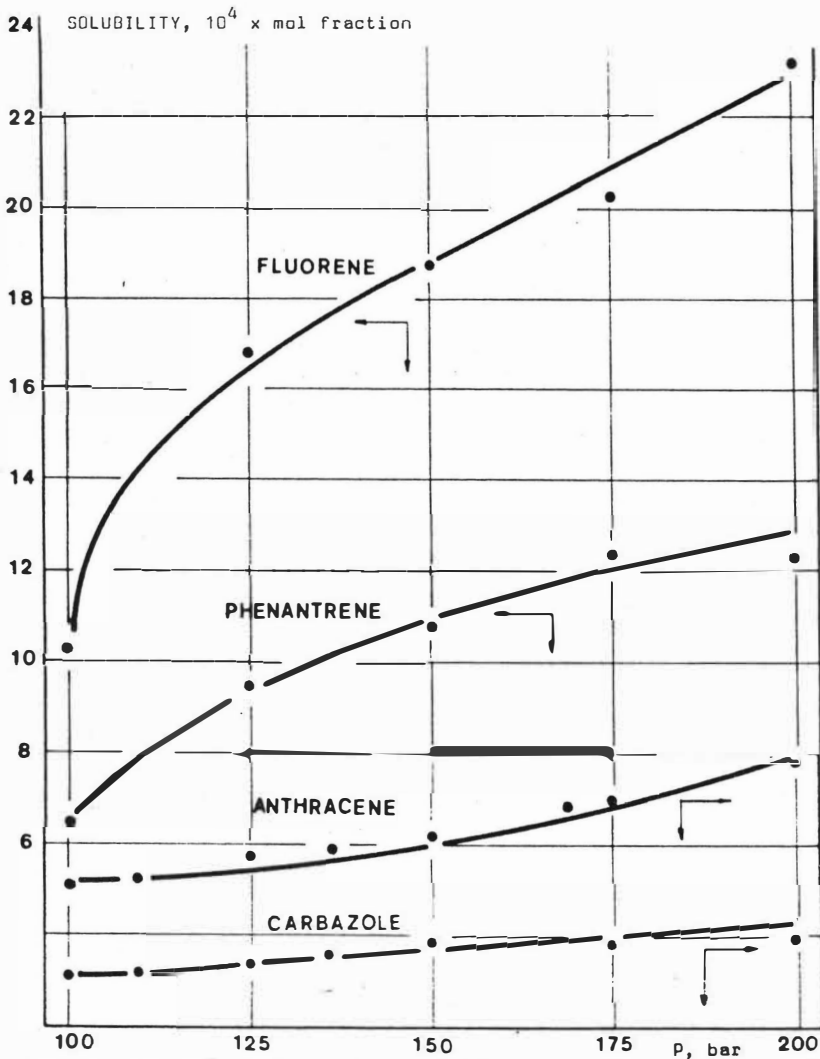


Fig. 2. The solubility of trinuclear hydrocarbons in CO_2 at 313.1 K.

SOLUBILITY, $10^4 \times$ mol fraction

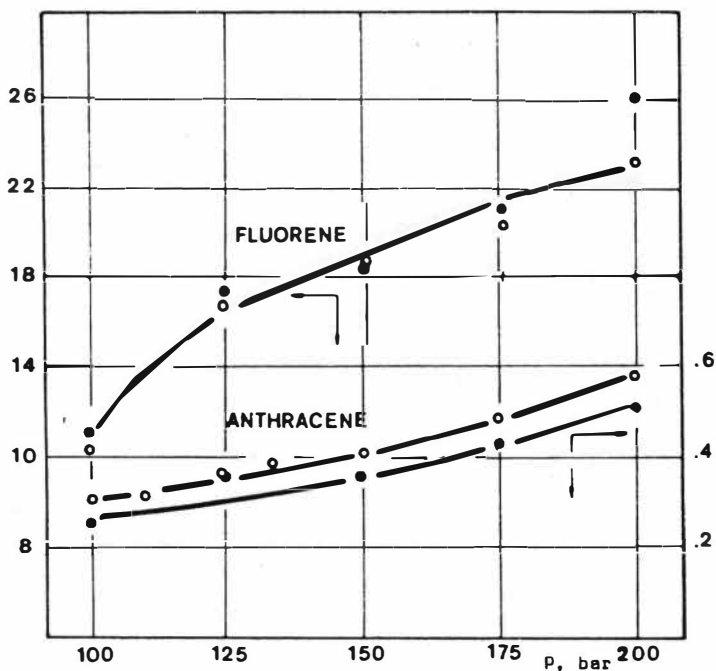


Fig. 3. The solubility of fluorene and anthracene in CO_2 at 313.1 K. o - binary system; • - ternary system.

REFERENCES

1. Kurnik, R.T., S.J. Holla, R.C. Reid, *J.Chem.Eng.Data*, **B6**, 47 (1981).
2. Kwiatkowski, J., Z. Lisicki, W. Majewski, *Ber.Bunsenges.Phys.Chem.*, **88**, 865 (1984).
3. Lebowitz, J.L., J.S. Rowlinson, *J.Chem.Phys.*, **41**, 133 (1964).
4. Mansoori, G.A., N.F. Carnahan, K.E. Starling, T.W. Leland, *J.Chem.Phys.*, **54**, 1523 (1971).
5. Mansoori, G.A., T.W. Leland, *J.Chem.Phys.*, **53**, 1931 (1970).
6. Mansoori, G.A., J.F. Ely, *Density Expansion (DEX) Mixing Rules*, IX Intern. CODATA Conf., Jerusalem, June 1984.
7. Prausnitz, J.M., *Molecular Thermodynamics of Fluid Phase Equilibria* Prentice Hall, Englewood Cliffs, N.J., 1969.
8. Reid, R.C., J.M. Prausnitz, T.K. Sherwood, *The Properties of Gases and Liquids*, 3rd ed., McGraw-Hill, N.Y., 1977.
9. Sievers, U., S. Schulz, *VDI-Forsch.-Heft No. 609*, 45 (1982).
10. Szafranski, A.M., D. Wyrzykowska-Stankiewicz, *IChP Report 1982*.
11. Szafranski, A.M., D. Wyrzykowska-Stankiewicz, unpublished work.

SOLUBILITY, $10^4 \times$ mol fraction

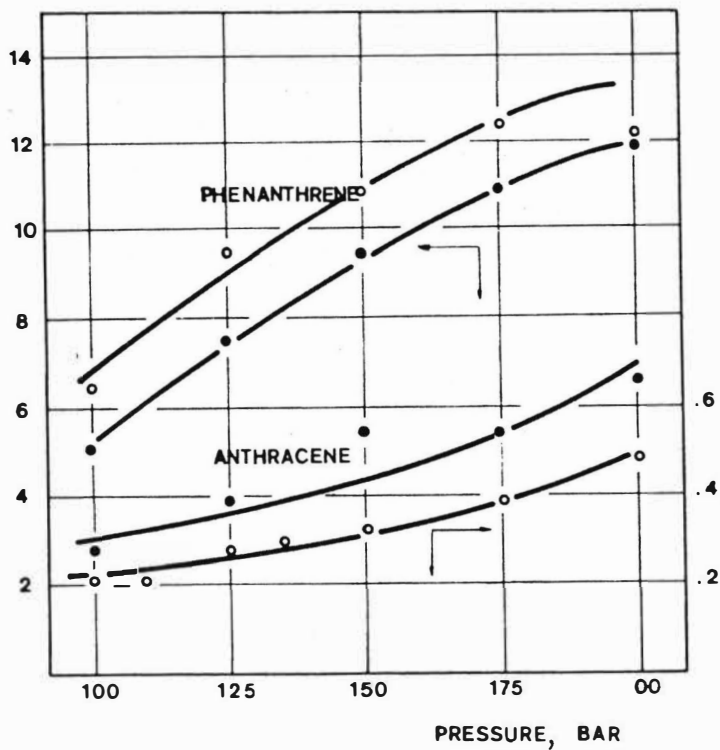


Fig. 4. The solubility of phenanthrene and anthracene in CO_2 at 313.1 K. o - binary system; • - ternary system.

SOLUBILITY, $10^4 \times$ mol fraction

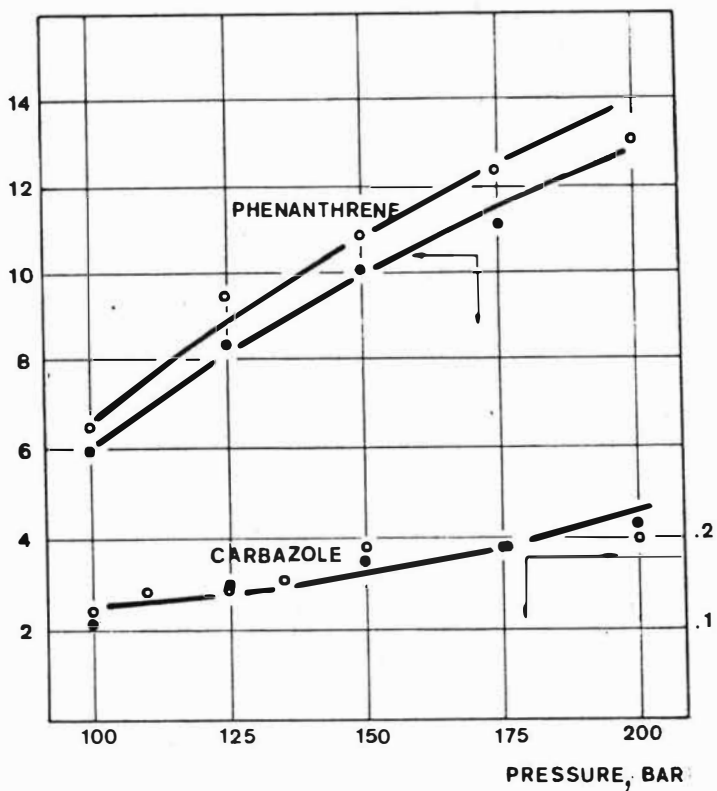


Fig. 5. The solubility of phenanthrene and carbazole in CO_2 at 313.1 K. o - binary system; ● - ternary system

High Pressure Extraction of Chemically Similar Substances

G. Braun, Hoechst AG, Frankfurt (M), FRG

Some of the reasons for the lively interest in high pressure extraction as an alternative to conventional separation processes like distillation and solvent extraction are the relatively low operating costs and the simple recovery of the solvent from the extract.

Therefore, in addition to applying high pressure extraction to food processing (coffee, hops, and spices) (1) increasing attempts have been made in the past years to apply this method to separation problems which are typical in the field of traditional industrial chemistry, like the purification of crude montan wax (2), the fractionation of polymeres (3) and above all the separation of chemical products from aqueous solutions (4, 5) and from solid and liquid wastes (6).

In high pressure extraction even chemically very similar substances may have significantly different extractabilities. E.g. from a mixture of α -olefines certain homologues can be selectively extracted (7). In many supercritical gases twice as much α -naphthol as the β -isomere is dissolved (8). Even in CO_2 at 150 bar and 40 °C the solubility of o-hydrobenzoic acid is 200 times that of the p-compound (9).

In this paper the separation of isophthalic acid dimethylester (DMI) from terephthalic acid dimethylester (DMT) and, respectively, of 5-oxohexanoic acid (OHA) from 1,3-cyclohexanedione (CD) will be reported on.

EXPERIMENTAL

High pressure extraction was carried out in a 4 l laboratory apparatus (fig. 1) at pressures of 100 to 300 bar and temperatures of 20 to 80 °C. The solvents used were CO_2 and ethylene as well as the fluorinated hydrocarbons Frigen R 13 (CClF_3) and R 23 (CHF_3).

The supercritical gas was passed for extraction through a bed of DMI/DMT ground to about 0.1 mm particle size or through a CD/OHA mother liquor in the extraction vessel. The extract was recovered at subcritical

pressure and temperature in a separation vessel, allowing the extract-free solvent to be recirculated.

RESULTS

To study the solubility of DMI and DMT in supercritical CO_2 first a mixture with 50 wt.% DMI was treated at 100 to 200 bar and 40 °C with 10 kg CO_2 /kg of mixture. By raising the pressure the percentage of DMI extracted increased from 15 to 92, whereas simultaneously 2 to 50 % of DMT were extracted (fig. 2). Correspondingly the loading capacity of CO_2 with DMI and DMT increased from 7.6 to 46 g DMI/kg CO_2 and from 1 to 25 g DMT/kg CO_2 , respectively. At 200 bar the content of DMI in the residue was only 13.3 wt.%. The separation factor $\alpha_{\text{DMI,DMT}}$ had values from 9 to 13.5.

Using Frigen 23 which is more polar than CO_2 it was possible already at 100 bar to extract 96 % of DMI and only 6 % of DMT (fig. 2). This corresponds to a separation factor of 360. Increasing pressures mainly resulted in higher fractions of DMT being coextracted. The same effect was observed by changing the temperature. Raising the temperature from 40 to 80 °C at 150 bar more than doubled the extractability of DMT ($\varphi = 45\%$), with the DMI values remaining almost constant. This corresponds to an increase of DMT dissolved in the Frigen 23 from 10 to 22.4 g DMT/kg and a decrease of the separation factor to 45.

It was also found that the results strongly depend on the composition of the starting material (fig. 3). Both with an initial DMI content of 20 wt.% and of 80 wt.%, DMI was almost totally extracted at 200 bar and 40 °C with 10 kg CO_2 /kg of mixture. Since at the same time the fraction of DMT extracted increased from 21 to 98 % the separation factor dropped from 1 170 (calculated with 0.1 wt.% DMI in the residue) to 1.1. Changing the initial DMI content from 20 to 80 wt.% the loading capacity of CO_2 with DMI increased to the fourfold. This indicates that an almost quantitative and perhaps more selective extraction of DMI from a 20 wt.% DMI starting material should be possible with solvent ratios smaller than 10 kg CO_2 /kg of mixture.

Similar results with different initial DMI contents were obtained for the extraction with Frigen 23 at 150 bar and 40 °C. However, because of the lower fraction of DMT being coextracted the separation factors for 20 to 50 wt.% initial DMI content are higher (2 850 and 5 000, resp.) compared with CO₂. If the starting material contained 80 wt.% DMI a separation from DMT was impossible ($\alpha = 1$) even with Frigen 23.

1,3-Cyclohexanedione (CD), which is a chemical intermediate in the production of resorcinol, can be obtained by cyclisation of 5-oxohexanoic acid (OHA). CD is crystallized from a solution of the reaction products in toluene and a mother liquor remains, still containing 10 to 20 wt.% CD along with 25 to 55 wt.% OHA and 5 to 10 wt.% enole-lactone of OHA. An attempt was made to extract CD from such mother liquors with CO₂ and ethylene as well as with Frigen 13 and 23 at 22 to 40 °C and 150 to 300 bar.

With CO₂ and ethylene extraction yields of 41 to 68 wt.% were obtained (tab. 1). With Frigen 13 as much as 89 wt.% of the mother liquor were dissolved in the supercritical phase, but only 2 wt.% with the more polar Frigen 23. With CO₂ about 25 % of the CD and 51 to 64 % of the OHA were extracted (tab. 2). This corresponds to separation factors $\alpha_{OHA,CD}$ of 3.3 to 6.7. In ethylene, as opposed to CO₂, the solubility of CD was higher than that of OHA ($\alpha_{CD,OHA} = 5.4$).

By high pressure extraction using CO₂ or ethylene 90 to 100 % of the less polar toluene and DHA enole-lactone could be separated from the mother liquors. However, Frigen 13 which is of medium polarity dissolved only about 50 % of toluene, but 95 % of CD and 98 % of DHA. The even more polar Frigen 23 would extract neither CD nor OHA and only 12 % of toluene.

SUMMARY

The results of the high pressure extraction studies indicate that with supercritical gases it is quite possible to separate chemically very similar substances or at least to enrich one of them.

Both with CO₂ and preferably with Frigen 23 dimethylisophthalate can be completely separated from dimethylterephthalate at 150 bar and 40 °C, if the initial material contains 20 to 50 wt.% DMI. However, starting with a mixture of nearly eutectical composition (83 wt.% DMI) a separation

of DMI from DMT by high pressure extraction is no longer possible.

The strong influence of the supercritical solvent used is demonstrated by the studies on the high pressure extraction of technical grade mother liquors of 1,3-cyclohexanedione and 5-oxohexanoic acid. Using CO₂ and Frigen 13 OHA is preferably extracted compared to CD, whereas ethylene dissolves better CD than OHA. Toluene can be separated from the mother liquor almost quantitatively with CO₂ and ethylene, but with the more polar Frigen types R 13 and R 23 only up to 50 and 12 %, respectively, can be achieved.

REFERENCES

- (1) Chem. Ind. (London) 12 (1982) 385.
- (2) G. Braun, H. Schmidt; Ber. Bunsenges. Phys. Chem. 88 (1984) 891.
- (3) G. Braun; Chem.-Ing.-Tech. 56 (1984) 856.
- (4) M. E. Paulaitis, R. G. Kander, J. R. DiAndreth; Ber. Bunsenges. Phys. Chem. 88 (1984) 869.
- (5) G. Brunner, K. Kreim; Chem.-Ing.-Tech. 57 (1985) 550.
- (6) Critical Fluid Systems, Inc.; Chem. Engng. (1985) 24.06., 27.
- (7) K. Zosel; Angew. Chem. 90 (1978) 748.
- (8) H. Brogle; Chem.-Anl. u. Verf. (1981) 5, 58.
- (9) E. Stahl, W. Schilz, E. Schütz, E. Willing; Angew. Chem. 90 (1978) 778.

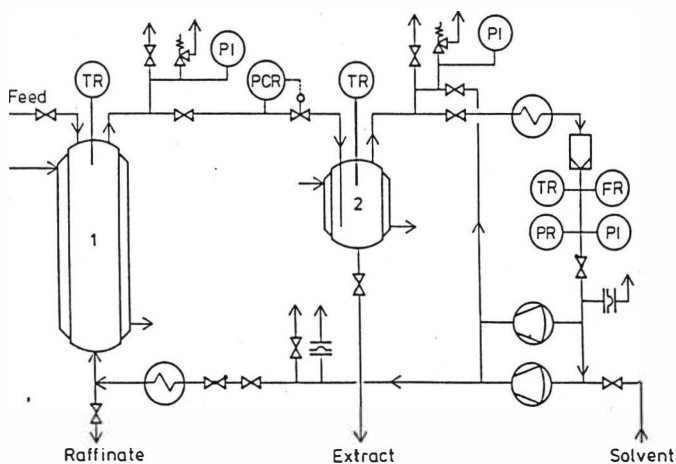


Fig. 1 Flow sheet of the high pressure extraction unit
(1: extractor, 2: separator)

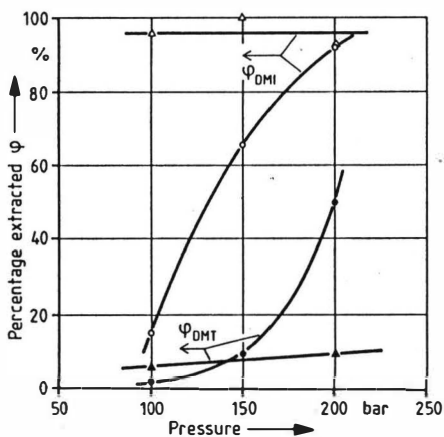


Fig. 2 High pressure extraction of DMI and DMT at 40 °C
($c_0 = 50\%$ DMI) using CO₂ (○,●) and Frigen 23 (△,▲)

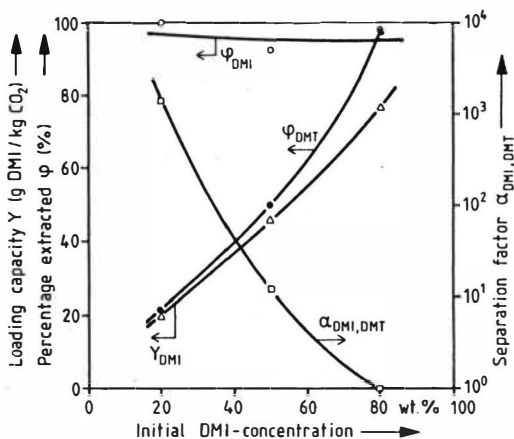


Fig. 3 High pressure extraction of DMI and DMT with CO_2 at 40°C and 200 bar

Tab. 1 HP extraction of CD mother liquors

Solvent		Extraction		Separation		
-type	-ratio (solvent/sample)	p_1 (bar)	T_1 ($^\circ\text{C}$)	p_2 (bar)	T_2 ($^\circ\text{C}$)	Yield (wt. %)
CO_2	24.7	150	40	45	24	55.8
CO_2	15.5	300	40	50	24	57.4
CO_2	22.3	300	35	50	22	67.8
C_2H_6	~15.0	300	22	35	5	51.2
F 13	~25.0	300	38	30	22	89.0
F 23	~20.0	300	35	40	22	2.0

Tab. 2 Degrees of extraction and separation factors attained by high pressure extraction of CD mother liquors (ELO: enol-lactone of OHA, α : separation factor)

Gas	Degree of extraction (%)				$\alpha_{\text{OHA,CD}}$
	CD	OHA	ELO	Toluene	
CO ₂	21.6	51.4	98.0	98.1	3.83
CO ₂	29.9	58.4	100.0	97.0	3.29
CO ₂	25.0	64.1	96.5	95.9	6.71
C ₂ H ₆	31.4	19.4	89.5	98.4	0.18
F 13	94.6	98.3		~50.0	3.31
F 23	0	0		12.1	

CPF : Continuous Polymer Fractionation

H. Geerßen, P. Schützeichel, B.A. Wolf; University of Mainz

It is well known how to fractionate polymers on a gram-scale^{1,2)}, but in most cases the expenditure of time and solvent forbids such procedures as soon as more than ca. 10 gram of the final product are required.

It has now been found^{3,4)} that a special form of counter-current extraction, the continuous polymer fractionation (CPF), can be used to obtain practically any amount of polymeric material with adequately narrow molecular weight distribution. This method does not make use of a miscibility gap between two low molecular weight liquids like a normal extraction, but functions on the basis of a solubility gap that is bound to the presence of the extract, i.e. of the polymer (intrinsic extraction).

Principle of the CPF :

A comparatively concentrated polymer solution (ca. 15 wt-% polymer) is used as feed (FD) and a suitable solvent/non-solvent mixture as extracting agent (EA).

The solvent components and the compositions of FD and EA are chosen such that

- (1) the low molecular weight liquids are miscible over the whole concentration range,
- (2) the entire system formed by the starting polymer and the mixed solvent exhibits a miscibility gap at the temperature of operation,
- (3) the composition of the FD corresponds to a point outside of this miscibility gap in the Gibb's phase triangle, and
- (4) the straight line drawn between FD and EA intersects the miscibility gap.

If these requirements are fulfilled and the corresponding flows \dot{V} of FD and EA are selected properly, the FD (depleted of the short polymeric chains) leaves the counter-current column as the polymer rich gel phase (GL) and the EA (now containing the short polymer chains) as the polymer-poor sol-phase (SL). The situation is shown in Fig. 1a schematically for the normally used mixed solvents. In addition Fig. 1b gives the situation with the special case of the CPF in which a single (theta-) solvent is used.

Apart from the composition of EA and FD, the main independent variable of the CPF is $\dot{q} = \dot{V}^{EA} / \dot{V}^{FD}$, the ratio of the flows entering the column. Among the important dependent variables are the corresponding ratio $\dot{r} = \dot{V}^{SL} / \dot{V}^{GL}$ of the flows leaving the column and $\dot{G} = \dot{m}_p^{SL} / \dot{m}_p^{GL}$, the ratio of the masses of polymer discharged per unit of time in these phases.

Fig. 1 a/b :

Schematic phase diagrams showing the composition of the flows entering and leaving the CPF-column in the case of mixed (1a) and single (1b) solvents.

- L : Solvent
- F : Precipitant
- P : Polymer
- T_0 : working temperature
- : working point, composition of the entire content of the column.

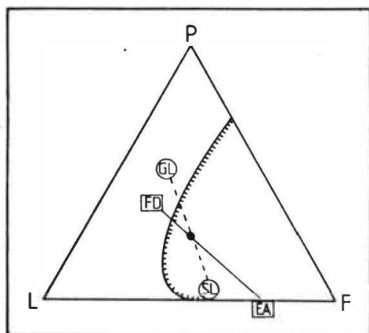


Fig. 1 a

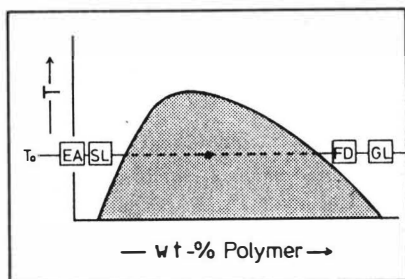


Fig. 1 b

M_w , the weight average molecular weight of the fractions constitutes the simplest measure of the effectiveness of a fractionation.

In the case of stationary states, the following equation must be valid:

$$\dot{m}_p^{FD} \cdot M_w^{FD} = \dot{m}_p^{GL} \cdot M_w^{GL} + \dot{m}_p^{SL} \cdot M_w^{SL}$$

or in terms of \dot{G} :

$$(\dot{G} + 1) \cdot M_w^{FD} = M_w^{GL} + \dot{G} \cdot M_w^{SL}$$

Criteria for the applicability of the CPF :

The most important prerequisite for a successful CPF is the availability of a suitable

solvent/non-solvent-system. As a rule these two components should thermodynamically be as similar as possible. An optimum mixed solvent in this respect is the system ethylmethyl ketone/acetone, used for the CPF of polystyrene (PS)³. However, such an ideal combination of a solvent plus a precipitant can hardly be found for most polymers.

Other criteria for the selection of the low molecular weight liquids are

- (i) rate of phase-separation
- (ii) difference in the densities of the GL- and the SL-phase
- (iii) sensitivity of the system against fluctuation in temperature and composition and of course
- (iiii) economic aspects.

Aids to find out the best mixed solvents are: cloudpoint-titrations to determine the miscibility gap, determination of the composition of the phases that coexist under equilibrium conditions as well as GPC-measurements of the polymers contained in it.

CPF-Apparatus^{3,4} :

Central component of the CPF-apparatus is a commercially available sieve bottom column with pulsator (Fa. Quickfit), which was slightly modified (fully thermostatted, spindle valves at the lower subsider). The separating column with a length of 100 cm and a volume of about 1200 cm³ (total volume = 2500 cm³) is suitable for the fractionation of a max. of 1 g polymer per minute. A pump permits a pulsation from 0 to 60 cm³ (linearly scaled from A = 1 to 20) with a frequency from 0 to 2,5 Hz (scaled from $\nu = 1$ to 10). For the transport of FD and EA (stored in thermostatable and calibrated reservoirs) valveless FMI wobble plunger pumps were used.

Application of the CPF to PVC :

PVC was the first polymer fractionated on a preparative scale. With regard to the choice of the solvent/non-solvent-mixture PVC constitutes an exception because of the strong tendency to form associates and gels (physical networks). Therefore we had to employ tetrahydrofuran as a very good solvent and water as a strong non-solvent. The special aptitude of this combination can be explained in terms of a pronounced preferential solvation of PVC by tetrahydrofuran, which hinders the formation of associates via intersegmental contacts.

The polymer sample used for fractionation was Vestolit H 5867 (Chemische Werke Hüls); its M_w -value is 67 000 and its non-uniformity $U (=M_w/M_n - 1) = 0.95$ (M_w = weight average of the molecular weight, M_n = number average).

At first some systematic explorative fractionations, in which the working point (cf. Fig. 1 a) was changed via a variation of \dot{q} and the water content of EA (w_F^{EA} , w = weight fraction), were carried out.

With increasing \dot{q} -value and increasing solvent quality of the EA the \dot{G} -ratio can be shifted to higher values. Like all other polymers under investigation, a change of w_F^{EA} leads to a greater range of experimentally accessible \dot{G} -values; for example: For $\dot{q} = 11$ and $w_F^{EA} = 0.15 - 0.158$, one obtains \dot{G} -values between 2.3 and 0.4, whereas in the case of a constant value of $w_F^{EA} = 0.155$ and $\dot{q} = 4 - 22$ \dot{G} only ranges from 0.9 to 1.85.

On the basis of this knowledge PVC was fractionated preparatively; for the working parameters see the legend of Fig. 2. The so obtained GL ($M_w = 90000$, $U = 0.32$) - and SL ($M_w = 32000$, $U = 0.46$) - fractions were again subjected to the CPF, yielding four PVC-samples (of ca. 100 g each) with M_w -values lying between 20000 and 100000 and non-uniformities of about 0.2.

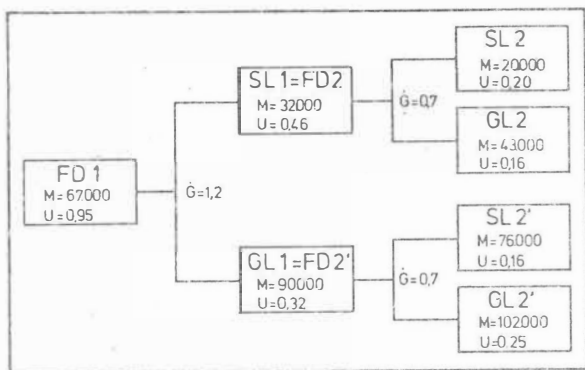


Fig. 2 : Flow chart of the preparative CPF of PVC (Vestolit M 5867).

All experiments were carried out with $\dot{m}_p^{FD} = 0.43$ g / min ($w_p^{FD} = 0.15$);

The other working parameters ($w_F^{EA}/\dot{q}/A/\dot{v}$) for the various steps are:

Step 1 : 0.155/11/7/4.5, Step 2 : 0.142/11/7/4.5, Step 2' : 0.168/6.4/5/3.5.

Application of the CPF to PIB :

The majority of the CPF-experiments was carried out with Oppanol B 15 (Fa. BASF):

$M_w = 98000$, $U = 1.4$.

Prior to the CPF, the fractionation effects were studied⁵⁾ by means of equilibrium experiments in numerous solvent|non-solvent-combinations, for example toluene|ethylmethylketon, toluene|2-propanol, heptane|ethylmethylketon. Based on the criteria mentioned above, the mixed solvent toluene|ethylmethylketon was chosen for the performance of the CPF. After some orienting experiments (determination of the operation parameters leading to $\hat{G} = 1$) Oppanol B 15 was fractionated on a large scale.

Because of the relatively high non-uniformity ($U = 1.4$) of the starting material, three fractionation steps had to be performed in order to get samples with $U \approx 0.2$. Since the SL-phase of the first run was not worked up, four PIB-samples (of ca. 200 g each) with M_w -values between ca. 80000 and 260000 and non-uniformities of about 0.25 were obtained (cf. Fig. 3).

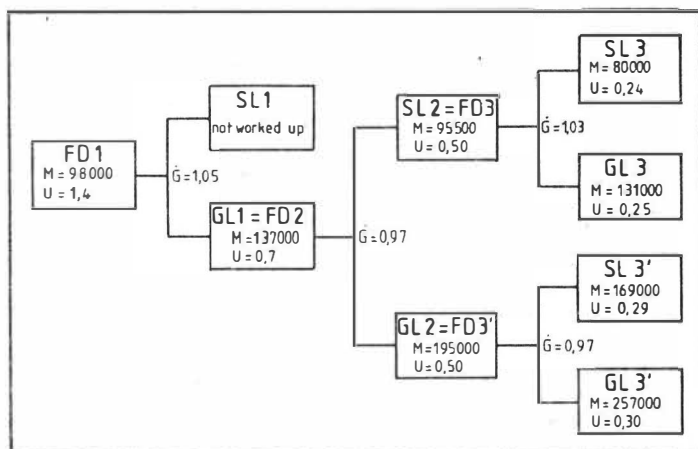


Fig. 3 : Flow chart of the preparative CPF of PIB (Oppanol B 15).

The various steps were carried out under the following conditions

$(\dot{m}_p^{FD}, \dot{m}_p^{FD}, \dot{m}_p^{EA} | \dot{q}_p | \Delta T)$,

Step 1 : 0.64 g · cm⁻³ | 0.15 | 0.25 | 5.3 | 5 | 3.5

Step 2 : 0.50 g · cm⁻³ | 0.148 | 0.225 | 6.3 | 5 | 3.5

Step 3 : 0.42 g · cm⁻³ | 0.123 | 0.218 | 6.3 | 5 | 4.0

Step 4 : 0.50 g · cm⁻³ | 0.149 | 0.235 | 5.5 | 5 | 4.0

The comparison of the present separation effects with the above CPF of PVC shows less favourable results for PIB. The reason seems to be the extraordinary stability of the gel-droplets, which hinders the exchange of polymer molecules of different chain length between the counter-current phases.

An improvement of the degree of dispersion can be reached not only by a higher pulsation intensity (limited by damming up) but also by shifting the working point closer to the critical point of the system, since the interfacial tension, like many other physical properties, vanishes as the phases become identical. Because of the small differences of the densities of the components in the system toluene|ethylmethylketon|PIB the mixed solvent was replaced by heptane|ethylmethylketon (which yields identical fractionation effects in equilibrium experiments).

With this new combination CPF-runs were carried out, in which \dot{q} -values down to 0.8, corresponding to working points up to ca. 8 wt.-% of polymer, could be reached. In spite of this high polymer concentration, a remarkable enhancement of the fractionation quality was reached. This means that large amounts of solvent can be saved whenever it is possible to operate close to the critical point.

Diese Arbeit wurde im Rahmen der industriellen Gemeinschaftsforschung aus Mitteln des Bundesministers für Wirtschaft gefördert, wofür wir herzlich danken.

- 1) M.J.R. Cantow: Polymer Fractionation; Academic Press N.Y. 1967
- 2) G. Glöckner: Polymercharakterisierung durch Flüssigkeitschromatographie; Hüthig Verlag Heidelberg 1982
- 3) B.A. Wolf, H. Geeriben, J. Roos, P. Amareshwar; Dt. Pat. Anm. P 32|42|130.3
- 4) H. Geeriben, J. Roos, B.A. Wolf: Makromol. Chem. 186, 735 (1985)
- 5) P. Schützeichel, Diplomarbeit, Mainz (1985)

Special Applications: Inorganic Products

SOLVENT EXTRACTION OF PHOSPHORIC ACID WITH LONG CHAIN TERTIARY AMINES

Stig Stenström, Dept. of Chem. Eng. 1, Lund Inst. of Techn., Lund, Sweden

Stig Wingefors, Swedish Nuclear Power Inspectorate, Stockholm, Sweden

Gharib Aly, Dept. of Chem. Eng. 1, Lund Inst. of Techn., Lund Sweden

During the development of a process for cadmium removal from WPA (wet process phosphoric acid) by extraction with trialkyl amines(1) it was found necessary to get a better understanding of acid extraction in these systems. This can only be achieved by considering all acids present in WPA, i.e. H_3PO_4 , H_2SO_4 , HCl , HF and H_2SiF_6 . In that way it would be possible to calculate and minimize acid losses and also to investigate the possibility to produce streams of refined phosphoric acid. Of course, the individual extraction isotherm for each acid is needed as a point of departure for such calculations. This paper describes the results for phosphoric acid.

Rather few studies(2-6) have been performed on the solvent extraction of phosphoric acid with long chain tertiary amines. The most complete investigation of these systems seems to be the work by Marcus et al(5-6). A large number of experimental data were measured for aqueous H_3PO_4 concentrations between 0.022 and 7.13 M H_3PO_4 and amine concentrations from 0.1 to 0.7 M Alamine 335. In the aqueous phase phosphoric acid is considered to exist as H_3PO_4 , H^+ and $H_2PO_4^-$ and in the organic phase species with one amine and one or two phosphoric acid molecules are identified. For the dissociation of phosphoric acid the activity data were taken from Elmore(7) and the activity coefficients calculated with the model of Van Rysselberghe and Eisenberg(8). The agreement between experimental and calculated distribution coefficients is generally good, however, at very low aqueous concentrations the model predicts too high distribution coefficients and above 4.2 M, as pointed out by Marcus and Asher, it is necessary to include species with 3 phosphoric acid molecules. Thus the proposed constants can not be used for solvent extraction of phosphoric acid from standard WPA ~ 5.5 M H_3PO_4 and the problems at low concentrations limits the usefulness in stripping calculations of phosphoric acid.

For these reasons it was decided to further investigate the solvent extraction of H_3PO_4 with tertiary amines and try to resolve the problems noted above.

Aqueous phase model

The aqueous phase model was based on the model presented by Elmore et al(7) and involves the following equilibria:





with the thermodynamic equilibrium constants K_1 , K_2 and K_3 , thus

$$K_1 = \frac{(\text{H}_3\text{PO}_4)}{(\text{H}^+) (\text{H}_2\text{PO}_4^-)} = \frac{y_u}{y_{\text{H}^+} y_{\text{H}_2\text{PO}_4^-}} \frac{[\text{H}_3\text{PO}_4]}{[\text{H}^+] [\text{H}_2\text{PO}_4^-]} \quad (4)$$

$$K_2 = \frac{(\text{H}_5\text{P}_2\text{O}_8^-)}{(\text{H}^+) (\text{H}_2\text{PO}_4^-)^2} = \frac{y_{\text{H}_5\text{P}_2\text{O}_8^-}}{y_{\text{H}^+} y_{\text{H}_2\text{PO}_4^-}^2} \frac{[\text{H}_5\text{P}_2\text{O}_8^-]}{[\text{H}^+] [\text{H}_2\text{PO}_4^-]^2} \quad (5)$$

$$K_3 = \frac{(\text{H}_6\text{P}_2\text{O}_8)}{(\text{H}^+)^2 (\text{H}_2\text{PO}_4^-)^2} = \frac{y_{\text{H}_6\text{P}_2\text{O}_8}}{y_{\text{H}^+}^2 y_{\text{H}_2\text{PO}_4^-}^2} \frac{[\text{H}_6\text{P}_2\text{O}_8]}{[\text{H}^+]^2 [\text{H}_2\text{PO}_4^-]^2} \quad (6)$$

K_1 was taken as reported by Bates(9), = 140.7 and K_2 and K_3 was taken as given by Elmore(7), $K_2 = 177.7$, $K_3 = 592.3$. The molar activity coefficient for the undissociated phosphoric acid, y_u , was taken from Elmore(7). By least square fitting the following polynomial in molar ionic strength (I_c) was found to reproduce these data up to 6.7 M H_3PO_4

$$\log y_u = -0.006537 + 1.0760 I_c - 0.34797 I_c^2 + 0.16204 I_c^3 - 0.025644 I_c^4 \quad (7)$$

Also $y_{\text{H}_6\text{P}_2\text{O}_8}$ was set equal to y_u .

The extraction isotherm must include a model that relates the activity of extractable components to their concentration. In order to be useful for multicomponent systems such a model should be based on theoretically sound assumptions. For this work Bromley's model (10) was selected. In a three component electrolyte the single ion activity coefficients for the ions H^+ , H_2PO_4^- , $\text{H}_5\text{P}_2\text{O}_8^-$ are calculated as

$$\log f_1 = \frac{-A \sqrt{I_m}}{1 + \sqrt{I_m}} + B_{12} m_2 + B_{14} m_4 \quad 1 = \text{H}^+ \quad (8)$$

$$\log f_2 = \frac{-A \sqrt{I_m}}{1 + \sqrt{I_m}} + B_{12} m_1 \quad 2 = \text{H}_2\text{PO}_4^- \quad (9)$$

$$\log f_4 = \frac{-A \sqrt{I_m}}{1 + \sqrt{I_m}} + B_{14} m_1 \quad 4 = \text{H}_5\text{P}_2\text{O}_8^- \quad (10)$$

$$B_{ij} = \frac{0.06 + 0.6 B_{ij}}{(1 + 1.5 I_m)^2} + B_{ij} \quad (11)$$

Converting to molar activity coefficients the equations contain two constants, B_{12} and B_{14} , to be determined. A procedure was set-up in a computer program to

minimize the following squared deviation.

$$\Phi = \left[\frac{I - I_{\text{calc}}}{I} \right]^2 \quad (12)$$

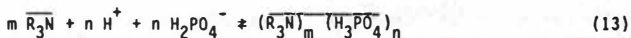
where I is the ionic strength of the solution and equal to the degree of dissociation, α . The α -value was taken as given by Elmore(7). The result on minimizing Φ was $B_{12} = -0.0180$, $B_{14} = 0.1232$.

The excellent agreement with the values of Elmore(7) is shown in Figure 1.

The extraction isotherm

Initial measurements with 0.1 M Alamine 336 produced distribution data that did not differ more than the experimental error from the values presented by Marcus and Asher(5). Their data from 39 measurements (except one measurement with an aqueous concentration above 6.7 M) for 0.1, 0.4 and 0.7 M Alamine 336 could thus be used for the calculation of the extraction constants. In order to get more data at low and very high (4.5-6.7 M) phosphoric acid concentrations additional distribution data were measured for 0.1, 0.5 and 1.0 M Alamine 336 in toluene. The result is shown in Table 1.

Extraction of phosphoric acid with tertiary alkyl amines can be assumed to be described by the general equilibria,



with the thermodynamic equilibrium constants given by

$$K_{mn} = \frac{y_{mn}}{y_{R_3N}^m y_1^n y_2^n [\overline{R_3N}]^m [H^+]^n [H_2PO_4^-]^n} \quad (14)$$

where y_{R_3N} is the activity coefficient for the free amine and y_{mn} the activity coefficients for the complexes in the organic phase.

Following Marcus and Asher (5) it can tentatively be assumed that $m=1$. However, in order to include higher concentrations than they did, $n=1, 2$ and 3 .

For low acid concentrations where the acid concentration is less than half the amine concentration, the distribution equilibrium should be described with $n=1$. This hypothesis was tested by calculating $K_{11} \cdot y_{R_3N}/y_{11}$ from experimental values of the organic phase acid concentration and solving the equations of the aqueous phase model. A plot of $K_{11} \cdot y_{R_3N}/y_{11}$ vs the organic acid concentrations, c_{org} , is shown in Figure 2.

The only explanation of this very strong dependence of $K_{11} \cdot y_{R_3N}/y_{11}$ on c_{org} is the formation of higher aggregates, i.e. $m \gg 1$ with $m/n=1$. This means that the assumption of $m=1$ by Marcus and Asher seems questionable. They tried to describe this discrepancy by letting $K_{11} \cdot y_{R_3N}/y_{11}$ vary proportionally to c_A , the total

amine concentration. It is here shown that it infact varies almost linearly with c_{org} .

The following empirical function was found to best correlate the data in Figure 2:

$$y_{R_3N}/y_{11} = 1 + K_y c_{org}^{0.9} \quad (15)$$

Further, it was concluded that the amount and quality of available distribution data did not allow a more refined analysis of the dependence of $K_{12} \cdot y_{R_3N}/y_{12}$ and $K_{13} \cdot y_{R_3N}/y_{13}$ on concentration. Therefore, y_{12} and y_{13} were set equal to y_{11} . Infact, this is equivalent not only to assume that the activity coefficients of the corresponding monomers are equal: it also implies that the mean aggregation number is independent of n . In these respects the proposed model is only empirical.

The constants K_y , K_{11} , K_{12} and K_{13} were determined by lease square minimisation of the relative error in calculated organic acid concentration.

The constants were determined as $K_y = 98.9$, $K_{11} = 112$, $K_{12} = 4060$, $K_{13} = 6860$. For 0.1 M, 0.4 M and 1.0 M Alamine 336 the result is shown in Figures 3-5.

The relative amounts of acid bound in the three different complexes can be calculated by the relationship:

$$\beta_{mn} = \frac{n K_{mn} (y_B/y_{11})^m (y_1 y_2)^n [R_3N]^m [H^+]^n [H_2PO_4^-]^n}{c_{org}} \quad (16)$$

with $m = 1$ and $n = 1, 2, 3$. The result is shown in Figure 6.

Conclusions

The solvent extraction model includes species with one amine and one, two or three phosphoric acid molecules. The presented model can be used for calculation of solvent extraction from 0.02 - 6.7 M aqueous phosphoric acid concentrations. The prediction at < 0.02 M H_3PO_4 is too low mainly due to impurities present in Alamine 336 affecting the distribution of phosphoric acid. For 0.02 - 0.2 M H_3PO_4 the model predicts values more accurate than what has been previously published. In the range 0.2 - 4 M the model predicts results with the same accuracy as the model presented by Marcus and Asher(5). Finally at high acidities inclusion of a third complex provides possibilities for calculation of phosphoric acid extraction up to 6.7 M. The non-ideal behaviour of the organic phase is described by expressing activity coefficients as a function of the total organic phase concentration of phosphoric acid. Better understanding of amine salt aggregation is needed before a more rigorous method can be used. In order to further develop the model TOA should be used for the modelling or the effect of impurities be included in the model.

REFERENCES

1. Stenström, S., Aly, G., Hydrometallurgy 14 (1985) 231-255.
2. Sato, T., J. Appl. Chem. 15 (1965) 10-16.
3. Smirnov, V.F., Gorlov, E.E., Russ. J. Inorg. Chem., 12 (1967) 428-429.
4. Baranov, Yu. I., Malysheva, L.P., Krivokhatskii, A.S., Savoskina, G.P., Smirnova, E.A., Soviet Radiochemistry, 22 (1980) 363-368.
5. Marcus, Y., Asher, L.E., J. Inorg. Nucl. Chem., 39 (1977) 2035-2040.
6. Marcus, Y., Asher, L.E., Barak, H., J. Inorg. Nucl. Chem., 40 (1978) 325-329.
7. Elmore, K.L., Hatfield, J.D., Dunn, R.L., Jones, A.D., J. Phys. Chem., 69 (1965) 3520-3525.
8. Van Rysselberghe, P., Eisenberg, S., J. Am. Chem. Soc., 61 (1939) 3030-3037.
9. Bates, R.G., J. Res. Natl. Bur. Std., 47 (1951) 127.
10. Bromley, L.A., AIChE, 19 (1973) 313-20.

Table 1: Distribution coefficients for solvent extraction of phosphoric acid with Alamine 336 and TOA dissolved in toluene.

c_A (molar)	c_{aq} (molar)	D	c_A (molar)	c_{aq} (molar)	D	
0.1	Alamine 336		1.0	Alamine 336		
	0.0097	0.036		0.0095	1.53	
	0.0233	0.075		0.0178	4.49	
	0.0455	0.099		0.0355	12.6	
	0.0667	0.103		0.096	9.01	
	0.0890	0.129		3.71	0.412	
	0.167	0.195		4.63	0.384	
	0.251	0.206		5.12	0.355	
	3.86	0.048		5.58	0.335	
	4.41	0.045		6.46	0.303	
	4.88	0.041				
	5.25	0.041				
5.85	0.039					
0.5	0.0115	1.10	0.1	0.100	0.020	
	0.0193	1.54		0.5	0.0615	2.29
	0.0319	2.09		1.0	0.0265	0.815
	0.0488	3.01				
	3.74	0.237				
	4.35	0.211				
	4.84	0.199				
	5.24	0.195				
	6.27	0.179				

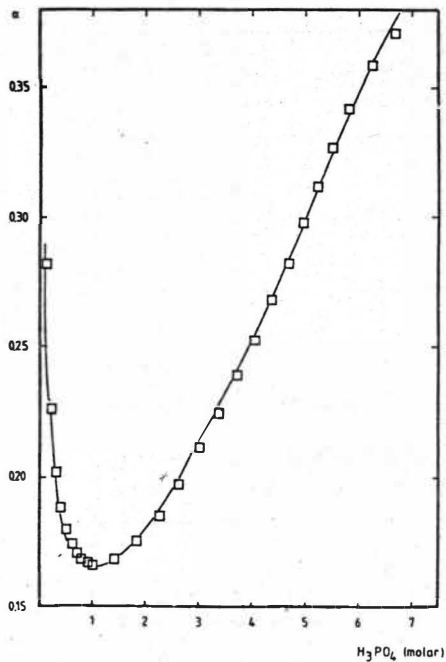


Figure 1. Degree of dissociation, α , for 0.1 - 6.7 M H_3PO_4 according to Elmore.

□ calc with $B_{12} = -0.018, B_{14} = 0.1232$

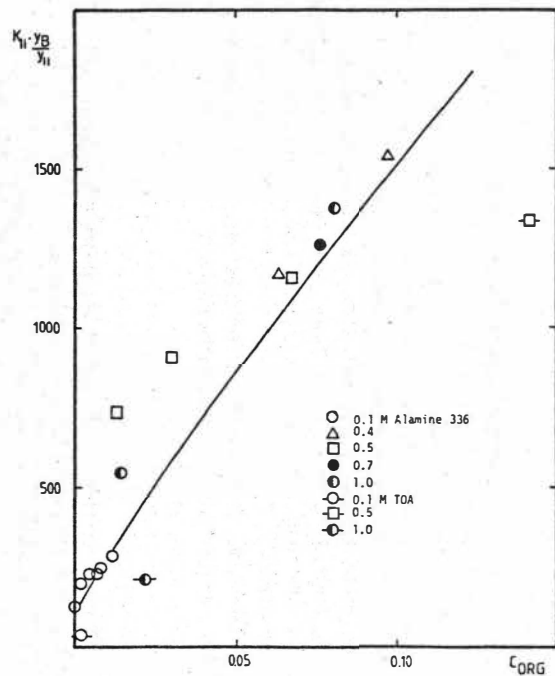


Figure 2. Activity coefficient quotient in the organic phase for $c_{\text{ORG}} < 0.15$ M H_3PO_4 . Line calculated with $K_y = 98.9, R_{11} = 112$.

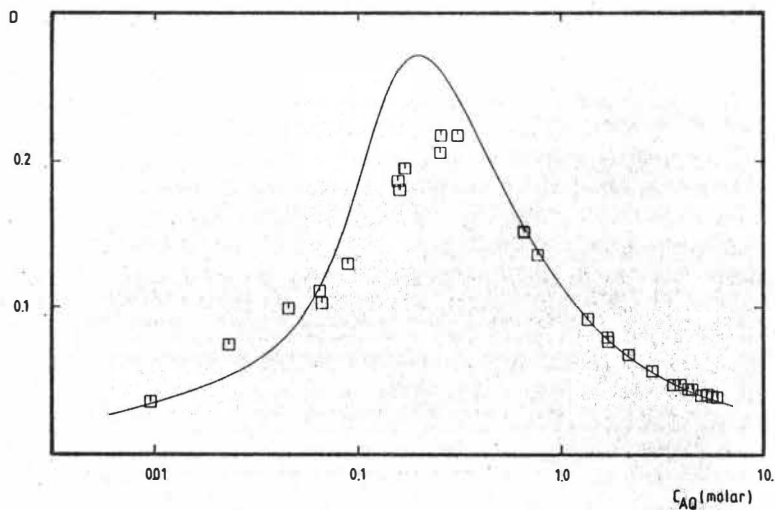


Figure 3. Distribution coefficient for H_3PO_4 for solvent extraction with 0.1 M Alamine in toluene calculated with $K_1=98.9, K_{11}=112, K_{12}=4060, K_{13}=6860$. \square experimental data. y

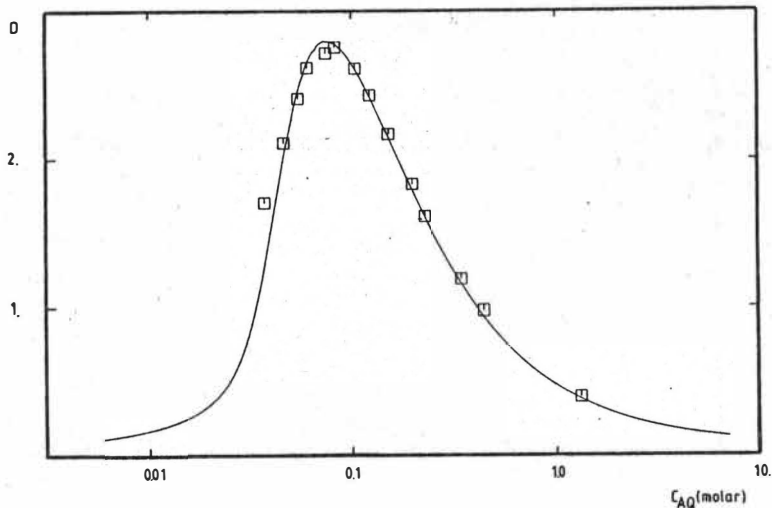


Figure 4. Distribution coefficient for H_3PO_4 for solvent extraction with 0.4 M Alamine 336 in toluene calculated with $K_1=98.9, K_{11}=112, K_{12}=4060, K_{13}=6860$. \square experimental data. y

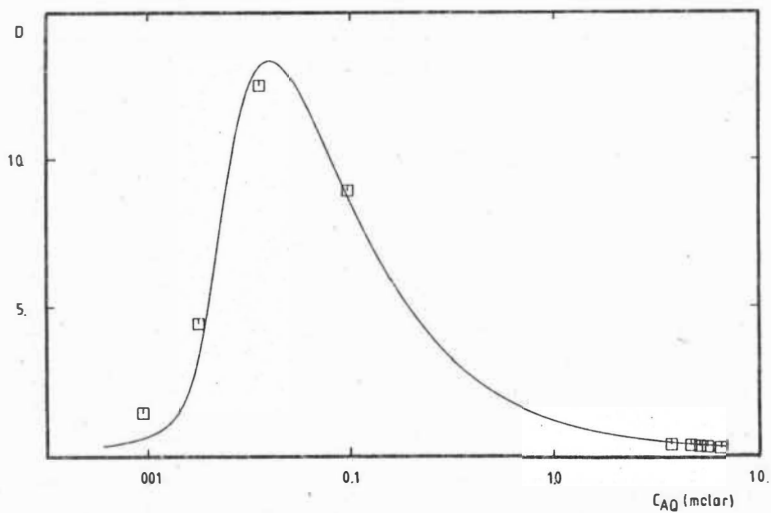


Figure 5. Distribution coefficient for H_3PO_4 for solvent extraction with 1.0 M Alamine 336 in toluene calculated with $K_y=98.9, K_{11}=112, K_{12}=4060, K_{13}=6860$. \square experimental data.

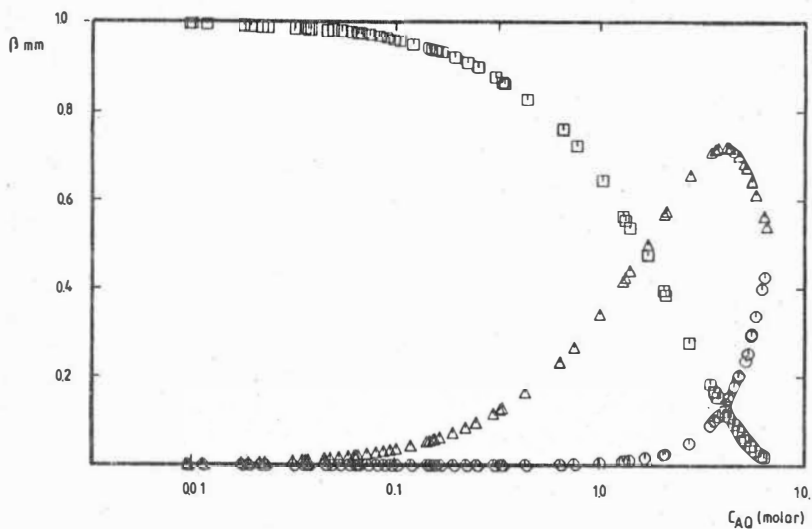


Figure 6. β_{mn} for solvent extraction with 0.1 - 1.0 M Alamine 336 in toluene.
 \square β_{11} , Δ β_{12} , \circ β_{13} .

On the modelling of multicomponent acid extraction from wet process phosphoric acid with trialkyl amines in kerosene

Stig Wingefors, Swedish Nuclear Power Inspectorate, Stockholm and Stig Stenström, Lund Institute of Technology, Lund, Sweden.

1. Introduction

In an investigation of Cd removal from wet process phosphoric acid (WPA) by extraction with trialkyl amines in kerosene (1,2) it was found desirable to get a better understanding of the extraction behaviour of all acids present in WPA. Apart from phosphoric acid (4-7 M), WPA may contain significant amounts of H_2SO_4 (0.1-0.5 M), HCl (0.001-0.05 M), HF (0.1-1M) and H_2SiF_6 (0.05-0.2 M). Since at least some of these (HF and H_2SiF_6) are undesirable contaminants, much work has been done in order to find methods for their separation from phosphoric acid. Solvent extraction belongs to the methods explored and also utilized in full scale for that purpose.

Results from the studies of Cd extraction from WPA with Alamine 336 in aromatic kerosene indicated possibilities to combine the removal of Cd with a flowsheet for production of purified H_3PO_4 . For this purpose, but also in order to explain and optimize Cd extraction, the equilibria for extraction of the major acid components would have to be incorporated into a multicomponent extraction model.

In the present paper the general outlines for that work are described and some preliminary results are given.

2. General considerations

2.1. Extraction equilibria and organic phase interactions

The acid-base neutralization reaction that governs extraction of acids (HL) with alkyl amines (B) might be described by various sets of equilibria. In this context we have chosen to include the aggregation to dimers and higher polymers of amine salts in the extraction equilibrium, i.e.,



The thermodynamic equilibrium constant for this reaction is,

$$K_{mn} = \bar{a}_{mn} (\bar{a}_B)^{-m} (a_{HL})^{-n} \quad (2)$$

where the bars denote activities of species in the organic phase and a_{HL} is the activity of acid in the aqueous phase.

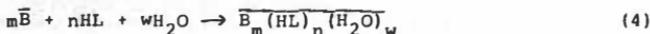
Equation (2) can be rewritten in molar concentrations for the organic phase species, thereby defining a "mixed" conditional equilibrium constant for Eq. (1),

$$k_{mn} = \bar{y}_B (\bar{y}_{mn})^{-1} k_{mn} = \bar{c}_{mn} b^{-m} (a_{HL})^{-n} \quad (3)$$

where \bar{y}_b and \bar{y}_{mn} are the activity coefficients of free amine and the amine salt aggregates, respectively, and b is the concentration of free amine. When aggregation is included in the model, experience shows that correlated values of k_{mn} might be regarded as constants independent of organic phase composition.

However, for phosphoric acid the available equilibrium data do not permit inclusion of aggregation. Instead \bar{y}_{mn} , or rather k_{mn} , has been described as an empirical function of organic phase composition (3,8). Although similar difficulties could be expected for hexafluorosilicic acid this did not occur (11). Therefore, extraction of H_2SiF_6 is treated by letting k_{mn} be constants even when aggregation is neglected, see section 4.

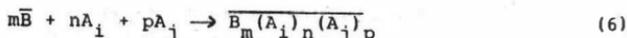
In careful modelling the hydration of species in the organic phase should be included (4),



$$K_{mnw} = \bar{a}_{mnw} (\bar{a}_B)^{-m} (a_{HL})^{-n} (a_{H_2O})^{-w} \quad (5)$$

Hydration might have a significant influence on the formation of aggregates. This means that complications can arise when isotherms for extraction of single acids without hydration are combined in a model for extraction of several acids - the activity of water in the multicomponent system could be less than in the range where the single acid isotherms are valid. This difficulty has not been further elaborated on in the present work, partly due to the scarcity of reliable hydration data.

When several acids are present mixed aggregates are likely to be formed (5). This might be taken into account by assuming the formation of binary aggregates with the acids A_i and A_j ,



$$k_{mnp}^{ij} = \bar{c}_{mnp}^{ij} b^{-m} (a_i)^{-n} (a_j)^{-p} \quad (7)$$

In principle, it could well be that more than two different acids are present in a mixed aggregate, but for the mathematical description of these systems the inclusion of

binary aggregates would probably be sufficient. Of course, this belief should as yet be regarded as a working hypothesis needing confirmation.

The extraction equilibrium for any acid (i) in a multicomponent system would then be described by the following set of equations.

$$a_i = f(c_i, \dots, c_j, \dots) \quad (8)$$

i.e. the aqueous phase model, cf next section,

$$\bar{c}_{i, \text{tot}} = \sum_{m,n} nk_{mn}^i b_{mn}^m a_i^n + \sum_{j \neq i} \sum_{m,n,p} nk_{mnp}^{ij} b_{mnp}^m a_i^n a_j^p \quad (9)$$

i.e. the isotherm of acid (i), and the mass balance of amine,

$$\bar{c}_B = b + \sum_i \sum_{m,n} mk_{mn}^i b_{mn}^m a_i^n + \sum_{i,j} \sum_{m,n,p} mk_{mnp}^{ij} b_{mnp}^m a_i^n a_j^p \quad (10)$$

For a given equilibrium composition of the aqueous phase Eqs (8) to (10) are sufficient for calculation of the acid concentrations in the organic phase. For given initial phase compositions these equations have to be solved simultaneously for all components together with the mass balances over phases.

2.2 Aqueous phase interactions

Ideally, the aqueous phase model should provide for calculation of activities of all components, including water. This last requirement has not been considered in the present work, however. The interest has been focused on a realistic calculation of ionic strength taking into account dissociation/association equilibria.

Bromley's model for multicomponent electrolyte solutions is used for correlation and calculation of ionic activity coefficients. According to Bromley (6) the molal activity coefficient f_i of an ion with charge Z_i is given by

$$\log f_i = - \frac{0.511 Z_i^2 \sqrt{I}}{1 + \sqrt{I}} + \sum_j B_{ij} \bar{z}_{ij}^2 m_j \quad (11)$$

$$B_{ij} = \frac{(0.06 + 0.6 B_{ij}) |Z_i Z_j|}{\left(1 + \frac{1.5I}{|Z_i Z_j|}\right)^2} + B_{ij} \quad (12)$$

$$\bar{z}_{ij} = (|Z_i| + |Z_j|) / 2 \quad (13)$$

$$I = \frac{1}{2} \left(\sum_i m_i Z_i^2 + \sum_j m_j Z_j^2 \right) \quad (14)$$

It should be noted that $B_{ij}=B_{ji}$. Only interactions between ions i and j with opposite sign of charge are taken into account. The model might be used successfully for ionic strengths up to about 3 m, thereby covering the range expected to be of importance in the present application. However, for sulphuric acid Eq.(12) had to be extended by an extra term $C_{ij}I$ (7).

In addition to Eqs (11)-(14) the aqueous model is comprised by a set of mass balance equations, one for each acid and one for hydrogen ion. The appropriate dissociation/association equilibria are treated under the separate headings for each acid in section 3. Conversion between molal and molar activity coefficients is performed according to

$$y_i c_i = \rho_w f_i m_i \quad (15)$$

3. Aqueous phase modelling

In this section hydrogen ion is denoted by subscript 1.

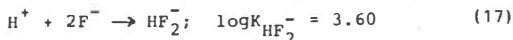
Phosphoric acid. The aqueous phase model for phosphoric acid is described in a separate paper of these proceedings(8).

Sulphuric acid. The first dissociation stage is assumed complete, and for the second stage the thermodynamic constant $K_2= 0.0102$ has been chosen from ref. 9. Denoting bisulphate and sulphate with 2 and 4, respectively, $B_{12}= 0.1944$, $B_{14}= -0.096$, $C_{12}= 0.00022$ and $C_{14}= 0.0120$. These values were obtained(7) from a combined least square minimization of the relative errors in mean ionic activity coefficients(9) and free sulphate concentration in solutions of pure sulphuric acid(10). The activity of $H_2SO_4 = y_4^2 y_4 c_4^2 c_4$.

Hydrochloric acid. The interaction constant is taken as given by Bromley(6), $B_{16}= 0.1433$. The activity of $HCl = y_1 y_6 c_1 c_6$.

Hexafluorosilicic acid. Due to lack of suitable activity data the same model, B- and C-values are used for this acid as for sulphuric acid(11). The second dissociation constant $K_2= 0.0148$ (12).

Hydrofluoric acid. The following equilibria in HF solutions are considered(13),



Denoting F^- with 8 and HF_2^- with 10, the values $B_{1g} = 0.250$ and $B_{1,10} = 0.050$ were obtained after minimization of the error in calculated stoichiometric activity coefficients(14) of HF solutions. The activity coefficient of HF is assumed to be 1, since the maximum ionic strength utilized in the correlation was less than 0.2. This means that the obtained results should be used with caution in trying to describe the behaviour of HF in multicomponent electrolyte solutions.

4. Single acid isotherms.

Phosphoric acid is treated in another paper of these proceedings(8).

Sulphuric acid. The model by Högfeldt et al.(15) for extraction with trilauryl amine in toluene has been adopted(7). After comparison with other studies by Wilson (16) on extraction with TOA in benzene, and by Bertocci and Rolandi(17) on extraction with TOA in xylene, it was concluded that the difference in chain-length and diluent would probably be of less importance in the present application. Högfeldt et al. included coextraction of water in their model. However, calculations showed that water extraction could be excluded, thereby setting water activity = 1 (cf Eq.5), without serious loss of accuracy. Thus, the following constants k_{mn} (cf Eq. 3) were employed, $\log k_{21} = 7.52$, $\log k_{42} = 16.89$, $\log k_{54} = 27.88$, $\log k_{33} = 17.40$ and $\log k_{23} = 7.43$.

Hydrochloric acid. Studies on the extraction of HCl by TOA in aromatic diluents are abundant, but no strictly thermodynamic study on the extraction with Alamine 336 is available. In this work the constants given by Aguilar and Högfeldt (18) for extraction of HCl with TOA in toluene from 1 M LiCl have been employed after conversion to zero ionic strength (7) according to Bromley (6). The resulting values of k_{mn} (Eq.3) are, $\log k_{11} = 3.87$, $\log k_{22} = 9.65$ and $\log k_{55} = 25.86$.

Hexafluorosilicic acid. Extraction of this acid with Alamine 336 in aromatic kerosene has been studied earlier and a model proposed for explanation of the experimental results (11). By utilizing the refined aqueous model for sulphuric acid, as explained above, the following constants k_{mn} (Eq.3) has been obtained, $\log k_{21} = 7.61$ and $\log k_{11} = 3.45$ (7).

Hydrofluoric acid. Only a limited number of measurements have been reported for amine extraction of HF. The results by Bertocci and Rolandi for extraction with TOA in xylene (17) were used for calculation of the following constants k_{mn} (Eq.3), $\log k_{12} = 1.40$ and $\log k_{14} = 0.14$ (7).

5. Multicomponent equilibria

5.1 Binary systems with phosphoric acid

As a point of departure the four binary systems with phosphoric acid have been investigated. The prime reason for this is that phosphoric acid would most probably be the dominating component in the loaded organic phase after extraction of acids from WPA. Also, in that case the formation of mixed aggregates with $(n + p) > m$ would be of importance in the first place.

A series of experiments were performed, where 0.5 M Alamine 336 in toluene were equilibrated with solutions of phosphoric acid together with each of the other four acids. The results are given in Table 1. Comparison of these values with those calculated assuming only single acid isotherms clearly indicated the need for addition of mixed species to the model. The as yet limited set of experimental data has not permitted inclusion of more than one such species for each binary with $m = n = p = 1$ ($p = 2$ for HF). A least square minimization of the error in per cent extraction gave the following values of $\log k_{11}^{ij}$ (cf Eq. 7; $i = H_3PO_4$), 5.46 ($j = H_2SO_4$), 4.36 ($j = HCl$), and 5.06 ($j = H_2SiF_6$). For $j = HF$ $\log k_{12}^{ij} = 3.76$. Results from calculations with these constants are shown in Table 1.

5.2 The multicomponent system

The now available binary constants have been employed tentatively for calculation of multicomponent equilibria, and a comparison with experiment is given in Table 2. The agreement is acceptable in view of the fact that only binary species with phosphoric acid are included in the model.

6. Conclusions

Not unexpectedly the development of a multicomponent equilibrium model of this kind has shown to be quite an arduous task. It was realized from the outset that such a model must rely on a careful description of interactions founded on thermodynamically defensible concepts. In that sense there are still room for improvements, e.g. regarding the formation of binary aggregates - one possibility would be inclusion of species with $(n + p) = m$. A better description of the behaviour of HF and H_2SiF_6 in electrolyte solutions is also needed.

Although these and many other difficulties remain to be solved, the results achieved so far seem to indicate a feasible way to deal with complicated equilibria of this kind.

Table 1. Comparison of experimental and calculated equilibria for binary combinations of phosphoric acid and other acids A_j at different initial aqueous concentrations. Organic phase 0.5 M Alamine 336 in toluene, equal phase volumes, 20-23 °C.

A_j	C_{in}, M		%E(H_3PO_4)		%E(A_j)	
	H_3PO_4	A_j	exp	calc	exp	calc
H_2SO_4	0.1	0.1	67	51	99+	99.8
	0.1	0.5	15	11	75	73
	5.0	0.1	17	17	92	86
	5.0	0.5	8	13	64	75
HCl	0.1	0.1	65	62	89	99
	0.1	0.5	8	8	97	97
	5.0	0.1	15	17	67	98
	5.0	0.5	9	11	90	90
H_2SiF_6	0.1	0.1	57	51	97	99.5
	0.1	0.5	-	29	67	53
	5.0	0.1	16	18	98	77
	5.0	0.5	2	14	74	67
HF	0.1	0.1	67	76	78	70
	0.1	1.0	72	98	83	71
	5.0	0.1	20	18	72	50
	5.0	1.0	14	13	64	69

Table 2. Comparison of experimental and calculated equilibria for multicomponent extraction. Initial concentrations are, (1) all acids 0.1 M; (2) H_2SO_4 0.5 M all other acids 0.1 M; (3) H_3PO_4 5 M, H_2SO_4 0.5 M, HCl 0.1 M, H_2SiF_6 0.5 M, and HF 1 M. Other conditions according to Table 1.

Exp. no	H_3PO_4		H_2SO_4		HCl		H_2SiF_6		HF	
	exp	cal	exp	cal	exp	cal	exp	cal	exp	cal
1	25	32	96	94	96	97	>96	84	61	46
2	13	33	52	61	83	88	58	11	75	13
3	8	10	30	41	79	81	8	26	-	14

References

1. Stenström, S., Aly, G., Hydrometallurgy 14 (1985) 231.
2. Stenström, S., Aly, G., Hydrometallurgy 14 (1985) 257.
3. Stenström, S., Aly, G., Wingefors, S., Solv. Extn. Ion Exch., submitted for publication.
4. Chekmarev, A.M., Ochkin, A.V., Sergievsky, V.V., Tarasov, V.V., Yagodin, G.A., Proc. ISEC 80, Liège 6-12 September 1980, 80-158.
5. Orlandini, F., Danesi, P.R., Basol, S., Scibona, G., Solvent Extraction Chemistry (Dyrssen, D., Liljenzin, J.-O., Rydberg, J., eds), North-Holland Publ. Co, Amsterdam 1967, p. 408.
6. Bromley, L.A., AIChE J., 19 (1973) 313.
7. Stenström, S., Wingefors, S., to be published.
8. Stenström, S., Aly, G., Wingefors, S., Proc. ISEC 86
9. Covington, A.K., Dobson, J.V., Wynne-Jones, W.F.K., Trans. Farad. Soc. 61 (1965) 2050.
10. Chen, H., Irish, D.E., J. Phys. Chem. 75 (1971) 2672.
11. Stenström, S., Wingefors, S., Can. J. Chem. Eng., in press.
12. Sudakova, T.N., Krasnoshchekov, V.V., Frolov, Y.G., Russ. J. Inorg. Chem. 23 (1978) 2092.
13. Hefter, G.T., J. Sol. Chem. 13 (1984) 457.
14. Hamer, W.J., Wu, Y.-C., J. Res. Natl. Bur. Stand. Sect. A 74 (1970) 761.
15. Högfeldt, E., Madaragia, J.M., Muhammed, M., Acta Chem. Scand. A 39 (1985) 805.
16. Wilson, A.S., ref. 5, p. 369.
17. Bertocci, U., Rolandi, G., J. Inorg. Nucl. Chem. 23 (1961) 323.
18. Aguilar, M., Högfeldt, E., Chemica Scripta 2 (1972) 149.

The Extraction Characteristic of silicic Acid in the different Systems

O.A.Sinegribova, A.Yu.Bobirenko, The Mendeleev Institute of Chemical Technology, Moscow, USSR.

The silicic acid species in an aqueous solution are subdivided into three types: α -species - a monomer and a dimer, β -species - from a trimer up to an octamer and γ -species - silicic acid high polycondensated (1). The content of different species depends on solution's "age". The change of different species concentrations in the solution contained $1.35 \text{ g}\cdot\text{l}^{-1} \text{ SiO}_2$ and $2 \text{ mol}\cdot\text{l}^{-1} \text{ HNO}_3$ for times to 6 hr is shown in Fig.1. α - and β -species concentrations were determined by colourimetric method (2). The data of Fig.1 show that the silicic acid polycondensation ($\alpha \rightarrow \beta \rightarrow \gamma$) is rather slow process. When extracting into tri-n-butylphosphate (TBP) and tri-n-octylphosphineoxide (TOPO) the distribution coefficient of silicic acid ceases to change after 5-7 min agitating. It means that there is no substantial transformation of silicic acid species during the agitation period and that after 5-7 min contact the extraction system reaches its pseudo-equilibrium state.

The dependence of silicic acid concentration in TBP on its concentration in $1 \text{ mol}\cdot\text{l}^{-1} \text{ HNO}_3$ (Fig.2) may be expressed as a polynomial:

$$y = -0.016 + 0.184x - 0.023x^2$$

The distribution coefficients of silicic acid are small and decrease after preliminary duration of aqueous phase (Fig.3, curve 1) similarly to a decrease in α -species concentration (Fig.1). It leads to a fact of priority extraction of α -species into TBP. When extracting into TOPO solution ($0.5 \text{ mol}\cdot\text{l}^{-1}$ in heptane) the dependence of silicic acid distribution coefficient on the period of preliminary duration (Fig.3, curve 2) is very similar to a change of β -species concentration in the aqueous phase (Fig.1). The analysis of the solution obtained by stripping of silicic acid extract also indicated that in TBP silicic acid mainly (90%) consisted of α -species. The stripping has been realized by dilute HNO_3 (pH 2) because at such acidity the silicic acid polycondensation rate is minimum.

The plot of silicic acid concentration in the organic phase vs the extractant concentration is linear (Fig.4 "a" for TBP and "b" for TOPO). However, the possibility of a pure solvation mechanism of silicic acid extraction does not conform to the data of Fig.2: silicic

acid is extracted even into 100% TBP only up to the concentration in the organic phase equal to $0.3 \text{ g}\cdot\text{l}^{-1}$ (the plot of isotherm gives a line parallel to X-axis beginning from the concentration $\sim 2 \text{ g}\cdot\text{l}^{-1}$ SiO_2 in the aqueous phase. The content of silicic acid in an organic phase is probably limited by the content of water there. The concentration of water in the organic phase (curves in Fig.4) was determined by Fisher method. The plot of water concentration vs the extractant concentration is linear, the plot of silicic acid amount in the organic phase vs water concentration is also linear. The interaction of silicic with water in TBP is suggested to take place. Under experimental conditions the concentration of water in the organic phase contained TBP was greater than in the organic phase contained TOPO. It is known that dehydration leads to a polycondensation of silicic acid (1). Therefore the lower concentration of water in TOPO solutions is the reason of the presence of β -species in the extract phase. In general at high concentration of water the α -species of silicic acid are present but the decreasing water content results in the polycondensation of silicic acid up to β -species. So after diluting of 100% TBP contained silicic acid (mainly α -species) to 30% TBP with heptane silicic acid consisted of β -species (32%) along with α -species has been obtained. At higher concentration of water in TOPO α -species of silicic acid may present in organic phase along with β -species. For example, when extracting of silicic acid (initial concentration $1.27 \text{ g}\cdot\text{l}^{-1}$) contained 26% α -species, 67% β -species and 7% γ -species into 100% TOPO melt (at 60°C) the next distribution coefficients were determined:

$$D_\alpha = 0.38; D_\beta = 0.61; D_\gamma = 0.$$

The mechanism of silicic acid transfer into organic phase containing neutral phosphororganic compounds (NPOC) is apparently identical with "back solubilization": the hydrate molecule (monomer or polymer) of silicic acid interacts with NPOC (or its hydrate) by means of hydrogen bond. The presence of an extractant in the compound promotes its dissolution in the organic phase. The hydrate number of silicic acid is 9.9 ± 3.1 in TBP (100%) and it is 3.8 ± 0.6 in the solution of TOPO ($0.5 \text{ mol}\cdot\text{l}^{-1}$ in heptane).

It can be noted that if silicic acid concentration in the extract phase was determined not by stripping and following analysis of reextract but by calculation of decrease in its concentration in the aqueous phase due to the extraction, the plot of silicic acid concentration vs the extractant concentration has the difference at the low concentration of an extractant (dotted lines in Fig.4). We suppose

that the cause of the divergence from the linearity consists in concentrating of silicic acid at the interface appreciable at low concentrations of silicic acid and an extractant in the organic phase. The compound of silicic acid with extractant has probably some surfactive properties.

The interfacial tension in the system "aqueous solution of silicic and nitric acids - organic phase containing TBP" was measured by "drop"-method at the different phase compositions (Table 1). The organic and aqueous phase were preliminarily contacted to get extraction equilibrium and to exclude the mass transfer when measuring the interfacial tension.

Table 1

DEPENDENCE OF INTERFACIAL TENSION ($\sigma \cdot 10^3 \text{H/m}$) ON COMPOSITION OF AQUEOUS AND ORGANIC PHASES^a

Aqueous phase:	pH 2		: 2 mol/liter HNO ₃		: 5 mol/liter HNO ₃	
Org. phase	: 2 g/liter:	4g/liter:	2g/liter:	4g/liter :	2g/liter:	4g/liter
	SiO ₂	SiO ₂	SiO ₂	SiO ₂	SiO ₂	SiO ₂
100% TBP	5.3	6.5	8.0(110)	8.3(90)	9.7	10.8
70% TBP	9.3	9.4	12.0(35)	10.7(50)	12.2	11.7
30% TBP	13.0	12.4	14.8(7)	13.2(20)	16.8	15.1

^a Diluent is heptane. The separation time (c) is in brackets

The interfacial tension is decreased by an increasing acidity (HNO₃). The effect of silicic acid concentration upon the interfacial tension depends on TBP concentration: the interfacial tension is increased for 100% TBP and decreased for 30% TBP by the increasing silicic acid concentration (from 2 to 4 g·l⁻¹ SiO₂ in the aqueous phase). It has been caused by the difference in relative amounts of TBP, HNO₃·TBP and the compound of TBP with silicic acid hydrate at the interface. These substances have the different surfactive properties. In studied systems the interfacial tension correlates the time of phase separation. 4 hours duration of silicic acid solutions before measurement of interfacial tension was almost without effect on the value of interfacial tension. It was pointed out (3,4) that the formation of structural silicic acid films at the unmoving interface took more than 1 hr. It is considerably greater than the residence time of the interface in the experiments for a measurement of interfacial tension by "drop"-method therefore in our experiments the film formation at the interface didn't take part in the interfacial tension and had no influence on the phase separation time.

The silicic acid extraction into di-2-ethylhexylphosphoric acid (HDEHP) is poorer than into TBP. The β -species of silicic acid are mainly extracted into HDEHP in heptane ($0.75 \text{ mol} \cdot \text{l}^{-1}$) because of the low content of water in the organic phase. The water concentration was equal to $0.55 \text{ g} \cdot \text{l}^{-1}$. It is lower than in the solutions of TBP and TOPO in our experiments. The extraction of silicic acid only at high acidity of an aqueous phase (Table 2) indicates that the interaction of silicic acid with undissociated HDEHP takes place as with NPOC through a phosphoryl oxygen atom.

Table 2
DISTRIBUTION OF α - AND β -SILICIC ACID SPECIES EXTRACTED INTO HDEHP FROM HNO_3 OF VARIOUS CONCENTRATIONS^a

Aqueous phase : distr. coefficient	pH 2	2 mol/liter HNO_3	5 mol/liter HNO_3
D_α	$< 1.8 \cdot 10^{-4}$	$3.1 \cdot 10^{-3}$	$4.5 \cdot 10^{-3}$
D_β	$< 2.1 \cdot 10^{-4}$	$4.7 \cdot 10^{-3}$	$5.0 \cdot 10^{-3}$

^a The initial concentration of SiO_2 in the aq. phase is $1.8 \text{ g} \cdot \text{l}^{-1}$; the initial org. solution is $0.75 \text{ mol} \cdot \text{l}^{-1}$ HDEHP in heptane; O:A = 1:1. In the experiments with HDEHP the silicic acid concentration in the organic phase was determined after its stripping by dilute HNO_3 (pH 2). The preliminary prolonged contact of silicic acid solution and the solution of HDEHP without agitation (for times to 72 hr) resulted in the formation of the precipitate at the interface when following mixing (Table 3). The amount of silicic acid in the precipitate was determined after its soluting in the volume of alkali equal to the volume of the aqueous phase (ΔC in Table 3).

Table 3
DISTRIBUTION OF SILICIC ACID ($\text{g} \cdot \text{l}^{-1}$) BETWEEN ORGANIC, AQUEOUS PHASES AND INTERFACIAL PRECIPITATE^a

Period: of con- tact (hr)	HDEHP, mol/liter								
	0.485			0.24			0.12		
	C_{org}	C_{aq}	$\Delta C_{\text{(pr)}}$	C_{org}	C_{aq}	$\Delta C_{\text{(pr)}}$	C_{org}	C_{aq}	$\Delta C_{\text{(pr)}}$
2	$8.2 \cdot 10^{-3}$	1.81	-	$6.5 \cdot 10^{-3}$	1.47	0.34	$5.5 \cdot 10^{-3}$	1.37	0.44
6	$7.0 \cdot 10^{-3}$	1.42	0.39	$5.2 \cdot 10^{-3}$	1.36	0.45	$4.7 \cdot 10^{-3}$	1.24	0.57
24	$4.4 \cdot 10^{-3}$	1.22	0.59	$4.8 \cdot 10^{-3}$	1.18	0.63	$3.5 \cdot 10^{-3}$	1.05	0.76
72	$4.4 \cdot 10^{-3}$	1.20	0.61	$4.0 \cdot 10^{-3}$	1.13	0.68	$3.2 \cdot 10^{-3}$	0.92	0.89

^a The initial concentration: SiO_2 is $1.82 \text{ g} \cdot \text{l}^{-1}$; HNO_3 is $5.7 \text{ mol} \cdot \text{l}^{-1}$
O:A = 1:1

The precipitation of silicic acid indicates that it may polycondense at the interface. An increase in the period of contacting (an increase in the extent of polycondensation) and a decrease in the ext-

ractant concentration (hence an decrease in water concentration in the organic phase) promote to precipitate of silicic acid at the interface.

The behaviour of silicic acid in the extraction systems with 40% tri-n-octylamine and tetralcylammonium nitrate in benzene was also studied. It was pointed out earlier (5) that silicic acid was extracted from sulfate media by toluene solutions of tetraoctylammonium bromide trialcylmethylammonium sulfate, tri-n-alcylamine sulfate. However we didn't observe the silicic acid extraction into tri-n-alcylamine and tetralcylmethylammonium nitrate from nitrate media (pH 2 - 7).

References

1. R.K.Iler, The chemistry of silica. 1979, N.-Y. A Wiley Interscience Publication.
2. A.A.Nemodruk, E.V.Bezrogova, *Jurn.analit.khimii*, 25(8), 1587(1970).
3. S.V.Chizhevskaja, O.A.Sinegribova, S.S.Danilova et al., *Izv.vuzov, Chimija i chim.technologija*, 20(5), 694(1977).
4. E.G.Kudriavtsev, O.A.Sinegribova, *Tr.MChTI im.D.I.Mendeleeva*, № 114, 49(1980).
5. N.N.Golovnev, in "Sedmaja vsesojuznaja konf. po chimii extractsii. Tezisi dokladov", Moscow, Nauka, 1984, p.94.

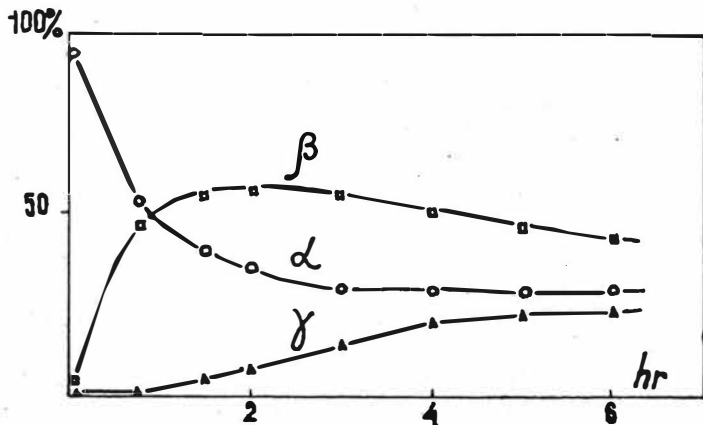


Fig.1. Plot of α -, β - and γ -species amount as a function of duration (hr.).

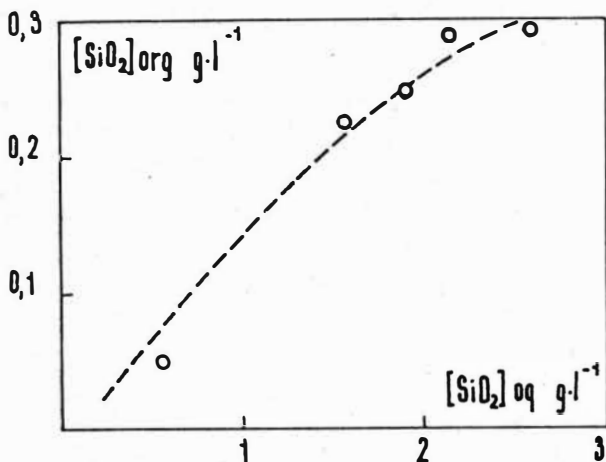


Fig. 2. Distribution isotherm for silicic acid.

Aq. phase - 1mol/l HNO_3 , org. phase - 100%TBP.

(The dashed curve is that calculated).

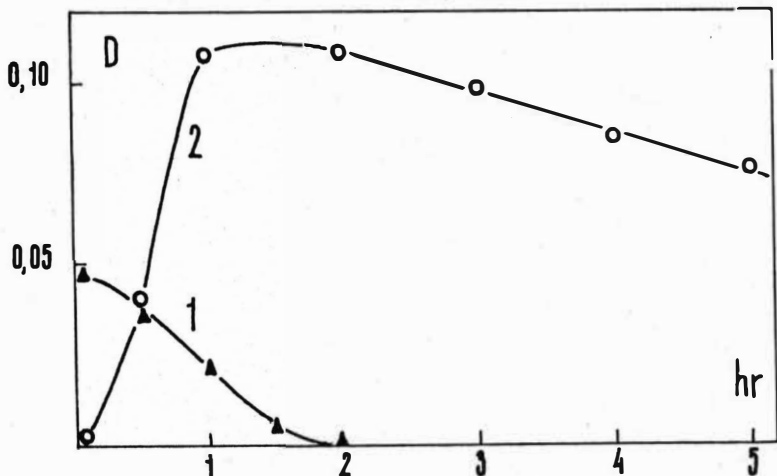


Fig. 3. Plot of silicic acid distribution coefficient for TBP(1)

and TOPO(2) as a function of duration (hr.) before

extraction. Aq. phase: 1.28g/l SiO_2 , 2mol/l HNO_3 .

Curve 1 - 1.33mol/l TBP, O:A=5:1.

Curve 2 - 0.5mol/l TOPO, O:A=1:1.

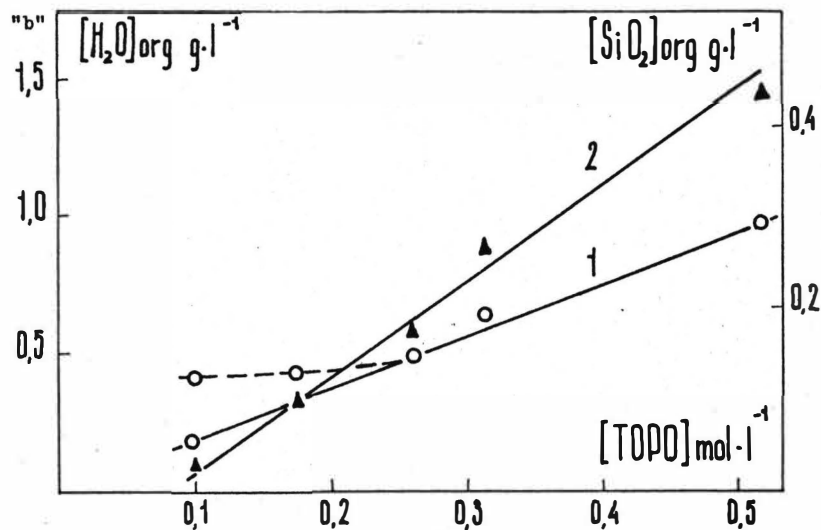
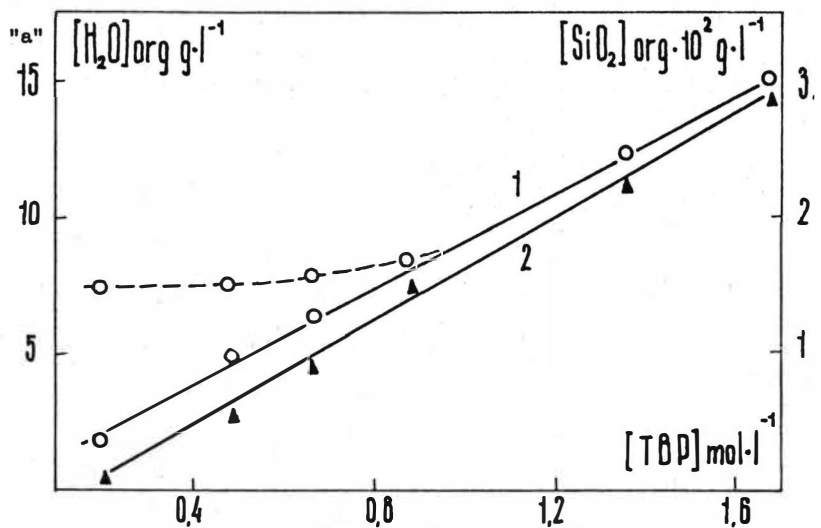


Fig.4. Plot of silicic acid and water concentrations in org. phase as a function of TBP("a") and TOPO("b") concentrations in heptane. Aq. phase: 3.02g/l SiO_2 , 2mol/l HNO_3 .
Curve1 - silicic acid.
Curve2 - water.

The Extraction of Sulfuric Acid by Primene-JMT dissolved in Toluene. Emf and Batch Studies at 25°C.

J.C.Blazquez, J.M.Madariaga and M.C.A.Sandino,
Kimika Departamendua, Euskal Herriko Unibertsitatea, Apt.644,
48080, Bilbo, Spain.

The extraction of sulfuric acid by tertiary long-chain amines has re- ceipt the attention of many authors [1]. In sulfate media primary amines are better extractants than secondary and tertiary ones [2]. Recently the extraction of water and sulfuric acid by trilaurylamine dissolved in toluene has been studied [3]. In this work the extraction of water and sulfuric acid by the primary amine, Primene-JMT, (PJMT), dissolved in toluene at 25°C, using both batch experiments [4] and the two-phase emf titration method [5], is presented.

Batch Experiments

Samples of the amine dissolved in toluene were equilibrated with the same volume of pure sulfuric acid solutions. After equilibrium was attained both phases were analysed for acid by titrating with alcaly. Water in the organic phase was analysed using the Karl-Fischer method. From the equilibrium concentration of sulfuric acid in water, the corresponding activities of water and acid were obtained from data by Giaque et al. [6].

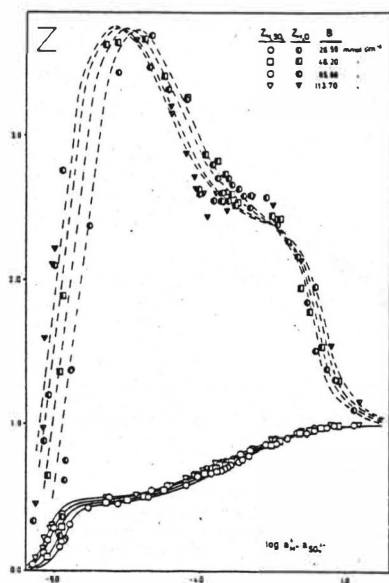


Fig.1 $Z_{H_2SO_4}$ and Z_{H_2O} plotted against $\log(H^+)^2 (SO_4^{2-})$ for the aqueous acidity range studied ($10^{-3} < |H_2SO_4| < 8.0 \text{ mol.dm}^{-3}$). The full drawn curves refer to H_2SO_4 , the dashed ones refer to H_2O . The curves have been computed from the model in Table 1.

The functions $Z_{H_2SO_4}$ and Z_{H_2O} are defined by

$$Z_{H_2SO_4} = \frac{|H_2SO_4|_{org} - |H_2SO_4|_{dil}}{B} \quad (1); \quad Z_{H_2O} = \frac{|H_2O|_{org} - |H_2O|_{dil}}{B} \quad (2)$$

The amine concentrations in toluene used in this work are : 26.59, 46.20, 85.86, 113.70 mmol.dm⁻³. Toluene does not extract sulfuric acid in the range of aqueous sulfuric acid concentration studied. However, the diluent extracts water by a simple partition equilibrium [7]. The presence of systematic errors in the whole sets of ($Z_{H_2SO_4}, \log(H^+)^2 \cdot (SO_4^{2-})_B$) data has been detected.

Fig.1, shows a plot of the $Z_{H_2SO_4}$ and Z_{H_2O} corrected values, against $\log(H^+)^2 \cdot (SO_4^{2-})_B$.

In order to obtain information about the general composition of the complexes in the organic phase, the general integration method developed by Sillén [8], has been applied to the whole sets of data, considering, as a first approximation, the (H_2O) constant. This data have been introduced in the computer program MESAK [9] and the values of \bar{p} and \bar{q} (the mean number of sulfuric acid and amine per complex respectively) have been calculated. Fig.2 gives a plot of \bar{p} against \bar{q} , for the four amine concentrations studied. This is an indication of the presence of two Core+Links families of complexes.

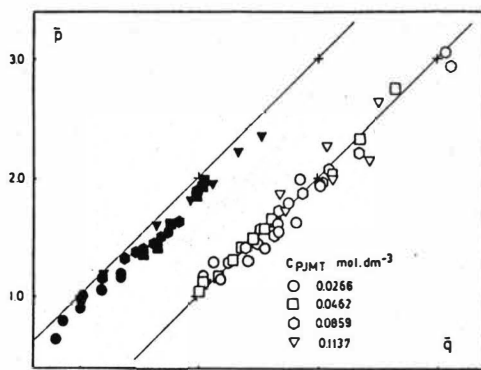


Fig.2 \bar{p} and \bar{q} values obtained by the MESAK program. White circles refer to $Z_{H_2SO_4} < 0.55$; black circles refer to $Z_{H_2SO_4} > 0.65$

The curves in Fig.1, have been computed with the species and equilibrium constants given in Table 1. This model was arrived at by using the version ZEHTA [10] of the computer program LETAGROP [11]. The constants K_{pqn} given in Table 1, refer to the reaction



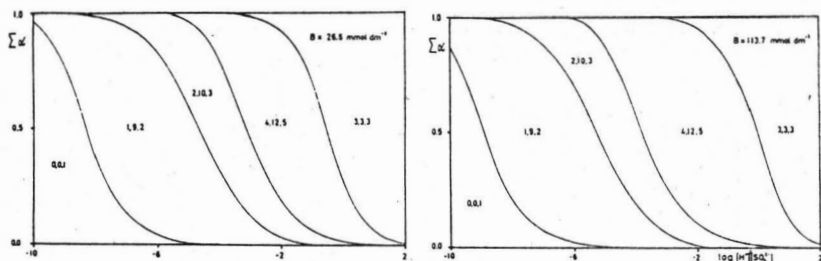


Fig.3 The fraction of amine present in each species, α_{pqn} , is plotted against $\log(H^+)^2(SO_4^{2-})$

The quantity, α_{pqn} , is given by

$$\alpha_{pqn} = \frac{q | (H_2SO_4)_p (PJMT)_q (H_2O)_n |}{B} \quad (4)$$

The α_{pqn} values have been computed using the COMPLEX-80 program [12].

Table 1.-Semi-stoichiometric formation constants, K_{pqn} , for reaction (3) in toluene.

Species (p,q,n)	$\log K_{pqn}$
$(H_2SO_4)_1 (PJMT)_2 (H_2O)_9$	9.91 ± 0.07
$(H_2SO_4)_2 (PJMT)_3 (H_2O)_{10}$	18.23 ± 0.25
$(H_2SO_4)_4 (PJMT)_5 (H_2O)_{12}$	34.36 ± 0.26
$(H_2SO_4)_3 (PJMT)_3 (H_2O)_3$	19.98 ± 0.21

Emf-Work

In order to find support for the existence of the species found at low acidities, an emf study was performed at 25°C using the two-phase emf titration technique at 1.0 mol.dm.⁻³ (Na,H)SO₄ of constant ionic strength.

Before analysing the data for the composition of the complexes, the range $Z < 0.1$ was investigated for systematic errors in Z, using the curve-fitting method proposed by Högfeldt [13]. Systematic errors have been detected in all the data series, probably due to an incorrect determination of the total amine concentration. In Fig.4, the Z corrected values have been plotted against $\log |H_2SO_4|$ for the following amine concentrations: 22.94, 34.07, 76.29, 117.65 mmol.dm.⁻³ in toluene.

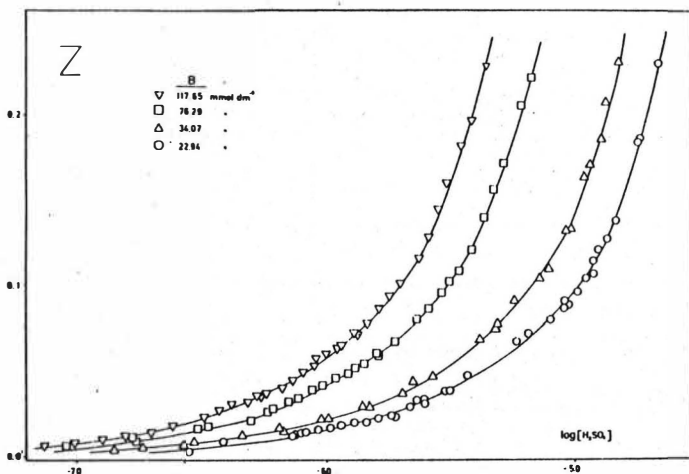
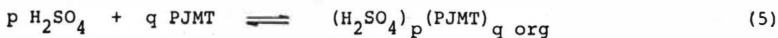


Fig.4 Z plotted against $\log|H_2SO_4|$ for the four amine concentrations studied. The curves have been computed from the model in Table 2.

The extraction of sulfuric acid by Primene-JMT can be expressed by the reaction



Since the water activity is kept constant by the ionic medium, no information about water in the species is obtained from the emf study. For that reason water is excluded from reaction (5).

The evaluation of \bar{p} and \bar{q} was performed by using the computer program MESAK. The results suggest a Core+Links behaviour, in agreement with the batch work, being $B(AB)_n$ the general formula of the complexes, with $p = q-1$, ($A \equiv H_2SO_4$, $B \equiv PJMT$). This fact is confirmed by the plot shown in Fig.5, where $X = \log B + \log|H_2SO_4|$, $|14|$.

Table 2.-Stoichiometric equilibrium constants for reaction (5) in toluene.

Species (p,q)	$\log \beta_{pq}$
$(H_2SO_4) (PJMT)_2$	5.80 ± 0.02
$(H_2SO_4)_6 (PJMT)_7$	37.43 ± 0.22
$(H_2SO_4)_7 (PJMT)_8$	43.60 ± 0.30

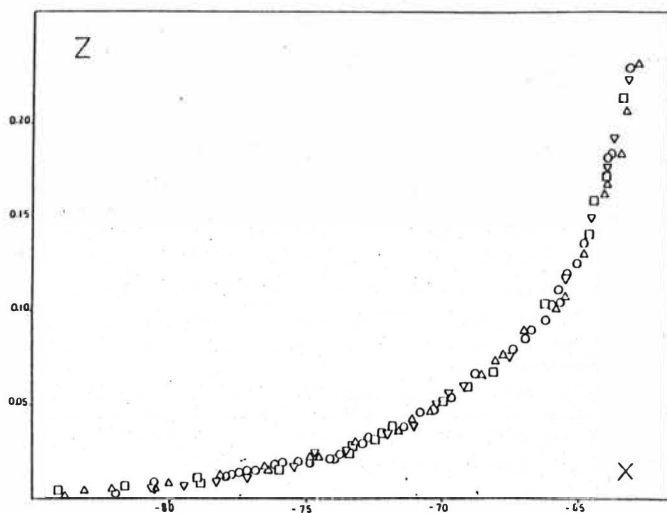


Fig.5 Z plotted against the variable X, for the four amine concentrations studied.

Then a Core+Links treatment as well as a standard graphical treatment were carried out. Finally a numerical treatment was performed using the ZETA version [15] of LETAGROP [10]. All the treatments gave the same set of species (1,2), (6,7) and (7,8). The values of proposed formation constants are given in Table 2.

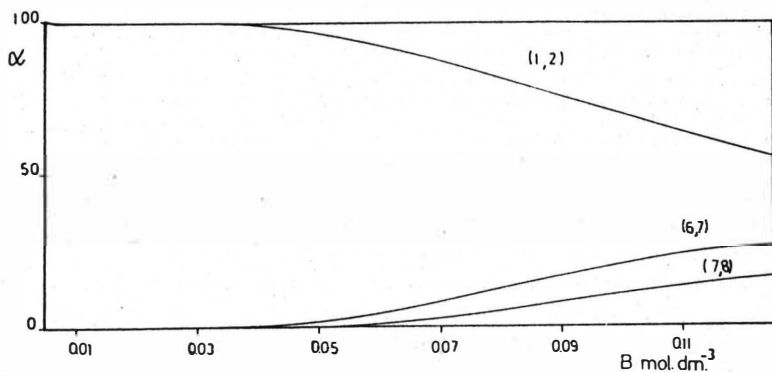


Fig.6 The molar fractions of the species (1,2), (6,7) and (7,8), plotted against B for $[\text{H}_2\text{SO}_4] = 10^{-5.35} \text{ mol.dm}^{-3}$:

In Fig.6 the fraction of amine present in each species, α_{pq} , is plotted against B. The α_{pq} values have been computed with the stoichiometric formation constants, given in Table 2, using the COMPLEX-80 program.

Discussion

The analysis of both, batch and emf work, has shown the same family of Core+Links complexes at the beginning of the extraction. The first species is always the monomeric ammonium sulfate : $AB_2 \equiv (RH_2NH^+)_2SO_4^{2-}$. When the quantity of sulfuric acid increases in the organic phase, species like $B(AB)_n$ are formed. These species can be formulated as $(AB_2) \cdot (AB)_{n-1} \equiv [(RH_2NH^+)_2SO_4^{2-}] \cdot [(RH_2NH^+)HSO_4^-]_{n-1}$, that is a solvated species between the monomeric ammonium sulfate and a polymeric ammonium bisulfate.

The extraction of water can be explained with the same kinds of species having 9 molecules of water per sulfuric acid in the ammonium sulfate and 1 molecule of water per sulfuric acid in the ammonium bisulfate, i.e. $[(RH_2NH^+)_2SO_4^{2-} \cdot (H_2O)_9] \cdot [(RH_2NH^+)HSO_4^- \cdot (H_2O)]_{n-1}$

However, in this region, the stoichiometries of the species obtained in the batch work are not the same than those obtained in the emf work. In the first case, $n=1,2$ and 4, and in the second one, $n=1,6$ and 7. From our point of view this second model seems to be more realistic because the uncertainty observed in the batch work at very low acidities of sulfuric acid in the aqueous phase is too high. Moreover the correlation between $[H_2SO_4]$ and $\{H^+\}^2(SO_4^{2-})$ is not so well defined than in moderate or high aqueous sulfuric concentration.

The distribution of species containing sulfuric acid in the organic phase should be remarked. As seen in Figure 3, the species containing ammonium sulfate in the organic phase predominate in the range

$[H_2SO_4]_{aq} < 3.5 \text{ mol.dm}^{-3}$. From both Figures 3 and 6, the monomeric ammonium sulfate seem to be a high predominant region, independently on the amine concentration. This amine does not form species with stoichiometries acid:amine higher than 1:1 ($Z > 1.0$).

Comparing these results with those obtained in a previous work [3], when triaurylamine was used as the extractant, important differences are observed. With the tertiary amine the monomeric ammonium sulfate is a minor species and the ammonium bisulfate predominates in the region $0.8 < [H_2SO_4]_{aq} < 6 \text{ mol.dm}^{-3}$, being the most important species.

Moreover at $[H_2SO_4]_{aq} > 4.0 \text{ mol.dm}^{-3}$, Z values higher than 1.0 are obtained indicating that an excess of sulfuric acid is extracted.

Primene-JMT, at 0.1 mol.dm^{-3} , begins to extract acid when $[H_2SO_4]_{aq} = 10^{-8} \text{ mol.dm}^{-3}$, while triaurylamine, at the same concentration, needs $[H_2SO_4]_{aq} = 10^{-4} \text{ mol.dm}^{-3}$ to extract sulfuric acid. Also the amount of water extracted in the region where ammonium sulfate species predominate is different with both kinds of amines. The water extraction is more important when Primene-JMT is used. With this amine the maximum value $Z_{H_2O} \approx 4$ is obtained, while the triaurylamine gives $Z_{H_2O} = 2$ as the maximum one.

Two similar behaviours can be observed when comparing the extraction of sulfuric acid by Primene-JMT and trilaurylamine dissolved in toluene. In both cases the species with the highest stoichiometry is more important as the concentration of the amine increases and the ammonium bisulfate is completely aggregated, namely trimerized.

The range of aqueous sulfuric concentration in which the aggregated ammonium bisulfate are formed can explain how primary amines are better extractants of metals than tertiary ones. The presence of a completely aggregated ammonium salt inhibits the extraction of metal-anionic species. In fact 1.0 mol.dm.⁻³ sulfuric acid is a good stripping reagent for metals previously extracted by tertiary ammonium salts in other forms than sulfate or bisulfate [16]. At this aqueous sulfuric concentration, trilaurylamine dissolved in toluene is practically as trilaurylammonium bisulfate. However, primary amines, e.g., Primene-JMT, need more than 3.5 mol.dm.⁻³ in H₂SO₄ to form the corresponding ammonium bisulfate salt.

Finally the use of a technical grade reagent, like Primene-JMT, without further purification should be commented. The presence of systematic errors have been detected in all the data series collected. However after correction of its, the experimental information can be treated in terms of solution equilibria analysis as if p.a. reagents were used.

References

- 1.- M.Cox and D.S.Flett in "Handbook of Solvent Extraction", (eds. T.C. Lo, M.H.I.Baird and C.Hanson), pag.64, Wiley, New York, 1983.
- 2.- F.G.Seeley and D.J.Crouse, J.Chem.Eng.Data, 16, 393(1971)
- 3.- E.Högfeldt, J.M.Madariaga and M.Muhammed, Acta Chem.Scand., 139, 805 (1985).
- 4.- J.C.Blazquez and J.M.Madariaga, to be published
- 5.- M.C.A.Sandino and J.M.Madariaga, to be published.
- 6.- W.F.Giauque, E.W.Hornung, J.E.Kunzler and T.R.Rubin, J.Am.Chem.Soc. 92, 62 (1960)
- 7.- J.M.Madariaga, M.Muhammed and E.Högfeldt, Solv.Ext.Ion Exchange, in press 1986.
- 8.- L.G.Sillén, Acta Chem.Scand., 15, 1981(1961).
- 9.- J.M.Madariaga, CPL-20, Kim.Dept., UPV-EHU, March 1985 and references therein.
- 10.- L.G.Sillén, Acta Chem.Scand., 16, 159 (1962).
- 11.- B.Warnquist, "The ZEHFA program", Dept.Inorg.Chem., KTH, Stockholm, (1972).
- 12.- J.M.Madariaga and A.García, Comput.& Chem., 8, 187 (1984).
- 13.- E.Högfeldt and F.Fredlund, Trans.Royal Inst. Technol., (1964), No.226.
- 14.- E.Högfeldt in "Treatise on Analytical Chemistry" (eds.I.M.Kolthoff and P.J.Elving), vol.2, Part.I, pag 117, 2nd Edition, Wiley, New York, 1979.
- 15.- R.Arnek, L.G.Sillén and O.Wahlberg, Arkiv Kemi, 31, 365 (1969)
- 16.- J.M.Madariaga, R.M.Jimenez, M.D.Ruiz and M.Aguilar, Proc.ISEC'83, pag.495, Denver, (1983).

Flow of Power-Law Fluid Spheres through Newtonian Fluids:
Hydrodynamics and Mass Transfer

Türker Gürkan

Middle East Technical University
Chemical Engineering Department
Ankara-TURKEY

The equations of motion for the flow of a power-law fluid sphere in a newtonian continuous phase have been approximately satisfied by using Galerkin's method. External and internal stream function expressions have been obtained, the constants of which vary with the Reynolds number, the viscosity ratio parameter X , and the dispersed phase power-law index, n_i . Calculated results indicate that the droplet drag coefficients decrease with decreases in n_i for $X \leq 1$ and increase with decreases in n_i for $X \geq 10$. Decreases in the value of the dispersed phase power-law index result in significant decreases in the circulation within the droplet for $X \geq 10$. Calculated results compare favorably with the available experimental data.

The convective diffusion equations for mass transfer with or without a second order chemical reaction inside a fluid sphere have been solved for the purpose of determining the effect of the power-law behavior in the dispersed phase on the dispersed phase mass transfer mechanism. Stream function expressions obtained in the first part of the study have been used for this purpose. The results are presented in terms of the total amount of mass transferred to the droplet, \bar{C}_{1t} , as a function of the dimensionless time of contact, τ , n_i , X , Re , Pe and k_R . Calculated results indicate that increased pseudoplasticity in the dispersed phase causes decreases in \bar{C}_{1t} because of reduced internal circulation velocities. Maximum decreases in \bar{C}_{1t} with decreases in n_i are calculated to be realized for larger values of Pe and X and smaller values of Re . The continuous phase Sherwood number, on the other hand, is calculated to be slightly enhanced with decreasing n_i . Calculated results compare favorably with the available experimental data.

As the manuscript was not available at the 28th May 1986, the deadline for printing this book, we only print the short abstract of the paper.

A Predictive Approach for the Determination of Composition and Temperature Dependence of Liquid Diffusivities

T. Gürkan, E. Eroglu, METU, Ankara, Turkey

The necessity of predicting liquid diffusivities often arises because of the lack of liquid diffusion coefficient data in literature especially as a function of composition and temperature. In addition, liquid state theories are not satisfactory in providing relations for the calculation of liquid diffusivities for highly nonideal and associating systems. Thus, it is unavoidable to use semi-empirical methods for the determination of composition and temperature dependence of liquid diffusion coefficients.

Sanchez and Clifton [1] proposed an empirical correlation of the form

$$D_{AB} = (X_A D_B^0 + X_B D_A^0)(1 - m + m\beta) \quad (1)$$

to represent the variation of diffusion coefficients with composition. In this expression D_A^0 and D_B^0 are diffusion coefficients at infinite dilution and m is an empirical constant evaluated from the slope of a $D_{AB}/(X_A D_B^0 + X_B D_A^0)$ versus β plot. The thermodynamic correction factor, β , is defined by:

$$\beta = (\partial \ln a_A / \partial \ln X_A)_{T,P} \quad (2)$$

The values of m for certain binaries were calculated by Sanchez and Clifton only at 298 K. Since one value of D_{AB} in the middle of the concentration range is enough in order to calculate m , they found the values of D_{AB} and β at the concentration for which β reaches a maximum or minimum value, and combining these with the literature values of D_A^0 and D_B^0 , they evaluated m . A comparison of their predictions with those of Darken, Vignes and Rathbun and Babb indicated that their correlation gives much better results. Sanchez and Clifton were not able to determine the temperature variation of m since this necessitates experimental data of diffusivities and activity coefficients as a function of composition over a range of temperatures.

The determination of the temperature dependence of m is the primary objective of the present study. For the highly non-ideal systems acetone-water, ethanol-water and acetone-chloroform measured values of diffusion coefficients as a function of both temperature and composition are available [2]. The second set of data needed for the evaluation of m is the constant temperature vapor-liquid equilibrium data at the same temperature of the diffusion data. However, vapor-liquid equilibrium data are available in literature only at certain temperatures for the above systems. Thus β is calculated at the desired temperatures by a predictive algorithm which includes a constant temperature bubble point computation. The virial equation of state truncated after the second term together with Pitzer and Curl correlations for the evaluation of second virial coefficients are used to

take into account the vapor phase nonidealities, and the UNIQUAC method is used for the liquid phase nonidealities.

Numerical values of UNIQUAC binary interaction parameters for the systems under study are available in literature [3]. Using these, vapor-liquid equilibria is predicted and compared with available experimental data. The deviation between the experimental and predicted values are small enough to conclude that β can be accurately predicted at any desired temperature with the chosen computational method [4].

Using the values of UNIQUAC binary interaction parameters available in literature their temperature dependence are determined. The form suggested by Prausnitz et al. [3]

$$A_{ij} = a_{ij} + b_{ij}/T \quad (3)$$

is used. The resultant correlations are given in Table 1.

Table 1. Correlations for Temperature Dependence of A_{ij}

System	A_{12}	A_{21}
Acetone(1)-Water(2)	$2.92228 \times 10^5 / T - 3.43711 \times 10^2$	$-1.26823 \times 10^5 / T + 2.85808 \times 10^2$
Acetone(1)-Chloroform(2)	$4.432395 \times 10^4 / T - 2.91476 \times 10^2$	$-1.944441 \times 10^5 / T + 6.69877 \times 10^2$
Ethanol(1)-Water(2)	$1.039376 \times 10^5 / T - 3.711 \times 10^2$	$-2.547163 \times 10^5 / T + 1.13207 \times 10^3$

After calculating temperature dependent UNIQUAC binary parameters, values of β as a function of liquid composition are evaluated applying the bubble point computation at the desired temperatures. Plots of D_{AB} / D_{AB}^{id} versus β are thus prepared. D_{AB}^{id} is given by :

$$D_{AB}^{id} = X_A D_B^0 + X_B D_A^0 \quad (4)$$

D_{AB} / D_{AB}^{id} and β show negative deviations from ideality for acetone-water and ethanol-water, whereas they show positive deviations for the system acetone-chloroform.

Instead of Eqn(1), a new approach is used for correlating D_{AB} as a function of β . We have used

$$D_{AB} / D_{AB}^{id} = m\beta + g \quad (5)$$

where the slope, m , and the intercept, g , are calculated by fitting the best straight line to the data of D_{AB} / D_{AB}^{id} versus β by the least squares method. The forms of the plots of D_{AB} / D_{AB}^{id} versus β suggested that two different straight lines could be drawn through a set of data points, a line for the data points up to a

mole fraction where the plot reaches a minimum or a maximum (from $X_A = 0$ to $X_{A,\min}$ or $X_{A,\max}$) and a second line for the remaining data points (from $X_{A,\min}$ or $X_{A,\max}$ to $X_A = 1.0$). Thus two correlations are obtained for the lower and higher concentration ranges. The resulting correlations for the prediction of composition dependence of D_{AB} at the specified temperatures for each system are given in Table 2. Correlations for other temperatures are available in [4].

Table 2. Predictive Correlations for Determination of Composition Dependence of D_{AB}

	<u>Composition Range</u>	<u>Correlation for D_{AB}/D_{AB}^{id}</u>
Acetone (A)-Water (B) (298 K)	$X_A < 0.3$	$0.8793\beta + 0.05$
	$X_A > 0.5$	$1.1067\beta + 0.0793$
	$0.4 < X_A < 0.5$	0.2460
Acetone (A)-Chloroform (B) (298 K)	$X_A < 0.4$	$0.2535\beta + 0.7602$
	$X_A > 0.4$	$0.2561\beta + 0.7341$
Ethanol (A)-Water (B) (313 K)	$X_A < 0.4$	$1.0121\beta + 0.0106$
	$X_A > 0.4$	$1.039\beta - 0.0299$

The predicted values of the diffusion coefficients are compared with experimental data. The averages of the percent deviations between experimental and predicted D_{AB}/D_{AB}^{id} values are given in Table 3.

Table 3. Comparison of Predictions of Correlations of this Study and Experimental Data

<u>System</u>	<u>Temperature, K</u>	<u>AAPD, Average Absolute Percent Deviations</u>
Acetone-Water	298	3.9
	308	3.6
	318	2.6
	328	1.4
Acetone-Chloroform	298	0.5
	313	0.2
	328	0.3
Ethanol-Water	313	1.0
	331	1.5
	346	1.7

The use of two equations for each system at a certain temperature decrease the percent deviations to very small values when compared with the Sanchez and Clifton

correlations. Table 4 clearly indicate the improvement. One should especially note the remarkable improvement for ethanol-water.

Table 4. Comparison of the Accuracy of the Correlations Given in this Study with those of Sanchez and Clifton [1].

	<u>This work, AAPD</u>	<u>Sanchez Clifton, AAPD</u>
Acetone-Water (298 K)	3.9	6.9
Acetone-Chloroform (298 K)	0.5	1.5
Ethanol-Water (313 K)	1.0	18.5

Quantitative determination of the temperature dependence of empirical constants of the predictive equations is aimed in this study. When slope and intercept values are plotted against temperature, it is seen that the slope, m , is inversely proportional to temperature, while the intercept, g , is directly proportional to temperature for systems acetone-water and ethanol-water for which β values are less than 1.0; and for acetone-chloroform with β values greater than 1.0, the trends are just the opposite. Correlations are obtained according to these trends by fitting straight lines to the data of m and g versus temperature. These correlations enable one to obtain the predictive equations for the composition dependence of diffusivity at any desired temperature in the range studied. These correlations are given in Table 5.

Table 5. Correlations for the Temperature Dependence of m and g .

<u>System</u>	<u>Composition Range</u>	<u>Slope, m</u>	<u>Intercept, g</u>
Acetone-Water (A) (B)	$X_A < 0.3$	$304.78/T - 0.1386$	$4.049 \times 10^{-3}T - 1.161$
	$X_A > 0.5$	$756.07/T - 1.4349$	$3.429 \times 10^{-3}T - 0.9477$
Acetone-Chloroform (A) (B)	$X_A < 0.4$	$8.5133 \times 10^{-3}T - 2.2841$	$899.53/T - 2.2562$
	$X_A > 0.4$	$6.46 \times 10^{-3}T - 1.6562$	$637.43/T - 1.4177$
Ethanol-Water (A) (B)	$X_A < 0.3$	$737.63/T - 1.3245$	$5.9819 \times 10^{-3}T - 1.8692$
	$X_A > 0.4$	$712.48/T - 1.2563$	$5.75 \times 10^{-3}T - 1.8184$

Predictive equations of the present study are used to compute the diffusion coefficients of acetone-water at 303 K and the results compared with literature values [5]. These are given in Table 6.

Table 6. Comparison of Predictions of this Study with Experimental Data [5].
(System : Acetone-Water at 303 K)

Mole Fraction <u>Acetone</u>	(D_{AB}/D_{AB}^{id}) exp <u>cm²/sec</u>	(D_{AB}/D_{AB}^{id}) pred <u>cm²/sec</u>	Percent <u>Deviation</u>
0.059	0.6556	0.6506	-0.8
0.2315	0.2977	0.3178	6.7
0.3499	0.2542	0.2575	1.3
0.5990	0.3582	0.3482	-2.8
0.8060	0.5843	0.5395	-7.7

The differences between the experimental and predicted values are small with an AAPD of 3.9 percent. This value is of the same order of magnitude with the AAPD values at 298 K and 308 K. Therefore the temperature dependence of empirical constants of predictive correlations are represented within a reasonable accuracy and the correlations can be used for temperatures other than the ones studied.

If a similar approach as the one used in this study is to be used to evaluate the predictive equations for the temperature and composition dependence of liquid diffusivities for binary systems other than the ones studied, one should find experimental diffusion coefficient data at two levels of temperatures and at each level at four compositions, so that two predictive equations will be obtained : one for lower concentrations and one for higher. From this set of data, the correlations for temperature dependence of m and g will be found.

Literature Cited

- [1] Sanchez, V., Clifton, M., Ind.Eng.Chem., Fundam., 16, 318 (1977).
- [2] Tyn, M.T., Calus, W.F., J.Chem.Eng.Data, 20, 310 (1975).
- [3] Prausnitz, J.M., Anderson, T.F., Grens, E.A., Eckert, C.A., Hsieh, R., O'Connell, J.P., Computer Calculations for Multi-Component Vapor-Liquid and Liquid-Liquid Equilibria, Prentice-Hall, Inc., Englewood Cliffs, N.J. (1980).
- [4] Eroglu, E., Measurement and Prediction of Composition and Temperature Dependence of Liquid Diffusivities, M.Sc. Thesis, METU, Ankara, Turkey (1984).
- [5] Baldauf, W., Knapp, H., Proceedings of Phase Equilibria and Fluid Properties in the Chemical Industry, Part I, Berlin, 121 (1980).

Ab Initio Calculation of Distribution Coefficients of Tetraalkylammonium Salts

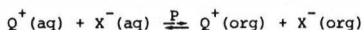
Stephen Jones, Simi Khan and Bryan G. Reuben
South Bank Polytechnic, London SE1 0AA, UK

INTRODUCTION

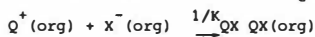
The principle aim of this project was to investigate the removal of phenolic compounds and thiocyanate ions from the waste water from coal gasification processes (1). As part of the work, we have measured the distribution of many tertiary and quaternary alkylammonium thiocyanates between organic solvents - in most cases dichloromethane - and water. We have also tried to calculate distribution coefficients and this aspect of the work is reported here.

The ab initio calculation of distribution coefficients for covalent molecules between water and organic solvents has been an intractable problem, although the application of the solubility parameter concept has had some success. The calculation of distribution coefficients for ions is apparently more open to theoretical analysis. Starting with Born (2), there have been numerous calculations on ionic solvation including a series of papers by Abraham and Liszi (3, 4) where further references may be found. The extraction of ion pairs from aqueous solution has also been widely studied (5 - 9).

Tetraalkylammonium salts (QX) are ionised in water [$Q^+(aq) + X^-(aq)$] but dissolve in organic solvents as ion pairs [QX(org)] which may dissociate slightly to $Q^+(org) + X^-(org)$. The process may be represented as two stages:

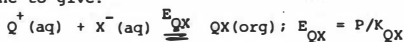


Standard free energy of phase transfer, $\Delta G_t^\circ = -RT \ln P$, and



Standard free energy of dissociation, $\Delta G_{QX}^\circ = -RT \ln K_{QX}$

These combine to give:



where E_{QX} is the thermodynamic extraction constant defined by Brändström (8) as

$$E_{QX} = \frac{a_{QX(org)}}{a_{Q^+(aq)} a_{X^-(aq)}}$$

The experimentally measured quantity is the distribution coefficient, D, given by:

$$D_{QX} = \frac{[X^-(aq)]^{\frac{1}{2}} [Q^+(aq)]^{\frac{1}{2}}}{[QX(org)]}$$

The derivation of extraction constants from distribution coefficients is complicated by side reactions such as ion pair and micelle formation in the aqueous layer and dimerization, adduct formation and reverse micelle formation in the organic layer.

In dilute solutions, these are unimportant and are usually ignored, while activity coefficients are assumed to be unity. Brändström (8) has shown how K_{QX} values can be obtained without any use of the activity constant in the actual solution. By these methods, the inter-related quantities P , E_{QX} , K_{QX} and the associated standard free energies can be derived for D_{QX} measurements.

Equally, if ΔG_t° and ΔG_{QX}° could be calculated, values of D_{QX} could be derived. The ab initio calculation of distribution coefficients, therefore, reduces to the prediction of these two quantities. Following Abraham and Liszi (9) we point out that ΔG_t° refers to partition of ions and ion pairs between pure water and pure solvent whereas the distribution coefficients are measured between two solvents each saturated with the other. For relatively immiscible solvents, this difference may be ignored.

CALCULATION OF FREE ENERGY OF PHASE TRANSFER OF IONS

The standard free energy of phase transfer ΔG_t° of an ion from water to an organic solvent is given by:

$$\Delta G_t^\circ = \Delta G_s^\circ - \Delta G_h^\circ$$

where ΔG_s° and ΔG_h° are the standard free energies of phase transfer of the ion from the gas phase into organic solvent and water respectively. ΔG_h° has been determined experimentally for many ions including the halides and tetramethyl and tetraethylammonium. Abraham and Liszi have estimated values for higher quaternaries (9).

ΔG_s° was calculated by Born (2) on the basis of a simple electrostatic model. If an ion of radius a is transferred from the gas phase to a solvent of dielectric constant D , then:

$$\Delta G_s^\circ = - \frac{Nz^2e^2}{8\pi\epsilon_0 a} \left[1 - \frac{1}{D} \right] \quad \dots\dots (1)$$

where N is Avagadro's number, z the charge on the ion, e the electronic charge and ϵ_0 the permittivity of vacuum.

Prediction versus experiment is shown in Figure 1. Agreement is poor. There are two defects in Born's simple model. First, no allowance is made for the disruption of the solvent caused by the ion because of its size rather than its charge. This has been calculated from the solubilities of non-polar gaseous molecules of similar size to the ions. Abraham and Liszi (9) followed Siekeirski (10) in splitting ΔG_s° into an electrostatic term ΔG_{el}° and a "neutral" term ΔG_n° . Values of ΔG_n° were calculated by Abraham and Liszi, the data for tetraalkylammonium ions being generated by interpolation of data on higher alkanes, and we have also used this method. Theory versus prediction is shown in Figure 1 and agreement is again poor.

The second defect of Born's model is that it assumes a homogeneous (unstructured) solvent of uniform dielectric constant whereas the dielectric constant of solvent

molecules near an ion must be less than in the bulk of the solvent because they are oriented by the intense electric field in its neighbourhood. Abraham and Liszi assume a structured solvent in which each ion is surrounded by a local layer of solvent of dielectric constant D_1 ($D_1 = 2$) and thickness b_0 , where b_0 is the radius of a solvent molecule. The ion plus solvation shell then has an effective radius $b = a + b_0$. On this assumption, the electrostatic standard free energy of solvation is given by:

$$\Delta G_{el}^{\circ} = -\frac{Nz^2e^2}{8\pi\epsilon_0} \left[\left(\frac{1}{D_1} - 1 \right) \left(\frac{1}{a} - \frac{1}{b} \right) + \left(\frac{1}{D} - 1 \right) \frac{1}{b} \right] \quad \dots\dots (2)$$

Values for ΔG_{el}° predicted by this model are shown in Figure 1 and are well within experimental error.

We conclude that the method of Abraham and Liszi is a useful way of predicting the free energies of phase transfer of tetraalkylammonium and other ions. The inter-relations between the various free energies are shown in Figure 2.

CALCULATION OF DISSOCIATION CONSTANTS OF ION PAIRS

The dissociation constant K_{QX} of an ion pair and the associated standard free energy change ΔG_{QX}° may be calculated by a method due to Bjerrum (11). He assumed an unstructured solvent and obtained the relationship:

$$\frac{1}{K_{QX}} = \frac{4\pi N}{1000} \int_{a_1+a_2}^q r^2 \exp(z'e^2/4\pi\epsilon_0 DkTr) dr \quad \dots\dots (3)$$

where a_1 and a_2 are the radii of the ions making up the ion pair and the distance q is defined by $q = e^2/2DkT$. Oppositely charged ions closer than q are defined as ion pairs; the remainder are free ions. A statistical mechanical treatment gives the same result (12). The integral may be evaluated on a microcomputer. For tetraalkylammonium salts in non-polar solvents where no structuring of solvent would be expected, the equation seems to give good results:

Salt	Solvent	a_1	a_2	b_0	K_{QX} (moles dm^{-3})	
					Experimental (14, 15)	Predicted
$(i-C_4H_9)_4NI$	benzene	0.352*	0.220	.2648	5.0×10^{-18}	5.2×10^{-18}
$(i-C_4H_9)_4NBr$	benzene	0.352*	0.195	.2648	3.5×10^{-18}	0.86×10^{-18}

* based on molar volumes (13).

For tetraalkylammonium salts in dichloromethane, equation 3 gives results which agree acceptably with the experimental results of Gustavii and Tivert, re-calculated by Brändström (8) (Figure 3). Hence, equations 2 and 3 appear to provide a means by which ΔG_{QX}° and ΔG_{el}° may be calculated. The drawback is that the two models are wholly inconsistent; the Abraham and Liszi model assumes a structured solvent whereas the Bjerrum solvent is homogeneous.

Bjerrum assumes a potential energy function between two oppositely charged ions of $- Nz^2 e^2 / 8\pi\epsilon_0 D r$ (Figure 4). This could be adapted to Abraham and Liszi's model by assuming a sharp change in dielectric constant when the positive and negative ions approached within a solvent diameter of one another. Thus, the potential energy function would coincide with that of Bjerrum until $r = a_1 + a_2 + 2b_0$, and would then follow a function related to $- Nz^2 e^2 / 8\pi\epsilon_0 D_1 r$ where $D_1 = 2$. This "close approach" potential energy function must coincide with the function at greater distances when $r = a_1 + a_2 + 2b_0$, hence it can be shown that its equation is $-\frac{Nz^2 e^2}{8\pi\epsilon_0 r} \left[\frac{1}{D_1 r} + \frac{1}{a_1 + a_2 + 2b_0} \left(\frac{1}{D} - \frac{1}{D_1} \right) \right]$ and this function is also shown in Figure 3. It gives a much

deeper potential well than the Bjerrum model and equation 3 may be modified to give:

$$\frac{1000}{4\pi N K Q X} = \int_{a_1+a_2}^{a_1+a_2+2b_0} \frac{z^2 e^2}{r^2} \exp \left[\frac{1}{4\pi\epsilon_0 k T} \left[\frac{1}{D_1 r} + \frac{1}{a_1+a_2+2b_0} \left(\frac{1}{D} - \frac{1}{D_1} \right) \right] \right] dr$$

$$+ \int_{a_1+a_2+2b_0}^q \frac{z^2 e^2}{r^2} \exp (z^2 e^2 / 4\pi\epsilon_0 D k T r) dr$$

..... (4)

The second term is usually very small in comparison with first, even for low values of D . If we ignore it, we are redefining an ion pair as being two oppositely charged ions within a single solvent diameter of each other. This new definition gets rid of the arbitrary distance q which is seen as a drawback to the Bjerrum model. When applied to tetraalkylammonium salts, however, it gives poor results (Figure 3).

Although this model allows for a structured solvent, it ignores the additional structuring which occurs when two solvated ions of opposite charge approach one another. If the solvent is reasonably polar, then the solvent molecule in the complex $Q^+ \text{---} \text{solvent} \text{---} X^-$ will be highly polarised. For the ions to approach closer, the solvent molecule must be forced out, a process which, as has been pointed out by Lee and Wheaton (16), may be energetically unfavourable. The stable species is then a solvent-separated ion pair. Lee and Wheaton cite considerable kinetic and spectroscopic evidence for such species and themselves adduce further evidence. If the existence of a potential energy minimum at an interionic distance of $a_1 + a_2 + 2b_0$ is accepted, then perhaps the step change in dielectric constant implied in the Abraham and Liszi model occurs at $a_1 + a_2 + 4b_0$. Bjerrum's model may then be reworked on the following assumptions:

- a. The anion and cation never approach closer than a single solvent diameter,
- b. the ions are surrounded by polarised solvent molecules as in the Abraham and Liszi model,
- c. an ion pair is said to exist when the ions are within two solvent diameters of each other.

The equation for the dissociation constant then becomes:

$$\frac{1}{K_{QX}} = \frac{4\pi N}{1000} \int_{a_1+a_2+2b_0}^{a_1+a_2+4b_0} r^2 \exp \left[\frac{z^2 e^2}{4\pi \epsilon_0 kT} \left[\frac{1}{D_1 r} + \frac{1}{a_1+a_2+2b_0} \left(\frac{1}{D} - \frac{1}{D_1} \right) \right] \right] dr$$

..... (5)

The values of ΔG_{QX}° generated by this equation are shown in Figure 3. The agreement is acceptable and the model wholly consistent with that of Abraham and Liszi. If a value of $D_1 = 2.5$ rather than $D_1 = 2$ is taken, agreement with experiment is substantially better, but the two models are no longer consistent.

APPLICATION TO THIOCYANATES

The thiocyanate ion is the ion of particular interest in this work. Experimental values for ΔG_t° (SCN^-) were obtained by measurement of the distribution of tetraalkylammonium thiocyanates between water and dichloromethane. Analysed by Brändström's method, it appears that ΔG_t° for the compound is zero. Assuming, ΔG_t° for tetraalkylammonium to be $-19.0 \text{ kJ mole}^{-1}$ (8), the value for thiocyanate is $19.0 \pm 0.8 \text{ kJ mole}^{-1}$. $\Delta G_{QX}^\circ = 19.3 \pm 0.5 \text{ kJ mole}^{-1}$. This makes it about 5 kJ mole^{-1} more lipophilic than iodide.

Attempts were also made to measure ΔG_t° by the competition for phase transfer between thiocyanate and halide ions. Figure 5 shows percentage extraction of thiocyanate ions into dichloromethane from a solution of $4.13 \times 10^{-4} \text{ M}$ tetrabutylammonium thiocyanate (solubility 1.1 g dm^{-3}) in the presence of varying concentrations of chloride, bromide and iodide ions. It was intended to analyse for halide ions in order to permit accurate calculation of ΔG_t° values, but problems with ion-sensitive electrodes made this impossible (17). Maximum and minimum values may, nonetheless, be obtained from the data in Figure 5 and they lead to a probable value for ΔG_t° (SCN^-) between 16 and 20 kJ mole^{-1} , in broad agreement with the value given above. It is slightly lower than the figure given by Thyron et al (21) for extraction into dichloromethane of $21.6 \text{ kJ mole}^{-1}$.

It is of interest to see how closely these figures agree with calculated values. The ionic radius of the thiocyanate ion is 0.195 nm , identical with that of bromide, consequently $\Delta G_s^\circ = -225.4 \text{ kJ mole}^{-1}$. Values of ΔG_h° (SCN^-) are not given in the literature, but may be calculated from ΔH_h° and ΔS_h° .

The gas phase entropy of the thiocyanate ion may be derived by statistical mechanics. The Sackur Tetrode equation gives $S_{trans}^\circ = 159.3 \text{ JK}^{-1} \text{ mole}^{-1}$. S_{rot}° (based on moment of inertia $= 1.253 \times 10^{-38} \text{ g cm}^2$) $= 65.1 \text{ JK}^{-1} \text{ mole}^{-1}$ and S_{vib}° (based on $\nu_1 = 750 \text{ cm}^{-1}$, $\nu_2 = 398 \text{ cm}^{-1}$, $\nu_3 = 2066 \text{ cm}^{-1}$) $= 8.4 \text{ JK}^{-1} \text{ mole}^{-1}$, so the gas phase entropy $= 232.8 \text{ JK}^{-1} \text{ mole}^{-1}$. This is close to Altschuller's value of 232.1 (18). The entropy of SCN^- in solution $= 144.3 \text{ JK}^{-1} \text{ mole}^{-1}$ (19), hence $\Delta S_h^\circ = -88.5 \text{ JK}^{-1} \text{ mole}^{-1}$.

ΔH_h° (SCN^-) is recorded by Vasilev et al (20) as $-305.5 \text{ kJ mole}^{-1}$. This value is based on different assumptions from those of Noyes (21) and Abraham (9) and adjustment to the latter's convention gives a value of $-260.3 \text{ kJ mole}^{-1}$, whence ΔG_h° (SCN^-) = $-234 \text{ kJ mole}^{-1}$ and $\Delta G_t^\circ = 8.6 \text{ kJ mole}^{-1}$. Correction to the molar scale gives $\Delta G_t^\circ = 11.7 \text{ kJ mole}^{-1}$. This is about 7 kJ mole^{-1} lower than the experimental value, which, as it is the difference between two large numbers, is certainly within the experimental errors of the various measurements.

The values of ΔG_t° and E_{QX} for the thiocyanate ion, therefore, fit in with the theories developed above. The value of K_{QX} , however, is almost an order of magnitude higher than that for the corresponding bromide (4×10^{-4} against $5 \times 10^{-5} \text{ mole dm}^{-3}$). Part of the reason may be that SCN^- is not spherically symmetrical. If the tetrabutyl group and bridging solvent molecule attach to the end of the thiocyanate ion, the distance between the charge centres will be larger than in the bromide. It may be estimated as follows: The sulfur atom has a Van der Waals radius of 0.185 nm and the S^{4-} ion a radius of 0.184 nm . The average of various radii for neutral and charged nitrogen is 0.155 nm . In SCN^- the S-C distance is 0.169 nm and the C-N distance 0.115 nm . The effective length of the ion will be approximately the sum of these distances, that is 0.614 nm . Equation 5 then predicts a value of $10^{-4} \text{ moles dm}^{-3}$ with $D_1 = 2.5$, which gives the best line through the other experimental points. The experimental value is still four times too large. Possibly other polarisation factors are at work. Also, K_{QX} is estimated from a small intercept on the y-axis and is liable to serious errors. Further work is needed on this topic.

CONCLUSION

The model of Abraham and Liszi, involving a structured dielectric of thickness equal to a solvent radius, gives excellent values for the free energies of solvation of tetraalkylammonium, halide and thiocyanate ions. Bjerrum's model for the dissociation constant of tetraalkylammonium halides gives acceptable results but assumes an unstructured solvent. Attempts to reconcile the two models leads to the suggestion of a structured solvent containing solvent-separated ion pairs and this too gives acceptable predictions of dissociation constants.

1. S. Jones, N. Kaur and B. G. Reuben, Chem. Ind. 14 (1985)
2. M. Born, z.Phys 1, 45 (1920)
3. M. H. Abraham and J. Liszi, J. Chem. Soc. (Faraday I) 74, 1604, 2858 (1978); 76 1219 (1980)
4. M. H. Abraham, J. Liszi and L. Meszaros, J. Chem. Phys. 70, 2491 (1979)
5. A. Brändström, Adv. Phys. Org. Chem. 15, 267 (1977)
6. T. Sekine and Y. Hasegawa, Solvent Extraction Chemistry, Dekker, New York, 1977
7. Y. Marcus and A. S. Kertes, Ion Exchange and Solvent Extraction of Metal Complexes, Wiley, New York, 1969
8. A. Brändström, Pure & Appl. Chem. 54, 1769 (1982)

9. M. H. Abraham and J. Liszi, *J. inorg. nucl. Chem.* 43, 143 (1981)
10. S. Siekeirski, *J. Radioanalyt. Chem.* 21, 9 (1974)
11. N. Bjerrum, *Kgt. danske Vidensk. Selsk.*, 7, 9 (1926)
12. R. Fowler and E. A. Guggenheim, *Statistical Thermodynamics*, OUP, 1939
13. F. J. Millero, *Chem. Revs.*, 71, 147 (1971)
14. R. M. Fuoss and C. A. Kraus, *J. Am. Chem. Soc.*, 55, 3614 (1933)
15. M. H. Abraham, *J. Chem. Soc. (Perkin II)* 1343 (1972)
16. W. H. Lee and R. J. Wheaton, *J. Chem. Soc. (Faraday II)* 1128 (1979)
17. S. A. Khan and B. G. Reuben, *J. App. Electrochem.* 15, 969 (1985)
18. A. P. Altschuller, *J. Chem. Physics*, 28, 1254 (1958)
19. Selected values of chemical thermodynamic properties, NBS Technical Note 270-3, NBS, Washington, 1968.
20. V. P. Vasilev et al, *Zhur, Fiz. Chim.* 34, 1763 (1960)
21. J. P. Antoine, I. De Aguirre, F. Janssens and F. Thyron, *Bull. Soc. Chim. France* 5-6 pt 2, 207 (1980).

We thank the British Gas Corporation, London Research Station, for their support of this work.

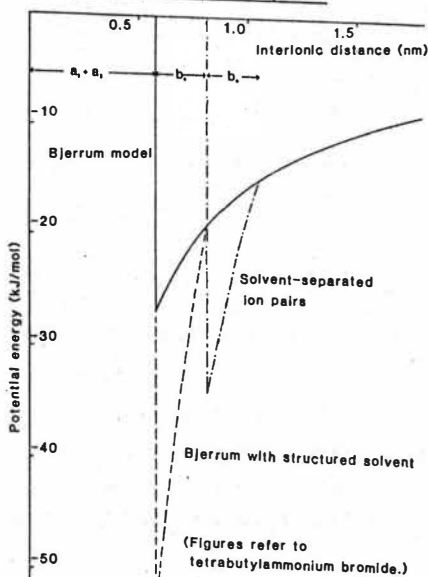
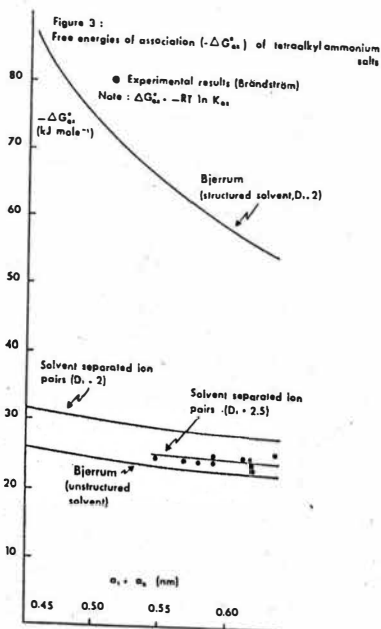
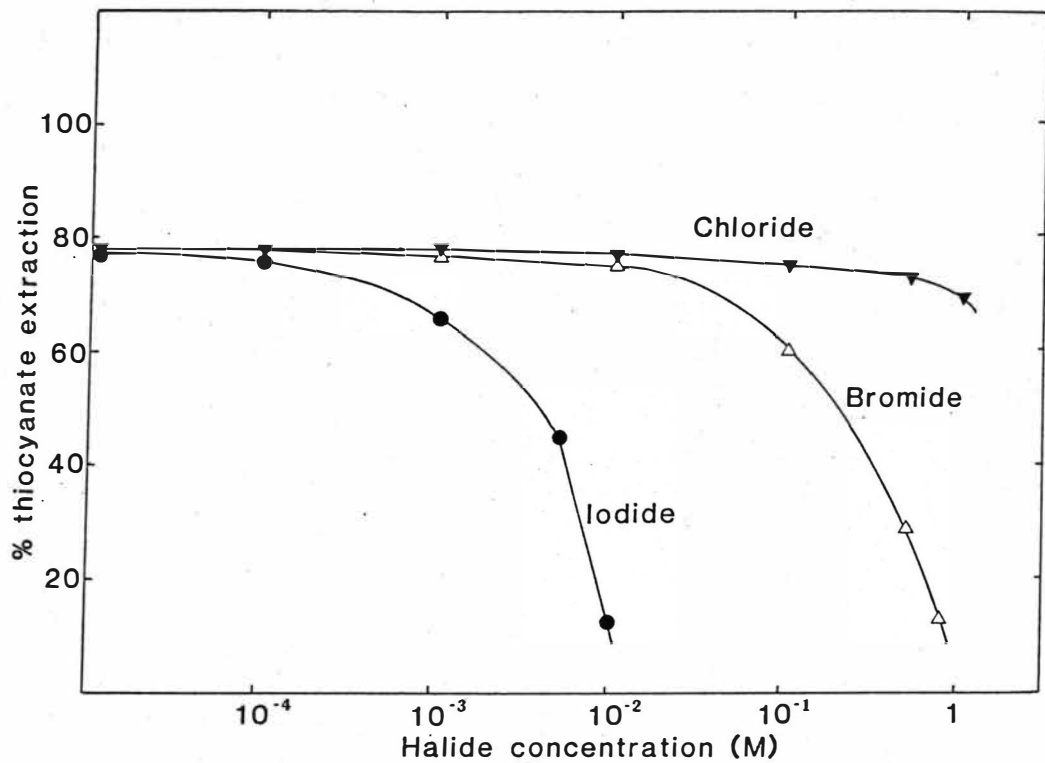


Figure 4: Potential energy functions between ions

Figure 5: Effect of added halide on thiocyanate extraction



INFLUENCE OF THE IONIC CHLORIDE MEDIUM
ON THE TRANSPORT OF HCl THROUGH A SUPPORTED LIQUID MEMBRANE
CONTAINING TRI-N-LAuryLAMINE IN CUMENE AS CARRIER

M. Valiente, A. Fernández and M. Muñoz

Department of Chemistry, Analytical Division
U.A.B. Bellaterra (Barcelona). Spain.

The use of solid supported membrane (SSM) on the extraction of inorganic acids from aqueous solutions has been already reported (1,2). In these cases different long-chain amines were employed as carriers for the extraction of nitric acid. Diffusional parameters have been determined to contribute to the overall mass transfer in these processes.

In the present work solid supported membranes containing Tri-n-dodecyl amine as carrier have been used on the extraction of hydrochloric acid from sodium chloride media. The study has been addressed to determine the influence of the ionic strength on the aqueous phase to the mass transfer process. Both diffusional and chemical kinetic parameters were considered in the analysis of the experimental data.

Reagents, Solutions and Membranes

The feed HCl solutions are prepared by diluting adequate amounts of concentrated HCl (Merck, p.a.) at the desired ionic strength by adding NaCl purified as in (3).

The preparation and purification of TLA has been already reported (4). Solutions of TLA in isopropylbenzene (IPB) were prepared on a weight basis using calibrated volumetric flasks.

The IPB was washed before use with 0.5 mol.dm^{-3} NaOH, distilled water, 0.5 mol.dm^{-3} HCl and water repeatedly. The flat film membranes used as solid support were Millipore (GVHP09050, $125 \mu\text{m}$ thickness and 75% porosity).

The liquid membrane was prepared by impregnating of the porous film with the corresponding TLA solution.

Experimental Technique

The experiments were carried out by using the cell described previously (5). This cell is provided with a rectangular window where the liquid membrane is placed. So, the membrane separates the compartments containing the feed and the stripping solutions respectively.

The concentration of H^+ of the feed solutions was monitored potentiometrically as a function of time by measuring the e.m.f., E , of the cell: Glass electrode/feed solution/reference electrode.

Different TLA concentrations ranging from 20 to 200 mM were employed for each ionic strength studied.

The different ionic strengths were 0.1, 0.5, 1.0, 2.0, 3.0 in the molar scale. The feed solution containing NaCl as ionic medium and the stripping solution containing NaOH were kept at equal concentration to avoid the transfer of water by osmotic pressure effect.

Results

The experimental data collected in the form E v.s. time (fig. 1a) at the different conditions have been transformed to permeability values, P_0 (defined below). The different parameters affecting the rate of mass transfer have been evaluated.

Preliminary experiments were carried out in order to establish the adequate hydrodynamic conditions. In this sense the permeability of the membrane was studied as a function of the rpm impeller agitation of the feed solution. The rpm at the stripping solution was kept constant at 200. These data are collected in fig. 2. As seen the permeability at the different ionic strengths is not depending of the hydrodynamic conditions in the range 200-400 rpm. Thus the data for the different conditions have been generated at 400 rpm.

Flux Equations

The mass transfer of H^+ is described considering the diffusional and reaction kinetics parameters. In this sense, the flux of H^+ crossing the membrane has been derived considering:

- a linear concentration gradient in the aqueous-membrane interface (first Fick's law)
- the interfacial flux due to the chemical reaction rate
- the diffusion across the organic membrane is due to the TLA-HCl species.

Thus, the derived flux equation is (6):

$$J = \frac{D|H^+|}{D\Delta a + \Delta o + k_2^{-1}(k_3 + |TLA|)} \quad (1)$$

where:

$\Delta a = \frac{da}{D_a}$: mass transfer coefficient in the aqueous phase

$\Delta o = \frac{do}{D_o}$: " " " " " organic "

D_a : diffusion coefficient in the aqueous phase

D_o : " " " " organic "

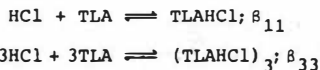
da: thickness of aqueous diffusion layer

do: " " organic " "

k_3, k_2 : true kinetic constants of the reaction mechanism determined previously (7).

D: distribution coefficient.

The TLA has been evaluated at the experimental conditions taken into account the formation of the amine salt in the organic solution considering the following reactions at the different ionic strength (8)



Substituting the distribution coefficient the flux equation can be written as:

$$J = \frac{|TLA| \beta_{11} |H^+| + 3|TLA|^3 \beta_{33} |H^+|^3}{|TLA| \beta_{11} \Delta a + 3|TLA|^3 \beta_{33} |H^+|^2 \Delta a + \Delta o + k_2^{-1}(k_3 + |TLA|)} \quad (2)$$

The initial permeability P_o is defined by (2):

$$P_o = \frac{J}{|H^+|_o} \quad (3)$$

and then:

$$P_o = \frac{|TLA| \beta_{11} + 3|TLA|^3 \beta_{33} |H^+|^2}{|TLA| \beta_{11} \Delta a + 3|TLA|^3 \beta_{33} |H^+|^2 \Delta a + \Delta o + k_2^{-1} (k_3 + |TLA|)} \quad (4)$$

The values of Δa and Δo have been determined by fitting equation (4) to the experimental data (fig. 3) using the program BMDP (9). The results obtained are given in Table I.

Additional data were generated in order to directly determine the contribution of the organic species diffusion to the HCl mass transfer. Thus, taken into account the flux equation (1) and considering negligible the contribution of D_a and $k_2^{-1} (k_3 + |TLA|)$ terms (2), the equation takes the form:

$$J = \frac{k_1 |H^+| |TLA|}{\Delta o} \quad (5)$$

To this purpose the experimental data were obtained at 0.1M $|H^+|$. Under this conditions: $D_a \Delta a \ll \Delta o$ (1). By integration of eq. (5) the following expression is obtained:

$$\frac{Q}{V} \frac{\Delta o}{|TLA|} t = (|H|_o - |H^+|) \quad (6)$$

The experimental data plotted in the form $|H^+|$ v.s. t are given in fig. 1b. As seen linear relationship are found for the different ionic strength. This results are consistent with the previous assumption. Table I give the D_o values obtained from these data.

Conclusions

The data obtained by e.m.f. measurements as well as titration procedures have shown to be reproducible for the different experimental conditions described. The results determined from these data give a good agreement with the proposed model which take into account both the diffusional effect of the species considered and the kinetics of the chemical reaction taking place on the mass transfer process. These two effects were considered to be independent in order to give evidence of their specific contribution to the overall process. In Table I the results obtained for the different ionic strength studied are given in the form of diffusional parameters affecting both the aqueous and the organic phase. As seen in this Table, the thickness of the aqueous boundary layer, d_a , decreases with the increase of ionic strength,

this fact may be due to the electrostatic contribution of the aqueous phase to the interfacial potential which determines the exchange of HCl.

On the other hand the diffusion coefficient of the organic species has been determined to be independent of the composition of the aqueous solution. Furthermore, the agreement observed between the calculated value of D_o from data at low H^+ concentration and those determined at the extreme conditions (fig. 1b), D_o^* , gives a good consistency to our theoretical model.

Table I.- Results of the different diffusional parameters obtained by using eq. (4).

I (M NaCl)	Δa	d_a	D_a	Δo	D_o
0.1	7.35	6.55×10^{-3}	8.91×10^{-4}	266 ± 160	4.7×10^{-5} ---*
0.5	7.32 ± 3.3	$(4.83 \pm 2.2) \times 10^{-3}$	6.61×10^{-4}	714 ± 141	$(1.75 \pm 0.35) \times 10^{-5}$ $(1.79 \pm 0.33) \times 10^{-5*}$
1.0	6.73 ± 2.0	$(2.49 \pm 0.74) \times 10^{-3}$	3.72×10^{-4}	852 ± 105	$(1.46 \pm 0.20) \times 10^{-5}$ $(1.57 \pm 0.33) \times 10^{-5*}$
2.0	7.47 ± 2.0	$(6.81 \pm 1.82) \times 10^{-4}$	9.12×10^{-5}	720 ± 107	$(1.73 \pm 0.30) \times 10^{-5}$ $(1.66 \pm 0.33) \times 10^{-5*}$
3.0	7.94 ± 1.2	$(1.78 \pm 0.27) \times 10^{-4}$	2.24×10^{-5}	671 ± 61	$(1.86 \pm 0.17) \times 10^{-5}$ ---*

* values determined from the data in fig. 1b.

Acknowledgements

The authors wish to thank the support given by the Research Council of Catalonia (C.I.R.I.T.) providing A. Fernández a scholarship to develop this work. The Spanish National Committee for the Research Development (CAICYT) is acknowledged for financial help on the materials part. Thank are due to Manel Escalada for his valuable help on the computer treatment.

Bibliography

- 1 - P.R. Danesi, C. Cianetti and E.P. Horwitz, Solvent Extraction and Ion Exchange, 1(2), 299-309 (1983).
- 2 - C. Cianetto and P.D. Danesi, Solvent Extraction an Ion Exchange, 1(3), 565-583 (1983).

- 3 - Some Laboratory Methods, Mimeograph 1959, Inorganic Chemistry, Royal Institute of Technology, Stockholm.
- 4 - M. Muhammed, H. Szabon and E. Högfeldt, Chem. Scripta 6, 61 (1974).
- 5 - P.R. Danesi, R. Chiarizia and A. Castanyola, J. Membr. Sci., 14, 161 (1983).
- 6 - L.A. Fernández, J.L. Aparicio and M. Muhammed, submitted to Sep. Sci. and Technol.
- 7 - P.R. Danesi, R. Chiarizia and M. Muhammed, J. Inorg. Nucl. Chem., 40, 1581 (1978).
- 8 - M. Valiente, A. Fernández, M. Muñoz, to be publish.
- 9 - M.B. Brown et.al. BMDP Statistical Software. University of California Press. 1983.

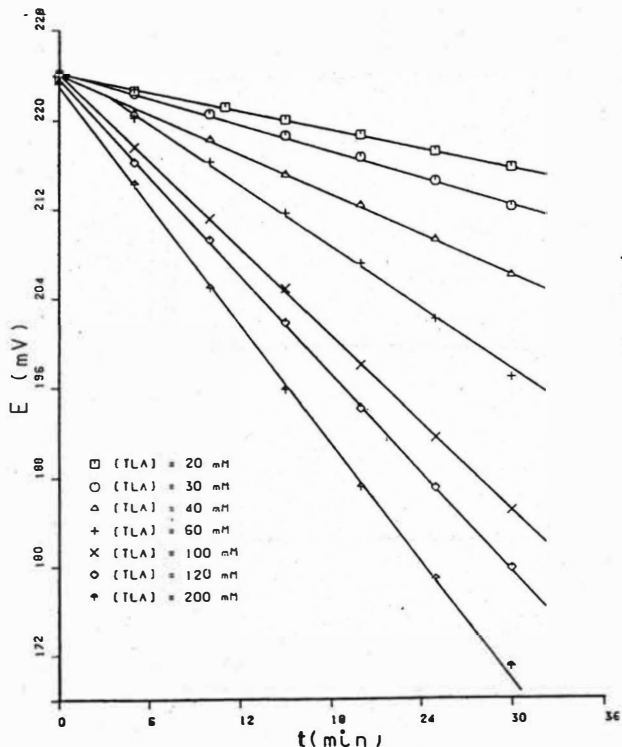


Fig. 1a).- E(mV) v.s. time (min).
 The experimental conditions were $|\text{H}^+|_0 = 10^{-3}$ M and 400 r.p.m. in all cases.

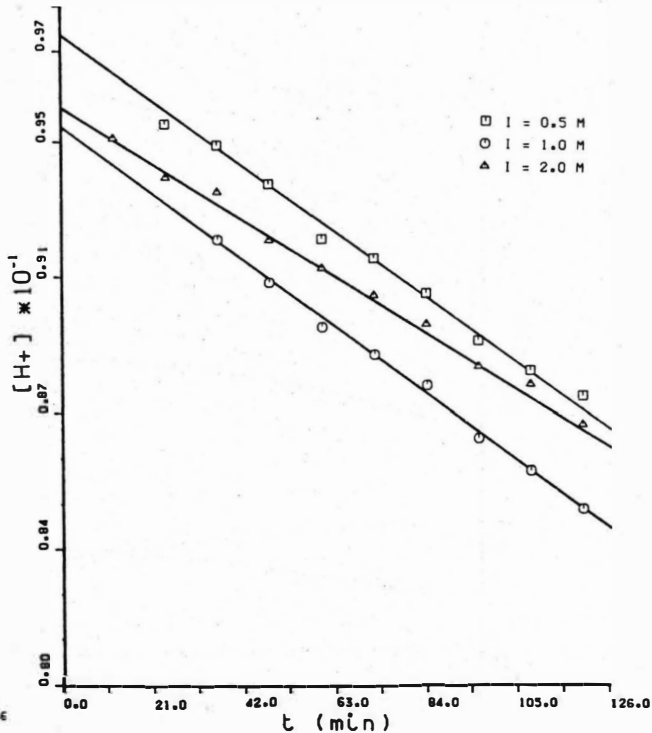


Fig. 1b).- H^+ (M) v.s. time.
 The experimental conditions were $|\text{I}^+|_0 = 0.1$ M and 400 r.p.m. in all cases.

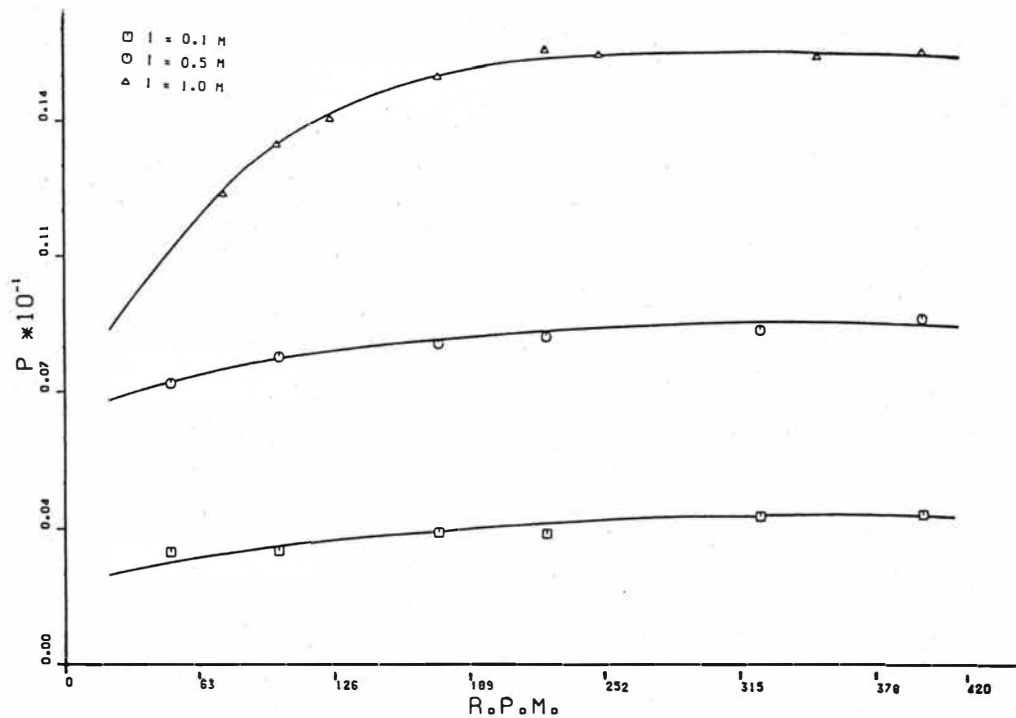


Fig. 2.- The influence of r.p.m. on the Permeability (cm. seg^{-1}) for different ionic strength.

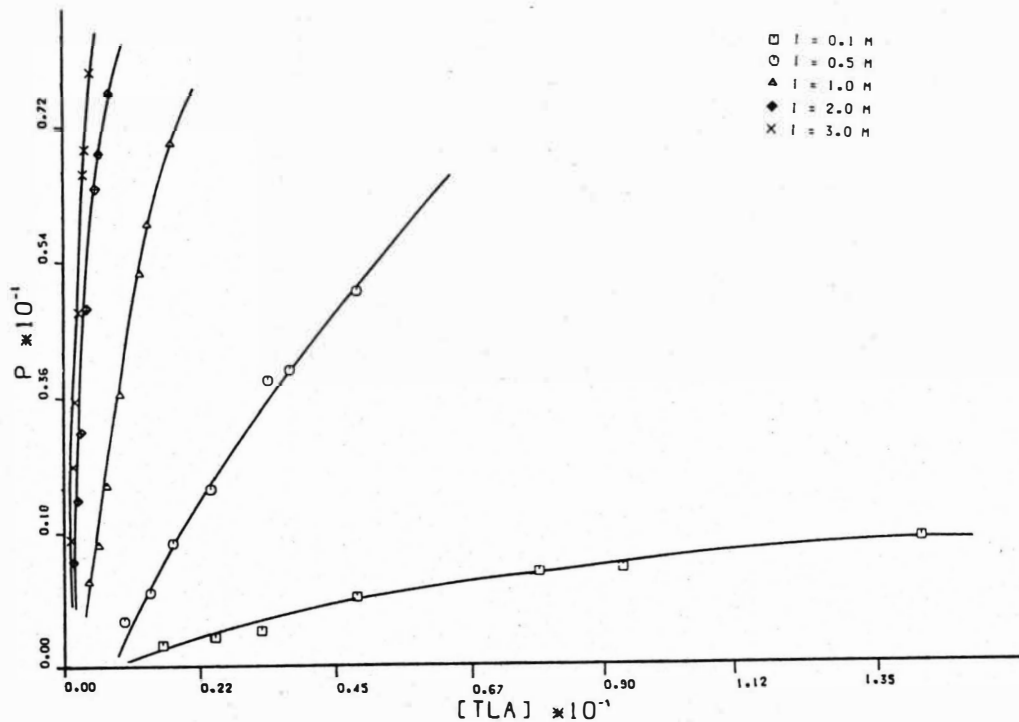


Fig. 3.- The Permeability ($\text{cm} \cdot \text{sec}^{-1}$) (eq. 4) is plotted v.s. $|TLA|$ for the different ionic strenght. Solid lines have been calculated using eq. 4.

Facilitated Transport of Acid Gases in Ion Exchange Membranes

J. D. Way, R. D. Noble, NBS, Center for Chemical Engineering, Boulder, CO/USA

A recent approach to solve solvent loss and carrier loss problems with immobilized liquid membranes (ILMs) has been to use ion exchange membranes as a support for complexation agents [1-2]. A cationic or anionic carrier is exchanged into an appropriate nonporous ion exchange membrane (IEM) to form the facilitated transport membrane. This configuration has the advantage that the carrier cannot easily be forced out of the support since the carrier is retained by strong electrostatic forces. Ion exchange membrane supports may provide longer operating lifetimes where conventional ILMs may be subject to carrier or solvent loss.

In this study, monopositive ethylene diamine (EDA) ions were exchanged into perfluorosulfonic acid ionomer films to prepare facilitated transport membranes. The flux of CO_2 and H_2S was measured with and without carrier present at ambient conditions as a function of the acid gas mole fraction in the feed gas stream. The selectivity of these membranes was determined by simultaneous measurements of acid gas and CH_4 fluxes from binary mixtures as a function of composition.

Facilitated transport of gases has been the subject of numerous review articles in recent years [3-7]. Much of the work in the literature deals with facilitated transport of CO_2 , both from an engineering and a physiological standpoint. Many of these studies have examined CO_2 transport through immobilized liquid membranes using aqueous carbonate and bicarbonate solutions immobilized in a variety of microporous substrates such as ultrafiltration membranes, reverse osmosis membranes and common filter paper [8-12]. Matson et al. [13] immobilized a carbonate solution in a microporous polymer film to prepare an ILM for the removal of H_2S from synthetic gas derived from coal gasification. LeBlanc et al. [1] demonstrated the feasibility of facilitated transport of ethylene and CO_2 in ion exchange membranes.

The kinetics of the reaction of CO_2 with EDA has been studied by several authors for possible applications in gas absorption [14-16]. The principal reaction is the formation of a carbamate zwitterion:

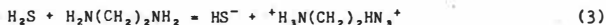


The equilibrium constant for the reaction is $1 \times 10^5 \text{ M}^{-1}$ [17]. The forward rate constant is $1.75 \cdot 10^4 \text{ M}^{-1}\text{s}^{-1}$ [16].

Fewer data are available on the H_2S -EDA reaction. Gioia and Astarita [18] and Astarita [19] have reported that the reaction of H_2S with all bases in solution is a proton transfer reaction:



These reactions are extremely fast with second order rate constants on the order of $10^{11} \text{ M}^{-2} \text{ s}$ [20]. Astarita [19] assumes these reactions to be essentially instantaneous and, therefore, at equilibrium everywhere in the liquid phase. Consequently, there is considerable evidence to conclude that the reaction of H_2S with EDA in solution is:



The apparatus and procedure used to measure membrane fluxes were described in detail by Bateman et al. [21]. The gas streams were saturated with water upstream of the membrane cell. A cold trap removed the water prior to chromatographic analysis. All measurements were made at ambient conditions of 298 K and 84.0 kPa. The chromatograph was calibrated by injecting 1.0 cm^3 aliquots of premixed gases of interest (1.0% in He).

The perfluorosulfonic acid ion exchange films (1100 g equivalent molecular weight, 170 μm thickness) were obtained from the manufacturer in the acid form. The mechanical, chemical, and ionic transport properties of these membranes have been extensively studied [22-24]. The membranes were converted to the Na salt form by soaking them in NaOH solutions overnight. The Na salt form was used as a non-reactive membrane for measurements of the diffusive contributions of the individual gases necessary to calculate the facilitation factor. After the transport measurements were made, the Na membrane was converted to reactive EDA salt form by soaking the membrane in an aqueous solution of EDA overnight. To create the monovalent ion of EDA, one equivalent of HCl was added to the solution prior to the exchange. The extent of exchange was measured by analysis of the exchange solutions for Na by atomic emission spectroscopy. The water content of the membranes at equilibrium was measured using the gravimetric method of Yeager and Steck [24]. The average water content of the Na and EDA forms of the membrane were 0.17 and 0.11 cm^3/g dry mass, respectively. The water content of the EDA membranes was used to calculate an effective EDA carrier concentrations of 8.3 M. The thickness of the water swollen membranes was 200 μm .

Figure 1 is a plot of steady-state CO_2 flux versus CO_2 feed gas mole fraction for both the EDA membrane and the Na membrane. The Na membrane flux is a linear function of feed gas concentration which is evidence of Fickian diffusion. The data are fit well by a least-squares line which is shown in Figure 1. The presence of EDA in the membrane markedly increases the fluxes which range from 5.22×10^{-10} to $2.82 \times 10^{-9} \text{ gmol}/(\text{cm}^2 \cdot \text{s})$, and the fluxes are a highly nonlinear function of feed gas mole fraction. The nonlinearity is an indication that a reaction is taking place within the membrane which is consistent with the facilitated transport mechanism. The flux versus feed mole fraction curve flattens out for higher CO_2 mole fractions indicating saturation of the carrier at the feed gas interface.

The ratio of the flux with EDA present to the flux without the carrier is called the facilitation factor F , which is a measure of the flux enhancement. The facilitation factor is 1.44 for a mole fraction of 1.0, increasing to 3.68 at $y = 0.25$. Facilitation factors continue to increase with decreasing feed gas mole fraction to a value of 26.7 at a CO_2 mole fraction of 0.01. This is further evidence that facilitated transport is most effective for dilute solutes. These very high facilitation factors are primarily due to two factors. The inverse Damkohler number, $D_{AB}/(k_r L^2)$, the ratio of reaction time to diffusion time, is 1.39×10^{-4} . Therefore, mass transport is limited only by the diffusion rate because of fast kinetics which maximizes the facilitation effect. Secondly, the carrier loading in the membrane is limited by the ion exchange site density in the ionomer support rather than the carrier solubility in a solvent phase.

The H_2S flux data for the Na IEM in Fig. 2 are a linear function of the log-mean mole fraction driving force. Fluxes range from 2.68×10^{-11} to 1.38×10^{-10} gmol/($\text{cm}^2 \cdot \text{s}$). The data are fit well by a least-squares line. The flux data in Fig. 2 for the EDA IEM are an order of magnitude greater than the Na membrane fluxes which clearly demonstrates that EDA facilitates the transport of H_2S . Comparing the shape of the EDA flux curve for H_2S to that for CO_2 in Fig. 1, the data for H_2S appear almost linear because of the low H_2S driving forces used in the experiments. The carrier saturation phenomena observed for the CO_2 data are not seen for H_2S also because of the small feed gas mole fractions studied. The carrier concentration is much greater than the H_2S concentration for all the experimental points. Due to the low H_2S mole fractions in the feed gas, the facilitation factors are high, ranging from 15.8 to 24.1 for feed gases containing 5% to 1% H_2S , respectively. Facilitation factors of this order of magnitude indicate that the presence of EDA greatly enhances the H_2S flux and that facilitated transport is most effective for dilute solutes.

The results of the CO_2/CH_4 binary mixture transport experiments are shown in Fig. 3. The ratio of the CO_2 flux to the CH_4 flux is plotted against the feed gas CH_4 concentration. The solid points represent data for an EDA membrane while the open square is the flux ratio for a Na membrane. The flux ratios increased from 29.0 to 264 for feed gases of 0.05 $\text{CO}_2/0.95 \text{CH}_4$ and 0.75 $\text{CO}_2/0.25 \text{CH}_4$, respectively. These flux ratios can be converted to separation factors (permeability of CO_2 /permeability of CH_4) of 87.9 to 551 corresponding to flux ratios of 264 to 29.0, respectively.

Figure 4 gives the results of the $\text{H}_2\text{S}/\text{CH}_4$ experiments. The ratio of the steady-state H_2S flux to the steady-state CH_4 flux was plotted as a function of the log-mean mole fraction driving forces of CH_4 and H_2S . The behavior of the flux ratio is similar to that for CO_2/CH_4 . Even at a very small H_2S mole fraction driving force of 1.85×10^{-3} and a large CH_4 driving force of 0.898, the H_2S flux was 2.47 times the CH_4 flux. The flux ratio increases with increasing H_2S driving force to

a value of 55.7 for a CH_4 feed mole fraction of 0.2 and an H_2S feed mole fraction of 0.04. Converting the flux ratios to separation factors by normalizing the fluxes with the driving forces, separation factors of 792-1200 are obtained corresponding to flux ratios of 55.7 and 2.47, respectively.

Table 1 compares these separation factors to those for cellulose ester hollow fiber and silicone rubber membranes.

Table 1
Comparison of Separation Factors Between Polymer Membranes
and the EDA IEM Facilitated Transport Membrane

Membrane	Separation Factor		Reference
	CO_2/CH_4	$\text{H}_2\text{S}/\text{CH}_4$	
Cellulose esters	26-30	12 ($\text{H}_2\text{S}/\text{N}_2$)	Berry [25], Kimura et al. [4]
Silicon rubber	--	23 ($\text{H}_2\text{S}/\text{N}_2$)	Kimura et al. [4]
EDA IEM	87.9-551	792-1200	present work

The range of separation factors obtainable with the polymer membranes was 12-30. The very high selectivities that can be obtained with facilitated transport membranes are what makes them potentially attractive for industrial application.

This is the first study of facilitated transport in perfluorosulfonic acid ionomer films. Fluxes of CO_2 , H_2S , and CH_4 were measured through ion exchange membranes containing organic amine carriers at ambient conditions. Facilitation factors up to 26.7 and 24.1 were observed for CO_2 and H_2S , respectively. Separation factors up to 1200 for $\text{H}_2\text{S}/\text{CH}_4$ and 551 for CO_2/CH_4 were calculated from ratios of steady-state acid gas flux to CH_4 flux. It can be concluded from the data that facilitated transport membranes can achieve a high degree of facilitation and high selectivities.

The authors would like to acknowledge the support of the U.S. Dept. of Energy for this work under DOE Contract DE-AC21-84MC21271.

- [1] LeBlanc, O.H., Ward, W.J. III, Matson, S.L., and S.G. Kimura, *J. Mem. Sci.*, 6, 339-343 (1980).
- [2] Way, J.D., Noble, R.D., and B.R. Bateman, in "Materials Science of Synthetic Membranes," ACS Symposium Series No. 269, D.L. Lloyd, editor, 1985.
- [3] Smith, D.R., Lander, R.J., and J.A. Quinn, in N.N. Li, Ed., *Recent Developments in Separation Science*, Vol. 3, CRC Press, Cleveland, OH, 1977.
- [4] Kimura, S.G., Matson, S.L., and W.J. Ward III, in: N.N. Li, Ed., *Recent Developments in Separation Science*, Vol. 5, CRC Press, Cleveland, Ohio, 1979.

- [5] Way, J.D., Noble, R.D., Flynn, T.M., and E.D. Sloan, J. Mem. Sci., 12, 239-259 (1982).
- [6] Matson, S.L., Lopez, J. and J.A. Quinn, Chem. Eng. Sci., 38, 503-524 (1983).
- [7] Noble, R.D., Way, J.D., and A.L. Bunge, in Y. Marcus, Ed., Solvent Extraction and Ion Exchange, 10, in press, 1986a.
- [8] Enns, T., Science, 155, 44-47 (1967).
- [9] Ward, W.J. and W.L. Robb, Science, 156, 1481-1484 (1967).
- [10] Otto, N.C. and J.A. Quinn, Chem. Eng. Sci., 26, 949-961 (1971).
- [11] Suchdeo, S.R. and J.S. Schultz, Chem. Eng. Sci., 29, 13-23 (1974).
- [12] Donaldson, T.L. and J.A. Quinn, Chem. Eng. Sci., 39, 103-115 (1975).
- [13] Matson, S.L., C.S. Herrick and W.J. Ward III, Ind. Eng. Chem., Process Des. Dev., 16, 370 (1977).
- [14] Weiland, R.H. and O. Trass, Can. J. Chem. Eng., 49, 767-772 (1971).
- [15] Hikita, H., Asai, S., Ishikawa, H., and M. Honda, Chem. Eng. J., 14, 27-30 (1977).
- [16] Sada, E., Kumazawa, H., and M.A. Butt, Chem. Eng. J., 13, 213-217 (1977).
- [17] Jensen, A. and R. Christensen, Acta Chemica Scandinavica, 9, 486-492 (1955).
- [18] Gioia, F. and G. Astarita, Ind. Eng. Chem. Fund., 6, 370 (1967).
- [19] Astarita, G., D.W. Savage, and A. Bisio, "Gas Treating with Chemical Solvents," Wiley-Interscience: New York, 1983.
- [20] Eigen, H., Suomen Kemistilehti, A34, 25 (1961).
- [21] Bateman, B.R., Way, J.D., and K.M. Larson, Sep. Sci. & Tech., 19, 21-32 (1984).
- [22] Grot, W.G.F., Munn, G.E., and P.N. Wainsley, paper presented at the 141st National Meeting of the Electrochemical Society, Houston, TX, May, 1972.
- [23] Yeo, S.C. and A. Eisenberg, J. Appl. Polymer Sci., 21, 875 (1977).
- [24] Yeager, H.L. and A. Steck, J. Electrochem. Soc., 129, 328-332 (1981).
- [25] Berry, R.I., Chem. Eng., 88, 63 (1981).

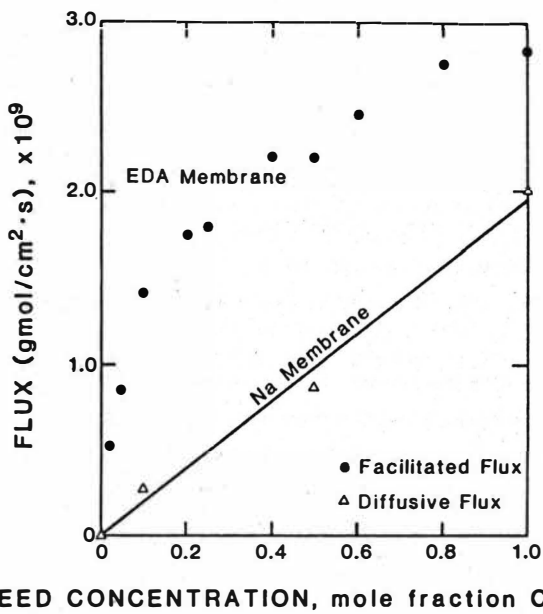


Figure 1. The CO₂ flux as a function of the CO₂ mole fraction in the feed gas.

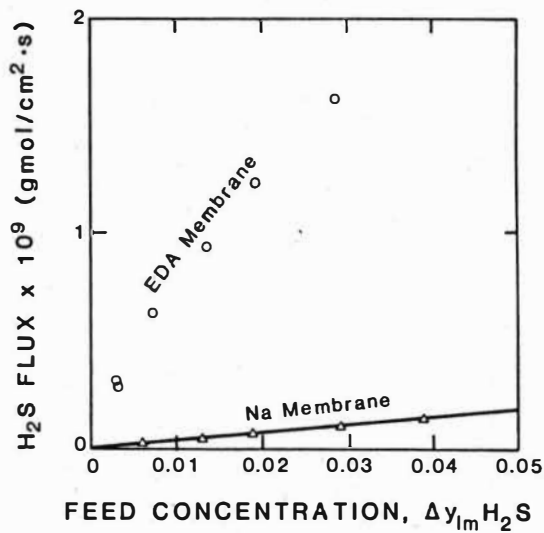


Figure 2. The H_2S flux as a function of the log-mean mole fraction driving force

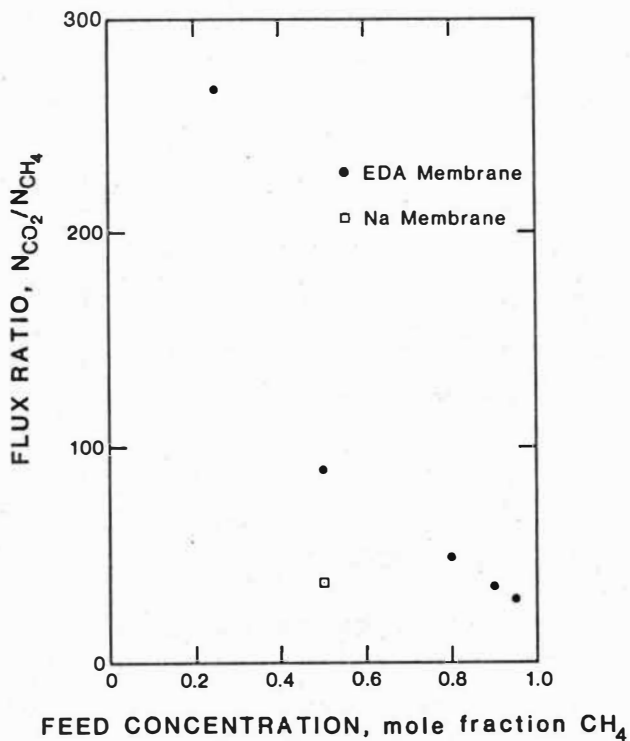


Figure 3. The ratio of the CO_2 flux to the CH_4 flux as a function of the CH_4 mole fraction in the feed gas CO_2/CH_4 binary mixture.

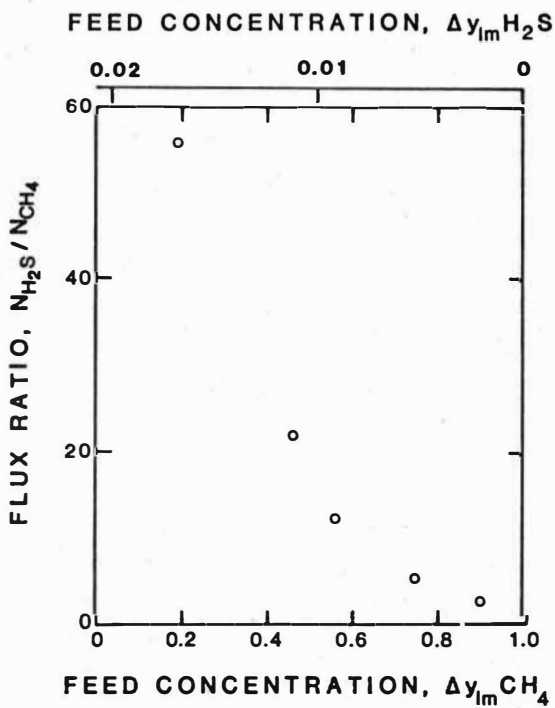


Figure 4. The ratio of the H_2S flux to the CH_4 flux as a function of the CH_4 log-mean mole fraction driving force.

Special Applications: Effluents

A Simple and Complete Recovery of Phenol from Waste Water by Tertiary Amines in Form of Sulfates - A New Powerful Extractant

G. Braun, W. Grünbein*, M. Mayer, B. Wojtech
Hoechst AG (* Cassella AG), Frankfurt (M), FRG

The separation of phenol from waste waters and its recovery is both an economical and environmental task. Legal regulations enforce almost complete recovery of phenol from waste waters. This can be achieved very economically by solvent extraction if a highly selective extractant having a boiling point distinctly above that of phenol (bp. 182 °C) is used. The resulting extracting costs are low and the phenol is easily separated from the extract by distillation.

Most extractants commonly used for extracting phenol from water exhibit increasing solubility in water with increasing extraction power, due to higher polarity. For instance, while the distribution coefficient (D) of diisopropyl ether, butyl acetate, and methyl isobutyl ketone rises from 29 to 71 up to 82 their solubility in water also increases from 0.7 to 1.9 wt.%, respectively.

Also amines in general and tertiary amines in particular associate as basic components with the acidic phenol. With trioctyl- and tridecyl amine, respectively, dissolved in benzene distribution coefficients of up to 11 are attained depending on the amine content. Using [®]Hostarex A 327 from Hoechst AG, which contains these two components in equal parts, and which has a boiling point of over 350 °C and a solubility in water of less than 1 ppm, distribution coefficients from 11 to 13 were obtained for phenol contents ranging from 0.1 to 2 wt.% in the aqueous phase.

If, however, the tertiary amine is converted to amine sulfate (R_3NH)₂SO₄, the ion pair formed is so activated that the distribution coefficients increase to values higher than 800. As the amines have a high affinity for H₂SO₄ (equilibrium constant for tertiary amines: 10⁶ to 10¹¹ (mol/l)⁻²) the formation of amine sulfate is achieved easily by contacting the amine with a stoichiometrical amount of H₂SO₄ in an aqueous solution. Because of its high viscosity the

amine sulfate may be diluted with an inert solvent before use as extractant. In order to be able to recover the phenol from the extract by direct distillation, a diluent boiling higher than phenol should be used. Advantageously, by only partial conversion of the amine to the sulfate form the amine itself may act as diluent.

Our experiments were done with Hostarex A 327 having a 70 % sulfate conversion, which is the optimal composition as just about 30 % of free Hostarex A 327 are soluble in the Hostarex A sulfate. For this extractant fig. 1 shows the very high extraction power for phenol corresponding to distribution coefficients of up to 850 (s. fig. 2). This value decreases gradually as the phenol content in the amine phase exceeds 5 wt.%. In comparison the distribution coefficient of phenol in free amine is smaller by a factor of about 100 at low phenol concentrations of the aqueous phase. As the amount of phenol dissolved in the organic phase increases the extraction power of both extractants becomes almost the same.

The effect on extraction power of phenol contained in the amine sulfate is demonstrated by fig. 3. As the phenol content increases from 0 to 4 moles of phenol per mole of amine sulfate the distribution coefficient drops from about 800 to below 100. Beyond this point the extraction power decreases only slowly.

The extractive properties of the amine complex are easily understood if the part of the water in the extraction process is considered. During the formation of a long chain tertiary amine sulfate a $(R_3NH)_2SO_4 \cdot 8 H_2O$ complex containing 8 molecules of constitutional water is obtained. This clearly demonstrates that a number of active sites for association exists in the amine sulfate molecule. Because of the higher acidity of phenol and the stronger interaction between the phenyl group and the amine sulfate, water is replaced by phenol during extraction.

The correlation between the amounts of water and phenol contained in a mole of amine sulfate is demonstrated by fig. 4. When in equilibrium with water pure amine sulfate contains 8 moles of water per mole amine sulfate. During the extraction water from the inner

districts is replaced successively by phenol. Simultaneously some water from the outer districts is imported by phenol. This amount of water increases linearly with the amount of phenol taken up (1 mole of water per 5 moles of phenol). If this quantity is subtracted from the total amount of water, it can be realized that 8 moles of constitutional water have been replaced by 4 moles of phenol. The inner district then is saturated with phenol. Consequently, the distribution coefficient drops from above 800 down to below 100, and the affinity of the extractant complex for further adding of phenol is markedly lowered.

The very high extraction power of amine sulfate at low phenol concentrations can be utilized for complete separation of phenol from water. Thus, the following results have been attained by simply contacting various waste waters (W) containing different amounts of phenol with Hostarex A 327 (X) converted by 70 % to sulfate:

wt.% phenol in waste water	Phase ratio W/X	ppm phenol in raffinate	Percentage extracted
5.0	2	210	99.58
5.0	1	80	99.81
1.0	1	13	99.97
0.15	1	2	99.99

Further studies using this extractant have been performed in order

- to test the extractant in a pilot plant and
- to study the effect of initial phenol content of the extractant.

Test runs were made at 25°C in a 3-stage mixer-settler made of glass and equipped with a PTFE-stirrer (rotation speed: 355 rpm). The volumetric flow rate was adjusted in such a way that a residence time of 30 min in the settlers resulted.

The aqueous feed contained about 5 wt.% of phenol. The effect of initial extractant concentration (0 and 2 wt.% of phenol) and of the feed-to-extractant phase ratio (varying between 1 and 2) was investigated. The results are given below:

Phase ratio W/X	P h e n o l c o n t e n t		
	Extractant Feed (wt.%)	Aqueous phase	
		Feed (wt.%)	Raffinate (ppm)
1	-	4.7	2
2	-	4.7	3
1	2.1	4.9	28
2	2.1	4.9	33

Besides the extraction power of Hostarex A 327 sulfate the recovery of the extractant is decisive for the whole separation process. The amine sulfate can be easily recovered both by re-extraction of phenol using a sodium hydroxide solution and, more economically, by distillation of phenol, since the extractant consists of a non-volatile component and one having a much higher boiling point than phenol has.

Obviously, high temperature and low pressure will help to reduce the phenol content. Experiments showed, however, that residual water content (s. fig. 4) limits the pressure attainable in single stage thin film evaporation. Therefore, the evaporation was performed in two stages (s. fig. 5). First, in a falling film evaporator at normal pressure and 200 °C heating steam temperature about 90 % of the water and 10 % of phenol were distilled off from 70 % Hostarex A 327 sulfate initially containing about 10 wt.% of water and 10 wt.% of phenol. Then, in a second stage consisting of a rigid rotor thin film evaporator the remaining phenol is reduced to a value which depends on evaporation conditions (temperature and pressure, s. fig. 6). E.g. at 240 °C heating temperature and at a pressure of 1 mbar a 0.05 wt.% residual phenol content was attained. This value should be sufficiently low for most applications of Hostarex A 327 sulfate as extractant.

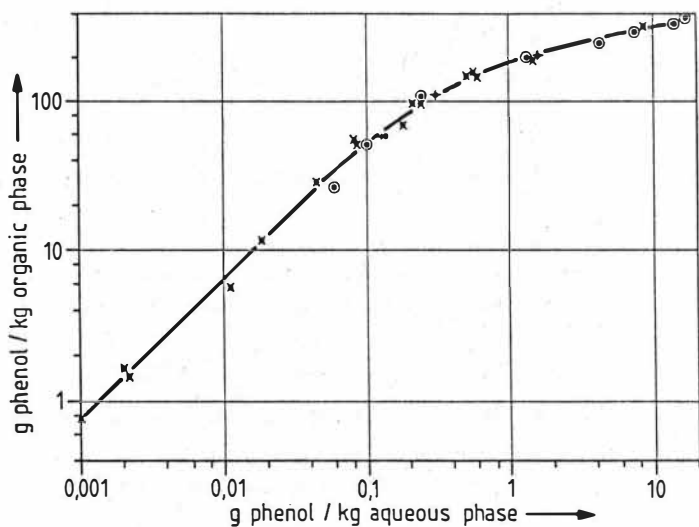


Fig. 1 Distribution of Phenol in Hostarex A 327 70% Converted to Sulfate Form

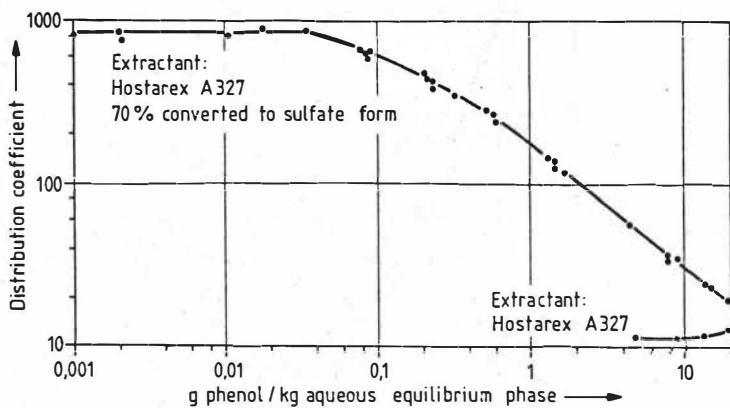


Fig. 2 Distribution Coefficient of Phenol

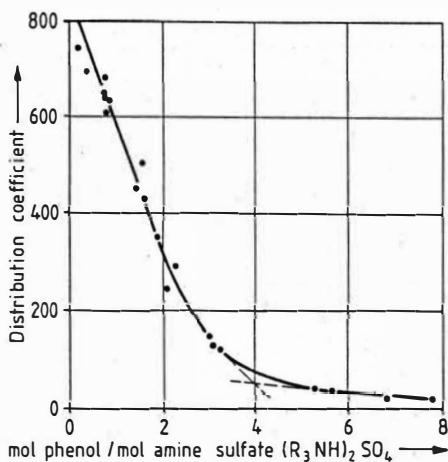


Fig. 3 Influence of the Phenol Content in the Amine Sulfate on the Distribution Coefficient

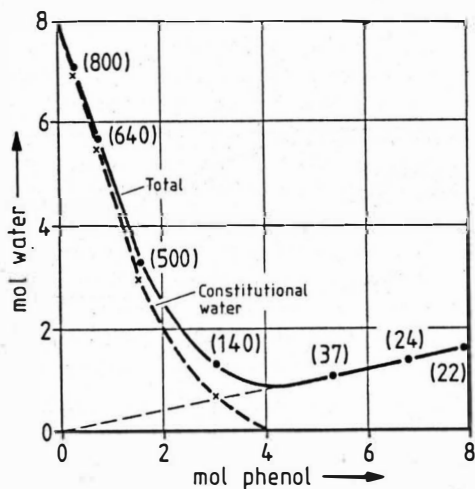


Fig. 4 Phenol and Water Content of the Amine Sulfate Complex (Distribution coefficients in brackets)

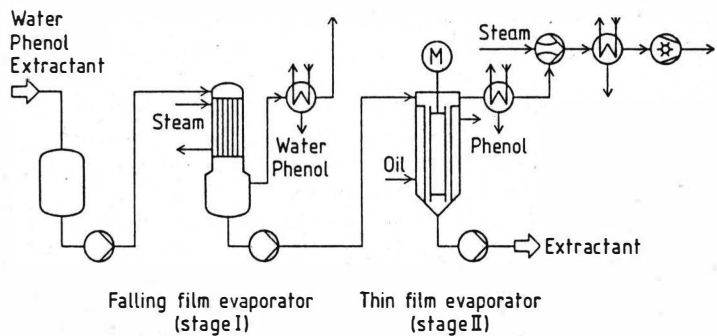


Fig.5 Two-Stage Recovery of the Extractant

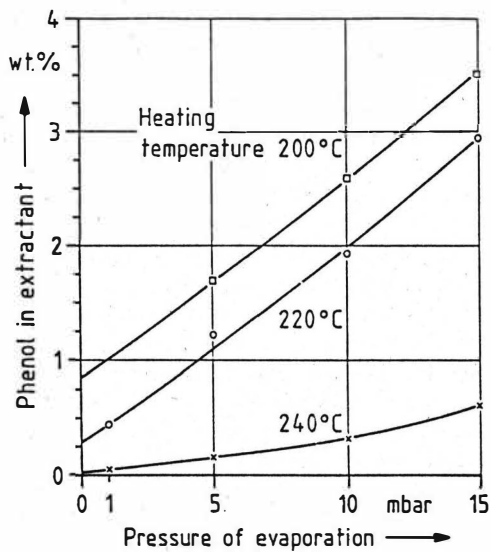


Fig.6 Extractant Recovery by Thin Film Evaporation

Phenol Extraction from Cokery Waste Waters with TAME. Development of the Process. Phase Equilibrium in the Water-TAME-Phenols Systems.

K. Zięborak, T. Porębski, S. Tomzik, Research Institute of Chemical Industry, Warszawa, Poland

Coking is accompanied by formation of a considerable amount of ammonia liquor contaminated with organic and inorganic compounds. These contaminations comprise mainly phenols, hydrocarbons, cyanides, as well as ammonium and sulphur containing compounds. Before further utilization of coking plant waste water or before its introduction to a sewer, it should be purified so as to remove all contaminations mainly phenols, by extraction, ammonia by stripping. This process is accomplished by biological treatment. Among recovery processes solvent extraction is the method generally preferred for phenols removal from ammonia waste waters. At present, diisopropyl ether /DIPE/ is generally used to this purposes as solvent. [1]

Recently at the Research Institute of Chemical Industry, Warsaw, a new extraction process for removal of phenols from phenols containing waste waters has been developed. In this process tert-amyl methyl ether TAME is used as a phenol solvent. Tertiary ether TAME is now used as gasoline additive and easily accessible on the chemical market. [2,3]

First, extraction ability of TAME and DIPE solvents was compared. To this end a cokery effluent and technical-grade solvents were applied. The solvents were above 98 % by weight purity as determined by gas chromatography. Cokery waste water used in experiments contained about 1600 ppm of phenols and had pH equal to 8.5-9.5. For the determination of the effect of pH on the distribution coefficient of different phenols between TAME and water, chemically pure substances and buffered water solution were used. The laboratory experiments were carried out at constant temperature 298 K and 323 K. The mixtures of buffered water acid component solution and TAME were shaken in a 250 ml capacity funnel. The desired level of pH was adjusted by additions of small amounts of sodium hydroxide or sulphuric acid. The remaining phenols concentration and pH was determined in the water phase after separation of mixture.

A Hitachi Model 356 spectrophotometer was applied for colorimetric phenol determinations, pH was measured with MERA-ELWRO NSA type pehameter.

In Table 1 short summary of distribution coefficient data for phenols between TAME and buffered water solution at 298 K are presented.

The K-coefficient for phenols as a function of pH of the water phase are measured experimentally in the pH range 5-12. At pH below 8 dissociation of phenols is negligible and the K value remains practically constant. The extrapolated values of $K_{\text{low pH}}$ for different phenols are listed in column 2 of Table 1. In column 3 the same Table K data for pH equal 10, corresponding to the cokery effluent, are presented.

Table 1. Distribution coefficient for phenols between TAME and water at 298 K.

Substance	$K_{\text{low pH 5-6}}$	$K_{\text{pH 10}}$
1	2	3
Phenol	56.6	25.2
p-Cresol	150.5	82.7
2,6-Dimethylphenol	468.1	356.0
Resorcinol	3.7	1.4

With all the studied systems the dependence of K as a function of pH had the same character. At pH between 8.5-10.5 a rapid decrease of K value takes place. The K-data fits the Treybal model well. For cokery effluents having pH about 10, average distribution coefficient K related to mixture of phenols present in water was found to be 38 and 20 for TAME and DIFE, respectively. In Figure 1 the experimentally measured phase-equilibrium curve for waste water- phenols- TAME and DIPE systems are shown at 293 K. Measurements taken at 323 K showed that temperature increase had only small influence on distribution coefficient. Generally, within this temperature range K values decrease by 5-10 %. The solubility of extractant in water or effluent is important in the regeneration step. In the case of TAME-water systems the solubility of TAME in the water phase decreases when the temperature of solution increases. The solubility data of TAME in cokery effluent measured experimentally are shown below:

Temperature, K	293	313	323	343
Solubility, % by wt.	0.775	0.512	0.420	0.375

At the process conditions solubility of TAME in cokery waste water is about 0.4 % by wt.

The extraction process was tested in a countercurrent Kerr type extractor delivered by the Quickfit Glasstechnik GmbH. The column efficiency was determined to be equivalent to three extraction stages. The water flow rate was $0.02 \text{ m}^3 \text{ h}^{-1}$. The typical examples from the

sets of experiments are presented in Table 2.

Table 2. The continuous extraction of phenol waste waters with TAME.

Water/solvent vol. ratio	Phenol content raw material	ppm in raffinate	Phenol recovery, %
10	1550	52	96.8
12	1600	70	95.6
15	1450	61	95.9
15	1550	83	94.8

In all experiments phenols were found to be recovered above 95 % of their initial weight content from waste water of pH values 8.5-9.6.

For testing the technology a pilot plant was constructed in a cokery plant. The throughput of the pilot plant was $1.5 \text{ m}^3 \text{ h}^{-1}$. A flowsheet is presented in Figure 2. The extractor, rectifying columns and washer were packed with ceramic Rasching rings. The extraction process was carried at 313 K. The results of the six months pilot plant test were as follows: Phenols were recovered in 98 % and their final concentration in the waste raffinate were between 50 to 60 ppm. The reduction of chemical oxygen demand was about 75 % as related to the initial value. The crude phenols mixture obtained from the bottom of rectifying column contained about 85 % of acid components and below 0.1 % by weight of solvent TAME. In the pilot plant test the simple stripping with steam at atmospheric pressure was applied to remove and to recover TAME from the raffinate. In the process inert-gas stripping or vacuum steam stripping can optionally be applied to prevent TAME losses. As proven in the pilot plant test TAME losses were below 0.2 kg per m^3 processing water.

In Table 3 the most important data for both the solvents TAME and DIPE are listed for comparison. Thanks to this lower solubility in the effluent, higher distribution coefficient for phenols and some higher boiling point TAME may be considered as having some advantages over DIPE.

Table 3. Selected properties of TAME and DIPE as phenols extractants.

Formula	TAME	DIPE
Molecular weight	102	102
Boiling point, K	359.2	342.0
Density at 293 K, kg/m ³	776	725
Vapour pressure at 293 K, kPa	9.4	16.1
Solubility in water at 293 K, % by wt.	1.2	1.2
Heat vaporization kJ/mol	33.3	29.2
K - for cokery effluent	38	22

The chemical stability of both the solvents in the cokery effluents is of the same range. TAME as a tertiary ether is not able to form peroxides. Finally, it should be emphasized, that TAME may be applied instead of DIPE used in the very well known Lurgi process. In this case the investment expenses and running costs of commercial plant should be diminished, as TAME in relation to DIPE has almost twice as high K-distribution coefficient - thus reducing the solvent stream, dimensions of the apparatus and energy expenses.

References

- [1] D.C. Greminger at all., Ind. Eng. Chem. Process Des. Dev. 1982, 21, 51-54
 [2] A. Chauvel, Rev. Inst. Francais Petrole, 1981, 36, No. 6, 682-733
 [3] J. Hervig, at all., Hydrocarbon Processing, 1984, une, 86-88

Nomenclature

TAME - tert-amylmethylether $\text{CH}_3.\text{O}.\text{C}/\text{CH}_3/2 \text{ C}_2\text{H}_5$

DIPE - diisopropylether $/\text{CH}_3/2\text{CH}.\text{O}.\text{CH}/\text{CH}_3/2$

K - distribution coefficient expressed as a ratio of phenols concentration /% by weight/ in organic to phenols concentration in aqueous phases

$K_{\text{low pH}}$ - K-coefficient at pH below 6

$K_{\text{pH } 10}$ - K-coefficient at pH equal 10.

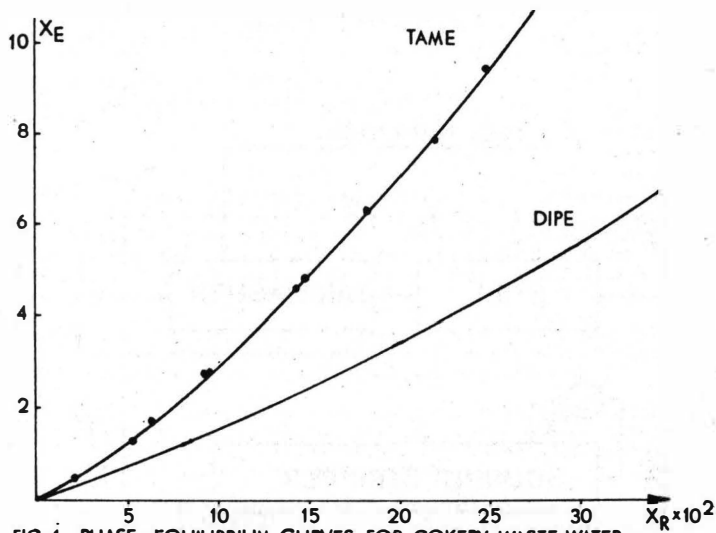
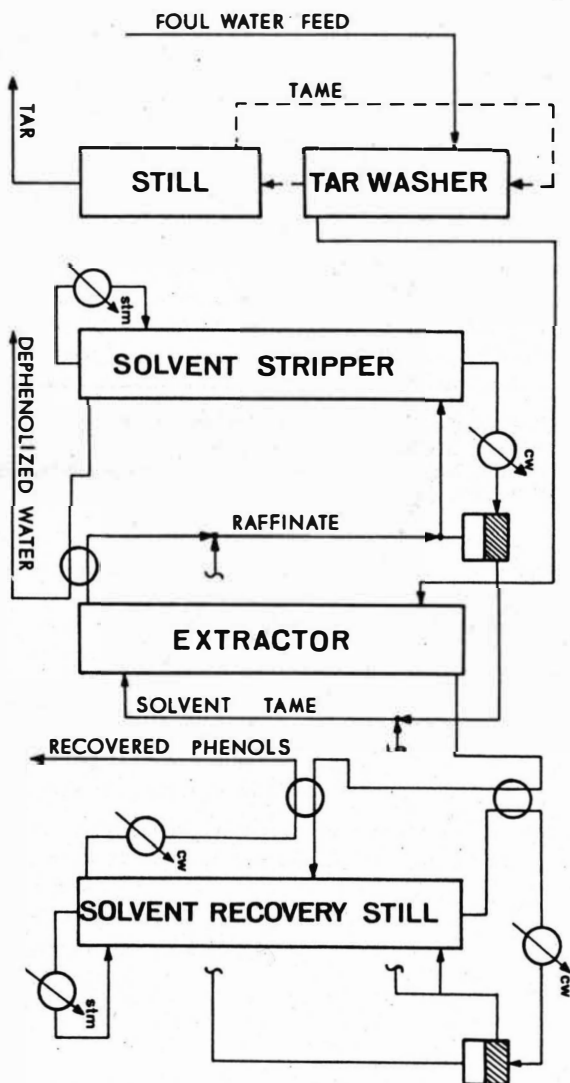


FIG. 1 . PHASE-EQUILIBRIUM CURVES FOR COKERY WASTE WATER - PHENOLS - ORGANIC SOLVENT SYSTEM AT 298 K.
 X_E , X_R - PHENOLS CONTENT IN EXTRACT AND RAFFINATE, RESPECTIVELY BOTH IN WT. %.

FIG. 2 SCHEME OF THE DEPHENOLIZATION PROCESS WITH TAME.



**Acetic acid recovery by liquid-liquid extraction
or azeotropic distillation?**

Dr.-Ing. habil. Th. Pilhofer,
QVF Glastechnik GmbH, 6200 Wiesbaden 13

In a lot of pharmaceutical processes dilute aqueous acetic solutions are produced. Recovery of nearly glacial acetic acid is possible by three processes: distillation, azeotropic distillation and liquid-liquid extraction. Because of the low relative volatility of the system water/acetic acid, distillation is only applied in very special cases.

In this paper a comparison is made between azeotropic distillation and liquid-liquid extraction. In the beginning the characteristics of the two processes are presented.

The typical feature of an azeotropic distillation process is the cycle of the entrainer on the top of the column and the high relative volatility resulting in a rather low acetic acid concentration of the top product water.

For extractive recovery of acetic acid different solvents are available. The characteristic data of these solvents are presented and discussed. A complete liquid-liquid plant consists of three columns: extraction column, solvent/solute distillation and water stripper. Thus, the costs of investment are higher than for azeotropic distillation.

In a following step the energy costs per ton acetic acid are evaluated for both processes. Together with the costs of investment, it is possible to calculate the total costs. These results will be discussed. Finally, recommendations are given for typical areas of application for both processes.

9.7.1985
Pi-Ce

As the manuscript was not available at the 28th May 1986, the deadline for printing this book, we only print the short abstract of the paper.

Process Calculations with Liquid Ion Exchangers

H.J.Bart, R.Wachter and R.Marr
Techn.University Graz, A-8010 Graz, Austria

Introduction

Hydrometallurgical processes for recovery of metals from low grade sources are very sensitive to economical factors. A large number of processes, like cementation, solvent extraction (SX), ion exchange, solvent-in-pulp processes etc., have been proposed to handle this problem. In this paper a comparison between SX and liquid membrane permeation (LMP) will be made with copper as an example.

SX of copper is well documented over a variety of copper feeds. Additionally, economical calculations can be found in literature too /1,2/. For purpose of comparison a 27 m³/h feed stream (Phase III) was considered with either 0,8 g/l copper at pH = 1,5 and 1,5 g/l copper at pH = 2, respectively. The cost calculations in this papers include costs of the SX or LMP plant as well as solvent inventory and make-up. Prices for leaching, electrowinning etc. are not included. Calculation of the SX circuit was done on the basis of conventional horizontal mixer settler (MS). LMP process was calculated when using MS and columns.

It is convenient to use columns with LMP technique. Counter current columns show a distinct concentration profile over the height of the column. This phenomenon allows a recovery of metals down to a region at about 10 ppm. In plant practice this is already demonstrated with zinc recovery from a waste water stream of an artificial fiber factory /3/.

The use of MS is an alternative procedure to solve this problem. They are commonly used in copper recovery plants. However, conventional horizontal MS do not work satisfactory with LMP. This is due to hydrodynamic problems in the settler /4/. Liquid membrane emulsions show segregation effects when moving in a conventional horizontal settler. This effect is enhanced with long residence times (too long settler, dead zones etc.). The final result of the segregation effect is a pure kerosene like organic phase and a heavier dense emulsion phase. The later one, containing all internal stripping phase droplets and the whole tensid acts as a sludge. It cannot be disemulsified and reused. One can overcome this effect with settler types where the coalescing area is under agitation. Therefore the sludge is redispersed and the emulsion phase stays homogeneous. This can be achieved in MS like the combined MS of Davy McKee, that of IMI etc. /4,5/.

The organic phase (Phase II) which was used in SX and FMP calculation procedure is very similar. The ion exchanger which we used was in all cases an aldoxime, as e.g. from Acorga P50 series. All balances where calculated on a stripping phase (Phase I) with 30 g/l copper and 180 g/l H₂SO₄ which is enriched to 45 g/l copper.

SX/MS-circuit

Specific plant data of the SX/MS circuit is shown in Tab.1. The SX-circuit consists of 2 extraction and 2 stripping stages. In every mixer the mean residence time was assumed to be 3 minutes. Raffinate concentrations are calculated according to data supplied by Acorga Ltd. /8/. In this way a solution containing less than 1 g/l copper may be successfully treated with an organic phase of 4 % Acorga P 5100. An organic phase with 5 % PT 5050 was suggested for treatment of about 1,5 g/l copper. The specific flow in settlers q_s is reported

to be in a region from 0,06 to 0,08 m³/m².min. /5/, so 0,075 was chosen /6/.

Table 1: SX/MS circuit

aqu.feed (g/l Cu)	0,8	1,5
aqu.raffinate (g/l Cu)	0,06	0,08
org.phase	4 % P 5100	5 % PT 5050
Cu (kg/h)	20	38,3
V _I (m ³ /h)	1,33	2,56
V _{II} (m ³ /h)	36,45	29,43
V _{III} (m ³ /h)	27	27
V _M (m ³)	10	9
A _S (m ²)	44	39
V _S (m ³)	40	35
V _{org} (m ³)	20	18

Mixer volume was calculated with two units as follows

$$V_M = 2 \cdot (V_{III} + V_{II} + V_{II} + V_I) \cdot \bar{t} \quad (1)$$

Total settler area was calculated for a plant with 2 extraction and stripping units as follows

$$A_S = (V_{II} + V_I + V_{II} + V_{III}) \cdot 2 / q_S \quad (2)$$

Settler depth was assumed to be 0,9 m. With this total amount of the organic phase was related to the total volume of the MS plant, as to $V_{org} = 0,4 V_M$ /5/. Organic phase inventory was calculated to be 20 m³ and 18 m³.

LMP/MS-circuit

The organic phase which is used in all LMP circuits contains 2 % surfactant for emulsion stabilization. It is a polyamine, Paranox 100 (Esso Chem.). Additionally 2 % ion exchanger, pure 5-nonyl-salicylaldoxime (Acorga P 50) is diluted in kerosene (Shellsol T).

The LMP/MS-process is done in two counter current units. Specific plant data are shown in Tab.2, which are calculated from experiments in a small unit ($V_M = 0,001$ m³).

Table 2: LMP/SX circuit

org.phase	2 % P 50, 2 % Paranox 100, 96 % Shellsol T	
aqu.feed (g/l Cu)	0,8	1,5
aqu.raff. (g/l Cu)	0,04	0,06
Cu (kg/h)	20,5	38,9
V _I (m ³ /h)	1,3	2,6
V _{II} (m ³ /h)	6,8	12,9
V _{III} (m ³ /h)	27	27
t _{III} (min)	8	8
t _{II+I} (min)	6,4	5,3
K	0,23	0,29
A _S (m ² /m ² .min)	0,166	0,108
V _S (m ²)	15,6	18,8
V _{org}	13,8	17,2

Total mixer volume was calculated for 2 units to:

$$V_M = 2 \cdot (V_{III} \cdot \bar{t}_{III}) / (1-X) \quad (3)$$

Mean residence time of Phase III, \bar{t}_{III} was held constant at 8 minutes. X denotes the hold-up ($X = V_{II+I} / V_M$) which was actually measured. Specific flow in the settler compartment, q_S was varied in a range from 0,108 to 0,24. For save plant lay-out a value of 0,075 was used. The organic phase volume was calculated from the hold-up in the mixer and the volume in the settler.

$$A_S = 2 \cdot (V_{III} + V_{II} + V_I) / q_S \quad (4)$$

$$V_{org,S} = 0,45 \cdot A_S$$

$$V_{org,M} = X \cdot V_M$$

We used a factor of 1,5 for volumes of storage piping etc., thus

$$V_{org} = 1,5 (V_{org,M} + V_{org,S}) \quad (5)$$

The total organic inventor is 13,8 and 17,2 m³, respectively.

LMP column circuit

In the LMP circuit an equal organic phase was used as in the LMP/SX circuit.

Specific plant data for the FMP-column system are shown in Tab.3.

Tab. 3: FMP/column circuit

org.phase	2 % P 50, 2 % Paranox 100, 96 % Shellsol T
aqu.feed (g/l Cu)	0,8
aqu.raff. (g/l Cu)	0,05
Cu (g/h)	20,2
V _{III} (m ³ /h)	27
V _{II} (m ³ /h)	6,7
V _I (m ³ /h)	1,35
X ^I	0,1
H _C (m)	5,9
D _C (m)	1,6
V _C (m ³)	20
A _C (m)	7,8
V _S (m ³)	8,25
V _{org} (m ³)	12

The total specific flow in the column is 17,5 m³/m².h. At this flow conditions entrainment is at 25 ppm. The settler area of the column is calculated with $q_S = 0,075$ m³/m².min. Diameter of the column are 1,6 and 2,5 m. The total height is 10 m including settling zones. V_{org} was calculated according to hold up in the column and a 0,45 m organic settler layer. Factor of 1,5 is again used for piping etc.

$$A_S = (V_{III} + V_{II} + V_I) / q_S \quad (6)$$

$$V_{org} = 1,5 (V_C \cdot X + A_S \cdot 0,45) \quad (7)$$

Cost calculation

A cost comparison between SX and FMP is presented in Tab. 4

Tab. 4: Cost calculation

163.000 kg Cu/a	SX/MS	FMP/MS	FMP/column
org.Phase	8.800	7.000	4.100
Plant	146.290	40.000	900.000
313.000 kg Cu/a			
org.Phase	8.100	9.100	6.000
Plant	126.750	61.100	1,000.000

Plant costs were calculated to be 2500 US\$/m² settler area. These data are from 1977 /6/, corrected with an index factor of 1,3. The costs of the organic phase were calculated at prices valied in Austria as to:

- organic phase, 4 % P 5100	0,44 US\$/l
- organic phase, 4 % PT 5050	0,45 US\$/l
- membrane phase, 2 % P 50 + 2 % Paranox	0,50 US\$/l

The amortization periode was assumed to be 5 years. Specific costs per kg copper are in Tab. 5.

Entrainment for SX and FMP is calculated at the basis of 75 ppm. An annual demand of 17 m³ Phase II is considered as make-up at an aqueous feed stream of 27 m³/h.

Tab. 5: Specific costs (US\$/kg Cu) Capital + Operating costs

Cu Feed (g/l)	SX/MS	FMP/MS	FMP/column
0,8	0,18+0,05	0,06+0,05	1,1+0,05
1,5	0,08+0,02	0,04+0,03	0,6+0,03

As can be seen LMP/MS process show disinct advantages at low tenor operations. This calculation is done on the assumption of an ideal behaviour of the LMP process. Up till now, there are some problems to be solved. Osmosis and degradation of the organic membrane phase cause additional costs. Phase I can enlarge in volume at a factor of 1,3 due to osmosis. A reduction of this volume is necessary and can be done e.g. with a solvent vapor condensor. Specific capital and operating costs are about 0,02 + 0,03 US\$/kg Cu. Costs due to degradation of the organic phase may be about 0,1 US\$/kg Cu. Tests in order to minimize osmosis and degradation are currently under operation /9/. Reduction of these additional cost factors should therefore be possible.

As can be seen from this table, FMP/column processes offer no advantage with copper recovery. This may be due to the effect that copper separation is kinetically controlled. Kinetics of copper extraction is known to be slow. (In contrary this is not true with zinc permeation.) As a result copper permeation needs long residence times which do not encourage the use of permeation columns.

Conclusions

LMP technique offers economical advantages at low tenor operations as is shown with copper as an example. This fact is mainly due to reduction of settler area in the process since extraction and reextraction step are situated in the membrane phase of the emulsion globule. Additionally since the organic phase acts only as a membrane, solvent inventory can be kept low. A problem is still up to now the degradation of the organic phase and the osmosis. Osmosis is a function of ion exchanger, tensid, modifier, and ionic strength in the aqueous phases. Osmosis is negligible when Phase I and Phase III have equal ionic strength, which is seldom true at low tenor operations.

Acknowledgement

We wish to thank Acorga Ltd. for supplement of product samples.

Symbols

A	area
D	diameter
H	height
M	mixer
S	settler
t	time
V	volume
X	hold-up

Indices

I	feed phase
II	organic phase
III	stripping phase
C	column
M	mixer
S	settler

Literature

- /1/ C.R.Merigold et al., Paper at Copper Technol.Seminar, Dez.1985, Washington, D.C.
- /2/ J.A.Tumilty et al., Paper at Advances in Extractive Metal, 1977, Ed. IMM
- /3/ J.Draxler et al., Paper at ISEC '86, Munich
- /4/ H.Lackner et al., Paper ISEC '86, Munich
- /5/ Handbook of SX, Ed.Lo et al., John Wiley, 1983
- /6/ J.A.Tumilty et al., Paper at ISEC '77, CIM Vol.21, 1979, Toronto
- /7/ A.Wolf, Master-thesis, TU Graz, 1986
- /8/ Acorga Ltd. Data of P 5000 series
- /9/ R.Wachter, Thesis for doctorate, TU Graz, 1986

Recovery of Furfural from Papermill-Effluents by Liquid-Liquid-Extraction - Economical and Technical Considerations

G.Bunzenberger, M.Siebenhofer, R.Marr, Technische Universität Graz, Graz/Austria

Furfural was discovered by Oobereiner in 1821. But there was no use for the next 90 years. In 1922 the first drum of furfural was produced by the Quaker Oats company and the first important commercial use was in the production of phenolic resins.

Furfural (2-furancarboxaldehyde) is a water white liquid when freshly distilled but darkens on standing in contact with air.

molekular weight:	96,08
101,3 kPa	161,7° C
freezing point	-36,5° C
water solubility at 20° C	8,3 Gew%
viscosity at 25° C	1,49 mPa.s
surface tension at 30° C	40,7 mN/m

Tab.1: Selected physical properties of furfural

At the absence of oxygen furfural is thermally stable up to 230° C (except colour). It is miscible with most of the common organic solvents, but only slightly misible with saturated aliphatic hydrocarbons. Today furfural is a well known solvent and used for separation processes. The principle usage of furfural is as selective solvent for separating saturated from unsaturated compounds in petroleum refining, gas oils and diesel fuel; for the extractive distillation of butadiene and other C₄ hydrocarbons, for the manufacture of synthetic rubber and the production of light colored wood rosins. Furthermore it is a versatile basic material for a whole palette of products.

Usually furfural is produced from annually renewable agricultural sources such as corn cobs, bagasse, husks and wood wastes. The pentosane content of this vegetable materials is hydrolyzed in the presence of inorganic acids to pentoses and the pentoses subsequently cyclodehydrated to furfural.

From the hydrolyses digester furfural usually as steam distilled. The simplest process for furfural isolation can be seen from Fig. 1. The condensed reactor vapors are fed to a stripping column from which an enriched furfural water distillate is withdrawn and

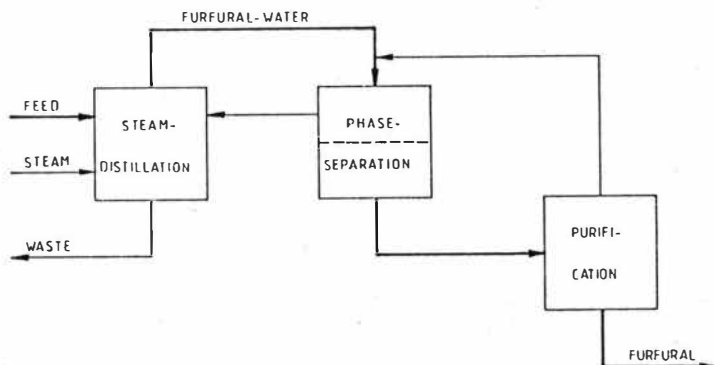


Fig. 1: Conventional furfural separation process

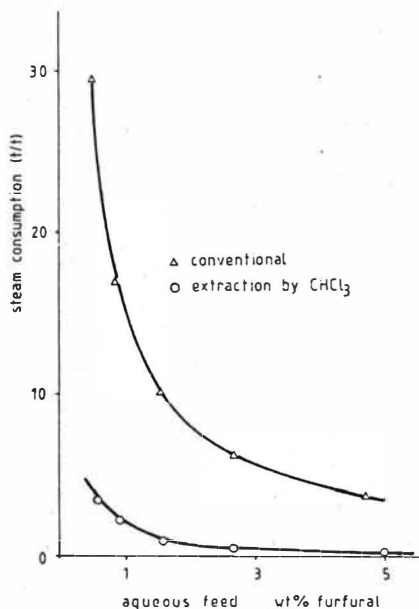


Fig.2: Comparison of steam consumption per ton furfural for conventional furfural separation process and extraction with CHCl_3

condensed in a decanter where it separates into two layers. The furfural rich layer contains about 6% water and is purified in a distillation column to commercial standard. The water rich layer is recycled to the steam distillation as reflux. These and similar processes have a steam consumption according to the upper graph in fig.2. The lower the feed concentration of furfural, the higher purification costs. Usually feed concentrations are higher than 4% weight.

But there is another big furfural source in the waste water of pulp and paper industry. The condensate of the vapor of the pulp digesters contains furfural, carboxylic acids (mainly acetic acid), methanol and some other.

A typical content is 0,3 to 0,5 % for the furfural and up to 2 % for the acids. It is not possible to obtain furfural out of this

waste water stream economically with the conventional process. On the other hand the new process must include both furfural and acid recovery as to refer also to environmental protection. The main idea of the new process is the selective and quantitative separation of the furfural from the waste water and the extraction of the carboxylic-acids as described in previous work /1,2/. In this paper liquid-liquid extraction of the aqueous furfural content in papermill effluents was investigated. A process description for the overall process (furfural and acids) is given.

In the search of a proper solvent we looked for a low boiling solvent with

- * high selectivity for furfural
- * high distribution coefficient in order to operate at low phase ratios
- * easy separation of the solute by distillation
- * no azeotrope between furfural and solute
- * easy solvent stripping from raffinate phase

Chloroform proved to be the best solution (see also /3/) to fulfill the points above. Even it has a solubility in the raffinate of 9,3 g/l reextraction with a solvent containing aliphatic hydrocarbons with a boiling point of about 186° C to 240° C (40 % decane, 60 % undecane). The solubility of this extractant in the water is so low (ppb-range), that no pollution is caused by this reextraction step.

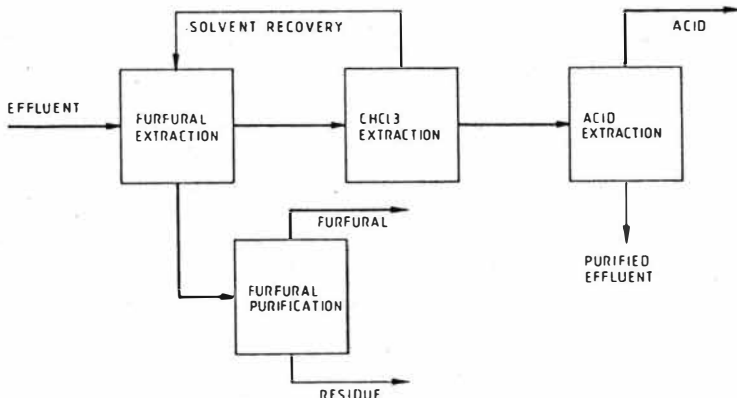


Fig. 3: Basic steps for furfural and acid recovery by liquid-liquid extraction

The separation process demands the following steps as can be seen in Fig. 3.

- a) selective extraction of furfural with solvent 1 (chloroform)
- b) separation of furfural and lower boiling solvent 1 by distillation and furfural purification
- c) selective reextraction of the chloroform content in the raffinate of furfural extraction step with the high boiling solvent 2 (Shellsol T) and separation of solvent 1 and 2 by distillation
- d) acid extraction with high boiling solvent 3 a mixture of tertiary amines as a reactive component, a modifier and a diluent with very low water solubility and easy separation of solvent solute by distillation /1,2/

Furfural has a distribution coefficient between chloroform and water of more than 20. With a phase ratio of 14 (aqueous/organic) and extraction column needs only 6 theoretical stages with a raffinate concentration of less than 100 ppm.

Furfural chloroform can be separated by distillation. E.g. separation of a mixture containing 14 % furfural effords less than 5 theoretical stages.

Chloroform has a distribution coefficient between solvent 2 and water of 67. Therefore the phase ratio can be kept very little, that means, that the solvent regeneration column (distillation) is of a small diameter.

Description of the developed extraction process: Fig. 4 shows the flow sheet of the process. It contains of three extraction columns:

EF - Furfural extraction, ES - solvent reextraction, EA - acid extraction and three distillation columns: D_F - furfural-solvent 1, D_S - solvent 2 - solvent 1, D_A - solvent 3 - acids.

In pulp and paper industry a standard volume of the furfural and acid containing waste water stream is 100 m³/h. So there is the potential to produce 2.000 to 3.000 metric tons of furfural (stream 8) with 99 % wt and 8.000 to 12.000 metric tons of acids (stream 12) - mainly acetic acid per year - with this process.

Economical Consideration

In Fig. 1 the comparison of conventional furfural production (distillation process) and extraction with chloroform is shown. As can be seen even in the region of low furfural concentration it can be produced with a steam consumption ten times less to the distillation process.

The distillation process can only be economically applied to feed concentrations less than 2 - 3 % wt. Regarding our new process about the same steam ratio is given in acid recovery. Helsel /4/ reports a steam consumption for conventional acid recovery systems of 20 tons per ton acetic acid out of aqueous solution with 2 wt% acetic acid. In our process steam consumption is about 10 times lower depending on the desired acid quality.

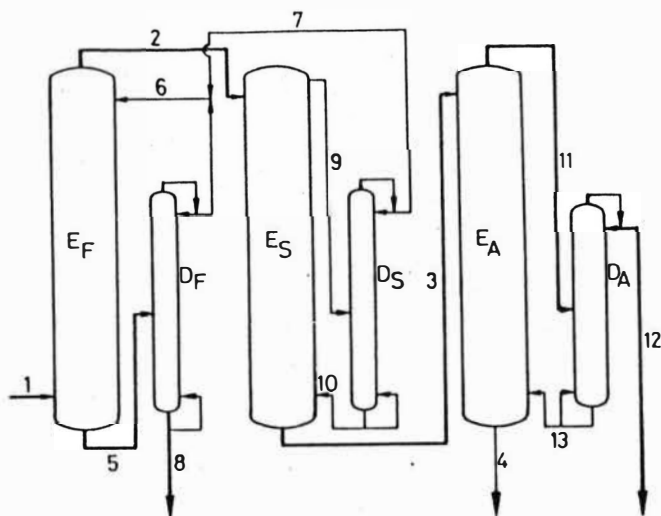


Fig. 4: Flow sheet of developed extraction process

1 aqueous waste stream, 2 raffinate (after furfural extraction containing solvent 1), 3 raffinate (without solvent 1), 4 raffinate (after acid extraction), 5 loaden solvent 1, 6 regenerated solvent 1, 7 solvent 1 recycling stream, 8 furfural product stream, 9 solvent 2 loaden with the re-extracted solvent 1, 10 solvent 2, 11 solvent 3 loaden with acids, 12 raw acid product stream

References

- /1/ Siebenhofer, M., R.Marr: Acid Extraction by Amines, ISEC '83, Denver, Col., 26.Aug.-2.Sept.1983, paper 18e
- /2/ Siebenhofer, M.: Thesis TU Graz, 1983
- /3/ Wennersten, R., Zacchi, G. and Aly, G.: Paper presented at the Symposium "Thermal Separation of Gas and Liquid Mixtures", European Federation of Chemical Eng., Cologne, 6.-8.5.1981
- /4/ Helsel, R.W.:Chem.Eng.Progr., May 1977,(73) p 55

The application of extraction methods in post-distillation residues elimination

M. Żak, Warszawa/IL

The industrial chemical technology produces many difficult to handle residues. This problem especially takes place during solvent regeneration processes. Methods of elimination or utilization of post-distillation residues as direct combustion/1,2/, storage/3/, pouring into canalisation systems/3/ produce serious, both technical and environmental problems. Some of them are:

- difficulties with evacuation from distillation vessels. Semi-liquid, easy solidifying materials are difficult to handle in large-scale installations,
- necessity of leaving some part of regenerated solvent decreases regeneration effectiveness,
- direct pouring into canalisation produces its rapid clogging,
- carrying out and storage in any place makes risk of serious environmental pollution.

The One Stage Double Extraction/OSDE/ method eliminates the majority of difficulties mentioned above. The OSDE method depends on extraction of post-distillation residues by the means of both water and combustible lyphophylic solvent. Water dissolves organic hydrophylic matter and inorganic substances, organic solvent dissolves organic matter, especially polymers and high boilers responsible for rapid solidifying the post-distillation mixtures and clogging pipelines. Adding of water to post-distillation residues produces the total precipitation of organic lyphophylic substances, which are immediately dissolved in organic solvent. When the extraction processes are over, water layer can be poured to canalisation without risk of clogging. Organic layer can be easily burnt. As organic solvent can be of very poor quality, and the OSDE method requires only minimal quantities of it, the described processes are not only very simple, but both environmentally and economically attractive.

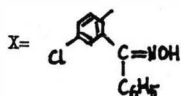
Materials and methods

The experiments had to prove the effectiveness of the OSDE treatment in two difficult cases, when a great amount of both salts and high boilers were crystallising and solidifying. Samples of post-distillation residues were taken directly from industrial installations, immediately when the distillation processes were over.

The OSDE procedure was the same in both cases and depended on:

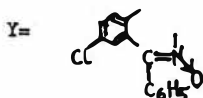
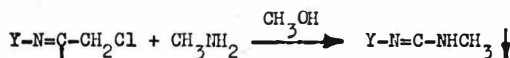
- pouring hot post-distillation residues into a glass reactor,
- adding lyphophylic solvent,
- adding water/in some cases NaOH or Na₂CO₃ aqueous solution/,
- extraction and cooling,
- separation of phases.

The distilled mixture I/experiment I/ was taken from organic synthesis, based on reaction/4/:



After separation of the precipitated product liquid phase was taken to distillation and acetic acid was regenerated in the process. Liquid phase before distillation consisted of: acetic acid/70% by weight appr./, chloroacetic acid/5% by weight appr./, zinc chloride/15% by weight appr./ and unidentified organic substances/10% by weight appr./. The above mixture in a quantity of 600 l. was loaded to distillation vessel. When the industrial distillation process was finished/ the residue was still liquid in high temperature, but continuing of distillation could cause crystallisation, solidifying and clogging the bottom outlet of the vessel/ the residues were poured out to containers. Samples were taken in this moment.

The distilled mixture II/experiment II/ was taken from organic synthesis, based on reaction/4/:



After separation of the precipitated product liquid phase was taken to distillation and both methylamine and methanol were obtained in the regeneration process. Liquid phase before distillation consisted of: methanol/80% by weight appr./, methylamine/14% by weight appr./, and unidentified substances/6% by weight appr./. The above mixture in a quantity of 800 l. was loaded to distillation vessel. The distillation was finished when there still was possibility of evacuation from the reactor the post-distillation residues as a liquid. Samples were taken in this moment.

Experimental

In both cases the OSDE method was applied to post-distillation residues treatment. The results are shown in a Table 1/experiment I/ and a Table 2/experiment II/.

Neutralisation by the means of basic solutions/ Table 1/ was carried out in order to protect incineration installations from high temperature corrosion. However, neutralisation caused creation of emulsions.

A routine OSDE treatment was applied in the experiment II. However, before the OSDE treatment the distillation was continued in a labo-

ratory scale/ Table 2, No 4, 5, 6/ up to the point, when the residues became oily and dense. This procedure was very convenient, because the emulsions creation tendency substantially decreased. The increase of solvent regeneration efficiency was observed in these cases.

In all cases the post-distillation residues were dark-brown. After the OSDE treatment water phase was of light pink colour. The colour of organic phase was similar to that of residues before treatment.

Further adding water to water phase after the OSDE treatment never caused any additional precipitation of solids or oily products. It is of great importance, as the water phase is to be poured into canalisation systems.

Ethyl acetate was used in the experiment II/ Table 2, No 6/. Extraction properties of this solvent were even better than these of toluene.

Toluene was used in a majority of the experiments. It was caused by local circumstances. The use of other lyphophylic liquids/ ex. ethyl acetate/ is possible.

As any crystallisation took place in organic phase, further diminishing of quantity of lyphophylic solvent was possible. It is of great importance when the technological experiments will be carried out in order to elaborate industrial processes based on the OSDE method.

Conclusions

The One Stage Double Extraction method can be perfectly applied in post-distillation residues treatment. Organic phase can be easily combusted, water phase can be poured into canalisation systems without risk of clogging.

As the OSDE method replaces storing of post-distillation residues it is much more safe to the natural environment. Incineration of organic phase may produce energy. It increases the efficiency of the process.

The OSDE method enables continuing distillation processes to dry residue allowing total regeneration of distilled substances. It can be of great importance when valuable substances are distilled.

After the OSDE treatment easy to handle liquids are obtained in contrary to traditional methods, which produce semi-liquid and solidifying materials.

In contrary to traditional methods of post-distillation residue treatment, the OSDE method works better when only a minimum of residual solvent remains in a distillation vessel.

A lyphophylic solvent used in the OSDE treatment can be of poor quality. It can contain water.

Colouring substances are extracted mainly to organic phase. It is

also convenient to environmental protection.

References

1. Koziarowski B. Oczyszczanie ścieków przemysłowych. W. N. T. Warszawa 1980.
2. Process design manual for sludge treatment and disposal. U.S. Environmental Protection Agency. 1974.
3. Meinck F., Stoof H., Koilschutter H. Industrie-Abwasser. Gustav Fischer Verlag. Stuttgart 1968.
4. German Patent No 1096362/1959/ and U.S. Patent No 2893992/1959/.

Table 2. The application of OSDE method in post-distillation residue treatment. Experiment II.

No	Residues from vessel /l/	Sample /ml/	Toluene /ml/	Water /ml/	Organic phase /ml/g/	Remarks
1.	300	100	50	300	70/65	Emulsions in both phases
2.	300	100	50	300	50/44	Emulsions in toluene phase
3.	300	100	50	300	46/42	Emulsions in toluene phase
4.	300	300	50	350	85/88	Before the CSDE treatment 190 ml of methanol/methylamine was distilled to nearly dry residue. Good separation of phases. No emulsions.
5.	300	300	50	350	88/89	Before the OSDE treatment 205 ml of methanol/methylamine was distilled to nearly dry residue. Good separation of phases. No emulsions.
6.	300	300	50 /ethyl acetate/	350	104/107	Before the OSDE treatment 220 ml of methanol/methylamine was distilled to nearly dry residue. Good separation of phases. No emulsions.

Table 1. The application of OSDE method in post-distillation residue treatment. Experiment I.

No	Residues from vessel	Sample /l/	Toluene /ml/	Water /ml/	Others /ml/	Organic phase /ml/g/	Water phase /pH/	Remarks
1.1	200	100	40	350		46/40	2,1	
1.2	the same	100	30	350		34/34	2,1	
1.3	the same	100	30	300	50 of 40% NaOH	37/34	3,5	Emulsions in both phases
2.1	200	100	40	350		41/38	2,0	
2.2	the same	100	30	350		32/30	2,0	
2.3	the same	100	30	250	100 of 20% NaOH			Strong emulsions. No possibility of separation
3.1	170	100	30	350		32/30	2,0	
3.2	the same	100	30	325	25 of 40% NaOH	36/34	2,5	Emulsions in organic phase
3.3	the same	100	50	250	100 of 20% Na ₂ CO ₃	49/44	2,5	Emulsions in organic phase
4.1	150	100	30	350		36/34	2,0	
4.2	the same	100	30	300	50 of 40% NaOH	32/30	2,5	Emulsions in organic phase
4.3	the same	100	30	250	100 of 20% Na ₂ CO ₃	46/36	2,5	Emulsions in organic phase
5.1	100	100	30	350		49/48	2,0	
5.2	the same	100	30	250	100 of 20% Na ₂ CO ₃	93/111	2,5	Emulsions in organic phase

LIQUID-LIQUID EXTRACTION AND TRANSPORT THROUGH LIQUID MEMBRANES OF METAL CYANIDE COMPLEXES ($KAu(CN)_2$ and $KAg(CN)_2$) BY MACROCYCLIC EXTRACTANTS.

M. TROMP, M. BURGARD, M.J.F. LEROY.

Laboratoire de Chimie Minérale E.N.S.C.S., Associé au C.N.R.S. U.A. 405,
1, Rue Blaise Pascal 67008 STRASBOURG Cedex (France).

M. PREVOST.

Institut National de Recherche Chimique Appliquée, Centre du Bouchet
91710 VERT LE PETIT (France).

I) - Introduction

The use of the liquid membrane technique for the extraction of metallic species has been widely investigated during the last decade and many applications in hydrometallurgy have been proposed (1).

In our laboratory we are interested in developing the liquid membrane technique in various processes related to the recovery and separation of precious metals (2).

This paper deals with the solvent extraction and the transport through a supported liquid membrane of metal cyanide complex salts of gold I and silver I by macrocyclic extractant carriers.

II - Determination of the extractant carrier.

Aqueous cyanide leaching solutions are common in the hydrometallurgy of gold and silver. These metals are present in the solutions as dicyanoaurate and dicyanoargentate anions $[M(CN)_2]^-$, $M = Au, Ag$ which can be extracted via an ion pair extraction process. The corresponding co-cation can be of various types (3).

1) **A quaternary ammonium.**

In this case, the extraction is pH independent but the stripping can be difficult. Hence, quaternary ammonium salts cannot be used as carriers.

2) **A protonated amine.**

Amines are able to extract dicyanometallic acids $[H M(CN)_2]$ and can therefore be envisaged as carriers in pH pump processes, in which the precious metal is extracted from acidic media.

This procedure is obviously not suitable in the presence of an excess of cyanide.

3) **A solvated cation.**

It has been shown that neutral solvents extract alkali dicyanometallates as well as the corresponding acids [3b, 3c].

Their significant solubility in water can cause depletions of the polymeric support.

As a result, the current extractants mentioned above have some disadvantages which make them unusable as carriers of dicyanometallates in supported liquid membranes.

An alternative possibility is proposed here. Strong alkali complexing agents (L) [e.g. Kryptofix 22 DD, see figure 1] dissolved in low polar diluents [e. g. decanol] are able to extract dicyanometallate salts [e.g. $\text{KM}(\text{CN})_2$] according to the equilibrium



[equilibrium constants see table 1).

The organic phase containing the complex salt can be stripped with water. The low polarity of the diluent ensures a high extraction selectivity with respect to common anions which can be present in the leaching solution [OH^- and/or CN^-], hence, an efficient driving force can be generated by the concentration gradient of the alkali ion between the aqueous feed and the aqueous stripping solution [see figure 2].

III - Supported liquid membranes (SLM)

Experimental.

The transport through a supported liquid membrane of potassium dicyanoaurate and dicyanoargentate has been investigated by using types of microporous polypropylene sheets having very different characteristics [see table 2]. These were filled by submersion in the macrocyclic carrier decanol solutions and fixed between the two chambers of a diaphragm cell [see figure 3]. The cell was immersed in a thermostated bath [$t=25^\circ\text{C}$]. The macroscopic area of the membrane was $9,1 \text{ cm}^2$. Equal volumes [80ml] of the aqueous phases were placed in the two chambers and were stirred [400 rpm]. The feed aqueous solution contained potassium dicyanometallate in the presence of an excess of potassium supplied by KOH or (and) KCN. The aqueous stripping phase was distilled water. The mass transfer was studied by plotting the solute concentrations in the aqueous stripping phase as a function of time.

Results and discussion.

The experimental flux for gold and silver has been found to be of the same order of magnitude as those generally observed for other metal transfers (4). As illustrated here (see figure 4) with Celgard 2500 and Accurel^R, the

characteristics of the microporous films greatly affect the mass transfer rate. As a result, the effect of the support thickness on the rate is offset by the larger pore size. Furthermore minimum membrane depletions have been observed with the Accurel^R supports containing the carrier decanol solutions.

Fresh tributylphosphate (TBP) SLM's also exhibit interesting transport properties however the semi permeability property of the membrane disappears within a few days.[approximatly 3 days]].

Two features have been observed in this case.

- 1) Loss of the impermeability with respect to KOH which leads to a pH equilibration in the two aqueous phases and which stops the precious metal transfer process.
- 2) Membrane depletion due to a too high TBP solubility in water.

Among all the tested systems the 22 DD-decanol-Accurel^R SLM offered the best compromise. It appears to be a promising SLM system for dicyanometallate recovery from KCN-KOH media. The semi permeability of the membrane remained constant for a period of about two weeks. This motivates a closer look at the industrial applicability of such membranes which are able to concentrate precious metal cyanide salts [see figure 5].

References :

- 1) a) D. PEARSON in "Ion Exchange Membranes", (D.S. FLETT ed, Ellis Horwood Ltd, 1983) chap. 4, p.55.
b) P.R. DANESI. Sep. Sc. Techn. 19, p.857, (1984-1985).
c) R. MARR and A. KOPP. Int. Chem. Eng. 22, 1, p.44 (1982)
- 2) a) M. BURGARD, P. ELISOAMIADANA, M.J.F. LEROY and H.S. PARK.
Int. Solv. Extr. Conf., I.S.E.C.'83, (A.I.Ch.E. publ.) p.399.
b) J.C. DUPUY, B. PONTVIANNE, M. PREVOST, M. BURGARD, M.J.F. LEROY, C.SIRLIN.
E.E.C. Publication (to be published).
"Application des membranes liquides dans le traitement des métaux précieux".
c) P. ELISOAMIADANA, M. BURGARD, M.J.F. LEROY.
Contrat C.N.R.S., A.T.P. - P.I.R.S.E.M.. N° 268.
Rapport final "Transport contre le gradient de concentration d'anions polychlorométallates de métaux précieux".
- 3) a) J.D. MILLER and M.B. MOOIMAN.
Sep. Sc. Techn. 19, (11-12), p. 895 (1985) and ref. therein.

b) C.M. RITLEY and A.W. ASHBROOK.

"Solvent Extraction Principles and Applications to Process Metallurgy, Part. II, (Elsevier 1977) p. 381-385.

c) M.B. MOOIMAN, J.D. MILLER and M.M. MENA.

Int. Solv. Extr. Conf., ISEC 83, (A.I. Ch. E. publ.) p. 530.

4) E. DRIOLI, R. CAMMAROTA, D.G. KI and F. PERONE,

Galvanotechnica 34, p. 183, (1983).

M	Au	Ag
$\log K_e$	2.38 ± 0.03	1.52 ± 0.03

Table 1: Extraction constant $K_e = \frac{|M_{org}| \cdot |M_{aq}|^{-1} \cdot |K^+|^{-1} \cdot |L^-|^{-1}}{}$
(in mole⁻². liter⁻²)

Diluent = decanol ; extractant = 22DD ;

ionic strength: KOH 0.1N

support	thickness	pore diameter	porosity
Celgard 2500	25 μm	0.04 μm	0.45
Accurel ^R	160 μm	0.2 μm	

Table 2. Support Characteristics

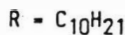
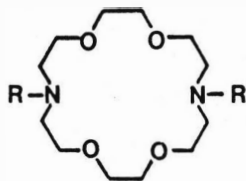


Figure 1. Kryptofix 22DD.

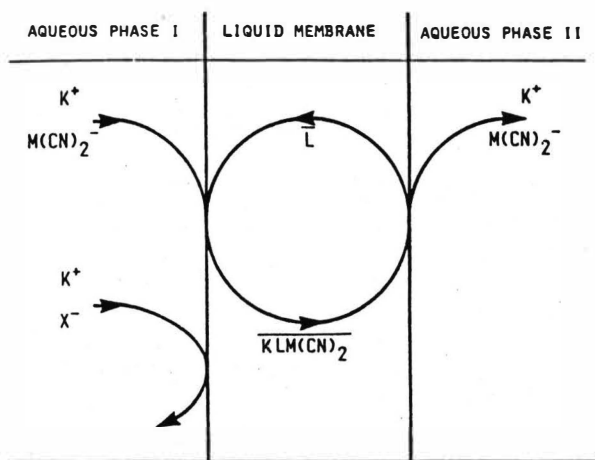
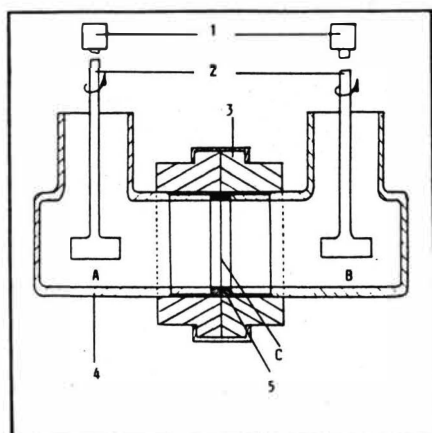


Figure 2. Simplified representation of the transport of a dicyanometallate facilitated by a neutral carrier.
(feed: aqu. phase I; stripping: aqu. phase II)



- | | |
|------------|-----------------------------|
| 1. Motor | A,B :aqueous phase chambers |
| 2. Stirrer | C :impregnated support |
| 3. Ring | |
| 4. Gell | |
| 5. Joint | |

Figure 3: Experimental setting up.

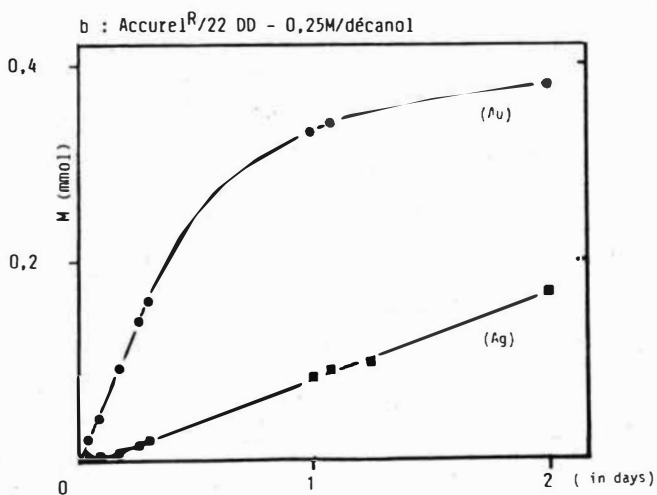
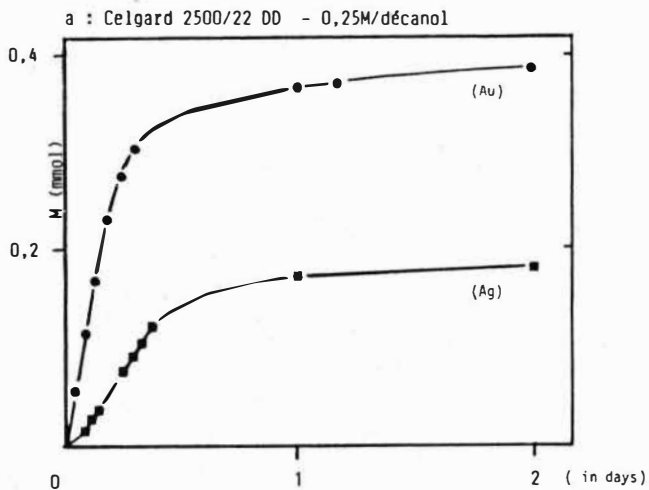


Figure 4: Gold and silver concentrations in the stripping aqueous phase vs. time.
 Liquid membrane: 0.25M Kryptofix 22DD in decanol. a) Celgard 2500 b) Accurel^R.

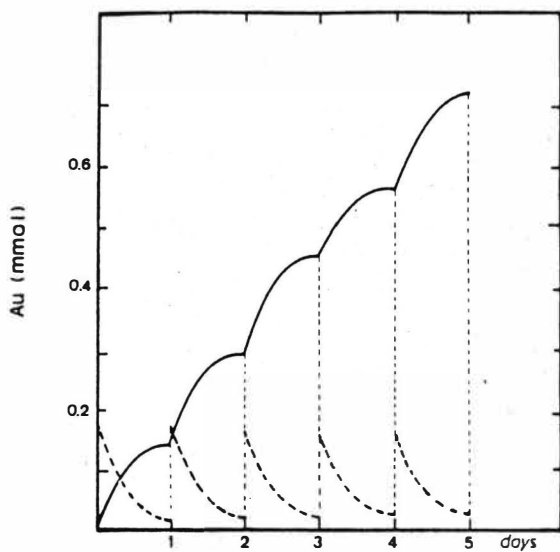


Figure 5: Gold recovery and concentration by means of an Accurel^R - 22DD(0.25M) -Decanol SLM. The feed aqueous solution is periodically replaced.
 Feed: $\text{KAu}(\text{CN})_2$; $2.1 \cdot 10^{-3}\text{M}$ ($0.17 \cdot 10^{-3}$ mole). KOH 1M.
 - - - - - gold quantity in the aqueous feed phase.
 ————— gold quantity in the aqueous stripping ph.

Behavior of Mass Transfer by Liquid Surfactant Membrane in a Continuous Separation Column

Jae-Hyung Yoo, Hyun-Soo Park, In-Suk Suh
Korea Advanced Energy Research Institute
Dae-Duk Research Town, Chung-Nam 300-31 Korea

ABSTRACT

A numerical model for simulation of steady-state operation of a separation column in liquid surfactant membrane process was developed. This model was made on the basis of the mass transfer kinetics for a single emulsion drop as well as the flow patterns of both continuous and dispersed phases. The predicted results calculated by this model were found to be in fairly good agreement with the experimental results in the aniline separation process of $C_6H_5NH_2$ (external phase)-liquid paraffin(membrane)-HCl(internal phase) system.

1. INTRODUCTION

A liquid surfactant membrane is prepared by forming an emulsion mixture of two immiscible phases and then dispersing the emulsion into a third phase(external phase). In most of the studies on liquid surfactant membrane processes up to the present, only batch-type equipments were used as extractors. However, the behaviors of a multi-stage continuous separation process would be needed for process design and scale-up calculations. Thus, in this study, a numerical model was developed for estimating the steady-state behaviors of a multi-stage column in the separation process of aniline. On the other hand, a multi-stage column was made in order to investigate the flow patterns of both continuous and dispersed phases and to verify the usefulness of this model. This column was modified from the conventional extraction columns in such a way that the interior part should be suitable for treating the viscous emulsion phase. The flow patterns of continuous(water) and dispersed(emulsion) phases were examined by means of the stagewise backmixing model (2) and the gamma distribution model(3) respectively.

In parallel with this work, the rate equation of mass transfer for a single emulsion drop was made because the model was based on the mass transfer kinetics together with the flow patterns of both phases. In formulation of W/O(water in oil)type emulsion, mineral oil(S 100 N) in which the solute aniline can be dissolved was used as membrane phase. Hydrochloric acid was added in the internal aqueous phase in order to trap aniline. Since the encapsulated hydrochloric acid converts aniline to the anilinium ion which is nonsoluble in the membrane phase, it acts as sinks of the extracted aniline. This type of mass transfer mechanism is the same as that of separation of acidic compounds such as phenol with aqueous bases(1).

2. MASS TRANSFER RATE

2.1 Assumption

The following assumptions, based on the membrane extraction system, were made to describe the rate of mass transfer.

- * There is no internal circulation within the emulsion drops because of the strong presence of surfactant in the membrane phase.
- * Since the interfacial tension around drop surface is low due to the surfactant, there is no coalescence and redispersion of the emulsion drops in the course of agitation.
- * The mass transfer resistance in film of the external phase around each drop is negligible because the external solution is continuously agitated.

2.2 Mathematical Description

The rate of mass transfer can be defined as

$$J = D \frac{\Delta C}{\Delta x} \quad (1)$$

where ΔC is the concentration difference of the extracted species on either side of the membrane, Δx is the membrane thickness, and D is the diffusion coefficient of the permeating species. In fact, the membrane thickness in this system is obscure to define. Therefore the term $D/\Delta x$ has been replaced by $k(C_R/C_{e0}) (1-\bar{C}_i/C_R)^q$. Since the term $(C_R/C_{e0}) (1-\bar{C}_i/C_R)^q$ is another driving force in this type of separation system, it may be reasonable to consider in describing the rate of mass transfer. When a reactant is present in the internal phase and the reaction with the extracted species is instantaneously fast, the term C can be reduced to C_e , and hence equation (1) is rearranged to give

$$J = kC_e(C_R/C_{e0}) (1-\bar{C}_i/C_R)^q \quad (2)$$

If we plot $\ln(-1/KC_e \cdot dC_e/dt)$ vs. $\ln(1-\bar{C}_i/C_R)$, where $K = (3k/R) (V_1/V_e) (C_R/C_{e0})$, we can obtain the value of q from the slope of the line. The value of k can be determined by the curve fitting method.

In a batch extractor, the change of solute concentration in the external phase can be described as follows:

$$-V_e \frac{dC_e}{dt} = \left(\frac{3V_d}{4\pi R^3} \right) (4\pi R^2) (J) \quad (3)$$

where the group $(3V_d/4\pi R^3)$ represents the number of emulsion drops in the system when it is assumed that the size of the drops is uniform. Equation (3) can be rewritten by substituting equation (2).

$$-\frac{dC_e}{dt} = \left(\frac{3k}{R} \frac{C_e}{C_{e0}} \right) \left(\frac{V_d}{V_e} \right) \left(\frac{C_R}{C_{e0}} \right) \left(1 - \frac{\bar{C}_i}{C_R} \right)^q \quad (4)$$

$C_e = C_{e0} \quad (t = 0)$

3. NUMERICAL MODEL

Behaviors of the liquid membrane process is significantly different to those of the conventional extraction processes because of the properties of emulsion as described in the assumptions. The most important thing is that a single emulsion drop can be treated as an aggregate of macro-fluid without coalescence and redispersion, and hence each drop has different residence time in every stage of a separation column. Thus each of the emulsion drops must be independently sought for the behavior during its lifetime inside the column.

3.1 Material balance

The material balance for a solute in n th stage is as follows:

$$v_c(1+f) x_{n-1} + v_c f x_{n+1} + v_d y_{n+1} = v_c(1+2f) x_n + v_d y_n \quad (5)$$

The boundary conditions for equation (5) are given by

$$\left. \begin{aligned} (1+f) x_0 &= x_f + f x_1 \\ y_0 &= y_1 \end{aligned} \right\} (n=0) \quad (6)$$

$$\left. \begin{aligned} x_N &= x_{N+1} \\ y_f &= y_{N+1} \end{aligned} \right\} (n=N+1) \quad (7)$$

From equations (6&7), equation(5) can be rearranged by deviding the terms according to x and y .

$$\left. \begin{aligned} v_c x_f - v_c(1+f) x_1 + v_c f x_2 &= v_d y_1 & (n=1) \\ v_c(1+f) x_{n-1} - v_c(1+2f) x_n + v_c f x_{n+1} &= v_d y_n & (n=2:N-1) \\ v_c(1+f) x_{N-1} - v_c(1+f) x_N &= v_d y_N & (n=N) \end{aligned} \right\} (8)$$

where

$$Y_n = y_n - y_{n+1} \quad (n=1:N) \quad (9)$$

Since each of the emulsion drops dispersed in the continuous phase is different in residence time, the amount of solute transferred into the emulsion phase must be calculated by summing the amount for each drop as follows :

$$Y_n = \frac{4\pi R^2}{V_d} \sum_{k=1}^P \left(\int_0^{\tau_i} j_{nk} dt \right) E_k \Delta t \quad (10)$$

where τ_i is the mean residence time of the drops belong to a group i . A major technique of calculating this is the Monte-Carlo method : the method is to sample a set of drops of which number is P by selecting them at random and assigning a group number to each drop according to the corresponding random number. Once the group number is fixed, then i can be automatically determined as shown in Fig.1.

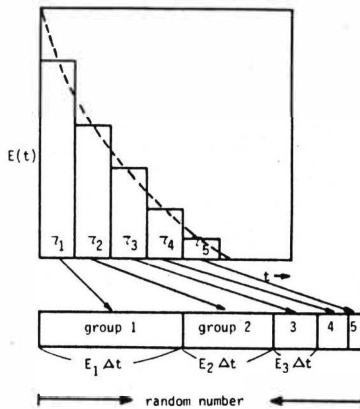


Fig.1. Grouping of emulsion drops with random numbers

3.2 Flow chart for calculation

The flow chart for simulation of the separation process is illustrated in Fig.2. An iterative trial and error procedure is used in this calculation. The aniline concentration in the last stage is guessed and then $Y(N)$ is calculated by equation (10). Once the value of $Y(N)$ is known, $x(N-1)$ can be obtained and plugged into equation(10) again in order to calculate $Y(N-1)$. This procedure is repeated stage by stage to the first stage. Finally if x_f converges to the value of C_{ef} , it will be satisfied. If not, however, a new guess of $x(N)$ is made and the whole process is repeated until the iteration converges to the right value.

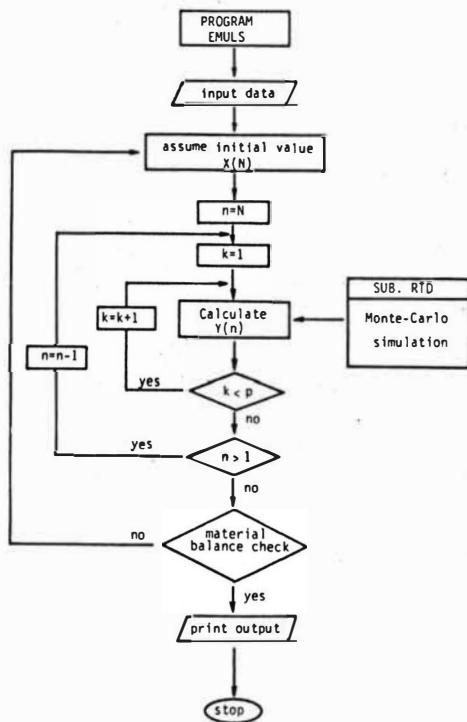


Fig.2. Flow chart of the numerical model

4. FLOW PATTERNS

4.1 Continuous Phase

The stagewise backmixing model (2) was used to represent the flow pattern of the continuous phase. The age distribution curves were obtained by the impulse-response technique.

As a tracer, KCl solution (0.2M) was used and the conductivity of the output solution was continuously checked and recorded. The value of backmixing coefficient f was determined by the following equation which was derived using the moment matching method.

$$\frac{\sigma_N^2}{\tau^2} = \frac{1+2f+2f^2}{N} - \frac{2f+2f^2}{N^2} \quad (11)$$

4.2 Dispersed Phase

Since the movement of the emulsion drops back to a lower stage was not found in normal operation, the gamma distribution model, which is one of the mathematical distribution models, was used for expressing the flow behavior of the emulsion phase. A mathematical description of the gamma distribution model(3) is given by

$$E(t) = \frac{(g)^g}{(\tau - \tau_p)^g \Gamma(g)} (t - \tau_p)^{g-1} e^{-\frac{g(t - \tau_p)}{\tau - \tau_p}} \quad (12)$$

where

$$r(g) = \int_0^{\infty} (t)^{g-1} e^{-t} dt \quad (13)$$

τ_p is the dead time of a given system. The value of g , which is related to the intensity of axial dispersion, was determined by the following equation which was derived from equation (12).

$$g = \tau^2 / \sigma^2 \quad (14)$$

Equation (12) is the age distribution function for the whole stages. However, in the numerical model, the age distribution for a single stage will be needed and it can be derived from equation (14) as follows :

$$E'(t) = \frac{(g')^{g'}}{(\tau' - \tau_p')^{g'} \Gamma(g')} (t - \tau_p')^{g'-1} e^{-\frac{g'(t - \tau_p')}{\tau' - \tau_p'}} \quad (15)$$

where $g' = g/N$, $\tau' = \tau/N$ and $\tau_p' = \tau_p/N$

5. EXPERIMENTAL WORK AND RESULTS

5.1 Emulsion Formulation

W/O emulsions were prepared by adding an appropriate amount of internal solution dropwise to the mineral oil containing 2-3% by weight of SPAN 80 with vigorous stirring.

5.2 Drop Size

The size of the emulsion drops were measured by a photographic method, and the Sauter mean diameter was calculated as the size of uniform drops. In table 1, the Sauter mean diameters were given at the various agitation speeds.

Table 1. Mean drop sizes with agitation speeds

agitation speed (rpm)	mean diameter (mm)	surface area (mm ²)	volume (mm ³)
200	0.99	3.1	0.51
220	0.85	2.3	0.33
240	0.76	1.8	0.23

5.3 Batch Extraction

A batch-type vessel with a marine-type impeller was used for extraction. Four intermediate baffles were equipped between the wall and center of the vessel in order to prevent the emulsion phase from remaining at the surface of solution as a layer. The emulsion was added in the external phase without containing aniline under the agitation speed of 200-300 rpm and then concentrated aniline solution was poured instantaneously. The continuous phase was sampled periodically for analysis. The concentration of aniline was measured using a UV-VIS spectrophotometer (HITACHI MODEL 100-60). The comparison of the experimental and predicted results for the external aniline concentration vs. time is shown in Fig.3. The values of q and k were found to be 1.0 and 6.4×10^{-3} respectively. The value of k was estimated by the curve fitting method.

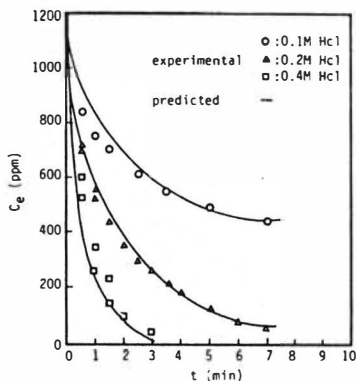


Fig.3. Comparison of predicted and experimental results for batch extraction of aniline; $V_i/V_d = 0.5$, $V_e/V_d = 5.6$, span 80=2 wt%, $D_m = 0.1$ cm

5.4 Extraction Column

A twelve-stage continuous separation column was used in this work. This equipment was made by modifying the conventional impeller-type extraction columns in such a way that the viscous emulsion phase can move up easily without sticking to the plates. The doughnut-type rings, each of which has tapered interior, were equipped instead of the perforated plates. This type of the rings has a great effect on diminishing the sticking trend of the emulsion drops when they reach under a flat board. Stirring was carried out using turbine impellers with four flat blades connected with a speed controller.

5.5 Flow Patterns

For the continuous phase, the values of f was significantly affected by the agitation speed. However, the flow rates of the continuous and dispersed phases had little influence on the backmixing. The average values of f with the change of agitation speed were given in Table 2.

Table 2. Effect of agitation speed on the backmixing coefficient

agitation speed (rpm)	f
150	0.4
200	0.7
250	1.0
300	1.3

On the other hand, the age distribution for the dispersed phase was investigated using the step-response technique. As a tracer, small quantity of xylenol orange was added in the internal phase so as to be 0.1% solution. This tracer-containing emulsion was supplied at the lowest stage of the column by a step change during steady operation and then the mixed phase (emulsion and water) was taken periodically at the highest stage. An automatic sampler (IS MODEL 328) was used for sampling.

In order to break the emulsion of the sample solution, 1 ml of xylene and 10 ml of buffer solution (PH 13) were added and left for a day. Because the internal phase containing xylenol orange is miscible with the aqueous continuous phase, A series of color intensities of the samples indicates the response. The intensity of reddish purple color was measured by colorimetric technique. The value of g was found to be 3.2 and the influence of both flow rates of the continuous and dispersed phases as well as the agitation speed were negligible under the operating conditions taken in this experiment.

5.6 Continuous Operation of the Column and Results

The emulsion formulation conditions were same in both cases of batch and continuous extractions. However the sizes of the emulsion drops were measured separately because the mixing condition in the extraction column is not exactly same as that in the batch extractor. The continuous phase was sampled at several stages during the steady operation. The concentration of aniline was measured using the UV spectrophotometer as carried out in the batch extraction. The predicted results obtained by the computer simulations and experimental results were compared in Fig.4 and Fig. 5. They were found to be in fairly good agreement, which implies that the present model can be utilized for predicting the behaviors of this type of membrane extraction column.

As shown in Fig.4, the mass transfer rate is enhanced with increase of the HCl concentration in the internal phase of the emulsion, which will be due to the high value of C_R in equation (2). Fig. 5 is illustrating the result for the change of emulsion flow rate. As the emulsion flow rate is increased, the rate of mass transfer is also increased. This result is showing a similar trend as that for the change of HCl concentration in the internal phase, which will be due to the greater trapping ability of aniline in both cases.

6. CONCLUSION

A numerical model for simulation of steady-state operation of a separation column in liquid surfactant membrane process was presented. This model was based on the properties of emulsion, the flow patterns of both continuous and dispersed phases together with the mass transfer kinetics for a single emulsion drop. The experimental and analytical studies were also performed to describe the extraction rate in the aniline extraction system and flow patterns of both phases. Consequently, the validity of the present model was verified by comparing the predicted results with the experimental results.

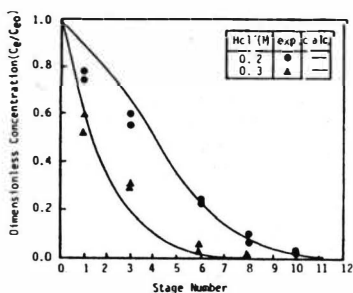


Fig.4. Comparison of experimental and calculated results for steady-state concentration profiles; effect of internal reactant concentration

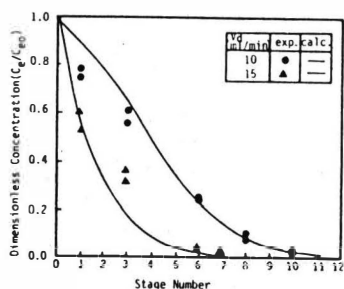


Fig.5. Comparison of experimental and calculated results for steady-state concentration profiles; effect of emulsion flow rate

7. NOMENCLATURE

C = concentration of solute (mol/cm^3)
 C_j = mean conc. of solute in the intergal phase (mol/cm^3)
 C_R = initial conc. of reactant (mol/cm^3)
 D = diffusion coefficient (cm^2/sec)
 d = diameter of drop (cm)
 $E(t)$ = age distribution fnc. for single stage (sec^{-1})
 $E(t)$ = age distribution fnc. (sec^{-1})
 f = backmixing coefficient
 J = mass flux ($\text{mol}/\text{cm}^2 \text{ sec}$)
 k = a coefficient related to mass transfer (cm/sec)
 n = number of stages
 R = radius of drop
 t = time (sec)
 v = flow rate (cm^3/sec)
 τ = mean residence time (sec)
 V = volume (cm^3)

x = solute conc. in the continuous phase (mol/cm^3)
 y = solute conc. in the dispersed phase (mol/cm^3)

(Subscripts)

c = continuous phase
 d = dispersed phase
 e = external phase
 f = feed
 m = mean
 o = initial value
 n = stage number
 σ^2 = variance (sec^2)
 D = dead time (sec)

8. REFERENCES

- (1) R.P.Cahn and N.N.Li, Sep. Sci., 9, 505 (1974)
- (2) J.C.Mecklenburgh and S.Hartland, "The Theory of Backmixing", John Wiley and Sons (1974)
- (3) C.Y.Wen, L.T.Fan, "Models for Flow Systems and Chemical Reactors", Marcel Dekker, Inc., New York (1975)

Pertraction of Ammonia from Waste Waters

Štefan Schlosser and Elemír Kossaczký

Department of Chemical Engineering, Slovak Technical University,
Kollárovo nám.9, 81237 Bratislava, Czechoslovakia

Pertraction through liquid membranes is a promising process which is suitable especially for recovery of solutes with lower concentration. Mechanism of pertraction is discussed in papers [1,2].

The recovery of ammonia by solvent extraction is economically unrealistic because of low values of distribution coefficient of ammonia in common solvents which are from 0.01 to 0.03. Ion-exchange is disadvantageous for solutions with higher concentration of other electrolytes. Steam stripping is a much heat consuming process. Pertraction can be an alternative process. Downs and Li [3] published the results of an extensive research devoted to the removal of ammonia from municipal waste waters. Ammonia was pertracted into an emulsion of 20 % H_2SO_4 from a feed containing 4 g/l ammonia. The yield of 97.7 % was reached at residence time of 30 min. The continual laboratory equipment used consisted of two stirred columns with co-current flow of phases. Pertraction is cheaper in comparison with tertial biological denitrification [3].

The aim of the present work was to test additives of the membrane phase which increase the rate of pertraction of ammonia.

Theory

In modelling batch pertraction the back transport of permeante from the emulsion due to its breaking during pertraction was taken into account. The braking of stable emulsions can be described by equation

$$\Theta = (V_{Ro} - V_R) / V_{Ro} = \gamma \tau_p \quad /1/$$

In pertraction of weak acids or bases these are transported through the membrane without carrier only in a molecular form. The influence of swelling of emulsion on mass-transfer was neglected. Combining flux equation, mass balance, equilibrium of permeante dissociation and eqn/1/ one gets differential equation [5,6]

$$(V_{Fo} + \gamma \tau_p V_{Ro}) \frac{dC_F}{d\tau_p} + \left[\frac{K_{A_E}}{1 + (K_b/K_w) 10^{-pH_F}} + \gamma (V_{Fo} + V_{Ro}) \right] C_F - \gamma V_{Fo} C_{Fo} = 0 \quad /2/$$

Function pH_F / τ_p was described by empirical equation. It is preferable to estimate the value of γ independently and by numerical solution of eqn/2/ determine only the parameter K_{A_E} .

Kinetics of coalescence of droplets in the emulsion is closely related to the number and size of droplets. The estimation of these values, however, is difficult. In paper [7] is given a relation for the description of the breaking of the emulsion in an electric field:

$$V_{Rc} = V_{RM} [1 - \exp(-v\zeta_D)] \quad /3/$$

Exponent v is a normalized initial rate of the breaking of emulsion.

Experimental

In the factory producing fertilizers are more sources of waste waters containing ammonia. A typical composition of one of these waters is following: 1.6 g/l NH_4^+ , salinity 5 g/l and pH = 10.2. Second type of waters are condensing ones with minimal salinity and with the content of NH_3 about 0.4 g/l. The pertraction rate increases with an increase of the content of salts in water [4]. With respect to this fact, the experiments were carried out with a solution of NH_4OH in distilled water with an addition of 0.001 mol/l NaOH. In case of pertraction into emulsion stabilized by SPAN 80, the feed contained 0.2 mol/l NaCl in order to suppress the swelling of the emulsion.

The membrane phase was composed of n-alkanes, a surfactant and in some cases of an additive. The fraction of n-alkanes $\text{C}_{10}-\text{C}_{13}$ has at 25 °C the density and dynamic viscosity 743 kg/m³ and $1.66 \cdot 10^{-6}$ m²/s, respectively. For stabilization of the emulsion sorbitan monooleate, SPAN 80 or the mixture of 97 vol.% SPAN 80 and 3 vol.% Tween 80 /an ethoxylated sorbitan monooleate both produced by ATLAS Chem.Ind./ were used. Further, a polyamine emulsifier ECA 4360 / according to the producer Exxon Chem.Corp. a solution of 50 wt.% of polyamine in oil/ was utilized. Two samples of polyamine, marked as I and II, were used. Hydroxyoxime LIX 64N /Henkel Corp./ or a new additive AFS were used as additives of the membrane phase. The stripping solution in the emulsion was H_3PO_4 1 mol/l.

The continual pertraction was carried out in a 4-stage cascade of mixers with a settler at the end. The working volume of one mixer of 8 x 8 cm cross-section was 409 cm³. Four blade turbines 4 cm in diameter served as stirrers. Water and emulsion were fed to the bottom of the first mixer. The dispersion overflowed the separation wall to the second mixer etc. The dispersion from the fourth mixer passed through a hole at the bottom to the settler of volume 800 cm³. Batch pertractions were conducted in one mixer of the cascade.

The emulsion was prepared by means of a high-speed two-blade stirrer with diameter of 4 cm which rotated in a stator ring with radial slots in it. Conditions of emulgation and pertraction are given in Table 1.

Table 1. Conditions in emulgation and in pertraction, if not otherwise stated.

Surfactant	Emulgation	Pertraction
	H_3PO_4 , 1 mol/l	$pH_{Fo} = 11$
SPAN 80 or SPAN 80 + Tween 80 1.5 vol.%	$n_e = 3500 \text{ min}^{-1}$ $\phi_{Ro} = 0.50$	$n_p = 210 \text{ min}^{-1}$ ϕ_{Eo} or $\varphi_{Eo} = 0.10$ 0.2 mol/l NaCl in feed
ECA 4360	$n_e = 6500 \text{ min}^{-1}$ $\phi_{Ro} = 0.33$	$n_p = 300 \text{ min}^{-1}$ ϕ_{Eo} or $\varphi_{Eo} = 0.14$

The emulsion was broken in an alternating electric field with high voltage /15 kV/. The electrode, insulated by PVC, was located in the centre and the second one was on the outer circumference of a glass cylindrical vessel with diameter of 4 cm.

Concentrations of ammonia and phosphates were determined spectrophotometrically. Coalesced ratio was calculated from mass balance of PO_4^{3-} anion assuming that it enters raffinate only due to emulsion breaking. The magnitude of emulsion globules and droplets in it was estimated from photographs. Apparent dynamic viscosity of the emulsion was measured by a rotary viscosimeter. The interfacial tension was measured by the drop volume method.

Results and Discussion

Influence of surfactant. Addition of a small amount of Tween 80 into membrane phase significantly increased the rate of pertraction of ammonia, see Fig.5. Emulsions stabilized by SPAN 80 or its blend significantly swell. By using polyamine emulsifier the swelling of the emulsion was substantially suppressed, see Fig.2 and Table 3. The rate of pertraction and values KA_E and K in Table 2, however, also decreased significantly, see Fig.1. Surfactants used increase the value of the distribution coefficient of ammonia, see Table 3. The rate of the breaking of the emulsion in ac electric field decreased as much as by two orders of magnitude, see Fig.7 and Table 5. Likewise the breaking of the emulsion during pertraction significantly slowed down /the decrease of the value of γ /, see Table 2. From this one can consider a change of the structure of the adsorption film on interfaces. The lipophilic chain of SPAN 80 is formed by oleoyl / C_{17} / group with a double bond in the middle. In polyamine ECA 4360 there is a lipophilic polyisobutylene chain which contains about 24 carbons in

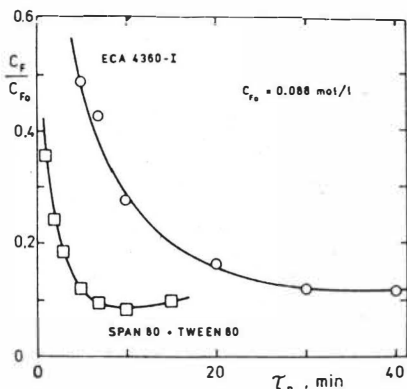


Fig.1. Influence of surfactant on batch pertraction of ammonia. Conditions for ECA 4360-I are given under Fig.2.

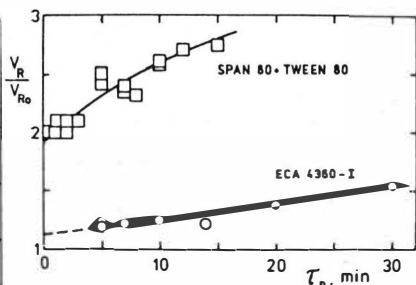


Fig.2. Influence of surfactant on swelling of emulsion. Conditions for ECA 4360-I:
 $\phi_{R_0} = 0.50$ $\phi_{E_0} = 0.10$
 $n_e = 5000 \text{ min}^{-1}$ $n_p = 400 \text{ min}^{-1}$
 $X_S = 0.04$

the main chain. With respect to the double bond SPAN 80 forms more expanded films [8] which have a smaller resistance against mass-transfer than the condensed film from the saturated straight chains in polyamine. This opinion is supported also by measurements of pertraction of cobalt through flat interface [11,12]. By the addition of polyamine instead of SPAN 80 into the bulk membrane, the rate of transport of cobalt significantly decreased [12].

Influence of additive. By the addition of LIX 64N or additive AFS into the membrane phase, pertraction of ammonia was significantly accelerated, see Fig.3,4,6 and Table 2. By the addition of 5 wt.% LIX 64N or 1 wt.% AFS into the solution of 4 wt.% ECA 4360-I in n-alkanes the interfacial tension with an aqueous solution containing 0.09 mol/l NH_3 decreased from 27.66 to 20.87 g.s^{-1} or 26.16 g.s^{-1} , respectively. Hence, both additives are adsorbed on the interface. HLB of LIX 64N is 1.53 [9]. The lipophilic chain of LIX 64N and AFS is formed by nonyl chain and polypropylene chain with about five carbons in the main chain, respectively. In mixed films with a different length of chains the distance between the molecules in the film is enlarged due to an increased mobility of fragments of longer chain which are above the height of the adjoined molecules [10]. In this way the rigidity of film as well as its resistance against mass-transfer are decreased. This is confirmed also by an increase of the rate of the breaking of the emulsion in electric field, see Fig.7 and Table 5. The advantage of additive AFS in comparison with LIX 64N is that the first one less decreases the stability of the emulsion during pertraction, see

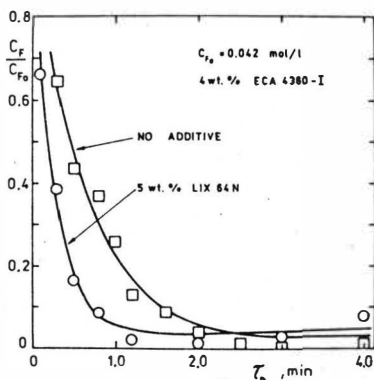


Fig.3. Influence of additive LIX 64N on batch pertraction. Lines are correlated by eqn/2/.

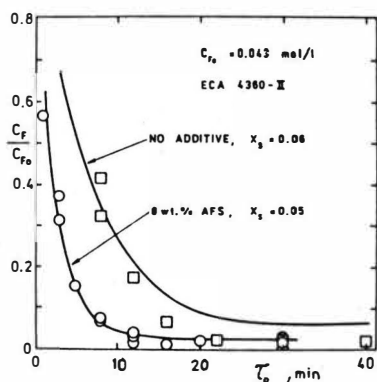


Fig.4. Influence of additive AFS on batch pertraction. Lines are correlated by eqn/2/.

Table 2. Properties of the emulsion and parameters of model eqn/2/

X_S	Additive	X_A	μ_E mPas	d_d μm	$C_{F0} \cdot 10^3$ mol/l	$^{++}d_E$ mm	$\gamma \cdot 10^6$ s^{-1}	$KA_E \cdot 10^7$ m^3/s	$K \cdot 10^6$ m/s
0.015 vol.% SPAN 80 + Tween 80									
	-	-	10.72	1	89.6	0.25	548.2 ^x	59.8	6.09
ECA 4360-I									
0.04	-	-			87.8 ^a		36.77 ^x	7.88	
"	-	-	5.74	4.59	87.3	0.867	9.08	6.02	1.52
"	LIX64N	0.05	5.83	3.75	"	0.744	9.48	10.08	2.18
"	"	"			42.3		10.06	21.38	
"	-	-			41.5		5.72	8.77	
ECA 4360-II									
0.06	-	-	5.96		43.1		1.97	7.93	
"	LIX64N	0.04			42.9		16.00	20.13	
"	"	0.05	7.07	2.68	43.0		15.02	21.28	
0.07	"	0.04	6.82	2.51	42.9		11.37	20.59	
0.05	AFS	0.04	6.21	"	"		2.85	17.61	
"	"	0.08	7.49	2.31	"	0.761	2.74	24.10	5.34

⁺ Values at the shear rate 720 s^{-1}

⁺⁺ Value for $\tau_p = 4 \text{ min}$

^a Conditions given under Fig.2

^x Estimated by correlation with model eqn/2/

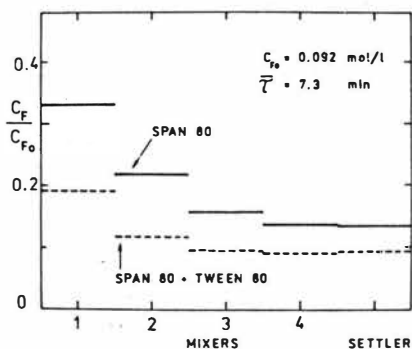


Fig. 5. Influence of surfactant on continual pertraction of ammonia from aqueous solution with 0.2 mol/l NaCl.

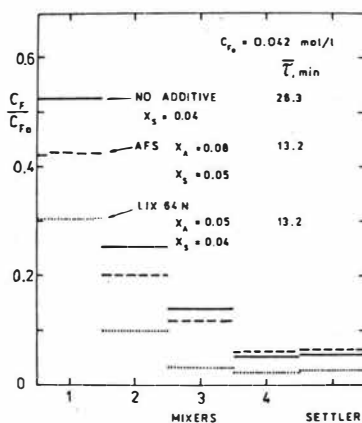


Fig. 6. Influence of additive on continual pertraction of ammonia. ECA 4360-I, with AFS ECA 4360-II.

Table 3. Swelling of the emulsion and its breaking in continual pertraction. Refer to Fig. 5 and 6.

Surfactant	Additive	$\bar{\tau}$ min	$\frac{V_R}{V_{R0}}$	PO_4^{3-} in raffinate mg/l	$\odot \cdot 10^2$
SPAN 80	-	7.3	2.27 ⁺		
SPAN 80 + Tween 80	-	7.3	2.40 ⁺		
ECA 4360-I	-	26.3	1.08	63.1	1.23
"	LIX64N	13.2	1.34	26.9	0.53
ECA 4360-II	AFS	13.2	1.14	12.5	0.24

⁺ 0.2 mol/l NaCl in the feed

Table 2 and 3. It seems that also the swelling of the emulsion with AFS will be smaller, see Table 3.

Conclusions

The resistance of the adsorption film on interfaces has a significant influence on the rate of pertraction of ammonia. Suitable additives of the membrane phase which substantially accelerate the pertraction were found. They enable to shorten the mean residence time in the cascade of mixers as much as 50 %.

Table 4. Influence of surfactant and additive on the distribution coefficient of ammonia in system water-n-alkanes at 25°C.

Surfactant	Additive	pH _F [*]	C _F [*] .10 ³	m
No	No	10.47	87.41	0.011
		10.52	45.83	0.027
SPAN 80, 1.5 vol.%	-	10.33	71.64 ⁺	0.0383
SPAN 80+Tween 80, 1.5 vol.%	-	10.05	67.85 ⁺	0.0510
ECA 4360-I, 4 wt.%	-	10.71	74.68	0.0268
"	5wt.% LIX64N	10.56	67.24	0.0542
ECA 4360-II, 5 wt.%	8wt.% AFS	10.68	75.33	0.0485

⁺ 0.2 mol/l NaCl in the aqueous phase

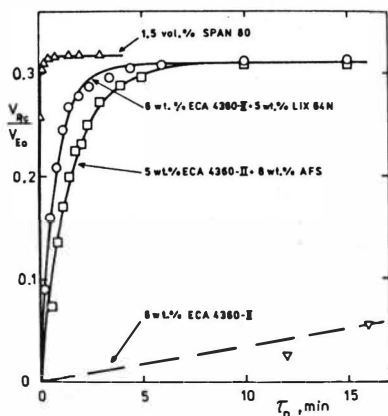


Fig. 7. Kinetics of the breaking of emulsions in an electric field. Lines are correlated by eqn/3/
 $\phi_{Ro} = 0.33$ $U = 15$ kV

Table 5. Influence of surfactant and additive on the initial rate of the breaking of the emulsion in the electric field. Refer to Fig. 7.
 $\phi_{Ro} = 0.33$; $U = 15$ kV

Surfactant	Additive	n _e min ⁻¹	v.10 ³ s ⁻¹
SPAN 80	-	3500	278.0
SPAN 80 + Tween 80	-	3500	15.8
ECA4360-II	-	6500	0.17
"	LIX64N	"	20.4
"	AFS	"	10.9

Notation

A_E surface area of globules, m²
 C overall concentration of permeante, kmol m⁻³
 d_d Sauter mean diameter of droplets in emulsion, μm
 d_E Sauter mean diameter of emulsion globules, μm

V_{RM} maximum volume of coalesced solution, m³
 V̇ volume flow rate, m³s⁻¹
 X_A weight fraction of additive, -
 X_S weight fraction of surfactant, -

K	overall mass-transfer coefficient, $m s^{-1}$	γ	coefficient of coalescence, eqn/l/, s^{-1}
K_b	dissociation constant of permeant	Θ	coalesced ratio, eqn/l/
K_w	ionic product of water	μ_E	apparent dynamic viscosity of emulsion, Pas
m	distribution coefficient	τ_D	time of deemulgation, s
n_e	frequency of emulgator stirrer, min^{-1}	τ_P	time of pertraction, s
n_p	frequency of pertractor stirrer, min^{-1}	$\bar{\tau}$	mean residence time in cascade of mixers, s
v	initial rate of emulsion breaking, eqn/3/, s^{-1}	γ_{Eo}	volume ratio defined as $\dot{V}_{Eo}/(\dot{V}_{Fo} + \dot{V}_{Eo})$, -
V	volume, m^3	ϕ_E	volume fraction of emulsion in pertractor
V_{Rc}	volume of coalesced stripping solution in deemulsifier, cm^3	ϕ_R	volume fraction of stripping solution in emulsion

Indices

F	aqueous phase	o	at the beginning of pertraction; input
R	stripping solution		
*	in equilibrium		

References

1. R.Marr und A.Kopp, Chem.Eng.Tech.,50/1980/399.
2. Š.Schlosser end E.Kossaczky, submitted for publication in J.Nuclear Redioanalyt.Chem.
3. H.H.Downs and N.N.Li, J.Separ.Proc.Technol.,2/1981/19.
4. Š.Schlosser und E.Kosseczky, Pertrektion von Amoniek, Depot-system 13/83, Chem.Technik,35/1983/373.
5. Š.Schlosser, V.Porubenský and E.Kosseczky, Pertraction of ammonia, paper No.C3.3, 8th Congress CHISA'84, Praha, Sept.1984.
6. Š.Schlosser and E.Kossaczky, Pertraction of ammonia / in Slovak/, Proc. 12th Conf.OSCHI, p.309, Štiavnické Bane, May 1985.
7. Š.Schlosser, E.Kossaczky and M.Kapecová, Breaking of W/O emulsions in electric field /in Slovak/, Proc. 13th Conf.OSCHI, Štiavnické Bane, May 1986.
8. D.O.Shah and J.H.Schulman, J.Colloid Interface Sci., 25/1967/107.
9. J.Szymanowski, M.Cox and C.G.Hirons, J.Chem.Tech.Biotechnol., 34A /1984/218.
10. M.K.Sharma, S.Y.Shiao, V.K.Bansal and D.O.Shah, in: Macro- and Microemulsions, ACS Symp.Ser., No272/1985/87.
11. J.Strzelbicky and W.Charewicz, Hydrometalurgy, 13/1984/89.
12. Š.Schlosser, J.Strzelbicky and W.Charewicz, unpubl. results /1985/

Scaleup and Performance of 5 Ft. (1.52 m) Diameter Reciprocating Plate Extraction Column

A. E. Karr, S. Ramanujam, Chem-Pro, Parsippany, NJ/USA

The waste water from a coke oven plant at the LTV Steel Flat Rolled and Bar Company contained 400 to 1100 ppm phenol. The average waste water rate was 350 gpm (79.5 m³/Hr.). Environmental considerations dictated the necessity of reducing the phenol content to 1 ppm or less. Liquid-liquid extraction was selected as the optimum procedure for effecting this reduction. The feed to the extraction unit was to come from a free ammonia stripping column and had a pH of approximately 9.0. Since the feed was available at a temperature of 105°C it was decided to operate the extraction column at that temperature for purposes of heat economy.

Planning the Pilot Scale Tests

Methylisobutyl ketone (MIBK) was selected as the solvent. This was based on several references and our own experience indicating that MIBK is an excellent and economical solvent for this extraction (1-4). MIBK is the solvent employed in the Chem-Pro dephenolization process, licensed from the Jones & Laughlin Steel Corp.

Preliminary calculations indicated that the production column would have to be approximately 1.5 m in diameter. Therefore in order to stay with a 30:1 scaleup of diameter, which was known to be possible based on previous experience (5), a nominal 50 mm diameter Reciprocating Plate Extraction Column was selected for the test unit. In order to estimate the height of column required in the test unit calculations were made assuming the test column would have 6 to 7 theoretical stages. Based on previous experience the plate stack height selected was 3.66 m (12 Ft.) and the solvent to aqueous feed ratio selected was 1:15 on a weight basis or 1:12 on a volume basis.

Pilot Scale Operation

Tests were conducted in a 52 mm diameter column. The column was constructed of type 316 stainless steel and the design pressure was 10 atm. A Dover seal, which is employed in reciprocating compressors, was used as the seal at the top of the column. The upper 0.61 m of the plate stack had 101.6 mm plate spacing and the remaining 3.05 m of the plate stack had 76.2 mm plate spacing. The plates had 13.5 mm diameter holes or partial holes and the open area was 61%. The upper disengaging section was 52 mm in diameter but the lower disengaging section was 100 mm in diameter. The disengaging chambers were fitted with sight glasses. The operating pressure was two atm., maintained by nitrogen pressure at the top of the column. The interface was control-

led in the top disengaging section by a D/P cell.

As previously indicated the pilot scale column should be optimized with respect to plate spacing and volumetric efficiency (5,6). The plate spacing selected was based on variations in physical properties and previous experience with a similar system. Total throughputs of 40.7, 53.0, and 61.1 m³/m²(hr.) were tested. The temperature of the feed, solvent, and column were maintained at 105°C. The solvent was "doped" with 5 ppm phenol to simulate expected operation in the solvent recovery section of the plant. The concentration of phenol in the feed was 440 ppm. The analysis was done by the 4-aminoantipyrine colorimetric method.

In Fig. 1 the concentration of phenol in the raffinate is plotted against the speed of reciprocation. As shown the specification of 1 ppm in the raffinate was just about achieved at total flow rates of 40.7 and 53.0 m³/m²(hr.) but could not be achieved at 61.1 m³/m²(hr.).

The data used for calculating the number of theoretical stages under optimum operating conditions in the 52 mm were as follows:

operating temperature = 105°C
distribution coefficient = 34 on a weight ratio basis
ppm phenol in feed = 440
ppm phenol in raffinate = 1
ppm phenol in entering solvent = 5
weight ratio of solvent to feed = 1/15

Employing the above values the number of theoretical stages was calculated to be 6.61.

$$\text{Therefore HETS} = \frac{3.66}{6.61} = 0.554 \text{ m}$$

Design of Production Unit

The requirement for the production unit was to process 350 gpm of waste water having a phenol content of 700 ppm and produce a raffinate with a maximum of 1 ppm phenol. In addition the column should be capable of processing 425 gpm of feed and produce a raffinate with a maximum of 2 ppm phenol. Based on these requirements a 1.52 m diameter column was selected. At feed rates of 350 gpm and 425 gpm the total specific throughput was 47.23 and 57.33 m³/m²(hr.) respectively.

The scaleup procedure has been described previously (5,7). When scaling up from 52 mm to 1.52 m the calculated HETS of the production column would be:

$$\left(\frac{1520}{52}\right)^{0.38} \times 0.554 = 2.00 \text{ m}$$

To reduce the phenol content from 700 ppm to 1 ppm 7.63 theoretical stages are required. Therefore the theoretical height of the production unit is 15.26 m.

However, it was considered prudent to increase the height about 20% for the following reasons:

- (1) The calculated height was based on the very best performance in the 52 mm diameter column. Therefore there would be no room for error or for possible future variations in feed composition, including surface active materials.
- (2) The requirement that 425 gpm be processed and produce a raffinate of no worse than 2 ppm was in an area that was not actually tested. Therefore it was felt that some safety factor was justified.
- (3) The 1.52 m column would be the largest to be built up to that time. Therefore a design factor was justified.

It was decided to employ a plate stack 18.29 m (60 Ft.) long. The plate stack consists of 3.05 m of 101.6 mm spacing and 15.24 m of 76.2 mm spacing. The plates had 14.29 mm holes on 17.46 mm centers and the total open area was 57.3%. Doughnut type baffles having the same open area as the plates were provided periodically in the plate stack to minimize axial mixing. A photograph of the plate stack is shown in Fig. 2 and a photograph of the installation is shown in Fig. 3. The drive for the extraction column can be seen above the top platform. Chem-Pro designed and provided the entire skid mounted unit including the solvent and phenol recovery columns.

Production Column Results

The column was operated at 105°C and 1.7 atm. pressure. Data were obtained at feed rates up to 350 gpm, which corresponds to 47.2 m³/m² (hr.). By interpolating in Fig. 1 the optimum reciprocating speed at 47.2 m³/m² (hr.) would be expected to be approximately 176 strokes per minute in the 52 mm column. The optimum reciprocating speed for the production column is given by the following equation:

$$\frac{SPM_2}{SPM_1} = \left(\frac{D_1}{D_2} \right)^{0.14} \left(\frac{(1-\epsilon)_2^2}{\epsilon_2} \times \frac{\epsilon_1}{(1-\epsilon)_1^2} \right)^{1/3} \quad (5,8)$$

where D = Diameter Column

SPM = Strokes per Minute

ε = Open Area of Perforated Plates

The ratios in the second brackets correct for variations in open area to normalize power per unit volume.

Therefore $SPM_2 = 103$. This calculated value should be close to the optimum.

Runs were made at 350 gpm when the feed contained 640 ppm phenol and the following results were obtained:

SPM	PPM Phenol in Recycle Solvent	Raffinate, ppm Phenol	Number of Theoretical Stages	HETS m
118	2	0.1	11.08	1.65
103	5	0.2	<u>10.78</u>	<u>1.70</u>
		Average	10.93	1.67

At feed flows of around 175 gpm raffinates containing 0.1 to 0.2 ppm phenol were obtained consistently. Thus the turn down is at least 2 to 1 and from prior experience it is probably at least 4 to 1.

Discussion of Results

The HETS increased from 0.554 m in the 52 mm column to 1.67 m in the 1.52 m column. Therefore the exponent, n , in the scaleup equation below is 0.326.

$$\frac{HETS_2}{HETS_1} = \left(\frac{D_2}{D_1} \right)^n$$

Thus the "normal" scaleup procedure, which employs an exponent of 0.38 appears to be somewhat conservative. As previously mentioned some design factor on calculated height was added because of the requirement to design for operation at 425 gpm and for other conservative considerations. In the future less conservatism will be needed for low interfacial tension systems.

Effect of Temperature

Runs were made in a 25 mm diameter column at temperatures ranging from 28 to 70°C. It was found that although the distribution coefficient decreases rapidly with increasing temperature the optimum HETS decreases more rapidly so that the percent phenol removal increases. From 70°C to 105°C the percent removal of phenol is only slightly improved while the distribution coefficient decreases sharply.

Literature Cited

1. Lauer, F. C., E. J. Littlewood, J. J. Butler, Iron and Engineer Reprint based on presentation at Eastern States Blast Furnace and Coke Oven Association Meeting in Pittsburgh, PA, Feb. 14, 1969.
2. Greminger, D. C.; G. P. Burns, S. Lynn, D. N. Hanson and C. J. King, Ind. eng. Chem. Process Des. Dev. 21, 51 (1982).

3. King, D. J., T. A. Barbari, D. K. Joshi, N. E. Bell and J. J. Senetar, National technical Information Service report No. EPA-600/2-84-060a, Feb., 1984.
4. Medzadourian, M. L., L. J. Durlofsky, and T. R. Thomason, Oak Ridge National Laboratory Report MIT-363, "Solvent Extraction for Treating Wastewater", July, 1983.
5. Karr, A. E., Separation Science and Technology 15 (4), 877 (1980).
6. Karr, A. E., A. I. C. H. E. Journal 5 (4), 446 (1959).
7. Karr, A. E., A. I. C. H. E. Journal 31 (4), 690 (1985).
8. Hafez, M. M. and M. H. I. Baird, Trans I Chem E 56 229 (1978).

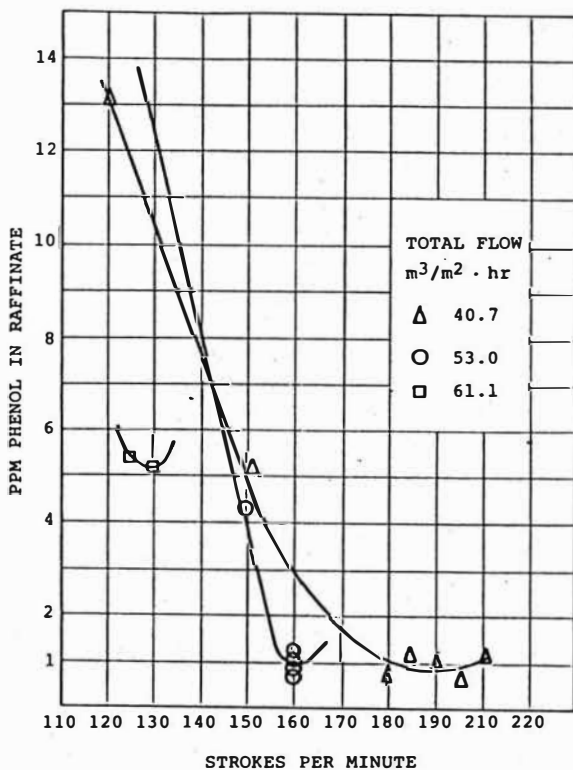


Fig. 1
EFFECT OF RECIPROCATING SPEED ON
52 mm COLUMN PERFORMANCE

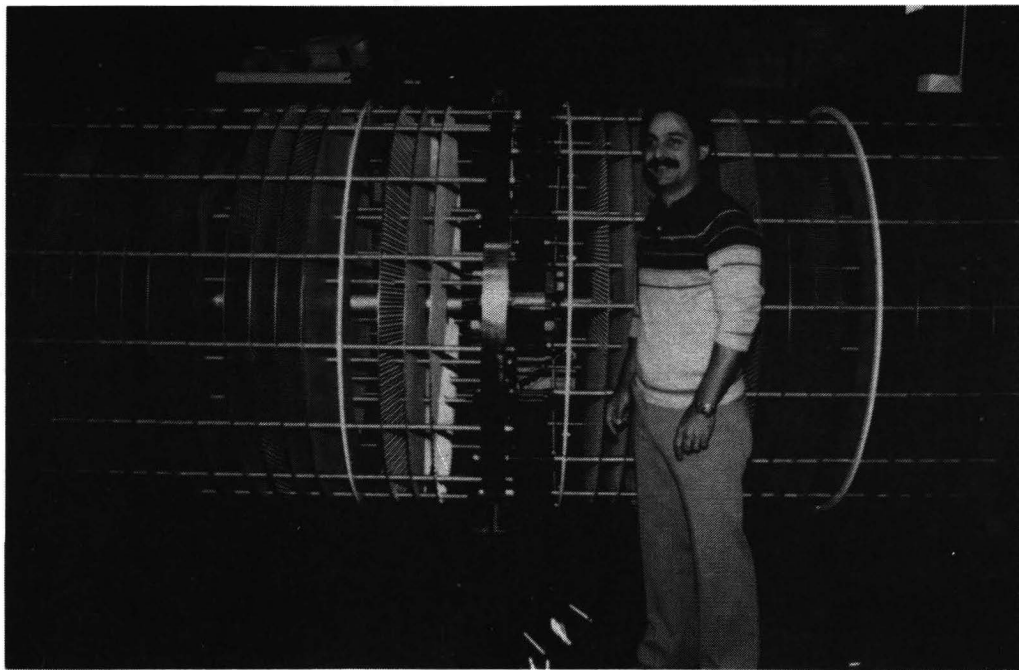


FIG. 2 - PLATE STACK



FIG. 3 - DEPHENOLIZATION UNIT

Author Index

A

Abbruzzese, C., Rome/I	
Afanasjev, A.V., Moscow/USSR	I-593
Afzaletdinova, N.G., Ufa/USSR	II-527
Aguilar, M., Barcelona/E	II-239
Al Khani, A., Toulouse/F	I-151
Al-Bazi, S.J., Tucson, AZ/USA	II-393
Alessi, P., Trieste/I	III-479, III-715
Alper, E. Dharan/Saudi Arabia	III-469
Aly, G., Lund/S	III-815
Aly, H.F., Cairo/ET	II-539
Ammon von, R., Karlsruhe/D	I-223
Angelino, H., Toulouse/F	II-139
Aparcio, J. L., Stockholm/S	I-611, II-239
Aprahamian Jr., E. Tucson, AZ/USA	II-385
Aquilar, M., Barcelona/E	II-165
Arai, K., Sendai/J	III-507
Archambault, D.A., Pinawa, Manitoba/CDN	I-441
Arenson, D. R., Berkeley, CA/USA	III-741
Aufderheide, E., Clausthal-Zellerfeld/D	III-247

B

Baba, Y., Saga/J	II-65, II-263
Bae, K., Syracuse, NY/USA	III-129
Bagreev, V.V., Moscow/USSR	I-499
Bailes, P.J., Bradford/UK	III- 63
Baird, M.H.I., Hamilton, ONT/CDN	I- 41
Balasubramanian, G.R., Kalpakkam/IND	I-413
Baradel, A., Milano/I	II-401
Bart, H.J., Graz/A	I-567, II-643, III-293, III-339, III-907
Bartsch, R.A., Lubbock, TX/USA	I-581
Bassey, E. N., Bradford/UK	III-755
Batey, W., Caithness/UK	I-371
Bathelier, A., Bessines sur Gartempe/F	I-285
Bauer, D., Paris/F	II- 91, II-463, II-503
Baumgärtner, F., Garching/D	I-253, I-293
Bautista, R. G., Nevada-Reno, NV/USA	II-107
Bautz, H., Karlsruhe/D	II-239
Becker, R., Karlsruhe/D	I-239
Beklemishev, M.K., Moscow/USSR	II-559
Bensalem, A. K., Zürich/CH	III- 99, III-191
Berger, R., Ludwigshafen/D	III- 3
Bes, R.S., Toulouse/F	III-239
Beutler, H.J., Krefeld/D	III- 51
Bhaskara Sarma, P.V.R., Bhubabeswar/IND	II-625
Billet, R., Bochum/D	III-115, III-123
Blázquez, J.C., Bilbao/E	III-839
Blaß, E., München/D	III- 11, III-379, III-387, III-445
Bleyl, H.-J., Karlsruhe/D	I-333, I-399
Bliznakovska, B., Skopje/YU	III-481

Boase, D.G., Pinawa, Manitoba/CDN	I-441
Bobirenko, A.Yu. Moscow/USSR	III-831
Bokobza, L., Paris/F	II-131
Bonnet, J.C., Syracuse, NY/USA	III-135
Borchardt, J., Jülich/D	I-325
Bouwmans, I., Delft/NL	III-317
Braun, Chr., Bochum/D	III-123
Braun, G., Frankfurt am Main-Höchst/D	III-799, III-877
Brignole, E.A., Bahia Blanca/RA	I- 63
Brown, T.J., Niagara Falls, ONT/CDN	III-775
Brunette, J.P., Strasbourg/F	II-481
Brunner, G., Hamburg/D	III-783
Bryan, S.A., Oak Ridge, TN/USA	I-477
Bühlmann, U., Allschwil/CH	III-167
Bukin, V.I., Moscow/USSR	I-621, III-621
Bunge, A.L., Golder, CO/USA	I-519
Bunzenberger, G., Graz/A	III-907
Burgard, M., Strasbourg/F	III-919
Byeseda, J.J., Tulsa, OK/USA	II-611

C

Caldentey-Navick, M., Paris/F	II- 91
Campbell, D.O., Oak Ridge, TN/USA	I-301
Carlini, D., Rome/I	I-355
Carnahan, T.G., Reno, NV/USA	I-572
Carvalho de, J.M.R., Lisboa/P	II-295
Casamatta, G., Toulouse/F	I-151, II-139, III-353, III-361
Casarci, M., Rome/I	I-107, I-355
Casas, I., Barcelona/E	II-165
Case, G.N., Oak Ridge, TN/USA	I-477
Chachaty, C., Fontenay-aux-Roses/F	I-267
Chadwick, A.T., Oxon, OX/UK	II-589
Chadwick, R.B., Oak Ridge, TN/USA	I-477
Chaiko, D.J., University Park, PA/USA	II-409
Chao, Shou-bai, Beijing/China	III-437
Charbonnel, M.-C., Fontenay-aux-Roses/F	I-261
Charewicz, W.A., Lubbock, TX/USA	I-581
Chekmercv, A.M., Moscow/USSR	II-195
Chen, Changqing, Beijing/China	II-339
Chen, Chia-yong, Beijing/China	II-447, II-565
Chen, Haijie, Shanghai/China	III-183
Chen, Jiayong, Beijing/China	II-573
Chen, Jinbang, Beijing/China	III-667
Chen, Zhichuan, Changchun/China	II-651
Chen, Zhifu, Changchun, Jilin/China	II-231
Chernysheva, M.F., Kuibyshev/USSR	III-747
Chesné, A., Stains/F	III-739
Chiang, H.W., Pinawa, Manitoba/CDN	III-369
Cichocki, M., Wrocław/PL	III-669
Coello, J., Stockholm/S	II-239
Colussi, I., Trieste/I	II-173, III-199
Cong, Jingyang, Beijing/China	II-605
Cote, G., Paris/F	II-91, II-131, II-463
Cox, M., Hatfield, Herts./UK	I-537

D

Dai, Ge-sheng, Shanghai/China	II-271
Dalton, R.F., Blackeley, Manchester/UK	II- 11
Danesi, P.R., Vienna/ A	I-527, II-255
Danilov, N.A., Moscow/USSR	II-236
Davies, G.R., Saginaw, MI/USA	III-345
Davister, A., Engis/B	I-177
Deák, Gy., Veszprém/H	III-515
Demopoulos, G.P., Montreal, QUE/CDN	II-581
Diantouba, B., Strasbourg/F	II-481
Dichtl, G., Wiesbaden/D	III-723
Ding, Hong-bing, Beijing/China	II-122
Ding, Jian-ping, Guangzhou/China	II-222
Dmitrienko, S.G., Moscow/USSR	II-559
Dobrowsky, B., Zalec, YU	III-639
Dohrn, R., Hamburg/D	III-783
Doyle, F.M., Berkeley, CA/USA	II-99
Draxler, J., Graz/A	I-553
Dupire, S., Louvain-La-Neuve/B	III-613
Dvorak, Z., Praha/CS	III-765

E

Eccles, H., Preston/UK	I- 13
Eiben, K., Leopoldshafen/D	I-317, I-393
Eid, K., Toulouse/F	III-353
Eisele, J.A., Reno, NV/USA	I-572
El-Dessouky, M.M., Cairo/ET	II-539
Eldridge, R.B., Austin, TX/USA	III- 55
Elsässer, K.H., Allschwil/CH	III-167
Elutin, A.V., Moscow/USSR	II-425
Enmrich, G., Essen/D	III-491
Eroglu, E., Ankara/TR	III-847
Ertel, D., Karlsruhe/D	I-399
Evers, H., Leopoldshafen/D	I-393

F

Fair, J.R., Austin/TX/USA	III- 39, III- 55
Fan, Zheng, Beijing/China	III-437
Fatović, I., Zagreb/YU	I-275
Faure, A., Fontenay-aux-Roses/F	I-267
Fei, Weiyang, Beijing/China	III-215
Feng, Hanzhen, Shanghai/China	II-495
Fermiglia, M., Trieste/I	III-715
Fernandez, L. A., Stockholm/S	I-611, II-239, III-863
Feucht, P., Karlsruhe/D	I-317, I-393
Figuerola, E., Barcelona/E	II-165
Fischer, K., Dresden/DDR	I-499
Fitzpatrick, L.M., Melbourne, Vic/AUS	III-175, III-325
Flett, D.S., Stevenage/UK	I- 3, II- 3
Flory, K., Karlsruhe/D	I-309
Fortuin, J.M.H., Amsterdam/NL	III- 31
Fredenslund, A., Lyngby/DK	I- 63
Freiser, H., Tucson, AZ/USA	II-385, II-393
Friehmelt, V., Berlin (West)	I-245
Fröhlich, M., Garching/D	III-301
Frydrych, Ch., Berlin (West)	I-245
Fürst, W., Graz/A	I-553

G

Gähns, H.J., Krefeld/D	III- 51
Gai, Huifa, Shandong/China	II-279
Galla, U., Karlsruhe/D	I-309
Gallo, V., Trieste/I	II-173, III-199, III-255
Gao, Haoqi, Shanghai/China	II-301
Gao, Zili, Shandong/China	II-279, II-287
Gaonkar, A.G., Auburn, AL/USA	II-361
Garcia, D.J., Cartagena/E	II-613
Gasparini, G.M., Rome/I	I-107, I-355
Gauglitz, R., Berlin (West)	I-245
Gaunand, A., Fontainebleau/F	II-511
Geerßen, H., Mainz/D	III-807
Gelfort, E., Hannover/D	I-427
Germain, M., Fontenay-aux-Roses/F	I-137
Geyer, H., Potsdam/DDR	II-537
Gilles, E.D., Stuttgart/D	I-161
Gloe, K., Dresden/DDR	II-537
Goebel, J.C., Amsterdam/NL	III- 31
Goetz-Grandmont, G.J., Strasbourg/F	II-481
Goklen, K.E., Cambridge, MA/USA	III-587
Goldacker, Karlsruhe/D	I-117
Goldmann, G., München/D	III- 11
Golubkov, A.S., Moscow/USSR	III-677
Goswami, A.N., Dehra Dun/IND	III-539
Goto, M., Fukuoka/J	I-573
Gourdon, C., Toulouse/F	III-353, III-361
Grabas, K., Wrocław/PL	I-347
Graham, F.R., Aiken, SC/USA	I-381
Grilc, V., Ljubljana/YU	III-639
Grizo, A., Skopje/YU	III-481
Grosch, A., Bochum/D	III-115
Grossi, Rome/I	I-107, I-355
Grünbein, W., Frankfurt am Main-Höchst/D	III-877
Guerkan, T., Ankara/TR	III-846, III-847
Guerriero, R., Venezia/I	I-585, II-401
Gutknecht, W., Hannover/D	I-601

H

Haberland, K., Leopoldshafen/D	I-317
Hänsel, R., Hannover/D	III-623
Hamburger, E., Karlsruhe/D	I-399
Hamza, A., Garching/D	I-459
Hancil, V., Praha/CS	II-57, III- 81
Harada, M., Kyoto/J	II-309
Harrison, J.W., Harwell, Oxon/UK	I-131
Hartland, S., Zürich/CH	III- 99, III-191, III-309, III-453
Hassan, F.M., Kuwait/State of Kuwait	II-113
Hatton, T.A., Cambridge, MA/USA	III- 89, III-587, III-685
Hauertamnn, H.-B., Hannover/D	I-601
Haydar, F., Kuwait/State of Kuwait	II-113
He, Chunfu, Changchun/China	II-651
Hedden, K., Karlsruhe/D	III-499
Heddur, R.B., Bombay/IND	II-439
Heilgeist, M., Karlsruhe/D	I-309

Heits, B., Hannover/D	I-427
Hemonic, D., Vert-le-Petit/F	II-511
Heng, R., Frankfurt am Main/D	II-613
Hodges, M.E., Aiken, SC/USA	III-421
Hoecker, J., Clausthal-Zellerfeld/D	III-523
Holdich, R.G., Birmingham/UK	II- 19
Holt, D.L., Aiken, SC/USA	I-381
Homolka, D., Darmstadt /D	II-369
Horwitz, Ph., Argonne, IL/USA	I- 81
Hu, Shuisheng, Shanghai/China	II-487
Hua, Tingting, Beijing/China	II-605
Huang, Chunhui, Beijing/China	II-215
Huang, Jin-wang, Guangzhou/China	II-431
Huber, A., Garching/D	I-253
Hughes, M.A., Bradford/UK	I- 23, III-755
Humphrey, J.L., Austin, TX/USA	III- 39, III- 55
Hunag, Shulan, Beijing/China	II-597
Hund, M., Saint-Etienne/F	I-511
Hussain, A., Bradford/UK	III-149
Hustedt, K.H., Braunschweig/D	III-597, III-703

I/J

Ihle, E., Garching/D	I-169
Ilic, Z., Beograd/YU	I-209
Inomata, H., Sendai/J	III-507
Inoue, K., Saga/J	II-65, II-263
Irie, J., Fukuoka/J	I-573
Ishikawa, I., Hamamatsu/J	II-159
Islanova, T. Yu., Moscow/USSR	II-377
Ivakhno, S.YU., Moscow/USSR	I-593
Jalhoom, M.G., Baghdad/Iraq	I-193
Jayasankar, P., Madras/IND	I-457
Jedináková, V., Praha/CS	III-765
Jeelani, S.A.K., Zürich /CH	III-453
Jeffreys, G.V., Birmingham/UK	III-157
Jenkins, J.A., Harwell, OX/UK	I-379
Ji, Liang-nian, Guangzhou/China	II-431
Jiang Dehua, Shandong/China	II-279
Jiang, Yu Ming, Shanghai/China	III-143, III-225
Jin, Tienzhou, Beijing/China	II-215
Jing, Pinlin, Shanghai/China	II-495
Jones, St., London/UK	III-853

K

Khan, S., London/UK	III-853
Kafarski, P., Wrocław/PL	III-669
Kalichkin, S.V., Moscow/USSR	II-197
Kanellakopulos, B., Karlsruhe/D	I-293
Kang, Sang Ihn, Lubbock, TX/USA	I-581
Karr, A.E., Parsippany, N.J. /USA	I- 41, III-943
Kása, Z., Veszprém/H	III-515
Kassaczky, E., Bratislava/CS	III-935
Katayama, Y., Kyoto/J	I-545
Kayahara, Y., Kyoto/J	II-309

Kedem, O., Rehovot/IL	I-525
Keimirov, M.A., Moscow/USSR	II-236
Kertes, A.S., Jerusalem/IL	III-631, III-741
Keymiriv, M.A., Moscow/USSR	II-236
Khalifa, S.M., Cairo/ET	II-539
Khisamutdinov, R.A., Ufa/USSR	II-527
Khopkar, S.M., Bombay/IND	II-439
Kikic, I., Trieste/I	II-173, III-479, III-715
Kim, J.I., Garching/D	I-293
Kim, K.W., Chung-Nam/Korea	I-215
King, C.J., Berkeley, CA/USA	III-631, III-741
Kirgios, I., Hannover/D	III-623
Kirkopru, A., Boulder, CO/USA	I-519
Kirou, V., Syracuse, NY/USA	III-135
Kiwan, A.M., Kuwait/State of Kuwait	II-113
Kluth, M., Karlsruhe/D	I-399
Knittel, G., Karlsruhe/D	I-223
Koganti, S.B., Kalpakkam/IND	I-413
Kojima, A., Kyoto/J	I-545
Kolarik, Z., Karlsruhe/D	I-333
Kolycheva, N.V., Moscow/USSR	II-197
Kondo, K., Fukuoka/J	I-573
Korchinsky, W.J., Manchester/UK	III-265
Korolkova, O.V., Moscow/USSR	II-197
Korpusov, G.V., Moscow/USSR	II-236
Koyama, K., Ibaraki-ken/J	I-91
Kreysa, G., Frankfurt am Main/D	III-461, III-767
Kriegel, S., Berlin (West)	I-245
Krishna, R., Dehra Dun/IND	III-539
Kroner, K.H., Braunschweig/D	III-597, III-703
Krylov, Yu.S., Moscow/USSR	II-236
Kube, B., Hannover/D	I-99
Kühl, H., Titz-Rödingen/D	I-427
Kula, M.-R., Düsseldorf/D	III-567
Kuzmin, N.M., Moscow/USSR	II-559
Kuznetsov, A.H., Moscow/USSR	I-433
Kwiatkowski, J., Warszawa/PL	III-791

L

Lack, E., Graz/A	III-645
Lackner, H., Graz/A	III-339
Lackner, K., Essen/D	III-491
Lahiere, R.J., Austin, TX/USA	III-39
Lancelot, F., Saint-Etienne/F	I-511
Lange, H.A., Saginaw, MI/USA	III-345
Lann Le, M.V., Toulouse/F	I-151
Laso, M., Zürich/CH	III-309
Lauprêtre, F., Paris/F	II-131
Lawson, G.J., Birmingham/UK	II-19
Lawson, P.N.E. Bradford/UK	I-23
Lehmann, R., Frankfurt am Main/D	II-613
Lei, Xia, Beijing/China	III-215
Leif, V.E., Moscow/USSR	III-223
Lejczak, B., Wrocław/PL	III-669
Lenhard, U., Krefeld/D	III-51
Leroy, M.J.F., Strasbourg/F	II-481, III-919

Li, Biaoguo, Beijing/China	II-215
Li, Dequian, Changchun, Jilin/China	II-231
Li, Han, Changchun/China	II-651
Li, Ji-ding, Beijing/China	II-121
Li, Jinshan, Beijing/China	II-597
Li, Jokang, Shanghai/China	III-423
Li, Junran, Beijing/China	II-215
Li, Shushen, Shanghai/China	II-487
Li, Yi-gui, Beijing/China	II-121, II-122
Li, Yuan-ying, Guangzhou/China	II-222
Likidis, Z., Hannover/D	III-695
Linzbach, G., Frankfurt am Main/D	III-767
Lisicki, Z., Warszawa/PL	III-764, III-791
Lo, T.C., Nutley, N.J./USA	I-41
Logsdail, D.H., Harwell, OX/UK	I-379, II-589
Long, Haiyan, Shanghai/China	II-495
Lonie, S.J., Caithness/UK	I-371
Lorbach, D., Cambridge, MA/USA	III-293
Lu, Jiu-fang, Beijing/China	II-121, II-122
Luciani, C., Trieste/I	III-199
Luerken, F., Krefeld/D	III-51
Ly, J., Gif-sur-Yvette/F	I-483
Lyall, E., Harwell, OX/UK	I-379
Lyaudet, G., Bessines sur Gartempe/F	I-285

M

Ma, Enxin, Shanghai/China	II-495
Maćkowiak, J., Bochum/D	III-115
Macasek, F., Bratislava/CS	I-363
Madariaga, J.M., Bilbao/E	III-839
Maier, A., Chatenay-Malabry/F	I-231
Majewski, W., Warszawa/PL	III-791
Makryaleas, K., Hannover/D	III-695
Maljković, Da., Zagreb/YU	II-471
Maljković, Du., Zagreb/YU	II-471
Marr, R., Graz/A	I-553, II-643, III-281, III-293, III-339, III-645 III-653, III-901, III-907
Marrocchelli, A., Rome/I	III-149
Martin, C.G., Pinawa, Manitoba/CDN	I-441
Martin, G., Engis/B	I-177
Martin, P.D., Harwell, OX/UK	II-589, III-331
Martinez, M., Barcelona/E	II-165
Marx, G., Berlin (West)	I-245
Mas, C., Karlsruhe/D	I-223
Masloboeva, S.M., Moscow/USSR	III-223
Massana, A., Bellaterra/E	II-239
Matsubara, K., Kawasaki/J	III-507
Matsumoto, M., Fukuoka/J	I-573
Matt, K., Garching/D	I-459
Mayer, M., Frankfurt am Main-Höchst/D	III-877
McCray, C.W., Idaho Falls, ID/USA	I-143
McDoughall, T.E., Pinawa, Manitoba/CDN	I-441
McDowell, W.J., Oak Ridge, TN/USA	I-477
Mead, D.A., Hatfield, Herts./UK	I-537
Mehandjiev, M.R., Sofia/BG	II-331
Mehandjieva, K.R., Sofia/BG	II-331
Meles, S., Zagreb/YU	I-275

Melling, J., Stevenage, Herts./UK	I-537
Melnyk, A.J., Pinawa, Manitoba/CON	III-405
Mendes Tasis, M.A., London/UK	II- 27
Meng, Shulan, Changchun, Jilin/China	II-651
Meng, Xi-quan, Beijing/China	II-565
Meng, Xiangsheng, Notre Dame, IN/USA	II-223
Meon, W., München/D	III-379
Meregalli, L., Venezia/I	I-585, II-401
Merz, A., Karlsruhe/D	I-317, III-207, III-413
Mesko, V., Skopje/YU	III-481
Meyer, E.-R., Hannover/D	III-695
Michel, P., Velizy-Villacoublay/F	I-285
Michel, Th., Garching/D	I-459
Mikéta, Gy., Budapest/H	II-519
Mikhailichenko, A.I., Moscow/USSR	II-425
Mikucki, B.A., University Park, PA/USA	I-561
Miller, J.D., Salt Lake City, UT/USA	II-187
Mills, A.L., Harwell, Oxon/UK	I-301, I-131, I-421
Milonjic, S., Beograd/YU	I-209
Miralles, N., Barcelona/E	II-165
Misek, T., Praha/CS	III- 71
Missal, P., Karlsruhe/D	III-499
Miyake, Y., Kyoto/J	II-309, II-323
Moccia, A., Rome/I	I-107
Mohan, V., Madras/IND	I-457
Molinier, J., Toulouse/F	III-239
Mollère, P. D., Belle Chasse, LA/USA	II- 49
Moore, R.J., Melbourne, Vic/AUS	III-549
Mora, J.C., Odeillo/F	III-239
Morosanova, E.I., Moscow/USSR	II-559
Mou, Xiru, Beijing/China	III-667
Moyer, B.A., Oak Ridge, TN/USA	I-477
Mrnka, M., Praha/CS	II-195
Mueller, P., Dresden/DOR	II-537
Muhammed, M., Stockholm/S	I-611, II-237, II-239
Mumford, C.J., Birmingham/UK	III-157
Munoz, M., Bellaterra/E	III-863
Muratet, G., Paris/F	III-353, III-361
Murinov, Y.I., Ufa/USSR	II- 75, II-527
Murthy, C.V.R., London /UK	II-353
Musikas, C., Fontenay-aux-Roses/F	I-261, I-267, II-479
Myers, P.E., Harwell, Ox/UK	I-379

N

Nagata, T., Kyoto/J	II-323
Najim, K., Toulouse/F	I-151
Nakai, M., Kyoto/J	II-323
Nakashio, F., Fukuoka/J	I-573
Navratil, J.D., Golden CO/USA	I-343, II-539
Naylor, A., Preston/UK	I- 13
Negri, E.D., Manchester/UK	III-265
Nekovár, P., Praha/CS	II-195
Neuman, R.D., Auburn, AL/USA	I-467, II-361
Ngoc Anh, V., Bratislava/CS	I-363
Nikitin, Yu. E., Ufa/USSR	II- 75
Nilsen, D.N., Albany, OR/USA	II-455
Nitsch, W., Garching/D	I-169, I-459, III-225, III-301
Noble, R.D., Boulder, CO/USA	I-451, I-519, III-865
Noïrot, P.A., Villeneuve D'Ascq/F	I-491
Nothhaft, A., Stuttgart/D	I- 99, I-161
Nowottny, Ch., Hannover/D	III-695

O

Ochkin, A.V., Moscow/USSR	II-195, II-196
Ollenik, R., Garching/D	I-169
Oloidi, J.O., Birmingham/UK	III-157
Olson, A.L., Idaho Falls, ID/USA	I-143, I-387
Orth, D.A., Aiken, SC/USA	I- 75, I-381
Osseo-Asare, K., University Park, PA/USA	I-561, II-175, II-345, II-409
Otillinger, F., München/D	III-445
Ovejero-Escudero, F.J., Toulouse/F	II-139
Ozawa, M., Ibaraki-ken/J	I- 91
Ozerov, R.P., Moscow/USSR	I-433, II-197

P

Paatero, E., Abo/SF	II-317
Padmanabhan, K., Madras/IND	I-457
Pajak, M., Bochum/D	III-115
Papamichael, Braunschweig/D	III-597
Pareau, D., Chatenay-Malabry/F	I-231, III-739
Park, Hyun-Soo, Chung-Nam/Korea	I-215, III-927
Patel, A.N., Nsukka/Nigeria	III-731
Pattee, D., Fontenay-aux-Roses/F	I-267
Pavasovic, V., Beograd/YU	I-209, III-107
Perez de Ortiz, E.S., London/UK	II-27, II-345, II-353
Pescher-Cluzeau, Y., Paris/F	II-503
Peter, S., Erlangen/D	III-605
Petrich, G., Karlsruhe/D	I- 31, I-393, I-399
Petrukhin, O.M., Moscow/USSR	II- 75, II-197, II-553
Pilhofer, Th., Wiesbaden/D	III-723, III-899
Piotrowicz, J., Wrocław/PL	II-205
Pitsch, H., Gif-sur-Yvette/F	I-483
Plawsky, J. L., Cambridge, MA/USA	III- 89
Plucinski, P., Wrocław/PL	III-531, III-669
Poddubnykh, L.P., Moscow/USSR	II-559
Poehlein, S.R., Atlanta, GA/USA	III-659
Poitrenaud, C., Gif- sur-Yvette/F	I-483
Poposka, F., Skopje/YU	III-481
Popov, S.O., Moscow/USSR	I-499
Porebski, T., Warszawa/PL	III-885
Porta, J.J. Karlsruhe/D	III-207, III-413
Pouillon, D., Berkeley, CA/USA	II- 99
Pouskouleli, Ottawa, ONT/CDN	II-581
Powers, L.A., Albany, OR/USA	II-455
Pratt, H.R.C., Melbourne, Vic/AUS	III-175, III-325, III-549
Preez du, A.C., Randburg/ZA	II- 83
Preston, J.S., Randburg/ZA	II- 83
Preti, U., Trieste/I	III-199
Prevost, M., Vert-le-Petit/F	III-919
Prior, A., Gerolfingen-Biel/CH	II-643
Procházka, J., Praha/CS	III-107, III-231
Prochaska, K., Poznań/PL	II-35
Prostenik, M.V., Zagreb/YU	I-275

R

Rajec, P., Bratislava/CS	I-363
Ramanujam, S., Parsippany, NJ/USA	I- 41, III-935
Ramm, H., Stuttgart/D	I-161
Rashid, Z.A., Poznań/PL	II- 35
Rebelein, F., München/D	III-387
Rehacek, V., Bratislava/CS	I-363
Reicheley-Yinger, L., Argonne, IL/USA	II-255
Renon, H., Fontainbleau/F	II-511
Reuben, B. G., London/UK	III-853
Reznicková, J., Praha/CS	III- 81
Reznik, A.M., Moscow/USSR	I-621, II-377, III-621
Rhein, H.-B., Hannover/D	III-273, III-623
Rice, N.M., Leeds/UK	II-633
Rickel, R.L., Albany, OR/USA	II-455
Rickelton, W.A., Niagara Falls, ONT/CDN	III-775
Riffel, W., Karlsruhe/D	I-399
Ritcey, G.M., Nepean, ONT/CDN	I- 51, II-581
Robertson, A.J., Niagara Falls, ONT/CDN	III-775
Rod, V., Praha/CS	II- 57, III- 81
Rodrigues de Carvalho, J.M. Lisboa/P	II-295
Romano, J., Zagreb/YU	I-275
Ross, R., Oxford/UK	I-421
Rückl, W., Graz/A	III-653
Russell, J.H., Albany, OR/USA	II-455
Rydberg, J., Göteborg/S	III- 21

S

Saito, S., Sendai/J	III-507
Sakuramoto, T., Kyoto/J	I-545
Sandino, M.C., Bilbao/E	III-839
Sandoval, S.P. Reno, NV/USA	I-572
Sastre, A., Barcelona/E	II-165
Sato, K., Hamamatsu/J	II-153, II-159
Sato, T., Tokyo/J	II-153, II-159
Savastano, C.A. London/UK	II-345
Sazonov, V.P., Kuibyshev/USSR	III-747
Schaekers, J.M., Pretoria/ZA	I-185
Schaller, C., Frankfurt am Main/D	III-461
Schein, R., Graz/A	II-643
Scheper, T., Hannover/D	III-695
Schlosser, St., Bratislava/CS	III-935
Schmidt, H., Karlsruhe/D	I-405
Schmieder, H., Karlsruhe/D	I- 33, I-117, I-309
Schoen, J., Karlsruhe/D	I-399
Schouteeten, A., Stains/F	III-739
Schrötterová, D., Praha/CS	II-195
Schügerl, K., Hannover/D	I-601, III-273, III-577, III-623, III-695
Schützeichel, P., Mainz/D	III-807
Schultze, L. E., Reno, NV/USA	I-572
Schulz, W.W., Richland, WA/USA	I- 81

Seekamp, M., Erlangen/D	III-605
Sekine, T., Tokyo/J	II-179
Semenov, S.A., Moscow/USSR	I-621, II-377, III-621
Seregina, I.P., Moscow/USSR	II-553
Serjogina, I.F., Moscow/USSR	II- 75
Seward, G.W., Phoenix, AR/USA	II- 11
Shehata, F.A., Cairo/ET	II-539
Shen, Jinglan, Shandong/China	II-279, II-287
Shen, Haihua, Shanghai/China	III-431
Shen, Zujun, Shanghai/China	III-431
Shikinev, V.M., Moscow/USSR	II-547
Shin, Y.J., Chung-Nam/Korea	I-215
Shkil, A.N., Moscow/USSR	II-553
Shuquistedt, L., Abo/SF	II-247
Sibrell, P.L. Salt Lake City, UT/USA	II-187
Siebenhofer, M., Graz/A	III-281, III-653, III-907
Simons, A.J. F., Geleen/NL	III- 31
Sinegribova, O.A., Moscow/USSR	I-433, I-593, III-831
Singh, D., Pinawa, Manitoba/CDN	III-369
Skarnemark, Göteborg/S	III- 21
Sklokin, L.I. Moscow/USSR	III-223
Slater, M.J., Bradford/UK	III-149
Sluys, van, R., Geleen/NL	III- 31
Smith, D.C., Leeds/UK	II-633
Smith, J.K., Cumbria/UK	I-201
Smith, J.M., Delft/NL	III-317
Soldenhoff, K.H., Randburg/ZA	II-123
Sovilj, M., Novi Sad/YU	III-557
Sovová, H., Praha/CS	III-231
Spivakov, B. Ya., Moscow/USSR	II-547
Sreedharan, V., Kalpakkam/IND	I-413
Srinivas, V.K., Madras/IND	I-475
Srinivasan, D., Madras/IND	I-475
Steiner, L., Zürich/CH	III- 99, III-191, III-309
Stenström, S., Lund/S	III-815, III-823
Stephan, K., Garching/D	I-293
Stepniak-Biniakiewicz, D., Poznań/PL	II-35
Stevanovic, R., Beograd/YU	I-209, III-107
Stevens, G.W., Melbourne, Vic/AUS	III-175, III-325, III-549
Stieglitz, L., Karlsruhe/D	I-239
Stitt, E.H., Bradford/UK	III- 63
Stockwell, C.L., Oxon, DX/UK	III-331
Su, Li-Min, Beijing/China	III-397
Su, Yuanfu, Shanghai/China	II-271, II-301, III-285, III-423
Suh, In-Suk, Chung-Nam/Korea	III-927
Sun, Sixiu, Shandong/China	II-279, II-287
Sun, Bing Yao, Shanghai/China	III-143, III-225
Szafranski, A., Warszawa/PL	III-764, III-791
Sze, Y., Pinawa, Manitoba/CDN	I-441
Szilassy, I., Budapest/H	II-519
Szust, J., Wrocław/PL	III-531
Szymanowski, J., Poznań/PL	II- 35, II-415

T

Takaya, H., Kyoto/J	I-545
Takeda, T., Kyoto/J	II-323
Takeuchi, Y., Hamamatsu/J	II-153
Tamada, J.A., Berkeley, CA/USA	III-631
Tavlarides, L.L., Syracuse, NY/USA	III-129, III-135
Tawfik, W.Y., Atlanta, GA/USA	III-659
Tayeb, A., Strasbourg/F	II-481
Tedder, D.W., Atlanta, GA/USA	III-659
Teng Teng, Beijing/China	II-121, II-122
Teramoto, M., Kyoto/J	I-545, II-323
Textoris, A., Bessines sur Gartempe/F	I-285
Thien, M.P., Cambridge, MA/USA	III-685
Thompson, P.J., Caithness/UK	I-371
Thornton, J.D., Caithness/UK	I-371
Thyrion, F.C., Louvain-la-Neuve/B	III-613
Tiegs, C., Erlangen/D	III-605
Todd, D.B., Saginaw, MI /USA	III-345
Todd, T.A., Idaho Falls, ID/USA	I-387
Tolic, A., Belgrade/YU	III-557
Tolstikov, G. A., Ufa/USSR	II- 75
Tomzik, S., Warszawa/PL	III-885
Torri, G., Rome/I	I-355
Tromp, M., Strasbourg/F	III-919
Tsien, H.H., Strasbourg/F	II-481
Tzirel'son, V.G., Moscow/USSR	II-197

U /V

Ueda, T., Kawasaki/J	III-507
Uhlemann, E., Potsdam/DDR	II-537
Vadasdi, K., Budapest/H	I-519
Valiente, M., Bellaterra/E	II-237, II-239, III-863
Varnek, A.A., Moscow/USSR	I-433, II-197
Vernadsky, V.I., Moscow/USS	I-499
Vialard, E., Fontenay-aux-Roses/F	I-137
Vijayan, S., Pinawa, Manitoba/CDN	III-369, III-405
Villegas, E.A., Minas Gerais/BR	II- 99
Vinogradova, J.N., Moscow/USSR	II-236
Vitart, X., Fontenay-aux-Roses/F	II-479
Vittadini, I., Venezia/I	I-585, II-401
Vogelpohl, A., Clausthal-Zellerfeld/D	III-247, III-523
Vorob'eva, G.A., Moscow/USSR	II-547

W

Wachter, R., Graz/A	I-567, III-901
Wärnheim, T., Stockholm/S	II-317
Walker, R.D., Inman, SC/USA	II-107
Walkowiak, W., Lubbock, TX/USA	I-581
Walter, R., Karlsruhe/D	I-317, III-413
Wang, Chenguo, Changchun, Jilin/China	II-232
Wang, D.I.C., Cambridge, MA/USA	III-685
Wang, Jiading, Beijing/China	III-215
Wang, Wenqing Xiaobo, Beijing/China	I-175
Wang, Z.M., Shanghai/China	III-285
Wang, Zhonghuai, Changchun, Jilin/China	II-231

Warmoeskerken, M.M.C.G., Deft/NL	III-317
Warshawsky, A., Rehovot/IL	I-525
Wasylkiewicz, St., Wrocław/PL	II-205
Watson, E.K., Niagara Falls, DNT/CDN	III-775
Waubke, M., Garching/D	III-255
Way, J.D., Boulder, CO/USA	III-865
Weidner, E., Erlangen/D	III-605
Wendt, H., Darmstadt/D	II-369
West, D.W., Stevenage/UK	II- 3
Westerholm, K., Abo/SF	II-247
Weyer, W., Titz-Rödingen/D	I-427
Wichterlová, J., Praha/CS	II- 57
Wilkins, M., Harwell, Oxon/UK	I-131
Will, R., Karlsruhe/D	I-239
Wilson, P.D., Cumbria/UK	I-201
Wingefors, S., Lund/S	III-815, III-823
Wisniewski, M., Poznan/PL	II-415
Wojtech, Frankfurt am Main-Höchst/D	III-877
Wolf, B.A., Mainz/D	III-807
Wozniak, M., Villeneuve D'Ascq/F	I-491
Wu, Fubing, Shanghai/China	II-495
Wu, Zhi-chun, Beijing/China	II-447

X/Y

Xi, Deli, Beijing/China	II-605
Xi, Zhengkai, Shandong/China	II-287
Xia, Jing-mao, Guangzhou/China	II-431
Xu, Guangxian, Beijing/China	II-215
Xu, Zhihong, Beijing/China	II-223
Yagodin, G.A., Moscow/USSR	I-433, I-593, II-197, III-622, III-627, III-677
Yamanouchi, T., Ibaraki-ken/J	I- 91
Yan, Jinying, Shanghai/China	II-495
Yan, Xiaomin, Shanghai/China	II-495
Yanagiuchi, M., Kawasaki/J	III-507
Yang, Yan-sheng, Guangzhou/China	II-222
Ye, Weizhen, Shanhai/China	II-495
Yoo, Jae-Hyung, Chung-Nam/Korea	I-215, III-927
Young, C.H., Manchester/UK	III-265
Yu Ming, Jiang, Shanghai/China	III-143
Yu, Han-chang, Guangzhou/China	II-431
Yu, Kening, Beijing/China	II-573
Yu, Qian, Beijing/China	III-215
Yu, Shu-qui, Beijing/China	II-447, II-565, II-573
Yuan, Chengye, Shanghai/China	II-487
Yurchenko, L.D., Moscow/USSR	I-621, II-377, III-621
Yurtov, E.V., Moscow/USSR	III-622, III-677

Z

Zak, M., Warszawa/PL	III-913
Zha, Jinrong, Beijing/China	II-223
Zhang, Shouhua, Shanghai/China	III-285
Zhang, Weixing, Changchun/China	II-651
Zhang, X., Beijing/China	I-585
Zhao, Qi, Shanghai/China	III-225
Zheng, Y., Beijing/China	II-175
Zhong, Yun Xiaon, Beijing/China	I-175, III-667

Zhou, Xuexi, Beijing/China
Zhu Jiawen, Shanghai/China
Zhu, Tun, Beijing/China
Zieborak, K., Warszawa/PL
Zimmer, E., Jülich/D
Zolotov, Yu. A., Moscow/USSR
Zvarova, T.I., Moscow/USSR

II-597
III-423
II-339, II-597
III-885
I-325
II- 75, I-499, II-547, II-553, II-559
II-547